Zur Chemie des Chlortrifluorids und der Fluoride des Urans, Neptuniums und Plutoniums

Kumulative Dissertation zur Erlangung des

Doktorgrades der Naturwissenschaften

(Dr. rer. nat.)

dem Fachbereich Chemie

der Philipps-Universität Marburg

(Hochschulkennziffer 1180)

vorgelegt von

Benjamin Scheibe, M. Sc.

aus

Lübbecke

Marburg (Lahn) 2020

Die Dissertation wurde am 08.12.2020 beim Fachbereich Chemie der Philipps-Universität Marburg eingereicht und am 08.01.2021 angenommen.

Datum der Disputation: 13.01.2021

Erstgutachter: Prof. Dr. Florian Kraus

Zweitgutachter: Dr. Frank Tambornino

Diese Arbeit wurde im Zeitraum von April 2017 bis November 2020 unter der wissenschaftlichen Anleitung von Prof. Dr. Florian Kraus am Fachbereich Chemie der Philipps-Universität Marburg angefertigt.

“Chlorine trifluoride, ClF_3, or "CTF" as the engineers insist on calling it, is a colorless gas, a greenish liquid, or a white solid. […] It is also quite probably the most vigorous fluorinating agent in existence — much more vigorous than fluorine itself. […] It is hypergolic with every known fuel, and so rapidly hypergolic that no ignition delay has ever been measured. It is also hypergolic with such things as cloth, wood, and test engineers, not to mention asbestos, sand, and water — with which it reacts explosively. It can be kept in some of the ordinary structural metals — steel, copper, aluminum, etc. — because of the formation of a thin film of insoluble metal fluoride which protects the bulk of the metal, just as the invisible coat of oxide on aluminum keeps it from burning up in the atmosphere. If, however, this coat is melted or scrubbed off, and has no chance to reform, the operator is confronted with the problem of coping with a metal-fluorine fire. For dealing with this situation, I have always recommended a good pair of running shoes.”

John D. Clark in Ignition!: An Informal History of Liquid Rocket Propellants.[1]

Erklärung

Ich erkläre, dass eine Promotion noch an keiner anderen Hochschule als der Philipps-Universität Marburg, Fachbereich Chemie, versucht wurde.

Ich versichere, dass ich meine vorgelegte Dissertation mit dem Titel

„Zur Chemie des Chlortrifluorids und der Fluoride des Urans, Neptuniums und Plutoniums“

selbst und ohne fremde Hilfe verfasst, nicht andere als die in ihr angegebenen Quellen oder Hilfsmittel benutzt, alle vollständig oder sinngemäß übernommenen Zitate als solche gekennzeichnet sowie die Dissertation in der vorliegenden oder einer ähnlichen Form noch bei keiner anderen in- oder ausländischen Hochschule anlässlich eines Promotionsgesuchs oder zu anderen Prüfungszwecken eingereicht habe.

Marburg, den

Benjamin Scheibe

Ich versichere, dass die im kumulativen Teil der Dissertation mit dem Titel „Zur Chemie des Chlortrifluorids und der Fluoride des Urans, Neptuniums und Plutoniums“ aufgeführten Anteile der Autoren an den verfassten Publikationen korrekt und vollständig dargelegt sind. Der kumulative Teil umfasst die Abschnitte 4.2 und 5.2. Die verfassten Publikationen sind im Abschnitt 7 abgedruckt.

Marburg, den

Benjamin Scheibe

Marburg, den

Prof. Dr. Florian Kraus (Betreuer)

Danksagung

Ein großer Dank geht an meinen Doktorvater Prof. Dr. Florian Kraus, dafür, dass er mir die Durchführung dieser Arbeit in seinen Laboren ermöglichte, die gewährten Freiheiten, das stete Interesse an meiner Forschung und für die sehr gute Betreuung.

Dr. Frank Tambornino danke ich für die Übernahme des Zweitgutachtens.

Prof. Dr. Antti Karttunen danke ich für die Einführung in quantenchemische Computerprogramme, die Entwicklung und Bereitstellung der Basissätze für CRYSTAL17, die gute Zeit in Finnland, die Diskussionsbereitschaft und die vielen beantworteten Fragen. PD Dr. Florian Weigend danke ich für die Durchführung von quantenchemischen Rechnungen.

Dr. Sergei I. Ivlev danke ich für die Hilfestellungen bei kristallographischen Fragestellungen, seiner Diskussionsbereitschaft und für eine reibungslose Leitung der kristallographischen Abteilung. Den Herren Radostan Riedel und Michael Marsch danke ich für die Pflege und Wartung der Einkristalldiffraktometer.

Prof. Dr. Thorsten Stumpf, PD Dr. Moritz Schmidt, Dr. Juliane März und Dr. Peter Kaden danke ich für die Ermöglichung mit Transuranelementen am Institut für Ressourcenökologie am Helmholtz-Zentrum Dresden-Rossendorf arbeiten zu können. Weiter danke ich allen Mitarbeitern der Abteilung Chemie der f-Elemente für ihre Unterstützung und den reibungslosen Ablauf im Kontrollbereich.

Der feinmechanischen Werkstatt des Fachbereichs Chemie danke ich für die zügige Anfertigung von Apparaturen.

Einem deutschen Professor danke ich für die Bereitstellung von Chlortrifluorid.

Den aktuellen und ehemaligen Mitgliedern der Arbeitsgruppen Kraus und Buchner, vor allem Dr. Stefan Rudel, Dr. Matthias Müller, Dr. Riane Stene und Jasmin Schönzart, danke ich für die gute Arbeitsatmosphäre und die fachlichen und außerfachlichen Gespräche.

Riane danke ich weiterhin für die Unterstützung und die gemeinsamen Aktivitäten. Meiner Mutter und Lotta danke ich für den Rückhalt und die stete Unterstützung während meines Studiums.

Lebenslauf

Persönliche Daten

Name	Benjamin Scheibe
Geburtsdatum	17.07.1992
Geburtsort	Lübbecke

Schul- und Hochschulausbildung

04/2017 – 01/2021	Promotion am Fachbereich Chemie Philipps-Universität Marburg Betreuer: Prof. Dr. F. Kraus „*Zur Chemie des Chlortrifluorids und der Fluoride des Urans, Neptuniums und Plutoniums*“
10/2014 – 03/2017	Masterstudium Chemie Philipps-Universität Marburg Betreuer der Abschlussarbeit: Prof. Dr. F. Kraus „*Darstellung und Charakterisierung von Hexafluoridouranaten(V)*“
10/2011 – 09/2014	Bachelorstudium Chemie Philipps-Universität Marburg Betreuer der Abschlussarbeit: Prof. Dr. J. Sundermeyer „*Synthese von Hexaalkylguanidinium-chalkogeniden und Untersuchungen zur Darstellung von Molybdän(IV)-sulfid aus Sulfid-basierten ionischen Flüssigkeiten*“
08/2008 – 07/2011	Leo-Sympher Berufskolleg Minden, Fachhochschulreife und staatlich geprüfter Chemisch-technischer Assistent
08/2002 – 07/2008	Jahn-Realschule Lübbecke, Mittlerer Schulabschluss

Publikationsverzeichnis

1.) L. H. Finger, B. Scheibe, J. Sundermeyer, *Synthesis of Organic (Trimethylsilyl)chalcogenolate Salts Cat[TMS-E] (E = S, Se, Te): the Methylcarbonate Anion as a Desilylating Agent*, *Inorg. Chem.* **2015**, *54*, 9568–9575.

2.) B. Scheibe, S. Lippert, S. S. Rudel, M. R. Buchner, O. Burghaus, C. Pietzonka, M. Koch, A. J. Karttunen, F. Kraus, *$NOUF_6$ Revisited: A Comprehensive Study of a Hexafluoridouranate(V) Salt*, *Chem. Eur. J.* **2016**, *22*, 12145–12153.

3.) B. Scheibe, S. S. Rudel, M. R. Buchner, A. J. Karttunen, F. Kraus, *A 1D Coordination Polymer of UF_5 with HCN as a Ligand, Chem. Eur. J.* **2017**, *23*, 291–295.

4.) S. S. Rudel, H. L. Deubner, B. Scheibe, M. Conrad, F. Kraus, *Facile Syntheses of pure Uranium(III) Halides: UF_3, UCl_3, UBr_3, and UI_3*, *Z. Anorg. Allg. Chem.* **2018**, *644*, 323–329.

5.) S. S. Rudel, S. A. Baer, P. Woidy, T. G. Müller, H. L. Deubner, B. Scheibe, F. Kraus, *Recent advances in the chemistry of uranium halides in anhydrous ammonia*, *Z. Kristallogr. - Cryst. Mater.* **2018**, *233*, 817–844.

6.) B. Scheibe, C. Pietzonka, O. Mustonen, M. Karppinen, A. J. Karttunen, M. Atanasov, F. Neese, M. Conrad, F. Kraus, *The $[U_2F_{12}]_2^-$ Anion of $Sr[U_2F_{12}]$*, *Angew. Chem.* **2018**, *130*, 2964–2968; *Angew. Chem. Int. Ed.* **2018**, 57, 2914–2918.

7.) B. Scheibe, M. R. Buchner, *Carboxylic Acid Ester Adducts of Beryllium Chloride and Their Role in the Synthesis of Beryllium Nitrates*, *Eur. J. Inorg. Chem.* **2018**, 2300–2308.

8.) L. V. Skripnikov, S. Schmidt, J. Ullmann, C. Geppert, F. Kraus, B. Kresse, W. Nörtershäuser, A. F. Privalov, B. Scheibe, V. M. Shabaev, M. Vogel, A. V. Volotka, *New Nuclear Magnetic Moment of ^{209}Bi: Resolving the Bismuth Hyperfine Puzzle*, *Phys. Rev. Lett.* **2018**, *120*, 093001.

9.) R. E. Stene, B. Scheibe, C. Pietzonka, A. J. Karttunen, W. Petry, F. Kraus, MoF_5 Revisited. *A Comprehensive Study of MoF_5*, *J. Fluorine Chem.* **2018**, *211*, 171–179.

10.) W. Nörtershäuser, J. Ullmann, L. V. Skripnikov, Z. Andelkovic, C. Brandau, A. Dax, W. Geithner, C. Geppert, C. Gorges, M. Hammen, V. Hannen, S. Kaufmann, K. König, F. Kraus, B. Kresse, Y. A. Litvinov, M. Lochmann, B. Maaß, J. Meisner, T. Murböck, A. F. Privalov, R. Sánchez, B. Scheibe, M. Schmidt, S. Schmidt, V. M. Shabaev, M. Steck, T. Stöhlker, R. C. Thompson, C. Trageser, M. Vogel, J. Vollbrecht, A. V. Volotka, C. Weinheimer, *The Hyperfine Puzzle of Strong-Field Bound-State QED*, *Hyperfine Interact.* **2019**, *240*, 51.

11.) B. Scheibe, J. Bruns, G. Heymann, M. Sachs, A. J. Karttunen, C. Pietzonka, S. I. Ivlev, H. Huppertz, F. Kraus, *UF_4 and the High-Pressure Polymorph HP-UF_4*, *Chem. Eur. J.* **2019**, *25*, 7366–7374.

12.) R. E. Stene, B. Scheibe, A. J. Karttunen, W. Petry, F. Kraus, *Lewis Acidic Behavior of $MoOF_4$ towards the Alkali Metal Fluorides in Anhydrous Hydrogen Fluoride Solutions*, *Eur. J. Inorg. Chem.* **2019**, *2019*, 3672–3682.

13.) B. Scheibe, S. I. Ivlev, A. J. Karttunen, F. Kraus, *Synthesis and Characterization of the Tetrafluoridochlorates(III) $A[ClF_4]$ (A = K, Rb, Cs)*, *Eur. J. Inorg. Chem.* **2020**, *2020*, 1319–1324.

14.) B. Scheibe, J. März, M. Schmidt, T. Stumpf, F. Kraus, *Synthesis and Crystal Structures of Transition Metal(II) Fluoridometallate(IV) Hydrates of Neptunium and Plutonium: $A^{II}M^{IV}F_6 \cdot 3H_2O$ (A^{II} = Mn, Zn; M^{IV} = Np, Pu)*, *Eur. J. Inorg. Chem.* **2020**, *2020*, 2279-2284.

15.) B. Scheibe, A. J. Karttunen, U. Müller, F. Kraus, *$Cs[Cl_3F_{10}]$: A Propeller-Shaped $[Cl_3F_{10}]^-$ Anion in a Peculiar $A^{[5]}B^{[5]}$ Structure Type*, *Angew. Chem.* **2020**, *132*, 18272–18276; *Angew. Chem. Int. Ed.* **2020**, *59*, 18116–18119.

16.) R. E. Stene, B. Scheibe, W. Petry, F. Kraus, *Synthesis and Characterization of the Hexafluoridomolybdates(V) $A[MoF_6]$ (A = Li – Cs)*, *Eur. J. Inorg. Chem.* **2020**, *19*, 1834-1843.

17.) R. E. Stene, B. Scheibe, A. J. Karttunen, W. Petry, F. Kraus, *Synthesis and Characterization of $A[W_2O_2F_9]$ (A = Li – Cs)*, *Eur. J. Inorg. Chem.* **2020**, *23*, 2260-2269.

18.) B. Scheibe, M. Patzschke, J. März, M. Conrad, F. Kraus, *A Molecular Octafluoridoneptunate(IV) Anion in $(NH_4)_4[NpF_8]$ and Theoretical Investigations of the $[MF_8]^{4-}$ System (M = Th - Bk)*, *Eur. J. Inorg. Chem.* **2020**, *39*, 3753-3759.

19.) B. Scheibe, A. J. Karttunen, F. Weigend, F. Kraus, *Photochemistry with Chlorine Trifluoride: Syntheses and Characterization of Difluorooxychloronium(V) Hexafluorido(non)metallates(V), $[ClOF_2][MF_6]$ (M = V, Nb, Ta, Ru, Os, Ir, P, Sb)*, *Chem. Eur. J.* **2020**, DOI 10.1002/chem.202003629.

20.) B. Scheibe, R. Haiges, S. I. Ivlev, U. Müller, A. J. Karttunen, K. O. Christe, F. Kraus, *Difluorochloronium(III) Fluoridometallates $ClF_2[MF_6]$ – From Molecular Building Blocks to (Helical) Chains*, *Eur. J. Inorg. Chem.* **2020**, DOI 10.1002/ejic.202000845.

21.) B. Scheibe, A. J. Karttunen, F. Kraus, *Reactions of ClF_3 with Main Group and Transition Metal Oxides: Access to Dioxychloronium(V) Fluoridometallates and Oxidofluoridometallates*, *Eur. J. Inorg. Chem.* **2020**, DOI 10.1002/ejic.202000908.

Die Veröffentlichungen 6.), 11.), 13.)-15.) und 18.)-21.) sind aus dieser Arbeit hervorgegangen, Abdrucke dieser befinden sich im Abschnitt 7.

Tagungsbeiträge

1.) 17. Deutscher Fluortag, Schmitten, **2016**, Vortrag: *Some chemistry of β−uranium(V) fluoride and uranium(VI) fluoride*.

2.) 18. Vortragstagung der Wöhlervereinigung für Anorganische Chemie, Berlin, **2016**, Kurzvortrag und Posterpräsentation: *Chemistry and properties of hexafluoridouranates(V)*, B. Scheibe, S. Lippert, S. S. Rudel, M. R. Buchner, O. Burghaus, C. Pietzonka, M. Koch, A. J. Karttunen, F. Kraus.

3.) 43. Hirschegg-Seminar Festkörperchemie, Hirschegg (Österreich), **2017**, Vortrag: *Synthese und Eigenschaften von Hexafluoridouranaten(V)*.

4.) GDCh-Wissenschaftsforum Chemie, Berlin, **2017**, Posterpräsentation: *Properties of hexafluoridouranates(V) MUF_6*, B. Scheibe, O. Mustonen, A. J. Karttunen, M. Karppinen, F. Kraus.

5.) 44. Hirschegg-Seminar Festkörperchemie, Hirschegg (Österreich), **2018**, Vortrag: *Photochemie mit Chlortrifluorid - Zugang zu $ClOF_2^+$-Salzen*.

6.) 22nd International Symposium on Fluorine Chemistry, Oxford (England), **2018**, Posterpräsentation: *Synthesis and crystallographic properties of $ClOF_2^+$ salts*, B. Scheibe, S. Ivlev, A. J. Karttunen, F. Kraus.

7.) 18. Deutscher Fluortag, Schmitten, **2018**, Vortrag: *Photochemical synthesis of $ClOF_2^+$ salts*.

8.) 19. Vortragstagung der Wöhlervereinigung für Anorganische Chemie Regensburg, **2018**, Posterpräsentation: *Photochemical synthesis of $ClOF_2^+$ salts*, B. Scheibe, A. J. Karttunen, F. Kraus.

9.) 24th Winter Fluorine Conference, Clearwater (Florida, USA), **2019**, Posterpräsentation: *Photochemistry with chlorine trifluoride - compounds with the $ClOF_2^+$ cation*, B. Scheibe, A. J. Karttunen, F. Kraus.

10.) GDCh-Wissenschaftsforum Chemie, Aachen, **2019**, Posterpräsentation: *Fluoridometallates(IV) of Neptunium and Plutonium - Synthesis, structures and theoretical investigations*, B. Scheibe, J. März, M. Patzschke, T. Stumpf, F. Kraus.

11.) Fachgruppentagung Nuklearchemie, Dresden, **2019**, Posterpräsentation: *Fluoridometallates(IV) of Neptunium and Plutonium - Synthesis, structures and theoretical investigations*, B. Scheibe, J. März, M. Patzschke, T. Stumpf, F. Kraus.

12.) Online-Vortragstagung für Anorganische Chemie der Fachgruppen Wöhler-Vereinigung und Festkörperchemie und Materialforschung, **2020**, Posterpräsentation: *To be or not to be fluorinated - chemistry of and with chlorine trifluoride*, B. Scheibe, F. Kraus.

Abkürzungsverzeichnis

aHF	*anhydrous hydrogen fluoride*, wasserfreier Fluorwasserstoff
Äq.	Äquivalente
CASSCF	*complete active space self consistent field*
CMOS	*complementary metal-oxide-semiconductor*
DFT	Dichtefunktionaltheorie
FEP	Tetrafluorethylen-Hexafluorpropylen-Copolymer
FT-IR	Fourier-Transform-Infrarot
FWHM	*full width at half maximum*, Halbwertsbreite
IR	Infrarot
LUMO	*lowest unoccupied molecular orbital*, niedrigstes unbesetztes Molekülorbital
PE	Polyethylen
PFA	Perfluoralkoxy-Polymer
PCTFE	Polychlortrifluorethylen
PP	Polypropylen
PTFE	Polytetrafluorethylen
VSEPR	*valence shell electron-pair repulsion*, Valenzschalen-Elektronenpaar-Abstoßung

Kurzzusammenfassung

Im Rahmen dieser Arbeit wurden Umsetzungen von Chlortrifluorid mit verschiedenen Verbindungsklassen untersucht. Die Reaktion von Alkalimetallfluoriden mit flüssigem Chlortrifluorid bei Raumtemperatur führt zur Bildung von Alkalimetallfluoridochloraten(III), $A[ClF_4]$ (A = K, Rb, Cs), deren Kristallstrukturen erstmalig aufgeklärt wurden. In diesen liegen planare, (fast) quadratische Tetrafluoridochlorat(III)-Anionen vor. Schwingungsspektroskopische Untersuchungen zeigten, dass Fluorwasserstoffaddukte der Alkalimetallfluoride häufig als Verunreinigungen vorliegen.

Die Umsetzung von Cäsiumfluorid mit einem Überschuss an Chlortrifluorid bei tiefen Temperaturen ermöglichte die Isolation eines Salzes mit dem ersten mehrkernigen Fluoridochlorat(III)-Anion, dem propellerförmigen $[Cl_3F_{10}]^-$-Anion. Die Kristallstruktur von $Cs[Cl_3F_{10}]$ kann dabei als ein Vertreter des seltenen $A^{[5]}B^{[5]}$-Strukturtyps beschrieben werden. Quantenchemische Rechnungen für gasförmige $[X_3F_{10}]^-$-Anionen (X = Cl, Br, I) zeigen, dass die X−F-Bindungen stark ionisch oder polar-kovalenter Natur sind.

Reaktionen von Metallpulvern, Fluoriden oder Chloriden mit überschüssigem Chlortrifluorid führen zur Bildung von Difluorochloronium(III)-Salzen, falls die Edukte stabile Fluoridometallat-Anionen ausbilden. Die Kristallstrukturen der erhaltenen Verbindungen zeigen, dass stets ein gewinkeltes ClF_2^+-Kation vorliegt, aber eine Vielzahl von Strukturmotiven ausgebildet wird. Diese reichen von molekularen Baueinheiten bis hin zu verschiedenen Ketten, welche linear, zick-zack-artig oder helical sein können.

Photochemische Umsetzungen von Oxiden, Metallpulvern oder Chloriden mit Chlortrifluorid, gegebenenfalls unter weiterer Zugabe gasförmigen Sauerstoffs, führen zur Bildung von Difluorooxychloronium(V)-Salzen, falls die Edukte stabile Fluoridometallat- oder Fluoridooxidometallat-Anionen ausbilden können. Die Kristallstrukturen dieser Verbindungen zeigen, dass stets ein pyramidales $ClOF_2^+$-Kation vorliegt, dessen Cl−O- und Cl−F-Abstände je nach Anion stark variieren.

Hydrolysereaktionen von Difluorochloronium(III)-Verbindungen oder Umsetzungen von Oxiden mit Chlortrifluorid führen zur Bildung von Dioxychloronium(V)-Salzen, falls die Edukte stabile Fluoridometallat- oder Fluoridooxidometallat-Anionen ausbilden können. In den Kristallstrukturen liegen gewinkelte ClO_2^+-Kationen vor und die Bandbreite ausgebildeter Strukturmotive der Salze ist groß.

In einem weiteren Projekt wurden die Lewis-Säure-Eigenschaften von Uranpentafluorid untersucht. Durch Umsetzungen mit verschiedenen Fluoridionendonoren wie Strontium- oder Bariumfluorid oder Hydraziniumdifluorid konnten Fluoridouranate(V) mit neuen Strukturmotiven erhalten werden. So liegt ein isoliertes Anion im Salz $Sr[UF_5(HF_2)_2]$ vor, ein zweikerniges Anion im Salz $Sr[U_2F_{12}]$ und komplexere, schichtartige Anionen in den Salzen $Ba(HF)_2U_2F_{12}$ und $(N_2H_6)U_2F_{10}(HF_2)_2$.

Die Reaktion von Uranhexafluorid mit Schwefel in wasserfreiem Fluorwasserstoff führt zur Bildung von Urantetrafluorid, welches nach der Entfernung von flüchtigen Bestandteilen eine hohe Reinheit aufweist und frei von oxidischen und sulfidischen Verunreinigungen ist. Durch Umsetzungen von Urantetrafluorid bei hohen Drücken und Temperaturen gelang die Synthese einer Hochdruckmodifikation, HP-UF_4 (*high pressure*-UF_4), welches eine komplexe Struktur aufweist.

Einkristalline Fluoridometallate(IV) des Neptuniums und Plutoniums konnten durch Reaktionen der Actinoid(IV)-oxide in Flusssäure mit Fluoridionendonoren bei Raumtemperatur oder unter hydrofluorothermalen Bedingungen erhalten werden. Die dargestellten Verbindungen kristallisieren isotyp zu den Uranverbindungen. Die Actinoid-Fluorabstände in den Salzen nehmen mit höherer Ordnungszahl ab, was durch die Actinoidenkontraktion erklärt werden kann.

Durch Oxidation des Hexafluoridouranats(V) $RbUF_6$ mit Chlortrifluorid, konnte einkristallines Rubidiumheptafluoridouranat(VI) erhalten werden. In der Kristallstruktur liegen isolierte $[UF_7]^-$-Anionen vor, welche erstmalig strukturell charakterisiert wurden.

Abstract

The reactions of chlorine trifluoride with a variety of compounds were studied in the course of this work. The reactions of alkali metal fluorides with liquid chlorine trifluoride at room temperature lead to the formation of alkali metal tetrafluoridochlorates(III), $A[ClF_4]$ (A = K, Rb, Cs). Their crystal structures were determined for the first time and they indicate the presence of planar (almost) square tetrafluoridochlorate(III) anions. Vibrational spectra of the compounds show, that hydrogen fluoride adducts of the alkali metal fluorides occur as impurities.

The reaction of cesium fluoride with an excess of chlorine trifluoride leads to the formation of a salt with a polynuclear fluoridochlorate(III) anion. The propeller-shaped $[Cl_3F_{10}]^-$ anion is obtained in the $Cs[Cl_3F_{10}]$ salt. The crystal structure of this compound can be regarded as a representative of the rare $A^{[5]}B^{[5]}$ structure type. Quantum-chemical calculations for $[X_3F_{10}]^-$ anions in the gas-phase indicate ionic or polar, covalent X−F bonds.

The reactions of metal powders, fluorides, or chlorides with an excess of chlorine trifluoride lead to the formation of difluorochloronium(III) salts if the starting material can form a stable fluoridometallate anion. A bent ClF_2^+ cation is present in the crystal structures of these compounds and a variety of structural motifs are observed. They range from molecular building blocks to linear, zig-zag, or helical chains.

Reactions of oxides, metal powders, or chlorides with chlorine trifluoride, and in some cases additional oxygen, under photochemical conditions lead to the formation of difluorooxychloronium(V) salts. The starting material has to have the ability to form stable fluoridometallate or fluoridooxidometallate anions. Pyramidal $ClOF_2^+$ cations are present in the crystal structures and the Cl−O and Cl−F distances within these cations strongly depend on the anion.

Dioxychloronium(V) salts can be obtained from the hydrolysis reactions of difluorochloronium(III) compounds, or, if the starting material can form a stable fluoridometallate or fluoridooxidometallate anion, from the reaction of oxides with chlorine trifluoride.

The Lewis acid properties of uranium pentafluoride were studied in another project. Fluoridouranates(V) were obtained from reactions of fluoride ion donors such as strontium or barium fluoride, or hydrazinium difluoride with uranium pentafluoride in anhydrous hydrogen fluoride. The obtained compounds show novel structure motifs, which were previously unknown for the fluoridouranates(V). An isolated anion is observed in the salt $Sr[UF_5(HF_2)_2]$, a dinuclear one in $Sr[U_2F_{12}]$, and more complex, layer-like anions in the salts $Ba(HF)_2U_2F_{12}$ and $(N_2H_6)U_2F_{10}(HF_2)_2$.

The reaction of uranium hexafluoride with sulfur in anhydrous hydrogen fluoride leads to the formation of uranium tetrafluoride, which can be obtained in pure form after removal of volatiles in vacuo. It has a high purity and is free from oxidic or sulfidic impurities. Under the impact of high pressure and temperature, a novel high-pressure modification of uranium tetrafluoride could be obtained. Hp-UF_4 shows a complex structure.

The reaction of neptunium or plutonium dioxide with fluoride ion donors in hydrofluoric acid at room temperature or hydrofluorothermal conditions leads to the formation of single-crystalline fluoridometallates(IV). The characterized compounds are isotypic with the respective uranium compounds and the actinoid fluorine distances tend to decrease with increasing atomic number, which is likely due to the actinoid contraction.

Single-crystalline rubidium heptafluoridouranate(VI) could be obtained from the oxidation of the hexafluoridouranate(V) $RbUF_6$ with chlorine trifluoride. Isolated $[UF_7]^-$ anions are present in the crystal structure, which could be structurally characterized for the first time.

Inhaltsverzeichnis

1. Einleitung 1
1.1. Die Halogenfluoride 1
1.1.1. Halogen(I)-fluoride 2
1.1.2. Halogen(III)-fluoride 4
1.1.3. Halogen(V)-fluoride 8
1.1.4. Halogen(VII)-fluoride 10
1.2. Die Halogenoxidfluoride 12
1.2.1. Halogen(III)-oxidfluoride 13
1.2.2. Halogen(V)-oxidfluoride 13
1.2.3. Halogen(VII)-oxidfluoride 17
2. Arbeitsmethoden 20
2.1. Arbeiten unter Luftausschluss 20
2.1.1. Handschuhkästen 20
2.2. Arbeiten mit Fluor und flüchtigen Fluoriden 20
2.2.1. Reaktionsgefäße und geeignete Materialien 20
2.2.2. Arbeiten mit Chlortrifluorid 22
2.2.3. Fluor und flüchtige Fluoride 23
2.2.4. Arbeiten mit wasserfreiem Fluorwasserstoff 24
2.2.5. UV-Reaktor für photochemische Umsetzungen 25
2.3. Arbeiten mit Transuranelementen 26
3. Analytische Methoden und quantenchemische Festkörperrechnungen 27
3.1. Einkristallstrukturanalyse 27
3.2. Infrarotspektroskopie 29
3.3. Raman-Spektroskopie 30
3.4. Quantenchemische Festkörperrechnungen 30
4. Chemie des Chlortrifluorids 32
4.1. Motivation und Zielsetzung 32
4.2. Kumulativer Teil 33

4.2.1. Synthesis and Characterization of the Tetrafluoridochlorates(III) *A*[ClF_4] (*A* = K, Rb, Cs) ... 33

4.2.2. Cs[Cl_3F_{10}]: A Propeller-Shaped [Cl_3F_{10}]$^-$ Anion in a Peculiar $A^{[5]}B^{[5]}$ Structure Type ... 35

4.2.3. Difluorochloronium(III) Fluoridometallates ClF_2[*M*F_6] – From Molecular Building Blocks to (Helical) Chains ... 37

4.2.4. Photochemistry with Chlorine Trifluoride: Syntheses and Characterization of Difluorooxychloronium(V) Hexafluorido(non)metallates(V), $ClOF_2$[*M*F_6] (*M* = V, Nb, Ta, Ru, Os, Ir, P, Sb) ... 39

4.2.5. Reactions of ClF_3 with Main Group and Transition Metal Oxides: Access to Dioxychloronium(V) Fluoridometallates and Oxidofluoridometallates .. 41

4.3. Difluorooxychloronium(V)-Verbindungen − Unveröffentlichte Ergebnisse 43

4.3.1. Darstellung und Charakterisierung von $(ClOF_2)_2$[*M*F_6] (*M* = Cr, Rh, Ge) 43

4.3.2. Darstellung und Charakterisierung von $(ClOF_2)_2$[*M*F_6] (*M* = Pd, Pt, Sn) 50

4.3.3. Darstellung und Charakterisierung von $ClOF_2$*M*F_5 (*M* = Sn, Pb) ... 57

4.3.4. Darstellung und Charakterisierung von $ClOF_2$[BF_4] ... 64

4.3.5. Darstellung und Charakterisierung von $ClOF_2$[$Mo_3O_3F_{13}$] ... 70

4.3.6. Darstellung und Charakterisierung von $(ClOF_2[OsO_3F_3])_2OsF_6$ ... 76

4.3.7. Darstellung und Charakterisierung von $(ClOF_2)_2$[AuF_4][SbF_6] ... 82

4.3.8. Vergleich der Difluorooxychloronium(V)-Verbindungen ... 87

4.4. Zusammenfassung ... 93

4.5. Ausblick ... 98

5. Fluoride und Fluoridometallate des Urans, Neptuniums und Plutoniums ... 100

5.1. Motivation und Zielsetzung ... 100

5.2. Kumulativer Teil ... 101

5.2.1. The [U_2F_{12}]$^{2-}$ Anion of Sr[U_2F_{12}] ... 101

5.2.2. UF_4 and the High-Pressure Polymorph HP-UF_4 ... 103

5.2.3. Synthesis and Crystal Structures of Transition Metal(II) Fluoridometallate(IV) Hydrates of Neptunium and Plutonium: $A^{II}M^{IV}F_6 \cdot 3H_2O$ (A^{II} = Mn, Zn; M^{IV} = Np, Pu) ... 105

5.2.4. A Molecular Octafluoridoneptunate(IV) Anion in $(NH_4)_4[NpF_8]$ and Theoretical Investigations of the $[MF_8]^{4-}$ System (M = Th - Bk) 107

5.3. Fluoridometallate(IV) des Neptuniums und Plutoniums − Unveröffentlichte Ergebnisse 108

5.3.1. Darstellung und Charakterisierung von NH_4PuF_5 und $TlMF_5$ (M = Np, Pu) 108

5.3.2. Darstellung und Charakterisierung von APu_2F_9 (A = Na, K) 113

5.4. Fluoridouranate(V) − Unveröffentlichte Ergebnisse 117

5.4.1. Darstellung und Charakterisierung von $Sr[UF_5(HF_2)_2]$ 117

5.4.2. Darstellung und Charakterisierung von $Ba(HF)_2U_2F_{12}$ 120

5.4.3. Darstellung und Charakterisierung von $(N_2H_6)U_2F_{10}(HF_2)_2$ 123

5.5. Fluoridouranate(VI) − Unveröffentlichte Ergebnisse 127

5.5.1. Darstellung und Charakterisierung von $Rb[UF_7]$ 127

5.6. Zusammenfassung 132

5.7. Ausblick 136

6. Literaturverzeichnis 138

7. Abdrucke der Publikationen 152

7.1. Synthesis and Characterization of the Tetrafluorido-chlorates(III) $A[ClF_4]$ (A = K, Rb, Cs) 152

7.2. $Cs[Cl_3F_{10}]$: A Propeller-Shaped $[Cl_3F_{10}]^-$ Anion in a Peculiar $A^{[5]}B^{[5]}$ Structure Type 171

7.3. Difluorochloronium(III) Fluoridometallates $ClF_2[MF_6]$ – From Molecular Building Blocks to (Helical) Chains 191

7.4. Photochemistry with Chlorine Trifluoride: Syntheses and Characterization of Difluorooxychloronium(V) Hexafluorido(non)metallates(V), $[ClOF_2][MF_6]$ (M = V, Nb, Ta, Ru, Os, Ir, P, Sb) 233

7.5. Reactions of ClF_3 with Main Group and Transition Metal Oxides: Access to Dioxychloronium(V) Fluoridometallates and Oxidofluoridometallates 284

7.6. The $[U_2F_{12}]^{2-}$ Anion of $Sr[U_2F_{12}]$ 334

7.7. UF_4 and the High-Pressure Polymorph HP-UF_4 365

7.8. Synthesis and Crystal Structures of Transition Metal(II) Fluoridometallate(IV) Hydrates of Neptunium and Plutonium: $A^{II}M^{IV}F_6{\cdot}3H_2O$ (A^{II} = Mn, Zn; M^{IV} = Np, Pu) 386

7.9. A Molecular Octafluoridoneptunate(IV) Anion in $(NH_4)_4[NpF_8]$ and Theoretical Investigations of the $[MF_8]^{4-}$ System (M = Th - Bk) 402
8. Anhang 420
8.1. Atomkoordinaten und kristallographische Daten 420
8.1.1. Verbindungen aus Abschnitt 4.3 420
8.1.2. Verbindungen aus Abschnitt 5.3 444
8.1.3. Verbindungen aus Abschnitt 5.4 454
8.1.4. Verbindungen aus Abschnitt 5.5 460
8.2. Basissatzdetails und optimierte Strukturen (CRYSTAL17) 462
8.2.1. Basissatzdetails für Cr, Pd und Rh 462
8.2.2. Strukturen der Verbindungen aus Abschnitt 4.3 466
8.2.3. Strukturen der Verbindungen aus Abschnitt 5.5 472
8.2.4. Mulliken-Populationsanalysen der optimierten Strukturen 473
8.3. Abbildungsverzeichnis 474
8.4. Tabellenverzeichnis 480

1. Einleitung

1.1. Die Halogenfluoride

Bisher wurde über die Existenz von zehn Halogenfluoriden berichtet, deren Zentralatome die Oxidationsstufen von +I bis +VII aufweisen (Tabelle 1).[2–15] Die Eigenschaften der Halogenfluoride unterscheiden sich dabei je nach Zentralatom und Oxidationsstufe teilweise sehr stark voneinander. Unterschiede ergeben sich vor allem in der Stabilität gegenüber Disproportionierung, Oxidations- und Fluorierungskraft und möglicher Substitutionsreaktionen. Die Halogenfluoride wurden teilweise in Übersichtsartikeln behandelt, die teilweise jedoch bereits veraltet sind und daher nicht den aktuellen Stand, vor allem bezüglich der von den Halogenfluoriden abgeleiteten Kationen und Anionen, widerspiegeln.[15–20]

Tabelle 1. Bisher beschriebene Halogenfluoride und formal durch Fluoridionenabstraktion abgeleitete Kationen oder Fluoridionenaufnahme abgeleitete Anionen. Zusätzlich ist die Klassifikation der Spezies nach dem VSEPR-Modell angegeben (bei mehrkernigen Spezies für Halogenatome ungleich Fluor). Dabei steht *A* für das Zentralatom, *B* für die Liganden und *E* für ein freies Elektronenpaar.

Abgeleitetes Kation		Halogenfluorid		Abgeleitetes Anion	
Summenformel	VSEPR	Summenformel	VSEPR	Summenformel	VSEPR
$[X_2F]^+$ (X = Cl[21,22])	AB_2E_2	XF (X = Cl[2], Br[4,5], I[7,23])	ABE_3	$[XF_2]^-$ (X = Cl[24,25], Br[26,27], I[28,29])	AB_2E_3
XF_2^+ (X = Cl[30,31], Br[32,33], I[6,23])	AB_2E_2	XF_3 (X = Cl[8], Br[9], I[6])	AB_3E_2	$[XF_4]^-$ (X = Cl[28,35,36], Br[37,38], I[6,28])	AB_4E_2
$[X_2F_5]^+$ (X = Br[34])	AB_3E_2			$[XF_5]^{2-}$ (X = I[39])	AB_5E_2
$[X_3F_8]^+$ (X = Br[34])	AB_3E_2 & AB_4E_2			$[X_2F_7]^-$ (X = Br[40,41])	AB_4E_2
				$[X_3F_{10}]^-$ (X = Cl[42], Br[41])	AB_4E_2
				$[X_4F_{13}]^-$ (X = Br[43])	AB_4E_2
XF_4^+ (X = Cl[44–46], Br[47,48], I[48,49])	AB_4E	XF_5 (X = Cl[11], Br[12], I[13])	AB_5E	$[XF_6]^-$ (X = Cl[50], Br[51], I[52–54])	AB_6E
				$[X_2F_{12}]^{2-}$ (X = I[55,56])	AB_7E
				$[X_3F_{16}]^-$ (X = I[51,54])	AB_6E
				$[X_4F_{24}]^{4-}$ (X = I[55])	AB_8E
XF_6^+ (X = Cl[57,58], Br[58–60], I[58,61,62])	AB_6	XF_7 (X = I[14])	AB_7	$[XF_8]^-$ (X = I[63,64])	AB_8

Sowohl die Halogenfluoride, als auch von ihnen durch formale Fluoridionenabstraktion bzw. -aufnahme abgeleitete Kationen bzw. Anionen sind Paradebeispiele für das Valenzelektronen-Paar-Abstoßungs-Modell (VSEPR-Modell), da die vorhergesagten Strukturen des Modells quasi immer ausgebildet werden.[65–67] Die Ionen $[ClF_6]^-$ und $[BrF_6]^-$ sind Beispiele, die nicht dem Modell folgen. Sie stellen AB_6E-Spezies dar, dabei steht *A* für das Zentralatom, *B* für die Liganden und *E* für ein freies Elektronenpaar.[51,68–70] Das VSEPR-Modell sagt für diese Ionen eine verzerrt oktaedrische Struktur voraus, es wurde jedoch berechnet, dass diese Ionen quasi oktaedrisch gebaut sind.[69,70] Im Festkörper scheint das $[BrF_6]^-$-Anion nur leicht verzerrt zu sein.[51,68] Dagegen ist das $[IF_6]^-$-Anion verzerrt oktaedrisch aufgebaut, was durch Rechnungen und schwingungsspektroskopische Untersuchungen bestätigt wurde, und für ein sterisch-aktives freies Elektronenpaar spricht.[70,71] Die Verzerrung des „$[IF_6]^-$-Anions“ ist in den bisher berichteten Kristallstrukturen auf eine Assoziation der $[IF_6]^-$-Anionen zurückzuführen, mit erhöhter Koordinationszahl der Iodatome. Zwischen diesen liegen dann μ-verbrückende Fluoratome vor und es werden beispielsweise $[I_2F_{12}]^{2-}$- oder $[I_4F_{24}]^{4-}$-Anionen ausgebildet.[55,56]

Im Folgenden wird ein Überblick über die bisher beschriebenen Halogenfluoride, deren Synthese und chemischen Eigenschaften gegeben.

1.1.1. Halogen(I)-fluoride

Die Halogenmonofluoride, *X*F, wurden für Chlor, Brom und Iod beschrieben.[2,4,7] Chlormonofluorid ist ein recht starkes Oxidationsmittel und tritt häufig als Reaktionsprodukt von höheren Chlorfluoriden und -oxyfluoriden auf. Es kann entweder aus den Elementen gewonnen werden oder aber durch Komproportionierungsreaktionen von ClF_3 mit Chlor oder Quecksilber(II)-chlorid (Gleichungen 1 bis 3).[2,72,73]

$$Cl_2 + F_2 \longrightarrow 2\ ClF \qquad (1)$$

$$Cl_2 + ClF_3 \longrightarrow 3\ ClF \qquad (2)$$

$$HgCl_2 + 2\ ClF_3 \longrightarrow 4\ ClF + HgF_2 \qquad (3)$$

Brom- und Iodmonofluorid sind thermodynamisch instabil gegenüber Disproportionierung in Brom und Bromtrifluorid beziehungsweise Iod und Iodpentafluorid.[4,5,7,23] Es wurden jedoch keine verlässlichen Angaben zu den Zersetzungstemperaturen gemacht. Brommonofluorid wurde unter anderem mittels Matrixisolationsspektroskopie bei tiefen Temperaturen nachgewiesen sowie im Festkörper mit Chlormethan als Cokristallisat.[5,74] Die Existenz des reinen Iodmonofluorids ist fragwürdig, da die berichteten Darstellungsmethoden von IF nicht reproduzierbar seien und bisherige Versuche der Cokristallisation mit inerten Lösungsmitteln scheiterten.[5,23] Es kann jedoch für beide angenommen werden, dass sie als Intermediate von Komproportionierungsreaktionen von Br_2/BrF_3 und I_2/IF_5 oder anderen Reaktionen entstehen, da formale Additionsprodukte der Monofluoride an Moleküle mit Mehrfachbindungen so erhalten werden konnten (Gleichungen 4 und 5).[75–79]

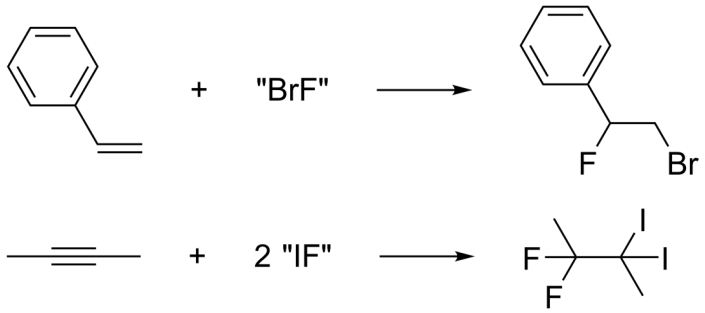

4

5

Vom ClF kann das gewinkelte $[Cl_2F]^+$-Kation abgeleitet werden, welches sich bei der Reaktion von ClF mit starken Lewis-Säuren wie BF_3 oder AsF_5 bei tiefen Temperaturen bildet (Abbildung 1 und Gleichung 6).[21,22,80,81] Ein formales Cl^+-Kation würde kein Elektronenoktett aufweisen. Für Brom und Iod wurden solche Kationen bisher nicht beschrieben.

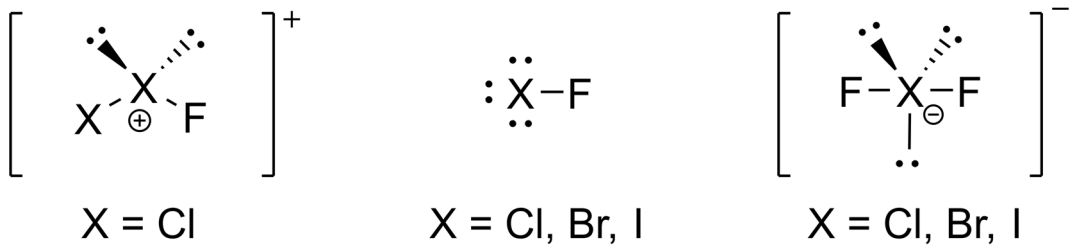

Abbildung 1. Lewis-Formeln der Halogenmonofluoride sowie davon abgeleiteter Ionen. Freie Elektronenpaare (Doppelpunkte) sind nur für das zentrale Halogenatom gezeigt.

$$AsF_5 + 2\ ClF \longrightarrow [Cl_2F][AsF_6] \qquad 6$$

Von den Halogenmonofluoriden können weiterhin die linearen $[XF_2]^-$-Anionen (AB_2E_3-Spezies, Abbildung 1), abgeleitet werden, welche im Falle des Chlors durch die direkte Reaktion von ClF mit Alkalimetallfluoriden zugänglich sind (Gleichung 7).[24,82,83] Sie sind auch indirekt durch die Fluorierung von Halogenid-Salzen, häufig mit organischen Kationen, mit (verdünntem) Fluor oder Xenondifluorid in geeigneten oxidationsstabilen Lösungsmitteln wie Acetonitril bei tiefen Temperaturen darstellbar.[25,27,28,84]

$$AF + ClF \longrightarrow A[ClF_2] \qquad (7)$$

A = K, Rb, Cs, NO

1.1.2. Halogen(III)-fluoride

Die Halogentrifluoride unterscheiden sich von den Monofluoriden in ihrer Stabilität gegenüber Disproportionierung sowie in ihrer Reaktivität.[6–9,17,23] Die Trifluoride sind aus den Elementen zugänglich (Gleichung 8), wobei unterschiedliche Temperaturen zur Darstellung verwendet werden müssen, da zum Beispiel IF_3 bereits ab −28 °C disproportioniert oder neben ClF_3 auch ClF gebildet wird. ClF_3 kann auch photochemisch aus den Elementen dargestellt werden.[85] ClF_3 und BrF_3 sind in der Gasphase und im Festkörper, wie IF_3, T-förmig (AB_3E_2-Spezies), wobei im festen Zustand die XF_3-Moleküle miteinander wechselwirken und durch Fluoratome verbrückt sind (Abbildung 2).[10,86–90]

$$X_2 + 3\,F_2 \longrightarrow 2\,XF_3 \qquad (8)$$

X = Cl, Br, I

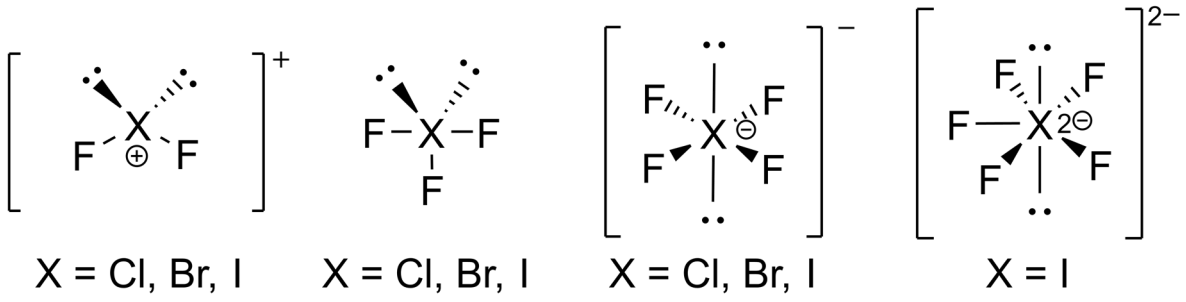

Abbildung 2. Lewis-Formeln der Halogentrifluoride sowie davon abgeleiteter Ionen. Freie Elektronenpaare (Doppelpunkte) sind nur für das zentrale Halogenatom gezeigt.

Chlor- und Bromtrifluorid sind sehr starke Oxidationsmittel, welche mit vielen Elementen und Verbindungen reagieren und sie in Fluoride hoher und höchster Oxidationsstufen überführen. Chlortrifluorid ist vermutlich das stärkste Oxidations- und Fluorierungsmittel unter den Halogenfluoriden.[8,15,17,91,92] Es reagiert leicht mit vielen Edelmetallen, wie Gold, Osmium und Iridium.[31,93] Weiterhin überführt es verschiedenste Uranverbindungen wie das Uranmetall, UO_2 oder UO_2F_2 in das Hexafluorid (Gleichungen 9 und 10).[94,95]

$$UO_2 + 3\,ClF_3 \longrightarrow UF_6 + ClO_2F + 2\,ClF \qquad 9$$

$$UO_2F_2 + 2\,ClF_3 \longrightarrow UF_6 + ClO_2F + ClF \qquad 10$$

Seine Reaktivität übertrifft meist die des reinen Fluors und das über große Temperaturbereiche, vor allem wenn ClF_3 flüssig vorliegt. Dies kann hauptsächlich auf die asymmetrische Elektronendichteverteilung des T-förmigen ClF_3-Moleküls und die Teilchendichte im flüssigen Zustand zurückgeführt werden. Chlor- und Bromtrifluorid können auch als Fluorierungsmittel zur mehr oder minder selektiven Fluorierung organischer Substrate verwendet werden.[96,97] Im Falle von ClF_3 muss jedoch mit äußerster Vorsicht, häufig verdünnt und im gasförmigen Zustand, gearbeitet werden, da dieses sonst mitunter explosiv mit organischer Materie reagieren kann.[8,98–100] Weiterhin sind Bromtrifluorid und Iodtrifluorid in der Lage metastabile Lewis-Säure-Base-Addukte mit organischen Stickstoffbasen wie Pyridin auszubilden.[6,7,101,102]

Chlortrifluorid wurde aufgrund seiner Reaktivität als chemischer Kampfstoff, Brandwaffe und Raketentreibstoff erprobt.[1,103,104] Die Verwendung als chemischer Kampfstoff beruht zum einen auf der hohen Reaktivität sowie der Toxizität des Chlortrifluorids und seiner Hydrolyseprodukte.[105–108] Je nach Bedingungen entstehen bei der Hydrolyse unter anderem Fluorwasserstoff, Chlor und Chlordioxid, vor allem wenn Wasser im Überschuss vorliegt.[105,108–110] Als Oxidationsmittel in Raketentreibstoffen ist es so reaktiv, dass es quasi mit allen gängigen Reduktionsmitteln spontan zündet.[1,111] Das Versuchsstadium hat Chlortrifluorid vermutlich aufgrund der schwierigen Handhabung und Lagerung, vor allem großer Mengen, nie verlassen. Heutzutage wird es noch in der Halbleiterindustrie als Ätzmittel und in der Nuklearindustrie als Fluorierungsmittel verwendet.[94,112–116]

Von den Trifluoriden lassen sich die gewinkelten Difluorohalonium(III)-Kationen, XF_2^+, ableiten, welche AB_2E_2-Spezies darstellen.[6,7,23,30,31,33,80,93] Die Synthese gelingt durch Umsetzung der Trifluoride mit starken Lewis-Säuren wie den Pentafluoriden, unter anderem AsF_5 und SbF_5, welche auch intermediär in Oxidationsreaktionen gebildet werden können (Gleichung 11).

$$XF_3 + MF_5 \longrightarrow XF_2[MF_6] \qquad (11)$$

X = Cl, Br, I
M = As, Sb

Das XF_2^+-Kation kann im Falle des Broms selbst als Lewis-Base reagieren und die mehrkernigen Kationen $[Br_2F_5]^+$ (AB_3E_2-Spezies) und $[Br_3F_8]^+$ (2×AB_3E_2- und AB_4E_2-Spezies), mit μ_2-verbrückenden Fluoratomen bilden (Gleichungen 12 und 13 sowie Abbildung 3).[34] Solche mehrkernigen Kationen sind für das Chlor und Iod bisher nicht bekannt.

$$BrF_2[SbF_6] + BrF_3 \longrightarrow [Br_2F_5][SbF_6] \qquad (12)$$

$$[Br_2F_5][SbF_6] + BrF_3 \longrightarrow [Br_3F_8][SbF_6] \qquad (13)$$

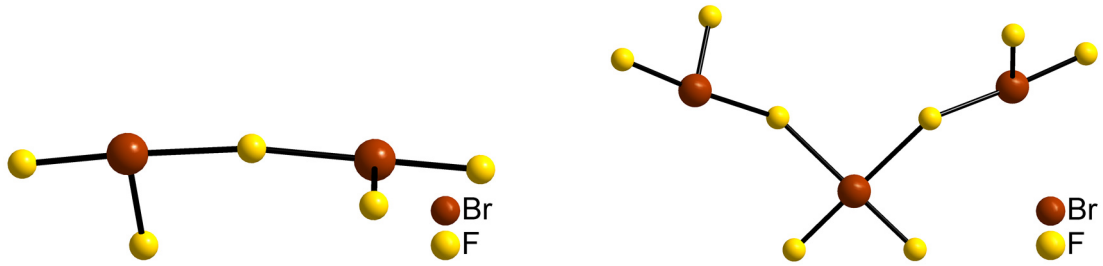

Abbildung 3. Ausschnitte aus den Kristallstrukturen von $[Br_2F_5][SbF_6]$ (links) und $[Br_3F_8][SbF_6]$ (rechts), es sind jeweils die Kationen gezeigt.[34]

Mit Fluoridionendonoren können die planaren Tetrafluoridohalogenat(III)-Anionen, $[XF_4]^-$ erhalten werden, welche AB_4E_2-Spezies darstellen (Gleichung 14).[28,36,40,117,118] Mit einem Überschuss an Trifluorid sind auch mehrkernige Anionen der Form $[X_2F_7]^-$ für X = Br und $[X_3F_{10}]^-$ mit X = Cl, Br darstellbar (Gleichungen 15 und 16 sowie Abbildung 4).[40–42]

$$XF_3 + AF \longrightarrow A[XF_4] \qquad (14)$$

X = Cl, Br, I
A = Cs, $N(CH_3)_4$

$$2\,BrF_3 + AF \longrightarrow A[Br_2F_7] \qquad (15)$$

A = Rb, Cs

$$3\,XF_3 + CsF \longrightarrow Cs[X_3F_{10}] \qquad (16)$$
X = Cl, Br

Die Chlor- bzw. Bromatome sind jeweils planar von vier Fluoratomen umgeben (AB_4E_2-Spezies). Das $[Cl_3F_{10}]^-$-Anion wurde im Rahmen dieser Arbeit im Salz $Cs[Cl_3F_{10}]$ erhalten. Im $[Br_2F_7]^-$-Anion liegt dabei ein μ_2-verbrückendes Fluoratom vor und in den $[X_3F_{10}]^-$-Anionen je ein μ_3-verbrückendes Fluoratom.

Das Goldtrifluorid verhält sich ähnlich zu den Halogentrifluoriden, da es ebenfalls $[AuF_4]^-$- und $[Au_2F_7]^-$-Anionen ausbildet.[119]

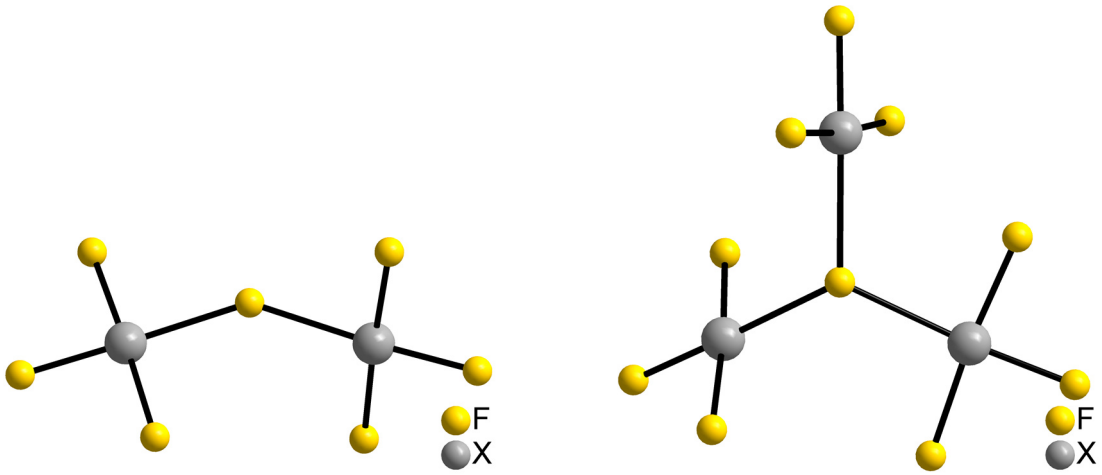

Abbildung 4. Strukturen der $[X_2F_7]^-$- (X = Au, Br) bzw. $[X_3F_{10}]^-$-Anionen (X = Cl, Br).[41,42,119]

Für Brom sind auch zwei isomere $[Br_4F_{13}]^-$-Anionen bekannt, in welchem entweder drei μ_2-verbrückende oder je ein μ_2- und μ_3-verbrückendes Fluoratom vorliegen.[43] Diese Konstitutionsisomere wurden auch quantenchemisch vorhergesagt (Abbildung 5).[120] Im Falle des Iods kann auch ein pentagonal-planares Pentafluoridoiodat(III)-Anion (AB_5E_2-Spezies) ausgehend vom $[IF_4]^-$-Anion gebildet werden (Gleichung 17).[39]

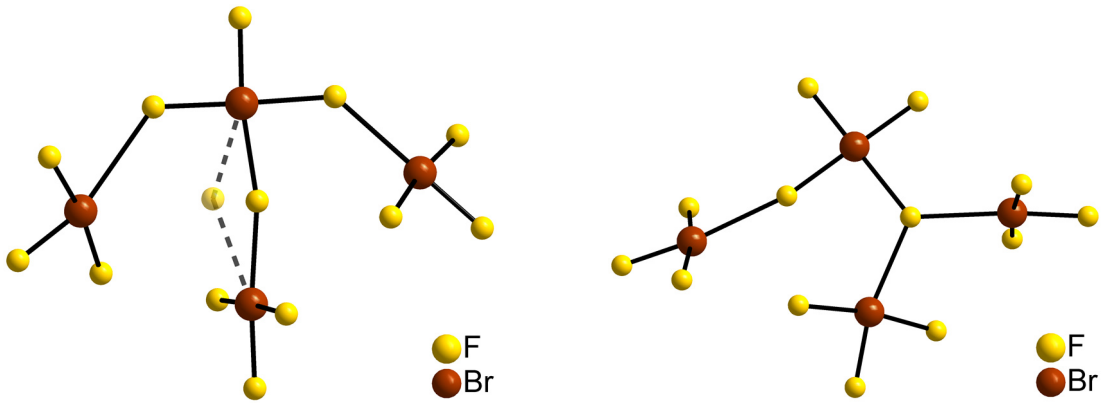

Abbildung 5. Die beiden Konstitutionsisomere des $[Br_4F_{13}]^-$-Anions.[43] Beim linken Anion ist eines der Fluoratome fehlgeordnet und das Fluoratom mit dem kleineren Besetzungsfaktor transparent dargestellt.

$$N(CH_3)_4[IF_4] \quad + \quad N(CH_3)_4F \longrightarrow (N(CH_3)_4)_2[IF_5] \qquad 17$$

1.1.3. Halogen(V)-fluoride

Die quadratisch-pyramidalen Halogenpentafluoride, XF_5 (AB_5E-Spezies, Abbildung 6), können, im Falle von Chlor und Brom, durch Fluorierung der Trifluoride mit Fluor erhalten werden, wobei hohe Temperaturen und/oder Drücke nötig sind (Gleichung 18).[11,12,121–124] ClF_5 kann dabei auch photochemisch dargestellt werden und Iodpentafluorid ist schon bei niedrigen Temperaturen aus den Elementen zugänglich.[13,125] Die Halogenpentafluoride sind im Vergleich zu den Mono- und Trifluoriden stabil gegenüber Disproportionierung. ClF_5 und BrF_5 sind gute Oxidations- und Fluorierungsmittel, ClF_5 ist dabei ein schwächeres Oxidationsmittel als ClF_3, was auf eine kinetische Hemmung aufgrund der pseudo-oktaedrischen Struktur zurückgeführt werden kann.[126] Sowohl ClF_5, als auch BrF_5 wurden als Oxidationsmittel in Raketentreibstoffen erprobt.[1,111]

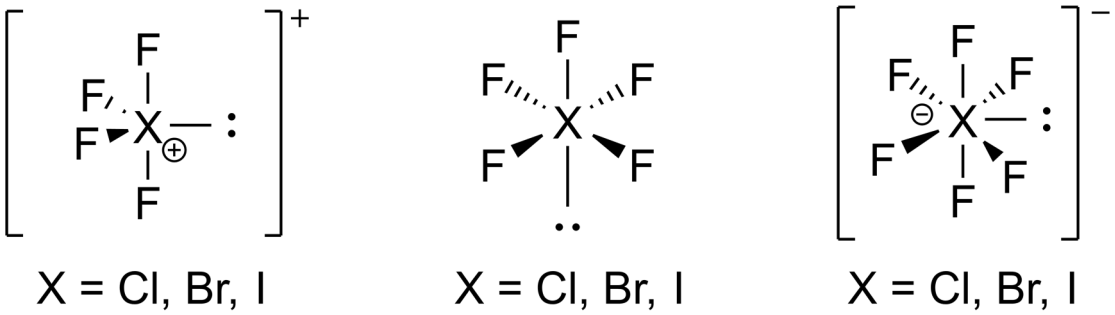

Abbildung 6. Lewis-Formeln der Halogenpentafluoride sowie davon abgeleiteter Ionen. Freie Elektronenpaare sind nur für das zentrale Halogenatom gezeigt.

$$XF_3 + F_2 \longrightarrow XF_5 \qquad (18)$$
X = Cl, Br

Mit Fluoridionenakzeptoren bilden die Pentafluoride die disphenoidalen, „wippenförmigen“, XF_4^+-Kationen aus, welche AB_4E-Spezies darstellen.[48] Sie können durch direkte Reaktionen von XF_5 mit AsF_5 oder SbF_5 gewonnen werden (Gleichung 19).[46,48] Bisher wurden keine mehrkernigen Kationen der Form $[X_2F_{11}]^+$ oder ähnliche beschrieben.

$$XF_5 + SbF_5 \longrightarrow XF_4[SbF_6] \qquad (19)$$
X = Cl, Br, I

Mit Fluoridionendonoren wie Alkalimetallfluoriden oder Tetramethylammoniumfluorid werden Hexafluoridohalogenate(V), $[XF_6]^-$, ausgebildet (AB_6E-Spezies), welche jedoch unterschiedliche thermische Stabilitäten aufweisen (Gleichung 20).[50,53,118,127] Die Hexafluoridochlorat(V)-Salze zersetzen sich sehr leicht, selbst bei tiefen Temperaturen. Am stabilsten scheinen die entsprechenden Iodverbindungen zu sein.

$$XF_5 + AF \longrightarrow A[XF_6] \qquad (20)$$
X = Cl, Br, I
A = Cs, $N(CH_3)_4$

Wie oben bereits beschrieben, ist das freie Elektronenpaar in den $[ClF_6]^-$- und $[BrF_6]^-$-Anionen, im Vergleich zum $[IF_6]^-$-Anion, nicht teil der Valenzschale und somit sterisch inaktiv.[51,68–70,128,129] Für das System Fluoridionendonor/Iodpentafluorid wurde eine Vielzahl mehrkerniger Anionen strukturell charakterisiert: $[I_3F_{16}]^-$, $[I_2F_{12}]^{2-}$, $[I_2F_{10}(HF_2)_2]^{2-}$ und $[I_4F_{24}]^{4-}$ (Abbildung 7).[51,55,56] Komplexe polymere Anionen sind ebenfalls bekannt.[56] Die Koordinationszahl der Iodatome beträgt in diesen Anionen sieben oder acht, sodass formal AB_7E- oder AB_8E-Spezies vorliegen.

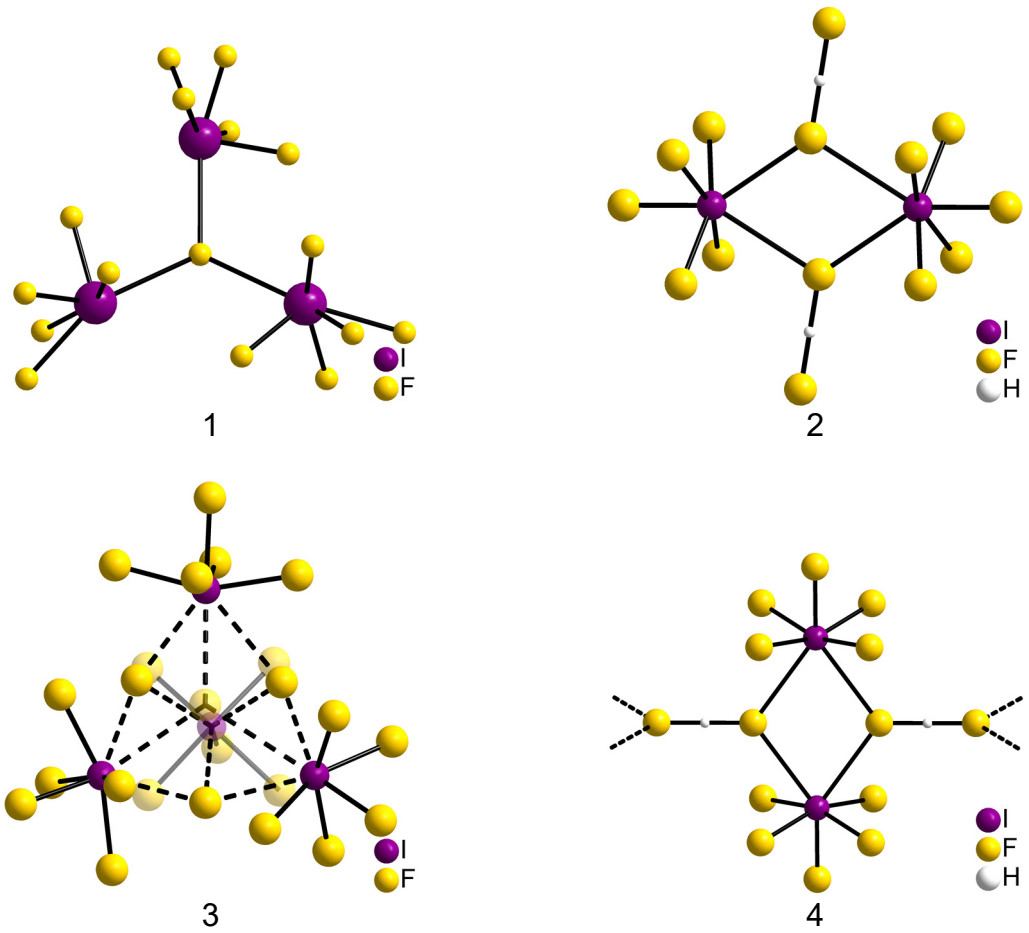

Abbildung 7. Verschiedene mehrkernige Fluoridoiodate(V): $[I_3F_{16}]^-$ (1), $[I_2F_{12}(HF_2)_2]^{2-}$ (2) $[I_4F_{24}]^{4-}$ (3) und ein Ausschnitt aus einem polymeren Anion (4) mit verbrückenden $[HF_2]^-$-Anionen.[51,55,56]

1.1.4. Halogen(VII)-fluoride

Das einzig bisher bekannte Halogenheptafluorid ist das IF_7, welches pentagonal-bipyramidal aufgebaut ist und eine *AB*$_7$-Spezies darstellt (Abbildung 8).[130] Es ist durch Fluorierung von IF_5 zugänglich.[14] Von diesem Heptafluorid kann durch Fluoridionenabstraktion mit zum Beispiel SbF_5 das oktaedrische IF_6^+-Kation erhalten werden (Gleichung 21).[58,61] Entsprechende XF_6^+-Kationen sind auch für Chlor und Brom bekannt, aufgrund der (bisherigen) Nichtexistenz des ClF_7 und BrF_7 müssen diese jedoch indirekt dargestellt werden. Dies gelingt durch Fluorierung der Pentafluoride mit sehr starken Fluorierungsmitteln wie KrF^+- und $[Kr_2F_3]^+$-Kationen, PtF_6 oder in situ erzeugten NiF_3^+-Kationen in Lösungen oder Suspensionen in den reinen Pentafluoriden oder wasserfreiem Fluorwasserstoff als Lösungsmittel (Gleichungen 22 bis 24).[57–60,131]

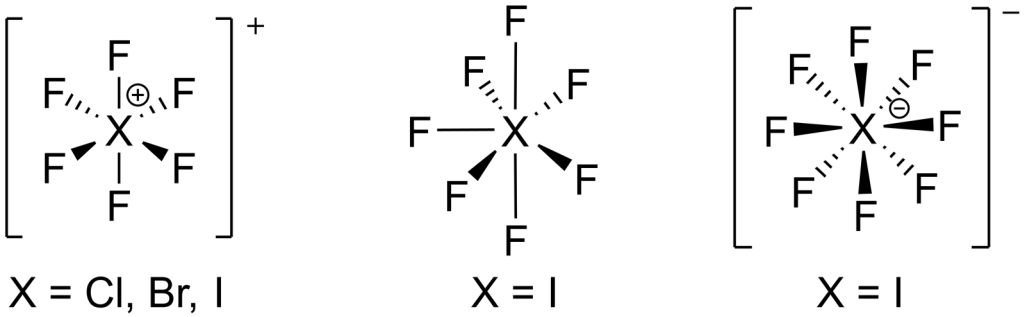

Abbildung 8. Lewis-Formeln des bekannten Halogenheptafluorids sowie davon abgeleiteter Ionen.

$$IF_7 + SbF_5 \longrightarrow IF_6[SbF_6] \qquad 21$$

$$2\ ClF_5 + 2\ PtF_6 \xrightarrow{h\nu} ClF_2[PtF_6] + ClF_6[PtF_6] + F_2 \qquad 22$$

$$XF_5 + KrF^+ \longrightarrow XF_6^+ + Kr \qquad 23$$

X = Cl, Br

$$XF_5 + NiF_3^+ \longrightarrow XF_6^+ + NiF_2 \qquad 24$$

X = Cl, Br

Entsprechende Versuche die Heptafluoride durch Verdrängungsreaktionen mit starken Lewis-Basen wie NOF aus den XF_6^+-Salzen auszutreiben scheiterten, es wurde Zersetzung zu Fluor und dem Halogenpentafluorid beobachtet, was mit den berechneten geringen energetischen Barrieren für eine Fluorabspaltung der hypothetischen ClF_7- und BrF_7-Moleküle übereinstimmt (Gleichungen 25 und 26).[57–60,70,131]

$$ClF_6[PtF_6] + NOF \longrightarrow NO[PtF_6] + ClF_5 + F_2 \qquad 25$$

$$BrF_6[AsF_6] + NOF \longrightarrow NO[AsF_6] + BrF_5 + F_2 \qquad 26$$

Die Umsetzung von Iodheptafluorid mit einem starken Fluoridionendonor wie Tetramethylammoniumfluorid führt zur Bildung des quadratisch-antiprismatischen Octafluoridoiodat(VII)-Anions, $[IF_8]^-$ (AB_8-Spezies).[63,132] Die Existenz solcher Ionen für Chlor und Brom ist fragwürdig, da zumindest im Falle des Chlors eine so hohe Koordinationszahl sehr ungünstig ist und indirekte Syntheserouten, gegebenenfalls durch Fluorierung von $[XF_6]^-$-Salzen in der Präsenz eines Fluoridionendonors, ausgenutzt werden müssten.

1.2. Die Halogenoxidfluoride

Von den Halogenoxidfluoriden wurden bisher dreizehn beschrieben, deren Zentralatome die Oxidationsstufen von +III bis +VII aufweisen (Tabelle 2). Von diesen sind einige jedoch sehr instabil gegenüber Disproportionierung, teilweise sehr kurzlebig oder deren Existenz fragwürdig.[133–139] Weiterhin können sich vor allem die Bromoxidfluoride spontan und explosiv zersetzen, eine Eigenschaft, die bereits die Bromoxide zeigen.[137,140] Die Halogenoxidfluoride und davon abgeleitete Ionen wurden teilweise in Übersichtsartikeln behandelt, welche jedoch im Bereich der abgeleiteten Ionen meist nicht auf dem aktuellen Stand sind.[18,20,141–143]

Tabelle 2. Bisher beschriebene Halogenoxidfluoride und durch Fluoridionenabstraktion abgeleitete Kationen und durch Fluoridionenaufnahme abgeleitete Anionen. Zusätzlich ist die Klassifikation der Spezies nach dem VSEPR-Modell angegeben. Dabei steht *A* für das Zentralatom, *B* für die Liganden und *E* für ein freies Elektronenpaar.

Abgeleitetes Kation		Halogenfluorid		Abgeleitetes Anion	
Summenformel	VSEPR	Summenformel	VSEPR	Summenformel	VSEPR
unbekannt	-	XOF (X = Cl[133–136])	AB_2E_2	unbekannt	-
XOF_2^+ (X = Cl[144–146], Br[147–149], I[139,150])	AB_3E	XOF_3 (X = Cl[151,152], Br[147,153], I[154,155])	AB_4E	$[XOF_4]^-$ (X = Cl[146,156], Br[157–159], I[160])	AB_5E
				$[XOF_5]^{2-}$ (X = I[161])	AB_6E
				$[XOF_6]^{3-}$ (?) (X = I[161])	AB_7E
XO_2^+ (X = Cl[162,163], Br[164,165], I[138,139])	AB_2E	XO_2F (X = Cl[166,167], Br[147,168], I[138,154])	AB_3E	$[XO_2F_2]^-$ (X = Cl[169,170], Br[158,159], I[171,172])	AB_4E_2
				$[XO_2F_3]^{2-}$ (X = I[173])	
unbekannt	-	XOF_5 (X = I[174,175])	AB_6	$[XOF_6]^-$ (X = I[132,176])	AB_6
$XO_2F_2^+$ (X = Cl[177,178], I(?)[139,179])	AB_4	XO_2F_3 (X = Cl[180,181], I[182,183])	AB_5	$[XO_2F_4]^-$ (X = I[179,184])	AB_6
				$[XO_2F_5]^{2-}$ (X = I[184])	AB_7
unbekannt	-	XO_3F (X = Cl[167,185], Br[186], I(?)[138,139])	AB_4	$[XO_3F_2]^-$ (X = Br[187])	AB_5

1.2.1. Halogen(III)-oxidfluoride

Das einzige sicher nachgewiesene Halogenoxidfluorid in der Oxidationsstufe +III ist das Chloroxidfluorid, ClOF, welches auch als Chlorosylfluorid bezeichnet wird.[133–136] Es entsteht vor allem als Intermediat bei der Umsetzung von Chlortrifluorid mit sauerstoffhaltigen Verbindungen wie Wasser.[109,110,133] Die Lebenszeit ist sehr kurz und es disproportioniert zu Chlordioxidfluorid, ClO_2F, und Chlormonofluorid (Gleichung 27).

$$2\ ClOF \longrightarrow ClO_2F + ClF \qquad 27$$

1.2.2. Halogen(V)-oxidfluoride

Es sind zwei mögliche Zusammensetzungen für Halogenoxidfluoride der Oxidationsstufe +V möglich: XOF_3 und XO_2F. Die disphenoidalen Halogenoxidtrifluoride (AB_4E-Spezies) sind für Chlor, Brom und Iod bekannt und bei Standardbedingungen flüssig ($ClOF_3$ und $BrOF_3$) oder fest (IOF_3) (Abbildung 9).[147,151–154,188,189]

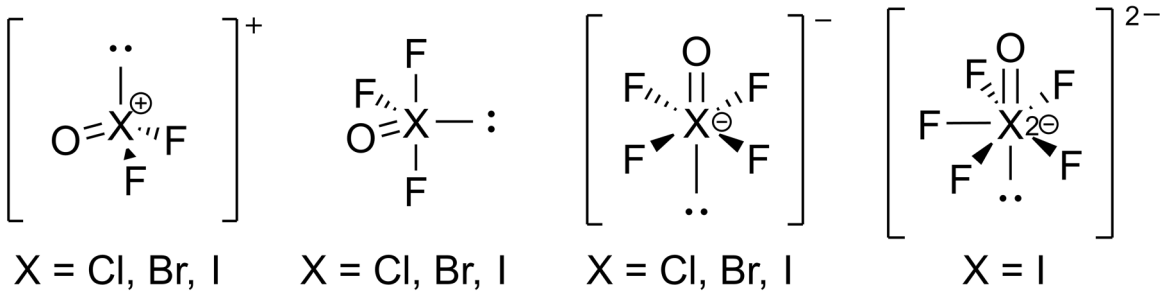

Abbildung 9. Lewis-Formeln der bekannten Halogenoxidtrifluoride sowie davon abgeleiteter Ionen. Freie Elektronenpaare sind nur für das zentrale Halogenatom gezeigt.

$ClOF_3$ ist durch Tieftemperaturfluorierung von Chlor(I)-oxid beziehungsweise -nitrat erhältlich (Gleichungen 28 und 29) und photochemische Synthesemethoden wurden ebenfalls beschrieben, welche jedoch eine aufwändige Trennung von Nebenprodukten erfordern.[151,152,190–192] $ClOF_3$ soll reaktiver als ClF_3 sein und wurde ebenso als Oxidationsmittel in Raketentreibstoffen erprobt.[1,152,193] $BrOF_3$ kann entweder indirekt durch Verdrängungsreaktionen des Salzes $K[BrOF_4]$, welches durch die vorsichtige Hydrolyse von $K[BrF_6]$ zugänglich ist, mit Fluorwasserstoff oder durch Sauerstoff/Fluor-Austausch von BrF_5 dargestellt werden (Gleichungen 30 und 31).[147,153]

IOF_3 kann durch die Reaktion von IF_5 und I_2O_5 bei höheren Temperaturen synthetisiert werden, wobei unter Umständen auch IO_2F entstehen kann (Gleichung 32).[154,194]

$$2\,F_2 + Cl_2O \xrightarrow{\text{NaF/CsF, } -78\,°C} ClOF_3 + ClF \qquad 28$$

$$2\,F_2 + ClONO_2 \xrightarrow{-35\,°C} ClOF_3 + NO_2F \qquad 29$$

$$K[BrOF_4] + HF \longrightarrow BrOF_3 + K[HF_2] \qquad 30$$

$$BrF_5 + LiNO_3 \longrightarrow BrOF_3 + LiF + NO_2F \qquad 31$$

$$3\,IF_5 + I_2O_5 \longrightarrow 5\,IOF_3 \qquad 32$$

Die Halogenoxidtrifluoride können wie die Halogenfluoride sowohl als Lewis-Basen als auch als Lewis-Säuren reagieren. Durch Fluoridionenabstraktion sind die pyramidalen XOF_2^+-Kationen zugänglich (*AB*$_3$*E*-Spezies, Gleichung 33) und durch formale Fluoridionenaufnahme die quadratisch-pyramidalen $[XOF_4]^-$-Anionen (*AB*$_5$*E*-Spezies, Gleichungen 34 bis 37).[139,145,146,149,156,157,159,195,196] Für Iod ist auch das pentagonal-pyramidale $[IOF_5]^{2-}$-Anion (*AB*$_6$*E*-Spezies) bekannt (Gleichung 42).

$$XOF_3 + SbF_5 \longrightarrow XOF_2[SbF_6] \qquad 33$$
X = Cl, Br, I

$$CsF + ClOF_3 \longrightarrow Cs[ClOF_4] \qquad 34$$

$$K[BrF_6] + H_2O \longrightarrow K[BrOF_4] + 2\,HF \qquad 35$$

$$ANO_3 + IF_5 \longrightarrow A[IOF_4] + NO_2F \qquad 36$$
A = Li, K, Cs

$$10\,CsF + I_2O_5 + 3\,IF_5 \longrightarrow 5\,Cs_2[IOF_5] \qquad 37$$

Weiterhin wurde über die Existenz eines $[IOF_6]^{3-}$-Anions spekuliert.[161] Ein mehrkerniges komplexes Anion, bestehend aus $[BrF_4]^-$-Anionen, welche an $BrOF_3$-Moleküle koordinieren, liegt in der Verbindung $NO_2Br_3O_2F_{10}$ vor (Abbildung 10).[189] Die Fluoratome der $[BrF_4]^-$-Anionen sind dabei terminal gebunden oder wirken μ_2- oder μ_3-verbrückend.

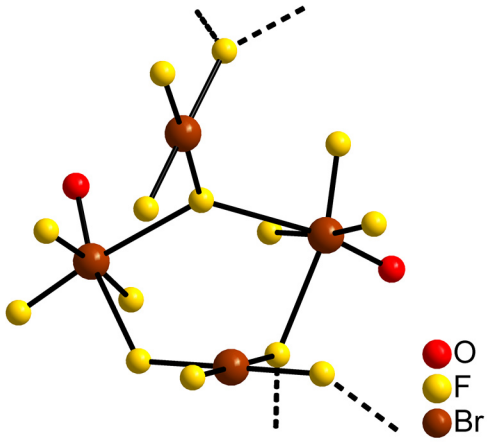

Abbildung 10. Ausschnitt aus dem komplexen Anion der Verbindung $NO_2Br_3O_2F_{10}$.[189] Die Fluoratome der $[BrF_4]^-$-Anionen sind μ_2- oder μ_3-verbrückend.

Die pyramidalen Halogendioxidfluoride, XOF_2, sind für Chlor, Brom und Iod bekannt (*AB*$_3$*E*-Spezies, Abbildung 11).[138,154,166,168,194,197] Sie werden häufig als Halogenylfluoride bezeichnet und unterscheiden sich sowohl in ihren physikalischen als auch chemischen Eigenschaften voneinander. ClO_2F und BrO_2F sind beides Gase bei Standardbedingungen, wohingegen IO_2F fest vorliegt.[154,166,168] Das endotherme BrO_2F kann sich spontan ab 10 °C, mitunter explosiv, zersetzen.[70,137] ClO_2F und IO_2F sind dagegen thermodynamisch deutlich stabiler.[137]

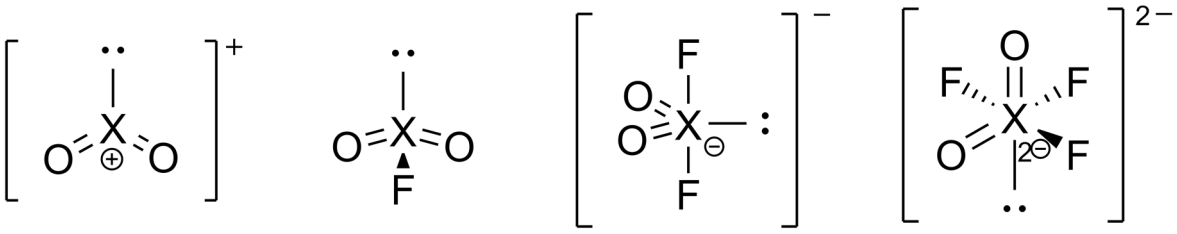

Abbildung 11. Lewis-Formeln der bekannten Halogendioxidfluoride sowie davon abgeleiteter Ionen. Freie Elektronenpaare sind nur für das zentrale Halogenatom gezeigt.

Für die Synthese der Dioxidfluoride werden je recht unterschiedliche Edukte und Bedingungen benötigt. Zum einen können ClO_2F und BrO_2F durch Fluorierung der instabilen Dioxide bei tiefen Temperaturen erhalten werden, zum anderen durch Fluorierung der Chlorate beziehungsweise Bromate (Gleichungen 38 bis 40).[137,141,198] Im Falle des IO_2F kann Iod(V)-oxid mit Iodpentafluorid bei erhöhter Temperatur umgesetzt werden, wobei sich zunächst IOF_3 bildet, welches leicht zu IO_2F und IF_5 pyrolysierbar ist (Gleichung 41).[154,194]

$$2\,XO_2 + F_2 \longrightarrow 2\,XO_2F \qquad (38)$$
X = Cl, Br

$$6\,A[ClO_3] + 4\,ClF_3 \longrightarrow 6\,AF + 2\,Cl_2 + 3\,O_2 + 6\,ClO_2F \qquad (39)$$
A = Na, K

$$2\,Na[BrO_3] + BrF_5 + 2\,HF \longrightarrow 3\,BrO_2F + 2\,Na[HF_2] \qquad (40)$$

$$IF_5 + 2\,I_2O_5 \longrightarrow 5\,IO_2F \qquad (41)$$

Die Halogendioxidfluoride können sowohl als Lewis-Basen als auch als Lewis-Säuren reagieren. Mit Fluoridionenakzeptoren wie AsF_5 oder SbF_5 bilden die Halogendioxidfluoride die gewinkelten Dioxyhalonium-Kationen, XO_2^+, welche AB_2E-Spezies darstellen (Gleichung 42).[138,139,143,147,163,165,168,199,200]

$$XO_2F + MF_5 \longrightarrow XO_2[MF_6] \qquad (42)$$
X = Cl, Br, I; M = As, Sb

Neben Fluoridometallat- oder Fluoridooxidometallat-Anionen sind für das ClO_2^+-Kation auch Salze mit Perchloratometallat-Anionen, das heißt Salze, in denen $[ClO_4]^-$-Anionen als Liganden fungieren, bekannt.[201–209] Im Falle des Iods wurden bisher keine Kristallstrukturen mit dem IO_2^+-Kation berichtet und die Salze zersetzen sich leicht im Vergleich zu den Chlor- und Bromhomologen.[139] Mehrkernige Kationen der Form $[Br_3O_6]^+$ und $[BrCl_2O_6]^+$ wurden erst kürzlich beschrieben und können als ein zentrales $[BrO_2]^-$-Anion, welches von zwei ClO_2^+- oder BrO_2^+-Kationen umgeben ist, aufgefasst werden (Abbildung 12).[137]

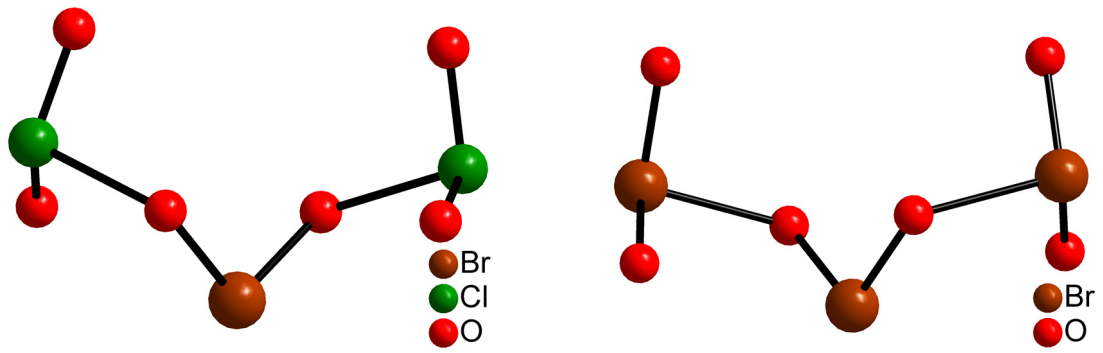

Abbildung 12. Die mehrkernigen $[BrCl_2O_6]^+$- und $[Br_3O_6]^+$-Kationen.[137]

Von den Halogendioxidfluoriden können die bisphenoidalen $[XO_2F_2]^-$-Anionen (*AB*$_4$*E*-Spezies) abgeleitet werden.[158,170,172,210] Die Synthese gelingt entweder durch Umsetzung des Halogendioxidfluorids mit einem Fluoridionendonor oder durch Fluorierung von Halogenaten(V), $[XO_3]^-$, mit BrF_5 oder Flusssäure (Gleichungen 43 bis 45).[158,159,169–172,210,211] Manche Salze mit dem $[IO_2F_2]^-$-Anion zeigen dabei nicht-lineare optische Eigenschaften.[212] Das $[IO_2F_2]^-$-Anion kann nochmals als Lewis-Säure agieren und ein weiteres Fluoridion, unter der Bildung des cis-$[IO_2F_3]^{2-}$-Anions (*AB*$_5$*E*-Spezies), aufnehmen (Gleichung 46).[173]

$$CsF + ClO_2F \longrightarrow Cs[ClO_2F_2] \qquad 43$$

$$2\,K[BrO_3] + 2\,BrF_5 \longrightarrow 2\,K[BrO_2F_2] + 2\,BrF_3 + O_2 \qquad 44$$

$$A[IO_3] + 2\,HF \longrightarrow A[IO_2F_2] + H_2O \qquad 45$$

A = Li, Na, K, Rb, Cs, NH_4

$$N(CH_3)_4[IO_2F_2] + N(CH_3)_4F \longrightarrow (N(CH_3)_4)_2[IO_2F_3] \qquad 46$$

1.2.3. Halogen(VII)-oxidfluoride

Drei verschiedene Halogenoxidfluoride mit dem Zentralatom in der Oxidationsstufe +VII wurden bisher beschrieben. Diese sind jedoch (bisher) nicht für alle Halogene bekannt. Ein Halogenoxidtetrafluorid ist bisher nur für Iod bekannt, welches durch die Hydrolyse von IF_7 erhalten werden kann (Gleichung 47) und eine oktaedrische *AB*$_6$-Spezies darstellt (Abbildung 13).[174,175] Die Lewis-Base-Eigenschaften sind nicht gesichert, aber es ist bekannt, dass es als Lewis-Säure reagieren kann und ein pentagonal-bipyramidales $[IOF_6]^-$-Anion bildet.[139,176,213]

$$IF_7 + H_2O \longrightarrow IOF_5 + 2\,HF \qquad 47$$

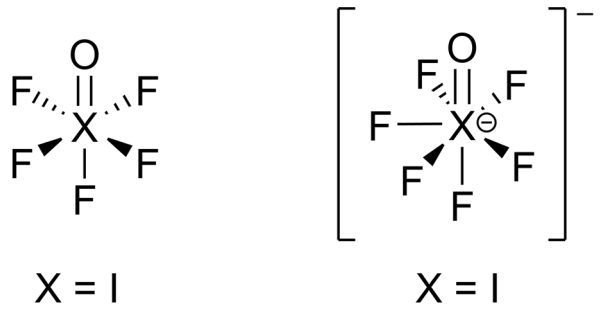

Abbildung 13. Lewis-Formeln des bekannten Halogenoxidtetrafluorids sowie des davon abgeleiteten Anions.

Die Halogendioxidtrifluoride, XO_2F_3, sind nur für Chlor und Iod bekannt und pentagonal-bipyramidal gebaut (*AB*$_5$-Spezies, Abbildung 14). ClO_2F_3 ist bisher nur mit dem sehr starken Oxidationsmittel PtF_6 zugänglich und muss aus dem Salz $ClO_2F_2[PtF_6]$ mit einer starken Lewis-Base wie NO_2F ausgetrieben werden (Gleichungen 48 und 49).[177,178,180,181] IO_2F_3 kann durch Entwässerung von HIO_2F_4 mit SO_3 erhalten werden, eine Existenz eines isolierten $IO_2F_2^+$-Kations ist fragwürdig (Gleichung 50).[179,182,214] Mit Fluoridionendonoren kann IO_2F_3 sowohl $[IO_2F_4]^-$- als auch $[IO_2F_5]^{2-}$-Anionen bilden, welche oktaedrische *AB*$_6$-Spezies oder pentagonal-bipyramidale *AB*$_7$-Spezies darstellen.[179,184]

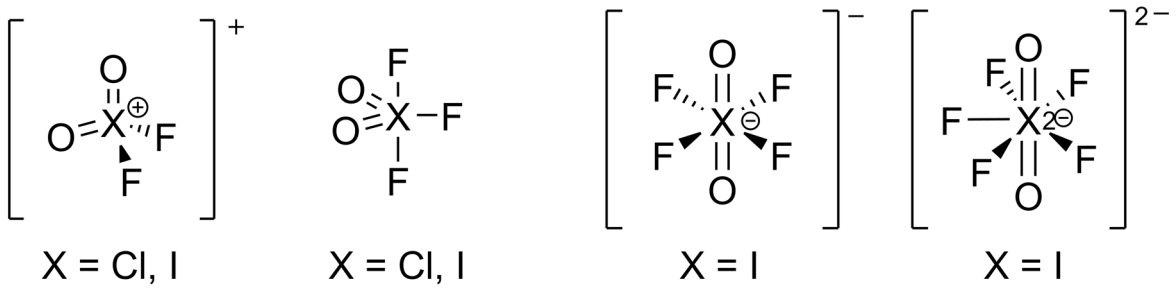

Abbildung 14. Lewis-Formeln der bekannten Halogendioxidtrifluoride sowie davon abgeleiteter Ionen.

$$2\ ClO_2F + 2\ PtF_6 \longrightarrow ClO_2F_2[PtF_6] + ClO_2[PtF_6] \qquad 48$$

$$ClO_2F_2[PtF_6] + NO_2F \longrightarrow ClO_2F_3 + NO_2[PtF_6] \qquad 49$$

$$HIO_2F_4 + SO_3 \longrightarrow IO_2F_3 + HSO_3F \qquad 50$$

Die Halogentrioxidfluoride, XO_3F, besitzen den höchsten Sauerstoffgehalt unter den Halogenoxidfluoriden, sind für Chlor und Brom bekannt und tetraedrisch gebaut (*AB*$_4$-Spezies, Abbildung 15). Die Existenz von IOF_3 ist nicht gesichert.[138,139] ClO_3F ist durch Fluorierung von Chloraten(V) bei tiefen Temperaturen und BrO_3F durch Fluorierung von Perbromaten(VII), $[BrO_4]^-$, zugänglich (Gleichungen 51 und 52).[167,185,186]

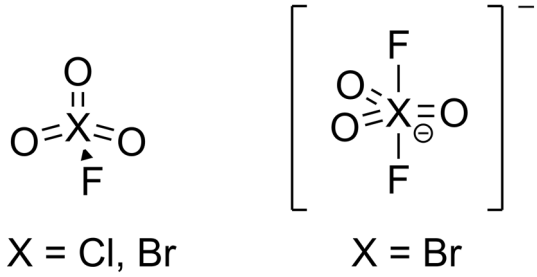

Abbildung 15. Lewis-Formeln der bekannten Halogentrioxidfluoride sowie des davon abgeleiteten Anions.

$$K[ClO_3] + F_2 \longrightarrow KF + ClO_3F \qquad 51$$

$$K[BrO_4] + AsF_5 + 2\,HF \longrightarrow BrO_3F + H_3O[AsF_6] + K[HF_2] \qquad 52$$

ClO_3F wurde wie viele andere Chlorfluoride und -oxidfluoride als Oxidationsmittel in Raketentreibstoffen erprobt, aber es ist deutlich unreaktiver als diese, was mit der tetraedrischen Gestalt des Moleküls und einer damit einhergehenden kinetischen Stabilität erklärt werden kann.[1,142] Das $[BrO_3F_2]^-$-Anion ist durch Umsetzung von BrO_2F_3 mit Fluoridionen erhältlich und mit Lewis-Säuren wie SbF_5 reagieren die Halogentrioxidfluoride unter Sauerstoffabspaltung zu XO_2^+-Salzen.[187,201]

2. Arbeitsmethoden

2.1. Arbeiten unter Luftausschluss

2.1.1. Handschuhkästen

Die Handhabung von luft- und hydrolyseempfindlichen Substanzen erfolgte in den Handschuhkästen MB10 compact und Labstar des Herstellers M. Braun Inertgas-Systeme GmbH. Die Handschuhkästen wurden mit Argon der Reinheit 5.0 als Schutzgas betrieben. Das Argon wurde mit den Reinigungssystemen der Handschuhkästen, BTS-Katalysator und Molekularsieb 3 Å, von möglichen Sauerstoff- und Wasserspuren weitgehend befreit. Geräte und Reaktionsgefäße wurden vor dem Einbringen in den Handschuhkasten dreimal in der entsprechenden Schleuse sekuriert.

2.2. Arbeiten mit Fluor und flüchtigen Fluoriden

2.2.1. Reaktionsgefäße und geeignete Materialien

Die Auswahl geeigneter Materialien für die Handhabung und Aufbewahrung von Fluor und anderer (reaktiver) Fluoride wie Uranhexafluorid oder Chlortrifluorid ist beschränkt, da diese Stoffe mit gängigen Laborgläsern und vielen anderen Materialien reagieren und so zwangsläufig zu Verunreinigungen oder unerwünschten Nebenreaktionen führen.[198,215,216] Unter den Gläsern ist einzig ein scharf ausgeheiztes Kieselglas bedingt für die Handhabung dieser Fluoride geeignet. Dieses reagiert jedoch mit der Zeit meist auch, aufgrund der nichtentfernbaren Restmenge an Wasser. Als geeignet erweisen sich jene Metalle, welche eine unlösliche und chemisch- sowie mechanisch-stabile Fluoridschicht bilden können und so gegenüber einer weiteren Reaktion mit Fluoriden passiviert sind. Weiterhin sind die Materialien den Reaktionsbedingungen entsprechend auszuwählen, die Temperatur und der Druck spielen dabei eine entscheidende Rolle. Für die meisten Arbeiten bei niedrigen bis mäßig hohen Temperaturen kann ein kohlenstoffarmer Edelstahl (316 oder 316L), Nickel oder Kupfer verwendet werden, wobei letzteres meist nur als Dichtungsmaterial oder für Rohrleitungen eingesetzt wird. Für hohe Temperaturen und/oder hohe Drücke eignen sich Nickellegierungen wie Inconel® (SPECIAL METALS) und Monel, welche auch im Vergleich zu Edelstahl sehr beständig gegenüber Korrosion bei Feuchtigkeitskontakt sind.

Weiterhin können fluorierte oder perfluorierte Kunststoffe wie Tetrafluorethylen-Hexafluorpropylen-Copolymer (FEP), Perfluoralkoxy-Polymer (PFA), Polychlortrifluorethylen (PCTFE) und Polytetrafluorethylen (PTFE) als Materialien für Reaktionsgefäße eingesetzt werden. Dabei ist zu beachten, dass diese Kunststoffe nur metastabil gegenüber Fluor und starken Fluorierungsmitteln sind und bei falscher Reaktionsführung mit diesen reagieren.

In dieser Arbeit wurden Reaktionsgefäße aus FEP und PFA verwendet, welche durch Heißbearbeitung von 1/4“-, 3/8“- oder 3/4“-Kunststoffrohren hergestellt wurden. Im Falle von 1/4“- und 3/8“-Rohren wurden diese auf einer Seite zusammengeschmolzen, auf der anderen Seite Edelstahl- oder Monel-Klemmringe angebracht und die Rohre dann mit Edelstahlfaltenbalgventilen (Typ SS-4BRW, Swagelok oder Typ SWSS-FFR4-2, Fitok GmbH) verschlossen. Für Reaktionsgefäße mit 3/4“-Kunstoffrohren wurden die Rohre auf einer Seite zusammengeschmolzen und die andere Seite konusartig aufgeweitet, sodass eine entsprechende Überwurfmutter mit einem Edelstahladapter das Rohr abdichtete (Abbildung 16). Alle Reaktionsgefäße wurden vor der Verwendung mit Petrolether entfettet, getrocknet, mehrfach sekuriert und dann mit Fluor oder gasförmigen Chlortrifluorid passiviert.

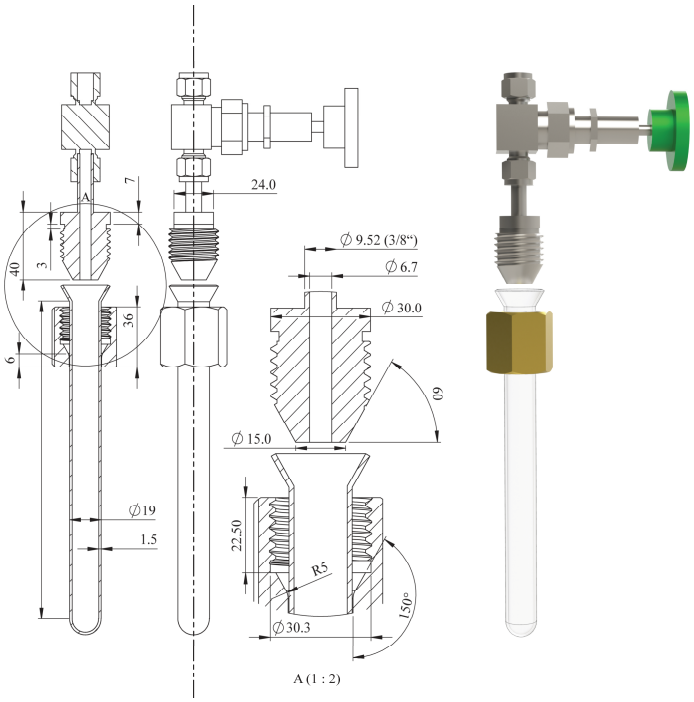

Abbildung 16. Konstruktionsskizze eines PFA- oder FEP-Reaktionsgefäßes, bestehend aus einem 3/4“-Kunststoffrohr, Faltenbalgventil und entsprechenden Adaptern.[217] Die Bemaßung ist in Millimetern angegeben.

2.2.2. Arbeiten mit Chlortrifluorid

Chlortrifluorid reagiert mit vielen Verbindungen und Elementen und wirkt dabei als starkes Oxidations- und Fluorierungsmittel (Abschnitt 1.1). Für die Handhabung können die in Abschnitt 2.2.1 erwähnten Materialien verwendet werden.[91,216,218] Die Arbeiten mit Chlortrifluorid erfolgten an einer Metallanlage aus 1/4"-Monelrohr, welche mit Faltenbalgventilen aus Edelstahl oder Monel und Membranventilen aus Monel bestückt war (Abbildung 17). Als Reaktionsgefäße wurden FEP- oder PFA-Rohre verwendet. Diese wurden mit Edelstahlfaltenbalgventilen verschlossen.

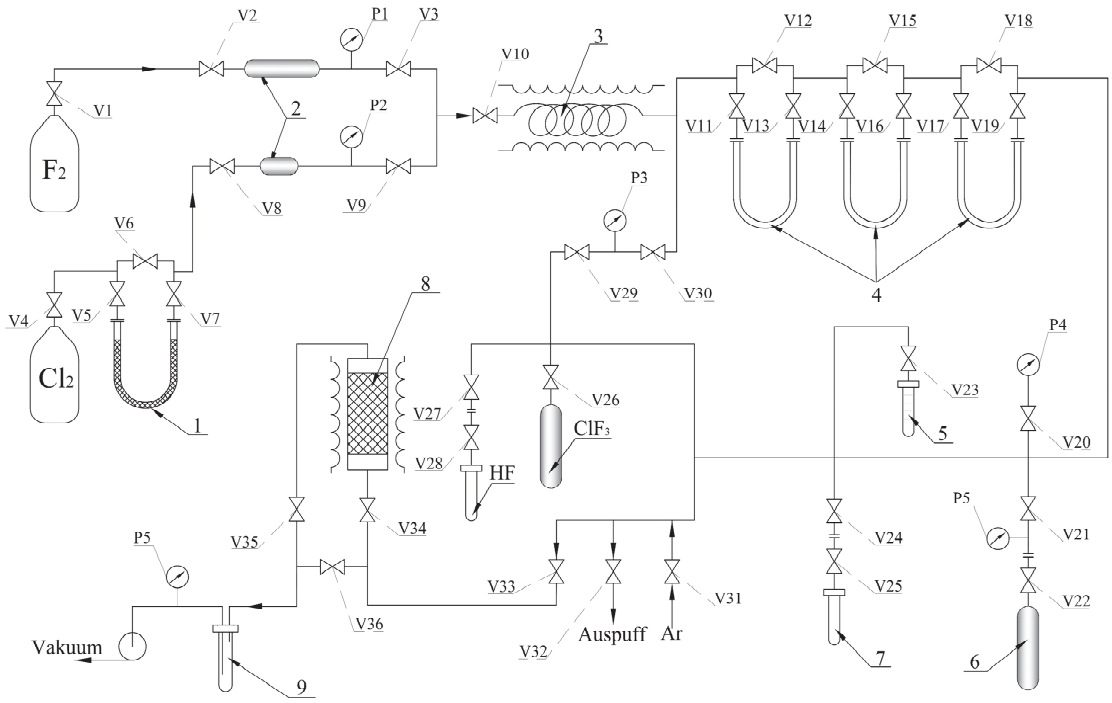

Abbildung 17. Schematischer Aufbau der Metallanlage für die Handhabung von Chlortrifluorid, die Abbildung wurde von Dr. Sergei Ivlev (Philipps-Universität Marburg) erstellt. 1: Trocknungsrohr, gefüllt mit P_2O_5; 2: Monel- und Edelstahlgefäß mit definiertem Volumen; 3: Beheizbare Monelspirale; 4: U-Rohre aus PFA; 5: Graduierter Kühlfinger aus PFA; 6: Monelzylinder; 7: Reaktionsgefäß aus PFA oder FEP; 8: Beheizbarer Natronkalk(„Sodalime“)-Absorber; 9: Kühlfalle aus PFA; Ar: Argon der Qualität 5.0; P1: Monel-Rohrfedermanometer (AIR PRODUCTS); P2: Edelstahl-Rohrfedermanometer (UNION CARBIDE); P3: Kapazitätsmanometer Baratron 627F (MKS Instruments Deutschland GmbH; P4: Monel-Rohrfedermanometer (Acco); P5: Pirani-Manometer VD84 (Thyracont Vacuum Instruments GmbH); V: Faltenbalgventil aus Edelstahl oder Monel (Typ SS- oder M-4BRW, Swagelok) oder Membranventil aus Monel (4600er Serie, HOKE); Vakuum: Zweistufige Drehschieberpumpe (Typ RV5F mit perfluoriertem Öl und Fluorelastomeren als Dichtungen, Edwards).

Bei Umsetzungen mit Chlortrifluorid ist stets Vorsicht geboten, da die Edukte teilweise unter Funkenbildung und starker Wärmetönung mit diesem reagieren. Dies gilt vor allem für flüssiges Chlortrifluorid und sehr reaktive Edukte wie feinverteilte Metallpulver. Außerdem kann der Druckanstieg bei den Reaktionen sehr rasch erfolgen und die Reaktionsgefäße gegebenenfalls bersten. Weiterhin können stark exotherme Reaktionen zum Erweichen des Kunststoffes führen. Eine Reaktion des Kunststoffes mit Chlortrifluorid ist ebenfalls möglich, was häufig in einer Explosion resultierte.

Die folgenden Schritte haben sich für Umsetzungen mit Chlortrifluorid bewährt. Das mit Edukt beschickte Reaktionsgefäß wird evakuiert und wenige Millibar ClF_3 in die Gasphase gegeben. Falls eine Reaktion unter Lichtemission erfolgt, wird so lange schrittweise gasförmiges ClF_3 zugegeben, bis diese ausbleibt. Ansonsten wird das Reaktionsgefäß mit flüssigem Stickstoff eingekühlt und wenig ClF_3 kondensiert. Das Reaktionsgefäß wird langsam über einem mit flüssigem Stickstoff gefüllten Dewar-Gefäß aufgetaut. Falls eine heftige Reaktion beim Auftauen eintritt, wird sofort wieder gekühlt und diese Schritte solange wiederholt, bis diese ausbleibt. Bei einigen Oxiden wie Sb_2O_3 und P_2O_5 oder Fluoriden wie SbF_3 ist die Reaktion mit ClF_3 dennoch so heftig, dass stets nur wenige Millibar ClF_3 hinzugegeben werden sollten. Falls keine photochemische Reaktion durchgeführt werden soll, so können stattdessen auch Monel- oder Edelstahl-Reaktionsgefäße verwendet werden.

2.2.3. Fluor und flüchtige Fluoride

Die Metallanlage für die Arbeiten mit verdünntem (20/80 Fluor:Argon) und unverdünntem Fluor sowie anderer flüchtiger Fluoride ähnelt im Aufbau der ClF_3-Anlage (Abbildung 18). Die Anlage besteht aus 3/8"-Monelrohr und Nadelventilen aus Monel (30VM608x-MO, Autoclave Engineers). Für die Arbeiten stehen zwei Abgriffe zur Verfügung und es können Drücke bis zu 28 bar reinen Fluors gehandhabt werden. Die Druckmessung erfolgte mit Kapazitätsmanometern (MKS Baratron 626C, je eins für 1 bis 1000 mbar und 10^{-3} bis 1 mbar, MKS Instruments Deutschland GmbH) oder Monel-Rohrfedermanometern. Als Pumpe kam eine zweistufige Drehschieberpumpe (Typ RV5F, Edwards) mit perfluoriertem Öl und Fluorelastomeren als Dichtungen zum Einsatz.

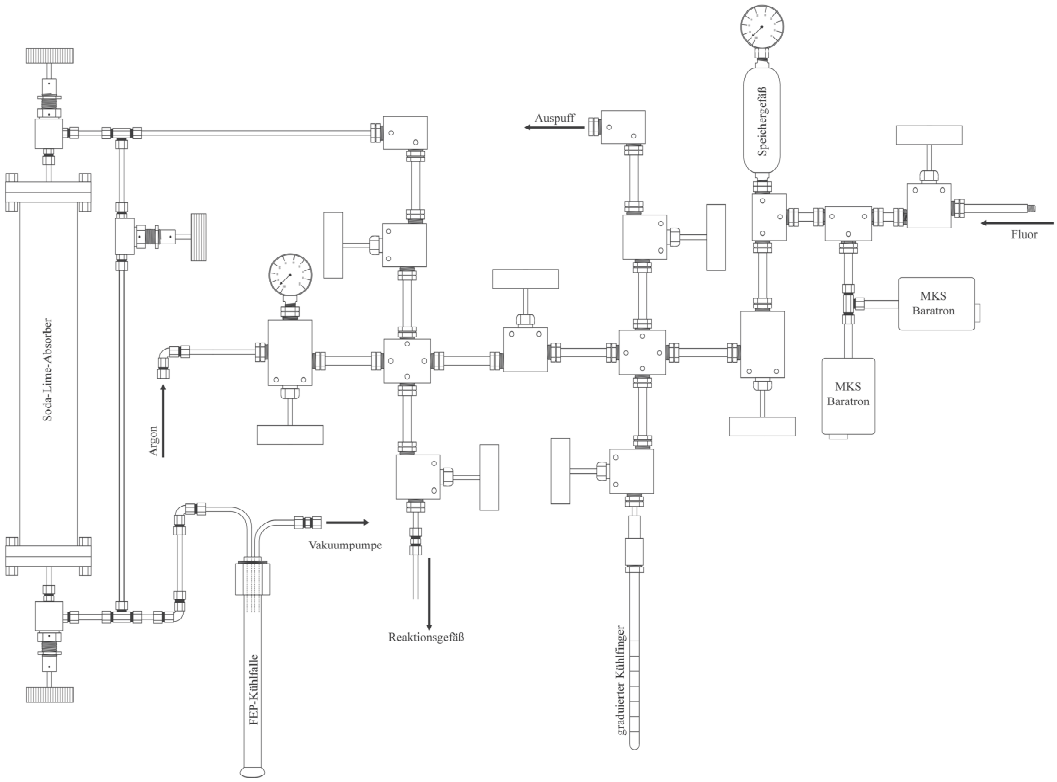

Abbildung 18. Schematischer Aufbau der Metallanlage für die Handhabung von Fluor und flüchtigen Fluoriden.[217]

2.2.4. Arbeiten mit wasserfreiem Fluorwasserstoff

Für die Arbeiten mit wasserfreiem Fluorwasserstoff wurde eine Anlage bestehend aus 3/8"- und 1/2"-Edelstahlrohr (316L) verwendet, die im Aufbau den ClF_3- und F_2-Anlagen ähnelt (Abbildung 19). Als Ventile wurden Edelstahlfaltenbalgventile mit PCTFE-Spindelspitze (SS-8BAK-V19, Swagelok) verwendet. Für die Druckmessungen wurden Kapazitätsmanometer (MKS Baratron 626C, je eins für 1 bis 1000 mbar und 10^{-3} bis 1 mbar, MKS Instruments Deutschland GmbH) oder ein Edelstahl-Rohrfedermanometer (UNION CARBIDE) verwendet. Die Hauptteile der Anlage waren mit Heizband umwickelt, sodass schwerflüchtige Fluoride wie IF_5 leichter gehandhabt werden können. Als Pumpe kam eine zweistufige Drehschieberpumpe (Duo 10 M, Pfeiffer Vacuum GmbH) zum Einsatz. Fluorwasserstoff wurde vor der Verwendung über Kalium-Hexafluoridoniccolat(IV) getrocknet.

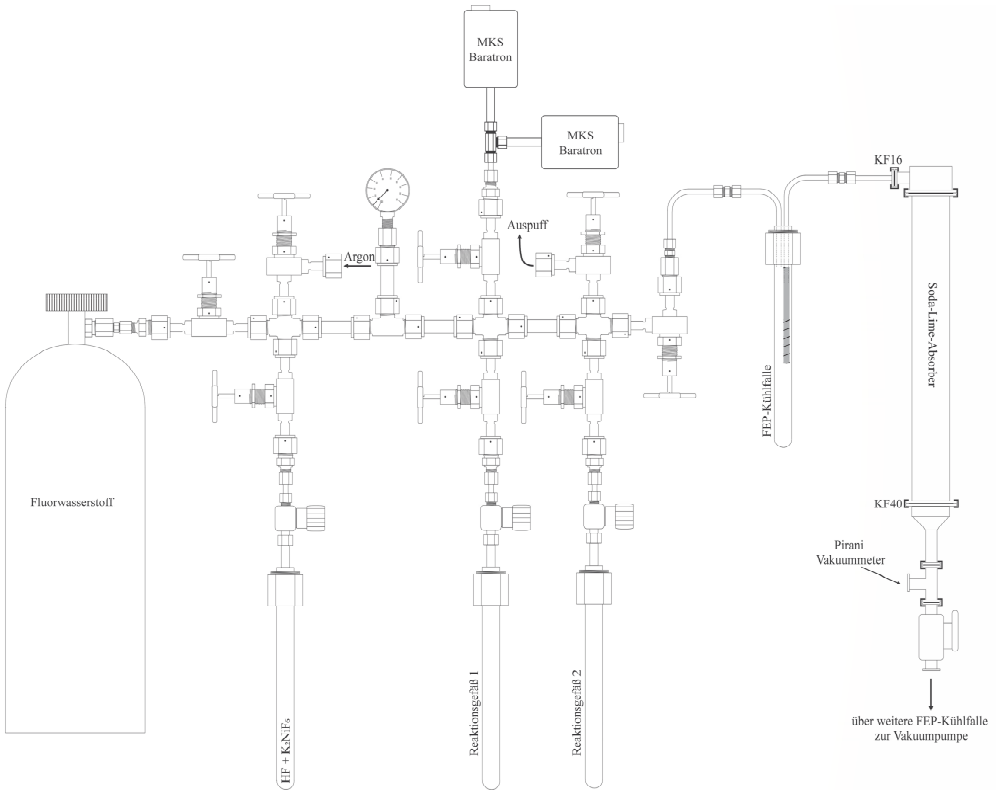

Abbildung 19. Schematischer Aufbau der Metallanlage für die Handhabung von wasserfreiem Fluorwasserstoff. (Abbildung verändert nach [217])

2.2.5. UV-Reaktor für photochemische Umsetzungen

Photochemische Umsetzungen mit Chlortrifluorid erfolgten in einem UV-Reaktor mit Messinggehäuse und einem Lüfter im Boden des Gehäuses. Der Reaktor war mit sechs Niederdruck-Quecksilberdampflampen des Typs PURITEC HNS S 11 W (OSRAM GmbH) bestückt (Abbildung 20). Die Lampen sind dabei kreisförmig um die zentrale Öffnung angeordnet und besitzen je eine Strahlungsleistung von 3 W im UVC-Bereich (200-280 nm) mit der Hauptemissionslinie bei 254 nm.

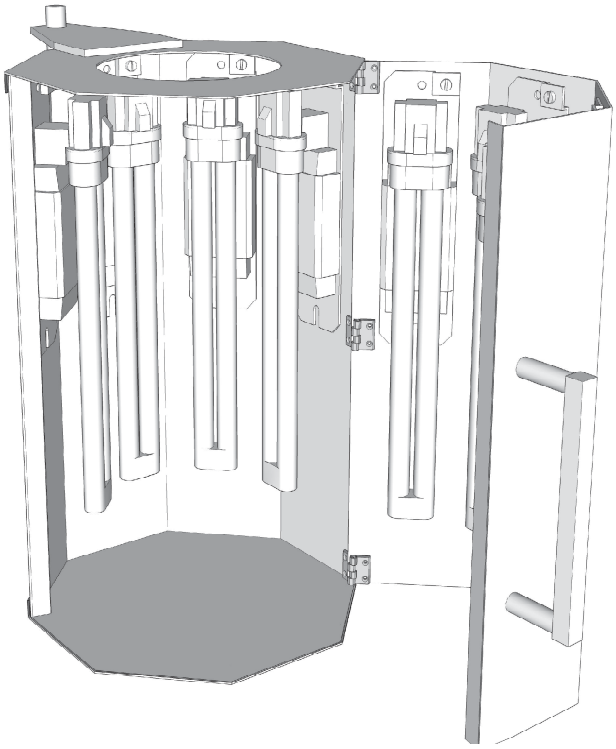

Abbildung 20. Aufbau des verwendeten UV-Reaktors.[217]

2.3. Arbeiten mit Transuranelementen

Die Arbeiten mit den Transuranelementen ^{237}Np (α: $t_{1/2}$ = 2,144×10^6 a) und ^{242}Pu (α: $t_{1/2}$ = 3,73×10^5 a) erfolgten im Kontrollbereich des Instituts für Ressourcenökologie des Helmholtz-Zentrums Dresden-Rossendorf (HZDR).[216,219,220] Die Handhabung der beiden Alphastrahler erfolgte in einem Unterdruck-Handschuhkasten (MBraun Inertgas-Systeme GmbH) mit Schwebstofffilter. Kristalline Proben der dargestellten Fluoridometallate(IV) wurden außerhalb des Handschuhkastens nur als Suspension (Wasser und/oder perfluoriertes Öl) gehandhabt. Die hydrofluorothermalen Reaktionen der Oxide NpO_2 oder PuO_2 mit Fluoriden und Flusssäure erfolgten in Säureaufschlussgefäßen (Modell 4749, Parr Instrument GmbH) mit PTFE-Einsätzen (Modell A280AC3, V = 10 mL, Parr Instrument GmbH).

3. Analytische Methoden und quantenchemische Festkörperrechnungen

Die in diesem Kapitel beschriebenen analytischen Methoden und Details zu den quantenchemischen Festkörperrechnungen gelten für die unveröffentlichten Ergebnisse in den Abschnitten 4.3 und 5.3. Weitere Details zu den eingesetzten Methoden finden sich in den entsprechenden Veröffentlichungen des kumulativen Teils dieser Arbeit.

3.1. Einkristallstrukturanalyse

Die Intensitätsdaten für die Einkristallstrukturanalysen wurden an vier verschiedenen Einkristalldiffraktometern gemessen: D8 Quest (Bruker AXS GmbH), D8 Venture (Bruker AXS GmbH), IPDS2 (STOE & Cie GmbH) und IPDS2T (STOE & Cie GmbH). Alle Messungen wurden mit monochromatisierter Molybdän-Strahlung, λ(Mo-K$_\alpha$) = 0,71073 Å, durchgeführt, als Röntgenquellen kamen dabei Mikrofokusquellen (D8 Quest und D8 Venture) oder eine Röntgenröhre (IPDS2 und IPDS2T) zum Einsatz.[221] Die Monochromatisierung erfolgte mit Vielschicht-Optiken (D8 Quest und D8 Venture) oder Graphit (IPDS2 und IPDS2T). Die Diffraktometer waren entweder mit einem PHOTON 100-CMOS-Detektor (D8 Quest und D8 Venture) oder einem Bildplattendetektor (IPDS2 und IPDS2T) ausgestattet. Die Messungen wurden in der Regel bei 100 K durchgeführt und die Kristalle mit einem kalten Stickstoffstrom der Kühleinheiten Cryostream 700 oder 800 (Oxford Cryosystems) gekühlt.

Die Messdaten wurden mit den jeweiligen herstellereigenen Programmpaketen, APEX3 (Bruker AXS GmbH) und X-Area (STOE & Cie GmbH) ausgewertet, integriert und reduziert sowie Lorentz- und Polarisationseffekte korrigiert.[222,223] Die Absorptionskorrektur erfolgte nach dem Multi-Scan-Verfahren (SADABS und TWINABS, Bruker AXS GmbH) oder mittels Gaußscher Integration (X-Shape und X-Red32, STOE & Cie GmbH).[224–227] Die Strukturlösungen erfolgten mit dem Programm SHELXT (*dual-space*-Methode) und die Strukturverfeinerungen gegen F_{obs}^2 mit SHELXL in der graphischen Benutzeroberfläche ShelXle.[228–231]

Im Falle nicht-meroedrischer Verzwillingung wurde der Datensatz mit dem Programm HKLF5Tools bearbeitet.[232] Die Strukturlösungen wurden abschließend auf mögliche übersehene höhere Symmetrie mit dem Programm Addsym des Programmpakets PLATON überprüft.[233,234] Abbildungen der Kristallstrukturen wurden mit dem Programm Diamond erstellt.[235]

Die Kristalle der in dieser Arbeit beschriebenen Verbindungen waren häufig sehr feuchtigkeitsempfindlich, sodass die entsprechende Selektion unter perfluorierten Ölen (Fomblin YR1800 für die Raumtemperaturpräparation oder Galden HT270 für die Tieftemperaturpräparation, beide SOLVAY GmbH), welche über Molekularsieb 3 Å getrocknet wurden, durchgeführt wurde. Die Kristalle wurden dann je auf einer Polymerschlaufe (“Loop”, MiTeGen) aufgenommen und auf dem Goniometerkopf des Diffraktometers platziert.

Im Falle von temperatur- und luftempfindlichen Verbindungen erfolgte die Kristallpräparation bei tiefen Temperaturen von circa −40 °C Öltemperatur, unter einem Strom gekühlten Stickstoffs mit einer speziellen Apparatur (Abbildung 21).[236] Die Kristallpräparationseinheit besteht aus einem Kupferstab, welcher mit einem Kühlmedium wie einer Trockeneis/Isopropanol-Suspension gekühlt werden kann und auf dem ein kleiner Kupferblock mit Vertiefungen aufgebracht ist. Dieser Stab ist in einem 3D-gedruckten Gerüst eingefasst, an welches seitlich eine bewegliche Düse angebracht ist. Über einen Adapter kann mit flüssigem Stickstoff vorgekühlter gasförmiger Stickstoff an die Düse angeschlossen werden.

Auf dem Kupferblock kann nun perfluoriertes Öl vorgelegt werden, welches zum einen gekühlt und zum anderen mit einem schützenden Polster kalten Stickstoffs umströmt wird. Die empfindlichen Kristalle können dann mit einem vorgekühlten Spatel und etwas Öl rasch auf den Kupferblock transferiert und selektiert werden. Mit einem MiTeGen-Loop können geeignete Kristalle aufgenommen, das Öl im kalten Stickstoffstrom schockgefroren und der Loop mit einer vorgekühlten Zange platziert werden. Die Zange wird im Anschluss mit flüssigem Stickstoff gekühlt und der Loop rasch auf den Goniometerkopf gesetzt.

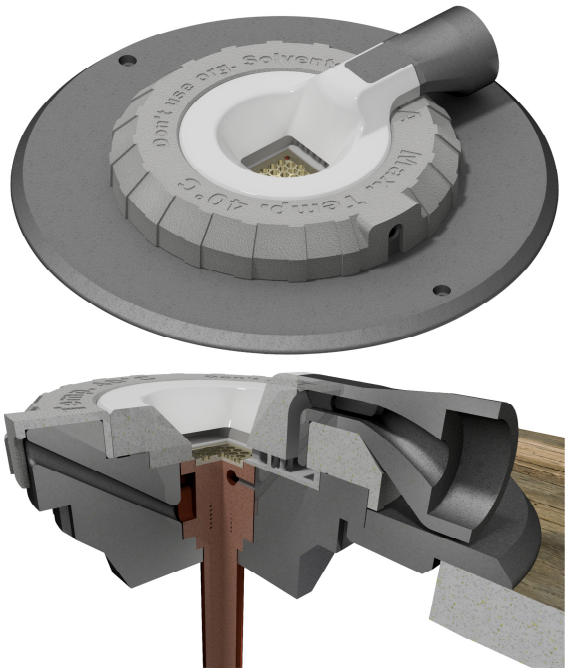

Abbildung 21. Kristallpräparationseinheit für temperatur- und luftempfindliche Kristalle.[236]

3.2. Infrarotspektroskopie

Die Infrarotspektren der untersuchten Feststoffe wurden mit einem Alpha FT-IR-Spektrometer (Bruker Optik GmbH) bei Raumtemperatur durchgeführt, welches in einem Handschuhkasten mit Argonatmosphäre platziert war. Die Messungen erfolgten in abgeschwächter Totalreflexion (*attenuated total reflection*, ATR) mit einer Diamant-ATR-Einheit. Der Messbereich betrug 400-4000 cm^{-1} mit einer Auflösung von 4 cm^{-1}. Die Spektren sind untergrundkorrigiert und die Auswertung erfolgte mit den Programmen OPUS und OriginPro2017.[237,238]

3.3. Raman-Spektroskopie

Die Raman-Spektren wurden mit einem konfokalen Raman-Mikroskop (MonoVista CRS+, Spectroscopy & Imaging GmbH) gemessen. Dabei kamen zwei verschiedene Gitter zum Einsatz: Eines für Messungen in niedriger Auflösung (300 Furchen pro Millimeter) und eines für Messungen in hoher Auflösung (1800 Furchen pro Millimeter). Für die Messungen wurde ein 532 nm Festkörper-Laser verwendet und die Auflösung (Halbwertsbreite, FWHM) betrug < 4,62 cm^{-1} bei niedriger Auflösung und < 0,368 cm^{-1} bei hoher Auflösung. Die Proben wurden entweder in ausgeheizten Glasgefäßen oder perfluoriertem Öl gemessen, dabei wurde der Fokus stets auf die Probenoberfläche gesetzt, um Raman-Banden des Glases oder Öls zu minimieren. Die Spektren wurden mit den Programmen VistaControl und OriginPro2017 ausgewertet.[238,239]

3.4. Quantenchemische Festkörperrechnungen

Quantenchemische Rechnungen, basierend auf atomzentrierten, gaußförmigen Basisfunktionen, mit periodischen Randbedingungen für den Festkörper wurden mit dem Programmpaket CRYSTAL17 durchgeführt.[240,241] Für die Rechnungen wurden die Dichtefunktionaltheorie, DFT, mit dem Hybrid-Funktional PBE0 angewendet und für alle Atome Basissätze mit Triple-ζ Valenzpolarisierung (TZVP) verwendet, welche von Prof. Dr. Antti Karttunen (Aalto-Universität, Espoo, Finnland) von def2-TZVP-Basissätzen abgeleitet wurden (Tabelle 3).[242–244] Die Gitter- und Lageparameter wurden im Rahmen der durch die Raumgruppensymmetrie vorgegebenen Einschränkungen vollständig optimiert, die im Abschnitt 8.2 aufgeführt sind. Dabei wurden die Standardeinstellungen für die Konvergenzkriterien der Integration und Optimierungen verwendet. Die Brillouin-Zonen wurden mit *k*-Punkten eines Monkhorst-Pack-Schemas beschrieben und sind jeweils in den Abschnitten 8.2.2 und 8.2.3 angegeben.[245] Die Toleranzfaktoren für die Coulomb- und Austauschintegrale (TOLINTEG) wurden als 8, 8, 8, 8, 16 für alle Rechnungen gesetzt. Falls ein magnetisches System vorlag, wurde ein entsprechender Grundzustand als Startwert gesetzt. Für alle untersuchten Systeme wurden Populationsanalysen nach Mulliken berechnet (Abschnitt 8.2.4).[246]

Harmonische Schwingungsfrequenzen, Infrarot-Absorptionen und Raman-Intensitäten wurden mit den in CRYSTAL17 implementierten Funktionen berechnet.[247–249] Die Raman-Intensitäten wurden für ein polykristallines Pulver mit isotropen Intensitäten berechnet. Die berechneten Raman-Spektren wurden mit einer Pseudo-Voigt-Funktion (50/50-Verhältnis von Lorentz- und Gauß-Funktionen) und einer Halbwertsbreite von 8 cm^{-1} simuliert. Für die Berechnungen wurden die experimentellen Parameter von 293,15 K für die Temperatur und 532 nm für die Wellenlänge des Lasers berücksichtigt. Die Bandenzuordnungen der berechneten Spektren erfolgte durch die Betrachtung der Normalmoden mit dem Programm Jmol.[250]

Tabelle 3. Verwendete Basissätze für die quantenchemischen Festkörperrechnungen mit dem Programmpaket CRYSTAL17.

Element	Basissatz	Quelle
Au	TZVP	[251]
B	TZVP	[31]
Cl	TZVP	[252]
Cr	TZVP	Abschnitt 8.2.1
F	TZVP	[253]
Ge	TZVP	[254]
Mo	TZVP	[255]
O	TZVP	[253]
Os	TZVP	[31]
Pb	TZVP	[256]
Pd	TZVP	Abschnitt 8.2.1
Pt	TZVP	[252]
Rb	TZVP	[36]
Rh	TZVP	Abschnitt 8.2.1
Sb	TZVP	[31]
Sn	TZVP	[257]
U	TZVP	[258]

4. Chemie des Chlortrifluorids

4.1. Motivation und Zielsetzung

Im Rahmen dieser Arbeit sollte die fundamentale Chemie des Chlortrifluorids in Reaktionen mit verschiedenen Verbindungen und Elementen untersucht werden, um so direkte oder indirekte Zugänge zu zuvor unbekannten oder ansonsten schwieriger zugänglichen Salzen mit Kationen oder Anionen des Chlors in den Oxidationsstufen +III und +V zu etablieren. So sollten auch Umsetzungen mit Chlortrifluorid unter UV-Bestrahlung durchgeführt werden, um eine mögliche Reaktivitätssteigerung zu erreichen. Chlortrifluorid absorbiert dabei Licht ab einer Wellenlänge von 460 nm bis unterhalb von 220 nm.[259] Es kann unter anderem mit Fluor unter photochemischen Bedingungen zu Chlorpentafluorid oxidiert werden.[125] Weiterhin wurde es unter anderem mit Sauerstoff oder Sauerstoffdifluorid unter photochemischen Bedingungen zu Chloroxidtrifluorid umgesetzt.[151,190,192,260] Dieses wird auch bei photochemischen Umsetzungen anderer Chloroxidfluoride gebildet.[192,260] Bisher wurden diese Umsetzungen jedoch nicht in der Gegenwart von starken Lewis-Säuren durchgeführt, was den Zugang zu $ClOF_2^+$-Salzen erleichtern sollte.

Die dargestellten Verbindungen sollten unter anderem mittels der Einkristallstrukturanalyse charakterisiert werden, da zuvor nur über wenige Kristallstrukturen von Tetrafluoridochlorat(III)-,[25,28] Difluorochloronium(III)-,[208,261–266] Dioxychloronium(V)-[201,206,208,209] und Difluorooxychloronium(V)-Verbindungen[267] berichtet wurde. Eine weitere Charakterisierung sollte durch die Aufnahme von Raman-Spektren erfolgen, die mittels periodischer quantenchemischer Rechnungen reproduziert werden sollten.

4.2. Kumulativer Teil

4.2.1. Synthesis and Characterization of the Tetrafluoridochlorates(III) *A*[ClF_4] (*A* = K, Rb, Cs)

Benjamin Scheibe, Sergei I. Ivlev, Antti J. Karttunen, Florian Kraus

Eur. J. Inorg. Chem. **2020**, *2020*, 1319–1324.
DOI: 10.1002/ejic.202000106

Siehe Abschnitt 7.1.

Die Verbindungen *A*[ClF_4] (*A* = K, Rb, Cs) konnten in einkristalliner Form durch Solvolysereaktionen der Alkalimetallfluoride in einem Überschuss an flüssigem Chlortrifluorid dargestellt werden. Das Lewis-Säure-Verhalten von ClF_3 ähnelt denen der Trifluoride AuF_3, BrF_3 und IF_3. Die Strukturaufklärung mittels Einkristallstrukturanalyse zeigte, dass K[ClF_4] im K[BrF_4]-Strukturtyp kristallisiert, wohingegen die entsprechenden Rubidium- und Cäsium-Verbindungen im Li[AuF_4]-Strukturtyp kristallisieren. In den Kristallstrukturen liegen isolierte, fast quadratische, planare $[ClF_4]^-$-Anionen vor. Die Cl−F-Bindungslängen werden kaum durch die verschiedenen Kationen beeinflusst, sie betragen 1,7982(6) Å im Kaliumsalz, 1,7930(9) und 1,8034(9) Å im Rubidiumsalz und 1,792(4) und 1,794(4) Å im Cäsiumsalz. Die Metallatome sind im Kaliumsalz von acht Fluoratomen in der Form eines quadratischen Antiprismas und im Rubidium- und Cäsiumsalz von zwölf Fluoratomen in Form eines verzerrten Antikuboktaeders umgeben. Die Verbindungen wurden weiter mittels Infrarot- und Raman-Spektroskopie analysiert und die Spektren durch quantenchemische Festkörperrechnungen reproduziert. Die Banden konnten auf Basis der berechneten Spektren zugeordnet werden und es konnte gezeigt werden, dass Spuren von Fluorwasserstoff-Addukten der Alkalimetallfluoride der Form *A*[H_nF_{1+n}] (*n* = 1, 2, 3) häufig in den Produkten vorliegen. Spuren von Wasser sind vermutlich die Quelle des Fluorwasserstoffs, welcher eine stärkere Lewis-Säure als Chlortrifluorid ist und dieses somit aus den Salzen verdrängt.

Beiträge der Autoren:

B. Scheibe synthetisierte die Verbindungen $K[ClF_4]$ und $Rb[ClF_4]$, charakterisierte alle Verbindungen mittels Infrarot- und Raman-Spektroskopie, bestimmte die Kristallstrukturen von $K[ClF_4]$ und $Rb[ClF_4]$ und führte die quantenchemischen Festkörperrechnungen durch. S. I. Ivlev synthetisierte die Verbindung $Cs[ClF_4]$ und bestimmte die Kristallstruktur. A. J. Karttunen entwickelte die verwendeten Basissätze für das Programmpaket CRYSTAL17. B. Scheibe analysierte und interpretierte die Ergebnisse. B. Scheibe verfasste das Manuskript in Absprache mit den Coautoren. F. Kraus leitete das Projekt.

4.2.2. $Cs[Cl_3F_{10}]$: A Propeller-Shaped $[Cl_3F_{10}]^-$ Anion in a Peculiar $A^{[5]}B^{[5]}$ Structure Type

Benjamin Scheibe, Antti J. Karttunen, Ulrich Müller, Florian Kraus

Angew. Chem. **2020**, *132*, 18272–18276.
Angew. Chem. Int. Ed. **2020**, *59*, 18116–18119.
DOI:10.1002/ange.202007019.
DOI: 10.1002/anie.202007019

Siehe Abschnitt 7.2.

Die Reaktion von Cäsiumfluorid und einem Überschuss an flüssigem Chlortrifluorid bei Temperaturen von 0°C oder −37°C führen zur Bildung der Verbindung $Cs[Cl_3F_{10}]$. Die Kristalle der Verbindung konnten bei tiefen Temperaturen von −37°C aus flüssigem Chlortrifluorid isoliert und für die Einkristallstrukturanalyse präpariert werden. Die Verbindung ist thermisch deutlich instabiler als $Rb[Br_3F_{10}]$ und $Cs[Br_3F_{10}]$, welche bei Raumtemperatur gehandhabt werden können. In der Kristallstruktur der Verbindung liegt ein propellerförmiges $[Cl_3F_{10}]^-$-Anion mit einem μ_3-verbrückenden Fluoratom vor, welches das erste mehrkernige Fluoridochlorat(III)-Anion ist. Das Anion ist ähnlich zum $[Br_3F_{10}]^-$-Anion aufgebaut, kristallisiert jedoch nicht isotyp mit den entsprechenden Rubidium- und Cäsium-Verbindungen. Das $[Cl_3F_{10}]^-$-Anion kann auch als ein zentrales Fluoridatom, welches von drei planaren Chlortrifluorid-Molekülen, mit Cl−μ_3-F-Abständen von 2,243(2) bis 2,265(2) Å umgeben ist, beschrieben werden.

Diese Beschreibung wird durch die Cl−F-Bindungslängen innerhalb der ClF_3-Einheiten unterstützt, welche mit 1,730(2) bis 1,747(2) Å für die cis-gebundenen und 1,600(2) bis 1,615(2) Å für die trans-gebundenen Fluoratome ähnlich zu denen in der orthorhombischen Modifikation des Chlortrifluorids von 1,716 und 1,621 Å sind. Die Cl−F-Bindungslängen unterscheiden sich deutlich von denen der Tetrafluoridochlorate(III). Die Struktur kann als einfacher AB-Strukturtyp beschrieben werden, in dem die Cs^+-Kationen, A, von fünf $[Cl_3F_{10}]^-$-Anionen, B, via der cis-gebundenen und μ_3-verbrückenden Fluoratome umgeben sind. Die Anionen sind ebenfalls von fünf Kationen umgeben, sodass die Packung als ein Vertreter des seltenen $A^{[5]}B^{[5]}$-Strukturtyps klassifiziert werden kann.

Quantenchemische Rechnungen in der Gasphase für die homologen $[X_3F_{10}]^-$-Anionen (X = Cl, Br, I) zeigen, dass die X−μ_3-F-Bindungen ionisch sind, wohingegen die anderen X−F-Bindungen polar-kovalenter Natur sind. Das erhaltene Produkt wurde weiter mit Tieftemperatur-Raman-Spektroskopie charakterisiert und das Raman-Spektrum für $Cs[Cl_3F_{10}]$ mittels quantenchemischer Festkörperrechnungen berechnet. Die Spektren zeigen, dass unter den gewählten Reaktionsbedingungen nur $Cs[Cl_3F_{10}]$ erhalten wird, Hinweise für die Bildung anderer möglicher mehrkerniger Fluoridochlorate(III) wie $[Cl_2F_7]^-$ oder $[Cl_4F_{13}]^-$ liegen nicht vor.

Beiträge der Autoren:

B. Scheibe entwickelte und erprobte Darstellungsmethoden von $Cs[Cl_3F_{10}]$, charakterisierte die Verbindung mittels Raman-Spektroskopie, bestimmte die Kristallstruktur und führte quantenchemische Festkörperrechnungen durch. A. J. Karttunen entwickelte die verwendeten Basissätze für das Programmpaket CRYSTAL17 und führte quantenchemische Gasphasenrechnungen durch. B. Scheibe analysierte und interpretierte die Ergebnisse. U. Müller stellte den Bärnighausen-Stammbaum auf. F. Kraus interpretierte die Kristallstruktur und klassifizierte die Kristallstruktur als einen Vertreter eines $A^{[5]}B^{[5]}$-Strukturtyps. B. Scheibe und F. Kraus verfassten das Manuskript in Absprache mit den Coautoren. F. Kraus leitete das Projekt.

4.2.3. Difluorochloronium(III) Fluoridometallates $ClF_2[MF_6]$ – From Molecular Building Blocks to (Helical) Chains

Benjamin Scheibe, Ralf Haiges, Sergei I. Ivlev, Ulrich Müller, Antti J. Karttunen, Karl O. Christe, Florian Kraus

Eur. J. Inorg. Chem. **2020**.
DOI: 10.1002/ejic.202000845

Siehe Abschnitt 7.3.

Difluorochloronium(III)-Verbindungen konnten durch Umsetzungen von Edelmetallpulvern (Ru, Os, Ir und Au), Fluoriden (NbF_5, SbF_3 und BiF_5) sowie des Chlorids $TaCl_5$ mit einem Überschuss an flüssigem Chlortrifluorid synthetisiert werden. Die kristallinen Verbindungen $ClF_2[AuF_4]$, $ClF_2[MF_6]$ (M = Nb, Ta, Ru, Os, Ir, Sb, Bi) und $ClF_2[Ta_2F_{11}]$ wurden mittels Einkristallstrukturanalyse untersucht. In allen Kristallstrukturen liegt ein gewinkeltes ClF_2^+-Kation mit F−Cl−F-Winkeln im Bereich von 95,4(2) bis 97.5(4)° vor. Die Bindungslängen der zwei kurzen, polar-kovalenten Cl−F-Bindungen liegen im Bereich von 1,538(4) bis 1,578(4) Å. Weiterhin sind zwei freie, sterisch aktive Valenzelektronenpaare am Cl(III)-Atom vorhanden, sodass eine pseudotetraedrische AX_2E_2-Struktur vorliegt. Das Cl(III)-Atom ist von zwei weiteren Fluoratomen in größerem Abstand von 2,170(4) bis 2,312(4) Å umgeben und diese Cl···μ-F-Wechselwirkungen können als ionisch klassifiziert werden, was durch quantenchemische Rechnungen für den Festkörper sowie für Gasphasenmodelle gezeigt werden konnte. Somit resultiert unter Berücksichtigung der Valenzelektronenpaare eine Koordinationszahl von sechs für das Chloratom. Durch die Cl···μ-F-Wechselwirkungen werden verschiedene Strukturmotive erhalten, welche von molekularen, dimeren Baueinheiten der Form $(ClF_2[AuF_4])_2$ und $(ClF_2[Ta_2F_{11}])_2$, zu kettenartigen Motiven bei den Verbindungen $ClF_2[MF_6]$ (M = Nb, Ta, Ru, Os, Ir, Sb, Bi) reichen. Die $[MF_6]^-$-Anionen in den Verbindungen mit Kettenmotiv können entweder cis- oder trans-verbrückend sein. Trans-verbrückende Anionen werden für M = Ir, Sb, Bi beobachtet und die Ketten können linear oder zick-zack-artig sein.

Cis-Verbrückung führt zu chiralen Ketten, aber aufgrund der entsprechenden Raumgruppen liegen Racemate mit links- und rechtsgängigen Ketten vor. Unter Annahme der Ketten als Polymere, können diese auch als Helices klassifiziert werden. Es werden verschiedene Helices beobachtet, welche von 2/1-Helices für *M* = Nb, Ta, einer stark verzerrten pseudo-3/1-Helix bei *M* = Os, bis hin zu einer 4/1-Helix bei *M* = Ru reichen.

Beiträge der Autoren:

Die Publikation entstand als Kooperation der Arbeitsgruppen Christe und Kraus. B. Scheibe synthetisierte die Verbindungen $ClF_2[MF_6]$ (*M* = Nb, Ta, Bi) und $ClF_2[Ta_2F_{11}]$ und bestimmte deren Kristallstrukturen. R. Haiges synthetisierte die Verbindungen $ClF_2[AuF_4]$ und $ClF_2[MF_6]$ (*M* = Ru, Ir, Os) und bestimmte deren Kristallstrukturen. S. I. Ivlev synthetisierte die Verbindung $ClF_2[SbF_6]$ und bestimmte die Kristallstruktur. B. Scheibe führte die quantenchemischen Rechnungen durch. B. Scheibe analysierte und interpretierte die Ergebnisse. U. Müller trug den Abschnitt zur Symmetrie polymerer, kettenartiger Moleküle bei und ermittelte die Balkengruppen der Ketten. A. J. Karttunen entwickelte die verwendeten Basissätze für das Programmpaket CRYSTAL17. K. O. Christe trug zum Abschnitt zu den Bindungen im ClF_2^+-Kation bei. B. Scheibe verfasste das Manuskript in Absprache mit den Coautoren. K. O. Christe und F. Kraus leiteten das Projekt.

4.2.4. Photochemistry with Chlorine Trifluoride: Syntheses and Characterization of Difluorooxychloronium(V) Hexafluorido(non)metallates(V), $ClOF_2[MF_6]$ (*M* = V, Nb, Ta, Ru, Os, Ir, P, Sb)

Benjamin Scheibe, Antti J. Karttunen, Florian Weigend, Florian Kraus

Chem. Eur. J. **2020**.
DOI: 10.1002/chem.202003629

Siehe Abschnitt 7.4.

Die Umsetzung der Oxide M_2O_5 (*M* = V, Nb, Ta, P), $RuO_2 \cdot xH_2O$ ($x \approx 2$) und Sb_2O_4 mit Chlortrifluorid und anschließender Bestrahlung mit UV-Licht führt zur Bildung von Difluorooxychloronium(V)-Verbindungen mit Hexafluoridometallat(V)-Anionen, $ClOF_2[MF_6]$. Die Umsetzungen von Os- und Ir-Pulver mit ClF_3, zusätzlicher Sauerstoffzugabe und anschließender UV-Bestrahlung führen ebenfalls zur Bildung von Verbindungen dieses Typs. Die Kristallstrukturen der erhaltenen Salze wurden mittels Einkristallstrukturanalyse bestimmt und es wurden zwei verschiedene Strukturtypen, mit gleichem Raumgruppentyp $Pna2_1$ (Nr. 33), aber unterschiedlichen Gitterparametern und Zellvolumina, beobachtet. Diese stellen verschiedene Stapelvarianten dar. Im Strukturtyp mit kleineren Zellvolumina von 578,2(2) bis 661,0(1) $Å^3$ kristallisieren die Verbindungen mit *M* = V, Nb, Ta, P, Sb sowie die vorher in der Literatur beschriebene Verbindung mit *M* = As. Eine Stapelvariante, mit in etwa verdoppelter *a*-Achse und Zellvolumina von 1328,67(8) und 1338,96(12) $Å^3$, wird für *M* = Nb, Ta beobachtet. In den Kristallstrukturen liegt ein pyramidales $ClOF_2^+$-Kation vor, welches eine AX_3E-Spezies mit pseudotetraedrischer Struktur ist. Die Cl−O-Bindungslängen liegen im Bereich von 1,436(2) bis 1,477(4) Å für *M* = V, Nb, Ta, P, As, Sb und der effektive Ionenradius des Zentralatoms des $[MF_6]^-$-Anions scheint einen Einfluss auf diese zu haben. Kein konsistenter Einfluss des Radius ist hingegen für die Cl−F-Bindungslängen zu beobachten, welche im Bereich von 1,486(6) bis 1,537(2) Å liegen. Quantenchemische Rechnungen für den Festkörper und für Gasphasenmodelle der Form $[ClOF_2[MF_6]_3]^{2-}$ können die experimentellen Beobachtungen einer möglichen Abhängigkeit der Cl−O- und Cl−F-Bindungslängen von den Radien nicht reproduzieren.

In den Kristallstrukturen von $ClOF_2[NbF_6]$ und $ClOF_2[TaF_6]$ wird eine teilweise oder vollständige O/F-Fehlordnung in den $ClOF_2^+$-Kationen beobachtet.

Die Cl(V)-Atome sind in beiden Strukturtypen von drei weiteren Fluoratomen der benachbarten Anionen in der Form Cl···μ-F umgeben, sodass die Koordinationszahl des Cl-Atoms 3+3 beträgt. Werden diese Kontakte berücksichtigt, so wird ein Schichtstrukturmotiv welches mit der Niggli-Formel ${}^{2}_{\infty}\left[\langle ClF_{\underset{1+1}{3}}F_{\underset{1}{2}}O_{\underset{1}{1}}\rangle\langle MF_{\underset{1+1}{3}}F_{\underset{1}{3}}\rangle\right]$ beschrieben werden kann, erhalten. Die Produkte wurden weiter mit Hilfe der Raman-Spektroskopie charakterisiert und die Raman-Spektren mit quantenchemischen Festkörperrechnungen berechnet. Die Rechnungen zeigen weiterhin, dass die Cl−O- und Cl−F-Bindungen kovalenter und die Cl···μ-F-Wechselwirkungen ionischer Natur sind.

Beiträge der Autoren:

B. Scheibe entwickelte und erprobte die photochemische Darstellung von $ClOF_2^+$-Verbindungen, charakterisierte diese mittels Raman-Spektroskopie und bestimmte deren Kristallstrukturen. B. Scheibe führte die quantenchemischen Festkörperrechnungen durch. B. Scheibe interpretierte und analysierte die Ergebnisse. A. J. Karttunen entwickelte die verwendeten Basissätze für das Programmpaket CRYSTAL17. F. Weigend führte die quantenchemischen Gasphasenrechnungen durch, interpretierte die Ergebnisse und trug den entsprechenden Abschnitt im Manuskript bei. B. Scheibe verfasste das Manuskript in Absprache mit den Coautoren. F. Kraus leitete das Projekt.

4.2.5. Reactions of ClF_3 with Main Group and Transition Metal Oxides: Access to Dioxychloronium(V) Fluoridometallates and Oxidofluoridometallates

Benjamin Scheibe, Antti J. Karttunen, Florian Kraus

Eur. J. Inorg. Chem., **2020**.
DOI 10.1002/ejic.202000908

Siehe Abschnitt 7.5.

Die Umsetzung von Hauptgruppen- und Übergangsmetalloxiden wie TiO_2, MoO_3, Re_2O_7, SnO, P_2O_5, As_2O_5 oder Niobpulver mit Oxidschicht mit einem Überschuss an Chlortrifluorid führt zur Bildung von Verbindungen mit dem Dioxychloronium(V)-Kation, ClO_2^+. Die Hydrolysereaktion von $ClF_2[IrF_6]$ führte zur Bildung von $ClO_2[IrF_6]$. Die Kristallstrukturen der erhaltenen Salze wurden mittels Einkristallstrukturanalyse aufgeklärt und es hat sich gezeigt, dass sich je nach Startmaterial Verbindungen mit Fluoridometallat- oder Oxidofluoridometallat-Anion gebildet haben. Es wurden Salze mit den folgenden Anionen erhalten: $[[TiF_{3/2}F_{3/1}]_2]^-$, $[Nb_3F_{16}]^-$, $[IrF_6]^-$, $[SnF_{2/2}F_{4/1}]^-$ $[PF_6]^-$, $[AsF_6]^-$, $[Mo_3O_3F_{13}]^-$ und $[Re_3O_6F_{10}]^-$. In allen Salzen liegen gewinkelte ClO_2^+-Kationen vor, mit O−Cl−O-Winkeln im Bereich von 117,37(10) bis 119,65(10)° und Cl−O-Abständen von 1,384(4) bis 1,418(4) Å. Die Chloratome sind stets von verbrückenden Fluoratomen der Anionen umgeben, sodass Cl···μ-F-Wechselwirkungen vorliegen. Es resultieren unter der Berücksichtigung dieser Wechselwirkungen die Koordinationszahlen 2+4 oder 2+6 für die Chloratome, mit oktaederähnlichen oder verzerrt-quadratisch antiprismatischen Ligandenanordnungen. Von den meisten Verbindungen wurden Raman-Spektren aufgenommen, welche auf der Basis von quantenchemischen Rechnungen für den Festkörper interpretiert werden konnten. Mulliken-Populationsanalysen der optimierten Strukturen deuten auf polar-kovalente Cl−O-Bindungen und ionische Cl···μ-F-Wechselwirkungen hin, welche im Einklang mit den entsprechenden Bindungslängen und Atomabständen sind.

Beiträge der Autoren:

B. Scheibe entwickelte und erprobte die Synthese von ClO_2^+-Verbindungen basierend auf der Umsetzung von Oxiden mit Chlortrifluorid, charakterisierte die Verbindungen mittels Raman-Spektroskopie und bestimmte deren Kristallstrukturen. B. Scheibe führte die quantenchemischen Festkörperrechnungen durch. B. Scheibe analysierte und interpretierte die Ergebnisse. A. J. Karttunen entwickelte die verwendeten Basissätze für das Programmpaket CRYSTAL17. B. Scheibe verfasste das Manuskript in Absprache mit den Coautoren. F. Kraus leitete das Projekt.

4.3. Difluorooxychloronium(V)-Verbindungen − Unveröffentlichte Ergebnisse

In diesem Kapitel werden photochemische Umsetzungen verschiedener Metalle, Oxide und Fluoride mit Chlortrifluorid und gegebenenfalls zusätzlichem Sauerstoff beschrieben. Die Produkte dieser Umsetzungen sind Difluorooxychloronium(V)-Verbindungen, deren Kristallstrukturen mittels Einkristalldiffraktometrie aufgeklärt wurden. Sie wurden weiterhin mit Hilfe der Schwingungsspektroskopie charakterisiert und auf Basis von quantenchemischen Festkörperrechnungen deren Schwingungsspektren berechnet wurden. Die optimierten Strukturen wurden weiterhin mit Mulliken-Populationsanalysen analysiert (Abschnitt 8.2.4).

4.3.1. Darstellung und Charakterisierung von $(ClOF_2)_2[MF_6]$ (*M* = Cr, Rh, Ge)

$(ClOF_2)_2[CrF_6]$: Ein PFA-Reaktionsgefäß ($V \approx 38$ mL) wurde mit 60,0 mg (1,15 mmol, 1 Äq.) Chrompulver beschickt, mit einem Edelstahlfaltenbalgventil verschlossen und an der ClF_3-Anlage mehrfach sekuriert. ClF_3 (0,53 g, 5,7 mmol, 5 Äq.) wurde bei 77 K auf den Feststoff kondensiert, die Kühlung entfernt und sofort 1,1 bar Sauerstoff hinzugegeben, das Reaktionsgefäß in einem Edelstahl-Dewargefäß platziert und langsam auf Raumtemperatur erwärmt. Bei Raumtemperatur war keine Reaktion erkennbar. Das Reaktionsgefäß wurde dann im UV-Reaktor für elf Tage bestrahlt. Im Anschluss wurden flüchtige Bestandteile im Vakuum entfernt und Chrompulver, auf dem rosafarbene Kristalle aufgewachsen waren, im Handschuhkasten isoliert. Ein Teil des isolierten Produkts wurde in perfluoriertem Öl suspendiert, unter dem Mikroskop selektiert und ein rosafarbener Kristall röntgenographisch untersucht. Für den untersuchten Kristall wurde die Zusammensetzung $(ClOF_2)_2[CrF_6]$ erhalten. Die Bildung dieser Verbindung kann mit Gleichung 53 beschrieben werden.

$$O_2 + Cr + 4\,ClF_3 \xrightarrow{hv} (ClOF_2)_2[CrF_6] + 2\,ClF \qquad 53$$

Eine vollständige Reaktion des Chrompulvers wurde unter den oben aufgeführten oder ähnlichen Bedingungen nicht beobachtet. Eventuell ist die Löslichkeit der auf dem Chrompulver kristallisierten Verbindung in Chlortrifluorid so gering, dass eine vollständige Reaktion des Chroms aufgrund von Passivierung verhindert wird.

Ähnliche Versuche der photochemischen Umsetzung von Chrompulver mit Chlortrifluorid, jedoch ohne zusätzliche Zugabe von Sauerstoff, führten ebenfalls zur Bildung rosafarbener Kristalle auf dem Chrompulver. Dies ist vermutlich auf die Diffusion von Sauerstoff durch den perfluorierten Kunststoff und die Oxidschicht auf dem Chrompulver zurückzuführen. Fluorierte Kunststoffe (PCTFE, PFA, FEP und PTFE) sind, wie andere Kunststoffe (Butylkautschuk, PP, PE) auch, permeabel für Sauerstoff.[268–271]

$(ClOF_2)_2[RhF_6]$: Ein PFA-Reaktionsgefäß wurde mit 28,0 mg (0,27 mmol, 1 Äq.) Rhodiumpulver beschickt, mit einem Edelstahlfaltenbalgventil verschlossen und an der ClF_3-Anlage mehrfach sekuriert. ClF_3 (0,29 g, 3,1 mmol, 11,5 Äq.) wurde bei 77 K auf den Feststoff kondensiert, das Reaktionsgefäß in einem Edelstahl-Dewargefäß platziert und langsam auf Raumtemperatur erwärmt. Bei Raumtemperatur war keine Reaktion erkennbar. Das Reaktionsgefäß wurde dann im UV-Reaktor für eine Woche bestrahlt. Im Anschluss wurden flüchtige Bestandteile im Vakuum entfernt und optisch unverändertes Rhodiumpulver im Handschuhkasten isoliert. Ein Teil des Pulvers wurde in perfluoriertem Öl suspendiert und unter dem Mikroskop betrachtet. Neben nicht umgesetzten Rhodiumpulver, waren auch farblose Kristalle erkennbar, von denen einer röntgenographisch untersucht wurde. Für den untersuchten Kristall wurde die Zusammensetzung $(ClOF_2)_2[RhF_6]$ erhalten. Die Bildung einer $ClOF_2^+$-Verbindung kann auch hier vermutlich auf die Diffusion von Sauerstoff durch den Kunststoff zurückgeführt werden, siehe oben. Die Gleichung 54 beschreibt die Bildung von $(ClOF_2)_2[RhF_6]$.

$$O_2 + Rh + 4\,ClF_3 \xrightarrow{hv} (ClOF_2)_2[RhF_6] + 2\,ClF \qquad 54$$

$(ClOF_2)_2[GeF_6]$: Ein PFA-Reaktionsgefäß wurde mit 32,0 mg (0,31 mmol, 1 Äq.) GeO_2 beschickt, mit einem Edelstahlfaltenbalgventil verschlossen und an der ClF_3-Anlage mehrfach sekuriert. ClF_3 (0,64 g, 6,9 mmol, 22 Äq.) wurde bei 77 K auf den Feststoff kondensiert, das Reaktionsgefäß in einem Edelstahl-Dewargefäß platziert und langsam auf Raumtemperatur Erwärmen lassen. Bei Raumtemperatur war keine Reaktion erkennbar. Das Reaktionsgefäß wurde dann im UV-Reaktor für 87 Stunden bestrahlt. Im Anschluss wurden flüchtige Bestandteile im Vakuum entfernt und ein weißer, kristalliner Feststoff blieb danach im Reaktionsgefäß zurück, welcher im Handschuhkasten isoliert wurde (5,8 mg).

Ein Teil des Produktes wurde in perfluoriertem Öl suspendiert und unter dem Mikroskop betrachtet, ein farbloser Kristall wurde röntgenographisch untersucht. Für den untersuchten Kristall wurde die Zusammensetzung $(ClOF_2)_2[GeF_6]$ erhalten. Die Bildung dieser Verbindung kann mit Gleichung 55 beschrieben werden.

$$GeO_2 + 4\,ClF_3 \xrightarrow{hv} (ClOF_2)_2[GeF_6] + 2\,ClF \qquad 55$$

Bis(difluorooxychloronium(V))-hexafluoridochromat(IV), -rhodat(IV) und -germanat(IV) kristallisieren isotyp in der monoklinen Raumgruppe *C*2/*m* (Nr. 12) mit zwei Formeleinheiten pro Elementarzelle, Pearson-Symbol *mS*30 und Wyckoff-Sequenz 12.ji^4hc. Die Gitterparameter und Zellvolumina der Verbindungen sind in Tabelle 4 aufgelistet. Ausgewählte kristallographische Daten, Details der Strukturbestimmungen sowie äquivalente isotrope und anisotrope Auslenkungsparameter sind in den Abschnitten 8.1.1.1 bis 8.1.1.3 aufgeführt.

Tabelle 4. Gitterparameter, Zellvolumina und Besetzungsfaktoren (S.O.F.) der O/F-mischbesetzten Lage der isotypen Verbindungen $(ClOF_2)_2[MF_6]$ (*M* = Cr, Rh, Ge)

Parameter	$(ClOF_2)_2[CrF_6]$	$(ClOF_2)_2[RhF_6]$	$(ClOF_2)_2[GeF_6]$
a / Å	9,2613(15)	9,3751(11)	9,2914(19)
b / Å	6,7573(7)	6,8244(7)	6,7050(13)
c / Å	7,2877(11)	7,3202(9)	7,2694(14)
β / °	117,190(11)	116,542(9)	116,75(3)
V / Å³	405,68(11)	418,98(9)	404,41(17)
S.O.F. (O/F(1))	0,36(5), 0,64	0,51(7), 0,49	0,43(4), 0,57

Das Chloratom Cl(1) besetzt die spezielle Lage 4*i* (Lagesymmetrie *m*) und ist von den Atomen O/F(1), O/F(1)#1 und F(2) umgeben (Abbildung 22). Im $ClOF_2^+$-Kation liegt aufgrund der Spiegelebene eine O/F-mischbesetzte Lage vor, die Besetzungsfaktoren sind in Tabelle 4 aufgeführt. Die Cl−O/F(1)-Abstände in den Verbindungen sind mit 1,492(2) Å (**Cr**), 1,483(3) Å (**Rh**) und 1,482(2) Å (**Ge**) deutlich kleiner als die Cl−F(2)-Abstände von 1,568(3) Å (**Cr**), 1,582(5) Å (**Rh**) und 1,578(2) Å (**Ge**), entsprechen aber in etwa dem arithmetischen Mittel der Cl−O- und Cl−F-Abstände der $ClOF_2^+$-Kationen anderer Salze, siehe Abschnitt 4.3.8 und die Literatur.[267] O/F-Mischbesetzung oder -Fehlordnung wurde auch für die Verbindungen $ClOF_2[BF_4]$ (Abschnitt 4.3.4) und $ClOF_2[MF_6]$ (*M* = Nb, Ta) (Abschnitt 7.4) sowie in der Kristallstruktur von $ClOF_3$, beobachtet.[189] Für das homologe $BrOF_2^+$-Kation in $BrOF_2[AsF_6]$ wurde eine symmetriebedingte O/F-Mischbesetzung berichtet.[267]

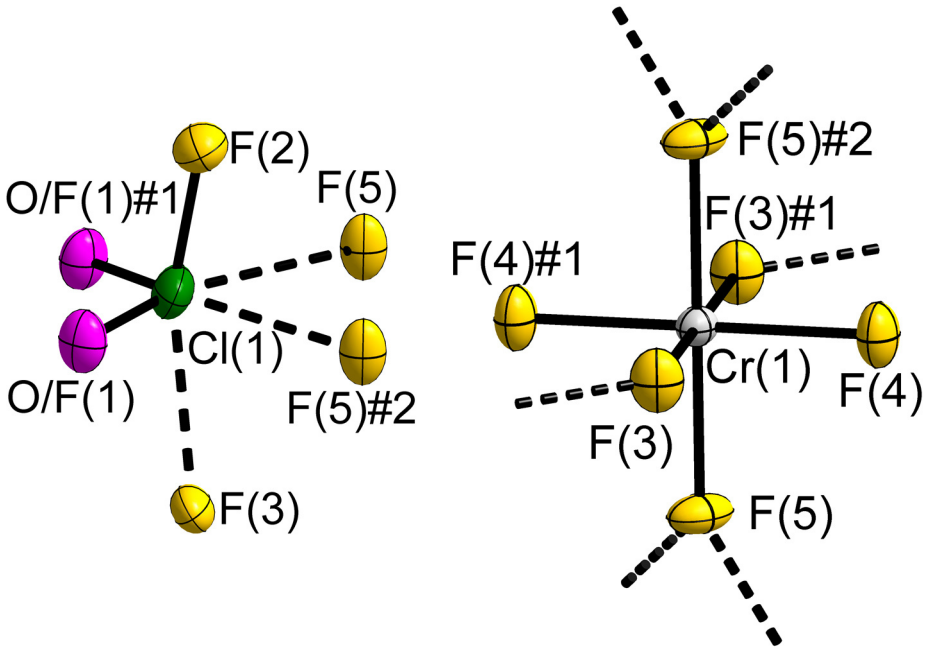

Abbildung 22. Ausschnitte aus der Kristallstruktur von $[ClOF_2]_2[CrF_6]$. Links ist das $ClOF_2^+$-Kation mit verbrückenden Fluoratomen abgebildet, rechts das $[CrF_6]^{2-}$-Anion. Die gestrichelten Bindungen stehen für kurze Kontakte der Form Cl···μ-F verbrückender Fluoratome des Anions mit den Chloratomen. Die Auslenkungsellipsoide sind mit 70% Aufenthaltswahrscheinlichkeit bei 100 K dargestellt. Symmetrietransformationen (links): #1 *x*, 1 − *y*, *z*; #2 1/2 − *x*, 3/2 − *y*, 1 − *z*; (rechts): #1 1 − *x*, *y*, 1 − *z*; #2 1 − *x*, 1 − *y*, 1 − *z*. Die Verbindungen $(ClOF_2)_2[MF_6]$ (*M* = Rh, Ge) kristallisieren isotyp zur Chromverbindung.

Das Metallatom *M*(1) (*M* = Cr, Rh, Ge) besetzt die spezielle Lage 2*c* (Lagesymmetrie 2/*m*) und ist von sechs Fluoratomen oktaederähnlich mit *M*−F-Abständen von 1,769(3)-1,865(3) Å (**Cr**), 1,869(4)-1,914(4) Å (**Rh**) und 1,760(2)-1,816(2) Å (**Ge**) umgeben. Diese sind vergleichbar mit denen in Salzen wie $Li_2[CrF_6]$ (1.812(4) und 1.829(3) Å bei 200 K), $K_2[CrF_6]\cdot 2HF$ (1.793(2)-1.8814(18) Å bei 200 K), $Li_2[RhF_6]$ (1,903 und 1,914 Å bei Raumtemperatur) und $Li_2[GeF_6]$ (1,792 und 1,804 Å bei Raumtemperatur).[272–274] Vier der sechs Fluoratome verbrücken zu benachbarten Chloratomen, wobei F(3) μ_2- und F(5) μ_3-verbrückt. Das Fluoratom F(4) ist terminal gebunden und die *M*−F(4)-Abstände sind deutlich kleiner als die der verbrückenden Fluoratome. Die Cl···μ-F-Abstände betragen 2,328(3) und 2,442(2) Å für *M* = Cr, 2,285(4) und 2,472(3) Å für *M* = Rh sowie 2,321(2) und 2,502(2) Å für *M* = Ge.

Die verbrückenden Fluoratome führen zur Koordinationszahl 3+3 für das Chloratom, mit einer oktaederähnlichen Anordnung der Liganden. Werden die Cl···μ-F-Kontakte berücksichtigt, so werden Schichten parallel zur *ab*-Ebene erhalten, welche mit der Niggli-Formel $^{2}_{\infty}\left[\langle ClF_{\frac{2}{2+1}}F_{\frac{1}{1+1}}F_{\frac{2}{1}}O_{\frac{1}{1}}\rangle_2\langle MF_{\frac{2}{1+2}}F_{\frac{2}{1+1}}F_{\frac{2}{1}}\rangle\right]$ beschrieben werden können (Abbildung 23). Die Schreibweise der Niggli-Formel erfolgt gemäß dem Vorschlag in der Literatur.[275] Die Chloratome sind pseudo-kubisch primitiv und die Metallatome pseudo-kubisch dicht gepackt. Die Metallatome sind somit würfelartig von Chloratomen und letztere tetraederähnlich von Metallatomen umgeben. Die Anordnung der Metall- und Chloratome ist damit ähnlich zu denen der Calcium- und Fluoratome im CaF_2-Typ.[276]

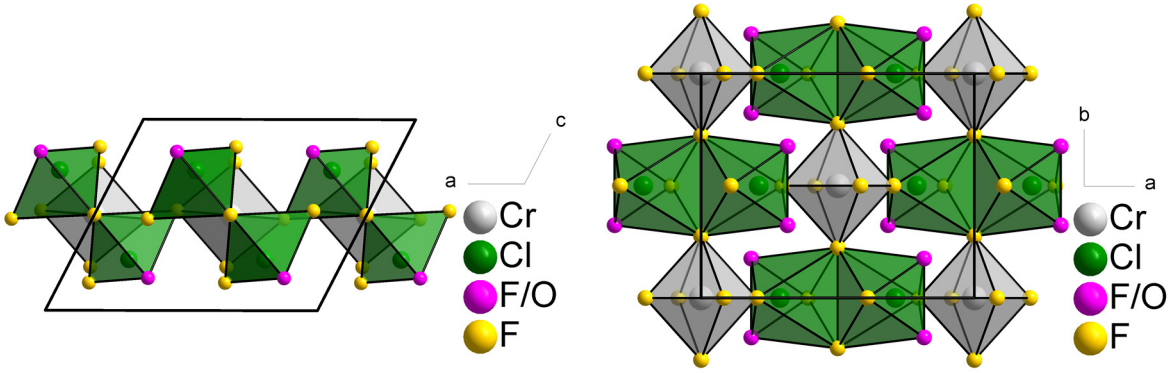

Abbildung 23. Kristallstruktur von $(ClOF_2)_2[CrF_6]$, projiziert entlang der *b*-Achse (links) oder der *c*-Achse (rechts). Die ersten Koordinationssphären der Chloratome sind als grüne und die der Chromatome als graue Polyeder dargestellt. Die Atome sind mit willkürlichen Radien abgebildet. Die Verbindungen $(ClOF_2)_2[MF_6]$ (*M* = Rh, Ge) kristallisieren isotyp zur Chromverbindung.

Von den Kristallstrukturen von $(ClOF_2)_2[MF_6]$ (*M* = Cr, Rh, Ge) in dem Raumgruppentyp *C*2/*m* (Nr. 12) wurden je Strukturmodelle mit geordneten $ClOF_2^+$-Kationen in der Untergruppe *C*2 (Nr. 5) abgeleitet, welche als Grundlage für periodische quantenchemische Rechnungen mit dem Programmpaket CRYSTAL17 (DFT-PBE0/TZVP) dienten.[242,243] Die optimierten Gitterparameter und Atompositionen dieser Modelle sind in den Abschnitten 8.2.2.1 bis 8.2.2.3 aufgeführt. Die optimierten Gitterparameter stimmen gut mit den experimentell ermittelten überein, was ebenso für die Cr−F-Abstände von 1,77-1,89 Å, die Rh−F-Abstände von 1,88-1,96 Å, als auch die Ge−F-Abstände von 1,76-1,87 Å, zutrifft. Ein Vergleich der berechneten und experimentell ermittelten Abstände und Winkel des $ClOF_2^+$-Kations erfolgt im Abschnitt 4.3.8.

Auf Basis der optimierten Struktur von $(ClOF_2)_2[GeF_6]$ wurde ein Raman-Spektrum für den Festkörper berechnet. Von $(ClOF_2)_2[CrF_6]$ und $(ClOF_2)_2[RhF_6]$ konnten keine Raman-Spektren erhalten werden, da diese sich im Laserlicht zersetzten oder kein Raman-Signal gemessen wurde. Gemessene und berechnete Raman-Spektren von $(ClOF_2)_2[GeF_6]$ sind in Abbildung 24 dargestellt und die Bandenzuordnungen in Tabelle 5 aufgeführt. Das hochaufgelöste Raman-Spektrum stimmt gut mit dem berechneten überein. Die Lagen der Banden, die dem $[GeF_6]^{2-}$-Anion zugeordnet werden können, stimmen mit denen in der Literatur berichteten von 621, 489 und 325 cm^{-1} für $(N_2H_6)_2[GeF_6]$ oder für in Wasser gelöste $[GeF_6]^{2-}$-Salze von 627, 454 und 318 cm^{-1} überein.[277,278]

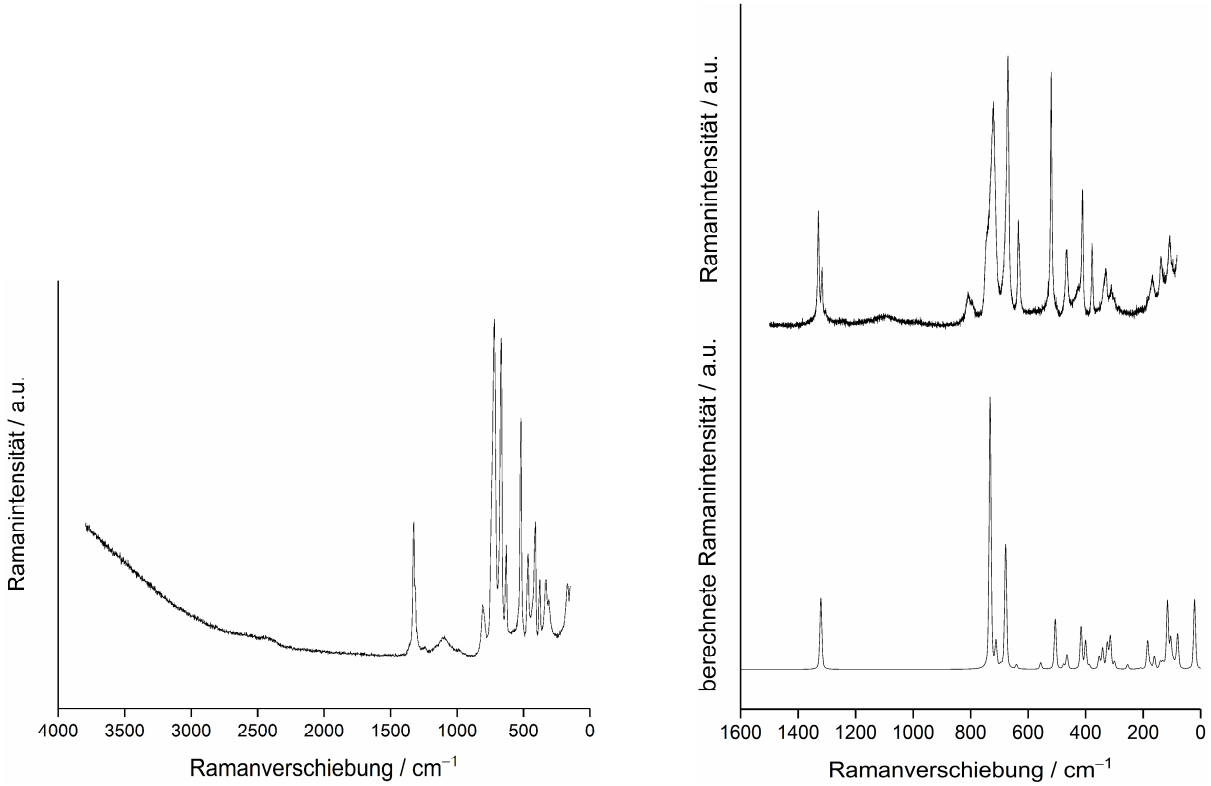

Abbildung 24. Links: Niedrigaufgelöstes Raman-Spektrum (532 nm Laser) von festem $(ClOF_2)_2[GeF_6]$. Rechts: Hochaufgelöstes (oben, 532 nm Laser) und berechnetes (unten) Raman-Spektrum von festem $(ClOF_2)_2[GeF_6]$. Das berechnete Spektrum basiert auf einem geordneten Modell von $(ClOF_2)_2[GeF_6]$ in der Raumgruppe *C*2 (Nr. 5), siehe Abschnitt 8.2.2.3. Die Banden bei circa 1000 und 800 cm^{-1} stellen vermutlich Kombinationsbanden oder Obertöne dar. Die Raman-Intensitäten sind in willkürlichen Einheiten (a.u.) angegeben.

Tabelle 5. Bandenlagen und -zuordnungen der Raman-Spektren von $(ClOF_2)_2[GeF_6]$, basierend auf dem berechneten Raman-Spektrum. (> 300 cm^{-1}) Das berechnete Spektrum basiert auf einem geordneten Modell von $(ClOF_2)_2[GeF_6]$ in der Raumgruppe *C*2 (Nr. 5), siehe Abschnitt 8.2.2.3. (*v*: Streckschwingung, *δ*: Deformationsschwingung, *π*: Inversionsschwingung, *s*: Symmetrisch, *as*: Asymmetrisch)

$\nu_{ber.}$ / cm^{-1}	$\nu_{gem.}$ / cm^{-1}	Zuordnung
1320	1329, 1316	$v(ClOF_2)$ – Cl−O-Streckschwingung des $ClOF_2^+$-Kations
732, 712	742, 721	$v_s(ClOF_2)$ – Symmetrische Streckschwingung der Fluoratome des $ClOF_2^+$-Kations
679, 678	670	$v_{as}(ClOF_2)$ – Asymmetrische Streckschwingung der Fluoratome des $ClOF_2^+$-Kations
695, 640, 556, 541	634	$v(GeF_6)$ – Streckschwingungen des $[GeF_6]^{2-}$-Anions
505, 476, 465	520, 468	$\pi(ClOF_2)$ + $v(GeF_6)$ – Inversionsschwingung des $ClOF_2^+$-Kations gekoppelt mit Streckschwingungen des $[GeF_6]^{2-}$-Anions
415, 400, 399	412	$\delta(ClOF_2)$ + $v(GeF_6)$ – Scherschwingung des O-Atoms des $ClOF_2^+$-Kations gekoppelt mit Streckschwingungen des $[GeF_6]^{2-}$-Anions
387, 353, 352, 341, 325, 321, 314	376, 330, 310	$\delta(ClOF_2)$ + $\delta(GeF_6)$ – Scherschwingung der F-Atome des $ClOF_2^+$-Kations gekoppelt mit Scherschwingungen des $[GeF_6]^{2-}$-Anions

4.3.2. Darstellung und Charakterisierung von $(ClOF_2)_2[MF_6]$ (*M* = Pd, Pt, Sn)

$(ClOF_2)_2[PdF_6]$: Ein PFA-Reaktionsgefäß (*V* ≈ 30 mL) wurde mit 27,0 mg (0,25 mmol, 1 Äq.) Palladiumschwamm beschickt, mit einem Edelstahlfaltenbalgventil verschlossen und an der ClF_3-Anlage mehrfach sekuriert. ClF_3 (0,36 g, 3,9 mmol, 15,6 Äq.) wurde bei 77 K auf den Feststoff kondensiert, die Kühlung entfernt und sofort 1,1 bar Sauerstoff hinzugegeben, das Reaktionsgefäß in einem Edelstahl-Dewargefäß platziert und langsam auf Raumtemperatur Erwärmen lassen. Bei Raumtemperatur war keine Reaktion erkennbar. Das Reaktionsgefäß wurde dann im UV-Reaktor für zwölf Tage bestrahlt. Im Anschluss wurden flüchtige Bestandteile im Vakuum entfernt und unverändertes Palladiumpulver sowie gelb-orange Kristalle im Handschuhkasten isoliert. Ein Teil des isolierten Produkts wurde in perfluoriertem Öl suspendiert und unter dem Mikroskop betrachtet, ein oranger Kristall wurde röntgenographisch untersucht. Die Zusammensetzung $(ClOF_2)_2[PdF_6]$ wurde für den Kristall erhalten.

Eine vollständige Reaktion des Palladiums wurde unter oben genannten oder ähnlichen Bedingungen nicht beobachtet. Die Bildung von $(ClOF_2)_2[PdF_6]$ kann mit der Gleichung 56 beschrieben werden.

$$O_2 + Pd + 4\,ClF_3 \xrightarrow{hv} (ClOF_2)_2[PdF_6] + 2\,ClF \qquad 56$$

$(ClOF_2)_2[PtF_6]$: Ein PFA-Reaktionsgefäß (*V* ≈ 30 mL) wurde mit 42,0 mg (0,16 mmol, 1 Äq.) *α*-$PtCl_2$ beschickt, mit einem Edelstahlfaltenbalgventil verschlossen und an der ClF_3-Anlage mehrfach sekuriert. ClF_3 (0,38 g, 4,1 mmol, 25,6 Äq.) wurde bei 77 K auf den Feststoff kondensiert, die Kühlung entfernt und sofort 1,1 bar Sauerstoff hinzugegeben, das Reaktionsgefäß in einem Edelstahl-Dewargefäß platziert und langsam auf Raumtemperatur erwärmt. Bei Raumtemperatur war keine Reaktion erkennbar. Das Reaktionsgefäß wurde dann im UV-Reaktor für elf Tage bestrahlt. Im Anschluss wurden flüchtige Bestandteile im Vakuum entfernt und ein dunkeloranger Feststoff im Handschuhkasten isoliert. Ein Teil des Feststoffs wurde in perfluoriertem Öl suspendiert und unter dem Mikroskop betrachtet. Es waren orange Kristalle erkennbar, von denen einer röntgenographisch untersucht wurde. Die Zusammensetzung $(ClOF_2)_2[PtF_6]$ wurde für den Kristall erhalten. Die Bildung von $(ClOF_2)_2[PtF_6]$ kann mit Gleichung 57 beschrieben werden.

$$O_2 + PtCl_2 + 5\,ClF_3 \xrightarrow{hv} (ClOF_2)_2[PtF_6] + 5\,ClF \qquad 57$$

$(ClOF_2)_2[SnF_6]$: Ein PFA-Reaktionsgefäß wurde mit 8,5 mg (0,06 mmol, 1 Äq.) SnO beschickt, mit einem Edelstahlfaltenbalgventil verschlossen und an der ClF_3-Anlage mehrfach sekuriert. ClF_3 (0,24 g, 2,6 mmol, 43,3 Äq.) wurde bei 77 K auf den Feststoff kondensiert, das Reaktionsgefäß in einem Edelstahl-Dewargefäß platziert und langsam auf Raumtemperatur erwärmt. Der Feststoff reagierte heftig mit Chlortrifluorid, sobald dieses aufgetaut war. Das Reaktionsgefäß wurde dann im UV-Reaktor für zwei Tage bestrahlt. Im Anschluss wurden flüchtige Bestandteile im Vakuum entfernt und ein farbloser Feststoff im Handschuhkasten isoliert (26,7 mg). Ein Teil des Feststoffs wurde in perfluoriertem Öl suspendiert und unter dem Mikroskop betrachtet. Es waren farblose Kristalle erkennbar, von denen einer röntgenographisch untersucht wurde. Die Zusammensetzung $(ClOF_2)_2[SnF_6]$ wurde für den Kristall erhalten. Die Bildung der Verbindung mit einem 2:1-Verhältnis von $ClOF_2^+$-Kation zu $[SnF_6]^-$-Anion kann auch hier vermutlich auf die Diffusion von Sauerstoff durch den Kunststoff zurückgeführt werden, siehe oben. Die Bildung der Verbindung kann mit Gleichung 58 beschrieben werden.

$$O_2 + 2\,SnO + 8\,ClF_3 \xrightarrow{hv} 2\,(ClOF_2)_2[SnF_6] + 4\,ClF \qquad 58$$

Bis(difluorooxychloronium(V))-hexafluoridopalladat(IV), -platinat(IV) und -stannat(IV) kristallisieren isotyp in der orthorhombischen Raumgruppe *Pnnm* (Nr. 58) mit zwei Formeleinheiten pro Elementarzelle, Pearson-Symbol *oP*30 und Wyckoff-Sequenz 58.h^2g^3b. Die Verbindungen kristallisieren isotyp zu $(SF_3)_2[GeF_6]$.[206] Die Gitterparameter und Zellvolumina der Verbindungen sind in Tabelle 6 aufgelistet. Ausgewählte kristallographische Daten, Details der Strukturbestimmungen sowie äquivalente isotrope und anisotrope Auslenkungsparameter sind in den Abschnitten 8.1.1.4 bis 8.1.1.6 aufgeführt.

Tabelle 6. Gitterparameter und Zellvolumina der isotypen Verbindungen $(ClOF_2)_2[MF_6]$ (M = Pd, Pt, Sn)

Parameter	$(ClOF_2)_2[PdF_6]$	$(ClOF_2)_2[PtF_6]$	$(ClOF_2)_2[SnF_6]$
a / Å	7,4491(15)	7,4807(15)	7,5859(4)
b / Å	9,4636(19)	9,4651(19)	9,7473(5)
c / Å	5,9111(12)	5,9950(12)	6,0864(3)
V / Å^3	416,70(15)	424,48(15)	450,04(4)

Das Chloratom Cl(1) besetzt die spezielle Lage 4*g* (Lagesymmetrie ..*m*) und ist von dem Sauerstoffatom O(1) sowie den Fluoratomen F(1) und F(1)#1 umgeben (Abbildung 25). Die Cl−O-Abstände in den pyramidalen $ClOF_2^+$-Kationen betragen 1,439(4) Å (**Pd**), 1,442(4) Å (**Pt**) und 1,481(2) Å (**Sn**), die Cl−F-Abstände sind mit 1,552(3) Å (**Pd**), 1,540(3) Å (**Pt**) und 1,532(2) Å (**Sn**) signifikant größer als die ersteren. Die Abstände entsprechen denen der anderen hier berichteten $ClOF_2^+$-Verbindungen sowie den in der Literatur genannten.[267]

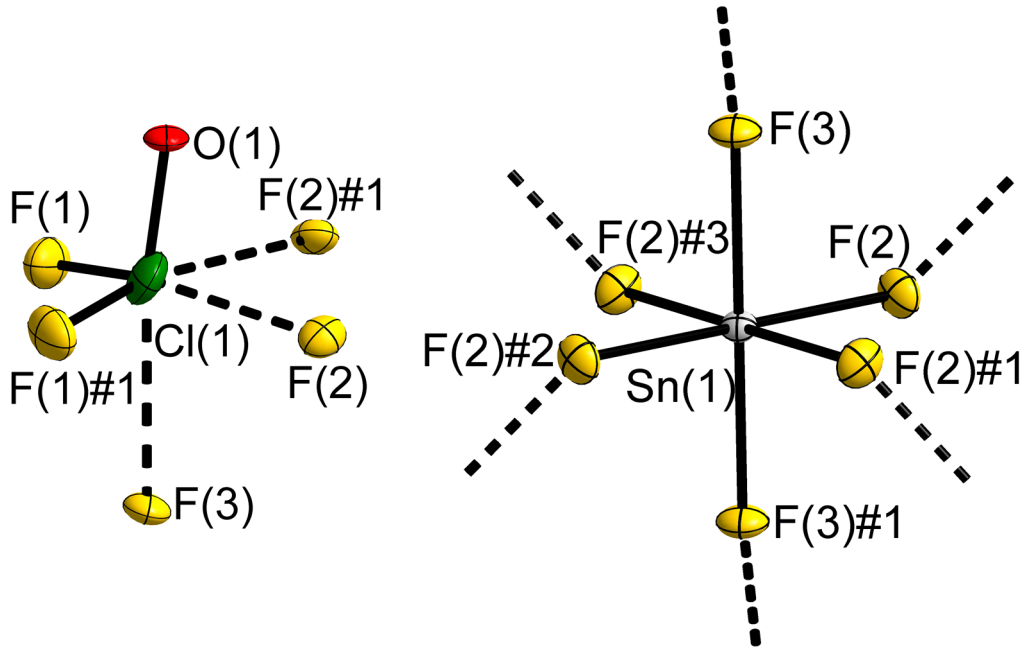

Abbildung 25. Ausschnitte aus der Kristallstruktur von $[ClOF_2]_2[SnF_6]$. Links ist das $ClOF_2^+$-Kation mit verbrückenden Fluoratomen abgebildet, rechts das $[SnF_6]^{2-}$-Anion. Die gestrichelten Bindungen stehen für kurze Kontakte der Form Cl···μ-F verbrückender Fluoratome des Anions mit den Chloratomen. Die Auslenkungsellipsoide sind mit 70% Aufenthaltswahrscheinlichkeit bei 100 K dargestellt. Symmetrietransformationen (links): #1 *x*, *y*, 1 − *z*; (rechts): #1 1 − *x*, 1 − *y*, *z*; #2 1 − *x*, 1 − *y*, −*z*; #3 *x*, *y*, −*z*. Die Verbindungen $(ClOF_2)_2[MF_6]$ (*M* = Pd, Pt) kristallisieren isotyp zur Zinnverbindung.

Das Metallatom *M*(1) (*M* = Pd, Pt, Sn) besetzt die spezielle Lage 2*b* (Lagesymmetrie 2/*m*) und ist von sechs Fluoratomen oktaederähnlich mit *M*−F-Abständen von 1,898(3) und 1,896(4) Å (**Pd**), 1,923(3) und 1,930(2) Å (**Pt**) und 1,953(2) und 1,958(1) Å (**Sn**) umgeben. Die *M*−F-Abstände sind vergleichbar mit denen in anderen Salzen wie $Li_2[PdF_6]$ (1,899(4) Å bei 299 K), $Li_2[PtF_6]$ (1,936(4) und 1,942(6) Å bei 150 K) und $Ag[SnF_6]$ (1,921(3)-1,983(3) Å bei Raumtemperatur).[279–281] Alle Fluoratome der $[MF_6]^{2-}$-Anionen sind μ_2-verbrückend zu benachbarten Chloratomen, welche somit die Koordinationszahl 3+3 mit einer oktaederähnlichen Ligandenanordnung aufweisen. Die Cl···μ-F-Abstände betragen dabei 2,396(3) und 2,452(4) Å für *M* = Pd, 2,391(3) und 2,440(4) Å für *M* = Pt und 2,394(1) und 2,421(2) Å für *M* = Sn.

Die Cl···μ-F(2)-Abstände sind quasi unabhängig von *M*, wohingegen die Cl···μ-F(3)-Abstände in der Reihe Pd > Pt > Sn abnehmen, was wiederum einen Einfluss auf die Cl−O- und Cl−F-Abstände innerhalb der $ClOF_2^+$-Kationen hat. Erstere nehmen in der Reihe zu und letztere nehmen ab.

Werden die Cl···μ-F-Kontakte berücksichtigt, so wird eine Gerüststruktur erhalten, welche mit der Niggli-Formel ${}^{3}_{\infty}\left[\langle ClF_{\underset{1+1}{3}}F_{\underset{1}{2}}O_{\underset{1}{1}}\rangle_2\langle MF_{\underset{1+1}{6}}\rangle\right]$ beschrieben werden kann, siehe Abbildung 26. Die Chloratome sind pseudo-kubisch primitiv und die Metallatome pseudo-kubisch dicht gepackt. Die Metallatome sind somit würfelartig von Chloratomen und letztere tetraederähnlich von Metallatomen umgeben. Die Anordnung der Metall- und Chloratome ist damit ähnlich zu denen der Calcium- und Fluoratome im CaF_2-Typ.[276]

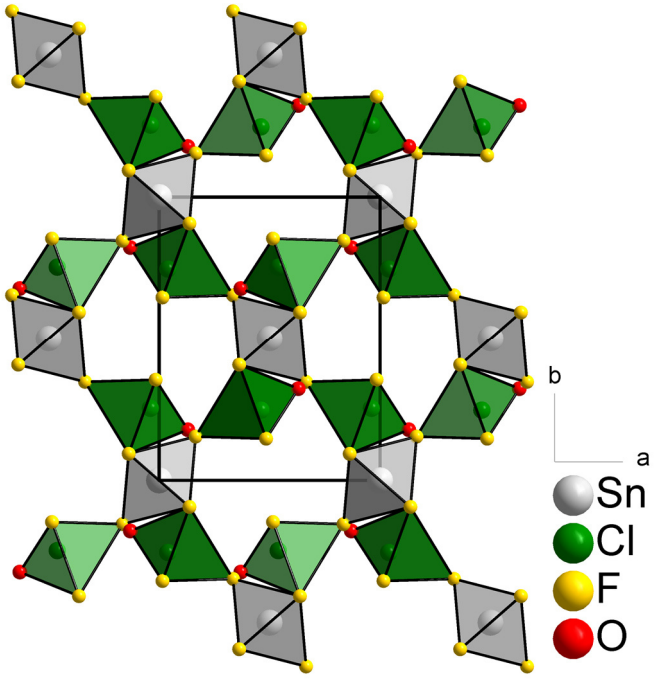

Abbildung 26. Kristallstruktur von $[ClOF_2]_2[SnF_6]$, projiziert entlang der *c*-Achse. Die ersten Koordinationssphären der Chloratome sind als grüne und die der Zinnatome als graue Polyeder dargestellt. Die Atome sind mit willkürlichen Radien abgebildet. Die Verbindungen $(ClOF_2)_2[MF_6]$ (*M* = Pd, Pt) kristallisieren isotyp zur Zinnverbindung.

Die Kristallstrukturen von $(ClOF_2)_2[MF_6]$ (M = Pd, Pt, Sn) dienten als Grundlagen für periodische quantenchemische Rechnungen mit dem Programmpaket CRYSTAL17 (DFT-PBE0/TZVP).[242,243] Die optimierten Gitterparameter und Atompositionen sind in den Abschnitten 8.1.1.4 bis 8.1.1.6 aufgeführt. Die berechneten und experimentell ermittelten Gitterparameter stimmen gut überein, ebenso die Pd−F-Abstände von 1,92 Å, die Pt−F-Abstände von 1,96 und 1,97 Å sowie die Sn−F-Abstände von 1,95 und 1,99 Å. Ein Vergleich berechneter und experimentell ermittelter Abstände und Winkel in den $ClOF_2^+$-Kationen erfolgt im Abschnitt 4.3.8. Auf Basis der optimierten Strukturen von $(ClOF_2)_2[PtF_6]$ und $(ClOF_2)_2[SnF_6]$ wurden je Raman-Spektren für den Festkörper berechnet. Gemessene und berechnete Raman-Spektren von $(ClOF_2)_2[PtF_6]$ sind in Abbildung 27 und die von $(ClOF_2)_2[SnF_6]$ in Abbildung 28 dargestellt. Von $(ClOF_2)_2[PdF_6]$ konnte kein Raman-Spektrum gemessen werden, da dieses sich im Laserlicht zersetzte. Die Bandenzuordnungen sind in Tabelle 7 und Tabelle 8 aufgeführt. Die hochaufgelösten Raman-Spektren stimmen gut mit den berechneten überein. Die Bandenlagen, die den $[PtF_6]^{2-}$- und $[SnF_6]^{2-}$-Anionen zugeordnet werden können, stimmen mit denen in der Literatur berichteten von 591, 577, 566 und 267 cm^{-1} für $Cs_2[PtF_6]$ oder 596, 557, 480, 420, 367 und 257 cm^{-1} für $Na_2[SnF_6]$ überein.[282,283]

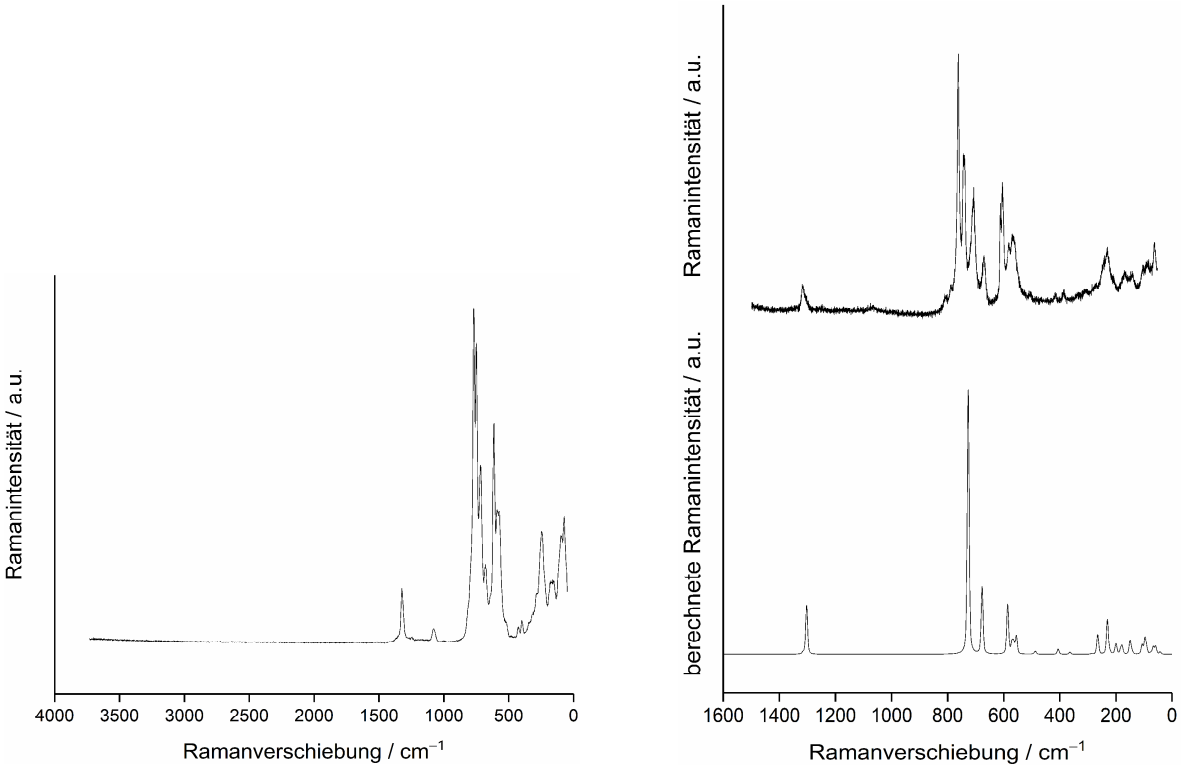

Abbildung 27. Links: Niedrigaufgelöstes Raman-Spektrum (532 nm Laser) von festem $(ClOF_2)_2[PtF_6]$. Rechts: Hochaufgelöstes (oben, 532 nm Laser) und berechnetes (unten) Raman-Spektrum von festem $(ClOF_2)_2[PtF_6]$. Die Raman-Intensitäten sind in willkürlichen Einheiten (a.u.) angegeben.

Tabelle 7. Bandenlagen und -zuordnungen der Raman-Spektren von $(ClOF_2)_2[PtF_6]$, basierend auf dem berechneten Raman-Spektrum. (> 300 cm^{-1}) (*v*: Streckschwingung, *δ*: Deformationsschwingung, *π*: Inversionsschwingung, *s*: Symmetrisch, *as*: Asymmetrisch)

$\nu_{ber.}$ / cm^{-1}	$\nu_{gem.}$ / cm^{-1}	Zuordnung
1315, 1302	1316	$v(ClOF_2)$ – Cl−O-Streckschwingung des $ClOF_2^+$-Kations
771, 726	763, 742, 739	$v_s(ClOF_2)$ – Symmetrische Streckschwingung der Fluoratome des $ClOF_2^+$-Kations
677, 672	707, 671	$v_{as}(ClOF_2)$ – Asymmetrische Streckschwingung der Fluoratome des $ClOF_2^+$-Kations
586, 585, 571, 564, 555	612, 605, 581, 566	$v(PtF_6)$ – Streckschwingungen des $[PtF_6]^{2-}$-Anions
494, 487	507	$\pi(ClOF_2)$ – Inversionsschwingung des $ClOF_2^+$-Kations
406, 404	418	$\delta(ClOF_2)$ – Scherschwingung des O-Atoms des $ClOF_2^+$-Kations
365, 364	386	$\delta(ClOF_2)$ – Scherschwingung der F-Atome des $ClOF_2^+$-Kations

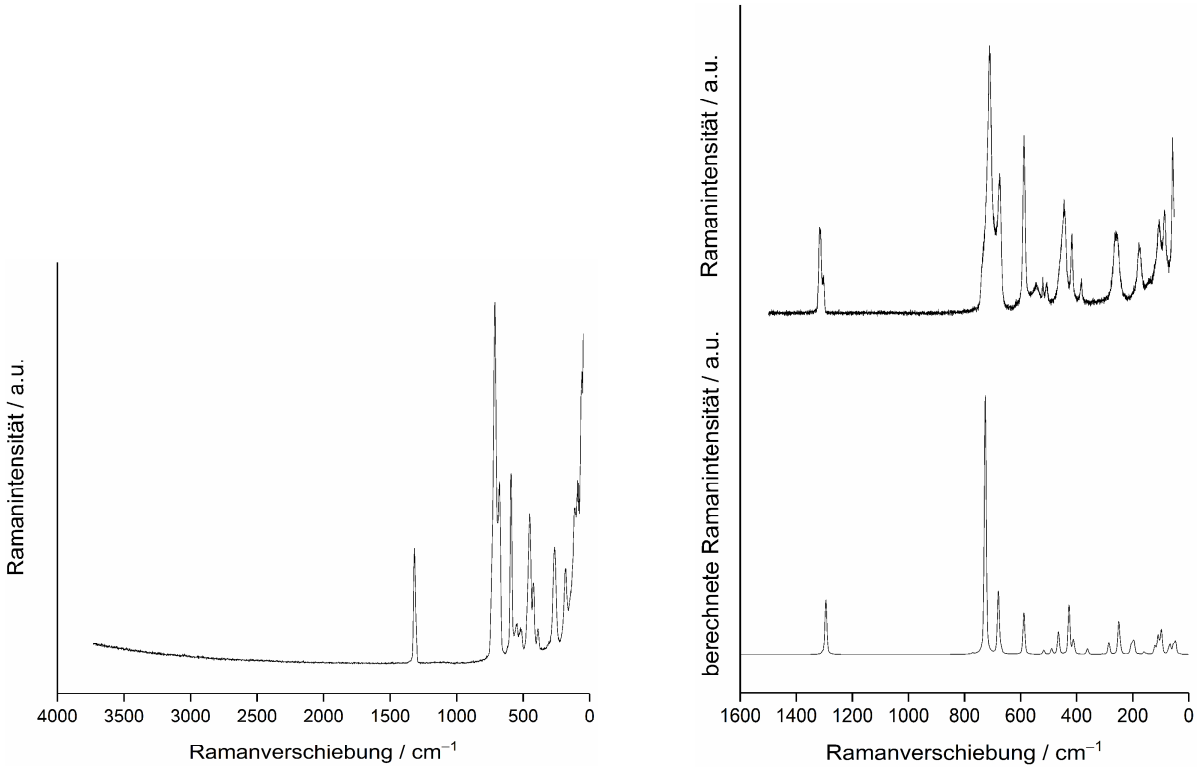

Abbildung 28. Links: Niedrigaufgelöstes Raman-Spektrum (532 nm Laser) von festem $(ClOF_2)_2[SnF_6]$. Rechts: Hochaufgelöstes (oben, 532 nm Laser) und berechnetes (unten) Raman-Spektrum von festem $(ClOF_2)_2[SnF_6]$. Die Raman-Intensitäten sind in willkürlichen Einheiten (a.u.) angegeben.

Tabelle 8. Bandenlagen und -zuordnungen der Raman-Spektren von $(ClOF_2)_2[SnF_6]$, basierend auf dem berechneten Raman-Spektrum. (> 300 cm^{-1}) (*v*: Streckschwingung, *δ*: Deformationsschwingung, *π*: Inversionsschwingung, *s*: Symmetrisch, *as*: Asymmetrisch)

$\nu_{ber.}$ / cm^{-1}	$\nu_{gem.}$ / cm^{-1}	Zuordnung
1307, 1294	1315, 1303	$\nu(ClOF_2)$ – Cl−O-Streckschwingung des $ClOF_2^+$-Kations
771, 726	709	$\nu_s(ClOF_2)$ – Symmetrische Streckschwingung der Fluoratome des $ClOF_2^+$-Kations
679, 669	675	$\nu_{as}(ClOF_2)$ – Asymmetrische Streckschwingung der Fluoratome des $ClOF_2^+$-Kations
588, 586	587, 545	$\nu_s(SnF_6)$ – Symmetrische Streckschwingungen des $[SnF_6]^{2-}$-Anions
517, 489	520, 507	$\pi(ClOF_2)$ – Inversionsschwingung des $ClOF_2^+$-Kations
471, 465, 427	445	$\nu(SnF_6)$ – Streckschwingungen des $[SnF_6]^{2-}$-Anions
412, 408	417	$\delta(ClOF_2)$ – Scherschwingung des O-Atoms des $ClOF_2^+$-Kations
363, 361	383	$\delta(ClOF_2)$ – Scherschwingung der F-Atome des $ClOF_2^+$-Kations

4.3.3. Darstellung und Charakterisierung von $ClOF_2MF_5$ (*M* = Sn, Pb)

$ClOF_2SnF_5$: Ein PFA-Reaktionsgefäß wurde mit 76 mg (0,49 mmol, 1 Äq.) SnF_2 beschickt, mit einem Edelstahlfaltenbalgventil verschlossen und an der ClF_3-Anlage mehrfach sekuriert. ClF_3 (0,77 g, 8,3 mmol, 16,9 Äq.) wurde bei 77 K auf den Feststoff kondensiert, das Reaktionsgefäß in einem Edelstahl-Dewargefäß platziert und langsam auf Raumtemperatur erwärmt. Der Feststoff reagierte heftig mit Chlortrifluorid, sobald dieses aufgetaut war. Das Reaktionsgefäß wurde dann im UV-Reaktor für 63 Stunden bestrahlt. Im Anschluss wurden flüchtige Bestandteile im Vakuum entfernt und ein farbloser Feststoff im Handschuhkasten isoliert (101 mg). Ein Teil des Feststoffs wurde in perfluoriertem Öl suspendiert und unter dem Mikroskop betrachtet. Es waren farblose Kristalle erkennbar, von denen einer röntgenographisch untersucht wurde. Die Zusammensetzung $ClOF_2SnF_5$ wurde für den Kristall erhalten.

Die Bildung einer $ClOF_2^+$-Verbindung kann vermutlich auf die Diffusion von Sauerstoff durch den Kunststoff und/oder Spuren von Wasser im SnF_2 zurückgeführt werden. Letztere führen in Verbindung mit Chlortrifluorid zur Bildung von Chlordioxidfluorid und Fluorwasserstoff, welcher zur Isolierung einer Verbindung mit dem SnF_5^--Anion durch eine Verdrängungsreaktion geführt haben könnte.[109,110,142] Verbindungen mit SnF_5^--Anionen, wie NF_4SnF_5 und $N_2F_3SnF_5$, wurden durch Metathese-Reaktionen in wasserfreiem Fluorwasserstoff dargestellt und selbst bei entsprechenden Stoffmengenverhältnissen der Edukte wurden keine Salze mit $[SnF_6]^{2-}$-Anionen erhalten.[284,285] Dies wurde auf Verdrängungsreaktionen des Fluorwasserstoffs mit potentiell gebildeten Verbindungen der Form $(NF_4)_2[SnF_6]$ und $(N_2F_3)_2[SnF_6]$, bei denen labiles $NF_4[HF_2]$ oder flüchtiges N_2F_4 durch Fluorwasserstoff freigesetzt wird, zurückgeführt.[284,285] Ähnliche Verdrängungsreaktionen wurden auch für $(O_2)_2[PdF_6]$, mit der Freisetzung von „O_2F“, welches sich zu O_2 und F_2 zersetzt, beschrieben.[286] $ClOF_3$ ist ebenfalls flüchtig, es besitzt einen Siedepunkt von 29°C (Druck nicht berichtet) und könnte entsprechend aus Salzen durch Fluorwasserstoff unter Erhöhung des Kondensationsgrades des Anions verdrängt werden.[152] Die Bildung von $ClOF_2SnF_5$ kann mit Gleichung 59 beschrieben werden.

$$O_2 + 2\,SnF_2 + 4\,ClF_3 \xrightarrow{hv} 2\,ClOF_2SnF_5 + 2\,ClF \qquad 59$$

$ClOF_2PbF_5$: Ein PFA-Reaktionsgefäß (V ≈ 28 mL) wurde mit 40,2 mg (0,14 mmol, 1 Äq.) PbF_4 im Handschuhkasten beschickt, mit einem Edelstahlfaltenbalgventil verschlossen und an der ClF_3-Anlage mehrfach sekuriert. ClF_3 (0,35 g, 3,8 mmol, 27,1 Äq.) wurde bei 77 K auf den Feststoff kondensiert, die Kühlung entfernt und sofort 0,84 bar Sauerstoff hinzugegeben, das Reaktionsgefäß in einem Edelstahl-Dewargefäß platziert und langsam auf Raumtemperatur erwärmt. Bei Raumtemperatur war keine Reaktion erkennbar. Das Reaktionsgefäß wurde dann im UV-Reaktor für zwei Stunden bestrahlt. Das Reaktionsgefäß wurde auf 77 K gekühlt, flüchtige Bestandteile im Vakuum entfernt, nochmals ClF_3 (0,34 g, 3,7 mmol, 26,4 Äq.) kondensiert, die Kühlung entfernt und 0,88 bar O_2 zugegeben. Das Reaktionsgefäß wurde bei Raumtemperatur für 16 Stunden bestrahlt. Im Anschluss wurden flüchtige Bestandteile im Vakuum entfernt. Ein farbloser, kristalliner Feststoff wurde im Handschuhkasten isoliert. Ein Teil des isolierten Produkts wurde in perfluoriertem Öl suspendiert, unter dem Mikroskop betrachtet und ein farbloser Kristall röntgenographisch untersucht. Die Zusammensetzung $ClOF_2PbF_5$ wurde für den Kristall erhalten. Vermutlich führten Spuren von Wasser zur Bildung von Fluorwasserstoff und dieser zu einer Verdrängungsreaktion, sodass eine Verbindung mit dem PbF_5^--Anion erhalten wurde, siehe oben. Die Bildung von $ClOF_2PbF_5$ kann mit Gleichung 60 beschrieben werden.

$$O_2 + 2\,PbF_4 + 2\,ClF_3 \xrightarrow{hv} 2\,ClOF_2PbF_5 \qquad 60$$

Difluorooxychloronium(V)-pentafluoridostannat(IV) und -plumbat(IV) kristallisieren isotyp in der monoklinen Raumgruppe $C2$ (Nr. 5) mit vier Formeleinheiten pro Elementarzelle, Pearson-Symbol $mS40$ und Wyckoff-Sequenz $5.c^{10}$. Die Gitterparameter und Zellvolumina der Verbindungen sind in Tabelle 9 aufgelistet. Ausgewählte kristallographische Daten, Details der Strukturbestimmungen sowie äquivalente isotrope und anisotrope Auslenkungsparameter sind in den Abschnitten 8.1.1.7 und 8.1.1.8 aufgeführt.

Tabelle 9. Gitterparameter und Zellvolumina der isotypen Verbindungen $ClOF_2MF_5$ (M = Sn, Pb)

Parameter	$ClOF_2SnF_5$	$ClOF_2PbF_5$
a / Å	15,828(3)	16,1838(12)
b / Å	5,0614(10)	5,1546(4)
c / Å	7,4425(15)	7,5376(5)
β / °	111,25(3)	111,932(2)
V / Å^3	555,7(2)	583,29(7)

Das Chloratom Cl(1) besetzt die allgemeine Lage 4*c* und ist von dem Sauerstoffatom O(1) und den zwei Fluoratomen F(1) und F(2) umgeben, siehe Abbildung 29. Die Cl−O-Abstände in den pyramidalen $ClOF_2^+$-Kationen betragen 1,418(9) (**Sn**) und 1,405(5) Å (**Pb**), die Cl−F-Abstände betragen 1,544(7) und 1,564(8) Å (**Sn**) und 1,569(4) und 1,582(4) Å (**Pb**). Die Cl−O-Abstände in den Kationen der beiden Verbindungen sind mit die kürzesten der in dieser Arbeit oder in der Literatur berichteten $ClOF_2^+$-Verbindungen (Abschnitt 4.3.8).[267] Sie sind ähnlich mit dem für das freie $ClOF_2^+$-Kation auf CCSD(T)/aug-ccpVTZ/aug-cc-pVTZ-PP-Niveau berechneten von 1,3921 Å.[70]

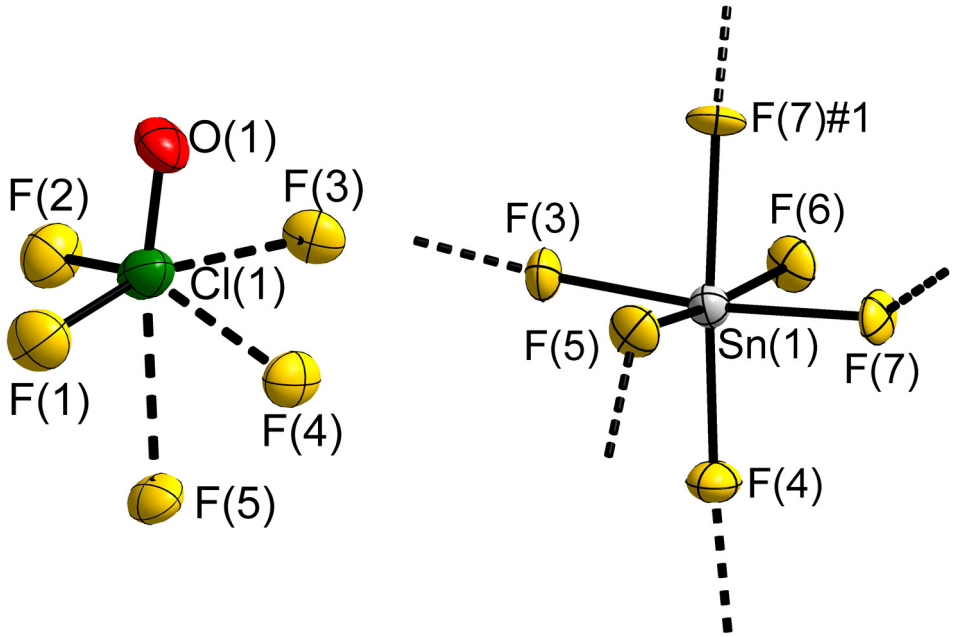

Abbildung 29. Ausschnitte aus der Kristallstruktur von $ClOF_2SnF_5$. Links ist das $ClOF_2^+$-Kation mit verbrückenden Fluoratomen abgebildet, rechts die Koordinationssphäre des Sn(1)-Atoms. Die gestrichelten Bindungen stehen für kurze Kontakte der Form Cl···μ-F verbrückender Fluoratome des Anions mit den Chloratomen oder zu weiteren Zinnatomen verbrückender Fluoratome (F(7)). Die Auslenkungsellipsoide sind mit 70% Aufenthaltswahrscheinlichkeit bei 100 K dargestellt. Symmetrietransformation (rechts): #1 3/2 − x, 1/2 + y, 1 − z. $ClOF_2PbF_5$ kristallisiert isotyp zur Zinnverbindung.

Das Metallatom *M*(1) (*M* = Sn, Pb) besetzt ebenfalls die allgemeine 4*c*-Lage und ist von sechs Fluoratomen oktaederähnlich umgeben. Die Fluoratome F(7) und F(7)#1 sind μ$_2$-verbrückend zwischen Metallatomen, sodass das MF_5^--Anion mit cis-verbrückenden [MF_6]-Polyedern erhalten wird. Die MF_5^--Anionen bilden Zick-Zack-Ketten entlang der *b*-Achse aus und können mit der Niggli-Formel ${}^{1}_{\infty}\left[MF_{\frac{4}{1}}F_{\frac{2}{2}}\right]^-$ beschrieben werden.

Drei der sechs Fluoratome der ${}^{1}_{\infty}\left[MF_{\frac{4}{1}}F_{\frac{2}{2}}\right]^-$-Anionen verbrücken jeweils zu benachbarten Chloratomen mit Cl···μ-F-Abständen von 2,377(7)-2,511(7) Å (**Sn**) und 2,351(4)-2,501(4) Å (**Pb**). Die *M*−F-Abstände betragen für die terminal-gebundenen Fluoratome 1,901(6) (**Sn**) und 1,979(3) Å (**Pb**) und für die zwischen Metallatomen verbrückenden Fluoratome 2,041(6) und 2,061(5) Å (**Sn**) und 2,134(4) und 2,156(3) Å (**Pb**). Für die zu Chloratomen verbrückenden Fluoratome liegen die entsprechenden Abstände in den Bereichen von 1,936(6)-1,951(6) Å (**Sn**) und 2,001(3)-2,040(4) Å (**Pb**). Die Sn−F-Abstände stimmen mit denen im ClO_2SnF_5 (1,9047(13)-2,0627(13) Å bei 100 K, Abschnitt 8.1.1.7) überein.[257] In der Literatur wurden bisher keine Kristallstrukturen mit PbF_5^--Anionen berichtet. Die Sn−F-Abstände sind vergleichbar mit denen für $O_2Sn_2F_9$ (1,898(2)-2,0374(4) Å bei 200 K), $O_2[Sn_2F_9]\cdot 0.9HF$ (1,880(4)-2,095(4) Å bei 150 K) und $(XeF_5)_4[Sn_5F_{24}]$ (1.879(6)-2.101(5) Å bei 150 K) berichteten.[287,288] In allen genannten Verbindungen sind terminal gebundene und zwischen Zinnatomen verbrückende Fluoratome präsent.

Verbindungen mit PbF_5^--Anionen oder anderen komplexeren Anionen mit verbrückenden Fluoratomen wurden vorher noch nicht beschrieben und es sind bisher nur Verbindungen mit $[PbF_6]^{2-}$-Anionen bekannt.[289–291] Die Pb−F-Abstände in Salzen mit $[PbF_6]^{2-}$-Anionen betragen 1,997(7) Å in $Li_2[PbF_6]$ bei 293 K, 2,042(4) und 2,060(4) Å in $Sr[PbF_6]$ bei 293 K und 2,048(2)-2,054(3) Å in $[Xe_2F_{11}]_2[PbF_6]$ bei 150 K.[288,291]

Werden die Cl···μ-F-Kontakte der Anionen berücksichtigt, so resultiert die Koordinationszahl 3+3 für das Chloratom und eine oktaederähnliche Anordnung der Liganden. Die Kontakte führen zu Schichten, die parallel zur (101)-Ebene angeordnet sind und mit der Niggli-Formel $^{2}_{\infty}\left[\langle ClF_{\frac{3}{1+1}}F_{\frac{2}{1}}O_{\frac{1}{1}}\rangle\langle MF_{\frac{3}{1+1}}F_{\frac{2}{2}}F_{\frac{1}{1}}\rangle\right]$ beschrieben werden können (Abbildung 30).

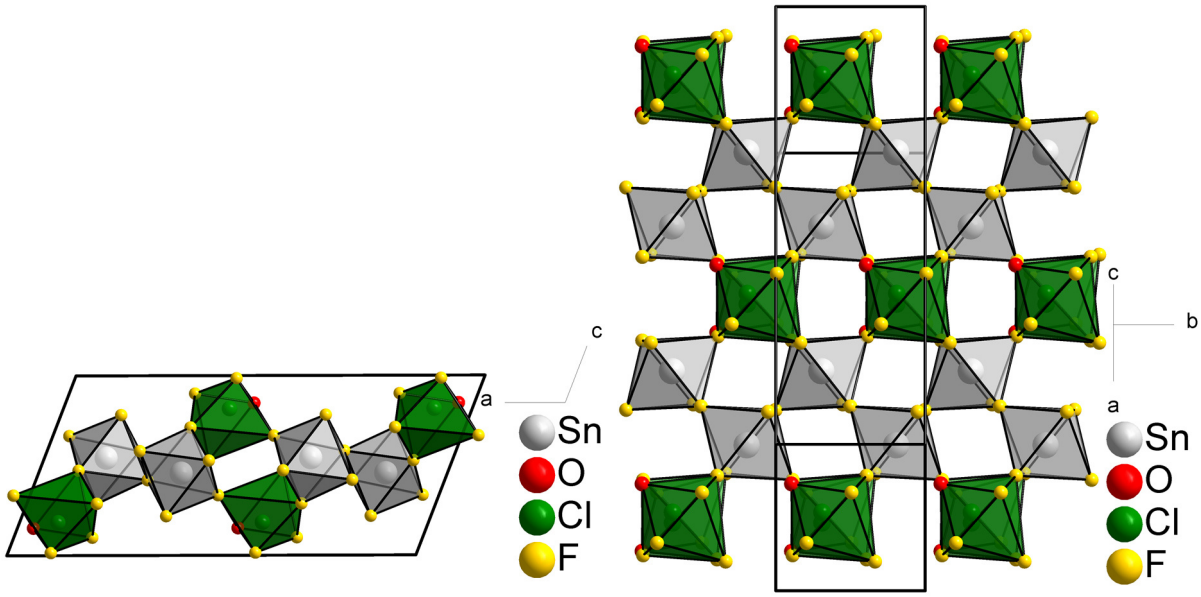

Abbildung 30. Kristallstruktur von $ClOF_2SnF_5$, projiziert entlang der *b*-Achse (links) oder auf die (101)-Ebene (rechts). Die ersten Koordinationssphären der Chloratome sind als grüne und die der Zinnatome als graue Polyeder dargestellt. Die Atome sind mit willkürlichen Radien abgebildet.

Die Chloratome bilden gewellte Schichten („4^4-Netz“) parallel zu der *ab*-Ebene aus, wenn Cl−Cl-Abstände von 4,57-5,06 Å (**Sn**) oder 4,62-5,16 Å (**Pb**) berücksichtigt werden. Wenn *M*−*M*-Abstände von 3,89-5,06 Å (**Sn**) oder 4,04-5,16 Å (**Pb**) berücksichtigt werden, bilden die Metallatome leicht gewellte Schichten ($3^3.4^2$-Netz) parallel zu der *ab*-Ebene aus. Die Metallatome und Chloratome umgeben sich jeweils in der Form eines leicht verzerrten Gyrobifastigiums (Johnson-Körper J_{26}) mit *M*−Cl-Abständen von 4,00-5,45 Å (**Sn**) und 4,08-5,50 Å (**Pb**).[292]

Die Kristallstrukturen von $ClOF_2SnF_5$ und $ClOF_2PbF_5$ dienten als Grundlagen für periodische quantenchemische Rechnungen mit dem Programmpaket CRYSTAL17 (DFT-PBE0/TZVP).[242,243] Die optimierten Gitterparameter und Atompositionen sind in den Abschnitten 8.2.2.7 und 8.2.2.8 aufgeführt. Die berechneten Gitterparameter stimmen gut mit den experimentell bestimmten überein, was auch auf die Sn−F-Abstände von 1,91-2,08 Å beziehungsweise Pb−F-Abstände von 1,99-2,18 Å zutrifft.

Ein Vergleich der berechneten und experimentell ermittelten Abstände und Winkel im $ClOF_2^+$-Kation erfolgt im Abschnitt 4.3.8. Auf Basis der optimierten Struktur von $ClOF_2PbF_5$ wurde ein Raman-Spektrum für den Festkörper berechnet. Gemessene und berechnete Raman-Spektren von $ClOF_2PbF_5$ sind in Abbildung 31 dargestellt und die Bandenzuordnungen in Tabelle 10 aufgeführt. Das hochaufgelöste Raman-Spektrum stimmt gut mit dem berechneten überein.

Bisher wurden keine Schwingungsspektren für Pentafluoridoplumbate(IV) berichtet, sodass nur ein Vergleich mit denen von Hexafluoridoplumbaten(IV) vorgenommen werden kann. Für $Li_2[PbF_6]$ wurden folgende Bandenlagen berichtet: 546, 457, 286, 232 und 161 cm^{-1}.[291] Die Anzahl der Banden des PbF_5^--Anions stimmt mit denen des Homologen SnF_5^--Anions in NF_4SnF_5 überein.[284]

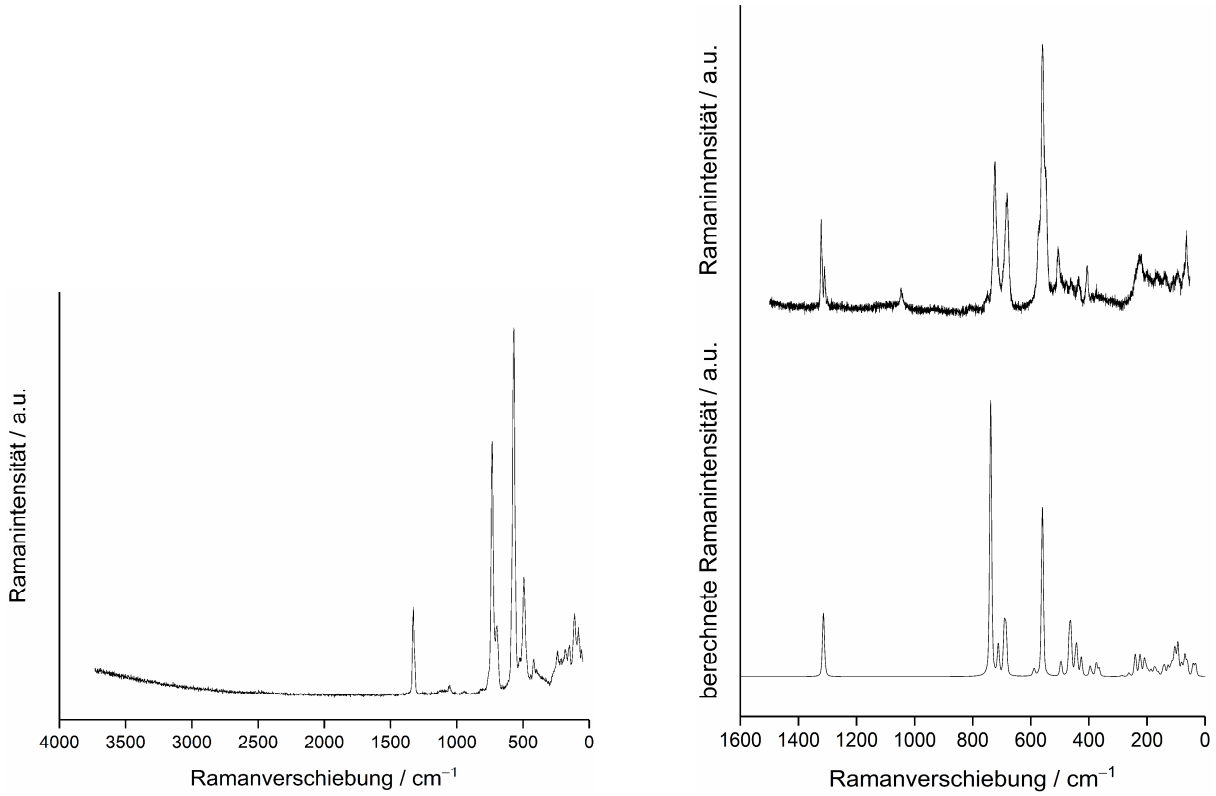

Abbildung 31. Links: Niedrigaufgelöstes Raman-Spektrum (532 nm Laser) von festem $ClOF_2PbF_5$. Rechts: Hochaufgelöstes (oben, 532 nm Laser) und berechnetes (unten) Raman-Spektrum von festem $ClOF_2PbF_5$. Die Raman-Intensitäten sind in willkürlichen Einheiten (a.u.) angegeben.

Tabelle 10. Bandenlagen und -zuordnungen der Raman-Spektren von $ClOF_2PbF_5$, basierend auf dem berechneten Raman-Spektrum. (> 300 cm^{-1}) (*v*: Streckschwingung, *δ*: Deformationsschwingung, *π*: Inversionsschwingung, *s*: Symmetrisch, *as*: Asymmetrisch)

$\nu_{ber.}$ / cm^{-1}	$\nu_{gem.}$ / cm^{-1}	Zuordnung
1314, 1307	1321, 1310	$v(ClOF_2)$ – Cl−O-Streckschwingung des $ClOF_2^+$-Kations
738, 712	724	$v_s(ClOF_2)$ – Symmetrische Streckschwingung der Fluoratome des $ClOF_2^+$-Kations
691, 685	683	$v_{as}(ClOF_2)$ – Asymmetrische Streckschwingung der Fluoratome des $ClOF_2^+$-Kations
592, 588, 563, 560	559	$v(PbF_6)$ – Streckschwingungen der $[PbF_6]$-Einheiten
498, 495, 467, 462	506	$\pi(ClOF_2)$ + $v(PbF_6)$ – Inversionsschwingung des $ClOF_2^+$-Kations gekoppelt mit Streckschwingungen der $[PbF_6]$-Einheiten
446, 442, 426	435	$v(PbF_6)$ – Streckschwingungen der μ-F-Atome der $[PbF_6]$-Einheiten
396, 389	407	$\delta(ClOF_2)$ + $v(PbF_6)$ – Scherschwingung des O-Atoms des $ClOF_2^+$-Kations gekoppelt mit Streckschwingungen der $[PbF_6]$-Einheiten
374, 365	374	$\delta(ClOF_2)$ + $v(PbF_6)$ – Scherschwingung der F-Atome des $ClOF_2^+$-Kations gekoppelt mit Streckschwingungen der $[PbF_6]$-Einheiten

4.3.4. Darstellung und Charakterisierung von $ClOF_2[BF_4]$

Ein PFA-Reaktionsgefäß wurde mit 53 mg (0,76 mmol) B_2O_3 beschickt, mit einem Edelstahlfaltenbalgventil verschlossen und an der ClF_3-Anlage mehrfach sekuriert. ClF_3 (0,28 g, 3,0 mmol) wurde bei 77 K auf den Feststoff kondensiert, das Reaktionsgefäß in einem Edelstahl-Dewargefäß platziert und langsam auf Raumtemperatur erwärmt. Der Feststoff löste sich rasch unter heftiger Reaktion, sobald das Chlortrifluorid aufgetaut war. Das Reaktionsgefäß wurde dann im UV-Reaktor für eine Woche bestrahlt. Im Anschluss wurden flüchtige Bestandteile im Vakuum entfernt und ein weißer, kristalliner Feststoff blieb danach im Reaktionsgefäß zurück, welcher im Handschuhkasten isoliert wurde (95 mg). Ein Teil des Produktes wurde in perfluoriertem Öl suspendiert und unter dem Mikroskop betrachtet. Es waren farblose Kristalle vorhanden, von denen einer röntgenographisch untersucht wurde. Die Zusammensetzung $ClOF_2[BF_4]$ wurde für den Kristall erhalten. Die Bildung der Verbindung kann mit Gleichung 61 erklärt werden. $ClOF_2[BF_4]$ kann auch durch die direkte Reaktion von $ClOF_3$ mit BF_3 erhalten werden.[146]

$$6\ B_2O_3 + 10\ ClF_3 \xrightarrow{hv} 2\ ClOF_2[BF_4] + ClO_2F + 5\ ClF \qquad 61$$

Difluorooxychloronium(V)-tetrafluoridoborat(III) kristallisiert in der orthorhombischen Raumgruppe *Pnma* (Nr. 62) mit a = 9,4367(4) Å, b = 5,5593(3) Å, c = 8,8592(4) Å, V = 464,77(4) Å^3, vier Formeleinheiten pro Elementarzelle, Pearson-Symbol *oP*36 und Wyckoff-Sequenz 62.d^2c^5. Die Verbindung kristallisiert isotyp zu $SF_3[BF_4]$.[293,294] In einer früheren Studie wurden folgende Gitterparameter aus einem Pulver-Röntgendiffraktogramm (Raumtemperatur) bestimmt: a = 13,21 Å, b = 13,62 Å, c = 9.63 Å und $V \approx$ 1733 Å^3.[146] Weiterhin wurden mögliche Kristallstrukturen auf Basis von DFT-Rechnungen vorhergesagt.[295] Die vorhergesagten Raumgruppen und Gitterparameter weichen jedoch von den hier berichteten ab. Ausgewählte kristallographische Daten, Details der Strukturbestimmung sowie äquivalente isotrope und anisotrope Auslenkungsparameter sind im Abschnitt 8.1.1.9 aufgeführt.

Das Chloratom Cl(1) besetzt die spezielle Lage 4*c* (Lagesymmetrie *m*) und ist von den Atomen O/F(1), O/F(1)#1 und F(2) umgeben (Abbildung 32). Im $ClOF_2^+$-Kation liegt aufgrund der Spiegelebene eine O/F-mischbesetzte Lage mit den Besetzungsfaktoren O(0,44(2))/F(0,56) vor. Der Cl−O/F-Abstand beträgt 1,4816(9) Å und ist deutlich kürzer als der Cl−F(2)-Abstand von 1,5356(11) Å, entspricht aber in etwa dem arithmetischen Mittel der Cl−O- und Cl−F-Abständen anderer $ClOF_2^+$-Salze, siehe Abschnitt 4.3.8 und die Literatur.[267] O/F-Mischbesetzung oder -Fehlordnung wurde auch für die Verbindungen $ClOF_2[MF_6]$ (*M* = Cr, Rh, Ge) und $ClOF_2[MF_6]$ (*M* = Nb, Ta) beobachtet (Abschnitt 4.3.1).[296]

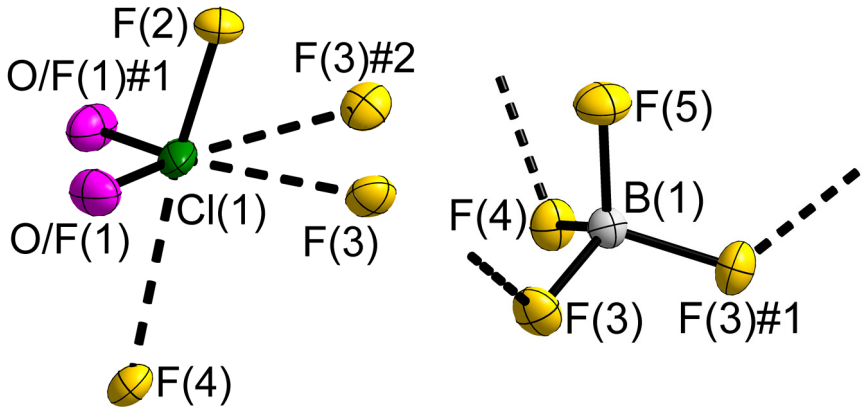

Abbildung 32. Ausschnitte aus der Kristallstruktur von $ClOF_2[BF_4]$. Links ist das $ClOF_2^+$-Kation mit verbrückenden Fluoratomen abgebildet, rechts das $[BF_4]^-$-Anion. Die gestrichelten Bindungen stehen für kurze Kontakte der Form Cl···μ-F verbrückender Fluoratome des Anions mit den Chloratomen. Die Auslenkungsellipsoide sind mit 70% Aufenthaltswahrscheinlichkeit bei 100 K dargestellt. Die Besetzungsfaktoren der gemischtbesetzten Lage sind: O(0,44(2))/F(0,56). Symmetrietransformationen (links): #1 *x*, 3/2 − *y*, *z*; #2 1 − *x*, 1/2 + *y*, 1 − *z*; (rechts): #1 *x*, 3/2 − *y*, *z*.

Das Boratom B(1) besetzt ebenfalls die spezielle 4*c*-Lage und ist von vier Fluoratomen, F(3), F(3)#1, F(4) und F(5), in der Form eines Tetraeders umgeben. Die B−F-Abstände liegen im Bereich von 1,392(2) bis 1,402(2) Å, wobei der B(1)−F(5)-Abstand deutlich kürzer ist als die restlichen. Sie sind vergleichbar zu denen im $Li[BF_4]$ bei 200 K von 1,387(3) und 1,391(3) Å.[297] Drei der vier Fluoratome des $[BF_4]^-$-Anions sind μ_2-verbrückend zu Chloratomen, was die etwas längeren B−F-Abstände dieser Fluoratome erklärt. Die Cl···μ-F-Abstände betragen dabei 2,5763(12) und 2,6134(9) Å und führen zu der Koordinationszahl 3+3 für das Chloratom, welches damit oktaederähnlich von Liganden umgeben ist.

Unter Berücksichtigung der Cl···μ-F-Wechselwirkungen wird ein Leitermotiv entlang der *b*-Achse erhalten, welches mit der Niggli-Formel $^{1}_{\infty}\left[\langle ClF_{\frac{3}{1+1}}F_{\frac{2}{1}}O_{\frac{1}{1}}\rangle\langle BF_{\frac{3}{1+1}}F_{\frac{1}{1}}\rangle\right]$ beschrieben werden kann, siehe Abbildung 33. Die Chloratome bilden eine hexagonal dichte Kugelpackung mit Cl−Cl-Abständen von 5,23-5,97 Å. Die Boratome sind von weiteren vier Boratomen tetraedrisch umgeben, mit B−B-Abständen von 4,07-4,94 Å. Die Chloratome sind von sechs Boratomen in der Form einer einfach überkappten tetragonalen Pyramide umgeben und die Boratome oktaederähnlich von sechs Chloratomen, wenn Cl−B-Abstände von 3,41-4,53 Å betrachtet werden.

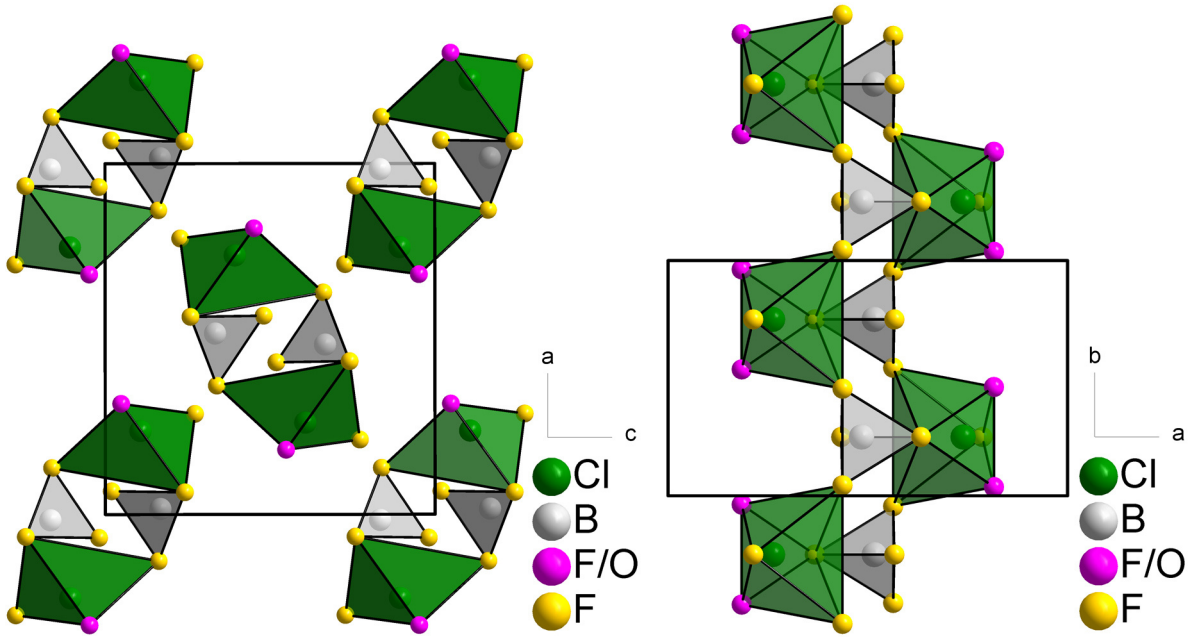

Abbildung 33. Kristallstruktur von $ClOF_2[BF_4]$, projiziert entlang der *b*-Achse (links) oder der *c*-Achse (rechts). Die ersten Koordinationssphären der Chloratome sind als grüne und die der Boratome als graue Polyeder dargestellt. Die Atome sind mit willkürlichen Radien abgebildet.

Von der Kristallstruktur von $ClOF_2[BF_4]$ in der Raumgruppe *Pnma* (Nr. 62) wurde ein Strukturmodell mit geordnetem $ClOF_2^+$-Kation in der Untergruppe $Pna2_1$ (Nr. 33) abgeleitet, welches als Grundlage für periodische quantenchemische Rechnungen mit dem Programmpaket CRYSTAL17 (DFT-PBE0/TZVP) diente.[242,243] Die optimierten Gitterparameter und Atompositionen dieses Modells sind in Abschnitt 8.2.2.9 aufgeführt. Die berechneten Gitterparameter stimmen gut mit den experimentellen ein, was auch auf die B−F-Abstände von 1,38-1,42 Å zutrifft. Ein Vergleich der berechneten und experimentellen Abstände und Winkel im $ClOF_2^+$-Kation erfolgt in Abschnitt 4.3.8.

Auf Basis des optimierten, geordneten Strukturmodells von $ClOF_2[BF_4]$ wurden ein Infrarot- und Raman-Spektrum für den Festkörper berechnet. Die gemessenen und berechneten Spektren sind in Abbildung 34 dargestellt. Die Bandenzuordnungen sind in Tabelle 11 und Tabelle 12 aufgeführt. Die gemessenen Spektren stimmen sehr gut mit den berechneten überein sowie mit vorher in der Literatur berichteten.[195] Die Bandenlagen $[BF_4]^-$-Anions im Infrarotspektrum sind vergleichbar mit denen von 1076, 1036, 779, 770, 551, 522 und 518 cm^{-1} für $Na[BF_4]$ berichteten.[298] Die Bandenlagen im Raman-Spektrum sind vergleichbar mit denen von 1100, 984, 786, 769, 541, 524, 369 und 353 cm^{-1} für in Wasser gelöste $[BF_4]^-$-Salze berichteten.[299,300]

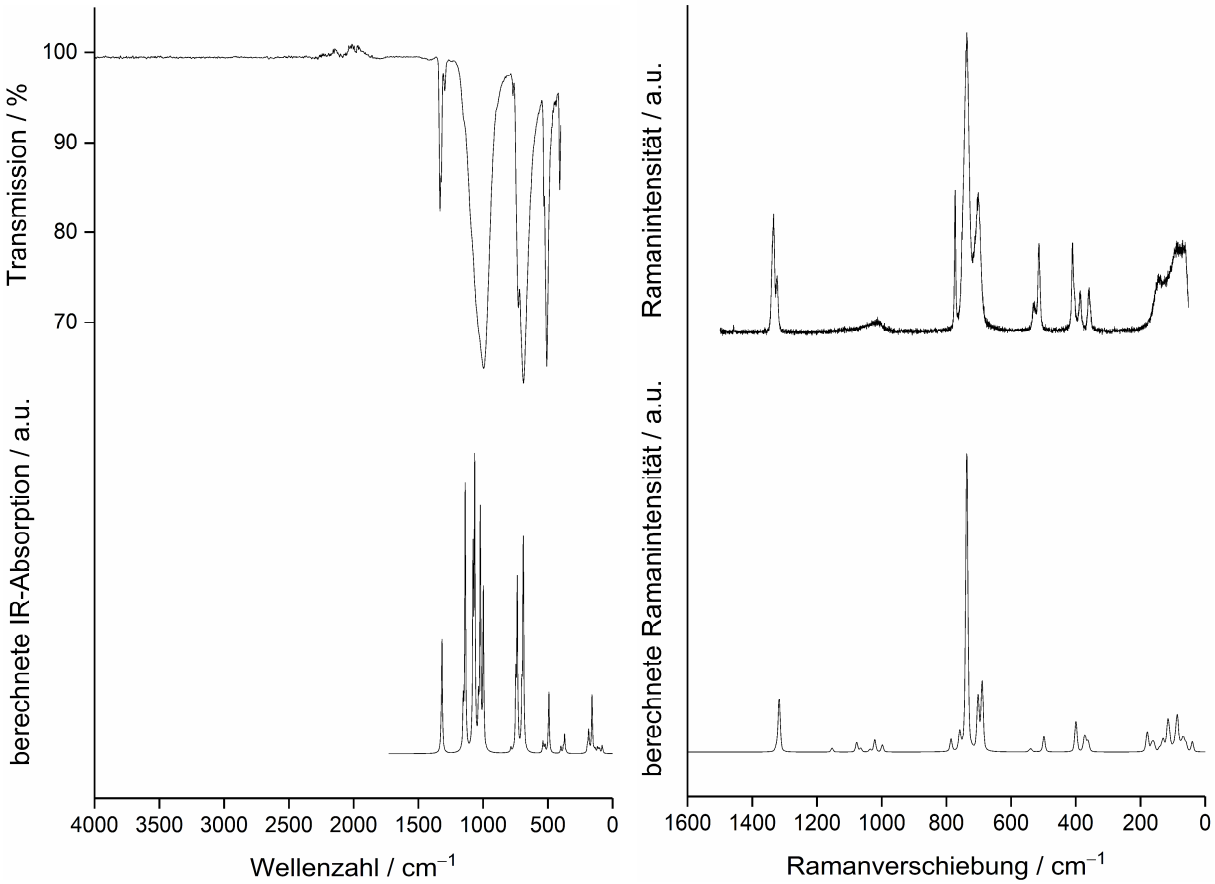

Abbildung 34. Infrarotspektren (links) und Raman-Spektren (rechts, 532 nm Laser) von festem $ClOF_2[BF_4]$. Oben ist jeweils das gemessene Spektrum und unten das berechnete abgebildet. Die berechneten Spektren basieren auf einem geordneten Modell von $ClOF_2[BF_4]$ in der Raumgruppe $Pna2_1$ (Nr. 33), siehe Abschnitt 8.2.2.9. Die berechnete IR-Absorption und die Raman-Intensitäten sind in willkürlichen Einheiten angegeben (a.u.).

Tabelle 11. Bandenlagen und -zuordnungen der Infrarotspektren von festem $ClOF_2[BF_4]$, basierend auf dem berechneten Spektrum. (> 400 cm^{-1}) Das berechnete Spektrum basiert auf einem geordneten Modell von $ClOF_2[BF_4]$ in der Raumgruppe *Pna*2_1 (Nr. 33), siehe Abschnitt 8.2.2.9. (*v*: Streckschwingung, *δ*: Deformationsschwingung, *π*: Inversionsschwingung, *s*: Symmetrisch, *as*: Asymmetrisch, n.b.: nicht beobachtet)

$\nu_{ber.}$ / cm^{-1}	$\nu_{gem.}$ / cm^{-1}	$\nu_{Lit.}$ / cm^{-1} [195]	Zuordnung
1326, 1318, 1317	1334, 1295	1334, 1322, 1295	$v(ClOF_2)$ – Cl−O-Streckschwingung des $ClOF_2^+$-Kations
1153, 1147, 1138, 1131, 1077, 1065, 1036, 1021, 998	995	1150-990	$v(BF_4)$ – Streckschwingung des $[BF_4]^-$-Anions (Boratom vs. Fluoratome)
786, 785	771	772	$v_s(BF_4)$ – Symmetrische Streckschwingung des $[BF_4]^-$-Anions
747, 736	728	734	$v_s(ClOF_2)$ – Symmetrische Streckschwingung der Fluoratome des $ClOF_2^+$-Kations
701, 691, 689	687	694	$v_{as}(ClOF_2)$ – Asymmetrische Streckschwingung der Fluoratome des $ClOF_2^+$-Kations
539, 538, 535, 533, 530, 529	n.b.	534	$\delta(BF_4)$ – Scherschwingung des $[BF_4]^-$-Anions
522	n.b.	521	$\delta(BF_4)$ – Wippschwingung des $[BF_4]^-$-Anions
498, 492	510	514	$\pi(ClOF_2)$ – Inversionsschwingung des $ClOF_2^+$-Kations
401, 399	408	405	$\delta(ClOF_2)$ + $\delta(BF_4)$ – Scherschwingung des O-Atoms des $ClOF_2^+$-Kations gekoppelt mit Wippschwingungen des $[BF_4]^-$-Anions

Tabelle 12. Bandenlagen und -zuordnungen der Raman-Spektren von festem $ClOF_2[BF_4]$, basierend auf dem berechneten Spektrum. (> 300 cm^{-1}) Das berechnete Spektrum basiert auf einem geordneten Modell von $ClOF_2[BF_4]$ in der Raumgruppe *Pna*2_1 (Nr. 33), siehe Abschnitt 8.2.2.9. (*v*: Streckschwingung, *δ*: Deformationsschwingung, *π*: Inversionsschwingung, *s*: Symmetrisch, *as*: Asymmetrisch, n.b.: nicht beobachtet)

$\nu_{ber.}$ / cm^{-1}	$\nu_{gem.}$ / cm^{-1}	$\nu_{Lit.}$ / cm^{-1} [195]	Zuordnung
1326, 1325, 1318, 1317	1334, 1323	1333, 1321	$v(ClOF_2)$ – Cl−O-Streckschwingung des $ClOF_2^+$-Kations
1159, 1153, 1147, 1138, 1131, 1077, 1065, 1036, 1021, 998	1018	1020	$v(BF_4)$ – Streckschwingung des $[BF_4]^-$-Anions (Boratom vs. Fluoratome)
786, 785	772	771	$v_s(BF_4)$ – Symmetrische Streckschwingung des $[BF_4]^-$-Anions
758, 747, 736	737	731	$v_s(ClOF_2)$ – Symmetrische Streckschwingung der Fluoratome des $ClOF_2^+$-Kations
703, 701, 691, 689	701	695	$v_{as}(ClOF_2)$ – Asymmetrische Streckschwingung der Fluoratome des $ClOF_2^+$-Kations
544, 539, 538, 535, 533, 530, 529	532	530	$\delta(BF_4)$ – Scherschwingung des $[BF_4]^-$-Anions
524, 522	n.b.	519	$\delta(BF_4)$ – Wippschwingung des $[BF_4]^-$-Anions
507, 498, 492	514	513	$\pi(ClOF_2)$ – Inversionsschwingung des $ClOF_2^+$-Kations
401, 399	410	404	$\delta(ClOF_2)$ + $\delta(BF_4)$ – Scherschwingung des O-Atoms des $ClOF_2^+$-Kations gekoppelt mit Wippschwingungen des $[BF_4]^-$-Anions
380, 376, 373, 371, 370, 365, 364, 362, 361, 359, 355, 353	386, 360	384, 356	$\delta(ClOF_2)$ + $\delta(BF_4)$ – Scherschwingung der F-Atome des $ClOF_2^+$-Kations gekoppelt mit Wippschwingungen des $[BF_4]^-$-Anions

4.3.5. Darstellung und Charakterisierung von $ClOF_2[Mo_3O_3F_{13}]$

Ein PFA-Reaktionsgefäß wurde mit 15 mg (0,10 mmol) MoO_3 beschickt, mit einem Edelstahlfaltenbalgventil verschlossen und an der ClF_3-Anlage mehrfach sekuriert. ClF_3 (0,08 g, 0,9 mmol) wurde bei 77 K auf den Feststoff kondensiert, das Reaktionsgefäß in einem Edelstahl-Dewargefäß platziert und langsam auf Raumtemperatur erwärmt. Das Reaktionsgefäß wurde dann im UV-Reaktor für zehn Tage bestrahlt. Im Anschluss wurden flüchtige Bestandteile im Vakuum entfernt und ein weißer, kristalliner Feststoff blieb danach im Reaktionsgefäß zurück, welcher im Handschuhkasten isoliert wurde (10,2 mg). Ein Einkristall wurde röntgenographisch untersucht und die Zusammensetzung $ClOF_2[Mo_3O_3F_{13}]$ für die Verbindung erhalten. Die Bildung dieser Verbindung kann mit Gleichung 62 erklärt werden.

$$6\,MoO_3 + 14\,ClF_3 \xrightarrow{hv} 2\,ClOF_2[Mo_3O_3F_{13}] + 5\,ClO_2F + 7\,ClF \qquad 62$$

Difluorooxychloronium(V)-tridecafluoridotrioxidotrimolybdat(VI) kristallisiert in der triklinen Raumgruppe $P\bar{1}$ (Nr. 2) mit a = 8,6464(4) Å, b = 8,6704(4) Å, c = 9,9748(4) Å, α = 66,074(3)°, β = 81,794(3)°, γ = 87,833(3)°, V = 676,37(5) Å^3, zwei Formeleinheiten pro Elementarzelle, Pearson-Symbol $aP46$ und Wyckoff-Sequenz $2.i^{23}$. Ausgewählte kristallographische Daten, Details der Strukturbestimmung sowie äquivalente isotrope und anisotrope Auslenkungsparameter sind im Abschnitt 8.2.2.10 aufgeführt.

Das Chloratom Cl(1) besetzt die allgemeine Lage 2*i* und ist von dem Sauerstoffatom O(1) und den zwei Fluoratomen F(1) und F(2) umgeben (Abbildung 35). Der Cl−O-Abstand im $ClOF_2^+$-Kation beträgt 1,4630(14) Å und ist etwas länger als in anderen $ClOF_2^+$-Verbindungen und die Cl−F-Abstände betragen 1,4968(14) und 1,5554(12) Å, wobei ersterer etwas kürzer ist als in anderen $ClOF_2^+$-Verbindungen. Ein Vergleich erfolgt in Abschnitt 4.3.8.[267]

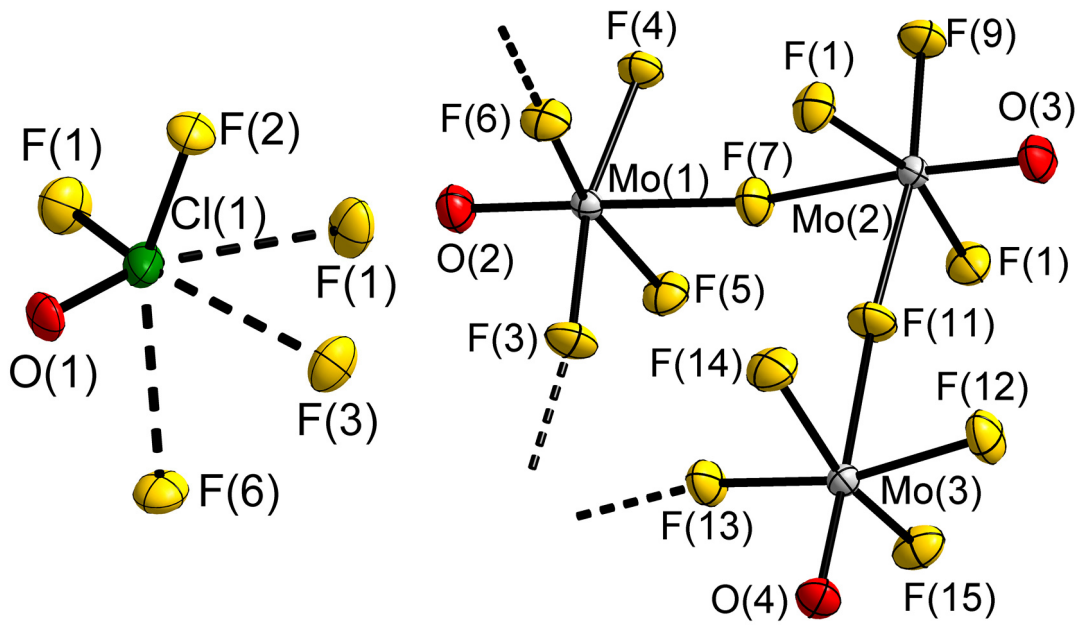

Abbildung 35. Ausschnitte aus der Kristallstruktur von $ClOF_2[Mo_3O_3F_{13}]$. Links ist das $ClOF_2^+$-Kation mit verbrückenden Fluoratomen abgebildet, rechts das $[Mo_3O_3F_{13}]^-$-Anion. Die gestrichelten Bindungen stehen für kurze Kontakte der Form Cl···μ-F verbrückender Fluoratome des Anions mit den Chloratomen. Die Auslenkungsellipsoide sind mit 70% Aufenthaltswahrscheinlichkeit bei 100 K dargestellt.

Die Molybdänatome Mo(1), Mo(2) und Mo(3) besetzen jeweils allgemeine Lagen und sind je von einem Sauerstoffatom und fünf Fluoratomen in der Form eines verzerrten Oktaeders umgeben. Die Fluoratome F(7) und F(11) sind μ_2-verbrückend zwischen Molybdänatomen, wodurch das $[Mo_3O_3F_{13}]^-$-Anion mit einem zentralen cis-verbrückenden $[MoOF_5]$-Polyeder erhalten wird. Die Mo−O-Abstände im Anion liegen im Bereich von 1,6499(14) bis 1,6607(15) Å, die Mo−F-Abstände im Bereich von 1,8311(12) bis 1,8791(12) Å und die Mo−μ_2-F-Abstände im Bereich von 1,9564(12) bis 2,2420(12) Å. Sie sind vergleichbar mit den entsprechenden Abständen in den Verbindungen $ClO_2[Mo_3O_3F_{13}]$ (Abschnitt 7.5) und $[BrCl_2O_6][Mo_3O_3F_{13}]$.[137] Ähnliche Abstände werden für die Alkalimetallsalze $A[Mo_2O_2F_9]$ (A = Li - Cs) beobachtet.[301] Das $[Mo_3O_3F_{13}]^-$-Anion kann auch als ein $[Mo_2O_2F_9]^-$-Anion, an welches eine $MoOF_4$-Einheit (Mo(3)) koordiniert, beschrieben werden.

Die Fluoratome F(3), F(6) und F(13) sind μ_2-verbrückend zu Chloratomen mit Cl···μ-F-Abständen von 2,4939(13) bis 2,5076(13) Å und die Koordinationszahl des Chloratoms ist somit 3+3. Werden diese Kontakte berücksichtigt, so wird ein Dimer der Form $(ClOF_2[Mo_3O_3F_{12}])_2$ erhalten, welches mit der Niggli-Formel ${}^{0}_{\infty}\left[\left(\langle ClF_{\frac{3}{1+1}}F_{\frac{2}{1}}O_{\frac{1}{1}}\rangle\langle MoF_{\frac{1}{1+1}}F_{\frac{1}{2}}F_{\frac{3}{1}}O_{\frac{1}{1}}\rangle\langle MoF_{\frac{2}{2}}F_{\frac{3}{1}}O_{\frac{1}{1}}\rangle\langle MoF_{\frac{2}{1+1}}F_{\frac{1}{2}}F_{\frac{2}{1}}O_{\frac{1}{1}}\rangle\right)_2\right]$ beschrieben werden kann (Abbildung 36). Ein solches Dimer ist von zwölf weiteren umgeben, wenn Zentrum-zu-Zentrum-Abstände von 8,65 bis 12,23 Å berücksichtigt werden. Die Zentren spannen dabei ein Kuboktaeder auf und die Struktur mit dem Cu-Typ verwandt.[302] Ein Dimer wird auch von $ClO_2[Mo_3O_3F_{13}]$ ausgebildet (Abschnitt 7.5).

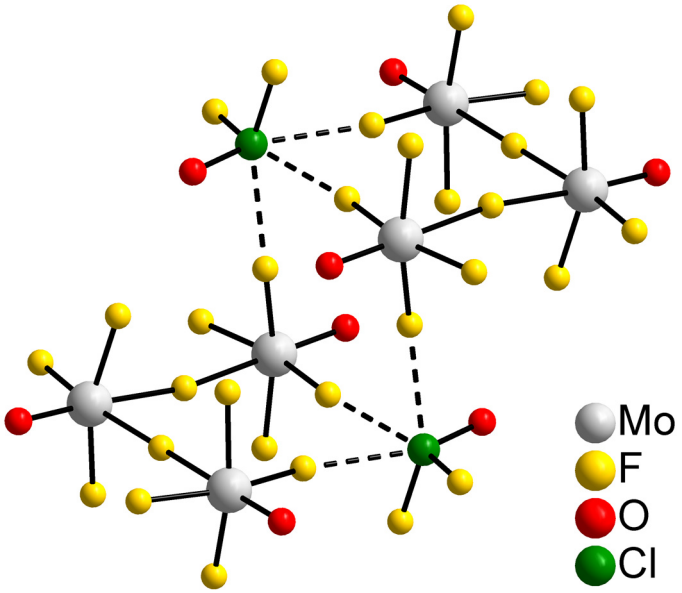

Abbildung 36. Dimeres $ClOF_2[Mo_3O_3F_{13}]$, welches durch die Berücksichtigung der Cl···μ-F-Kontakte erhalten wird.

Die Kristallstruktur von $ClOF_2[Mo_3O_3F_{13}]$ diente als Grundlage für periodische quantenchemische Rechnungen mit dem Programmpaket CRYSTAL17 (DFT-PBE0/TZVP).[242,243] Die optimierten Gitterparameter und Atompositionen sind in Abschnitt 8.2.2.10 aufgeführt. Die optimierten und gemessen Gitterparameter stimmen gut überein, ebenso stimmen die Mo−O- und Mo−F-Abstände von 1,66 Å beziehungsweise 1,85-2,27 Å mit den experimentell bestimmten überein. Ein Vergleich der berechneten und experimentellen Abstände und Winkel im $ClOF_2^+$-Kation erfolgt im Abschnitt 4.3.8. Auf Basis der optimierten Struktur von $ClOF_2[Mo_3O_3F_{13}]$ wurden ein Infrarot- und Raman-Spektrum für den Festkörper berechnet.

Die gemessenen und berechneten Spektren sind in Abbildung 37 dargestellt. Die Bandenzuordnungen für die berechneten Spektren sind in Tabelle 13 und Tabelle 14 aufgeführt. Die gemessenen Spektren stimmen sehr gut mit den berechneten überein. Die Bandenlagen des $[Mo_3O_3F_{13}]^-$-Anions im Raman-Spektrum sind mit denen der Verbindung $ClO_2[Mo_3O_3F_{13}]$ (Abschnitt 7.5) vergleichbar. Für die Mo−O- und Mo−F-Streckschwingungen werden in Salzen mit $[MoOF_5]^-$- und $[Mo_2O_2F_9]^-$-Anionen ähnliche Bandenlagen beobachtet.[301,303]

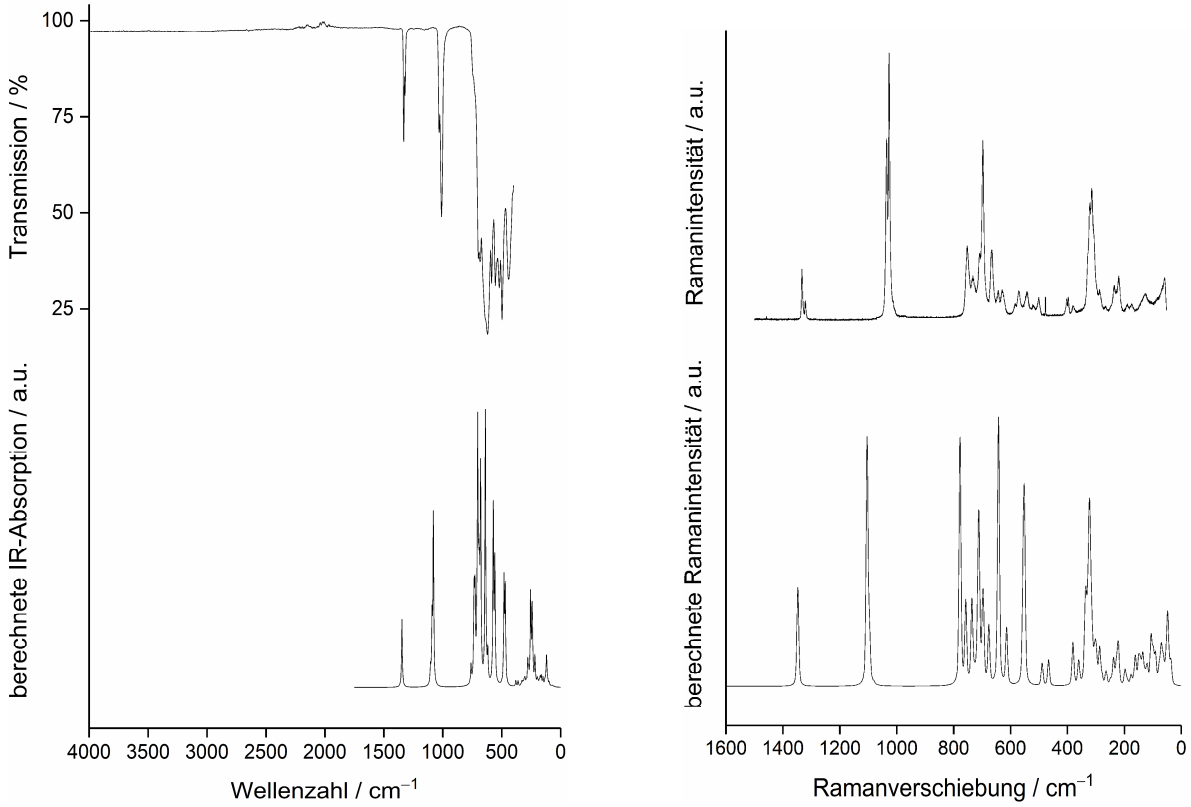

Abbildung 37. Infrarotspektren (links) und Raman-Spektren (rechts, 532 nm Laser) von festem $ClOF_2[Mo_3O_3F_{13}]$. Oben ist jeweils das gemessene Spektrum und unten das berechnete abgebildet. Die berechnete IR-Absorption und die Raman-Intensitäten sind in willkürlichen Einheiten angegeben (a.u.).

Tabelle 13. Bandenlagen und -zuordnungen der Infrarotspektren von $ClOF_2[Mo_3O_3F_{13}]$, basierend auf dem berechneten Spektrum. (> 400 cm^{-1}) (*v*: Streckschwingung, *δ*: Deformationsschwingung, *π*: Inversionsschwingung, *s*: Symmetrisch, *as*: Asymmetrisch, n.b.: nicht beobachtet)

$\nu_{ber.}$ / cm^{-1}	$\nu_{gem.}$ / cm^{-1}	Zuordnung
1346	1330, 1320	$v(ClOF_2)$ – Cl−O-Streckschwingung des $ClOF_2^+$-Kations
1104, 1091, 1080	1030, 1012	$v(MoOF_4)$ – Mo−O-Streckschwingung der $[MoOF_4]$-Einheiten
761	n.b.	$v_s(ClOF_2)$ + $v(MoOF_4)$ – Symmetrische Streckschwingung der Fluoratome des $ClOF_2^+$-Kations gekoppelt mit Mo−F-Streckschwingungen der $[MoOF_4]$-Einheiten
737, 734, 727, 724, 711, 704, 695, 689, 679, 639, 619, 571, 558	691, 620, 585, 555	$v_{as}(ClOF_2)$ + $v(MoOF_4)$ – Asymmetrische Streckschwingung der Fluoratome des $ClOF_2^+$-Kations gekoppelt mit den Mo−F-Streckschwingungen der $[MoOF_4]$-Einheiten
480, 470	520, 498, 440	$\pi(ClOF_2)$ + $v(MoOF_4)$ – Inversionsschwingung des $ClOF_2^+$-Kations gekoppelt mit Mo−μ-F-Streckschwingungen der $[MoOF_4]$-Einheiten

Tabelle 14. Bandenlagen und -zuordnungen der Raman-Spektren von $ClOF_2[Mo_3O_3F_{13}]$, basierend auf dem berechneten Spektrum. (> 300 cm^{-1}) (*v*: Streckschwingung, *δ*: Deformationsschwingung, *π*: Inversionsschwingung, *s*: Symmetrisch, *as*: Asymmetrisch)

$\nu_{ber.}$ / cm^{-1}	$\nu_{gem.}$ / cm^{-1}	Zuordnung
1348	1333, 1321	$v(ClOF_2)$ – Cl−O-Streckschwingung des $ClOF_2^+$-Kations
1104, 1096, 1080	1036, 1027	$v(MoOF_4)$ – Mo−O-Streckschwingung der $[MoOF_4]$-Einheit
777	752	$v_s(ClOF_2)$ + $v(MoOF_4)$ – Symmetrische Streckschwingung der Fluoratome des $ClOF_2^+$-Kations gekoppelt mit Mo−F-Streckschwingungen der $[MoOF_4]$-Einheiten
757, 736, 729, 725, 716, 711, 698, 696, 676, 642, 614, 571, 555, 551	733, 709, 697, 666, 644, 629, 585, 571, 542	$v_{as}(ClOF_2)$ + $v(MoOF_4)$ – Asymmetrische Streckschwingung der Fluoratome des $ClOF_2^+$-Kations gekoppelt mit den Mo−F-Streckschwingungen der $[MoOF_4]$-Einheiten
489, 466	521, 500, 478	$\pi(ClOF_2)$ + $v(MoOF_4)$ – Inversionsschwingung des $ClOF_2^+$-Kations gekoppelt mit Mo−μ-F-Streckschwingungen der $[MoOF_4]$-Einheiten
381	403, 397	$\delta(ClOF_2)$ – Scherschwingung des O-Atoms des $ClOF_2^+$-Kations
360	381	$\delta(ClOF_2)$ – Scherschwingung der F-Atome des $ClOF_2^+$-Kations
339, 335, 330	322	$\delta(ClOF_2)$ + $\delta(MoOF_4)$ – Scherschwingung des O-Atoms des $ClOF_2^+$-Kations gekoppelt mit Scherschwingungen der μ-F-Atome der $[MoOF_4]$-Einheiten
342, 321, 319, 314, 306, 301	315	$\delta(ClOF_2)$ + $\delta(MoOF_4)$ – Scherschwingung des O-Atoms des $ClOF_2^+$-Kations gekoppelt mit Scherschwingungen der F-Atome der $[MoOF_4]$-Einheiten

4.3.6. Darstellung und Charakterisierung von $(ClOF_2[OsO_3F_3])_2OsF_6$

Ein PFA-Reaktionsgefäß wurde im Handschuhkasten mit 28,5 mg (0,112 mmol) OsO_4 beschickt und mit einem Edelstahlfaltenbalgventil verschlossen. An der ClF_3-Anlage wurden bei 77 K 0,15 g (1,6 mmol) ClF_3 auf den Feststoff kondensiert, das Reaktionsgefäß in einem Edelstahl-Dewargefäß platziert und langsam auf Raumtemperatur erwärmt. Das Reaktionsgefäß wurde dann im UV-Reaktor für 17,5 Stunden bestrahlt. Im Anschluss wurden flüchtige Bestandteile im Vakuum entfernt und gelbe und orange Kristalle blieben danach im Reaktionsgefäß zurück. Die Kristalle wurden in perfluoriertem Öl suspendiert und röntgenographisch untersucht.

Neben Kristallen von $OsOF_5$, dessen Kristallstruktur bekannt ist, waren Kristalle einer bisher unbekannten Verbindung vorhanden.[304,305] Ein Einkristall der letzteren wurde röntgenographisch untersucht und die Zusammensetzung $(ClOF_2[OsO_3F_3])_2OsF_6$ erhalten. Die Bildung dieser Verbindung kann mit Gleichung 63 erklärt werden.

$$12\,OsO_4 + 32\,ClF_3 \xrightarrow{hv} 4\,(ClOF_2[OsO_3F_3])_2{\cdot}OsF_6 + 4\,ClOF_3 + 20\,ClF + 6\,O_2 \qquad 63$$

Bis(difluorooxychloronium(V)-trifluoridotrioxidoosmat(VIII))-Osmiumhexafluorid(1/1) kristallisiert in der triklinen Raumgruppe $P\bar{1}$ (Nr. 2) mit a = 5,6262(4) Å, b = 7,4973(5) Å, c = 10,2444(6) Å, α = 106,076(2)°, β = 97,064(2)°, γ = 96,846(2)°, V = 406,72(5) Å^3, einer Formeleinheit pro Elementarzelle, Pearson-Symbol *aP*29 und Wyckoff-Sequenz $2.i^{14}a$. Ausgewählte kristallographische Daten, Details der Strukturbestimmung sowie äquivalente isotrope und anisotrope Auslenkungsparameter sind im Abschnitt 8.1.1.11 aufgeführt.

Das Chloratom Cl(1) besetzt die allgemeine Lage 2*i* und ist von dem Sauerstoffatom O(1) und den Fluoratomen F(1) und F(2) umgeben (Abbildung 38). Der Cl−O-Abstand im pyramidalen $ClOF_2^+$-Kation beträgt 1,475(3) Å und die Cl−F-Abstände betragen 1,506(2) und 1,573(2) Å. Diese sind vergleichbar mit denen anderer in dieser Arbeit beschriebenen $ClOF_2^+$-Salze sowie mit denen in der Literatur berichteten, ein Vergleich erfolgt in Abschnitt 4.3.8.[267]

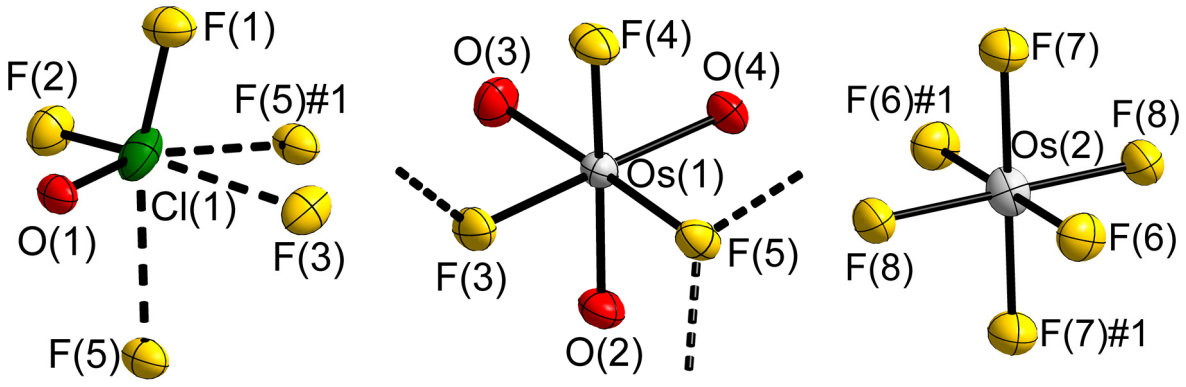

Abbildung 38. Ausschnitte aus der Kristallstruktur von $(ClOF_2[OsO_3F_3])_2OsF_6$. Links ist das $ClOF_2^+$-Kation mit verbrückenden Fluoratomen abgebildet, in der Mitte das $[OsO_3F_3]^-$-Anion und rechts das OsF_6-Molekül. Die gestrichelten Bindungen stehen für kurze Kontakte der Form Cl···μ-F verbrückender Fluoratome des Anions mit den Chloratomen. Die Auslenkungsellipsoide sind mit 70% Aufenthaltswahrscheinlichkeit bei 100 K dargestellt. Symmetrietransformationen (links): #1 −1 + *x*, *y*, *z*; (rechts): #1 −*x*, −*y*, −*z*.

Das Osmiumatom Os(1) ist von drei Fluoratomen und drei Sauerstoffatomen in der Form eines verzerrten Oktaeders umgeben. Das Osmiumatom ist dabei leicht aus dem Zentrum des Polyeders hin zu den Sauerstoffatomen ausgelenkt. Die Os−O-Abstände im $[OsO_3F_3]^-$-Anion betragen 1,718(3) bis 1,730(2) Å und die Os−F-Abstände 1,924(2) bis 2,023(2) Å. Diese sind vergleichbar mit denen in $(N(CH_3)_4)[OsO_3F_3]$, $XeF_5[OsO_3F_3]$ und $[Xe_2F_{11}][OsO_3F_3]$.[306,307] Zwei der Fluoratome, F(3) und F(5), sind verbrückend zu Chloratomen mit Cl···μ-F-Abständen von 2,330(2) bis 2,502(2) Å, wobei F(3) μ_2 verbrückend und F(5) μ_3-verbrückend wirkt. Für das Chloratom resultiert unter Berücksichtigung dieser Atome die Koordinationszahl 3+3 und eine oktaederähnliche Anordnung der Liganden. Die Cl···μ-F-Kontakte führen zu Strängen, welche entlang der *a*-Achse verlaufen und mit der Niggli-Formel $^{1}_{\infty}\left[\langle ClF_{\frac{2}{2+1}}F_{\frac{1}{1+1}}F_{\frac{2}{1}}O_{\frac{1}{1}}\rangle\langle OsF_{\frac{1}{1+2}}F_{\frac{1}{1+1}}O_{\frac{3}{1}}F_{\frac{1}{1}}\rangle\right]$ beschrieben werden können, siehe Abbildung 39.

Das Osmiumatom Os(2) besetzt die spezielle Lage 1*a* (Lagesymmetrie $\bar{1}$) und ist von sechs Fluoratomen oktaedrisch umgeben. Die Os−F-Abstände betragen 1,797(2) bis 1,837(2) Å und sind vergleichbar mit denen für die orthorhombische Modifikation von OsF_6 bei 133 K berichteten von 1,822(2)-1,833(2) Å.[308] Das Os(2)-Atom zeigt keine weiteren Kontakte zu benachbarten Atomen im Bereich bis zu 3.6 Å und das OsF_6-Molekül liegt somit isoliert vor. Eine solche Co-Kristallisation eines Hexafluorids wurde bisher noch nicht beschrieben.

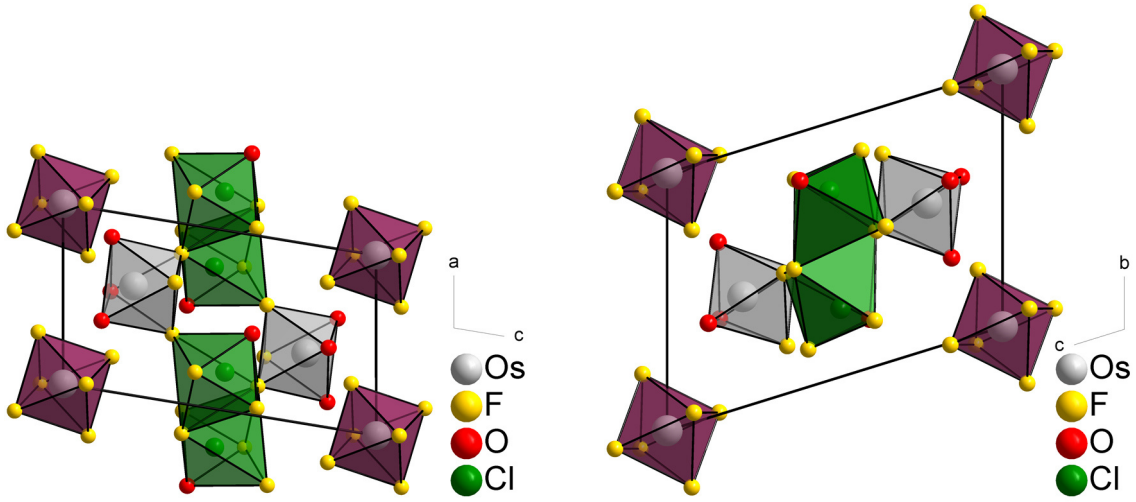

Abbildung 39. Kristallstruktur von $(ClOF_2[OsO_3F_3])_2OsF_6$, projiziert entlang der *b*-Achse (links) oder der *a*-Achse (rechts). Die ersten Koordinationssphären der Chloratome sind als grüne, die des Os(1)-Atoms ($[OsO_3F_3]^-$) als graue und die des Os(2)-Atoms (OsF_6) als pflaumenfarbene Polyeder dargestellt. Die Atome sind mit willkürlichen Radien abgebildet.

Die Chloratome bilden Schichten (3^6-Netz) parallel zu der *ab*-Ebene aus, wenn Cl−Cl-Abstände von 3,92-5,63 Å berücksichtigt werden. Die Os(1)-Atome sind von zehn weiteren Os(1)-Atomen in der Form eines stark verzerrten zweifach überkappten Würfels umgeben, mit Os(1)−Os(1)-Abständen von 4,42 bis 7,11 Å. Die Os(2)-Atome sind ebenfalls von zehn weiteren Os(2)-Atomen in der Form eines zweifach-überkappten Würfels umgeben, mit Os(2)−Os(2)-Abständen von 4,92 bis 5,68 Å. Das Chloratom ist von acht Os-Atomen (6×Os(1) und 2×Os(2)) in der Form eines verzerrten verdrehten Doppelkeils (Johnson-Körper J_{26}) mit Cl−Os-Abständen von 3,95 bis 6,18 Å umgeben.[292]

Die Kristallstruktur von $(ClOF_2[OsO_3F_3])_2OsF_6$ diente als Grundlage für periodische quantenchemische Rechnungen mit dem Programmpaket CRYSTAL17 (DFT-PBE0/TZVP).[242,243] Die optimierten Gitterparameter und Atomkoordinaten sind in Abschnitt 8.2.2.11 aufgeführt. Die optimierten Gitterparameter stimmen gut mit den ermittelten überein. Dies gilt ebenso für die Os−F-Abstände von 1,84-1,87 Å des OsF_6-Moleküls, wie für die Os−F- und Os−O-Abstände von je 1,94-2,11 Å beziehungsweise 1,69-70 Å des $[OsO_3F_3]^-$-Anions. Ein Vergleich der berechneten und gemessenen Abstände des $ClOF_2^+$-Kations erfolgt im Abschnitt 4.3.8. Auf Basis der optimierten Struktur von $(ClOF_2[OsO_3F_3])_2OsF_6$ wurde ein Raman-Spektrum für den Festkörper berechnet. Die Raman-Spektren sind in Abbildung 40 dargestellt, und die Bandenzuordnung des berechneten Spektrums ist in Tabelle 15 aufgeführt.

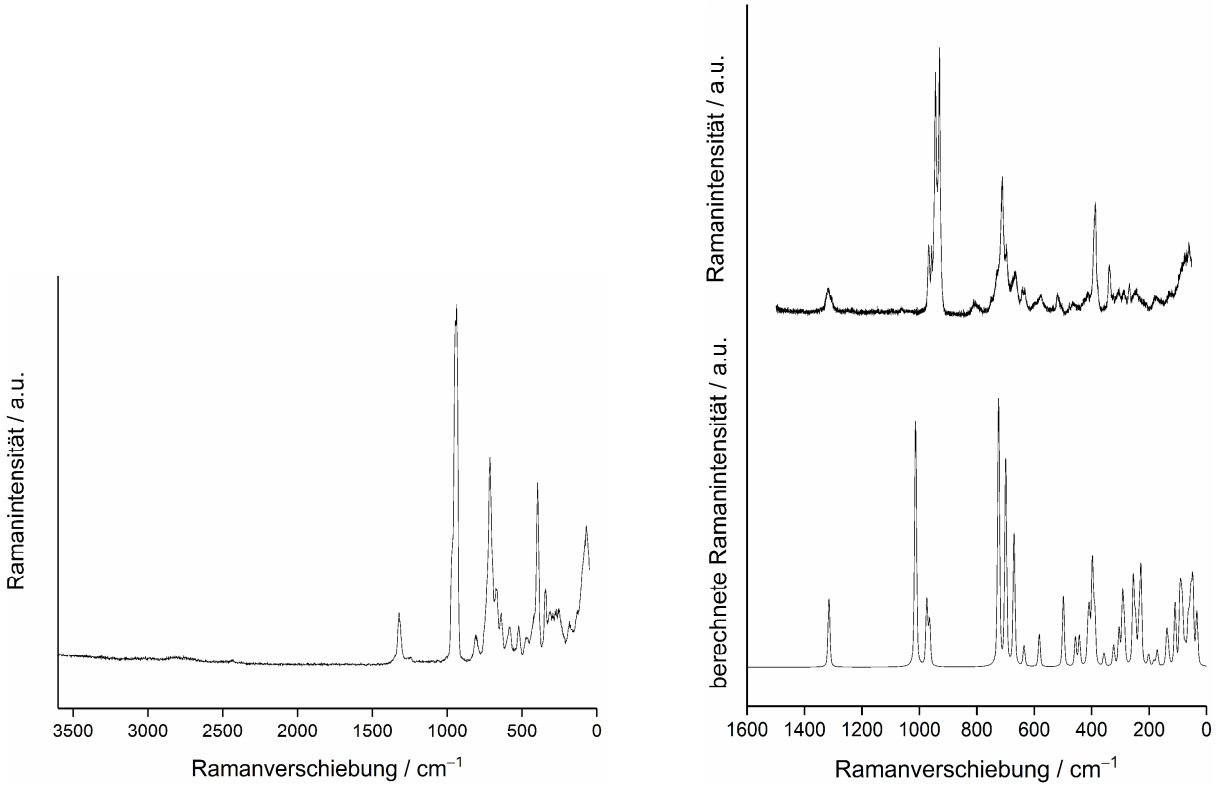

Abbildung 40. Links: Niedrigaufgelöstes Raman-Spektrum (523 nm Laser) von festem $(ClOF_2[OsO_3F_3])_2OsF_6$. Rechts: Hochaufgelöstes (oben, 532 nm Laser) und berechnetes (unten) Raman-Spektrum von festem $(ClOF_2[OsO_3F_3])_2OsF_6$. Die Raman-Intensitäten sind in willkürlichen Einheiten (a.u.) angegeben.

Beide Spektren stimmen gut überein und die Bandenlagen des $ClOF_2^+$-Kations sowie des $[OsO_3F_3]^-$-Anions (Tabelle 16) als auch des OsF_6-Moleküls (Tabelle 17) stimmen gut mit in der Literatur berichteten überein.[296,305–307,309,310]

Im Vergleich mit den Raman-Spektren des festen, flüssigen und gasförmigen OsF_6, ist die $\nu_s(OsF_6)$-Bande ist im $(ClOF_2[OsO_3F_3])_2OsF_6$ leicht zu niedrigeren Wellenzahlen verschoben, die restlichen Banden sind kaum von denen des „reinen“ OsF_6 verschieden, jedoch wird eine Aufspaltung der sonst dreifach entarteten T_{2g}-Bande ($\delta(OsF_6)$) beobachtet, was aufgrund der niedrigen Lagesymmetrie des Os-Atoms zu erwarten ist.[305,309,310] Daraus lässt sich ableiten, wie aus dem Vergleich der Os−F-Abstände ersichtlich wird, dass das OsF_6-Molekül wenig von umgebenden Atomen beeinflusst wird.

Tabelle 15. Bandenlagen und -zuordnungen der Raman-Spektren von $(ClOF_2[OsO_3F_3])_2OsF_6$, basierend auf dem berechneten Spektrum. (> 300 cm^{-1}) (*v*: Streckschwingung, *δ*: Deformationsschwingung, *π*: Inversionsschwingung, *s*: Symmetrisch, *as*: Asymmetrisch, n.b.: nicht beobachtet)

$\nu_{ber.}$ / cm^{-1}	$\nu_{gem.}$ / cm^{-1}	Zuordnung
1315	1318	$v(ClOF_2)$ – Cl−O-Streckschwingung des $ClOF_2^+$-Kations
1013, 974, 965	977, 958, 944, 930	$v(OsO_3F_3)$ – Os−O-Streckschwingungen des $[OsO_3F_3]^-$-Anions
724, 696	711, 668	$v_s(ClOF_2)$ – Symmetrische Streckschwingung der Fluoratome des $ClOF_2^+$-Kations
699	696	$v_s(OsF_6)$ – Symmetrische Streckschwingung des OsF_6-Moleküls
670	641	$v_{as}(ClOF_2)$ – Asymmetrische Streckschwingung der Fluoratome des $ClOF_2^+$-Kations
635	633	$v_{as}(OsF_6)$ – Asymmetrische Streckschwingung des OsF_6-Moleküls
582	577	$v_{as}(OsO_3F_3)$ – Asymmetrische Os−F-Streckschwingung des $[OsO_3F_3]^-$-Anions
456, 443	518	$\pi(ClOF_2)$ + $v(OsO_3F_3)$ – Inversionsschwingung des $ClOF_2^+$-Kations gekoppelt mit Os−F-Streckschwingungen des $[OsO_3F_3]^-$-Anions
413	413	$v_{as}(OsO_3F_3)$ – Asymmetrische Os−F-Streckschwingung des $[OsO_3F_3]^-$-Anions
408, 398, 397	388	$\delta(ClOF_2)$ + $\delta(OsO_3F_3)$ – Scherschwingung des O-Atoms des $ClOF_2^+$-Kations gekoppelt mit Scherschwingungen der O-Atome des $[OsO_3F_3]^-$-Anions
389	n.b.	$\delta(OsO_3F_3)$ – Wippschwingung der O-Atome des $[OsO_3F_3]^-$-Anions
357	338	$\delta(ClOF_2)$ – Scherschwingung der F-Atome des $ClOF_2^+$-Kations
323, 305	309	$\delta(OsO_3F_3)$ – Scherschwingungen der F-Atoms des $[OsO_3F_3]^-$-Anions

Tabelle 16. Raman-aktive Streck- und Scherschwingungen des $[OsO_3F_3]^-$-Anions verschiedener $[OsO_3F_3]^-$-Salze. (>300 cm^{-1}) (*v*: Streckschwingung, *δ*: Scherschwingung)

Verbindung	$v(Os\underline{\mathbf{O}}_3F_3)$	$v(OsO_3\underline{\mathbf{F}}_3)$	$\delta(Os\underline{\mathbf{O}}_3F_3)$	$\delta(OsO_3\underline{\mathbf{F}}_3)$	Quelle
$(ClOF_2[OsO_3F_3]_2)OsF_6$	977, 958, 944, 930	577, 518, 413	388	309	diese Arbeit
$(N(CH_3)_4)[OsO_3F_3]$	920, 912, 908	573, 504, 493	402, 385	316, 310, 301	[306]
$NO[OsO_3F_3]$	934, 920	555, 483	386	307	[306]
$(XeF_5)[OsO_3F_3]$	955, 951, 948, 946, 940	585, 457, 447	411, 402, 390, 386	<300	[307]
$(Xe_2F_{11})[OsO_3F_3]$	945, 942, 936, 933	591, 585, 448, 426, 422	401, 386, 381	306	[307]

Tabelle 17. Raman-aktive Streck- und Scherschwingungen des OsF_6-Moleküls. (*v*: Streckschwingung, *δ*: Scherschwingung, s: Symmetrisch, as: Asymmetrisch)

Verbindung	$v_s(OsF_6)$	$v_{as}(OsF_6)$	$\delta(OsF_6)$	Quelle
$(ClOF_2[OsO_3F_3]_2)OsF_6$	696	633	288, 268, 246	diese Arbeit
OsF_6[a]	731	643	272	[309]
OsF_6[b]	733	632	252	[310]
OsF_6[c]	731	620	321	[305]

a: Gasförmig; *b*: Flüssig; *c*: Fest, bei 133 K.

4.3.7. Darstellung und Charakterisierung von $(ClOF_2)_2[AuF_4][SbF_6]$

Ein PFA-Reaktionsgefäß ($V \approx 4$ mL) wurde mit 13,77 mg (0,045 mmol) Sb_2O_4 und 17,78 mg (0,090 mmol) Goldpulver beschickt, mit einem Edelstahlfaltenbalgventil verschlossen und an der ClF_3-Anlage mehrfach sekuriert. An der ClF_3-Anlage wurden bei 77 K 0,26 g (2,8 mmol) ClF_3 auf die Feststoffe kondensiert, die Kühlung entfernt und sofort 1,1 bar Sauerstoff hinzugegeben, das Reaktionsgefäß in einem Edelstahl-Dewargefäß platziert und langsam auf Raumtemperatur erwärmt. Das Reaktionsgefäß wurde dann im UV-Reaktor für 84 Stunden bestrahlt. Im Anschluss wurden flüchtige Bestandteile im Vakuum entfernt und es blieb danach ein gelber Feststoff im Reaktionsgefäß zurück, welcher im Handschuhkasten isoliert wurde (63,7 mg). Ein Einkristall wurde röntgenographisch untersucht und die Zusammensetzung $(ClOF_2)_2[AuF_4][SbF_6]$ für die Verbindung erhalten. Die Bildung dieser Verbindung kann mit Gleichung 64 erklärt werden.

$$2\ Au + Sb_2O_4 + 12\ ClF_3 \xrightarrow{h\nu} 2\ (ClOF_2)_2[AuF_4][SbF_6] + 8\ ClF \qquad 64$$

Bis(difluorooxychloronium(V))-tetrafluoridoaurat(III)-hexafluoridoantimonat(V) kristallisiert in der monoklinen Raumgruppe $P2_1/c$ (Nr. 14) mit a = 5,8201(3) Å, b = 9,2247(5) Å, c = 11,5058(6) Å, β = 103,299(2)°, V = 601,17(6) Å^3, zwei Formeleinheiten pro Elementarzelle, Pearson-Symbol $mP40$ und Wyckoff-Sequenz $14.e^9ca$. Ausgewählte kristallographische Daten, Details der Strukturbestimmung sowie äquivalente isotrope und anisotrope Auslenkungsparameter sind im Abschnitt 8.1.1.12 aufgeführt.

Das Chloratom Cl(1) besetzt die allgemeine Lage 4*e* und ist von dem Sauerstoffatom O(1) und den Fluoratomen F(1) und F(2) umgeben (Abbildung 41). Der Cl−O-Abstand im pyramidalen $ClOF_2^+$-Kation beträgt 1,432(3) Å und die Cl−F-Abstände betragen 1,546(2) und 1,564(2) Å. Die Abstände entsprechen denen in anderen $ClOF_2^+$-Verbindungen (Abschnitte 4.2.4 und 7.4).[307]

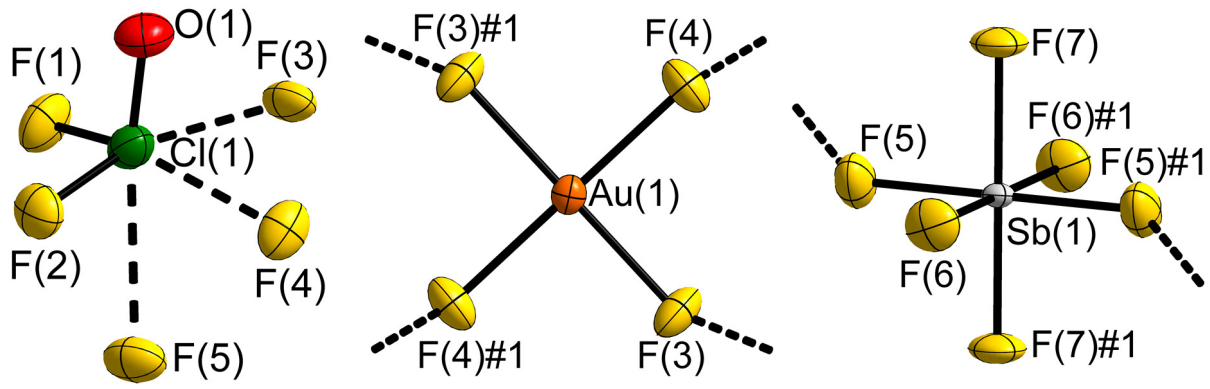

Abbildung 41. Ausschnitte aus der Kristallstruktur von $(ClOF_2)_2[AuF_4][SbF_6]$. Links ist das $ClOF_2^+$-Kation mit verbrückenden Fluoratomen abgebildet, in der Mitte das $[AuF_4]^-$-Anion und rechts das $[SbF_6]^-$-Anion. Die gestrichelten Bindungen stehen für kurze Kontakte der Form Cl···μ-F verbrückender Fluoratome des Anions mit den Chloratomen. Die Auslenkungsellipsoide sind mit 70% Aufenthaltswahrscheinlichkeit bei 100 K dargestellt. Symmetrietransformationen (Mitte): #1 −*x*, 1 − *y*, −*z*; (rechts): #1 2 − *x*, 1 − *y*, 1 − *z*.

Das Goldatom Au(1) besetzt die spezielle Lage 2*c* (Lagesymmetrie $\bar{1}$) und ist von vier Fluoratomen quadratisch-planar mit Abständen von 1,913(2) und 1,917(2) Å umgeben. Die Au−F-Abstände stimmen mit denen in anderen Salzen wie $Li[AuF_4]$ (1,890(7)-1,965(6) Å) und $Rb[AuF_4]$ (1,915(3) Å), welche bei Raumtemperatur bestimmt wurden, überein.[311] Alle Fluoratome des $[AuF_4]^-$-Anions sind verbrückend zu benachbarten Chloratomen mit Cl···μ-F-Abständen von 2,341(2) und 2,380(2) Å.

Das Antimonatom Sb(1) besetzt ebenfalls eine spezielle Lage (2*a*, Lagesymmetrie $\bar{1}$) und ist von sechs Fluoratomen oktaedrisch mit Sb−F-Abständen von 1,861(2) bis 1,888(2) Å umgeben. Der Sb(1)−F(5)-Abstand ist etwas größer als die anderen, vermutlich aufgrund der kurzen Cl···μ-F-Kontakte von 2,608(2) Å zu umgebenden Chloratomen, wobei die $[SbF_6]$-Polyeder dabei trans-verknüpfend sind. Die Sb−F-Abstände sind vergleichbar mit denen in anderen $[SbF_6]^-$-Salzen wie $Rb[SbF_6]$ (1,868(2) Å, Raumtemperatur) und $Cs[SbF_6]$ (1,875(9) Å, Raumtemperatur).[312,313]

Die Cl···μ-F-Kontakte der Fluoratome der $[AuF_4]^-$- und $[SbF_6]^-$-Anionen führen zu der Koordinationszahl 3+3 für das Chloratom mit einer oktaederähnlichen Ligandenanordnung. Es resultieren Schichten parallel zur *ac*-Ebene, wenn diese Kontakte berücksichtigt werden (Abbildung 42). Die Schichten können auch mit der Niggli-Formel $^{2}_{\infty}\left[\langle ClF_{\frac{3}{1+1}}F_{\frac{2}{1}}O_{\frac{1}{1}}\rangle_2\langle AuF_{\frac{4}{1+1}}\rangle\langle SbF_{\frac{2}{1+1}}F_{\frac{4}{1}}\rangle\right]$ beschrieben werden.

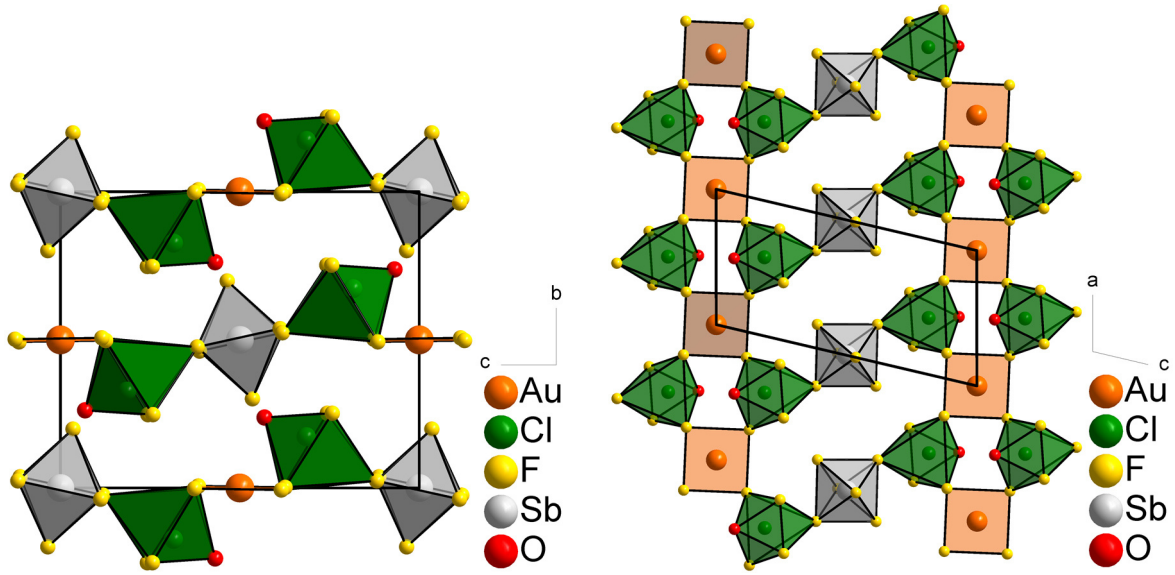

Abbildung 42. Kristallstruktur von $(ClOF_2)_2[AuF_4][SbF_6]$, projiziert entlang der *a*-Achse (links) oder der *b*-Achse (rechts). Die ersten Koordinationssphären der Chloratome sind als grüne, die der Goldatome als orange und die der Antimonatome als graue Polyeder dargestellt. Die Atome sind mit willkürlichen Radien abgebildet.

Die Chloratome sind von zwölf weiteren Chloratomen in der Form eines Antikuboktaeders umgeben, wenn Cl−Cl-Abstände von 5,00-7,32 Å berücksichtigt werden. Die Goldatome sind von weiteren Goldatomen oktaedrisch mit Au−Au-Abständen von 5,82-7,37 Å umgeben. Die Antimonatome sind ebenfalls oktaedrisch von Antimonatomen mit Sb−Sb-Abständen von 5,82-7,37 Å umgeben. Beide Atomsorten sind für sich jeweils pseudo-kubisch primitiv gepackt und die Gitter durchdringen sich gegenseitig. Das Chloratom ist entsprechend von acht Atomen (4×Au und 4×Sb) würfelartig mit Atomabständen von 3,90-6,27 Å umgeben. Die Gold- und Antimonatome sind für sich jeweils würfelartig von Chloratomen mit Au−Cl-Abständen von 3,90-6,27 Å oder Sb−Cl-Abständen von 4,19-5,73 Å umgeben. Die Atomanordnungen sind ähnlich zu denen der Cs- und Cl-Atome im CsCl-Typ.[314]

Die Kristallstruktur von $(ClOF_2)_2[AuF_4][SbF_6]$ diente als Grundlage für periodische quantenchemische Rechnungen mit dem Programmpaket CRYSTAL17 (DFT-PBE0/TZVP).[242,243] Die optimierten Gitterparameter und Atomkoordinaten sind in 8.2.2.12 aufgeführt. Die gemessenen und berechneten Gitterparameter stimmen gut überein, ebenso die berechneten Au−F-Abstände von 1,96 Å und Sb−F-Abstände von 1,88 bis 1,91 Å, welche etwas größer als die oben genannten ermittelten Abstände sind. Ein Vergleich von berechneten und ermittelten Abständen und Winkeln im $ClOF_2^+$-Kation erfolgt im Abschnitt 4.3.8. Auf Basis der optimierten Struktur von $(ClOF_2)_2[AuF_4][SbF_6]$ wurde das Raman-Spektrum für den Festkörper berechnet.

Die Raman-Spektren sind in Abbildung 43 dargestellt und zeigen eine gute Übereinstimmung. Die Bandenzuordnung des berechneten Raman-Spektrums ist in Tabelle 18 aufgeführt. Sowohl die Banden die dem $ClOF_2^+$-Kation zugeordnet werden können als auch die, die den $[AuF_4]^-$- und $[SbF_6]^-$-Anionen zugewiesen werden können (Tabelle 19 und Tabelle 20), stimmen gut mit den in der Literatur berichteten Bandenlagen überein.[201,296,315–318]

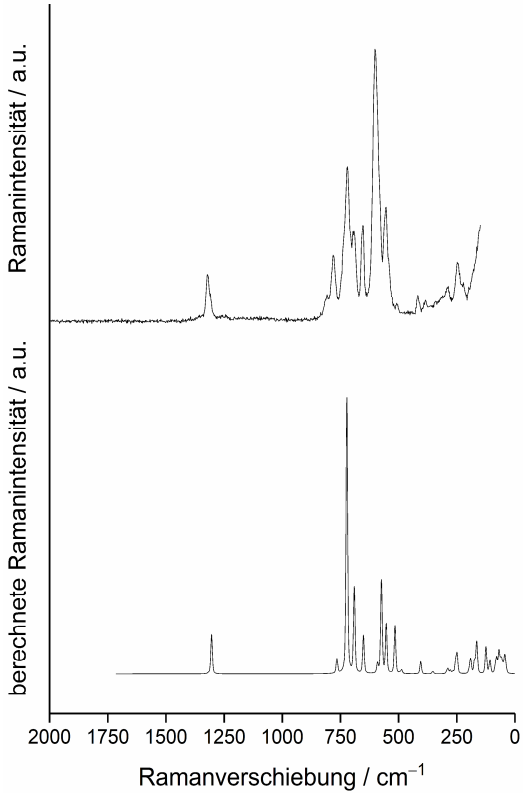

Abbildung 43. Niedrigaufgelöstes (oben, 532 nm Laser) und berechnetes (unten) Raman-Spektrum von festem $(ClOF_2)_2[AuF_4][SbF_6]$. Die Raman-Intensitäten sind in willkürlichen Einheiten (a.u.) angegeben.

Tabelle 18. Bandenlagen und -zuordnungen der Raman-Spektren von $(ClOF_2)_2[AuF_4][SbF_6]$, basierend auf dem berechneten Spektrum. (> 300 cm^{-1}) (*v*: Streckschwingung, *δ*: Deformationsschwingung, *π*: Inversionsschwingung, *s*: Symmetrisch, *as*: Asymmetrisch, n.b.: nicht beobachtet)

$\nu_{ber.}$ / cm^{-1}	$\nu_{gem.}$ / cm^{-1}	Zuordnung
1318, 1303	1322	$v(ClOF_2)$ – Cl−O-Streckschwingung des $ClOF_2^+$-Kations
765, 722	781, 722	$v_s(ClOF_2)$ – Symmetrische Streckschwingung der Fluoratome des $ClOF_2^+$-Kations
690	694	$v_{as}(ClOF_2)$ – Asymmetrische Streckschwingung der Fluoratome des $ClOF_2^+$-Kations
650	653	$v_s(SbF_6)$ – Symmetrische Streckschwingung des $[SbF_6]^-$-Anions
594, 590, 574, 571, 562, 553	599	$v(SbF_6)$ + $v(AuF_4)$ – Streckschwingungen des $[SbF_6]^-$-Anions gekoppelt mit Streckschwingungen des $[AuF_4]^-$-Anions
515	556	$v_{as}(AuF_4)$ – Asymmetrische Streckschwingung des $[AuF_4]^-$-Anions
495, 487	508	$\pi(ClOF_2)$ – Inversionsschwingung des $ClOF_2^+$-Kations
405	418	$\delta(ClOF_2)$ – Scherschwingung des O-Atoms des $ClOF_2^+$-Kations gekoppelt
355, 352	385, 342	$\delta(ClOF_2)$ – Scherschwingung der F-Atome des $ClOF_2^+$-Kations

Tabelle 19. Raman-aktive Streck- und Scherschwingungen des $[AuF_4]^-$-Anions in Tetrafluoridoauraten(III). (*v*: Streckschwingung, *δ*: Scherschwingung, s: Symmetrisch, as: Asymmetrisch)

Verbindung	$v_s(AuF_4)$	$v_{as}(AuF_4)$	$\delta(AuF_4)$	Quelle
$(ClOF_2)_2[AuF_4][SbF_6]$	599	556	244	diese Arbeit
$Cs[AuF_4]$	590	562	238, 230	[315]
$(N(CH_3)_4)[AuF_4]$	594	569	232	[315]
$(N(C_2H_5)_4)[AuF_4]$	592	570	234	[315]
$(XeF_5)[AuF_4]$	582	552	240	[316]

Tabelle 20. Raman-aktive Streck- und Scherschwingungen des $[SbF_6]^-$-Anions in Hexafluoridoantimonaten(V). (*v*: Streckschwingung, *δ*: Scherschwingung)

Verbindung	$v(SbF_6)$	$\delta(SbF_6)$	Quelle
$(ClOF_2)_2[AuF_4][SbF_6]$	653, 599	286	diese Arbeit
$ClOF_2[SbF_6]$	675, 662, 643, 560	288, 281	[296]
$SF_4[SbF_6]$	680, 652, 582, 554	288	[317]
$ClO_2[SbF_6]$	668, 654, 661, 574, 552	285, 281	[201]
$BrO_2[SbF_6]$	673, 665, 651, 638, 563, 551	284, 280	[201]
$K[SbF_6]$	661, 575	294, 278	[318]

4.3.8. Vergleich der Difluorooxychloronium(V)-Verbindungen

Die Cl−O-, Cl−F- und die Cl···F-Abstände der in dieser Arbeit charakterisierten $ClOF_2^+$-Verbindungen unterscheiden sich je nach Anion teilweise sehr stark voneinander. Die experimentell bestimmten und berechneten (CRYSTAL17, DFT-PBE0/TZVP) Abstände sind in Tabelle 21 aufgeführt. Die Abstände variieren stark und im Falle von $[MF_6]^-$-Anionen (*M* = V, Nb, Ta, Ru, Os, Ir, P, As, Sb) kann der Cl−O-Abstand bedingt mit dem effektiven Ionenradius des *M*(V)-Zentralatoms korreliert werden.[296,319]

In den mit CRYSTAL17 auf DFT-PBE0/TZVP-Niveau optimierten Strukturen sind die Cl−F-Abstände mit circa 1,62 bis 1,65 Å stets länger und die Cl−O-Abstände mit Ausnahme von $ClOF_2PbF_5$ mit 1,41 Å kürzer als die experimentell ermittelten Abstände. Dies ist nicht im Einklang mit den experimentellen Befunden, da für die jeweiligen Abstände je nach Anion eine große Variation beobachtet wird. Quantenchemische Gasphasenrechnungen für das isolierte $ClOF_2^+$-Kation haben gezeigt, dass eine Erhöhung der Elektronendichte in den niedrigsten unbesetzten Molekülorbitalen (LUMOs) sowohl zu einer Verlängerung der Cl−O-Bindung als auch der Cl−F-Bindung führt, da die Orbitale antibindend bezüglich dieser Bindungen sind (Abbildung 44).[296]

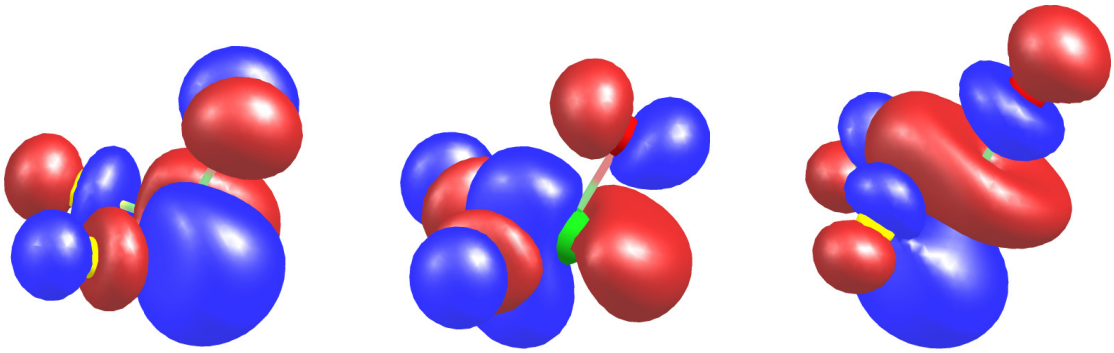

Abbildung 44. Niedrigste unbesetzte Molekülorbitale (LUMO) des freien $ClOF_2^+$-Kations.[296] Fluoratome sind in gelb, Chloratome in grün und Sauerstoffatome in rot dargestellt.

Die Erhöhung der Elektronendichte entspricht dabei einer Wechselwirkung des $ClOF_2^+$-Kations mit den μ-verbrückenden Fluoratomen der Anionen, die im Festkörper gegeben ist, da stets drei weitere Fluoratome das Chloratom umgeben. So sollte eine besonders starke Wechselwirkung des Chloratoms mit den μ-Fluoratomen zu einer Verlängerung der Cl−O- und Cl−F-Abstände führen.

Unter dieser Annahme sollten Anionen mit einer hohen Elektronegativitätsdifferenz von Zentralatom und Fluoratom zu großen Cl−O- und Cl−F-Abständen im $ClOF_2^+$-Kation führen. Ebenso sollten auch kurze Cl···F-Abstände die Abstände im $ClOF_2^+$-Kation beeinflussen. Dem entgegen stehen unterschiedliche Verläufe dieser Abstände. So kann der Cl−O-Abstand relativ klein sein und die Cl−F-Abstände groß, wie in der Kristallstruktur von $ClOF_2[PF_6]$. Ebenso führen die Vergleiche von F···Cl···O- oder F···Cl···F-Winkeln zu keinem Trend, der die Abstände im $ClOF_2^+$-Kation erklären könnte. Die unterschiedlichen Abstände spiegeln sich weiterhin nicht in den Bandenlagen der $ClOF_2^+$-Kationen in den Raman-Spektren bei Raumtemperatur wider, da keine Korrelation dieser vorliegt (Tabelle 23). Über die entsprechenden Ursachen der teilweise großen Unterschiede der Cl−O- und Cl−F-Abstände innerhalb der $ClOF_2^+$-Kationen kann somit nur spekuliert werden.

Tabelle 21. Gemessene und berechnete Cl−O-, Cl−F- und Cl···F-Abstände in Difluorooxychloronium(V)-Verbindungen. Die berechneten Abstände stammen aus den mit CRYSTAL17 optimierten Strukturen (DFT-PBE0/TZVP).

Verbindung	Atomabstände / Å			Methode[a]	Quelle
	Cl−O	Cl−F	Cl···F		
$ClOF_2[PF_6]$	1,4364(17)	1,5233(19), 1,5367(17)	2,4766(17)-2,6061(16)	gem.	b, [296]
	1,41	1,62, 1,62	2,39-2,65	ber.	b, [296]
$ClOF_2[AsF_6]$	1,455(2)	1,522(2), 1,543(2)	2,476(2)-2,598(2)	gem.	[267]
	1,41	1,62, 1,63	2,37-2,62	ber.	b, [296]
$ClOF_2[VF_6]$	1,465(2)	1,528(2), 1,531(3)	2,362(2)-2,512(2)	gem.	b, [296]
	1,41	1,62, 1,63	2,28-2,58	ber.	b, [296]
$ClOF_2[RuF_6]$	1,461(3)	1,509(3), 1,533(3)	2,418(2)-2,522(3)	gem.	b, [296]
	1,41	1,62, 1,63	2,33-2,58	ber.	b, [296]
$ClOF_2[IrF_6]$	1,444(5)	1,486(6), 1,514(5)	2,401(5)-2,487(5)	gem.	b, [296]
	1,41	1,63, 1,63	2,29-2,55	ber.	b, [296]
$ClOF_2[OsF_6]$	1,477(4)	1,508(3), 1,532(4)	2,442(3)-2,520(3)	gem.	b, [296]
	1,41	1,63, 1,63	2,36-2,52	ber.	b, [296]
$ClOF_2[SbF_6]$	1,476(3)	1,497(3), 1,529(3)	2,458(3)-2,531(3)	gem.	b, [296]
	1,41	1,62, 1,63	2,36-2,57	ber.	b, [296]

$ClOF_2[NbF_6]$	1,487(2)-1,511(2)	1,503(3)-1,516(2)	2,413(2)-2,484(2)	gem.	b, [296]
	1,41, 1,41	1,63-1,64	2,30-2,55	ber.[c]	b, [296]
$ClOF_2[TaF_6]$	1,488(4)-1,512(4)	1,488(4)-1,521(4)	2,423(4)-2,484(4)	gem.	b, [296]
	1,41, 1,41	1,62-1,63	2,31-2,54	ber.[c]	b, [296]
$(ClOF_2)_2[CrF_6]$	1,492(2)	1,492(2), 1,568(3)	2,328(3), 2,442(2)	gem.	b
	1,41	1,65	2,15-2,64	ber.[c]	b
$(ClOF_2)_2[RhF_6]$	1,483(3)	1,483(3), 1,582(5)	2,285(4), 2,472(3)	gem.	b
	1,41	1,65	2,16-2,62	ber.[c]	b
$(ClOF_2)_2[GeF_6]$	1,482(2)	1,482(2), 1,578(2)	2,321(2), 2,502(2)	gem.	b
	1,41	1,64	2,25-2,59	ber.[c]	b
$(ClOF_2)_2[PdF_6]$	1,439(4)	1,552(3)	2,396(3), 2,452(4)	gem.	b
	1,41	1,64	2,31, 2,51	ber.	b
$(ClOF_2)_2[PtF_6]$	1,442(4)	1,540(3)	2,391(3), 2,440(4)	gem.	b
	1,41	1,64	2,31, 2,49	ber.	b
$(ClOF_2)_2[SnF_6]$	1,481(2)	1,532(2)	2,394(1), 2,421(2)	gem.	b
	1,42	1,64	2,28, 2,52	ber.	b
$ClOF_2SnF_5$	1,418(9)	1,544(7), 1,564(8)	2,377(7)-2,511(7)	gem.	b
	1,41	1,63	2,31-2,47	ber.	b
$ClOF_2PbF_5$	1,405(5)	1,569(4), 1,582(4)	2,351(4)-2,501(4)	gem.	b
	1,41	1,64	2,28-2,49	ber.	b
$ClOF_2[BF_4]$	1,4816(9)	1,4816(9), 1,5356(11)	2,5763(12), 2,6134(9)	gem.	b
	1,41	1,62	2,42-2,71	ber.[c]	b
$ClOF_2[Mo_3O_3F_{13}]$	1,4630(14)	1,4968(14), 1,5554(12)	2,4939(13)-2,5076(13)	gem.	b
	1,41	1,63	2,38-2,51	ber.	b
$(ClOF_2[OsO_3F_3])_2OsF_6$	1,475(3)	1,506(2), 1,573(2)	2,330(2)-2,502(2)	gem.	b
	1,41	1,64	2,25-2,60	ber.	b
$(ClOF_2)_2[AuF_4][SbF_6]$	1,432(3)	1,546(2), 1,564(2)	2,341(2), 2,380(2)	gem.	b
	1,41	1,63	2,28-2,57	ber.	b

a: Gemessen (gem.) und berechnet (ber.); b: diese Arbeit; c: Modell ohne O/F-Fehlordnung.

Tabelle 22. Ausgewählte gemessene und berechnete Winkel in Difluorooxychloronium(V)-Verbindungen. Die berechneten Winkel stammen aus den mit CRYSTAL17 optimierten Strukturen (DFT-PBE0/TZVP).

Verbindung	Winkel / °				Methode[a]	Quelle
	F−Cl−F	F−Cl−O	F···Cl···O	F···Cl···F		
$ClOF_2[PF_6]$	98,00(10)	105,23(11), 105,46(11)	169,47(9)	79,99(6)	gem.	b, [296]
	93,0	106,1, 106,9	175,2	85,7	ber.	b, [296]
$ClOF_2[AsF_6]$	98,7(1)	104,2(1), 105,5(1)	168,5(1)	88,48(10)	gem.	[267]
	93,0	106,1, 106,5	174,0	85,9	ber.	b, [296]
$ClOF_2[VF_6]$	98,53(14)	102,70(14), 104,83(14)	169,12(12)	84,42(8)	gem.	b, [296]
	90,1	105,0, 105,6	174,0	90,3	ber.	b, [296]
$ClOF_2[RuF_6]$	99,69(16)	103,51(16), 104,25(16)	167,33(14)	81,60(9)	gem.	b, [296]
	92,5	105,7, 106,4	173,2	87,7	ber.	b, [296]
$ClOF_2[IrF_6]$	100,0(3)	103,5(3), 104,1(3)	167,0(3)	80,36(17)	gem.	b, [296]
	92,7	105,6, 106,4	171,9	84,1	ber.	b, [296]
$ClOF_2[OsF_6]$	100,4(2)	103,3(2), 104,15(19)	166,84(17)	80,33(10)	gem.	b, [296]
	92,4	106,0, 106,4	168,9	85,6	ber.	b, [296]
$ClOF_2[SbF_6]$	100,66(19)	102,90(19), 104,57(18)	166,87(16)	79,85(10)	gem.	b, [296]
	92,9	106,3, 106,4	172,1	85,2	ber.	b, [296]
$(ClOF_2)_2[CrF_6]$	99,49(12), 105,43(18)		164,58(11)	84,30(6)	gem,	b
	91,2	103,5, 106,4	171,9	88,9	ber.[c]	b
$(ClOF_2)_2[RhF_6]$	99,27(17), 106,8(3)		163,05(15)	83,33(9)	gem,	b
	91,3	103,5, 106,9	169,2	87,0	ber.[c]	b
$(ClOF_2)_2[GeF_6]$	99,44(9), 106,62(14)		163,99(11	84,42(5)	gem.	b
	91,9	104,5, 106,0	170,2	87,0	ber.[c]	b
$(ClOF_2)_2[PdF_6]$	96,2(2)	103,44(17)	172,7(2)	85,34(14)	gem.	b
	91,3	104,7	176,6	89,6	ber.	b
$(ClOF_2)_2[PtF_6]$	96,2(3)	103,12(19)	171,9(2)	86,33(12)	gem.	b
	91,3	104,7	175,7	89,2	ber.	b
$(ClOF_2)_2[SnF_6]$	98,88(12)	102,34(7)	172,28(9)	87,65(6)	gem.	b
	91,3	104,1	178,1	93,1	ber.	b
$ClOF_2SnF_5$	95,0(4)	103,5(4), 105,7(5)	171,3(4)	97,5(2)	gem.	b
	91,1	104,7, 105,7	173,9	98,9	ber.	b
$ClOF_2PbF_5$	92,5(2)	104,5(2), 106,5(3)	171,1(2)	97,54(13)	gem.	b
	90,6	104,5, 105,5	174,2	99,2	ber.	b
$ClOF_2[BF_4]$	100,73(5), 105,80(8)		165,89(4)	100,16(3)	gem.	b

	91,6	105,4, 105,5	171,9	105,1	ber.[c]	b
$ClOF_2[Mo_3O_3F_{13}]$	99,51(8)	102,21(8), 106,93(8)	163,30(7)	79,39(4)	gem.	b
	92,1	106,9, 107,1	168,5	84,5	ber.	b
$(ClOF_2[OsO_3F_3])_2OsF_6$	98,49(14)	100,41(14), 105,63(14)	164,58(12)	85,86(8)	gem.	b
	90,9	104,5, 105,6	169,7	91,1	ber.	b
$(ClOF_2)_2[AuF_4][SbF_6]$	96,20(13)	102,22(14), 105,03(14)	171,42(13)	82,73(8)	gem.	b
	92,2	104,9, 105,6	173,0	84,1	ber.	b

a: Gemessen (gem.) und berechnet (ber.); b: diese Arbeit; c: Modell ohne O/F-Fehlordnung.

Tabelle 23. Vergleich der Raman-aktiven Banden (Bandenlagen in cm^{-1}) des $ClOF_2^+$-Kations in verschiedenen Difluorooxychloronium(V)-Verbindungen. (*v*: Streckschwingung, *δ*: Scherschwingung, *π*: Inversionsschwingung, s: Symmetrisch, as: Asymmetrisch, n.b: nicht beobachtet)

Verbindung	v(Cl<u>O</u>)	v_s(Cl<u>F</u>$_2$)	v_{as}(Cl<u>F</u>$_2$)	π($ClOF_2$)	δ(Cl<u>O</u>)	δ(Cl<u>F</u>$_2$)	Quelle
$ClOF_2[PF_6]$	1332, 1321	732	710	508	401	382	a, [296]
$ClOF_2[VF_6]$	1322	750	712	506	401	345	a, [296]
$ClOF_2[RuF_6]$	1323, 1311	742	714	503	401	375	a, [296]
$ClOF_2[IrF_6]$	1324, 1313	737	713	503	400	374	a, [296]
$ClOF_2[OsF_6]$	1325, 1313	740	716	503	402	375	a, [296]
$ClOF_2[SbF_6]$	1330, 1318	747	715	507	402	377	a, [296]
$ClOF_2[NbF_6]$	1325, 1313	744	n.b.	499	405	377	a, [296]
$ClOF_2[TaF_6]$	1327, 1315	741	n.b.	500	404	376	a, [296]
$(ClOF_2)_2[GeF_6]$	1329, 1316	742, 721	670, 634	520, 468	412	376, 330, 310	a
$(ClOF_2)_2[PtF_6]$	1316	763, 742, 739	707, 671	507	418	386	a
$(ClOF_2)_2[SnF_6]$	1315, 1303	709	675	520, 507	417	383	a
$ClOF_2PbF_5$	1321, 1310	724	683	506	407	374	a
$ClOF_2[BF_4]$	1334, 1323	737	701	514	410	386, 360	a
$ClOF_2[Mo_3O_3F_{13}]$	1333, 1321	752	733, 709, 697	512, 500, 478	403, 397	381	a
$(ClOF_2[OsO_3F_3])_2OsF_6$	1318	711, 668	696, 641	518	388	338	a
$(ClOF_2)_2[AuF_4][SbF_6]$	1322	781, 722	694	508	418	385, 342	a

a: Diese Arbeit.

4.4. Zusammenfassung

Die Chemie des Chlortrifluorids ist vielfältig und es konnte gezeigt werden, dass es sich als Edukt für verschiedenste Verbindungsklassen eignet. Diese können, wie das ClF_2^+-Kation oder $[ClF_4]^-$-Anion, durch Lewis-Säure-Base-Reaktionen von ClF_3 abgeleitet werden. Unter bestimmten Bedingungen sind auch Salze mit $ClOF_2^+$- oder ClO_2^+-Kationen zugänglich. Eine Übersicht über die Reaktionspfade des Chlortrifluorids ist in Abbildung 45 gegeben.

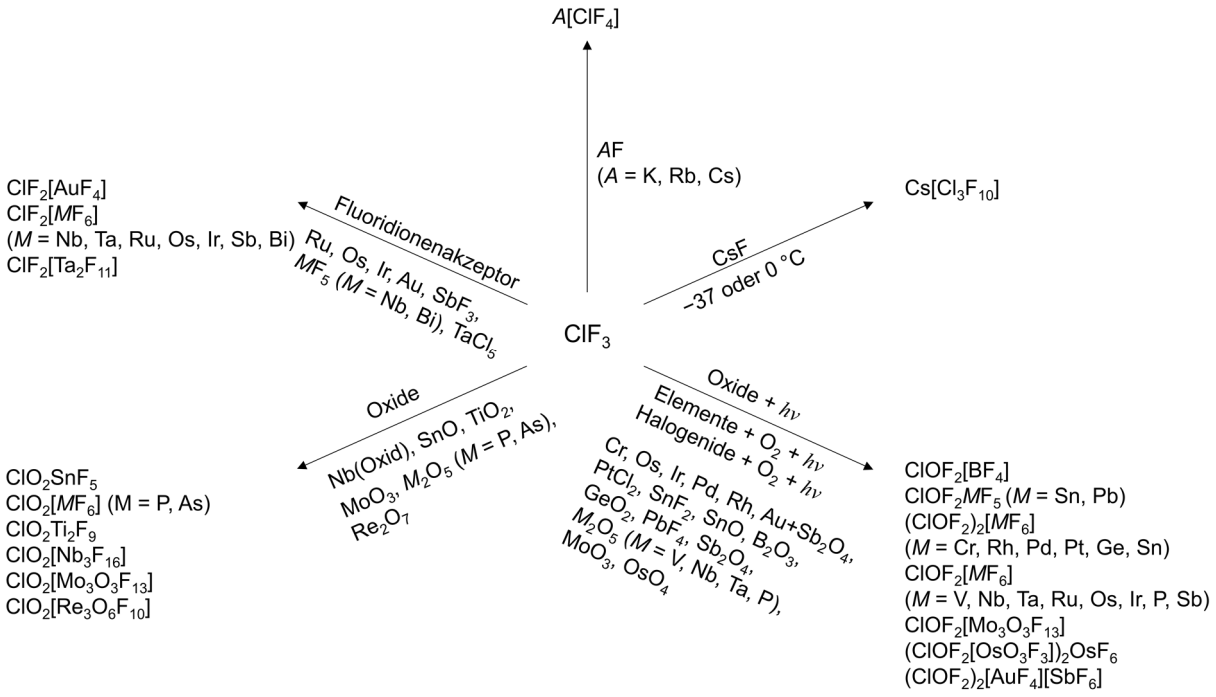

Abbildung 45. Übersicht über die durch Reaktionen mit Chlortrifluorid dargestellten Verbindungen. Die Reaktionen sind der Übersichtlichkeit halber nicht ausgeglichen.

<u>Fluoridochlorate(III)</u>

Die Solvolysereaktionen von Alkalimetallfluoriden in flüssigem Chlortrifluorid stellen einen Zugang zu verschiedenen Fluoridochloraten(III) dar. Umsetzungen von Kalium-, Rubidium- und Cäsiumfluorid mit Chlortrifluorid und die Entfernung des überschüssigen Lösungsmittels bei Raumtemperatur führen zu der Bildung von Salzen mit dem planaren $[ClF_4]^-$-Anion. Die Kristallstrukturen dieser Verbindungen konnten erstmalig mittels Einkristallstrukturanalyse aufgeklärt und eine Isotypie zum $K[BrF_4]$-Typ im Falle des $K[ClF_4]$ oder zum $Li[AuF_4]$-Typ für $Rb[ClF_4]$ und $Cs[ClF_4]$ aufgezeigt werden. Weiterhin konnten die Schwingungsspektren mit Hilfe quantenchemischer Rechnungen interpretiert werden.

Bei tiefen Temperaturen hingegen führt die Umsetzung von Cäsiumfluorid mit einem Überschuss an Chlortrifluorid zu der Bildung des Salzes $Cs[Cl_3F_{10}]$, welches das vorher unbekannte propellerförmige $[Cl_3F_{10}]^-$-Anion enthält. Die temperaturempfindliche Verbindung und sehr reaktive wurde sowohl mittels Einkristallstrukturanalyse als auch Raman-Spektroskopie charakterisiert. Die Kristallstruktur dieses Salzes kann als ein Vertreter des seltenen $A^{[5]}B^{[5]}$-Strukturtyps klassifiziert werden. Die Cl−F-Abstände im $[Cl_3F_{10}]^-$-Anion sind sehr verschieden und es kann als ein zentrales Fluorid-Ion, welches an drei ClF_3-Moleküle koordiniert, aufgefasst werden. Quantenchemische Rechnungen zeigen, dass die Cl−μ_3-F-Bindungen stark ionisch im Vergleich zu denen in den „ClF_3-Untereinheiten“ sind.

<u>Difluorochloronium(III)-Verbindungen</u>

In Kooperation mit der Arbeitsgruppe von Prof. Dr. Karl O. Christe wurden Umsetzungen von Edelmetallen wie Iridium, Fluoriden wie NbF_5 und Chloriden wie $TaCl_5$ mit Überschüssen an Chlortrifluorid untersucht. Diese Reaktionen führten zu der Bildung von ClF_2^+-Salzen, falls die entsprechenden Edukte stabile Fluoridometallat-Anionen bilden können. Die Kristallstrukturen der erhaltenen Salze wurden mittels Einkristallstrukturanalyse aufgeklärt. Dabei wurden teilweise bereits berichtete Strukturmodelle verbessert oder korrigiert. Allen Kristallstrukturen ist ein gewinkeltes ClF_2^+-Kation mit polar-kovalenten Cl−F-Bindungen gemein. Das Chloratom des ClF_2^+-Kations ist stets von zwei zusätzlichen Fluoratomen der Anionen in der Form ionischer Cl···F-Brücken umgeben. Daher resultiert die Koordinationszahl 2+2 für das Chloratom. Für die Salze konnte eine große Anzahl verschiedener Strukturmotive beobachtet werden (Tabelle 24).

Die $[MF_6]^-$-Anionen können cis- oder trans-verbrückend sein und zu unterschiedlichen Strukturmotiven, wie Ketten oder Helices, führen. Die Salze mit $[MF_6]^-$-Anionen können mit der allgemeinen Niggli-Formel ${}^{1}_{\infty}\left[\langle ClF_{\frac{2}{1+1}}F_{\frac{2}{1}}\rangle\langle MF_{\frac{2}{1+1}}F_{\frac{4}{1}}\rangle\right]$ beschrieben werden.

Die verschiedenen Strukturmotive können weder mit den effektiven Ionenradien der *M*(V)-Zentralatome noch den Elektronegativitäten in Verbindung gebracht werden und eine mögliche Ursache für die strukturelle Vielfalt wurde noch nicht identifiziert.

Tabelle 24. Übersicht über die Strukturmotive, die Art der Verbrückung des Anions und die Niggli-Formeln der charakterisierten ClF_2^+-Verbindungen. Die Koordinationszahl der Chloratome beträgt in allen aufgelisteten Verbindungen 2+2.

Verbindung	Verbrückung	Strukturmotiv	Niggli-Formel
$ClF_2[AuF_4]$	cis	Dimere	${}^{0}_{\infty}\left[\left(\langle ClF_{\frac{2}{1+1}}F_{\frac{2}{1}}\rangle\langle AuF_{\frac{2}{1+1}}F_{\frac{2}{1}}\rangle\right)_2\right]$
$ClF_2[Ta_2F_{11}]$	cis	Dimere	${}^{0}_{\infty}\left[\left(\langle ClF_{\frac{2}{1+1}}F_{\frac{2}{1}}\rangle\langle TaF_{\frac{1}{1+1}}F_{\frac{1}{2}}F_{\frac{4}{1}}\rangle_2\right)_2\right]$
$ClF_2[IrF_6]$	trans	Ketten	${}^{1}_{\infty}\left[\langle ClF_{\frac{2}{1+1}}F_{\frac{2}{1}}\rangle\langle IrF_{\frac{2}{1+1}}F_{\frac{4}{1}}\rangle\right]$
$ClF_2[MF_6]$ (M = Sb, Bi)	trans	Zick-Zack-Ketten	${}^{1}_{\infty}\left[\langle ClF_{\frac{2}{1+1}}F_{\frac{2}{1}}\rangle\langle MF_{\frac{2}{1+1}}F_{\frac{4}{1}}\rangle\right]$
$ClF_2[MF_6]$ (M = Nb, Ta)	cis	2/1-Helices	${}^{1}_{\infty}\left[\langle ClF_{\frac{2}{1+1}}F_{\frac{2}{1}}\rangle\langle MF_{\frac{2}{1+1}}F_{\frac{4}{1}}\rangle\right]$
$ClF_2[OsF_6]$	cis	„3/1-Helices“	${}^{1}_{\infty}\left[\langle ClF_{\frac{2}{1+1}}F_{\frac{2}{1}}\rangle\langle OsF_{\frac{2}{1+1}}F_{\frac{4}{1}}\rangle\right]$
$ClF_2[RuF_6]$	cis	4/1-Helices	${}^{1}_{\infty}\left[\langle ClF_{\frac{2}{1+1}}F_{\frac{2}{1}}\rangle\langle RuF_{\frac{2}{1+1}}F_{\frac{4}{1}}\rangle\right]$

Difluoroxychloronium(V)-Verbindungen

Die photochemische Umsetzung von Chlortrifluorid mit Oxiden führt, falls stabile Anionen gebildet werden können, zur Bildung von Salzen mit dem pyramidalen $ClOF_2^+$-Kation. Dies gilt ebenfalls für photochemische Reaktionen von Chlortrifluorid mit Elementen wie Osmium oder Iridium und zusätzlicher Sauerstoffzugabe. Die Salze wurden mittels Einkristallstrukturanalyse charakterisiert. Die Synthese von solchen Verbindungen gelingt somit indirekt, ohne Verwendung von $ClOF_3$, welches ansonsten durch Fluorierung von $ClONO_2$ oder Cl_2O dargestellt werden muss. Werden Metalle wie Chrom oder Palladium unter oben genannten Bedingungen umgesetzt, so erfolgt Oxidation bis zur Oxidationsstufe +IV unter Bildung von $[MF_6]^{2-}$-Anionen. Metalle wie Iridium oder Osmium werden bis zur Oxidationsstufe +V oxidiert und bilden $[MF_6]^-$-Anionen.

Allen hier beschriebenen Salzen ist das pyramidale $ClOF_2^+$-Kation gemein, dessen Chloratom stets von drei weiteren Fluoratomen umgeben und die Koordinationszahl entsprechend 3+3 ist. Eine Übersicht über die dargestellten Verbindungen und deren Strukturmotive ist in Tabelle 25 gegeben. Mit dem $ClOF_2^+$-Kation konnten Verbindungen mit unterschiedlichen und vorher selten oder gar nicht strukturchemisch charakterisierten Anionen erhalten werden, unter anderem die SnF_5^-- und PbF_5^--Anionen. Weitere ungewöhnliche Verbindungen stellen $(ClOF_2[OsO_3F_3])_2OsF_6$ und $(ClOF_2)_2[AuF_4][SbF_6]$ dar, in welchen entweder Osmiumhexafluorid cokristallisiert, was vorher noch nicht für ein Hexafluorid beschrieben wurde, oder ein Doppelsalz mit dem $ClOF_2^+$-Kation vorliegt. Die Cl−O- und Cl−F-Abstände der $ClOF_2^+$-Kationen variieren je nach Anion stark und teilweise liegt symmetriebedingte O/F-Mischbesetzung wie in $ClOF_2[BF_4]$ oder O/F-Fehlordnung wie in $ClOF_2[NbF_6]$ vor.

Tabelle 25. Übersicht über die Strukturmotive und die Niggli-Formeln der in dieser Arbeit beschriebenen $ClOF_2^+$-Verbindungen. Die Koordinationszahl der Chloratome beträgt in allen aufgelisteten Verbindungen 3+3.

Verbindung	Strukturmotiv	Niggli-Formel
$ClOF_2[Mo_3O_3F_{13}]$	Dimere	${}^{0}_{\infty}\left[\left(\langle ClF_{\frac{3}{1+1}}F_{\frac{2}{1}}O_{\frac{1}{1}}\rangle\langle MoF_{\frac{1}{1+1}}F_{\frac{1}{2}}F_{\frac{3}{1}}O_{\frac{1}{1}}\rangle\langle MoF_{\frac{2}{2}}F_{\frac{3}{1}}O_{\frac{1}{1}}\rangle\langle MoF_{\frac{2}{1+1}}F_{\frac{1}{2}}F_{\frac{2}{1}}O_{\frac{1}{1}}\rangle\right)_2\right]$
$ClOF_2[BF_4]$	Leitern	${}^{1}_{\infty}\left[\langle ClF_{\frac{3}{1+1}}F_{\frac{2}{1}}O_{\frac{1}{1}}\rangle\langle BF_{\frac{3}{1+1}}F_{\frac{1}{1}}\rangle\right]$
$(ClOF_2[OsO_3F_3])_2OsF_6$	Stränge	${}^{1}_{\infty}\left[\langle ClF_{\frac{2}{2+1}}F_{\frac{1}{1+1}}F_{\frac{2}{1}}O_{\frac{1}{1}}\rangle\langle OsF_{\frac{1}{1+2}}F_{\frac{1}{1+1}}O_{\frac{3}{1}}F_{\frac{1}{1}}\rangle\right]$
$ClOF_2[MF_6]$ (M = V, Nb, Ta Ru, Os, Ir, P, Sb)	Schichten	${}^{2}_{\infty}\left[\langle ClF_{\frac{3}{1+1}}F_{\frac{2}{1}}O_{\frac{1}{1}}\rangle\langle MF_{\frac{3}{1+1}}F_{\frac{3}{1}}\rangle\right]$
$(ClOF_2)_2[MF_6]$ (M = Cr, Rh, Ge)	Schichten	${}^{2}_{\infty}\left[\langle ClF_{\frac{2}{2+1}}F_{\frac{1}{1+1}}F_{\frac{2}{1}}O_{\frac{1}{1}}\rangle_2\langle MF_{\frac{2}{1+2}}F_{\frac{2}{1+1}}F_{\frac{2}{1}}\rangle\right]$
$ClOF_2MF_5$ (M = Sn, Pb)	Schichten	${}^{2}_{\infty}\left[\langle ClF_{\frac{3}{1+1}}F_{\frac{2}{1}}O_{\frac{1}{1}}\rangle\langle MF_{\frac{3}{1+1}}F_{\frac{2}{2}}F_{\frac{1}{1}}\rangle\right]$
$(ClOF_2)_2[AuF_4][SbF_6]$	Schichten	${}^{2}_{\infty}\left[\langle ClF_{\frac{3}{1+1}}F_{\frac{2}{1}}O_{\frac{1}{1}}\rangle_2\langle AuF_{\frac{4}{1+1}}\rangle\langle SbF_{\frac{2}{1+1}}F_{\frac{4}{1}}\rangle\right]$
$(ClOF_2)_2[MF_6]$ (M = Pd, Pt, Sn)	Gerüst	${}^{3}_{\infty}\left[\langle ClF_{\frac{3}{1+1}}F_{\frac{2}{1}}O_{\frac{1}{1}}\rangle_2\langle MF_{\frac{6}{1+1}}\rangle\right]$

Dioxychloronium(V)-Verbindungen

Eine weitere Verbindungsklasse, die ausgehend von Chlortrifluorid erhalten werden kann, sind die ClO_2^+-Verbindungen. Diese können durch Umsetzungen von ClF_3 mit Oxiden von Elementen, welche stabile Fluoridometallat- oder Oxidofluoridometallat-Anionen bilden, erhalten werden. Initial wird bei diesen Umsetzungen vermutlich das instabile ClOF gebildet, welches in ClF und ClO_2F disproportioniert. Das gebildete ClO_2F reagiert entsprechend mit den in situ erzeugten Fluoriden oder Oxidfluoriden und bildet so die ClO_2^+-Salze. Die erhaltenen Salze wurden mittels Einkristallstrukturanalyse und Raman-Spektroskopie charakterisiert.

In den Salzen liegt stets ein gewinkeltes ClO_2^+-Kation vor, welches je nach Anion zusätzlich von vier oder sechs Fluoratomen umgeben ist, sodass die Koordinationszahl des Chloratoms 2+4 oder 2+6 beträgt (Tabelle 26). Quantenchemische Festkörperrechnungen zeigen, dass die Cl−O-Bindungen polar-kovalent und die Cl···F-Wechselwirkungen ionisch sind.

Tabelle 26. Übersicht über die Koordinationszahlen der Chloratome (KZ(Cl)), der Strukturmotive und der Niggli-Formeln der in dieser Arbeit beschriebenen ClO_2^+-Verbindungen.

Verbindung	KZ(Cl)	Strukturmotiv	Niggli-Formel
$ClO_2[Mo_3O_3F_{13}]$	2+4	Dimere	${}^{0}_{\infty}\left[\left[\langle ClF_{\frac{4}{1+1}}O_{\frac{2}{1}}\rangle\langle MoF_{\frac{2}{1+1}}F_{\frac{1}{2}}F_{\frac{2}{1}}O_{\frac{1}{1}}\rangle\langle MoF_{\frac{2}{2}}F_{\frac{3}{1}}O_{\frac{1}{1}}\rangle\langle MoF_{\frac{1}{1+1}}F_{\frac{1}{2}}F_{\frac{3}{1}}O_{\frac{1}{1}}\rangle\right]_2\right]$
$ClO_2[AsF_6]$	2+4	Säulen	${}^{1}_{\infty}\left[\langle ClF_{\frac{2}{2+1}}F_{\frac{2}{1+1}}O_{\frac{2}{1}}\rangle\langle AsF_{\frac{1}{1+2}}F_{\frac{2}{1+1}}F_{\frac{3}{1}}\rangle\right]$
$ClO_2[TiF_{3/2}F_{3/1}]_2$	2+4	Säulen	${}^{1}_{\infty}\left[\langle ClF_{\frac{4}{1+1}}O_{\frac{2}{1}}\rangle\langle TiF_{\frac{2}{1+1}}F_{\frac{3}{2}}F_{\frac{1}{1}}\rangle_2\right]$
$ClO_2[Re_3O_6F_{10}]$	2+4	Säulen	${}^{1}_{\infty}\left[\langle ClF_{\frac{4}{1+1}}O_{\frac{2}{1}}\rangle\langle ReF_{\frac{2}{1+1}}F_{\frac{1}{2}}F_{\frac{1}{1}}O_{\frac{2}{1}}\rangle_2\langle ReF_{\frac{2}{2}}F_{\frac{2}{1}}O_{\frac{2}{1}}\rangle\right]$
$ClO_2[Nb_3F_{16}]$	2+4	Leitern	${}^{1}_{\infty}\left[\langle ClF_{\frac{4}{1+1}}O_{\frac{2}{1}}\rangle\langle NbF_{\frac{2}{1+1}}F_{\frac{1}{2}}F_{\frac{3}{1}}\rangle_2\langle NbF_{\frac{2}{2}}F_{\frac{4}{1}}\rangle\right]$
$ClO_2[IrF_6]$	2+4	Schichten	${}^{2}_{\infty}\left[\langle ClF_{\frac{4}{1+1}}O_{\frac{2}{1}}\rangle\langle IrF_{\frac{4}{1+1}}F_{\frac{2}{1}}\rangle\right]$
$ClO_2[SnF_{2/2}F_{4/1}]$	2+4	Schichten	${}^{2}_{\infty}\left[\langle ClF_{\frac{2}{2+1}}F_{\frac{2}{1+1}}O_{\frac{2}{1}}\rangle\langle SnF_{\frac{1}{1+2}}F_{\frac{2}{1+1}}F_{\frac{2}{2}}F_{\frac{1}{1}}\rangle\right]$
$ClO_2[PF_6]$	2+6	Gerüst	${}^{3}_{\infty}\left[\langle ClF_{\frac{2}{2+1}}F_{\frac{4}{1+1}}O_{\frac{2}{1}}\rangle\langle PF_{\frac{1}{1+2}}F_{\frac{4}{1+1}}F_{\frac{1}{1}}\rangle\right]$

4.5. Ausblick

Lewis-Säure-Base-Reaktionen

Die in dieser Arbeit beschriebenen $[ClF_4]^-$-, ClF_2^+-, $ClOF_2^+$- und ClO_2^+-Verbindungen könnten als Ausgangsstoffe für weitere Untersuchungen dienen. Das Lewis-Säure-Verhalten der Kationen könnte untersucht werden, unter anderem durch Umsetzung mit N-Donor-Liganden wie Acetonitril oder Edelgasfluoriden wie XeF_2 und KrF_2, was im Falle organischer Liganden zu hochenergetischen Materialien führen würde (Gleichungen 65 und 66). Für das $BrOF_2^+$-Kation wurde unter anderem gezeigt, dass mit XeF_2 und KrF_2 Lewis-Säure-Base-Addukte gebildet werden können, $[BrOF_2(XeF_2)_n]^+$ (n = 1,2) und $[BrOF_2(KrF_2)_2]^+$.[267,320] Bisher gibt es jedoch keine Berichte über eine entsprechende Reaktivität des $ClOF_2^+$-Kations.

$$ClF_2^+ + 2\,CH_3CN \longrightarrow [ClF_2(CH_3CN)_2]^+ \qquad 65$$

$$ClOF_2^+ + n\,XF_2 \longrightarrow [ClOF_2(XF_2)_n]^+ \qquad 66$$

n = 1, 2
X = Kr, Xe

Einfacherer Zugang zu Difluorooxychloronium(V)-Verbindungen

Erstrebenswert wäre es auch den Zugang von $ClOF_2^+$-Salzen durch photochemische Umsetzungen von Chlor/Fluor/Sauerstoff-Mischungen mit Lewis-Säuren wie BF_3 oder AsF_5 zu untersuchen, sodass nicht mehr auf Chlortrifluorid als Startmaterial zurückgegriffen werden muss (Gleichung 67). Umsetzungen mit BF_3 wären dabei besonders geeignet, da die möglichen Nebenprodukte $ClO_2[BF_4]$ und $ClF_2[BF_4]$ bei Raumtemperatur einen hohen Dampfdruck besitzen und einfach vom raumtemperaturstabilen $ClOF_2[BF_4]$ entfernt werden könnten.[206,321]

$$2\,BF_3 + 3\,F_2 + Cl_2 + O_2 \xrightarrow{hv} 2\,ClOF_2[BF_4] \qquad 67$$

Ligandenaustauschreaktionen

Hochenergetische Materialien könnten durch mögliche Ligandenaustauschreaktionen des $[ClF_4]^-$-Anions oder der ClF_2^+- und $ClOF_2^+$-Kationen mit Trimethylsilylazid erhalten werden. Denkbare Ionen, welche bisher noch nicht beschrieben wurden, wären unter anderem $[Cl(N_3)_4]^-$, $Cl(N_3)_2^+$ oder $ClO(N_3)_2^+$ (Gleichungen 68 bis 70).

$$[ClF_4]^- + 4\ Si(CH_3)_3N_3 \longrightarrow [Cl(N_3)_4]^- + 4\ Si(CH_3)_3F \qquad 68$$

$$ClF_2^+ + 2\ Si(CH_3)_3N_3 \longrightarrow Cl(N_3)_2^+ + 2\ Si(CH_3)_3F \qquad 69$$

$$ClOF_2^+ + 2\ Si(CH_3)_3N_3 \longrightarrow ClO(N_3)_2^+ + 2\ Si(CH_3)_3F \qquad 70$$

Mehrkernige Kationen und Anionen

Versuche mehrkernige Kationen wie $[Cl_2F_5]^+$ oder $[Cl_3F_8]^+$ in Salzen mit dem $[IrF_6]^-$-Anion bei tiefen Temperaturen zu isolieren schlugen bisher fehl. Gegebenenfalls muss auf ein anderes, größeres Anion wie $[Sb_2F_{11}]^-$- oder $[Sb_3F_{16}]^-$ ausgewichen werden, um entsprechende Verbindungen bei tiefen Temperaturen stabilisieren zu können (Gleichung 71).

$$ClF_2[Sb_2F_{11}] + n\ ClF_3 \longrightarrow [Cl_{1+n}F_{2+3n}][Sb_2F_{11}] \qquad 71$$

$n = 1, 2$

Weiterhin könnten die mit den $[Br_3O_6]^+$- oder $[BrCl_2O_6]^+$-Kationen verwandten $[Cl_3O_6]^+$- oder $[ClBr_2O_6]^+$-Kationen bei tiefen Temperaturen durch Umsetzungen von ClO_2^+-Salzen mit Chlor- oder Bromdioxid zugänglich sein (Gleichung 72).[137]

$$ClO_2^+ + n\ XO_2 \longrightarrow [ClX_2O_6]^+ \qquad 72$$

$n = 1, 2$
$X = Cl, Br$

Auf der Seite der Anionen könnten auch die $[Cl_2F_7]^-$- oder $[Cl_4F_{13}]^-$-Anionen durch geschickte Temperatur- und Kationenwahl zugänglich sein, die entsprechenden Brom-basierten Anionen sind bereits bekannt (Gleichung 73).[41,43]

$$[ClF_4]^- + n\ ClF_3 \longrightarrow [Cl_{1+n}F_{4+3n}]^- \qquad 73$$

$n = 1, 3$

5. Fluoride und Fluoridometallate des Urans, Neptuniums und Plutoniums

5.1. Motivation und Zielsetzung

Im Rahmen dieser Arbeit sollten die Lewis-Säure-Eigenschaften verschiedener Uranfluoride, vor allem die des Uranpentafluorids, untersucht werden. Diese Arbeiten bauen auf denen der vorherigen Masterarbeit auf.[322] Durch Umsetzungen mit Fluoridionendonoren wie den Erdalkalimetallfluoriden sollte versucht werden Fluoridouranate(V) mit neuartigen Strukturmotiven zu stabilisieren.

Weiterhin sollten ternäre Fluoridometallate(IV) des Neptuniums und Plutoniums dargestellt und strukturchemisch charakterisiert werden, um zum einen neue Zugänge auf der Basis hydrofluorothermaler Umsetzungen, welche für ternäre und quarternäre Fluoridothorate(IV)- und -uranate(IV) beschrieben sind, zu etablieren und zum anderen mögliche strukturelle Unterschiede zu analogen Thorium- und Uranverbindungen aufzuzeigen.[323–327] Bisher wurden ternäre Fluoridoneptunate(IV)- und -plutonate(IV) meist durch Festkörperreaktionen der Fluoride oder Hydrofluorierungen bei hohen Temperaturen synthetisiert.[328–330]

Im Falle des Plutoniums sollte weiterhin untersucht werden, ob Fluoridoplutonate(III) unter hydrofluorothermalen Bedingungen zugänglich sind, da Plutonium(III) im wässrigen System thermodynamisch stabil ist und Plutoniumtrifluorid aus wässriger Lösung gefällt werden kann.[331–333]

5.2. Kumulativer Teil

5.2.1. The $[U_2F_{12}]^{2-}$ Anion of $Sr[U_2F_{12}]$

Benjamin Scheibe, Clemens Pietzonka, Otto Mustonen, Maarit Karppinen, Antti J. Karttunen, Mihail Atanasov, Frank Neese, Matthias Conrad, Florian Kraus

Angew. Chem. **2018**, *130*, 2964–2968
Angew. Chem. Int. Ed. **2018**, 57, 2914–2918.
DOI: 10.1002/ange.201800743
DOI: 10.1002/anie.201800743

Siehe Abschnitt 7.6.

Die Umsetzung von zwei Äquivalenten *β*-Uranpentafluorid mit Strontiumfluorid in wasserfreiem Fluorwasserstoff führt zu Bildung von $Sr[U_2F_{12}]$. Zu einem geringen Anteil liegt die Verbindung $Sr[UF_5(HF_2)_2]$ als Verunreinigung vor. In der Kristallstruktur von $Sr[U_2F_{12}]$ liegt ein hochsymmetrisches $[U_2F_{12}]^{2-}$-Anion mit μ_2-verbrückenden Fluoratomen vor. Die Uranatome sind jeweils von sieben Fluoratomen in der Form eines einfach überkappten trigonalen Prismas umgeben und diese sind über eine gemeinsame Kante verknüpft. Das Anion kann auch als „Kondensationsprodukt“ zweier $[UF_6]^-$-Anionen aufgefasst werden. Die U−F-Bindungslängen der terminal gebundenen Fluoratome betragen 2,079(10) und 2,081(4) Å, die der μ_2-verbrückenden Fluoratome 2,281(4) Å. Die Struktur kann mit dem einfachen AB-Strukturtyp CsCl in Verbindung gebracht werden. Die Verbindung zeigt, bedingt durch die magnetische Kopplung der beiden $5f^1$-Elektronen der Uran(V)-Atome, molekularen Antiferromagnetismus, welcher durch die μ_2-F-Atome vermittelt wird. Aufgrund der einfachen Liganden und Struktur des Anions wurden *Complete Active Space Self-Consistent Field*-Rechnungen zur Interpretation der magnetischen und spektroskopischen Eigenschaften durchgeführt. Die Rechnungen an dem Modell $[U_2F_{12}]^{2-}$ reproduzieren diese Eigenschaften gut und ein Vergleich mit weiteren Rechnungen an dem einkernigen Modell $[UF_7]^{2-}$ zeigen den Einfluss der Wechselwirkung zweier Uran(V)-Zentren.

Die Verbindung wurde weiter mittels Infrarot- und Raman-Spektroskopie charakterisiert und die Spektren durch quantenchemische Festkörperrechnungen reproduziert. Quantenchemische Rechnungen zeigen, dass die U−μ_2-F-Bindung ionischer ist als die U−F-Bindungen.

Beiträge der Autoren:

Die Publikation baut auf den Ergebnissen der Masterarbeit von B. Scheibe auf, weitere Untersuchungen wurden während der Promotion durchgeführt.[322] B. Scheibe entwickelte und erprobte die Darstellung von $Sr[U_2F_{12}]$, charakterisierte die Verbindung und bestimmte die Kristallstruktur. B. Scheibe analysierte und interpretierte die Ergebnisse. M. Conrad half bei kristallographischen Fragestellungen. C. Pietzonka, O. Mustonen und M. Karppinen führten die magnetischen Messungen durch und interpretierten die Ergebnisse. A. J. Karttunen entwickelte die verwendeten Basissätze für das Programmpaket CRYSTAL14, führte die quantenchemischen Festkörperrechnungen durch und interpretierte die Ergebnisse. M. Atanasov und F. Neese interpretierten die magnetischen und spektroskopischen Messdaten, führten die CASSCF-Rechnungen durch, interpretierten die Ergebnisse und trugen die entsprechenden Abschnitte zum Manuskript bei. B. Scheibe verfasste das Manuskript in Absprache mit den Coautoren. F. Kraus leitete das Projekt.

5.2.2. UF_4 and the High-Pressure Polymorph HP-UF_4

Benjamin Scheibe, Jörn Bruns, Gunter Heymann, Malte Sachs, Antti J. Karttunen, Clemens Pietzonka, Sergei I. Ivlev, Hubert Huppertz, Florian Kraus

Chem. Eur. J. **2019**, *25*, 7366–7374.
DOI: 10.1002/chem.201900639

Siehe Abschnitt 7.7.

Die Umsetzung von einem Überschuss Schwefel mit Uranhexafluorid in flüssigem Fluorwasserstoff bei Raumtemperatur führt zur Bildung von grünem Urantetrafluorid. Schwefelreste können aus dem Rohprodukt durch Vakuumsublimation entfernt werden. Das erhaltene UF_4 ist frei von schwefelhaltigen und oxidischen Verunreinigungen, was durch Röntgen-Pulverdiffraktometrie, Mikroröntgenfluoreszenzanalyse, Infrarot- und Raman-Spektroskopie sowie magnetische Messungen gezeigt werden konnte. Ausgehend von dem reinen UF_4 wurden Hochdruckexperimente in einer Vielstempel-Presse durchgeführt und so eine Hochdruckmodifikation, HP-UF_4, synthetisiert. Die Kristallstruktur wurde mittels Einkristallstrukturanalyse aufgeklärt. In der Kristallstruktur liegen zwei symmetrieunabhängige Uranatome vor, die entweder von neun oder elf Fluoratomen umgeben sind. Die Fluoratome sind entweder μ_2- oder μ_3-verbrückend zwischen den Urantatomen und insgesamt liegt eine komplexe Gerüststruktur vor, die mit der Niggli-Formel ${}^{3}_{\infty}\left[\langle UF_{\frac{6}{3}}F_{\frac{5}{2}}\rangle\,\langle UF_{\frac{6}{3}}F_{\frac{3}{2}}\rangle\right]$ beschrieben werden kann. Die Kristallstruktur von HP-UF_4 repräsentiert einen neuen Strukturtypen, der strukturell nicht mit Hochdruckmodifikationen des Zirkoniumtetrafluorids verwandt ist. Weiterhin ist es die erste strukturell charakterisierte Hochdruckmodifikation eines Actinoidtetrafluorids. Magnetische Messungen der Verbindung zeigen, dass das magnetische Verhalten bei hohen Temperaturen dem des UF_4 ähnlich ist. Bei tiefen Temperaturen werden Sättigungseffekte beobachtet, welche typisch für Uran(IV)-Verbindungen sind. Quantenchemische Festkörperrechnungen zeigen einen geringen Energieunterschied zwischen HP-UF_4 und der Normaldruckmodifikation.

Beiträge der Autoren:

Die Publikation entstand in Kooperation der Arbeitsgruppen Huppertz und Kraus. B. Scheibe entwickelte und erprobte die neue Darstellungsmethode von UF_4. J. Bruns führte die Hochdruckexperimente mit UF_4 durch und synthetisierte die Hochdruckmodifikation HP-UF_4. G. Heynmann bestimmte die Kristallstruktur von HP-UF_4. M. Sachs und C. Pietzonka führten magnetische Messungen der Verbindungen durch, interpretierten die Daten und trugen entsprechende Teile zum Manuskript bei. S. I. Ivlev führte die Rietveldverfeinerungen durch. B. Scheibe charakterisierte die Verbindungen weiter und interpretierte und analysierte die Ergebnisse. B. Scheibe verfasste das Manuskript in Absprache mit den Coautoren. H. Huppertz und F. Kraus leiteten das Projekt.

5.2.3. Synthesis and Crystal Structures of Transition Metal(II) Fluoridometallate(IV) Hydrates of Neptunium and Plutonium: $A^{II}M^{IV}F_6{\cdot}3H_2O$ (A^{II} = Mn, Zn; M^{IV} = Np, Pu)

Benjamin Scheibe, Juliane März, Moritz Schmidt, Thorsten Stumpf, Florian Kraus
Eur. J. Inorg. Chem. **2020**, *2020*, 2279-2284.
DOI: 10.1002/ejic.202000298

Siehe Abschnitt 7.8.

Die Umsetzung von Suspensionen der Übergangsmetallchloride Mangan(II)- und Zink(II)-chlorid und der Oxide Neptunium(IV)- und Plutonium(IV)-oxid in Flusssäure bei Raumtemperatur oder 60°C führt zur Bildung von „Hydraten“ der Zusammensetzung $A^{II}M^{IV}F_6{\cdot}3H_2O$ (A^{II} = Mn, Zn; M^{IV} = Np, Pu) in kristalliner Form. Die Kristallstrukturen der Verbindungen wurden mit Einkristallstrukturanalyse bestimmt. Die Verbindungen kristallisieren isotyp zu den Uranverbindungen. In den Kristallstrukturen liegen oktaederähnlich von vier Fluoratomen und zwei Wassermolekülen umgebene A^{II}-Kationen vor. Die M^{IV}-Atome sind von acht Fluoratomen und einem Wassermolekül in der Form eines verzerrten dreifach überkappten trigonalen Prismas umgeben. Vier der Fluoratome sind μ_2-verbrückend zwischen M^{IV}-Atomen, wodurch eindimensionale Stränge trans-kantenverknüpfter $[M^{IV}F_8(H_2O)]$-Polyeder entlang der *c*-Achse erhalten werden. Die anderen vier Fluoratome sind μ_2-verbrückend zwischen A^{II}- und M^{IV}-Atomen, sodass eine Gerüststruktur, welche mit der Niggli-Formel ${}^{3}_{\infty}\left[\langle A^{II}F_{\frac{4}{1+1}}(H_2O)_{\frac{2}{1}}\rangle\langle M^{IV}F_{\frac{4}{1+1}}F_{\frac{4}{2}}(H_2O)_{\frac{1}{1}}\rangle\right]$ beschrieben werden kann, erhalten wird. Die Zellvolumina und M^{IV}−F-Bindungslängen zeigen eine Abhängigkeit von der Ordnungszahl und verringern sich entlang der Reihe Uran, Neptunium und Plutonium aufgrund der Actinoidenkontraktion. Eine solche Verkleinerung wird jedoch nicht für die M^{IV}−O-Abstände beobachtet.

Beiträge der Autoren:

Die Publikation entstand in Kooperation mit der Abteilung Chemie der f-Elemente des Instituts für Ressourcenökologie am Helmholtz-Zentrum Dresden-Rossendorf und der Arbeitsgruppe Kraus. B. Scheibe entwickelte und erprobte die Darstellung der Fluoridometallate(IV) des Neptuniums und Plutoniums, bestimmte die Kristallstrukturen der Verbindungen und analysierte und interpretierte die Ergebnisse. B. Scheibe verfasste das Manuskript in Absprache mit den Coautoren. J. März und M. Schmidt koordinierten das Projekt. T. Stumpf und F. Kraus leiteten das Projekt.

5.2.4. A Molecular Octafluoridoneptunate(IV) Anion in $(NH_4)_4[NpF_8]$ and Theoretical Investigations of the $[MF_8]^{4-}$ System (*M* = Th - Bk)

Benjamin Scheibe, Michael Patzschke, Juliane März, Matthias Conrad, Florian Kraus

Eur. J. Inorg. Chem, **2020**, *39*, 3753-3759.
DOI: 10.1002/ejic.202000565

Siehe Abschnitt 7.9.

Durch Umsetzung von Neptunium(IV)-oxid mit Flusssäure wird ein grünes Neptunium(IV)-fluorid-Hydrat erhalten, welches umgesetzt mit gesättigter Ammoniumfluorid-Lösung, Einkristalle der Verbindung $(NH_4)_4[NpF_8]$ ergibt. Die Kristallstruktur der Verbindung wurde mit Einkristallstrukturanalyse aufgeklärt. Sie kristallisiert isotyp zu der Uranverbindung. In der Kristallstruktur liegen isolierte $[NpF_8]^{4-}$-Anionen vor, die entweder als ein verzerrtes quadratisches Antiprisma oder als ein zweifach überkapptes trigonales Prisma beschrieben werden können. Zu den NH_4^+-Kationen werden Wasserstoffbrückenbindungen ausgebildet. Quanten-chemische Gasphasenrechnungen für die $[MF_8]^{4-}$-Anionen mit *M* = Th bis Bk zeigen, dass die *M*−F-Bindungen ionisch sind und die Energieunterschiede verschiedener Ligandenanordnungen (würfelartig, quadratisch-antiprismatisch oder trigonal-dodekaedrisch) gering sind.

Beiträge der Autoren:

Die Publikation entstand in Kooperation mit der Abteilung Chemie der f-Elemente des Instituts für Ressourcenökologie am Helmholtz-Zentrum Dresden-Rossendorf und der Arbeitsgruppe Kraus. B. Scheibe entwickelte und erprobte die Darstellung von $(NH_4)_4[NpF_8]$, bestimmte die Kristallstruktur und analysierte und interpretierte die Ergebnisse. M. Patzschke führte die quantenchemischen Rechnungen durch, interpretierte die Ergebnisse und trug den entsprechenden Teil zum Manuskript bei. M. Conrad zeigte die Strukturverwandtschaft auf. B. Scheibe verfasste das Manuskript in Absprache mit den Coautoren. J. März koordinierte und F. Kraus leitete das Projekt.

5.3. Fluoridometallate(IV) des Neptuniums und Plutoniums − Unveröffentlichte Ergebnisse

5.3.1. Darstellung und Charakterisierung von NH_4PuF_5 und $TlMF_5$ (*M* = Np, Pu)

NH_4PuF_5: In dem PTFE-Einsatz (Modell A280AC3, *V* = 10 mL, Parr Instrument GmbH) eines Säureaufschlussgefäßes (Modell 4749, Parr Instrument GmbH) wurden 0,6 mg (2 µmol, 1 Äq.) $^{242}PuO_2$ und 45,5 mg (1,22 mmol, 610 Äq.) NH_4F in 0,2 mL 48%iger Flusssäure suspendiert. Das Säureaufschlussgefäß wurde verschlossen und auf einer Heizplatte für 20,5 Stunden auf circa 190°C erhitzt. Danach wurde die Heizplatte ausgeschaltet und das Säureaufschlussgefäß auf der Heizplatte auf Raumtemperatur abgekühlt. Im PTFE-Einsatz waren orange Kristalle gewachsen, welche mehrmals mit entionisiertem Wasser gewaschen und anschließend in perfluoriertes Öl transferiert wurden. Die Kristalle wurden unter einem Mikroskop begutachtet und ein oranger Kristall röntgenographisch untersucht. Es wurde die Zusammensetzung NH_4PuF_5 für den Kristall erhalten.

$TlNpF_5$: Es wurden 1,8 mg (6,7 µmol, 1 Äq.) $^{237}NpO_2$ und 23,4 mg (0,10 mmol, 15 Äq.) TlF in einem PTFE-Einsatz in 0,2 mL 48%iger Flusssäure suspendiert. Das verschlossene Säureaufschlussgefäß wurde auf einer Heizplatte für 68 Stunden auf circa 200°C erhitzt, die Heizplatte ausgeschaltet und das Gefäß auf der Heizplatte langsam auf Raumtemperatur abgekühlt. Es waren olivgrüne Kristalle gewachsen, welche mehrmals mit entionisiertem Wasser gewaschen und in perfluoriertes Öl transferiert wurden. Ein olivgrüner Kristall wurde röntgenographisch untersucht und die Zusammensetzung $TlNpF_5$ erhalten.

$TlPuF_5$: Es wurden 1,3 mg (4,7 µmol, 1 Äq.) $^{242}PuO_2$ und 10,5 mg (0,05 mmol, 11 Äq.) TlF in einem PTFE-Einsatz in 0,2 mL 48%iger Flusssäure suspendiert. Das verschlossene Säureaufschlussgefäß wurde für 46 Stunden auf circa 200°C erhitzt, die Heizplatte ausgeschaltet und das Gefäß auf der Heizplatte langsam auf Raumtemperatur abgekühlt. Es waren orange Kristalle gewachsen, welche mehrmals mit entionisiertem Wasser gewaschen und in perfluoriertes Öl transferiert wurden. Ein oranger Kristall wurde röntgenographisch untersucht und die Zusammensetzung $TlPuF_5$ erhalten. Die Bildung dieser Verbindungen kann mit Gleichung 74 beschrieben werden.

$$AF + PuO_2 + 4\,HF \longrightarrow AMF_5 + 2\,H_2O \qquad 74$$

A = NH_4 (M = Np), Tl (M = Np, Pu)

Ammoniumpentafluoridoplutonat(IV) und Thallium(I)-pentafluoridoneptunat(IV)- und -plutonat(IV) kristallisieren im β-NH_4UF_5-Typ in der monoklinen Raumgruppe $P2_1/c$ (Nr. 14) mit vier Formeleinheiten pro Elementarzelle, Pearson-Symbol $mP28$ und Wyckoff-Sequenz $14.e^7$ (ohne H-Atome im Falle von NH_4PuF_5).[334] $TlThF_5$ und $CsThF_5$ kristallisieren ebenfalls im β-NH_4UF_5-Typ.[334–337] Die entsprechenden Zirkonium- und Hafniumverbindungen NH_4MF_5 (M = Zr, Hf), $TlMF_5$ (M = Zr, Hf) und $RbHfF_5$ kristallisieren im $TlZrF_5$-Typ, welcher isopuntal zum β-NH_4UF_5-Typ ist, jedoch mit Koordinationszahl acht für die M(IV)-Atome.[338–341] Die Gitterparameter und Zellvolumina der hier dargestellten und untersuchten Verbindungen sind in Tabelle 27 aufgelistet. Ausgewählte kristallographische Daten, Details der Strukturbestimmungen sowie äquivalente isotrope und anisotrope Auslenkungsparameter sind in den Abschnitten 8.1.2.1 bis 8.1.2.3 aufgeführt.

Tabelle 27. Gitterparameter und Zellvolumina der isotypen Verbindungen NH_4MF_5 (M = U, Pu) und $TlMF_5$ (M = Th, Np, Pu).

Parameter	NH_4UF_5[335]	NH_4PuF_5	$TlThF_5$[336]	$TlNpF_5$	$TlPuF_5$
a / Å	7,785(2)	7,6965(5)	8,1128(5)	8,0218(4)	8,0129(17)
b / Å	7,1665(17)	7,0413(5)	7,2250(4)	7,0653(3)	7,0041(15)
c / Å	8,747(2)	8,6402(6)	8,8493(6)	8,7431(4)	8,676(3)
β / °	116,089(7)	115,982(2)	116,683(3)	117,1510(10)	116,966(6)
V / Å^3	438,27(19)	420,92(5	463,46(5)	440,92(4)	433,97(19)
T / K	296	100	296	293	289

Die Metallatome M(1) (M = Np, Pu) besetzen die allgemeine Lage 4e und sind von neun Fluoratomen in der Form eines dreifach überkappten trigonalen Prismas umgeben (Abbildung 46). Das Fluoratom F(5) ist terminal gebunden und die restlichen Fluoratome wirken μ_2-verbrückend zu weiteren Metallatomen. Die entsprechenden M−F-Abstände sind mit denen für NHF_4UF_5 und $TlThF_5$ berichteten in Tabelle 28 aufgelistet.

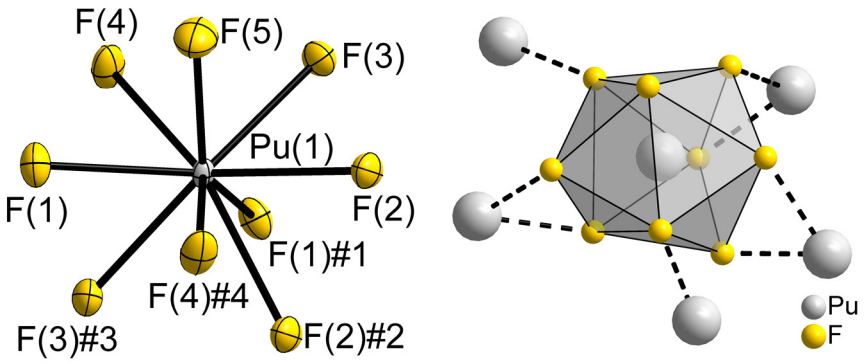

Abbildung 46. Ausschnitte aus der Kristallstruktur von $TlPuF_5$. Links ist die Umgebung des Plutoniumatoms dargestellt und rechts das Koordinationspolyeder mit umgebenden Plutoniumatomen. Links sind die Auslenkungsellipsoide mit 70% Aufenthaltswahrscheinlichkeit bei 289 K dargestellt. Rechts sind die Atome mit willkürlichen Radien abgebildet. Symmetrietransformationen: #1 2 − *x*, −1/2 + *y*, 3/2 − *z*; #2 2 − *x*, 1 −*y*, 1 − *z*; #3 2 − *x*, 1/2 + *y*, 3/2 − *z*; #4 *x*, 3/2 −*y*, −1/2 + *z*. Die Verbindungen NH_4PuF_5 und $TlNpF_5$ und kristallisieren isotyp zu $TlPuF_5$.

Tabelle 28. Vergleich der *M*−F-Abstände in NH_4MF_5 (*M* = U, Pu) und $TlMF_5$ (*M* = Th, Np, Pu) des *β*-NH_4UF_5-Typs.[334]

Verbindung	$d(M-F_{terminal})$ / Å	$d(M-\mu\text{-}F)$ / Å	*T* / K
NH_4UF_5[335]	2,181(3)	2,308(3)-2,407(3)	296
NH_4PuF_5	2,1689(16)	2,2806(16)-2,3583(15)	100
$TlThF_5$[336]	2,214(14)	2,365(9)-2,404(11)	296
$TlNpF_5$	2,161(2)	2,316(2)-2,395(2)	293
$TlPuF_5$	2,146(3)	2,300(2)-2370(2)	289

Die *M*−F-Abstände der terminal gebundenen Fluoratome sind signifikant kleiner als die *M*−μ_2-F-Abstände, was aufgrund der unterschiedlichen Koordinationszahlen der Fluoratome zu erwarten ist. Mit steigender Ordnungszahl nehmen die Atomabstände ab, was zum einen an der Actinoidenkontraktion (Atomradien: Th: 2,88, U: 2,83, Np: 2,81, Pu: 2,78 Å) liegt und im Falle der Ammoniumverbindungen auch zusätzlich durch unterschiedliche Messtemperaturen hervorgerufen wird.[330,342,343]

Die [MF_9]-Polyeder sind von fünf weiteren solcher Polyeder umgeben, mit denen sie entweder Ecken (2×) oder Kanten (3×) teilen und so zu leicht gewellten Schichten, welche parallel zu der *bc*-Ebene verlaufen, führen (Abbildung 47). Die Metallatome spannen dabei ein 3^2.4.3.4-Netz auf (Abbildung 48), welches häufig in Kristallstrukturen von Fluoridometallaten(IV), unter anderem im $LiUF_5$-Typ, $TlZrF_5$-Typ und KU_2F_9-Typ sowie in intermetallischen Verbindungen wie U_2Si_3 und $CuAl_2$ beobachtet wird.[338,344–348]

Das Anion kann mit der Niggli-Formel ${}^{2}_{\infty}\left[MF_{\frac{1}{1}}F_{\frac{8}{2}}\right]^{-}$ beschrieben werden und unterscheidet sich von dem im $TlUF_5$-Typ, in welchem ein komplexeres Anion der Form ${}^{2}_{\infty}\left[\langle UF_{\frac{2}{1}}F_{\frac{4}{2}}F_{\frac{3}{3}}\rangle_2 \langle UF_{\frac{2}{1}}F_{\frac{3}{2}}F_{\frac{4}{3}}\rangle\right]^{11/6-}$ vorliegt und ein $3^3.4^2$-Netz von den *M*(IV)-Atomen aufgespannt wird.[349]

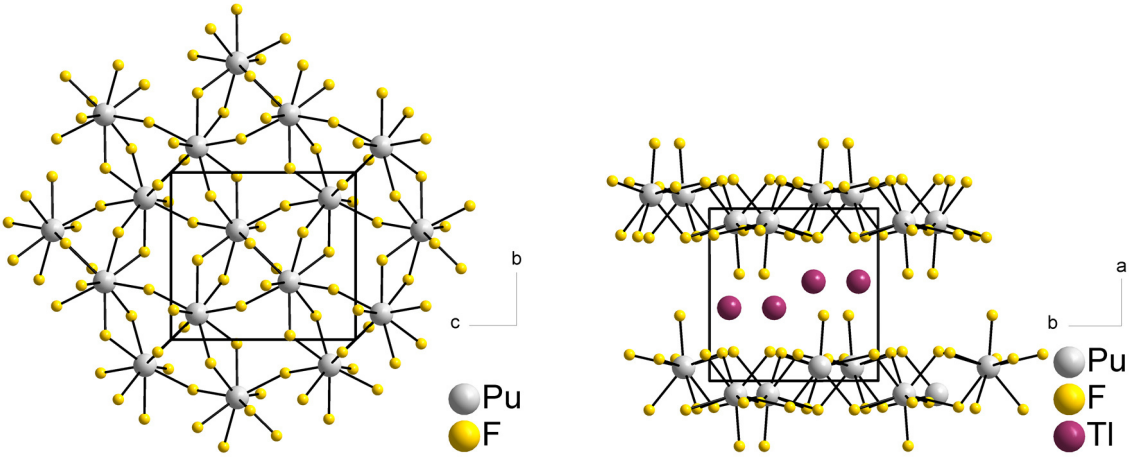

Abbildung 47. Kristallstruktur von $TlPuF_5$, projiziert entlang der *a*-Achse (links) oder der *c*-Achse (rechts). Die Atome sind mit willkürlichen Radien abgebildet. Die Verbindungen NH_4PuF_5 und $TlNpF_5$ kristallisieren isotyp zu $TlPuF_5$.

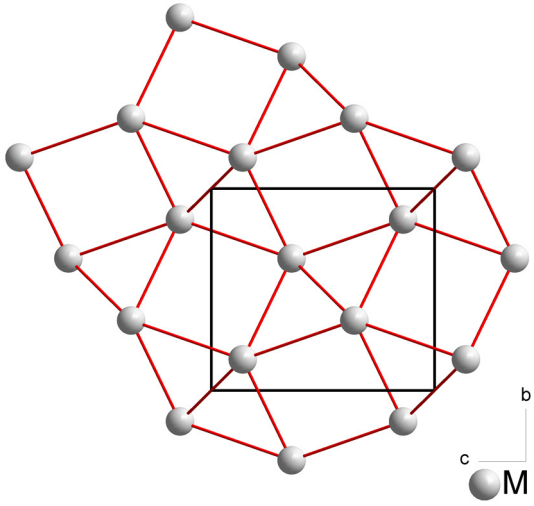

Abbildung 48. $3^2.4.3.4$-Netz, welches von den Metallatomen (*M* = Np, Pu) im $Tl\mathit{M}F_5$ parallel zur *bc*-Ebene aufgespannt wird.

Die Ammonium- oder Thallium(I)-Ionen besetzen eine allgemeine Lage (4*c*) und sind zwischen den ${}^{2}_{\infty}\left[MF_{\frac{1}{1}}F_{\frac{8}{2}}\right]^{-}$-Anionen angeordnet. Sie bilden ebenfalls ein 3^2.4.3.4-Netz aus (N−N- bzw. Tl−Tl-Kontakte).

Im Falle des Ammioniumions (Abbildung 49) werden N−H···F-Wasserstoffbrücken mit N−F-Abständen im Bereich von 2,747(3)-3,072(3) und N−H···F-Winkeln von 120(4)-152(4)°Å ausgebildet.

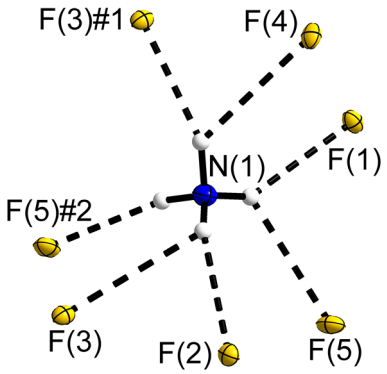

Abbildung 49. Wasserstoffbrückenbindungen der Form N−H···F des Ammoniumions in NH_4PuF_5. Die Auslenkungsellipsoide sind mit 70% Aufenthaltswahrscheinlichkeit bei 100 K dargestellt. Wasserstoffatome (weiß) sind isotrop mit willkürlichen Radien abgebildet. Symmetrietransformationen: #1 *x*, 1/2 − *y*, 1/2 + *z*; #2 −1 + *x*, *y*, *z*.

5.3.2. Darstellung und Charakterisierung von APu_2F_9 (*A* = Na, K)

Es wurden 1,3 mg (***A* = Na**, 4,7 µmol, 1 Äq.) und 1,2 mg (***A* = K**, 4,4 µmol, 1 Äq.) $^{242}PuO_2$ in zwei verschiedenen PTFE-Einsätzen vorgelegt und in je 0,1 mL 48%iger Bromwasserstoffsäure suspendiert. Die Säureaufschlussgefäße wurden verschlossen und auf einer Heizplatte für zwei Stunden auf circa 140°C erhitzt. Danach wurde die Heizplatte ausgeschaltet und die Säureaufschlussgefäße auf der Heizplatte auf Raumtemperatur abgekühlt. In den PTFE-Einsätzen war je ein blauvioletter Feststoff vorhanden. Zu den PTFE-Einsätzen wurden nun 5,8 mg (0,14 mmol, 30 Äq.) NaF oder 3,8 mg (0,065 mmol, 15 Äq.) KF, je 0,1 mL 48%ige Bromwasserstoffsäure und je 0,2 mL 48%ige Flusssäure gegeben. Die Säureaufschlussgefäße wurden wieder verschlossen und für 64 Stunden auf circa 200°C erhitzt. Danach wurde die Heizplatte ausgeschaltet und die Säureaufschlussgefäße auf der Heizplatte auf Raumtemperatur abgekühlt. In beiden Einsätzen waren orange Kristalle gewachsen, welche mehrmals mit entionisiertem Wasser gewaschen und anschließend in perfluoriertes Öl transferiert wurden. Die Kristalle wurden unter einem Mikroskop begutachtet und je ein oranger Kristall röntgenographisch untersucht. Es wurden die Zusammensetzungen $NaPu_2F_9$ und KPu_2F_9 für die Kristalle erhalten.

Ziel der Umsetzungen war Fluoridoplutonate(III) darzustellen, welche wie andere Plutonium(III)-Verbindungen, unter anderem PuF_3, violett sein sollten.[330,350] Die Reduktion von Plutonium höherer Oxidationsstufen zu Pu(III) mit Bromwasserstoffsäure wurde bereits in der Literatur beschrieben.[351] Während der hydrofluorothermalen Synthesen wurde das Plutonium vermutlich wieder oxidiert und orange Fluoridoplutonate(IV) isoliert. Die Bildung dieser Verbindungen kann mit den Gleichungen 75 bis 78 erklärt werden.

$$2\,PuO_2 + 8\,HBr \longrightarrow 2\,PuBr_3 + 4\,H_2O + Br_2 \qquad 75$$

$$PuBr_3 + 3\,HF \longrightarrow PuF_3 + 3\,HBr \qquad 76$$

$$O_2 + 4\,PuF_3 + 4\,HF \longrightarrow 4\,PuF_4 + 2\,H_2O \qquad 77$$

$$2\,PuO_2 + AF + 8\,HF \longrightarrow APu_2F_9 + 4\,H_2O \qquad 78$$

A = Na, K

Natrium- und Kaliumnonafluoridodiplutonat(IV) kristallisieren im KU_2F_9-Typ in der orthorhombischen Raumgruppe *Pnma* (Nr. 62) mit vier Formeleinheiten pro Elementarzelle, Pearson-Symbol *oP*48 und Wyckoff-Sequenz 62.d^5c^2. Weiterhin kristallisieren die Verbindungen NaM_2F_9 (M = U, Np) und KM_2F_9 (M = Th, U) im KU_2F_9-Typ.[323,327,352] Die Gitterparameter und Zellvolumina der hier dargestellten und untersuchten Verbindungen sowie der in der Literatur berichteten isotypen Actinoidverbindungen sind in Tabelle 29 aufgelistet. Ausgewählte kristallographische Daten, Details der Strukturbestimmungen sowie äquivalente isotrope und anisotrope Auslenkungsparameter sind in den Abschnitten 8.1.2.4 und 8.1.2.5 aufgeführt.

Tabelle 29. Gitterparameter und Zellvolumina der isotypen Verbindungen NaM_2F_9 (M = U, Np, Pu) und KM_2F_9 (M = Th, U, Pu) des KU_2F_9-Typs.[353]

Parameter	NaU_2F_9[327]	$NaNp_2F_9$[352]	$NaPu_2F_9$
a / Å	8,6362(2)	8,617(5)	8,5121(4)
b / Å	11,1390(3)	11,274(9)	10,9891(5)
c / Å	6,9996(2)	6,955(4)	6,8845(3)
V / Å³	673,35(3)	676	643,98(5)
T / K	300	Raumtemperatur	100
Parameter	KTh_2F_9[327]	KU_2F_9[323]	KPu_2F_9
a / Å	8,8479(13)	8,6923(6)	8,6013(7)
b / Å	11,6515(17)	11,4542(8)	11,3374(9)
c / Å	7,1757(11)	7,0132(5)	6,9113(5)
V / Å³	739,75(19)	698,26(8)	673,97(9)
T / K	302	100	100

Die Plutoniumatome Pu(1) besetzen die allgemeine Lage 8*d* und sind von neun Fluoratomen in der Form eines verzerrten dreifach überkappten trigonalen Prismas umgeben, siehe Abbildung 50. Alle Fluoratome sind μ_2-verbrückend zwischen *M*(IV)-Atomen, die *M*−F-Abstände der isotypen Verbindungen NaM_2F_9 (M = U, Np, Pu) und KM_2F_9 (M = Th, U, Pu) sind in Tabelle 30 aufgelistet. Die Abstände für die Natrium- und Kaliumsalze sind vergleichbar und in der jeweiligen Reihe wird eine Abnahme der *M*−F-Abstände mit steigender Ordnungszahl aufgrund der Actinoidenkontraktion beobachtet.[330,342,343] Zusätzlich werden auch die unterschiedlichen Messtemperaturen einen Einfluss auf die Abstände haben.

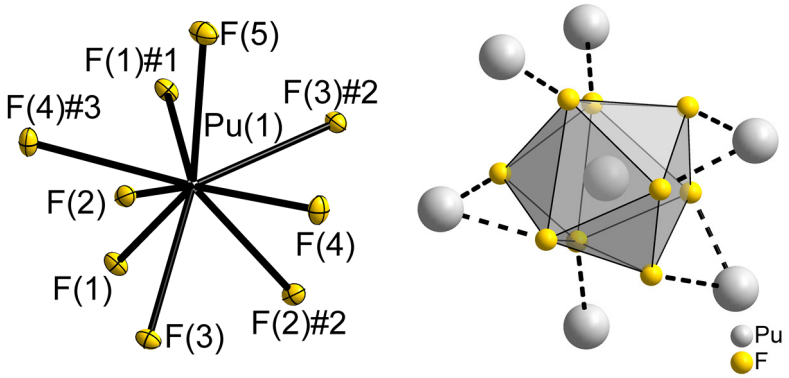

Abbildung 50. Ausschnitte aus der Kristallstruktur von KPu_2F_9. Links ist die Umgebung des Plutoniumatoms dargestellt und rechts das Koordinationspolyeder mit umgebenden Plutoniumatomen. Links sind die Auslenkungsellipsoide mit 70% Aufenthaltswahrscheinlichkeit bei 100 K dargestellt. Rechts sind die Atome mit willkürlichen Radien abgebildet. Symmetrietransformationen: #1 1 − *x*, 1 − *y*, −*z*; #2 1/2 − *x*, 1 −*y*, −1/2 + *z*; #3 1/2 + *x*, *y*, 1/2 − *z*. Die Verbindung $NaPu_2F_9$ kristallisiert isotyp zu KPu_2F_9.

Tabelle 30. Vergleich der *M*−F-Abstände in NaM_2F_9 (*M* = U, Np, Pu) und KM_2F_9 (*M* = Th, U, Pu) des KU_2F_9-Typs.[353]

Verbindung	$d(M-F_{verbrückend})$ / Å	*T* / K
NaU_2F_9[327]	2,2478(2)-2,418(2)	300
$NaNp_2F_9$[352]	2,260(5)-2,371(5)	Raumtemperatur
$NaPu_2F_9$	2,22193(14)-2,3710(15)	100
KTh_2F_9[327]	2,3252(4)-2,4311(19)	302
KU_2F_9[323]	2,2879(2)-2,385(3)	100
KPu_2F_9	2,2707(2)-2,3475(18)	100

Die $[PuF_9]$-Polyeder sind von sechs weiteren Polyedern umgeben, mit denen sie entweder eine Ecke (3×) oder eine Kante (3×) teilen. Es werden Schichten parallel zur *ac*-Ebene ausgebildet, welche jeweils untereinander verbunden sind und so resultiert insgesamt eine Netzwerkstruktur, welche mit der Niggli-Formel ${}^{3}_{\infty}\left[MF_{\frac{9}{2}}\right]^{1/2-}$ beschrieben werden kann (Abbildung 51). Wie auch im *β*−NH_4UF_5-Typ, wird von den *M*(IV)-Atomen ein $3^2.4.3.4$-Netz parallel zu der *ac*-Ebene aufgespannt (Abbildung 52).[334] Im Vergleich zum *β*−NH_4UF_5-Typ ist der „Kondensationsgrad“ der $[MF_9]$-Polyeder jedoch größer, da alle Fluoratome verbrückend sind.[334]

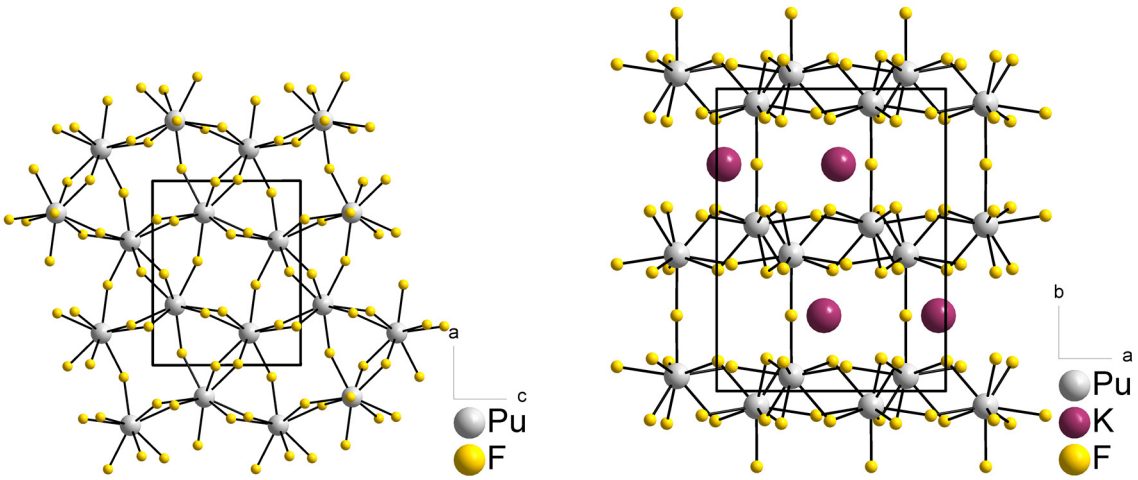

Abbildung 51. Kristallstruktur von KPu_2F_9, projiziert entlang der *b*-Achse (links) oder der *c*-Achse (rechts). Die Atome sind mit willkürlichen Radien abgebildet. Die Verbindung $NaPu_2F_9$ kristallisiert isotyp zu KPu_2F_9.

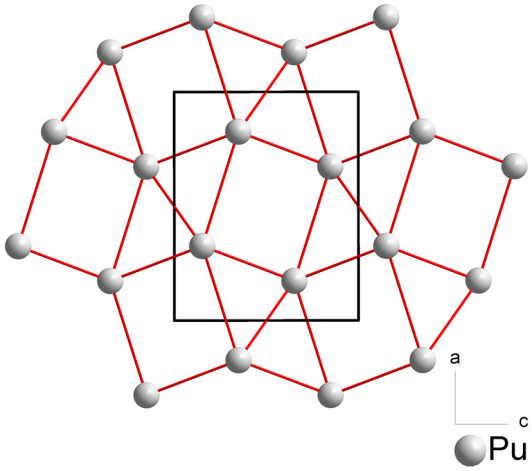

Abbildung 52. 3^2.4.3.4-Netz, welches von den Plutoniumatomen in APu_2F_9 (*A* = Na, K) parallel zur *ac*-Ebene aufgespannt wird.

Die Kationen *A*(1) (*A* = Na, K) besetzen die spezielle Lage 4*c* (Lagesymmetrie *.m.*) und sind von elf Fluoratomen in der Form eines einfach überkappten pentagonalen Prismas umgeben. Die Kationen sind von zehn Plutoniumatomen verzerrt pentagonal-prismatisch und die Plutoniumatome von fünf Kationen verzerrt pentagonal-pyramidal mit *A*−Pu-Abständen von 3,94-4,42 (*A* = Na) und 4,10-4,40 Å (*A* = K) umgeben. Die Kationen sind von vier weiteren tetraedrisch mit *A*−*A*-Abständen von 4,44-5,95 (*A* = Na) und 4,58-6,00 Å (*A* = K) umgeben. Die Plutoniumatome sind von fünf weiteren in der Form einer verzerrten pentagonalen Pyramide mit Pu−Pu-Abständen von 3,81-4,44 (*A* = Na) und 3,82-4,54 Å (*A* = K) umgeben.

5.4. Fluoridouranate(V) − Unveröffentlichte Ergebnisse

5.4.1. Darstellung und Charakterisierung von $Sr[UF_5(HF_2)_2]$

Ein FEP-Rohr wurde im Handschuhkasten mit 101,4 mg (0,81 mmol, 1 Äq.) SrF_2 und 268,9 mg (0,81 mmol, 1 Äq.) *β*-UF_5 beschickt und mit einem Edelstahlfaltenbalgventil verschlossen. An der HF-Anlage wurden etwa 7 mL aHF auf das Gemenge unter Stickstoffkühlung kondensiert. Das Reaktionsgefäß wurde auf Raumtemperatur erwärmt, wobei sich die Feststoffe rasch unter Bildung einer türkisenen Lösung auflösten. Das Lösungsmittel wurde langsam im Vakuum entfernt und es blieben türkise Kristalle zurück, welche im Handschuhkasten isoliert wurden (340 mg). Ein Teil dieser wurde in perfluoriertem Öl suspendiert und unter dem Mikroskop selektiert. Einer der Kristalle wurde röntgenographisch untersucht und die Zusammensetzung $Sr[UF_5(HF_2)_2]$ erhalten. Die Bildung der Verbindung kann mit Gleichung 79 erklärt werden.

$$SrF_2 + UF_5 + 2\,HF \longrightarrow Sr[UF_5(HF_2)_2] \qquad 79$$

Strontiumpentafluoridobis(hydrogendifluorido)uranat(V) kristallisiert in der monoklinen Raumgruppe $P2_1/c$ (Nr. 14), mit a = 5,9752(5) Å, b = 11,1917(9) Å, c = 10,3409(9) Å, β = 95,649(7)°, V = 688,17(10) Å^3, mit vier Formeleinheiten pro Elementarzelle, Pearson-Symbol *mP*44 und Wyckoff-Sequenz 14.e^{11} (beide ohne Wasserstoffatome). Ausgewählte kristallographische Daten, Details der Strukturbestimmung sowie äquivalente isotrope und anisotrope Auslenkungsparameter sind im Abschnitt 8.1.3.1 aufgeführt.

Das Uranatom U(1) besetzt die allgemeine Lage 4*e* und ist von sieben Fluoratomen in der Form eines einfach überkappten trigonalen Prismas umgeben (Abbildung 53). Das Koordinationspolyeder des Uranatoms ist somit ähnlich zu dem des Uranatoms in $Sr[U_2F_{12}]$.[354,355] Zwei der Fluoratome, F(1) und F(3), sind je von einem weiteren Fluoratom, F(2) oder F(4), mit Abständen von 2,406(7) und 2,493(7) Å umgeben. Dies spricht für das Vorliegen von $[HF_2]^-$-Anionen, welche auch für den Ladungsausgleich benötigt werden.

Die F···F-Abstände sind etwas länger als in Bifluoridsalzen mit Alkali- oder Erdalkalimetallkationen ($Na[HF_2]$: 2.277(1) Å bei 140 K, $Rb[HF_2]$: 2.280(4) Å bei 150 K, $Ca[HF_2]_2$: 2,283(2) Å bei 200 K), jedoch vergleichbar mit Übergangsmetallkomplexen in denen $[HF_2]^-$-Anionen als Liganden vorliegen ($[Ru(P(CH_3)_3)_4(HF_2)_2]$: 2,323(8) und 2,329(8) Å bei 150 K, $[Ir(HF_2)(cod)(I^iPr)]$ H_2O·(cod: 1,5-Cyclooctadien, I^iPr: 1,3-Diisopropylimidazol-2-yliden): 2,457(6) und 2,587(6) Å bei 93 K).[356–359] Weitere Übergangsmetallverbindungen mit $[HF_2]^-$-Liganden sind in einem Übersichtsartikel zusammengefasst.[360]

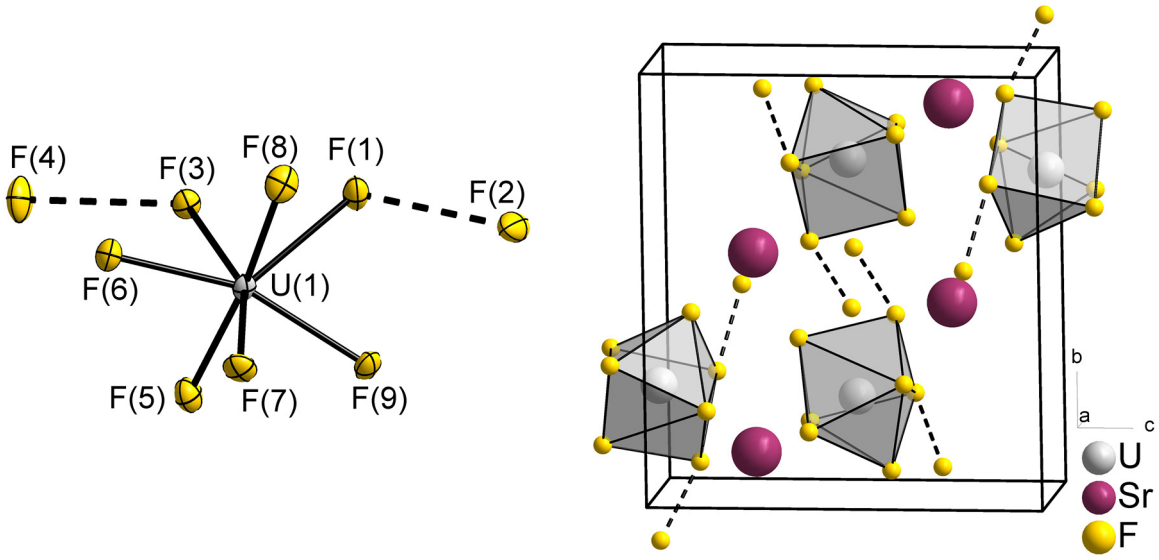

Abbildung 53. Ausschnitte aus der Kristallstruktur von $Sr[UF_5(HF_2)_2]$. Links ist das $[UF_5(HF_2)_2]^-$-Anion dargestellt und rechts ein Strukturausschnitt mit der ersten Koordinationssphären der Uranatome als graue Polyeder. Links sind die Auslenkungsellipsoide mit 70% Aufenthaltswahrscheinlichkeit bei 100 K dargestellt. Rechts sind die Atome mit willkürlichen Radien abgebildet.

Die U−F-Abstände der terminal gebundenen F-Atome liegen im Bereich von 2,072(5)-2,113(5) Å und stimmen gut mit denen anderer Fluoridouranate(V) wie $Cs[UF_6]$ (2,057(6) Å, Temperatur nicht angegeben), $NO[UF_6]$ (2,0671(9) Å bei 100 K) oder $(PPh_4)[UF_6]$ (2,0650(2) und 2,0768(4) Å bei 20 K) überein.[258,361,362] Im Vergleich dazu sind die Abstände zwischen den U-Atomen und den F-Atomen der $[HF_2]^-$-Anionen mit 2,198(5) und 2,314(5) Å deutlich größer, was vermutlich auf die höhere Koordinationszahl und die verringerte Ladungsdichte dieser Fluoratome zurückgeführt werden kann.

Das Strontiumatom Sr(1) besetzt ebenfalls die allgemeine Lage 4*e* und ist von neun Fluoratomen in der Form eines dreifach überkappten trigonalen Prismas mit Sr−F-Abständen von etwa 2,47 bis 2,63 Å umgeben. Die Strontiumatome sind von sechs Uranatomen trigonal-prismatisch und die Uranatome von sechs Strontiumatomen oktaedrisch mit Sr−U-Abständen von etwa 4,02-4,69 Å umgeben. Die Strontiumatome sind von zwölf weiteren Strontiumatomen antikuboktaedrisch mit Sr−Sr-Abständen von circa 5,83-7,06 Å umgeben. Die Uranatome sind ebenfalls von zwölf weiteren Uranatomen mit U−U-Abständen von 5,18-7,56 Å antikuboktaedrisch umgeben.

Das Infrarotspektrum von festem $Sr[UF_5(HF_2)_2]$ ist in Abbildung 54 dargestellt. Es sind Banden bei 2408, 1850 und 1560 cm^{-1} beobachtbar, letztere kann den asymmetrischen Streckschwingungen der $[HF_2]^-$-Liganden zugeordnet werden und die anderen beiden stellen vermutlich Kombinationsbanden dar.[360,363,364] Die Banden bei 1220, 1133 und 1031 cm^{-1} können den Deformationsschwingungen der $[HF_2]^-$-Liganden zugeordnet werden.[360,363,364] Im Vergleich zu den Infrarotspektren der salzartigen Bifluoride $Na[HF_2]$ und $K[HF_2]$ liegt keine große Verschiebung der Bandenlagen vor.[363] Die Banden bei 598, 535, 516, 466 und 439 können den U−F-Streckschwingungen zugeordnet werden und die Lagen sind vergleichbar mit denen von Hexafluoridouranaten(V) wie $Li[UF_6]$ (515 cm^{-1}) und $NO[UF_6]$ (528 und 479 cm^{-1}).[258,365]

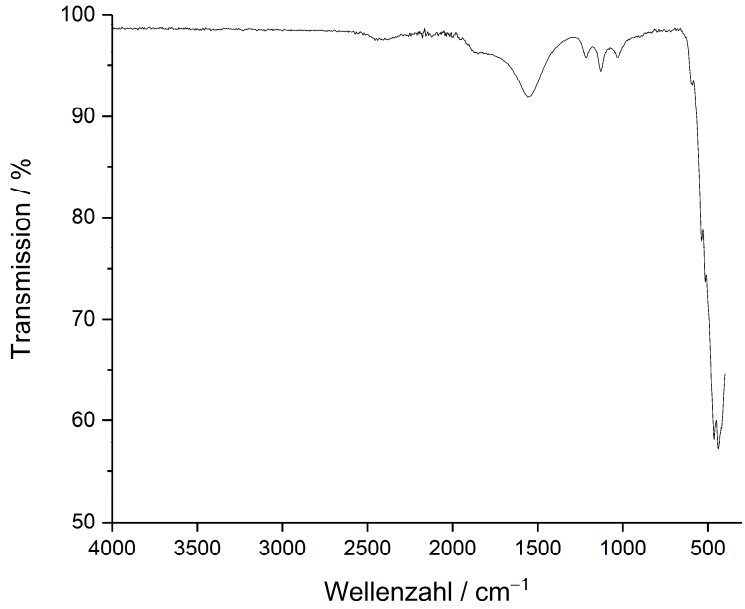

Abbildung 54. Infrarotspektrum von festem $Sr[UF_5(HF_2)_2]$.

5.4.2. Darstellung und Charakterisierung von $Ba(HF)_2U_2F_{12}$

Ein FEP-Rohr wurde im Handschuhkasten mit 14,0 mg (0,08 mmol, 1 Äq.) BaF_2, 54,0 mg (0,16 mmol, 2 Äq.) *β*-UF_5 und 55,0 mg (0,32 mmol, 4 Äq.) XeF_2 beschickt und mit einem Edelstahlfaltenbalgventil verschlossen. An der HF-Anlage wurden etwa 4 mL aHF auf das Gemenge unter Stickstoffkühlung kondensiert. Das Reaktionsgefäß wurde auf Raumtemperatur erwärmt, wobei sich die Lösung schwach bläulich färbte und die Feststoffe zunächst unverändert aussahen. Die Lösung hat sich nach etwa 30 Minuten bei Raumtemperatur entfärbt, wobei gelbe Kristalle gewachsen sind. Der Großteil des Lösungsmittels wurde im Vakuum entfernt, ein Teil der Kristalle isoliert und in perfluoriertem Öl suspendiert. Unter dem Mikroskop wurden die Kristalle selektiert, wobei zwei verschiedene Arten vorlagen, farblose und gelbe. Die röntgenographische Untersuchung zeigte, dass neben XeF_2 (farblos), eine bisher unbekannte Verbindung vorlag, für die die Zusammensetzung $Ba(HF)_2U_2F_{12}$ erhalten wurde. Die Bildung dieser Verbindung kann mit Gleichung 80 erklärt werden.

$$BaF_2 + 2\,UF_5 + 2\,HF \longrightarrow Ba(HF)_2U_2F_{12} \qquad 80$$

Bis(hydrogenfluorid)bariumdodecafluoridodiuranat(V) kristallisiert in der orthorhombischen Raumgruppe *Pnma* (Nr. 62), mit a = 8,5422(2) Å, b = 12,9933(5) Å, c = 9,5306(3) Å, V = 688,17(10) Å^3, mit vier Formeleinheiten pro Elementarzelle, Pearson-Symbol *oP*68 und Wyckoff-Sequenz 62.d^7c^3 (beide ohne Wasserstoffatome). Ausgewählte kristallographische Daten, Details der Strukturbestimmung sowie äquivalente isotrope und anisotrope Auslenkungsparameter sind im Abschnitt 8.1.3.2 aufgeführt.

Das Uranatom U(1) besetzt die allgemeine Lage 8*d* und ist von acht Fluoratomen in der Form eines zweifach überkappten trigonalen Prismas umgeben, siehe Abbildung 55. Vier der Fluoratome sind μ_2-verbrückend zwischen Uranatomen und wenn nur zwei dieser berücksichtigt werden, F(1) und F(1)#1, so wird ein $[U_2F_{12}]^{2-}$-Anion ähnlich zu dem im $Sr[U_2F_{12}]$ erhalten.[354,355] Die U−F-Abstände der terminal gebundenen Fluoratome liegen im Bereich von 2,047(4) bis 2,075(4) Å, die der μ_2-verbrückenden im Bereich von 2,114(4)-2,638(3) Å. Der U(1)−F(3)#2-Abstand ist mit 2,638(3) Å dabei für μ_2-verbrückende Fluoratome besonders groß.

Im Vergleich betragen die U−F-Abstände im NO[UF_6] 2,0671(9) Å bei 100 K und im Sr[U_2F_{12}] 2,079(10) und 2,081(4) Å für die terminalen und 2,281(4) Å für die μ_2-verbrückenden Fluoratome bei 100 K.[258,354,355]

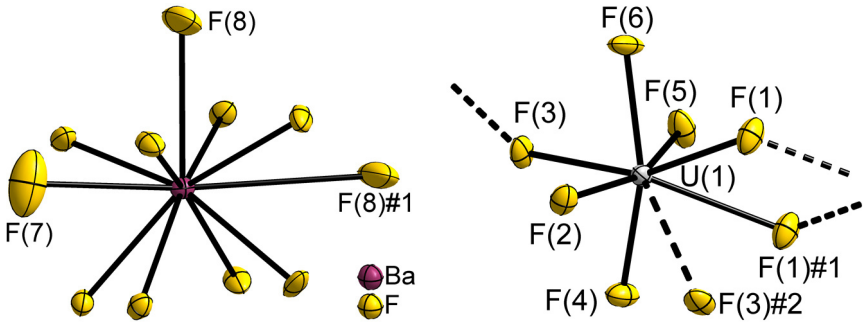

Abbildung 55. Ausschnitte aus der Kristallstruktur von $Ba(HF)_2U_2F_{12}$. Links ist die Umgebung des Bariumkations dargestellt und rechts die Umgebung des Uranatoms. Die Auslenkungsellipsoide sind mit 70% Aufenthaltswahrscheinlichkeit bei 100 K dargestellt. Gestrichelte Bindungen stehen für Bindungen zu weiteren Uranatomen der verbrückenden Fluoratome. Symmetrietransformationen (links): #1 1/2 + *x*, 1/2 − *y*, 3/2 − *z*; (rechts): #1 1 − *x*, 1 − *y*, 1 − *z*; #2 1/2 + *x*, *y*, 1/2 − *z*.

Die Berücksichtigung aller Fluoratome führt zur entsprechenden Koordinationszahl acht und einem komplexen Anion mit Schichtstrukturmotiv parallel zu der *ac*-Ebene (Abbildung 56). Das Anion kann mit der Niggli-Formel ${}^{2}_{\infty}\left[UF_{\frac{4}{1}}F_{\frac{4}{2}}\right]^{-}$ beschrieben werden. Die Uranatome spannen dabei ein 3^2.4.3.4-Netz auf in der *ac*-Ebene auf. Es stellt das erste komplexere Fluoridouranat(V) mit einem Schichtstrukturmotiv dar, da vorher beschriebene Verbindungen nur isolierte $[UF_6]^-$- oder $[U_2F_{12}]^{2-}$-Anionen oder strangartige ${}^{1}_{\infty}\left[UF_{\frac{4}{1}}F_{\frac{4}{2}}\right]^{-}$-Anionen enthielten.[258,322,354,355,361,362,366]

Das Bariumatom Ba(1) besetzt die spezielle Lage 4*c* (Lagesymmetrie .*m*.) und ist von elf Fluoratomen in der Form eines dreifach überkappten Würfels umgeben. Die Bariumatome befinden sich dabei zwischen den ${}^{2}_{\infty}\left[UF_{\frac{4}{1}}F_{\frac{4}{2}}\right]^{-}$-Schichten. Die Ba−F-Abstände liegen im Bereich von 2,671(4) bis 2,848(8) Å. Die Auslenkungsellipsoide der Fluoratome F(7) und F(8) sind dabei deutlich größer als die der anderen Fluoratome, welche zusammen mit für den Ladungsausgleich nötigen Wasserstoffatome das Vorliegen von an das Bariumatom gebundene HF-Liganden wahrscheinlich macht. Die Ba(1)−F(7)- und Ba(1)−F(8)-Abstände betragen dabei 2,796(8) und 2,848(8) Å.

Verbindungen, in denen Fluorwasserstoff als Ligand für Erdalkalimetallkationen wirkt, wurden bereits beschrieben, unter anderem $Sr(HF)_3[TaF_6]_2$, $Sr(HF)[BF_4]_2$ und $Ba(HF)[MF_6]_2$ (M = As, Sb).[367–369] In $Ba(HF)[AsF_6]_2$ beträgt der Ba−FH-Abstand 2,629(6) Å und in der Sb-Verbindung 2,618(4) Å, jeweils bei 200 K und Koordinationszahl zehn für die Ba-Atome.[367]

Die Bariumatome sind von weiteren Bariumatomen mit Ba−Ba-Abständen von 4,29-4,81 Å oktaedrisch umgeben. Eine Ähnlichkeit zum CsCl-Typ kann aufgezeigt werden, wenn die Bariumatome und die „verknüpften $[U_2F_{12}]^{2-}$-Anionen“ des ${}^{2}_{\infty}\left[UF_{\frac{4}{1}}F_{\frac{4}{2}}\right]^{-}$-Anions betrachtet werden. Für die Bariumatome und die Schwerpunkte der „$[U_2F_{12}]^{2-}$-Anionen“ liegt so eine Anordnung wie für die Cs- und Cl-Atome vor, mit Abständen von 5,24-6,04 Å.[276]

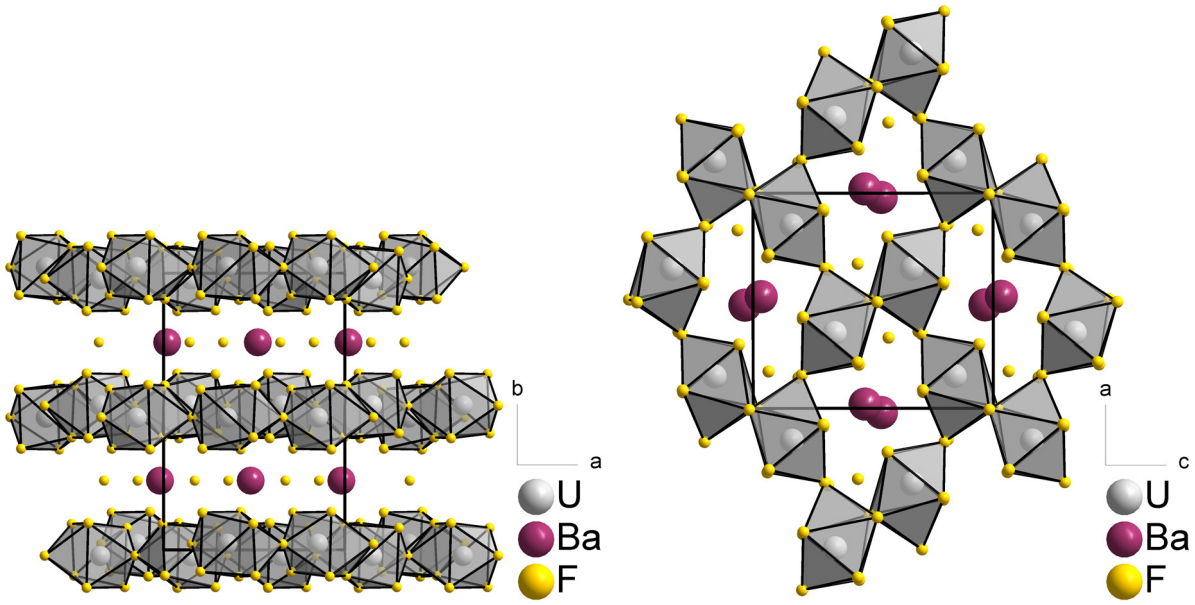

Abbildung 56. Kristallstruktur von $Ba(HF)_2U_2F_{12}$, projiziert entlang der *c*-Achse (links) oder der *b*-Achse (rechts). Die ersten Koordinationssphären der Uranatome sind als graue Polyeder dargestellt. Die Atome sind mit willkürlichen Radien abgebildet.

5.4.3. Darstellung und Charakterisierung von $(N_2H_6)U_2F_{10}(HF_2)_2$

Ein PFA-Rohr wurde mit 23,98 mg (0,23 mmol, 1 Äq.) $N_2H_6Cl_2$ beschickt, mit einem Edelstahlfaltenbalgventil verschlossen und an der HF-Anlage mehrfach sekuriert. Es wurden etwa 0,5 mL aHF auf den Feststoff unter Stickstoffkühlung kondensiert und das Reaktionsgefäß auf Raumtemperatur erwärmt. Nach etwa zehn Minuten bei Raumtemperatur wurden flüchtige Bestandteile im Vakuum entfernt, woraufhin ein farbloser Feststoff zurückblieb. Im Handschuhkasten wurden 152,50 mg (0,46 mmol, 2 Äq.) β-UF_5 zugegeben und an der HF-Anlage etwa 2 mL aHF auf das Gemenge unter Stickstoffkühlung kondensiert. Das Reaktionsgefäß wurde auf Raumtemperatur erwärmt, wobei sich die Feststoffe unter Bildung einer türkisenen Lösung auflösten. Das Reaktionsgefäß wurde dann bei −37 °C gelagert, woraufhin hellblaue Kristalle nach einigen Stunden wuchsen. Ein Teil der Kristalle wurde bei tiefen Temperaturen isoliert und präpariert. Ein Kristall wurde röntgenographisch untersucht und es wurde die Zusammensetzung $(N_2H_6)U_2F_{10}(HF_2)_2$ für diesen erhalten. Die Bildung der Verbindung kann mit den Gleichungen 81 und 82 erklärt werden.

$$N_2H_6Cl_2 + 2\,HF \longrightarrow N_2H_6F_2 + 2\,HCl \qquad 81$$

$$N_2H_6F_2 + 2\,UF_5 + 2\,HF \longrightarrow (N_2H_6)U_2F_{10}(HF_2)_2 \qquad 82$$

Hydrazinium(2+)-decafluoridobishydrogendifluoridodiuranat(V) kristallisiert in der monoklinen Raumgruppe *C*2/*c* (Nr. 15), mit a = 16,1264(8) Å, b = 9,7986(5) Å, c = 8,4047(4) Å, β = 118,530(2)°, V = 1166,81(10) Å^3, mit vier Formeleinheiten pro Elementarzelle, Pearson-Symbol *mS*72 und Wyckoff-Sequenz 15.f^9 (beide ohne Wasserstoffatome). Ausgewählte kristallographische Daten, Details der Strukturbestimmung sowie äquivalente isotrope und anisotrope Auslenkungsparameter sind im Abschnitt 8.1.3.3 aufgeführt.

Das Uranatom U(1) besetzt die allgemeine Lage 8*f* und ist von acht Fluoratomen in der Form eines zweifach überkappten trigonalen Prismas umgeben (Abbildung 57). Das Fluoratom F(1) gehört dabei zu einem $[HF_2]^-$-Anion, mit einem F(1)−F(7)-Abstand von 2,4731(14) Å, einem F(7)−H-Abstand von 0,76(4) Å, einem F(1)···H−Abstand von 1,72(4) Å sowie einem F(1)−H−F(7)-Winkel von 170(4)°. Die F···F-Abstände sind etwas länger als in Bifluoridsalzen mit Alkali- oder Erdalkalimetallkationen ($Na[HF_2]$: 2.277(1) Å bei 140 K, $Rb[HF_2]$: 2.280(4) Å bei 150 K, $Ca[HF_2]_2$: 2,283(2) Å bei 200 K), jedoch vergleichbar mit denen in Übergangsmetallkomplexen mit $[HF_2]^-$-Liganden ($[Ru(P(CH_3)_3)_4(HF_2)_2]$: 2,323(8) und 2,329(8) Å bei 150 K, $[Ir(HF_2)(cod)(I^iPr)]\ H_2O$·(cod: 1,5-Cyclooctadien, I^iPr: 1,3-Diisopropylimidazol-2-yliden): 2,457(6) und 2,587(6) Å bei 93 K).[356–359] Sie stimmen jedoch gut mit denen im $[UF_5(HF_2)_2]^{2-}$-Anion von 2,406(7) und 2,493(7) Å bei 100 K überein (Abschnitt 5.4.1).

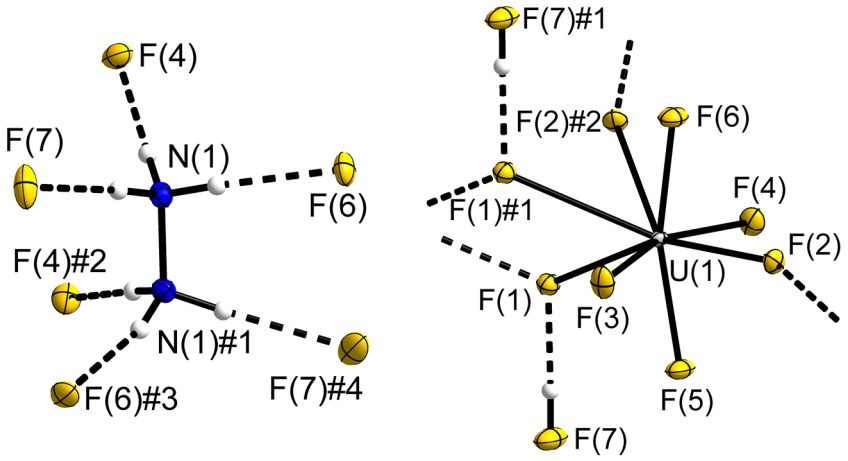

Abbildung 57. Ausschnitte aus der Kristallstruktur von $(N_2H_6)U_2F_{10}(HF_2)_2$. Links ist das Hydrazinium(2+)-Kation dargestellt und rechts die Umgebung des Uranatoms. Die Auslenkungsellipsoide sind mit 70% Aufenthaltswahrscheinlichkeit bei 100 K dargestellt. Wasserstoffatome (weiß) sind isotrop mit willkürlichen Radien abgebildet. Gestrichelte Bindungen stehen für Wasserstoffbrückenbindungen der Formen F−H···F und N−H···F oder Bindungen zu weiteren Uranatomen der verbrückenden Fluoratome. Symmetrietransformationen (links): #1 −*x*, *y*, 1/2 − *z*; #2 −1/2 + *x*, 1/2 + *y*, −1 + *z*; #3 −*x*, 1 − *y*, 1 − *z*; #4 1/2 − *x*, 3/2 − *y*, 1 − *z*; (rechts): #1 1/2 − *x*, 3/2 − *y*, 2 − *z*; #2 *x*, 1 − *y*, 1/2 + *z*.

Die Wasserstoffbrückenbindung im $[HF_2]^-$-Anion in $(N_2H_6)U_2F_{10}(HF_2)_2$ ist aufgrund der unterschiedlichen H−F-Abstände asymmetrisch, symmetrische Wasserstoffbrückenbindungen werden unter anderem in $A[HF_2]$ (A = Li, Na, K, NH_4) beobachtet.[356,370–372] Asymmetrische Wasserstoffbrückenbindungen wurden weiterhin in $Rb[HF_2]$ und einer Vielzahl von Verbindungen, in denen $[HF_2]^-$-Anionen als Liganden auftreten, beobachtet.[356,360,373]

Die U−F-Abstände der terminal gebundenen Fluoratome liegen im Bereich von 2,0390(10) bis 2,0819(9) Å, die der μ_2-verbrückenden betragen 2,1531(9) und 2,5040(9) Å und die der zum $[HF_2]^-$-Anion gehörenden 2,2700(9) und 2,5971(9) Å. Die U−μ_2-F···HF-Abstände sind etwas länger als die der anderen μ_2-verbrückenden Fluoratome, was mit der höheren Koordinationszahl und der Wechselwirkung des Fluoratoms mit dem HF-Molekül erklärt werden kann. Weiterhin sind die μ_2-verbrückenden Fluoratome asymmetrisch verbrückend zwischen Uranatomen, mit einem kleinen und einem deutlich längeren Abstand.

Die Abstände der terminal gebundenen Fluoratome stimmen mit denen in $Cs[UF_6]$ (2,057(6) Å, Temperatur nicht angegeben), $NO[UF_6]$ (2,0671(9) Å bei 100 K) oder $(PPh_4)[UF_6]$ (2,0650(2) und 2,0768(4) Å bei 20 K) überein.[258,361,362] Im Vergleich dazu stimmen die kleineren Abstände der μ_2-verbrückenden Fluoratome mit dem im $Sr[U_2F_{12}]$ (2,281(4) Å bei 100 K) überein, jedoch liegt eine symmetrische Verbrückung der Fluoratome vor.[354,355]

Das Anion kann auch mit der Niggli-Formel ${}^{2}_{\infty}\left[UF_{\frac{4}{1}}F_{\frac{2}{2}}(HF_2)_{\frac{2}{2}}\right]^-$ beschrieben werden, wobei die Schichten parallel zur *bc*-Ebene angeordnet sind (Abbildung 58). Die Uranatome spannen dabei ein $3^2.4.3.4$-Netz auf. Zwischen den Schichten befinden sich die Hydrazinium(2+)-Kationen, mit dem N(1)-Atom auf der allgemeinen 8*f*-Lage. Der der N−N-Abstand beträgt 1,446(3) Å und stimmt gut mit denen in Salzen wie $(N_2H_6)Cl_2$ (1,4302(10) Å bei 291 K), $(N_2H_6)[SiF_6]$ (1,428(2) Å bei Raumtemperatur), $(N_2H_6)[SbF_6]_2$ (1,457(8) Å bei 150 K) und $(N_2H_6)[Sb_2F_{11}]_2$ (1,439(8) Å bei 150 K) überein.[374–376] Das N_2H_6-Kation liegt in ekliptischer Konformation vor, welche auch für die Kationen im $(N_2H_6)[SbF_6]_2$, $(N_2H_6)_2[SnF_6]F_2$ und $(N_2H_6)_2[TiF_6]F_2$ beobachtet wurde.[376–378]

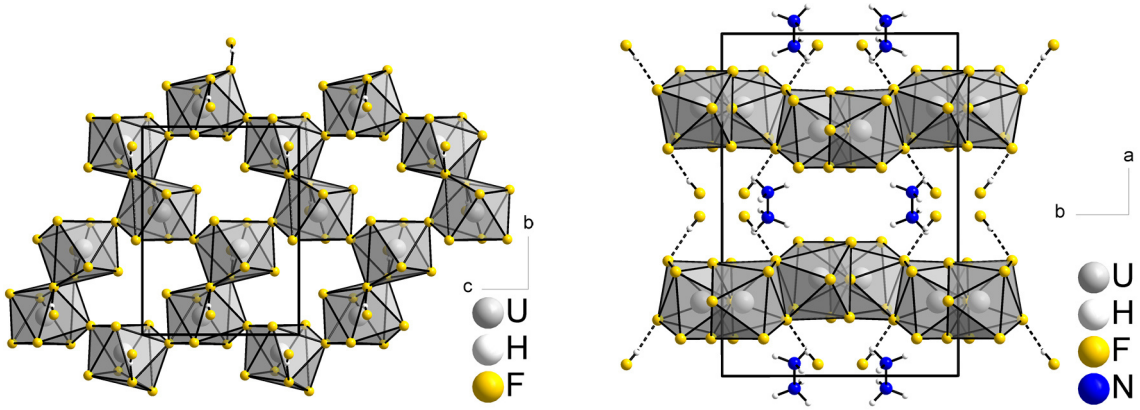

Abbildung 58. Kristallstruktur von $(N_2H_6)U_2F_{10}(HF_2)_2$, projiziert entlang der *a*-Achse (links) oder der *c*-Achse (rechts). Die Atome sind mit willkürlichen Radien abgebildet. Gestrichelte Bindungen stehen für Wasserstoffbrückenbindungen der Form F−H···F.

Zu Fluoratomen des $^{2}_{\infty}\left[UF_{\frac{4}{1}}F_{\frac{2}{2}}(HF_2)_{\frac{2}{2}}\right]^{-}$-Anions werden N−H···F-Wasserstoffbrückenbindungen ausgebildet, wobei sowohl terminal an das Uranatom gebundene Fluoratome (4×) und HF-Moleküle (2×) als Akzeptoren wirken. Details zu den Wasserstoffbrückenbindungen sind in Tabelle 31 aufgeführt. Die N···F-Abstände sind dabei vergleichbar mit denen anderer Hydrazinium(2+)-Salze wie $(N_2H_6)[SiF_6]$ (2,714(4)-2,768(4) Å bei Raumtemperatur), $(N_2H_6)_2[SnF_6]F_2$ (2,57(2)-2,75(2) Å bei 123 K) und $(N_2H_6)_2[TiF_6]F_2$ (2,568(5)-2,765(5) Å bei Raumtemperatur).[375,377,378]

Tabelle 31. Details zu den N−H···F-Wasserstoffbrückenbindungen in $(N_2H_6)U_2F_{10}(HF)_2$.

Wasserstoffbrückenbindung	*d*(N−H) / Å	*d*(H···F) / Å	*d*(N···F) / Å	$\angle_{NHF}$ / °
N(1)−H(1)···F(4)	0,85(3)	1,92(3)	2,7754(17)	177(3)
N(1)−H(2)···F(6)	0,86(3)	1,84(3)	2,6897(16)	167(3)
N(1)−H(3)···F(7)	0,88(3)	1,90(3)	2,7837(17)	177(3)

Die Schwerpunkte der Hydrazinium(2+)-Kationen umgeben einander in der Form einer hexagonalen Bipyramide, wenn Schwerpunkt-zu-Schwerpunkt-Abstände von 5,67 bis 8,41 Å berücksichtigt werden. Die Schwerpunkte sind von acht Uranatomen in der Form eines quadratischen Antiprismas mit Abständen von 4,63-5,19 Å und die Uranatome von acht Schwerpunkten in Form eines Würfels mit Abständen von 4,63-8,19 Å umgeben.

5.5. Fluoridouranate(VI) − Unveröffentlichte Ergebnisse

5.5.1. Darstellung und Charakterisierung von $Rb[UF_7]$

Ein FEP-Rohr wurde im Handschuhkasten mit 65,8 mg (0,15 mmol, 1 Äq.) $RbUF_6$ beschickt und mit einem Edelstahlfaltenbalgventil verschlossen. An der ClF_3-Anlage wurden 0,61 g (6,6 mmol, 44 Äq.) ClF_3 auf den Feststoff unter Stickstoffkühlung kondensiert. Das Reaktionsgefäß wurde langsam auf Raumtemperatur erwärmt, woraufhin sich der türkise Feststoff rasch entfärbte. Nach sechs Tagen bei Raumtemperatur haben sich farblose Kristalle gebildet. Flüchtige Bestandteile wurden im Vakuum entfernt und die Kristalle im Handschuhkasten isoliert (54,6 mg). Ein Teil dieser wurde in perfluoriertem Öl suspendiert und unter dem Mikroskop selektiert. Ein Kristall wurde röntgenographisch untersucht und die Zusammensetzung $Rb[UF_7]$ für diesen erhalten. Die Bildung der Verbindung kann mit Gleichung 83 erklärt werden.

$$2\,RbUF_6 + ClF_3 \longrightarrow 2\,Rb[UF_7] + ClF \qquad 83$$

Berichtete Versuche entsprechende Einkristalle von Heptafluoridouranaten(VI) aus Acetonitril-Suspensionen zu züchten schlugen fehl, da diese eine zu geringe Löslichkeit aufweisen oder Reduktion eintritt.[379]

Andere Hexafluoride neben UF_6, wie MoF_6, WF_6, ReF_6, TeF_6 und XeF_6, können ebenfalls als Fluoridionenakzeptoren wirken und Hepta- oder Octafluoridometallate(VI), $[MF_7]^-$ und $[MF_8]^{2-}$, mit Lewis-Basen wie den Alkalimetallfluoriden bilden.[380–382,176,379,383] Die restlichen Hexafluoride zeigen hingegen keine Tendenz Fluoridionen aufzunehmen.[384–387]

Die Alkalimetallfluoride Natrium- und Kaliumfluorid wurden häufig als Absorbermaterial für Uranhexafluorid eingesetzt, wobei entweder Hepta- oder Octafluoridouranate(VI) gebildet werden.[94,388,389] Durch thermische Zersetzung dieser Verbindungen ist Uranhexafluorid wieder zugänglich.

Für die Heptafluoridouranate(VI) $A[UF_7]$ (A = Na, K, Rb, Cs, NO) wurde Dimorphismus berichtet, mit je einer kubischen Hochtemperaturmodifikation und niedersymmetrischen Tieftemperaturmodifikation.[390–395] Die Pulverröntgendiffraktogramme der Tieftemperaturmodifikationen wurden jedoch nicht indiziert, die Gitterparameter der kubischen Modifikationen dieser Salze sind in Tabelle 32 aufgeführt.

Rubidiumheptafluoridouranat(VI) kristallisiert in der monoklinen Raumgruppe $P2_1/c$ (Nr. 14), mit a = 5,0825(10) Å, b = 10,594(2) Å, c = 10,755(2) Å, β = 95,15(3)°, V = 576,8(2) Å^3, mit vier Formeleinheiten pro Elementarzelle, Pearson-Symbol $mP36$ und Wyckoff-Sequenz $14.e^9$. Ausgewählte kristallographische Daten, Details der Strukturbestimmung sowie äquivalente isotrope und anisotrope Auslenkungsparameter sind im Abschnitt 8.1.4.1 aufgeführt.

Tabelle 32. Gitterparameter der kubischen Modifikationen der Heptafluoridouranate $A[UF_7]$ (A = Na, K, Rb, Cs, NO) bei Raumtemperatur.[395]

Verbindung	a / Å
$Na[UF_7]$ (cF)	8,511(8)
$K[UF_7]$ (cP)	5,22(1)
$Rb[UF_7]$ (cP)	5,385(5)
$Cs[UF_7]$ (cP)	5,517(5)
$NO[UF_7]$ (cP)	5,334(7)

Das Uranatom U(1) besetzt die allgemeine Lage 4e und ist von sieben Fluoratomen in der Form eines einfach überkappten trigonalen Prismas umgeben (Abbildung 59). Für die Koordinationszahl sieben gibt es drei mögliche Ligandenanordnungen, die idealen Polyeder sind das einfach überkappte trigonale Prisma (C_{2v}, 1/4/2-Anordnung), das einfach überkappte Oktaeder (C_{3v}, 1/3/3-Anordnung) sowie die pentagonale Bipyramide (D_{5h}, 1/5/1-Anordnung), siehe Abbildung 60. Die Anordnung wird dabei von einer Spitze des Polyeders aus betrachtet, bei dem einfach überkappten trigonalen Prisma wird von dem überkappenden Punkt („Ligand“) ausgegangen, darunter liegen zunächst vier Punkte („Liganden“) und unter diesen zwei weitere Punkte („Liganden“), was zur Bezeichnung 1/4/2-Anordnung führt. Einige Beispiele mit solchen Ligandenanordnungen sind in Tabelle 33 gegeben.

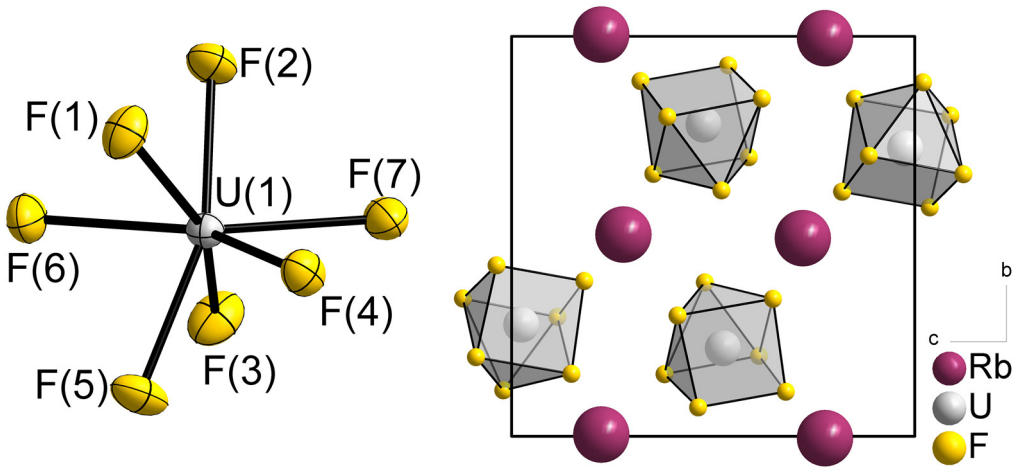

Abbildung 59. Ausschnitte aus der Kristallstruktur von $Rb[UF_7]$. Links ist das $[UF_7]^-$-Anion dargestellt und rechts ein Strukturausschnitt mit der ersten Koordinationssphären der Uranatome als graue Polyeder. Links sind die Auslenkungsellipsoide mit 70% Aufenthaltswahrscheinlichkeit bei 100 K dargestellt. Rechts sind die Atome mit willkürlichen Radien abgebildet.

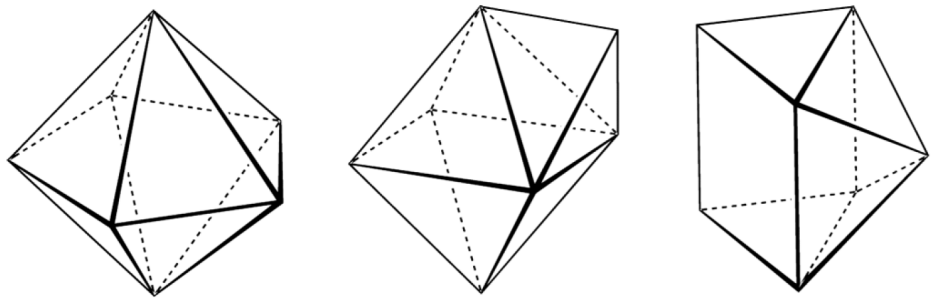

D_{5h}, 1/5/1-Anordnung C_{3v}, 1/3/3-Anordnung C_{2v}, 1/4/2-Anordnung

Abbildung 60. Die möglichen Ligandenanordnungen für Koordinationszahl sieben. (Abbildung verändert nach [396])

Tabelle 33. Moleküle (ReF_7 und IF_7) und homoleptische Komplexe mit Koordinationszahl sieben für das Zentralatom. (1/4/2-Anordnung: einfach überkapptes trigonales Prisma; 1/3/3-Anordnung: einfach überkapptes Oktaeder; 1/5/1-Anordnung: pentagonale Bipyramide)

1/4/2-Anordnung	1/3/3-Anordnung	1/5/1-Anordnung
$[NbF_7]^{2-}$ [397], $[Nb(N_3)_7]^{2-}$ [398], $[TaF_7]^{2-}$ [397], $[Ta(N_3)_7]^{2-}$ [398], $[UF_7]^-$ (diese Arbeit)	$[MoF_7]^-$ [381], $[Mo(CH_3)_7]^-$ [399], $[WF_7]^-$ [381], $[W(CH_3)_7]^-$ [400] $[U(N_3)_7]^{3-}$ [401], $[XeF_7]^-$ [383]	$[U(N_3)_7]^{3-}$ [401], ReF_7 [402], $[SbF_7]^{2-}$ [403], $[TeF_7]^-$ [176], IF_7 [130], $[XeF_7]^+$ [404],

Die Energieunterschiede zwischen den verschiedenen Anordnungen sind für Fluoridoliganden meist gering und generell können neben der Ligandenabstoßung auch elektronische Effekte einen Einfluss auf die Anordnung haben.[66,405] Das $[UF_7]^-$-Anion im $Rb[UF_7]$ unterscheidet sich dabei mit der 1/4/2-Anordnung von anderen Heptafluoridometallaten(VI), welche 1/3/3-Anordnungen (*M* = Mo, W, Xe) oder 1/5/1-Anordnungen (*M* = Te) zeigen.[176,381,383,404]

Die U−F-Abstände im $[UF_7]^-$-Anion liegen im Bereich von 2,019(3) bis 2,068(3) Å, sie sind vergleichbar zu denen in festem UF_6 (2,023(6) Å bei 77 K) und $(NO)_2[UF_8]$ (2,070(5)-2,151(4) Å bei 120 K), wobei diese in letzterem vermutlich aufgrund der höheren Koordinationszahl des Uranatoms teilweise größer sind.[406,407] Das Rubidiumkation besetzt ebenfalls die allgemeine 4*e*-Lage und ist von dreizehn Fluoratomen in der Form eines Prismatoids umgeben. Die Rubidium- und Uranatome sind jeweils pseudokubisch primitiv gepackt und die Gitter ineinander verschoben, die Atome sind entsprechend ähnlich zu den Cs- und Cl-Atomen im CsCl-Strukturtyp angeordnet.[314]

Auf Grundlage der Kristallstruktur von $Rb[UF_7]$ wurden periodische quantenchemische Rechnungen mit dem Programmpaket CRYSTAL17 durchgeführt (DFT-PBE0/TZVP).[242,243] Die optimierten Gitterparameter und Atomkoordinaten sind in 8.2.3.1 aufgeführt. Sie stimmen gut mit denen aus der Einkristallstrukturanalyse überein. Dies gilt auch für die berechneten U−F-Abstände, welche im Bereich von 2,022 bis 2,075 Å liegen. Auf der Grundlage der optimierten Struktur wurde ein Raman-Spektrum für festes $Rb[UF_7]$ berechnet. Die Raman-Spektren von $Rb[UF_7]$ sind in Abbildung 61 dargestellt. Die Bandenzuordnungen sind in Tabelle 33 aufgeführt, ebenso wie in der Literatur für Heptafluoridouranate(VI) berichtete Bandenlagen. Das Raman-Spektrum von $Rb[UF_7]$ stimmt sehr gut mit denen der anderen Heptafluoridouranate(VI) sowie mit dem berechneten Spektrum überein. Daraus ist ersichtlich, dass Kationen nur einen geringen Einfluss auf die Streck- und Scherschwingungen des $[UF_7]^-$-Anions haben.

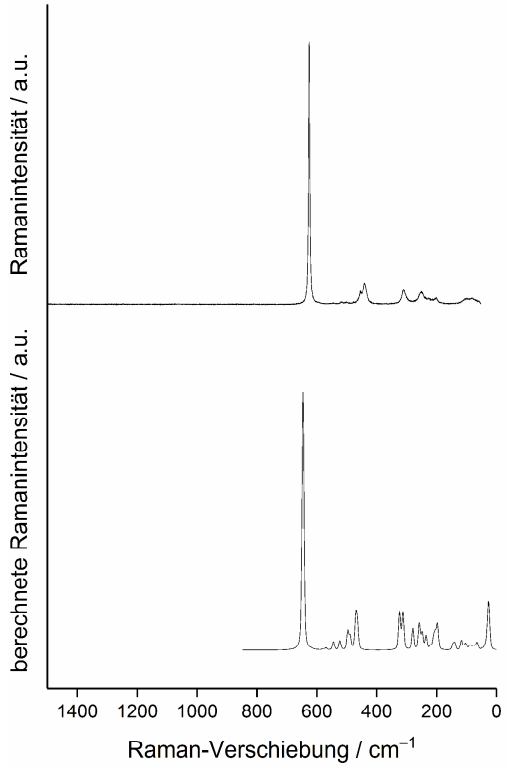

Abbildung 61. Hochaufgelöstes (oben, 532 nm Laser) und berechnetes (unten) Raman-Spektrum von $Rb[UF_7]$. Die Raman-Intensitäten sind in willkürlichen Einheiten (a.u.) angegeben.

Tabelle 34. Bandenlagen und -zuordnungen der Raman-Spektren von Heptafluoridouranaten(VI). (>240 cm^{-1}) (*v*: Streckschwingung, *δ*: Scherschwingung, s: Symmetrisch, as: Asymmetrisch)

Verbindung	$v_s(UF_7)$	$v_{as}(UF_7)$	$\delta(UF_7)$	Quelle
$Na[UF_7]^a$	633	554, 552, 450	310, 242	[395]
$K[UF_7]^b$	623	544, 517, 502, 455, 440	311, 253	[395]
$Rb[UF_7]^b$	625	518, 501, 455, 441	311, 251	diese Arbeit
$Rb[UF_7]$	648, 646	618, 579, 569, 545, 525, 523, 497, 488, 471, 469, 466, 463	324, 314, 312, 279, 259, 258,	berechnet
$Rb[UF_7]^b$	625	520, 443	310, 248	[395]
$Cs[UF_7]^b$	622	462, 444	312, 249	[408]
$NO[UF_7]^b$	627	446, 434	310, 240	[408]
$NH_4[UF_7]^b$	625	447	314, 250	[395]

a: Feststoff, kubische Modifikation, *b*: Feststoff, bei Raumtemperatur gemessen.

5.6. Zusammenfassung

Fluoridouranate(V)

Die Umsetzungen von Erdalkalimetallfluoriden wie Strontium- oder Bariumfluorid mit Uranpentafluorid in wasserfreiem Fluorwasserstoff bieten einen Zugang zu neuen Fluoridouranat(V)-Ionen (Abbildung 62).

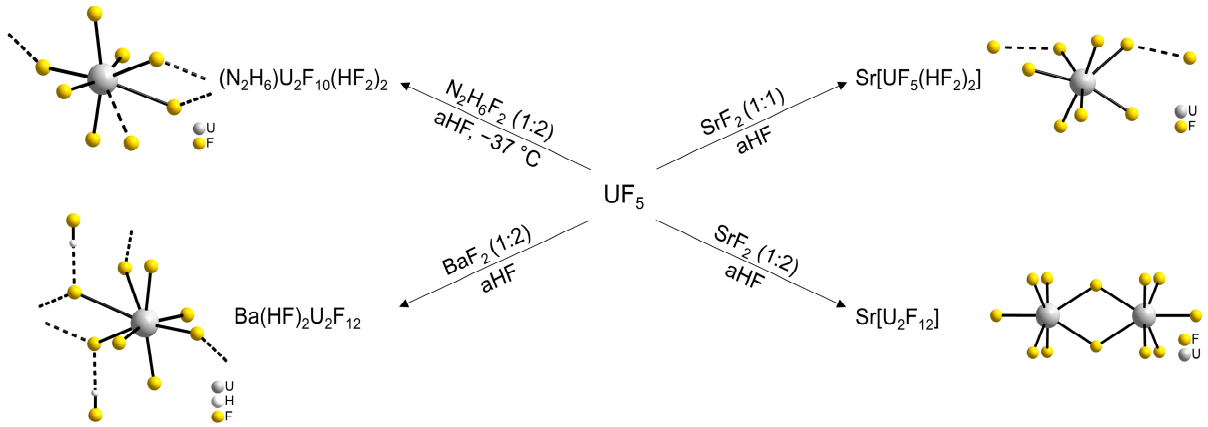

Abbildung 62. Übersicht über die dargestellten und charakterisierten Verbindungen mit Fluoridouranat(V)-Anionen. Die Reaktionen sind der Übersichtlichkeit halber nicht ausgeglichen.

Mit Strontiumfluorid konnte das Salz $Sr[U_2F_{12}]$ mit dem molekularen zweikernigen $[U_2F_{12}]^{2-}$-Anion erhalten werden, in welchem die Uranatome über zwei verbrückende Fluoratome verbunden sind. Die magnetischen Messungen der Verbindung zeigen, dass eine antiferromagnetische Wechselwirkung bei tiefen Temperaturen vorliegt, welche, wie auch die Absorptionsspektren, mit CASSCF-Rechnungen erklärt werden konnten. Als Verunreinigung lag stets etwas $Sr[UF_5(HF_2)_2]$ vor, dessen Kristallstruktur ebenso aufgeklärt werden konnte. In der Verbindung liegt ein molekulares $[UF_5(HF_2)_2]^{2-}$-Anion mit terminal gebundenen Hydrogendifluorid-Anionen vor. Die Wasserstoffatome konnten nicht lokalisiert werden, das Infrarotspektrum zeigt jedoch, dass $[HF_2]^-$-Anionen enthalten sind.

Durch die Reaktion von BaF_2 mit UF_5 in wasserfreiem Fluorwasserstoff konnte die Verbindung $Ba(HF)_2U_2F_{12}$ erhalten werden, in welcher ein komplexes schichtartiges Anion vorliegt, welches mit der Niggli-Formel ${}^{2}_{\infty}\left[UF_{\frac{4}{1}}F_{\frac{4}{2}}\right]^{-}$ beschrieben werden kann. Das Bariumatom ist dabei unter anderem von Fluorwasserstoffliganden umgeben, deren Wasserstoffatome nicht lokalisiert werden konnten.

Die Umsetzung von Hydraziniumdifluorid mit UF_5 in wasserfreiem Fluorwasserstoff bei tiefen Temperaturen und entsprechender Tieftemperaturkristallpräparation führte zur Isolierung der Verbindung $(N_2H_6)U_2F_{10}(HF_2)_2$, in welcher verbrückende Hydrogendifluorid-Liganden mit asymmetrischer F···H···F-Brücke vorliegen (Gleichung 89). Es liegt ebenfalls ein schichtartiges Anion vor, welches mit der Niggli-Formel ${}^{2}_{\infty}\left[UF_{4\,\frac{1}{1}}F_{2\,\frac{2}{2}}(HF_2)_{2\,\frac{2}{2}}\right]^{-}$ beschrieben werden kann. Die beiden Fluoridouranate(V) stellen die ersten strukturell charakterisierten dar, in denen die Anionen Schichten ausbilden. Bisher waren nur Fluoridouranate(V) mit molekularen oder kettenartigen Anionen bekannt.

Hochdruckmodifikation von Urantetrafluorid

Die Reaktion von Schwefel mit Uranhexafluorid in wasserfreiem Fluorwasserstoff führt zur Bildung von Urantetrafluorid (Gleichung 84). Im dynamischen Vakuum können flüchtige Bestandteile entfernt und unter Erwärmen überschüssiger Schwefel sublimiert werden. Das erhaltene Urantetrafluorid ist frei von oxidischen oder sulfidischen Verunreinigungen und eignet sich unter anderem für die Darstellung von Urantrifluorid, bei welcher diese sonst stören. Durch hohen Druck und Temperatur konnte eine vorher unbekannte Hochdruckmodifikation von UF_4 erhalten und charakterisiert werden (Gleichung 85).

$$2\ UF_6 + 1/8\ S_8 \xrightarrow{aHF} 2\ UF_4 + SF_4 \qquad 84$$

$$UF_4 \xrightarrow{9{,}5\ GPa,\ 600\ °C} HP\text{-}UF_4 \qquad 85$$

In der Kristallstruktur besitzen die Uranatome hohe Koordinationszahlen von neun oder elf, mit ungewöhnlichen prismatoiden Ligandenanordnungen (Abbildung 63). Die ausgebildete Gerüststruktur kann mit der Niggli-Formel ${}^{3}_{\infty}\left[\langle UF_{6\,\frac{6}{3}}F_{5\,\frac{5}{2}}\rangle\,\langle UF_{6\,\frac{6}{3}}F_{3\,\frac{3}{2}}\rangle\right]$ beschrieben werden.

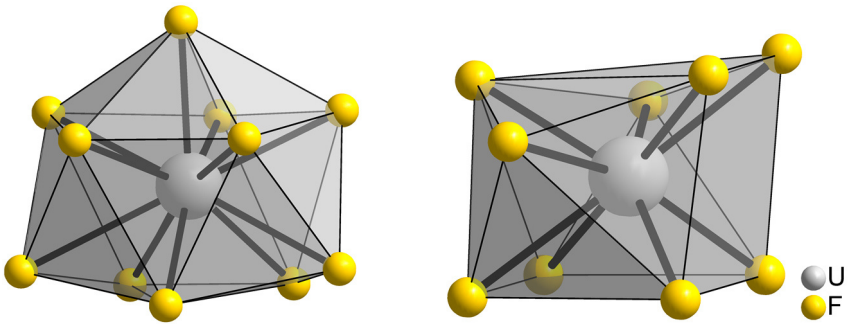

Abbildung 63. Erste Koordinationssphären der beiden kristallographisch-unabhängigen Uranatome in HP-UF_4.

Fluoridoneptunate(IV)- und -plutonate(IV)

Einkristalline Fluoridoneptunate(IV) und -plutonate(IV) konnten durch Umsetzungen von Neptunium(IV)- oder Plutonium(IV)-oxid mit Fluoridionendonoren wie Alkalimetallfluoriden oder *in situ* erzeugten Übergangsmetallfluoriden in Flusssäure erhalten werden. Bei Raumtemperatur wurden so Einkristalle von $(NH_4)_4[NpF_8]$ oder $AMF_6{\cdot}3H_2O$ (A = Mn, Zn; M = Np, Pu)) erhalten und unter hydrofluorothermalen solche von NH_4PuF_5, $TlMF_5$ (M = Np, Pu), APu_2F_9 (A = Na, K).

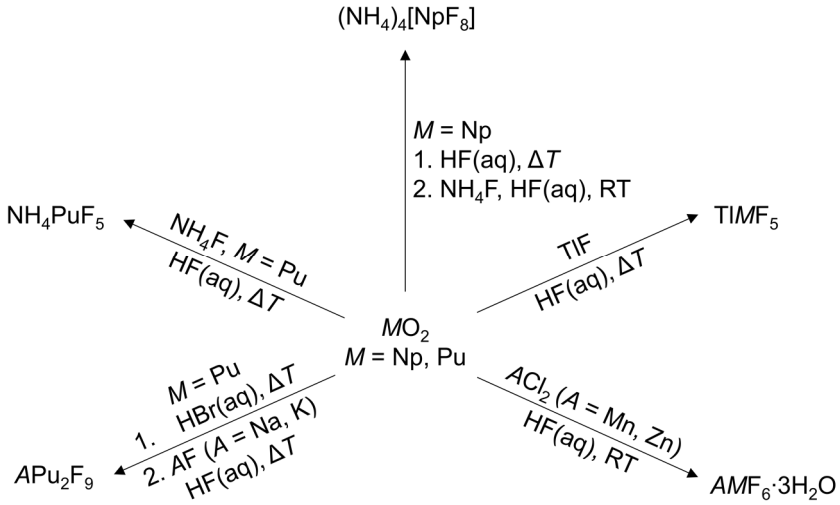

Abbildung 64. Übersicht über die dargestellten und charakterisierten Fluoridoneptunate(IV) und -plutonate(IV). Die Reaktionen sind der Übersichtlichkeit halber nicht ausgeglichen.

Die entsprechenden Kristallstrukturen sind isotyp zu denen der Uranverbindungen, wobei die Actinoid-Fluor-Abstände entsprechend der Actinoidenkontraktion mit höherer Ordnungszahl abnehmen. Die Actinoidatome sind dabei in den Kristallstrukturen von neun Fluoratomen in der Form dreifach überkappter trigonaler Prismen umgeben, mit der Ausnahme des $[NpF_8]^{4-}$-Anions, welches entweder als verzerrtes quadratisches Antiprisma oder zweifach überkapptes trigonales Prisma beschrieben werden kann. Quantenchemische Rechnungen für die Gasphase zeigen, dass die Energieunterschiede für unterschiedliche Ligandenanordnungen der $[MF_8]^{4-}$-Anionen (*M* = Th-Bk) gering sind und vermutlich leicht durch die Gitterenergie im Festkörper kompensiert werden können.

Darstellung und Charakterisierung von Rubidiumhexafluoridouranat(V)

Die Oxidation von Rubidiumhexafluoridouranat(V) mit flüssigem Chlortrifluorid führte zur Isolation von einkristallinem Rubidiumheptafluoridouranat(VI) (Gleichung 86). In der Kristallstruktur liegen isolierte $[UF_7]^-$-Anionen vor, welche erstmalig strukturell charakterisiert wurden. Das Uranatom ist dabei in Form eines einfach überkappten trigonalen Prismas von Fluoratomen umgeben.

$$2\ RbUF_6 + ClF_3 \longrightarrow 2\ Rb[UF_7] + ClF \qquad 86$$

5.7. Ausblick

Azido- und Cyanidouranate

Die Fluoridouranate in den Oxidationsstufen +IV, +V und +VI könnten als Ausgangsmaterialien für homoleptische Azido- oder Cyanidokomplexe dienen, welche gegebenenfalls durch Ligandenaustauschreaktionen mit Trimethylsilylverbindungen wie Trimethylsilylazid oder Trimethylsilylcyanid zugänglich sind (Gleichungen 87 bis 89).

$$[UF_6]^{2-} + 6\ Si(CH_3)_3X \longrightarrow [UX_6]^{2-} + 6\ Si(CH_3)_3F \qquad (87)$$
X = CN, N_3

$$[UF_6]^{-} + 6\ Si(CH_3)_3X \longrightarrow [UX_6]^{-} + 6\ Si(CH_3)_3F \qquad (88)$$
X = CN, N_3

$$[UF_7]^{-} + 7\ Si(CH_3)_3X \longrightarrow [UX_7]^{-} + 7\ Si(CH_3)_3F \qquad (89)$$
X = CN, N_3

Diese Synthesestrategie hat sich bisher für die Darstellung von Cyaniden, Aziden sowie entsprechenden Komplexen bewährt, sowohl bei Elementen der Haupt- als auch Nebengruppen.[409–415] Bisher ist nur ein homoleptisches Azidouranat(IV)-Anion bekannt, $[U(N_3)_7]^{3-}$, welches durch Metathese-Reaktionen von $[UX_6]^{2-}$ (X = Cl, Br) mit Silberazid erhalten wurde.[401] Denkbar wären auch Versuche zur Darstellung binärer Uranazide und -cyanide, da diese Verbindungen bisher noch unbekannt sind.

Hochdruckchemie

Die Hochdruckchemie könnte mit großer Wahrscheinlichkeit auch auf entsprechende Fluoridometallate des Urans, Neptuniums und Plutoniums übertragen werden, um so höchstmögliche Koordinationszahlen zu erreichen oder spektroskopische Eigenschaften der Verbindungen unter extremen Bedingungen zu untersuchen. Weiterhin könnten sich die Bindungseigenschaften ändern, was erst kürzlich für eine Cm(III)-Verbindung gezeigt wurde.[416]

Charakterisierung der Fluoridoneptunate(IV)- und plutonate(IV)

Die weitere magnetische und spektroskopische Charakterisierung der Fluoridoneptunate(IV) und -plutonate(IV) könnte weitere Einblicke in die Eigenschaften von $5f^3$- und $5f^4$-Systemen geben. Vor allem das Np(IV)-Ion, welches bei allen Temperaturen ein ungepaartes Elektron aufweist, sollte zu antiferromagnetischen oder ferromagnetischen Systemen führen. Bisher wurde der Magnetismus nur weniger Fluoridoneptunate(IV) untersucht.[330,417,418]

Neue Strukturmotive bei Fluoridouranate(V)

Mögliche neue Strukturmotive bei den Fluoridouranaten(V) sollten weiter durch Umsetzungen mit Fluoriden der Nebengruppe sowie mit organischen Kationen zugänglich sein. Eventuell sind so weitere Verbindungen mit ungewöhnlichen mehrkernigen molekularen Anionen zugänglich. Diese Systeme könnten zu besonderen magnetischen und spektroskopischen Eigenschaften führen, wie sie auch für das $[U_2F_{12}]^{2-}$-Anion beobachtet wurden. Durch die „einfache“ Elektronenkonfiguration des Uran(V)-Ions, $[Rn]5f^1$, könnten entsprechende Verbindungen auch als „Benchmark“ für quantenchemische Rechnungen dienen.

6. Literaturverzeichnis

Die zitierten Fachzeitschriften wurden nach den Vorgaben des *Chemical Abstracts Service Source Index* (CASSI) abgekürzt.[419] Technische Berichte über militärische Auftragsforschung, vor allem der Firma Rocketdyne, wie das *chlorine trifluoride handling manual*, können über das *Defense Technical Information Center* (DTIC) erhalten werden.[420]

[1] J. D. Clark, *Ignition! An Informal History of Liquid Rocket Propellants*, Rutgers University Press, New Brunswick, New Jersey, **1972**.
[2] O. Ruff, E. Ascher, J. Fischer, F. Laass, *Z. Anorg. Allg. Chem.* **1928**, *176*, 258–270.
[3] O. Ruff, *Z. Angew. Chem.* **1928**, *41*, 1289–1292.
[4] O. Ruff, A. Braida, *Z. Anorg. Allg. Chem.* **1933**, *214*, 81–90.
[5] T. Drews, K. Seppelt, *Z. Anorg. Allg. Chem.* **2012**, *638*, 2106–2110.
[6] M. Schmeisser, W. Ludovici, D. Naumann, P. Sartori, E. Scharf, *Chem. Ber.* **1968**, *101*, 4214–4220.
[7] M. Schmeisser, P. Sartori, D. Naumann, *Chem. Ber.* **1970**, *103*, 590–593.
[8] O. Ruff, H. Krug, *Z. Anorg. Allg. Chem.* **1930**, *190*, 270–276.
[9] P. Lebeau, *Ann. Chim. Phys.* **1906**, *9*, 241–263.
[10] S. Hoyer, K. Seppelt, *Angew. Chem. Int. Ed.* **2000**, *39*, 1448–1449.
[11] D. F. Smith, *Science* **1963**, *141*, 1039–1040.
[12] O. Ruff, W. Menzel, *Z. Anorg. Allg. Chem.* **1931**, *202*, 49–61.
[13] H. Moissan, *Ann. Chim. Phys.* **1891**, *6*, 224–232.
[14] O. Ruff, R. Keim, *Z. Anorg. Allg. Chem.* **1930**, *193*, 176–186.
[15] H. Simmons. Booth, J. Turner. Pinkston, *Chem. Rev.* **1947**, *41*, 421–439.
[16] H. Meinert, *Z. Chem.* **1967**, *7*, 41–57.
[17] K. O. Christe, in *XXIVth International Congress of Pure and Applied Chemistry*, Butterworth-Heinemann, Oxford, **1974**, pp. 115–141.
[18] K. Seppelt, *Angew. Chem. Int. Ed. Engl.* **1979**, *18*, 186–202.
[19] I. C. Tornieporth-Oetting, T. M. Klapötke, *Heteroatom Chem.* **1993**, *4*, 543–552.
[20] T. A. Engesser, M. R. Lichtenthaler, M. Schleep, I. Krossing, *Chem. Soc. Rev.* **2016**, *45*, 789–899.
[21] K. O. Christe, W. Sawodny, *Inorg. Chem.* **1969**, *8*, 212–219.
[22] G. Frenking, W. Koch, *Inorg. Chem.* **1990**, *29*, 4513–4517.
[23] S. Hoyer, Strukturchemie von Iodverbindungen in den Oxidationsstufen +1/7 bis +5, Dissertation, Freie Universität Berlin, **2004**.
[24] K. O. Christe, J. P. Guertin, *Inorg. Chem.* **1965**, *4*, 905–908.
[25] P. Pröhm, J. R. Schmid, K. Sonnenberg, P. Voßnacker, S. Steinhauer, C. J. Schattenberg, R. Müller, M. Kaupp, S. Riedel, *Angew. Chem. Int. Ed.* **2020**, *59*, 16002–16006.
[26] J. H. Miller, L. Andrews, *Inorg. Chem.* **1979**, *18*, 988–992.
[27] R. Minkwitz, R. Bröchler, R. Ludwig, *Inorg. Chem.* **1997**, *36*, 4280–4283.
[28] X. Zhang, K. Seppelt, *Z. Anorg. Allg. Chem.* **1997**, *623*, 491–500.
[29] K. O. Christe, W. W. Wilson, G. W. Drake, M. A.Petrie, J. A. Boatz, *J. Fluorine Chem.* **1998**, *88*, 185–189.
[30] K. O. Christe, W. Sawodny, *Inorg. Chem.* **1967**, *6*, 313–318.

[31] B. Scheibe, R. Haiges, S. I. Ivlev, A. J. Karttunen, U. Müller, K. O. Christe, F. Kraus, *Eur. J. Inorg. Chem.* **2020**, DOI 10.1002/ejic.202000845.
[32] A. A. Woolf, H. J. Emeléus, *J. Chem. Soc.* **1949**, 2865–2871.
[33] A. J. Edwards, G. R. Jones, *J. Chem. Soc. A* **1969**, *0*, 1467–1470.
[34] S. I. Ivlev, A. J. Karttunen, M. R. Buchner, M. Conrad, F. Kraus, *Angew. Chem.* **2018**, *130*, 14850–14855.
[35] E. Dow. Whitney, R. O. MacLaren, C. E. Fogle, T. J. Hurley, *J. Am. Chem. Soc.* **1964**, *86*, 2583–2586.
[36] B. Scheibe, S. I. Ivlev, A. J. Karttunen, F. Kraus, *Eur. J. Inorg. Chem.* **2020**, *2020*, 1319–1324.
[37] K. O. Christe, C. J. Schack, *Inorg. Chem.* **1970**, *9*, 1852–1858.
[38] A. J. Edwards, G. R. Jones, *J. Chem. Soc. A* **1969**, 1936–1938.
[39] K. O. Christe, W. W. Wilson, G. W. Drake, D. A. Dixon, J. A. Boatz, R. Z. Gnann, *J. Am. Chem. Soc.* **1998**, *120*, 4711–4716.
[40] S. Ivlev, P. Woidy, V. Sobolev, I. Gerin, R. Ostvald, F. Kraus, *Z. Anorg. Allg. Chem.* **2013**, *639*, 2846–2850.
[41] S. I. Ivlev, A. J. Karttunen, R. V. Ostvald, F. Kraus, *Chem. Commun.* **2016**, *52*, 12040–12043.
[42] B. Scheibe, A. J. Karttunen, U. Müller, F. Kraus, *Angew. Chem.* **2020**, *132*, 18272–18276.
[43] J. Bandemehr, S. I. Ivlev, A. J. Karttunen, F. Kraus, *Eur. J. Inorg. Chem.* **2020**, DOI 10.1002/ejic.202000875.
[44] K. O. Christe, D. Pilipovich, *Inorg. Chem.* **1969**, *8*, 391–393.
[45] K. O. Christe, W. Sawodny, *Inorg. Chem.* **1973**, *12*, 2879–2885.
[46] K. O. Christe, X. Zhang, J. A. Sheehy, R. Bau, *J. Am. Chem. Soc.* **2001**, *123*, 6338–6348.
[47] M. D. Lind, K. O. Christe, *Inorg. Chem.* **1972**, *11*, 608–612.
[48] A. Vij, F. S. Tham, V. Vij, W. W. Wilson, K. O. Christe, *Inorg. Chem.* **2002**, *41*, 6397–6403.
[49] A. J. Edwards, P. Taylor, *J. Chem. Soc., Dalton Trans.* **1975**, 2174–2177.
[50] K. O. Christe, W. W. Wilson, R. V. Chirakal, J. C. P. Sanders, G. J. Schrobilgen, *Inorg. Chem.* **1990**, *29*, 3506–3511.
[51] A. R. Mahjoub, A. Hoser, J. Fuchs, K. Seppelt, *Angew. Chem.* **1989**, *101*, 1528–1529.
[52] S. P. Beaton, D. W. A. Sharp, A. J. Perkins, I. Sheft, H. H. Hyman, K. Christe, *Inorg. Chem.* **1968**, *7*, 2174–2176.
[53] K. O. Christe, J. P. Guertin, W. Sawodny, *Inorg. Chem.* **1968**, *7*, 626–628.
[54] K. O. Christe, *Inorg. Chem.* **1972**, *11*, 1215–1219.
[55] A. R. Mahjoub, K. Seppelt, *Angew. Chem. Int. Ed. Engl.* **1991**, *30*, 323–324.
[56] A. R. Mahjoub, D. Leopold, K. Seppelt, *Eur. J. Solid State Inorg. Chem.* **1992**, *29*, 635–648.
[57] K. O. Christe, *Inorg. Nucl. Chem. Lett.* **1972**, *8*, 741–745.
[58] J. F. Lehmann, G. J. Schrobilgen, K. O. Christe, A. Kornath, R. J. Suontamo, *Inorg. Chem.* **2004**, *43*, 6905–6921.
[59] G. J. Schrobilgen, Fluorocations of Krypton, Xenon and Bromine(VII), Dissertation, McMaster University (Canada), **1973**.
[60] R. J. Gillespie, G. J. Schrobilgen, *Inorg. Chem.* **1974**, *13*, 1230–1235.
[61] K. O. Christe, W. Sawodny, *Inorg. Chem.* **1967**, *6*, 1783–1788.
[62] E. Goreshnik, Z. Mazej, *Acta Cryst.* **2006**, *C62*, i59–i60.
[63] A.-R. Mahjoub, K. Seppelt, *Angew. Chem.* **1991**, *103*, 844–845.

[64] A. Ellern, K. Seppelt, *Z. Anorg. Allg. Chem.* **2001**, *627*, 234–237.
[65] R. J. Gillespie, R. S. Nyholm, *Q. Rev., Chem. Soc.* **1957**, *11*, 339–380.
[66] R. J. Gillespie, E. A. Robinson, *Angew. Chem.* **1996**, *108*, 539–560.
[67] R. J. Gillespie, *Coord. Chem. Rev.* **2008**, *252*, 1315–1327.
[68] A. R. Mahjoub, X. Zhang, K. Seppelt, *Chem. Eur. J.* **1995**, *1*, 261–265.
[69] D. A. Dixon, D. J. Grant, K. O. Christe, K. A. Peterson, *Inorg. Chem.* **2008**, *47*, 5485–5494.
[70] K. S. Thanthiriwatte, M. Vasiliu, D. A. Dixon, K. O. Christe, *Inorg. Chem.* **2012**, *51*, 10966–10982.
[71] K. O. Christe, W. W. Wilson, *Inorg. Chem.* **1989**, *28*, 3275–3277.
[72] C. J. Schack, R. D. Wilson, *Synth. React. Inorg. Met.-Org. Chem.* **1973**, *3*, 393–396.
[73] C. J. Schack, R. D. Wilson, D. D. Desmarteau, in *Inorganic Syntheses* (Ed.: J.M. Shreeve), John Wiley & Sons, Inc., Hoboken, NJ, USA, **1986**, pp. 1–3.
[74] R. R. Smardzewski, W. B. Fox, *J. Fluorine Chem.* **1976**, *7*, 453–455.
[75] B. Baasner, Ed. , *Houben-Weyl Methods of Organic Chemistry - Organo-Fluorine Compounds - Fluorinating Agents and Their Application in Organic Synthesis*, Thieme, **2014**.
[76] S. Rozen, M. Brand, *J. Org. Chem.* **1986**, *51*, 222–225.
[77] R. E. A. Dear, *J. Org. Chem.* **1970**, *35*, 1703–1705.
[78] S. Rozen, in *Encyclopedia of Reagents for Organic Synthesis* (Ed.: John Wiley & Sons, Ltd), John Wiley & Sons, Ltd, Chichester, UK, **2001**, p. rb263.
[79] S. Rozen, in *Encyclopedia of Reagents for Organic Synthesis* (Ed.: John Wiley & Sons, Ltd), John Wiley & Sons, Ltd, Chichester, UK, **2001**, p. ri015.
[80] L. Stein, *Science* **1964**, *143*, 1058–1060.
[81] R. J. Gillespie, M. J. Morton, *Inorg. Chem.* **1970**, *9*, 811–814.
[82] K. O. Christe, W. Sawodny, J. P. Guertin, *Inorg. Chem.* **1967**, *6*, 1159–1162.
[83] K. O. Christe, J. P. Guertin, *Inorg. Chem.* **1965**, *4*, 1785–1787.
[84] J. R. Schmid, P. Pröhm, P. Voßnacker, G. Thiele, M. Ellwanger, S. Steinhauer, S. Hasenstab-Riedel, *Eur. J. Inorg. Chem.* **2020**, DOI 10.1002/ejic.202000847.
[85] E. A. S. Román, H. J. Schumacher, *Z. Phys. Chem.* **1970**, *71*, 153–162.
[86] R. D. Burbank, F. N. Bensey, *J. Chem. Phys.* **1953**, *21*, 602–608.
[87] M. Y. Antipin, A. M. Ellern, V. F. Sukhoverkhov, Y. T. Struchkov, *Russ. J. Inorg. Chem.* **1989**, *34*, 459–461.
[88] D. F. Smith, *J. Chem. Phys.* **1953**, *21*, 609–614.
[89] D. W. Magnuson, *J. Chem. Phys.* **1957**, *27*, 223–226.
[90] A. M. Ellern, M. Yu. Antipin, Yu. T. Struchkov, V. F. Sukhoverkhov, *Russ. J. Inorg. Chem.* **1991**, *36*, 792–794.
[91] *Interhalogen Handbook, Technical Report AFRPL-TR-67-276*, Rocketdyne, Canoga Park, California, **1967**.
[92] D. Naumann, *Fluor und Fluorverbindungen*, Springer, Berlin, Heidelberg, **1980**.
[93] R. Haiges, in *Efficient Preparations of Fluorine Compounds* (Ed.: H.W. Roesky), John Wiley & Sons, Inc., Hoboken, NJ, USA, **2012**, pp. 100–107.
[94] W. Bacher, E. Jacob, *Gmelin-Handbuch der anorganischen Chemie Teil: System-Nr. 55., Uran : U / Erg.-Bd. / C. / 8. Verbindungen mit Fluor*, Springer-Verlag, Berlin Heidelberg New York, **1980**.
[95] R. C. Shrewsberry, E. L. Williamson, *J. Inorg. Nucl. Chem.* **1966**, *28*, 2535–2539.

[96] S. Rozen, *Adv. Synth. Catal.* **2010**, *352*, 2691–2707.
[97] S. Rozen, in *Efficient Preparations of Fluorine Compounds* (Ed.: H.W. Roesky), John Wiley & Sons, Inc., Hoboken, NJ, USA, **2012**, pp. 154–172.
[98] C. B. Baddiel, C. F. Cullis, *Symp. (Int.) Combust., [Proc.]* **1961**, *8*, 1089–1095.
[99] Kh. Bromme, B. Cornils, D. Fritze, G. Schiemann, *Chemie Ing. Techn.* **1965**, *37*, 843–848.
[100] K. R. Brower, *J. Org. Chem.* **1987**, *52*, 798–802.
[101] Y. Hagooly, S. Rozen, *Org. Lett.* **2012**, *14*, 1114–1117.
[102] S. I. Ivlev, M. R. Buchner, A. J. Karttunen, F. Kraus, *J. Fluorine Chem.* **2018**, *215*, 17–24.
[103] F. Schmaltz, *Kampfstoff-Forschung im Nationalsozialismus - Zur Kooperation von Kaiser-Wilhelm-Instituten, Militär und Industrie*, Wallstein Verlag, Göttingen, **2005**.
[104] F. Kraus, *Nachr. Chem.* **2019**, *67*, 17–22.
[105] F. N. Dost, D. J. Reed, V. N. Smith, C. H. Wang, *Toxicol. Appl. Pharmacol.* **1974**, *27*, 527–536.
[106] H. N. MacFarland, W. J. Watson, J. C. Paterson, *Toxicol. Appl. Pharmacol.* **1962**, *4*, 504–521.
[107] W.-T. Tsai, *J. Hazard. Mater.* **2011**, *190*, 1–7.
[108] National Research Council (U.S.), Committee on Acute Exposure Guideline Levels, *Eighteenth Interim Report of the Committee on Acute Exposure Guideline Levels*, **2010**.
[109] R. Bougon, M. Carles, J. Aubert, *C. R. Seances Acad. Sci., Ser. C* **1967**, *265*, 179–182.
[110] K. O. Christe, *Inorg. Chem.* **1972**, *11*, 1220–1222.
[111] A. Dadieu, R. Damm, E. W. Schmidt, *Raketentreibstoffe*, Springer, Wien, New York, **1968**.
[112] Y. Hijikata, Ed. , *Physics and Technology of Silicon Carbide Devices*, InTech, **2012**.
[113] Y. Saito, *J. Vac. Sci. Technol. B* **1991**, *9*, 2503.
[114] F. Ishii, Y. Kita, in *Advanced Inorganic Fluorides*, Elsevier, **2000**, pp. 625–660.
[115] J. VanOmmeren, *J. ASTM Int.* **2009**, *6*, JAI102215.
[116] H. A. Bernhardt, E. J. Barber, R. A. Gustison, *Ind. Eng. Chem.* **1959**, *51*, 179–184.
[117] K. O. Christe, D. Naumann, *Inorg. Chem.* **1973**, *12*, 59–62.
[118] W. W. Wilson, K. O. Christe, *Inorg. Chem.* **1989**, *28*, 4172–4175.
[119] R. Schmidt, B. G. Müller, *Z. Anorg. Allg. Chem.* **2004**, *630*, 2393–2397.
[120] J. Linnera, S. I. Ivlev, F. Kraus, A. J. Karttunen, *Z. Anorg. Allg. Chem.* **2019**, *645*, 284–291.
[121] G. A. Hyde, M. M. Boudakian, *Inorg. Chem.* **1968**, *7*, 2648–2649.
[122] M. Drifford, R. Rousson, J. M. Weulersse, *Can. J. Phys.* **1978**, *56*, 1353–1357.
[123] R. D. Burbank, F. N. Bensey, *J. Chem. Phys.* **1957**, *27*, 982–983.
[124] R. D. Burbank, G. R. Jones, *Inorg. Chem.* **1974**, *13*, 1071–1074.
[125] R. L. Krieger, R. Gatti, H. J. Schumacher, *Z. Phys. Chem.* **1966**, *51*, 240–254.
[126] D. Pilipovich, W. Maya, E. A. Lawton, H. F. Bauer, D. F. Sheehan, N. N. Ogimachi, R. D. Wilson, F. C. Gunderloy, V. E. Bedwell, *Inorg. Chem.* **1967**, *6*, 1918–1919.
[127] H. Meinert, U. Groß, *Z. Chem.* **1971**, *11*, 469–469.
[128] E. A. Robinson, R. J. Gillespie, *Inorg. Chem.* **2003**, *42*, 3865–3872.
[129] J. Pilmé, E. A. Robinson, R. J. Gillespie, *Inorg. Chem.* **2006**, *45*, 6198–6204.

[130] R. D. Burbank, F. N. Bensey, *J. Chem. Phys.* **1957**, *27*, 981–982.
[131] K. O. Christe, *Inorg. Chem.* **1973**, *12*, 1580–1587.
[132] K. O. Christe, J. C. P. Sanders, G. J. Schrobilgen, W. W. Wilson, *J. Chem. Soc., Chem. Commun.* **1991**, 837–840.
[133] T. D. Cooper, F. N. Dost, C. H. Wang, *J. Inorg. Nucl. Chem.* **1972**, *34*, 3564–3567.
[134] L. Andrews, F. K. Chi, A. Arkell, *J. Am. Chem. Soc.* **1974**, *96*, 1997–2000.
[135] H. S. P. Müller, *Chem. Phys. Lett.* **1999**, *314*, 396–402.
[136] H. S. P. Müller, E. A. Cohen, *J. Chem. Phys.* **2002**, *116*, 2407–2416.
[137] K. Seppelt, *Angew. Chem. Int. Ed.* **2019**, *58*, 18928–18930.
[138] M. Schmeisser, K. Lang, *Angew. Chem.* **1955**, *67*, 156–156.
[139] J. J. Krasznai, Oxo and Oxyfluoro Complexes of Iodine (V) and (VII), Dissertation, McMaster University (Canada), **1975**.
[140] I.-C. Hwang, R. Kuschel, K. Seppelt, *Z. Anorg. Allg. Chem.* **1997**, *623*, 379–383.
[141] M. Schmeisser, K. Brändle, in *Advances in Inorganic Chemistry and Radiochemistry*, Academic Press, New York, London, **1963**, pp. 41–89.
[142] K. O. Christe, C. J. Schack, in *Advances in Inorganic Chemistry and Radiochemistry*, Academic Press, New York, London, **1976**, pp. 319–398.
[143] R. J. Gillespie, P. H. Spekkens, *Isr. J. Chem.* **1978**, *17*, 11–19.
[144] R. Bougon, J. Isabey, P. Plurien, *C. R. Seances Acad. Sci., Ser. C* **1971**, *273*, 415–417.
[145] R. Bougon, T. Bui Huy, A. Cadet, P. Charpin, R. Rousson, *Inorg. Chem.* **1974**, *13*, 690–695.
[146] K. O. Christe, C. J. Schack, D. Pilipovich, *Inorg. Chem.* **1972**, *11*, 2205–2208.
[147] R. J. Gillespie, P. H. Spekkens, *J. Chem. Soc., Dalton Trans.* **1977**, 1539–1546.
[148] M. Adelhelm, E. Jacob, *Angew. Chem. Int. Ed. Engl.* **1977**, *16*, 461–461.
[149] R. Bougon, T. Bui Huy, P. Charpin, R. J. Gillespie, P. H. Spekkens, *J. Chem. Soc., Dalton Trans.* **1979**, 6–12.
[150] R. J. Gillespie, J. P. Krasznai, D. R. Slim, *J. Chem. Soc., Dalton Trans.* **1980**, 481–483.
[151] R. Bougon, J. Isabey, P. Plurien, *C. R. Seances Acad. Sci., Ser. C* **1970**, *271*, 1366–1369.
[152] D. Pilipovich, C. B. Lindahl, C. J. Schack, R. D. Wilson, K. O. Christe, *Inorg. Chem.* **1972**, *11*, 2189–2192.
[153] R. Bougon, T. Bui Huy, *C. R. Seances Acad. Sci., Ser. C* **1976**, *283*, 461–463.
[154] E. E. Aynsley, R. Nichols, P. L. Robinson, *J. Chem. Soc.* **1953**, 623.
[155] A. J. Edwards, P. Taylor, *J. Fluorine Chem.* **1974**, *4*, 173–179.
[156] K. O. Christe, E. C. Curtis, *Inorg. Chem.* **1972**, *11*, 2209–2211.
[157] R. Bougon, T. Bui Huy, P. Charpin, G. Tantot, *C. R. Seances Acad. Sci., Ser. C* **1976**, *283*, 71–74.
[158] R. Bougon, P. Joubert, G. Tantot, *J. Chem. Phys.* **1977**, *66*, 1562–1565.
[159] R. J. Gillespie, P. Spekkens, *J. Chem. Soc., Dalton Trans.* **1976**, 2391–2396.
[160] R. R. Ryan, L. B. Asprey, *Acta Cryst. B* **1972**, *28*, 979–981.
[161] K. O. Christe, W. W. Wilson, D. A. Dixon, J. A. Boatz, *J. Am. Chem. Soc.* **1999**, *121*, 3382–3385.
[162] K. O. Christe, C. J. Schack, D. Pilipovich, W. Sawodny, *Inorg. Chem.* **1969**, *8*, 2489–2494.
[163] A. A. Woolf, *J. Chem. Soc.* **1954**, 4113–4116.

[164] E. Jacob, *Angew. Chem.* **1976**, *88*, 189–190.
[165] P. H. Spekkens, Oxyfluoro Compounds of Bromine, Dissertation, McMaster University (Canada), **1977**.
[166] H. Schmitz, H. J. Schumacher, *Z. Anorg. Allg. Chem.* **1942**, *249*, 238–244.
[167] H. Bode, E. Klesper, *Z. Anorg. Allg. Chem.* **1951**, *266*, 275–280.
[168] M. Schmeisser, E. Pammer, *Angew. Chem.* **1955**, *67*, 156–156.
[169] D. K. Huggins, W. B. Fox, *Inorg. Nucl. Chem. Lett.* **1970**, *6*, 337–339.
[170] K. O. Christe, E. C. Curtis, *Inorg. Chem.* **1972**, *11*, 35–39.
[171] R. F. Weinland, O. Lauenstein, *Z. Anorg. Chem.* **1899**, *20*, 30–39.
[172] L. Helmholz, M. T. Rogers, *J. Am. Chem. Soc.* **1940**, *62*, 1537–1542.
[173] J. P. Mack, J. A. Boatz, M. Gerken, *Inorg. Chem.* **2008**, *47*, 3243–3247.
[174] N. Bartlett, L. E. Levchuk, *Proc. Chem. Soc.* **1963**, 342–343.
[175] K. O. Christe, E. C. Curtis, D. A. Dixon, *J. Am. Chem. Soc.* **1993**, *115*, 9655–9658.
[176] A.-R. Mahjoub, K. Seppelt, *J. Chem. Soc., Chem. Commun.* **1991**, 840.
[177] K. O. Christe, *Inorg. Nucl. Chem. Lett.* **1972**, *8*, 453–455.
[178] K. O. Christe, R. D. Wilson, E. C. Curtis, *Inorg. Chem.* **1973**, *12*, 1358–1362.
[179] R. J. Gillespie, J. P. Krasznai, *Inorg. Chem.* **1977**, *16*, 1384–1392.
[180] K. O. Christe, *Inorg. Nucl. Chem. Lett.* **1972**, *8*, 457–459.
[181] K. O. Christe, R. D. Wilson, *Inorg. Chem.* **1973**, *12*, 1356–1357.
[182] A. Engelbrecht, P. Peterfy, E. Schandara, *Z. Anorg. Allg. Chem.* **1971**, *384*, 202–210.
[183] I. R. Beattie, G. J. Van Schalkwyk, *Inorg. Nucl. Chem. Lett.* **1974**, *10*, 343–347.
[184] J. A. Boatz, K. O. Christe, D. A. Dixon, B. A. Fir, M. Gerken, R. Z. Gnann, H. P. A. Mercier, G. J. Schrobilgen, *Inorg. Chem.* **2003**, *42*, 5282–5292.
[185] A. Engelbrecht, H. Atzwanger, *Monatsh. Chem.* **1952**, *83*, 1087–1089.
[186] E. H. Appelman, M. H. Studier, *J. Am. Chem. Soc.* **1969**, *91*, 4561–4562.
[187] J. F. Lehmann, G. J. Schrobilgen, *J. Am. Chem. Soc.* **2005**, *127*, 9416–9427.
[188] H. Oberhammer, K. O. Christe, *Inorg. Chem.* **1982**, *21*, 273–275.
[189] A. Ellern, J. A. Boatz, K. O. Christe, T. Drews, K. Seppelt, *Z. Anorg. Allg. Chem.* **2002**, *628*, 1991–1999.
[190] D. Pilipovich, R. D. Wilson, *Synthesis of Oxychlorine Trifluoride (North American Rockwell Corporation)*, **1972**, US-3,697,394.
[191] D. Pilipovich, R. D. Wilson, H. F. Bauer, *Oxychlorine Trifluoride and Alkali Fluoride-Cl2O Complex (North American Rockwell Corporation)*, **1973**, US-3,733,392.
[192] R. D. Wilson, A. E. Axworthy, K. O. Christe, *J. Argent. Chem. Soc.* **2005**, *93*, 1–20.
[193] C. J. Schack, C. B. Lindahl, D. Pilipovich, K. O. Christe, *Inorg. Chem.* **1972**, *11*, 2201–2205.
[194] R. Minkwitz, M. Berkei, R. Ludwig, *Inorg. Chem.* **2001**, *40*, 6493–6495.
[195] K. O. Christe, E. C. Curtis, C. J. Schack, *Inorg. Chem.* **1972**, *11*, 2212–2215.
[196] K. O. Christe, W. W. Wilson, R. D. Wilson, *Inorg. Chem.* **1989**, *28*, 904–908.
[197] H. S. P. Müller, *J. Mol. Struct.* **2000**, *517–518*, 335–350.
[198] K. O. Christe, R. D. Wilson, C. J. Schack, *Inorg. Synth.* **1986**, *24*, 3–6.
[199] M. Schmeisser, F. L. Ebenhöch, *Angew. Chem.* **1954**, *66*, 230–231.
[200] E. Jacob, *Angew. Chem. Int. Ed. Engl.* **1976**, *15*, 158–158.
[201] J. F. Lehmann, S. Riedel, G. J. Schrobilgen, *Inorg. Chem.* **2008**, *47*, 8343–8356.

[202] F. Cunin, C. Deudon, F. Favier, B. Mula, J. L. Pascal, *Inorg. Chem.* **2002**, *41*, 4173–4178.
[203] M. Fourati, M. Chaabouni, C. H. E. Belin, J. L. Pascal, J. Potier, *New J. Chem.* **1990**, *14*, 695–700.
[204] K. M. Tobias, M. Jansen, *Angew. Chem. Int. Ed. Engl.* **1986**, *25*, 993–994.
[205] K. M. Tobias, M. Jansen, *Z. Anorg. Allg. Chem.* **1987**, *550*, 16–26.
[206] T. E. Mallouk, G. L. Rosenthal, G. Mueller, R. Brusasco, N. Bartlett, *Inorg. Chem.* **1984**, *23*, 3167–3173.
[207] T. E. Mallouk, B. Desbat, N. Bartlett, *Inorg. Chem.* **1984**, *23*, 3160–3166.
[208] R. Bougon, W. V. Cicha, M. Lance, L. Meublat, M. Nierlich, J. Vigner, *Inorg. Chem.* **1991**, *30*, 102–109.
[209] A. J. Edwards, R. J. C. Sills, *J. Chem. Soc., Dalton Trans.* **1974**, 1726–1729.
[210] G. Tantot, R. Bougon, P. Plurien, *C. R. Seances Acad. Sci., Ser. C* **1975**, *281*, 271–273.
[211] M. Gerken, J. P. Mack, G. J. Schrobilgen, R. J. Suontamo, *J. Fluorine Chem.* **2004**, *125*, 1663–1670.
[212] M. Zhang, C. Hu, T. Abudouwufu, Z. Yang, S. Pan, *Chem. Mater.* **2018**, *30*, 1136–1145.
[213] K. O. Christe, D. A. Dixon, A. R. Mahjoub, H. P. A. Mercier, J. C. P. Sanders, K. Seppelt, G. J. Schrobilgen, W. W. Wilson, *J. Am. Chem. Soc.* **1993**, *115*, 2696–2706.
[214] A. Engelbrecht, P. Peterfy, *Angew. Chem.* **1969**, *81*, 753–753.
[215] M. Jaccaud, R. Faron, D. Devilliers, R. Romano, S. Riedel, H. Pernice, in *Ullmann's Encyclopedia of Industrial Chemistry*, American Cancer Society, **2020**, pp. 1–19.
[216] Georg Brauer, *Handbuch der präparativen anorganischen Chemie*, Ferdinand Enke Verlag, Stuttgart, **1975**.
[217] S. S. Rudel, Ammonolyse von Uranhalogeniden und Beiträge zur Chemie der Platinfluoride, Dissertation, Philipps-Universität Marburg, **2019**.
[218] *Chlorine Trifluoride Handling Manual, Technical Report AF/SSD-TR-61-9*, Rocketdyne, Canoga Park, California, **1961**.
[219] I. M. Lowles, T. D. Mac Mahon, R. A. P. Wiltshire, D. Crossley, A. J. Fudge, *Nucl. Instrum. Methods Phys. Res., Sect. A* **1992**, *312*, 339–345.
[220] J. P. Butler, M. Lounsbury, J. S. Merritt, *Can. J. Chem.* **1956**, *34*, 253–258.
[221] *International Tables for Crystallography Volume C*, Kluwer Academic Publishers, Dordrecht, Boston, London, **2004**.
[222] *APEX3*, Bruker AXS Inc., Madison, Wisconsin, USA, **2018**.
[223] *X-Area*, STOE & Cie GmbH, Darmstadt, Germany, **2018**.
[224] *SADABS*, Bruker AXS Inc., Madison, Wisconsin, USA, **2016**.
[225] *TWINABS*, Bruker AXS Inc., Madison, Wisconsin, USA, **2012**.
[226] *X-Shape*, STOE & Cie GmbH, Darmstadt, Germany, **2017**.
[227] *X-RED32*, STOE & Cie GmbH, Darmstadt, Germany, **2018**.
[228] G. M. Sheldrick, *Acta Crystallogr., Sect. A: Found. Adv.* **2015**, *71*, 3–8.
[229] G. M. Sheldrick, *Acta Crystallogr., Sect. C: Struct. Chem.* **2015**, *71*, 3–8.
[230] G. M. Sheldrick, *SHELXL-2016/6*, Göttingen, Germany, **2016**.
[231] C. B. Hübschle, G. M. Sheldrick, B. Dittrich, *J. Appl. Crystallogr.* **2011**, *44*, 1281–1284.
[232] S. I. Ivlev, M. Conrad, F. Kraus, *Z. Kristallogr. - Cryst. Mater.* **2019**, *234*, 415–418.
[233] A. L. Spek, *Acta Crystallogr., Sect. C: Struct. Chem.* **2015**, *71*, 9–18.

[234] A. L. Spek, *PLATON - A Multipurpose Crystallographic Tool*, Utrecht University, Utrecht, The Netherlands, **2019**.
[235] K. Brandenburg, H. Putz, *Diamond - Crystal and Molecular Structure Visualization*, Crystal Impact GbR, Bonn, **2019**.
[236] M. Müller, Die Chemie des Berylliums: Bio-Anorganische Grundlagenforschung, Dissertation, Philipps-Universität Marburg, **2020**.
[237] *OPUS V7.2*, Bruker Optik GmbH, Ettlingen, Germany, **2012**.
[238] *OriginPro 2017*, OriginLAb Corporation, **2017**.
[239] *VistaControl*, Spectroscopy And Imaging GmbH, Warstein, Germany, **2018**.
[240] R. Dovesi, A. Erba, R. Orlando, C. M. Zicovich-Wilson, B. Civalleri, L. Maschio, M. Rérat, S. Casassa, J. Baima, S. Salustro, B. Kirtman, *Wiley Interdiscip. Rev.: Comput. Mol. Sci.* **2018**, e1360.
[241] R. Dovesi, V. R. Saunders, R. Roetti, R. Orlando, C. M. Zicovich-Wilson, F. Pascale, B. Civalleri, K. Doll, N. M. Harrison, I. J. Bush, P. D'Arco, M. Llunell, M. Causa, Y. Noel, L. Maschio, A. Erba, M. Rerat, S. Casassa, *CRYSTAL17 User's Manual*, University Of Torino, Torino, **2017**.
[242] J. P. Perdew, K. Burke, M. Ernzerhof, *Phys. Rev. Lett.* **1996**, *77*, 3865–3868.
[243] C. Adamo, V. Barone, *J. Chem. Phys.* **1999**, *110*, 6158–6170.
[244] F. Weigend, R. Ahlrichs, *Phys. Chem. Chem. Phys.* **2005**, *7*, 3297–3305.
[245] H. J. Monkhorst, J. D. Pack, *Phys. Rev. B* **1976**, *13*, 5188–5192.
[246] R. S. Mulliken, *J. Chem. Phys.* **1955**, *23*, 1833–1840.
[247] C. M. Zicovich-Wilson, F. Pascale, C. Roetti, V. R. Saunders, R. Orlando, R. Dovesi, *J. Comput. Chem.* **2004**, *25*, 1873–1881.
[248] F. Pascale, C. M. Zicovich-Wilson, F. López Gejo, B. Civalleri, R. Orlando, R. Dovesi, *J. Comput. Chem.* **2004**, *25*, 888–897.
[249] L. Maschio, B. Kirtman, M. Rérat, R. Orlando, R. Dovesi, *J. Chem. Phys.* **2013**, *139*, 164101.
[250] *Jmol: an open-source Java viewer for chemical structures in 3D. http://www.jmol.org/*, Jmol Team, **2019**.
[251] K. Eklund, M. S. Kuklin, F. Kraus, A. J. Karttunen, *ChemPhysChem* **2020**, *21*, 802–808.
[252] V. Sivchik, R. K. Sarker, Z.-Y. Liu, K.-Y. Chung, E. V. Grachova, A. J. Karttunen, P.-T. Chou, I. O. Koshevoy, *Chem. Eur. J.* **2018**, *24*, 11475–11484.
[253] A. J. Karttunen, T. Tynell, M. Karppinen, *J. Phys. Chem. C* **2015**, *119*, 13105–13114.
[254] L. M. Scherf, A. J. Karttunen, O. Pecher, P. C. M. M. Magusin, C. P. Grey, T. F. Fässler, *Angew. Chem. Int. Ed.* **2016**, *55*, 1075–1079.
[255] R. E. Stene, B. Scheibe, C. Pietzonka, A. J. Karttunen, W. Petry, F. Kraus, *J. Fluorine Chem.* **2018**, *211*, 171–179.
[256] H. L. Deubner, M. Sachs, J. Bandemehr, S. I. Ivlev, A. J. Karttunen, S. R. Kachel, B. P. Klein, L. Ruppenthal, M. Schöniger, C. K. Krug, J. Herritsch, J. M. Gottfried, J. M. N. Aman, J. Schmedt auf der Günne, F. Kraus, *Chem. Eur. J* **2019**, *25*, 15656–15661.
[257] B. Scheibe, A. J. Karttunen, F. Kraus, *Eur. J. Inorg. Chem.* **2020**, DOI https://doi.org/10.1002/ejic.202000908.
[258] B. Scheibe, S. Lippert, S. S. Rudel, M. R. Buchner, O. Burghaus, C. Pietzonka, M. Koch, A. J. Karttunen, F. Kraus, *Chem. Eur. J.* **2016**, *22*, 12145–12153.
[259] H. Schmitz, H. J. Schumacher, *Z. Naturforsch.* **1947**.
[260] D. Pilipovich, H. H. Rogers, R. D. Wilson, *Inorg. Chem.* **1972**, *11*, 2192–2195.

[261] H. Lynton, J. Passmore, *Can. J. Chem.* **1971**, *49*, 2539–2543.
[262] A. J. Edwards, R. J. C. Sills, *J. Chem. Soc., A* **1970**, 2697–2699.
[263] M. Y. Antipin, A. M. Ellern, V. F. Sukhoverkhov, Y. T. Struchkov, Y. A. Buslaev, *Russ. J. Inorg. Chem.* **1988**, *33*, 171–173.
[264] A. M. Ellern, M. N. Sinitsyn, M. Y. Antipin, A. V. Sharabarin, Y. T. Struchkov, *Koord. Khim.* **1991**, *17*, 1686–1688.
[265] A. M. Ellern, M. Y. Antipin, A. V. Sharabarin, Y. T. Struchkov, *Russ. J. Inorg. Chem.* **1991**, *36*, 1278–1280.
[266] A. M. Ellern, M. Y. Antipin, A. V. Sharabarin, Y. T. Struchkov, *Russ. J. Inorg. Chem.* **1992**, *37*, 46–47.
[267] D. S. Brock, J. J. Casalis de Pury, H. P. A. Mercier, G. J. Schrobilgen, B. Silvi, *Inorg. Chem.* **2010**, *49*, 6673–6689.
[268] P. Kjeldsen, *Water Res.* **1993**, *27*, 121–131.
[269] E. I. Hormats, F. C. Unterleitner, *J. Phys. Chem.* **1965**, *69*, 3677–3681.
[270] F. W. Giacobbe, *J. Appl. Polym. Sci.* **1990**, *39*, 1121–1132.
[271] C. W. Extrand, L. Monson, *J. Appl. Polym. Sci.* **2006**, *100*, 2122–2125.
[272] Z. Mazej, E. Goreshnik, *Eur. J. Inorg. Chem.* **2008**, *11*, 1795–1812.
[273] H. Fitz, B. G. Müller, O. Graudejus, N. Bartlett, *Z. Anorg. Allg. Chem.* **2002**, *628*, 133–137.
[274] F. Averdunk, R. Hoppe, *Z. Anorg. Allg. Chem.* **1990**, *582*, 111–120.
[275] W. B. Jensen, in *Cohesion and Structure* (Eds.: J. Hafner, F. Hulliger, W.B. Jensen, J.A. Majewski, K. Mathis, P. Villars, P. Vogl), North-Holland, **1989**, pp. 105–146.
[276] W. L. Bragg, *Proc. R. Soc. London, Ser. A* **1914**, *89*, 468–489.
[277] T. F. Antokhina, N. N. Savchenko, S. B. Ivanov, L. N. Ignat'eva, V. Ya. Kavun, V. I. Sergienko, *Russ. Chem. Bull.* **1992**, *41*, 1941–1949.
[278] J. E. Griffiths, D. E. Irish, *Inorg. Chem.* **1964**, *3*, 1134–1137.
[279] O. Graudejus, A. P. Wilkinson, L. C. Chacón, N. Bartlett, *Inorg. Chem.* **2000**, *39*, 2794–2800.
[280] F. Kraus, *Acta Crystallogr., Sect. E: Struct. Rep. Online* **2014**, *70*, i43–i43.
[281] R. Fischer, B. G. Müller, *Z. Anorg. Allg. Chem.* **2001**, *627*, 445–452.
[282] P. Erlhöfer, W. Preetz, *Z. Naturforsch., B: Anorg. Chem., Org. Chem.* **1989**, *44*, 1214–1220.
[283] H. A. Carter, A. M. Qureshi, J. R. Sams, F. Aubke, *Can. J. Chem.* **1970**, *48*, 2853–2859.
[284] K. O. Christe, C. J. Schack, R. D. Wilson, *Inorg. Chem.* **1977**, *16*, 849–854.
[285] K. O. Christe, C. J. Schack, *Inorg. Chem.* **1978**, *17*, 2749–2754.
[286] G. M. Lucier, C. Shen, S. H. Elder, N. Bartlett, *Inorg. Chem.* **1998**, *37*, 3829–3834.
[287] Z. Mazej, E. Goreshnik, *Inorg. Chem.* **2020**, *59*, 2092–2103.
[288] Z. Mazej, E. Goreshnik, *Eur. J. Inorg. Chem.* **2019**, 1265–1272.
[289] R. Hoppe, K. Blinne, *Z. Anorg. Allg. Chem.* **1958**, *293*, 251–263.
[290] R. Hoppe, B. G. Müller, *Naturwissenschaften* **1969**, *56*, 35–35.
[291] J. Bandemehr, H. L. Deubner, M. Sachs, F. Kraus, *Z. Anorg. Allg. Chem.* **2018**, *644*, 1721–1726.
[292] N. W. Johnson, *Can. J. Math.* **1966**, *18*, 169–200.
[293] D. D. Gibler, C. J. Adams, M. Fischer, Allan. Zalkin, Neil. Bartlett, *Inorg. Chem.* **1972**, *11*, 2325–2329.
[294] L. D. Calvert, J. R. Morton, *Acta Cryst.* **1964**, *17*, 613–613.

[295] H. Du, G. Wang, X. Gong, H. Xiao, *Int. J. Quantum Chem.* **2012**, *112*, 1291–1298.
[296] B. Scheibe, A. J. Karttunen, F. Weigend, F. Kraus, *Chem. - Eur. J.* **2020**, DOI 10.1002/chem.202003629.
[297] K. Matsumoto, R. Hagiwara, Z. Mazej, E. Goreshnik, B. Žemva, *J. Phys. Chem. B* **2006**, *110*, 2138–2141.
[298] G. L. Cote, H. W. Thompson, *Proc. Roy. Soc. (London)* **1951**, *210*, 217–223.
[299] J. O. Edwards, G. C. Morrison, V. F. Ross, J. W. Schultz, *J. Am. Chem. Soc.* **1955**, *77*, 266–268.
[300] J. Goubeau, W. Bues, *Z. Anorg. Allg. Chem.* **1952**, *268*, 221–228.
[301] R. E. Stene, B. Scheibe, A. J. Karttunen, W. Petry, F. Kraus, *Eur. J. Inorg. Chem.* **2019**, *2019*, 3672–3682.
[302] W. L. Bragg, *Philos. Mag. (1798-1977)* **1914**, *28*, 355–360.
[303] M. R. Bortolus, H. P. A. Mercier, G. J. Schrobilgen, *Chem. Eur. J.* **2020**, *26*, 8935–8950.
[304] N. Bartlett, J. Trotter, *J. Chem. Soc., A* **1968**, 543.
[305] H. Shorafa, K. Seppelt, *Inorg. Chem.* **2006**, *45*, 7929–7934.
[306] M. Gerken, D. A. Dixon, G. J. Schrobilgen, *Inorg. Chem.* **2000**, *39*, 4244–4255.
[307] M. J. Hughes, H. P. A. Mercier, G. J. Schrobilgen, *Inorg. Chem.* **2010**, *49*, 3501–3515.
[308] T. Drews, J. Supeł, A. Hagenbach, K. Seppelt, *Inorg. Chem.* **2006**, *45*, 3782–3788.
[309] H. H. Claassen, H. Selig, *Isr. J. Chem.* **1969**, *7*, 499–504.
[310] B. Weinstock, H. H. Claassen, J. G. Malm, *J. Chem. Phys.* **1960**, *32*, 181–185.
[311] U. Engelmann, B. G. Müller, *Z. Anorg. Allg. Chem.* **1991**, *598*, 103–110.
[312] C. Röhr, S. Loss, *Z. Naturforsch., B: J. Chem. Sci.* **1998**, *53*, 75–80.
[313] M. M. Steyn, A. M. Heyns, R. B. English, *J. Crystallogr. Spectrosc. Res.* **1984**, *14*, 505–512.
[314] W. P. Davey, *Phys. Rev.* **1923**, *21*, 143–161.
[315] M. A. Ellwanger, S. Steinhauer, P. Golz, H. Beckers, A. Wiesner, B. Braun-Cula, T. Braun, S. Riedel, *Chem. Eur. J.* **2017**, *23*, 13501–13509.
[316] K. Lutar, A. Jesih, I. Leban, B. Žemva, N. Bartlett, *Inorg. Chem.* **1989**, *28*, 3467–3471.
[317] M. Azeem, M. Brownstein, R. J. Gillespie, *Can. J. Chem.* **1969**, *47*, 4159–4167.
[318] H. A. Carter, F. Aubke, *Can. J. Chem.* **1970**, *48*, 3456–3459.
[319] R. D. Shannon, *Acta Crystallogr., Sect. A: Cryst. Phys., Diffr., Theor. Gen. Crystallogr.* **1976**, *32*, 751–767.
[320] D. S. Brock, J. J. Casalis de Pury, H. P. A. Mercier, G. J. Schrobilgen, B. Silvi, *J. Am. Chem. Soc.* **2010**, *132*, 3533–3542.
[321] H. Selig, J. Shamir, *Inorg. Chem.* **1964**, *3*, 294–294.
[322] B. Scheibe, Darstellung und Charakterisierung von Hexafluoridouranaten(V), Masterarbeit, Philipps-Universität Marburg, **2017**.
[323] J. Yeon, M. D. Smith, J. Tapp, A. Möller, H.-C. zur Loye, *Inorg. Chem.* **2014**, *53*, 6289–6298.
[324] J. Yeon, M. D. Smith, J. Tapp, A. Möller, H.-C. zur Loye, *J. Am. Chem. Soc.* **2014**, *136*, 3955–3963.
[325] J. Yeon, M. D. Smith, G. Morrison, H.-C. zur Loye, *Inorg. Chem.* **2015**, *54*, 2058–2066.

[326] J. Felder, J. Yeon, M. Smith, H.-C. zur Loye, *Inorg. Chem. Front.* **2017**, *4*, 368–377.
[327] V. V. Klepov, J. B. Felder, H.-C. zur Loye, *Inorg. Chem.* **2018**, *57*, 5597–5606.
[328] C. Keller, H. Schmutz, *Inorg. Nucl. Chem. Lett.* **1966**, *2*, 355–358.
[329] R. A. Penneman, T. K. Keenan, L. B. Asprey, in *Lanthanide/Actinide Chemistry* (Eds.: P.R. Fields, T. Moeller), AMERICAN CHEMICAL SOCIETY, WASHINGTON, D.C., **1967**, pp. 248–255.
[330] L. R. Morss, N. M. Edelstein, J. Fuger, J. J. Katz, Eds. , *The Chemistry of the Actinide and Transactinide Elements*, Springer, Dordrecht, **2006**.
[331] P. Vitorge, H. Capdevila, S. Maillard, M.-H. Faure, T. Vercouter, *J. Nucl. Sci. Technol.* **2002**, *39*, 713–716.
[332] R. E. Wilson, P. M. Almond, P. C. Burns, L. Soderholm, *Inorg. Chem.* **2006**, *45*, 8483–8485.
[333] G. A. Burney, F. W. Tober, *Ind. Eng. Chem. Proc. Des. Dev.* **1965**, *4*, 28–32.
[334] R. A. Penneman, R. R. Ryan, A. Rosenzweig, *Acta Cryst. B* **1974**, *30*, 1966–1970.
[335] A. T. Chemey, J. M. Sperling, C. J. Windorff, D. E. Hobart, T. E. Albrecht-Schmitt, *Cryst. Growth Des.* **2020**, *20*, 2998–3006.
[336] A. Oudahmane, M. El-Ghozzi, L. Jouffret, D. Avignant, *J. Solid State Chem.* **2015**, *232*, 73–78.
[337] C. C. Underwood, M. Mann, C. D. McMillen, J. D. Musgraves, J. W. Kolis, *Solid State Sci.* **2012**, *14*, 574–579.
[338] D. Avignant, I. Mansouri, R. Chevalier, J. C. Cousseins, *J. Solid State Chem.* **1981**, *38*, 121–127.
[339] C. Plitzko, G. Meyer, *Z. Anorg. Allg. Chem.* **1998**, *624*, 169–170.
[340] D. Koller, B. G. Müller, *Z. Anorg. Allg. Chem.* **2002**, *628*, 575–579.
[341] J. Lima-de-Faria, E. Hellner, F. Liebau, E. Makovicky, E. Parthé, *Acta Cryst. A* **1990**, *46*, 1–11.
[342] M. Rahm, R. Hoffmann, N. W. Ashcroft, *Chem. Eur. J.* **2016**, *22*, 14625–14632.
[343] M. Seth, M. Dolg, P. Fulde, P. Schwerdtfeger, *J. Am. Chem. Soc.* **1995**, *117*, 6597–6598.
[344] G. Brunton, *Acta Cryst.* **1966**, *21*, 814–817.
[345] G. Brunton, *Acta Cryst. B* **1969**, *25*, 1919–1921.
[346] J. B. Friauf, *J. Am. Chem. Soc.* **1927**, *49*, 3107–3114.
[347] R. C. Birtcher, M. H. Mueller, J. W. Richardson, J. Faber, *MRS Online Proc. Libr.* **1989**, *166*, 437–441.
[348] D. E. Laughlin, K. Hono, Eds. , *Physical Metallurgy*, Elsevier, Amsterdam, **2014**.
[349] D. Avignant, I. Mansouri, R. Sabatier, J. C. Cousseins, R. Chevalier, *Acta Cryst. B* **1980**, *36*, 664–666.
[350] G. Koch, *Transurane Teil C: Die Verbindungen*, Springer Berlin Heidelberg, Berlin, Heidelberg, **1972**.
[351] J. N. Cross, T.-H. Lee, C.-J. Kang, Y.-X. Yao, S. K. Cary, J. T. Stritzinger, M. J. Polinski, C. D. McKinley, T. E. Albrecht Schmitt, N. Lanata, *Chem. Sci.* **2019**, *10*, 6508–6518.
[352] A. Cousson, H. Abazli, A. Tabuteau, M. Pagès, M. Gasperin, *Acta Cryst. B* **1982**, *38*, 1801–1803.
[353] W. H. Zachariasen, *J. Am. Chem. Soc.* **1948**, *70*, 2147–2151.

[354] B. Scheibe, C. Pietzonka, O. Mustonen, M. Karppinen, A. J. Karttunen, M. Atanasov, F. Neese, M. Conrad, F. Kraus, *Angew. Chem.* **2018**, *130*, 2964–2968.
[355] B. Scheibe, C. Pietzonka, O. Mustonen, M. Karppinen, A. J. Karttunen, M. Atanasov, F. Neese, M. Conrad, F. Kraus, *Angew. Chem. Int. Ed.* **2018**, *57*, 2914–2918.
[356] S. I. Troyanov, *Crystallogr. Rep.* **2005**, *50*, 773–778.
[357] T. Bunič, M. Tramšek, E. Goreshnik, B. Žemva, *J. Solid State Chem.* **2008**, *181*, 2318–2324.
[358] N. A. Jasim, R. N. Perutz, S. P. Foxon, P. H. Walton, *J. Chem. Soc., Dalton Trans.* **2001**, 1676–1685.
[359] B. J. Truscott, F. Nahra, A. M. Z. Slawin, D. B. Cordes, S. P. Nolan, *Chem. Commun.* **2015**, *51*, 62–65.
[360] F. Nahra, M. Brill, A. Gómez-Herrera, C. S. J. Cazin, S. P. Nolan, *Coord. Chem. Rev.* **2016**, *307*, 65–80.
[361] A. Rosenzweig, D. T. Cromer, *Acta Crystallogr.* **1967**, *23*, 865–867.
[362] C. G. Gianopoulos, V. V. Zhurov, S. G. Minasian, E. R. Batista, C. Jelsch, A. A. Pinkerton, *Inorg. Chem.* **2017**, *56*, 1775–1778.
[363] V. C. Epa, W. R. Thorson, *J. Chem. Phys.* **1990**, *93*, 3773–3786.
[364] G. L. Coté, H. W. Thompson, *Proc. R. Soc. Lond. A* **1951**, *210*, 206–216.
[365] H. G. Hecht, J. G. Malm, J. Foropoulos, W. T. Carnall, *J. Chem. Phys.* **1986**, *84*, 3653.
[366] M. P. Eastman, P. Gary Eller, G. W. Halstead, *J. Inorg. Nucl. Chem.* **1981**, *43*, 2839–2842.
[367] M. Tramšek, Z. Mazej, E. Goreshnik, G. Tavčar, *J. Fluorine Chem.* **2015**, *175*, 18–21.
[368] T. Bunič, M. Tramšek, E. Goreshnik, B. Žemva, *Acta Chim. Slov.* **2008**, *55*, 788–792.
[369] M. Tramšek, E. Goreshnik, M. Lozinšek, B. Žemva, *J. Fluorine Chem.* **2009**, *130*, 1093–1098.
[370] L. K. Frevel, H. W. Rinn, *Acta Cryst.* **1962**, *15*, 286–286.
[371] J. A. Ibers, *J. Phys. (Paris)* **1964**, *25*, 474–477.
[372] J. A. Ibers, *J. Chem. Phys.* **1964**, *40*, 402–404.
[373] S. Grabowski, *Crystals* **2015**, *6*, 3.
[374] R. Kruszynski, A. Trzesowska, *Acta Crystallogr., Sect. E: Struct. Rep. Online* **2007**, *63*, i179–i179.
[375] T. S. Cameron, O. Knop, L. A. MacDonald, *Can. J. Chem.* **1983**, *61*, 184–188.
[376] Z. Mazej, E. A. Goreshnik, *Z. Anorg. Allg. Chem.* **2015**, *641*, 1216–1219.
[377] C. Garcia, D. Barbusse, R. Fourcade, B. Ducourant, *J. Fluorine Chem.* **1991**, *51*, 245–256.
[378] L. Golič, V. Kaučič, B. Kojić-Prodić, *Acta Crystallogr., Sect. B: Struct. Crystallogr. Cryst. Chem.* **1980**, *36*, 659–661.
[379] I.-C. Hwang, Strukturchemie von Rhenium-, Uran- und Goldfluoriden, Dissertation, Freie Universität Berlin, **2001**.
[380] I. Peka, F. Sýkora, J. Vachuška, *Collect. Czech. Chem. Commun.* **1969**, *34*, 2857–2864.
[381] S. Giese, K. Seppelt, *Angew. Chem.* **1994**, *106*, 473–475.
[382] A. Beuter, W. Kuhlmann, W. Sawodny, *J. Fluorine Chem.* **1975**, *6*, 367–378.
[383] A. Ellern, A.-R. Mahjoub, K. Seppelt, *Angew. Chem. Int. Ed. Engl.* **1996**, *35*, 1123–1125.

[384] R. Craciun, R. T. Long, D. A. Dixon, K. O. Christe, *J. Phys. Chem. A* **2010**, *114*, 7571–7582.
[385] R. Craciun, D. Picone, R. T. Long, S. Li, D. A. Dixon, K. A. Peterson, K. O. Christe, *Inorg. Chem.* **2010**, *49*, 1056–1070.
[386] M. J. Molski, K. Seppelt, *Dalton Trans.* **2009**, 3379.
[387] K. Seppelt, *Chem. Rev.* **2015**, *115*, 1296–1306.
[388] R. Cui, Z. Cheng, J. Dai, Q. Dou, Q. Li, *ACS Omega* **2020**, *5*, 5651–5656.
[389] R. Cui, Z. Cheng, Q. Dou, Q. Li, *J. Radioanal. Nucl. Chem.* **2020**, *326*, 603–610.
[390] J. R. Geichman, E. A. Smith, P. R. Ogle, *Inorg. Chem.* **1963**, *2*, 1012–1015.
[391] J. G. Malm, H. Selig, S. Siegel, *Inorg. Chem.* **1966**, *5*, 130–132.
[392] N. S. Nikolaev, A. I. Sadikova, *At. Energy* **1968**, *25*, 1232–1233.
[393] A. T. Sadikova, G. G. Sadikov, N. S. Nikolaev, *At. Energy* **1969**, *26*, 313–314.
[394] A. Paillet, Contribution a l'etude des interactions entre l'hexafluorure d'uranium et les fluorures alcalins, Dissertation, Université Claude-Bernard (Frankreich), **1972**.
[395] R. Bougon, P. Charpin, J. P. Desmoulin, J. G. Malm, *Inorg. Chem.* **1976**, *15*, 2532–2540.
[396] A. Sattler, S. Ruccolo, G. Parkin, *Dalton Trans.* **2011**, *40*, 7777.
[397] C. C. Torardi, L. H. Brixner, G. Blasse, *J. Solid State Chem.* **1987**, *67*, 21–25.
[398] R. Haiges, J. A. Boatz, M. Yousufuddin, K. O. Christe, *Angew. Chem.* **2007**, *119*, 2927–2932.
[399] B. Roessler, K. Seppelt, *Angew. Chem.* **2000**, *112*, 1326–1329.
[400] V. Pfennig, K. Seppelt, N. Robertson, *Angew. Chem.* **1997**, *109*, 1410–1412.
[401] M.-J. Crawford, A. Ellern, P. Mayer, *Angew. Chem.* **2005**, *117*, 8086–8090.
[402] T. Vogt, A. N. Fitch, J. K. Cockcroft, *Science* **1994**, *263*, 1265–1267.
[403] G. W. Drake, D. A. Dixon, J. A. Sheehy, J. A. Boatz, K. O. Christe, *J. Am. Chem. Soc.* **1998**, *120*, 8392–8400.
[404] K. O. Christe, D. A. Dixon, J. C. P. Sanders, G. J. Schrobilgen, W. W. Wilson, *J. Am. Chem. Soc.* **1993**, *115*, 9461–9467.
[405] M. Kaupp, *Angew. Chem. Int. Ed.* **2001**, *40*, 3534.
[406] J. H. Levy, J. C. Taylor, A. B. Waugh, *J. Fluorine Chem.* **1983**, *23*, 29–36.
[407] I.-C. Hwang, K. Seppelt, *J. Fluorine Chem.* **2000**, *102*, 69–72.
[408] R. Bougon, R. M. Costes, J. P. Desmoulin, J. Michel, J. L. Person, *J. Inorg. Nucl. Chem.* **1976**, *28*, 99–105.
[409] R. Haiges, J. A. Boatz, T. Schroer, M. Yousufuddin, K. O. Christe, *Angew. Chem.* **2006**, *118*, 4948–4953.
[410] T. Saal, P. Deokar, K. O. Christe, R. Haiges, *Eur. J. Inorg. Chem.* **2019**, *2019*, 2388–2391.
[411] R. Haiges, *Dalton Trans.* **2019**, *48*, 806–813.
[412] R. Haiges, M. Rahm, D. A. Dixon, E. B. Garner, K. O. Christe, *Inorg. Chem.* **2012**, *51*, 1127–1141.
[413] J. Liu, K. S. Pedersen, S. M. Greer, I. Oyarzabal, A. Mondal, S. Hill, F. Wilhelm, A. Rogalev, A. Tressaud, E. Durand, J. R. Long, R. Clérac, *Angew. Chem.* **2020**, *132*, 10392–10396.
[414] R. Haiges, P. Deokar, M. Vasiliu, T. H. Stein, D. A. Dixon, K. O. Christe, *Chem. Eur. J.* **2017**, *23*, 8991–8991.
[415] Z. M. Smallwood, M. F. Davis, J. G. Hill, L. J. R. James, P. Portius, *Inorg. Chem.* **2019**, *58*, 4583–4591.

[416] J. M. Sperling, E. J. Warzecha, C. Celis-Barros, D.-C. Sergentu, X. Wang, B. E. Klamm, C. J. Windorff, A. N. Gaiser, F. D. White, D. A. Beery, A. T. Chemey, M. A. Whitefoot, B. N. Long, K. Hanson, P. Kögerler, M. Speldrich, E. Zurek, J. Autschbach, T. E. Albrecht-Schönzart, *Nature* **2020**, *583*, 396–399.
[417] H. Abazli, A. Cousson, J. Jové, M. Pagès, M. Gasperin, *J. Less-Common Met.* **1984**, *96*, 23–33.
[418] H. Abazli, A. Cousson, J. Jove, M. Pages, *J. Fluorine Chem.* **1980**, *16*, 647–648.
[419] *Chemical Abstracts Service Source Index (CASSI), https://cassi.cas.org/search.jsp*, **2020**.
[420] *Defense Technical Information Center (DTIC), https://discover.dtic.mil/technical-reports/*, **2020**.

7. Abdrucke der Publikationen

7.1. Synthesis and Characterization of the Tetrafluoridochlorates(III) *A*[ClF_4] (*A* = K, Rb, Cs)

Benjamin Scheibe, Sergei I. Ivlev, Antti J. Karttunen, Florian Kraus

Eur. J. Inorg. Chem. **2020**, *2020*, 1319–1324.
DOI: 10.1002/ejic.202000106

© 2020 The Authors. Published by Wiley-VCH Verlag GmbH & Co. KGaA.

Open access article distributed under the Creative Commons CC BY 4.0 license.
The original licensed material is shown.
(https://creativecommons.org/licenses/by/4.0/legalcode)

EurJIC
European Journal of Inorganic Chemistry

Full Paper
doi.org/10.1002/ejic.202000106

Interhalogen Chemistry

Synthesis and Characterization of the Tetrafluoridochlorates(III) $A[ClF_4]$ (A = K, Rb, Cs)

Benjamin Scheibe,[a] Sergei I. Ivlev,[a] Antti J. Karttunen,[b] and Florian Kraus*[a]

Abstract: Single-crystalline tetrafluoridochlorates(III) $A[ClF_4]$ (A = K, Rb, Cs) were synthesized from solvolysis reactions of alkali metal fluorides in liquid chlorine trifluoride. The structures were examined by means of single-crystal X-ray diffraction. $K[ClF_4]$ crystallizes in the $K[BrF_4]$ structure type, whereas the Rb and Cs compounds crystallize in the $Li[AuF_4]$ structure type. The compounds were further characterized by Raman and IR spectroscopy. Solid state quantum chemical calculations with hybrid density functional methods reproduced the experimental structures and enabled the interpretation of the experimental Raman and IR spectra.

Introduction

The first preparation of tetrafluoridochlorates(III) of the alkali metals, $A[ClF_4]$ (A = K, Rb, Cs), was probably accomplished by direct fluorination of the respective chlorides.[1–3] The authors first discussed a possible formation of polyfluorides of the type "AF_2" (A = K, Rb) and "AF_3" (A = Rb, Cs).[1–3] These results were disputed at a meeting of the Gesellschaft Deutscher Chemiker in 1950 and later revised by the same authors, who showed that the products contained alkali metal fluoridochlorates(III) as well as the alkali metal fluorides.[2,4] Polyfluorides have so far only been obtained under cryogenic conditions with the matrix isolation technique.[5–7]

Others have also prepared tetrafluoridochlorate(III)-containing products by fluorination of alkali metal chlorides at high pressures and/or temperatures.[8–10] The syntheses of tetrafluoridochlorates(III) are also possible by solvolysis reactions of alkali metal fluorides, AF (A = K, Rb, Cs) in ClF_3.[11–13] This approach is also commonly used for the syntheses of tetrafluoridobromates(III), see Equation (1).[14,15] The $[MF_4]^-$-compounds of iodine, gold and silver are also known.[15–17]

More complex anions with higher MF_3 content, such as $[M_2F_7]^-$ and $[M_3F_{10}]^-$, have been reported and are so far limited to the BrF_3 and AuF_3 systems.[18–22] The $[M_2F_7]^-$ anions show a μ_2-bridging fluorine atom and have been obtained in the compounds $A[Br_2F_7]$ (A = Rb, Cs, PbF) and $Cs[Au_2F_7]$.[18–22] Thus far, the $[Br_3F_{10}]^-$ anion has the highest MF_3 content, exhibiting a central μ_3-bridging F atom, and was obtained as the Rb and Cs salts.[20] The possibility of anions of the composition $[M_4F_{13}]^-$ for Au and Br has been the subject of a theoretical study.[23]

$$AF + MF_3 \xrightarrow{MF_3} A[MF_4] \quad (1)$$

A = e.g. K, Rb, Cs

M = Cl, Br

Here, we report on the syntheses, structure determinations, vibrational spectroscopic characterizations and hybrid density functional theory calculations of the tetrafluoridochlorates(III), $A[ClF_4]$ (A = K, Rb, Cs).

Results and Discussion

The tetrafluoridochlorates(III) of K, Rb and Cs were synthesized by a solvolysis reaction of the respective alkali metal fluoride in liquid ClF_3, see Equation (2).

$$AF + ClF_3 \xrightarrow{ClF_3} A[ClF_4] \quad (2)$$

A = K, Rb, Cs

Single crystals of $K[ClF_4]$ and $Rb[ClF_4]$ were obtained by carefully heating suspensions of the alkali metal fluorides in ClF_3 up to 50 °C in an air bath. In the case of $Cs[ClF_4]$, single crystals were obtained by slowly removing excess ClF_3 from solutions in vacuo.

Single Crystal X-ray Diffraction

Potassium tetrafluoridochlorate(III) crystallizes in the tetragonal space group $I4/mcm$ (No. 140) with four formula units per unit cell, Pearson symbol $tI24$ and Wyckoff sequence 140, lda. The compound is isotypic to $K[BrF_4]$.[24,25] See Table 1 for selected

[a] Fachbereich Chemie, Philipps-Universität Marburg, Hans-Meerwein-Straße 4, 35032 Marburg, Germany
E-mail: f.kraus@uni-marburg.de
[b] Department of Chemistry and Materials Science, Aalto University, 00076 Aalto, Finland

Supporting information and ORCID(s) from the author(s) for this article are available on the WWW under https://doi.org/10.1002/ejic.202000106.

© 2020 The Authors. Published by Wiley-VCH Verlag GmbH & Co. KGaA. • This is an open access article under the terms of the Creative Commons Attribution License, which permits use, distribution and reproduction in any medium, provided the original work is properly cited.

© 2020 The Authors. Published by Wiley-VCH Verlag GmbH & Co. KGaA, Weinheim

EurJIC
European Journal of Inorganic Chemistry

Full Paper
doi.org/10.1002/ejic.202000106

Chemistry Europe
European Chemical Societies Publishing

Table 1. Selected crystallographic data and details of the structure determinations of the compounds $A[ClF_4]$ (A = K, Rb, Cs).

	[K][ClF_4]	Rb[ClF_4]	Cs[ClF_4]
Formula	$KClF_4$	$RbClF_4$	$CsClF_4$
Molar mass / g mol^{-1}	150.55	196.92	244.35
Space group (No.)	*I*4/*mcm* (140)	*C*2/*c* (15)	*C*2/*c* (15)
a/Å	6.0372(3)	10.4131(8)	10.908(2)
b/Å	*a*	4.8957(4)	5.4275(11)
c/Å	10.7566(6)	8.4012(7)	8.4068(17)
β/°	90	103.843(3)	108.98(3)
V/Å^3	392.05(4)	415.85(6)	470.67(18)
Z	4	4	4
Pearson symbol	*tI*24	*mS*24	*mS*24
ρ_{calc}/g cm^{-3}	2.55	4.55	3.45
μ/mm^{-1}	1.97	3.15	8.38
Color	colorless	colorless	colorless
Crystal morphology	block	block	block
Crystal size/mm^3	0.104 × 0.152 × 0.168	0.050 × 0.051 × 0.074	0.007 × 0.037 × 0.075
T/K	100	100	100
λ/Å	0.71073 (Mo-K_α)	0.71073 (Mo-K_α)	0.71073 (Mo-K_α)
No. of reflections	4904	9473	1449
θ range/°	3.79–39.35	4.03–37.82	3.95–26.71
Range of Miller indices	$-10 \le h \le 10$	$-17 \le h \le 17$	$-13 \le h \le 11$
	$-10 \le k \le 10$	$-8 \le k \le 8$	$-6 \le k \le 6$
	$-18 \le l \le 19$	$-14 \le l \le 14$	$-10 \le l \le 10$
Absorption correction	multi-scan	multi-scan	integration
T_{max}, T_{min}	0.77, 0.67	0.54, 0.45	0.37, 0.31
R_{int}, R_σ	0.030, 0.012	0.034, 0.020	0.071, 0.055
Completeness of the data set	1.000	1.000	0.998
No. of unique reflections	339	1122	502
No. of parameters	13	31	30
No. of restraints	0	0	0
No. of constraints	0	0	0
S (all data)	1.15	1.07	1.06
R(*F*) ($I \ge 2\sigma(I)$, all data)	0.017, 0.023	0.022, 0.029	0.035, 0.049
wR(F^2) ($I \ge 2\sigma(I)$, all data)	0.035, 0.036	0.037, 0.038	0.061, 0.065
Extinction coefficient	0.0113(16)	0.0033(4)	–
$\Delta\rho_{max}$, $\Delta\rho_{min}$/e Å^{-3}	0.39, −0.27	0.58, −0.61	0.88, −0.80

crystallographic data and details of the structure determinations. Atom coordinates and isotropic displacement parameters are given in Table 2. Anisotropic displacement parameters are reported in the Supporting Information.

Table 2. Atomic coordinates and equivalent isotropic displacement parameters U_{iso} of K[ClF_4].

Atom	Position	*x*	*y*	*z*	U_{iso}/Å^2
[K](1)	4*a*	1/2	1/2	1/4	0.00868(9)
Cl(1)	4*d*	1/2	0	1/2	0.00649(9)
F(1)	16*l*	0.64919(7)	0.14919(7)	0.38201(5)	0.01265(12)

The chlorine atom occupies the Wyckoff position 4*d* (site symmetry *m.mm*) and is surrounded by the fluorine atom F(1) and its three symmetry-equivalent F atoms, F(1)#1-F(1)#3, forming the almost square but planar [ClF_4]$^-$ anion, see Figure 1. The Cl–F distance is 1.7982(6) Å and the F–Cl–F angles are 89.79(4) and 90.21(4)°. These values nicely agree with structure determinations on other [ClF_4]$^-$ salts, which were measured at 130 K: NO[ClF_4] (1.727(1) and 1.874(1) Å; 89.36(5)-91.32(9)° and 179.33(7)°) and 1,1,3,3,5,5-hexamethylpiperidinium[ClF_4] (1.759(2)-1.814(1) Å, 88.90(7)-91.16(7)°, 178.42(7)° and 178.68(8)°).[17]

The potassium atom occupies the Wyckoff position 4*a* (site symmetry 422) and is surrounded by eight fluorine atoms in

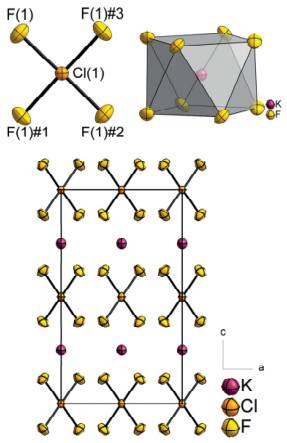

Figure 1. Top: Left: Tetrafluoridochlorate(III) anion observed in K[ClF_4]. Symmetry transformations for the generation of equivalent atoms: #1 1 − *x*, −*y*, *z*; #2 1/2 − *y*, 1/2 − *x*, 1 − *z*; #3 1/2 + *y*, −1/2 + *x*, 1 − *z*. Right: Coordination polyhedron of K(1) in K[ClF_4]. Bottom: Crystal structure of K[ClF_4] projected along the *b* axis. The displacement ellipsoids are shown at the 90 % probability level at 100 K.

© 2020 The Authors. Published by Wiley-VCH Verlag GmbH & Co. KGaA, Weinheim

EurJIC
European Journal of Inorganic Chemistry

Full Paper
doi.org/10.1002/ejic.202000106

Chemistry Europe
European Chemical Societies Publishing

the shape of a distorted square antiprism. A projection of the crystal structure of $K[ClF_4]$ is shown in Figure 1.

The $[ClF_4]^-$ anions are isolated and are superimposed when viewed along the *a* axis. Along the *c* axis, the anions are oriented at 90° towards one another. The fluorine atoms of the $[ClF_4]^-$ anion each coordinate to two potassium atoms. The Cl atoms are each surrounded by eight K atoms in the shape of a cube and vice versa, being similarly arranged like the Cs and Cl atoms in CsCl.[26]

The salts $Rb[ClF_4]$ and $Cs[ClF_4]$ are isotypic and crystallize in the monoclinic space group *C*2/*c* (No. 15) with four formula units per unit cell, Pearson code *mS*24 and Wyckoff sequence 15, f^2ed. Therefore, the compounds are isotypic to $Li[AuF_4]$.[16] See Table 1 for selected crystallographic data and details of the structure determinations. Atom coordinates and isotropic displacement parameters are given in Table 3 and Table 4. Anisotropic displacement parameters are reported in the Supporting Information. The chlorine atom occupies the Wyckoff position 4*d* (site symmetry $\bar{1}$) and is surrounded by the fluorine atoms F(1) and F(2) and its symmetry-equivalent atoms F(1)#1 and F(2)#1, see Figure 2. The Cl(1)–F(1) distance is 1.8034(9) Å in the Rb and 1.794(4) Å in the Cs compound, respectively. The Cl(1)–F(2) distance is 1.7930(9) Å in the Rb and 1.792(4) Å in the Cs salt, respectively. The Cl–F distances of the latter salt are equal within the tripled standard uncertainties. The F(1)–Cl(1)–F(2) angles are 89.33(4) and 90.67(4)° in $Rb[ClF_4]$ and 89.14(19) and 90.9(2)° in $Cs[ClF_4]$. The F–Cl–F angles of the two salts are equal within the tripled standard uncertainties and nicely agree with the above-mentioned data of other $[ClF_4]^-$ salts.

Table 3. Atomic coordinates and equivalent isotropic displacement parameters U_{iso} of $Rb[ClF_4]$.

Atom	Position	*x*	*y*	*z*	U_{iso}/Å^2
Rb(1)	4*e*	1/2	0.22368(4)	1/4	0.01348(6)
Cl(1)	4*d*	3/4	3/4	1/2	0.01066(8)
F(1)	8*f*	0.57241(8)	0.72418(18)	0.43421(11)	0.01627(16)
F(2)	8*f*	0.76854(9)	0.47384(19)	0.36710(11)	0.02005(18)

Table 4. Atomic coordinates and equivalent isotropic displacement parameters U_{iso} of $Cs[ClF_4]$.

Atom	Position	$Cs[ClF_4]$			
		x	*y*	*z*	U_{iso}/Å^2
Cs(1)	4*e*	1/2	0.20405(12)	1/4	0.0177(2)
Cl(1)	4*d*	3/4	3/4	1/2	0.0153(5)
F(1)	8*f*	0.5787(4)	0.6935(8)	0.4368(5)	0.0242(9)
F(2)	8*f*	0.7725(4)	0.4850(7)	0.3844(5)	0.0268(10)

The Rb/Cs atom occupies the Wyckoff position 4*e* (site symmetry 2) and is coordinated by twelve fluorine atoms in the shape of a distorted anti-cuboctahedron. The crystal structure of $Rb[ClF_4]$ is shown in Figure 2. The fluorine atoms of the $[ClF_4]^-$ anion each coordinate to three different alkali metal cations. The Cl atoms are surrounded by six alkali metal cations in the shape of a distorted octahedron and vice versa. The Rb/Cs and Cl atoms thus have a similar arrangement to the Na and Cl atoms in NaCl.[27]

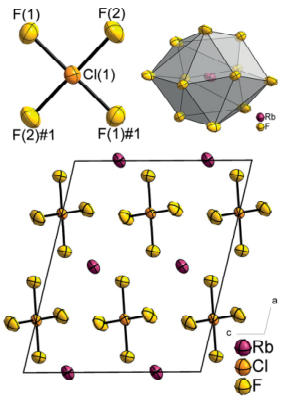

Figure 2. Top: Left: Tetrafluoridochlorate(III) anion observed in $Rb[ClF_4]$ and in the isotypic $Cs[ClF_4]$. Symmetry transformation for the generation of equivalent atoms: #1 3/2 – *x*, 3/2 – *y*, 1 – *z*. Right: Coordination polyhedron of Rb(1) in $Rb[ClF_4]$. Bottom: Crystal structure of $Rb[ClF_4]$ projected along the *b* axis. The displacement ellipsoids are shown at the 90 % probability level at 100 K. $Cs[ClF_4]$ is isotypic to $Rb[ClF_4]$.

The lattice parameters and atomic positions of the three compounds reported here were fully optimized with the DFT-PBE0 method using the CRYSTAL17 program package.[28,29] The lattice parameters and the *xyz* coordinates of the optimized structures are given in the Supporting Information. The cell volumes of the optimized structures are bigger than the experimentally obtained ones: 4 % for $K[ClF_4]$, and 6.5 % for both $Rb[ClF_4]$ and $Cs[ClF_4]$. Thus, the interaction between the alkali metal cations and the $[ClF_4]^-$ anions is probably somewhat underestimated by the DFT-PBE0 method that was employed. The calculated Cl–F distances are only slightly longer than the experimental ones: 1.82 Å in $K[ClF_4]$; 1.81 and 1.83 Å in $Rb[ClF_4]$; 1.82 Å in $Cs[ClF_4]$.

Vibrational Spectroscopy

The experimental Raman and IR spectra of the tetrafluoridochlorates(III) are shown in Figure 3. Values and band assignments are given in Table 5 and Table 6. The Raman and IR spectra of the compounds were also calculated with the DFT-PBE0 method and the calculated band positions, assignments and figures are given in the Supporting Information. The $[ClF_4]^-$ ion has D_{2h} (*mmm*) symmetry in $K[ClF_4]$ and C_i ($\bar{1}$) symmetry in $Rb[ClF_4]$ and $Cs[ClF_4]$, deviating from the ideal D_{4h} (4/*mmm*) symmetry.

In the Raman spectra, the symmetric in-phase Cl–F stretching modes, $\nu s(ClF_4)$, are observed at slightly above 500 cm^{-1} and the symmetric out-of-phase Cl–F stretching modes, $\nu s(ClF_4)$, at approximately 415 cm^{-1}. The values shift towards lower energy with increasing cation size. The scissoring vibration of the $[ClF_4]^-$ ion is observed in the range of 290–260 cm^{-1}, showing no dependency on the cation size. Below 150 cm^{-1}, further deformation vibrational modes – twisting, umbrella bending and rocking – of the $[ClF_4]^-$ ion are observed,

© 2020 The Authors. Published by Wiley-VCH Verlag GmbH & Co. KGaA, Weinheim

EurJIC
European Journal of Inorganic Chemistry

Full Paper
doi.org/10.1002/ejic.202000106

Chemistry Europe
European Chemical Societies Publishing

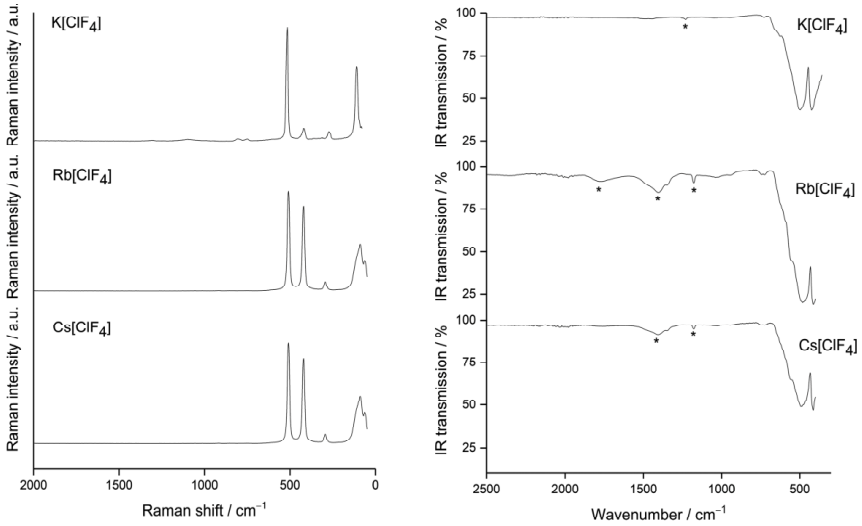

Figure 3. Left: Low-resolution (300/mm grating) Raman spectra of $A[ClF_4]$ (A = K, Rb, Cs) measured at room temperature under perfluorinated oil (K) or in glass vials (Rb, Cs). Single crystal of $K[ClF_4]$ and powder samples of $Rb[ClF_4]$ and $Cs[ClF_4]$. Right: ATR-IR spectra of $A[ClF_4]$ (A = K, Rb, Cs) measured at room temperature. Asterisks denote bands that stem from hydrogen fluoride adduct impurities of the alkali metal fluorides, $[AF(HF)_n]$.

Table 5. Comparison and assignment of Raman-active bands of tetrafluoridochlorates(III), $A[ClF_4]$ (A = K, Rb, Cs). All values in cm^{-1}.

Compound	$\nu_s(ClF_4)$ in phase	$\nu_s(ClF_4)$ out of phase	$\delta(ClF_4)$ scissoring	Reference
$[ClF_4]$	515	416	272, 265	this work
	530, 529	424	275, 263	DFT-PBE0
$Rb[ClF_4]$	503	415	288	this work
	505	417	288	[30]
	502	414	287	[10]
	518, 517	422	281, 280	DFT-PBE0
$Cs[ClF_4]$	501	411	284	this work
	507	418	290	[31]
	518, 517	422, 417	279, 278	DFT-PBE0

Table 6. Comparison and assignment of IR-active bands of tetrafluoridochlorates(III), $A[ClF_4]$ (A = K, Rb, Cs). All values in cm^{-1}.

Compound	$\nu_{as}(ClF_4)$	$\delta(ClF_4)$ umbrella bending	Reference
$K[ClF_4]$	498	424	this work
	563, 540	429	DFT-PBE0
$Rb[ClF_4]$	559 (shoulder), 482	413	this work
	486	430	[32]
	627, 534, 522	422, 421	DFT-PBE0
$Cs[ClF_4]$	552 (shoulder), 491	414	this work
	590	425	[13]
	541	436	[30]
	478	425	[32]
	595, 556, 538, 523	424, 420	DFT-PBE0

which are coupled with the respective cation. These values nicely agree with our calculated values and Raman spectra that have been reported thus far.[10,30,31]

As was previously mentioned, the reported IR data of the tetrafluoridochlorates(III) are not as consistent as the Raman data.[15] In most studies Pyrex glass Schlenk lines were used for the handling of ClF_3 or the products were not handled under inert conditions, leading to impure compounds.[8,13,30,32] We also observed impurity bands in the IR spectra, especially when the ClF_3 used was not free from traces of HF. These bands are observed above 1000 cm^{-1} and are caused by HF-adducts of the alkali metal fluorides, $[AF(HF)_n]$, (A = K, Rb, Cs; n being usually 1–3).[33,34] This highlights the fact that HF is a stronger Lewis-base than ClF_3 and thus displaces it from the tetrafluoridochlorates(III).[35]

Nevertheless, in the IR spectra two broad bands are seen in the region of 600 to 400 cm^{-1} which can be attributed to the $[ClF_4]^-$ ion. The first one, with a maximum at approximately 500 cm^{-1}, can be assigned to the asymmetric Cl–F stretching mode, $\nu_{as}(ClF_4)$, and the latter one at circa 420 cm^{-1} to the umbrella bending vibration of the $[ClF_4]^-$ ion. The calculated frequencies for the stretching modes are somewhat overestimated by the DFT-PBE0 method that was employed. The calculated Raman and IR spectra otherwise nicely agree with our experimental results.

Conclusions

The tetrafluoridochlorates(III), $A[ClF_4]$ (A = K, Rb, Cs), were synthesized from solvolysis reactions of the alkali metal fluorides in liquid ClF_3 in single-crystalline form. Structure determination by single-crystal X-ray diffraction showed that $K[ClF_4]$ is isotypic to $K[BrF_4]$, whereas $Rb[ClF_4]$ and $Cs[ClF_4]$ are isotypic to $Li[AuF_4]$.

© 2020 The Authors. Published by Wiley-VCH Verlag GmbH & Co. KGaA, Weinheim

EurJIC
European Journal of Inorganic Chemistry

Full Paper
doi.org/10.1002/ejic.202000106

Chemistry Europe
European Chemical Societies Publishing

The Raman and IR spectra could be interpreted on the basis of quantum-chemical solid-state calculations.

Experimental Section

General: All operations were performed on a Monel metal Schlenk line, which was passivated with 100 % fluorine and chlorine trifluoride at various pressures before use. Moisture-sensitive compounds were stored and handled in an Ar-filled glove box (MBraun). Reaction vessels were made out of fluoropolymer (perfluoroalkoxy alkanes, PFA) and passivated with fluorine before use. Preparations were carried out in an atmosphere of dry and purified argon (5.0, Praxair). Chlorine trifluoride was stored over NaF to remove traces of HF. Caution! Fluorine, chlorine trifluoride, and tetrafluoridochlorates(III) must be handled using appropriate protective gear with ready access to proper emergency treatment procedures in the event of contact. The aforementioned are potent oxidative fluorinators that are only stable under the rigorously anhydrous conditions employed in the experimental procedures outlined in the Experimental Section. They react vigorously to explosively upon hydrolysis or contact with organic materials. The utmost precautions must be taken when disposing of these materials and their derivatives.

Synthesis: $K[ClF_4]$: A PFA reaction vessel was loaded with 12.3 mg KF (0.218 mmol) inside a glove box and attached to a stainless-steel valve. An excess of ClF_3 (approximately 0.35 g, 3.8 mmol) was then condensed onto the solid at 77 K. The resulting suspension was gently heated in an air bath to approximately 50 °C for two hours. The remaining ClF_3 was then slowly pumped off and the colorless product (21.2 mg isolated, calculated: 31.87 mg) was transferred into the glove box. $Rb[ClF_4]$: A PFA reaction vessel was loaded with 28.1 mg RbF (0.269 mmol) inside a glove box and attached to a stainless-steel valve. An excess of ClF_3 (approximately 0.40 g, 4.3 mmol) was then condensed onto the solid at 77 K. The resulting suspension was gently heated in an air bath to approximately 50 °C for one hour. The remaining ClF_3 was then slowly pumped off and the colorless product (43.2 mg isolated, calculated: 52.97 mg) was transferred into the glove box. $Cs[ClF_4]$: A PFA reaction vessel was loaded with 20.9 mg CsF (0.138 mmol) inside a glove box and attached to a stainless-steel valve. An excess of ClF_3 (approximately 0.25 g, 2.7 mmol) was then condensed onto the solid at 77 K. The resulting solution was kept at room temperature for several hours. The remaining ClF_3 was then slowly pumped off and the colorless product (28.3 mg isolated, calculated: 33.61 mg) was transferred into the glove box. The mass balances of the three reactions indicate that a full conversion of the alkali metal fluorides to the respective tetrafluoridochlorates(III) was not achieved under the chosen conditions. Also, not all of the solid product could be isolated from the reaction vessels.

Single-Crystal X-ray Diffraction: Crystals of the moisture sensitive compounds were selected under dried perfluorinated oil (Fomblin YR1800, Solvay, stored over molecular sieves 3 Å) and mounted on a MiTeGen loop. Intensity data of suitable crystals were recorded with a D8 Quest diffractometer (Bruker) or an IPDS2T diffractometer (STOE). The diffractometers were operated with monochromatized Mo-K_α radiation (0.71073 Å, multi layered optics (D8 Quest) or graphite monochromator (IPDS2T)) and equipped with a PHOTON 100 CMOS detector (D8 Quest) or an image plate detector (IPDS2T). Evaluation, integration and reduction of the diffraction data was carried out with the APEX3 software suite (D8 Quest) or the X-Area software suite (IPDS2T).[36,37] The diffraction data was corrected for absorption utilizing the multi-scan method of SADABS within the APEX3 software suite (D8 Quest) or the integration method with the modules X-Shape and X-Red32 of the X-Area software suite (IPDS2T). The structures were solved with dual-space methods (SHELXT) and refined against F^2 (SHELXL).[38,39] For $Rb[ClF_4]$ one systematic absence violation ($[I > 3\sigma(I)]$ is observed for space group $C2/c$ (No. 15). Solution and refinement in the subgroups Cc (No. 9) and $C2$ (No. 5) showed correlation for some atoms. Subsequently, space group $C2/c$ was chosen, which was also indicated by the Addsym function in PLATON.[40,41] The highest residual electron densities after the final refinements were the following: $K[ClF_4]$: 0.68 Å distant from atom Cl(1); $Rb[ClF_4]$: 1.58 Å distant from atom F(2); $Cs[ClF_4]$: 1.05 Å distant from atom Cs(1). Representations of the crystal structures were created with the Diamond software.[42]

CCDC 1980748 (for $Cs[ClF_4]$), 1980749 (for $Rb[ClF_4]$), and 1980750 (for $K[ClF_4]$) contain the supplementary crystallographic data for this paper. These data can be obtained free of charge from The Cambridge Crystallographic Data Centre.

IR and Raman spectroscopy: The IR spectra were recorded on a Bruker alpha FT-IR spectrometer using an ATR Diamond module with a resolution of 4 cm^{-1}. The spectrometer was located inside a glovebox (MBraun) under argon atmosphere. The spectra were processed with the OPUS software package.[43] The Raman spectra were measured at room temperature with a Monovista CRS+ confocal Raman microscope (Spectroscopy & Imaging GmbH) using a 532 nm solid-state laser and either a 300 grooves/mm (low-resolution mode, FWHM: <4.62 cm^{-1}) or a 1800 grooves/mm (high-resolution mode, FWHM: <0.368 cm^{-1}) grating.

Density Functional Calculations: Periodic quantum-chemical calculations were carried out for the $A[ClF_4]$ (A = K, Rb, Cs) salts using the PBE0 density functional method (DFT-PBE0).[28,29] A triple-zeta-valence + polarization (TZVP) level basis set was applied for F and Cl and split-valence + polarization (SVP) level basis sets were applied for K, Rb and Cs. The basis sets were derived from the Karlsruhe def2 basis sets and taken from previous studies (F, Cl, K, Cs) or listed in the Supporting Information (Rb).[44–47] All calculations were carried out with the CRYSTAL17 program package.[48] The reciprocal space for the salts was sampled using the following Monkhorst-Pack-type k-point grids: $K[ClF_4]$: 4×4×4, $Rb[ClF_4]$: 5×5×3, $Cs[ClF_4]$: 5×5×3. For the evaluation of the Coulomb and exchange integrals (TOLINTEG), tight tolerance factors of 8, 8, 8, 8, 16 were used for all calculations. Both the atomic positions and lattice parameters were fully optimized within the constraints imposed by the space group symmetry. Default DFT integration grids and optimization convergence thresholds were applied in all calculations. The xyz coordinates used in the calculations of each salt are given in the Supporting information. The harmonic vibrational frequencies, IR intensities and Raman intensities were obtained through usage of the computational scheme implemented in CRYSTAL17.[49–52] The Raman intensities were calculated for a polycrystalline powder sample (total isotropic intensity in arbitrary units). The Raman spectra were obtained by using a pseudo Voigt band profile (50:50 Lorentzian:Gaussian) and an FWHM of 8 cm^{-1}. The Raman spectra were simulated taking into account the experimental setup (T = 298.15 K, λ = 532 nm). For the IR spectra, a Lorentzian lineshape and an FWHM of 8 cm^{-1} was used. The band assignments were carried out by visual inspection of the normal modes using the J mol program package.[53]

Acknowledgments

We thank the Deutsche Forschungsgemeinschaft (DFG) for generous funding.

 © 2020 The Authors. Published by Wiley-VCH Verlag GmbH & Co. KGaA, Weinheim

EurJIC
European Journal of Inorganic Chemistry

Full Paper
doi.org/10.1002/ejic.202000106

Chemistry Europe
European Chemical Societies Publishing

Keywords: Density Functional Theory Calculations · Chlorine · Fluorine · Interhalogen Compounds

[1] H. Bode, *Naturwissenschaften* **1950**, *37*, 477–477.
[2] H. Bode, *Angew. Chem.* **1950**, *62*, 449.
[3] H. Bode, E. Klesper, *Z. Anorg. Allg. Chem.* **1952**, *267*, 97–112.
[4] H. Bode, E. Klesper, *Z. Anorg. Allg. Chem.* **1961**, *313*, 161–169.
[5] W. F. Howard, L. Andrews, *J. Am. Chem. Soc.* **1973**, *95*, 3045–3046.
[6] T. Vent-Schmidt, F. Brosi, J. Metzger, T. Schlöder, X. Wang, L. Andrews, C. Müller, H. Beckers, S. Riedel, *Angew. Chem. Int. Ed.* **2015**, *54*, 8279–8283; *Angew. Chem.* **2015**, *127*, 8397.
[7] S. Hasenstab-Riedel, K. Sonnenberg, L. Mann, F. A. Redeker, B. Schmidt, *Angew. Chem. Int. Ed.* **2019**, DOI –000; *Angew. Chem.* **2019**, *131*, 000https://doi.org/10.1002/anie.201903197.
[8] L. B. Asprey, J. L. Margrave, M. F. Silverthorn, *J. Am. Chem. Soc.* **1961**, *83*, 2955–2956.
[9] D. H. Kelly, B. Post, R. W. Mason, *J. Am. Chem. Soc.* **1963**, *85*, 307–308.
[10] J. Shamir, N. Parchi, *Spectrosc. Lett.* **1971**, *4*, 57–58.
[11] E. Dow, Whitney, R. O. MacLaren, C. E. Fogle, T. J. Hurley, *J. Am. Chem. Soc.* **1964**, *86*, 2583–2586.
[12] E. Dow, Whitney, R. O. MacLaren, T. J. Hurley, C. E. Fogle, *J. Am. Chem. Soc.* **1964**, *86*, 4340–4342.
[13] K. O. Christe, W. Sawodny, *Z. Anorg. Allg. Chem.* **1970**, *374*, 306–309.
[14] H. Meinert, *Z. Chem.* **1967**, *7*, 41–57.
[15] J. Shamir, *Isr. J. Chem.* **1978**, *17*, 37–47.
[16] R. Hoppe, R. Homann, *Z. Anorg. Allg. Chem.* **1970**, *379*, 193–198.
[17] X. Zhang, K. Seppelt, *Z. Anorg. Allg. Chem.* **1997**, *623*, 491–500.
[18] S. Ivlev, P. Woidy, V. Sobolev, I. Gerin, R. Ostvald, F. Kraus, *Z. Anorg. Allg. Chem.* **2013**, *639*, 2846–2850.
[19] S. I. Ivlev, P. Woidy, I. I. Zherin, R. V. Ostvald, F. Kraus, M. Yu. Voytenko, V. V. Shagalov, *Procedia Chem.* **2014**, *11*, 35–42.
[20] S. I. Ivlev, A. J. Karttunen, R. V. Ostvald, F. Kraus, *Chem. Commun.* **2016**, *52*, 12040–12043.
[21] J. Bandemehr, M. Sachs, S. I. Ivlev, A. J. Karttunen, F. Kraus, *Eur. J. Inorg. Chem.* **2020**, *2020*, 64–70.
[22] R. Schmidt, B. G. Müller, *Z. Anorg. Allg. Chem.* **2004**, *630*, 2393–2397.
[23] J. Linnera, S. I. Ivlev, F. Kraus, A. J. Karttunen, *Z. Anorg. Allg. Chem.* **2019**, *645*, 284–291.
[24] S. Siegel, *Acta Crystallogr.* **1957**, *10*, 380–380.
[25] S. I. Ivlev, F. Kraus, *IUCrData* **2018**, *3*, x180646.
[26] W. P. Davey, F. G. Wick, *Phys. Rev.* **1921**, *17*, 403–404.
[27] W. L. Bragg, *Proc. R. Soc. London Ser. A* **1914**, *89*, 468–489.
[28] J. P. Perdew, K. Burke, M. Ernzerhof, *Phys. Rev. Lett.* **1996**, *77*, 3865–3868.
[29] C. Adamo, V. Barone, *J. Chem. Phys.* **1999**, *110*, 6158–6170.
[30] K. O. Christe, W. Sawodny, *Z. Anorg. Allg. Chem.* **1968**, *357*, 125–133.
[31] K. O. Christe, W. W. Wilson, R. V. Chirakal, J. C. P. Sanders, G. J. Schrobilgen, *Inorg. Chem.* **1990**, *29*, 3506–3511.
[32] K. O. Christe, J. P. Guertin, *Inorg. Chem.* **1966**, *5*, 473–476.
[33] L. H. Jones, R. A. Penneman, *J. Chem. Phys.* **1954**, *22*, 781–782.
[34] K. M. Harmon, R. R. Lovelace, *J. Phys. Chem.* **1982**, *86*, 900–903.
[35] T. Surles, L. A. Quarterman, H. H. Hyman, *J. Fluorine Chem.* **1974**, *3*, 293–306.
[36] *APEX3*, Bruker AXS Inc., Madison, Wisconsin, USA, **2018**.
[37] *X-Area*, STOE & Cie GmbH, Darmstadt, Germany, **2018**.
[38] G. M. Sheldrick, *Acta Crystallogr., Sect. A: Found. Adv.* **2015**, *71*, 3–8.
[39] G. M. Sheldrick, *Acta Crystallogr., Sect. C: Struct. Chem.* **2015**, *71*, 3–8.
[40] A. L. Spek, *PLATON - A Multipurpose Crystallographic Tool*, Utrecht University, Utrecht, The Netherlands, **2019**.
[41] A. L. Spek, *Acta Crystallogr., Sect. D: Biol. Crystallogr.* **2009**, *65*, 148–155.
[42] K. Brandenburg, H. Putz, *Diamond - Crystal and Molecular Structure Visualization*, Crystal Impact GbR, Bonn, **2019**.
[43] *OPUS V7.2*, Bruker Optik GmbH, Ettlingen, Germany, **2012**.
[44] F. Weigend, R. Ahlrichs, *Phys. Chem. Chem. Phys.* **2005**, *7*, 3297–3305.
[45] V. Sivchik, R. K. Sarker, Z.-Y. Liu, K.-Y. Chung, E. V. Grachova, A. J. Karttunen, P.-T. Chou, I. O. Koshevoy, *Chem. Eur. J.* **2018**, *24*, 11475–11484.
[46] R. E. Stene, B. Scheibe, A. J. Karttunen, W. Petry, F. Kraus, *Eur. J. Inorg. Chem.* **2019**, *2019*, 3672–3682.
[47] A. J. Karttunen, T. Tynell, M. Karppinen, *J. Phys. Chem. C* **2015**, *119*, 13105–13114.
[48] R. Dovesi, A. Erba, R. Orlando, C. M. Zicovich-Wilson, B. Civalleri, L. Maschio, M. Rérat, S. Casassa, J. Baima, S. Salustro, et. al, *Wiley Interdiscip. Rev.: Comput. Mol. Sci.* **2018**, e1360.
[49] C. M. Zicovich-Wilson, F. Pascale, C. Roetti, V. R. Saunders, R. Orlando, R. Dovesi, *J. Comput. Chem.* **2004**, *25*, 1873–1881.
[50] F. Pascale, C. M. Zicovich-Wilson, F. López Gejo, B. Civalleri, R. Orlando, R. Dovesi, *J. Comput. Chem.* **2004**, *25*, 888–897.
[51] L. Maschio, B. Kirtman, M. Rérat, R. Orlando, R. Dovesi, *J. Chem. Phys.* **2013**, *139*, 164101.
[52] L. Maschio, B. Kirtman, M. Rérat, R. Orlando, R. Dovesi, *J. Chem. Phys.* **2013**, *139*, 164102.
[53] Jmol: An Open-Source Java Viewer for Chemical Structures in 3D. Jmol.Org/Jmol Team, **2019**.

Received: February 2, 2020

 © 2020 The Authors. Published by Wiley-VCH Verlag GmbH & Co. KGaA, Weinheim

EurJIC European Journal of Inorganic Chemistry

Supporting Information

Synthesis and Characterization of the Tetrafluoridochlorates(III) A[ClF_4](*A* =K,Rb, Cs)

Benjamin Scheibe, Sergei I. Ivlev, Antti J. Karttunen, and Florian Kraus*

Contents

Selected crystallographic data of the compounds *A*[ClF_4] (*A* = K, Rb, Cs) 1
Quantum chemical solid-state calculations of *A*[ClF_4] (*A* = K, Rb, Cs) 2
Lattice parameters and *xyz* coordinates of the optimized structure of K[ClF_4] 2
Lattice parameters and *xyz* coordinates of the optimized structure of Rb[ClF_4] 2
Lattice parameters and *xyz* coordinates of the optimized structure of Cs[ClF_4] 2
Band assignments for the calculated IR and Raman spectra of K[ClF_4] 3
Band assignments for the calculated IR and Raman spectra of Rb[ClF_4] 4
Band assignments for the calculated IR and Raman spectra of Cs[ClF_4] 5
Experimental and computationally calculated IR and Raman spectra of *A*[ClF_4] (*A* = K, Rb, Cs) 6
Basis set definition for Rb 9
References 10

Selected crystallographic data of the compounds *A*[ClF$_4$] (*A* = K, Rb, Cs)

Table S1. Anisotropic displacement parameters of K[ClF$_4$] at 100 K.

Atom	U_{11} / Å^2	U_{22} / Å^2	U_{33} / Å^2	U_{23} / Å^2	U_{13} / Å^2	U_{12} / Å^2
K(1)	0.00843(11)	0.00843(11)	0.00919(14)	0.000	0.000	0.000
Cl(1)	0.00642(11)	0.00642(11)	0.00661(14)	0.000	0.000	0.00050(12)
F(1)	0.01281(15)	0.01281(15)	0.0123(2)	0.00389(15)	0.00389(15)	−0.0001(2)

Table S2. Anisotropic displacement parameters of Rb[ClF$_4$] at 100 K.

Atom	U_{11} / Å^2	U_{22} / Å^2	U_{33} / Å^2	U_{23} / Å^2	U_{13} / Å^2	U_{12} / Å^2
Rb(1)	0.01647(9)	0.01121(8)	0.01484(9)	0	0.00785(6)	0
Cl(1)	0.01187(17)	0.01099(18)	0.01001(16)	0.00091(12)	0.00435(13)	0.00047(12)
F(1)	0.0122(4)	0.0194(4)	0.0173(4)	−0.0004(3)	0.0039(3)	0.0001(3)
F(2)	0.0205(4)	0.0195(4)	0.0229(5)	−0.0088(3)	0.0106(4)	−0.0018(3)

Table S3. Anisotropic displacement parameters of Cs[ClF$_4$] at 100 K.

Atom	U_{11} / Å^2	U_{22} / Å^2	U_{33} / Å^2	U_{23} / Å^2	U_{13} / Å^2	U_{12} / Å^2
Cs(1)	0.0212(4)	0.0156(3)	0.0182(3)	0	0.0088(2)	0
Cl(1)	0.0182(11)	0.0133(13)	0.0163(10)	−0.0029(8)	0.0083(9)	−0.0008(8)
F(1)	0.019(2)	0.025(2)	0.029(2)	−0.0031(19)	0.0083(17)	0.000(2)
F(2)	0.033(3)	0.023(2)	0.030(2)	−0.0093(17)	0.016(2)	−0.0026(18)

Quantum chemical solid-state calculations of *A*[ClF$_4$] (*A* = K, Rb, Cs)

Lattice parameters and *xyz* coordinates of the optimized structure of K[ClF$_4$]

Space group *I*4/*mcm* (No. 140)
a = 6.09351754 Å, *c* = 10.97569811 Å

Table S4. The *xyz* coordinates of the optimized structure of K[ClF$_4$].

Atom	*x*	*y*	*z*
K(1)	9.414869808519E−21	−9.414869808519E−21	2.500000000000E−01
Cl(1)	−5.000000000000E−01	−9.414869808519E−21	0.000000000000E+00
F(2)	1.494050156263E−01	3.505949843737E−01	−3.830337576994E−01

Lattice parameters and *xyz* coordinates of the optimized structure of Rb[ClF$_4$]

Space group *C*2/*c* (No. 15)
a = 10.76501715 Å, *b* = 4.84458355 Å, *c* = 8.66542143 Å, *β* = 101.695251°

Table S5. The *xyz* coordinates of the optimized structure of Cs[ClF$_4$].

Atom	*x*	*y*	*z*
Rb(1)	−6.938893903907E−18	−2.347332293531E−01	2.500000000000E−01
Cl(1)	2.500000000000E−01	2.500000000000E−01	−5.000000000000E−01
F(1)	7.761645936897E−02	2.636137510726E−01	4.367025928662E−01
F(2)	2.670584464940E−01	−4.714292788442E−01	3.660863812182E−01

Lattice parameters and *xyz* coordinates of the optimized structure of Cs[ClF$_4$]

Space group *C*2/*c* (No. 15)
a = 11.24929075 Å, *b* = 5.51706851 Å, *c* = 8.50257760 Å, *β* = 108.129730°

Table S6. The *xyz* coordinates of the optimized structure of Cs[ClF$_4$].

Atom	*x*	*y*	*z*
Cs(1)	6.938893903907E−18	−2.871344472296E−01	2.500000000000E−01
Cl(1)	2.500000000000E−01	2.500000000000E−01	−5.000000000000E−01
F(1)	8.152331039980E−02	2.021108515210E−01	4.343341374473E−01
F(2)	2.718950540875E−01	−1.728342620927E−02	3.870834000912E−01

Band assignments for the calculated IR and Raman spectra of $K[ClF_4]$

Table S7. Band assignments for the calculated IR and Raman frequencies for $K[ClF_4]$. The notation for band assignments is the following: ν – stretching, δ – deformation, s – symmetric, as – asymmetric.

ν / cm^{-1}	IR active	Raman active	Irrep (D_{2h})	Assignment
563	X		A_{2u}	$\nu_{as}(ClF_4)$
540	X		E_u	$\nu_{as}(ClF_4)$
530		X	B_{2g}	$\nu_s(ClF_4)$ – in-phase
529		X	A_{1g}	$\nu_s(ClF_4)$ – in-phase
429	X		E_u	$\delta(ClF_4)$ – umbrella bending
424		X	E_g	$\nu_s(ClF_4)$ – out-of-phase
275		X	A_{1g}	$\delta(ClF_4)$ –scissoring
263		X	B_{2g}	$\delta(ClF_4)$ – scissoring
211	X		A_{2u}	$\delta(ClF_4)$ –scissoring coupled with K atoms
205	X		E_u	$\delta(ClF_4)$ –scissoring coupled with K atoms
151	X		E_u	Lattice vibrations
147		X	E_g	$\delta(ClF_4)$ – umbrella bending coupled with K atoms
126	X		A_{2u}	Lattice vibrations
119		X	E_g	$\delta(ClF_4)$ – umbrella bending coupled with K atoms
117		X	B_{1g}	$\delta(ClF_4)$ – umbrella bending coupled with K atoms
81	X		E_u	Lattice vibrations
54		X	E_g	$\delta(ClF_4)$ – rocking coupled with K atoms

Band assignments for the calculated IR and Raman spectra of $Rb[ClF_4]$

Table S8. Band assignments for the calculated IR and Raman frequencies for $Rb[ClF_4]$. The notation for band assignments is the following: ν – stretching, δ – deformation, s – symmetric, as – asymmetric.

ν / cm^{-1}	IR active	Raman active	Irrep (C_i)	Assignment
627	X		A_u	$\nu_{as}(ClF_4)$
534	X		A_u	$\nu_{as}(ClF_4)$
522	X		A_u	$\nu_{as}(ClF_4)$
519		X	B_g	$\nu_s(ClF_4)$ – in-phase
517		X	A_g	$\nu_s(ClF_4)$ – in-phase
514	X		B_u	$\nu_{as}(ClF_4)$ – coupled with Rb atoms
422		X	A_g	$\nu_s(ClF_4)$ – out-of-phase
422	X		B_u	$\delta(ClF_4)$ – umbrella bending
421	X		A_u	$\delta(ClF_4)$ – umbrella bending
281		X	B_g	$\delta(ClF_4)$ –scissoring
280		X	A_g	$\delta(ClF_4)$ –scissoring
235	X		A_u	$\delta(ClF_4)$ –scissoring coupled with Rb atoms
227	X		B_u	$\delta(ClF_4)$ –scissoring coupled with Rb atoms
212	X		A_u	$\delta(ClF_4)$ – twisting coupled with Rb atoms
208	X		B_u	$\delta(ClF_4)$ – twisting coupled with Rb atoms
205	X		A_u	$\delta(ClF_4)$ – twisting coupled with Rb atoms
204	X		B_u	$\delta(ClF_4)$ – twisting coupled with Rb atoms
134		X	A_g	$\delta(ClF_4)$ – twisting coupled with Rb atoms
130		X	B_g	$\delta(ClF_4)$ – umbrella bending coupled with Rb atoms
120		X	B_g	$\delta(ClF_4)$ – umbrella bending coupled with Rb atoms
105	X		A_u	Lattice vibrations
99	X		B_u	Lattice vibrations
97		X	A_g	$\delta(ClF_4)$ – twisting coupled with Rb atoms
92	X		A_u	Lattice vibrations
89		X	B_g	$\delta(ClF_4)$ – umbrella bending coupled with Rb atoms
89		X	A_g	$\delta(ClF_4)$ – umbrella bending coupled with Rb atoms
86	X		B_u	Lattice vibrations
77	X		B_u	Lattice vibrations
75		X	B_g	$\delta(ClF_4)$ – umbrella bending coupled with Rb atoms
60		X	B_g	$\delta(ClF_4)$ – umbrella bending coupled with Rb atoms
55	X		A_u	Lattice vibrations
54		X	A_g	$\delta(ClF_4)$ – umbrella bending coupled with Rb atoms

Band assignments for the calculated IR and Raman spectra of $Cs[ClF_4]$

Table S9. Band assignments for the calculated IR and Raman frequencies for $Cs[ClF_4]$. The notation for band assignments is the following: ν – stretching, δ – deformation, s – symmetric, as – asymmetric.

ν / cm^{-1}	IR active	Raman active	Irrep (C_i)	Assignment
595	X		A_u	ν_{as}(Cl−F)
556	X		A_u	ν_{as}(Cl−F)
538	X		B_u	ν_{as}(Cl−F)
523	X		B_u	ν_{as}(Cl−F)
518		X	B_g	ν_s(Cl−F) – in-phase
517		X	A_g	ν_s(Cl−F) – in-phase
424	X		A_u	$\delta(ClF_4)$ – umbrella bending
422		X	A_g	ν_s(Cl−F) – out-of-phase
420	X		B_u	$\delta(ClF_4)$ – umbrella bending
417		X	B_g	ν_s(Cl−F) – out-of-phase
279		X	A_g	$\delta(ClF_4)$ –scissoring
278		X	B_g	$\delta(ClF_4)$ –scissoring
239	X		A_u	$\delta(ClF_4)$ –scissoring coupled with Cs atoms
231	X		B_u	$\delta(ClF_4)$ –scissoring coupled with Cs atoms
203	X		A_u	$\delta(ClF_4)$ – twisting coupled with Cs atoms
199	X		B_u	$\delta(ClF_4)$ – twisting coupled with Cs atoms
198	X		A_u	$\delta(ClF_4)$ – twisting coupled with Cs atoms
196	X		B_u	$\delta(ClF_4)$ – twisting coupled with Cs atoms
107		X	A_g	$\delta(ClF_4)$ – twisting coupled with Cs atoms
91		X	B_g	$\delta(ClF_4)$ – twisting coupled with Cs atoms
90		X	B_g	$\delta(ClF_4)$ – twisting coupled with Cs atoms
89	X		A_u	Lattice vibrations
85		X	B_g	$\delta(ClF_4)$ – umbrella bending coupled with Cs atoms
81		X	B_g	$\delta(ClF_4)$ – umbrella bending coupled with Cs atoms
79	X		B_u	Lattice vibrations
78	X		A_u	Lattice vibrations
72		X	A_g	$\delta(ClF_4)$ – twisting coupled with Cs atoms
71	X		B_u	Lattice vibrations
60	X		B_u	Lattice vibrations
57		X	B_g	$\delta(ClF_4)$ – umbrella bending coupled with Cs atoms
55	X		A_u	Lattice vibrations
46		X	B_g	$\delta(ClF_4)$ – umbrella bending coupled with Cs atoms
41		X	A_g	$\delta(ClF_4)$ – umbrella bending coupled with Cs atoms

Experimental and computationally calculated IR and Raman spectra of *A*[ClF$_4$] (*A* = K, Rb, Cs)

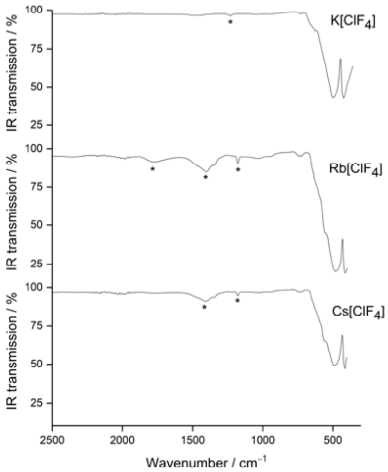

Figure S1. ATR-IR spectra of the tetrafluoridochlorates *A*[ClF$_4$] (*A* = K, Rb, Cs) measured at room temperature in an Ar-filled glove box. Asterisks denote bands that stem from hydrogen fluoride adduct impurities of the alkali metal fluorides [*A*F(HF)n] (n = 1-3).[1,2]

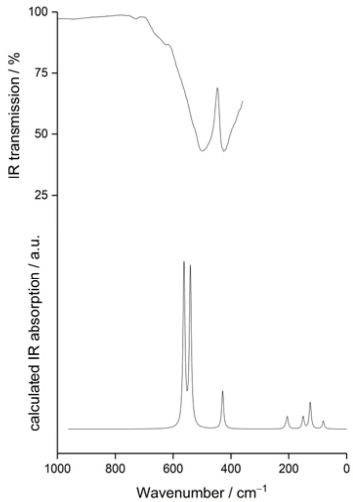

Figure S2. Top: Measured room-temperature ATR-IR spectrum of K[ClF$_4$]. Bottom: Calculated solid-state IR spectrum of K[ClF$_4$].

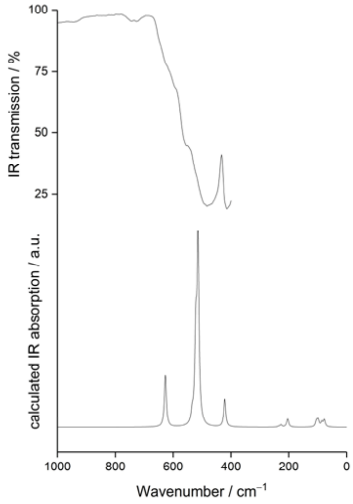

Figure S3. Top: Measured room-temperature ATR-IR spectrum of $Rb[ClF_4]$. Bottom: Calculated solid-state IR spectrum of $Rb[ClF_4]$.

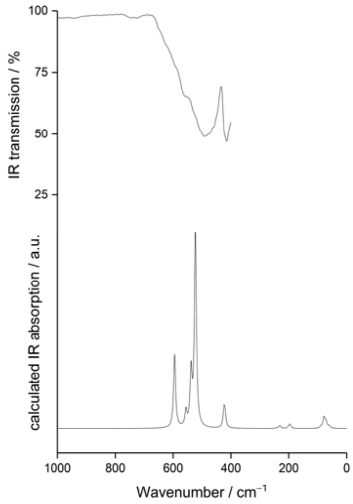

Figure S4. Top: Measured room-temperature ATR-IR spectrum of $Cs[ClF_4]$. Bottom: Calculated solid-state IR spectrum of $Cs[ClF_4]$.

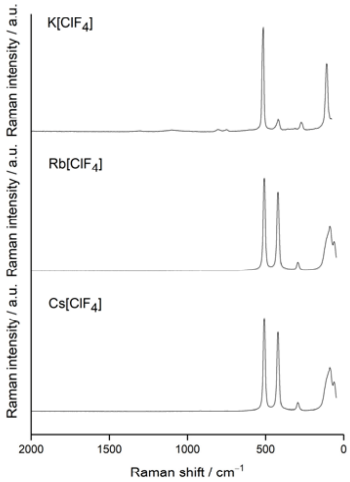

Figure S5. Low-resolution (300/mm grating) Raman spectra of tetrafluoridochlorates *A*[ClF_4] (*A* = K, Rb, Cs) measured at room temperature under perfluorinated oil (K) or in glass vials (Rb, Cs). (Single crystal of K[ClF_4] and powder samples of Rb[ClF_4] and Cs[ClF_4])

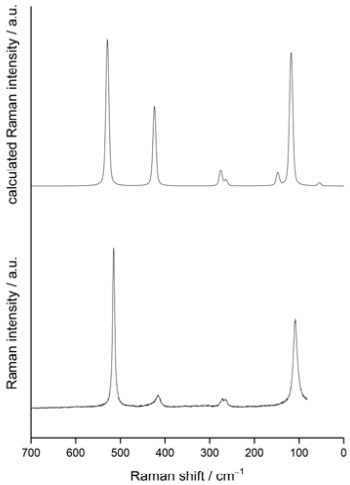

Figure S6. Top: Calculated solid-state Raman spectrum of K[ClF_4]. Bottom: High resolution (1800/mm grating) room-temperature Raman spectrum of a [$KClF_4$] single crystal measured under perfluorinated oil (Fomblin YR1800).

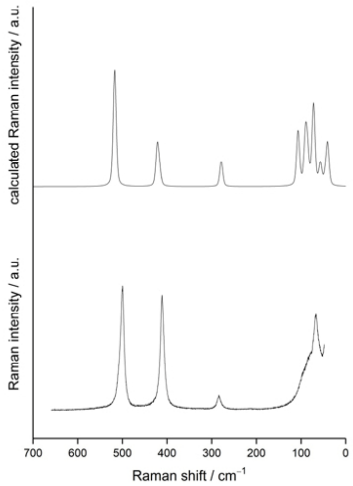

Figure S7. Top: Calculated solid-state Raman spectrum of Rb[ClF_4]. Bottom: High-resolution (1800/mm grating) room-temperature Raman spectrum of a powder sample of Rb[ClF_4] measured in a glass vial.

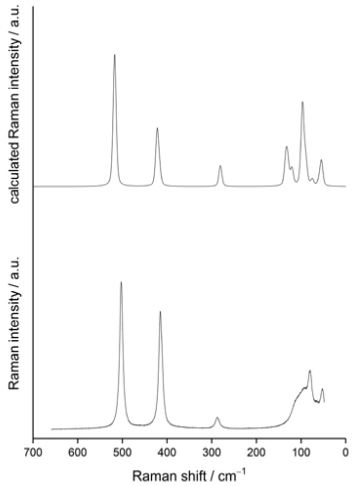

Figure S8. Top: Calculated solid-state Raman spectrum of Cs[ClF_4]. Bottom: High-resolution (1800/mm grating) room-temperature Raman spectrum of a powder sample of Cs[ClF_4] measured in a glass vial.

Basis set definition for Rb

The all-electron def2-SVP basis set was used as a starting point (28 core electrons described by a pseudopotential). The most diffuse s- and p-type functions were removed (exponents 0.014 and 0.021, respectively). The exponents of the two outermost s-functions were increased from 0.032 to 0.111 and from 0.216 to 0.226. The exponent of the p-polarization function was decreased from 0.13 to 0.11. The

outermost s and p functions were combined into an sp-type function. The diffuse d-polarization function with an exponent of 0.027 was removed. The full basis set is listed below in CRYSTAL input format.

```
237 6
INPUT
9. 0 2 2 2 1 0
5.03655181 89.50019822 0
1.97084963 0.49376198 0
4.25834119 58.56897492 0
1.47070961 0.43179108 0
3.02312774 26.22489809 0
0.65038346 0.96283950 0
3.84311471 -12.31690065 0
0 0 3 2.0 1.0
  4.6687885071      0.29008526793
  2.9442428420     -0.67740090428
  0.58171262989     0.45712389487
0 0 1 1.0 1.0
  0.45147933555     1.0000000000
0 0 1 0.0 1.0
  0.225739668       1.0000000000
0 1 1 0.0 1.0
  0.11              1.0 1.0
0 2 4 6.0 1.0
  5.5234179480      0.51234729472E-01
  3.4120149646     -0.17337025646
  0.76899021792     0.43339683188
  0.33008071786     0.55354332721
0 3 1 0.0 1.0
  0.226             1.0000000
```

References

[1] L. H. Jones, R. A. Penneman, *J. Chem. Phys.* **1954**, *22*, 781–782.
[2] K. M. Harmon, R. R. Lovelace, *J. Phys. Chem.* **1982**, *86*, 900–903.

7.2. $Cs[Cl_3F_{10}]$: A Propeller-Shaped $[Cl_3F_{10}]^-$ Anion in a Peculiar $A^{[5]}B^{[5]}$ Structure Type

Benjamin Scheibe, Antti J. Karttunen, Ulrich Müller, Florian Kraus

Angew. Chem. **2020**, *132*, 18272–18276.
Angew. Chem. Int. Ed. **2020**, *59*, 18116–18119.
DOI:10.1002/ange.202007019
DOI: 10.1002/anie.202007019

© 2020 The Authors. Published by Wiley-VCH Verlag GmbH & Co. KGaA.

Open access article distributed under the Creative Commons CC BY 4.0 license.
The original licensed material is shown.
(https://creativecommons.org/licenses/by/4.0/legalcode)

GDCh Communications Angewandte International Edition Chemie

Check for updates

Interhalogen Compounds

How to cite: *Angew. Chem. Int. Ed.* **2020**, *59*, 18116–18119
International Edition: doi.org/10.1002/anie.202007019
German Edition: doi.org/10.1002/ange.202007019

$Cs[Cl_3F_{10}]$: A Propeller-Shaped $[Cl_3F_{10}]^-$ Anion in a Peculiar $A^{[5]}B^{[5]}$ Structure Type

*Benjamin Scheibe, Antti J. Karttunen, Ulrich Müller, and Florian Kraus**

Abstract: *Reaction of CsF with ClF_3 leads to $Cs[Cl_3F_{10}]$. It contains a molecular, propeller-shaped $[Cl_3F_{10}]^-$ anion with a central μ_3-F atom and three T-shaped ClF_3 molecules coordinated to it. This anion represents the first example of a heteropolyhalide anion of higher ClF_3 content than $[ClF_4]^-$ and is the first Cl-containing interhalogen species with a μ-bridging F atom. The chemical bonds to the central μ_3-F atom are highly ionic and quite weak as the bond lengths within the coordinating XF_3 units (X = Cl, and also calculated for Br, I) are almost unchanged in comparison to free XF_3 molecules. $Cs[Cl_3F_{10}]$ crystallizes in a very rarely observed $A^{[5]}B^{[5]}$ structure type, where cations and anions are each pseudohexagonally close packed, and reside, each with coordination number five, in the trigonal bipyramidal voids of the other.*

Fluorine containing interhalogen cations and anions derive from the neutral halogen fluorides. Those containing bridging μ-F atoms are very scarce. Overviews of (homo and hetero) polyhalogen cations and anions have been given in recent review articles.[1–5] So far, the only known species with μ-bridging F atoms were reported for Br(III) and I(V). These are $[Br_2F_5]^+$, $[Br_3F_8]^+$, $[Br_2F_7]^-$, $[Br_3F_{10}]^-$, and $[I_3F_{16}]^-$.[6–13] To the best of our knowledge, not a single Cl-containing species, regardless of the oxidation state, with μ-bridging F atoms is known. For the cationic side of Cl(III), only the $[ClF_2]^+$ cation is known and for the anionic side only tetrafluoridochlorates(III), $A[ClF_4]$, have been reported (A = K, Rb, Cs, NO, 1,1,3,3,5,5-hexamethylpiperidinium).[14–18] We present the synthesis and characterization of the first fluoridochlorate(III) anion with μ-bridging F atoms. Figure 1 shows the Lewis structure of the propeller-shaped $[Cl_3F_{10}]^-$ anion and its molecular structure in the salt $Cs[Cl_3F_{10}]$.

Single crystals of the compound were obtained by reaction of CsF with excess liquid chlorine trifluoride at temperatures at or below 0 °C, see Equation 1.

$$3\,ClF_3 + CsF \xrightarrow{ClF_3} Cs[Cl_3F_{10}] \qquad (1)$$

These crystals were directly isolated from cold ClF_3 suspensions and handled at low temperatures under a nitrogen atmosphere. The crystals rapidly deteriorate upon warming to room temperature and/or moisture from air contact, releasing ClF_3 and/or hydrolysis products. Further details on the synthesis are given in the Supporting Information. Single-crystal X-ray diffraction on $Cs[Cl_3F_{10}]$ shows it to crystallize in the monoclinic space group $P12_1/n1$ ($mP56$, 14, e^{14}). The lattice parameters are $a = 9.0949(7)$, $b = 15.3652(12)$, $c = 6.8841(5)$ Å, $\beta = 91.314(2)°$, $V = 961.77(13)$ Å^3, and $Z = 4$ at $T = 100$ K. Further crystallographic details are given in the Supporting Information, Tables S1–S5.

The compound contains the propeller-shaped $[Cl_3F_{10}]^-$ anion in C_1 symmetry (Figure 1). However, the deviation of the molecule from C_3 symmetry is small. The anion can be thought of as a central fluoride ion which is coordinated by the Cl atoms of three surrounding ClF_3 molecules. The central μ_3-bridging F atom (F(1) in Figure 1) lies 0.522(2) Å above a virtual plane formed by the Cl atoms with Cl-μ_3-F-Cl angles from 113.53(9) to 116.12(8)°. Its structure is correctly predicted by VSEPR theory and there seems to be an additional interaction to the Cs^+ counterion residing above the apex of the trigonal-pyramidal anion (Figure 1).

In contrast, the quantum-chemically calculated gas-phase minimum structure is D_3-symmetric (TURBOMOLE, DFT-PBE0/TZVP, see Supporting Information), that is the μ_3-F atom and the Cl atoms reside within a plane and the Cl-μ_3-F-Cl angles are 120°.[19–22] Even when the geometry optimization is started from C_3 symmetry, where the μ_3-F atom is displaced from the virtual plane formed by the Cl atoms, the D_3-symmetric structure is reobtained.

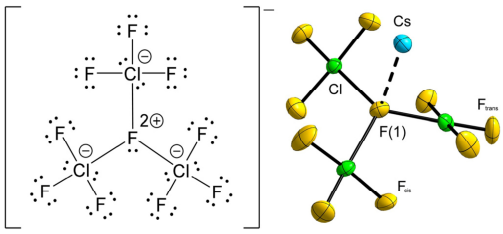

Figure 1. The Lewis structure of the $[Cl_3F_{10}]^-$ anion and its structure in the salt $Cs[Cl_3F_{10}]$. The displacement ellipsoids are shown at the 70% probability level at 100 K. Fluorine atoms drawn in yellow, chlorine atoms in green, and caesium atoms in sky blue. [41]

[*] M. Sc. B. Scheibe, Prof. em. Dr. U. Müller, Prof. Dr. F. Kraus
Fachbereich Chemie, Philipps-Universität Marburg
Hans-Meerwein-Straße 4, 35032 Marburg (Germany)
E-mail: f.kraus@uni-marburg.de
Prof. Dr. A. J. Karttunen
Department of Chemistry and Materials Science, Aalto University
00076 Aalto (Finland)
Supporting information and the ORCID identification number(s) for the author(s) of this article can be found under:
https://doi.org/10.1002/anie.202007019.

© 2020 The Authors. Published by Wiley-VCH GmbH. This is an open access article under the terms of the Creative Commons Attribution License, which permits use, distribution and reproduction in any medium, provided the original work is properly cited.

In the crystal structure, the ClF_3 units are essentially planar and are rotated around the μ_3-F–Cl bond in the same direction, which leads to the propeller shape of the anion. That is, the ClF_3 units are tilted in comparison to the virtual plane formed by the Cl atoms by 33.34(7), 36.41(6), and 44.77(6)°. The anion is thus similarly shaped as the $[Br_3F_{10}]^-$ anion, see below.[10] The Cl atoms are surrounded by four F atoms each in a quadrilateral, almost planar manner. The μ_3-F–Cl distances are in the range of 2.243(2) to 2.265(2) Å. The F atoms *cis*-bound relative to μ_3-F show F_{cis}–Cl distances from 1.730(2) to 1.747(2) Å, while the *trans*-bound F atoms show F_{trans}–Cl distances of 1.600(2) to 1.615(2) Å. These are comparable with the F–Cl distances reported for the orthorhombic modification of ClF_3 (1.716 and 1.621 Å) and thus support the description of the anion having a central fluoride anion coordinated by three ClF_3 molecules.[23] We will see below that the chemical bond between the μ_3-F atom and the three chlorine atoms is almost ionic. Also, a comparison with F–Cl distances in $[ClF_4]^-$ salts (1.794(4) to 1.8034(9) Å) shows significant differences which we attribute to the same reason.[17,18] In the structurally closely related $[Br_3F_{10}]^-$ anions, the μ_3-F–Br distances range from 2.238(10) to 2.248(2) Å, the F_{cis}–Br distances from 1.824(10) to 1.878(7) Å, and the F_{trans}–Br distances from 1.745(2) to 1.767(7) Å.[10] So, unexpectedly, the observed μ_3-F-X distances are essentially similar. This is likely to be due to the direct interaction of the Cs^+ cation with the μ_3-F atom in $Cs[Cl_3F_{10}]$ leading to coordination number 3 + 1 for it, while such an interaction is absent in the crystal structure of $Cs[Br_3F_{10}]$ and the coordination number of that μ_3-F atom is only three. The F_{cis}-X and F_{trans}-X atomic distances are circa 0.1 Å longer for X = Br compared to the Cl-case, which agrees with the expectation.

As mentioned above, quantum-chemical gas-phase calculations for the homologous anions $[X_3F_{10}]^-$ (X = Cl, Br, I) show them to be D_3-symmetric even when the geometry optimization is started from the pyramidal C_3 symmetry around the μ_3-F atom as in the crystal structure. Except for the pyramidalization around the μ_3-F atom, the calculated structure of the D_3-symmetric $[Cl_3F_{10}]^-$ anion nicely agrees with the atomic distances and angles reported here. The same is true for X = Br with the previously reported $[Br_3F_{10}]^-$ anion in its Rb and Cs salts.[10] To the best of our knowledge, a compound containing $[I_3F_{10}]^-$ anions is not known yet. The calculated X-F distances within the XF_3 subunits are very similar to those in the solid-state structures of the halogen trifluorides.[23–25] This indicates a rather weak interaction of the XF_3 units with the central μ_3-F atom. The calculated X-μ_3-F distances of 2.22, 2.30 and 2.44 Å for X = Cl, Br, I, respectively, also support this.

To obtain a qualitative picture of the bonding situation in these anions we carried out an intrinsic atomic orbital (IAO) analysis to obtain partial atomic charges (Table S6) and generated the intrinsic bonding orbitals (IBOs), see Figure 2 and Figures S2–S4, which give information about the polarization and contribution of the atoms to the respective bond.[26,27] Further details are given in the Supporting Information. The obtained partial atomic charges from the IAO analysis show that the μ_3-F atom has the most negative partial charge in all three anions, followed by the F_{cis} atom of the XF_3 units. The F_{trans} atoms are the least negatively partially charged F atoms. The partial charges of the atoms follow the expected trend in line with decreasing electronegativities $\chi_{AR}(Cl) > \chi_{AR}(Br) > \chi_{AR}(I)$, that is, the iodine atoms are more positively partially charged than the Cl atoms and the F atoms are most negatively partially charged in $[I_3F_{10}]^-$.[28]

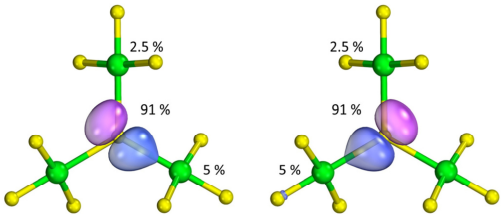

Figure 2. The two intrinsic bond orbitals (IBOs) showing the Cl-μ_3-F-Cl bonds in the $[Cl_3F_{10}]^-$ anion.[27] The percentages indicate the contribution of the Cl atoms and of the μ_3-F atom to the IBO. The larger the percentage, the more polarized the bond. For comparison: For a gas-phase NaF molecule, in which the bond should be highly ionic, the contribution of the F atom is 96%. In the H_2 molecule, which has a purely covalent bond, the contribution of each atom is 50%. If the summation of the percentages does not add up to 100%, then other atoms contribute—less than 1%—to the IBO. For further details, see the Supporting Information. F atoms: yellow, Cl atoms: green.

The two IBOs representing the Cl-μ_3-F-Cl bond in the $[Cl_3F_{10}]^-$ anion are shown in Figure 2. Further IBOs showing the other F–Cl bonds, as well as the respective IBOs for $[Br_3F_{10}]^-$ and $[I_3F_{10}]^-$ are reported in the Supporting Information. The percentages next to the atoms show the contribution of each atom to the IBO. The higher the contribution of an atom to the IBO in %, the more ionic is the bond. The contribution of the μ_3-F atom to the respective IBO is above 90% in all three anions, showing a highly polarized covalent, that is essentially ionic, bond (Figure 2 and Figures S2–S4). The heavier halogen atoms only have minor contributions to the IBO. Within the series, the contributions of the atoms follow the expected trend, which is due to the decrease of the electronegativities from Cl to I.

After the description of the molecular structure of the anion we come to the description of the crystal structure of $Cs[Cl_3F_{10}]$.

Surprisingly, $Cs[Cl_3F_{10}]$ can be regarded as a simple AB structure type. The Cs^+ cations ("A") are coordinated by five $[Cl_3F_{10}]^-$ anions ("B"), that is C. N. (Cs^+) = 5, and that exclusively via the F_{cis} and μ_3-F atoms. The arrangement of the Cs cations corresponds to the hexagonal-close packing with the layers arranged perpendicular to the c axis (Figure 3). Into the empty channels (parallel to the c axis), the terminally bound F_{ter} atoms protrude (see center of Figure 3). The μ_3-F atoms, which may be seen as the centers of gravity of the $[Cl_3F_{10}]^-$ anions ("B"), are also arranged in a hexagonal-close packed manner with the layers also perpendicular to the c axis. Their coordination number is also five. Thus, the two pseudohexagonal-close packed lattices of A and B interpenetrate in such a way that each ion is surrounded by five of its counterions in a trigonal bipyramidal manner. That is, the

 © 2020 The Authors. Published by Wiley-VCH GmbH

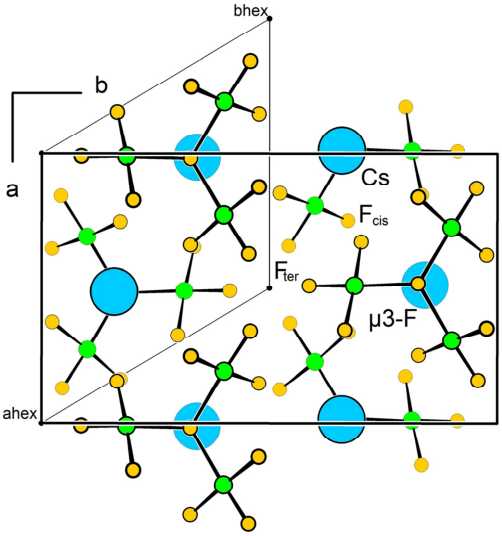

Figure 3. The crystal structure of $Cs[Cl_3F_{10}]$ viewed along the *c* axis and its relation to the hexagonal aristotype. Cs atoms are shown in sky-blue, Cl atoms in green, and F atoms in yellow. All atoms are drawn as spheres with arbitrary radii. Note the pseudohexagonal arrangement of the Cs^+ cations and the $[Cl_3F_{10}]^-$ anions. If the atoms in the pseudohexagonal cell would fulfil trigonal symmetry, the space group would be $P\bar{3}$.[41]

packing of $Cs[Cl_3F_{10}]$ can be described as a simple $A^{[5]}B^{[5]}$ structure type. Of course, the situation is somewhat more complicated because the $[Cl_3F_{10}]^-$ ion is not spherical. But if we take idealized planar $[Cl_3F_{10}]^-$ ions, the resulting space group is that of the hexagonal-close packing, $P6_3/mmc$ (aristotype). Distortion of the planar $[Cl_3F_{10}]^-$ ions to their real structure entails a symmetry reduction to the actual space group $P12_1/n1$; that can be represented by the Bärnighausen tree[29–33] shown in Figure S1. The crystal structure of the compound and its relation to the hexagonal aristotype is shown in Figure 3 and explained in detail in the Supporting Information.

A related structural motif of an $A^{[5]}B^{[5]}$ structure type is known to occur as a substructure in the Ni_2In structure type, where one kind of Ni atoms reside in the octahedral voids and the other kind of Ni atoms in the trigonal bipyramidal voids of hexagonal-close packed In atoms.[34] The reported orthoselenate $Li_4{}^{[5]}Se^{[5]}O_5{}^{[5]}$ is an ordered variant of the $A^{[5]}B^{[5]}$ aristotype.[35,36] Also, such a 5-5 coordination has been quantum-chemically predicted for a low temperature modification of sodium chloride $Na^{[5]}Cl^{[5]}$, and later also for magnesium oxide $Mg^{[5]}O^{[5]}$.[37,38] To the best of our knowledge, no binary compound with such a $A^{[5]}B^{[5]}$ crystal structure exists yet, and $Cs[Cl_3F_{10}]$ appears to be one of the very rare examples of this type.

The recorded Raman spectrum of $Cs[Cl_3F_{10}]$ along with a calculated one obtained from quantum-chemical solid-state calculations (CRYSTAL17, DFT-PBE0/TZVP) is shown in Figure 4.[21,22,39]

A detailed comparison of the Raman spectra with the ones of $Cs[ClF_4]$ and liquid ClF_3 as well as further details are given in the Supporting Information, Table S8 and Figure S5. The calculated Raman spectrum nicely agrees with the measured one, indicating that the main product obtained under the experimental conditions is $Cs[Cl_3F_{10}]$. The two main features of the Raman spectrum are the bands above 690 cm^{-1} and the band at approximately 500 cm^{-1}. The first can be attributed to the Cl-F_{trans} symmetric stretching mode and the latter to the Cl-F_{cis} symmetric stretching mode.

In summary, we obtained the compound $Cs[Cl_3F_{10}]$ which crystallizes in the very rarely observed $A^{[5]}B^{[5]}$ structure type. The cations and anions of $Cs[Cl_3F_{10}]$ form interpenetrated hexagonal-close packed layers. The coordination number of each cation and anion is five. The $[Cl_3F_{10}]^-$ anion is propeller-shaped with a symmetry close to C_3 as the central μ_3-F atom is surrounded in trigonal-pyramidal manner by the three Cl atoms, while quantum-chemical gas-phase calculations predict the anion to be D_3-symmetric with the μ_3-F atom in plane with the Cl atoms. The recorded Raman spectrum of $Cs[Cl_3F_{10}]$ is in excellent agreement with the quantum-chemically calculated one for the solid-state. So far there is no experimental evidence for the existence of a $[Cl_2F_7]^-$ anion

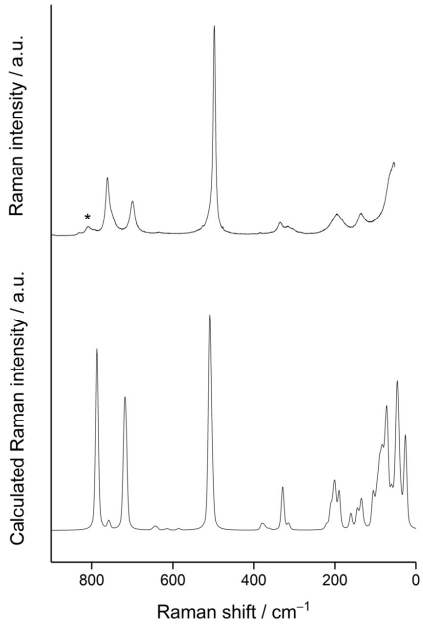

Figure 4. Top: The Raman spectrum of $Cs[Cl_3F_{10}]$ recorded at circa −66 °C. The asterisk denotes a band caused by the perfluoropolyether used for the immersion of the sample. Bottom: Computational solid-state Raman spectrum of $Cs[Cl_3F_{10}]$. The Raman intensities are given in arbitrary units, a.u. Further details are given in the Supporting Information.

 © 2020 The Authors. Published by Wiley-VCH GmbH

that would be the analogue to the known $[Br_2F_7]^-$ anion, or for anions with an even higher ClF_3 content than $[Cl_3F_{10}]^-$, such as a $[Cl_4F_{13}]^-$ anion. Investigations to obtain compounds containing such anions are ongoing, as well as analogous ones that derive from ClF_5.

Acknowledgements

We thank the Deutsche Forschungsgemeinschaft (DFG) for generous funding. A. J. K thanks CSC—the Finnish IT Center for Science for computational resources. We thank Dr. Sergei Ivlev, Marburg, for the development of the program HKLF5Tools,[40] Dr. Matthias Conrad, Marburg, and Prof. em. Dr. Martin Jansen, Dresden, for helpful discussions. Open access funding enabled and organized by Projekt DEAL.

Conflict of interest

The authors declare no conflict of interest.

Keywords: density functional theory calculations · fluorides · halogens · interhalogen compound · X-ray diffraction

[1] I. C. Tornieporth-Oetting, T. M. Klapötke, *Heteroat. Chem.* **1993**, *4*, 543 – 552.
[2] S. Brownridge, I. Krossing, J. Passmore, H. D. B. Jenkins, H. K. Roobottom, *Coord. Chem. Rev.* **2000**, *197*, 397 – 481.
[3] H. Haller, S. Riedel, *Nachr. Chem.* **2012**, *60*, 865 – 867.
[4] H. Haller, S. Riedel, *Z. Anorg. Allg. Chem.* **2014**, *640*, 1281 – 1291.
[5] K. Sonnenberg, L. Mann, F. A. Redeker, B. Schmidt, S. Riedel, *Angew. Chem. Int. Ed.* **2020**, *59*, 5464 – 5493; *Angew. Chem.* **2020**, *132*, 5506 – 5535.
[6] S. I. Ivlev, A. J. Karttunen, M. R. Buchner, M. Conrad, F. Kraus, *Angew. Chem. Int. Ed.* **2018**, *57*, 14640 – 14644; *Angew. Chem.* **2018**, *130*, 14850 – 14855.
[7] K. O. Christe, C. J. Schack, *Inorg. Chem.* **1970**, *9*, 1852 – 1858.
[8] L. Stein, *J. Fluorine Chem.* **1985**, *27*, 249 256.
[9] S. Ivlev, P. Woidy, V. Sobolev, I. Gerin, R. Ostvald, F. Kraus, *Z. Anorg. Allg. Chem.* **2013**, *639*, 2846 – 2850.
[10] S. I. Ivlev, A. J. Karttunen, R. V. Ostvald, F. Kraus, *Chem. Commun.* **2016**, *52*, 12040 – 12043.
[11] K. O. Christe, *Inorg. Chem.* **1972**, *11*, 1215 – 1219.
[12] A. R. Mahjoub, A. Hoser, J. Fuchs, K. Seppelt, *Angew. Chem. Int. Ed. Engl.* **1989**, *28*, 1526 – 1527; *Angew. Chem.* **1989**, *101*, 1528 – 1529.
[13] J. Bandemehr, M. Sachs, S. I. Ivlev, A. J. Karttunen, F. Kraus, *Eur. J. Inorg. Chem.* **2020**, 64 – 70.
[14] L. B. Asprey, J. L. Margrave, M. E. Silverthorn, *J. Am. Chem. Soc.* **1961**, *83*, 2955 – 2956.
[15] E. D. Whitney, R. O. MacLaren, C. E. Fogle, T. J. Hurley, *J. Am. Chem. Soc.* **1964**, *86*, 2583 – 2586.
[16] E. D. Whitney, R. O. MacLaren, T. J. Hurley, C. E. Fogle, *J. Am. Chem. Soc.* **1964**, *86*, 4340 – 4342.
[17] X. Zhang, K. Seppelt, *Z. Anorg. Allg. Chem.* **1997**, *623*, 491 – 500.
[18] B. Scheibe, S. I. Ivlev, A. J. Karttunen, F. Kraus, *Eur. J. Inorg. Chem.* **2020**, 1319 – 1324.
[19] TURBOMOLE V7.3, a Development of University of Karlsruhe and Forschungszentrum Karlsruhe GmbH, 1989 – 2007, TURBOMOLE GmbH, since 2007., **2018**.
[20] F. Weigend, R. Ahlrichs, *Phys. Chem. Chem. Phys.* **2005**, *7*, 3297 – 3305.
[21] J. P. Perdew, K. Burke, M. Ernzerhof, *Phys. Rev. Lett.* **1996**, *77*, 3865 – 3868.
[22] C. Adamo, V. Barone, *J. Chem. Phys.* **1999**, *110*, 6158 – 6170.
[23] R. D. Burbank, F. N. Bensey, *J. Chem. Phys.* **1953**, *21*, 602 – 608.
[24] R. D. Burbank, F. N. Bensey, *J. Chem. Phys.* **1957**, *27*, 982 – 983.
[25] S. Hoyer, K. Seppelt, *Angew. Chem. Int. Ed.* **2000**, *39*, 1448 – 1449; *Angew. Chem.* **2000**, *112*, 1512 1514.
[26] G. Knizia, *J. Chem. Theory Comput.* **2013**, *9*, 4834 – 4843.
[27] G. Knizia, J. E. M. N. Klein, *Angew. Chem. Int. Ed.* **2015**, *54*, 5518 – 5522; *Angew. Chem.* **2015**, *127*, 5609 – 5613.
[28] A. L. Allred, E. G. Rochow, *J. Inorg. Nucl. Chem.* **1958**, *5*, 264 – 268.
[29] H. Bärnighausen, *MATCH* **1980**, *9*, 139 – 175.
[30] *International Tables for Crystallography*, *Volume A1: Symmetry Relations Between Space Groups* (Eds.: H. Wondratscheck, U. Müller), Springer, Dordrecht, **2010**.
[31] U. Müller, *Symmetry Relationships between Crystal Structures: Applications of Crystallographic Group Theory in Crystal Chemistry*, Oxford University Press, Oxford, **2013**.
[32] U. Müller, *Symmetriebeziehungen zwischen verwandten Kristallstrukturen*, Vieweg + Teubner, Wiesbaden, **2012**.
[33] U. Müller, *Relaciones de Simetría Entre Estructuras Cristalinas*, Editorial Síntesis, Madrid, **2013**.
[34] F. Laves, H. J. Wallbaum, *Z. Angew. Mineral.* **1942**, *4*, 17 – 46.
[35] H. Haas, M. Jansen, *Angew. Chem. Int. Ed.* **1999**, *38*, 1909 – 1911; *Angew. Chem.* **1999**, *111*, 2033 – 2035.
[36] H. Haas, M. Jansen, *Z. Anorg. Allg. Chem.* **2000**, *626*, 1174 – 1178.
[37] J. C. Schön, M. Jansen, *Angew. Chem. Int. Ed. Engl.* **1996**, *35*, 1286 – 1304; *Angew. Chem.* **1996**, *108*, 1358 – 1377.
[38] S. Limpijumnong, W. R. L. Lambrecht, *Phys. Rev. B* **2001**, *63*, 104103.
[39] R. Dovesi, A. Erba, R. Orlando, C. M. Zicovich-Wilson, B. Civalleri, L. Maschio, M. Rérat, S. Casassa, J. Baima, S. Salustro, et al., *Wiley Interdiscip. Rev.: Comput. Mol. Sci.* **2018**, *8*, e1360.
[40] S. I. Ivlev, M. Conrad, F. Kraus, *Z. Kristallogr. - Cryst. Mater.* **2019**, *234*, 415 – 418.
[41] Deposition Number(s) 1992456 contain(s) the supplementary crystallographic data for this paper. These data are provided free of charge by the joint Cambridge Crystallographic Data Centre and Fachinformationszentrum Karlsruhe Access Structures service www.ccdc.cam.ac.uk/structures.

Manuscript received: May 15, 2020
Accepted manuscript online: June 30, 2020
Version of record online: August 17, 2020

 © 2020 The Authors. Published by Wiley-VCH GmbH

Angewandte Chemie
Eine Zeitschrift der Gesellschaft Deutscher Chemiker

Supporting Information

$Cs[Cl_3F_{10}]$: A Propeller-Shaped $[Cl_3F_{10}]^-$ Anion in a Peculiar $A^{[5]}B^{[5]}$ Structure Type

*Benjamin Scheibe, Antti J. Karttunen, Ulrich Müller, and Florian Kraus**

anie_202007019_sm_miscellaneous_information.pdf

Supporting Information
©Wiley-VCH 2019
69451 Weinheim, Germany

Table of Contents

Experimental Procedures 2
Selected crystallographic data of $Cs[Cl_3F_{10}]$ 3
Crystallographic Considerations 7
Gas-phase quantum-chemical calculations of $[X_3F_{10}]^-$ (X = Cl, Br, I) anions 8
Solid-state quantum-chemical calculations of $Cs[Cl_3F_{10}]$ 11
Band assignments for the calculated Raman spectrum of $Cs[Cl_3F_{10}]$ and comparison of Raman spectra 12
References 14
Author Contributions 14

Experimental Procedures

General: All operations were performed on a Monel metal Schlenk line, which was passivated with undiluted fluorine and chlorine trifluoride at various pressures before use. Moisture-sensitive compounds were stored and handled in an Ar-filled glove box (MBraun). Reaction vessels were made out of fluoropolymer (perfluoroalkoxy alkanes, PFA) and passivated with fluorine before use. Preparations were carried out in an atmosphere of dry and purified argon (5.0, Praxair). Chlorine trifluoride was stored over NaF to remove traces of HF. **Caution!** Fluorine, chlorine trifluoride, and fluoridochlorates(III) must be handled using appropriate protective gear with ready access to proper emergency treatment procedures in the event of contact. The aforementioned are potent oxidative fluorinators that are only stable under the rigorously anhydrous conditions employed in the experimental procedures outlined in the Experimental Section. They react vigorously to explosively upon hydrolysis or contact with organic materials. The utmost precautions must be taken when disposing of these materials and their derivatives.

Synthesis of $Cs[Cl_3F_{10}]$: In a typical experiment a PFA reaction vessel was loaded with 46.8 mg CsF (0.308 mmol) inside a glove box and attached to a stainless-steel valve. An excess of ClF_3 (approximately 0.13 g, 1.4 mmol) was then condensed onto the solid at 77 K. The reaction mixture was slowly warmed to room-temperature, at which point the CsF completely dissolved. The resulting solution was then stored at −37 °C. Colorless crystals of $Cs[Cl_3F_{10}]$ grew from the solution after several hours at this temperature. Similar experiments were conducted at a temperature of 0 °C and the isolated crystals were determined to be $Cs[Cl_3F_{10}]$. The crystals were then transferred from the cold chlorine trifluoride suspensions into cold (<0 °C) Galden HT270 (perfluoropolyether, Solvay). Note that the crystals of $Cs[Cl_3F_{10}]$ were observed to be only stable at low temperatures (≤0 °C) and/or when suspended in chlorine trifluoride. The crystals of $Cs[Cl_3F_{10}]$ rapidly deteriorate upon warming to room temperature and air contact. When excess chlorine trifluoride was removed in vacuo, $Cs[ClF_4]$ was obtained, which was identified by Raman spectroscopy.

Single-crystal X-ray diffraction: Crystals of $Cs[Cl_3F_{10}]$ were selected in the absence of air under dried, cooled perfluoropolyether (Galden HT270, Solvay, stored over molecular sieves 3 Å) and mounted on a MiTeGen loop. Intensity data of suitable crystals were recorded with a D8 Quest diffractometer (Bruker). The diffractometer was operated with monochromatized Mo-K_α radiation (0.71073 Å, multi layered optics) and equipped with a PHOTON 100 CMOS detector. Evaluation, integration, and reduction of the diffraction data was carried out with the APEX3 software suite.[1] Split reflections were observed for multiple specimens, which indicate non-merohedral twinning. The measured crystal was a non-merohedral twin with three components. The cell constants and twin laws were determined with the program CELL_NOW.[2] The diffraction data were corrected for absorption utilizing the multi-scan method of TWINABS within the APEX3 software suite. For the structure solution only the non-overlapping reflections of the major twin component were used. The structure was solved with dual-space methods (SHELXT).[3] The data were initially refined with the HKLF5 format option in SHELXL with all reflections (overlapping reflections and non-overlapping reflections of the three twin components).[4] The data were then processed with the HKLF5Tools program: the non-overlapping reflections of the weaker diffracting twin components were removed, the non-overlapping reflections of the major twin component were merged in point group 2/*m* and the overlapping reflections were merged in point group 1. The final refinement was carried out against the detwinned dataset (created by SHELXL with the LIST 8 option as a FCF file and converted to a HKL file with HKLF5Tools).[5] The highest residual electron density after the final refinement was 0.78 Å distant from atom Cs(1). Representations of the crystal structure were created with the Diamond software.[6] CCDC 1992456 contains the supplementary crystallographic data for this paper. These data are provided free of charge by The Cambridge Crystallographic Data Centre.

Raman spectroscopy: The Raman spectra were measured with a Monovista CRS+ confocal Raman microscope (Spectroscopy & Imaging GmbH) using a 532 nm solid-state laser and either a 300 grooves/mm (low-resolution mode, FWHM: <4.62 cm^{-1}) or an 1800 grooves/mm (high-resolution mode, FWHM: <0.368 cm^{-1}) grating. Sample preparation of $Cs[Cl_3F_{10}]$: A crop of colorless crystals was quickly transferred from a cold chlorine trifluoride suspension (ca. −37 °C) into Galden HT270 (perfluoropolyether, Solvay) on a microscope slide with a recess. The microscope slide was located slightly above a small Dewar vessel, which was filled with liquid nitrogen. Raman spectra of the crystals were recorded as soon as the perfluoropolyether was a viscous liquid (approximately −66 °C, which is the pour point of Galden HT270).

Selected crystallographic data of $Cs[Cl_3F_{10}]$

Determination of the cell constants and twin law using CELL_NOW[2]

CELL_NOW output:

The following cells would appear to be plausible, but should be checked using XPREP because they are not necessarily the conventional cells.

FOM, % within 0.2, a..gamma, volume and lattice type for potential unit-cells:

```
 1 1.000  78.1   6.887  15.380   9.089   90.01   91.21   89.93    962.5  P
 2 0.651  78.1   6.887  15.380  11.288   90.02  126.41   89.93    962.3  P
 3 0.494  79.7   6.887   9.089  16.848   89.50   65.93   88.79    962.7  P
 4 0.420  79.3   6.887   9.089  17.868   59.43   89.44   88.79    962.8  P
 5 0.416  80.6   6.887   9.089  19.215   61.27   68.44   88.79    962.9  P
 6 0.393  77.5   6.887   9.089  16.856   89.48   65.82   88.79    962.3  P
 7 0.330  78.2   6.887   9.089  19.082  117.94  110.60   91.21    962.6  P
 8 0.327  77.9  11.523  15.380  16.343   90.03   94.16   89.97   2888.9  P
 9 0.324  79.8   6.887  11.288  16.848   75.99   65.93   53.59    962.5  P
10 0.315  76.5   6.887   9.089  17.865   59.41   89.34   88.79    962.4  P
11 0.305  77.2  11.288  15.380  16.669   90.04   93.34   89.98   2888.9  P
12 0.301  77.4   6.887  15.380  22.575   90.04  126.41   89.93   1924.7  P
-----------------------------------------------------------------------------

Cell for domain 1:   6.887   15.380   9.089   90.01   91.21   89.93

Figure of merit: 0.845   %(0.1):  74.7   %(0.2):  78.1   %(0.3):  82.7

Orientation matrix:
0.09446988 -0.02510910  0.07350846
0.02914441 -0.04837650 -0.06969371
0.10637643  0.03545101 -0.04302402

Percentages of reflections in this domain not consistent with lattice types:
A: 36.2,  B: 51.0,  C: 49.1,  I: 48.8,  F: 68.1,  O: 66.9  and  R: 67.2%

Percentages of reflections in this domain that do not have:
h=2n: 49.9,  k=2n: 51.4,  l=2n: 49.6,  h=3n: 67.3,  k=3n: 68.0,  l=3n: 66.8%

19783 reflections within tolerance assigned to domain 1,
19783 of them exclusively; 4897 reflections not yet assigned to a domain
-----------------------------------------------------------------------------

Cell for domain 2:   6.887   15.380   9.089   90.01   91.21   89.93

Figure of merit: 0.470   %(0.1):  46.7   %(0.2):  52.7   %(0.3):  63.4

Orientation matrix:
0.09041524 -0.02595982 -0.07266141
0.02975903  0.05938596 -0.03815977
0.10967856  0.00518869  0.07332070

Rotated from first domain by 118.8 degrees about
reciprocal axis  1.000  0.002 -0.028  and real axis  1.000  0.000  0.000

Twin law to convert hkl from first to this domain (SHELXL TWIN matrix):
1.000   0.000   0.000
-0.038  -0.482  -1.483
-0.042   0.518  -0.482

12849 reflections within tolerance assigned to domain 2,
2828 of them exclusively; 2069 reflections not yet assigned to a domain
-----------------------------------------------------------------------------

Cell for domain 3:   6.887   15.380   9.089   90.01   91.21   89.93

Figure of merit: 0.704   %(0.1):  69.7   %(0.2):  71.2   %(0.3):  76.5

Orientation matrix:
-0.09413844  0.04955499 -0.00076555
-0.02969191 -0.01075762 -0.10662626
-0.10651876 -0.04069526  0.02724020

Rotated from first domain by 179.9 degrees about
reciprocal axis -0.014  0.961  1.000  and real axis  0.003  0.335  1.000

Twin law to convert hkl from first to this domain (SHELXL TWIN matrix):
-1.000  -0.007  -0.020
0.007  -0.513   1.453
0.004   0.507   0.513

10441 reflections within tolerance assigned to domain 3,
1505 of them exclusively; 564 reflections not yet assigned to a domain
```

Compared to the output of CELL_NOW the unit cell was transformed according to **c**, −**b**, **a** and correspondingly l −k, h . This way, the monoclinic c axis coincides with the pseudohexagonal c axis and the monoclinic unit cell corresponds to the orthohexagonal cell. The axes of the twin domains mentioned in the output of CELL_NOW have to be relabeled accordingly.

Table S1. Selected crystallographic data and details of the structure determination of $Cs[Cl_3F_{10}]$.

Formula	$CsCl_3F_{10}$
Molar mass / g·mol^{-1}	429.26
Space group (No.)	$P12_1/n1$ (14)
a / Å	9.0949(7)
b / Å	15.3652(12)
c / Å	6.8841(5)
β / °	91.314(2)
V / Å^3	961.77(13)
Z	4
Pearson symbol	$mP56$
$\rho_{calc.}$ / g·cm^{-3}	2.97
μ / mm^{-1}	4.795
Color	colorless
Crystal morphology	block
Crystal size / mm^3	0.060 · 0.082 · 0.170
T / K	100
λ / Å	0.71073 (Mo-K$_\alpha$)
No. of reflections	72465
θ range / °	2.60-30.50
Range of Miller indices	$-12 \leq h \leq 12$
	$-21 \leq k \leq 21$
	$-9 \leq l \leq 9$
Absorption correction	multi-scan
T_{max}, T_{min}	0.75, 0.51
R_{int}, R_σ	0.050, 0.0471
Completeness of the data set	0.996
No. of unique reflections	2915
No. of parameters	127
No. of restraints	0
No. of constraints	0
S (all data)	1.09
$R(F)$ ($I \geq 2\sigma(I)$, all data)	0.0353, 0.0459
$wR(F^2)$ ($I \geq 2\sigma(I)$, all data)	0.0819, 0.0863
Extinction coefficient	not refined
$\Delta\rho_{max}$, $\Delta\rho_{min}$ / e·Å^{-3}	2.29, −1.26

Table S2. Atomic coordinates and equivalent isotropic displacement parameters U_{iso} of $Cs[Cl_3F_{10}]$ at 100 K.

Atom	Position	*x*	*y*	*z*	U_{iso} / Å^2
Cs(1)	4*e*	0.01291(2)	0.34115(2)	0.26558(3)	0.02195(9)
Cl(1)	4*e*	0.00999(7)	0.18673(5)	0.79210(11)	0.01919(16)
Cl(2)	4*e*	0.22709(8)	0.39970(5)	0.77877(11)	0.01866(16)
Cl(3)	4*e*	−0.19246(8)	0.40043(5)	0.75364(10)	0.01628(15)
F(1)	4*e*	0.0182(2)	0.32657(13)	0.6995(3)	0.0238(4)
F(2)	4*e*	−0.1537(2)	0.16571(15)	0.6662(4)	0.0417(6)
F(3)	4*e*	0.0091(2)	0.08724(12)	0.8674(3)	0.0352(5)
F(4)	4*e*	0.1731(2)	0.20129(14)	0.9274(3)	0.0338(5)
F(5)	4*e*	0.3386(3)	0.32653(14)	0.6604(4)	0.0402(6)
F(6)	4*e*	0.3719(2)	0.45434(14)	0.8376(3)	0.0364(5)
F(7)	4*e*	0.1245(2)	0.47666(14)	0.9043(3)	0.0283(5)
F(8)	4*e*	−0.1472(2)	0.47675(14)	0.5765(3)	0.0298(5)
F(9)	4*e*	−0.3422(2)	0.45278(14)	0.7841(3)	0.0327(5)
F(10)	4*e*	0.2477(2)	0.32775(13)	0.9320(3)	0.0329(5)

Table S3. Anisotropic displacement parameters of $Cs[Cl_3F_{10}]$ at 100 K.

Atom	U_{11} / Å^2	U_{22} / Å^2	U_{33} / Å^2	U_{23} / Å^2	U_{13} / Å^2	U_{12} / Å^2
Cs(1)	0.02457(12)	0.02174(13)	0.01951(12)	0.00040(7)	−0.00004(8)	−0.00298(7)
Cl(1)	0.0185(3)	0.0186(4)	0.0202(3)	−0.0026(3)	−0.0047(3)	0.0022(2)
Cl(2)	0.0193(3)	0.0165(4)	0.0205(4)	0.0012(3)	0.0067(3)	0.0026(3)
Cl(3)	0.0149(3)	0.0159(3)	0.0179(3)	−0.0002(2)	−0.0024(2)	−0.0002(2)
F(1)	0.0217(9)	0.0226(10)	0.0269(10)	0.0031(8)	−0.0015(7)	0.0053(7)
F(2)	0.0291(12)	0.0431(14)	0.0521(16)	−0.0145(11)	−0.0209(11)	−0.0006(9)
F(3)	0.0389(12)	0.0168(10)	0.0497(14)	0.0020(10)	−0.0023(10)	0.0002(9)
F(4)	0.0285(11)	0.0343(13)	0.0378(12)	0.0115(9)	−0.0177(9)	−0.0046(9)
F(5)	0.0434(14)	0.0261(11)	0.0521(15)	−0.0031(10)	0.0274(12)	0.0092(10)
F(6)	0.0194(9)	0.0311(12)	0.0591(16)	−0.0026(10)	0.0092(10)	−0.0078(8)
F(7)	0.0239(10)	0.0283(11)	0.0328(11)	−0.0117(9)	0.0030(9)	0.0053(8)
F(8)	0.0335(11)	0.0240(11)	0.0317(11)	0.0090(9)	−0.0014(9)	0.0005(9)
F(9)	0.0192(9)	0.0345(12)	0.0445(13)	0.0025(10)	0.0016(9)	0.0098(8)
F(10)	0.0344(12)	0.0338(12)	0.0306(12)	0.0094(9)	0.0071(9)	−0.0024(9)

Table S4. Selected experimental and computational (DFT-PBE0/TZVP, solid-state and DFT-PBE0/TZVP, gas-phase, D_3 symmetry) atom distances for the $[Cl_3F_{10}]^-$ anion.

	d (experimental) / Å	*d* (DFT-PBE0, solid-state) / Å	*d* (DFT-PBE0, gas-phase) / Å
Cl(1)−F(1)	2.243(2)		
Cl(2)−F(1)	2.263(2)	2.24-2.27	2.22
Cl(3)−F(1)	2.265(2)		
Cl(1)−F(2)	1.736(2)		
Cl(1)−F(4)	1.747(2)		
Cl(2)−F(5)	1.730(2)	1.74-1.76	1.73
Cl(2)−F(7)	1.747(2)		
Cl(3)−F(8)	1.747(2)		
Cl(3)−F(10)	1.743(2)		
Cl(1)−F(3)	1.615(2)		
Cl(2)−F(6)	1.606(2)	1.60-1.62	1.64
Cl(3)−F(9)	1.600(2)		

Table S5. Selected experimental and computational (DFT-PBE0/TZVP, solid-state and DFT-PBE0/def2-TZVP, gas-phase D_3 symmetry) angles for the $[Cl_3F_{10}]^-$ anion.

	∡ (experimental) / °	∡ (DFT-PBE0, solid-state) / °	∡ (DFT-PBE0, gas-phase) / °
Cl(1)−F(1)−Cl(2)	116.12(8)	109.8-115.5	120
Cl(2)−F(1)−Cl(3)	114.83(9)		
Cl(3)−F(1)−Cl(1)	113.52(9)		
F(1)−Cl(1)−F(3)	177.29(10)	177.2-178.1	180
F(1)−Cl(2)−F(6)	178.03(10)		
F(1)−Cl(3)−F(9)	178.03(10)		
F(2)−Cl(1)−F(4)	176.13(12)	176.1-176.7	174.5
F(5)−Cl(2)−F(7)	176.42(12)		
F(8)−Cl(3)−F(10)	176.47(11)		
F(2)−Cl(1)−F(3)	88.50(11)	87.8-88.6	87.3
F(3)−Cl(1)−F(4)	87.73(11)		
F(5)−Cl(2)−F(6)	88.41(12)		
F(6)−Cl(2)−F(7)	88.05(11)		
F(8)−Cl(3)−F(9)	88.19(11)		
F(9)−Cl(3)−F(10)	88.28(11)		

Crystallographic Considerations

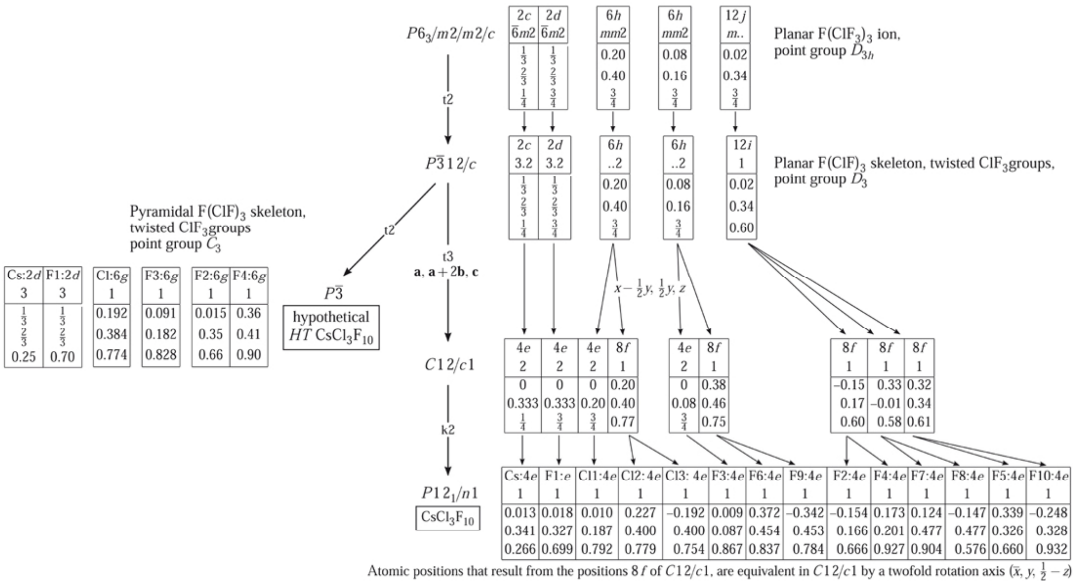

Figure S1. Bärnighausen tree showing the group–subgroup relations from a hexagonal aristotype with Cs atoms arranged as in the Mg type and with planar $[Cl_3F_{10}]^-$ in its trigonal pyramidal voids to the real structure of. $Cs[Cl_3F_{10}]$. The branch to the space group $P\bar{3}$ shows the relation to a hypothetical high-temperature form of $Cs[Cl_3F_{10}]$.

The actual crystal structure corresponds in good approximation to a hypothetical structure in the space group $P\bar{3}$, which is another subgroup of $P6_3/mmc$ (Figure S1). It seems probable that this could be a trigonal high-temperature modification of $Cs[Cl_3F_{10}]$ that, however, possibly cannot be obtained because of its instability at temperatures higher than 0 °C. This is in accordance with the observed twinning. As mentioned above (Selected crystallographic data), there exists a twin domain 3 rotated by 180° about *a* and another twin domain 2 rotated by 120° about *c*. That is exactly what is to be expected from the Bärnighausen tree, where we have a *translationengleiche* subgroup of index 2 (marked t2) giving rise to twins, and another one of index 3 (t3) giving rise to triplet twinning. Since the space group $P\bar{3}$ is not a direct supergroup of $P12_1/n1$, a phase transformation from the real to the hypothetical high-temperature form could only be a first-order transformation.

Gas-phase quantum-chemical calculations of $[X_3F_{10}]^-$ (X = Cl, Br, I) anions

Gas-phase quantum-chemical calculations for the anions $[X_3F_{10}]^-$ (X = Cl, Br, I) were carried out with the TURBOMOLE program package (version 7.3.) using the PBE0 hybrid density functional method and Karlsruhe triple-zeta-valence + polarization basis sets (def2-TZVP for Cl and Br, dhf-TZVP for I).[7–9] The resolution-of-the-identity technique was used to speed up the calculations.[10,11] All calculations were done in the gas phase without any solvent models. A full geometry optimization was carried out in the D_3 point group. All structures were confirmed to be true local minima by harmonic frequency calculations. The bonding in the studied species was investigated with the help of Intrinsic Atomic Orbitals (IAOs) and Intrinsic Bond Orbitals (IBOs) using the program package IboView.[12,13] The plotted IBO isosurfaces enclose 80% of the total electron density of the IBO.

XYZ coordinates of the geometry-optimized $[Cl_3F_{10}]^-$ anion

```
Cl   1.1077871  −1.9187436   0.0000000
Cl   1.1077871   1.9187436   0.0000000
F    0.0000000   0.0000000   0.0000000
F    0.1358137   2.5755586  −1.2780215
F    1.9275393  −3.3385960   0.0000000
F    2.1625923   1.4053974   1.2780215
F    2.1625923  −1.4053974  −1.2780215
F    0.1358137  −2.5755586   1.2780215
F    1.9275393   3.3385960   0.0000000
Cl  −2.2155742   0.0000000   0.0000000
F   −3.8550786   0.0000000   0.0000000
F   −2.2984060   1.1701612   1.2780215
F   −2.2984060  −1.1701612  −1.2780215
```

XYZ coordinates of the geometry-optimized $[Br_3F_{10}]^-$ anion

```
Br   1.1496286  −1.9912152   0.0000000
Br   1.1496286   1.9912152   0.0000000
F   −0.0000000   0.0000000   0.0000000
F    0.1667520   2.6976675  −1.3923404
F    2.0305703  −3.5170509   0.0000000
F    2.2528726   1.4932452   1.3923404
F    2.2528726  −1.4932452  −1.3923404
F    0.1667520  −2.6976675   1.3923404
F    2.0305703   3.5170509   0.0000000
Br  −2.2992573   0.0000000   0.0000000
F   −4.0611406   0.0000000   0.0000000
F   −2.4196246   1.2044223   1.3923404
F   −2.4196246  −1.2044223  −1.3923404
```

XYZ coordinates of the geometry-optimized $[I_3F_{10}]^-$ anion

```
I    1.2209583  −2.1147618   0.0000000
I    1.2209583   2.1147618   0.0000000
F    0.0000000   0.0000000   0.0000000
F    0.3666149   2.8334558  −1.6241675
F    2.1708407  −3.7600063   0.0000000
F    2.2705373   1.7342257   1.6241675
F    2.2705373  −1.7342257  −1.6241675
F    0.3666149  −2.8334558   1.6241675
F    2.1708407   3.7600063   0.0000000
I   −2.4419166   0.0000000   0.0000000
F   −4.3416813   0.0000000   0.0000000
F   −2.6371521   1.0992301   1.6241675
F   −2.6371521  −1.0992301  −1.6241675
```

Table S6. Partial atomic charges for the $[X_3F_{10}]^-$ (X = Cl, Br, I) anions from Intrinsic Atomic Orbital (IAO) analysis (e^- units).

Atom	$[Cl_3F_{10}]^-$	$[Br_3F_{10}]^-$	$[I_3F_{10}]^-$
X	1.29	1.44	1.68
μ_3-F	−0.60	−0.62	−0.67
F_{trans}	−0.39	−0.45	−0.55
F_{cis}	−0.52	−0.56	−0.62

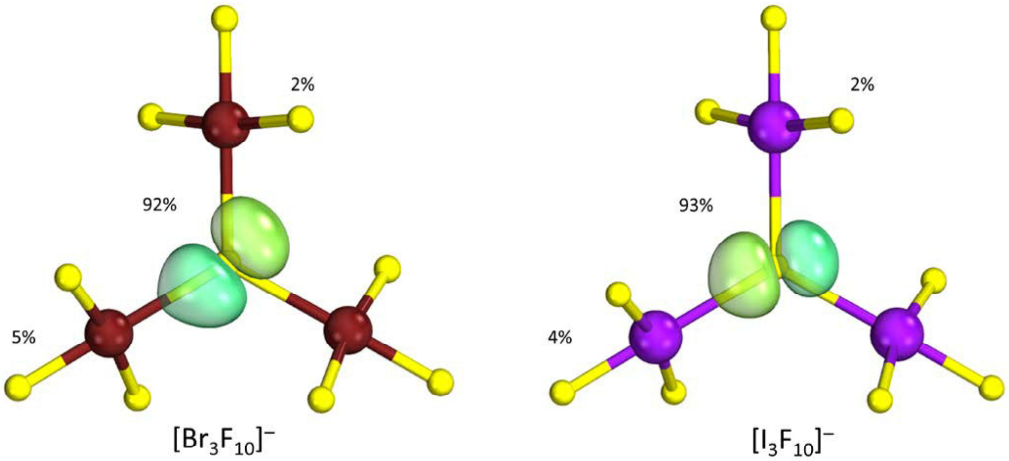

Figure S2. One of the two intrinsic bond orbitals (IBOs) showing the μ_3-F–*X* bonds in the $[Br_3F_{10}]^-$ and $[I_3F_{10}]^-$ anions (*X* = Br, I).[22] The percentages indicate the contribution of the halogen atoms and the μ_3-F atom to the IBO. The larger the percentage, the more polarized the bond. For comparison: For a gas-phase NaF molecule, in which the bond should be highly ionic, the contribution of the F atom is 96 %. In the H_2 molecule, which has a purely covalent bond, the contribution of each atom is 50 %. If the summation of the percentages does not add up to 100 %, then other atoms contribute – less than 1 % – to the IBO. F atoms: yellow, Br atoms: reddish brown, I atoms: purple.

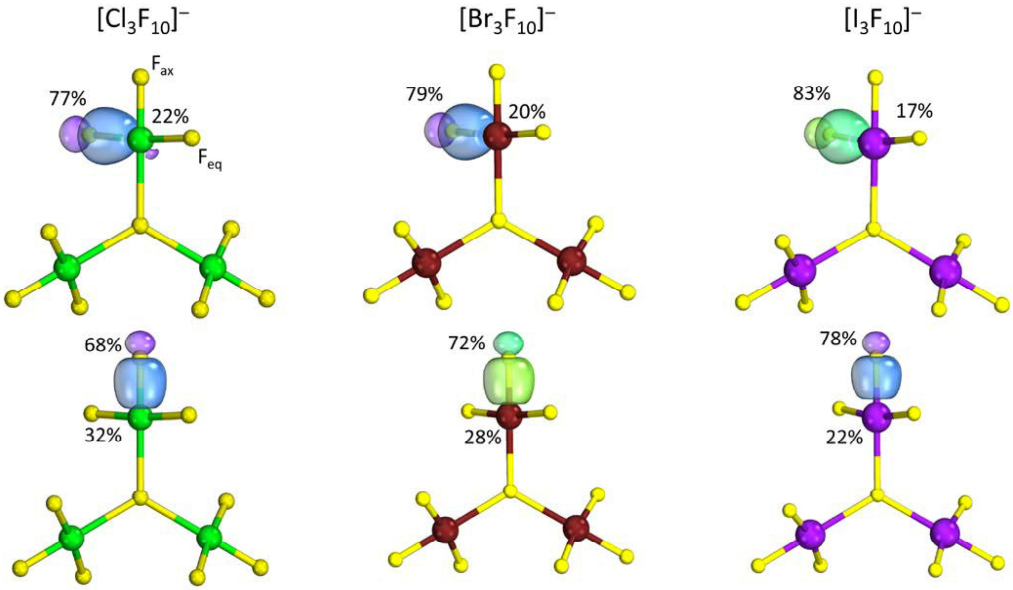

Figure S3. Intrinsic Bond Orbitals (IBOs) showing *X*–F_{cis} (top) and *X*–F_{trans} (bottom) bonds in the $[X_3F_{10}]^-$ anions (*X* = Cl, Br, I). Percentages indicate the contribution of each atom to the IBO. The larger the percentage, the more polarized the bond. For comparison: For a gas-phase NaF molecule, in which the bond should be highly ionic, the contribution of the F atom is 96 %. In the H_2 molecule, which has a purely covalent bond, the contribution of each atom is 50 %. If the summation of the percentages does not add up to 100 %, then other atoms contribute – less than 1 % – to the IBO. F atoms: yellow, Cl atoms: green, Br atoms: reddish brown, I atoms: purple.

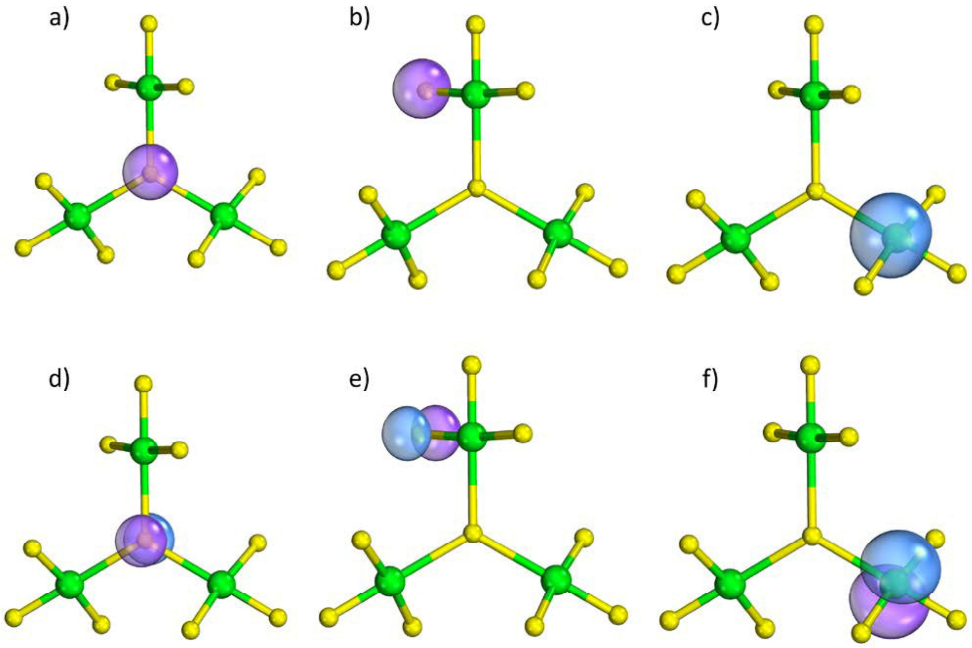

Figure S4. Examples of non-bonding Intrinsic Bond Orbitals (IBOs) in the $[Cl_3F_{10}]^-$ anion. s-orbital-like IBOs are shown in a)-c). p-orbital-like IBOs are shown in d)-f). F atoms in yellow, Cl atoms in green.

Solid-state quantum-chemical calculations of $Cs[Cl_3F_{10}]$

Periodic quantum-chemical calculations were carried out for $Cs[Cl_3F_{10}]$ with the PBE0 hybrid density functional theory method (DFT-PBE0).[14,15] A triple-zeta-valence + polarization (TZVP) level basis set was applied for F and Cl and a split-valence + polarization (SVP) level basis set was applied for Cs. The basis sets were derived from the Karlsruhe def2 basis sets and taken from previous studies.[9,16–18] All calculations were carried out with the CRYSTAL17 program package.[19] The reciprocal space was sampled with a 4×2×3 Monkhorst-Pack-type *k*-point grid. For the evaluation of the Coulomb and exchange integrals (TOLINTEG), tight tolerance factors of 8, 8, 8, 8, 16 were used for all calculations. Both the atomic positions and lattice parameters were fully optimized within the constraints imposed by the space group symmetry. Default DFT integration grids and optimization convergence thresholds were applied in all calculations. The harmonic vibrational frequencies and Raman intensities were obtained through usage of the computational scheme implemented in CRYSTAL17.[20–23] The Raman intensities were calculated for a polycrystalline powder sample (total isotropic intensity in arbitrary units). The Raman spectra were obtained by using a pseudo-Voigt band profile (50:50 Lorentzian:Gaussian) and an FWHM of 8 cm^{-1}. The Raman spectra were simulated taking into account the experimental setup (T = 207.15 K, λ = 532 nm). The band assignments were carried out by visual inspection of the normal modes with the Jmol program package.[24]

Lattice parameters and atomic coordinates of the optimized solid-state structure of $Cs[Cl_3F_{10}]$

Space group $P2_1/n$ (No. 14) – here, a different space group setting was used, so lattice parameters and atomic coordinates are interchanged compared to the deposited crystal structure. However, the results are of course identical.
a = 7.29891298 Å, b = 15.29673244 Å, c = 9.12132812 Å, β = 93.243220°, V = 1016.760812 $Å^3$

Table S7. Atomic coordinates of the optimized structure of $Cs[Cl_3F_{10}]$.

Atom	*x*	*y*	*z*
Cs(1)	2.762404704911E−01	3.487537724337E−01	−4.851377917018E−01
Cl(1)	−2.499977788070E−01	3.955001550605E−01	3.214039278472E−01
Cl(2)	−2.064146484759E−01	1.831217546430E−01	−4.824472805740E−01
Cl(3)	−2.060477666329E−01	3.962893633638E−01	−2.590965482665E−01
F(1)	−3.040827548803E−01	3.229303714803E−01	−4.672212545441E−01
F(2)	−8.247541012499E−02	4.685669529561E−01	−3.710187149355E−01
F(3)	−2.222373885948E−01	4.480775087627E−01	1.683737183078E−01
F(4)	−4.298632094940E−01	4.701207408601E−01	3.563317591261E−01
F(5)	−6.719095268031E−02	3.257530157643E−01	2.773161315502E−01
F(6)	−3.224952817150E−01	3.292216490220E−01	−1.376579378583E−01
F(7)	−1.277514849546E−01	4.531752927419E−01	−1.171161103897E−01
F(8)	−1.259557260578E−01	8.312380724319E−02	−4.867301386579E−01
F(9)	−9.138593581981E−02	1.949154564508E−01	−3.070629551867E−01
F(10)	−3.152329059001E−01	1.650743845394E−01	3.414527937302E−01

Band assignments for the calculated Raman spectrum of $Cs[Cl_3F_{10}]$ and comparison of Raman spectra

Table S8. Band assignments for the calculated Raman spectrum (>300 cm^{-1}) of $Cs[Cl_3F_{10}]$. The notation for band assignments is the following: ν – stretching, δ – deformation, s – symmetric, as – asymmetric. The irreducible representation is given for the point group $C2/m$ (C_{2h}) of the space group $P2_1/n$ (No. 14). The point group of the $[Cl_3F_{10}]^-$ anion in the crystal structure is C_1.

ν (calculated) / cm^{-1}	ν (experimental) / cm^{-1}	irrep	Assignment
787	761 & 699	A_g	ν_s – Symmetric stretching of F_{trans}–Cl
779		B_g	
758		B_g	
719		A_g	
719		B_g	
715		A_g	
650	not observed	B_g	ν_{as} – Antisymmetric stretching of F_{cis}–Cl
645		B_g	
639		A_g	
619		B_g	
613		A_g	
586		A_g	
510	498	A_g	ν_s – Symmetric stretching of F_{cis}–Cl coupled with the central μ_3-F atom
509		B_g	
509		A_g	
508		B_g	
503		A_g	
503		B_g	
381	not observed	B_g	δ – scissoring of F_{trans}–Cl, coupled with the central μ_3-F atom
381		A_g	
377		B_g	
376		B_g	
373		B_g	
372		A_g	
367	334	B_g	δ – out-of-plane bending of the ClF_3 groups, coupled with the central μ_3-F atom
364		A_g	
363		B_g	
361		A_g	
360		A_g	
360		B_g	
341		B_g	
329		A_g	
323	315	B_g	δ – scissoring of F_{cis}–Cl, coupled with the central μ_3-F atom
316		A_g	
315		B_g	
313		A_g	

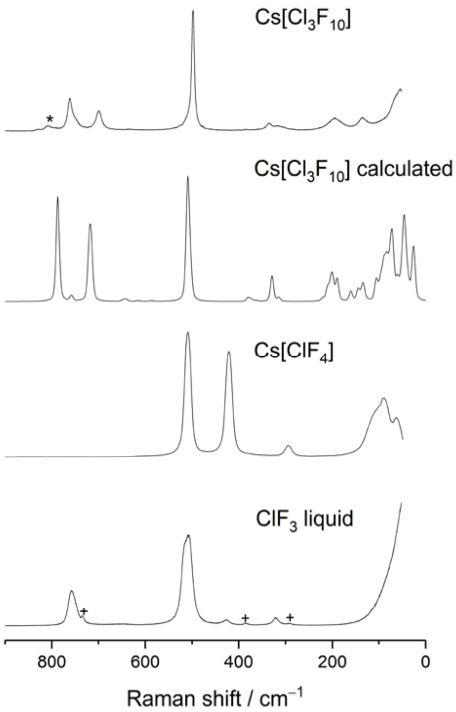

Figure S5. Comparison of experimental and calculated Raman spectra. **$Cs[Cl_3F_{10}]$:** Experimental high-resolution Raman spectrum of crystalline $Cs[Cl_3F_{10}]$ measured at ca. −66 °C under the perfluoropolyether Galden HT270. The asterisk denotes a band caused by Galden HT270. **$Cs[Cl_3F_{10}]$ calculated:** Calculated (DFT-PBE0) solid-state Raman spectrum of $Cs[Cl_3F_{10}]$ taking into account the experimental temperature of −66 °C and the used laser wavelength of 532 nm. **$Cs[ClF_4]$:** Experimental low-resolution Raman spectrum of powdered $Cs[ClF_4]$ measured in a glass vial. **ClF_3 liquid:** Experimental high-resolution Raman spectrum of liquid ClF_3 measured in an FEP (fluorinated ethylene propylene copolymer) sample tube. The plus signs denote bands that are caused by the FEP tube. The Raman intensities are given in arbitrary units.

References

[1] *APEX3*, Bruker AXS Inc., Madison, Wisconsin, USA, **2018**.
[2] G. M. Sheldrick, *CELL_NOW*, Göttingen (Germany), **2008**.
[3] G. M. Sheldrick, *Acta Crystallogr., Sect. A: Found. Adv.* **2015**, *71*, 3–8.
[4] G. M. Sheldrick, *Acta Crystallogr., Sect. C: Struct. Chem.* **2015**, *71*, 3–8.
[5] S. I. Ivlev, M. Conrad, F. Kraus, *Z. Kristallogr. - Cryst. Mater.* **2019**, *234*, 415–418.
[6] K. Brandenburg, H. Putz, *Diamond - Crystal and Molecular Structure Visualization*, Crystal Impact GbR, Bonn, **2019**.
[7] R. Ahlrichs, M. Bär, M. Häser, H. Horn, C. Kölmel, *Chem. Phys. Lett.* **1989**, *162*, 165–169.
[8] *TURBOMOLE V7.3, a Development of University of Karlsruhe and Forschungszentrum Karlsruhe GmbH, 1989-2007, TURBOMOLE GmbH, since 2007.*, **2018**.
[9] F. Weigend, R. Ahlrichs, *Phys. Chem. Chem. Phys.* **2005**, *7*, 3297–3305.
[10] K. Eichkorn, O. Treutler, H. Öhm, M. Häser, R. Ahlrichs, *Chem. Phys. Lett.* **1995**, *240*, 283–290.
[11] F. Weigend, *Phys. Chem. Chem. Phys.* **2006**, *8*, 1057–1065.
[12] G. Knizia, *J. Chem. Theory Comput.* **2013**, *9*, 4834–4843.
[13] G. Knizia, J. E. M. N. Klein, *Angew. Chem. Int. Ed.* **2015**, *54*, 5518–5522.
[14] J. P. Perdew, K. Burke, M. Ernzerhof, *Phys. Rev. Lett.* **1996**, *77*, 3865–3868.
[15] C. Adamo, V. Barone, *J. Chem. Phys.* **1999**, *110*, 6158–6170.
[16] V. Sivchik, R. K. Sarker, Z.-Y. Liu, K.-Y. Chung, E. V. Grachova, A. J. Karttunen, P.-T. Chou, I. O. Koshevoy, *Chem. Eur. J.* **2018**, *24*, 11475–11484.
[17] R. E. Stene, B. Scheibe, A. J. Karttunen, W. Petry, F. Kraus, *Eur. J. Inorg. Chem.* **2019**, *2019*, 3672–3682.
[18] A. J. Karttunen, T. Tynell, M. Karppinen, *J. Phys. Chem. C* **2015**, *119*, 13105–13114.
[19] R. Dovesi, A. Erba, R. Orlando, C. M. Zicovich-Wilson, B. Civalleri, L. Maschio, M. Rérat, S. Casassa, J. Baima, S. Salustro, et al., *Wiley Interdiscip. Rev.: Comput. Mol. Sci.* **2018**, e1360.
[20] C. M. Zicovich-Wilson, F. Pascale, C. Roetti, V. R. Saunders, R. Orlando, R. Dovesi, *J. Comput. Chem.* **2004**, *25*, 1873–1881.
[21] F. Pascale, C. M. Zicovich-Wilson, F. López Gejo, B. Civalleri, R. Orlando, R. Dovesi, *J. Comput. Chem.* **2004**, *25*, 888–897.
[22] L. Maschio, B. Kirtman, M. Rérat, R. Orlando, R. Dovesi, *J. Chem. Phys.* **2013**, *139*, 164101.
[23] L. Maschio, B. Kirtman, M. Rérat, R. Orlando, R. Dovesi, *J. Chem. Phys.* **2013**, *139*, 164102.
[24] *Jmol: An Open-Source Java Viewer for Chemical Structures in 3D. Http://Www.Jmol.Org/*, Jmol Team, **2019**.

Author Contributions

Benjamin Scheibe: Planning and conducting the experiments, main data acquisition and interpretation, quantum-chemical solid-state calculations, manuscript preparation.

Antti J. Karttunen: Quantum-chemical gas-phase calculations and solid-state calculations in CsF polymorphs, Quantum-chemical gas-phase calculations, CRYSTAL17 basis set development, intrinsic atomic orbital (IAO) and intrinsic bond orbital (IBO) analysis, manuscript preparation.

Ulrich Müller: Data interpretation, preparation of the Bärnighausen tree, crystallographic considerations, manuscript preparation.

Florian Kraus: Project administration, data interpretation, structure chemistry, manuscript preparation.

7.3. Difluorochloronium(III) Fluoridometallates $ClF_2[MF_6]$ – From Molecular Building Blocks to (Helical) Chains

Benjamin Scheibe, Ralf Haiges, Sergei I. Ivlev, Ulrich Müller, Antti J. Karttunen, Karl O. Christe, Florian Kraus

Eur. J. Inorg. Chem. **2020**
DOI: 10.1002/ejic.202000845

© 2020 The Authors. Published by Wiley-VCH Verlag GmbH & Co. KGaA.

Open access article distributed under the Creative Commons CC BY 4.0 license.
The original licensed material is shown.
(https://creativecommons.org/licenses/by/4.0/legalcode)

EurJIC
European Journal of Inorganic Chemistry

Chemistry Europe
European Chemical Societies Publishing

Accepted Article

Title: Difluorochloronium(III) Fluoridometallates – From Molecular Building Blocks to (Helical) Chains

Authors: Benjamin Scheibe, Ralf Haiges, Sergei I Ivlev, Antti J Karttunen, Ulrich Müller, Karl O Christe, and Florian Kraus

This manuscript has been accepted after peer review and appears as an Accepted Article online prior to editing, proofing, and formal publication of the final Version of Record (VoR). This work is currently citable by using the Digital Object Identifier (DOI) given below. The VoR will be published online in Early View as soon as possible and may be different to this Accepted Article as a result of editing. Readers should obtain the VoR from the journal website shown below when it is published to ensure accuracy of information. The authors are responsible for the content of this Accepted Article.

To be cited as: *Eur. J. Inorg. Chem.* 10.1002/ejic.202000845

Link to VoR: https://doi.org/10.1002/ejic.202000845

WILEY-VCH

European Journal of Inorganic Chemistry 10.1002/ejic.202000845

WILEY-VCH

FULL PAPER

Difluorochloronium(III) Fluoridometallates – From Molecular Building Blocks to (Helical) Chains

Benjamin Scheibe[a], Ralf Haiges[b], Sergei I. Ivlev[a], Antti J. Karttunen[c], Ulrich Müller[a], Karl O. Christe[b], and Florian Kraus*[a]

[a] B. Scheibe M. Sc., Dr. S. I. Ivlev, Prof. em. Dr. U. Müller, Prof. Dr. F. Kraus
Fachbereich Chemie
Philipps-Universität Marburg
Hans-Meerwein-Straße 4
35032 Marburg (Germany)
E-mail: f.kraus@uni-marburg.de
Homepage: https://www.uni-marburg.de/en/fb15/researchgroups/ag-kraus

[b] Prof. Dr. R. Haiges, Prof. Dr. K. O. Christe,
Department of Chemistry
University of Southern California
Los Angeles, CA 90089 (USA)

[c] Prof. Dr. A. J. Karttunen
Department of Chemistry and Materials Science
Aalto University
00076 Aalto (Finland)

Supporting information for this article is given via a link at the end of the document.

Abstract: Difluorochloronium(III) compounds were synthesized from the reaction of metal powders (Ru, Os, Ir, Au), metal fluorides (NbF_5, SbF_3, BiF_5) or a metal chloride ($TaCl_5$) with excess liquid chlorine trifluoride. The compounds $ClF_2[AuF_4]$, $ClF_2[MF_6]$ (M = Nb, Ta, Ru, Os, Ir, Sb, Bi) and $ClF_2[Ta_2F_{11}]$ were obtained in crystalline form and their crystal structures were determined by single-crystal X-ray diffraction. The ClF_2^+ cations in the investigated compounds are bent, containing two strong, short, mainly covalent Cl−F bonds and two sterically active, free valence electron pairs in a pseudo-tetrahedral arrangement. The coordination around the Cl atom is extended by two highly ionic, long fluorine bridges to neighboring fluoridometallate anions, resulting in a total coordination number of six. The crystal structures vary among the ClF_2^+ compounds and range from molecular building blocks, such as dimeric $(ClF_2[AuF_4])_2$ and $(ClF_2[Ta_2F_{11}])_2$, to chains, some of which being helical, as in $(ClF_2[MF_6]$, M = Nb, Ta, Ru, Os, Ir, Sb, Bi). Quantum-chemical solid-state and gas-phase calculations were carried to elucidate the bonding within the ClF_2^+ cations and their interactions with the bridging F atoms.

Introduction

Chlorine trifluoride is one of the most reactive compounds and reacts vigorously with many metals, metal oxides and especially with most organic compounds, if the reaction conditions are not well controlled.[1–4] The reactivity of ClF_3 at ambient temperature surpasses that of elemental fluorine. The products from reactions of ClF_3 with metals, such as Mo, W, U, and metal oxides, such as UO_2, ReO_3, OsO_4, are usually fluorides (MF_6, M = Mo, W, U) and oxyfluorides ($ReOF_5$, OsO_3F_2), respectively, in high or highest oxidation states.[5–8]

If ClF_3 is used in excess and reacted with a fluoride that has an appreciable fluoride ion affinity, such as AsF_5 or SbF_5, a difluorochloronium(III) compound is formed.[9,10] With weaker Lewis acids, such as BF_3 and PF_5, thermally unstable ClF_2^+ salts, are formed.[11] This amphoteric character is common for all halogen trifluorides, XF_3 (X = Cl, Br, I). They can form bent, C_{2v}-symmetric XF_2^+ cations and square planar D_{4h}-symmetric $[XF_4]^-$ anions, see Equations 1 and 2 and Scheme 1.[9,10,12–20]

$$XF_3 + MF_5 \longrightarrow XF_2[MF_6] \quad (1)$$

X = Cl, Br, I; M = As, Sb

$$XF_3 + AF \longrightarrow A[XF_4] \quad (2)$$

X = Cl, Br, I; A = K, Rb, Cs

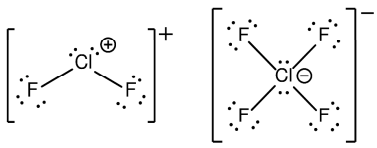

Scheme 1. Lewis structures of the ClF_2^+ cation and the ClF_4^- anion.

Fluorohalonium(III) cations with higher nuclearity have recently been reported for the BrF_3 system: $[Br_2F_5]^+$ and $[Br_3F_8]^+$ are formed according to Equation 3.[21] In these cations, μ_2-bridging fluorine atoms are present, but so far no evidence for such type cations has been reported for ClF_3 and IF_3.

$$BrF_2[SbF_6] + n\,BrF_3 \longrightarrow [Br_{1+n}F_{2+3n}][SbF_6] \quad (3)$$

n = 1, 2

Several ClF_2^+ salts have previously been structurally characterized by single-crystal X-ray diffraction. Crystal structures were reported for $ClF_2[BF_4]$ and $ClF_2[MF_6]$ (M = Nb, Ta, Ru, Os, As, Sb, Bi).[9,10,22–26] In the reported crystal structure of $ClF_2[OsF_6]$, a disordered ClF_2^+ cation was proposed, which prompted us to redetermine some of the reported crystal structures.

Accepted Manuscript

This article is protected by copyright. All rights reserved.

European Journal of Inorganic Chemistry 10.1002/ejic.202000845

WILEY-VCH

FULL PAPER

Here, we report on the syntheses of several ClF_2^+ compounds ($ClF_2[MF_6]$, M = Nb, Ta, Ru, Os, Ir, Sb, Bi; $ClF_2[Ta_2F_{11}]$; $ClF_2[AuF_4]$) and the determination of their crystal structures by single-crystal X-ray diffraction. Some of the crystal structures were redetermined with higher precision than before to see if the reported space groups or structural models were correct. For example, the previously reported crystal structure of $ClF_2[OsF_6]$ with a disordered ClF_2^+ cation seemed questionable. Furthermore, quantum-chemical calculations are presented for the solid-state crystal structures as well as for the corresponding free gas-phase fragments, $[ClF_2[MF_6]_2]^-$ (M = Nb, Ta, Ru, Os, Ir, As, Sb, Bi), $[ClF_2(HF)_2]^+$, $(ClF_2[Ta_2F_{11}])_2$, $(ClF_2[AuF_4])_2$, and $(ClF_2[BF_4])_2$, to elucidate the chemical bonding. The ClF_2^+ containing compounds reported here are enormously powerful oxidizers. One of the authors (KOC) has demonstrated in classified unpublished work at Rocketdyne the potential of ClF_2^+ salts as an incendiary for Diesel fuel.

Results and Discussion

Synthesis of difluorochloronium(III) compounds

Difluorochloronium(III) compounds were synthesized by either reacting metal powders (Ru, Os, Ir, Au), (**Caution!** ***The reactions of metal powders with ClF_3 are highly exothermic and can result in explosions when scaled up)***, metal fluorides (NbF_5, BiF_5, SbF_3) or a chloride ($TaCl_5$) with an excess of liquid chlorine trifluoride. The reactions can be described by the following idealized Equations 3 to 8. The compounds were isolated in crystalline form from the respective solutions or suspensions by slow removal of excess ClF_3 in vacuo. The crystal structures were subsequently determined by single-crystal X-ray diffraction.

The transition metals Ru, Os and Ir react with ClF_3 at room temperature and are oxidized to the +V oxidation state, giving $ClF_2[MF_6]$ (Equation 4).

Gold also reacts with ClF_3 at room temperature and is oxidized to the +III oxidation state, yielding $ClF_2[AuF_4]$ (Equation 5).

Reactions of metals with ClF_3:

$$2\,M + 7\,ClF_3 \longrightarrow 2\,ClF_2[MF_6] + 5\,ClF \quad (4)$$

M = Ru, Os, Ir

$$2\,Au + 5\,ClF_3 \longrightarrow 2\,ClF_2[AuF_4] + 3\,ClF \quad (5)$$

The reactions of the fluorides NbF_5 and BiF_5 with ClF_3 lead directly to the formation of the $ClF_2[MF_6]$ compounds (Equation 6). When SbF_3 is reacted with ClF_3, $ClF_2[SbF_6]$ is formed in a vigorous and strongly exothermic reaction (Equation 7).

Reactions of fluorides with ClF_3:

$$MF_5 + ClF_3 \longrightarrow ClF_2[MF_6] \quad (6)$$

M = Nb, Bi

$$SbF_3 + 2\,ClF_3 \longrightarrow ClF_2[SbF_6] + ClF \quad (7)$$

From the reaction of $TaCl_5$ with ClF_3 both $ClF_2[TaF_6]$ and $ClF_2[Ta_2F_{11}]$ could be obtained (Equation 8 and 9).

Reactions of chlorides with ClF_3:

$$TaCl_5 + 6\,ClF_3 \longrightarrow ClF_2[TaF_6] + 10\,ClF \quad (8)$$

$$2\,TaCl_5 + 11\,ClF_3 \longrightarrow ClF_2[Ta_2F_{11}] + 20\,ClF \quad (9)$$

Idealized equations are given for all the reactions as for simplicity the exclusive formation of ClF was assumed. The formation of Cl_2 is also possible, as ClF can also act as an oxidizer and fluorinating agent.[27] Any formed Cl_2 might react with excess ClF_3 to give ClF, although the reaction is slow, even at elevated temperature and pressure.[28–30]

Table 1. Selected crystallographic data and details of the structure determinations of difluorochloronium(III) hexafluoridometallates(V).

	$ClF_2[IrF_6]$	$ClF_2[SbF_6]$	$ClF_2[BiF_6]$	$ClF_2[NbF_6]$	$ClF_2[TaF_6]$
Formula	$ClIrF_8$	$ClSbF_8$	$ClBiF_8$	$ClNbF_8$	$ClTaF_8$
Molar mass / g·mol^{-1}	379.66	309.20	455.97	280.35	368.39
Space group (No.)	$P12/n1$ (13)	$P\bar{1}$ (2)	$P\bar{1}$ (2)	$Pcca$ (54)	$Pcca$ (54)
a / Å	6.832(2)	5.1571(5)	5.1564(4)	9.9239(4)	9.9577(6)
b / Å	5.5944(16)	5.5369(5)	5.6670(4)	5.7712(3)	5.7530(3)
c / Å	7.571(2)	10.4111(10)	10.5324(8)	10.4941(4)	10.5389(6)
α / °	90	91.576(8)	91.285(2)	90	90
β / °	94.450(4)	93.507(8)	94.197(2)	90	90
γ / °	90	91.386(7)	92.093(2)	90	90
V / Å^3	288.50(14)	296.51(5)	306.64(4)	601.03(5)	603.74(6)
Z	2	2	2	4	4
Pearson symbol	$mP20$	$aP20$	$aP20$	$oP40$	$oP40$
$\rho_{calc.}$ / g·cm^{-3}	4.370	3.463	4.294	3.10	4.053
μ / mm^{-1}	23.703	5.200	29.278	2.5 42	18.743
Color	yellow	colorless	colorless	colorless	colorless
Crystal morphology	prism	block	block	block	block
Crystal size / mm^3	0.084×0.109×0.166	0.072×0.075×0.092	0.077×0.082×0.198	0.059×0.126×0.135	0.117×0.131×0.206
T / K	100	100	100	100	100
λ / Å	0.71073 (Mo K_α)	0.71073 (Mo K_α)	0.71073 (Mo K_α)	0.71073 (Mo K_α)	0.71073 (Mo K_α)

This article is protected by copyright. All rights reserved.

Accepted Manuscript

European Journal of Inorganic Chemistry 10.1002/ejic.202000845

WILEY-VCH

FULL PAPER

No. of reflections	6587	6712	22457	32885	9729
θ range / °	3.64 to 30.54	3.682 to 32.178	3.599 to 32.691	3.530 to 35.052°	3.541 to 35.027
Range of Miller indices	$-9 \le h \le 9$	$-7 \le h \le 7$	$-7 \le h \le 7$	$-16 \le h \le 16$	$-16 \le h \le 14$
	$-7 \le k \le 7$	$-8 \le k \le 8$	$-8 \le k \le 8$	$-9 \le k \le 9$	$-9 \le k \le 9$
	$-10 \le l \le 10$	$-15 \le l \le 15$	$-15 \le l \le 15$	$-16 \le l \le 16$	$-17 \le l \le 17$
Absorption correction	multi-scan	integration	multi-scan	multi-scan	multi-scan
$Trans._{max}$, $Trans._{min}$	0.24, 0.12	0.706, 0.646	0.143, 0.033	0.791, 0.721	0.213, 0.097
R_{int}, R_{σ}	0.0281, 0.0084	0.0532, 0.0558	0.0246, 0.0350	0.0269, 0.0084	0.0335, 0.0198
Completeness of the data set	0.998	0.989	0.999	0.998	0.999
No. of unique reflections	877	3930	2704	1335	1337
No. of parameters	47	96	94	48	48
No. of restrains	0	0	0	0	0
No. of constrains	0	0	0	0	0
S (all data)	1.255	0.935	1.059	1.255	1.243
$R(F)$ ($I \ge 2\sigma(I)$, all data)	0.0168, 0.0169	0.0363, 0.0542	0.0233, 0.0405	0.0158, 0.0181	0.0199, 0.0237
$wR(F^2)$ ($I \ge 2\sigma(I)$, all data)	0.0434, 0.0434	0.0880, 0.0936	0.0442, 0.0486	0.0360, 0.0367	0.0443, 0.0458
Extinction coefficient	not refined	not refined	not refined	0.0045(5)	0.0065(4)
$\Delta\rho_{max}$, $\Delta\rho_{min}$ / e·Å^{-3}	1.375, −1.710	1.853, −2.120	1.617, −1.943	0.473, −0.438	2.258, −1.658

A short introduction to the symmetry of polymeric chainlike molecules

In all the studied difluorochloronium(III) compounds, the ClF_2^+ cations are associated with the anions resulting in dimeric or polymeric molecules. For the crystallographer these would be one-dimensional infinite strands, however, for reasons that will become clear below, we will use here terms common in polymer chemistry. Some of the polymeric molecules adopt helical configurations. That means there is a *polymer main chain* consisting of atoms held together by a continuous sequence of covalent bonds or similar atomic contacts. The atoms of the main chain are situated on imagined interleaving spirals, one spiral for each kind of atoms. Each spiral is a continuous line that winds at a constant distance around a straight line, the *spiral axis*. The helix consists of *chemically* equivalent *repeating units*. In polymer chemistry, according to the *equivalence postulate*, it is assumed that the repeating units can be treated as if they were symmetry equivalent, even if this is only approximately true.[31,32]

The chemical configuration of a helical molecule is specified as an N/r helix. N is the number of repeating units per translation period, and r is the number of the corresponding coil turns (360° turns). N and r are positive integers without a common divisor. An additional letter P or M indicates whether the spiral is right- or left-handed.

The term *molecular symmetry* usually refers to the symmetry of an isolated non-polymeric or polymeric molecule, meaning that the influence of any surroundings of the molecule is neglected. The molecular symmetry of a chainlike polymeric molecule that has translational symmetry in only one unique direction is designated by a *rod group*.[33] It is specified in the same way as a space group by its Hermann-Mauguin symbol, but beginning with a script style $\mathcal{P}$ and referring to c as the unique direction. Crystallographic rod groups have been compiled in the *International Tables for Crystallography*, Volume E.[33] They contain rotation or screw axes of the orders 1, 2, 3, 4, and 6. However, in a rod group the order of a symmetry axis that points in the unique direction is not restricted to these numbers. Being defined differently, the handedness of the chemical helix and of the corresponding screw axis can be opposite; for example, a chemically left-handed $3/2M$ helix has a right-handed 3_1 screw axis. For more details concerning the symmetry of helical molecules see the literature.[34]

The symmetry of a molecule in a crystal must conform to the crystal symmetry. For a non-polymeric molecule that is the site symmetry (point group) of its Wyckoff position. For a chainlike polymeric molecule it is its rod-site symmetry, called *penetration rod group*.[33] The site symmetry or the penetration rod group is a common subgroup of the space group and of the point group or rod group of the molecular symmetry, respectively.

The crystal structures of difluorochloronium(III) compounds

The crystal structure of $ClF_2[IrF_6]$

Difluorochloronium(III) hexafluoridoiridate(V) crystallizes in the monoclinic space group $P12/n1$ (No. 13) with two formula units per unit cell, Pearson code $mP20$ and Wyckoff sequence $13.g^4fe$. See

Table 1 for selected crystallographic data and details of the structure determination. Atomic coordinates, equivalent isotropic and anisotropic displacement parameters are reported in the Supporting Information.

The Cl atom occupies the Wyckoff position $2f$ (site symmetry 2) and is surrounded by the fluorine atoms F(1) and F(1)#1, forming the ClF_2^+ cation, see Figure 1. The Cl−F bond length is 1.573(3) Å and the F(1)−Cl(1)−F(1)#1 angle is 97.1(2)°. The Ir atom occupies the $2e$ position (site symmetry 2) and is surrounded by the fluorine atoms F(2) to F(4) and F(2)#2 to F(4)#2 in the shape of a distorted octahedron. The Ir−F bond lengths are 1.860(3)-1.913(3) Å. For comparison, the Ir−F bond length in $Li[IrF_6]$ is 1.879(5) Å at 299 K.[35] The Ir(1)−F(2) bond length of 1.913(3) Å is significantly longer than the other Ir−F bond lengths, due to a close contact of 2.300(3) Å to the Cl atom. The corresponding F(2)···Cl(1)···F(2)#1 angle is 90.38(14)°. The chlorine atom is thus surrounded by four fluorine atoms in a planar-quadrangular fashion (the distance of Cl(1) from the least-squares plane of the surrounding F atoms is 0 Å, due to symmetry).

This article is protected by copyright. All rights reserved.

Accepted Manuscript

European Journal of Inorganic Chemistry 10.1002/ejic.202000845

WILEY-VCH

FULL PAPER

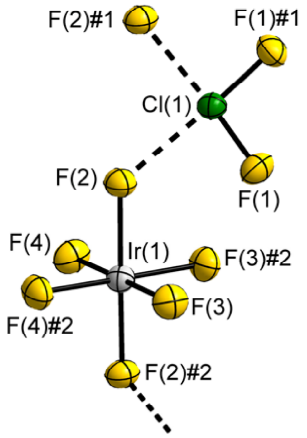

Figure 1. Section of the crystal structure of $ClF_2[IrF_6]$ showing the coordination sphere of the Cl and Ir atoms. Close contacts of F atoms to neighboring Cl atoms are shown as dashed bonds. Symmetry transformations: #1 1/2 − *x*, *y*, 3/2 − *z*, #2 3/2 − *x*, *y*, 3/2 − *z*. The displacement ellipsoids are shown at the 70% probability level at 100 K.

When these close Ir−F···Cl contacts are taken into account, a chain along the *a* axis with *trans*-bridging $[IrF_6]^-$ anions results, see Figure 2. The resulting chain has the rod group symmetry $p211$.[33] The Cl and Ir atoms each form a pseudo cubic primitive lattice. The Cl atoms are thus surrounded by eight Ir atoms in the shape of a distorted cube when Cl−Ir distances of approximately 3.8-5.2 Å are considered, and vice versa for the Ir atoms. The Cl and Ir atoms are hence similarly arranged as the Cs and Cl atoms in the CsCl structure type.[36]

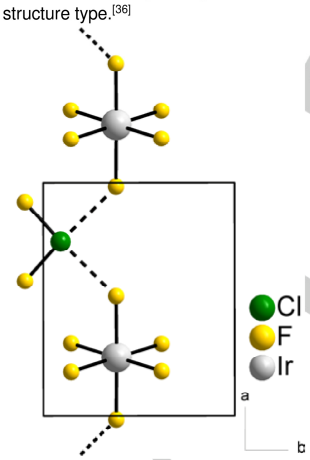

Figure 2. Crystal structure of $ClF_2[IrF_6]$ projected along the *c* axis. Close contacts of F atoms to neighboring Cl atoms are shown as dashed bonds. Atoms are shown with arbitrary radii.

The crystal structures of $ClF_2[SbF_6]$ and $ClF_2[BiF_6]$

The crystal structures of the isotypic salts difluorochloronium(III) hexafluoridoantimonate(V) and difluorochloronium(III) hexafluoridobismuthate(V) have been described previously.[10,25] The crystal structures were redetermined with higher precision of lattice parameters, atomic coordinates, bond lengths and angles. The space group was confirmed to be $P\bar{1}$ (No. 2). They crystallize with two formula units per unit cell, Pearson code *aP*20 and Wyckoff sequence $2.^{g}he$. See Table 1 for selected crystallographic data and details of the structure determination. Atomic coordinates, equivalent isotropic and anisotropic displacement parameters, as well as a comparison with previously reported interatomic distances are given in the Supporting Information.

The chlorine atom occupies the Wyckoff position 2*i* (site symmetry 1) and is surrounded by the fluorine atoms F(1) and F(2), see Figure 3. The Cl−F bond lengths are 1.555(4) and 1.560(4) Å in $ClF_2[SbF_6]$ and 1.568(3) and 1.573(3) Å in $ClF_2[BiF_6]$, respectively. The F(1)−Cl(1)−F(2) angle is 97.0(2)° in the Sb and 95.9(2)° in the Bi compound. There are two symmetry-independent *M* (*M* = Sb, Bi) atoms in the unit cell: *M*(1) on position 1*h* and *M*(2) on position 1*e* (both site symmetries $\bar{1}$).

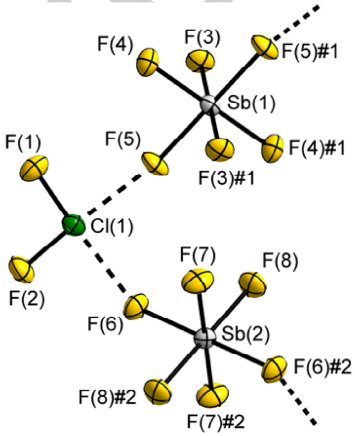

Figure 3. Section of the crystal structure of $ClF_2[SbF_6]$ showing the coordination sphere of the Cl and Sb atoms. Close contacts of F atoms to neighboring Cl atoms are shown as dashed bonds. Symmetry transformations: #1 1 − *x*, 1 − *y*, 1 − *z*, #2 1 − *x*, 1 − *y*, 2 − *z*. The displacement ellipsoids are shown at the 70% probability level at 100 K. $ClF_2[BiF_6]$ is isotypic with $ClF_2[SbF_6]$.

The *M*(1) atom is surrounded by the fluorine atoms F(3) to F(5) and F(3)#1 to F(5)#1 in the shape of a slightly distorted octahedron. The *M*(2) atom is surrounded similarly by the fluorine atoms F(6) to F(8) and F(6)#2 to F(8)#2. The Sb−F bond lengths lie in the range of 1.862(3)-1.901(3) Å and the Bi−F bond lengths in the range of 1.956(3)-2.026(3) Å. By comparison, in $Li[SbF_6]$ the Sb−F bond length is 1.877(6) Å at room temperature and in $Ag[BiF_6]_2$ the Bi−F bond lengths lie in the range of 1.939(10)-2.048(9) Å at 298 K.[37,38] The crystal structures of other $A^{I}[BiF_6]$ salts are of insufficient quality to allow for proper comparison.

The fluorine atoms F(5) and F(6) of the $[MF_6]^-$ anions show short contacts to the chlorine atoms of 2.312(4) and 2.302(4) Å in the Sb and 2.252(3) and 2.254(3) Å in the Bi compound. The chlorine atom is surrounded by four fluorine atoms in a planar-quadrangular fashion (the distance of Cl(1) from the least-squares plane of the surrounding F atoms is 0.003(2) Å for $ClF_2[SbF_6]$ and 0.001(2) Å for $ClF_2[BiF_6]$). The resulting F(5)···Cl(1)···F(6) angle is 90.66(14)° in $ClF_2[SbF_6]$ and 90.88(12)° in $ClF_2[BiF_6]$.

When the short *M*−F···Cl contacts are taken into account, a zig-zag chain with *trans*-bridging $[MF_6]^-$ anions along the *c* axis results, see Figure 4. The zig-zag chains have the rod group symmetry $p\bar{1}$.[33] The Cl and *M* atoms each form a pseudo cubic

This article is protected by copyright. All rights reserved.

Accepted Manuscript

European Journal of Inorganic Chemistry 10.1002/ejic.202000845

WILEY-VCH

FULL PAPER

primitive lattice. The Cl atoms are thus surrounded by eight *M* atoms in the shape of a distorted cube when Cl−*M* distances of approximately 3.9-5.2 Å are considered, and vice versa for *M*. The Cl and *M* atoms are consequently similarly arranged as the Cs and Cl atoms in the CsCl structure type.[36]

Table 2. Selected crystallographic data and details of the structure determinations of difluorochloronium(III) fluoridometallates.

	$ClF_2[OsF_6]$	$ClF_2[RuF_6]$	$ClF_2[Ta_2F_{11}]$	$ClF_2[AuF_4]$
Formula	$ClOsF_8$	$ClRuF_8$	$ClF_{13}Ta_2$	$ClAuF_6$
Molar mass / g·mol^{-1}	377.67	288.51	644.35	346.41
Space group (No.)	*P*2/*c* (13)	*Pcca* (54)	$P12_1/n1$ (14)	$P12_1/n1$ (14)
a / Å	15.584(2)	19.708(2)	7.6576(3)	4.4720(13)
b / Å	5.6370(9)	5.6153(6)	9.1844(4)	7.331(2)
c / Å	10.5162(16)	10.5024(12)	14.1108(6)	14.894(4)
α / °	90	90	90	90
β / °	107.903(2)	90	92.120(2)	97.580(5)
γ / °	90	90	90	90
V / Å^3	879.1(2)	1162.3(2)	991.74(7)	484.0(2)
Z	6	8	4	4
Pearson symbol	*mP*60	*oP*80	*mP*64	*mP*32
$\rho_{calc.}$ / g·cm^{-3}	4.280	3.298	4.316	4.754
μ / mm^{-1}	22.312	3.256	22.485	30.979
Color	colorless	pale green	colorless	pale yellow
Crystal morphology	prism	prism	block	prism
Crystal size / mm^3	0.223×0.290×0.310	0.080×0.100×0.150	0.093×0.096×0.139	0.010×0.030×0.180
T / K	100	143	100	100
λ / Å	0.71073 (Mo-K$_\alpha$)	0.71073 (Mo-K$_\alpha$)	0.71073 (Mo-K$_\alpha$)	0.71073 (Mo-K$_\alpha$)
No. of reflections	19970	14370	28468	11122
θ range / °	1.37 to 30.49	2.07 to 27.55°	2.647 to 35.035	3.10 to 30.58
Range of Miller indices	$-14 \le h \le 14$	$-6 \le h \le 7$	$-12 \le h \le 12$	$-6 \le h \le 6$
	$-8 \le k \le 8$	$-13 \le k \le 13$	$-14 \le k \le 14$	$-10 \le k \le 10$
	$-20 \le l \le 20$	$-25 \le l \le 25$	$-22 \le l \le 22$	$-21 \le l \le 20$
Absorption correction	multi-scan	multi-scan	multi-scan	multi-scan
$Trans._{max}$, $Trans._{min}$	0.08, 0.06	0.78, 0.67	0.249, 0.135	0.75, 0.22
R_{int}, R_σ	0.0694, 0.0368	0.0246, 0.0147	0.0229, 0.0343	0.0625, 0.0432
Completeness of the data set	0.973	0.994	0.999	0.994
No. of unique reflections	2607	1339	4378	1482
No. of parameters	138	92	146	73
No. of restrains	0	0	0	0
No. of constrains	0	0	0	0
S (all data)	1.082	1.159	1.158	1.075
$R(F)$ ($I \ge 2\sigma(I)$, all data)	0.0423, 0.0483	0.0174, 0.0200	0.0184, 0.0228	0.0261, 0.0342
$wR(F^2)$ ($I \ge 2\sigma(I)$, all data)	0.1177, 0.1237	0.0435, 0.0444	0.0318, 0.0326	0.0632, 0.0658
Extinction coefficient	0.0016(3)	not refined	0.00207(5)	not refined
$\Delta\rho_{max}$, $\Delta\rho_{min}$ / e·Å^{-3}	3.641, −3.971	0.317, −0.546	1.156, −1.594	1.884, −1.372

WILEY-VCH Accepted Manuscript

This article is protected by copyright. All rights reserved.

European Journal of Inorganic Chemistry 10.1002/ejic.202000845

WILEY-VCH

FULL PAPER

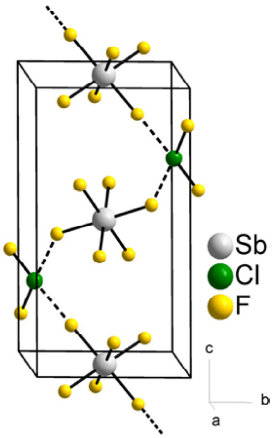

Figure 4. Crystal structure of $ClF_2[SbF_6]$. Close contacts of F atoms to neighboring Cl atoms are shown as dashed bonds. Atoms are shown with arbitrary radii. $ClF_2[BiF_6]$ is isotypic to $ClF_2[SbF_6]$.

The crystal structures of $ClF_2[NbF_6]$ and $ClF_2[TaF_6]$

The crystal structures of the isotypic salts difluorochloronium(III) hexafluoridoniobate(V) and difluorochloronium(III) hexafluoridotantalate(V) have been described previously.[23] The crystal structures were redetermined with higher precision of lattice parameters, atomic coordinates, bond lengths and angles. The space groups were confirmed to be *Pcca* (No. 54). They crystallize with four formula units per unit cell, Pearson symbol *oP*40 and Wyckoff sequence 54.f^4de. See Table 1 for selected crystallographic data and details of the structure determination. Atom coordinates, equivalent isotropic displacement parameters, anisotropic displacement parameters and a comparison with previously reported interatomic distances are given in the Supporting Information.

The chlorine atom occupies the Wyckoff position 4*d* (site symmetry 2) and is surrounded by the fluorine atom F(1) and a symmetry-generated F(1)#1 atom, forming the ClF_2^+ cation, see Figure 5. In $ClF_2[NbF_6]$, the Cl−F bond length is 1.571(1) Å and the F(1)−Cl(1)−F(1)#1 angle is 96.00(6)°. In $ClF_2[TaF_6]$, the respective values are 1.568(2) Å and 96.45(15)°. The *M* (*M* = Nb, Ta) atom occupies the 4*c* position (site symmetry 2) and is surrounded by six fluorine atoms, F(2) to F(4) and F(2)#2 to F(4)#2, in the shape of a distorted octahedron. The Nb−F bond lengths are 1.850(1)-1.949(1) Å and the Ta−F bond lengths are 1.862(2)-1.945(2) Å. In comparison, in the Li[*M*F$_6$] salts the Nb−F distance is 1.863(3) Å and the Ta−F distance is 1.859(4) Å at 299 K.[35]

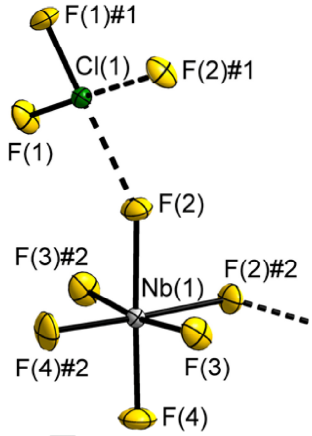

Figure 5. Section of the crystal structure of $ClF_2[NbF_6]$ showing the coordination sphere of the Cl and Nb atoms. Close contacts of F atoms to neighboring Cl atoms are shown as dashed bonds. Symmetry transformations: #1 1/2 − *x*, −*y*, *z*, #2 1 − *x*, *y*, 1/2 − *z*. The displacement ellipsoids are shown at the 70% probability level at 100 K. $ClF_2[TaF_6]$ is isotypic with $ClF_2[NbF_6]$.

The fluorine atoms of the $[MF_6]^-$ anion (*M* = Nb, Ta), F(2) and F(2)#2, are *cis*-bridging to the Cl atoms with a distance of 2.234(1) Å and an angle F(2)···Cl(1)···F(2)#2 of 93.62(4)°. In the Ta compound the corresponding values are 2.252(2) Å and 93.47(10)°. This leads to significantly longer Nb(1)−F(2) and Ta(1)−F(2) bond lengths in comparison to the *M*−F bond lengths of non-bridging F atoms. The chlorine atom is thus surrounded by four fluorine atoms in a planar-quadrangular fashion (the distance of Cl(1) from the least-squares plane of the surrounding F atoms is 0 Å for both compounds, due to symmetry).

When the short *M*−F···Cl contacts are taken into account, a helix with a translation period of *a* (9.9239(4) Å for Nb and 9.9577(6) Å for Ta) along the *a* axis results, see Figure 6. This helix can be described as a 2/1 helix with the rod group symmetry $\not{p}222_1$ (or $\not{p}_a2_122$ if *a* is taken as the unique rod group direction).[33] The isolated helix is chiral, but due to the symmetry of the space group, both *M* and *P* helices are present. The Cl and *M* (*M* = Nb, Ta) atoms each form a pseudo cubic primitive lattice. The Cl atoms are thus surrounded by eight *M* atoms in the shape of a distorted cube when Cl−*M* distances of approximately 4.1-5.2 Å are considered, and vice versa for *M* atoms. The Cl and *M* atoms are hence similarly arranged to the Cs and Cl atoms in the CsCl structure type.[36]

Accepted Manuscript

This article is protected by copyright. All rights reserved.

European Journal of Inorganic Chemistry 10.1002/ejic.202000845

WILEY-VCH

FULL PAPER

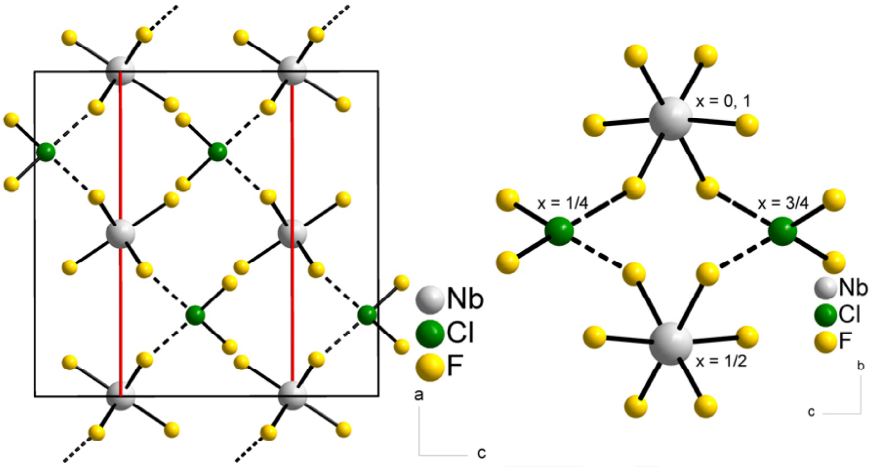

Figure 6. Left: Section of the crystal structure of $ClF_2[NbF_6]$. The red lines indicate the spiral axes running along the 2_1 axes of the space group *Pcca* at *x*,0,1/4 (*P* helix) and *x*,1,3/4 (*M* helix). Right: Projection of one *P* helix along its spiral axis parallel to the *a* axis. The *x* coordinates of the Cl and Nb atoms indicate the heights within the unit cell. Close contacts of F atoms to neighboring Cl atoms are shown as dashed bonds. Atoms are shown with arbitrary radii. $ClF_2[TaF_6]$ is isotypic to $ClF_2[NbF_6]$.

The crystal structure of $ClF_2[OsF_6]$

The reported crystal structure of $ClF_2[OsF_6]$ in the triclinic space group $P\bar{1}$ is questionable.[26] The authors first attempted the solution and refinement in the monoclinic space group *P*2/*m*, but then chose the space group $P\bar{1}$ instead, due to lower *R* values of the structural model. In the published structure, the ClF_2^+ ion is disordered, resulting in a too short Cl−F bond length of 1.38(7) Å. We observed that difluorochloronium(III) hexafluoridoosmate(V) crystallizes in the monoclinic space group *P*2/*c* (No. 13) with six formula units per unit cell, Pearson code *mP*60 and Wyckoff sequence 13.$g^{14}fe$. See Table 2 for selected crystallographic data and details of the structure determination. Atomic coordinates, equivalent isotropic and anisotropic displacement parameters are reported in the Supporting Information.

There are two different kinds of chlorine atoms: Cl(1), Wyckoff position 2*e* (site symmetry 2) and Cl(2), position 4*g* (site symmetry 1), see Figure 7. The atom Cl(1) is surrounded by the fluorine atom F(1) and the symmetry-equivalent F(1)#1 atom with a Cl−F bond length of 1.567(5) Å and an F(1)−Cl(1)−F(1)#1 angle of 97.5(4)°. The atom Cl(2) is surrounded by the two fluorine atoms F(2) and F(3). The bond lengths are 1.572(5) and 1.576(5) Å and the F(2)−Cl(1)−F(3) angle is 97.0(3)°. The shapes of the two ClF_2^+ cations are equal within the tripled standard uncertainties.

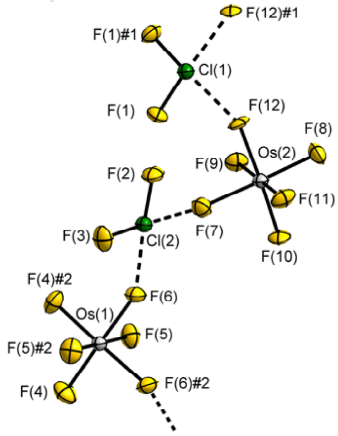

Figure 7. Section of the crystal structure of $ClF_2[OsF_6]$ showing the coordination sphere of the Cl and Os atoms. Close contacts of F atoms to neighboring Cl atoms are shown as dashed bonds. Symmetry transformations: #1 2 − *x*, *y*, 3/2 − *z*, #2 1 − *x*, *y*, 3/2 − *z*. The displacement ellipsoids are shown at the 70% probability level at 100 K.

The atom Os(1) occupies the 2*f* position (site symmetry 2) and is surrounded by six fluorine atoms, F(4) to F(6) and F(4)#2 to F(6)#2 in the shape of a distorted octahedron. The atom Os(2) occupies the 4*g* position (site symmetry 1) and is surrounded by the six fluorine atoms F(7) to F(12) in the shape of a distorted octahedron. The Os−F bond lengths in the $[Os(1)F_6]^-$ anion are 1.854(4)-1.910(4) Å and 1.852(4)-1.919(4) Å in the $[Os(2)F_6]^-$ anion. For comparison, the Os−F bond length in $Li[OsF_6]$ is 1.872(7) Å at 299 K.[35] In the previously reported crystal structure, the Os−F bond length was reported to be 1.84(3) Å.[26]

The Os(1)−F(6), Os(2)−F(7) and Os(2)−F(12) bond lengths are significantly longer than the other Os−F bond lengths, due to short contacts of the form Os−F···Cl to the ClF_2^+ cations. These contacts are 2.288(4) Å for Cl(1)···F(12), 2.260(5) Å for Cl(2)···F(6) and 2.269(5) Å for Cl(2)···F(7). The chlorine atoms are

This article is protected by copyright. All rights reserved.

Accepted Manuscript

European Journal of Inorganic Chemistry 10.1002/ejic.202000845

WILEY-VCH

FULL PAPER

thus surrounded by four fluorine atoms in a planar-quadrangular fashion (the distances of the Cl atoms from the least-squares plane of the surrounding F atoms are 0 Å for Cl(1), due to symmetry, and 0.004(3) Å for Cl(2)). The angle F(12)···Cl(1)···F(12)#1 is 90.8(2)° and the F(6)···Cl(2)···F(7) is 90.0(2)°.

Severely deformed *M* and *P* 3/1 helices along the *a* axis with a translation period of *a* (15.584(2) Å) result when Os−F···Cl contacts are taken into account, see Figure 8.[34] Ideal 3/1 helices would have the rod group symmetries $\not{p}3_1 21$ and $\not{p}3_2 21$. As can be seen from the projection along the helix axis (right part of Figure 8), actually there exists no threefold screw axis and the rod group symmetry is only $\not{p}121$. The twofold rotation axes are perpendicular to the rod axis and run through the atoms Os(1) and Cl(1). The two kinds of chemical repeating units are not symmetry equivalent such that the equivalence postulate cannot be applied. The Cl and Os atoms each form a pseudo cubic primitive lattice. The Cl atoms are thus surrounded by eight Os atoms in the shape of a distorted cube when Cl−Os distances of approximately 3.8-5.2 Å are considered, and vice versa for Os. The Cl and Os atoms are consequently similarly arranged as the Cs and Cl atoms in the CsCl structure type.[36]

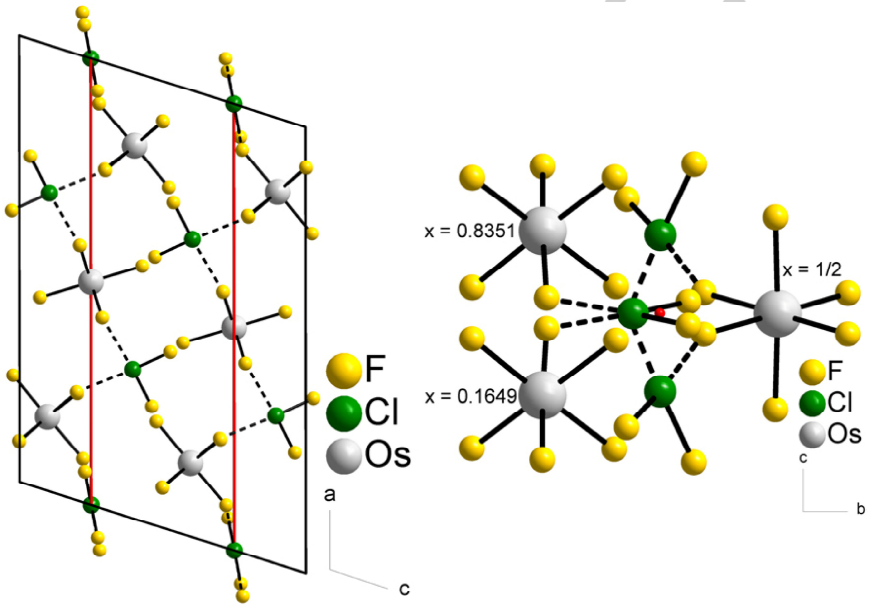

Figure 8. Left: Section of the crystal structure of $ClF_2[OsF_6]$. The red lines indicate the spiral axes of two helices running along *x*,1/2,1/4 (*M* helix) and *x*,1/2,3/4 (*P* helix). Right: Projection of one *P* helix along the *a* axis. For the sake of clarity, *x* coordinates indicating the height within the unit cell are only given for the Os atoms. Cl atoms are located at *x* = 0, 1/3, 2/3, 1. Close contacts of F atoms to neighboring Cl atoms are shown as dashed bonds. Atoms are shown with arbitrary radii.

The crystal structure of $ClF_2[RuF_6]$

The crystal structure of difluorochloronium(III) hexafluoridoruthenate(V) was redetermined.[24] The compound crystallizes in the orthorhombic space group *Pcca* (No. 54), Pearson code *oP*80 and Wyckoff sequence 54.f^3dc. See Table 2 for selected crystallographic data and details of the structure determination. Atomic coordinates, equivalent isotropic and anisotropic displacement parameters, as well as a comparison with previously reported interatomic distances are given in the Supporting Information.

There are two symmetry-independent kinds of chlorine atoms: Cl(1), Wyckoff position 4*d* and Cl(2), position 4*c* (both site symmetry 2), Figure 9. The atom Cl(1) is surrounded by the fluorine atom F(1) and the symmetry-equivalent F(1)#1 atom. The atom Cl(2) is surrounded by the atom F(2) and the symmetry-equivalent F(2)#2 atom. For the $Cl(1)F_2^+$ cation a Cl−F bond length of 1.565(2) Å and an F(1)−Cl(1)−F(1)#1 angle of 96.80(13)° are observed. For $Cl(2)F_2^+$ they are 1.568(1) Å and 96.29(11)°. The values of the two ClF_2^+ cations are equal within the tripled standard uncertainties.

This article is protected by copyright. All rights reserved.

Accepted Manuscript

European Journal of Inorganic Chemistry 10.1002/ejic.202000845

WILEY-VCH

FULL PAPER

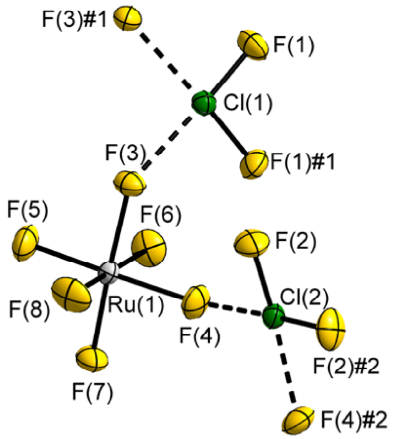

Figure 9. Section of the crystal structure of $ClF_2[RuF_6]$ showing the coordination sphere of the Cl and Ru atoms. Close contacts of F atoms to neighboring Cl atoms are shown as dashed bonds. Symmetry transformations: #1 1 − *x*, *y*, 3/2 − *z*, #2 1/2 − *x*, −*y*, *z*. The displacement ellipsoids are shown at the 70% probability level at 143 K.

The Ru atom occupies the 8*f* position (site symmetry 1) and is surrounded by six fluorine atoms, F(3)-F(8), in the shape of a distorted octahedron. The Ru−F bond lengths are 1.819(1)-1.896(1) Å. For comparison, in $Li[RuF_6]$ the Ru−F bond length is 1.851(8) Å at 299 K.[35]

The atoms F(3) and F(4) of the $[RuF_6]^-$ anion show close contacts to the Cl atoms of the ClF_2^+ cations and thus have significantly longer Ru−F bond lengths of 1.896(1) and 1.891(1) Å, respectively. The resulting Cl···F distances are: Cl(1)···F(3): 2.271(1) Å; Cl(2)···F(4): 2.248(2) Å. The chlorine atoms are thus surrounded by four fluorine atoms in a planar-quadrangular fashion (the distances of the Cl atoms from the least-squares plane of the surrounding F atoms are 0 Å for both Cl atoms, due to symmetry). The angle F(3)···Cl(1)···F(3)#1 of 89.92(8)° is significantly smaller than the F(4)···Cl(2)···F(4)#2 angle of 91.25(7)°. Taking into account the Ru−F···Cl contacts, both *M* and *P* 4/1 helices with a translation period of *a* (19.708(2) Å) along the *a* axis result, see Figure 10.[34] The ideal rod group symmetries of the helices are $\not{A}4_122$ and $\not{A}4_322$. The penetration rod group of the helices in the crystal structure is $\not{P}222_1$. The Cl and Ru atoms each form a pseudo cubic primitive lattice. The Cl atoms are thus surrounded by eight Ru atoms in the shape of a distorted cube when Cl−Ru distances of 3.8-5.2 Å are considered, and vice versa for Ru. The Cl and Ru atoms are hence arranged similar to the Cs and Cl atoms in the CsCl structure type.[36]

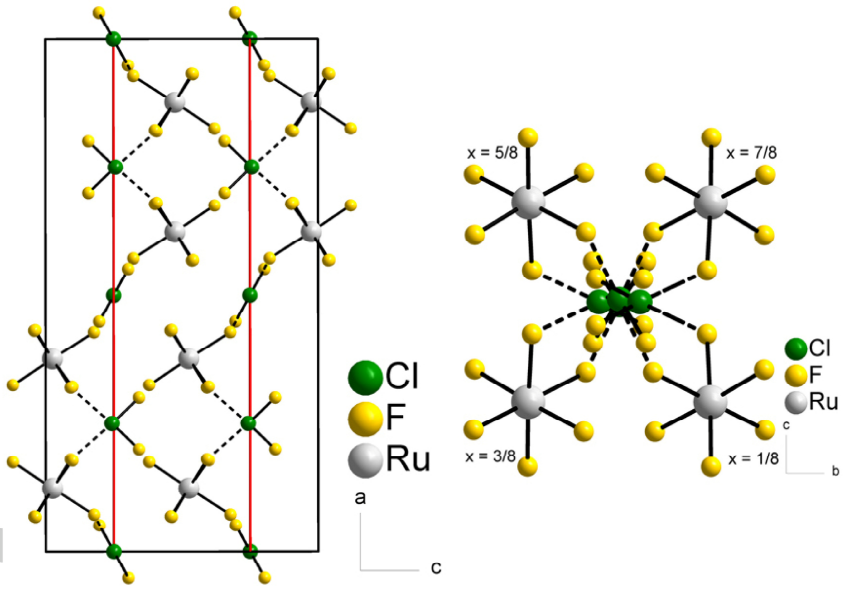

Figure 10. Left: Section of the crystal structure of $ClF_2[RuF_6]$. The red lines indicate two spiral axes of two helixes running along *x*,1,1/4 (*M* helix) and *x*,1,3/4 (*P* helix). Right: Projection of one *M* helix along the *a* axis. For the sake of clarity, idealized *x* coordinates indicating the heights within the unit cell are only given for the Ru atoms. Cl atoms are located at *x* = 0, 1/4, 1/2, 3/4, 1. Close contacts of F atoms to neighboring Cl atoms are shown as dashed bonds. Atoms are shown with arbitrary radii.

This article is protected by copyright. All rights reserved.

Accepted Manuscript

European Journal of Inorganic Chemistry 10.1002/ejic.202000845

WILEY-VCH

FULL PAPER

The crystal structure of $ClF_2[Ta_2F_{11}]$

Difluorochloronium(III) undecafluoridoditantalate(V) crystallizes in the monoclinic space group $P12_1/n1$ (No. 14), Pearson code $mP64$ and Wyckoff sequence $14.e^{16}$. See Table 2 for selected crystallographic data and details of the structure determination. Atomic coordinates, equivalent isotropic and anisotropic displacement parameters are reported in the Supporting Information.

The chlorine atom Cl(1) occupies the Wyckoff position 4*e* and is surrounded by the fluorine atoms F(1) and F(2) giving the ClF_2^+ cation (Figure 11). The Cl−F bonds lengths are 1.567(2) and 1.566(2) Å and the F(1)−Cl(1)−F(2) is 96.30(10)°. The two symmetry-independent Ta atoms, Ta(1) and Ta(2), both occupy the Wyckoff position 4*e*. The Ta(1) atom is surrounded by the terminal F atoms F(4) to F(8) and the Ta(2) atom by the atoms F(9) to F(13). The Ta−F bond lengths lie in the range of 1.835(2)-1.935(2) Å. The atom F(3) is μ-bridging between the two Ta atoms with bond lengths of 2.057(2) and 2.068(2) Å, giving the $[Ta_2F_{11}]^-$ anion, see Figure 11. The Ta−F bond lengths are comparable with the ones reported for $Cd[Ta_2F_{11}]_2$ of 1.821(4)-1.942(4) Å terminal F atoms and 2.056(4)-2.077(4) Å for μ-bridging F atoms.[39]

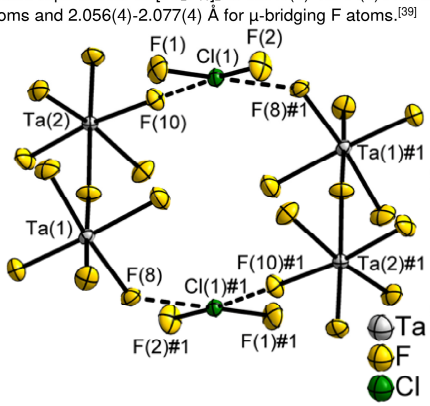

Figure 11. Molecular structure of the dimeric $ClF_2[Ta_2F_{11}]$. Symmetry transformation: #1 1 − *x*, 1 − *y*, 1 − *z*. The displacement ellipsoids are shown at the 70% probability level at 100 K. Close contacts of F atoms to neighboring Cl atoms are shown as dashed bonds. Atom labels are only given for certain atoms for the sake of clarity.

The atoms F(8) and F(10) of the $[Ta_2F_{11}]^-$ anion show close contacts to the Cl atom and thus the corresponding Ta−F bond lengths of 1.935(2) and 1.934(2) Å are significantly longer than the other bond lengths of terminal F atoms. The resulting Cl···F bond lengths are: Cl(1)···F(8): 2.292(2) Å and Cl(1)···F(10): 2.235(2) Å. The angle F(8)···Cl(1)···F(10) is 92.89(6)°. Consequently, the Cl(1) atom is surrounded by four fluorine atoms in an almost planar, quadrangular fashion (the distance of Cl(1) from the least-squares plane of the surrounding F atoms is 0.017(1) Å).

When the Ta−F···Cl contacts are considered, a dimer of the form $(ClF_2[Ta_2F_{11}])_2$ results, see Figure 11. Each of the dimers is surrounded by twelve further dimers in the shape of a cuboctahedron, when center-to-center distances of approximately 7.6-9.4 Å are considered.

The crystal structure of $ClF_2[AuF_4]$

Difluorochloronium(III) tetrafluoridoaurate(III) crystallizes in the monoclinic space group $P12_1/n1$ (No. 14) with four formula units per unit cell, Pearson code $mP32$ and Wyckoff sequence $14.e^8$. See Table 2 for selected crystallographic data and details of the structure determination. Atom coordinates, equivalent isotropic and anisotropic displacement parameters are reported in the Supporting Information. The chlorine atom occupies the Wyckoff position 4*e* (site symmetry 1) and is surrounded by the fluorine atoms F(1) and F(2), see Figure 12. The Cl−F bond lengths are 1.583(4) and 1.578(4) Å, respectively. The F(1)−Cl(1)−F(2) angle is 95.4(2)°.

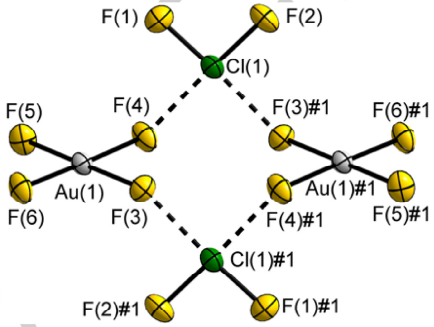

Figure 12. Molecular structure of the dimeric $ClF_2[AuF_4]$. Symmetry transformation: #1 −*x*, 1 − *y*, 1 − *z*. The displacement ellipsoids are shown at the 70% probability level at 100 K. Close contacts of F atoms to neighboring Cl atoms are shown as dashed bonds.

The gold atom occupies the position 4*e* and is surrounded by four fluorine atoms F(3)-F(6), giving the nearly square-planar $[AuF_4]^-$ anion (the distance of Au(1) from the least-squares plane of the surrounding F atoms is 0.015(2) Å). The Au−F bond lengths lie in the range of 1.903(4)-1.961(4) Å. For comparison, those in $Li[AuF_4]$ are 1.890(7)-1.965(6) Å at room temperature.[40]

The bond lengths Au(1)−F(3) and Au(1)−F(4) are significantly longer than the other two Au−F bond lengths, due to close contacts to the Cl atom. The fluorine atoms of the $[AuF_4]^-$ anions are cis-bridging and the Cl···F distances are 2.198(4) and 2.170(4) Å, respectively. The chlorine atom is thus surrounded by four fluorine atoms in an almost planar-quadrangular fashion (the distance of Cl(1) from the least-squares plane of the surrounding F atoms is 0.042(3) Å). The F(3)···Cl(1)···F(4) angle is 88.08(14)°. When these Au−F···Cl contacts are considered, a dimer of the form $(ClF_2[AuF_4])_2$ results, see Figure 12. Within this dimer, the $[AuF_4]^-$ units lie in a plane and the ClF_2^+ cations lie above and below this plane, leading to a "chair configuration" of the dimer. Each of the dimers is surrounded by eight further dimers in the shape of a hexagonal bipyramid, when center-to-center distances of approximately 4.5-8.3 Å are considered.

Quantum-chemical solid-state calculations

The crystal structures of all our ClF_2^+ compounds were investigated by quantum-chemical solid-state calculations using CRYSTAL17 (DFT-PBE0/TZVP level of theory).[41,42] The optimized structures are reported in the Supporting Information and a comparison of observed and calculated bond lengths, distances and angles are given in Tables 3-5.

The calculated Cl−F bond lengths are with approximately 1.60 Å quite similar to the experimentally determined values but are 2 to

This article is protected by copyright. All rights reserved.

Accepted Manuscript

European Journal of Inorganic Chemistry 10.1002/ejic.202000845

WILEY-VCH

FULL PAPER

4% longer. In contrast, the calculated Cl···F bridging distances are generally shorter and show a broad variation among the different compounds. The strength of the Cl−F bonds is thus somewhat underestimated by the used method and the strength of the Cl···F bridges is overestimated. The calculated F−Cl−F angles with circa 95.0° are also quite similar among all compounds and 1 to 8% smaller than the experimentally determined ones. The calculated F···Cl···F angles show a broad variation and usually are bigger than the observed ones. The calculated *M*−F bond lengths are longer than the experimentally determined ones and thus the interactions with the cations are in comparison underestimated.

To get a qualitative picture of the bonding in these compounds, the atomic partial charges and overlap populations between atoms were examined by Mulliken analysis. The average atomic partial charges are reported in the Supporting Information and the average overlap populations (AOP) are given in Table 6.

The most negatively charged F atoms are the μ-bridging F atoms of the fluoridometallate anions, followed by the non-bridging F atoms. This agrees nicely with the observed *M*−F bond lengths. The AOPs for the Cl−F bonds of ClF_2^+ are quite similar for all compounds and correlate well with the respective bond lengths. The AOPs for the Cl···F interactions are much smaller and support the assumption of a weak, mostly ionic interaction between Cl and the neighboring F atoms of the anions.

Overall, the anion has a minor impact on the calculated structural parameters of the ClF_2^+ cation, whereas the nature of the bridging *M*−F···Cl contacts depends much more on the anion.

Quantum-chemical modeling of the fluorine-bridging effect in the gas-phase

As has been previously shown in a detailed study of the closely related $ClF_4[SbF_6]$ salt, its anion-cation interactions strongly impact the structure.[43] Quantum-chemical modeling of this effect presented a major challenge. The assumption of simple ion pairs alters the nature of the fluorine bridges, and the modeling of infinite chains is computationally prohibitive. The use of trinuclear fragments with either ClF_4^+ or $[SbF_6]^-$ in the center results in incorrect overall charges, and chain termination becomes a major problem. The best approximation found for $ClF_4[SbF_6]$ was the use of ClF_4^+ capped by two neutral HF molecules with the Cl···F bridge bond length, observed in the crystal structure, used as the only constraint. This approach preserved the positive charge on ClF_4^+ and reduced the computational requirements.

In the present study, either trinuclear species with ClF_2^+ in the center of the form $[ClF_2[MF_6]_2]^-$ (*M* = Nb, Ta, Ru, Os, Ir, As, Sb, Bi) or dimers ($(ClF_2[Ta_2F_{11}])_2$, $(ClF_2[AuF_4])_2$, $(ClF_2[BF_4])_2$) were investigated by means of quantum-chemical gas-phase calculations with TURBOMOLE (DFT-PBE0/def2-TZVP level of theory).[44,45] The *xyz* coordinates of the optimized molecular structures, selected bond lengths, angles as well as partial atomic charges from a natural population analysis are reported in the Supporting Information.[46]

As can be seen from Table 8, the molecular structure of ClF_2^+ observed in the crystal structures is in excellent agreement with that predicted by high-level quantum chemical calculations at the CCSD(T) level for the free gaseous ion.[47] The DFT calculations for the solid salts are in fair agreement with the experimental crystallographic values but overestimate the Cl−F bond lengths and therefore underestimate the F−Cl−F bond angle. The DFT calculations for the gaseous state, using the trinuclear $[ClF_2[MF_6]_2]^-$ anion model, result in the same Cl−F bond length as the solid state calculations but show a further compression of the F−Cl−F bond angle. As for $ClF_4[SbF_6]$, the HF terminated ClF_2^+ model, $[ClF_2(HF)_2]^+$ gave the best results.

Atomic charges from natural population analyses show that the bridging F atoms of the fluoridometallate anions are usually the most negatively charged ones. They are followed by the non-bridging F atoms and the F atoms of the ClF_2^+ cation. The latter ones are the least negatively charged ones and the values are similar among the different bonding models, indicating only minor effects of the anions.

Bonding in the ClF_2^+ cation

Halogen fluorides offer a golden opportunity to study the influence of oxidation state, coordination number and sterically active free valence electron pairs on the structure and bonding.[4] Their oxidation states range from +1 to +7, they are amphoteric, capable of forming cations and anions, and in most cases possess sterically active free valence electron pairs and hyper valency. The only exceptions are ClF and ClF_2^+ which are not hypervalent, ClF_6^+ which does not possess a free valence electron pair, and $[ClF_6]^-$ which has a free valence electron pair, but which is sterically inactive.[48,49]

The underlying structural principles are rather simple.[4] When the Cl atom has a free valence electron pair, it seeks maximal *s* character to stay as close as possible to the nucleus. If the coordination number exceeds four, so many Cl−F bonds will form semi-ionic, three-center four-electron bonds, until the free pair can participate in a more desirable sp^n hybrid orbital. As a result, chlorine fluorides can possess two different kinds of Cl−F bonds, shorter, strong, mainly covalent bonds and longer, weaker, semi-ionic, 3c-4e bonds.

As already mentioned above, ClF_2^+ has two free valence electron pairs and is not hypervalent. Therefore, it can easily form an sp^3 hybrid orbital involving the two strong Cl−F bonds and the two free valence electron pairs, resulting in a pseudo-tetrahedral structure. The coordination sphere around the Cl atom is extended by two more, highly ionic fluorine bridges from neighboring anions. These fluorine bridges avoid the free valence electron pairs of the Cl atom and approach it in the ClF_2 plane, resulting in a total coordination number of six. It must be pointed out, however, that the two free valence electron pairs do not occupy the linear axial positions of an AX_4E_2-type VSEPR octahedron, as is present for example in $[ClF_4]^-$, but are strongly bent because they are part of the underlying AX_2E_2 pseudo-tetrahedron.[4,50]

Evidence for electron localization can be obtained computationally using, for example, the ELF (electron-localization function), the HELP (the High Electron Localization domain Population), or the MESP (molecular electrostatic potential) to "observe" increased electron density in the corresponding electron density basins.[51–53] HELP is a theoretically well defined (but non unique) qualitative measure of the number of localized and delocalized electrons in a region of space.[51,53] The ELF approach was chosen in our case for ClF_2^+ in the gaseous trinuclear $[ClF_2[SbF_6]_2]^-$ anion (Figure 13) and shows increased electron density in the basins attributed to the free valence electron pairs. [54,55] The ELF also shows the differences between the strong, polar covalent Cl−F bonds within the ClF_2^+ cation and the weak, highly ionic Cl···F bridge bonds.

Two attractors, that is maxima of ELF, which are located above and below the ClF_2^+ plane, are found, which correspond to the two lone pairs of the Cl(III) atom in the Lewis picture. These lone pair

This article is protected by copyright. All rights reserved.

Accepted Manuscript

European Journal of Inorganic Chemistry 10.1002/ejic.202000845

WILEY-VCH

FULL PAPER

domains were further analyzed by intra-basin partitioning of ELF (HELP and the High Electron Localization domain Volume (HELV)), see Table 7.[51] Among the investigated species the HELP values are similar with approximately 1.50 *e* per domain and the corresponding volumes of the localized electrons are circa 16 Bohr^3, which indicates that the different anions have minor effects on the lone pairs of the Cl(III) atom. For comparison, the values around 1.5 electrons are close to the value obtained for PH_3, lower than that of NH_3, and larger than that of AsH_3.[53]

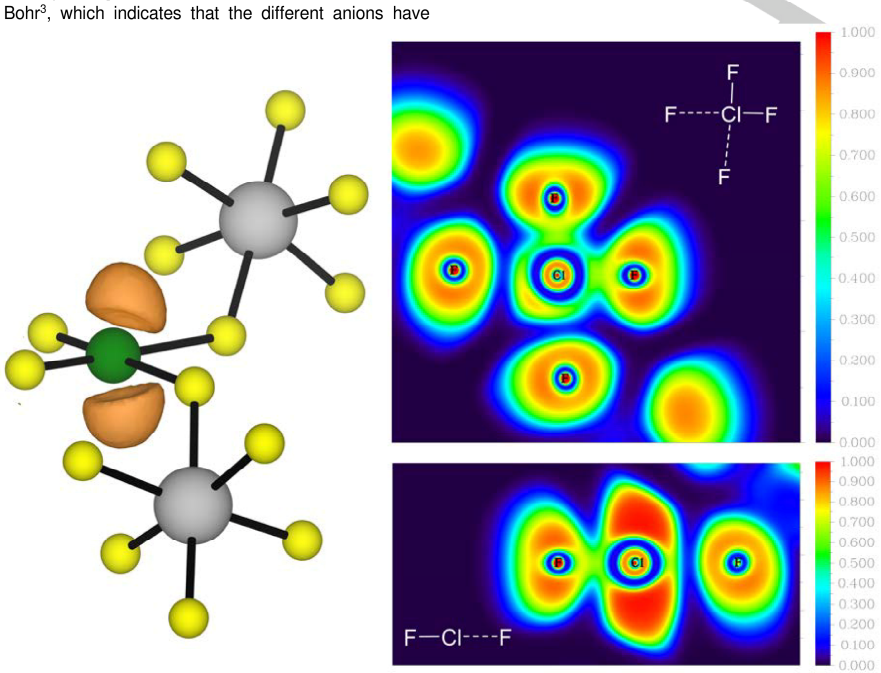

Figure 13. Left: Projection of the three-dimensional ELF (orange) of $[ClF_2[SbF_6]_2]^-$ with $\eta(r)$ = 0.9. The Cl atom is shown in green, the Sb atoms in grey and the F atoms in yellow. Right: Projections of the ELF of $[ClF_2[SbF_6]_2]^-$ of certain planes. The corresponding planes are indicated in white in the top right or bottom left corner. Top: Section through the plane of the ClF_2^+ cation, showing the ClF_2^+ cation and two bridging F atoms of $[SbF_6]^-$ units close to the Cl atom. Bottom: Section through the plane of F−Cl···F.

General remarks on the crystal structures of difluorochloronium(III) compounds

In the investigated and the previously reported difluorochloronium(III) compounds, the structures of the ClF_2^+ cations are similar with only minor differences in the Cl−F bond lengths and F−Cl−F bond angles. The Cl atoms are always coordinated by two additional F atoms from neighboring fluoridometallate anions, resulting in almost planar-quadrangular or planar-quadrangular planes.

Inspection of the Cl···F distances and F···Cl···F angles shows that they strongly vary with the fluoridometallate anion. The *M*−F···Cl interactions lead to either the formation of molecular building units in $(ClF_2[BF_4])_2$, $(ClF_2[AuF_4])_2$ and $(ClF_2[Ta_2F_{11}])_2$, or to chains in $ClF_2[MF_6]$, *M* = Nb, Ta, Ru, Os, Ir, As, Sb, Bi).[9,22]

For compounds containing $[MF_6]^-$ anions either *cis*- or *trans*-bridging of the F atoms is observed, but not both. When the $[MF_6]^-$ anions are *trans*-bridging (*M* = Ir, As, Sb, Bi), either linear (*M* = Ir), or zig-zag chains (*M* = As, Sb, Bi) are formed.[9] If the $[MF_6]^-$ anions are *cis*-bridging, chains with different shapes are formed. The chains are chiral, but both left- and right-handed chains are present, yielding racemates due to the centrosymmetric crystal structures. They are 2/1 helices for the Nb and Ta compounds and 4/1 helices for the Ru compound. For $ClF_2[OsF_6]$ the chain can be described as a severely deformed 3/1 helix. Regardless of the bridging-type, a pseudo-cubic primitive arrangement of the Cl and *M*(V) atoms is observed for all $ClF_2[MF_6]$ compounds, corresponding to the CsCl structure type. The observed crystal structures show no correlation with the effective ionic radii of the *M*(V) ions.[56] The two compounds with the smallest and biggest effective ionic radii, As(V) and Bi(V), show a zig-zag chain structure.[56] One could argue that in contrast to that, the bridging type of the $[MF_6]^-$ polyhedra might be correlated with the electronegativity (χ_{AR}) of the central atom, as *trans*-bridging is observed for the compounds containing the more electronegative elements (As, Sb, Bi, Ir), while *cis*-bridging is observed for those with the less electronegative ones (Nb, Ta, Ru, Os).[57,58] However, this correlation with electronegativity is not valid as *cis*-bridging Ru and Os and *trans*-bridging Ir have quite similar electronegativity values. Valence electron configuration of the *M*(V) atoms also does not play a clear role. So, one can only speculate what driving forces are responsible for the differences in the crystal structures.

This article is protected by copyright. All rights reserved.

Accepted Manuscript

European Journal of Inorganic Chemistry 10.1002/ejic.202000845

WILEY-VCH

FULL PAPER

Table 3. Experimentally determined and calculated Cl−F bond lengths as well as Cl···F distances of the bridging F atoms of the fluoridometallate anions in difluorochloronium(III) fluoridometallates.

Compound	bridging mode	*d* exp. / Å			*d* calc. (DFT-PBE0/TZVP, solid-state) / Å	
		Cl−F	Cl···F	Reference	Cl−F	Cl···F
$ClF_2[AsF_6]$	trans	1.541(14)	2.339(14)	[9]	1.59	2.28
$ClF_2[SbF_6]$	trans	1.555(4), 1.560(4)	2.302(4), 2.312(4)	this work	1.60	2.26
$ClF_2[IrF_6]$	trans	1.573(3)	2.300(3)	this work	1.61	2.24
$ClF_2[BiF_6]$	trans	1.568(3), 1.573(3)	2.252(3), 2.254(3)	this work	1.60	2.21, 2.23
$ClF_2[NbF_6]$	cis	1.571(1)	2.234(1)	this work	1.61	2.19
$ClF_2[TaF_6]$	cis	1.568(2)	2.252(2)	this work	1.61	2.20
$ClF_2[RuF_6]$	cis	1.565(2), 1.568(1)	2.248(2), 2.271(1)	this work	1.61	2.20, 2.23
$ClF_2[OsF_6]$	cis	1.567(5), 1.572(5), 1.576(5)	2.260(5), 2.269(5), 2.288(4)	this work	1.60	2.22-2.25
$ClF_2[Ta_2F_{11}]$	cis	1.566(2), 1.567(2)	2.235(2), 2.292(2)	this work	1.60	2.18, 2.26
$ClF_2[AuF_4]$	cis	1.538(4), 1.578(4)	2.170(4), 2.198(4)	this work	1.61, 1.62	2.16, 2.18
$ClF_2[BF_4]$	cis	1.562(1), 1.567(1)	2.270(1), 2.312(1)	[22]	1.60	2.24, 2.27

Table 4. Experimentally determined and calculated F−Cl−F angles as well as F···Cl···F angles of the bridging F atoms of the fluoridometallate anions in difluorochloronium(III) fluoridometallates.

Compound	bridging mode	∡ exp. / °			∡ calc. (DFT-PBE0/TZVP, solid-state) / °	
		F−Cl−F	F···Cl···F	Reference	F−Cl−F	F···Cl···F
$ClF_2[AsF_6]$	trans	103.2(7)	93.7(5)	[9]	95.6	99.7
$ClF_2[SbF_6]$	trans	97.0(2)	90.66(14)	this work	95.7	92.2
$ClF_2[IrF_6]$	trans	97.1(2)	90.38(14)	this work	95.1	91.3
$ClF_2[BiF_6]$	trans	95.90(19)	90.88(12)	this work	95.1	92.0
$ClF_2[NbF_6]$	cis	96.00(6)	93.62(4)	this work	94.6	94.5
$ClF_2[TaF_6]$	cis	96.45(15)	93.47(10)	this work	94.8	94.6
$ClF_2[RuF_6]$	cis	96.29(11), 96.80(13)	89.92(8), 91.25(7)	this work	94.8, 95.6	89.4, 93.6
$ClF_2[OsF_6]$	cis	97.0(3), 97.5(4)	90.0(2), 90.8(2)	this work	95.0, 95.8	92.6, 94.8
$ClF_2[Ta_2F_{11}]$	cis	96.30(10)	92.89(6)	this work	94.9	95.1
$ClF_2[AuF_4]$	cis	95.4(2)	88.1(1)	this work	94.5	88.3
$ClF_2[BF_4]$	cis	96.42(5)	99.11(3)	[22]	95.0	101.4

Table 5. Experimentally determined and calculated *M*−F distances of non-bridging and bridging F atoms of the fluoridometallate anions in difluorochloronium(III) fluoridometallates.

Compound	bridging mode	*d* exp. / Å			*d* calc. (DFT-PBE0/TZVP, solid-state) / Å	
		M−F(non-bridging)	*M*−F(bridging)	Reference	*M*−F(non-bridging)	*M*−F(bridging)
$ClF_2[AsF_6]$	trans	1.637(16)-1.694(12)	1.740(13)	[9]	1.71-1.72	1.77
$ClF_2[SbF_6]$	trans	1.862(3)-1.868(3)	1.896(3)-1.901(3)	this work	1.88	1.94
$ClF_2[IrF_6]$	trans	1.860(3)-1.871(2)	1.913(3)	this work	1.86-1.87	1.92
$ClF_2[BiF_6]$	trans	1.956(3)-1.964(3)	2.019(3)-2.026(3)	this work	1.98	2.05-2.06
$ClF_2[NbF_6]$	cis	1.850(1)-1.871(1)	1.9494(7)	this work	1.87-1.89	1.98
$ClF_2[TaF_6]$	cis	1.862(2)-1.881(2)	1.945(2)	this work	1.88-1.90	1.99
$ClF_2[RuF_6]$	cis	1.819(1)-1.841(1)	1.891(1)-1.896(1)	this work	1.84-1.87	1.930
$ClF_2[OsF_6]$	cis	1.852(4)-1.875(5)	1.910(4)-1.919(4)	this work	1.87-1.90	1.96
$ClF_2[Ta_2F_{11}]$	cis	1.835(2)-1.886(2) 2.057(2)-2.068(2)[a]	1.934(2)-1.935(2)	this work	1.85-1.91 2.08-2.09[a]	1.97
$ClF_2[AuF_4]$	cis	1.903(4)-1.905(3)	1.950(3)-1.961(4)	this work	1.92-1.94	1.99-2.00
$ClF_2[BF_4]$	cis	1.375(2)-1.378(2)	1.421(2)-1.425(2)	[22]	1.36-1.38	1.43

a: Parameter for the μ_2-F atom in the $[Ta_2F_{11}]^-$ anion.

Table 6. Average overlap population between two atoms from Mulliken population analysis of the optimized solid-state structures of difluorochloronium(III) fluoridometallates.

Compound	Bridging mode	average overlap population (DFT-PBE0/TZVP, solid-state) / *e*			
		Cl−F	Cl···F	*M*−F(non-bridging)	*M*−F(bridging)
$ClF_2[AsF_6]$	trans	0.05	0.02	0.28	0.22

This article is protected by copyright. All rights reserved.

Accepted Manuscript

European Journal of Inorganic Chemistry 10.1002/ejic.202000845

WILEY-VCH

FULL PAPER

$ClF_2[SbF_6]$	trans	0.05	0.01	0.23	0.18
$ClF_2[IrF_6]$	trans	0.05	0.02	0.13	0.10
$ClF_2[BiF_6]$	trans	0.05	0.01	0.19	0.13
$ClF_2[NbF_6]$	cis	0.05	0.01	0.10	0.07
$ClF_2[TaF_6]$	cis	0.05	0.01	0.14	0.09
$ClF_2[RuF_6]$	cis	0.05	0.01	0.08	0.06
$ClF_2[OsF_6]$	cis	0.05	0.01	0.09	0.08
$ClF_2[Ta_2F_{11}]$	cis	0.06	0.01	0.12, 0.06[a]	0.09
$ClF_2[AuF_4]$	cis	0.03	0.01	0.10	0.08
$ClF_2[BF_4]$	cis	0.05	0.02	0.29	0.22

a: Parameter for the μ_2-F atom in the $[Ta_2F_{11}]^-$ anion.

Table 7. Average high electron localization domain population (HELP) and average high electron localization domain volume (HELV) of the lone pair domains of the Cl atoms of ClF_2^+ in the optimized gas-phase, model structures of difluorochloronium(III) fluoridometallates.[51]

Model (Point group)	HELP / *e*	HELV / Bohr³
$[ClF_2[AsF_6]_2]^-$ (C_2)	1.50	15.9
$[ClF_2[SbF_6]_2]^-$ (C_1)	1.50	16.0
$[ClF_2[BiF_6]_2]^-$ (C_1)	1.51	16.1
$[ClF_2[IrF_6]_2]^-$ (C_2)	1.52	15.7
$[ClF_2[NbF_6]_2]^-$ (C_2)	1.50	16.1
$[ClF_2[TaF_6]_2]^-$ (C_2)	1.50	16.3
$[ClF_2[RuF_6]_2]^-$ (C_2)	1.50	15.8
$[ClF_2[OsF_6]_2]^-$ (C_1)	1.50	16.0
$[ClF_2[Ta_2F_{11}]]_2$ (C_i)	1.50	16.4
$[ClF_2[AuF_4]]_2$ (C_i)	1.52	17.2
$[ClF_2[BF_4]]_2$ (C_i)	1.51	16.9
ClF_2^+ (C_{2v})	1.61	27.2
$[ClF_2(HF)_2]^+$ (C_2)	1.53	19.7

Table 8. Comparison of the experimentally determined bond lengths and bond angles of ClF_2^+ with those calculated for the free gaseous cation, the solid salts, the gaseous trinuclear $[ClF_2[MF_6]_2]^-$ anions, and the gaseous $[ClF_2(HF_2)_2]^+$ cation.

Source	*d*(Cl−F) / Å	∡ F−Cl−F / °
Experimentally determined from crystal structures	1.54-1.57	95.9-103.2
Free, gaseous ClF_2^+ (CCSD(T)/aug-cc-pVTZ)[47]	1.552	101.7
Free, gaseous ClF_2^+ (DFT-PBE0/def2-TZVP)	1.54	102.5
Solid ClF_2^+ salts (DFT-PBE0/TZVP)	1.59-1.61	94.6-95.7
Gaseous $[ClF_2[MF_6]_2]^-$ (DFT-PBE0/def2-TZVP)	1.59-1.61	91.0-91.9
Gaseous $[ClF_2(HF_2)_2]^+$ (DFT-PBE0/def2-TZVP)	1.55	98.0

Conclusion

The difluorochloronium(III) compounds $ClF_2[MF_6]$ (M = Nb, Ta, Ru, Os, Ir, Sb, Bi), $ClF_2[Ta_2F_{11}]$, and $ClF_2[AuF_4]$ have been synthesized from reactions of metals, fluorides or chlorides with chlorine trifluoride. A similarly shaped ClF_2^+ cation is present in the crystal structures of all investigated compounds. This cation contains two strong, short, mainly covalent Cl−F, and two sterically active, free valence electron pairs in a pseudo-tetrahedral arrangement.[59] The coordination around the Cl atom is extended by two highly ionic, long fluorine bridges to neighboring fluoridometallate anions, resulting in a total coordination number of six. Regardless of the anion, the Cl atom and the four fluorine ligands form a perfect or almost perfect quadrangular plane. The bridging-modes of the $[MF_6]^-$ anions show neither a clear correlation with the effective ionic radii of the M atoms nor with their electronegativity. Quantum-chemical solid-state and gas-phase calculations were carried out and are in accord with the experimentally determined structures.

Experimental Section

General: Volatile materials were handled in either a Monel metal Schlenk line or a stainless steel/Teflon-FEP vacuum line, which were passivated with 100 % fluorine and/or chlorine trifluoride at various pressures before use.[5,60] Moisture-sensitive compounds were stored and handled in Ar- or N_2-filled glove boxes (MBraun, Vacuum Atmospheres Co). Reaction vessels were made of fluoropolymer (PFA or Teflon-FEP) or stainless steel (Hoke) that were closed by stainless steel valves. All reactors were passivated with fluorine or ClF_3 before use. Preparations were carried out in an atmosphere of dry and purified argon (5.0, Praxair). Chlorine trifluoride was stored over NaF to remove any traces of HF. **Caution!** ***Fluorine, chlorine trifluoride, and difluorochloronium(III) compounds***

This article is protected by copyright. All rights reserved.

Accepted Manuscript

European Journal of Inorganic Chemistry 10.1002/ejic.202000845

WILEY-VCH

FULL PAPER

are strong oxidative fluorinators. They react explosively upon hydrolysis or contact with organic materials and must be handled using appropriate protective gear.

Synthesis

$ClF_2[RuF_6]$, $ClF_2[OsF_6]$, $ClF_2[IrF_6]$, $ClF_2[AuF_4]$. A passivated 30 mL stainless steel cylinder was loaded outside the glove box with 1.0 mmol of the corresponding metal powder. The cylinder was connected to the stainless-steel vacuum line, evacuated and an excess of ClF_3 (5.0 g, 54 mmol) condensed in at 77 K. The reactor was warmed to room temperature over a period of two hours. After 8 hours, all volatile materials (ClF and ClF_3) were slowly pumped off. The ClF_2^+ salts were isolated as crystalline solids ($ClF_2[RuF_6]$ isolated: 281 mg, calculated 289 mg; $ClF_2[OsF_6]$ isolated: 375 mg, calculated 378 mg; $ClF_2[IrF_6]$ isolated: 377 mg, calculated 380 mg; $ClF_2[AuF_4]$ isolated: 342 mg, calculated 346 mg).

$ClF_2[NbF_6]$, $ClF_2[SbF_6]$, $ClF_2[TaF_6]$, $ClF_2[Ta_2F_{11}]$, $ClF_2[BiF_6]$. A PFA reaction vessel was loaded with the metal starting material in the glove box and attached to a stainless-steel valve. An excess of ClF_3 was then condensed onto the solid at 77 K. The vessel was warmed slowly to room temperature. The unreacted ClF_3 and ClF by-product were then slowly pumped off, and the colorless residue was removed in the glove box. $ClF_2[NbF_6]$: 20.6 mg NbF_5 (0.11 mmol) was reacted with approximately 0.07 g (0.8 mmol) of ClF_3. Volatiles were pumped off after a few hours at room temperature (29.2 mg isolated, calculated: 30.8 mg). $ClF_2[SbF_6]$: 0.407 g SbF_3 (2.3 mmol) was reacted with approximately 3 g (32 mmol) of ClF_3. Volatiles were removed after one hour at room temperature (0.641 g isolated, calculated: 0.704 g). $ClF_2[TaF_6]$: 21.0 mg $TaCl_5$ (0.059 mmol) was reacted with approximately 0.13 g (1.4 mmol) of ClF_3. Volatiles were removed after a few hours at room temperature. (19.0 mg isolated, 21.7 mg calculated). $ClF_2[Ta_2F_{11}]$: 29.6 mg $TaCl_5$ (0.083 mmol) was reacted with approximately 0.09 g (1 mmol) of ClF_3. Volatiles were removed after a few hours at room temperature. Crystals of both, $ClF_2[TaF_6]$ and $ClF_2[Ta_2F_{11}]$, were present in the product (29.7 mg isolated). $ClF_2[BiF_6]$: 35.2 mg BiF_5 (0.12 mmol) was reacted with approximately 0.09 g (1 mmol) of ClF_3. Volatiles were removed after a few hours at room temperature (40.9 mg isolated, calculated: 47.6 mg).

Single-crystal X-ray diffraction: Crystals of the moisture-sensitive compounds were selected under dried perfluorinated oil (Fomblin YR1800, Solvay, stored over molecular sieve 3 Å) and mounted on a MiTeGen loop. Intensity data of suitable crystals were recorded with a D8 Quest diffractometer (Bruker), an APEX II DUO diffractometer (Bruker) or an IPDS2 diffractometer (STOE). The diffractometers were operated with monochromatized Mo-K_α radiation (0.71073 Å), multi-layered optics (D8 Quest), a TRIUMPH curved crystal (APEX II DUO) or a graphite monochromator (IPDS2) and equipped with a PHOTON 100 CMOS detector (D8 Quest), a CCD detector (Apex II DUO) or an image plate detector (IPDS2). Evaluation, integration and reduction of the diffraction data was carried out with the APEX3 software suite (D8 Quest and Apex II DUO) or the X-Area software suite (IPDS2).[61,62] The diffraction data were corrected for absorption utilizing the multi-scan method of SADABS or TWINABS within the APEX3 software suite (D8 Quest and Apex II DUO) or the integration method with the modules X-Shape and X-Red32 of the X-Area software suite (IPDS2T). The structures were solved with dual-space methods (SHELXT) and refined against F^2 (SHELXL).[63,64] Systematic absence violations were observed for the space groups of the compounds $ClF_2[MF_6]$ (M = Nb, Ta, Ru, Os, Ir) and $ClF_2[Ta_2F_{11}]$. However, the very weak intensities of the corresponding reflections were very close to the tripled standard uncertainties. Solution and refinement of the structures in crystallographic subgroups resulted in significant correlations between atomic coordinates and non-positive definite displacement parameters for some atoms. The crystal structures were consequently solved and refined in the space groups reported here, which were also indicated by the Addsym feature of the program package PLATON when checking for additional symmetry within the subgroups.[65,66] The crystals of $ClF_2[SbF_6]$ and $ClF_2[BiF_6]$ used for the diffraction experiment were non-merohedral twins (three twin components in $ClF_2[SbF_6]$ and two twin components in $ClF_2[BiF_6]$). The lattice parameters and twin law of $ClF_2[BiF_6]$ were determined with the program CELL_NOW.[67] In the case of $ClF_2[SbF_6]$, the twin components were determined manually in the X-Area software. In both cases only the non-overlapping reflections of the major twin component were used for the structure solution. The data were initially refined with the HKLF5 format option in SHELXL with all reflections (overlapping reflections and non-overlapping reflections of all twin components). The data were then processed with the HKLF5Tools program: the non-overlapping reflections of the weaker diffracting twin component were removed, the non-overlapping reflections of the major twin component were merged in point group $\bar{1}$ and the overlapping reflections were merged in point group 1.[68] In the case of $ClF_2[BiF_6]$ the final refinement was carried out against the detwinned dataset (created by SHELXL with the LIST 8 option as a FCF file and converted to a HKL file with HKLF5Tools).The locations of highest residual electron densities after the final refinement were the following: $ClF_2[IrF_6]$: 0.78 Å from atom Ir(1), $ClF_2[SbF_6]$: 0.68 Å from atom Sb(2), $ClF_2[BiF_6]$: 0.82 Å from atom Bi(1), $ClF_2[NbF_6]$: 0.74 Å from atom Cl(1), $ClF_2[TaF_6]$: 0.70 Å from atom Ta(1), $ClF_2[OsF_6]$: 0.81 Å from atom Os(2), $ClF_2[RuF_6]$: 1.28 Å from atom F(3), $ClF_2[Ta_2F_{11}]$: 1.79 Å from atom F(7), $ClF_2[AuF_4]$: 1.13 Å from atom Au(1). Representations of the crystal structures were created with the Diamond software.[69] CCDC 2008578-2008586 contain the supplementary crystallographic data for this paper. These data are provided free of charge by The Cambridge Crystallographic Data Centre.

Solid-state quantum-chemical calculations: Periodic quantum-chemical calculations were carried out for difluorochloronium(III) fluoridometallates with the PBE0 hybrid density functional method (DFT-PBE0).[41,42] Triple-zeta-valence + polarization (TZVP) level basis sets were applied for all atoms. Details of the used basis sets are given in the Supporting Information. All calculations were carried out with the CRYSTAL17 program package.[70] The crystal structures of $ClF_2[AsF_6]$ and $ClF_2[BF_4]$ were taken from previous studies.[9,22] The reciprocal space was sampled with the following Monkhorst-Pack-type k-point grids: $ClF_2[AsF_6]$: 2×3×3, $ClF_2[IrF_6]$: 4×5×3, $ClF_2[SbF_6]$: 5×5×3, $ClF_2[BiF_6]$: 5×5×3, $ClF_2[NbF_6]$: 3×5×3, $ClF_2[TaF_6]$: 3×5×3, $ClF_2[OsF_6]$: 2×4×2, $ClF_2[RuF_6]$: 1×5×2, $ClF_2[Ta_2F_{11}]$: 3×3×2, $ClF_2[AuF_4]$: 5×3×2, $ClF_2[BF_4]$: 4×3×3. For the evaluation of the Coulomb and exchange integrals (TOLINTEG), tight tolerance factors of 8, 8, 8, 8, 16 were used for all calculations. Both the atomic positions and lattice parameters were fully optimized within the constraints imposed by the space group symmetry. Default DFT integration grids and optimization convergence thresholds were applied in all calculations. Mulliken population analyses were carried out for all compounds. For the magnetic systems $ClF_2[MF_6]$ (M = Ru, Os, Ir) a ferromagnetic ground state was employed. The resulting magnetic moments were 2.0 μB for the $[IrF_6]^-$ anion (1.4 μB contribution from Ir), 3.0 and 2.9 μB for the two independent $[OsF_6]^-$ anions (2.4 μB contribution from the respective Os atom) and 3.0 μB for the $[RuF_6]^-$ anion (2.3 μB contribution from Ru).

Gas-phase quantum-chemical calculations: Gas-phase quantum-chemical calculations were carried out with the TURBOMOLE program package (version 7.2.1) using the PBE0 hybrid density functional method and Karlsruhe triple-zeta-valence + polarization basis sets (def2-TZVP).[44,45,71] The basis sets of Nb, Ru and Sb include a 28-electron scalar relativistic effective core potential. The basis sets of Ta, Ir, Au, Bi include a 60-electron scalar relativistic effective core potential. The resolution-of-the-identity technique was used to speed up the calculations.[72,73] For the magnetic systems $[ClF_2[MF_6]_2]^-$ (M = Ir, Os, Ru) magnetic ground states were employed. The resulting magnetic moments from natural population analyses were 2.0 μB for the $[IrF_6]^-$ anion (1.5 μB contribution from Ir), 3.0 μB for each of the $[OsF_6]^-$ anions (2.4 μB contribution from the respective Os atom) and 3.0 μB for the $[RuF_6]^-$ anion (2.4 μB contribution from Ru). All calculations were done in the gas phase without any solvent models. A full geometry optimization was carried out in the stated point group. All structures were confirmed to be true local minima by harmonic frequency calculations. Natural population analyses were carried out with the scheme implemented in Turbomole.[46] Electron localization functions (ELF) were generated with the program package Multiwfn (version 3.7).[54,74] A 300×300 grid was used for the generation of

This article is protected by copyright. All rights reserved.

Accepted Manuscript

European Journal of Inorganic Chemistry 10.1002/ejic.202000845

WILEY-VCH

FULL PAPER

color-coded maps and a high-quality grid for the three-dimensional electron localization functions. The figure of the three-dimensional ELF was generated with the program package VESTA (version 3).[75,76] Analyses of the high electron localization domain population (HELP) and high electron localization domain volume (HELV)) were carried out with Multiwfn, medium-quality grids and standard settings were used for the basin analysis.[51]

Acknowledgements

We thank the Deutsche Forschungsgemeinschaft (DFG) for generous funding and another chemist, who wants to remain anonymous, for the donation of some ClF_3. We thank Prof. Dr. Martin Rahm, Chalmers University of Technology Gothenburg, Sweden for helpful discussions on HELP and HELV.

Keywords: difluorochloronium(III) cation • chlorine trifluoride • fluorine chemistry • single-crystal X-ray diffraction

[1] O. Ruff, H. Krug, *Z. Anorg. Allg. Chem.* **1930**, *190*, 270–276.
[2] *Interhalogen Handbook, Technical Report AFRPL-TR-67-276*, Rocketdyne, Canoga Park, California, **1967**.
[3] J. VanOmmeren, *J. ASTM Int.* **2009**, *6*, JAI102215.
[4] K. O. Christe, in *XXIVth International Congress of Pure and Applied Chemistry*, Butterworth-Heinemann, Oxford, **1974**, pp. 115–141.
[5] R. Haiges, in *Efficient Preparations of Fluorine Compounds* (Ed.: H.W. Roesky), John Wiley & Sons, Inc., Hoboken, NJ, USA, **2012**, pp. 100–107.
[6] L. Stein, R. C. Vogel, *Ind. Eng. Chem.* **1956**, *48*, 418–421.
[7] W. Bacher, E. Jacob, *Gmelin-Handbuch Der Anorganischen Chemie Teil: System-Nr. 55., Uran : U / Erg.-Bd. / C. / 8. Verbindungen Mit Fluor*, Springer-Verlag, Berlin Heidelberg New York, **1980**.
[8] R. Bougon, B. Buu, K. Seppelt, *Chem. Ber.* **1993**, *126*, 1331–1336.
[9] H. Lynton, J. Passmore, *Can. J. Chem.* **1971**, *49*, 2539–2543.
[10] A. J. Edwards, R. J. C. Sills, *J. Chem. Soc., A* **1970**, 2697–2699.
[11] K. O. Christe, A. E. Pavlath, *Z. Anorg. Allg. Chem.* **1965**, *335*, 210–216.
[12] M. Schmeißer, W. Ludovici, D. Naumann, P. Sartori, E. Scharf, *Chem. Ber.* **1968**, *101*, 4214–4220.
[13] A. J. Edwards, G. R. Jones, *J. Chem. Soc. A* **1969**, *0*, 1467–1470.
[14] K. O. Christe, C. J. Schack, *Inorg. Chem.* **1970**, *9*, 2296–2299.
[15] J. Shamir, in *Structural Problems*, Springer, Berlin, Heidelberg, **1979**, pp. 141–210.
[16] I. C. Tornieporth-Oetting, T. M. Klapötke, *Heteroatom Chem.* **1993**, *4*, 543–552.
[17] L. B. Asprey, J. L. Margrave, M. E. Silverthorn, *J. Am. Chem. Soc.* **1961**, *83*, 2955–2956.
[18] J. Shamir, *Isr. J. Chem.* **1978**, *17*, 37–47.
[19] B. Scheibe, S. I. Ivlev, A. J. Karttunen, F. Kraus, *Eur. J. Inorg. Chem.* **2020**, *2020*, 1319–1324.
[20] P. Pröhm, J. R. Schmid, K. Sonnenberg, P. Voßnacker, S. Steinhauer, C. J. Schattenberg, R. Müller, M. Kaupp, S. Riedel, *Angew. Chem. Int. Ed.* **2020**, *59*, 16002–16006.
[21] S. I. Ivlev, A. J. Karttunen, M. R. Buchner, M. Conrad, F. Kraus, *Angew. Chem. Int. Ed.* **2018**, *57*, 14640–14644.
[22] M. Y. Antipin, A. M. Ellern, V. F. Sukhoverkhov, Y. T. Struchkov, Y. A. Buslaev, *Russ. J. Inorg. Chem.* **1988**, *33*, 171–173.
[23] A. M. Ellern, M. Y. Antipin, A. V. Sharabarin, Y. T. Struchkov, *Russ. J. Inorg. Chem.* **1991**, *36*, 1278–1280.
[24] R. Bougon, W. V. Cicha, M. Lance, L. Meublat, M. Nierlich, J. Vigner, *Inorg. Chem.* **1991**, *30*, 102–109.
[25] A. M. Ellern, M. Y. Antipin, A. V. Sharabarin, Y. T. Struchkov, *Russ. J. Inorg. Chem.* **1992**, *37*, 46–47.
[26] A. M. Ellern, M. N. Sinitsyn, M. Y. Antipin, A. V. Sharabarin, Y. T. Struchkov, *Koord. Khim.* **1991**, *17*, 1686–1688.
[27] O. Ruff, E. Ascher, J. Fischer, F. Laass, *Z. Anorg. Allg. Chem.* **1928**, *176*, 258–270.
[28] H. Schmitz, H. J. Schumacher, *Z. Naturforsch., A: Astrophys., Phys. Phys. Chem.* **1947**, *2*, 359–362.
[29] C. J. Schack, R. D. Wilson, *Synth. React. Inorg. Met.-Org. Chem.* **1973**, *3*, 393–396.
[30] C. J. Schack, R. D. Wilson, D. D. Desmarteau, in *Inorganic Syntheses* (Ed.: J.M. Shreeve), John Wiley & Sons, Inc., Hoboken, NJ, USA, **1986**, pp. 1–3.
[31] G. Natta, P. Corradini, *J. Polym. Sci.* **1959**, *39*, 29–46.
[32] C. De Rosa, F. Auriemma, *Crystals and Crystallinity in Polymers: Diffraction Analysis of Ordered and Disordered Crystals*, Wiley, Hoboken, New Jersey, **2013**.
[33] V. Kopský, D. B. Litvin, Eds. , *International Tables for Crystallography. Vol. E: Subperiodic Groups*, Wiley, Chichester, **2010**.
[34] U. Müller, *Acta Crystallogr., Sect. B: Struct. Crystallogr. Cryst. Chem.* **2017**, *73*, 443–452.
[35] O. Graudejus, A. P. Wilkinson, L. C. Chacón, N. Bartlett, *Inorg. Chem.* **2000**, *39*, 2794–2800.
[36] W. P. Davey, *Phys. Rev.* **1923**, *21*, 143–161.
[37] J. H. Burns, *Acta Crystallogr.* **1962**, *15*, 1098–1101.
[38] G. Lucier, J. Muenzenberg, W. J. Casteel, N. Bartlett, *Inorg. Chem.* **1995**, *34*, 2692–2698.
[39] G. Tavčar, E. Goreshnik, *J. Fluorine Chem.* **2016**, *189*, 33–38.
[40] U. Engelmann, B. G. Müller, *Z. Anorg. Allg. Chem.* **1991**, *598*, 103–110.
[41] J. P. Perdew, K. Burke, M. Ernzerhof, *Phys. Rev. Lett.* **1996**, *77*, 3865–3868.
[42] C. Adamo, V. Barone, *J. Chem. Phys.* **1999**, *110*, 6158–6170.
[43] K. O. Christe, X. Zhang, J. A. Sheehy, R. Bau, *J. Am. Chem. Soc.* **2001**, *123*, 6338–6348.
[44] *TURBOMOLE V7.2.1, a Development of University of Karlsruhe and Forschungszentrum Karlsruhe GmbH, 1989-2007, TURBOMOLE GmbH, since 2007.*, **2017**.
[45] F. Weigend, R. Ahlrichs, *Phys. Chem. Chem. Phys.* **2005**, *7*, 3297–3305.
[46] A. E. Reed, R. B. Weinstock, F. Weinhold, *J. Chem. Phys.* **1985**, *83*, 735–746.
[47] K. S. Thanthiriwatte, M. Vasiliu, D. A. Dixon, K. O. Christe, *Inorg. Chem.* **2012**, *51*, 10966–10982.
[48] J. F. Lehmann, G. J. Schrobilgen, K. O. Christe, A. Kornath, R. J. Suontamo, *Inorg. Chem.* **2004**, *43*, 6905–6921.
[49] D. A. Dixon, D. J. Grant, K. O. Christe, K. A. Peterson, *Inorg. Chem.* **2008**, *47*, 5485–5494.
[50] R. J. Gillespie, R. S. Nyholm, *Q. Rev., Chem. Soc.* **1957**, *11*, 339–380.
[51] M. Rahm, Karl. O. Christe, *ChemPhysChem* **2013**, *14*, 3714–3725.
[52] A. Kumar, S. R. Gadre, N. Mohan, C. H. Suresh, *J. Phys. Chem. A* **2014**, *118*, 526–532.
[53] M. Rahm, *J. Chem. Theory Comput.* **2015**, *11*, 3617–3628.
[54] A. D. Becke, K. E. Edgecombe, *J. Chem. Phys.* **1990**, *92*, 5397–5403.
[55] A. Savin, R. Nesper, S. Wengert, T. F. Fässler, *Angew. Chem. Int. Ed.* **1997**, *36*, 1808–1832.
[56] R. D. Shannon, *Acta Crystallogr., Sect. A: Cryst. Phys., Diffr., Theor. Gen. Crystallogr.* **1976**, *32*, 751–767.
[57] J. B. Mann, T. L. Meek, L. C. Allen, *J. Am. Chem. Soc.* **2000**, *122*, 2780–2783.

This article is protected by copyright. All rights reserved.

Accepted Manuscript

European Journal of Inorganic Chemistry 10.1002/ejic.202000845

WILEY-VCH

FULL PAPER

[58] J. B. Mann, T. L. Meek, E. T. Knight, J. F. Capitani, L. C. Allen, *J. Am. Chem. Soc.* **2000**, *122*, 5132–5137.
[59] R. T. Sanderson, *Polar Covalence*, Academic Press, New York, **1983**.
[60] K. O. Christe, R. D. Wilson, C. J. Schack, *Inorg. Synth.* **1986**, *24*, 3–6.
[61] *APEX3*, Bruker AXS Inc., Madison, Wisconsin, USA, **2018**.
[62] *X-Area*, STOE & Cie GmbH, Darmstadt, Germany, **2018**.
[63] G. M. Sheldrick, *Acta Crystallogr., Sect. A: Found. Adv.* **2015**, *71*, 3–8.
[64] G. M. Sheldrick, *Acta Crystallogr., Sect. C: Struct. Chem.* **2015**, *71*, 3–8.
[65] A. L. Spek, *PLATON - A Multipurpose Crystallographic Tool*, Utrecht University, Utrecht, The Netherlands, **2019**.
[66] A. L. Spek, *Acta Crystallogr., Sect. D: Biol. Crystallogr.* **2009**, *65*, 148–155.
[67] G. M. Sheldrick, *CELL_NOW*, Göttingen (Germany), **2008**.
[68] S. I. Ivlev, M. Conrad, F. Kraus, *Z. Kristallogr. - Cryst. Mater.* **2019**, *234*, 415–418.
[69] K. Brandenburg, H. Putz, *Diamond - Crystal and Molecular Structure Visualization*, Crystal Impact GbR, Bonn, **2019**.
[70] R. Dovesi, A. Erba, R. Orlando, C. M. Zicovich-Wilson, B. Civalleri, L. Maschio, M. Rérat, S. Casassa, J. Baima, S. Salustro, B. Kirtman, *Wiley Interdiscip. Rev.: Comput. Mol. Sci.* **2018**, e1360.
[71] R. Ahlrichs, M. Bär, M. Häser, H. Horn, C. Kölmel, *Chem. Phys. Lett.* **1989**, *162*, 165–169.
[72] K. Eichkorn, O. Treutler, H. Öhm, M. Häser, R. Ahlrichs, *Chem. Phys. Lett.* **1995**, *240*, 283–290.
[73] F. Weigend, *Phys. Chem. Chem. Phys.* **2006**, *8*, 1057–1065.
[74] T. Lu, F. Chen, *J. Comput. Chem.* **2012**, *33*, 580–592.
[75] K. Momma, F. Izumi, *J. Appl. Crystallogr.* **2008**, *41*, 653–658.
[76] K. Momma, F. Izumi, *J. Appl. Crystallogr.* **2011**, *44*, 1272–1276.

WILEY-VCH

Accepted Manuscript

This article is protected by copyright. All rights reserved.

Supporting Information

Content

Selected crystallographic data of difluorochloronium(III) fluoridometallates 2

Comparison of Cl−F and *M*−F bond lengths and Cl···F distances as well as F−Cl−F and F···Cl···F angles of previously reported crystal structures and redetermined crystal structures of difluorochloronium(III) fluoridometallates 7

Basis set details for quantum-chemical solid-state calculations 8

Lattice parameters and atomic coordinates of optimized solid-state structures of difluorochloronium(III) fluoridometallates 14

XYZ coordinates of geometry-optimized structures of gas-phase quantum-chemical calculations..... 18

Bond lengths and angles of the ClF_2^+ cations of geometry-optimized structures from gas-phase quantum-chemical calculations..... 21

Partial atomic charges from Mulliken population analysis from quantum-chemical solid-state calculations 22

Partial atomic charges in geometry-optimized structures of gas-phase quantum-chemical calculations..... 22

References 23

Selected crystallographic data of difluorochloronium(III) fluoridometallates

Atomic coordinates and displacement parameters of $ClF_2[IrF_6]$

Table S1. Atomic coordinates and equivalent isotropic displacement parameters U_{iso} of $ClF_2[IrF_6]$ at 100 K.

Atom	Position	*x*	*y*	*z*	U_{iso} / Å^2
Ir(1)	2*e*	3/4	0.61744(3)	3/4	0.01914(7)
Cl(1)	2*f*	1/4	0.9094(2)	3/4	0.0198(2)
F(1)	4*g*	0.4191(4)	1.0956(4)	0.7948(4)	0.0281(5)
F(2)	4*g*	0.4841(4)	0.6196(4)	0.8125(4)	0.0258(5)
F(3)	4*g*	0.8123(4)	0.8550(5)	0.9190(3)	0.0274(5)
F(4)	4*g*	0.6902(4)	0.3821(4)	0.5808(4)	0.0294(5)

Table S2. Anisotropic displacement parameters of $ClF_2[IrF_6]$ at 100 K.

Atom	U_{11} / Å^2	U_{22} / Å^2	U_{33} / Å^2	U_{23} / Å^2	U_{13} / Å^2	U_{12} / Å^2
Ir(1)	0.01937(10)	0.02016(11)	0.01808(10)	0	0.00256(7)	0
Cl(1)	0.0192(5)	0.0214(5)	0.0192(5)	0	0.0030(4)	0
F(1)	0.0265(12)	0.0260(12)	0.0322(13)	−0.0070(9)	0.0058(10)	−0.0032(9)
F(2)	0.0213(11)	0.0285(12)	0.0280(12)	0.0016(9)	0.0054(9)	0.0030(9)
F(3)	0.0297(12)	0.0292(12)	0.0236(11)	−0.0009(10)	0.0031(9)	−0.0073(9)
F(4)	0.0299(12)	0.0300(13)	0.0286(13)	−0.0048(9)	0.0045(10)	−0.0088(9)

Atomic coordinates and displacement parameters of $ClF_2[SbF_6]$

Table S3. Atomic coordinates and equivalent isotropic displacement parameters U_{iso} of $ClF_2[SbF_6]$ at 100 K.

Atom	Position	*x*	*y*	*z*	U_{iso} / Å^2
Sb(1)	1*h*	1/2	1/2	1/2	0.01339(14)
Sb(2)	1*e*	1/2	1/2	1	0.01383(14)
Cl(1)	2*i*	0.0745(3)	0.0964(2)	0.74983(14)	0.0171(3)
F(1)	2*i*	−0.0883(7)	0.0262(7)	0.6231(4)	0.0237(8)
F(2)	2*i*	−0.0996(8)	−0.0401(7)	0.8430(4)	0.0251(8)
F(3)	2*i*	0.6195(7)	0.2255(6)	0.4174(4)	0.0202(7)
F(4)	2*i*	0.1916(7)	0.4769(6)	0.3960(4)	0.0206(7)
F(5)	2*i*	0.3533(7)	0.3008(6)	0.6240(4)	0.0209(7)
F(6)	2*i*	0.3265(7)	0.2133(6)	0.9334(4)	0.0214(7)
F(7)	2*i*	0.3447(8)	0.6760(7)	0.8671(4)	0.0251(8)
F(8)	2*i*	0.7770(7)	0.4351(7)	0.8983(4)	0.0253(8)

Table S4. Anisotropic displacement parameters of $ClF_2[SbF_6]$ at 100 K.

Atom	U_{11} / Å^2	U_{22} / Å^2	U_{33} / Å^2	U_{23} / Å^2	U_{13} / Å^2	U_{12} / Å^2
Sb(1)	0.0156(3)	0.0106(2)	0.0143(3)	0.0012(2)	0.0030(2)	0.00095(19)
Sb(2)	0.0157(3)	0.0126(3)	0.0133(3)	0.0003(2)	0.0010(2)	0.00146(19)
Cl(1)	0.0187(6)	0.0159(6)	0.0172(6)	0.0019(5)	0.0026(5)	0.0010(5)
F(1)	0.028(2)	0.0189(17)	0.0229(19)	−0.0024(14)	−0.0067(15)	0.0003(14)
F(2)	0.0269(19)	0.0222(18)	0.027(2)	0.0051(15)	0.0089(15)	−0.0047(14)
F(3)	0.0256(17)	0.0145(15)	0.0210(18)	−0.0040(13)	0.0057(14)	0.0043(13)
F(4)	0.0175(16)	0.0187(16)	0.0249(19)	0.0008(14)	−0.0033(14)	−0.0007(13)
F(5)	0.0262(18)	0.0159(16)	0.0219(18)	0.0056(14)	0.0109(14)	0.0003(13)
F(6)	0.0259(18)	0.0147(15)	0.0228(19)	−0.0024(14)	−0.0022(14)	−0.0022(13)
F(7)	0.031(2)	0.0230(18)	0.0215(19)	0.0067(15)	−0.0058(15)	0.0055(15)
F(8)	0.0216(17)	0.029(2)	0.026(2)	−0.0043(16)	0.0083(15)	0.0022(15)

Atomic coordinates and displacement parameters of $ClF_2[BiF_6]$

Table S5. Atomic coordinates and equivalent isotropic displacement parameters U_{iso} of $ClF_2[BiF_6]$ at 100 K.

Atom	Position	*x*	*y*	*z*	U_{iso} / Å²
Bi(1)	1*h*	1/2	1/2	1/2	0.00950(6)
Bi(2)	1*c*	1/2	1/2	1	0.01039(6)
Cl(1)	2*i*	0.0725(2)	0.0960(2)	0.74946(10)	0.0129(2)
F(1)	2*i*	−0.0924(6)	0.0327(6)	0.6214(3)	0.0205(6)
F(2)	2*i*	−0.1134(6)	−0.0386(6)	0.8378(3)	0.0221(7)
F(3)	2*i*	0.6178(6)	0.2163(5)	0.4149(3)	0.0164(6)
F(4)	2*i*	0.1711(6)	0.4698(6)	0.3934(3)	0.0180(6)
F(5)	2*i*	0.3559(6)	0.2911(5)	0.6329(3)	0.0173(6)
F(6)	2*i*	0.3156(6)	0.1973(5)	0.9304(3)	0.0174(6)
F(7)	2*i*	0.3350(7)	0.6751(6)	0.8598(3)	0.0219(7)
F(8)	2*i*	0.7891(6)	0.4372(6)	0.8953(3)	0.0216(7)

Table S6. Anisotropic displacement parameters of $ClF_2[BiF_6]$ at 100 K.

Atom	U_{11} / Å²	U_{22} / Å²	U_{33} / Å²	U_{23} / Å²	U_{13} / Å²	U_{12} / Å²
Bi(1)	0.00985(13)	0.00824(11)	0.01071(11)	0.00123(8)	0.00262(9)	0.00031(9)
Bi(2)	0.01099(13)	0.01057(12)	0.00980(11)	0.00058(8)	0.00136(9)	0.00135(10)
Cl(1)	0.0133(5)	0.0126(5)	0.0128(4)	0.0010(4)	0.0021(4)	0.0003(4)
F(1)	0.0218(17)	0.0181(15)	0.0202(14)	−0.0012(11)	−0.0058(12)	−0.0012(13)
F(2)	0.0197(16)	0.0226(16)	0.0251(15)	0.0074(12)	0.0098(12)	−0.0048(13)
F(3)	0.0174(15)	0.0147(14)	0.0176(13)	−0.0007(11)	0.0042(11)	0.0024(12)
F(4)	0.0127(14)	0.0218(16)	0.0185(14)	0.0000(11)	−0.0035(11)	−0.0012(12)
F(5)	0.0213(16)	0.0137(14)	0.0180(14)	0.0055(11)	0.0070(11)	0.0004(12)
F(6)	0.0207(16)	0.0113(13)	0.0194(14)	−0.0014(10)	−0.0009(11)	−0.0037(12)
F(7)	0.0271(18)	0.0208(16)	0.0176(14)	0.0079(12)	−0.0044(12)	0.0042(14)
F(8)	0.0150(15)	0.0283(17)	0.0224(15)	−0.0032(12)	0.0085(12)	0.0027(13)

Atomic coordinates and displacement parameters of $ClF_2[NbF_6]$

Table S7. Atomic coordinates and equivalent isotropic displacement parameters U_{iso} of $ClF_2[NbF_6]$ at 100 K.

Atom	Position	*x*	*y*	*z*	U_{iso} / Å²
Nb(1)	4c	1/2	0.39706(2)	1/4	0.00801(4)
Cl(1)	4d	1/4	0	0.46734(3)	0.00931(6)
F(1)	8f	0.34865(8)	0.11033(13)	0.56754(7)	0.01950(15)
F(2)	8f	0.38845(7)	0.15147(13)	0.32168(8)	0.01802(14)
F(3)	8f	0.39655(8)	0.37323(14)	0.10158(7)	0.02049(15)
F(4)	8f	0.61280(9)	0.62024(14)	0.18202(8)	0.02297(16)

Table S8. Anisotropic displacement parameters of $ClF_2[NbF_6]$ at 100 K.

Atom	U_{11} / Å²	U_{22} / Å²	U_{33} / Å²	U_{23} / Å²	U_{13} / Å²	U_{12} / Å²
Nb(1)	0.00865(6)	0.00720(6)	0.00819(6)	0	0.00052(4)	0
Cl(1)	0.00979(12)	0.00903(12)	0.00911(12)	0	0	−0.00014(11)
F(1)	0.0240(3)	0.0184(3)	0.0161(3)	−0.0040(3)	−0.0099(3)	−0.0026(3)
F(2)	0.0158(3)	0.0157(3)	0.0226(3)	0.0029(3)	0.0078(3)	−0.0029(2)
F(3)	0.0247(4)	0.0199(3)	0.0169(3)	−0.0003(3)	−0.0095(3)	−0.0017(3)
F(4)	0.0261(4)	0.0185(4)	0.0243(4)	0.0060(3)	0.0022(3)	−0.0109(3)

Atomic coordinates and displacement parameters of $ClF_2[TaF_6]$

Table S9. Atomic coordinates and equivalent isotropic displacement parameters U_{iso} of $ClF_2[TaF_6]$ at 100 K.

Atom	Position	*x*	*y*	*z*	U_{iso} / Å^2
Ta(1)	4*c*	1/2	0.39715(2)	1/4	0.00746(7)
Cl(1)	4*d*	1/4	0	0.46837(9)	0.00918(14)
F(1)	8*f*	0.3485(2)	0.1105(3)	0.5677(2)	0.0189(4)
F(2)	8*f*	0.3893(2)	0.1512(4)	0.3220(2)	0.0176(4)
F(3)	8*f*	0.3955(2)	0.3744(4)	0.1017(2)	0.0199(4)
F(4)	8*f*	0.6130(2)	0.6226(4)	0.1819(2)	0.0219(4)

Table S10. Anisotropic displacement parameters of $ClF_2[TaF_6]$ at 100 K.

Atom	U_{11} / Å^2	U_{22} / Å^2	U_{33} / Å^2	U_{23} / Å^2	U_{13} / Å^2	U_{12} / Å^2
Ta(1)	0.00852(9)	0.00643(9)	0.00743(9)	0	0.00055(4)	0
Cl(1)	0.0098(3)	0.0087(3)	0.0091(3)	0	0	−0.0001(3)
F(1)	0.0236(10)	0.0172(9)	0.0160(9)	−0.0032(7)	−0.0100(8)	−0.0031(7)
F(2)	0.0161(8)	0.0144(8)	0.0223(9)	0.0029(7)	0.0079(7)	−0.0026(7)
F(3)	0.0229(9)	0.0201(9)	0.0167(9)	−0.0006(7)	−0.0102(8)	−0.0024(8)
F(4)	0.0263(10)	0.0166(9)	0.0228(10)	0.0050(7)	0.0031(8)	−0.0097(8)

Atomic coordinates and displacement parameters of $ClF_2[OsF_6]$

Table S11. Atomic coordinates and equivalent isotropic displacement parameters U_{iso} of $ClF_2[OsF_6]$ at 100 K.

Atom	Position	*x*	*y*	*z*	U_{iso} / Å^2
Os(1)	2*f*	1/2	0.11041(6)	3/4	0.01423(15)
Os(2)	4*g*	0.83507(2)	0.88709(5)	0.90293(3)	0.01349(14)
Cl(1)	2*e*	1	0.5889(4)	3/4	0.0152(4)
Cl(2)	4*g*	0.66785(10)	0.4982(3)	0.60451(17)	0.0152(3)
F(1)	4*g*	0.9304(3)	0.4056(7)	0.7723(5)	0.0225(10)
F(2)	4*g*	0.7363(3)	0.6096(8)	0.5383(5)	0.0242(11)
F(3)	4*g*	0.6017(3)	0.3870(8)	0.4734(5)	0.0265(11)
F(4)	4*g*	0.4273(3)	−0.1214(8)	0.7885(6)	0.0281(11)
F(5)	4*g*	0.5718(3)	0.1180(8)	0.9287(5)	0.0264(11)
F(6)	4*g*	0.5729(3)	0.3548(8)	0.7107(5)	0.0244(10)
F(7)	4*g*	0.7586(3)	0.6448(8)	0.8008(5)	0.0226(10)
F(8)	4*g*	0.9106(3)	1.1201(8)	1.0011(5)	0.0246(11)
F(9)	4*g*	0.9092(3)	0.6499(8)	1.0024(5)	0.0217(9)
F(10)	4*g*	0.7670(3)	0.8875(8)	1.0222(5)	0.0229(10)
F(11)	4*g*	0.7610(3)	1.1200(8)	0.7982(5)	0.0247(11)
F(12)	4*g*	0.9031(3)	0.8738(7)	0.7788(5)	0.0203(10)

Table S12. Anisotropic displacement parameters of $ClF_2[OsF_6]$ at 100 K.

Atom	U_{11} / Å^2	U_{22} / Å^2	U_{33} / Å^2	U_{23} / Å^2	U_{13} / Å^2	U_{12} / Å^2
Os(1)	0.0129(2)	0.0147(2)	0.0171(2)	0	0.00749(16)	0
Os(2)	0.01222(19)	0.0148(2)	0.01500(18)	−0.00028(8)	0.00640(12)	0.00018(8)
Cl(1)	0.0140(10)	0.0162(10)	0.0162(10)	0	0.0057(8)	0
Cl(2)	0.0137(8)	0.0161(7)	0.0165(7)	−0.0006(5)	0.0058(6)	0.0001(6)
F(1)	0.022(2)	0.021(2)	0.028(3)	−0.0067(17)	0.013(2)	0.0002(17)
F(2)	0.025(2)	0.026(2)	0.028(3)	−0.0013(18)	0.019(2)	0.0011(18)
F(3)	0.027(2)	0.027(2)	0.020(2)	−0.0014(18)	−0.001(2)	−0.0031(17)
F(4)	0.030(3)	0.025(2)	0.031(3)	−0.0088(19)	0.012(2)	0.0045(19)
F(5)	0.031(3)	0.026(2)	0.020(2)	−0.0023(19)	0.005(2)	−0.0030(17)
F(6)	0.021(2)	0.024(2)	0.033(3)	−0.0022(18)	0.016(2)	0.000(2)
F(7)	0.019(2)	0.025(2)	0.023(2)	−0.0022(18)	0.0055(19)	−0.0011(19)
F(8)	0.026(2)	0.022(2)	0.025(3)	−0.0102(18)	0.006(2)	−0.0053(18)
F(9)	0.018(2)	0.024(2)	0.022(2)	0.0042(18)	0.0041(18)	0.0049(19)
F(10)	0.025(2)	0.027(2)	0.024(2)	−0.0033(18)	0.019(2)	0.0003(17)
F(11)	0.024(2)	0.025(2)	0.027(3)	0.0108(18)	0.011(2)	0.0072(18)
F(12)	0.021(2)	0.024(2)	0.023(2)	0.0038(17)	0.0182(19)	0.0010(17)

Atomic coordinates and displacement parameters of $ClF_2[RuF_6]$

Table S13. Atomic coordinates and equivalent isotropic displacement parameters U_{iso} of $ClF_2[RuF_6]$ at 143 K.

Atom	Position	*x*	*y*	*z*	U_{iso} / Å^2
Ru(1)	8*f*	0.37586(2)	0.38473(3)	0.52507(2)	0.01333(7)
Cl(1)	4*d*	1/2	0.08651(12)	3/4	0.01536(15)
Cl(2)	4*c*	1/4	0	0.74337(7)	0.01517(15)
F(1)	8*f*	0.55205(7)	−0.0998(2)	0.80308(14)	0.0256(3)
F(2)	8*f*	0.30012(7)	0.1118(2)	0.84233(15)	0.0299(3)
F(3)	8*f*	0.42728(7)	0.3694(2)	0.67744(13)	0.0220(3)
F(4)	8*f*	0.31967(7)	0.1422(2)	0.59192(15)	0.0264(3)
F(5)	8*f*	0.43147(8)	0.6153(2)	0.46247(15)	0.0305(4)
F(6)	8*f*	0.43068(7)	0.1502(2)	0.45851(14)	0.0264(3)
F(7)	8*f*	0.32474(7)	0.3876(2)	0.37973(14)	0.0279(3)
F(8)	8*f*	0.32168(7)	0.6113(3)	0.59807(16)	0.0315(4)

Table S14. Anisotropic displacement parameters of $ClF_2[RuF_6]$ at 143 K.

Atom	U_{11} / Å^2	U_{22} / Å^2	U_{33} / Å^2	U_{23} / Å^2	U_{13} / Å^2	U_{12} / Å^2
Ru(1)	0.01386(11)	0.01235(11)	0.01379(11)	−0.00052(6)	0.00003(7)	−0.00032(6)
Cl(1)	0.0168(3)	0.0151(3)	0.0142(3)	0	−0.0002(3)	0
Cl(2)	0.0164(3)	0.0134(3)	0.0157(3)	0	0	−0.0013(3)
F(1)	0.0308(7)	0.0207(7)	0.0253(8)	0.0015(6)	−0.0050(6)	0.0083(6)
F(2)	0.0370(8)	0.0286(8)	0.0242(8)	−0.0052(6)	−0.0137(7)	−0.0040(6)
F(3)	0.0238(6)	0.0228(7)	0.0195(7)	−0.0032(6)	−0.0060(6)	0.0033(5)
F(4)	0.0233(7)	0.0277(7)	0.0282(8)	0.0049(6)	0.0059(6)	−0.0088(6)
F(5)	0.0364(8)	0.0257(8)	0.0294(9)	0.0057(6)	0.0004(7)	−0.0144(6)
F(6)	0.0290(7)	0.0254(7)	0.0249(8)	−0.0058(6)	0.0071(6)	0.0065(6)
F(7)	0.0354(8)	0.0259(7)	0.0223(8)	0.0011(6)	−0.0132(7)	−0.0020(6)
F(8)	0.0329(8)	0.0303(8)	0.0314(9)	−0.0083(7)	−0.0017(7)	0.0155(6)

Atomic coordinates and displacement parameters of $ClF_2[Ta_2F_{11}]$

Table S15. Atomic coordinates and equivalent isotropic displacement parameters U_{iso} of $ClF_2[Ta_2F_{11}]$ at 100 K.

Atom	Position	*x*	*y*	*z*	U_{iso} / Å^2
Ta(1)	4*e*	0.65525(2)	0.80887(2)	0.41494(2)	0.00809(3)
Ta(2)	4*e*	0.37282(2)	0.53521(2)	0.24433(2)	0.00751(3)
Cl(1)	4*e*	0.72732(8)	0.30886(6)	0.41680(4)	0.01025(10)
F(1)	4*e*	0.8566(2)	0.40234(18)	0.35840(12)	0.0192(3)
F(2)	4*e*	0.8693(2)	0.2410(2)	0.48627(12)	0.0204(3)
F(3)	4*e*	0.4715(2)	0.69133(16)	0.33732(11)	0.0140(3)
F(4)	4*e*	0.8081(2)	0.76092(19)	0.32042(12)	0.0181(3)
F(5)	4*e*	0.8125(2)	0.91473(18)	0.48821(11)	0.0163(3)
F(6)	4*e*	0.5637(2)	0.96589(16)	0.34531(11)	0.0143(3)
F(7)	4*e*	0.7015(2)	0.62868(17)	0.47386(12)	0.0193(3)
F(8)	4*e*	0.4658(2)	0.82867(16)	0.50101(11)	0.0137(3)
F(9)	4*e*	0.5785(2)	0.58112(17)	0.18116(11)	0.0155(3)
F(10)	4*e*	0.5151(2)	0.40980(17)	0.32579(11)	0.0141(3)
F(11)	4*e*	0.1956(2)	0.51956(19)	0.33081(11)	0.0167(3)
F(12)	4*e*	0.2575(2)	0.68538(17)	0.18039(11)	0.0175(3)
F(13)	4*e*	0.3076(2)	0.38734(16)	0.16307(11)	0.0146(3)

Table S16. Anisotropic displacement parameters of $ClF_2[Ta_2F_{11}]$ at 100 K.

Atom	U_{11} / Å^2	U_{22} / Å^2	U_{33} / Å^2	U_{23} / Å^2	U_{13} / Å^2	U_{12} / Å^2
Ta(1)	0.00793(4)	0.00864(4)	0.00769(4)	−0.00042(3)	0.00037(3)	−0.00057(3)
Ta(2)	0.00709(4)	0.00775(4)	0.00766(4)	−0.00037(3)	−0.00015(3)	−0.00025(3)
Cl(1)	0.0092(2)	0.0109(2)	0.0107(2)	0.00169(18)	0.00128(18)	0.0009(2)
F(1)	0.0144(8)	0.0204(8)	0.0233(8)	0.0049(7)	0.0065(6)	−0.0050(7)
F(2)	0.0130(8)	0.0270(9)	0.0210(8)	0.0071(7)	−0.0041(6)	0.0053(7)
F(3)	0.0124(7)	0.0138(7)	0.0155(7)	−0.0054(6)	−0.0014(6)	−0.0014(6)
F(4)	0.0133(8)	0.0208(8)	0.0210(8)	−0.0032(6)	0.0088(6)	−0.0006(6)
F(5)	0.0144(8)	0.0188(7)	0.0153(7)	−0.0017(6)	−0.0034(6)	−0.0050(6)
F(6)	0.0150(7)	0.0123(7)	0.0154(7)	0.0033(6)	−0.0009(6)	0.0005(6)
F(7)	0.0279(9)	0.0125(7)	0.0173(8)	0.0024(6)	−0.0037(7)	0.0026(7)
F(8)	0.0143(7)	0.0145(7)	0.0127(7)	−0.0018(6)	0.0047(6)	−0.0015(6)
F(9)	0.0139(7)	0.0165(7)	0.0166(7)	−0.0008(6)	0.0064(6)	−0.0039(6)
F(10)	0.0134(7)	0.0137(7)	0.0148(7)	0.0027(6)	−0.0031(6)	0.0022(6)
F(11)	0.0113(7)	0.0237(8)	0.0153(7)	−0.0007(6)	0.0042(6)	−0.0010(6)
F(12)	0.0225(9)	0.0137(7)	0.0158(7)	0.0018(6)	−0.0044(6)	0.0064(6)
F(13)	0.0170(8)	0.0125(7)	0.0140(7)	−0.0036(6)	−0.0021(6)	−0.0023(6)

Atomic coordinates and displacement parameters of $ClF_2[AuF_4]$

Table S17. Atomic coordinates and equivalent isotropic displacement parameters U_{iso} of $ClF_2[AuF_4]$ at 100 K.

Atom	Position	*x*	*y*	*z*	U_{iso} / Å^2
Au(1)	4*e*	0.45927(4)	0.23866(3)	0.56562(2)	0.01665(9)
Cl(1)	4*e*	0.0915(3)	0.66158(17)	0.64362(11)	0.0183(3)
F(1)	4*e*	0.3961(7)	0.6583(5)	0.7111(3)	0.0235(8)
F(2)	4*e*	0.0171(8)	0.8681(5)	0.6608(3)	0.0271(8)
F(3)	4*e*	0.3342(7)	0.3563(4)	0.4484(3)	0.0204(7)
F(4)	4*e*	0.1550(7)	0.3723(4)	0.6215(3)	0.0234(8)
F(5)	4*e*	0.5834(8)	0.1256(5)	0.6794(3)	0.0237(8)
F(6)	4*e*	0.7634(7)	0.1122(5)	0.5122(3)	0.0235(8)

Table S18. Anisotropic displacement parameters of $ClF_2[AuF_4]$ at 100 K.

Atom	U_{11} / Å^2	U_{22} / Å^2	U_{33} / Å^2	U_{23} / Å^2	U_{13} / Å^2	U_{12} / Å^2
Au(1)	0.01710(12)	0.01611(12)	0.01718(14)	−0.00022(8)	0.00387(9)	0.00110(7)
Cl(1)	0.0190(6)	0.0170(6)	0.0196(7)	−0.0006(5)	0.0043(5)	0.0014(4)
F(1)	0.0208(16)	0.0289(19)	0.021(2)	0.0003(15)	0.0022(15)	−0.0017(13)
F(2)	0.0329(19)	0.0174(17)	0.032(2)	−0.0038(16)	0.0082(17)	0.0028(13)
F(3)	0.0200(15)	0.0240(17)	0.0173(19)	0.0018(14)	0.0029(14)	−0.0006(12)
F(4)	0.0190(15)	0.0200(16)	0.034(2)	−0.0014(15)	0.0126(15)	0.0019(12)
F(5)	0.0268(17)	0.0264(18)	0.019(2)	0.0029(15)	0.0086(15)	0.0037(13)
F(6)	0.0196(15)	0.0216(16)	0.032(2)	0.0005(15)	0.0112(15)	0.0046(12)

Comparison of Cl−F and *M*−F bond lengths and Cl···F distances as well as F−Cl−F and F···Cl···F angles of previously reported crystal structures and redetermined crystal structures of difluorochloronium(III) fluoridometallates

Table S19. Comparison of previously reported and redetermined bond lengths, distances and angles of ClF_2^+ cations in difluorochloronium(III) fluoridometallates. r.t.: room temperature.

Compound	*d*(Cl−F) / Å	*d*(Cl···F) / Å	∡(F−Cl−F) / °	∡(F···Cl···F) / °	*T* / K	Reference
$ClF_2[SbF_6]$	1.555(4), 1.560(4)	2.302(4), 2.312(4)	97.0(2)	90.66(14)	100	this work
$ClF_2[SbF_6]$	1.57(3), 1.58(3)	2.33(3), 2.43(3)	95.9(31)	89.9(19)	r.t.	[1]
$ClF_2[BiF_6]$	1.568(3), 1.573(3)	2.252(3), 2.254(3)	95.90(19)	90.88(12)	100	this work
$ClF_2[BiF_6]$	1.55(2), 1.55(2)	2.24(2), 2.25(2)	96.4(10)	90.4(10)	213	[2]
$ClF_2[NbF_6]$	1.5714(2)	2.2335(7)	96.00(6)	93.62(4)	100	this work
$ClF_2[NbF_6]$	1.574(4)	2.23(6)	96.4(3)	94.2(4)	r.t.	[3]
$ClF_2[TaF_6]$	1.5677(18)	2.252(2)	96.45(15)	93.47(10)	100	this work
$ClF_2[TaF_6]$	1.54(1)	2.24(6)	98.3(10)	96.5(5)	183	[3]
$ClF_2[OsF_6]$	1.567(5), 1.572(5), 1.576(5)	2.260(5), 2.269(5), 2.288(4)	97.5(4), 97.0(3)	90.0(2), 90.8(2)	100	this work
$ClF_2[OsF_6]$	1.38(7)	2.44, 2.52	125(3)	137	183	[4]
$ClF_2[RuF_6]$	1.565(2), 1.568(1)	2.248(2), 2.271(1)	96.80(13), 96.29(11)	89.92(8), 91.25(7)	143	this work
$ClF_2[RuF_6]$	1.565(3), 1.568(3)	2.297(3), 2.263(4)	96.4(3), 96.4(3)	90.9(2), 92.3(2)	r.t.	[5]

Table S20. Comparison of previously reported and redetermined *M*−F bond lengths in the fluoridometallate anions of different difluorochloronium(III) compounds. r.t.: room temperature.

Compound	*d*(*M*−F) / Å	*T* / K	Reference
$ClF_2[SbF_6]$	1.865(4)-1.901(3)	100	this work
$ClF_2[SbF_6]$	1.78(3)-1.93(3)	r.t.	[1]
$ClF_2[BiF_6]$	1.958(3)-2.026(3)	100	this work
$ClF_2[BiF_6]$	1.93(2)-2.01(2)	213	[2]
$ClF_2[NbF_6]$	1.850(1)-1.949(1)	100	this work
$ClF_2[NbF_6]$	1.847(4)-1.952(3)	r.t.	[3]
$ClF_2[TaF_6]$	1.862(2)-1.949(2)	100	this work
$ClF_2[TaF_6]$	1.82(2)-1.93(1)	183	[3]
$ClF_2[OsF_6]$	1.852(4)-1.919(4)	100	this work
$ClF_2[OsF_6]$	1.84(3)	183	[4]
$ClF_2[RuF_6]$	1.819(1)-1.896(1)	143	this work
$ClF_2[RuF_6]$	1.810(3)-1.886(3)	r.t.	[5]

Basis set details for quantum-chemical solid-state calculations

TZVP basis set for B

We modified the molecular def2-TZVP basis by removing the outermost s-function with an exponent of 0.06, leaving still three s-functions in the valence space. The exponents of the outermost s and p functions were fixed to 0.17 and the exponents of the other s and p functions in the valence space were reoptimized for the boron atom in its ground state. Finally, the outermost s and p functions were combined into a single sp-type function to increase the efficiency of the CRYSTAL code. The resulting energy loss w.r.t the unmodified basis set is 15 mH. The final basis set in CRYSTAL input format is as follows:

```
5 7
0 0 6 2.0 1.0
  8564.8660687      0.22837198155E-03
  1284.1516263      0.17682576447E-02
  292.27871604      0.91407080516E-02
  82.775469176      0.36342638989E-01
  27.017939269      0.11063458441
  9.8149619660      0.23367344321
0 0 2 2.0 1.0
  3.9295537119      0.41818777978
  1.6980409139      0.22325473798
0 0 1 0.0 1.0
 0.57483069645      1.0000000000
0 1 1 0.0 1.0
 0.17000000000      1.0 1.0
0 2 3 1.0 1.0
  28.577505088      0.50265575179E-02
  6.7104492541      0.32801738965E-01
  2.0721954358      0.13151230768
0 2 1 0.0 1.0
 0.64922416350      1.0000000000
0 3 1 0.0 1.0
 0.50000000000      1.0000000000
```

TZVP basis set for As

The starting point was the molecular def-TZVP basis. The exponents of the outermost s and p functions were fixed to 0.13 and the exponents of the other s and p functions in the valence space were reoptimized for the arsenic atom in its ground state. The exponent of the outermost d primitive was kept fixed, while the exponents of the other d functions were optimised for the arsenic atom in its ground state. An f-type polarization function with an exponent of 0.433 was added (def2-TZVP basis set). Finally, the outermost s and p functions were combined into a single sp-type function to increase the efficiency of the CRYSTAL code. The resulting energy loss w.r.t unmodified def2-TZVP basis set is 0.2 mH. The final basis set in CRYSTAL input format is as follows:

```
33 14
0 0 8 2.0 1.0
  498032.42158      0.22740196900E-03
  74656.868743      0.17632816413E-02
  16990.960004      0.91728040381E-02
  4809.6200321      0.37337829344E-01
  1566.2887055      0.12199536117
  563.21360499      0.29137475324
  219.11179978      0.42326351479
  86.866061030      0.22921464278
0 0 4 2.0 1.0
  538.19512479     -0.25254197297E-01
  167.14850224     -0.11915461115
  27.605517159      0.54628495980
  11.947858521      0.53001520976
0 0 2 2.0 1.0
  18.538023133     -0.23479188136
  3.2018985739      0.69167053428
0 0 1 2.0 1.0
  1.4362581800       1.0000000000
0 0 1 0.0 1.0
 0.35310762320       1.0000000000
0 1 1 0.0 1.0
 0.13000000000       1.0 1.0
0 2 6 6.0 1.0
  2678.9421546      0.23318955287E-02
  634.61765840      0.19042149977E-01
  203.93967606      0.90229744913E-01
  76.323890369      0.26169037693
  30.664124943      0.41857168155
  12.505056732      0.23447830190
0 2 4 6.0 1.0
  49.256229549     -0.21235539870E-01
  7.7274891466      0.30470206668
  3.5410493476      0.52888373107
```

8

```
  1.6985585501      0.37272250955
0 2 1 3.0 1.0
 0.80396418504       1.0000000000
0 2 1 0.0 1.0
 0.41045871535       1.0000000000
0 3 5 10.0 1.0
  139.05230680      0.99291144106E-02
  41.113850141      0.66568843496E-01
  15.035409461      0.22275768307
  5.9891096071      0.40309224382
  2.4322147899      0.41671667946
0 3 1 0.0 1.0
 0.96247584610       1.0000000000
0 3 1 0.0 1.0
 0.29300000000       1.0000000000
0 4 1 0.0 1.0
 0.43271941          1.0
```

TZVP basis set for F

The basis set for F was taken from a previous study.[6]

TZVP basis set for Cl

The basis set for Cl was taken from a previous study.[7]

TZVP basis set for Sb

The def2-TZVP basis set with a 28-electron effective core potential was used as a starting point. We fixed the exponents of the outermost s and p functions to 0.11 and reoptimized the exponents of the other s and p functions in the valence space for the antimony atom in its ground state. Finally, the outermost s and p functions were combined into one sp-type function. The resulting energy loss with respect to the original molecular basis set is 4.7 mH. The exponent of the outermost d-function was increased from 0.14 to 0.217. The energy cost of this change was only 0.14 mH. The steep f-type polarization function with an exponent of 1.1 was removed. The final basis set in CRYSTAL input format is as follows:

```
251 13
INPUT
23. 0 2 4 4 2 0
16.330865  281.071581 0
8.556542    61.716604 0
14.470337   67.457380 0
13.816194  134.933503 0
8.424924    14.716344 0
8.092728    29.518512 0
14.886331   35.447815 0
15.146319   53.143466 0
5.908267     9.179223 0
5.594322    13.240253 0
14.444978  -15.366801 0
14.449295  -20.296138 0
0 0 4 2.0 1.0
  1612.4199933      0.28540380783E-03
  238.84452097      0.13393778746E-02
  23.998118809     -0.49388154574E-01
  15.193124213      0.43392227254
0 0 2 2.0 1.0
  11.731361334      0.92125519965
  6.5268387226      0.79235280226
0 0 1 0.0 1.0
 2.0178590021       1.0000000000
0 0 1 0.0 1.0
 0.96219277446       1.0000000000
0 0 1 0.0 1.0
 0.28581551962       1.0000000000
0 1 1 0.0 1.0
 0.11                1.0 1.0
0 2 3 6.0 1.0
  215.68393354      0.26051823221E-03
  16.374479088      0.73728000195E-01
  9.7216283345     -0.27230028128
0 2 3 3.0 1.0
  2.7979771259      0.46472692374
  1.4696586758      0.50364242075
 0.74906751891      0.18706666294
0 2 1 0.0 1.0
  0.32300924430     1.0000000000
0 3 6 10.0 1.0
  115.90312253      0.53140915051E-03
  30.474233720      0.59411139166E-02
  18.228418239     -0.10563706947E-01
```

```
  4.3291456646      0.20348177341
  2.1294818496      0.42748378928
 0.99682636692      0.38539560809
0 3 1 0.0 1.0
 0.43347239863      1.0000000000
0 3 1 0.0 1.0
 0.216736199315     1.0000000000
0 4 1 0.0 1.0
 0.32369706         1.0000000000
```

TZVP basis set for Bi

The def2-TZVP basis set with a 60-electron effective core potential was used as a starting point.[8] We fixed the exponents of the outermost s and p functions to 0.10 and reoptimized the exponents of the other s and p functions in the valence space for the bismuth atom in its ground state. Finally, the outermost s and p functions were combined into one sp-type function. The resulting energy loss with respect to the original molecular basis set is 3.5 mH. The exponent of the outermost d-function was increased from 0.14 to 0.165. The energy cost of this change was only 0.03 mH. The steep f-type polarization function with an exponent of 1.05 was removed. The final basis set in CRYSTAL input format is as follows:

```
283 13
INPUT
23. 0 2 4 4 2 2
13.043090 283.264227 0
8.221682   62.471959 0
10.467777  72.001499 0
9.118901  144.002277 0
6.754791    5.007945 0
6.252592    9.991550 0
8.081474   36.396259 0
7.890595   54.597664 0
4.955556    9.984294 0
4.704559   14.981485 0
4.214546   13.713383 0
4.133400   18.194308 0
6.205709  -10.247443 0
6.227782  -12.955710 0
0 0 4 2.0 1.0
  716.41435310      0.31254307133E-03
  83.806059047      0.17624768946E-02
  21.116962853     -0.21910983437
  15.491448187      0.40411224931
0 0 2 2.0 1.0
  23.213322651     -0.68255758685E-01
  6.6412776932      0.97888046471
0 0 1 0.0 1.0
 1.7668753097       1.0000000000
0 0 1 0.0 1.0
 0.87636753866      1.0000000000
0 0 1 0.0 1.0
 0.26185055933      1.0000000000
0 1 1 0.0 1.0
 0.10               1.0 1.0
0 2 3 6.0 1.0
  15.249644669      0.74560356000
  14.846176053     -0.85578637338
  7.0636826784      0.40149159592
0 2 3 3.0 1.0
  2.5802708340      0.35542729633
  1.4990870077      0.63976991890
 0.75411119473      0.32332773839
0 2 1 0.0 1.0
  0.29617825843     1.0000000000
0 3 6 10.0 1.0
  66.404481948      0.38102878348E-03
  13.858426961      0.10746152442E-01
  7.0654519000     -0.71947646845E-01
  2.5252144035      0.26195974989
  1.3419585000      0.42594750000
 0.68340941000      0.33680325627
0 3 1 0.0 1.0
 0.32934755420      1.0000000000
0 3 1 0.0 1.0
 0.1646737771     1.0000000000
0 4 1 0.0 1.0
 0.31271            1.0000000000
```

10

TZVP basis set for Nb

The basis set was derived from the molecular Karlsruhe def2-TZVP basis set (28-electron effective core potential). The diffuse outermost s-exponents were increased from 0.033 and 0.086 to 0.13 and 0.30, respectively. The outermost p-type function with an exponent of 0.03 was removed and the exponents of the two remaining outermost p-type functions were changed from 0.09 to 0.13 and 0.2797 to 0.30. The two outermost s and p functions were both then combined into two sp-type functions. The most diffuse d-type function (exponent 0.10) was removed and the inner (3d) function was decontracted to (2d1d). The f-type polarization function was removed. The final basis set in CRYSTAL input format is as follows:

```
241 9
INPUT
13. 0 2 2 2 2 0
8.900000 165.179143 0
4.430000 21.992974 0
7.770000 111.794414 0
3.960000 16.633483 0
6.050000 38.112249 0
2.840000 8.039167 0
8.490000 -22.929550 0
4.250000 -3.666310 0
0 0 2 2.0 1.0
  12.000000000      -0.20219507530
  10.500000000       0.33640105939
0 0 1 2.0 1.0
  3.9276062854       1.0000000000
0 0 1 0.0 1.0
 0.85976543258       1.0000000000
0 1 1 0.0 1.0
 0.30                1.0 1.0
0 1 1 0.0 1.0
 0.13                1.0 1.0
0 2 4 6.0 1.0
  9.2056285646       0.43347689874E-01
  4.8679632125      -0.21302479233
  1.2442155792       0.48102127136
 0.60390590312       0.53917858960
0 3 2 3.0 1.0
  4.6170975867      -0.13574476955E-01
  1.5663438480       0.20374310496
0 3 1 0.0 1.0
 0.66952425826       0.42997453105
0 3 1 0.0 1.0
 0.27140946867       1.0000000000
```

TZVP basis set for Ta

The basis set was derived from the molecular Karlsruhe def2-TZVP basis set (60-electron effective core potential). The diffuse outermost s- and p-type functions with exponents of 0.039 and 0.065 were removed. The exponent of the outermost s-type function was increased from 0.10 and 0.11. The exponent of the outermost p-type function was changed from 0.27 to 0.11 and combined with the outermost s function into a single sp-type function. The most diffuse d-type function (exponent 0.088) was removed and the inner (3d) function was decontracted to (2d1d). The f-type polarization function was removed. The final basis set in CRYSTAL input format is as follows:

```
273 10
INPUT
13. 0 2 2 2 1 1
14.546408 1345.880647 0
7.273204 36.766806 0
9.935565 378.425301 0
4.967782 22.293091 0
6.347377 104.883956 0
3.173688 8.755848 0
2.017881 12.017961 0
3.040330 -11.728933 0
0 0 4 2.0 1.0
  24.473650944       0.20590322488
  18.721372549      -0.74670795514
  11.500000000        3.4071363897
  10.350000000       -2.8175487609
0 0 1 2.0 1.0
  3.8436180089        1.0000000000
0 0 1 0.0 1.0
  1.0202266016        1.0000000000
0 0 1 0.0 1.0
 0.46774781869        1.0000000000
0 1 1 0.0 1.0
  0.11                1.0 1.0
```

11

```
0 2 4 6.0 1.0
  17.000000000     -0.32577305616E-01
  12.008186536      0.10336287365
  5.0278760583     -0.28526521696
  1.1937124184      0.51790141155
0 2 1 0.0 1.0
 0.57889707053       1.0000000000
0 3 2 3.0 1.0
  3.9738796278     -0.52799310714E-01
  1.4528884813      0.18558319471
0 3 1 0.0 1.0
 0.61042908544      0.42959071631
0 3 1 0.0 1.0
 0.24216276510       1.0000000000
```

TZVP basis set for Ir

The basis set was derived from the molecular Karlsruhe def2-TZVP basis set (60-electron effective core potential). The diffuse outermost s- and p-type functions with exponents of 0.05 and 0.056 were removed. The exponent of the outermost p-type function was changed from 0.33 to 0.14 and it was combined with the outermost s function into a single sp-type function. The exponents of the two outermost d-type functions were increased to 0.18 and 0.36. The f-type polarization function was removed. The final basis set in CRYSTAL input format is as follows:

```
277 10
INPUT
17. 0 2 2 2 1 1
13.652203 732.269200 0
6.826101 26.484721 0
10.279868 299.489474 0
5.139934 26.466234 0
7.349859 124.457595 0
3.674929 14.035995 0
3.034072 21.531031 0
4.808857 -21.607597 0
0 0 3 2.0 1.0
  30.000000000      0.30797903228
  27.000000000     -0.46726361781
  13.961973911      0.47161003146
0 0 1 2.0 1.0
  5.3956977802       1.0000000000
0 0 1 0.0 1.0
  1.2149128721       1.0000000000
0 0 1 0.0 1.0
 0.55885743756       1.0000000000
0 1 1 0.0 1.0
 0.14097974313       1.0 1.0
0 2 4 6.0 1.0
  15.902664143     -0.16290720099
  14.415830698      0.23483212987
  5.7597608991     -0.30305337176
  1.5008913108      0.55512982069
0 2 1 0.0 1.0
 0.72348035957       1.0000000000
0 3 4 7.0 1.0
  8.6321692504      0.75000099949E-01
  6.5898192302     -0.17326965173
  1.5808379663      0.55065196913
 0.71827834905      0.85273641436
0 3 1 0.0 1.0
 0.36                1.0000000000
0 3 1 0.0 1.0
 0.18                1.0000000000
```

TZVP basis set for Ru

The basis set was derived from the molecular Karlsruhe def2-TZVP basis set (28-electron effective core potential). The diffuse outermost s-exponents were increased from 0.039 and 0.107 to 0.13 and 0.26, respectively. The outermost p-type function with an exponent of 0.037 was removed and the exponents of the two remaining outermost p-type functions were changed from 0.115 to 0.13 and 0.367 to 0.26. The two outermost s and p functions were then combined into two sp-type functions. The exponent of the outermost d-type function (exponent 0.15) increased to 0.20. The f-type polarization function was removed. The final basis set in CRYSTAL input format is as follows:

```
244 10
INPUT
16. 0 2 2 2 2 0
11.105269 209.822971 0
5.414745 30.654726 0
9.771271 146.336182 0
```

```
5.073991 24.127877 0
7.671423 67.515897 0
4.136565 9.870104 0
11.360000 -28.340616 0
5.680000 -4.944629 0
0 0 2 2.0 1.0
  16.000000000      -0.20634002919
  13.910581694       0.33550437725
0 0 1 2.0 1.0
  4.7967971407        1.0000000000
0 0 1 0.0 1.0
  1.1555425594        1.0000000000
0 0 1 0.0 1.0
 0.52455741182        1.0000000000
0 1 1 0.0 1.0
 0.26                1.0 1.0
0 1 1 0.0 1.0
 0.13                1.0 1.0
0 2 4 6.0 1.0
  11.187208671       0.53225073263E-01
  6.2477688734      -0.22731662050
  1.6279472859       0.47869486056
 0.79326493538       0.50213311567
0 3 3 6.0 1.0
  5.7341846619      -0.35266111560E-01
  2.2483686294       0.21802502222
 0.98376978359       0.44709565013
0 3 1 0.0 1.0
 0.40379445583       1.0000000000
0 3 1 0.0 1.0
 0.2                 1.0000000000
```

TZVP basis set for Os

The basis set was derived from the molecular Karlsruhe def2-TZVP basis set (60-electron effective core potential). The diffuse outermost s- and p-type functions with exponents of 0.047 and 0.052 were removed. The exponent of the outermost p-type function was changed from 0.31 to 0.13 and it was combined with the outermost s function into a single sp-type function. The most diffuse d-type function (exponent 0.11) was removed and the inner (4d) function was decontracted to (3d1d). The f-type polarization function was removed. The final basis set in CRYSTAL input format is as follows:

```
276 10
INPUT
16. 0 2 2 2 1 1
13.875754 885.405719 0
6.937877 25.967040 0
10.193793 320.083902 0
5.096896 26.148765 0
7.099238 115.044843 0
3.549619 13.622575 0
2.767075 18.909457 0
4.349905 -19.027595 0
0 0 3 2.0 1.0
  30.000000000       0.32213004804
  27.000000000      -0.47922918137
  13.524730005       0.47465946837
0 0 1 2.0 1.0
  5.2402883472        1.0000000000
0 0 1 0.0 1.0
  1.1306661245        1.0000000000
0 0 1 0.0 1.0
 0.51689966917        1.0000000000
0 1 1 0.0 1.0
 0.13222953545        1.0 1.0
0 2 4 6.0 1.0
  15.500000000       0.16016463376
  14.000000000      -0.23201520402
  5.5458290420       0.29772587274
  1.4139502215      -0.54253238176
0 2 1 0.0 1.0
 0.68136686765        1.0000000000
0 3 3 6.0 1.0
  8.2945059487       0.69648222110E-01
  6.3060397430      -0.16444229630
  1.4890109110       0.55154541033
0 3 1 0.0 1.0
 0.67315390607       0.88461370291
0 3 1 0.0 1.0
 0.22                1.0000000000
```

TZVP basis set for Au

The basis set for Au was taken from a previous study.[9]

Lattice parameters and atomic coordinates of optimized solid-state structures of difluorochloronium(III) fluoridometallates

Lattice parameters and atomic coordinates of the optimized solid-state structure of $ClF_2[AsF_6]$

The initial parameters for the optimization were taken from a previous study on the crystal structure of $ClF_2[AsF_6]$.[10]

Space group *A*2/*a* (No. 15)
a = 9.96746020 Å, *b* = 7.77648472 Å, *c* = 8.13775233 Å, *β* = 113.838954°, *V* = 576.95760553 Å^3

Table S21. Atomic coordinates of the optimized structure of $ClF_2[AsF_6]$.

Atom	*x*	*y*	*z*
As	1.407774254564E−20	−3.969122116057E−36	4.692873032087E−20
Cl	2.500000000000E−01	3.502486536049E−01	0.000000000000E+00
F	1.655574002924E−01	4.879221990369E−01	6.826589580577E−02
F	1.315209090597E−01	1.612039855302E−01	1.092623517970E−01
F	−3.166120581946E−02	−2.660924964998E−02	1.910606999496E−01
F	1.344348333220E−01	−1.528464639605E−01	7.727941401102E−02

Lattice parameters and atomic coordinates of the optimized solid-state structure of $ClF_2[SbF_6]$

Space group $P\bar{1}$ (No. 2)
a = 5.10740984 Å, *b* = 5.55662938 Å, *c* = 10.42149237 Å, *α* = 91.55214°, *β* = 94.21963°, *γ* = 94.21963°,
V = 294.673966 Å^3

Table S22. Atomic coordinates of the optimized structure of $ClF_2[SbF_6]$.

Atom	*x*	*y*	*z*
Sb	5.000000000000E−01	5.000000000000E−01	5.000000000000E−01
Sb	5.000000000000E−01	−5.000000000000E−01	−1.734723475977E−18
Cl	7.899141083252E−02	1.022957239390E−01	2.499951830422E−01
F	−3.303679670522E−01	3.338377771682E−01	−3.648939005436E−01
F	2.201532507940E−01	−4.448797604339E−01	−3.965889629050E−01
F	3.299141853448E−01	2.011124688114E−01	4.328398808398E−01
F	3.816580978285E−01	−2.270844139986E−01	8.591461512382E−02
F	3.611250070055E−01	2.930382003278E−01	1.270820549105E−01
F	−1.817958450578E−01	−4.722221915539E−01	1.032986309440E−01
F	−1.088460022539E−01	−3.181228191653E−02	3.432762167410E−01
F	−9.594713520301E−02	3.319654253396E−02	1.201886682221E−01

Lattice parameters and atomic coordinates of the optimized solid-state structure of $ClF_2[IrF_6]$

Space group *P*2/*n* (No. 13)
a = 6.76710531 Å, *b* = 5.61408895 Å, *c* = 7.59698521 Å, *β* = 94.728842°, *V* = 294.673966 Å^3

Table S23. Atomic coordinates of the optimized structure of $ClF_2[IrF_6]$.

Atom	*x*	*y*	*z*
Ir	−2.500000000000E−01	−3.764029688914E−01	−2.500000000000E−01
Cl	2.500000000000E−01	−9.766436081064E−02	−2.500000000000E−01
F	4.204351347737E−01	9.543702515543E−02	−1.997750252732E−01
F	4.816557538337E−01	−3.770058222953E−01	−1.844025219336E−01
F	−1.818677719188E−01	−1.433726987656E−01	−7.936078194352E−02
F	−3.150102964609E−01	3.936791723262E−01	−4.217092287333E−01

Lattice parameters and atomic coordinates of the optimized solid-state structure of $ClF_2[BiF_6]$

Space group $P\bar{1}$ (No. 2)
a = 5.17385522 Å, b = 5.67173636 Å, c = 10.60118031 Å, α = 91.134784°, β = 94.402826°, γ = 92.173406°,
V = 309.867180 Å^3

Table S24. Atomic coordinates of the optimized structure of $ClF_2[BiF_6]$.

Atom	*x*	*y*	*z*
Bi	−5.000000000000E−01	−5.000000000000E−01	5.000000000000E−01
Bi	−5.000000000000E−01	−5.000000000000E−01	−1.355252715607E−19
Cl	8.118861083488E−02	1.015000509084E−01	−2.492635862241E−01
F	−8.871092536118E−02	3.838425754563E−02	−3.792996142739E−01
F	−1.117857883388E−01	−3.451788293174E−02	−1.614221580022E−01
F	−3.832782287672E−01	2.134379969121E−01	4.149513950445E−01
F	3.605192492447E−01	2.912459275118E−01	−3.623777497121E−01
F	1.667465250802E−01	4.677711988322E−01	3.942411188935E−01
F	3.290097942853E−01	−3.284477630907E−01	−1.420590035762E−01
F	−2.088742580367E−01	4.398984368206E−01	−1.059224981674E−01
F	3.185118013241E−01	1.905683963064E−01	−6.950610782578E−02

Lattice parameters and atomic coordinates of the optimized solid-state structure of $ClF_2[NbF_6]$

Space group Pcca (No. 54)
a = 9.90628565 Å, b = 5.81344175 Å, c = 10.50747802 Å, V = 605.121610 Å^3

Table S25. Atomic coordinates of the optimized structure of $ClF_2[NbF_6]$.

Atom	*x*	*y*	*z*
Nb	−5.000000000000E−01	3.974050766058E−01	2.500000000000E−01
Cl	2.500000000000E−01	0.000000000000E+00	4.653771889127E−01
F	3.501782947433E−01	1.107426896912E−01	−4.307033844844E−01
F	3.860195814465E−01	1.508075264452E−01	3.240496565045E−01
F	3.966357988433E−01	3.675184306410E−01	9.933800065631E−02
F	−3.841482204764E−01	−3.782067930929E−01	1.839623508743E−01

Lattice parameters and atomic coordinates of the optimized solid-state structure of $ClF_2[TaF_6]$

Space group Pcca (No. 54)
a = 9.91526412 Å, b = 5.78853361 Å, c = 10.55467008 Å, V = 605.783596 Å^3

Table S26. Atomic coordinates of the optimized structure of $ClF_2[TaF_6]$.

Atom	*x*	*y*	*z*
Ta	5.000000000000E−01	3.987403645311E−01	2.500000000000E−01
Cl	2.500000000000E−01	0.000000000000E+00	4.661805390966E−01
F	3.508366968864E−01	1.093820589685E−01	−4.307008731769E−01
F	3.869786977302E−01	1.509489284430E−01	3.250126821870E−01
F	3.943503864887E−01	3.702323985269E−01	1.006898545536E−01
F	−3.850356664682E−01	−3.754371907812E−01	1.823460156949E−01

Lattice parameters and atomic coordinates of the optimized solid-state structure of $ClF_2[RuF_6]$

Space group *P*cca (No. 54)
a = 19.62352498 Å, *b* = 5.67906871 Å, *c* = 10.55942761 Å, *V* = 1176.777952 Å^3

Table S27. Atomic coordinates of the optimized structure of $ClF_2[RuF_6]$.

Atom	*x*	*y*	*z*
Ru	3.760633111161E−01	3.815413059646E−01	−4.763623236917E−01
Cl	−5.000000000000E−01	9.578327011849E−02	−2.500000000000E−01
Cl	2.500000000000E−01	−7.011798060205E−20	−2.633090614837E−01
F	4.259044114363E−01	3.646656061046E−01	−3.190611486010E−01
F	3.015613520933E−01	1.100562250774E−01	−1.611344861520E−01
F	4.327726017204E−01	−3.843369945738E−01	4.645226156640E−01
F	3.189863908606E−01	1.327934404731E−01	−4.116733279607E−01
F	4.339651539104E−01	1.499608507601E−01	4.595126929519E−01
F	3.189153243324E−01	−3.950886276747E−01	−4.044012059828E−01
F	3.257509116280E−01	3.818622106460E−01	3.755336466210E−01
F	−4.461768318830E−01	−9.553118836647E−02	−1.997481053055E−01

Lattice parameters and atomic coordinates of the optimized solid-state structure of $ClF_2[OsF_6]$

Space group *P*2/*c* (No. 13)
a = 15.46839150 Å, *b* = 5.70840375 Å, *c* = 10.56789104 Å, *β* = 108.040419°, *V* = 887.268015 Å^3

Table S28. Atomic coordinates of the optimized structure of $ClF_2[OsF_6]$.

Atom	*x*	*y*	*z*
Os	−5.000000000000E−01	1.171883877137E−01	−2.500000000000E−01
Os	−1.651861936572E−01	−1.182275396901E−01	−9.513455152138E−02
Cl	−6.938893903907E−18	−4.031923558963E−01	−2.500000000000E−01
Cl	−3.289359609589E−01	4.991307351921E−01	−3.918109705774E−01
F	−7.232587257715E−02	4.070134163337E−01	−2.338580113340E−01
F	−2.503353319632E−01	−3.964666893166E−01	−4.448480019470E−01
F	−3.887357963250E−01	3.932757887536E−01	4.681856489095E−01
F	4.363631977037E−01	−1.117752991780E−01	−1.878700836873E−01
F	−4.078531709601E−01	1.246477241023E−01	−8.303621726198E−02
F	−4.375086949102E−01	3.665461342076E−01	−3.141245174713E−01
F	−2.471032957819E−01	−3.637950817813E−01	−1.928810389363E−01
F	−8.549676837996E−02	1.150975478979E−01	−2.479965096732E−03
F	−8.644138097050E−02	−3.564576376047E−01	1.142051398120E−03
F	−2.276841618310E−01	−1.162631476393E−01	3.147488055583E−02
F	−2.438241183072E−01	1.115372444419E−01	−1.980499007033E−01
F	−1.015180101339E−01	−1.369159478510E−01	−2.289240507879E−01

Lattice parameters and atomic coordinates of the optimized solid-state structure of $ClF_2[Ta_2F_{11}]$

Space group $P2_1/n$ (No. 14)
a = 7.64426077 Å, b = 9.20654475 Å, c = 14.0934171 Å, β = 92.87489°, V = 990.607324 Å^3

Table S29. Atomic coordinates of the optimized structure of $ClF_2[Ta_2F_{11}]$.

Atom	*x*	*y*	*z*
Ta	−3.418742080497E−01	−1.819841101271E−01	4.153948314722E−01
Ta	3.708534550108E−01	−4.650538031935E−01	2.423574714950E−01
Cl	−2.761079215982E−01	3.104360843153E−01	4.186739563322E−01
F	−1.448115929614E−01	4.058311945751E−01	3.590845274681E−01
F	−1.254705387824E−01	2.426150659468E−01	4.882576941438E−01
F	−1.916289787288E−01	−7.222830967676E−02	4.937703506352E−01
F	−1.831687596293E−01	−2.229445350978E−01	3.221323651722E−01
F	4.809340653822E−01	−3.054604055206E−01	3.325976123661E−01
F	−2.924314444075E−01	−3.645008873944E−01	4.729126894811E−01
F	−4.460043286915E−01	−2.804283892197E−02	3.446572899482E−01
F	−4.224295091804E−01	−4.220677293931E−01	1.774588288927E−01
F	4.609573353138E−01	−1.720181037945E−01	4.999614740555E−01
F	−4.812491327755E−01	4.124470520119E−01	3.285521945617E−01
F	2.000843978496E−01	−4.740209322751E−01	3.331882367565E−01
F	2.532808033505E−01	−3.147229622382E−01	1.765777820819E−01
F	3.013411558098E−01	3.811803453573E−01	1.652932501023E−01

Lattice parameters and atomic coordinates of the optimized solid-state structure of $ClF_2[AuF_4]$

Space group $P2_1/n$ (No. 14)
a = 4.53736957 Å, b = 7.36687133 Å, c = 14.88353039 Å, β = 97.928216°, V = 492.744851 Å^3

Table S30. Atomic coordinates of the optimized structure of $ClF_2[AuF_4]$.

Atom	*x*	*y*	*z*
Au	4.523547008176E−01	2.339633345233E−01	−4.358315218318E−01
Cl	8.547429294033E−02	−3.477932489622E−01	−3.564035688324E−01
F	3.957305057106E−01	−3.494018092128E−01	−2.885402742407E−01
F	3.359881235377E−01	3.627012144144E−01	4.462137278633E−01
F	1.399926127732E−02	−1.377615492169E−01	−3.379382378241E−01
F	1.434028051209E−01	3.672470472734E−01	−3.790611729806E−01
F	−2.405544244278E−01	1.096435283300E−01	−4.901269606933E−01
F	−4.314776796913E−01	1.134408174392E−01	−3.219267221362E−01

Lattice parameters and atomic coordinates of the optimized solid-state structure of $ClF_2[BF_4]$

The initial parameters for the optimization were taken from a previous study on the crystal structure of $ClF_2[BF_4]$.[11]

Space group $P2_1/c$ (No. 14)
a = 5.54722926 Å, b = 8.81209969 Å, c = 9.79693154 Å, β = 114.949886°, V = 434.208409 Å^3

Table S31. Atomic coordinates of the optimized structure of $ClF_2[BF_4]$.

Atom	*x*	*y*	*z*
B	−4.284788789383E−01	2.760149877712E−03	−1.802627986438E−01
CL	−1.694966089704E−01	2.188478708633E−01	1.151938687161E−01
F	−6.541076339537E−02	3.492594476082E−01	3.954928308500E−02
F	1.936606068491E−02	2.662184853066E−01	2.845127993837E−01
F	−3.507411892992E−01	−3.678593828630E−03	−2.947919721709E−01
F	2.988933730300E−01	−4.116696302980E−02	−2.333925002897E−01
F	−2.788928641418E−01	−8.812178521459E−02	−6.020995968458E−02
F	−4.142507683915E−01	1.560160334199E−01	−1.297185206882E−01

XYZ coordinates of geometry-optimized structures of gas-phase quantum-chemical calculations

XYZ coordinates of geometry-optimized $[ClF_2[AsF_6]_2]^-$ (C_2 point group)

Cl	0.0000000	−0.0000000	1.2095232
F	−1.4869455	−0.5677655	−0.1934962
F	1.4869455	0.5677655	−0.1934962
F	−1.0753396	−0.3949188	2.3223010
F	1.0753396	0.3949188	2.3223010
As	−3.1542547	0.2053383	−0.4374766
As	3.1542547	−0.2053383	−0.4374766
F	−3.4984168	−1.0938099	−1.5046659
F	−2.6371974	1.4302764	0.6733000
F	−4.6959963	0.9227304	−0.6430144
F	−2.4687894	1.1033602	−1.7288163
F	−3.6929540	−0.7444070	0.8956042
F	3.4984168	1.0938099	−1.5046659
F	2.6371974	−1.4302764	0.6733000
F	4.6959963	−0.9227304	−0.6430144
F	2.4687894	−1.1033602	−1.7288163
F	3.6929540	0.7444070	0.8956042

XYZ coordinates of geometry-optimized $[ClF_2[SbF_6]_2]^-$ (C_1 point group)

Sb	−0.0869903	−0.1653929	−3.3438191
F	1.5452833	−0.8627714	−2.6989150
F	−1.7347122	0.6234200	−3.7626223
F	0.2037761	−0.7923505	−5.0865709
F	−0.3438838	0.5016087	−1.4812376
F	−0.9543289	−1.7431097	−2.8234212
F	0.7818861	1.4636119	−3.7002915
Cl	1.0689951	0.5127866	0.1057741
F	−0.0262627	−0.7158590	1.4553253
F	1.9451898	1.4398166	−0.8511807
F	2.1732235	0.5629018	1.2556091
Sb	−0.6907751	−0.2114293	3.2667015
F	−1.2840128	0.3070894	4.9677610
F	−0.1951006	1.5457238	2.7832623
F	−1.0882980	−2.0232021	3.5376077
F	1.0623821	−0.5037399	3.8819513
F	−2.3763716	0.0608961	2.4940661

XYZ coordinates of geometry-optimized $[ClF_2[BiF_6]_2]^-$ (C_1 point group)

Bi	−0.1418662	−0.2049600	−3.4183648
F	1.6606193	−0.8039606	−2.8357412
F	−1.9611612	0.4958028	−3.7318736
F	0.0862831	−0.8740315	−5.2659492
F	−0.3126170	0.5123529	−1.4352574
F	−0.8967801	−1.9134123	−2.7792699
F	0.6202195	1.5653292	−3.8677514
Cl	1.1130487	0.5081428	0.0942939
F	0.0488951	−0.7069517	1.4326356
F	1.9861206	1.4410864	−0.8731991
F	2.2464662	0.5510283	1.2275232
Bi	−0.6678080	−0.1720974	3.3498762
F	−1.2949715	0.3943579	5.1387348
F	−0.0737344	1.6529462	2.8347330
F	−1.1523116	−2.0693151	3.6084518
F	1.1589792	−0.5509956	4.0115692
F	−2.4193816	0.1746778	2.5095889

XYZ coordinates of geometry-optimized $[ClF_2[IrF_6]_2]^-$ (C_2 point group)

Cl	0.0000000	−0.0000000	1.1992171
F	1.0132248	−0.5403958	2.3188449
F	−1.0132248	0.5403958	2.3188449
F	1.3895875	−0.7716870	−0.2007795
F	−1.3895875	0.7716870	−0.2007795
Ir	3.2109508	−0.0551772	−0.4253759
Ir	−3.2109508	0.0551772	−0.4253759
F	4.9401826	0.6134565	−0.6366889
F	3.7592439	−1.1615470	0.9465162
F	2.7864481	1.2943564	0.8443554
F	2.5725227	1.0282815	−1.7686613
F	3.6165519	−1.4076414	−1.6778194
F	−4.9401826	−0.6134565	−0.6366889
F	−2.7864481	−1.2943564	0.8443554
F	−3.7592439	1.1615470	0.9465162
F	−3.6165519	1.4076414	−1.6778194
F	−2.5725227	−1.0282815	−1.7686613

XYZ coordinates of geometry-optimized $[ClF_2[NbF_6]_2]^-$ (C_2 point group)

Nb	2.5289329	2.2039616	−0.4562030
F	1.4993535	0.4669079	−0.1129188
F	3.6368910	1.1482648	−1.5375264
F	1.3807182	2.5060318	−1.9090491
F	3.5867919	1.7612272	1.0400274
F	3.4394117	3.8011671	−0.7313920
F	1.2381926	2.9365050	0.7130920
Cl	−0.0000000	0.0000000	1.2443098
F	1.0959983	0.3389041	2.3713360
F	−1.0959983	−0.3389041	2.3713360
F	−1.4993535	−0.4669079	−0.1129188
Nb	−2.5289329	−2.2039616	−0.4562030
F	−3.4394117	−3.8011671	−0.7313920
F	−1.2381926	−2.9365050	0.7130920
F	−1.3807182	−2.5060318	−1.9090491
F	−3.5867919	−1.7612272	1.0400274
F	−3.6368910	−1.1482648	−1.5375264

XYZ coordinates of geometry-optimized $[ClF_2[TaF_6]_2]^-$ (C_2 point group)

Ta	2.5444021	2.2136527	-0.4485924
F	1.5010796	0.4842462	-0.1472619
F	3.6648323	1.1909273	-1.5722979
F	1.3902783	2.5705008	-1.9017488
F	3.6041335	1.7169059	1.0453390
F	3.4762118	3.8216067	-0.6781874
F	1.2598016	2.9496077	0.7472330
Cl	-0.0000000	0.0000000	1.2228803
F	1.0941081	0.3443574	2.3435972
F	-1.0941081	-0.3443574	2.3435972
F	-1.5010796	-0.4842462	-0.1472619
Ta	-2.5444021	-2.2136527	-0.4485924
F	-3.4762118	-3.8216067	-0.6781874
F	-1.2598016	-2.9496077	0.7472330
F	-1.3902783	-2.5705008	-1.9017488
F	-3.6041335	-1.7169059	1.0453390
F	-3.6648323	-1.1909273	-1.5722979

XYZ coordinates of geometry-optimized $[ClF_2[RuF_6]_2]^-$ (C_2 point group)

Cl	0.0000000	0.0000000	−1.1064597
F	1.0874218	−0.3622226	−2.2219599
F	−1.0874218	0.3622226	−2.2219599
F	1.4974685	−0.5119373	0.2864275
F	−1.4974685	0.5119373	0.2864275
Ru	2.4010235	−2.2465960	0.4066084
Ru	−2.4010235	2.2465960	0.4066084
F	1.3161109	−2.6773005	1.8281105
F	3.2397883	−3.8632192	0.4956426
F	3.6176748	−1.4839385	1.5543469
F	1.1184817	−2.8997396	−0.7619120
F	3.4392533	−1.7413551	−1.0340298
F	−1.3161109	2.6773005	1.8281105
F	−3.2397883	3.8632192	0.4956426
F	−3.6176748	1.4839385	1.5543469
F	−1.1184817	2.8997396	−0.7619120
F	−3.4392533	1.7413551	−1.0340298

XYZ coordinates of geometry-optimized $[ClF_2[OsF_6]_2]^-$ (C_1 point group)

F	1.7413092	0.2978346	−1.8180420
Cl	0.3463926	0.0020805	−1.0989122
F	−0.3683783	−0.2959619	−2.4956833
F	−3.4470413	−3.7212107	−0.5052844
Os	−2.5353981	−2.1129745	−0.3673747
F	−0.9770368	−2.8446257	−1.1326723
F	−1.9077614	−2.5716272	1.3337600
F	−3.1110292	−1.5930453	−2.0768615
F	−1.5526821	−0.4064939	−0.2384786
F	−4.0289703	−1.2841434	0.3921372
F	1.3866499	0.4140581	0.7082502
Os	2.2832489	2.1119981	1.1618349
F	3.1251870	3.7127425	1.5665152
F	3.0456016	1.2849989	2.6550257
F	0.7897846	2.5970384	2.1779226
F	1.4706355	2.8434682	−0.3727902
F	3.7394880	1.5658633	0.1106534

XYZ coordinates of geometry-optimized $[ClF_2[Ta_2F_{11}]]_2$ (C_i point group)

Ta	1.3286620	3.0932841	−1.2322869
F	2.1003522	4.1242328	0.0861530
F	2.7953379	3.0858510	−2.3639230
F	0.3531133	1.8901812	−2.6221608
F	1.7868906	1.4180424	−0.4897745
F	0.4620375	4.4759423	−2.1353785
F	−0.3500844	2.9040678	−0.1840113
Ta	−0.8044965	0.3608500	−3.4263518
Cl	−1.7684405	1.7494707	0.9954678
F	0.6617704	0.1333469	−4.5635246
F	0.2040028	−0.7855807	−2.1546492
F	−1.9101325	0.7701282	−1.9544953
F	−1.6107384	1.6203033	−4.5170090
F	−1.7843832	−1.0795163	−4.0262171
F	−2.7974423	0.9493985	1.8858332
F	−2.8792268	2.4965829	0.1636713
F	−0.2040028	0.7855807	2.1546492
Cl	1.7684405	−1.7494707	−0.9954678
Ta	0.8044965	−0.3608500	3.4263518
F	2.7974423	−0.9493985	−1.8858332
F	2.8792268	−2.4965829	−0.1636713
F	0.3500844	−2.9040678	0.1840113
F	−0.3531133	−1.8901812	2.6221608
F	−0.6617704	−0.1333469	4.5635246
F	1.9101325	−0.7701282	1.9544953
F	1.6107384	−1.6203033	4.5170090
F	1.7843832	1.0795163	4.0262171
Ta	−1.3286620	−3.0932841	1.2322869
F	−2.1003522	−4.1242328	−0.0861530
F	−2.7953379	−3.0858510	2.3639230
F	−1.7868906	−1.4180424	0.4897745
F	−0.4620375	−4.4759423	2.1353785

XYZ coordinates of geometry-optimized $[ClF_2[AuF_4]]_2$ (C_i point group)

Au	1.8450859	−1.8928616	1.0186790
F	1.2847542	−0.7327096	−0.4835819
F	0.6399316	−0.8857970	2.2278341
F	2.9545546	−2.8703727	−0.1405136
F	2.3940957	−2.9447996	2.4722352
Cl	−0.0626851	−1.1011969	−2.0697821
Cl	0.0626851	1.1011969	2.0697821
F	−1.0706377	−1.3735424	−3.2807710
F	0.3887756	−2.6378260	−2.0054336
F	−0.6399316	0.8857970	−2.2278341
F	1.0706377	1.3735424	3.2807710
F	−1.2847542	0.7327096	0.4835819
F	−0.3887756	2.6378260	2.0054336
Au	−1.8450859	1.8928616	−1.0186790
F	−2.9545546	2.8703727	0.1405136
F	−2.3940957	2.9447996	−2.4722352

XYZ coordinates of geometry-optimized $[ClF_2[BF_4]]_2$ (C_i point group)

Cl	1.3295505	1.8825180	0.9827582
F	2.2576938	3.0162363	0.3636843
F	1.5500507	2.4050320	2.4678739
F	0.1493258	0.3909512	1.9694831
F	1.0938157	1.3268613	−1.0846390
B	−1.2104674	0.0348486	1.5812250
B	1.2104674	−0.0348486	−1.5812250
F	−2.0046569	0.0530152	2.6671875
F	−1.5924359	0.8444749	0.5502597
F	−1.0938157	−1.3268613	1.0846390
F	2.0046569	−0.0530152	−2.6671875
F	−0.1493258	−0.3909512	−1.9694831
F	1.5924359	−0.8444749	−0.5502597
Cl	−1.3295505	−1.8825180	−0.9827582
F	−2.2576938	−3.0162363	−0.3636843
F	−1.5500507	−2.4050320	−2.4678739

XYZ coordinates of geometry-optimized ClF_2^+ (C_{2v} point group)

Cl	0.0000000	0.0000000	0.6412708
F	-1.1974809	0.0000000	-0.3206461
F	1.1974809	0.0000000	-0.3206461

XYZ coordinates of geometry-optimized $[ClF_2(HF)_2]^+$ (C_2 point group)

Cl	0.0000000	0.0000000	-0.7732273
F	-1.1703094	0.0696115	-1.7926807
F	1.1703094	-0.0696115	-1.7926807
F	1.6702885	0.0349491	0.8826976
F	-1.6702885	-0.0349491	0.8826976
H	-2.2277041	0.5846572	1.2965928
H	2.2277041	-0.5846572	1.2965928

Bond lengths and angles of the ClF_2^+ cations of geometry-optimized structures from gas-phase quantum-chemical calculations

Table S32. Experimentally determined and calculated Cl−F bond lengths as well as Cl···F distances of the bridging F atoms of the fluoridometallate anions in difluorochloronium(III) fluoridometallates.

Compound	*d* exp. / Å			*d* calc. (DFT-PBE0/def2-TZVP, gas-phase) / Å		
	Cl−F	Cl···F	Reference	Model (Point group)	Cl−F	Cl···F
$ClF_2[AsF_6]$	1.541(14)	2.339(14)	[10]	$[ClF_2[AsF_6]_2]^-$ (C_2)	1.60	2.12
$ClF_2[SbF_6]$	1.555(4), 1.560(4)	2.302(4), 2.312(4)	this work	$[ClF_2[SbF_6]_2]^-$ (C_1)	1.59	2.13
$ClF_2[IrF_6]$	1.573(3)	2.300(3)	this work	$[ClF_2[BiF_6]_2]^-$ (C_1)	1.60	2.10
$ClF_2[BiF_6]$	1.568(3), 1.573(3)	2.252(3), 2.254(3)	this work	$[ClF_2[IrF_6]_2]^-$ (C_2)	1.60	2.12
$ClF_2[NbF_6]$	1.571(1)	2.234(1)	this work	$[ClF_2[NbF_6]_2]^-$ (C_2)	1.61	2.08
$ClF_2[TaF_6]$	1.568(2)	2.252(2)	this work	$[ClF_2[TaF_6]_2]^-$ (C_2)	1.60	2.09
$ClF_2[RuF_6]$	1.565(2), 1.568(1)	2.248(2), 2.271(1)	this work	$[ClF_2[RuF_6]_2]^-$ (C_2)	1.60	2.11
$ClF_2[OsF_6]$	1.567(5), 1.572(5), 1.576(5)	2.260(5), 2.269(5), 2.288(4)	this work	$[ClF_2[OsF_6]_2]^-$ (C_1)	1.60	2.13
$ClF_2[Ta_2F_{11}]$	1.566(2), 1.567(2)	2.235(2), 2.292(2)	this work	$[ClF_2[Ta_2F_{11}]]_2$ (C_i)	1.58	2.18
$ClF_2[AuF_4]$	1.538(4), 1.578(4)	2.170(4), 2.198(4)	this work	$[ClF_2[AuF_4]]_2$ (C_i)	1.60	2.10
$ClF_2[BF_4]$	1.562(1), 1.567(1)	2.270(1), 2.312(1)	[11]	$[ClF_2[BF_4]]_2$ (C_i)	1.59	2.15

Table S33. Experimentally determined and calculated F−Cl−F angles as well as F···Cl···F angles of the bridging F atoms of the fluoridometallate anions in difluorochloronium(III) fluoridometallates.

Compound	∡ exp. / °			∡ calc. (DFT-PBE0/def2-TZVP, gas-phase) / °		
	F−Cl−F	F···Cl···F	Reference	Model (Point group)	F−Cl−F	F···Cl···F
$ClF_2[AsF_6]$	103.2(7)	93.7(5)	[10]	$[ClF_2[AsF_6]_2]^-$ (C_2)	91.7	97.2
$ClF_2[SbF_6]$	97.0(2)	90.66(14)	this work	$[ClF_2[SbF_6]_2]^-$ (C_1)	91.9	97.4
$ClF_2[IrF_6]$	97.1(2)	90.38(14)	this work	$[ClF_2[BiF_6]_2]^-$ (C_1)	91.5	97.0
$ClF_2[BiF_6]$	95.90(19)	90.88(12)	this work	$[ClF_2[IrF_6]_2]^-$ (C_2)	91.4	97.3
$ClF_2[NbF_6]$	96.00(6)	93.62(4)	this work	$[ClF_2[NbF_6]_2]^-$ (C_2)	91.0	98.3
$ClF_2[TaF_6]$	96.45(15)	93.47(10)	this work	$[ClF_2[TaF_6]_2]^-$ (C_2)	91.3	98.0
$ClF_2[RuF_6]$	96.29(11), 96.80(13)	89.92(8), 91.25(7)	this work	$[ClF_2[RuF_6]_2]^-$ (C_2)	91.6	97.3
$ClF_2[OsF_6]$	97.0(3), 97.5(4)	90.0(2), 90.8(2)	this work	$[ClF_2[OsF_6]_2]^-$ (C_1)	91.8	97.5
$ClF_2[Ta_2F_{11}]$	96.30(10)	92.89(6)	this work	$[ClF_2[Ta_2F_{11}]]_2$ (C_i)	94.5	93.2
$ClF_2[AuF_4]$	95.4(2)	88.1(1)	this work	$[ClF_2[AuF_4]]_2$ (C_i)	92.6	93.3
$ClF_2[BF_4]$	96.42(5)	99.11(3)	[11]	$[ClF_2[BF_4]]_2$ (C_i)	92.8	101.7

Partial atomic charges from Mulliken population analysis from quantum-chemical solid-state calculations

Table S34. Average partial atomic charges from Mulliken population analysis of the optimized solid-state structures of difluorochloronium(III) fluoridometallates.

Compound	average partial atomic charge (DFT-PBE0/TZVP, solid-state) / *e*				
	M	Cl	F(ClF_2^+)	F(non-bridging)	F(bridging)
$ClF_2[AsF_6]$	1.59	1.10	−0.18	−0.38	−0.42
$ClF_2[SbF_6]$	2.07	1.14	−0.19	−0.46	−0.50
$ClF_2[IrF_6]$	1.68	1.13	−0.20	−0.39	−0.42
$ClF_2[BiF_6]$	1.99	1.14	−0.20	−0.43	−0.50
$ClF_2[NbF_6]$	2.64	1.18	−0.22	−0.49	−0.56
$ClF_2[TaF_6]$	2.51	1.18	−0.22	−0.53	−0.57
$ClF_2[RuF_6]$	1.97	1.15	−0.21	−0.44	−0.50
$ClF_2[OsF_6]$	1.85	1.15	−0.20	−0.42	−0.47
$ClF_2[Ta_2F_{11}]$	2.54	1.16	−0.20	−0.52, −0.56[a]	−0.56
$ClF_2[AuF_4]$	1.19	1.10	−0.22	−0.45	−0.48
$ClF_2[BF_4]$	1.04	1.11	−0.20	−0.44	−0.44

a: Parameter for the μ_2-F atom in the $[Ta_2F_{11}]^-$ anion.

Partial atomic charges in geometry-optimized structures of gas-phase quantum-chemical calculations

Table S35. Average partial atomic charges from natural population analysis of the optimized gas-phase model structures of difluorochloronium(III) fluoridometallates.[12]

Model (Point group)	average partial atomic charge (DFT-PBE0/def2-TZVP, gas-phase) / *e*				
	M	Cl	F(ClF_2^+)	F(non-bridging)	F(bridging)
$[ClF_2[AsF_6]_2]^-$ (C_2)	2.83	1.38	−0.33	−0.62	−0.61
$[ClF_2[SbF_6]_2]^-$ (C_1)	3.13	1.38	−0.33	−0.67	−0.66
$[ClF_2[BiF_6]_2]^-$ (C_1)	2.99	1.37	−0.34	−0.64	−0.64
$[ClF_2[IrF_6]_2]^-$ (C_2)	2.21	1.35	−0.34	−0.50	−0.56
$[ClF_2[NbF_6]_2]^-$ (C_2)	2.53	1.37	−0.35	−0.55	−0.61
$[ClF_2[TaF_6]_2]^-$ (C_2)	2.68	1.37	−0.34	−0.58	−0.62
$[ClF_2[RuF_6]_2]^-$ (C_2)	2.08	1.37	−0.33	−0.48	−0.55
$[ClF_2[OsF_6]_2]^-$ (C_1)	2.30	1.37	−0.33	−0.52	−0.57
$[ClF_2[Ta_2F_{11}]]_2$ (C_i)	2.71	1.40	−0.30	−0.54; −0.63[a]	−0.63
$[ClF_2[AuF_4]]_2$ (C_i)	1.60	1.35	−0.33	−0.53	−0.61
$[ClF_2[BF_4]]_2$ (C_i)	1.33	1.38	−0.32	−0.52	−0.52
ClF_2^+ (C_{2v})	-	1.40	−0.20	-	-
$[ClF_2(HF)_2]^+$ (C_2)	-	1.40	−0.25	-	−0.56

a: Parameter for the μ_2-F atom in the $[Ta_2F_{11}]^-$ anion.

References

[1] A. J. Edwards, R. J. C. Sills, *J. Chem. Soc., A* **1970**, 2697–2699.
[2] A. M. Ellern, M. Y. Antipin, A. V. Sharabarin, Y. T. Struchkov, *Russ. J. Inorg. Chem.* **1992**, *37*, 46–47.
[3] A. M. Ellern, M. Y. Antipin, A. V. Sharabarin, Y. T. Struchkov, *Russ. J. Inorg. Chem.* **1991**, *36*, 1278–1280.
[4] A. M. Ellern, M. N. Sinitsyn, M. Y. Antipin, A. V. Sharabarin, Y. T. Struchkov, *Koord. Khim.* **1991**, *17*, 1686–1688.
[5] R. Bougon, W. V. Cicha, M. Lance, L. Meublat, M. Nierlich, J. Vigner, *Inorg. Chem.* **1991**, *30*, 102–109.
[6] A. J. Karttunen, T. Tynell, M. Karppinen, *J. Phys. Chem. C* **2015**, *119*, 13105–13114.
[7] V. Sivchik, R. K. Sarker, Z.-Y. Liu, K.-Y. Chung, E. V. Grachova, A. J. Karttunen, P.-T. Chou, I. O. Koshevoy, *Chem. Eur. J.* **2018**, *24*, 11475–11484.
[8] F. Weigend, R. Ahlrichs, *Phys. Chem. Chem. Phys.* **2005**, *7*, 3297–3305.
[9] K. Eklund, M. S. Kuklin, F. Kraus, A. J. Karttunen, *ChemPhysChem* **2020**, *21*, 802–808.
[10] H. Lynton, J. Passmore, *Can. J. Chem.* **1971**, *49*, 2539–2543.
[11] M. Y. Antipin, A. M. Ellern, V. F. Sukhoverkhov, Y. T. Struchkov, Y. A. Buslaev, *Russ. J. Inorg. Chem.* **1988**, *33*, 171–173.
[12] A. E. Reed, R. B. Weinstock, F. Weinhold, *J. Chem. Phys.* **1985**, *83*, 735–746.
[13] G. Knizia, *J. Chem. Theory Comput.* **2013**, *9*, 4834–4843.
[14] G. Knizia, J. E. M. N. Klein, *Angew. Chem. Int. Ed.* **2015**, *54*, 5518–5522.

7.4. Photochemistry with Chlorine Trifluoride: Syntheses and Characterization of Difluorooxychloronium(V) Hexafluorido(non)metallates(V), $[ClOF_2][MF_6]$ (*M* = V, Nb, Ta, Ru, Os, Ir, P, Sb)

Benjamin Scheibe, Antti J. Karttunen, Florian Weigend, Florian Kraus

Chem. Eur. J. **2020**
DOI: 10.1002/chem.202003629

© 2020 The Authors. Published by Wiley-VCH Verlag GmbH & Co. KGaA.

Open access article distributed under the Creative Commons CC BY 4.0 license.
The original licensed material is shown.
(https://creativecommons.org/licenses/by/4.0/legalcode)

Chemistry
A European
Journal

Chemistry Europe
European Chemical Societies Publishing

Accepted Article

Title: Photochemistry with Chlorine Trifluoride: Syntheses and Characterization of Difluorooxychloronium(V) Hexafluorido(non)metallates(V), [ClOF2][MF6] (M = V, Nb, Ta, Ru, Os, Ir, P, Sb)

Authors: Benjamin Scheibe, Antti J. Karttunen, Florian Weigend, and Florian Kraus

This manuscript has been accepted after peer review and appears as an Accepted Article online prior to editing, proofing, and formal publication of the final Version of Record (VoR). This work is currently citable by using the Digital Object Identifier (DOI) given below. The VoR will be published online in Early View as soon as possible and may be different to this Accepted Article as a result of editing. Readers should obtain the VoR from the journal website shown below when it is published to ensure accuracy of information. The authors are responsible for the content of this Accepted Article.

To be cited as: *Chem. Eur. J.* 10.1002/chem.202003629

Link to VoR: https://doi.org/10.1002/chem.202003629

WILEY-VCH

Chemistry - A European Journal 10.1002/chem.202003629

WILEY-VCH

FULL PAPER

Photochemistry with Chlorine Trifluoride: Syntheses and Characterization of Difluorooxychloronium(V) Hexafluorido(non)metallates(V), $[ClOF_2][MF_6]$ (*M* = V, Nb, Ta, Ru, Os, Ir, P, Sb)

Benjamin Scheibe,[a] Antti J. Karttunen,[b] Florian Weigend,[a] and Florian Kraus*[a]

[a] B. Scheibe M. Sc., Priv.-Doz. Dr. F. Weigend, Prof. Dr. F. Kraus
Fachbereich Chemie
Philipps-Universität Marburg
Hans-Meerwein-Straße 4, 35032 Marburg (Germany)
E-mail: f.kraus@uni-marburg.de

[b] Prof. Dr. A. J. Karttunen
Department of Chemistry and Materials Science
Aalto University
00076 Aalto (Finland)

Supporting information for this article is given via a link at the end of the document.

Abstract: A photochemical route to salts consisting of difluorooxychloronium(V) cations, $[ClOF_2]^+$, and hexafluorido(non)metallate(V) anions, $[MF_6]^-$ (*M* = V, Nb, Ta, Ru, Os, Ir, P, Sb) is presented. As starting materials, either metals, oxygen and ClF_3 or oxides and ClF_3 are used. The prepared compounds were characterized by single-crystal X-ray diffraction and Raman spectroscopy. The crystal structures of $[ClOF_2][MF_6]$ (*M* = V, Ru, Os, Ir, P, Sb) are layer structures that are isotypic with the previously reported compound $[ClOF_2][AsF_6]$, whereas for *M* = Nb and Ta, similar crystal structures with a different stacking variant of the layers are observed. Additionally, partial or full O/F disorder within the $[ClOF_2]^+$ cations of the Nb and Ta compounds occurs. In all compounds reported here, a trigonal pyramidal $[ClOF_2]^+$ cation with three additional Cl···F contacts to neighboring $[MF_6]^-$ anions is observed, resulting in an pseudo-octahedral coordination sphere around the Cl atom. The Cl−F and Cl−O bond lengths of the $[ClOF_2]^+$ cations seem to correlate with the effective ionic radii of the *M*(V) ions. Quantum-chemical, solid-state calculations well reproduce the experimental Raman spectra and show, as do quantum-chemical gas phase calculations, that the secondary Cl···F interactions are ionic in nature. However, both solid-state and gas-phase quantum-chemical calculations fail to reproduce the increases in the Cl−O bond lengths with increasing effective ionic radius of *M* in $[MF_6]^-$ and the Cl−O Raman shifts also do not generally follow this trend.

Introduction

Chlorine oxide trifluoride, $ClOF_3$,[1–3] is one of the currently known four stable chlorine oxyfluorides with the other three being ClO_2F, ClO_3F and ClO_2F_3.[4–9] Chlorosyl fluoride, ClOF, is unstable towards disproportionation into ClF and ClO_2F, and is formed as an intermediate during the hydrolysis of ClF_3.[10–14] Perchloryl hypofluorite, ClO_4F, does not have a Cl−F bond and is thus different from the above mentioned oxyfluorides.[3,15] Several synthetic routes for $ClOF_3$ have been described. The first synthesis of $ClOF_3$ was likely carried out by Rocketdyne in 1965, a few years before the first publications on $ClOF_3$ appeared in the open literature.[1,2,16–18] It can either be synthesized by the fluorination of $ClONO_2$ or of Cl_2O at low temperatures according to Equations (1) and (2).[2,17]

$$2\,F_2 + ClONO_2 \xrightarrow{-35\,°C} ClOF_3 + NO_2F \quad (1)$$

$$2\,F_2 + Cl_2O \xrightarrow{NaF/CsF,\ -78\,°C} ClOF_3 + ClF \quad (2)$$

A photochemical synthesis of $ClOF_3$ is also possible.[1,16,18,19] $ClOF_3$ can be obtained at room temperature by UV irradiation of ClF_3/OF_2 mixtures.[1] It can also be obtained at low temperatures by irradiating mixtures of $Cl_2/F_2/O_2$, ClF_3/O_2, ClO_2F/ClF_5, ClO_3F/ClF_5, ClO_3F/F_2, or of ClF/IOF_5 with UV light.[18,19] Usually a range of side products is obtained in such photochemical reactions, with yields of $ClOF_3$ that are low to good with, for example, up to a 79% yield for the mixture ClO_3F/ClF_5.[19]

$ClOF_3$ shows Lewis-amphoteric behavior, thus it forms adducts with both Lewis acids and Lewis bases.[20–22] The higher homologues, $BrOF_3$ and IOF_3, are known to exhibit similar reactivities towards Lewis acids and bases.[23–31] For example, with Lewis bases, alkali metal fluorides and $ClOF_3$ form compounds containing the tetrafluoridooxidochlorate(V) anion, $[ClOF_4]^-$, which is likely tetragonal-pyramidal like the homologous $[XOF_4]^-$ (*X* = Br, I) anions are.[22,23,31,32] However, a crystal structure containing $[ClOF_4]^-$ anions has yet to be determined.

Compounds with the trigonal pyramidal difluoroxychloronium(V) cation, $[ClOF_2]^+$, are obtained in reactions with Lewis acids, such as the pentafluorides MF_5 (Equation (3)).[20–22,33–35]

This article is protected by copyright. All rights reserved.

Accepted Manuscript

Chemistry - A European Journal 10.1002/chem.202003629

$$ClOF_3 + MF_5 \longrightarrow ClOF_2[MF_6] \quad (M = P, As, Sb, V, Nb, Ta, Pt, Au, Bi, U) \tag{3}$$

The initially undesirable formation of a $[ClOF_2]^+$ salt, $[ClOF_2]_2[SiF_6]$, was also reported.[36,37] It was obtained serendipitously by the photochemical reaction of ClF_5/OF_2 mixtures in quartz vessels (Equation (4)).

$$2\ ClF_5 + 2\ OF_2 + SiF_4 \xrightarrow{h\nu} (ClOF_2)_2[SiF_6] + 4\ F_2 \tag{4}$$

Thus far, the only reported crystal structure of a $[ClOF_2]^+$ compound is that of $[ClOF_2][AsF_6]$.[38] We therefore report on the photochemical syntheses of the difluorooxychloronium(V) hexafluorido(non)metallates(V), $[ClOF_2][MF_6]$ (M = V, Nb, Ta, Ru, Os, Ir, P, Sb) under UV irradiation from the reactions of the respective elements with O_2 and ClF_3, or with metal and nonmetal oxides and chlorine trifluoride. The products were characterized by single-crystal X-ray diffraction, Raman spectroscopy and quantum-chemical solid-state and gas phase calculations.

Results and Discussion

Photochemical syntheses of $[ClOF_2][MF_6]$ (M = V, Nb, Ta, Ru, Os, Ir, P, Sb)

Our difluorooxychloronium(V) compounds have been prepared from either the photochemical reaction of ClF_3 with metals (Os, Ir) and O_2, or from the oxides M_2O_5 (M = P, V, Nb, Ta), $RuO_2{\cdot}xH_2O$ ($x \approx 2$), and Sb_2O_4 (Equations (5) to (8)). The starting materials were first reacted with ClF_3 and, in the case of the metals Os and Ir, oxygen gas was also added to the reaction vessels before UV irradiation. ***Caution!*** *The reaction between metal powders or oxides with liquid/gaseous ClF_3 can be vigorous to explosive.* The reaction mixtures were then irradiated with UV light from low-pressure Hg lamps (main emission line of 254 nm) for half a day to two weeks. Crystalline difluorooxychloronium(V) compounds were obtained in all cases from ClF_3 solutions or suspensions.
The overall reaction between Os or Ir metal with ClF_3 and O_2 under UV irradiation can be rationalized according to Equation (5).

$$2\ M + 7\ ClF_3 + O_2 \xrightarrow{h\nu} 2\ ClOF_2[MF_6] + 5\ ClF \quad (M = Os, Ir) \tag{5}$$

The initial step is likely the oxidation of the metal, followed by a Lewis acid-base reaction between excess ClF_3 and the metal pentafluoride intermediate, to give $ClF_2[MF_6]$ (M = Os, Ir). Such compounds and oxidation reactions have been previously reported for Ru, Os and Ir.[39–41] In a photochemical reaction, $ClOF_3$ is formed, which then likely displaces ClF_2^+ as ClF_3, resulting in the formation of the $[ClOF_2]^+$ compound. Single-crystal X-ray diffraction and Raman spectroscopy do not indicate the presence of ClF_2^+ compounds in the isolated products.
In the case of the oxides, the initial reaction is likely the formation of ClO_2F and the dissolved pentafluoride, which subsequently will form a solvated $ClO_2[MF_6]$ (M = V, Nb, Ta, Ru, P, Sb) salt. The formation of ClO_2F from the reaction of ClF_3 with oxides such as H_2O, $A[ClO_3]$ (A = Na, K), $[UO_2]F_2$ and $Cs[IOF_4]$ has been reported.[10,42–45] The Lewis-base character of ClO_2F has been previously described, where a range of Lewis-acids, compounds, such as $ClO_2[BF_4]$, ClO_2GeF_5 and $ClO_2[MF_6]$ (M = Ru, P, As, Sb), were obtained.[39,46–49] As mentioned above, $ClOF_3$ is formed in photochemical reactions, which will then likely displaces ClO_2^+ as ClO_2F to form a $[ClOF_2]^+$ salt. Single-crystal X-ray diffraction and Raman spectroscopy do not indicate the presence of ClO_2^+ salts in the isolated products. The overall proposed reactions can be described in terms of Equation (6) for M_2O_5 (M = P, V, Nb, Ta), Equation (7) for $RuO_2{\cdot}xH_2O$ ($x \approx 2$) and Equation (8) for Sb_2O_4.

$$2\ M_2O_5 + 14\ ClF_3 \xrightarrow{h\nu} 4\ ClOF_2[MF_6] + 3\ ClO_2F + 7\ ClF \quad (M = P, V, Nb, Ta) \tag{6}$$

$$2\ RuO_2{\cdot}xH_2O + (7+x)\ ClF_3 \xrightarrow{h\nu} 2\ ClOF_2[RuF_6] + (1+0.5x)\ ClO_2F + (4+0.5x)\ ClF + 2x\ HF \tag{7}$$

$$Sb_2O_4 + 7\ ClF_3 \xrightarrow{h\nu} 2\ ClOF_2[SbF_6] + ClO_2F + 4\ ClF \tag{8}$$

The thermal stabilities of $[ClOF_2]^+$ salts may be correlated with the Lewis acidity of the free parent fluoride of the anion.[3] The $[ClOF_2][MF_6]$ salts derived from AsF_5 and SbF_5 are more stable than those derived from VF_5 and PF_5.[33,34] The aforementioned salts are more stable than $[ClOF_2]_2[SiF_6]$.[36,37]

Crystal structures of $[ClOF_2][MF_6]$ (M = P, Sb, V, Ru, Os, Ir)

Powder X-ray diffraction patterns were previously reported for $[ClOF_2][MF_6]$ (M = V, Nb, Ta, P, As, Sb, Bi), but no lattice parameters were determined.[34] Isotypism was assumed for these compounds and preliminary results of a study on single crystals of $[ClOF_2][VF_6]$ indicated an orthorhombic unit cell.[34] Furthermore, powder X-ray diffraction patterns of $[ClOF_2][AsF_6]$ and $[ClOF_2][PtF_6]$ were indexed with orthorhombic unit cells in separate studies and the resulting lattice parameters, likely determined at room temperature, were a =

This article is protected by copyright. All rights reserved.

Accepted Manuscript

Chemistry - A European Journal 10.1002/chem.202003629

WILEY-VCH

FULL PAPER

9.94, b = 10.78, c = 8.16 Å, V ≈ 874 Å^3 and a = 9.94, b = 11.12, c = 8.21 Å^3, V ≈ 907 Å^3, respectively.[21,22] In the case of $[ClOF_2][AsF_6]$, the reported cell volume is a factor of ca. $\sqrt{2}$ larger than the cell volume determined by single-crystal X-ray diffraction at 100 K.[22,38]
To sort out these discrepancies we determined the crystal structures of the difluorooxychloronium(V) hexafluorido(non)metallates(V), $[ClOF_2][MF_6]$ (M = V, Ru, Os, Ir, P, Sb), by single-crystal X-ray diffraction. The compounds are isotypic with the previously described hexafluoridoarsenate(V) salt, $[ClOF_2][AsF_6]$.[38] They crystallize with four formula units per unit cell in the orthorhombic space group $Pna2_1$ (No. 33), Pearson code $oP44$ and Wyckoff sequence 33,a^{11}. See Table 1 for selected crystallographic data and details of the structure determinations. Atomic coordinates, equivalent isotropic and anisotropic displacement parameters are reported in the Supporting Information.

Table 1. Selected crystallographic data and details of the structure determinations of $[ClOF_2][MF_6]$ (M = P, V, Ru, Ir, Os, Sb). Columns are arranged in order of increasing $r_{eff}(M(V))$.

Compound	$[ClOF_2][PF_6]$	$[ClOF_2][VF_6]$	$[ClOF_2][RuF_6]$	$[ClOF_2][IrF_6]$	$[ClOF_2][OsF_6]$	$[ClOF_2][SbF_6]$
Molar mass / g·mol^{-1}	234.42	254.39	304.52	395.65	393.65	325.20
Space group (No.)			$Pna2_1$ (33)			
a / Å	14.322(3)	14.7272(9)	14.882(3)	14.7229(15)	15.0037(6)	15.1032(6)
b / Å	5.1046(10)	5.1331(2)	5.1859(10)	5.1304(8)	5.2277(2)	5.2766(3)
c / Å	7.9096(16)	8.1446(4)	8.2299(16)	8.1328(8)	8.2816(3)	8.2943(3)
V / Å^3	578.2(2)	615.70(5)	635.2(2)	614.31(13)	649.57(4)	661.00(5)
Z			4			
Pearson symbol			$oP44$			
$\rho_{calc.}$ / g·cm^{-3}	2.69	2.74	3.19	4.28	4.03	3.27
μ / mm^{-1}	1.060	2.159	2.999	22.284	20.150	4.685
Color	colorless	colorless	colorless	yellow	colorless	colorless
Crystal morphology	block	block	block	plate	plate	plate
Crystal size / mm^3	0.27·0.28·0.41	0.22·0.23·0.34	0.13·0.16·0.22	0.04·0.09·0.11	0.06·0.16·0.17	0.03·0.04·0.12
T / K			100			
λ / Å			0.71073 (Mo K_α)			
No. of reflections	6097	10498	8305	8014	9961	9139
θ range / °	2.85-32.03	2.77-32.03	2.74-31.45	2.77-31.87	2.72-36.40	2.70-33.33
Range of Miller indices	$-21 \le h \le 21$	$-21 \le h \le 21$	$-21 \le h \le 21$	$-21 \le h \le 21$	$-25 \le h \le 24$	$-23 \le h \le 23$
	$-7 \le k \le 7$	$-7 \le k \le 7$	$-7 \le k \le 7$	$-7 \le k \le 7$	$-8 \le k \le 8$	$-8 \le k \le 8$
	$-11 \le l \le 11$	$-12 \le l \le 10$	$-12 \le l \le 12$	$-10 \le l \le 12$	$-13 \le l \le 13$	$-12 \le l \le 12$
Absorption correction	integration	integration	integration	integration	multi-scan	integration
$Trans._{max}$, $Trans._{min}$	0.79, 0.71	0.70, 0.49	0.72, 0.62	0.50, 0.02	0.15, 0.07	0.91, 0.35
R_{int}, R_σ	0.0186, 0.0310	0.0290, 0.0495	0.0199, 0.0336	0.0112, 0.0193	0.0292, 0.0412	0.0153, 0.0250
Completeness of the data set	1.000	0.997	1.000	0.990	0.998	0.999
No. of unique reflections	2016	2030	2113	1884	3124	2474
No. of parameters	101	101	101	102	101	101
No. of restraints	1	1	1	1	1	1
No. of constraints	0	0	0	0	0	0
S (all data)	1.07	1.08	1.10	1.17	0.95	1.10
$R(F)$ ($I \ge 2\sigma(I)$, all data)	0.0261, 0.0270	0.0281, 0.0339	0.0216, 0.0230	0.0191, 0.0211	0.0197, 0.0242	0.0230, 0.0253
$wR(F^2)$ ($I \ge 2\sigma(I)$, all data)	0.0685, 0.0691	0.0659, 0.0686	0.0542, 0.0548	0.0492, 0.0513	0.0402, 0.0417	0.0576, 0.0590
Flack parameter x	0.29(9)	0.015(15)	−0.02(3)	0.136(16)	0.024(6)	0.22(3)
Extinction coefficient	not refined	0.007(2)	0.0018(6)	0.0009(2)	0.0040(3)	not refined
$\Delta\rho_{max}$, $\Delta\rho_{min}$ / e·Å^{-3}	0.30, −0.58	0.45, −0.63	0.59, −0.63	1.11, −1.03	1.48, −1.60	1.51, −0.81

The chlorine atom Cl(1) occupies the Wyckoff position 4a (site symmetry 1 / C_1) and is surrounded by the fluorine atoms F(1) and F(2) as well as the oxygen atom O(1), giving the trigonal pyramidal $[ClOF_2]^+$ cation, see Figure 1. Such a trigonal pyramidal geometry is also observed for the heavier homologues $[BrOF_2]^+$ in $[BrOF_2][AsF_6]$ and $[IOF_2]^+$ in $[IOF_2][IO_2F_4]$ as well as in the crystal structures of the valence isoelectronic chalcogen oxyfluorides SOF_2 and $SeOF_2$.[38,50–52]

This article is protected by copyright. All rights reserved.

Accepted Manuscript

Chemistry - A European Journal 10.1002/chem.202003629

WILEY-VCH

FULL PAPER

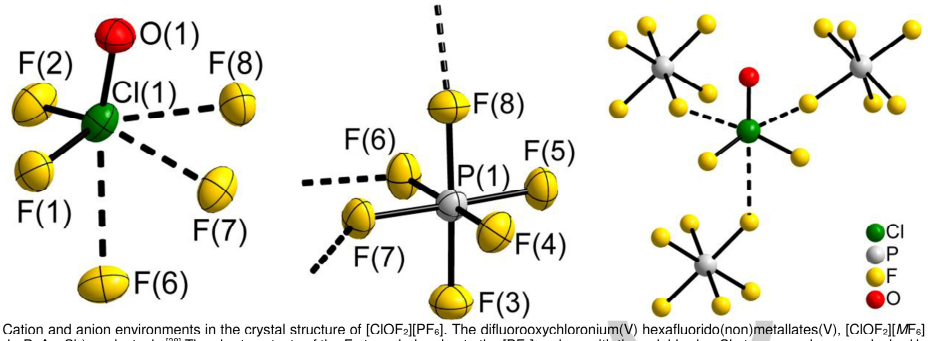

Figure 1. Cation and anion environments in the crystal structure of $[ClOF_2][PF_6]$. The difluorooxychloronium(V) hexafluorido(non)metallates(V), $[ClOF_2][MF_6]$ (M = V, Ru, Os, Ir, P, As, Sb) are isotypic.[38] The short contacts of the F atoms belonging to the $[PF_6]^-$ anions with the neighboring Cl atoms are shown as dashed bonds. On the left and in the middle atoms are shown with displacement ellipsoids at the 70% probability level at 100 K. On the right, atoms are shown as isotropic with arbitrary radii.

The respective Cl−O and Cl−F bond lengths within the $[ClOF_2]^+$ cations of the investigated compounds, along with the As compound from the literature, are stated in Table 2. The Cl−O bond lengths range from 1.4364(17) Å in $[ClOF_2][PF_6]$ to 1.477(4) Å in $[ClOF_2][OsF_6]$ and are longer than in gaseous $ClOF_3$ (1.405(3) Å, from electron diffraction at 238 K).[53] A comparison with the crystal structure of $ClOF_3$ is of limited use, because of O/F disorder, with averaged Cl−O/F bond lengths of 1.498(1) Å (data from single-crystal X-ray diffraction at 123 K) which is approximately the arithmetic mean of the Cl−O and Cl−F bond lengths from the electron-diffraction study on gaseous $ClOF_3$.[31]

Table 2. Experimental and calculated Cl−O and Cl−F bond lengths as well as Cl···F distances of the bridging F atoms of the fluoridometallate anions in $[ClOF_2][MF_6]$ (M = V, Nb, Ta, Ru, Os, Ir, P, As, Sb). Rows are listed according to increasing $r_{eff}(M(V))$.

Compound	exptl. bond lengths and distances / Å			calc. bond lengths and distances (DFT-PBE0/TZVP, solid-state) / Å		
	Cl−O	Cl−F	Cl···F	Cl−O	Cl−F	Cl···F
$[ClOF_2][PF_6]$	1.4364(17)	1.5233(19), 1.5367(17)	2.4766(17)-2.6061(16)	1.41	1.62, 1.62	2.39-2.65
$[ClOF_2][AsF_6]$[a]	1.455(2)	1.522(2), 1.543(2)	2.476(2)-2.598(2)	1.41	1.62, 1.63	2.37-2.62
$[ClOF_2][VF_6]$	1.465(2)	1.528(2), 1.531(3)	2.362(2)-2.512(2)	1.41	1.62, 1.63	2.28-2.58
$[ClOF_2][RuF_6]$	1.461(3)	1.509(3), 1.533(3)	2.418(2)-2.522(3)	1.41	1.62, 1.63	2.33-2.58
$[ClOF_2][IrF_6]$	1.444(5)	1.486(6), 1.514(5)	2.401(5)-2.487(5)	1.41	1.63, 1.63	2.29-2.55
$[ClOF_2][OsF_6]$	1.477(4)	1.508(3), 1.532(4)	2.442(3)-2.520(3)	1.41	1.63, 1.63	2.36-2.52
$[ClOF_2][SbF_6]$	1.476(3)	1.497(3), 1.529(3)	2.458(3)-2.531(3)	1.41	1.62, 1.63	2.36-2.57
$[ClOF_2][NbF_6]$[b]	1.487(2)-1.511(2)	1.503(3)-1.516(2)	2.413(2)-2.484(2)	1.41, 1.41	1.63-1.64	2.30-2.55
$[ClOF_2][TaF_6]$[b]	1.488(4)-1.512(4)	1.488(4)-1.521(4)	2.423(4)-2.484(4)	1.41, 1.41	1.62-1.63	2.31-2.54

[a]: Experimentally determined bond lengths taken from a previous study conducted at 100 K.[38]

[b]: Experimentally determined bond lengths include Cl−O/F bond lengths of disordered $[ClOF_2]^+$ cations. Calculated bond lengths are given for a fully ordered, minimum-energy model, see the Supporting Information.

The observed Cl−O bond lengths seem to correlate with the effective ionic radii of the M(V) atoms, $r_{eff}(M(V))$, within the $[MF_6]^-$ counter anions and seem to increase with increasing $r_{eff}(M(V))$. The effective ionic radii for M(V) atoms with coordination number six are: P: 0.38; As: 0.46; V: 0.54; Ru: 0.565; Ir: 0.57; Os: 0.575; Sb: 0.60 Å.[54] Plots of the respective bond lengths and bond angles versus $r_{eff}(M(V))$ are given in the Supporting Information.

In contrast no clear trend for the Cl−F bond lengths is observed, where the shortest value, 1.486(6) Å, is observed for $[ClOF_2][IrF_6]$ and the longest values, 1.5367(17) Å, for $[ClOF_2][PF_6]$. However, for M = Os, which one would expect to be very similar to M = Ir, the observed Cl−F bond length is 1.508(3) Å. The aforementioned are shorter than the Cl−F bonds in gaseous $ClOF_3$ with 1.603(4) Å (equatorial) and 1.713(3) Å (axial)) or in solid $ClOF_3$ with 1.498(1) Å (equatorial, O/F disorder) and 1.683(2)-1.818(2) Å (axial), as would be expected.[31,53]

One may attribute the elongation of the Cl−O bonds to interactions with the surrounding anions so that the coordination number of the Cl atom becomes 3 + 3 (see below) compared to gaseous $ClOF_3$ where the coordination number is only four. However, this is in contradiction to the observed shortening of the Cl−F bonds, which also should be elongated due to the increased coordination number. For the $[ClOF_2]^+$ cation one would expect shorter Cl−F and Cl−O bond lengths relative to $ClOF_3$ due to the smaller coordination number of the Cl atom, less steric repulsion of ligands, and the positive charge of the cation. The expectation is in line with the observed Cl−F distances that are shorter compared to those of $ClOF_3$, however, the observed Cl−O bond lengths contradict this expectation.

Correlations with $r_{eff}(M(V))$ are also observed for the F−Cl−O and F−Cl−F bond angles within the $[ClOF_2]^+$ cations, which are stated in Table 3. While the former decrease to some extent with increasing $r_{eff}(M(V))$, the latter increase.

This article is protected by copyright. All rights reserved.

Accepted Manuscript

Chemistry - A European Journal 10.1002/chem.202003629

Table 3. Selected experimental and calculated bond angles for $[ClOF_2][MF_6]$ (M = V, Ru, Os, Ir, P, As, Sb). Rows are arranged in order of increasing $r_{eff}(M(V))$.

Compound	exptl. bond angle / °				calc. bond angle (DFT-PBE0/TZVP, solid-state) / °			
	F–Cl–F	F–Cl–O	F(6)···Cl–O	F(7)···Cl···F(8)	F–Cl–F	F–Cl–O	F(6)···Cl–O	F(7)···Cl···F(8)
$[ClOF_2][PF_6]$	98.00(10)	105.23(11), 105.46(11)	169.47(9)	79.99(6)	93.0	106.1, 106.9	175.2	85.7
$[ClOF_2][AsF_6]$[a]	98.7(1)	104.2(1), 105.5(1)	168.5(1)	88.48(10)	93.0	106.1, 106.5	174.0	85.9
$[ClOF_2][VF_6]$	98.53(14)	102.70(14), 104.83(14)	169.12(12)	84.42(8)	90.1	105.0, 105.6	174.0	90.3
$[ClOF_2][RuF_6]$	99.69(16)	103.51(16), 104.25(16)	167.33(14)	81.60(9)	92.5	105.7, 106.4	173.2	87.7
$[ClOF_2][IrF_6]$	100.0(3)	103.5(3), 104.1(3)	167.0(3)	80.36(17)	92.7	105.6, 106.4	171.9	84.1
$[ClOF_2][OsF_6]$	100.4(2)	103.3(2), 104.15(19)	166.84(17)	80.33(10)	92.4	106.0, 106.4	168.9	85.6
$[ClOF_2][SbF_6]$	100.66(19)	102.90(19), 104.57(18)	166.87(16)	79.85(10)	92.9	106.3, 106.4	172.1	85.2

[a]: Experimental values are taken from a previous study conducted at 100 K.[38]

The M(V) atoms of the $[MF_6]^-$ anions occupy the general position 4a (site symmetry 1 / C_1). The observed M–F bond lengths are given in Table 4. Three of the six F atoms of the $[MF_6]^-$ anions – F(6), F(7) and F(8) – show M–μ-F···Cl contacts with the Cl atoms of the $[ClOF_2]^+$ cation (Figure 1). These Cl···μ-F distances lie in the range of approximately 2.4 to 2.6 Å within the series and are provided in Table 2. The corresponding M–F bond lengths of the bridging μ-F atoms are thus longer than the non-bridging, terminally bound F atoms (F(3), F(4) and F(5)). This is likely due to the higher effective coordination number of the bridging μ-F atoms in their interactions with the Cl atoms.

Table 4. Experimental and calculated M–F bond lengths of non-bridging and bridging F atoms of the fluorido(non)metallate anions in $[ClOF_2][MF_6]$ (M = V, Nb, Ta, Ru, Os, Ir, P, As, Sb). Rows are arranged in order of increasing $r_{eff}(M(V))$.

Compound	exptl. bond length / Å		calc. bond length (DFT-PBE0/TZVP, solid-state) / Å	
	M–F (non-bridging)	M–F (bridging)	M–F (non-bridging)	M–F (bridging)
$[ClOF_2][PF_6]$	1.5827(16)-1.5952(17)	1.6076(17)-1.6255(16)	1.61-1.62	1.64-1.67
$[ClOF_2][AsF_6]$[a]	1.709(2)-1.7149(19)	1.7313(19)-1.7474(19)	1.71-1.72	1.74-1.77
$[ClOF_2][VF_6]$	1.734(2)-1.748(2)	1.794(2)-1.820(2)	1.72-1.74	1.78-1.85
$[ClOF_2][RuF_6]$	1.832(2)-1.836(2)	1.867(2)-1.875(2)	1.85-1.86	1.89-1.91
$[ClOF_2][IrF_6]$	1.828(5)-1.841(4)	1.856(4)-1.869(4)	1.83-1.87	1.89-1.94
$[ClOF_2][OsF_6]$	1.855(3)-1.866(3)	1.882(3)-1.894(3)	1.88-1.89	1.92-1.94
$[ClOF_2][SbF_6]$	1.857(3)-1.863(3)	1.881(3)-1.893(2)	1.90-1.91	1.93-1.95
$[ClOF_2][NbF_6]$	1.857(2)-1.867(2)	1.913(2)-1.926(2)	1.87-1.89	1.92-1.97
$[ClOF_2][TaF_6]$	1.863(4)-1.872(4)	1.911(3)-1.923(3)	1.88-1.89	1.93-1.97

[a]: Experimental values are taken from a previous study conducted at 100 K.[38]

For the Cl atoms, an overall coordination number of six results with a coordination sphere that can be best described as distorted octahedral. If the lone-pair of the Cl atom is included, an AX_6E VSEPR arrangement of ligand atom-chlorine bond pairs and the valence electron pair on chlorine is obtained (A = Cl, X = ligand and E = lone pair). The VSEPR model predicts a distorted pentagonal-bipyramidal geometry for an AX_6E species.[55–57] However, no species with such an arrangement of the ligands is known.[58] Instead, two different structures of AX_6E species, octahedral or distorted octahedral, have been described.[58] An octahedral structure is observed, when the central atom has a sterically inactive lone pair, such as in $[BiCl_6]^{3-}$ and $[BrF_6]^-$.[59,60] A distorted octahedral structure is observed, when the central atom has a "weakly" sterically active lone pair, such as in $[IF_6]^-$ and XeF_6.[61–63]

In the case of the Cl atoms studied in these systems, a clear classification is difficult, because the ligands are different and the primary bond lengths of the $[ClOF_2]^+$ cation differ significantly from the Cl···μ-F distances. The lone pair of the Cl atom might be arranged as in the free $[ClOF_2]^+$ cation, which has a distorted tetrahedral structure (AX_3E VSEPR arrangement).[3] It might then point in the direction of the center of the three μ-F atoms, that is, to a wider face of the octahedron.

The Br atom in the homologous $[BrOF_2]^+$ cation of $[BrOF_2][AsF_6]$ has a similar distorted octahedral coordination environment with bridging μ-F atoms.[38] In the compound $[IOF_2][IO_2F_4]$, the I atom of the $[IOF_2]^+$ cation also exhibits a distorted octahedral coordination environment, but with close contacts to μ-O instead of μ-F atoms.[50]

In the compounds presented here, the bridging via μ-F atoms originates from three $[MF_6]^-$ anions (Figure 1). When these interactions are considered, a layer motif, with corrugated layers parallel to the bc plane, is obtained (Figure 2). The crystal structures of the compounds can thus be described as layered structures with the Niggli formula $^2_\infty\left[\langle ClO_{\frac{1}{1}}F_{\frac{2}{1}}F_{\frac{3}{1+1}}\rangle\langle MF_{\frac{3}{1}}F_{\frac{3}{1+1}}\rangle\right]$ (M = V, Ru, Os, Ir, P, As, Sb), where the notation of the Niggli formula is given according to the literature.[64]

This article is protected by copyright. All rights reserved.

Accepted Manuscript

Chemistry - A European Journal 10.1002/chem.202003629

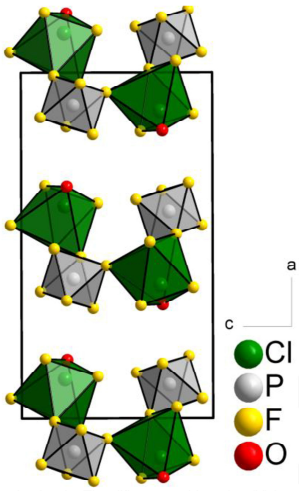

Figure 2. Crystal structure of $[ClOF_2][PF_6]$ projected along the *b* axis. The difluorooxychloronium(V) hexafluorido(non)metallates(V), $[ClOF_2][MF_6]$ (*M* = V, Ru, Os, Ir, P, As, Sb), are isotypic.[38] The coordination polyhedra of the Cl atoms are shown in green and those of the P atoms in grey. Atoms are shown as isotropic with arbitrary radii.

Crystal structures of $[ClOF_2][MF_6]$ (M = Nb, Ta)

The crystal structures of $[ClOF_2][MF_6]$ (*M* = Nb, Ta) were determined by single-crystal X-ray diffraction. Both crystallize with eight formula units per unit cell in the orthorhombic space group $Pna2_1$ (No. 33), Pearson code *oP*88 and Wyckoff sequence 33,a^{22}. See Table 5 for selected crystallographic data and details of the structure determinations. Atomic coordinates, equivalent isotropic and anisotropic displacement parameters are reported in the Supporting Information.

Table 5. Selected crystallographic data and details of the structure determinations of $[ClOF_2][MF_6]$ (*M* = Nb, Ta).

Compound	$[ClOF_2][NbF_6]$	$[ClOF_2][TaF_6]$
Molar mass / g·mol^{-1}	296.36	384.40
Space group (No.)	$Pna2_1$ (33)	
a / Å	30.1890(11)	30.2598(16)
b / Å	5.2653(2)	5.2923(3)
c / Å	8.3588(3)	8.3610(4)
V / Å^3	1328.67(8)	1338.96(12)
Z	8	
Pearson symbol	*oP*88	
$\rho_{calc.}$ / g·cm^{-3}	2.96	3.81
μ / mm^{-1}	2.320	16.922
Color	colorless	colorless
Crystal morphology	block	block
Crystal size / mm^3	0.11·0.15·0.17	0.07·0.10·0.10
T / K	100	
λ / Å	0.71073 (Mo-K$_\alpha$)	
No. of reflections	31305	21295
θ range / °	2.70-34.92	2.69-33.21
Range of Miller indices	$-48 \le h \le 47$	$-46 \le h \le 46$
	$-8 \le k \le 8$	$-7 \le k \le 8$
	$-13 \le l \le 13$	$-12 \le l \le 12$
Absorption correction	multi-scan	multi-scan
T_{max}, T_{min}	0.75, 0.68	0.30, 0.12
R_{int}, R_σ	0.0263, 0.0311	0.0313, 0.0313
Completeness of the data set	0.998	0.996
No. of unique reflections	5802	4982

This article is protected by copyright. All rights reserved.

WILEY-VCH Accepted Manuscript

Chemistry - A European Journal 10.1002/chem.202003629

No. of parameters	203	206
No. of restraints	2	3
No. of constraints	0	0
S (all data)	1.16	1.06
$R(F)$ ($I \geq 2\sigma(I)$, all data)	0.0293, 0.0356	0.0210, 0.0252
$wR(F^2)$ ($I \geq 2\sigma(I)$, all data)	0.0468, 0.0482	0.0417, 0.0432
Flack parameter x	0.013(11)	0.074(11)
Extinction coefficient	0.00299(15)	0.00142(9)
$\Delta\rho_{max}$, $\Delta\rho_{min}$ / e·Å^{-3}	1.08, −0.83	1.58, −1.83

The crystal structures of $[ClOF_2][NbF_6]$ and $[ClOF_2][TaF_6]$ are closely related to those described above, because the *a* axes of the former are approximately doubled. For example, a = 30.1890(11) Å for $[ClOF_2][NbF_6]$, whereas in $[ClOF_2][SbF_6]$ the *a* axis is 15.1032(6) Å long, resulting in a different stacking of layers.[38]

There are two symmetry-independent Cl atoms present, Cl(1) and Cl(2), which both occupy the general 4*a* position with site symmetry 1 / C_1. In case of $[ClOF_2][NbF_6]$, the $Cl(1)OF_2^+$ cation shows O/F disorder (Figure 3), where the Cl−O/F bond lengths of 1.501(2) to 1.511(2) Å are equal within the tripled standard uncertainties.

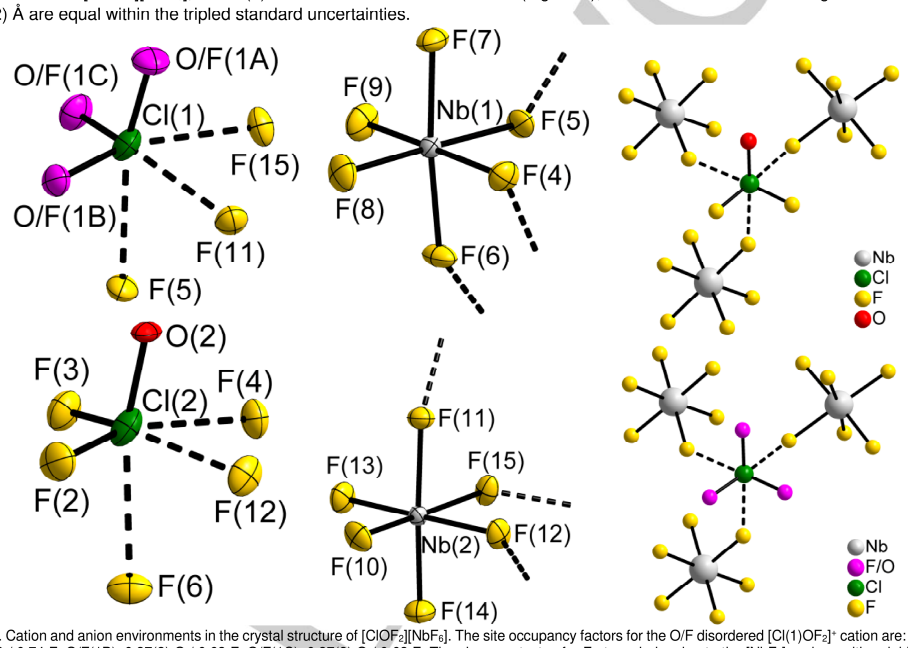

Figure 3. Cation and anion environments in the crystal structure of $[ClOF_2][NbF_6]$. The site occupancy factors for the O/F disordered $[Cl(1)OF_2]^+$ cation are: O/F(1A): 0.26(3) O / 0.74 F; O/F(1B): 0.37(3) O / 0.63 F; O/F(1C): 0.37(3) O / 0.63 F. The close contacts of μ-F atoms belonging to the $[NbF_6]^-$ anions with neighboring Cl atoms are shown as dashed bonds. On the left and in the middle, the atoms are shown with displacement ellipsoids at the 70% probability level at 100 K. On the right, atoms are shown isotropic with arbitrary radii.

For the homologous $[BrOF_2]^+$ cation in $[BrOF_2][AsF_6]$, which crystallizes in the cubic space group $P2_13$ (No. 198), O/F disorder was also observed.[38] Furthermore, O/F disorder was observed in the crystal structure of $ClOF_3$, as mentioned above. The Cl−O/F bond lengths of 1.498(1) Å (from single-crystal X-ray diffraction at 123 K) are close to the present reported values.[31] In contrast, the second cation, $[Cl(2)OF_2]^+$, does not show O/F disorder, because the Cl−O bond length of 1.487(2) Å is significantly shorter than the Cl−F bond lengths of 1.514(2) and 1.516(2) Å.

The $[ClOF_2]^+$ cations in $[ClOF_2][TaF_6]$ are either partially or fully O/F disordered (Figure 4). The $[Cl(1)OF_2]^+$ cation is partially O/F disordered with Cl−O/F bond lengths of 1.488(4) and 1.498(4) Å in comparison with the Cl−F bond length of 1.521(4) Å, whereas the $[Cl(2)OF_2]^+$ cation is fully disordered with Cl−O/F bond lengths of 1.493(4) to 1.512(4) Å.

This article is protected by copyright. All rights reserved.

Accepted Manuscript

Chemistry - A European Journal 10.1002/chem.202003629

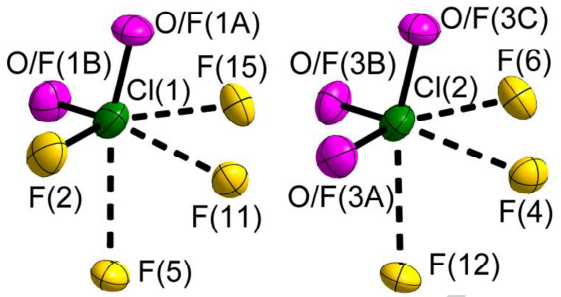

Figure 4. Cation environments in the crystal structure of $[ClOF_2][TaF_6]$. The site occupancy factors for the O/F disordered $Cl(1)OF_2^+$ cation are: O/F(1A): 0.58(3) O / 0.42 F; O/F(1B): 0.42(3) O / 0.58 F. The site occupancy factors for the O/F disordered $Cl(2)OF_2^+$ cation are: O/F(3A): 0.33(4) O / 0.67 F; O/F(3B): 0.38(4) O / 0.62 F; O/F(3C): 0.29(4) O / 0.71 F. The same numbering scheme of the F atoms in the $[NbF_6]^-$ anions in Figure 3 has been used for the F atoms in the $[TaF_6]^-$ anions of $[ClOF_2][TaF_6]$. The close contacts of μ-F atoms belonging to the $[TaF_6]^-$ anions with neighboring Cl atoms are shown as dashed bonds. The displacement ellipsoids are shown at the 70% probability level at 100 K.

It is unclear why both cations of the Ta compound show disorder. The chemical properties and effective ionic radii of Nb and Ta are similar, as are the $[ClOF_2]^+$ cation environments. The ordering of the cations may depend on temperature and cooling rate of the crystals, however the rate with which they were cooled for the diffraction experiment should be quite similar.

These observed Cl−O and Cl−F bond lengths nicely agree with the above-mentioned correlation of bond lengths with the effective ionic radii $r_{eff}(M(V))$ in the compounds $[ClOF_2][MF_6]$ (M = V, Ru, Os, Ir, P, As, Sb), as the former are increasing and the latter are decreasing with increasing $r_{eff}(M(V))$. Both Nb(V) and Ta(V) have an effective radius of 0.64 Å in coordination number six, which seemingly renders them to a border case, where O/F disorder can be observed.[54] In contrast, O/F disorder is neither observed for $[ClOF_2][OsF_6]$ ($r_{eff}(Os(V))$: 0.575 Å) nor for $[ClOF_2][SbF_6]$ ($r_{eff}(Sb(V))$: 0.60 Å), see above.[54]

A similar trend is also observed for the bond angles within the $[ClOF_2]^+$ cations. The O/F−Cl(1)−O/F bond angles in the Nb compound lie in the range of 102.03(14) to 102.75(14)°, whereas the F−Cl(2)−O bond angles with 102.29(14) and 103.57(15)° and the F−Cl(2)−F bond angle of 100.95(15)° are significantly different. In the Ta compound the respective O/F−Cl(1)−O/F bond angles are observed from 101.9(2) to 103.3(3)° and the O/F−Cl(2)−O/F bond angles from 101.3 to 103.3°.

In the crystal structures of both compounds two symmetry-independent M(V) ions of respective $[MF_6]^-$ anions are present, which both occupy general 4a positions. As in the crystal structures of the compounds reported above, three of the F atoms of the $[MF_6]^-$ anions show close contacts to the Cl atoms of the $[ClOF_2]^+$ cations, see Figure 3. Thus, the F atoms act in a bridging manner M−μ-F···Cl. The coordination sphere of the Cl atoms is thus pseudo-octahedral, as above. The respective Cl···μ-F distances range from 2.413(2) to 2.484(2) Å in $[ClOF_2][NbF_6]$ and from 2.423(4) to 2.484(4) Å in $[ClOF_2][TaF_6]$. The distances are shorter than in $[ClOF_2][PF_6]$ or $[ClOF_2][RuF_6]$ for example, see Table 2. The M−F bond lengths of the non-bridging, terminally bound F atoms, that is those not coordinating to Cl atoms, are shorter than the ones to the bridging μ-F atoms, as expected (see Table 4). This observation can likely be explained by the higher effective coordination number of these bridging μ-F atoms and their interaction with the Cl atoms. Similarly as in $[ClOF_2][MF_6]$ (M = V, Ru, Os, Ir, P, As, Sb), a layer motif with corrugated layers parallel to the bc plane is obtained when the M−μ-F···Cl interactions are taken into account, see Figure 5, and the crystal structure of the compounds can be described as a layer structure with the same Niggli formula as above. In contrast, every second layer is shifted (and rotated) which leads to the approximate doubling of the a axis. So, the Nb and Ta compound crystallize in a stacking variant of likely very similar lattice energy and therefore even more modifications, that is, more stacking variants of these compounds could be obtainable.

Accepted Manuscript

This article is protected by copyright. All rights reserved.

Chemistry - A European Journal 10.1002/chem.202003629

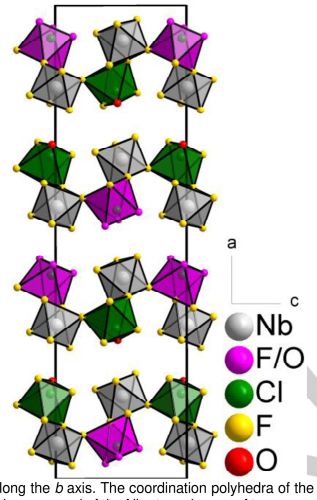

Figure 5. Crystal structure of $[ClOF_2][NbF_6]$ projected along the *b* axis. The coordination polyhedra of the Cl(1) atoms (O/F disordered $[ClOF_2]^+$ cation) are shown in pink, that of the Cl(2) atoms (ordered $[ClOF_2]^+$ cation) in green and of the Nb atoms in grey. Atoms are shown as isotropic with arbitrary radii.

Quantum chemical calculations

The crystal structures of all thus far reported and herein described $[ClOF_2][MF_6]$ compounds were investigated by means of quantum chemical solid-state calculations with CRYSTAL17 (DFT-PBE0/TZVP level of theory).[65,66] The optimized structures are reported in the Supporting Information and comparisons of observed and calculated bond lengths and angles are given in Tables 2 and 3.

For $[ClOF_2][MF_6]$ (M = Nb, Ta), several structural models with fully ordered $[ClOF_2]^+$ cations were optimized, that is, with full oxygen atom occupation on the possible positions. The structures of the respective models are reported in the Supporting Information. The energy differences of the two possible structural models of $[ClOF_2][NbF_6]$ in comparison with the lowest-energy model with full O atom occupation on the O/F(1C) position (Figure 3) are only ca. 6.0 and 6.6 kJ/mol. For $[ClOF_2][TaF_6]$, the energy differences lie in the range 4.7 to 9.6 kJ/mol with respect to the lowest-energy model with full O atom occupation on the O/F(1B) and O/F(3B) positions. See Figure 4 and model No. 5 in the Supporting Information.

Surprisingly, the calculated Cl−O bond lengths (ca. 1.41 Å) are similar for all compounds investigated in this study. The Cl−O interaction is somewhat overestimated by the employed method, giving calculated bond lengths that are 2 to 7% shorter than the observed values. The opposite trend is observed for the calculated Cl−F bond lengths, which are 5 to 9% longer than the experimentally determined values and thus the interaction is underestimated. The respective calculated values for the $[ClOF_2]^+$ cations are overall independent of the $[MF_6]^-$ anion. Thus, these results are not in accordance with the crystal structures. In contrast, the calculated Cl···F distances overall correlate with $r_{eff}(M(V))$ and tend to decrease with increasing $r_{eff}(M(V))$. This is therefore in agreement with the experimental observations.

To get a qualitative picture of the bonding in these compounds, the atomic partial charges and overlap populations between atoms were examined by Mulliken population analyses. The average atomic partial charges are reported in Table 6 and the average overlap populations in Table 7. As for the calculated primary Cl−O and Cl−F bond lengths of the $[ClOF_2]^+$ cations, the average partial charges and average overlap populations are similar among the investigated compounds. The Cl−F interaction is rather ionic in comparison with the Cl−O interaction. The interactions between the Cl atoms and the bridging μ-F atoms are by comparison also ionic. The values for the non-bridging and bridging F atoms are likely dependent on both the electronegativity (χ_{AR}) of M(V) and $r_{eff}(M(V))$.[67,68] The average partial charges of M(V), F(non-bridging) and μ-F atoms show correlations with χ_{AR} that are smaller, the higher $\chi_{AR}(M)$ is. Furthermore, the bridging μ-F atoms have more negative partial charges than the non-bridging F atoms, which is likely due to their higher coordination number.

Table 6. Average atomic partial charges from Mulliken population analyses of the optimized solid-state structures of $[ClOF_2][MF_6]$ (M = V, Nb, Ta, Ru, Os, Ir, P, As, Sb). Rows are arranged in order of increasing $r_{eff}(M(V))$.

Compound	average atomic partial charge / *e*					
	M(V)	Cl	O	F (of $[ClOF_2]^+$)	F (non-bridging)	μ-F (bridging)
$[ClOF_2][PF_6]$	+1.80	+1.40	−0.18	−0.20	−0.42	−0.46
$[ClOF_2][AsF_6]$	+1.62	+1.39	−0.18	−0.20	−0.38	−0.42
$[ClOF_2][VF_6]$	+1.82	+1.41	−0.20	−0.22	−0.39	−0.47
$[ClOF_2][RuF_6]$	+1.96	+1.40	−0.19	−0.21	−0.42	−0.49
$[ClOF_2][IrF_6]$	+1.68	+1.39	−0.19	−0.21	−0.38	−0.44

This article is protected by copyright. All rights reserved.

Accepted Manuscript

Chemistry - A European Journal 10.1002/chem.202003629

WILEY-VCH

FULL PAPER

$[ClOF_2][OsF_6]$	+1.84	+1.41	−0.18	−0.22	−0.41	−0.46
$[ClOF_2][SbF_6]$	+2.14	+1.40	−0.18	−0.21	−0.47	−0.51
$[ClOF_2][NbF_6]$[a]	+2.36	+1.42	−0.20	−0.22	−0.49	−0.55
$[ClOF_2][TaF_6]$[a]	+2.50	+1.42	−0.19	−0.22	−0.53	−0.57

[a]: Values for a fully ordered model (without O/F disorder); see the Supporting Information for further details.

Table 7. Average overlap population between two atoms from Mulliken population analyses of the optimized solid-state structures of $[ClOF_2][MF_6]$ (M = V, Nb, Ta, Ru, Os, Ir, P, As, Sb). Rows are arranged in order of increasing $r_{eff}(M(V))$.

Compound	average overlap population / e				
	Cl−O	Cl−F	Cl···μ-F	M−F (non-bridging)	M−μ-F (bridging)
$[ClOF_2][PF_6]$	0.25	0.01	0.01	0.25	0.20
$[ClOF_2][AsF_6]$	0.24	0.01	0.01	0.28	0.24
$[ClOF_2][VF_6]$	0.25	0.01	0.01	0.11	0.10
$[ClOF_2][RuF_6]$	0.25	0.01	0.01	0.09	0.07
$[ClOF_2][IrF_6]$	0.24	0.01	0.01	0.12	0.11
$[ClOF_2][OsF_6]$	0.24	0.01	0.01	0.09	0.08
$[ClOF_2][SbF_6]$	0.25	0.01	0.01	0.19	0.16
$[ClOF_2][NbF_6]$[a]	0.25	0.01	0.01	0.10	0.08
$[ClOF_2][TaF_6]$[a]	0.25	0.01	0.01	0.12	0.10

[a]: Values for a fully ordered model (without O/F disorder); see the Supporting Information for further details.

We note that the experimentally observed trend of increasing Cl−O bond lengths in $[ClOF_2]^+$ with increasing effective radius of the central M atom in the $[MF_6]^-$ anions is not reproduced in the calculations, where a value of 1.41 Å is obtained, independent from the choice of M. Moreover, the entire electronic structure of the cation does not show a significant dependence on M, as reflected by the almost identical numbers for the partial charges and the overlap populations in $[ClOF_2]^+$ for all choices of M in Tables 6 and 7. For additional insights, we carried out molecular DFT calculations using TURBOMOLE and the same settings as for the periodic calculations for a bare $[ClOF_2]^+$ cation as well as for $[[ClOF_2](MF_6)_3]^{2-}$ anions (M = P, Sb). For the latter, the atomic coordinates of the three $[MF_6]^-$ ions were fixed to those of the determined crystal structures. Like for the periodic treatment reported above, Mulliken analyses indicate charge being transferred from the anion to the cation, here amounting to 0.28 electrons for both types of MF_6^- anions. For the periodic treatment it is somewhat smaller, circa 0.2 electrons, see Table 6. This leads to partial occupations of the energetically lowest unoccupied orbitals of the bare $[ClOF_2]^+$ ion. The three energetically lowest of them are shown in Figure 6. These are the three energetically highest of the 16 molecular orbitals that may be constructed from the atomic valence s/p orbitals while the other thirteen molecular orbitals are occupied by the 26 valence electrons of the $[ClOF_2]^+$ cation. The three are all anti-bonding with respect to the Cl−O bond as well as to the Cl−F bonds. Consequently, both Cl−O and Cl−F bonds are longer in the embedded than in the bare cation. For M = P they amount to 1.384 Å (Cl−O) and 1.596 Å (mean value of the two Cl−F bond lengths), thus longer by 0.005 Å and 0.039 Å than for the bare $[ClOF_2]^+$ ion. On the other hand, the changes from M = P to M = As are small, +0.002 Å for Cl−O and +0.003 Å for Cl−F, as the amount of charge transferred is the same for both cases. So, whereas changes from the bare to the embedded cation as well as the weak dependence of the Cl−F bond lengths on the choice of M result from our calculations and can be rationalized within a simple orbital picture, this is not the case for the correlations of Cl−O distances with any property of M.

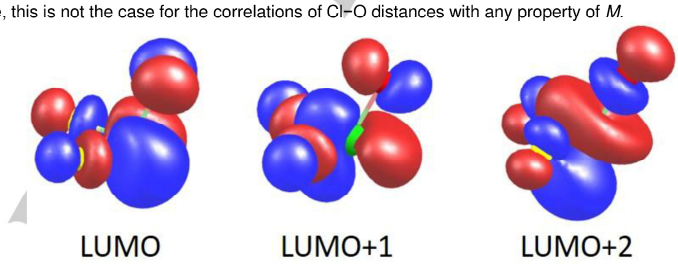

Figure 6. The three lowest unoccupied orbitals of $[ClOF_2]^+$. They are all anti-bonding with respect to the Cl−O bond and the Cl−F bonds. Contours for amplitudes are drawn at ± 0.05 atomic units.

Raman spectra of $[ClOF_2][MF_6]$ compounds

Compounds containing the $[ClOF_2]^+$ cation and a range of different anions, including "$[F(HF)_n]^-$", $[BF_4]^-$, $[MoOF_5]^-$, $[Mo_2O_2F_9]^-$, $[MF_6]^-$ (M = V, Nb, Ta, U, Pt, Au, P, As, Sb, Bi) and $[SiF_6]^{2-}$, were previously extensively studied by Raman spectroscopy in hydrogen fluoride solutions and/or in the solid-state.[3,20,21,33–38,69–71] In the previous studies, the band assignments were usually based on a C_s symmetry for the $[ClOF_2]^+$ cation either in solution or in the solid-state.

This article is protected by copyright. All rights reserved.

Accepted Manuscript

Chemistry - A European Journal 10.1002/chem.202003629

The Raman spectra of the presently investigated compounds are shown in Figure 7 and the respective low-resolution spectra are reported in the Supporting Information. Additionally, Raman spectra based on the optimized solid-state structures (DFT-PBE0/TZVP level of theory) were calculated. A comparison of the calculated and experimental Raman spectra, along with band assignments for the calculated Raman spectra, are given in the Supporting Information. Vibrational frequencies attributable to the $[ClOF_2]^+$ cation are listed in Table 8. The Raman spectra of the compounds $[ClOF_2][MF_6]$ (M = V, Nb, Ta, P, Sb) reported in this work nicely agree with the previously reported spectra.[34]

Generally, six bands are observed and attributed to the $[ClOF_2]^+$ cation in most Raman spectra: ν(ClO) at ≈ 1330 cm^{-1} (usually two separate bands due to the ^{35}Cl and ^{37}Cl isotopes), $\nu_s(ClF_2)$ at ≈ 740 cm^{-1}, $\nu_{as}(ClF_2)$ at ≈ 710 cm^{-1}, $\delta_{umbrella}([ClOF_2])$ at ≈ 510 cm^{-1}, δ_{sciss}(ClO) at ≈ 400 cm^{-1} and $\delta_{sciss}(ClF_2)$ at ≈ 380 cm^{-1}.[3,35] The frequencies that are assigned to these bands are similar among the $[ClOF_2][MF_6]$ compounds, indicating that the $[MF_6]^-$ anion has a minor effect. The bands attributable to ν(ClO) and ν(ClF) modes in the Raman spectrum of liquid $ClOF_3$ occur at 1224 and 689 cm^{-1}, respectively, and are shifted bathochromically when compared with the $[ClOF_2]^+$ cation, as may be expected.[72]

The calculated frequencies of $[ClOF_2][MF_6]$ compounds usually lie lower in energy and the band assignments of the calculated frequencies show that the vibrational modes of the $[MF_6]^-$ anions are vibrationally coupled to modes of the $[ClOF_2]^+$ cation. This was also shown for the calculated Raman spectrum for the hypothetical molecular anion, $[ClOF_2][AsF_6]_3^{2-}$, which was used to model a section of the crystal structure of $[ClOF_2][AsF_6]$.[38]

Bands assigned to the $[MF_6]^-$ anions are in agreement with those reported for their respective lithium salts $Li[MF_6]$ (M = V, Nb, Ta, Ru, Os, Ir, P, Sb).[73]

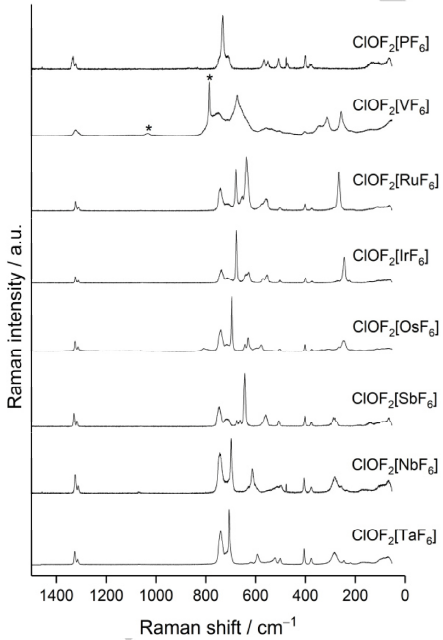

Figure 7. Recorded high-resolution Raman spectra of solid $[ClOF_2][MF_6]$ (M = V, Nb, Ta, Ru, Os, Ir, P, Sb). Asterisks denote bands that likely arise from hydrolysis products of the sample. Spectra are arranged in order of increasing $r_{eff}(M(V))$.

Table 8. Comparison of experimentally determined and calculated vibrational frequencies assigned to the $[ClOF_2]^+$ cation in $[ClOF_2][MF_6]$ (M = V, Nb, Ta, Ru, Os, Ir, P, Sb). Rows are arranged in order of increasing $r_{eff}(M(V))$.

Compound	ν(ClO) / cm^{-1}	$\nu_s(ClF_2)$ / cm^{-1}	$\nu_{as}(ClF_2)$ / cm^{-1}	$\delta_{umbrella}([ClOF_2])$ / cm^{-1}	δ_{sciss}(ClO) / cm^{-1}	$\delta_{sciss}(ClF_2)$ / cm^{-1}	Reference
$[ClOF_2][PF_6]$	1332, 1321	732	710	508	401	382	this work
	1329-1327	748-742	727-715	495-486	388-386	352-350	calculated
	1334, 1321	741	710	506	400	382, 377	[34]
	1334, 1325	740	713	511	403	380	[33]
$[ClOF_2][VF_6]$	1322	750	712	506	401	345	this work
	1312-1310	737	718-702	487	401-399	361-343	calculated
	1318, 1308	746	not observed	530	407	380	[34]
$[ClOF_2][RuF_6]$	1323, 1311	742	714	503	401	375	this work
	1317-1315	745	715	491-481	392-390	350-349	calculated

This article is protected by copyright. All rights reserved.

Accepted Manuscript

Chemistry - A European Journal 10.1002/chem.202003629

WILEY-VCH

$[ClOF_2][IrF_6]$	1324, 1313	737	713	503	400	374	this work
	1319-1317	743-737	727-708	491-481	390-384	349	calculated
$[ClOF_2][OsF_6]$	1325, 1313	740	716	503	402	375	this work
	1329-1323	757-735	699-692	486-476	386	348-347	calculated
$[ClOF_2][SbF_6]$	1330, 1318	747	715	507	402	377	this work
	1325-1324	751-743	727-714	494-484	389-388	348-347	calculated
	1327, 1316	742	715	508	402	377	[34]
	1330, 1319	748	709	509	404	378	[20]
$[ClOF_2][NbF_6]$	1325, 1313	744	not resolved	499	405	377	this work
	1317-1313	747-745	738-705	493-490	398-393	351-347	calculated
	1332, 1320	740	not observed	502	406	377	[34]
$[ClOF_2][TaF_6]$	1327, 1315	741	not resolved	500	404	376	this work
	1330-1316	765-741	722-711	500-468	395-388	350-349	calculated
	1324, 1313	737	not observed	502	406	377	[34]

Conclusion

The reactions of chlorine trifluoride with oxides or with metals and O_2 under UV irradiation led to the formation of the compounds $[ClOF_2][MF_6]$ (M = V, Nb, Ta, Ru, Os, Ir, P, Sb). The crystal structures determined by single-crystal X-ray diffraction show that two different structure types are formed as determined by different stacking variants among the layer structures. The sizes of the M(V) ions generally impact the primary Cl−O bond lengths of the $[ClOF_2]^+$ cations, which increase with increasing effective ionic radius $r_{eff}(M(V))$. Surprisingly, quantum-chemical calculations at the present level of theory did not reproduce the observed values, with longer Cl−F and much shorter Cl−O bond lengths. The Cl−O Raman shifts also generally do not to follow this trend. The calculations show that the Cl−O bonds have essentially covalent character, whereas the Cl−F bonds have a significantly higher degree of ionic character. The interactions of the μ-F atoms of the $[MF_6]^-$ anions that bridge to the Cl atoms are essentially electrostatic. Further investigations regarding the photochemical synthesis of new $[ClOF_2]^+$ compounds are ongoing.

Experimental Section

General: Volatile materials were handled in a Monel metal Schlenk line, which was passivated with undiluted fluorine and/or chlorine trifluoride at various pressures before use. Moisture-sensitive compounds were stored and handled in an Ar-filled glove box (MBraun). Reaction vessels were made out of fluoropolymer (PFA) that were closed by stainless steel valves. All reactors were passivated with fluorine before use. Preparations were carried out in an atmosphere of dry and purified argon (5.0, Praxair). Chlorine trifluoride was stored over NaF to remove traces of HF. Photochemical syntheses were carried out in a homemade UV reactor, which was equipped with eight low-pressure Hg lamps (OSRAM Puritec HNS S 11 W G23, main emission line 254 nm). ***Caution!*** *Fluorine, chlorine trifluoride, and difluorooxychloronium(V) compounds must be handled using appropriate protective gear with ready access to proper emergency treatment procedures in the event of contact. They are potent oxidative fluorinators that are only stable under the rigorously anhydrous conditions employed in the experimental procedures outlined in this section. They can react vigorously to explosively upon hydrolysis or contact with organic materials. The utmost precautions must be taken when disposing of these materials and their derivatives. The PFA reaction vessels occasionally became brittle after prolonged UV irradiation of the reaction mixtures due to stress cracking likely caused by highly reactive radicals formed in these reactions.*

The low yields are due to incomplete transfer of the products from the PFA tubes into the storage vessels. For $[ClOF_2][PF_6]$ and $[ClOF_2][VF_6]$, the yields are even lower due to the dissociation vapor pressures of these compounds at room temperature, which were reported to be approximately 4.7 and 3.3 mbar, respectively.[34]

Syntheses – General: A PFA reaction vessel was loaded with the solid starting material outside the glove box and attached to a stainless-steel valve. The valve was then connected to the Monel metal Schlenk line, the reaction vessel was evacuated and an excess of ClF_3 was condensed onto the solid at 77 K. The reaction vessel was then placed in a stainless-steel Dewar vessel and allowed to warm to room temperature over a period of several hours. After that, the reaction vessel was placed inside the UV reactor and irradiated. In the case of Os and Ir, the reaction mixtures were then cooled to 77 K, the liquid nitrogen cooling removed, and then O_2 was added to the reaction vessels. UV-irradiation was started while the reaction mixture warmed to room temperature. All volatiles were then pumped off and the product was isolated in the glove box.
$[ClOF_2][VF_6]$: 45 mg V_2O_5 (0.25 mmol) was reacted with 0.42 g ClF_3 (4.5 mmol) and the reaction mixture was then irradiated for five days (30.8 mg isolated, 127 mg calculated).
$[ClOF_2][NbF_6]$: 27 mg Nb_2O_5 (0.10 mmol) was reacted with 0.36 g ClF_3 (3.9 mmol) and the reaction mixture was then irradiated for four days (31.4 mg isolated, 60 mg calculated).
$[ClOF_2][TaF_6]$: 64 mg Ta_2O_5 (0.14 mmol) was reacted with 0.38 g ClF_3 (4.1 mmol) and the reaction mixture was then irradiated for seven days (100 mg isolated, 108 mg calculated).
$[ClOF_2][RuF_6]$: 18 mg $RuO_2 \cdot xH_2O$ (59.78% Ru, $x \approx 2$, 0.11 mmol) was reacted with 0.34 g ClF_3 (3.7 mmol) and the reaction mixture was then irradiated for thirteen days (28.4 mg isolated, 32 mg calculated).
$[ClOF_2][OsF_6]$: 37 mg Os powder (0.19 mmol) was reacted with 0.60 g ClF_3 (6.5 mmol), the reddish solution was frozen with liquid nitrogen, the cooling was removed and 0.7 bar O_2 was added to the reaction vessel. The reaction mixture was then irradiated for 16 h (55.6 mg isolated, 75 mg calculated).

This article is protected by copyright. All rights reserved.

Accepted Manuscript

Chemistry - A European Journal 10.1002/chem.202003629

WILEY-VCH

FULL PAPER

[ClOF$_2$][IrF$_6$]: 20 mg Ir powder (0.10 mmol) was reacted with 0.17 g ClF$_3$ (1.8 mmol), the red solution was frozen with liquid nitrogen, the cooling was removed and 1 bar O$_2$ was added to the reaction vessel. The reaction mixture was then irradiated for seven days (55.6 mg isolated, 75 mg calculated).
[ClOF$_2$][PF$_6$]: 38 mg P$_2$O$_5$ (0.27 mmol) was reacted with 0.36 g ClF$_3$ (3.9 mmol) and the reaction mixture was then irradiated for four days (66.7 mg isolated, 127 mg calculated).
[ClOF$_2$][SbF$_6$]: 18 mg Sb$_2$O$_4$ (0.058 mmol) was reacted with 0.14 g ClF$_3$ (1.5 mmol) and the reaction mixture was then irradiated for thirteen days (29.1 mg isolated, 38 mg calculated).

Single-crystal X-ray diffraction: Crystals of the moisture-sensitive compounds were selected under dried perfluorinated oil (Fomblin YR1800, Solvay, stored over molecular sieve 3 Å) and mounted on a MiTeGen loop. Intensity data of suitable crystals were recorded with a D8 Quest diffractometer (Bruker), an IPDS2 diffractometer (STOE) or an IPDS2T diffractometer (STOE). The diffractometers were operated with monochromatized Mo-K$_\alpha$ radiation (0.71073 Å), multi-layered optics (D8 Quest), or a graphite monochromator (IPDS2/IPDS2T) and equipped with a PHOTON 100 CMOS detector (D8 Quest) or an image plate detector (IPDS2/IPDS2T). Evaluation, integration and reduction of the diffraction data was carried out with the APEX3 software suite (D8 Quest) or the X-Area software suite (IPDS2/IPDS2T).[74,75] The diffraction data was corrected for absorption utilizing the multi-scan method of SADABS within the APEX3 software suite (D8 Quest) or the integration method with the modules X-Shape and X-Red32 of the X-Area software suite (IPDS2/IPDS2T).[76–78] The structures were solved with dual-space methods (SHELXT) and refined against F^2 (SHELXL).[79,80] For the compounds [ClOF$_2$][NbF$_6$] and [ClOF$_2$][TaF$_6$] partial or full O/F disorder was observed for the [ClOF$_2$]$^+$ cations. The *xyz* and U_{ij} parameters of the disordered O/F atoms were restrained with the EXYZ and EADP commands in SHELXL. The site occupancy factors among the possible O/F positions were restrained by the SUMP command in SHELXL. For [ClOF$_2$][NbF$_6$] the site occupation factors for the O/F disordered Cl(1)OF$_2^+$ cation are the following: O/F(1A): 0.26(3) O / 0.74 F; O/F(1B): 0.37(3) O / 0.63 F; O/F(1C): 0.37(3) O / 0.63 F. For [ClOF$_2$][TaF$_6$] the site occupancy factors for the O/F disordered Cl(1)OF$_2^+$ cation are the following: O/F(1A): 0.58(3) O / 0.42 F; O/F(1B): 0.42(3) O / 0.58 F. The site occupancy factors for the O/F disordered Cl(2)OF$_2^+$ cation are the following: O/F(3A): 0.33(4) O / 0.67 F; O/F(3B): 0.38(4) O / 0.62 F; O/F(3C): 0.29(4) O / 0.71 F. Weak systematic absence violations were observed for the space group *Pna*2$_1$ (No. 33) for all here investigated compounds. However, the intensities of the respective reflections were close to the tripled standard uncertainties. Solution and refinement of the structures in crystallographic subgroups resulted in correlations between atomic coordinates and non-positive definite displacement parameters for some atoms. The crystal structures were consequently solved and refined in the reported space groups, which were also indicated by the Addsym feature of the program package PLATON when searching for additional symmetry within the subgroups.[81,82] The locations of highest residual electron densities after the final refinement were the following: [ClOF$_2$][VF$_6$]: 0.44 Å from atom O(1), [ClOF$_2$][NbF$_6$]: 1.46 Å from atom F(10), [ClOF$_2$][TaF$_6$]: 1.30 Å from atom F(11), [ClOF$_2$][RuF$_6$]: 0.92 Å from atom Ru(1), [ClOF$_2$][OsF$_6$]: 0.70 Å from atom Os(1), [ClOF$_2$][IrF$_6$]: 1.03 Å from atom F(3), [ClOF$_2$][PF$_6$]: 0.51 Å from atom O(1), [ClOF$_2$][SbF$_6$]: 0.97 Å from atom Sb(1). Representations of the crystal structures were created with the Diamond software.[83] CCDC 2013082-2013089 contain the supplementary crystallographic data for this paper. These data are provided free of charge by The Cambridge Crystallographic Data Centre.

Raman spectroscopy: The Raman spectra were measured with a Monovista CRS+ confocal Raman microscope (Spectroscopy & Imaging GmbH) using a 532 nm solid-state laser and either a 300 grooves/mm (low-resolution mode, FWHM: <4.62 cm^{-1}) or a 1800 grooves/mm (high-resolution mode, FWHM: <0.368 cm^{-1}) grating. Samples were either transferred into dried glass vessels or immersed in perfluorinated oil (Fomblin YR1800, Solvay, stored over molecular sieve 3 Å) on a microscope slide.

Quantum-chemical calculations: Periodic quantum-chemical calculations were carried out for the difluorooxychloronium(V) hexafluorido(non)metallates(V) with the PBE0 hybrid density functional theory method (DFT-PBE0).[65,66] Triple-zeta-valence + polarization (TZVP) level basis sets were applied for all atoms. Details of the basis sets that were employed are given in the Supporting Information. All calculations were carried out with the CRYSTAL17 program package.[84] The crystal structure of [ClOF$_2$][AsF$_6$] was taken from a previous study.[38] The reciprocal space was sampled with the following Monkhorst-Pack-type *k*-point grids: [ClOF$_2$][VF$_6$]: 2×4×3, [ClOF$_2$][NbF$_6$]: 1×5×3, [ClOF$_2$][TaF$_6$]: 1×5×3, [ClOF$_2$][RuF$_6$]: 2×4×3, [ClOF$_2$][OsF$_6$]: 2×4×3, [ClOF$_2$][IrF$_6$]: 2×4×3, [ClOF$_2$][PF$_6$]: 2×4×3, [ClOF$_2$][AsF$_6$]: 2×4×3, [ClOF$_2$][SbF$_6$]: 2×4×3. For the evaluation of the Coulomb and exchange integrals (TOLINTEG), tight tolerance factors of 8, 8, 8, 8, 16 were used for all calculations. Both the atomic positions and lattice parameters were fully optimized within the constraints imposed by the space group symmetry. Default DFT integration grids and optimization convergence thresholds were applied in all calculations. Mulliken population analyses were carried out for all compounds. For the magnetic systems [ClOF$_2$][RuF$_6$], [ClOF$_2$][OsF$_6$] and [ClOF$_2$][IrF$_6$] a ferromagnetic ground state was employed. The resulting magnetic moments were 3.0 μB for the [RuF$_6$]$^-$ anion (2.3 μB contribution from Ru), 3.0 μB for the [OsF$_6$]$^-$ anion (2.4 μB contribution from the Os atom) and 2.0 μB for the [IrF$_6$]$^-$ anion (1.4 μB contribution from Ir). The harmonic vibrational frequencies and Raman intensities were obtained through usage of the computational scheme implemented in CRYSTAL17.[85–87,87] The Raman intensities were calculated for a polycrystalline powder sample (total isotropic intensity in arbitrary units). The Raman spectra were obtained by using a pseudo-Voigt band profile (50:50 Lorentzian:Gaussian) and an FWHM of 8 cm^{-1}. The Raman spectra were simulated taking the experimental setup (T = 207.15 K, λ = 532 nm) into account. The band assignments were carried out by visual inspection of the normal modes with the Jmol program package.[88] Molecular DFT calculations were carried out with TURBOMOLE with the same settings as the periodic calculations, orbitals were visualized with Chemcraft.[89,90]

Acknowledgements

We thank the Deutsche Forschungsgemeinschaft (DFG) for generous funding and Dr. Sergei Ivlev, Marburg, for helpful discussions. A. J. K. acknowledges computational resources provided by CSC, the Finnish IT Center for Science.

Keywords: chlorine trifluoride • difluorooxychloronium(V) cation • fluorine • photochemistry • single-crystal X-ray diffraction

[1] R. Bougon, J. Isabey, P. Plurien, *C. R. Seances Acad. Sci., Ser. C* **1970**, *271*, 1366–1369.
[2] D. Pilipovich, C. B. Lindahl, C. J. Schack, R. D. Wilson, K. O. Christe, *Inorg. Chem.* **1972**, *11*, 2189–2192.
[3] K. O. Christe, C. J. Schack, in *Advances in Inorganic Chemistry and Radiochemistry*, Elsevier, **1976**, pp. 319–398.
[4] H. Schmitz, H. J. Schumacher, *Z. Anorg. Allg. Chem.* **1942**, *249*, 238–244.
[5] H. Bode, E. Klesper, *Z. Anorg. Allg. Chem.* **1951**, *266*, 275–280.
[6] A. Engelbrecht, H. Atzwanger, *Monatsh. Chem.* **1952**, *83*, 1087–1089.

This article is protected by copyright. All rights reserved.

Accepted Manuscript

Chemistry - A European Journal 10.1002/chem.202003629

WILEY-VCH

FULL PAPER

[7] K. O. Christe, *Inorg. Nucl. Chem. Lett.* **1972**, *8*, 453–455.
[8] K. O. Christe, *Inorg. Nucl. Chem. Lett.* **1972**, *8*, 457–459.
[9] K. O. Christe, R. D. Wilson, *Inorg. Chem.* **1973**, *12*, 1356–1357.
[10] R. Bougon, M. Carles, J. Aubert, *C. R. Seances Acad. Sci., Ser. C* **1967**, *265*, 179–182.
[11] T. D. Cooper, F. N. Dost, C. H. Wang, *J. Inorg. Nucl. Chem.* **1972**, *34*, 3564–3567.
[12] L. Andrews, F. K. Chi, A. Arkell, *J. Am. Chem. Soc.* **1974**, *96*, 1997–2000.
[13] H. S. P. Müller, *Chem. Phys. Lett.* **1999**, *314*, 396–402.
[14] H. S. P. Müller, E. A. Cohen, *J. Chem. Phys.* **2002**, *116*, 2407–2416.
[15] G. H. Rohrback, G. H. Cady, *J. Am. Chem. Soc.* **1947**, *69*, 677–678.
[16] D. Pilipovich, R. D. Wilson, *SYNTHESIS OF OXYCHLORINE TRIFLUORIDE (North American Rockwell Corporation)*, **1972**, US-3,697,394.
[17] D. Pilipovich, R. D. Wilson, H. F. Bauer, *OXYCHLORINE TRIFLUORDE AND ALKALI FLUORDE-Cl2O COMPLEX (North American Rockwell Corporation)*, **1973**, US-3,733,392.
[18] R. D. Wilson, A. E. Axworthy, K. O. Christe, *J. Argent. Chem. Soc.* **2005**, *93*, 1–20.
[19] D. Pilipovich, H. H. Rogers, R. D. Wilson, *Inorg. Chem.* **1972**, *11*, 2192–2195.
[20] R. Bougon, J. Isabey, P. Plurien, *C. R. Seances Acad. Sci., Ser. C* **1971**, *273*, 415–417.
[21] C. J. Schack, C. B. Lindahl, D. Pilipovich, K. O. Christe, *Inorg. Chem.* **1972**, *11*, 2201–2205.
[22] K. O. Christe, C. J. Schack, D. Pilipovich, *Inorg. Chem.* **1972**, *11*, 2205–2208.
[23] R. Bougon, T. B. Huy, P. Charpin, G. Tantot, *C. R. Seances Acad. Sci., Ser. C* **1976**, *283*, 71–74.
[24] R. J. Gillespie, P. Spekkens, *J. Chem. Soc., Dalton Trans.* **1976**, 2391–2396.
[25] P. H. Spekkens, OXYFLUORO COMPOUNDS OF BROMINE, Dissertation, McMaster University (Canada), **1977**.
[26] R. J. Gillespie, P. H. Spekkens, *Isr. J. Chem.* **1978**, *17*, 11–19.
[27] R. Bougon, T. B. Huy, P. Charpin, R. J. Gillespie, P. H. Spekkens, *J. Chem. Soc., Dalton Trans.* **1979**, 6–12.
[28] J. J. Krasznai, OXO AND OXYFLUORO COMPLEXES OF IODINE (V) AND (VII), Dissertation, McMaster University (Canada), **1975**.
[29] K. Seppelt, *Angew. Chem.* **1979**, *91*, 199–214.
[30] K. Seppelt, *Angew. Chem. Int. Ed. Engl.* **1979**, *18*, 186–202.
[31] A. Ellern, J. A. Boatz, K. O. Christe, T. Drews, K. Seppelt, *Z. Anorg. Allg. Chem.* **2002**, *628*, 1991–1999.
[32] K. O. Christe, E. C. Curtis, *Inorg. Chem.* **1972**, *11*, 2209–2211.
[33] R. Bougon, *C. R. Seances Acad. Sci., Ser. C* **1972**, *274*, 696–698.
[34] R. Bougon, T. Bui Huy, A. Cadet, P. Charpin, R. Rousson, *Inorg. Chem.* **1974**, *13*, 690–695.
[35] Sh. Sh. Nabiev, I. I. Ostroukhova, N. V. Revina, L. P. Sukhanov, *Russ. Chem. Bull.* **1998**, *47*, 417–422.
[36] K. Züchner, O. Glemser, *Angew. Chem.* **1972**, *84*, 1147–1149.
[37] K. Züchner, O. Glemser, *Angew. Chem. Int. Ed. Engl.* **1972**, *11*, 1094–1095.
[38] D. S. Brock, J. J. Casalis de Pury, H. P. A. Mercier, G. J. Schrobilgen, B. Silvi, *Inorg. Chem.* **2010**, *49*, 6673–6689.
[39] R. Bougon, W. V. Cicha, M. Lance, L. Meublat, M. Nierlich, J. Vigner, *Inorg. Chem.* **1991**, *30*, 102–109.
[40] A. M. Ellern, M. N. Sinitsyn, M. Y. Antipin, A. V. Sharabarin, Y. T. Struchkov, *Koord. Khim.* **1991**, *17*, 1686–1688.
[41] R. Haiges, in *Efficient Preparations of Fluorine Compounds* (Ed.: H.W. Roesky), John Wiley & Sons, Inc., Hoboken, NJ, USA, **2012**, pp. 100–107.
[42] J. F. Ellis, C. W. Forrest, *J. Inorg. Nucl. Chem.* **1960**, *16*, 150–153.
[43] R. C. Shrewsberry, E. L. Williamson, *J. Inorg. Nucl. Chem.* **1966**, *28*, 2535–2539.
[44] K. O. Christe, R. D. Wilson, C. J. Schack, *Inorg. Chem.* **1981**, *20*, 2104–2114.
[45] K. O. Christe, R. D. Wilson, C. J. Schack, *Inorg. Synth.* **1986**, *24*, 3–6.
[46] M. Schmeisser, F. L. Ebenhöch, *Angew. Chem.* **1954**, *66*, 230–231.
[47] A. A. Woolf, *J. Chem. Soc.* **1954**, 4113–4116.
[48] J. F. Lehmann, S. Riedel, G. J. Schrobilgen, *Inorg. Chem.* **2008**, *47*, 8343–8356.
[49] T. E. Mallouk, G. L. Rosenthal, G. Mueller, R. Brusasco, N. Bartlett, *Inorg. Chem.* **1984**, *23*, 3167–3173.
[50] R. J. Gillespie, J. P. Krasznai, D. R. Slim, *J. Chem. Soc., Dalton Trans.* **1980**, 481–483.
[51] D. Mootz, L. Korte, *Z. Naturforsch., B: Anorg. Chem., Org. Chem.* **1984**, *39*, 1295–1299.
[52] J. C. Dewan, A. J. Edwards, *J. Chem. Soc., Dalton Trans.* **1976**, 2433–2435.
[53] H. Oberhammer, K. O. Christe, *Inorg. Chem.* **1982**, *21*, 273–275.
[54] R. D. Shannon, *Acta Crystallogr., Sect. A: Cryst. Phys., Diffr., Theor. Gen. Crystallogr.* **1976**, *32*, 751–767.
[55] R. J. Gillespie, R. S. Nyholm, *Q. Rev., Chem. Soc.* **1957**, *11*, 339–380.
[56] R. J. Gillespie, E. A. Robinson, *Angew. Chem.* **1996**, *108*, 539–560.
[57] R. J. Gillespie, *Coord. Chem. Rev.* **2008**, *252*, 1315–1327.
[58] J. Pilmé, E. A. Robinson, R. J. Gillespie, *Inorg. Chem.* **2006**, *45*, 6198–6204.
[59] F. Benachenhou, G. Mairesse, G. Nowogrocki, D. Thomas, *J. Solid State Chem.* **1986**, *65*, 13–26.
[60] A. R. Mahjoub, A. Hoser, J. Fuchs, K. Seppelt, *Angew. Chem.* **1989**, *101*, 1528–1529.
[61] A. R. Mahjoub, K. Seppelt, *Angewandte Chemie International Edition in English* **1991**, *30*, 323–324.
[62] S. Hoyer, T. Emmler, K. Seppelt, *Journal of Fluorine Chemistry* **2006**, *127*, 1415–1422.
[63] L. S. Bartell, R. M. Gavin, *J. Chem. Phys.* **1968**, *48*, 2466–2483.
[64] W. B. Jensen, in *Cohesion and Structure* (Eds.: J. Hafner, F. Hulliger, W.B. Jensen, J.A. Majewski, K. Mathis, P. Villars, P. Vogl), North-Holland, **1989**, pp. 105–146.
[65] J. P. Perdew, K. Burke, M. Ernzerhof, *Phys. Rev. Lett.* **1996**, *77*, 3865–3868.
[66] C. Adamo, V. Barone, *J. Chem. Phys.* **1999**, *110*, 6158–6170.
[67] J. B. Mann, T. L. Meek, L. C. Allen, *J. Am. Chem. Soc.* **2000**, *122*, 2780–2783.
[68] J. B. Mann, T. L. Meek, E. T. Knight, J. F. Capitani, L. C. Allen, *J. Am. Chem. Soc.* **2000**, *122*, 5132–5137.
[69] K. O. Christe, E. C. Curtis, C. J. Schack, *Inorg. Chem.* **1972**, *11*, 2212–2215.
[70] R. Bougon, T. Bui Huy, P. Charpin, *Inorg. Chem.* **1975**, *14*, 1822–1830.
[71] Sh. Sh. Nabiev, *Russ. Chem. Bull.* **1999**, *48*, 711–717.
[72] K. O. Christe, E. C. Curtis, *Inorg. Chem.* **1972**, *11*, 2196–2201.
[73] G. Tavčar, B. Žemva, *Inorg. Chem.* **2013**, *52*, 4319–4323.
[74] *APEX3*, Bruker AXS Inc., Madison, Wisconsin, USA, **2018**.
[75] *X-Area*, STOE & Cie GmbH, Darmstadt, Germany, **2018**.
[76] *SADABS*, Bruker AXS Inc., Madison, Wisconsin, USA, **2016**.
[77] *X-Shape*, STOE & Cie GmbH, Darmstadt, Germany, **2017**.
[78] *X-RED32*, STOE & Cie GmbH, Darmstadt, Germany, **2018**.
[79] G. M. Sheldrick, *Acta Crystallogr., Sect. A: Found. Adv.* **2015**, *71*, 3–8.
[80] G. M. Sheldrick, *Acta Crystallogr., Sect. C: Struct. Chem.* **2015**, *71*, 3–8.
[81] A. L. Spek, *PLATON - A Multipurpose Crystallographic Tool*, Utrecht University, Utrecht, The Netherlands, **2019**.
[82] A. L. Spek, *Acta Crystallogr., Sect. D: Biol. Crystallogr.* **2009**, *65*, 148–155.
[83] K. Brandenburg, H. Putz, *Diamond - Crystal and Molecular Structure Visualization*, Crystal Impact GbR, Bonn, **2019**.
[84] R. Dovesi, A. Erba, R. Orlando, C. M. Zicovich-Wilson, B. Civalleri, L. Maschio, M. Rérat, S. Casassa, J. Baima, S. Salustro, B. Kirtman, *Wiley Interdiscip. Rev.: Comput. Mol. Sci.* **2018**, e1360.
[85] C. M. Zicovich-Wilson, F. Pascale, C. Roetti, V. R. Saunders, R. Orlando, R. Dovesi, *J. Comput. Chem.* **2004**, *25*, 1873–1881.
[86] F. Pascale, C. M. Zicovich-Wilson, F. López Gejo, B. Civalleri, R. Orlando, R. Dovesi, *J. Comput. Chem.* **2004**, *25*, 888–897.
[87] L. Maschio, B. Kirtman, M. Rérat, R. Orlando, R. Dovesi, *J. Chem. Phys.* **2013**, *139*, 164101.
[88] *Jmol: An Open-Source Java Viewer for Chemical Structures in 3D. Http://Www.Jmol.Org/*, Jmol Team, **2019**.

This article is protected by copyright. All rights reserved.

Accepted Manuscript

Chemistry - A European Journal 10.1002/chem.202003629

[89] *TURBOMOLE V7.5, a Development of University of Karlsruhe and Forschungszentrum Karlsruhe GmbH, 1989-2007, TURBOMOLE GmbH, since 2007.*, **2020**.
[90] *Chemcraft - Graphical Software for Visualization of Quantum Chemistry Computations. Https://Www.Chemcraftprog.Com*, **2020**.

WILEY-VCH

Accepted Manuscript

This article is protected by copyright. All rights reserved.

Supporting Information

Content

Selected crystallographic data of difluorooxychloronium(V) fluoridometallates(V) 2

Plot of distances and angles within the $ClOF_2^+$ cations versus effective ionic radii of *M*(V) ions 8

Basis set details for quantum-chemical solid-state calculations 10

Lattice parameters and atomic coordinates of optimized solid-state structures of $ClOF_2[MF_6]$ (*M* = V, Nb, Ta, Ru, Os, Ir, P, As, Sb) 15

Comparison of low-resolution Raman spectra of $ClOF_2[MF_6]$ compounds (*M* = V, Nb, Ta, Ru, Os, Ir, P, Sb) 26

Raman spectra and band assignments for the calculated Raman spectra of $ClOF_2[MF_6]$ (*M* = V, Nb, Ta, Ru, Os, Ir, P, Sb) 27

References 34

Selected crystallographic data of difluorooxychloronium(V) fluoridometallates(V)

Atomic coordinates and displacement parameters of $ClOF_2[VF_6]$

Table S1. Atomic coordinates and equivalent isotropic displacement parameters U_{iso} of $ClOF_2[VF_6]$ at 100 K.

Atom	Position	*x*	*y*	*z*	U_{iso} / Å^2
V(1)	4*a*	0.39808(3)	0.39826(10)	0.72959(6)	0.01298(13)
Cl(1)	4*a*	0.39306(5)	0.10775(18)	0.27759(10)	0.0214(2)
O(1)	4*a*	0.34166(16)	0.3505(4)	0.2598(3)	0.0162(5)
F(1)	4*a*	0.32893(15)	−0.0769(4)	0.3681(3)	0.0230(5)
F(2)	4*a*	0.38619(15)	−0.0129(5)	0.1061(3)	0.0225(4)
F(3)	4*a*	0.33378(16)	0.1219(4)	0.7681(3)	0.0247(5)
F(4)	4*a*	0.30957(15)	0.5402(4)	0.6181(3)	0.0212(4)
F(5)	4*a*	0.36418(16)	0.5413(4)	0.9130(3)	0.0227(4)
F(6)	4*a*	0.49528(15)	0.2533(4)	0.8281(3)	0.0200(4)
F(7)	4*a*	0.43909(15)	0.2503(5)	0.5405(2)	0.0202(4)
F(8)	4*a*	0.46842(15)	0.6740(4)	0.6835(3)	0.0207(4)

Table S2. Anisotropic displacement parameters of $ClOF_2[VF_6]$ at 100 K.

Atom	U_{11} / Å^2	U_{22} / Å^2	U_{33} / Å^2	U_{23} / Å^2	U_{13} / Å^2	U_{12} / Å^2
V(1)	0.0120(2)	0.0145(2)	0.0125(2)	−0.0008(2)	−0.0003(2)	−0.00022(17)
Cl(1)	0.0133(3)	0.0300(4)	0.0209(4)	−0.0033(3)	−0.0028(3)	0.0002(3)
O(1)	0.0164(10)	0.0148(9)	0.0173(13)	0.0006(8)	−0.0020(9)	0.0050(8)
F(1)	0.0179(10)	0.0250(11)	0.0260(12)	0.0041(8)	0.0018(9)	−0.0034(8)
F(2)	0.0235(11)	0.0275(11)	0.0163(10)	−0.0053(9)	−0.0031(8)	−0.0001(9)
F(3)	0.0239(10)	0.0199(9)	0.0303(14)	0.0016(9)	0.0028(9)	−0.0070(8)
F(4)	0.0152(9)	0.0260(10)	0.0224(11)	0.0027(8)	−0.0025(9)	0.0028(8)
F(5)	0.0242(11)	0.0266(11)	0.0173(10)	−0.0060(9)	0.0031(9)	0.0021(9)
F(6)	0.0210(10)	0.0226(9)	0.0165(9)	−0.0006(8)	−0.0037(8)	0.0069(7)
F(7)	0.0190(9)	0.0270(10)	0.0146(10)	−0.0075(9)	−0.0011(7)	0.0020(8)
F(8)	0.0206(9)	0.0187(8)	0.0228(10)	0.0016(8)	−0.0012(8)	−0.0064(7)

Atomic coordinates and displacement parameters of $ClOF_2[PF_6]$

Table S3. Atomic coordinates and equivalent isotropic displacement parameters U_{iso} of $ClOF_2[PF_6]$ at 100 K.

Atom	Position	*x*	*y*	*z*	U_{iso} / Å^2
P(1)	4*a*	0.40302(4)	0.38662(11)	0.72980(7)	0.01791(12)
Cl(1)	4*a*	0.38681(4)	0.11177(11)	0.27429(8)	0.02260(13)
O(1)	4*a*	0.33048(12)	0.3438(3)	0.2620(2)	0.0232(3)
F(1)	4*a*	0.32779(11)	−0.0840(3)	0.3761(2)	0.0252(3)
F(2)	4*a*	0.37925(11)	−0.0211(4)	0.1024(2)	0.0287(3)
F(3)	4*a*	0.34159(12)	0.1345(3)	0.7644(2)	0.0283(3)
F(4)	4*a*	0.31949(11)	0.5163(3)	0.6259(2)	0.0253(3)
F(5)	4*a*	0.36850(11)	0.5177(3)	0.9002(2)	0.0257(3)
F(6)	4*a*	0.49026(11)	0.2551(3)	0.8287(2)	0.0265(3)
F(7)	4*a*	0.44176(11)	0.2541(3)	0.55662(19)	0.0248(3)
F(8)	4*a*	0.46730(12)	0.6375(3)	0.6904(2)	0.0276(3)

Table S4. Anisotropic displacement parameters of $ClOF_2[PF_6]$ at 100 K.

Atom	U_{11} / Å²	U_{22} / Å²	U_{33} / Å²	U_{23} / Å²	U_{13} / Å²	U_{12} / Å²
P(1)	0.0161(2)	0.0201(2)	0.0175(2)	−0.0011(2)	−0.00051(19)	0.00024(16)
Cl(1)	0.0172(2)	0.0281(3)	0.0225(2)	−0.0006(2)	−0.00145(18)	−0.00076(16)
O(1)	0.0232(7)	0.0202(6)	0.0262(9)	−0.0006(7)	−0.0027(7)	0.0047(6)
F(1)	0.0223(6)	0.0268(6)	0.0266(7)	0.0037(6)	0.0014(6)	−0.0035(5)
F(2)	0.0276(7)	0.0375(9)	0.0209(7)	−0.0057(7)	−0.0023(6)	0.0040(6)
F(3)	0.0300(7)	0.0246(6)	0.0304(9)	0.0017(6)	0.0021(7)	−0.0064(5)
F(4)	0.0200(6)	0.0305(7)	0.0254(7)	0.0028(6)	−0.0018(5)	0.0034(5)
F(5)	0.0243(7)	0.0311(8)	0.0218(7)	−0.0058(6)	0.0015(6)	0.0031(6)
F(6)	0.0243(7)	0.0327(8)	0.0226(6)	−0.0031(6)	−0.0039(5)	0.0091(5)
F(7)	0.0220(6)	0.0321(7)	0.0203(6)	−0.0074(6)	−0.0003(5)	0.0018(5)
F(8)	0.0254(7)	0.0261(6)	0.0314(8)	−0.0012(6)	0.0010(6)	−0.0066(6)

Atomic coordinates and displacement parameters of $ClOF_2[RuF_6]$

Table S5. Atomic coordinates and equivalent isotropic displacement parameters U_{iso} of $ClOF_2[RuF_6]$ at 100 K.

Atom	Position	*x*	*y*	*z*	U_{iso} / Å²
Ru(1)	4*a*	0.59850(2)	0.60283(4)	0.26989(5)	0.01684(9)
Cl(1)	4*a*	0.61128(7)	0.89502(19)	0.72628(13)	0.0241(2)
O(1)	4*a*	0.66233(18)	0.6553(5)	0.7395(3)	0.0202(6)
F(1)	4*a*	0.67455(18)	1.0741(5)	0.6320(3)	0.0273(5)
F(2)	4*a*	0.61831(17)	1.0147(6)	0.8930(3)	0.0273(5)
F(3)	4*a*	0.6672(2)	0.8886(4)	0.2290(4)	0.0276(6)
F(4)	4*a*	0.69248(16)	0.4554(5)	0.3805(3)	0.0244(5)
F(5)	4*a*	0.63578(18)	0.4594(5)	0.0779(3)	0.0256(5)
F(6)	4*a*	0.49976(17)	0.7507(5)	0.1653(3)	0.0242(5)
F(7)	4*a*	0.55784(17)	0.7529(5)	0.4637(3)	0.0242(5)
F(8)	4*a*	0.52723(17)	0.3154(5)	0.3152(3)	0.0247(5)

Table S6. Anisotropic displacement parameters of $ClOF_2[RuF_6]$ at 100 K.

Atom	U_{11} / Å²	U_{22} / Å²	U_{33} / Å²	U_{23} / Å²	U_{13} / Å²	U_{12} / Å²
Ru(1)	0.01711(12)	0.01689(12)	0.01652(12)	−0.00086(14)	−0.00027(11)	0.00002(7)
Cl(1)	0.0188(4)	0.0297(5)	0.0238(4)	−0.0011(3)	−0.0021(3)	−0.0005(3)
O(1)	0.0218(11)	0.0167(10)	0.0222(17)	−0.0017(9)	−0.0019(9)	0.0049(8)
F(1)	0.0222(12)	0.0292(12)	0.0304(14)	0.0045(9)	0.0014(9)	−0.0050(9)
F(2)	0.0282(11)	0.0317(13)	0.0221(11)	−0.0052(11)	−0.0029(9)	0.0006(10)
F(3)	0.0293(12)	0.0209(10)	0.0325(14)	0.0026(9)	0.0018(10)	−0.0083(8)
F(4)	0.0183(10)	0.0292(10)	0.0258(11)	0.0042(10)	−0.0030(9)	0.0048(9)
F(5)	0.0298(12)	0.0262(10)	0.0207(10)	−0.0062(9)	0.0043(9)	0.0020(10)
F(6)	0.0242(11)	0.0266(11)	0.0217(10)	−0.0011(9)	−0.0047(9)	0.0078(8)
F(7)	0.0269(11)	0.0280(11)	0.0177(10)	−0.0068(9)	0.0003(8)	0.0026(9)
F(8)	0.0248(11)	0.0222(10)	0.0270(11)	0.0017(9)	−0.0006(8)	−0.0074(9)

Atomic coordinates and displacement parameters of $ClOF_2[SbF_6]$

Table S7. Atomic coordinates and equivalent isotropic displacement parameters U_{iso} of $ClOF_2[SbF_6]$ at 100 K.

Atom	Position	*x*	*y*	*z*	U_{iso} / Å^2
Sb(1)	4*a*	0.59745(2)	0.60365(4)	0.26865(6)	0.01624(7)
Cl(1)	4*a*	0.61420(8)	0.8957(2)	0.73000(13)	0.0233(2)
O(1)	4*a*	0.6660(2)	0.6591(6)	0.7403(4)	0.0204(7)
F(1)	4*a*	0.6756(2)	1.0721(6)	0.6355(4)	0.0264(6)
F(2)	4*a*	0.6207(2)	1.0093(6)	0.8950(4)	0.0278(6)
F(3)	4*a*	0.6667(2)	0.8876(5)	0.2285(4)	0.0284(6)
F(4)	4*a*	0.69092(18)	0.4481(6)	0.3768(4)	0.0250(5)
F(5)	4*a*	0.6304(2)	0.4659(6)	0.0715(3)	0.0251(5)
F(6)	4*a*	0.4981(2)	0.7597(5)	0.1734(3)	0.0248(5)
F(7)	4*a*	0.5605(2)	0.7474(5)	0.4666(3)	0.0242(5)
F(8)	4*a*	0.52459(19)	0.3235(5)	0.3142(3)	0.0237(5)

Table S8. Anisotropic displacement parameters of $ClOF_2[SbF_6]$ at 100 K.

Atom	U_{11} / Å^2	U_{22} / Å^2	U_{33} / Å^2	U_{23} / Å^2	U_{13} / Å^2	U_{12} / Å^2
Sb(1)	0.01783(11)	0.01677(10)	0.01410(10)	−0.00120(15)	−0.00016(10)	0.00005(6)
Cl(1)	0.0195(4)	0.0285(5)	0.0218(5)	0.0000(3)	−0.0023(3)	−0.0011(3)
O(1)	0.0237(13)	0.0150(10)	0.023(2)	−0.0006(10)	−0.0031(10)	0.0047(9)
F(1)	0.0242(13)	0.0298(14)	0.0253(14)	0.0055(10)	0.0003(10)	−0.0038(10)
F(2)	0.0303(13)	0.0328(16)	0.0203(12)	−0.0046(12)	−0.0023(10)	0.0014(12)
F(3)	0.0311(15)	0.0230(12)	0.0311(16)	0.0022(10)	0.0030(11)	−0.0080(9)
F(4)	0.0191(12)	0.0308(13)	0.0252(13)	0.0031(11)	−0.0044(10)	0.0045(10)
F(5)	0.0317(14)	0.0266(13)	0.0170(11)	−0.0054(10)	0.0047(10)	0.0016(11)
F(6)	0.0281(13)	0.0255(13)	0.0208(11)	−0.0018(10)	−0.0047(10)	0.0094(10)
F(7)	0.0285(13)	0.0288(12)	0.0154(11)	−0.0067(10)	0.0007(9)	0.0012(10)
F(8)	0.0249(12)	0.0220(11)	0.0240(12)	0.0018(10)	0.0006(8)	−0.0067(10)

Atomic coordinates and displacement parameters of $ClOF_2[OsF_6]$

Table S9. Atomic coordinates and equivalent isotropic displacement parameters U_{iso} of $ClOF_2[OsF_6]$ at 100 K.

Atom	Position	*x*	*y*	*z*	U_{iso} / Å^2
Os(1)	4*a*	0.59708(2)	0.60243(3)	0.26912(4)	0.01137(5)
Cl(1)	4*a*	0.61312(9)	0.8971(3)	0.72704(14)	0.0188(2)
O(1)	4*a*	0.6641(2)	0.6561(7)	0.7398(4)	0.0153(7)
F(1)	4*a*	0.6759(2)	1.0728(7)	0.6321(4)	0.0232(7)
F(2)	4*a*	0.6202(2)	1.0142(7)	0.8930(4)	0.0221(6)
F(3)	4*a*	0.6662(3)	0.8896(6)	0.2288(4)	0.0237(7)
F(4)	4*a*	0.6924(2)	0.4525(6)	0.3787(4)	0.0197(6)
F(5)	4*a*	0.6335(2)	0.4615(7)	0.0734(3)	0.0205(6)
F(6)	4*a*	0.4976(2)	0.7532(6)	0.1664(3)	0.0198(6)
F(7)	4*a*	0.5580(2)	0.7496(6)	0.4657(3)	0.0190(6)
F(8)	4*a*	0.5264(2)	0.3139(6)	0.3143(3)	0.0193(6)

Table S10. Anisotropic displacement parameters of $ClOF_2[OsF_6]$ at 100 K.

Atom	U_{11} / Å^2	U_{22} / Å^2	U_{33} / Å^2	U_{23} / Å^2	U_{13} / Å^2	U_{12} / Å^2
Os(1)	0.00949(7)	0.01331(7)	0.01130(6)	−0.00101(15)	−0.00011(9)	0.00005(5)
Cl(1)	0.0113(5)	0.0256(6)	0.0195(4)	0.0001(4)	−0.0029(3)	−0.0009(4)
O(1)	0.0155(15)	0.0110(13)	0.0193(19)	−0.0013(10)	−0.0033(11)	0.0051(12)
F(1)	0.0130(15)	0.0294(19)	0.0272(16)	0.0049(12)	0.0026(11)	−0.0059(13)
F(2)	0.0211(16)	0.0270(18)	0.0182(13)	−0.0056(12)	−0.0038(11)	0.0015(15)
F(3)	0.0229(17)	0.0204(15)	0.0277(16)	0.0005(10)	0.0026(11)	−0.0064(12)
F(4)	0.0134(14)	0.0243(15)	0.0212(13)	0.0034(11)	−0.0032(10)	0.0032(12)
F(5)	0.0215(17)	0.0247(16)	0.0154(12)	−0.0055(11)	0.0042(11)	0.0024(13)
F(6)	0.0188(15)	0.0234(16)	0.0171(12)	−0.0007(10)	−0.0048(10)	0.0083(12)
F(7)	0.0172(15)	0.0254(16)	0.0143(11)	−0.0066(10)	−0.0002(9)	0.0009(12)
F(8)	0.0169(15)	0.0198(14)	0.0211(12)	−0.0008(10)	−0.0015(9)	−0.0040(14)

Atomic coordinates and displacement parameters of $ClOF_2[IrF_6]$

Table S11. Atomic coordinates and equivalent isotropic displacement parameters U_{iso} of $ClOF_2[IrF_6]$ at 100 K.

Atom	Position	*x*	*y*	*z*	U_{iso} / Å^2
Ir(1)	4*a*	0.40276(2)	0.39654(4)	0.73031(8)	0.01379(8)
Cl(1)	4*a*	0.38700(13)	0.1039(4)	0.2724(2)	0.0208(4)
O(1)	4*a*	0.3363(3)	0.3437(10)	0.2589(7)	0.0177(13)
F(1)	4*a*	0.3238(3)	−0.0734(10)	0.3676(7)	0.0230(10)
F(2)	4*a*	0.3799(3)	−0.0152(11)	0.1063(7)	0.0241(10)
F(3)	4*a*	0.3340(4)	0.1062(8)	0.7701(7)	0.0247(12)
F(4)	4*a*	0.3071(3)	0.5440(10)	0.6182(6)	0.0207(9)
F(5)	4*a*	0.3644(3)	0.5390(10)	0.9242(6)	0.0209(9)
F(6)	4*a*	0.5023(3)	0.2485(9)	0.8352(6)	0.0199(9)
F(7)	4*a*	0.4436(3)	0.2482(9)	0.5339(5)	0.0204(9)
F(8)	4*a*	0.4735(3)	0.6868(9)	0.6838(6)	0.0212(9)

Table S12. Anisotropic displacement parameters of $ClOF_2[IrF_6]$ at 100 K.

Atom	U_{11} / Å^2	U_{22} / Å^2	U_{33} / Å^2	U_{23} / Å^2	U_{13} / Å^2	U_{12} / Å^2
Ir(1)	0.01440(11)	0.01430(11)	0.01266(12)	−0.00086(19)	−0.00002(14)	0.00001(6)
Cl(1)	0.0157(6)	0.0265(8)	0.0201(10)	−0.0011(6)	−0.0023(5)	−0.0006(5)
O(1)	0.019(2)	0.0146(18)	0.019(4)	−0.0035(19)	−0.0030(18)	0.0059(16)
F(1)	0.018(2)	0.027(2)	0.024(3)	0.0038(18)	0.0032(18)	−0.0032(18)
F(2)	0.025(2)	0.030(3)	0.018(2)	−0.005(2)	−0.0037(18)	0.000(2)
F(3)	0.026(2)	0.0166(19)	0.031(4)	0.0014(16)	−0.0009(18)	−0.0084(15)
F(4)	0.0169(19)	0.025(2)	0.020(2)	0.0055(18)	−0.0043(17)	0.0066(17)
F(5)	0.027(2)	0.020(2)	0.015(2)	−0.0051(17)	0.0039(17)	0.0016(18)
F(6)	0.020(2)	0.022(2)	0.0171(19)	−0.0024(16)	−0.0046(16)	0.0099(16)
F(7)	0.023(2)	0.0246(19)	0.013(2)	−0.0064(18)	0.0019(16)	0.0026(18)
F(8)	0.0204(19)	0.0191(19)	0.024(2)	0.0006(16)	0.0009(15)	−0.0063(17)

Atomic coordinates and displacement parameters of $ClOF_2[NbF_6]$

Table S13. Atomic coordinates and equivalent isotropic displacement parameters U_{iso} of $ClOF_2[NbF_6]$ at 100 K.

Atom	Position	*x*	*y*	*z*	U_{iso} / Å^2
Nb(1)	4*a*	0.42532(2)	0.53321(5)	0.51021(4)	0.00988(6)
Nb(2)	4*a*	0.17377(2)	0.22516(4)	0.50189(4)	0.00963(6)
Cl(1)	4*a*	0.56853(3)	0.77234(17)	0.46699(11)	0.01819(18)
Cl(2)	4*a*	0.31949(3)	0.03073(18)	0.45880(11)	0.01803(17)
O/F(1A)	4*a*	0.56433(8)	0.8717(5)	0.6348(3)	0.0198(6)
O/F(1B)	4*a*	0.54739(7)	0.5131(4)	0.4807(3)	0.0162(6)
O/F(1C)	4*a*	0.53404(8)	0.9228(5)	0.3789(3)	0.0190(6)
O(2)	4*a*	0.29393(8)	−0.2095(4)	0.4738(3)	0.0119(5)
F(2)	4*a*	0.28851(8)	0.2040(5)	0.3668(3)	0.0218(5)
F(3)	4*a*	0.31588(8)	0.1416(5)	0.6254(3)	0.0199(4)
F(4)	4*a*	0.38612(7)	0.8110(4)	0.5525(3)	0.0175(4)
F(5)	4*a*	0.40645(7)	0.3793(4)	0.7077(2)	0.0169(4)
F(6)	4*a*	0.37546(8)	0.3686(4)	0.4128(3)	0.0180(4)
F(7)	4*a*	0.47015(7)	0.6989(5)	0.6234(3)	0.0188(4)
F(8)	4*a*	0.44239(8)	0.6738(4)	0.3156(3)	0.0210(5)
F(9)	4*a*	0.46102(7)	0.2516(4)	0.4717(3)	0.0223(6)
F(10)	4*a*	0.22156(7)	0.0760(4)	0.6077(3)	0.0191(4)
F(11)	4*a*	0.13808(7)	−0.0650(4)	0.5504(3)	0.0159(4)
F(12)	4*a*	0.15597(7)	0.3711(5)	0.7032(3)	0.0178(4)
F(13)	4*a*	0.18939(8)	0.0912(4)	0.3038(3)	0.0194(4)
F(14)	4*a*	0.20623(8)	0.5167(4)	0.4587(3)	0.0219(5)
F(15)	4*a*	0.12105(7)	0.3745(4)	0.4155(3)	0.0164(4)

Table S14. Anisotropic displacement parameters of $ClOF_2[NbF_6]$ at 100 K.

Atom	U_{11} / Å^2	U_{22} / Å^2	U_{33} / Å^2	U_{23} / Å^2	U_{13} / Å^2	U_{12} / Å^2
Nb(1)	0.00898(11)	0.01095(10)	0.00972(12)	0.00031(14)	0.00020(13)	−0.00001(8)
Nb(2)	0.00904(10)	0.01078(10)	0.00907(11)	−0.00162(14)	−0.00011(13)	−0.00003(8)
Cl(1)	0.0109(3)	0.0223(4)	0.0214(5)	−0.0017(3)	0.0047(3)	−0.0007(3)
Cl(2)	0.0108(3)	0.0254(4)	0.0179(4)	−0.0025(3)	0.0025(3)	0.0006(3)
O/F(1A)	0.0230(13)	0.0233(12)	0.0131(11)	−0.0053(9)	0.0041(9)	−0.0003(10)
O/F(1B)	0.0148(10)	0.0129(9)	0.0208(14)	−0.0003(8)	0.0034(8)	−0.0035(7)
O/F(1C)	0.0140(12)	0.0194(11)	0.0235(13)	0.0030(9)	−0.0025(9)	0.0054(9)
O(2)	0.0127(9)	0.0098(8)	0.0131(13)	−0.0008(8)	0.0035(8)	−0.0049(8)
F(2)	0.0167(11)	0.0235(11)	0.0252(12)	0.0058(9)	−0.0024(9)	0.0049(9)
F(3)	0.0195(11)	0.0248(11)	0.0153(10)	−0.0049(9)	0.0032(9)	0.0005(9)
F(4)	0.0154(10)	0.0166(9)	0.0204(11)	−0.0002(8)	−0.0013(8)	0.0058(8)
F(5)	0.0170(10)	0.0226(11)	0.0110(10)	0.0058(8)	−0.0004(8)	−0.0007(8)
F(6)	0.0188(11)	0.0205(10)	0.0148(10)	0.0018(8)	−0.0052(8)	−0.0079(8)
F(7)	0.0118(10)	0.0222(10)	0.0224(11)	−0.0062(9)	−0.0029(8)	−0.0018(8)
F(8)	0.0249(12)	0.0218(11)	0.0163(11)	0.0045(9)	0.0058(9)	−0.0039(9)
F(9)	0.0199(10)	0.0164(10)	0.0305(16)	−0.0055(8)	0.0028(10)	0.0052(8)
F(10)	0.0116(10)	0.0244(11)	0.0213(11)	0.0038(9)	−0.0039(8)	0.0028(8)
F(11)	0.0148(9)	0.0139(9)	0.0190(11)	0.0002(7)	−0.0003(7)	−0.0033(7)
F(12)	0.0179(10)	0.0238(11)	0.0117(10)	−0.0071(8)	0.0002(8)	0.0008(9)
F(13)	0.0219(11)	0.0230(11)	0.0134(10)	−0.0056(8)	0.0028(9)	0.0006(9)
F(14)	0.0228(11)	0.0156(10)	0.0272(13)	0.0003(8)	0.0038(9)	−0.0052(8)
F(15)	0.0169(10)	0.0171(10)	0.0152(10)	−0.0025(8)	−0.0049(8)	0.0054(8)

Atomic coordinates and displacement parameters of $ClOF_2[TaF_6]$

Table S15. Atomic coordinates and equivalent isotropic displacement parameters U_{iso} of $ClOF_2[TaF_6]$ at 100 K.

Atom	Position	*x*	*y*	*z*	U_{iso} / Å^2
Ta(1)	4*a*	0.42478(2)	0.53075(3)	0.51004(3)	0.01523(5)
Ta(2)	4*a*	0.17310(2)	0.22083(3)	0.50208(3)	0.01507(5)
Cl(1)	4*a*	0.56802(5)	0.7773(3)	0.4680(2)	0.0248(3)
Cl(2)	4*a*	0.31896(5)	0.0287(3)	0.4591(2)	0.0243(3)
O/F(1A)	4*a*	0.56345(15)	0.8735(8)	0.6344(5)	0.0233(9)
O/F(1B)	4*a*	0.53376(15)	0.9237(8)	0.3778(5)	0.0269(10)
O/F(3A)	4*a*	0.29342(13)	−0.2117(8)	0.4730(5)	0.0270(11)
O/F(3B)	4*a*	0.28817(14)	0.1994(8)	0.3670(5)	0.0244(9)
O/F(3C)	4*a*	0.31529(14)	0.1380(8)	0.6257(5)	0.0235(9)
F(2)	4*a*	0.54680(12)	0.5174(7)	0.4794(5)	0.0287(9)
F(4)	4*a*	0.38572(12)	0.8065(6)	0.5519(4)	0.0221(7)
F(5)	4*a*	0.40669(13)	0.3793(7)	0.7081(4)	0.0238(7)
F(6)	4*a*	0.37506(13)	0.3638(7)	0.4141(5)	0.0249(8)
F(7)	4*a*	0.46994(13)	0.6978(8)	0.6208(5)	0.0260(8)
F(8)	4*a*	0.44145(15)	0.6698(8)	0.3135(5)	0.0291(8)
F(9)	4*a*	0.46066(14)	0.2492(6)	0.4720(5)	0.0312(10)
F(10)	4*a*	0.22115(12)	0.0704(7)	0.6046(5)	0.0250(8)
F(11)	4*a*	0.13729(12)	−0.0684(6)	0.5506(4)	0.0209(7)
F(12)	4*a*	0.15608(13)	0.3655(7)	0.7038(4)	0.0246(8)
F(13)	4*a*	0.18835(14)	0.0891(7)	0.3020(5)	0.0267(8)
F(14)	4*a*	0.20568(14)	0.5115(7)	0.4583(5)	0.0280(8)
F(15)	4*a*	0.12052(13)	0.3712(7)	0.4162(5)	0.0235(7)

Table S16. Anisotropic displacement parameters of $ClOF_2[TaF_6]$ at 100 K.

Atom	U_{11} / Å^2	U_{22} / Å^2	U_{33} / Å^2	U_{23} / Å^2	U_{13} / Å^2	U_{12} / Å^2
Ta(1)	0.01457(9)	0.01628(8)	0.01484(9)	0.00053(12)	0.00061(13)	0.00048(5)
Ta(2)	0.01484(9)	0.01647(8)	0.01389(9)	−0.00175(12)	0.00019(13)	0.00049(6)
Cl(1)	0.0182(6)	0.0274(6)	0.0288(9)	−0.0026(5)	0.0052(5)	−0.0005(5)
Cl(2)	0.0165(6)	0.0316(7)	0.0247(7)	−0.0031(5)	0.0031(5)	0.0013(5)
O/F(1A)	0.028(2)	0.026(2)	0.0156(18)	−0.0049(16)	0.0033(16)	0.0009(17)
O/F(1B)	0.025(2)	0.026(2)	0.029(2)	0.0031(17)	−0.0032(18)	0.0062(16)
O/F(3A)	0.0268(18)	0.0233(16)	0.031(3)	0.0002(16)	0.0030(17)	−0.0037(14)
O/F(3B)	0.0191(19)	0.029(2)	0.025(2)	0.0062(16)	−0.0026(16)	0.0052(16)
O/F(3C)	0.027(2)	0.026(2)	0.0176(18)	−0.0051(15)	0.0018(16)	0.0017(16)
F(2)	0.0259(17)	0.0244(16)	0.036(3)	0.0009(17)	0.0057(17)	−0.0041(12)
F(4)	0.0226(17)	0.0206(15)	0.0230(18)	0.0004(13)	−0.0008(13)	0.0057(13)
F(5)	0.0244(18)	0.0306(19)	0.0164(16)	0.0069(14)	0.0005(14)	0.0019(15)
F(6)	0.0270(19)	0.0247(18)	0.0228(18)	0.0001(15)	−0.0056(15)	−0.0062(14)
F(7)	0.0185(18)	0.0296(18)	0.030(2)	−0.0048(16)	−0.0021(15)	−0.0016(15)
F(8)	0.035(2)	0.030(2)	0.0219(18)	0.0063(16)	0.0081(17)	−0.0017(17)
F(9)	0.035(2)	0.0212(18)	0.038(3)	−0.0030(15)	0.010(2)	0.0104(13)
F(10)	0.0173(17)	0.0293(19)	0.029(2)	0.0034(16)	−0.0039(15)	0.0031(14)
F(11)	0.0207(16)	0.0182(14)	0.0238(18)	0.0007(12)	−0.0022(13)	−0.0035(12)
F(12)	0.0270(19)	0.0297(19)	0.0172(17)	−0.0093(14)	0.0005(15)	−0.0010(15)
F(13)	0.034(2)	0.0284(19)	0.0177(17)	−0.0077(15)	0.0048(16)	0.0021(16)
F(14)	0.0297(19)	0.0225(17)	0.032(2)	0.0012(14)	0.0040(17)	−0.0081(14)
F(15)	0.0252(19)	0.0216(17)	0.0237(17)	−0.0013(14)	−0.0054(14)	0.0075(14)

Plot of distances and angles within the $ClOF_2^+$ cations versus effective ionic radii of *M*(V) ions

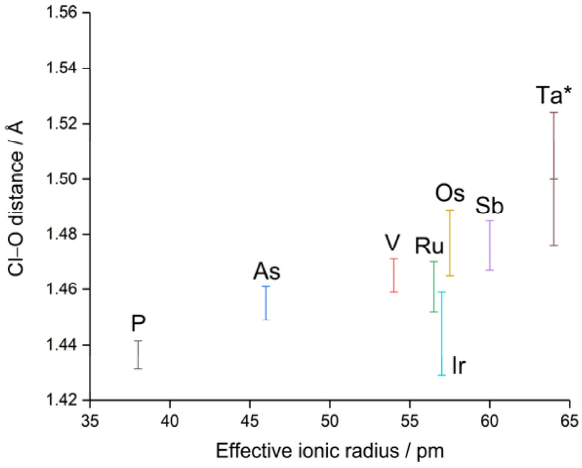

Figure S1. Plot of experimentally determined Cl–O distances obtained from single-crystal X-ray diffraction of the $ClOF_2^+$ cations versus effective ionic radii of *M*(V) ions.[1] The values of $ClOF_2[AsF_6]$ were taken from a previous study.[2] For $ClOF_2[TaF_6]$, the minimal and maximal Cl–O/F distances of the disordered cations were taken. Distances of $ClOF_2[NbF_6]$ are not plotted, as the values are very close to those of $ClOF_2[TaF_6]$. The error bars indicate the tripled standard uncertainties.

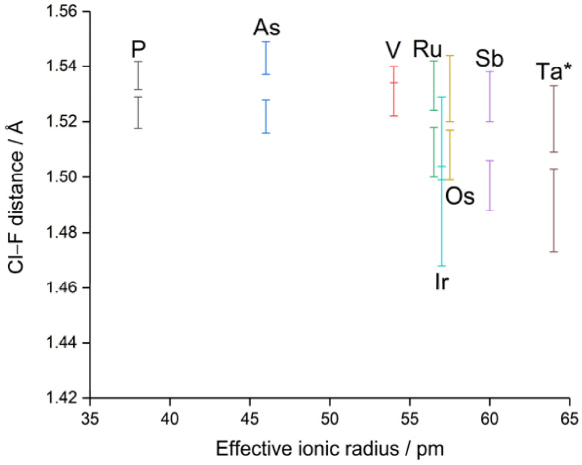

Figure S2. Plot of experimentally determined Cl–F distances obtained from single-crystal X-ray diffraction of the $ClOF_2^+$ cations versus effective ionic radii of *M*(V) ions.[1] The values of $ClOF_2[AsF_6]$ were taken from a previous study.[2] For $ClOF_2[TaF_6]$, the minimal and maximal Cl–O/F and Cl–F distances of the fully/partially disordered cations were taken. Distances of $ClOF_2[NbF_6]$ are not plotted, as the values are very close to those of $ClOF_2[TaF_6]$. The error bars indicate the tripled standard uncertainties.

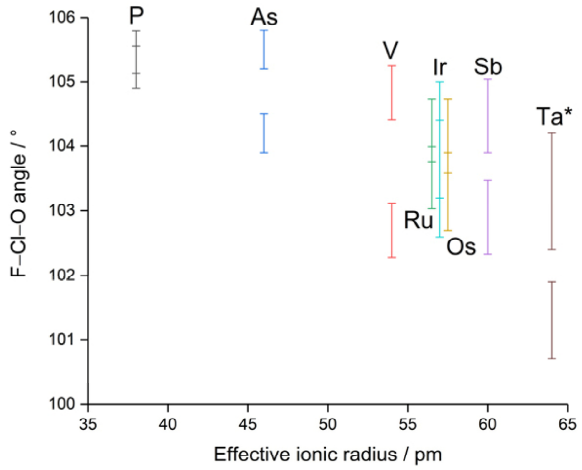

Figure S3. Plot of experimentally determined F−Cl−O angles obtained from single-crystal X-ray diffraction of the $ClOF_2^+$ cations versus effective ionic radii of *M*(V) ions.[1] The values of $ClOF_2[AsF_6]$ were taken from a previous study.[2] For $ClOF_2[TaF_6]$, the minimal and maximal O/F−Cl−O/F and O/F−Cl−F angles of the fully/partially disordered cations were taken. Angles of $ClOF_2[NbF_6]$ are not plotted, as the values are very close to those of $ClOF_2[TaF_6]$. The error bars indicate the tripled standard uncertainties.

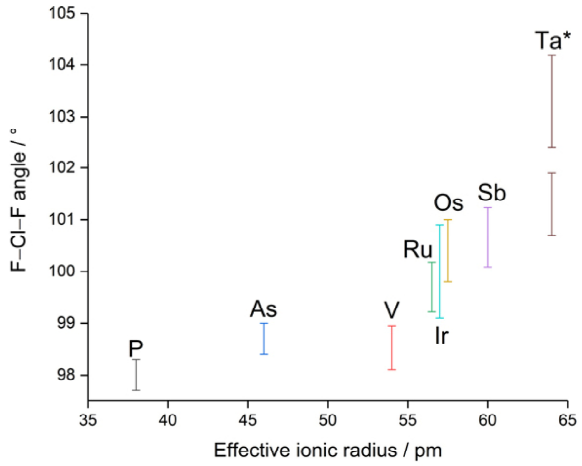

Figure S4. Plot of experimentally determined F−Cl−F angles obtained from single-crystal X-ray diffraction of the $ClOF_2^+$ cations versus effective ionic radii of *M*(V) ions.[1] The values of $ClOF_2[AsF_6]$ were taken from a previous study.[2] For $ClOF_2[TaF_6]$, the minimal and maximal O/F−Cl−O/F and O/F−Cl−F angles of the fully/partially disordered cations were taken. Angles of $ClOF_2[NbF_6]$ are not plotted, as the values are very close to those of $ClOF_2[TaF_6]$. The error bars indicate the tripled standard uncertainties.

Basis set details for quantum-chemical solid-state calculations

TZVP basis set for O

The basis set for O was taken from a previous study.[3]

TZVP basis set for F

The basis set for F was taken from a previous study.[3]

TZVP basis set for Cl

The basis set for Cl was taken from a previous study.[4]

TZVP basis set for V

The basis set for V was taken from a previous study.[5]

TZVP basis set for As

The starting point was the molecular def-TZVP basis set.[6] The exponents of the outermost s and p functions were fixed to 0.13 and the exponents of the other s and p functions in the valence space were reoptimized for the arsenic atom in its ground state. The exponent of the outermost d primitive was kept fixed, while the exponents of the other d functions were optimised for the arsenic atom in its ground state. An f-type polarization function with an exponent of 0.433 was added (def2-TZVP basis set). Finally, the outermost s and p functions were combined into a single sp-type function to increase the efficiency of the CRYSTAL code. The resulting energy loss w.r.t unmodified def2-TZVP basis set is 0.2 mH. The final basis set in CRYSTAL input format is as follows:

```
33 14
0 0 8 2.0 1.0
  498032.42158      0.22740196900E-03
  74656.868743      0.17632816413E-02
  16990.960004      0.91728040381E-02
  4809.6200321      0.37337829344E-01
  1566.2887055      0.12199536117
  563.21360499      0.29137475324
  219.11179978      0.42326351479
  86.866061030      0.22921464278
0 0 4 2.0 1.0
  538.19512479     -0.25254197297E-01
  167.14850224     -0.11915461115
  27.605517159      0.54628495980
  11.947858521      0.53001520976
0 0 2 2.0 1.0
  18.538023133     -0.23479188136
  3.2018985739      0.69167053428
0 0 1 2.0 1.0
  1.4362581800       1.0000000000
0 0 1 0.0 1.0
 0.35310762320       1.0000000000
0 1 1 0.0 1.0
 0.13000000000       1.0 1.0
0 2 6 6.0 1.0
  2678.9421546      0.23318955287E-02
  634.61765840      0.19042149977E-01
  203.93967606      0.90229744913E-01
  76.323890369      0.26169037693
  30.664124943      0.41857168155
  12.505056732      0.23447830190
0 2 4 6.0 1.0
  49.256229549     -0.21235539870E-01
  7.7274891466      0.30470206668
  3.5410493476      0.52888373107
  1.6985585501      0.37272250955
0 2 1 3.0 1.0
 0.80396418504       1.0000000000
0 2 1 0.0 1.0
 0.41045871535       1.0000000000
0 3 5 10.0 1.0
  139.05230680      0.99291144106E-02
  41.113850141      0.66568843496E-01
  15.035409461      0.22275768307
  5.9891096071      0.40309224382
  2.4322147899      0.41671667946
0 3 1 0.0 1.0
 0.96247584610       1.0000000000
0 3 1 0.0 1.0
 0.29300000000       1.0000000000
0 4 1 0.0 1.0
```

```
 0.43271941          1.0
```

TZVP basis set for Sb

The def2-TZVP basis set with a 28-electron effective core potential was used as a starting point.[6] We fixed the exponents of the outermost s and p functions to 0.11 and reoptimized the exponents of the other s and p functions in the valence space for the antimony atom in its ground state. Finally, the outermost s and p functions were combined into one sp-type function. The resulting energy loss with respect to the original molecular basis set is 4.7 mH. The exponent of the outermost d-function was increased from 0.14 to 0.217. The energy cost of this change was only 0.14 mH. The steep f-type polarization function with an exponent of 1.1 was removed. The final basis set in CRYSTAL input format is as follows:

```
251 13
INPUT
23. 0 2 4 4 2 0
16.330865  281.071581 0
8.556542    61.716604 0
14.470337   67.457380 0
13.816194  134.933503 0
8.424924    14.716344 0
8.092728    29.518512 0
14.886331   35.447815 0
15.146319   53.143466 0
5.908267     9.179223 0
5.594322    13.240253 0
14.444978  -15.366801 0
14.449295  -20.296138 0
0 0 4 2.0 1.0
  1612.4199933      0.28540380783E-03
  238.84452097      0.13393778746E-02
  23.998118809     -0.49388154574E-01
  15.193124213      0.43392227254
0 0 2 2.0 1.0
  11.731361334      0.92125519965
  6.5268387226      0.79235280226
0 0 1 0.0 1.0
 2.0178590021       1.0000000000
0 0 1 0.0 1.0
 0.96219277446       1.0000000000
0 0 1 0.0 1.0
 0.28581551962       1.0000000000
0 1 1 0.0 1.0
 0.11                1.0 1.0
0 2 3 6.0 1.0
  215.68393354      0.26051823221E-03
  16.374479088      0.73728000195E-01
  9.7216283345     -0.27230028128
0 2 3 3.0 1.0
  2.7979771259      0.46472692374
  1.4696586758      0.50364242075
 0.74906751891      0.18706666294
0 2 1 0.0 1.0
  0.32300924430     1.0000000000
0 3 6 10.0 1.0
  115.90312253      0.53140915051E-03
  30.474233720      0.59411139166E-02
  18.228418239     -0.10563706947E-01
  4.3291456646      0.20348177341
  2.1294818496      0.42748378928
 0.99682636692      0.38539560809
0 3 1 0.0 1.0
 0.43347239863      1.0000000000
0 3 1 0.0 1.0
 0.216736199315     1.0000000000
0 4 1 0.0 1.0
 0.32369706         1.0000000000
```

TZVP basis set for Nb

The basis set was derived from the molecular Karlsruhe def2-TZVP basis set (28-electron effective core potential).[6] The diffuse outermost s-exponents were increased from 0.033 and 0.086 to 0.13 and 0.30, respectively. The outermost p-type function with an exponent of 0.03 was removed and the exponents of the two remaining outermost p-type functions were changed from 0.09 to 0.13 and 0.2797 to 0.30. The two outermost s and p functions were both then combined into two sp-type functions. The most diffuse d-type function (exponent 0.10) was removed and the inner (3d) function was decontracted to (2d1d). The f-type polarization function was removed. The final basis set in CRYSTAL input format is as follows:

```
241 9
INPUT
13. 0 2 2 2 2 0
8.900000 165.179143 0
4.430000 21.992974 0
7.770000 111.794414 0
3.960000 16.633483 0
6.050000 38.112249 0
2.840000 8.039167 0
8.490000 -22.929550 0
4.250000 -3.666310 0
0 0 2 2.0 1.0
  12.000000000     -0.20219507530
  10.500000000      0.33640105939
0 0 1 2.0 1.0
  3.9276062854      1.0000000000
0 0 1 0.0 1.0
 0.85976543258      1.0000000000
0 1 1 0.0 1.0
 0.30               1.0 1.0
0 1 1 0.0 1.0
 0.13               1.0 1.0
0 2 4 6.0 1.0
  9.2056285646      0.43347689874E-01
  4.8679632125     -0.21302479233
  1.2442155792      0.48102127136
 0.60390590312      0.53917858960
0 3 2 3.0 1.0
  4.6170975867     -0.13574476955E-01
  1.5663438480      0.20374310496
0 3 1 0.0 1.0
 0.66952425826      0.42997453105
0 3 1 0.0 1.0
 0.27140946867      1.0000000000
```

TZVP basis set for Ta

The basis set was derived from the molecular Karlsruhe def2-TZVP basis set (60-electron effective core potential).[6] The diffuse outermost s- and p-type functions with exponents of 0.039 and 0.065 were removed. The exponent of the outermost s-type function was increased from 0.10 and 0.11. The exponent of the outermost p-type function was changed from 0.27 to 0.11 and combined with the outermost s function into a single sp-type function. The most diffuse d-type function (exponent 0.088) was removed and the inner (3d) function was decontracted to (2d1d). The f-type polarization function was removed. The final basis set in CRYSTAL input format is as follows:

```
273 10
INPUT
13. 0 2 2 2 1 1
14.546408 1345.880647 0
7.273204 36.766806 0
9.935565 378.425301 0
4.967782 22.293091 0
6.347377 104.883956 0
3.173688 8.755848 0
2.017881 12.017961 0
3.040330 -11.720933 0
0 0 4 2.0 1.0
  24.473650944      0.20590322488
  18.721372549     -0.74670795514
  11.500000000       3.4071363897
  10.350000000      -2.8175487609
0 0 1 2.0 1.0
  3.8436180089       1.0000000000
0 0 1 0.0 1.0
  1.0202266016       1.0000000000
0 0 1 0.0 1.0
 0.46774781869       1.0000000000
0 1 1 0.0 1.0
  0.11               1.0 1.0
0 2 4 6.0 1.0
  17.000000000     -0.32577305616E-01
  12.008186536      0.10336287365
  5.0278760583     -0.28526521696
  1.1937124184      0.51790141155
0 2 1 0.0 1.0
 0.57889707053       1.0000000000
```

```
0 3 2 3.0 1.0
  3.9738796278     -0.52799310714E-01
  1.4528884813      0.18558319471
0 3 1 0.0 1.0
 0.61042908544      0.42959071631
0 3 1 0.0 1.0
 0.24216276510       1.0000000000
```

TZVP basis set for Ir

The basis set was derived from the molecular Karlsruhe def2-TZVP basis set (60-electron effective core potential).[6] The diffuse outermost s- and p-type functions with exponents of 0.05 and 0.056 were removed. The exponent of the outermost p-type function was changed from 0.33 to 0.14 and it was combined with the outermost s function into a single sp-type function. The exponents of the two outermost d-type functions were increased to 0.18 and 0.36. The f-type polarization function was removed. The final basis set in CRYSTAL input format is as follows:

```
277 10
INPUT
17. 0 2 2 2 1 1
13.652203 732.269200 0
6.826101 26.484721 0
10.279868 299.489474 0
5.139934 26.466234 0
7.349859 124.457595 0
3.674929 14.035995 0
3.034072 21.531031 0
4.808857 -21.607597 0
0 0 3 2.0 1.0
  30.000000000      0.30797903228
  27.000000000     -0.46726361781
  13.961973911      0.47161003146
0 0 1 2.0 1.0
  5.3956977802       1.0000000000
0 0 1 0.0 1.0
  1.2149128721       1.0000000000
0 0 1 0.0 1.0
 0.55885743756       1.0000000000
0 1 1 0.0 1.0
 0.14097974313       1.0 1.0
0 2 4 6.0 1.0
  15.902664143     -0.16290720099
  14.415830698      0.23483212987
  5.7597608991     -0.30305337176
  1.5008913108      0.55512982069
0 2 1 0.0 1.0
 0.72348035957       1.0000000000
0 3 4 7.0 1.0
  8.6321692504      0.75000099949E-01
  6.5898192302     -0.17326965173
  1.5808379663      0.55065196913
 0.71827834905      0.85273641436
0 3 1 0.0 1.0
 0.36                1.0000000000
0 3 1 0.0 1.0
 0.18                1.0000000000
```

TZVP basis set for Ru

The basis set was derived from the molecular Karlsruhe def2-TZVP basis set (28-electron effective core potential).[6] The diffuse outermost s-exponents were increased from 0.039 and 0.107 to 0.13 and 0.26, respectively. The outermost p-type function with an exponent of 0.037 was removed and the exponents of the two remaining outermost p-type functions were changed from 0.115 to 0.13 and 0.367 to 0.26. The two outermost s and p functions were then combined into two sp-type functions. The exponent of the outermost d-type function (exponent 0.15) increased to 0.20. The f-type polarization function was removed. The final basis set in CRYSTAL input format is as follows:

```
244 10
INPUT
16. 0 2 2 2 2 0
11.105269 209.822971 0
5.414745 30.654726 0
9.771271 146.336182 0
5.073991 24.127877 0
7.671423 67.515897 0
4.136565 9.870104 0
11.360000 -28.340616 0
5.680000 -4.944629 0
0 0 2 2.0 1.0
  16.000000000     -0.20634002919
  13.910581694      0.33550437725
0 0 1 2.0 1.0
  4.7967971407       1.0000000000
0 0 1 0.0 1.0
  1.1555425594       1.0000000000
0 0 1 0.0 1.0
```

```
 0.52455741182       1.0000000000
0 1 1 0.0 1.0
 0.26                1.0 1.0
0 1 1 0.0 1.0
 0.13                1.0 1.0
0 2 4 6.0 1.0
  11.187208671       0.53225073263E-01
  6.2477688734      -0.22731662050
  1.6279472859       0.47869486056
 0.79326493538       0.50213311567
0 3 3 6.0 1.0
  5.7341846619      -0.35266111560E-01
  2.2483686294       0.21802502222
 0.98376978359       0.44709565013
0 3 1 0.0 1.0
 0.40379445503       1.0000000000
0 3 1 0.0 1.0
 0.2                 1.0000000000
```

TZVP basis set for Os

The basis set was derived from the molecular Karlsruhe def2-TZVP basis set (60-electron effective core potential).[6] The diffuse outermost s- and p-type functions with exponents of 0.047 and 0.052 were removed. The exponent of the outermost p-type function was changed from 0.31 to 0.13 and it was combined with the outermost s function into a single sp-type function. The most diffuse d-type function (exponent 0.11) was removed and the inner (4d) function was decontracted to (3d1d). The f-type polarization function was removed. The final basis set in CRYSTAL input format is as follows:

```
276 10
INPUT
16. 0 2 2 2 1 1
13.875754 885.405719 0
6.937877 25.967040 0
10.193793 320.083902 0
5.096896 26.148765 0
7.099238 115.044843 0
3.549619 13.622575 0
2.767075 18.909457 0
4.349905 -19.027595 0
0 0 3 2.0 1.0
  30.000000000       0.32213004804
  27.000000000      -0.47922918137
  13.524730005       0.47465946837
0 0 1 2.0 1.0
  5.2402883472       1.0000000000
0 0 1 0.0 1.0
  1.1306661245       1.0000000000
0 0 1 0.0 1.0
 0.51689966917       1.0000000000
0 1 1 0.0 1.0
 0.13222953545       1.0 1.0
0 2 4 6.0 1.0
  15.500000000       0.16016463376
  14.000000000      -0.23201520402
  5.5458290420       0.29772587274
  1.4139502215      -0.54253238176
0 2 1 0.0 1.0
 0.68136686765       1.0000000000
0 3 3 6.0 1.0
  8.2945059487       0.69648222110E-01
  6.3060397430      -0.16444229630
  1.4890109110       0.55154541033
0 3 1 0.0 1.0
 0.67315390607       0.88461370291
0 3 1 0.0 1.0
 0.22                1.0000000000
```

Lattice parameters and atomic coordinates of optimized solid-state structures of $ClOF_2[MF_6]$ (*M* = V, Nb, Ta, Ru, Os, Ir, P, As, Sb)

Lattice parameters and atomic coordinates of the optimized solid-state structure of $ClOF_2[PF_6]$

Space group $Pna2_1$ (No. 33)
a = 14.38025897 Å, b = 5.08846086 Å, c = 8.04744210 Å, V = 588.858579 Å^3

Table S17. Atomic coordinates of the optimized structure of $ClOF_2[PF_6]$.

Atom	*x*	*y*	*z*
P	4.062778554519E−01	3.864604967303E−01	−2.709139186074E−01
Cl	3.868244093407E−01	1.431994641732E−01	2.804371365093E−01
O	3.319807886150E−01	3.713200620399E−01	2.641350018282E−01
F	3.242535740893E−01	−7.163199477015E−02	3.785570542197E−01
F	3.781576290736E−01	−1.178668638641E−02	1.056809994518E−01
F	3.474471715323E−01	1.261369234349E−01	−2.291718044716E−01
F	3.189907454284E−01	−4.870781340849E−01	−3.695082726865E−01
F	4.419116123237E−01	2.484687947995E−01	−4.477141076297E−01
F	4.693615542443E−01	−3.537791654662E−01	−3.200683413392E−01
F	4.985362320363E−01	2.603065159246E−01	−1.806395844815E−01
F	3.755698206090E−01	−4.766600226452E−01	−9.933416279322E−02

Lattice parameters and atomic coordinates of the optimized solid-state structure of $ClOF_2[VF_6]$

Space group $Pna2_1$ (No. 33)
a = 14.83986594 Å, b = 5.12465376 Å, c = 8.27596028 Å, V = 629.379950 Å^3

Table S18. Atomic coordinates of the optimized structure of $ClOF_2[VF_6]$.

Atom	*x*	*y*	*z*
V	4.024998290335E−01	3.937739568582E−01	−2.801753905208E−01
Cl	3.924995245221E−01	1.478612410209E−01	2.706943344949E−01
O	3.424253932990E−01	3.805299848763E−01	2.537131057854E−01
F	3.249706786827E−01	−5.890449197671E−02	3.598530406277E−01
F	3.819653201076E−01	−1.220876943674E−03	9.786716679915E−02
F	3.135760380775E−01	−4.593801701868E−01	−3.854384080866E−01
F	3.394864720533E−01	1.160129713872E−01	−2.390124736320E−01
F	4.742453974179E−01	−3.285355864486E−01	−3.332821997414E−01
F	4.384012046849E−01	2.449971621154E−01	−4.735618915157E−01
F	3.737701582601E−01	−4.601780842940E−01	−9.820659039276E−02
F	−4.990168701804E−01	2.481531848385E−01	−1.935606938180E−01

Lattice parameters and atomic coordinates of the optimized solid-state structure of $ClOF_2[AsF_6]$

The initial parameters for the optimization were taken from a previous study on the crystal structure of $ClOF_2[AsF_6]$.[2]

Space group $Pna2_1$ (No. 33)
a = 14.63689586 Å, b = 5.10684533 Å, c = 8.16955416 Å, V = 610.660802 Å^3

Table S19. Atomic coordinates of the optimized structure of $ClOF_2[AsF_6]$.

Atom	*x*	*y*	*z*
As	9.361603309681E−02	3.877779212081E−01	1.407934084638E−01
Cl	1.137674315014E−01	1.443557424744E−01	−4.086145687992E−01
O	1.659085132510E−01	3.750982333500E−01	−3.926861526771E−01
F	−3.300954769340E−03	2.531855068144E−01	5.001142866646E−02
F	2.707357999303E−02	−3.390681248614E−01	1.925799618570E−01
F	5.755557699395E−02	2.436489846825E−01	3.264741000832E−01
F	1.550559099730E−01	1.119971681585E−01	9.752801597998E−02
F	1.843951808439E−01	−4.760404152474E−01	2.434188484937E−01
F	3.220920134006E−01	4.340715173744E−01	−3.933188277927E−03
F	3.757323073108E−01	3.129579804577E−02	4.599798774131E−01
F	3.770448115688E−01	4.915777576132E−01	2.642782687969E−01

Lattice parameters and atomic coordinates of the optimized solid-state structures of $ClOF_2[NbF_6]$

Model 1 (full oxygen occupation on position O(1A))

Energy difference relative to Model 3: 6.6 kJ/mol

Space group $Pna2_1$ (No. 33)
a = 30.32836377 Å, b = 5.23609528 Å, c = 8.45914808 Å, V = 1343.331347 Å^3

Table S20. Atomic coordinates of the optimized structure of $ClOF_2[NbF_6]$. (full oxygen occupation on position O(1A))

Atom	*x*	*y*	*z*
Nb	4.232274639452E−01	−4.741423061017E−01	−4.847162508938E−01
Nb	1.717776174416E−01	2.378287439949E−01	4.959365967078E−01
Cl	−4.310239782525E−01	−2.317179064533E−01	4.842073428372E−01
Cl	3.195935706686E−01	−7.683329970997E−03	4.541376706808E−01
O	−4.379782135432E−01	−1.436164773254E−01	−3.602351218474E−01
O	2.947084671817E−01	−2.348086997231E−01	4.662033179675E−01
F	−4.682685251491E−01	−9.191470030614E−02	3.758781615374E−01
F	2.867330095788E−01	1.985486904815E−01	3.675037526893E−01
F	−4.559905605881E−01	4.920113435762E−01	4.726051986008E−01
F	3.143649461809E−01	1.330448786616E−01	−3.754911927144E−01
F	3.834670480343E−01	−1.837928430226E−01	−4.452417297253E−01
F	4.060110271317E−01	3.876264871981E−01	−2.818461083765E−01
F	3.718643391636E−01	3.625234553947E−01	4.247942265021E−01
F	4.379166233748E−01	−3.421091652663E−01	3.144689773123E−01
F	4.694344737392E−01	−2.967840823168E−01	−3.835569498425E−01
F	2.201148245075E−01	8.247903889347E−02	−4.035230730011E−01
F	1.344085729118E−01	−5.125135884368E−02	−4.491218522782E−01
F	1.567076941377E−01	3.881686040143E−01	−2.983784415613E−01
F	1.852082376857E−01	1.045732394568E−01	2.962544767186E−01
F	2.027446107961E−01	−4.605658321338E−01	4.509004048581E−01
F	1.171030546968E−01	3.925485376831E−01	4.212132763261E−01
F	4.577910074127E−01	2.343334363421E−01	4.792973175025E−01

Lattice parameters and atomic coordinates of the optimized solid-state structures of $ClOF_2[NbF_6]$

Model 2 (full oxygen occupation on position O(1B))

Energy difference relative to Model 3: 6.0 kJ/mol

Space group $Pna2_1$ (No. 33)
a = 30.60513126 Å, b = 5.17841765 Å, c = 8.50529152 Å, V = 1347.970923 Å^3

Table S21. Atomic coordinates of the optimized structure of $ClOF_2[NbF_6]$. (full oxygen occupation on position O(1B))

Atom	*x*	*y*	*z*
Nb	4.229791707176E−01	−4.724010081077E−01	−4.952435232552E−01
Nb	1.726714892951E−01	2.412234140905E−01	−4.965366792128E−01
Cl	−4.314683452136E−01	−2.823565727950E−01	4.608922778962E−01
Cl	3.187258057045E−01	−8.741611494593E−03	4.606243867571E−01
O	2.946577283381E−01	−2.398254326739E−01	4.761840087935E−01
O	−4.534798343798E−01	4.787178461563E−01	4.730257608633E−01
F	−4.372813251818E−01	−1.440055126230E−01	−3.685070310017E−01
F	−4.662282346185E−01	−8.563270053139E−02	3.781648328090E−01
F	2.858239442573E−01	1.961583746758E−01	3.739386096608E−01
F	3.139989921629E−01	1.375105992617E−01	−3.708431134552E−01
F	3.844057911691E−01	−1.829532212109E−01	−4.436923230643E−01
F	4.079170170285E−01	3.766313526967E−01	−2.900472797954E−01
F	3.708028899258E−01	3.669705722341E−01	4.239395488084E−01
F	4.369483753179E−01	−3.295054433111E−01	3.084552128180E−01
F	4.697367327872E−01	−3.074200198248E−01	−3.912092685597E−01
F	2.203392737251E−01	7.731451369798E−02	−3.975041494055E−01
F	1.348954923362E−01	−5.193544249165E−02	−4.447534200711E−01
F	1.583434654047E−01	3.857475909264E−01	−2.890409239568E−01
F	1.854670546271E−01	1.029899853426E−01	3.048689578273E−01
F	2.047868665520E−01	−4.588557951756E−01	4.595884406436E−01
F	1.198097310822E−01	4.008746262185E−01	4.277310993401E−01
F	4.557119154256E−01	2.297277352011E−01	4.612545755605E−01

Lattice parameters and atomic coordinates of the optimized solid-state structures of $ClOF_2[NbF_6]$

Model 3 (full oxygen occupation on position O(1C))

Space group *Pna*2$_1$ (No. 33)
a = 30.58152116 Å, *b* = 5.22196635 Å, *c* = 8.46186047 Å, *V* = 1351.322514 Å^3

Table S22. Atomic coordinates of the optimized structure of $ClOF_2[NbF_6]$. (full oxygen occupation on position O(1C))

Atom	*x*	*y*	*z*
Nb	4.223718614085E−01	−4.536390078210E−01	−4.945076252371E−01
Nb	1.717784176120E−01	2.398917494018E−01	−4.948032456532E−01
Cl	−4.332217375744E−01	−2.299613183068E−01	4.479430447492E−01
Cl	3.183160082941E−01	4.553733052978E−03	4.608730558131E−01
O	−4.659030293543E−01	−8.472341704085E−02	3.713324243452E−01
O	2.941006447935E−01	−2.239725991816E−01	4.774391491541E−01
F	−4.373739326832E−01	−1.581887933056E−01	−3.654885043769E−01
F	2.856732781080E−01	2.068400114293E−01	3.713657990473E−01
F	−4.547020973042E−01	4.863404575349E−01	4.758256007658E−01
F	3.133654894660E−01	1.518878122977E−01	−3.706559558771E−01
F	3.841131158830E−01	−1.051736110091E−01	−4.417445088225E−01
F	4.080628529923E−01	4.048455108899E−01	−2.850491245341E−01
F	3.700960969055E−01	3.841623058914E−01	4.272545914293E−01
F	4.359702037101E−01	−3.145778522422E−01	3.075643169601E−01
F	4.698877655399E−01	−2.886594849586E−01	−3.950342350601E−01
F	2.206882882382E−01	8.594554346826E−02	−3.991169178898E−01
F	1.350169029018E−01	−4.864477525653E−02	−4.472338023059E−01
F	1.577639064852E−01	3.843277669442E−01	−2.860385799366E−01
F	1.847875032158E−01	1.166015602545E−01	3.024206866453E−01
F	2.020803353244E−01	−4.541564788684E−01	4.616003466913E−01
F	1.177301052609E−01	4.020119343878E−01	4.317451021735E−01
F	4.549391761342E−01	2.486022568836E−01	4.655983819191E−01

Lattice parameters and atomic coordinates of the optimized solid-state structure of $ClOF_2[RuF_6]$

Space group *Pna*2$_1$ (No. 33)
a = 15.05074141 Å, *b* = 5.17998973 Å, *c* = 8.40403396 Å, *V* = 655.201060 Å^3

Table S23. Atomic coordinates of the optimized structure of $ClOF_2[RuF_6]$.

Atom	*x*	*y*	*z*
Ru	−4.053834304356E−01	−3.953566547424E−01	2.829839056565E−01
Cl	−3.888657216199E−01	−1.409463153213E−01	−2.664503512197E−01
O	−3.397534963779E−01	−3.714661636097E−01	−2.495423382848E−01
F	−3.798890679127E−01	8.338666347106E−03	−9.724928461431E−02
F	−4.406445821760E−01	−2.419060475324E−01	4.799798859978E−01
F	−3.228162928861E−01	6.264745483152E−02	−3.557428378389E−01
F	4.931832811590E−01	−2.465517060903E−01	1.880289035556E−01
F	−3.737659248679E−01	4.573462064001E−01	9.078453534375E−02
F	−3.090496757371E−01	4.550994631337E−01	3.862675368404E−01
F	−4.769586951726E−01	3.124578320839E−01	3.352391347180E−01
F	−3.386109347436E−01	−1.053705567215E−01	2.370909078377E−01

Lattice parameters and atomic coordinates of the optimized solid-state structure of $ClOF_2[SbF_6]$

Space group *Pna*2_1 (No. 33)
a = 15.25805037 Å, *b* = 5.20681786 Å, *c* = 8.45561707 Å, *V* = 671.764017 Å^3

Table S24. Atomic coordinates of the optimized structure of $ClOF_2[SbF_6]$.

Atom	*x*	*y*	*z*
Sb	4.059946184780E−01	−1.085734416874E−01	4.534837768995E−01
Cl	−3.843194787899E−01	3.580474228628E−01	4.960763198278E−01
O	−3.358328181971E−01	1.286938819911E−01	4.815527957163E−01
F	−3.206003251700E−01	−4.369357943515E−01	−4.143463872163E−01
F	−4.893254416302E−01	−2.630290520820E−01	−4.609721116589E−01
F	4.382329359350E−01	−2.550039474741E−01	2.495975802462E−01
F	4.789600805580E−01	1.846893753411E−01	4.010829471841E−01
F	3.086262475702E−01	5.059884987259E−02	3.516879178981E−01
F	3.394975841132E−01	−4.086267402462E−01	4.980692531433E−01
F	3.782320725397E−01	3.394103852699E−02	−3.455846869947E−01
F	−3.757001365859E−01	−4.952806295422E−01	3.277225949545E−01

Lattice parameters and atomic coordinates of the optimized solid-state structures of $ClOF_2[TaF_6]$

Model 1 (full oxygen occupation on positions O(1A) and O(3A))

Energy difference relative to Model 5: 9.6 kJ/mol

Space group *Pna*2_1 (No. 33)
a = 30.40710140 Å, *b* = 5.22904067 Å, *c* = 8.46820243 Å, *V* = 1346.443932 Å^3

Table S25. Atomic coordinates of the optimized structure of $ClOF_2[TaF_6]$ (full oxygen occupation on positions O(1A) and O(3A)).

Atom	*x*	*y*	*z*
Ta	4.228748183414E−01	−4.745335309432E−01	−4.854440615671E−01
Ta	1.714705355059E−01	2.381716664734E−01	4.949702982445E−01
Cl	−4.315828845805E−01	−2.331892387869E−01	4.850429925984E−01
Cl	3.188610930987E−01	−8.931254857564E−03	4.547916139660E−01
O	−4.385298028561E−01	−1.446905476885E−01	−3.596913039092E−01
O	2.941042280161E−01	−2.365434783415E−01	4.661948515794E−01
F	−4.685402722415E−01	−9.279242654004E−02	3.763594765228E−01
F	−4.564732847694E−01	4.903087057983E−01	4.732358878672E−01
F	2.863473289977E−01	1.981380008449E−01	3.677497842375E−01
F	3.135579508882E−01	1.314030034252E−01	−3.750951810356E−01
F	3.830738300500E−01	−1.843826212448E−01	−4.447735784693E−01
F	4.069359722767E−01	3.892426377611E−01	−2.802886864492E−01
F	3.713120445901E−01	3.580095865255E−01	4.279384607143E−01
F	4.362076670358E−01	−3.430374919985E−01	3.118855888193E−01
F	4.228748183414E−01	−4.745335309432E−01	−4.854440615671E−01
F	1.714705355059E−01	2.381716664734E−01	4.949702982445E−01
F	−4.315828845805E−01	−2.331892387869E−01	4.850429925984E−01
F	3.188610930987E−01	−8.931254857564E−03	4.547916139660E−01
F	−4.385298028561E−01	−1.446905476885E−01	−3.596913039092E−01
F	2.941042280161E−01	−2.365434783415E−01	4.661948515794E−01
F	−4.685402722415E−01	−9.279242654004E−02	3.763594765228E−01
F	−4.564732847694E−01	4.903087057983E−01	4.732358878672E−01

Model 2 (full oxygen occupation on positions O(1A) and O(3B))

Energy difference relative to Model 5: 6.4 kJ/mol

Space group $Pna2_1$ (No. 33)
a = 30.45703786 Å, b = 5.26770955 Å, c = 8.40785604 Å, V = 1348.946579Å^3

Table S26. Atomic coordinates of the optimized structure of $ClOF_2[TaF_6]$ (full oxygen occupation on positions O(1A) and O(3B)).

Atom	*x*	*y*	*z*
Ta	4.222901365176E−01	−4.598849123116E−01	−4.837913362912E−01
Ta	1.707847088089E−01	2.334708493979E−01	4.952248110381E−01
Cl	−4.317713999744E−01	−2.315420539205E−01	4.859704092708E−01
Cl	3.176132809787E−01	5.427234922679E−02	4.419068745847E−01
O	−4.386878530455E−01	−1.427336787686E−01	−3.578644114272E−01
O	2.866433384170E−01	2.075208663360E−01	3.614898373137E−01
F	−4.685406623241E−01	−9.246144783253E−02	3.756137020128E−01
F	2.931867468320E−01	−2.187621499626E−01	4.681244440331E−01
F	−4.567435894686E−01	4.944879122683E−01	4.748234881952E−01
F	3.129992912914E−01	1.272015480960E−01	−3.711769139237E−01
F	3.836099674091E−01	−1.745400258153E−01	−4.488443529079E−01
F	4.067195250613E−01	4.031513027390E−01	−2.771893347121E−01
F	3.695991662039E−01	3.680472102534E−01	4.325573953582E−01
F	4.355612263479E−01	−3.469829735520E−01	3.079749814690E−01
F	4.700465007458E−01	−2.881429467087E−01	−3.903258924170E−01
F	2.203057025563E−01	7.885896978718E−02	−4.113046359878E−01
F	1.341545671618E−01	−5.638204664282E−02	−4.474139562861E−01
F	1.572101963533E−01	3.736762174989E−01	−2.933395509664E−01
F	1.831556507859E−01	1.042033920919E−01	2.924636702730E−01
F	2.013601725678E−01	−4.630788495274E−01	4.532164079796E−01
F	1.159847222577E−01	3.908234928526E−01	4.249305461210E−01
F	4.554812034081E−01	2.425668340235E−01	4.793738172703E−01

Model 3 (full oxygen occupation on positions O(1A) and O(3C))

Energy difference relative to Model 5: 7.9 kJ/mol

Space group *Pna*2$_1$ (No. 33)
a = 30.30441561 Å, *b* = 5.30144461 Å, *c* = 8.39435863 Å, *V* = 1348.613993 Å^3

Table S27. Atomic coordinates of the optimized structure of $ClOF_2[TaF_6]$ (full oxygen occupation on positions O(1A) and O(3C)).

Atom	*x*	*y*	*z*
Ta	4.226711960274E−01	−4.691457034604E−01	−4.925798243652E−01
Ta	1.712887891196E−01	2.437348699292E−01	−4.950583945174E−01
Cl	−4.307648110817E−01	−2.346042239848E−01	4.798865166984E−01
Cl	3.202992639418E−01	4.345680399707E−02	4.781406283122E−01
O	−4.382753738963E−01	−1.508280233500E−01	−3.630500499275E−01
O	3.134766708213E−01	1.328546522667E−01	−3.656288726913E−01
F	−4.675633650948E−01	−9.222984970652E−02	3.702798025859E−01
F	2.918995085979E−01	−2.173167674757E−01	4.648475279905E−01
F	−4.562417768672E−01	4.940211277671E−01	4.644800849989E−01
F	2.853359670321E−01	1.972634289371E−01	3.656772458098E−01
F	3.832701587509E−01	−1.848977495150E−01	−4.505793360676E−01
F	4.057558516247E−01	3.885029547760E−01	−2.889545706482E−01
F	3.696774503106E−01	3.667273038751E−01	4.203424306363E−01
F	4.364277153137E−01	−3.457420646494E−01	3.022710541251E−01
F	4.696414540369E−01	−2.975676369590E−01	−3.934892998738E−01
F	2.200020494038E−01	7.936855991747E−02	−4.022168689987E−01
F	1.334333852443E−01	−4.684402119718E−02	−4.510724930580E−01
F	1.552517142259E−01	3.788913315755E−01	−2.886033961672E−01
F	1.840160310968E−01	1.258468552408E−01	2.976413868436E−01
F	2.032720092745E−01	−4.580635846105E−01	4.661693272372E−01
F	1.169966599802E−01	4.019038571914E−01	4.240774270608E−01
F	4.562276377524E−01	2.377911433618E−01	4.698396740161E−01

Model 4 (full oxygen occupation on positions O(1B) and O(3A))

Energy difference relative to Model 5: 4.7 kJ/mol

Space group $Pna2_1$ (No. 33)
a = 30.63822175 Å, b = 5.21157319 Å, c = 8.47935533 Å, V = 1353.926944 Å^3

Table S28. Atomic coordinates of the optimized structure of $ClOF_2[TaF_6]$ (full oxygen occupation on positions O(1B) and O(3A)).

Atom	*x*	*y*	*z*
Ta	4.219653362156E−01	−4.551295623314E−01	−4.951760168421E−01
Ta	1.712651878335E−01	2.377434668366E−01	−4.956148391515E−01
Cl	−4.339979574936E−01	−2.300013377336E−01	4.490030298970E−01
Cl	3.176238975742E−01	2.418842090299E−03	4.617647324603E−01
O	−4.665214706466E−01	−8.491997238686E−02	3.718110592312E−01
O	2.935926898864E−01	−2.269530173419E−01	4.781741606746E−01
F	−4.383175732146E−01	−1.585487841952E−01	−3.650678439004E−01
F	−4.552068985717E−01	4.851674531254E−01	4.759628815176E−01
F	2.852096741278E−01	2.044889945360E−01	3.713472985348E−01
F	3.125549675282E−01	1.507102946588E−01	−3.706824524876E−01
F	3.838149433714E−01	−1.653714102240E−01	−4.416274677589E−01
F	4.086609038729E−01	4.044006921491E−01	−2.847090283306E−01
F	3.694673718497E−01	3.799416752193E−01	4.296824367510E−01
F	4.345478861820E−01	−3.169157479234E−01	3.055142636958E−01
F	4.699339894879E−01	−2.878267640441E−01	−3.991494866087E−01
F	2.206568025718E−01	8.078561336686E−02	−4.043996891577E−01
F	1.345934054870E−01	−5.281529639463E−02	−4.477487470538E−01
F	1.584032446165E−01	3.792944510710E−01	−2.853396146660E−01
F	1.832417904473E−01	1.167432682184E−01	2.999800357868E−01
F	2.016622277415E−01	−4.551669077969E−01	4.603804481228E−01
F	1.169942442160E−01	4.017054645262E−01	4.346796661705E−01
F	4.546797772095E−01	2.467612539089E−01	4.636351731147E−01

Model 5 (full oxygen occupation on positions O(1B) and O(3B))

Space group $Pna2_1$ (No. 33)
a = 30.69052327 Å, b = 5.25193804 Å, c = 8.42283279 Å, V = 1357.632001 Å^3

Table S29. Atomic coordinates of the optimized structure of $ClOF_2[TaF_6]$ (full oxygen occupation on positions O(1B) and O(3B)).

Atom	*x*	*y*	*z*
Ta	4.213576152608E−01	−4.416956311913E−01	−4.934392738326E−01
Ta	1.707350781252E−01	2.323614309034E−01	−4.953974850326E−01
Cl	−4.340045558084E−01	−2.292365487276E−01	4.494156272408E−01
Cl	3.165600162671E−01	6.204439997863E−02	4.474768258493E−01
O	−4.661938482657E−01	−8.613390642581E−02	3.694842704633E−01
O	2.855538753949E−01	2.107512106802E−01	3.651065317727E−01
F	−4.386505556627E−01	−1.550240981015E−01	−3.640727019383E−01
F	2.932831267261E−01	−2.125656221251E−01	4.783829339362E−01
F	−4.553379446638E−01	4.893762807856E−01	4.783666846370E−01
F	3.120724264864E−01	1.417383794873E−01	−3.668846665719E−01
F	3.842919433735E−01	−1.555695485061E−01	−4.442214627125E−01
F	4.087721508485E−01	4.197013528593E−01	−2.806089006868E−01
F	3.679311439194E−01	3.889358138032E−01	4.357551918744E−01
F	4.335875066438E−01	−3.194803555509E−01	3.019671642939E−01
F	4.703414007610E−01	−2.811425089803E−01	−4.022115491801E−01
F	2.207334501297E−01	7.661385025346E−02	−4.083198616927E−01
F	1.345638483284E−01	−5.721221188179E−02	−4.451012156257E−01
F	1.586738823221E−01	3.652129517579E−01	−2.806757215759E−01
F	1.821698455225E−01	1.135581926158E−01	2.986572166728E−01
F	2.010328589894E−01	−4.610228740436E−01	4.644463691373E−01
F	1.165743787632E−01	3.983138564731E−01	4.379173758496E−01
F	4.526744258573E−01	2.551881447279E−01	4.663766471219E−01

Model 6 (full oxygen occupation on positions O(1B) and O(3C))

Energy difference relative to Model 5: 8.7 kJ/mol

Space group $Pna2_1$ (No. 33)
a = 30.54138843 Å, b = 5.27351400 Å, c = 8.40013732 Å, V = 1352.929808 Å^3

Table S30. Atomic coordinates of the optimized structure of $ClOF_2[TaF_6]$ (full oxygen occupation on positions O(1B) and O(3C)).

Atom	*x*	*y*	*z*
Ta	4.212837457685E−01	−4.492359622129E−01	4.974228580069E−01
Ta	1.708930996086E−01	2.444614361563E−01	−4.860216625325E−01
Cl	−4.333224421775E−01	−2.320814559025E−01	4.440459609882E−01
Cl	3.187983166578E−01	5.477450663191E−02	4.845991571779E−01
O	−4.655068398381E−01	−8.544638660922E−02	3.658485392543E−01
O	3.122716234754E−01	1.483267494551E−01	−3.600019400217E−01
F	−4.384094052577E−01	−1.662917447577E−01	−3.679366289654E−01
F	2.913040498220E−01	−2.094432009773E−01	4.746438748036E−01
F	−4.554239861714E−01	4.870914184876E−01	4.670763152138E−01
F	2.839048682166E−01	2.037906915274E−01	3.707059802283E−01
F	3.838307661088E−01	−1.636065308125E−01	−4.460979634356E−01
F	4.074028282868E−01	4.047464705741E−01	−2.928442204225E−01
F	3.673454561180E−01	3.896770946774E−01	4.233909988486E−01
F	4.342849341029E−01	−3.170771235660E−01	2.957420988436E−01
F	4.696703506821E−01	−2.901712926897E−01	−4.053059782640E−01
F	2.202128001033E−01	8.027705282859E−02	−3.990258544139E−01
F	1.337401473368E−01	−4.623654361654E−02	−4.493273205822E−01
F	1.564326425644E−01	3.738810772964E−01	−2.763722690481E−01
F	1.829958689673E−01	1.376034984466E−01	3.033650451002E−01
F	2.024690733279E−01	−4.532141730656E−01	4.760998212002E−01
F	1.170537953834E−01	4.110158049705E−01	4.369969951256E−01
F	4.527992459758E−01	2.510748996249E−01	4.554161928946E−01

Lattice parameters and atomic coordinates of the optimized solid-state structure of $ClOF_2[OsF_6]$

Space group $Pna2_1$ (No. 33)
a = 15.25805037 Å, b = 5.20681786 Å, c = 8.45561707 Å, V = 671.764017 Å^3

Table S31. Atomic coordinates of the optimized structure of $ClOF_2[OsF_6]$.

Atom	*x*	*y*	*z*
Os	4.082386746445E−01	3.910123810543E−01	−4.977230922155E−01
Cl	1.097800733173E−01	−4.066583686038E−01	4.727802130408E−01
O	1.228511277670E−01	−4.952701100265E−01	−3.693247640527E−01
F	1.802746547484E−01	4.418563801279E−01	3.595521715724E−01
F	1.662636029880E−01	−1.457100526718E−01	4.594132356443E−01
F	3.101124312580E−01	−4.532033498061E−01	−3.991126071943E−01
F	3.407865298306E−01	9.977079523670E−02	4.645133892418E−01
F	4.802766000225E−01	−3.154966924896E−01	−4.542567016032E−01
F	3.756433868229E−01	−4.827545026842E−01	2.990204417516E−01
F	−4.875221667650E−01	2.382143857115E−01	4.054495199134E−01
F	4.447808671667E−01	2.539359565969E−01	−2.947018060987E−01

Lattice parameters and atomic coordinates of the optimized solid-state structure of $ClOF_2[IrF_6]$

Space group $Pna2_1$ (No. 33)
a = 15.09574775 Å, b = 5.13646909 Å, c = 8.31062347 Å, V = 644.396118 Å^3

Table S32. Atomic coordinates of the optimized structure of $ClOF_2[IrF_6]$.

Atom	*x*	*y*	*z*
Ir	4.048234990928E−01	3.814781207281E−01	−4.774094027396E−01
Cl	1.124653105106E−01	−3.637790224478E−01	−4.268981346726E−01
O	1.617912507093E−01	−1.319961740300E−01	−4.442404875151E−01
F	1.759311079238E−01	4.319746985017E−01	−3.315817462498E−01
F	1.234339077147E−01	4.816047346509E−01	4.033656108270E−01
F	3.684122913874E−01	−4.753185385918E−01	−2.807642728658E−01
F	3.053295049777E−01	−4.735738294498E−01	4.183902933915E−01
F	3.432311042832E−01	8.194495219675E−02	−4.346614076906E−01
F	4.444246755472E−01	2.312461746924E−01	3.214124682089E−01
F	−4.921152000784E−01	2.432560317700E−01	−3.737800439817E−01
F	4.707369954925E−01	−3.200142522967E−01	4.729771232878E−01

Comparison of low-resolution Raman spectra of $ClOF_2[MF_6]$ compounds (*M* = V, Nb, Ta, Ru, Os, Ir, P, Sb)

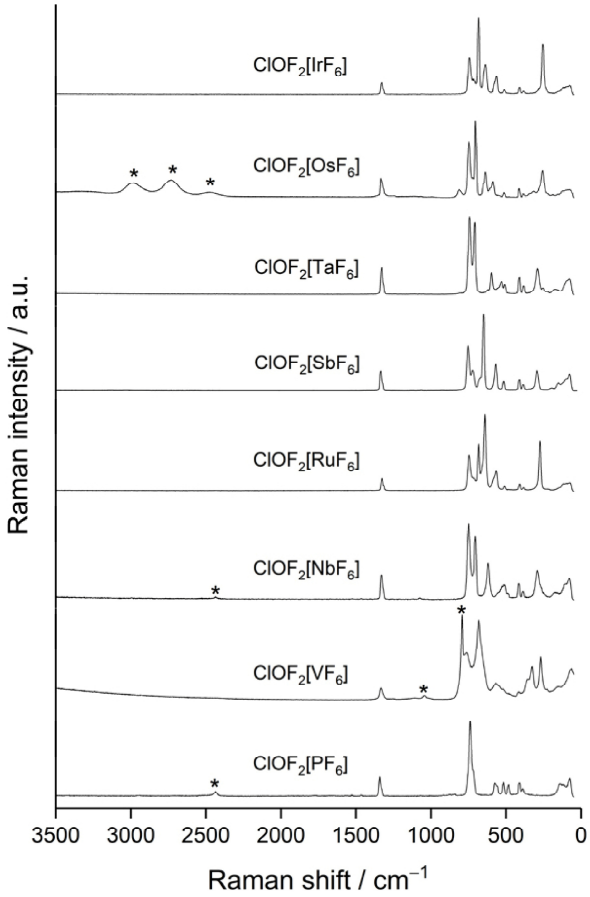

Figure S5. Comparison of low-resolution Raman spectra of $ClOF_2[MF_6]$ (*M* = P, V, Nb, Ru, Sb, Ta, Os, Ir) compounds. The Raman intensities are given in arbitrary units, a.u.. Samples were either measured in glass vessels or under perfluorinated polyether (Fomblin YR1800) on a microscope slide. The asterisks denote signals that are likely caused due to hydrolysis products of the samples.

Raman spectra and band assignments for the calculated Raman spectra of $ClOF_2[MF_6]$ (*M* = V, Nb, Ta, Ru, Os, Ir, P, Sb)

Raman spectra of $ClOF_2[PF_6]$

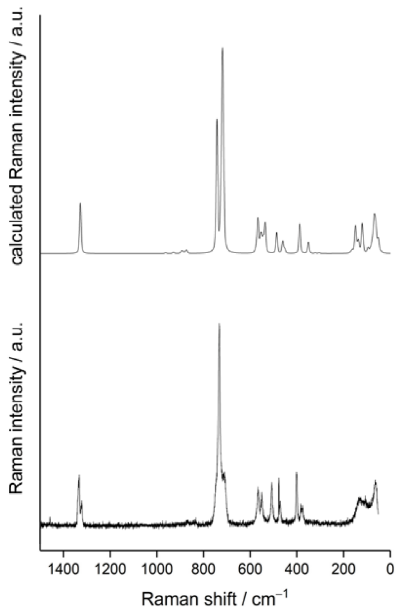

Figure S6. Comparison of the experimental high-resolution and calculated solid-state (DFT-PBE0/TZVP) Raman spectra of $ClOF_2[PF_6]$. The Raman intensities are given in arbitrary units, a.u..

Table S33. Band assignments for the calculated Raman spectrum (>300 cm^{-1}) of $ClOF_2[PF_6]$. The notation for band assignments is the following: *v* – stretching, *δ* – deformation, s – symmetric, as – asymmetric.

v (calculated) / cm^{-1}	*v* (experimental) / cm^{-1}	Assignment
1329-1327	1332, 1321	v(ClO) – Stretching of the O atom of the $ClOF_2^+$ cation
961-872	not observed	$v(ClF_2) + v(PF_6)$ –Stretching of F atoms of the $ClOF_2^+$ cation coupled with stretching modes of the $[PF_6]^-$ anion
748-742	732	$v_s(ClF_2) + v(PF_6)$ – Symmetric stretching of F atoms of the $ClOF_2^+$ cation coupled with stretching of the $[PF_6]^-$ anion
727-715	710	$v_{as}(ClF_2) + v(PF_6)$ – Asymmetric stretching of F atoms of the $ClOF_2^+$ cation coupled with stretching of the $[PF_6]^-$ anion
576-563	566	$v_{as}(PF_6)$ – Asymmetric stretching of the $[PF_6]^-$ anion
558-536	551	$\delta(PF_6)$ – Scissoring of the $[PF_6]^-$ anion
495-486	508	$\delta(ClOF_2) + \delta(PF_6)$ – Umbrella bending of the $ClOF_2^+$ cation coupled with scissoring of the $[PF_6]^-$ anion
464-451	478, 471	$\delta(PF_6)$ – Wagging of the $[PF_6]^-$ anion
388-386	401	δ(ClO) – Scissoring of the O atom of the $ClOF_2^+$ cation
352-350	382	$\delta(ClF_2)$ – Scissoring of the F atoms of the $ClOF_2^+$ cation
322-303	375	$\delta(PF_6)$ – Twisting of the $[PF_6]^-$ anion

Raman spectra of $ClOF_2[VF_6]$

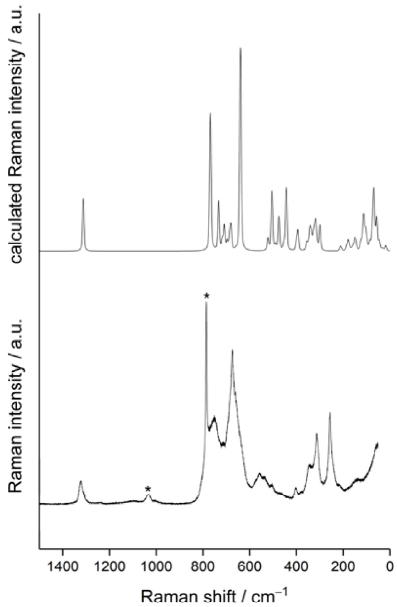

Figure S7. Comparison of the experimental high-resolution and calculated solid-state (DFT-PBE0/TZVP) Raman spectra of $ClOF_2[VF_6]$. The bands marked with an asterisk are likely caused by hydrolysis products. The Raman intensities are given in arbitrary units, a.u..

Table S34. Band assignments for the calculated Raman spectrum (>300 cm^{-1}) of $ClOF_2[VF_6]$. The notation for band assignments is the following: ν – stretching, δ – deformation, s – symmetric, as – asymmetric.

ν (calculated) / cm^{-1}	ν (experimental) / cm^{-1}	Assignment
1312-1310	1322	ν(ClO) – Stretching of the O atom of the $ClOF_2^+$ cation
798-642	750, 673	$\nu(ClF_2) + \nu(VF_6)$ –Stretching of F atoms of the $ClOF_2^+$ cation coupled with stretching modes of the $[VF_6]^-$ anion
521-434	558, 506	$\delta(ClOF_2) + \delta(VF_6)$ – Umbrella bending of the $ClOF_2^+$ cation coupled with scissoring of the $[VF_6]^-$ anion
401-399	401	$\delta(ClO) + \delta(VF_6)$ – Scissoring of the O atom of the $ClOF_2^+$ cation coupled with scissoring of the $[VF_6]^-$ anion
361-343	345	$\delta(ClF_2) + \delta(VF_6)$ – Scissoring of the F atom of the $ClOF_2^+$ cation coupled with scissoring of the $[VF_6]$ anion
331-302	313, 256	$\delta(ClOF_2) + \delta(VF_6)$ – Scissoring of the O and F atoms of the $ClOF_2^+$ cation coupled with scissoring of the $[VF_6]^-$ anion

Raman spectrum of $ClOF_2[NbF_6]$

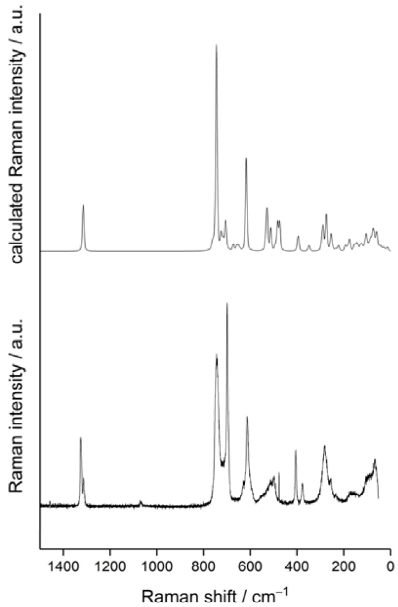

Figure S8. Comparison of the experimental high-resolution and calculated solid-state (DFT-PBE0/TZVP) Raman spectra of $ClOF_2[NbF_6]$. The Raman intensities are given in arbitrary units, a.u..

Table S35. Band assignments for the calculated Raman spectrum (>300 cm^{-1}) of $ClOF_2[NbF_6]$. The notation for band assignments is the following: ν – stretching, δ – deformation, s – symmetric, as – asymmetric.

ν (calculated) / cm^{-1}	ν (experimental) / cm^{-1}	Assignment
1317-1313	1325, 1313	ν(ClO) – Stretching of the O atom of the $ClOF_2^+$ cation
747-745	744	ν_s(ClF_2) – Symmetric stretching of F atoms of the $ClOF_2^+$ cation
738-705	not resolved due to overlapping bands	ν_{as}(ClF2) – Asymmetric stretching of F atoms of the $ClOF_2^+$ cation
701-510	698, 613	ν(NbF_6) – Stretching of the $[NbF_6]^-$ anion
493-490	499	δ($ClOF_2$) – Umbrella bending of the $ClOF_2^+$ cation
483-474	477	δ($ClOF_2$) + ν(NbF_6) – Umbrella bending of the $ClOF_2^+$ cation coupled with stretching of the $[NbF_6]^-$ anion
398-393	405	δ(ClO) – Scissoring of the O atom of the $ClOF_2^+$ cation
351-347	377	δ(ClF_2) – Scissoring of the F atoms of the $ClOF_2^+$ cation

Raman spectra of $ClOF_2[RuF_6]$

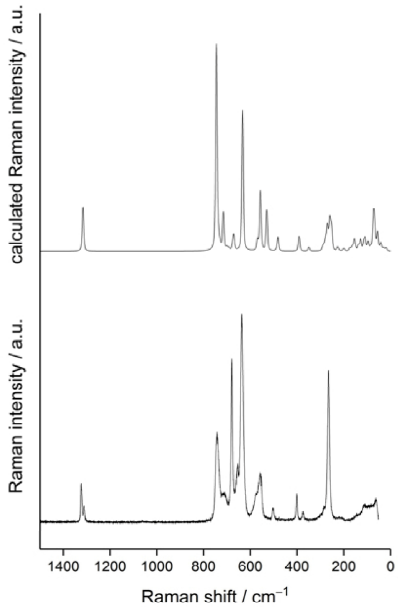

Figure S9. Comparison of the experimental high-resolution and calculated solid-state (DFT-PBE0/TZVP) Raman spectra of $ClOF_2[RuF_6]$. The Raman intensities are given in arbitrary units, a.u..

Table S36. Band assignments for the calculated Raman spectrum (>300 cm^{-1}) of $ClOF_2[RuF_6]$. The notation for band assignments is the following: ν – stretching, δ – deformation, s – symmetric, as – asymmetric.

ν (calculated) / cm^{-1}	ν (experimental) / cm^{-1}	Assignment
1317-1315	1323, 1311	ν(ClO) – Stretching of the O atom of the $ClOF_2^+$ cation
756-529	742, 714, 679, 654, 637, 558	$\nu(ClF_2)$ + $\nu(RuF_6)$ –Stretching of F atoms of the $ClOF_2^+$ cation coupled with stretching modes of the $[RuF_6]^-$ anion
491-481	503	$\delta(ClOF_2)$ + $\delta(RuF_6)$ – Umbrella bending of the $ClOF_2^+$ cation coupled with scissoring of the $[RuF_6]^-$ anion
392-390	401	δ(ClO) – Scissoring of the O atom of the $ClOF_2^+$ cation
350-349	375	$\delta(ClF_2)$ – Scissoring of the F atoms of the $ClOF_2^+$ cation

Raman spectra of $ClOF_2[SbF_6]$

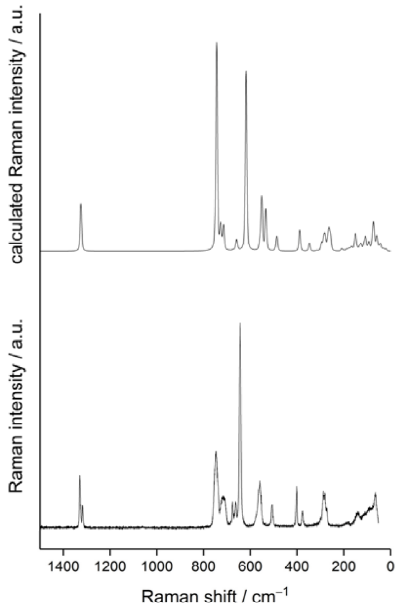

Figure S10. Comparison of the experimental high-resolution and calculated solid-state (DFT-PBE0/TZVP) Raman spectra of $ClOF_2[SbF_6]$. The Raman intensities are given in arbitrary units, a.u..

Table S37. Band assignments for the calculated Raman spectrum (>300 cm^{-1}) of $ClOF_2[SbF_6]$. The notation for band assignments is the following: ν – stretching, δ – deformation, s – symmetric, as – asymmetric.

ν (calculated) / cm^{-1}	ν (experimental) / cm^{-1}	Assignment
1325-1324	1330, 1318	ν(ClO) – Stretching of the O atom of the $ClOF_2^+$ cation
751-743	747	ν_s(ClF_2) – Symmetric stretching of F atoms of the $ClOF_2^+$ cation
727-714	715	ν_{as}(ClF_2) – Asymmetric stretching of F atoms of the $ClOF_2^+$ cation
688-533	675, 662, 643, 560	ν(SbF_6) –Stretching of the $[SbF_6]^-$ anion
494-484	507	δ($ClOF_2$) – Umbrella bending of the $ClOF_2^+$ cation
389-388	402	δ(ClO) – Scissoring of the O atom of the $ClOF_2^+$ cation
348-347	377	δ(ClF_2) – Scissoring of the F atoms of the $ClOF_2^+$ cation
316-303	288, 281	δ(SbF_6) – Scissoring of the $[SbF_6]^-$ anion

Raman spectrum of $ClOF_2[TaF_6]$

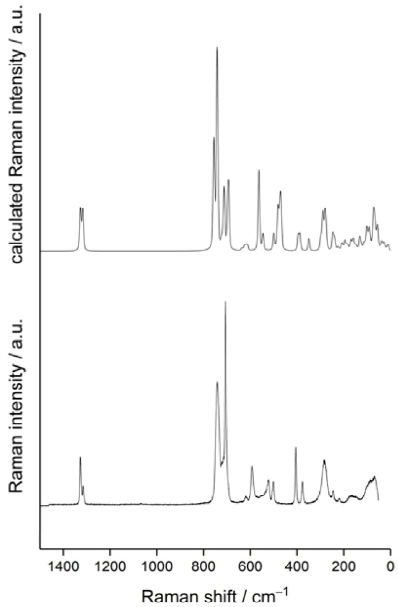

Figure S11. Comparison of the experimental high-resolution and calculated solid-state (DFT-PBE0/TZVP) Raman spectra of $ClOF_2[TaF_6]$. The Raman intensities are given in arbitrary units, a.u..

Table S38. Band assignments for the calculated Raman spectrum (>300 cm^{-1}) of $ClOF_2[TaF_6]$. The notation for band assignments is the following: ν – stretching, δ – deformation, s – symmetric, as – asymmetric.

ν (calculated) / cm^{-1}	ν (experimental) / cm^{-1}	Assignment
1330-1316	1327, 1315	ν(ClO) – Stretching of the O atom of the $ClOF_2^+$ cation
765-741	741	$\nu_s(ClF_2)$ – Symmetric stretching of F atoms of the $ClOF_2^+$ cation
722-711	not resolved due to overlapping bands	$\nu_{as}(ClF_2)$ – Asymmetric stretching of F atoms of the $ClOF_2^+$ cation
699-546	706, 617, 592, 522	$\nu(TaF_6)$ – Stretching of the $[TaF_6]^-$ anion
500-468	500	$\delta(ClOF_2) + \nu(TaF_6)$ – Umbrella bending of the $ClOF_2^+$ cation coupled with stretching of the $[TaF_6]^-$ anion
395-388	404	δ(ClO) – Scissoring of the O atom of the $ClOF_2^+$ cation
350-349	376	$\delta(ClF_2)$ – Scissoring of the F atoms of the $ClOF_2^+$ cation

Raman spectra of $ClOF_2[OsF_6]$

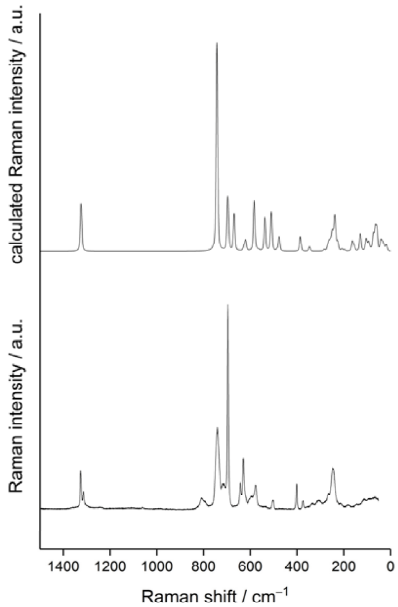

Figure S12. Comparison of the experimental high-resolution and calculated solid-state (DFT-PBE0/TZVP) Raman spectra of $ClOF_2[OsF_6]$. The Raman intensities are given in arbitrary units, a.u..

Table S39. Band assignments for the calculated Raman spectrum (>300 cm^{-1}) of $ClOF_2[OsF_6]$. The notation for band assignments is the following: ν – stretching, δ – deformation, s – symmetric, as – asymmetric.

ν (calculated) / cm^{-1}	ν (experimental) / cm^{-1}	Assignment
1329-1323	1325, 1313	ν(ClO) – Stretching of the O atom of the $ClOF_2^+$ cation
757-735	740	ν_s(ClF_2) – Symmetric stretching of F atoms of the $ClOF_2^+$ cation
699-692	716	ν_{as}(ClF_2) – Asymmetric stretching of F atoms of the $ClOF_2^+$ cation
673-510	696, 643, 631, 577	ν(OsF_6) – Stretching of the $[OsF_6]^-$ anion
486-476	503	δ($ClOF_2$) – Umbrella bending of the $ClOF_2^+$ cation
386	402	δ(ClO) – Scissoring of the O atom of the $ClOF_2^+$ cation
348-347	375	δ(ClF_2) – Scissoring of the F atoms of the $ClOF_2^+$ cation

Raman spectrum of $ClOF_2[IrF_6]$

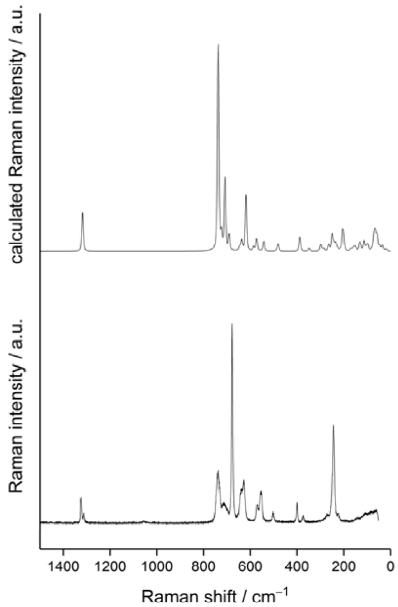

Figure S13. Comparison of the experimental high-resolution and calculated solid-state (DFT-PBE0/TZVP) Raman spectra of $ClOF_2[IrF_6]$. The Raman intensities are given in arbitrary units, a.u..

Table S40. Band assignments for the calculated Raman spectrum (>300 cm^{-1}) of $ClOF_2[IrF_6]$. The notation for band assignments is the following: ν – stretching, δ – deformation, s – symmetric, as – asymmetric.

ν (calculated) / cm^{-1}	ν (experimental) / cm^{-1}	Assignment
1319-1317	1324, 1313	ν(ClO) – Stretching of the O atom of the $ClOF_2^+$ cation
743-737	737	ν_s(ClF_2) – Symmetric stretching of F atoms of the $ClOF_2^+$ cation
727-708	713	ν_{as}(ClF_2) – Asymmetric stretching of F atoms of the $ClOF_2^+$ cation
692-542	677, 639, 628, 570, 555	ν(IrF_6) – Stretching of the $[IrF_6]^-$ anion
491-481	503	δ($ClOF_2$) – Umbrella bending of the $ClOF_2^+$ cation
390-384	400	δ(ClO) – Scissoring of the O atom of the $ClOF_2^+$ cation
349	374	δ(ClF_2) – Scissoring of the F atoms of the $ClOF_2^+$ cation

References

[1] R. D. Shannon, *Acta Crystallogr., Sect. A: Cryst. Phys., Diffr., Theor. Gen. Crystallogr.* **1976**, *32*, 751–767.
[2] D. S. Brock, J. J. Casalis de Pury, H. P. A. Mercier, G. J. Schrobilgen, B. Silvi, *Inorg. Chem.* **2010**, *49*, 6673–6689.
[3] A. J. Karttunen, T. Tynell, M. Karppinen, *J. Phys. Chem. C* **2015**, *119*, 13105–13114.
[4] V. Sivchik, R. K. Sarker, Z.-Y. Liu, K.-Y. Chung, E. V. Grachova, A. J. Karttunen, P.-T. Chou, I. O. Koshevoy, *Chem. Eur. J.* **2018**, *24*, 11475–11484.
[5] M. S. Kuklin, A. J. Karttunen, *J. Phys. Chem. C* **2018**, *122*, 24949–24957.
[6] F. Weigend, R. Ahlrichs, *Phys. Chem. Chem. Phys.* **2005**, *7*, 3297–3305.

7.5. Reactions of ClF_3 with Main Group and Transition Metal Oxides: Access to Dioxychloronium(V) Fluoridometallates and Oxidofluoridometallates

Benjamin Scheibe, Antti J. Karttunen, Florian Kraus

Eur. J. Inorg. Chem. **2020**.
DOI: 10.1002/ejic.202000908

© 2020 The Authors. Published by Wiley-VCH Verlag GmbH & Co. KGaA.

Open access article distributed under the Creative Commons CC BY 4.0 license.
The original licensed material is shown.
(https://creativecommons.org/licenses/by/4.0/legalcode)

European Journal of Inorganic Chemistry 10.1002/ejic.202000908

WILEY-VCH

FULL PAPER

Reactions of ClF_3 with Main Group and Transition Metal Oxides: Access to Dioxychloronium(V) Fluoridometallates and Oxidofluoridometallates

Benjamin Scheibe,[a] Antti J. Karttunen,[b] and Florian Kraus*[a]

[a] B. Scheibe M. Sc., Prof. Dr. F. Kraus
Fachbereich Chemie
Philipps-Universität Marburg
Hans-Meerwein-Straße 4, 35032 Marburg (Germany)
E-mail: f.kraus@uni-marburg.de

[b] Prof. Dr. A. J. Karttunen
Department of Chemistry and Materials Science
Aalto University
00076 Aalto (Finland)

Supporting information for this article is given via a link at the end of the document.

Abstract: Compounds containing the dioxychloronium cation, $[ClO_2]^+$, were obtained from reactions of ClF_3 with various oxides such as TiO_2, MoO_3, Re_2O_7, SnO, P_2O_5, As_2O_5, and Nb metal, as the latter contained oxide as an impurity. Partial hydrolysis of $[ClF_2][IrF_6]$ led to the formation of $[ClO_2][IrF_6]$. The crystal structures of the compounds were determined by single-crystal X-ray diffraction, which showed that depending on the starting material $[ClO_2]^+$ salts with the fluoridometallate anions $[[TiF_{3/2}F_{3/1}]_2]^-$, $[Nb_3F_{16}]^-$, $[IrF_6]^-$, $[SnF_{2/2}F_{4/1}]^-$ $[PF_6]^-$, and $[AsF_6]^-$, or with the oxidofluoridometallate anions $[Mo_3O_3F_{13}]^-$ and $[Re_3O_6F_{10}]^-$, were obtained. Bent $[ClO_2]^+$ cations with short Cl···μ-F contacts of surrounding F atoms of the anions with the Cl atom are present in the crystal structures, leading to coordination numbers of 2+4 or 2+6 for the Cl atom. Various structural motifs are observed, which range from molecular, columnar, ladder-like, to layer and framework structures. The salts were furthermore characterized by Raman spectroscopy and solid-state quantum-chemical calculations. Covalent Cl−O bonds and ionic Cl···μ-F interactions are indicated by the calculations.

Introduction

Chlorosyl fluoride, ClOF, has a short lifetime and disproportionates into ClF and ClO_2F.[1–4] The latter, called chlorine dioxide fluoride or chloryl fluoride, is one of the known stable oxyfluorides of chlorine.[5–8] The other ones are chlorine oxide trifluoride $ClOF_3$, perchloryl fluoride ClO_3F, and chlorine dioxide trifluoride ClO_2F_3.[9–14] Perchloryl hypofluorite, ClO_4F, does not possess a Cl−F bond, as indicated by the name, and is thus different from the oxyfluorides.[8,15] Structural formulas of these compounds are shown in Scheme 1.

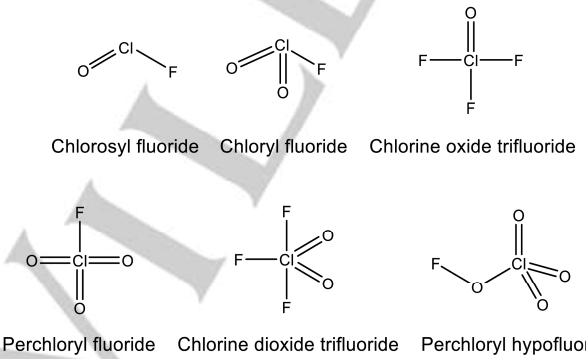

Scheme 1. Overview of the known hypofluorite and oxyfluorides of chlorine.

ClO_2F can be synthesized by different methods, the most important ones being the fluorination of ClO_2 (Equation (1)) or of chlorates, $A[ClO_3]$ (A = Na, K) (Equations (2) and (3)).[5,8,16–19]

$$2\ ClO_2 + F_2 \longrightarrow 2\ ClO_2F \quad (1)$$

$$6\ K[ClO_3] + 10\ BrF_3 \longrightarrow 6\ K[BrF_4] + 2\ Br_2 + 3\ O_2 + 6\ ClO_2F \quad (2)$$

This article is protected by copyright. All rights reserved.

Accepted Manuscript

European Journal of Inorganic Chemistry 10.1002/ejic.202000908

WILEY-VCH

FULL PAPER

$$6\,A[ClO_3] + 4\,ClF_3 \longrightarrow 6\,AF + 2\,Cl_2 + 3\,O_2 + 6\,ClO_2F \quad (3)$$
$$A = Na, K$$

Reactions involving the chlorine oxides ClO_2 or Cl_2O_6 are usually disadvantageous due to their preparation and handling.[5,16,20,21] Usage of BrF_3 usually leads to Br_2 impurities in the ClO_2F, in comparison to the fluorination with ClF_3, which gives more easily separable Cl_2 as a side product. If the chlorates are fluorinated with gaseous F_2, both ClO_2F and ClO_3F are formed.[6,22,23] ClO_2F is furthermore formed in the reactions of ClF, ClF_3, and ClF_5 with many oxygen-containing compounds.[8,24,25]

ClO_2F can act as an oxidizing and fluorinating agent, but it is much less oxidizing than ClF_3.[8] Like other halogen fluorides and oxyfluorides, it shows amphoteric behavior and thus can act as a Lewis acid or base.

The halogen dioxide fluorides, XO_2F (X = Cl, Br, I), form bent C_{2v} $[XO_2]^+$ cations with Lewis acids such as AsF_5 or SbF_5 (Equation (4)).[19,26–33]

$$XO_2F + MF_5 \longrightarrow [XO_2][MF_6] \quad (4)$$
$$X = Cl, Br, I;\ M = As, Sb$$

Compounds with $[ClO_2]^+$ or $[BrO_2]^+$ ions are furthermore obtained when XO_3F (X = Cl, Br) is reacted with strong Lewis acids.[34] In the case of $[ClO_2]^+$ cations, reactions of Cl_2O_6 ("$[ClO_2][ClO_4]$") with metals or chlorides often lead to the formation of dioxychloronium(V) perchloratometallates, where $[ClO_4]^-$ anions are bound as ligands.[35–40] Crystal structures of $[ClO_2]^+$ salts with the following anions have been reported: $[BF_4]^-$, $[GeF_{2/2}F_{4/1}]^-$, $[RuF_6]^-$, $[SbF_6]^-$, $[Sb_2F_{11}]^-$, $[ClO_4]^-$, $[Au(ClO_4)_4]^-$ and $[Sn(ClO_4)_6]^{2-}$.[34,37–44] Recently, compounds were published containing the complex $[Cl_2BrO_6]^+$ cation that might be considered as a central $[BrO_2]^-$ anion coordinating to two $[ClO_2]^+$ cations.[45]

Salts containing disphenoidal (seesaw) C_{2v} $[XO_2F_2]^-$ anions are also known but they are usually not formed by the direct reaction of XO_2F with a fluoride ion donor.[46–49] Thus far, only salts with $[IO_2F_2]^-$ anions have been structurally characterized by single-crystal X-ray diffraction.[49–52] For Cl, the direct reaction of ClO_2F with CsF, yielding $Cs[ClO_2F_2]$, is known, and for Br, the reaction of BrO_2F with KF, giving $K[BrO_2F_2]$, accompanied with the partial decomposition of BrO_2F during this reaction, has been reported.[47,48,53] The indirect formation via hydrolysis reactions of $K[BrF_6]$ or fluorination of $K[BrO_3]$ with BrF_5 is also possible, but $K[BrOF_4]$ is usually also formed.[29–31,48] The corresponding iodine compounds can be synthesized by dissolving an iodate, $A[IO_3]$ (A = Na, K, Rb, Cs, NH_4, $N(CH_3)_4$), in hydrofluoric acid.[50,54]

Here, we report on reactions of ClF_3 with the main group oxides SnO, P_2O_5, and As_2O_5, and with the transition metal oxides TiO_2, Nb/Nb_2O_5, MoO_3, and Re_2O_7, as well as on the hydrolysis reaction of $[ClF_2][IrF_6]$. These reactions lead to the formation of dioxychloronium(V) salts with the fluoridometallate anions $[Ti_2F_9]^-$, $[SnF_5]^-$, $[MF_6]^-$ (M = Ir, P, As), and $[Nb_3F_{16}]^-$ and to the oxidofluoridometallate anions $[Mo_3O_3F_{13}]^-$ and $[Re_3O_6F_{10}]^-$. Crystal structures were determined by single-crystal X-ray diffraction and the compounds were further characterized by Raman spectroscopy and quantum-chemical calculations.

Results and Discussion

Syntheses of $[ClO_2]^+$ compounds

Compounds containing the $[ClO_2]^+$ cation are usually synthesized by the reaction of ClO_2F with a Lewis acid.[7,8,26,55] It is known that ClF_3, when reacted with oxygen-containing compounds such as H_2O, forms ClO_2F along other side-products.[1,8,24,25] This might be attributed to the intermediate formation of ClOF, an elusive oxyfluoride that readily disproportionates into ClO_2F and ClF.[1–4] Furthermore, $[ClO_2]^+$ impurities were reported in reactions of ClF_3 with Lewis acids, where either ClF_3 was contaminated with ClO_2F, or when the starting material contained water or the equipment was not properly dried or "unsuitable" for the work with ClF_3, for example, apparatuses made out of glass.[8,55,56] The reactions of ClF_3 with main group (non)metal and transition metal oxides of elements that can form fluoridometallate or oxidofluoridometallate anions were studied(Equations (5) to (10)).

Caution! *We would like to stress that the reactions of ClF_3 with metal powders or oxides are highly exothermic and can result in explosions when scaled up.*

In all cases, salts containing the $[ClO_2]^+$ cation were obtained, as shown by single-crystal X-ray diffraction and Raman spectroscopy. Furthermore, the hydrolysis reaction of $[ClF_2][IrF_6]$ yielded $[ClO_2][IrF_6]$ and the reaction of Nb powder that had been stored on air, gave $[ClO_2][Nb_3F_{16}]$ along with $[ClF_2][NbF_6]$.[57] All given equations are idealized and assume that ClO_2F and/or ClF are the sole side-products in these reactions. ClO_2F and ClF are themselves oxidizing and fluorinating agents, and depending on the reaction conditions, O_2 and Cl_2 might also be formed.[8]

The reactions of M_2O_5 (M = P, As) with ClF_3 lead to the formation of $[ClO_2][MF_6]$ (Equation (5)). While the reaction of P_2O_5 with ClF_3 is highly exothermic and vigorous, the reaction with As_2O_5 is comparably slow. The dissociation pressure of the adduct $[ClO_2][PF_6]$ is high and it is unstable at room temperature.[26]

This article is protected by copyright. All rights reserved.

Accepted Manuscript

European Journal of Inorganic Chemistry 10.1002/ejic.202000908

WILEY-VCH

FULL PAPER

$$2\ M_2O_5 + 10\ ClF_3 \longrightarrow 4\ [ClO_2][MF_6] + ClO_2F + 5\ ClF \quad (5)$$

M = P, As, Nb, Ta

The reaction of SnO with ClF_3 in anhydrous HF (aHF) leads to the formation of $[ClO_2][SnF_5]$ and likely $[ClF_2][SnF_5]$ as well, as bands of the $[ClF_2]^+$ cation show up in the Raman spectrum (Equation (6)).

$$2\ SnO + 5\ ClF_3 \xrightarrow{aHF} [ClO_2][SnF_5] + [ClF_2][SnF_5] + 3\ ClF \quad (6)$$

If TiO_2 is reacted with ClF_3, then $[ClO_2][Ti_2F_9]$ is formed (Equation (7)).

$$2\ TiO_2 + 4\ ClF_3 \longrightarrow [ClO_2][Ti_2F_9] + ClO_2F + 2\ ClF \quad (7)$$

The reaction of MoO_3 with ClF_3 yields a salt containing the $[Mo_3O_3F_{13}]^-$ anion (Equation (8)). The reaction of $MoOF_4$ with ClF_3 also gave the compound $[ClO_2][Mo_3O_3F_{13}]$, assuming the formation of MoF_6 (Equation (9)).

$$3\ MoO_3 + 6\ ClF_3 \longrightarrow [ClO_2][Mo_3O_3F_{13}] + 2\ ClO_2F + 3\ ClF \quad (8)$$

$$5\ MoOF_4 + 2\ ClF_3 \longrightarrow [ClO_2][Mo_3O_3F_{13}] + 2\ MoF_6 + ClF \quad (9)$$

Carried out at −37 °C, the reaction of Re_2O_7 with ClF_3 leads to a salt with the $[Re_3O_6F_{10}]^-$ anion (Equation (10)). Crystals of the compound quickly decompose at room temperature. The reactions of Re_2O_7 with ClF_3 were reported previously and depending on the reaction conditions, ReO_2F_3 (at low temperatures) or $ReOF_5$ (room temperature) was formed.[58,59]

$$6\ Re_2O_7 + 18\ ClF_3 \longrightarrow 4\ [ClO_2][Re_3O_6F_{10}] + 5\ ClO_2F + 9\ ClF \quad (10)$$

During the attempted synthesis of a salt with a $[ClF_2(ClF_3)_n]^+$ cation that would be similar to the cations $[BrF_2(BrF_3)_n]^+$ (n = 1, 2), the salt $[ClO_2][IrF_6]$ was obtained as a hydrolysis product.[60] Hydrolysis reactions of $[ClF_2]^+$ salts, yielding $[ClO_2]^+$ salts, were previously reported.[25,61]

$$ClF_2[IrF_6] + 2\ H_2O + ClF_3 \longrightarrow [ClO_2][IrF_6] + 4\ HF + ClF \quad (11)$$

Crystal structures of $[ClO_2]^+$ compounds

The crystal structure of $[ClO_2][PF_6]$

Dioxychloronium(V) hexafluoridophosphate(V) crystallizes in the orthorhombic space group $P2_12_12_1$ (No. 19) with four formula units per unit cell, Pearson code *oP*40, and Wyckoff sequence 19.a^{10}. Selected crystallographic data and details of the structure determination are given in Table 1. Atomic coordinates, equivalent isotropic and anisotropic displacement parameters are reported in the Supporting Information. The Cl(1) atom occupies the Wyckoff position 4*a* (site symmetry 1) and is surrounded by the two oxygen atoms O(1) and O(2), giving the $[ClO_2]^+$ cation (Figure 1). The Cl−O bond lengths are 1.4077(8) and 1.4060(8) Å and the O−Cl−O angle is 119.75(5)°. A comparison of the Cl−O bond lengths of the investigated compounds and thus far reported $[ClO_2]^+$ salts is given in Table 2.
The P(1) atom also occupies a general position (4*a*) and is surrounded by the six fluorine atoms F(1) to F(6) in the shape of a distorted octahedron, yielding the $[PF_6]^-$ anion. The P−F bond lengths lie in the range from 1.5881(6) to 1.6197(6) Å and nicely agree with those in $Li[PF_6]$, which are 1.603(1) Å at room temperature.[62] Five of the six F atoms, F(1) and F(3) to F(6), show short Cl···μ-F contacts with the Cl atom with distances in the range of 2.6226(7) to 2.8797(7) Å. The F(4) atom shows contacts to two Cl atoms and is μ_3-bridging. With the P−μ_3-F bond being the longest, the P−μ-F bonds are significantly longer compared to the terminally bound F(2) atom with a P−F bond length of 1.5881(6) Å. They range from 1.5993(7) to 1.6197(6) Å. This is likely due to the higher effective coordination number of these μ-F atoms and their interaction with the Cl atom.

This article is protected by copyright. All rights reserved.

Accepted Manuscript

European Journal of Inorganic Chemistry 10.1002/ejic.202000908

WILEY-VCH

FULL PAPER

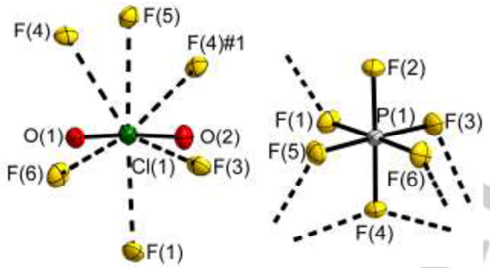

Figure 1. The coordination environment of the Cl and P atom in the crystal structure of $[ClO_2][PF_6]$. Short contacts of F atoms belonging to the $[PF_6]^-$ anions with neighboring Cl atoms are shown as dashed bonds. Symmetry transformation: #1 1/2 − *x*, 1 − *y*, 1/2 + *z*. Displacement ellipsoids are shown at the 70% probability level at 100 K.

The overall coordination number of the Cl atom is 2+6 if the μ-F atoms are considered and the F and O ligands are arranged in the shape of a distorted square antiprism (Figure 1). Due to the shorter Cl−O bonds in comparison to the much longer Cl···μ-F interactions, the Cl atom is displaced from the center of the coordination polyhedron. In comparison to previously reported crystal structures of $[ClO_2]^+$ compounds, such as $[ClO_2][BF_4]$, $[ClO_2][RuF_6]$, $[ClO_2][SbF_6]$, $[ClO_2][Sb_2F_{11}]$, or $[ClO_2][ClO_4]$, the coordination number of the Cl atom is unexpectedly high.[34,39,41,43,44] Usually, only four short contacts of O or F atoms from surrounding anions are observed. The only other example with such a coordination number for the Cl atom of a $[ClO_2]^+$ cation is the compound $[ClO_2][GeF_5]$, in which two symmetry-independent $[ClO_2]^+$ cations are present. There, one Cl atom has coordination number six (distorted octahedron) and the other one eight (square antiprism).[41]

When these Cl···μ-F contacts are considered, a framework structure is obtained (Figure 2). The structure can be described with the Niggli formula ${}^{3}_{\infty}\left[\langle ClF_{\frac{2}{2+1}}F_{\frac{4}{1+1}}O_{\frac{2}{1}}\rangle\langle PF_{\frac{1}{1+2}}F_{\frac{4}{1+1}}F_{\frac{1}{1}}\rangle\right]$, where the notation of the Niggli formula is given according to the literature.[63] Explained in short, this type of Niggli formula indicates for the cation that two F atoms bridge μ_3-like between two Cl and one P atoms, four F atoms bridge between the Cl and P atoms, and the two O atoms belong solely to the Cl atom. For the anion, there is one μ_3-like bridging F atom between one P and two Cl atoms, there are four μ-like bridging F atoms between a P and a Cl atom, and there is terminally bound F atom.

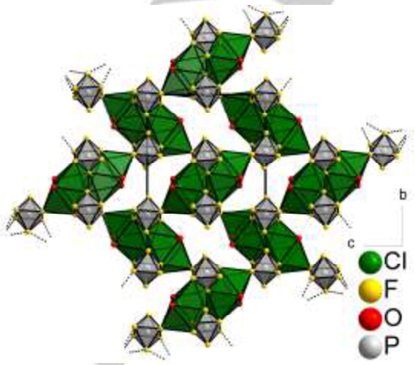

Figure 2. Crystal structure of $[ClO_2][PF_6]$ projected along the *a* axis. Coordination polyhedra of Cl atoms are shown in green and those of P atoms in grey. Short contacts of F atoms belonging to the $[PF_6]^-$ anions with neighboring Cl atoms are shown as dashed bonds. Atoms are shown as isotropic with arbitrary radii.

The Cl atoms form a hexagonal close packing, with Cl···Cl distances of *circa* 5.21 to 6.64 Å. When Cl···P distances of 3.64 to 5.11 Å are considered, a distorted octahedron for the P atom and a distorted trigonal prism for the Cl atom are obtained as the coordination polyhedra. The arrangement of the P and Cl atoms is therefore similar to the Ni and As atoms in the NiAs structure type.[64]

Table 1. Selected crystallographic data and details of the structure determinations of $[ClO_2][MF_6]$ (M = P, As, Ir), $[ClO_2][SnF_5]$, $[ClO_2][Ti_2F_9]$ and $[ClO_2][Nb_3F_{16}]$.

Compound	$[ClO_2][PF_6]$	$[ClO_2][AsF_6]$	$[ClO_2][IrF_6]$	$[ClO_2][SnF_5]$	$[ClO_2][Ti_2F_9]$	$[ClO_2][Nb_3F_{16}]$
Molar mass / g·mol^{-1}	212.42	256.37	373.65	281.14	334.25	650.18
Space group (No.)	$P2_12_12_1$(19)	$C2/m$(12)	$P12/n1$(13)	$P12_1/n1$(14)	$C2/c$(15)	$C2/c$(15)
a / Å	5.2060(3)	10.9411(6)	7.0660(4)	7.3673(4)	11.084(2)	9.6738(7)
b / Å	10.1459(5)	10.0225(5)	5.6559(3)	5.1042(3)	14.603(2)	14.4023(11)
c / Å	10.2172(5)	5.0773(3)	7.1583(4)	13.5108(8)	5.330(1)	10.0266(8)
β / °	90	97.680(5)	92.052(1)	93.026(2)	111.73(1)	97.142(3)
V / Å^3	539.67(5)	551.77(5)	285.90(3)	507.35(5)	801.4(2)	1386.1(2)

This article is protected by copyright. All rights reserved.

Accepted Manuscript

European Journal of Inorganic Chemistry 10.1002/ejic.202000908

WILEY-VCH

FULL PAPER

Z	4	4	2	4	4	4
Pearson symbol	$oP40$	$mS40$	$mP20$	$mP36$	$mS56$	$mS88$
$\rho_{calc.}$ / g·cm^{-3}	2.61	3.09	4.34	3.68	2.77	3.12
μ / mm^{-1}	1.084	6.722	23.891	5.606	2.459	2.816
Color	colorless	colorless	yellow	colorless	colorless	colorless
Crystal morphology	block	block	block	block	block	block
Crystal size / mm^3	0.39×0.46×0.49	0.10×0.15×0.26	0.15×0.24×0.27	0.05×0.06×0.12	0.09×0.13×0.25	0.18×0.18×0.23
T / K	100					
λ / Å	0.71073 (Mo-K$_\alpha$)					
No. of reflections	18116	6480	43352	9560	14689	47929
θ range / °	2.83-41.25	3.76-33.33	3.60-41.39	3.02-33.19	2.79-31.50	2.55-39.59
Range of Miller indices	$-9 \le h \le 8$	$-16 \le h \le 16$	$-13 \le h \le 13$	$-11 \le h \le 11$	$-16 \le h \le 14$	$-17 \le h \le 17$
	$-18 \le k \le 18$	$-15 \le k \le 15$	$-10 \le k \le 10$	$-7 \le k \le 7$	$-21 \le k \le 21$	$-25 \le k \le 25$
	$-18 \le l \le 18$	$-7 \le l \le 7$	$-13 \le l \le 13$	$-20 \le l \le 20$	$-7 \le l \le 7$	$-17 \le l \le 17$
Absorption correction	multi-scan	integration	multi-scan	multi-scan	integration	multi-scan
$Trans._{max}$, $Trans._{min}$	0.28, 0.22	0.56, 0.29	0.11, 0.01	0.75, 0.62	0.84, 0.58	0.44, 0.38
R_{int}, R_σ	0.0249, 0.0337	0.0186, 0.0373	0.0159, 0.0269	0.0315, 0.0355	0.0421, 0.475	0.0126, 0.291
Completeness of the data set	0.999	0.998	0.997	0.997	0.999	0.996
No. of unique reflections	3598	1126	1927	1934	1337	4167
No. of parameters	92	51	47	83	66	102
No. of restraints	0	0	0	0	0	0
No. of constraints	0	0	0	0	0	0
S (all data)	1.089	1.113	1.146	1.034	1.017	1.191
$R(F)$ ($I \ge 2\sigma(I)$, all data)	0.0203, 0.0240	0.0184, 0.0253	0.0216, 0.0225	0.0222, 0.0344	0.0452, 0.0616	0.0137, 0.0155
$wR(F^2)$ ($I \ge 2\sigma(I)$, all data)	0.0432, 0.0443	0.0410, 0.0435	0.0614, 0.0623	0.0403, 0.0434	0.1101, 0.1218	0.0310, 0.0315
Flack parameter x	0.00(2)	-	-	-	-	-
Extinction coefficient	0.064(3)	not refined	not refined	0.0040(3)	0.0097(18)	0.00189(8)
$\Delta\rho_{max}$, $\Delta\rho_{min}$ / e·Å^{-3}	0.38, −0.35	0.41, −0.65	4.30, −4.45	0.82, −0.90	0.82, −0.94	0.95, −0.65

Table 2. Experimental and calculated Cl−O bond lengths, as well as Cl···μ-F distances of bridging F atoms of fluoridometallate and oxidofluoridometallate anions in $[ClO_2]^+$ salts.

Compound	bond lengths and atomic distances / Å		calculated bond lengths and atomic distances (DFT-PBE0/TZVP, solid-state) / Å	
	Cl−O	Cl···μ-F	Cl−O	Cl···μ-F
$[ClO_2][PF_6]$	1.4060(8), 1.4077(8)	2.6226(7)-2.8797(7)	1.43, 1.44	2.50-2.82
$[ClO_2][AsF_6]$	1.4027(11)	2.7275(9), 2.7953(8)	1.44	2.58, 2.77
$[ClO_2][IrF_6]$	1.409(3)	2.467(2), 2.699(2)	1.44	2.32, 2.77
$[ClO_2]SnF_5$	1.4045(13), 1.4050(18)	2.3847(14)-2.6912(14)	1.44	2.30-2.68
$[ClO_2]Ti_2F_9$	1.401(3)	2.665(2), 2.708(2)	1.44	2.56, 2.66
$[ClO_2][Nb_3F_{16}]$	1.4084(6)	2.4904(5), 2.6554(6)	1.44	2.39, 2.63
$[ClO_2][Mo_3O_3F_{13}]$	1.3950(18), 1.4068(18)	2.4617(15)-2.9054(15)	1.43	2.39-2.85
$[ClO_2][Re_3O_6F_{10}]$	1.384(4), 1.418(4)	2.354(3)-2.749(3)	1.44	2.25-2.82

The crystal structure of $[ClO_2][AsF_6]$

To our surprise, dioxychloronium(V) hexafluoridoarsenate(V) is not isotypic to the $[PF_6]^-$ salt described above and crystallizes with four formula units per unit cell in the monoclinic space group $C2/m$ (No. 12), Pearson code $mS40$, and Wyckoff sequence $12j^3i^3h$. Selected crystallographic data and details of the structure determination are given in Table 1. Atomic coordinates, equivalent isotropic and anisotropic displacement parameters are reported in the Supporting Information. The Cl(1) atom occupies the Wyckoff position $4h$ (site symmetry 2) and is surrounded by the oxygen atoms O(1) and O(1)#1, giving the $[ClO_2]^+$ cation (Figure 3). The Cl−O bond length is 1.4027(11) Å and the O−Cl−O angle is 119.57(11)°. The As(1) atom occupies the Wyckoff position $4i$ (site symmetry m) and is surrounded by six F atoms in the shape of a distorted octahedron, resulting in the $[AsF_6]^-$ anion. The As−F bond lengths lie in the range of 1.7034(14) to 1.7418(13) Å and are comparable to those in $Li[AsF_6]$, which are 1.74(4) Å at room temperature.[62] The F atoms of the $[AsF_6]^-$ anion show short Cl···μ-F contacts of either 2.7275(9) or 2.7953(8) Å. One of the F atoms of the $[AsF_6]^-$ anion, F(4), is μ_3-bridging, two are μ-bridging, F(2) and F(2)#1, and the other three are terminally bound. The longest As−F bond is observed for the μ_3-F atom, whereas the As−μ_2-F bonds are unexpectedly shorter than those of the terminally bound F atoms.

This article is protected by copyright. All rights reserved.

Accepted Manuscript

European Journal of Inorganic Chemistry 10.1002/ejic.202000908

WILEY-VCH

FULL PAPER

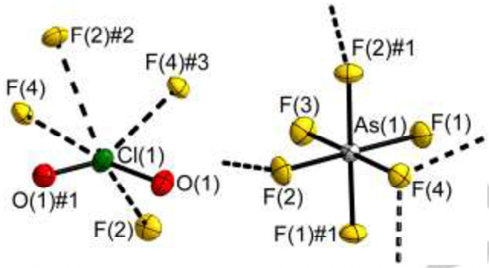

Figure 3. The coordination environment of the Cl and As atom in the crystal structure of $[ClO_2][AsF_6]$. Short contacts of F atoms belonging to the $[AsF_6]^-$ anions with neighboring Cl atoms are shown as dashed bonds. Symmetry transformations (left): #1 1 − *x*, *y*, 1 − *z*; #2 1/2 − *x*, 1/2 + *y*, −*z*; #3 1/2 − *x*, 1/2 + y, 1 − *z*. Symmetry transformation (right): #1 *x*, 1 − *y*, *z*. Displacement ellipsoids are shown at the 70% probability level at 100 K.

The overall coordination number of the Cl atom is 2+4, with a distorted octahedral arrangement of the ligands. The Cl atom is displaced from the center of the coordination polyhedron, which is of course due to the unequal Cl−O and Cl···F distances, see above. When the Cl···μ-F contacts are considered, isolated columns, which are arranged along the *c* axis, are obtained (Figure 4). The crystal structure can then be described with the Niggli formula $^{1}_{\infty}\left[\langle ClF_{\frac{2}{2+1}}F_{\frac{2}{1+1}}O_{\frac{2}{1}}\rangle\langle AsF_{\frac{1}{1+2}}F_{\frac{2}{1+1}}F_{\frac{3}{1}}\rangle\right]$. The homologous $[BrO_2][AsF_6]$ salt, in contrast, forms a layer structure.[45]

An analysis of the packing motif shows that a consideration of Cl···Cl distances of *circa* 4.56 to 5.49 Å leads to a distorted octahedron as the coordination polyhedron for the Cl atom. When As···As distances of approximately 4.83 to 6.77 Å are taken into account, a bicapped cube (BCCU-10) is obtained as the coordination polyhedron for the As atom.[65] For Cl···As distances of *circa* 4.00 to 5.41 Å, a distorted or severely distorted cube is obtained as a coordination polyhedron around the As or Cl atoms, respectively, with similar arrangements as the Cs and Cl atoms in the CsCl structure type.[66]

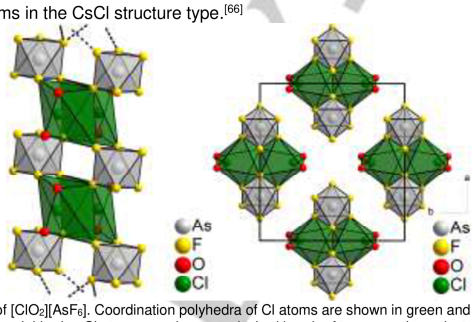

Figure 4. Sections of the crystal structure of $[ClO_2][AsF_6]$. Coordination polyhedra of Cl atoms are shown in green and those of As atoms in grey. Short contacts of F atoms belonging to the $[PF_6]^-$ anions with neighboring Cl atoms are shown as dashed bonds. Atoms are shown isotropic with arbitrary radii.

The crystal structure of $[ClO_2][IrF_6]$

Dioxychloronium(V) hexafluoridoiridate(V) crystallizes in the monoclinic space group *P*12/*n*1 (No. 13) with two formula units per unit cell, Pearson code *mP*20, and Wyckoff sequence 13.g^4fe. The compound is, as are $[ClO_2][SbF_6]$ and $[BrO_2][SbF_6]$, isotypic to $[ClO_2][RuF_6]$.[43] Selected crystallographic data and details of the structure determination are given in Table 1. Atomic coordinates, equivalent isotropic and anisotropic displacement parameters are reported in the Supporting Information. The Cl(1) atom occupies the Wyckoff position 2*f* (site symmetry 2) and is surrounded by the oxygen atoms O(1) and O(1)#1 (Figure 5). The Cl−O bond length is 1.409(3) Å and the O−Cl−O angle is 118.3(2)°. The Ir(1) atom occupies the Wyckoff position 2*e* (site symmetry 2) and is surrounded by six F atoms, giving the $[IrF_6]^-$ anion. The Ir−F bond lengths lie in the range of 1.868(2) to 1.892(2) Å and are comparable to those in $Li[IrF_6]$, which are 1.875 Å at room temperature.[67] Three of the six F atoms are terminally bound and the other three are μ-bridging to Cl atoms, which results in an elongation of the Ir−μ-F bond.

This article is protected by copyright. All rights reserved.

Accepted Manuscript

European Journal of Inorganic Chemistry 10.1002/ejic.202000908

WILEY-VCH

FULL PAPER

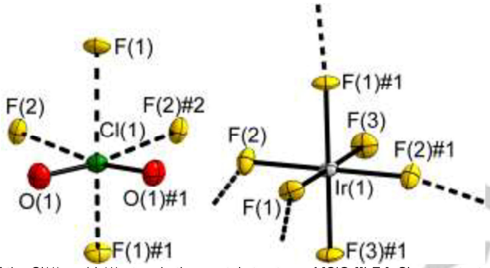

Figure 5. The coordination environment of the Cl(1) and Ir(1) atom in the crystal structure of $[ClO_2][IrF_6]$. Short contacts of F atoms belonging to the $[IrF_6]^-$ anions with neighboring Cl atoms are shown as dashed bonds. Symmetry transformations (left): #1 3/2 – *x*, *y*, 1/2 – *z*; #2 1/2 + *x*, 1 – *y*, −1/2 + *z*. Symmetry transformation (right): #1 3/2 – *x*, *y*, 3/2 – *z*. Displacement ellipsoids are shown at the 70% probability level at 100 K.

The consideration of Cl···μ-F contacts leads for the Cl atom to coordination number 2+4 with a distorted octahedral ligand arrangement. The Cl atom is again, see above, displaced from the center of the coordination polyhedron. A layer motif with layers parallel to the *ac* plane is obtained if Cl···μ-F contacts are taken into account (Figure 6). The crystal structure can be described with the Niggli formula $^{2}_{\infty}\left[\langle ClF_{\frac{4}{1+1}}O_{\frac{2}{1}}\rangle\langle IrF_{\frac{4}{1+1}}F_{\frac{2}{1}}\rangle\right]$. The Cl and Ir atoms both form a pseudo-cubic primitive lattice and are similarly arranged as the Cs and Cl atoms in the CsCl structure type, with Cl···Ir distances of *circa* 4.11 to 5.0 Å.[66]

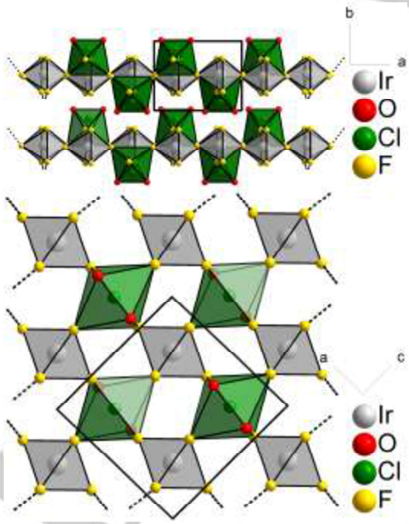

Figure 6. Crystal structure of $[ClO_2][IrF_6]$ projected along the *c* (top) or *b* (bottom) axis. Coordination polyhedra of Cl atoms are shown in green and those of Ir atoms in grey. Short contacts of F atoms belonging to the $[IrF_6]^-$ anions with neighboring Cl atoms are shown as dashed bonds. Atoms are shown as isotropic with arbitrary radii.

The crystal structure of $[ClO_2][SnF_{2/2}F_{4/1}]$

To the best of our knowledge, there are thus far no previously reported crystal structures of salts with a pentafluoridostannate(IV) anion, $[SnF_5]^-$. The latter forms one-dimensional infinite strands that can be described with the Niggli formula $^{1}_{\infty}[SnF_{2/2}F_{4/1}]^-$. In contrast the molecular hexafluoridostannate(IV) anion, $[SnF_6]^{2-}$, was structurally characterized by single-crystal X-ray diffraction in a multitude of salts, such as with alkali metal cations.[68,69] The structures of $[SnF_5]^-$ anions in the $[NF_4]^+$, $[N_2F_3]^+$, and $[N_5]^+$ salts were previously derived from vibrational and/or ^{19}F NMR spectroscopy in the solid-state or solution, respectively.[70–72] Only crystal structures with discrete $[SiF_5]^-$ anions have been reported for the homologous pentafluoridosilicate(IV) anion.[73–76] Whereas the homologous pentafluoridogermanate(IV) anion can either be discrete, as a $[GeF_5]^-$ anion in the 1,3-bis(2,6-diisopropylphenyl)imidazolium salt or a $[Ge_3F_{16}]^{4-}$ anion in $[C(NH_2)_2NH_3]_2[Ge_3F_{16}]\cdot nHF$ (n = 1, 2), or "polymerize" to form the $^{1}_{\infty}[GeF_{2/2}F_{4/1}]^-$ anion.[42,77,78] The $[GeF_6]$ polyhedra in the latter can either be trans-bridged to a linear chain as in $[XeF_5][GeF_{2/2}F_{4/1}]$ or cis-bridged to helical chains as in $[ClO_2][GeF_{2/2}F_{4/1}]$ or $O_2[GeF_5]\cdot HF$.[42,78] For the Sn system, anions with higher Sn content such as $[Sn_2F_9]^-$ and $[Sn_5F_{24}]^{4-}$ were described and they were either characterized by vibrational spectroscopy or single-crystal X-ray diffraction.[78–80] The $[Sn_2F_9]^-$ anion shows a ladder-like structure

This article is protected by copyright. All rights reserved.

Accepted Manuscript

European Journal of Inorganic Chemistry 10.1002/ejic.202000908

WILEY-VCH

FULL PAPER

motif in $O_2[Sn_2F_9]$ and a more complex layer-structure with hexa- and hepta-coordinated Sn(IV) atoms in $O_2[Sn_2F_9]\cdot 0.9HF$.[78] Similar coordination numbers are observed for the Sn(IV) atoms in $[XeF_5]_4[Sn_5F_{24}]$, in which the anion also forms a layer-motif.[80]

Dioxychloronium(V) pentafluoridostannate(V) crystallizes in the monoclinic space group $P12_1/n1$ (No. 14) with four formula units per unit cell, Pearson code *mP*36, and Wyckoff sequence 14.e^9. Selected crystallographic data and details of the structure determination are given in Table 1. Atomic coordinates, equivalent isotropic and anisotropic displacement parameters are reported in the Supporting Information. The Cl(1) atom occupies the Wyckoff position 4*e* (site symmetry 1) and is surrounded by the oxygen atoms O(1) and O(2), forming the $[ClO_2]^+$ cation (Figure 7).

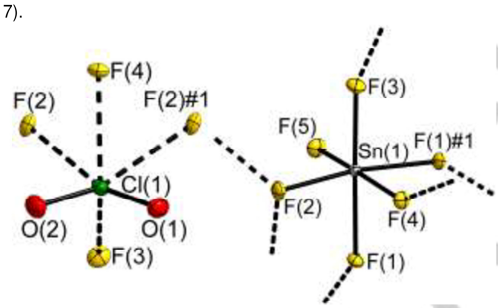

Figure 7. Cl and Sn atom environments in the crystal structure of $[ClO_2][SnF_{2/2}F_{4/1}]$. Short contacts of F atoms belonging to the $^1_\infty[SnF_{2/2}F_{4/1}]^-$ anions with neighboring Cl atoms are shown as dashed bonds. The atoms F(1) and F(1)#1 are μ-bridging between Sn atoms and their contacts are also shown as dashed bonds. Symmetry transformation (left): #1 1 − *x*, 1 − *y*, 1 − *z*. Symmetry transformation (right): #1 1/2 − *x*, 1/2 + *y*, 1/2 − *z*. Displacement ellipsoids are shown at the 70% probability level at 100 K.

The Cl−O bond lengths are 1.4045(13) and 1.4050(18) Å and the O−Cl−O angle is 117.37(10)°. The Sn(1) atom also occupies the Wyckoff position 4*e* and is surrounded by six F atoms in the shape of a distorted octahedron. The Sn−F bond lengths lie in the range of 1.9047(13) to 2.0627(13) Å. Two of the F atoms, F(1) and F(1)#1, are μ-bridging between Sn atoms, giving the $^1_\infty[SnF_{2/2}F_{4/1}]^-$ anion. The anion is a linear zig-zag chain formed by cis-bridged $[SnF_6]$ polyhedra (Figure 8). The F atoms F(2) to F(4) show short contacts with the Cl(1) atom with Cl···μ-F distances of 2.3847(14) to 2.6912(14) Å, whereas the F(2) atom is bridging to two Cl atoms and is thus μ_3-bridging. As in the previously described compounds, the Cl atom has the coordination number 2+4 and is surrounded by the ligands in a distorted octahedral manner. When the Cl···μ-F contacts are taken into account, a layer structure is obtained with layers in the (101)-plane, best described with the Niggli formula $^2_\infty\left[\langle ClF_{\frac{2}{2+1}}F_{\frac{2}{1+1}}O_{\frac{2}{1}}\rangle\langle SnF_{\frac{1}{1+2}}F_{\frac{2}{1+1}}F_{\frac{2}{2}}F_{\frac{1}{1}}\rangle\right]$.

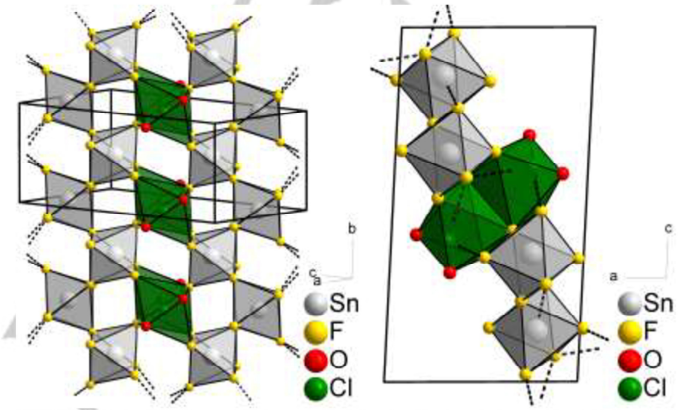

Figure 8. Crystal structure of $[ClO_2][SnF_{2/2}F_{4/1}]$, with the layer motif shown on the left and a side view of a layer on the right. Coordination polyhedra of the Cl atoms are shown in green and those of Sn atoms in grey. Short contacts of F atoms belonging to the $^1_\infty[SnF_{2/2}F_{4/1}]^-$ anions with neighboring Cl atoms and to further Sn atoms are shown as dashed bonds. Atoms are shown as isotropic with arbitrary radii.

The crystal structure of $[ClO_2][[TiF_{3/2}F_{3/1}]_2]$

Dioxychloronium(V) nonafluoridoititanate(IV) crystallizes in the monoclinic space group *C*2/*c* (No. 15) with four formula units per unit cell, Pearson code *mS*56, and Wyckoff sequence 15.f^6e^2. Selected crystallographic data and details of the structure determination are given in Table 1. Atomic coordinates, equivalent isotropic and anisotropic displacement parameters are reported in the Supporting Information. The Cl(1) atom occupies Wyckoff position 4*e* (site symmetry 2) and is surrounded by the oxygen atoms O(1) and O(2)#1,

This article is protected by copyright. All rights reserved.

Accepted Manuscript

European Journal of Inorganic Chemistry 10.1002/ejic.202000908

WILEY-VCH

FULL PAPER

giving a $[ClO_2]^+$ with a Cl−O bond length of 1.401(3) Å and an O−Cl−O angle of 118.7(2)° (Figure 9). The Ti(1) atom occupies the general position 8*f* and is surrounded by six F atoms in the shape of a distorted octahedron with Ti−F bond lengths of 1.776(2) to 1.980(2) Å.

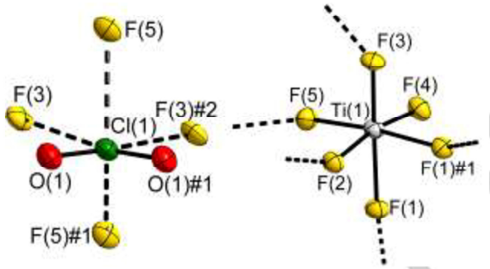

Figure 9. Cl and Ti atom environments in the crystal structure of $[ClO_2][[TiF_{3/2}F_{3/1}]_2]$. Short contacts of F atoms belonging to the $^1_\infty[[TiF_{3/1}F_{3/2}]_2]^-$ anions with neighboring Cl atoms are shown as dashed bonds (left). The atoms F(1), F(1)#1, and F(2) are μ_2-bridging between Ti atoms and these contacts are shown as dashed bonds (right). Symmetry transformations (left): #1 1 – *x*, *y*, 1/2 – *z*, #2 1 – *x*, *y*, 3/2 – *z*. Symmetry transformation (right): #1 *x*, 1 – *y*, 1/2 + *z*. Displacement ellipsoids are shown at the 70% probability level at 100 K.

Three of the F atoms, F(1), F(1)#1 and F(2), are μ-bridging between Ti atoms, resulting in the formation of the ladder-like anion running along the *c* axis with corner-sharing $[TiF_6]$ polyhedra, via "facial" F atoms (Figure 10). The anion can be described with the Niggli formula $^1_\infty[[TiF_{3/1}F_{3/2}]_2]^-$. The structural chemistry of fluoridotitanates(IV) is rich and many different structural motifs have been described.[81] The simplest discrete anion of the fluoridotitanates(IV) is the $[TiF_6]^{2-}$ anion, which has been observed in the crystal structures of salts such as $A^I_2[TiF_6]$ (A^I = Li – Cs) and $A^{II}[TiF_6]$ (A^{II} = Ag, Ca, Sr, Ba).[82–87] All other fluoridotitanate(IV) anions are derived from $[TiF_6]$ polyhedra by condensation and thus corner- or edge-sharing of such polyhedra is present. The structure motifs range from discrete anions as in $[TiF_2([15]crown\text{-}5)][Ti_4F_{18}]\cdot 0.5CH_3CN$, $[XeF_5][Ti_4F_{19}]$ and $K_4[Ti_8F_{36}]\cdot 8HF$, to one-dimensional chains or strands as in $K[TiF_5]$ and $Rb[Ti_2F_9]$, and even to a layer structure in $Cs[Ti_8F_{33}]$.[82,88–91] Compounds with similarly shaped $[Ti_2F_9]^-$ anions were described previously for the salts $A[Ti_2F_9]$ (A = Rb, Cs, H_3O, $C_3H_5N_2$).[82,92,93] The Ti−F bond lengths in $Na[Ti_2F_9]\cdot HF$ are 1.768(2)-1.974(1) Å at 200 K and in $Rb[Ti_2F_9]$ they are 1.762(2)-2.005(2) Å at 157 K.[82]

Two of the F atoms, F(3) and F(5), show short contacts to the Cl atom with Cl···μ-F distances of 2.665(2) and 2.708(2) Å. When the Cl···μ-F contacts are taken into account, the coordination number 2+4 results for the Cl atom with a distorted octahedral arrangement of the ligands. The Cl···μ-F interaction leads to a columnar structure along the *c* axis that can be described with the Niggli formula $^1_\infty\left[\langle ClF_{\frac{4}{1+1}}O_{\frac{2}{1}}\rangle\langle TiF_{\frac{2}{1+1}}F_{\frac{3}{2}}F_{\frac{1}{1}}\rangle_2\right]$ (Figure 10).

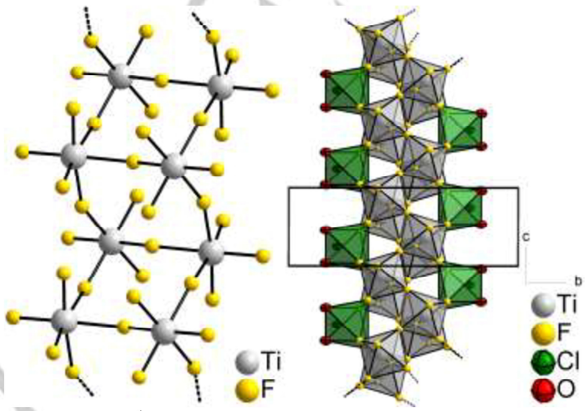

Figure 10. Crystal structure of $[ClO_2][[TiF_{3/2}F_{3/1}]_2]$. The $^1_\infty\left[\left[TiF_{\frac{3}{1}}F_{\frac{3}{2}}\right]_2\right]^-$ anion is shown on the left and the column obtained from the Cl···μ-F contacts on the right. Coordination polyhedra of Cl atoms are shown in green and those of Ti atoms in grey. Short contacts of F atoms belonging to the $^1_\infty\left[\left[TiF_{\frac{3}{1}}F_{\frac{3}{2}}\right]_2\right]^-$ anions with the neighboring Cl atoms and to further Ti atoms are shown as dashed bonds. Atoms are shown isotropic with arbitrary radii.

The crystal structure of $[ClO_2][Nb_3F_{16}]$

It is well-known that pentafluorides, MF_5 (M = e.g. As, Sb, Bi), can react with fluoride ion donors, such as AF, to give anions with higher nuclearity than $[MF_6]^-$ if appropriate ratios of AF and MF_5 are chosen for the reaction.[94] These bi- and polymetallic complex anions can

This article is protected by copyright. All rights reserved.

Accepted Manuscript

European Journal of Inorganic Chemistry 10.1002/ejic.202000908

WILEY-VCH

FULL PAPER

be described with the formula $[M_nF_{5n+1}]^-$ (n = 2, 3, 4) and can be considered as weakly coordinating anions, but not all anions are known for each pentafluoride.[94,95] For actinide pentafluorides no anions of the form $[M_nF_{5n+1}]^-$ (n = 2, 3, 4) have been reported as of yet, and these pentafluorides might differ in their reactivity and structural chemistry from main group and transition metal pentafluorides due to the higher possible coordination number for the central atom.[96] For example, in the compound $Sr[U_2F_{12}]$, the $[U_2F_{12}]^{2-}$ anion may be described as two condensed $[UF_6]^-$ anions, resulting in coordination number seven for the U atoms.[97]

The best-studied AF/MF_5 system is probably that of SbF_5, for which crystal structures of compounds containing all above-mentioned anions have been described.[94,98–100] In the crystal structures with the anions $[Sb_3F_{16}]^-$ and $[Sb_4F_{21}]^-$ almost exclusively *cis*-bridging central $[SbF_6]$ polyhedra are observed.[94,98,100] The only example of a *trans*-bridging central $[SbF_6]$ polyhedron seems to be $Br_2[Sb_3F_{16}]$.[101]

In contrast to that, the NbF_5 system is less studied and only the $[Nb_2F_{11}]^-$ anion was characterized by single-crystal diffraction.[102–104] Reports on the AF/NbF_5 system (A = Rb, Cs, Tl) exist. It was investigated by powder X-ray diffraction and differential thermal analysis and it was assumed that compounds of the composition $A[Nb_3F_{16}]$ (A = Rb, Tl) and $Cs[Nb_4F_{21}]$ form.[105]

Dioxychloronium(V) hexadecafluoridotriniobate(V) crystallizes in the monoclinic space group $C2/c$ (No. 15) with four formula units per unit cell, Pearson code $mS88$, and Wyckoff sequence $15.f^{10}e^2$. Selected crystallographic data and details of the structure determination are given in Table 1. Atomic coordinates, equivalent isotropic and anisotropic displacement parameters are reported in the Supporting Information. The Cl(1) atom occupies the Wyckoff position 4e (site symmetry 2) and is surrounded by the oxygen O(1) and O(1)#1 giving a $[ClO_2]^+$ cation with a Cl−O bond length of 1.4084(6) Å and an O−Cl−O angle of 119.06(5)°(Figure 11).

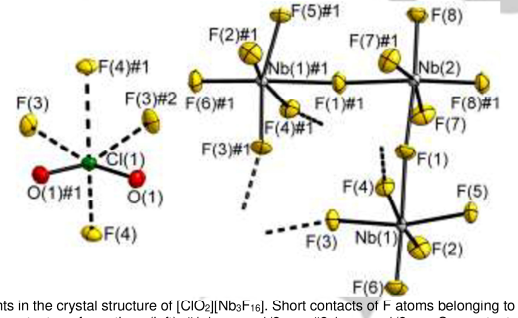

Figure 11. Cl and Nb atoms environments in the crystal structure of $[ClO_2][Nb_3F_{16}]$. Short contacts of F atoms belonging to the $[Nb_3F_{16}]^-$ anions with neighboring Cl atoms are shown as dashed bonds. Symmetry transformations (left): #1 1 − x, y, 1/2 − z; #2 1 − x, y, 1/2 − z. Symmetry transformation (right): #1 1 − x, y, 3/2 − z. Displacement ellipsoids are shown at the 70% probability level at 100 K.

The two symmetry-independent Nb atoms, Nb(1) and Nb(2), occupy the Wyckoff positions 8f and 4e (site symmetries 1 and 2), respectively. Each of the Nb atoms is surrounded by six fluorine atoms, of which F(1) and F(1)#1 are μ-bridging between Nb atoms. The resulting $[Nb_3F_{16}]^-$ anion consists of a *cis*-bridging central $[NbF_6]$ polyhedron and can be described with the Niggli formula $^0_\infty\left[\langle NbF_{\frac{1}{2}}F_{\frac{5}{1}}\rangle_2\langle NbF_{\frac{2}{2}}F_{\frac{4}{1}}\rangle\right]^-$. The Nb−F bond lengths lie in the range of 1.8183(5) to 1.9011(5) Å for terminally bound F atoms and 2.0298(5) and 2.1082(5) Å for the μ-bridging F atoms. They agree with previously reported Nb−F bond lengths for $[2,4\text{-}(OMe)_2C_6H_5][Nb_2F_{11}]$, which are 1.857(2) to 1.872(3) Å for the terminal and 2.0584(5) Å for the μ-bridging F atom at 100 K.[104] In comparison to $[Sb_3F_{16}]^-$ salts with cations such as Cs^+, $[Cl_3]^+$ $[OCNCO]^+$ or $[C_{10}Cl_{10}]^+$, in which the Sb−μ-F−Sb angles differ significantly from 180° and the $[SbF_6]$ polyhedra are tilted against each other, the Nb−μ-F−Nb angle in $[ClO_2][Nb_3F_{16}]$ is close to 180° with 175.13(3)° and the $[NbF_6]$ polyhedra are not tilted against each other.[98,106–108] This might be caused by the coordination number six of the Cl atom and the shape of the formed $[ClO_2F_4]$ polyhedron, see below.

Two of the F atoms, F(3) and F(4) atoms show short contacts to the Cl atom with Cl···μ-F distances of 2.4904(5) and 2.6554(6) Å. If these Cl···μ-F contacts are considered, the Cl atom is coordinated by 2+4 ligands in the shape of a distorted octahedron. Then, a ladder-like structure motif with interconnected $[ClO_2[Nb_3F_{16}]]$ units running along the c axis is obtained, with a $[ClO_2]^+$ cation coordinated by three $[Nb_3F_{16}]^-$ anions (Figure 12). The overall structure can then be described with the Niggli formula $^1_\infty\left[\langle ClF_{\frac{4}{1+1}}O_{\frac{2}{1}}\rangle\langle NbF_{\frac{2}{1+1}}F_{\frac{1}{2}}F_{\frac{3}{1}}\rangle_2\langle NbF_{\frac{2}{2}}F_{\frac{4}{1}}\rangle\right]$.

This article is protected by copyright. All rights reserved.

Accepted Manuscript

European Journal of Inorganic Chemistry 10.1002/ejic.202000908

WILEY-VCH

FULL PAPER

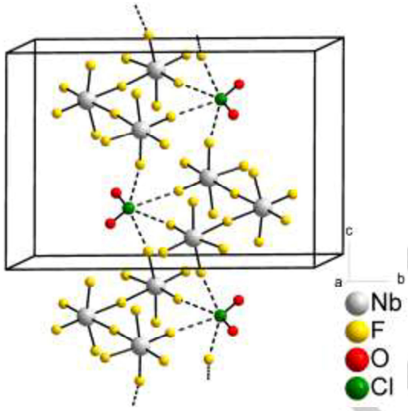

Figure 12. Section of the crystal structure of $[ClO_2][Nb_3F_{16}]$. Short contacts of F atoms belonging to the $[Nb_3F_{16}]^-$ anions with neighboring Cl atoms are shown as dashed bonds. Atoms are shown isotropic with arbitrary radii.

The crystal structure of $[ClO_2][Mo_3O_3F_{13}]$

Dioxychloronium(V) tridecafluoridotrioxidotrimolybdate(VI) crystallizes in the triclinic space group $P\bar{1}$ (No. 2) with two formula units per unit cell, Pearson code *aP*44 and Wyckoff sequence $2.i^{22}$. Selected crystallographic data and details of the structure determination are given in Table 3. Atomic coordinates, equivalent isotropic and anisotropic displacement parameters are reported in the Supporting Information. The Cl(1) atom occupies the general 2*i* position and is surrounded by the oxygen atoms O(1) and O(2), giving the $[ClO_2]^+$ cation, see Figure 13. The Cl−O bond lengths are 1.3950(18) and 1.4068(18) Å and the O−Cl−O angle is 119.65(10)°.

Three symmetry-independent Mo atoms are present, Mo(1) to Mo(3), which are each surrounded by one oxygen atom, and five fluorine atoms in the shape of a distorted octahedron. With a central *cis*-bridging $[MoOF_5]$ polyhedron, two of the F atoms, F(5) and F(9), are μ-bridging between the other two Mo atoms, resulting in the $[Mo_3O_3F_{13}]^-$ anion that can be described with the Niggli formula $^{0}_{\infty}\left[\langle MoF_{\frac{1}{2}}F_{\frac{4}{1}}O_{\frac{1}{1}}\rangle_2 \langle MoF_{\frac{2}{2}}F_{\frac{3}{1}}O_{\frac{1}{1}}\rangle\right]^-$ (Figure 13). Molybdenum oxide tetrafluoride, $MoOF_4$, can also form other anions of different nuclearity with fluoride ion donors, such as the mononuclear $[MoOF_5]^-$ and the dinuclear $[Mo_2O_2F_9]^-$ anion.[109,110]

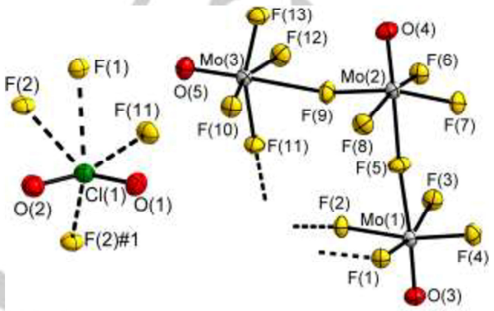

Figure 13. Cl and Mo atoms environments in the crystal structure of $[ClO_2][Mo_3O_3F_{13}]$. Short contacts of F atoms belonging to the $[Mo_3O_3F_{13}]^-$ anions with neighboring Cl atoms are shown as dashed bonds. Symmetry transformation: #1 1 − *x*, 1 − *y*, 1 − *z*. Displacement ellipsoids are shown at the 70% probability level at 100 K.

The Mo−O bond lengths lie in the range of 1.6435(17) to 1.6457(17) Å and the Mo−F bond lengths for terminally bound F atoms in the range of 1.8196(13) to 1.9288(13) Å and 2.1071(13) to 2.3161(13) Å for the μ-F atoms. They agree with the previously reported bond lengths for $[Cl_2BrO_6][Mo_3O_3F_{13}]$, which are 1.652(2)-1.662(2) Å (Mo−O), 1.819(2)-1.949(2) Å (Mo−F), and 2.102(2)-2.249(2) Å (Mo−μ-F) at 100 K.[45]

The $[Mo_3O_3F_{13}]^-$ anion can also be thought of as a $[Mo_2O_2F_9]^-$ anion that coordinates via the F(9) atom to a $MoOF_4$ unit. This becomes evident, as the Mo(3)−F(9) bond of 2.3161(13) Å is significantly longer than the Mo(1)−F(5) and Mo(2)−F(5) bonds of 2.1112(13) and 2.1071(13) Å, respectively. The latter nicely agree with the Mo−μ-F bond lengths in the alkali metal salts $A[Mo_2O_2F_9]$ (A = Li-Cs).[110]

Three of the F atoms of the anion, F(1), F(2), and F(11), show short contacts to the Cl atom with Cl···μ−F distances of 2.4617(15) to 2.9054(15) Å. In total, the Cl atom is then surrounded by six ligands in the form of a distorted octahedron. If the Cl···μ−F contacts are considered, a dimer of the form $[[ClO_2][Mo_3O_3F_{13}]]_2$ that can also be described with the Niggli formula

This article is protected by copyright. All rights reserved.

Accepted Manuscript

European Journal of Inorganic Chemistry 10.1002/ejic.202000908

WILEY-VCH

FULL PAPER

$^{0}_{\infty}\left[\left[\langle ClF_{\frac{4}{1+1}}O_{\frac{2}{1}}\rangle\langle MoF_{\frac{2}{1+1}}F_{1\frac{1}{2}}F_{2\frac{1}{1}}O_{1\frac{1}{1}}\rangle\langle MoF_{2\frac{1}{2}}F_{3\frac{1}{1}}O_{1\frac{1}{1}}\rangle\langle MoF_{\frac{1}{1+1}}F_{1\frac{1}{2}}F_{3\frac{1}{1}}O_{1\frac{1}{1}}\rangle\right]_{2}\right]$ is obtained (Figure 14). One of the dimers is surrounded by twelve further dimers in a cuboctahedron-like manner, and therefore the compound is related to the Cu structure type.[111]

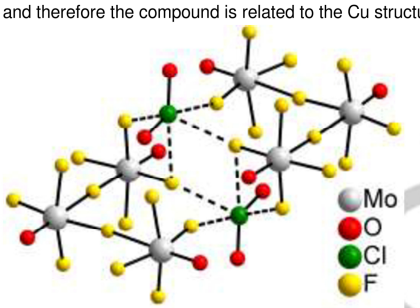

Figure 14. Dimer of $[ClO_2][Mo_3O_3F_{13}]$, which is obtained by taking the Cl···μ-F contacts into account. Atoms are shown as isotropic with arbitrary radii.

Table 3. Selected crystallographic data and details of the structure determinations of $[ClO_2][Mo_3O_3F_{13}]$ and $[ClO_2][Re_3O_6F_{10}]$.

Compound	$[ClO_2][Mo_3O_3F_{13}]$	$[ClO_2][Re_3O_6F_{10}]$
Molar mass / g·mol^{-1}	650.27	912.05
Space group (No.)	$P\bar{1}$(2)	$P\bar{1}$(2)
a / Å	7.8633(5)	8.6351(5)
b / Å	8.8097(6)	8.9888(6)
c / Å	10.1029(7)	9.0785(6)
α / °	73.285(5)	113.872(2)
β / °	84.923(5)	96.647(2)
γ / °	68.553(5)	98.259(2)
V / Å^3	623.77(8)	625.82(7)
Z	2	2
Pearson symbol	aP44	aP44
$\rho_{calc.}$ / g·cm^{-3}	3.46	4.84
μ / mm^{-1}	3.370	29.323
Color	colorless	colorless
Crystal morphology	block	block
Crystal size / mm^3	0.17×0.19×0.20	0.07×0.10×0.16
T / K	100	
λ / Å	0.71073 (Mo-K$_\alpha$)	
No. of reflections	13712	54494
θ range / °	2.11-32.58	2.43-33.47
Range of Miller indices	$-11 \le h \le 11$	$-13 \le h \le 12$
	$-13 \le k \le 13$	$-13 \le k \le 13$
	$-15 \le l \le 15$	$-13 \le l \le 13$
Absorption correction	integration	multi-scan
$Trans._{max}$, $Trans._{min}$	0.66, 0.51	0.38, 0.09
R_{int}, R_σ	0.0420, 0.0523	0.0548, 0.0371
Completeness of the data set	0.998	0.941
No. of unique reflections	4537	4604
No. of parameters	199	199
No. of restraints	0	0
No. of constraints	0	0
S (all data)	0.964	0.973
$R(F)$ ($I \ge 2\sigma(I)$, all data)	0.0245, 0.0345	0.0253, 0.0342
$wR(F^2)$ ($I \ge 2\sigma(I)$, all data)	0.0504, 0.0525	0.0500, 0.0517
Extinction coefficient	not refined	not refined
$\Delta\rho_{max}$, $\Delta\rho_{min}$ / e·Å^{-3}	0.88, −1.17	2.44, −2.77

This article is protected by copyright. All rights reserved.

Accepted Manuscript

European Journal of Inorganic Chemistry 10.1002/ejic.202000908

WILEY-VCH

FULL PAPER

The crystal structure of $[ClO_2][Re_3O_6F_{10}]$

Dioxychloronium(V) decafluoridohexaoxidotrirhenate(VII) crystallizes with two formula units per unit cell in the triclinic space group $P\bar{1}$ (No. 2), Pearson code *aP*44 and Wyckoff sequence $2.i^{2}$. Selected crystallographic data and details of the structure determination are given in Table 3. Atomic coordinates, equivalent isotropic and anisotropic displacement parameters are reported in the Supporting Information. The Cl(1) atom occupies the general 2*i* position and is surrounded by the oxygen atoms O(1) and O(2), giving the $[ClO_2]^+$ cation, see Figure 15. The Cl−O bond lengths are 1.384(4) and 1.418(4) Å and the O−Cl−O angle is 118.9(2)°.

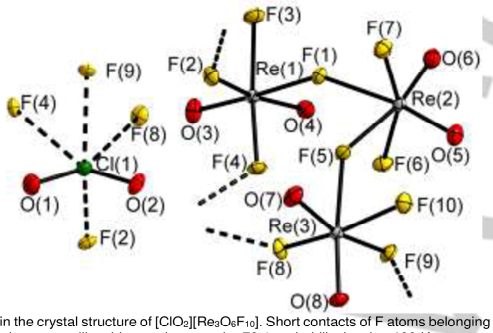

Figure 15. Cl and Re atoms environments in the crystal structure of $[ClO_2][Re_3O_6F_{10}]$. Short contacts of F atoms belonging to the $[Re_3O_6F_{10}]^-$ anions with neighboring Cl atoms are shown as dashed bonds. Displacement ellipsoids are shown at the 70% probability level at 100 K.

There are three symmetry-independent Re atoms present, Re(1) to Re(3), which are each surrounded by four F and two O atoms. Two of the F atoms are μ-bridging between Re atoms, resulting in the $[Re_3O_6F_{10}]^-$ anion. This anion contains a central *cis*-bridging $[ReO_2F_4]$ polyhedron and can also be described with the Niggli formula ${}^{0}_{\infty}\left[\langle ReF_{\frac{1}{2}}F_{\frac{3}{1}}O_{\frac{2}{1}}\rangle_2 \langle ReF_{\frac{2}{2}}F_{\frac{2}{1}}O_{\frac{2}{1}}\rangle\right]^-$. The Re−O bond lengths lie in the range of 1.652(3) to 1.692(3) Å, and the Re−F bond lengths range from 1.858(3) to 1.935(3) Å for the terminal and from 2.051(3) to 2.179(3) Å for the bridging F atoms. They agree with the reported bond lengths for $Cs[Re_3O_6F_{10}]$ which are 1.669(8) to 1.715(8) for Re−O, 1.848(6) to 1.936(7) for Re−F, and 2.039(6) to 2.213(6) Å for Re−μ-F, at 155 K.[112]
Four of the F atoms, F(2), F(4), F(8) and F(9), show short contacts to the Cl atom with Cl···μ−F distances of 2.354(3) to 2.749(3) Å. The resulting coordination number for the Cl atom is 2+4 and its coordination sphere is distorted octahedral. Overall, a column-like structure motif running along the *a* axis is obtained considering these Cl···μ−F interactions. The crystal structure can be described with the Niggli formula ${}^{1}_{\infty}\left[\langle ClF_{\frac{4}{1+1}}O_{\frac{2}{1}}\rangle \langle ReF_{\frac{2}{1+1}}F_{\frac{1}{2}}F_{\frac{1}{1}}O_{\frac{2}{1}}\rangle_2 \langle ReF_{\frac{2}{2}}F_{\frac{2}{1}}O_{\frac{2}{1}}\rangle\right]$ (Figure 16).

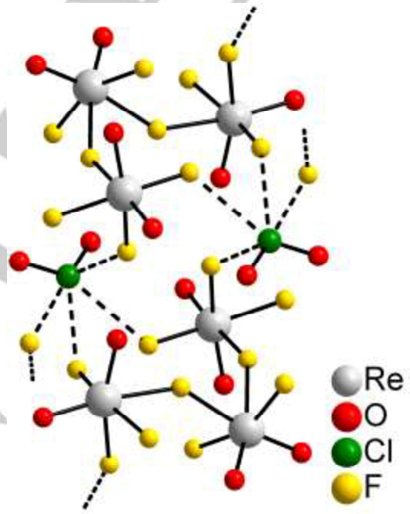

Figure 16. Section of the crystal structure of $[ClO_2][Re_3O_6F_{10}]$. Short contacts of F atoms belonging to the $[Re_3O_6F_{10}]^-$ anions with neighboring Cl atoms are shown as dashed bonds. Atoms are shown isotropic with arbitrary radii.

This article is protected by copyright. All rights reserved.

Accepted Manuscript

European Journal of Inorganic Chemistry 10.1002/ejic.202000908

WILEY-VCH

FULL PAPER

Quantum-chemical calculations

Quantum-chemical solid-state calculations were carried out for the investigated $[ClO_2]^+$ salts with CRYSTAL17 (DFT-PBE0/TZVP level of theory).[113,114] The optimized structures are reported in the Supporting Information and a comparison of experimental and calculated bond lengths, atomic distances, and angles are given in Tables 2 and 4 to 6. The calculated Cl−O bond lengths are ~1.44 Å and similar among the investigated compounds, being approximately 1.6 to 2.6% larger than the experimentally determined ones. The quantum-chemically calculated Cl···μ-F distances are generally shorter and the interaction of the Cl atom with the F atoms seems to be overestimated by the employed level of theory.

To get a qualitative picture of the bonding in these compounds, the atomic charges and overlap populations between atoms were examined by Mulliken population analyses. Average atomic charges are reported in Table 6 and the average overlap populations in Table 7. The atomic charges of the Cl atoms show only minor differences among the compounds. The lowest charge with +1.09 on the Cl atom is calculated for $[ClO_2][Mo_3O_3F_{13}]$ and the highest with +1.20 for $[ClO_2][Nb_3F_{16}]$. The most negatively charged F atoms are the bridging ones, whereas those bridging to the Cl atoms are more negatively charged than those bridging between *M* atoms. The average overlap populations indicate covalent Cl−O bonds and ionic Cl···μ-F interactions, which can be expected as the respective distances are quite large. Overall, the impact on the bonding within the $[ClO_2]^+$ cations by the fluoridometallate or oxidofluoridometallate anions is minor.

Table 4. Experimental and calculated O−Cl−O angles in $[ClO_2]^+$ salts.

Compound	∠O−Cl−O / °	calculated ∠O−Cl−O (DFT-PBE0/TZVP, solid-state) / °
$[ClO_2][PF_6]$	119.75(5)	117.7
$[ClO_2][AsF_6]$	119.57(11)	116.7
$[ClO_2][IrF_6]$	118.3(2)	116.6
$[ClO_2][SnF_{2/2}F_{4/1}]$	117.37(10)	115.3
$[ClO_2][[TiF_{3/2}F_{3/1}]_2]$	118.7(2)	116.1
$[ClO_2][Nb_3F_{16}]$	119.06(5)	116.5
$[ClO_2][Mo_3O_3F_{13}]$	119.65(10)	117.1
$[ClO_2][Re_3O_6F_{10}]$	118.9(2)	116.5

Table 5. Experimental and calculated *M*−O and *M*−F bond lengths (*M*: central atom of the anion) of fluoridometallate and oxidofluoridometallate anions in $[ClO_2]^+$ salts.

Compound	bond length / Å			calculated bond length (DFT-PBE0/TZVP, solid-state) / Å		
	M−O	*M*−F (non-bridging)	*M*−F (bridging)	*M*−O	*M*−F (non-bridging)	*M*−F (bridging)
$[ClO_2][PF_6]$	-	1.5881(6)	1.5993(7)-1.6197(6)	-	1.61	1.62-1.65
$[ClO_2][AsF_6]$	-	1.7034(14), 1.7231(9)	1.7208(9), 1.7418(13)	-	1.71	1.73-1.76
$[ClO_2][IrF_6]$	-	1.868(2)	1.873(2), 1.892(2)	-	1.85	1.88, 1.93
$[ClO_2][SnF_{2/2}F_{4/1}]$	-	1.9047(13)	1.9321(13)-1.9336(12), 2.0458(12)[a], 2.0627(13)[a]	-	1.91	1.95-1.96, 2.06[a], 2.08[a]
$[ClO_2][[TiF_{3/2}F_{3/1}]_2]$	-	1.776(2)	1.778(2), 1.787(2), 1.968(1)-1.980(2)[a]	-	1.78	1.79, 1.80, 1.98-1.99[a]
$[ClO_2][Nb_3F_{16}]$	-	1.8183(5)-1.8675(5)	1.8743(5), 1.9011(5), 2.0298(5)[a], 2.1082(5)[a]	-	1.84-1.87	1.90, 1.94, 2.06[a], 2.12[a]
$[ClO_2][Mo_3O_3F_{13}]$	1.6435(17)-1.6457(17)	1.8196(14)-1.8454(13)	1.8699(14)-1.8957(13), 1.9288(13)-2.3161(13)[a]	1.65-1.66	1.84-1.87	1.89-1.93, 1.94-2.33[a]
$[ClO_2][Re_3O_6F_{10}]$	1.652(3)-1.692(3)	1.858(3)-1.875(3)	1.859(3)-1.935(3), 2.051(3)-2.179(3)[a]	1.67-1.68	1.86-1.87	1.88-2.03, 2.12-2.18[a]

a: μ-bridging between *M* atoms.

Table 6. Average atomic charges from Mulliken population analyses of the optimized solid-state structures of $[ClO_2]^+$ salts.

Compound	average atomic charge / *e*					
	M[a]	Cl	O ($[ClO_2]^+$)	O (Anion)	F (non-bridging)	F (bridging)
$[ClO_2][PF_6]$	1.78	1.15	−0.17	-	−0.41	−0.44
$[ClO_2][AsF_6]$	1.62	1.15	−0.16	-	−0.36	−0.42
$[ClO_2][IrF_6]$	1.70	1.15	−0.22	-	−0.38	−0.42
$[ClO_2][SnF_{2/2}F_{4/1}]$	1.82	1.17	−0.23	-	−0.49	−0.52, −0.49[b]
$[ClO_2][[TiF_{3/2}F_{3/1}]_2]$	1.94	1.18	−0.18	-	−0.49	−0.51, −0.54[b]
$[ClO_2][Nb_3F_{16}]$	2.40	1.20	−0.21	-	−0.47	−0.53, −0.61[b]
$[ClO_2][Mo_3O_3F_{13}]$	2.02	1.09	−0.17	−0.38	−0.40	−0.46, −0.52[b]
$[ClO_2][Re_3O_6F_{10}]$	2.09	1.19	−0.22	−0.50	−0.36	−0.42, −0.44[b]

This article is protected by copyright. All rights reserved.

Accepted Manuscript

European Journal of Inorganic Chemistry 10.1002/ejic.202000908

WILEY-VCH

FULL PAPER

a: Central atom of the anion.
b: μ-bridging between *M* atoms.

Table 7. Average overlap population between two atoms from Mulliken population analyses of the optimized solid-state structures of $[ClO_2]^+$ salts.

Compound	average overlap population / *e*				
	Cl−O	Cl···μ-F	M^a−O	M^a −F (non-bridging)	M^a−F (bridging)
$[ClO_2][PF_6]$	0.17	0.01	-	0.25	0.22
$[ClO_2][AsF_6]$	0.17	0.01	-	0.29	0.26
$[ClO_2][IrF_6]$	0.17	0.01	-	0.13	0.11
$[ClO_2][SnF_{2/2}F_{4/1}]$	0.18	0.01	-	0.22	0.18, 0.12[b]
$[ClO_2][[TiF_{3/2}F_{3/1}]_2]$	0.18	0.01	-	0.11	0.11, 0.07[b]
$[ClO_2][Nb_3F_{16}]$	0.18	0	-	0.10	0.08, 0.04[b]
$[ClO_2][Mo_3O_3F_{13}]$	0.27	0.01	0.24	0.15	0.14, 0.09[b]
$[ClO_2][Re_3O_6F_{10}]$	0.19	0	0.19	0.13	0.12, 0.07[b]

a: Central atom of the anion.
b: μ-bridging between *M* atoms.

Raman spectra of $[ClO_2]^+$ compounds

The $[ClO_2]^+$ compounds presented here were furthermore investigated by Raman spectroscopy. An exemplary Raman spectrum of $[ClO_2][AsF_6]$ is shown in Figure 17 and low- and high-resolution Raman spectra of the other salts are reported in the Supporting Information. The Raman spectra were furthermore calculated by quantum-chemical calculations, which are based on the optimized structures. Band assignments for the calculated spectra are given in the Supporting Information.

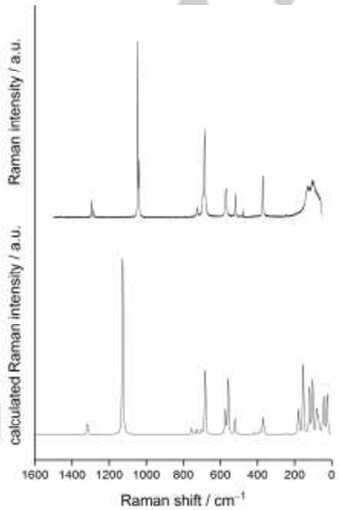

Figure 17. High-resolution (top) and calculated Raman spectrum (bottom) of $[ClO_2][AsF_6]$ with intensities given in arbitrary units.

In previous reports on the vibrational spectra of $[ClO_2]^+$ compounds, the symmetry of the $[ClO_2]^+$ cations was assumed to be C_{2v}, resulting in the three possible modes $\nu_3(B_1)$ ($\nu_{as}(ClO_2)$), $\nu_1(A_1)$ ($\nu_s(ClO_2)$) and $\nu_2(A_1)$ ($\delta_{sciss}(ClO_2)$) for the cation.[8] The characteristic and usually most pronounced features in the Raman spectra of the investigated compounds are the bands assigned to the Cl−O stretching modes, $\nu_{as}(ClO_2)$ and $\nu_s(ClO_2)$, which are located at 1283 to 1312 and at 1040 to 1078 cm^{-1}, respectively. The two naturally occurring Cl isotopes ^{35}Cl and ^{37}Cl lead to a splitting of the Cl−O bands, with differences of 13 to 15 cm^{-1} for $\nu_{as}(ClO_2)$ and of 5 to 6 cm^{-1} for $\nu_s(ClO_2)$.[55] The intensities of the bands of $\nu_s(ClO_2)$ is in all cases higher than those of $\nu_{as}(ClO_2)$. The third possible mode is the scissoring of $[ClO_2]^+$, $\delta_{sciss}(ClO_2)$, which can be observed in the range of 513 to 527 cm^{-1}. The experimental and calculated vibrational frequencies are listed in Table 8. Similar vibrational frequencies were reported for $[ClO_2]^+$ in compounds such as $[ClO_2][GeF_5]$, $[ClO_2][MF_6]$ (M = Ru, Pt, Au, Sb), $[ClO_2][ClO_4]$, $[ClO_2][Cd(ClO_4)_3]$, $[ClO_2][Au(ClO_4)_4]$ and $[ClO_2][M(ClO_4)_4]$ (M = In, Tl).[34,37,40,42,43,115–118] This indicates a minor effect of the anions and bridging atoms (O or F) on the vibrational frequencies of the $[ClO_2]^+$ cation.

This article is protected by copyright. All rights reserved.

Accepted Manuscript

European Journal of Inorganic Chemistry 10.1002/ejic.202000908

WILEY-VCH

FULL PAPER

Table 8. Comparison of experimental and calculated vibrational frequencies assigned to the $[ClO_2]^+$ cation in compounds with fluoridometallate or oxidofluoridometallate anions.

Compound	$\nu_{as}(ClO_2)$ / cm^{-1}	$\nu_s(ClO_2)$ / cm^{-1}	$\delta_{sciss}(ClO_2)$ / cm^{-1}	Reference
$[ClO_2][AsF_6]$	1296, 1283	1046, 1040	519	this work
	1317	1127	521	calculated
	1296	1044, 1039	521	[55]
	1296, 1281	1045	518	[119]
$[ClO_2][IrF_6]$	1290	1061, 1056	518	this work
	1319	1125	521	calculated
	1300, 1286	1057	518	[115]
$[ClO_2][SnF_{2/2}F_{4/1}]$	1303, 1289	1076, 1071	525, 515	this work
	1310, 1306	1136, 1135	532, 530, 520	calculated
$[ClO_2][[TiF_{3/2}F_{3/1}]_2]$	1293, 1280	1049, 1044	517	this work
	1310	1124	516	calculated
$[ClO_2][Nb_3F_{16}]$	1304, 1291	1060, 1054	519	this work
	1320	1135	524	calculated
$[ClO_2][Mo_3O_3F_{13}]$	1309, 1294	1061, 1056	513	this work
	1329	1140	523, 513	calculated
$[ClO_2][Re_3O_6F_{10}]$	1312, 1298	1078, 1072	527	this work
	1316	1135	528	calculated

The Raman spectra of the $[MF_6]^-$ anions in $[ClO_2][MF_6]$ (M = As, Ir) are similar to those of respective Li^+ salts, albeit with more bands due to lower symmetry of the $[MF_6]^-$ anion.[120,121] In the Raman spectrum of $[ClO_2][SnF_{2/1}F_{4/1}]$, an additional band of a $[ClF_2]^+$ cation at 783 cm^{-1} is present, likely due to an impurity of $[ClF_2][SnF_5]$.[122] The Raman spectrum is otherwise similar to the reported one of $[ClO_2]_2[SnF_6]$, which itself has too many bands for a $[SnF_6]^{2-}$ salt.[123] They are both similar to those reported for $[NF_4][SnF_5]$ and $[N_2F_3][SnF_5]$.[70,71] The bands assigned to the $[Ti_2F_9]^-$ anion in the Raman spectrum of $[ClO_2][[TiF_{3/2}F_{3/1}]_2]$ are similar to those of $A[Ti_2F_9]$ (A = Cs, NF_4).[92,124] The Raman spectrum of $[ClO_2][Nb_3F_{16}]$ is more complex than that of $Li[NbF_6]$, but similar to that of $[XeF][Nb_2F_{11}]$, with comparable vibrational frequencies for the $\nu(NbF_6)$ bands.[120,125] The Raman spectrum of $[ClO_2][Mo_3O_3F_{13}]$ is more complex for the anionic part than the reported ones for $A[MoOF_5]$ (A = Cs, Xe_2F_{11}) or $A[Mo_2O_2F_9]$ (A = Li – Cs), which is to be expected.[109,110,126] The Raman spectrum of $[ClO_2][Re_3O_6F_{10}]$ is similar to that of $Cs[Re_3O_6F_{10}]$.[112]

General remarks on the crystal structures of $[ClO_2]^+$ compounds

The $[ClO_2]^+$ cation is bent in the crystal structures of all herein described salts as well as in the previously reported ones. Its structure is in line with the VSEPR model for an AX_2E species.[127] The Cl–O bond lengths of the investigated salts range from 1.384(4) to 1.418(4) Å (Table 2) and are comparable to the Cl–O bond length of 1.418(2) Å determined from the microwave spectrum of gaseous ClO_2F. [128–130] They are much shorter than in solid ClO_2 (1.471(1) and 1.476(1) Å at 123 K).[131] The observed O–Cl–O angles range from 117.37(10) to 119.65(10)°, which is to be expected from the VSEPR model, which predicts an angle below 120° for such a species. In our quantum-chemical calculations, we also obtain angles below 120°. However, in $[ClO_2][Au(ClO_4)_4]$ and $[ClO_2][Sb_2F_{11}]$, the O–Cl–O angles were reported with 132(3) and 121.9(15)°, respectively, likely due to the quality of the structure determinations.[37,44]

The Cl atom of the $[ClO_2]^+$ cation is always surrounded by additional bridging ligands, either F atoms in fluoridometallate or oxidofluoridometallate salts or O atoms in perchlorate-containing compounds.[37–40] The coordination number of the Cl atom in the investigated compounds is usually 2+4, with a distorted octahedral arrangement of the ligands, see Table 9. The only exceptions are $[ClO_2][PF_6]$, in which the coordination number is 2+6 with a distorted square-antiprismatic ligand arrangement, and the previously reported $[ClO_2][GeF_{2/2}F_{4/1}]$ in which Cl atoms with both coordination number 2+4 and 2+6 are present.[42] A range of structural motifs is observed for the $[ClO_2]^+$ salts when the Cl···μ–F interactions are considered. These span from molecular, over column- and ladder-like ones, to layer-like and framework structures and are summarized in Table 9.

Table 9. Overview of coordination numbers (C. N.) of the Cl atoms and structure motifs in $[ClO_2]^+$ fluoridometallates and oxidofluoridometallates.

Compound	C. N. of Cl	Structure motif	Niggli formula
$[ClO_2][Mo_3O_3F_{13}]$	2+4	molecular structure (dimeric)	${}^{0}_{\infty}\left[\left[\langle ClF_{\frac{4}{1+1}}\,O_{\frac{2}{1}}\rangle\langle MoF_{\frac{2}{1+1}}\,F_{\frac{1}{2}}F_{\frac{2}{1}}O_{\frac{1}{1}}\rangle\langle MoF_{\frac{2}{2}}F_{\frac{3}{1}}O_{\frac{1}{1}}\rangle\langle MoF_{\frac{1}{1+1}}\,F_{\frac{1}{2}}F_{\frac{3}{1}}O_{\frac{1}{1}}\rangle\right]_2\right]$
$[ClO_2][AsF_6]$	2+4	columnar structure	${}^{1}_{\infty}\left[\langle ClF_{\frac{2}{2+1}}\,F_{\frac{2}{1+1}}\,O_{\frac{2}{1}}\rangle\langle AsF_{\frac{1}{1+2}}\,F_{\frac{2}{1+1}}\,F_{\frac{3}{1}}\rangle\right]$
$[ClO_2][[TiF_{3/2}F_{3/1}]_2]$	2+4	columnar structure	${}^{1}_{\infty}\left[\langle ClF^{-}_{\frac{4}{1+1}}\,O_{\frac{2}{1}}\rangle\langle TiF^{-}_{\frac{2}{1+1}}\,F_{\frac{3}{2}}F_{\frac{1}{1}}\rangle_2\right]$
$[ClO_2][Re_3O_6F_{10}]$	2+4	columnar structure	${}^{1}_{\infty}\left[\langle ClF_{\frac{4}{1+1}}\,O_{\frac{2}{1}}\rangle\langle ReF_{\frac{2}{1+1}}\,F_{\frac{1}{2}}F_{\frac{1}{1}}O_{\frac{2}{1}}\rangle_2\langle ReF_{\frac{2}{2}}F_{\frac{2}{1}}O_{\frac{2}{1}}\rangle\right]$

This article is protected by copyright. All rights reserved.

Accepted Manuscript

European Journal of Inorganic Chemistry 10.1002/ejic.202000908

WILEY-VCH

FULL PAPER

$[ClO_2][Nb_3F_{16}]$	2+4	ladder-like structure	$^{1}_{\infty}\left[\langle ClF_{\frac{4}{1+1}}O_{\frac{2}{1}}\rangle\langle NbF_{\frac{2}{1+1}}F_{\frac{1}{2}}F_{\frac{3}{1}}\rangle_2\langle NbF_{\frac{2}{2}}F_{\frac{4}{1}}\rangle\right]$
$[ClO_2][MF_6]$, M = Ru[43], Ir, Sb[34]	2+4	layer structure	$^{2}_{\infty}\left[\langle ClF_{\frac{4}{1+1}}O_{\frac{2}{1}}\rangle\langle IrF_{\frac{4}{1+1}}F_{\frac{2}{1}}\rangle\right]$
$[ClO_2][SnF_{2/2}F_{4/1}]$	2+4	layer structure	$^{2}_{\infty}\left[\langle ClF_{\frac{2}{2+1}}F_{\frac{2}{1+1}}O_{\frac{2}{1}}\rangle\langle SnF_{\frac{1}{1+2}}F_{\frac{2}{1+1}}F_{\frac{2}{2}}F_{\frac{1}{1}}\rangle\right]$
$[ClO_2][PF_6]$	2+6	framework structure	$^{3}_{\infty}\left[\langle ClF_{\frac{2}{2+1}}F_{\frac{4}{1+1}}O_{\frac{2}{1}}\rangle\langle PF_{\frac{1}{1+2}}F_{\frac{4}{1+1}}F_{\frac{1}{1}}\rangle\right]$
$[ClO_2][BF_4]$[41]	2+4	framework structure	$^{3}_{\infty}\left[\langle ClF_{\frac{4}{1+1}}O_{\frac{2}{1}}\rangle\langle BF_{\frac{4}{1+1}}\rangle\right]$
$[ClO_2][GeF_5]$[41,42]	2+4 & 2+6	framework structure	$^{3}_{\infty}\left[\langle ClF_{\frac{4}{2+1}}O_{\frac{2}{1}}\rangle\langle ClF_{\frac{4}{2+1}}F_{\frac{2}{1+1}}O_{\frac{2}{1}}\rangle\langle GeF_{\frac{2}{1+2}}F_{\frac{1}{1+1}}F_{\frac{2}{2}}F_{\frac{1}{1}}\rangle_2\right]$
$[ClO_2][Sb_2F_{11}]$[44]	2+4	framework structure	$^{3}_{\infty}\left[\langle ClF_{\frac{4}{1+1}}O_{\frac{2}{1}}\rangle\langle SbF_{\frac{2}{1+1}}F_{\frac{1}{2}}F_{\frac{3}{1}}\rangle_2\right]$

Conclusion

The reactions of the main group and transition metal oxides TiO_2, MoO_3, Re_2O_7, SnO, P_2O_5, and As_2O_5 with ClF_3 led to the formation of $[ClO_2]^+$ compounds with fluoridometallate ($[[Ti_{3/2}F_{3/1}]_2]^-$, $[SnF_{2/2}F_{4/1}]^-$, $[PF_6]^-$, $[AsF_6]^-$) or oxidofluoridometallate ($[Mo_3O_3F_{13}]^-$, $[Re_3O_6F_{10}]^-$) anions. The reaction of ClF_3 with oxygen-containing Nb powder, as well as the hydrolysis reaction of $[ClF_2][IrF_6]$, led to the formation of $[ClO_2][Nb_3F_{16}]$ and $[ClO_2][IrF_6]$, respectively. Bent $[ClO_2]^+$ cations, with Cl−O bond lengths from 1.384(4) to 1.418(4) Å, are present in the crystal structures of these compounds. The Raman bands of the $[ClO_2]^+$ cations are observed in the range from 1283 to 1312 ($\nu_{as}(ClO_2)$) and from 1040 to 1078 cm^{-1} ($\nu_s(ClO_2)$). The O−Cl−O angles are below 120° in all compounds with 117.37(10) to 119.65(10)°, which is in line with predictions based on the VSEPR model and quantum-chemical calculations. The Cl atom shows furthermore short Cl···μ-F contacts to F atoms from the neighboring anions, resulting in coordination numbers of 2+4 or 2+6 ($[ClO_2][PF_6]$) and distorted octahedral or distorted square-antiprismatic arrangements of the ligands. The structure motifs of the $[ClO_2]^+$ compounds differ a lot and seem to be dictated by the nature of the anion. Quantum-chemical calculations indicate that these Cl···μ-F interactions are weak and ionic. The $[ClO_2]^+$ cation seems to enable the isolation of rather unusual salts with mono-, bi- and polynuclear anions.

Experimental Section

General: Volatile materials were handled in a Monel metal Schlenk line, which was passivated with undiluted fluorine and/or chlorine trifluoride at various pressures before use. Moisture-sensitive compounds were stored and handled in an Ar-filled glove box (MBraun). Reaction vessels were made out of fluoropolymer (PFA) and closed by stainless steel valves (SS316 or 316L, Swagelok). All vessels were passivated with fluorine before use. Preparations were carried out in an atmosphere of dry and purified argon (5.0, Praxair). Chlorine trifluoride was stored over NaF to remove traces of HF. Hydrogen fluoride was stored over $K_2[NiF_6]$ to remove traces of moisture. **Caution!** *Fluorine, chlorine trifluoride, and dioxychloronium(V) compounds must be handled using appropriate protective gear with ready access to proper emergency treatment procedures in the event of contact. They are potent oxidizing agents that are only stable under the rigorously anhydrous conditions employed in the experimental procedures outlined in this section. They react vigorously to explosively upon hydrolysis or contact with organic materials. The utmost precautions must be taken when disposing of these materials and their derivatives.*

Syntheses - General: A PFA reaction vessel was loaded with the starting material and attached to a stainless-steel valve. The valve was then connected to the Monel metal Schlenk line, the reaction vessel was evacuated and an excess of ClF_3 was condensed onto the solid at 77 K. The reaction vessel was then placed in a stainless-steel Dewar vessel and allowed to warm to room temperature over a period of a few hours. The reaction vessel was then stored at room temperature for the time specified below. All volatiles were then pumped off and the product was isolated in a glove box.
$[ClO_2][AsF_6]$, $[ClO_2][SnF_5]$, $[ClO_2][Ti_2F_9]$, $[ClO_2][Nb_3F_{16}]$, $[ClO_2][Mo_3O_3F_{13}]$: $[ClO_2][AsF_6]$: 14 mg As_2O_5 (0.061 mmol) was reacted with 0.17 g of ClF_3 (1.8 mmol). The reaction vessel was stored at room temperature for two weeks. (25.5 mg isolated) $[ClO_2][SnF_5]$: 23.6 mg SnO (0.18 mmol) was reacted with 0.49 g of ClF_3 (5.3 mmol). After that, 0.5 mL of anhydrous HF were condensed on to the reaction mixture at 77 K. The reaction vessel was stored at room temperature for a few hours. Both $[ClO_2][SnF_5]$ and a $[ClF_2]^+$-containing compound were present in the product. $[ClO_2][Ti_2F_9]$: 20.0 mg TiO_2 (0.25 mmol) was reacted with 0.15 g of ClF_3 (1.6 mmol). The reaction vessel was stored at room temperature for four days (40.1 mg isolated). $[ClO_2][Nb_3F_{16}]$: 10.6 mg Nb powder (0.11 mmol) was reacted with 0.20 g of ClF_3 (2.2 mmol). The reaction vessel was stored at room temperature for one day. Both crystals of $[ClF_2][NbF_6]$ and $[ClO_2][Nb_3F_{16}]$ were present in the product. $[ClO_2][Mo_3O_3F_{13}]$: Method 1: 18.0 mg MoO_3 (0.13 mmol) was reacted with 0.13 g ClF_3 (1.4 mmol). The reaction vessel was stored at room temperature for 19 days (10.7 mg isolated). Method 2: 22.19 mg $MoOF_4$ (0.12 mmol) was reacted with 0.08 g of ClF_3 (0.9 mmol). The reaction vessel was stored at room temperature for eight days (16.0 mg isolated).
Low-temperature syntheses of $[ClO_2][PF_6]$ and $[ClO_2][Re_3O_6F_{13}]$: $[ClO_2][PF_6]$: 10.5 mg P_2O_5 (0.074 mmol) was reacted with 0.12 g of ClF_3 (1.3 mmol). The reaction vessel was then stored at −37 °C and colorless crystals grew at the top of the reaction vessel after a few hours at this temperature. The reaction vessel was then opened to the atmosphere at *circa* −40 °C to isolate some of the crystals for single-crystal X-ray diffraction. They were quickly transferred into cold (*circa* −40 °C) Galden HT270 (perfluoropolyether, Solvay) and handled under a stream of cold nitrogen. Crystals of $[ClO_2][PF_6]$

This article is protected by copyright. All rights reserved.

Accepted Manuscript

European Journal of Inorganic Chemistry 10.1002/ejic.202000908

WILEY-VCH

FULL PAPER

rapidly deteriorated at room temperature and contact to the atmosphere. $[ClO_2][Re_3O_6F_{13}]$: 19.7 mg Re_2O_7 (0.04 mmol) was reacted with 0.10 g of ClF_3 (1.1 mmol). The reaction vessel was then stored at −37 °C and colorless crystals grew from the yellowish solution after a few hours at this temperature. The reaction vessel was then opened to the atmosphere at < 0 °C to isolate some of the crystals for single-crystal X-ray diffraction. The crystals were handled under cold perfluorinated oil and a stream of cold nitrogen. Crystals of $[ClO_2][Re_3O_6F_{13}]$ rapidly deteriorated at room temperature and contact to the atmosphere.

Hydrolysis of $[ClF_2][IrF_6]$: $[ClO_2][IrF_6]$ was obtained as a hydrolysis product of $[ClF_2][IrF_6]$. 21.9 mg Ir powder (0.11 mmol) was reacted with 0.19 g of ClF_3 (2.1 mmol). The reaction vessel was then stored at −37 °C and yellow crystals grew from the red solution at that temperature after one hour. The reaction vessel was then opened to the atmosphere at < 0 °C to isolate some of the crystals for single-crystal X-ray diffraction. The crystals turned out to be of the compound $[ClF_2][IrF_6]$.[57,59] After that, the reaction vessel was closed again and stored at room temperature for ten days, after which yellow crystals of $[ClO_2][IrF_6]$ grew from the solution.

Single-crystal X-ray diffraction: Crystals of the moisture-sensitive compounds were selected under dried perfluoropolyether (Fomblin YR1800, Solvay, stored over molecular sieve 3 Å) and mounted on a MiTeGen loop. Crystals of $[ClO_2][PF_6]$ and $[ClO_2][Re_3O_6F_{10}]$ were selected in the absence of air under dried, cooled perfluoropolyether (Galden HT270, Solvay, stored over molecular sieves 3 Å) and mounted on a MiTeGen loop. Intensity data of suitable crystals were recorded with a D8 Quest diffractometer (Bruker), an IPDS2, or an IPDS2T diffractometer (STOE). The diffractometers were operated with monochromatized Mo-K_α radiation (0.71073 Å), multi-layered optics (D8 Quest), or a graphite monochromator (IPDS2 and IPDS2T) and equipped with a PHOTON 100 CMOS detector (D8 Quest) or an image plate detector (IPDS2 and IPDS2T). Evaluation, integration, and reduction of the diffraction data was carried out with the APEX3 software suite (D8 Quest) or the X-Area software suite (IPDS2 and IPDS2T).[132,133] The diffraction data were corrected for absorption utilizing the multi-scan method of SADABS or TWINABS within the APEX3 software suite (D8 Quest) or the integration method with the modules X-Shape and X-Red32 of the X-Area software suite (IPDS2 and IPDS2T). The structures were solved with dual-space methods (SHELXT) and refined against F^2 (SHELXL).[134,135] Systematic absence violations were observed for the space groups of the compounds $[ClO_2][PF_6]$ and $[ClO_2][Nb_3F_{16}]$. However, the very weak intensities of the corresponding reflections were very close to the tripled standard uncertainties. The solution and refinement of the structures in crystallographic subgroups resulted in significant correlations between atomic coordinates and non-positive definite displacement parameters for some atoms. The crystal structures were consequently solved and refined in the space groups reported here, which were also indicated by the Addsym feature of the program package PLATON when checking for additional symmetry within the subgroups.[136,137] The crystals of $[ClO_2][IrF_6]$, $[ClO_2][Ti_2F_9]$ and $[ClO_2][Re_3O_6F_{10}]$ used for the diffraction experiment were non-merohedral twins (two twin components in $[ClO_2][IrF_6]$, $[ClO_2][Ti_2F_9]$ and $[ClO_2][Re_3O_6F_{10}]$, respectively). The lattice parameters and twin laws of $[ClO_2][IrF_6]$ and $[ClO_2][Re_3O_6F_{10}]$ were determined with the program CELL_NOW.[138] In the case of $[ClO_2][Ti_2F_9]$, the twin components were determined manually in the X-Area software. In all cases, only the non-overlapping reflections of the major twin component were used for the structure solution. The data were initially refined with all reflections with the HKLF5 format option in SHELXL (overlapping reflections and non-overlapping reflections of all twin components). The data were then processed with the HKLF5Tools program: the non-overlapping reflections of the weaker diffracting twin component were removed, the non-overlapping reflections of the major twin component were merged in point groups $2/m$ ($[ClO_2][IrF_6]$ and $[ClO_2][Ti_2F_9]$) or $\bar{1}$ ($[ClO_2][Re_3O_6F_{10}]$ and the overlapping reflections were merged in point group 1.[139] The final refinements were carried out against the detwinned dataset (created by SHELXL with the LIST 8 option as an FCF file and converted to an HKL file with HKLF5Tools).The locations of highest residual electron densities after the final refinement were the following: $[ClO_2][PF_6]$: 0.38 Å from atom O(2), $[ClO_2][AsF_6]$: 0.76 Å from atom F(1), $[ClO_2][IrF_6]$: 0.63 Å from atom Ir(1), $[ClO_2][SnF_5]$: 0.79 Å from atom Cl(1), $[ClO_2][Ti_2F_9]$: 1.25 Å from atom F(2), $[ClO_2][Nb_3F_{16}]$: 0.57 Å from atom Cl(1), $[ClO_2][Mo_3O_3F_{13}]$: 0.70 Å from atom O(5) and $[ClO_2][Re_3O_6F_{10}]$: 0.70 Å from atom Re(1). Representations of the crystal structures were created with the Diamond software.[140] CCDC 2034213-2034220 contain the supplementary crystallographic data for this paper. These data are provided free of charge by The Cambridge Crystallographic Data Centre.

Raman spectroscopy: The Raman spectra were measured with a Monovista CRS+ confocal Raman microscope (Spectroscopy & Imaging GmbH) using a 532 nm solid-state laser and either a 300 grooves/mm (low-resolution mode, FWHM: <4.62 cm^{-1}) or a 1800 grooves/mm (high-resolution mode, FWHM: <0.368 cm^{-1}) grating. Samples were either transferred into dried glass vessels or immersed in perfluorinated oil (Fomblin YR1800, Solvay, stored over molecular sieve 3 Å) on a microscope slide.

Solid-state quantum-chemical calculations: Periodic quantum-chemical calculations were carried out with the PBE0 hybrid density functional method (DFT-PBE0).[113,114] Triple-zeta-valence + polarization (TZVP) level basis sets were applied for all atoms. Details of the basis sets that were employed are given in the Supporting Information. All calculations were carried out with the CRYSTAL17 program package.[141] The reciprocal space was sampled with the following Monkhorst-Pack-type *k*-point grids: $[ClO_2][PF_6]$: 4×2×2, $[ClO_2][AsF_6]$: 2×2×5, $[ClO_2][IrF_6]$: 3×4×3, $[ClO_2][SnF_5]$: 4×4×4, $[ClO_2][Ti_2F_9]$: 2×2×5, $[ClO_2][Nb_3F_{16}]$: 3×3×3, $[ClO_2][Mo_3O_3F_{13}]$: 3×3×3, $[ClO_2][Re_3O_6F_{10}]$: 3×3×3. For the evaluation of the Coulomb and exchange integrals (TOLINTEG), tight tolerance factors of 8, 8, 8, 8, 16 were used for all calculations. Both the atomic positions and lattice parameters were fully optimized within the constraints imposed by the space group symmetry. Default DFT integration grids and optimization convergence thresholds were applied in all calculations. Mulliken population analyses were carried out for all compounds. A ferromagnetic ground state was employed for $[ClO_2][IrF_6]$ and the resulting magnetic moment was 2.0 μB for the $[IrF_6]^-$ anion (1.4 μB contribution from Ir). The harmonic vibrational frequencies and Raman intensities were obtained through usage of the computational scheme implemented in CRYSTAL17.[142–144,144] The Raman intensities were calculated for a polycrystalline powder sample (total isotropic intensity in arbitrary units). The Raman spectra were obtained by using a pseudo-Voigt band profile (50:50 Lorentzian:Gaussian) and an FWHM of 8 cm^{-1}. The Raman spectra were simulated taking the experimental setup (T = 293.15 K, λ = 532 nm) into account. The band assignments were carried out by visual inspection of the normal modes with the Jmol program package.[145]

Acknowledgments

We thank the Deutsche Forschungsgemeinschaft (DFG) for generous funding and Dr. Sergei Ivlev (Marburg) for helpful discussions.

Keywords: Chlorine • Dioxychloronium(V) cation • Fluorine • Chlorine trifluoride • Single-crystal X-ray diffraction

[1] T. D. Cooper, F. N. Dost, C. H. Wang, *J. Inorg. Nucl. Chem.* **1972**, *34*, 3564–3567.
[2] L. Andrews, F. K. Chi, A. Arkell, *J. Am. Chem. Soc.* **1974**, *96*, 1997–2000.
[3] H. S. P. Müller, *Chem. Phys. Lett.* **1999**, *314*, 396–402.

This article is protected by copyright. All rights reserved.

Accepted Manuscript

European Journal of Inorganic Chemistry 10.1002/ejic.202000908

WILEY-VCH

FULL PAPER

[4] H. S. P. Müller, E. A. Cohen, *J. Chem. Phys.* **2002**, *116*, 2407–2416.
[5] H. Schmitz, H. J. Schumacher, *Z. Anorg. Allg. Chem.* **1942**, *249*, 238–244.
[6] H. Bode, E. Klesper, *Z. Anorg. Allg. Chem.* **1951**, *266*, 275–280.
[7] M. Schmeisser, K. Brändle, in *Advances in Inorganic Chemistry and Radiochemistry*, Elsevier, **1963**, pp. 41–89.
[8] K. O. Christe, C. J. Schack, in *Advances in Inorganic Chemistry and Radiochemistry*, Elsevier, **1976**, pp. 319–398.
[9] R. Bougon, J. Isabey, P. Plurien, *C. R. Seances Acad. Sci., Ser. C* **1970**, *271*, 1366–1369.
[10] D. Pilipovich, C. B. Lindahl, C. J. Schack, R. D. Wilson, K. O. Christe, *Inorg. Chem.* **1972**, *11*, 2189–2192.
[11] D. Pilipovich, R. D. Wilson, *Synthesis of Oxychlorine Trifluoride (North American Rockwell Corporation)*, **1972**, US-3,697,394.
[12] A. Engelbrecht, H. Atzwanger, *Monatsh. Chem.* **1952**, *83*, 1087–1089.
[13] K. O. Christe, *Inorg. Nucl. Chem. Lett.* **1972**, *8*, 457–459.
[14] K. O. Christe, R. D. Wilson, *Inorg. Chem.* **1973**, *12*, 1356–1357.
[15] G. H. Rohrback, G. H. Cady, *J. Am. Chem. Soc.* **1947**, *69*, 677–678.
[16] J. E. Sicre, H. J. Schumacher, *Z. Anorg. Allg. Chem.* **1956**, *286*, 232–236.
[17] D. F. Smith, G. M. Begun, W. H. Fletcher, *Spectrochim. Acta* **1964**, *20*, 1763–1770.
[18] K. O. Christe, R. D. Wilson, C. J. Schack, *Inorg. Nucl. Chem. Lett.* **1975**, *11*, 161–163.
[19] A. A. Woolf, *J. Chem. Soc.* **1954**, 4113–4116.
[20] A. J. Arvia, W. H. Basualdo, H. J. Schumacher, *Angew. Chem.* **1955**, *67*, 616–616.
[21] A. J. Arvia, W. H. Basualdo, H. J. Schumacher, *Z. Anorg. Allg. Chem.* **1956**, *286*, 58–80.
[22] H. Bode, E. Klesper, *Angew. Chem.* **1954**, *66*, 605–605.
[23] A. Engelbrecht, *Angew. Chem.* **1954**, *66*, 442–442.
[24] R. Bougon, M. Carles, J. Aubert, *C. R. Seances Acad. Sci., Ser. C* **1967**, *265*, 179–182.
[25] K. O. Christe, *Inorg. Chem.* **1972**, *11*, 1220–1222.
[26] M. Schmeisser, F. L. Ebenhöch, *Angew. Chem.* **1954**, *66*, 230–231.
[27] M. Schmeisser, E. Pammer, *Angew. Chem.* **1955**, *67*, 156–156.
[28] E. Jacob, *Angew. Chem. Int. Ed. Engl.* **1976**, *15*, 158–158.
[29] R. J. Gillespie, P. H. Spekkens, *J. Chem. Soc., Dalton Trans.* **1977**, 1539–1546.
[30] P. H. Spekkens, Oxyfluoro Compounds of Bromine, Dissertation, McMaster University (Canada), **1977**.
[31] R. J. Gillespie, P. H. Spekkens, *Isr. J. Chem.* **1978**, *17*, 11–19.
[32] M. Schmeisser, K. Lang, *Angew. Chem.* **1955**, *67*, 156–156.
[33] J. J. Krasznai, Oxo and Oxyfluoro Complexes of Iodine (V) and (VII), Dissertation, McMaster University (Canada), **1975**.
[34] J. F. Lehmann, S. Riedel, G. J. Schrobilgen, *Inorg. Chem.* **2008**, *47*, 8343–8356.
[35] J.-L. Pascal, J. Potier, C. S. Zhang, *J. Chem. Soc., Dalton Trans.* **1985**, 297.
[36] J.-L. Pascal, F. Favier, *Coord. Chem. Rev.* **1998**, *178–180*, 865–902.
[37] F. Cunin, C. Deudon, F. Favier, B. Mula, J. L. Pascal, *Inorg. Chem.* **2002**, *41*, 4173–4178.
[38] M. Fourati, M. Chaabouni, C. H. E. Belin, J. L. Pascal, J. Potier, *New J. Chem.* **1990**, *14*, 695–700.
[39] K. M. Tobias, M. Jansen, *Angew. Chem. Int. Ed. Engl.* **1986**, *25*, 993–994.
[40] K. M. Tobias, M. Jansen, *Z. Anorg. Allg. Chem.* **1987**, *550*, 16–26.
[41] T. E. Mallouk, G. L. Rosenthal, G. Mueller, R. Brusasco, N. Bartlett, *Inorg. Chem.* **1984**, *23*, 3167–3173.
[42] T. E. Mallouk, B. Desbat, N. Bartlett, *Inorg. Chem.* **1984**, *23*, 3160–3166.
[43] R. Bougon, W. V. Cicha, M. Lance, L. Meublat, M. Nierlich, J. Vigner, *Inorg. Chem.* **1991**, *30*, 102–109.
[44] A. J. Edwards, R. J. C. Sills, *J. Chem. Soc., Dalton Trans.* **1974**, 1726–1729.
[45] K. Seppelt, *Angew. Chem. Int. Ed.* **2019**, *58*, 18928–18930.
[46] K. S. Thanthiriwatte, M. Vasiliu, D. A. Dixon, K. O. Christe, *Inorg. Chem.* **2012**, *51*, 10966–10982.
[47] K. O. Christe, E. C. Curtis, *Inorg. Chem.* **1972**, *11*, 35–39.
[48] R. J. Gillespie, P. Spekkens, *J. Chem. Soc., Dalton Trans.* **1976**, 2391–2396.
[49] L. Helmholz, M. T. Rogers, *J. Am. Chem. Soc.* **1940**, *62*, 1537–1542.
[50] M. Gerken, J. P. Mack, G. J. Schrobilgen, R. J. Suontamo, *J. Fluorine Chem.* **2004**, *125*, 1663–1670.
[51] J.-P. Laval, N. Jennene Boukharrata, *Acta Crystallogr., Sect. C: Cryst. Struct. Commun.* **2008**, *64*, i47–i49.
[52] Q. Wu, H. Liu, F. Jiang, L. Kang, L. Yang, Z. Lin, Z. Hu, X. Chen, X. Meng, J. Qin, *Chem. Mater.* **2016**, *28*, 1413–1418.
[53] D. K. Huggins, W. B. Fox, *Inorg. Nucl. Chem. Lett.* **1970**, *6*, 337–339.
[54] R. F. Weinland, O. Lauenstein, *Z. Anorg. Chem.* **1899**, *20*, 30–39.
[55] K. O. Christe, C. J. Schack, D. Pilipovich, W. Sawodny, *Inorg. Chem.* **1969**, *8*, 2489–2494.
[56] J. D. Clark, *Ignition! An Informal History of Liquid Rocket Propellants*, Rutgers University Press, New Brunswick, New Jersey, **1972**.
[57] B. Scheibe, R. Haiges, S. I. Ivlev, A. J. Karttunen, U. Müller, K. O. Christe, F. Kraus, *Eur. J. Inorg. Chem.* **2020**, DOI 10.1002/ejic.202000845.
[58] J. Supeł, Ternäre Halogenverbindungen des Rheniums und Technetiums in der Oxidationsstufe +7, Freie Universität Berlin, **2007**.
[59] R. Haiges, in *Efficient Preparations of Fluorine Compounds* (Ed.: H.W. Roesky), John Wiley & Sons, Inc., Hoboken, NJ, USA, **2012**, pp. 100–107.
[60] S. I. Ivlev, A. J. Karttunen, M. R. Buchner, M. Conrad, F. Kraus, *Angew. Chem. Int. Ed.* **2018**, *57*, 14640–14644.
[61] M. Gerken, M. D. Moran, H. P. A. Mercier, B. E. Pointner, G. J. Schrobilgen, B. Hoge, K. O. Christe, J. A. Boatz, *J. Am. Chem. Soc.* **2009**, *131*, 13474–13489.
[62] C. Röhr, R. Knicp, *Z. Naturforsch., B: J. Chem. Sci.* **1994**, *49*, 650–654.
[63] W. B. Jensen, in *Cohesion and Structure* (Eds.: J. Hafner, F. Hulliger, W.B. Jensen, J.A. Majewski, K. Mathis, P. Villars, P. Vogl), North-Holland, **1989**, pp. 105–146.
[64] G. Aminoff, *Z. Kristallogr. - Cryst. Mater.* **1923**, *58*, 203–219.
[65] A. Ruiz-Martínez, S. Alvarez, *Chem. Eur. J.* **2009**, *15*, 7470–7480.
[66] W. P. Davey, *Phys. Rev.* **1923**, *21*, 143–161.
[67] H. Fitz, B. G. Müller, O. Graudejus, N. Bartlett, *Z. Anorg. Allg. Chem.* **2002**, *628*, 133–137.
[68] Ch. Hebecker, H. G. von Schnering, R. Hoppe, *Naturwissenschaften* **1966**, *53*, 154–154.
[69] Mm. J. Durand, J. L. Galigne, A. Lari-Lavassani, *J. Solid State Chem.* **1976**, *16*, 157–160.

This article is protected by copyright. All rights reserved.

Accepted Manuscript

European Journal of Inorganic Chemistry 10.1002/ejic.202000908

WILEY-VCH

FULL PAPER

[70] K. O. Christe, C. J. Schack, R. D. Wilson, *Inorg. Chem.* **1977**, *16*, 849–854.
[71] K. O. Christe, C. J. Schack, *Inorg. Chem.* **1978**, *17*, 2749–2754.
[72] W. W. Wilson, A. Vij, V. Vij, E. Bernhardt, K. O. Christe, *Chem. Eur. J.* **2003**, *9*, 2840–2844.
[73] D. Schomburg, R. Krebs, *Inorg. Chem.* **1984**, *23*, 1378–1381.
[74] F. Olbrich, R. J. Lagow, *Z. Anorg. Allg. Chem.* **1995**, *621*, 1929–1932.
[75] C. Bolli, J. Gellhaar, C. Jenne, M. Keßler, H. Scherer, H. Seeger, R. Uzun, *Dalton Trans.* **2014**, *43*, 4326–4334.
[76] B. Alič, M. Tramšek, A. Kokalj, G. Tavčar, *Inorg. Chem.* **2017**, *56*, 10070–10077.
[77] Y. Morgenstern, F. Zischka, A. Kornath, *Chem. Eur. J.* **2018**, *24*, 17311–17317.
[78] Z. Mazej, E. Goreshnik, *Inorg. Chem.* **2020**, *59*, 2092–2103.
[79] K. O. Christe, D. A. Dixon, D. J. Grant, R. Haiges, F. S. Tham, A. Vij, V. Vij, T.-H. Wang, W. W. Wilson, *Inorg. Chem.* **2010**, *49*, 6823–6833.
[80] Z. Mazej, E. Goreshnik, *Eur. J. Inorg. Chem.* **2019**, 1265–1272.
[81] R. L. Davidovich, D. V. Marinin, V. Stavila, K. H. Whitmire, *Coord. Chem. Rev.* **2015**, *299*, 61–82.
[82] I. M. Shlyapnikov, E. A. Goreshnik, Z. Mazej, *Inorg. Chem.* **2018**, *57*, 1976–1987.
[83] G. F. Schäfer, *Z. Kristallogr. - Cryst. Mater.* **1986**, *175*, 269–276.
[84] S. Siegel, *Acta Cryst.* **1952**, *5*, 683–684.
[85] D. Yu. Popov, V. Ya. Kavun, A. V. Gerasimenko, V. I. Sergienko, T. F. Antokhina, *Russ. J. Coord. Chem.* **2002**, *28*, 19–24.
[86] R. Fischer, B. G. Müller, *Z. Anorg. Allg. Chem.* **2001**, *627*, 445–452.
[87] J. Ravez, M. Vassiliadis, R. Von der Mühll, P. Hagenmüller, *Rev. Chim. Miner.* **1970**, 967–973.
[88] A. Decken, H. D. B. Jenkins, C. Knapp, G. B. Nikiforov, J. Passmore, J. M. Rautiainen, *Angew. Chem. Int. Ed.* **2005**, *44*, 7958–7961.
[89] Z. Mazej, E. Goreshnik, *Eur. J. Inorg. Chem.* **2009**, *2009*, 4503–4506.
[90] I. M. Shlyapnikov, E. A. Goreshnik, Z. Mazej, *Chem. Commun.* **2013**, *49*, 2703–2705.
[91] H. Bialowons, *Z. Anorg. Allg. Chem.* **1995**, *621*, 1223–1226.
[92] Z. Mazej, E. Goreshnik, *Inorg. Chem.* **2009**, *48*, 6918–6923.
[93] I. M. Shlyapnikov, H. P. A. Mercier, E. A. Goreshnik, G. J. Schrobilgen, Z. Mazej, *Inorg. Chem.* **2013**, *52*, 8315–8326.
[94] Z. Mazej, R. Hagiwara, *J. Fluorine Chem.* **2007**, *128*, 423–437.
[95] T. A. Engesser, M. R. Lichtenthaler, M. Schleep, I. Krossing, *Chem. Soc. Rev.* **2016**, *45*, 789–899.
[96] L. R. Morss, N. M. Edelstein, J. Fuger, J. J. Katz, Eds. , *The Chemistry of the Actinide and Transactinide Elements*, Springer, Dordrecht, **2006**.
[97] B. Scheibe, C. Pietzonka, O. Mustonen, M. Karppinen, A. J. Karttunen, M. Atanasov, F. Neese, M. Conrad, F. Kraus, *Angew. Chem.* **2018**, *130*, 2964–2968.
[98] P. Benkič, H. D. Brooke Jenkins, M. Ponikvar, Z. Mazej, *Eur. J. Inorg. Chem.* **2006**, *2006*, 1084–1092.
[99] E. Goreshnik, Z. Mazej, *J. Fluorine Chem.* **2020**, *236*, 109587.
[100] T. Drews, K. Seppelt, *Angew. Chem. Int. Ed.* **1997**, *36*, 273–274.
[101] A. J. Edwards, G. R. Jones, *J. Chem. Soc., A* **1971**, 2318.
[102] A. J. Edwards, G. R. Jones, *J. Chem. Soc. A* **1970**, 1491–1497.
[103] A. J. Edwards, P. Taylor, *J. Chem. Soc., Dalton Trans.* **1973**, 2150–2153.
[104] F. Marchetti, G. Pampaloni, C. Pinzino, S. Zacchini, *Eur. J. Inorg. Chem.* **2013**, *2013*, 5755–5761.
[105] D. Bizot, *J. Fluorine Chem.* **1978**, *11*, 497–507.
[106] T. Drews, W. Koch, K. Seppelt, *J. Am. Chem. Soc.* **1999**, *121*, 4379–4384.
[107] I. Bernhardi, T. Drews, K. Seppelt, *Angew. Chem. Int. Ed.* **1999**, *38*, 2232–2233.
[108] S. M. Rupf, P. Pröhm, M. Malischewski, *Chem. Commun.* **2020**, DOI 10.1039.D0CC04226A.
[109] M. R. Bortolus, H. P. A. Mercier, G. J. Schrobilgen, *Chem. Eur. J.* **2020**, *26*, 8935–8950.
[110] R. E. Stene, B. Scheibe, A. J. Karttunen, W. Petry, F. Kraus, *Eur. J. Inorg. Chem.* **2019**, *2019*, 3672–3682.
[111] W. L. Bragg, *Philos. Mag. (1798-1977)* **1914**, *28*, 355–360.
[112] W. J. Casteel, D. A. Dixon, N. LeBlond, P. E. Lock, H. P. A. Mercier, G. J. Schrobilgen, *Inorg. Chem.* **1999**, *38*, 2340–2358.
[113] J. P. Perdew, K. Burke, M. Ernzerhof, *Phys. Rev. Lett.* **1996**, *77*, 3865–3868.
[114] C. Adamo, V. Barone, *J. Chem. Phys.* **1999**, *110*, 6158–6170.
[115] K. O. Christe, *Inorg. Chem.* **1973**, *12*, 1580–1587.
[116] Sh. Sh. Nabiev, *Russ. Chem. Bull.* **1999**, *48*, 711–717.
[117] M. Fourati, M. Chaabouni, J.-L. Pascal, J. Potier, *Can. J. Chem.* **1987**, *65*, 2783–2790.
[118] M. Fourati, M. Chaabouni, H. F. Ayedi, J.-L. Pascal, J. Potier, *Can. J. Chem.* **1985**, *63*, 3499–3504.
[119] H. A. Carter, W. M. Johnson, F. Aubke, *Can. J. Chem.* **1969**, *47*, 4619–4625.
[120] G. Tavčar, B. Žemva, *Inorg. Chem.* **2013**, *52*, 4319–4323.
[121] O. Graudejus, A. P. Wilkinson, L. C. Chacón, N. Bartlett, *Inorg. Chem.* **2000**, *39*, 2794–2800.
[122] A. I. Popov, A. V. Scharabarin, V. F. Sukhoverkhov, N. A. Tchumaevsky, *Z. Anorg. Allg. Chem.* **1989**, *576*, 242–254.
[123] H. A. Carter, A. M. Qureshi, J. R. Sams, F. Aubke, *Can. J. Chem.* **1970**, *48*, 2853–2859.
[124] K. O. Christe, C. J. Schack, *Inorg. Chem.* **1977**, *16*, 353–359.
[125] B. Landa, Laser Raman Spectroscopic Investigations of Some Fluoroxenon Compounds, Dissertation, McMaster University (Canada), **1974**.
[126] A. Beuter, W. Sawodny, *Z. Anorg. Allg. Chem.* **1976**, *427*, 37–44.
[127] R. J. Gillespie, R. S. Nyholm, *Q. Rev., Chem. Soc.* **1957**, *11*, 339–380.
[128] C. R. Parent, M. C. L. Gerry, *J. Mol. Spectrosc.* **1974**, *49*, 343–364.
[129] A. G. Robiette, C. R. Parent, M. C. L. Gerry, *J. Mol. Spectrosc.* **1981**, *86*, 455–464.
[130] H. S. P. Müller, *J. Mol. Struct.* **2000**, *517–518*, 335–350.
[131] A. Rehr, M. Jansen, *Inorg. Chem.* **1992**, *31*, 4740–4742.
[132] *APEX3*, Bruker AXS Inc., Madison, Wisconsin, USA, **2018**.
[133] *X-Area*, STOE & Cie GmbH, Darmstadt, Germany, **2018**.
[134] G. M. Sheldrick, *Acta Crystallogr., Sect. A: Found. Adv.* **2015**, *71*, 3–8.
[135] G. M. Sheldrick, *Acta Crystallogr., Sect. C: Struct. Chem.* **2015**, *71*, 3–8.

This article is protected by copyright. All rights reserved.

Accepted Manuscript

European Journal of Inorganic Chemistry 10.1002/ejic.202000908

[136]A. L. Spek, *PLATON - A Multipurpose Crystallographic Tool*, Utrecht University, Utrecht, The Netherlands, **2019**.
[137]A. L. Spek, *Acta Crystallogr., Sect. D: Biol. Crystallogr.* **2009**, *65*, 148–155.
[138]G. M. Sheldrick, *CELL_NOW*, Göttingen (Germany), **2008**.
[139]S. I. Ivlev, M. Conrad, F. Kraus, *Z. Kristallogr. - Cryst. Mater.* **2019**, *234*, 415–418.
[140]K. Brandenburg, H. Putz, *Diamond - Crystal and Molecular Structure Visualization*, Crystal Impact GbR, Bonn, **2019**.
[141]R. Dovesi, A. Erba, R. Orlando, C. M. Zicovich-Wilson, B. Civalleri, L. Maschio, M. Rérat, S. Casassa, J. Baima, S. Salustro, B. Kirtman, *Wiley Interdiscip. Rev.: Comput. Mol. Sci.* **2018**, e1360.
[142]C. M. Zicovich-Wilson, F. Pascale, C. Roetti, V. R. Saunders, R. Orlando, R. Dovesi, *J. Comput. Chem.* **2004**, *25*, 1873–1881.
[143]F. Pascale, C. M. Zicovich-Wilson, F. López Gejo, B. Civalleri, R. Orlando, R. Dovesi, *J. Comput. Chem.* **2004**, *25*, 888–897.
[144]L. Maschio, B. Kirtman, M. Rérat, R. Orlando, R. Dovesi, *J. Chem. Phys.* **2013**, *139*, 164101.
[145]*Jmol: An Open-Source Java Viewer for Chemical Structures in 3D. Http://Www.Jmol.Org/*, Jmol Team, **2019**.

WILEY-VCH

Accepted Manuscript

This article is protected by copyright. All rights reserved.

Supporting Information

Content

Selected crystallographic data of $[ClO_2]^+$ compounds 3
Atomic coordinates and displacement parameters of $[ClO_2][PF_6]$ 3
Atomic coordinates and displacement parameters of $[ClO_2][AsF_6]$ 3
Atomic coordinates and displacement parameters of $[ClO_2][IrF_6]$ 4
Atomic coordinates and displacement parameters of $[ClO_2][SnF_5]$ 4
Atomic coordinates and displacement parameters of $[ClO_2][Ti_2F_9]$ 5
Atomic coordinates and displacement parameters of $[ClO_2][Nb_3F_{16}]$ 5
Atomic coordinates and displacement parameters of $[ClO_2][Mo_3O_3F_{13}]$ 6
Atomic coordinates and displacement parameters of $[ClO_2][Re_3O_6F_{10}]$ 7
Basis set details for quantum-chemical solid-state calculations 8
TZVP basis set for O 8
TZVP basis set for F 8
TZVP basis set for Cl 8
TZVP basis set for P 8
TZVP basis set for Ti 8
TZVP basis set for Sn 8
TZVP basis set for Mo 9
TZVP basis set for Re 9
TZVP basis set for As 9
TZVP basis set for Nb[9] 10
TZVP basis set for Ir[9] 12
Lattice parameters and atomic coordinates of optimized solid-state structures 13
Lattice parameters and atomic coordinates of the optimized solid-state structure of $[ClO_2][PF_6]$ 13
Lattice parameters and atomic coordinates of the optimized solid-state structure of $[ClO_2][AsF_6]$ 13
Lattice parameters and atomic coordinates of the optimized solid-state structure of $[ClO_2][IrF_6]$ 13
Lattice parameters and atomic coordinates of the optimized solid-state structure of $[ClO_2][SnF_5]$ 14
Lattice parameters and atomic coordinates of the optimized solid-state structure of $[ClO_2][Ti_2F_9]$ 14
Lattice parameters and atomic coordinates of the optimized solid-state structure of $[ClO_2][Nb_3F_{16}]$ 14
Lattice parameters and atomic coordinates of the optimized solid-state structure of $[ClO_2][Mo_3O_3F_{13}]$ 15
Lattice parameters and atomic coordinates of the optimized solid-state structure of $[ClO_2][Re_3O_6F_{10}]$ 16
Low-resolution Raman spectra 17
Raman spectrum of $[ClO_2][AsF_6]$ 17
Raman spectrum of $[ClO_2][IrF_6]$ 17
Raman spectrum of $[ClO_2][SnF_5]$ 18
Raman spectrum of $[ClO_2][Ti_2F_9]$ 18
Raman spectrum of $[ClO_2][Nb_3F_{16}]$ 19
Raman spectrum of $[ClO_2][Mo_3O_3F_{13}]$ 19
Raman spectrum of $[ClO_2][Re_3O_6F_{10}]$ 20
Comparison of calculated Raman spectra and high-resolution Raman spectra and band assignments for the calculated Raman spectra 21

Raman spectra and band assignment of $[ClO_2][AsF_6]$ 21
Raman spectra and band assignment of $[ClO_2][IrF_6]$ 22
Raman spectra and band assignment of $[ClO_2][SnF_5]$ 23
Raman spectra and band assignment of $[ClO_2][Ti_2F_9]$ 24
Raman spectra and band assignment of $[ClO_2][Nb_3F_{16}]$ 25
Raman spectra and band assignment of $[ClO_2][Mo_3O_3F_{13}]$ 26
Raman spectra and band assignment of $[ClO_2][Re_3O_6F_{10}]$ 27
References 28

Selected crystallographic data of $[ClO_2]^+$ compounds

Atomic coordinates and displacement parameters of $[ClO_2][PF_6]$

Table S1. Atomic coordinates and equivalent isotropic displacement parameters U_{iso} of $[ClO_2][PF_6]$ at 100 K.

Atom	Position	*x*	*y*	*z*	U_{iso} / Å^2
Cl(1)	4*a*	0.31253(4)	0.70671(2)	0.77191(2)	0.01194(4)
P(1)	4*a*	0.61838(4)	0.47969(2)	0.50033(3)	0.00994(5)
O(1)	4*a*	0.52119(14)	0.77682(8)	0.71870(8)	0.01571(13)
O(2)	4*a*	0.07165(14)	0.71161(8)	0.70988(8)	0.01698(13)
F(1)	4*a*	0.41193(13)	0.50840(7)	0.61524(7)	0.01677(12)
F(2)	4*a*	0.72120(13)	0.62663(6)	0.51137(7)	0.01659(12)
F(3)	4*a*	0.41187(14)	0.52252(6)	0.39254(7)	0.01713(12)
F(4)	4*a*	0.51227(12)	0.32985(6)	0.49204(7)	0.01490(11)
F(5)	4*a*	0.82111(13)	0.43229(6)	0.60960(6)	0.01592(11)
F(6)	4*a*	0.82232(14)	0.44815(6)	0.38729(6)	0.01764(12)

Table S2. Anisotropic displacement parameters of $[ClO_2][PF_6]$ at 100 K.

Atom	U_{11} / Å^2	U_{22} / Å^2	U_{33} / Å^2	U_{23} / Å^2	U_{13} / Å^2	U_{12} / Å^2
Cl(1)	0.01193(8)	0.01264(7)	0.01124(8)	0.00091(7)	0.00001(7)	0.00064(7)
P(1)	0.01120(9)	0.00944(8)	0.00919(9)	−0.00071(7)	0.00037(8)	−0.00010(6)
O(1)	0.0140(3)	0.0155(3)	0.0176(3)	−0.0011(3)	0.0030(3)	−0.0018(2)
O(2)	0.0132(3)	0.0201(3)	0.0176(3)	0.0015(3)	−0.0027(2)	−0.0005(3)
F(1)	0.0169(3)	0.0176(3)	0.0157(3)	−0.0038(2)	0.0061(2)	−0.0005(2)
F(2)	0.0222(3)	0.0108(2)	0.0168(3)	−0.0001(2)	−0.0002(2)	−0.00443(19)
F(3)	0.0185(3)	0.0163(3)	0.0166(3)	0.0011(2)	−0.0062(2)	0.0019(2)
F(4)	0.0190(3)	0.0102(2)	0.0155(3)	−0.0011(2)	−0.0010(2)	−0.00289(18)
F(5)	0.0155(3)	0.0176(2)	0.0147(3)	0.0029(2)	−0.0042(2)	−0.0004(2)
F(6)	0.0184(3)	0.0202(3)	0.0143(3)	−0.0013(2)	0.0066(3)	0.0011(3)

Atomic coordinates and displacement parameters of $[ClO_2][AsF_6]$

Table S3. Atomic coordinates and equivalent isotropic displacement parameters U_{iso} of $[ClO_2][AsF_6]$ at 100 K.

Atom	Position	*x*	*y*	*z*	U_{iso} / Å^2
Cl(1)	4*h*	1/2	0.77239(5)	1/2	0.01428(10)
As(1)	4*i*	0.22084(2)	0,5	0.12141(4)	0.00961(6)
O(1)	4*j*	0.46454(11)	0.70196(12)	0.7162(2)	0.0180(2)
F(1)	4*j*	0.27503(9)	0.62214(10)	0.34594(19)	0.01783(18)
F(2)	4*j*	0.16168(9)	0.37862(10)	−0.09933(18)	0.01782(19)
F(3)	4*i*	0.35715(13)	1/2	−0.0061(3)	0.0204(3)
F(4)	4*i*	0.08386(12)	1/2	0.2612(3)	0.0153(2)

Table S4. Anisotropic displacement parameters of $[ClO_2][AsF_6]$ at 100 K.

Atom	U_{11} / Å^2	U_{22} / Å^2	U_{33} / Å^2	U_{23} / Å^2	U_{13} / Å^2	U_{12} / Å^2
Cl(1)	0.0193(2)	0.0121(2)	0.0113(2)	0	0.00168(16)	0
As(1)	0.00874(9)	0.00985(9)	0.00990(9)	0	−0.00002(6)	0
O(1)	0.0186(5)	0.0214(5)	0.0139(5)	0.0020(4)	0.0014(4)	−0.0037(4)
F(1)	0.0198(4)	0.0159(4)	0.0169(4)	−0.0043(3)	−0.0009(3)	−0.0039(3)
F(2)	0.0193(4)	0.0160(4)	0.0174(4)	−0.0062(3)	−0.0004(3)	−0.0020(3)
F(3)	0.0141(6)	0.0247(7)	0.0237(7)	0	0.0073(5)	0
F(4)	0.0119(5)	0.0167(6)	0.0182(6)	0	0.0052(4)	0

Atomic coordinates and displacement parameters of $[ClO_2][IrF_6]$

Table S5. Atomic coordinates and equivalent isotropic displacement parameters U_{iso} of $[ClO_2][IrF_6]$ at 100 K.

Atom	Position	*x*	*y*	*z*	U_{iso} / Å^2
Cl(1)	2*f*	3/4	0.11456(14)	1/4	0.01044(12)
Ir(1)	2*e*	3/4	0.51359(2)	3/4	0.00846(4)
O(1)	4*g*	0.5802(4)	−0.0133(4)	0.2217(5)	0.0171(4)
F(1)	4*g*	0.7171(3)	0.2727(4)	0.5684(3)	0.0144(3)
F(2)	4*g*	0.4884(3)	0.5138(3)	0.7836(4)	0.0149(3)
F(3)	4*g*	0.7827(3)	0.7475(4)	0.9326(3)	0.0160(3)

Table S6. Anisotropic displacement parameters of $[ClO_2][IrF_6]$ at 100 K.

Atom	U_{11} / Å^2	U_{22} / Å^2	U_{33} / Å^2	U_{23} / Å^2	U_{13} / Å^2	U_{12} / Å^2
Cl(1)	0.0143(3)	0.0065(3)	0.0105(3)	0	0.0013(2)	0
Ir(1)	0.01199(6)	0.00491(5)	0.00850(6)	0	0.00074(3)	0
O(1)	0.0165(9)	0.0126(9)	0.0222(12)	0.0001(6)	0.0007(8)	−0.0038(6)
F(1)	0.0219(8)	0.0107(7)	0.0108(6)	−0.0041(5)	0.0017(5)	−0.0022(5)
F(2)	0.0107(7)	0.0110(7)	0.0232(10)	−0.0003(5)	0.0021(6)	0.0001(4)
F(3)	0.0236(8)	0.0101(7)	0.0143(7)	−0.0066(6)	0.0005(6)	−0.0004(6)

Atomic coordinates and displacement parameters of $[ClO_2][SnF_5]$

Table S7. Atomic coordinates and equivalent isotropic displacement parameters U_{iso} of $[ClO_2][SnF_5]$ at 100 K.

Atom	Position	*x*	*y*	*z*	U_{iso} / Å^2
Cl(1)	4*e*	0.29056(7)	1.00214(9)	0.60283(4)	0.00783(9)
Sn(1)	4*e*	0.27271(2)	0.48834(2)	0.35899(2)	0.00482(5)
O(1)	4*e*	0.3122(2)	0.8692(3)	0.69370(13)	0.0133(3)
O(2)	4*e*	0.1298(2)	1.1466(3)	0.58496(13)	0.0141(3)
F(1)	4*e*	0.31208(18)	0.2999(2)	0.22678(9)	0.0082(3)
F(2)	4*e*	0.37364(19)	0.1815(2)	0.42530(10)	0.0103(3)
F(3)	4*e*	0.22994(19)	0.6719(2)	0.48068(10)	0.0111(3)
F(4)	4*e*	0.51456(17)	0.6303(2)	0.35080(10)	0.0093(3)
F(5)	4*e*	0.02974(18)	0.3600(3)	0.34752(10)	0.0110(3)

Table S8. Anisotropic displacement parameters of $[ClO_2][SnF_5]$ at 100 K.

Atom	U_{11} / Å^2	U_{22} / Å^2	U_{33} / Å^2	U_{23} / Å^2	U_{13} / Å^2	U_{12} / Å^2
Cl(1)	0.0071(2)	0.0082(2)	0.0082(2)	−0.00060(19)	−0.00015(17)	−0.00038(18)
Sn(1)	0.00530(8)	0.00405(7)	0.00510(8)	0.00017(5)	0.00013(5)	−0.00023(5)
O(1)	0.0136(9)	0.0140(8)	0.0121(8)	0.0035(6)	−0.0001(7)	−0.0030(6)
O(2)	0.0098(9)	0.0132(7)	0.0192(9)	−0.0010(7)	0.0004(7)	0.0029(6)
F(1)	0.0097(7)	0.0075(5)	0.0073(6)	−0.0018(5)	0.0005(5)	−0.0010(5)
F(2)	0.0132(7)	0.0071(5)	0.0105(7)	0.0027(5)	−0.0001(5)	0.0020(5)
F(3)	0.0150(7)	0.0095(6)	0.0089(7)	−0.0033(5)	0.0016(5)	−0.0004(5)
F(4)	0.0076(7)	0.0091(6)	0.0110(7)	−0.0010(5)	0.0006(5)	−0.0031(5)
F(5)	0.0076(7)	0.0119(6)	0.0137(7)	−0.0013(5)	0.0012(5)	−0.0035(5)

Atomic coordinates and displacement parameters of $[ClO_2][Ti_2F_9]$

Table S9. Atomic coordinates and equivalent isotropic displacement parameters U_{iso} of $[ClO_2][Ti_2F_9]$ at 100 K.

Atom	Position	*x*	*y*	*z*	U_{iso} / Å^2
Cl(1)	4*e*	1/2	0.20992(7)	1/4	0.0177(2)
Ti(1)	8*f*	0.31891(5)	0.40469(4)	0.62705(10)	0.01490(18)
O(1)	8*f*	0.4090(2)	0.16103(18)	0.0375(5)	0.0246(5)
F(1)	8*f*	0.29524(18)	0.48287(12)	0.3113(4)	0.0179(4)
F(2)	4*e*	1/2	0.44747(18)	3/4	0.0182(5)
F(3)	8*f*	0.3540(2)	0.34589(14)	0.9381(4)	0.0215(4)
F(4)	8*f*	0.14839(18)	0.38659(14)	0.5040(4)	0.0207(4)
F(5)	8*f*	0.36090(19)	0.31003(14)	0.4631(4)	0.0209(4)

Table S10. Anisotropic displacement parameters of $[ClO_2][Ti_2F_9]$ at 100 K.

Atom	U_{11} / Å^2	U_{22} / Å^2	U_{33} / Å^2	U_{23} / Å^2	U_{13} / Å^2	U_{12} / Å^2
Cl(1)	0.0192(4)	0.0208(5)	0.0141(4)	0	0.0074(3)	0
Ti(1)	0.0185(3)	0.0161(3)	0.0109(3)	0.00002(18)	0.00634(18)	−0.00012(18)
O(1)	0.0252(11)	0.0305(13)	0.0173(10)	−0.0017(9)	0.0070(9)	−0.0010(9)
F(1)	0.0208(8)	0.0192(9)	0.0134(8)	0.0012(7)	0.0061(7)	−0.0003(7)
F(2)	0.0170(11)	0.0210(13)	0.0165(11)	0	0.0062(9)	0
F(3)	0.0282(10)	0.0234(10)	0.0153(8)	0.0055(7)	0.0107(7)	0.0029(7)
F(4)	0.0198(9)	0.0259(10)	0.0172(9)	−0.0005(7)	0.0081(7)	−0.0009(7)
F(5)	0.0280(10)	0.0169(8)	0.0197(9)	−0.0030(7)	0.0110(8)	−0.0011(7)

Atomic coordinates and displacement parameters of $[ClO_2][Nb_3F_{16}]$

Table S11. Atomic coordinates and equivalent isotropic displacement parameters U_{iso} of $[ClO_2][Nb_3F_{16}]$ at 100 K.

Atom	Position	*x*	*y*	*z*	U_{iso} / Å^2
Cl(1)	4*e*	1/2	0.35052(2)	1/4	0.00893(4)
Nb(1)	8*f*	0.76217(2)	0.41470(2)	0.62565(2)	0.00751(2)
Nb(2)	4*e*	1/2	0.21444(2)	3/4	0.00801(2)
O(1)	8*f*	0.40180(6)	0.30093(4)	0.31450(6)	0.01412(10)
F(1)	8*f*	0.62507(6)	0.31680(4)	0.69407(6)	0.01764(10)
F(2)	8*f*	0.85114(7)	0.40774(4)	0.79934(6)	0.01964(10)
F(3)	8*f*	0.63270(6)	0.49933(4)	0.67943(6)	0.01850(10)
F(4)	8*f*	0.64271(6)	0.40125(4)	0.46133(5)	0.01561(9)
F(5)	8*f*	0.85712(5)	0.30874(4)	0.57991(5)	0.01445(8)
F(6)	8*f*	0.87537(6)	0.50183(4)	0.56522(6)	0.01824(10)
F(7)	8*f*	0.59704(6)	0.23537(4)	0.91768(6)	0.02011(10)
F(8)	8*f*	0.37731(6)	0.12901(4)	0.80216(6)	0.01690(9)

Table S12. Anisotropic displacement parameters of $[ClO_2][Nb_3F_{16}]$ at 100 K.

Atom	U_{11} / Å^2	U_{22} / Å^2	U_{33} / Å^2	U_{23} / Å^2	U_{13} / Å^2	U_{12} / Å^2
Cl(1)	0.00941(8)	0.00812(8)	0.00900(8)	0	0.00010(6)	0
Nb(1)	0.00760(3)	0.00737(3)	0.00766(3)	−0.00051(2)	0.00132(2)	−0.00012(2)
Nb(2)	0.00772(3)	0.00793(3)	0.00876(4)	0	0.00258(3)	0
O(1)	0.0137(2)	0.0147(2)	0.0141(2)	0.00146(18)	0.00238(18)	−0.00305(18)
F(1)	0.0186(2)	0.0133(2)	0.0229(3)	0.00114(18)	0.0098(2)	−0.00491(17)
F(2)	0.0250(3)	0.0220(3)	0.0104(2)	−0.00176(17)	−0.00346(18)	0.0004(2)
F(3)	0.0173(2)	0.0140(2)	0.0253(3)	−0.00501(18)	0.00710(19)	0.00412(17)
F(4)	0.0149(2)	0.0181(2)	0.0125(2)	−0.00128(16)	−0.00369(16)	0.00094(17)
F(5)	0.0149(2)	0.01326(19)	0.0153(2)	−0.00163(16)	0.00233(16)	0.00513(16)
F(6)	0.0179(2)	0.0166(2)	0.0213(3)	0.00256(18)	0.00638(19)	−0.00644(18)
F(7)	0.0192(2)	0.0281(3)	0.0123(2)	−0.00173(19)	−0.00125(18)	−0.0034(2)
F(8)	0.0173(2)	0.0142(2)	0.0206(2)	−0.00008(17)	0.00786(18)	−0.00562(17)

Atomic coordinates and displacement parameters of $[ClO_2][Mo_3O_3F_{13}]$

Table S13. Atomic coordinates and equivalent isotropic displacement parameters U_{iso} of $[ClO_2][Mo_3O_3F_{13}]$ at 100 K.

Atom	Position	*x*	*y*	*z*	U_{iso} / Å^2
Cl(1)	2*i*	0.69793(7)	0.28547(6)	0.45349(5)	0.01439(9)
Mo(1)	2*i*	0.27179(2)	0.22350(2)	0.61884(2)	0.01230(4)
Mo(2)	2*i*	0.18126(2)	0.29898(2)	0.19590(2)	0.01198(4)
Mo(3)	2*i*	0.27978(2)	0.75792(2)	0.09219(2)	0.01248(4)
O(1)	2*i*	0.8781(2)	0.1713(2)	0.48671(18)	0.0202(3)
O(2)	2*i*	0.6285(2)	0.3291(2)	0.31990(18)	0.0195(3)
O(3)	2*i*	0.3100(2)	0.2001(2)	0.78223(18)	0.0195(3)
O(4)	2*i*	0.1378(2)	0.3341(2)	0.03120(17)	0.0192(3)
O(5)	2*i*	0.3225(2)	0.9348(2)	0.03722(19)	0.0205(3)
F(1)	2*i*	0.51570(17)	0.11372(17)	0.57534(14)	0.0159(3)
F(2)	2*i*	0.32845(19)	0.42315(16)	0.54891(14)	0.0164(3)
F(3)	2*i*	0.02927(18)	0.35142(17)	0.60472(15)	0.0179(3)
F(4)	2*i*	0.22832(18)	0.02842(16)	0.63567(14)	0.0181(3)
F(5)	2*i*	0.23735(19)	0.26152(18)	0.40540(14)	0.0187(3)
F(6)	2*i*	−0.05073(18)	0.41353(17)	0.24747(14)	0.0167(3)
F(7)	2*i*	0.14563(19)	0.09665(17)	0.26116(15)	0.0188(3)
F(8)	2*i*	0.43028(18)	0.19389(18)	0.19416(15)	0.0191(3)
F(9)	2*i*	0.22567(19)	0.50600(17)	0.17444(15)	0.0183(3)
F(10)	2*i*	0.50995(18)	0.60314(18)	0.08438(15)	0.0191(3)
F(11)	2*i*	0.3276(2)	0.70721(18)	0.28109(14)	0.0193(3)
F(12)	2*i*	0.03602(19)	0.84266(18)	0.13189(15)	0.0207(3)
F(13)	2*i*	0.2146(2)	0.73665(19)	−0.06926(15)	0.0215(3)

Table S14. Anisotropic displacement parameters of $[ClO_2][Mo_3O_3F_{13}]$ at 100 K.

Atom	U_{11} / Å^2	U_{22} / Å^2	U_{33} / Å^2	U_{23} / Å^2	U_{13} / Å^2	U_{12} / Å^2
Cl(1)	0.0159(2)	0.0129(2)	0.0154(2)	−0.00525(18)	0.00128(18)	−0.00553(18)
Mo(1)	0.01310(8)	0.01122(8)	0.01292(9)	−0.00379(6)	0.00022(6)	−0.00435(6)
Mo(2)	0.01282(8)	0.01118(8)	0.01203(9)	−0.00373(6)	0.00029(6)	−0.00397(6)
Mo(3)	0.01355(8)	0.01168(9)	0.01220(9)	−0.00360(6)	0.00063(6)	−0.00434(6)
O(1)	0.0168(8)	0.0220(9)	0.0224(9)	−0.0063(7)	−0.0010(7)	−0.0072(7)
O(2)	0.0221(8)	0.0184(8)	0.0189(8)	−0.0047(7)	−0.0001(6)	−0.0085(7)
O(3)	0.0216(8)	0.0222(9)	0.0153(8)	−0.0046(7)	−0.0011(6)	−0.0085(7)
O(4)	0.0222(8)	0.0190(8)	0.0148(8)	−0.0051(6)	−0.0001(6)	−0.0051(7)
O(5)	0.0219(8)	0.0168(8)	0.0227(9)	−0.0044(7)	0.0019(7)	−0.0078(7)
F(1)	0.0136(6)	0.0140(6)	0.0190(7)	−0.0052(5)	0.0016(5)	−0.0037(5)
F(2)	0.0185(6)	0.0121(6)	0.0197(7)	−0.0044(5)	0.0012(5)	−0.0069(5)
F(3)	0.0151(6)	0.0155(6)	0.0209(7)	−0.0048(5)	0.0013(5)	−0.0032(5)
F(4)	0.0183(6)	0.0126(6)	0.0241(7)	−0.0048(5)	−0.0006(5)	−0.0064(5)
F(5)	0.0236(7)	0.0200(7)	0.0128(6)	−0.0058(5)	−0.0016(5)	−0.0066(5)
F(6)	0.0134(6)	0.0159(6)	0.0196(7)	−0.0058(5)	0.0019(5)	−0.0035(5)
F(7)	0.0223(7)	0.0132(6)	0.0228(7)	−0.0053(5)	0.0012(6)	−0.0086(5)
F(8)	0.0141(6)	0.0195(7)	0.0212(7)	−0.0059(6)	0.0016(5)	−0.0031(5)
F(9)	0.0229(7)	0.0146(6)	0.0204(7)	−0.0049(5)	0.0019(5)	−0.0104(5)
F(10)	0.0156(6)	0.0165(7)	0.0229(7)	−0.0056(6)	0.0019(5)	−0.0035(5)
F(11)	0.0258(7)	0.0210(7)	0.0138(6)	−0.0054(5)	0.0000(5)	−0.0108(6)
F(12)	0.0160(6)	0.0210(7)	0.0223(7)	−0.0053(6)	0.0039(5)	−0.0045(5)
F(13)	0.0243(7)	0.0254(8)	0.0158(7)	−0.0064(6)	−0.0012(6)	−0.0090(6)

Atomic coordinates and displacement parameters of $[ClO_2][Re_3O_6F_{10}]$

Table S15. Atomic coordinates and equivalent isotropic displacement parameters U_{iso} of $[ClO_2][Re_3O_6F_{10}]$ at 100 K.

Atom	Position	*x*	*y*	*z*	U_{iso} / Å^2
Cl(1)	2*i*	0.71213(13)	0.39095(15)	0.63833(14)	0.0089(2)
Re(1)	2*i*	0.30998(2)	0.14147(2)	0.30182(2)	0.00643(4)
Re(2)	2*i*	0.22460(2)	0.22105(2)	0.75298(2)	0.00692(4)
Re(3)	2*i*	0.17081(2)	0.67841(2)	0.84334(2)	0.00639(4)
O(1)	2*i*	0.6398(4)	0.4842(5)	0.7687(4)	0.0142(8)
O(2)	2*i*	0.7193(4)	0.2289(5)	0.6094(4)	0.0146(8)
O(3)	2*i*	0.3041(4)	0.1247(5)	0.1087(4)	0.0141(8)
O(4)	2*i*	0.1530(4)	−0.0023(4)	0.2749(4)	0.0112(7)
O(5)	2*i*	0.1334(4)	0.2868(5)	0.9145(4)	0.0138(8)
O(6)	2*i*	0.2138(4)	0.0223(5)	0.7106(4)	0.0144(8)
O(7)	2*i*	0.3610(4)	0.7782(4)	0.8895(4)	0.0128(7)
O(8)	2*i*	0.0714(4)	0.8330(4)	0.8975(4)	0.0105(7)
F(1)	2*i*	0.3459(3)	0.1927(4)	0.5608(3)	0.0101(6)
F(2)	2*i*	0.4972(3)	0.3189(4)	0.4058(3)	0.0107(6)
F(3)	2*i*	0.4619(3)	0.0167(4)	0.3098(4)	0.0141(6)
F(4)	2*i*	0.2050(3)	0.3170(4)	0.3754(3)	0.0106(6)
F(5)	2*i*	0.2648(3)	0.4567(4)	0.7654(3)	0.0107(6)
F(6)	2*i*	0.0555(3)	0.1942(4)	0.5873(4)	0.0125(6)
F(7)	2*i*	0.4319(3)	0.2943(4)	0.8728(3)	0.0129(6)
F(8)	2*i*	0.1397(3)	0.6253(4)	0.6184(3)	0.0110(6)
F(9)	2*i*	−0.0202(3)	0.5064(4)	0.7729(3)	0.0108(6)
F(10)	2*i*	0.1875(3)	0.6499(4)	1.0377(3)	0.0132(6)

Table S16. Anisotropic displacement parameters of $[ClO_2][Re_3O_6F_{10}]$ at 100 K.

Atom	U_{11} / Å^2	U_{22} / Å^2	U_{33} / Å^2	U_{23} / Å^2	U_{13} / Å^2	U_{12} / Å^2
Cl(1)	0.0087(5)	0.0086(6)	0.0087(5)	0.0035(4)	0.0012(4)	0.0006(4)
Re(1)	0.00719(8)	0.00463(9)	0.00668(9)	0.00153(7)	0.00172(6)	0.00124(6)
Re(2)	0.00770(8)	0.00594(9)	0.00762(9)	0.00268(7)	0.00322(6)	0.00222(6)
Re(3)	0.00682(8)	0.00512(9)	0.00668(9)	0.00174(7)	0.00202(6)	0.00144(6)
O(1)	0.0170(18)	0.014(2)	0.0100(17)	0.0027(15)	0.0065(14)	0.0034(15)
O(2)	0.0187(19)	0.0074(18)	0.0132(18)	0.0015(15)	−0.0005(14)	0.0010(15)
O(3)	0.0149(18)	0.014(2)	0.0112(17)	0.0045(15)	0.0036(14)	−0.0017(15)
O(4)	0.0123(17)	0.0062(17)	0.0137(18)	0.0029(14)	0.0034(14)	0.0013(13)
O(5)	0.0141(17)	0.016(2)	0.0124(18)	0.0068(15)	0.0045(14)	0.0019(15)
O(6)	0.0140(18)	0.014(2)	0.0166(19)	0.0076(16)	0.0061(14)	0.0027(15)
O(7)	0.0091(16)	0.0090(18)	0.0162(18)	0.0022(15)	0.0025(13)	−0.0010(14)
O(8)	0.0109(16)	0.0079(18)	0.0117(17)	0.0021(14)	0.0034(13)	0.0045(13)
F(1)	0.0100(13)	0.0118(15)	0.0099(14)	0.0051(12)	0.0045(11)	0.0030(11)
F(2)	0.0103(13)	0.0077(14)	0.0124(14)	0.0042(12)	0.0006(11)	−0.0018(11)
F(3)	0.0147(15)	0.0113(16)	0.0180(16)	0.0052(13)	0.0075(12)	0.0073(12)
F(4)	0.0110(13)	0.0080(15)	0.0130(14)	0.0032(12)	0.0037(11)	0.0051(11)
F(5)	0.0090(13)	0.0092(15)	0.0154(15)	0.0057(12)	0.0050(11)	0.0027(11)
F(6)	0.0091(13)	0.0131(16)	0.0137(15)	0.0048(13)	0.0006(11)	0.0018(12)
F(7)	0.0103(14)	0.0156(17)	0.0120(15)	0.0053(13)	0.0018(11)	0.0024(12)
F(8)	0.0155(14)	0.0120(16)	0.0052(13)	0.0033(12)	0.0025(11)	0.0026(12)
F(9)	0.0072(13)	0.0103(15)	0.0141(15)	0.0043(12)	0.0041(11)	0.0003(11)
F(10)	0.0149(15)	0.0147(16)	0.0106(14)	0.0055(12)	0.0035(11)	0.0037(12)

Basis set details for quantum-chemical solid-state calculations

TZVP basis set for O

The basis set for O was taken from a previous study.[1]

TZVP basis set for F

The basis set for F was taken from a previous study.[1]

TZVP basis set for Cl

The basis set for Cl was taken from a previous study.[2]

TZVP basis set for P

The basis set for P was taken from a previous study.[3]

TZVP basis set for Ti

The basis set for Ti was taken from a previous study.[4]

TZVP basis set for Sn

We applied the 28-electron Stuttgart-Cologne scalar-relativistic pseudopotential to describe the 1s2s2p3s3p3d core electrons of tin.[5] The molecular def2-TZVP basis set[6] was modified by fixing the exponents of the outermost s and p functions to 0.09 and reoptimizing the exponents of the other s and p functions in the valence space for the tin atom in its ground state. The basis set optimization was performed with the TURBOMOLE program package.[7] The resulting energy loss with respect to the unmodified def2-TZVP basis set is 3.4 mH. The final basis set in CRYSTAL input format is as follows:

```
250 13
INPUT
22   0   2   4   4   2   0
17.4204140000000  279.988682000000  0
7.63115500000000  62.3778100000000  0
16.1310240000000  66.1625230000000  0
15.6280770000000  132.174396000000  0
7.32560800000000  16.3394170000000  0
6.94251900000000  32.4889590000000  0
15.5149760000000  36.3874410000000  0
15.1881600000000  54.5078410000000  0
5.45602400000000  8.69682300000000  0
5.36310500000000  12.8402080000000  0
12.2823480000000 -12.5763330000000  0
12.2721500000000 -16.5959440000000  0
0 0 4 2.0 1.0
  1577.0715931      0.17042767713E-03
  235.26601078      0.81467057272E-03
  38.206330645     -0.39057904293E-02
  13.097031765      0.53245922343
0 0 2 2.0 1.0
  11.673161352       1.5435287275
  5.9463871497      0.76421510041
0 0 1 0.0 1.0
 1.8924497043       1.0000000000
0 0 1 0.0 1.0
 0.88429486443       1.0000000000
0 0 1 0.0 1.0
 0.23543697233       1.0000000000
0 1 1 0.0 1.0
 0.09                1.0 1.0
0 2 3 6.0 1.0
  221.55767496      0.31125177983E-03
  21.084021433      0.31108097016E-01
  8.7600138521     -0.27571560918
0 2 3 2.0 1.0
  2.5902185134      0.45912328666
```

```
  1.3409064118      0.49682867217
 0.67241607517      0.18962377821
0 2 1 0.0 1.0
  0.27895803477     1.0000000000
0 3 6 10.0 1.0
  108.33210154      0.46561853277E-03
  23.703936630      0.54063163067E-01
  22.339843906     -0.58928768877E-01
  4.0874834028      0.19588500896
  1.9737354146      0.42301799185
 0.90158257692      0.39252716176
0 3 1 0.0 1.0
 0.38237153649      1.0000000000
0 3 1 0.0 1.0
 0.191185768245     1.0000000000
0 4 1 0.0 1.0
 0.293928485        1.0000000000
```

TZVP basis set for Mo

The basis set for Mo was taken from a previous study.[8]

TZVP basis set for Re

The basis set was derived from the molecular Karlsruhe def2-TZVP basis set (60-electron effective core potential). The diffuse outermost s- and p-type functions with exponents of 0.04 and 0.07 were removed. The exponent of the outermost p-type function was changed from 0.31 to 0.122 and it was combined with the outermost s function into a single sp-type function. The most diffuse d-function with an exponent of 0.1 was removed and the most diffuse primitive with an exponent of 0.62 was decontracted from the contracted d-function. The f-type polarization function was removed. The final basis set in CRYSTAL input format is as follows:

```
275 10
INPUT
15. 0 2 2 2 1 1
14.099305 1038.951572 0
7.049653 29.561738 0
10.107717 339.543510 0
5.053858 24.913696 0
6.848618 111.699653 0
3.424309 12.624329 0
2.508651 16.449852 0
3.901245 -16.501120 0
0 0 3 2.0 1.0
  30.000000000      0.31780717811
  27.000000000     -0.46492321332
  13.078045684      0.45723641305
0 0 1 2.0 1.0
  5.0352712861       1.0000000000
0 0 1 0.0 1.0
  1.0482706438       1.0000000000
0 0 1 0.0 1.0
 0.47708773413       1.0000000000
0 1 1 0.0 1.0
 0.12225857255       1.0 1.0
0 2 4 6.0 1.0
  18.000000000     -0.26890962397E-01
  12.318606250      0.99711498502E-01
  5.3719234505     -0.29289398145
  1.3506646748      0.51466301434
0 2 1 0.0 1.0
 0.66212816808       1.0000000000
0 3 3 5.0 1.0
  7.7352877672      0.83901798556E-01
  6.0949443610     -0.17722258734
  1.3871105497      0.55238259692
0 3 1 0.0 1.0
 0.62324027854      0.91980111239
0 3 1 0.0 1.0
 0.26517328547       1.0000000000
```

TZVP basis set for As

The starting point was the molecular def-TZVP basis. The exponents of the outermost s and p functions were fixed to 0.13 and the exponents of the other s and p functions in the valence space were reoptimized for the arsenic atom in its ground state using TURBOMOLE program package. The exponent of the outermost d primitive was kept fixed, while the exponents of the other d functions were optimised for the arsenic atom in its ground state. An f-type polarization function with an exponent of 0.433 was added (def2-TZVP basis set). Finally, the outermost s and p functions were combined into a single sp-type function to increase the efficiency of the CRYSTAL code. The resulting energy loss with respect to the unmodified def2-TZVP basis set is 0.2 mH. The final basis set in CRYSTAL input format is as follows:

```
33 14
0 0 8 2.0 1.0
  498032.42158      0.22740196900E-03
  74656.868743      0.17632816413E-02
  16990.960004      0.91728040381E-02
  4809.6200321      0.37337829344E-01
  1566.2887055      0.12199536117
  563.21360499      0.29137475324
  219.11179978      0.42326351479
  86.866061030      0.22921464278
0 0 4 2.0 1.0
  538.19512479     -0.25254197297E-01
  167.14050224     -0.11915461115
  27.605517159      0.54628495980
  11.947858521      0.53001520976
0 0 2 2.0 1.0
  18.538023133     -0.23479188136
  3.2018985739      0.69167053428
0 0 1 2.0 1.0
  1.4362581800       1.0000000000
0 0 1 0.0 1.0
 0.35310762320       1.0000000000
0 1 1 0.0 1.0
 0.13000000000       1.0 1.0
0 2 6 6.0 1.0
  2678.9421546      0.23318955287E-02
  634.61765840      0.19042149977E-01
  203.93967606      0.90229744913E-01
  76.323890369      0.26169037693
  30.664124943      0.41857168155
  12.505056732      0.23447830190
0 2 4 6.0 1.0
  49.256229549     -0.21235539870E-01
  7.7274891466      0.30470206668
  3.5410493476      0.52888373107
  1.6985585501      0.37272250955
0 2 1 3.0 1.0
 0.80396418504       1.0000000000
0 2 1 0.0 1.0
 0.41045871535       1.0000000000
0 3 5 10.0 1.0
  139.05230680      0.99291144106E-02
  41.113850141      0.66568843496E-01
  15.035409461      0.22275768307
  5.9891096071      0.40309224382
  2.4322147899      0.41671667946
0 3 1 0.0 1.0
 0.96247584610       1.0000000000
0 3 1 0.0 1.0
 0.29300000000       1.0000000000
0 4 1 0.0 1.0
 0.43271941          1.0
```

TZVP basis set for Nb[9]

The basis set was derived from the molecular Karlsruhe def2-TZVP basis set (28-electron effective core potential). The diffuse outermost s-exponents were increased from 0.033 and 0.086 to 0.13 and 0.30, respectively. The outermost p-type function with an exponent of 0.03 was removed and the exponents of the two remaining outermost p-type functions were changed from 0.09 to 0.13 and 0.2797 to 0.30. The two outermost s and p functions were both then combined into two sp-type functions. The most diffuse d-type function (exponent 0.10) was removed and the inner (3d) function was decontracted to (2d1d). The f-type polarization function was removed. The final basis set in CRYSTAL input format is as follows:

```
241 9
INPUT
13. 0 2 2 2 2 0
8.900000 165.179143 0
4.430000 21.992974 0
7.770000 111.794414 0
3.960000 16.633483 0
6.050000 38.112249 0
```

```
2.840000 8.039167 0
8.490000 -22.929550 0
4.250000 -3.666310 0
0 0 2 2.0 1.0
  12.000000000     -0.20219507530
  10.500000000      0.33640105939
0 0 1 2.0 1.0
  3.9276062854      1.0000000000
0 0 1 0.0 1.0
 0.85976543258      1.0000000000
0 1 1 0.0 1.0
 0.30               1.0 1.0
0 1 1 0.0 1.0
 0.13               1.0 1.0
0 2 4 6.0 1.0
  9.2056205646      0.43347609074E-01
  4.8679632125     -0.21302479233
  1.2442155792      0.48102127136
 0.60390590312      0.53917858960
0 3 2 3.0 1.0
  4.6170975867     -0.13574476955E-01
  1.5663438480      0.20374310496
0 3 1 0.0 1.0
 0.66952425826      0.42997453105
0 3 1 0.0 1.0
 0.27140946867      1.0000000000
```

TZVP basis set for Ir[9]

The basis set was derived from the molecular Karlsruhe def2-TZVP basis set (60-electron effective core potential). The diffuse outermost s- and p-type functions with exponents of 0.05 and 0.056 were removed. The exponent of the outermost p-type function was changed from 0.33 to 0.14 and it was combined with the outermost s function into a single sp-type function. The exponents of the two outermost d-type functions were increased to 0.18 and 0.36. The f-type polarization function was removed. The final basis set in CRYSTAL input format is as follows:

```
277 10
INPUT
17. 0 2 2 2 1 1
13.652203 732.269200 0
6.826101 26.484721 0
10.279868 299.489474 0
5.139934 26.466234 0
7.349859 124.457595 0
3.674929 14.035995 0
3.034072 21.531031 0
4.808857 -21.607597 0
0 0 3 2.0 1.0
  30.000000000      0.30797903228
  27.000000000     -0.46726361781
  13.961973911      0.47161003146
0 0 1 2.0 1.0
  5.3956977802       1.0000000000
0 0 1 0.0 1.0
  1.2149128721       1.0000000000
0 0 1 0.0 1.0
 0.55885743756       1.0000000000
0 1 1 0.0 1.0
 0.14097974313       1.0 1.0
0 2 4 6.0 1.0
  15.902664143     -0.16290720099
  14.415830698      0.23483212987
  5.7597608991     -0.30305337176
  1.5008913108      0.55512982069
0 2 1 0.0 1.0
 0.72348035957       1.0000000000
0 3 4 7.0 1.0
  8.6321692504      0.75000099949E-01
  6.5898192302     -0.17326965173
  1.5808379663      0.55065196913
 0.71827834905      0.85273641436
0 3 1 0.0 1.0
 0.36                1.0000000000
0 3 1 0.0 1.0
 0.18                1.0000000000
```

Lattice parameters and atomic coordinates of optimized solid-state structures

Lattice parameters and atomic coordinates of the optimized solid-state structure of $[ClO_2][PF_6]$

Space group $P2_12_12_1$ (No. 19)
a = 5.31160822 Å, b = 10.75042313 Å, c = 9.64845284 Å, V = 550.946300 Å^3

Table S17. Atomic coordinates of the optimized structure of $[ClO_2][PF_6]$.

Atom	*x*	*y*	*z*
P	−3.969171412604E−01	−4.624589276550E−01	4.998092986991E−01
Cl	3.261328776000E−01	2.859544486251E−01	2.414238187490E−01
O	9.222129090288E−02	2.913856301597E−01	3.153953490995E−01
O	−4.630871981911E−01	2.291928096836E−01	3.095629555418E−01
F	4.750973754309E−01	−3.235249115723E−01	−4.951677276592E−01
F	4.053174104345E−01	4.907228760403E−01	−3.837238252829E−01
F	−2.023265473761E−01	−4.099285458168E−01	3.799409429202E−01
F	−2.689143748746E−01	4.017029935600E−01	4.908346693591E−01
F	−1.976571054958E−01	−4.214626203345E−01	−3.807379405063E−01
F	4.057244867321E−01	4.985825774943E−01	3.766046797234E−01

Lattice parameters and atomic coordinates of the optimized solid-state structure of $[ClO_2][AsF_6]$

Space group $C2/m$ (No. 12)
a = 11.01430304 Å, b = 10.17487680 Å, c = 4.98083804 Å, β = 98.328442°, V = 552.31166200 Å^3,

Table S18. Atomic coordinates of the optimized structure of $[ClO_2][AsF_6]$.

Atom	*x*	*y*	*z*
As	−2.769516136598E−01	−2.365992167710E−17	1.050602508610E−01
Cl	−4.857225732735E−17	2.831875513850E−01	5.000000000000E−01
O	−3.991354645425E−02	2.092059928610E−01	−2.836578930121E−01
F	−2.226887560696E−01	1.215189081529E−01	3.329963360006E−01
F	−3.391425329574E−01	−1.198837900209E−01	−1.238290328901E−01
F	−4.135835931537E−01	−3.881485267634E−19	2.480929869234E−01
F	−1.432364992784E−01	−3.542981355579E−17	−2.984420466958E−02

Lattice parameters and atomic coordinates of the optimized solid-state structure of $[ClO_2][IrF_6]$

Space group $P12/n1$ (No. 13)
a = 7.18354747 Å, b = 5.76612983 Å, c = 7.07484191 Å, β = 92.991606°, V = 292.649549 Å^3

Table S19. Atomic coordinates of the optimized structure of $[ClO_2][IrF_6]$.

Atom	*x*	*y*	*z*
Ir	−2.500000000000E−01	4.869319711063E−01	−2.500000000000E−01
Cl	−2.500000000000E−01	1.488358444037E−01	2.500000000000E−01
O	−4.188411629921E−01	1.793691760215E−02	2.177843058463E−01
F	−2.885734970242E−01	2.442404705103E−01	−4.356334431853E−01
F	4.970070340909E−01	4.837830810452E−01	−2.114989563962E−01
F	−2.111950570200E−01	−2.832876090413E−01	−6.446995181708E−02

Lattice parameters and atomic coordinates of the optimized solid-state structure of $[ClO_2][SnF_5]$

Space group *P*2/*c* (No. 13)
a = 7.49430527 Å, *b* = 5.13550730 Å, *c* = 13.44793932 Å, *β* = 93.886869° *V* = 516.381143 Å^3

Table S20. Atomic coordinates of the optimized structure of $[ClO_2][SnF_5]$.

Atom	*x*	*y*	*z*
Sn	2.724572296487E−01	4.984766976939E−01	3.600956133862E−01
Cl	2.978208817626E−01	−1.265559782193E−04	−3.981349914954E−01
O	3.155692340213E−01	−1.441451037707E−01	−3.063538488361E−01
O	1.349040227610E−01	1.458655670815E−01	−4.144241680022E−01
F	3.112145238651E−01	3.146692611751E−01	2.255985357480E−01
F	2.324470572635E−01	−3.187860407937E−01	4.847269908280E−01
F	3.775422742585E−01	1.923739424397E−01	4.271356445328E−01
F	−4.881031804743E−01	−3.550509543919E−01	3.541333091280E−01
F	3.330106405755E−02	3.678458027570E−01	3.471002395405E−01

Lattice parameters and atomic coordinates of the optimized solid-state structure of $[ClO_2][Ti_2F_9]$

Space group *C*2/*c* (No. 15)
a = 11.29631100 Å, *b* = 14.77990658 Å, *c* = 5.31012255 Å, *β* = 108.605929°, *V* = 840.23346600 Å^3

Table S21. Atomic coordinates of the optimized structure of $[ClO_2][Ti_2F_9]$.

Atom	*x*	*y*	*z*
Ti	1.758114080840E−01	−9.506426012881E−02	3.583339847374E−01
Cl	0.000000000000E+00	−2.801954875728E−01	−2.500000000000E−01
O	4.201448666773E−01	1.683419190254E−01	−4.677627461779E−01
F	1.988874499267E−01	1.727017483083E−02	1.732254447001E−01
F	1.426655287319E−01	−1.517239595510E−01	4.615584741515E−02
F	3.393535848944E−01	−1.160340154567E−01	4.632303204736E−01
F	6.938893903907E−18	−5.208438322093E−02	2.500000000000E−01
F	1.293716992363E−01	−1.900586698104E−01	−4.814115392417E−01

Lattice parameters and atomic coordinates of the optimized solid-state structure of $[ClO_2][Nb_3F_{16}]$

Space group *C*2/*c* (No. 15)
a = 9.66875245 Å, *b* = 14.41237068 Å, *c* = 10.04838753 Å, *β* = 98.210022° *V* = 1385.88855320 Å^3

Table S22. Atomic coordinates of the optimized structure of $[ClO_2][Nb_3F_{16}]$.

Atom	*x*	*y*	*z*
Nb	−2.639971655454E−01	8.715756370934E−02	3.760849705834E−01
Nb	0.000000000000E+00	2.886688483992E−01	2.500000000000E−01
Cl	−1.387778780781E−17	−1.439332185567E−01	2.500000000000E−01
O	1.018349165122E−01	−1.963245260238E−01	1.908520115355E−01
F	−3.603948374923E−01	9.435711952846E−02	2.017043653197E−01
F	1.410287057880E−01	−3.071603194389E−01	4.266006912930E−01
F	−1.386635929453E−01	9.800623437906E−02	−4.561651045096E−01
F	−1.316007005649E−01	4.499974680213E−03	3.187927190232E−01
F	−3.730337653365E−01	−4.400324263343E−03	4.357260009944E−01
F	−1.287044243905E−01	1.870931984671E−01	3.089418302468E−01
F	−1.017265820673E−01	2.636946640835E−01	8.201571258118E−02
F	−3.783650957477E−01	−1.235674000067E−01	1.971556859509E−01

Lattice parameters and atomic coordinates of the optimized solid-state structure of $[ClO_2][Mo_3O_3F_{13}]$

Space group $P\bar{1}$ (No. 2)
a = 7.85096862 Å, b = 8.76666384 Å, c = 10.10058487 Å, α = 73.655583°, β = 84.754771°, γ = 67.913971°,
V = 618.064224 Å^3

Table S23. Atomic coordinates of the optimized structure of $[ClO_2][Mo_3O_3F_{13}]$.

Atom	*x*	*y*	*z*
Mo	−1.816708354931E−01	−2.987121487625E−01	−1.950783279114E−01
Mo	−2.791667956276E−01	2.388819432716E−01	−9.328666294581E−02
Mo	−2.709574995875E−01	−2.243666862996E−01	3.813000935961E−01
Cl	3.062595316269E−01	−2.890965594936E−01	−4.545854070399E−01
O	1.190535620257E−01	−1.751728590925E−01	−4.846656620883E−01
O	−3.139227783232E−01	−2.025625037696E−01	2.178922974214E−01
O	−3.199433301120E−01	5.960020711571E−02	−3.805753586748E−02
O	−1.351408321192E−01	−3.332831332848E−01	−2.990294288258E−02
O	3.724181225827E−01	−3.312862116709E−01	−3.163454747368E−01
F	−4.351700683113E−01	−1.887258180310E−01	−1.939609719156E−01
F	−2.266781774838E−01	4.930781303774E−01	−1.743659044079E−01
F	−2.404032050533E−02	−3.561420889641E−01	3.940816088041E−01
F	4.786628541594E−01	−1.173565767429E−01	4.293626610612E−01
F	−3.272095752196E−01	−4.280979301760E−01	4.536945613318E−01
F	−2.385799225934E−01	−2.612863779822E−01	−4.064127930062E−01
F	5.378087313576E−02	−4.126404665264E−01	−2.523520710740E−01
F	4.891780808460E−01	3.974214666151E−01	−7.780444972846E−02
F	−3.362632962451E−01	2.966017223255E−01	−2.829632885821E−01
F	−3.380943643460E−02	1.538596389170E−01	−1.424525104381E−01
F	−2.339254206258E−01	−2.405544067037E−02	3.646239346596E−01
F	−1.504294761418E−01	−9.189698013189E−02	−2.625162936857E−01
F	−2.019930335265E−01	2.566055574072E−01	6.723079811607E−02

Lattice parameters and atomic coordinates of the optimized solid-state structure of $[ClO_2][Re_3O_6F_{10}]$

Space group $P\bar{1}$ (No. 2)
a = 8.68021580 Å, b = 9.27410243 Å, c = 10.10058487 Å, α = 113.360852°, β = 98.848901°, γ = 96.622910°,
V = 671.727596 Å^3

Table S24. Atomic coordinates of the optimized structure of $[ClO_2][Re_3O_6F_{10}]$.

Atom	*x*	*y*	*z*
Re	−3.284748919983E−01	−3.305257139091E−01	−1.621171998487E−01
Re	−1.909386409457E−01	1.429260947966E−01	3.062729491933E−01
Re	−2.763266623969E−01	2.174812707259E−01	−2.495743652851E−01
Cl	2.152155849774E−01	3.929449502232E−01	−3.614059309200E−01
O	−1.951813835220E−01	1.266544345696E−01	1.195154105215E−01
O	−3.500149996324E−01	7.026270813100E−03	2.789462022304E−01
O	1.423539887401E−01	4.901589696739E−01	−2.382263643961E−01
O	−3.656294655359E−01	2.801391051759E−01	−9.448027279638E−02
O	−4.280373409164E−01	−1.816386004245E−01	−1.098752122604E−01
O	−2.835274224081E−01	2.679325826600E−02	−2.874552907819E−01
O	−1.399085528011E−01	−2.340610125296E−01	−1.140357809581E−01
O	2.206851791251E−01	2.363949873175E−01	−3.732160399430E−01
F	−4.468089236116E−01	1.901831278019E−01	−4.134931966617E−01
F	−6.652371289773E−02	2.949434375784E−01	−1.345179045399E−01
F	−2.899034716847E−01	3.191916252979E−01	3.770328993420E−01
F	−1.577892428791E−01	1.939592218330E−01	−4.392189472646E−01
F	3.607755610442E−03	3.153240689359E−01	4.135505785421E−01
F	−4.006142282494E−02	1.856030578355E−02	3.169539003476E−01
F	−2.421808663278E−01	4.509680714571E−01	−2.393433642335E−01
F	4.713364856617E−01	−4.999085687251E−01	−2.386968596944E−01
F	−3.589696029516E−01	−3.803325319947E−01	−3.825227704722E−01
F	−3.180847865739E−01	−3.659455410210E−01	2.386478149311E−02

Low-resolution Raman spectra

Raman spectrum of $[ClO_2][AsF_6]$

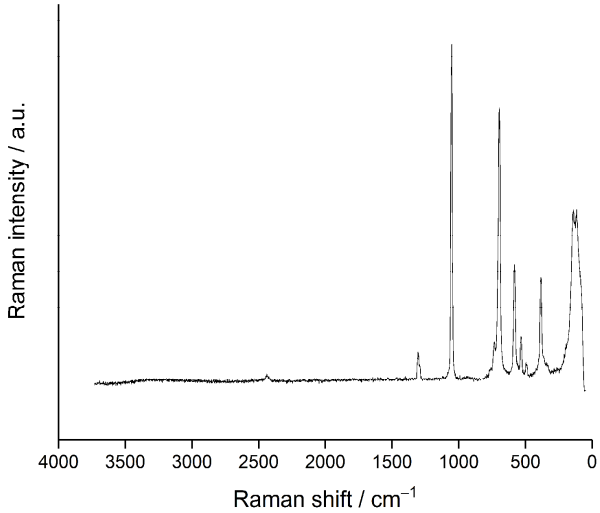

Figure S1. Low-resolution Raman spectrum of $[ClO_2][AsF_6]$ of a sample measured under perfluorinated oil (Fomblin YR1800) on a microscope slide. Raman intensities are given in arbitrary units, a.u..

Raman spectrum of $[ClO_2][IrF_6]$

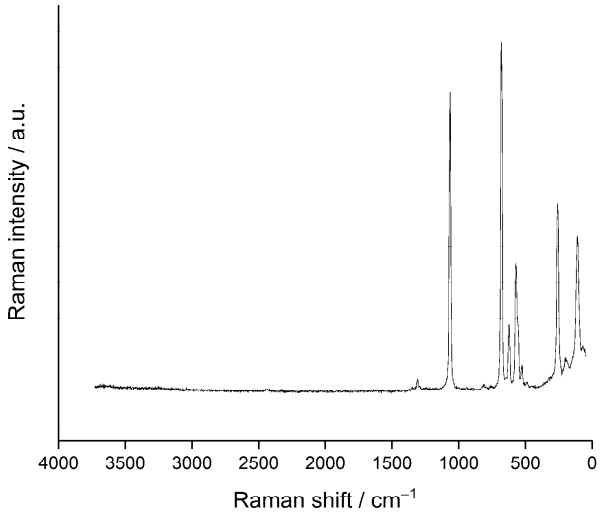

Figure S2. Low-resolution Raman spectrum of $[ClO_2][IrF_6]$ of a sample measured under perfluorinated oil (Fomblin YR1800) on a microscope slide. Raman intensities are given in arbitrary units, a.u..

Raman spectrum of $[ClO_2][SnF_5]$

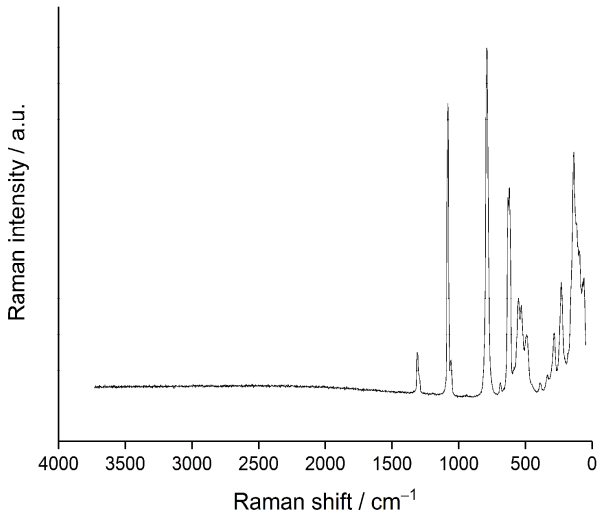

Figure S3. Low-resolution Raman spectrum of $[ClO_2][SnF_5]$ of a sample measured under perfluorinated oil (Fomblin YR1800) on a microscope slide. Raman intensities are given in arbitrary units, a.u..

Raman spectrum of $[ClO_2][Ti_2F_9]$

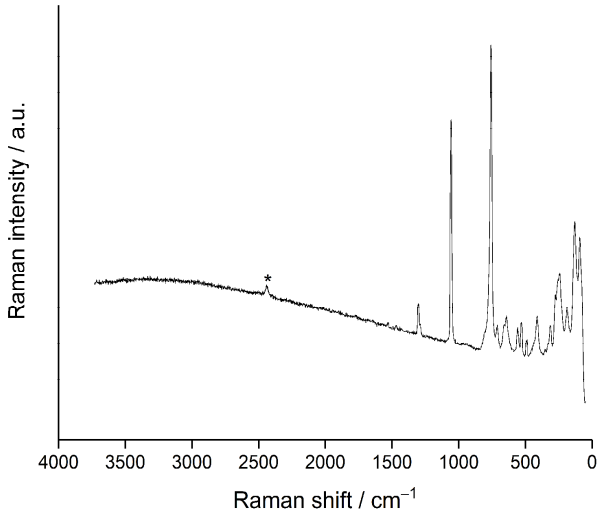

Figure S4. Low-resolution Raman spectrum of $[ClO_2][Ti_2F_9]$ of a sample measured in a glass vial. The asterisk denotes a band that is likely caused by hydrolysis products of the sample. Raman intensities are given in arbitrary units, a.u..

Raman spectrum of $[ClO_2][Nb_3F_{16}]$

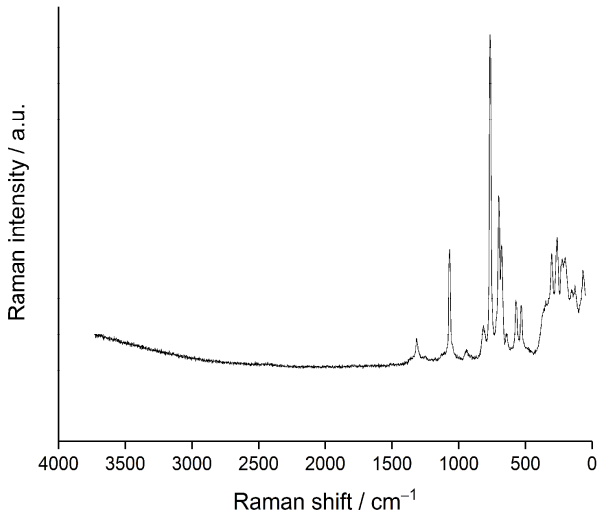

Figure S5. Low-resolution Raman spectrum of $[ClO_2][Nb_3F_{16}]$ of a sample measured under perfluorinated oil (Fomblin YR1800) on a microscope slide. Raman intensities are given in arbitrary units, a.u..

Raman spectrum of $[ClO_2][Mo_3O_3F_{13}]$

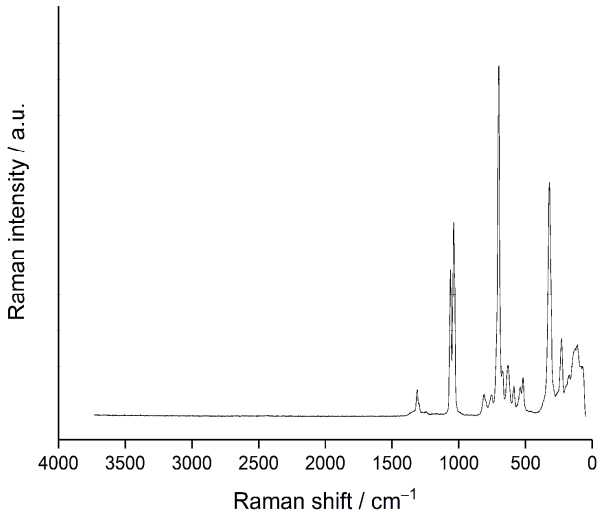

Figure S6. Low-resolution Raman spectrum of $[ClO_2][Mo_3O_3F_{13}]$ of a sample measured under perfluorinated oil (Fomblin YR1800) on a microscope slide. Raman intensities are given in arbitrary units, a.u..

Raman spectrum of $[ClO_2][Re_3O_6F_{10}]$

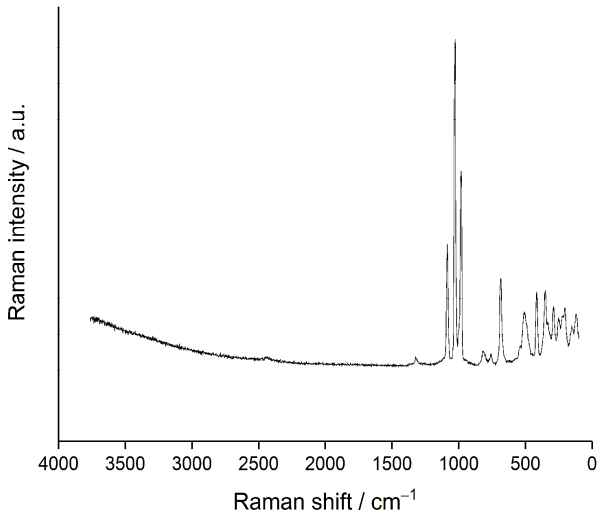

Figure S7. Low-resolution Raman spectrum of $[ClO_2][Re_3O_6F_{10}]$ of a sample measured under perfluorinated oil (Fomblin YR1800) on a microscope slide. Raman intensities are given in arbitrary units, a.u..

Comparison of calculated Raman spectra and high-resolution Raman spectra and band assignments for the calculated Raman spectra

Raman spectra and band assignment of $[ClO_2][AsF_6]$

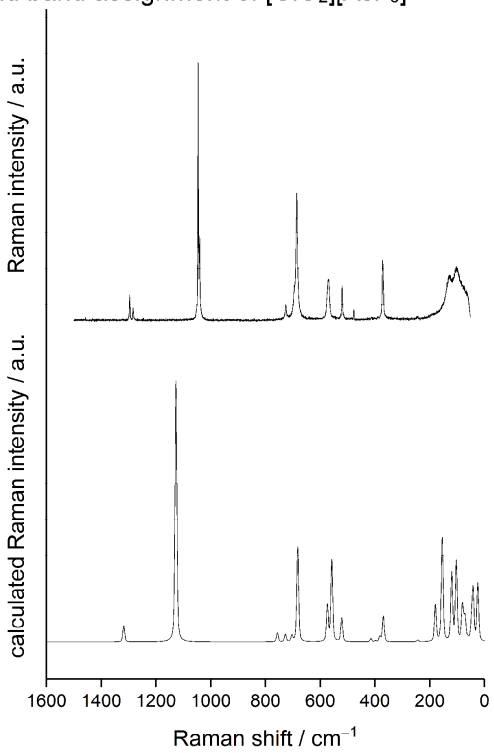

Figure S8. Comparison of the experimental high-resolution and calculated solid-state (DFT-PBE0/TZVP) Raman spectra of $[ClO_2][AsF_6]$. Raman intensities are given in arbitrary units, a.u..

Table S25. Band assignments for the calculated Raman spectrum (>300 cm^{-1}) of $[ClO_2][AsF_6]$. The notation for band assignments is the following: ν – stretching, δ – deformation, s – symmetric, as – asymmetric.

ν (calculated) / cm^{-1}	ν (experimental) / cm^{-1}	Assignment
1317	1296, 1283	$\nu_{as}(ClO_2)$ – Asymmetric stretching of the O atoms of the $[ClO_2]^+$ cation
1127	1046, 1040	$\nu_s(ClO_2)$ – Symmetric stretching of the O atoms of the $[ClO_2]^+$ cation
756, 727, 703, 682, 573, 557	725, 685, 570	$\nu(AsF_6)$ – Stretching of F atoms of the $[AsF_6]^-$ anion
521	519	$\delta(ClO_2)$ – Scissoring of the O atoms of the $[ClO_2]^+$ cation
414, 398, 382, 370, 369, 368	372	$\delta(AsF_6)$ – Wagging of the $[AsF_6]^-$ anion

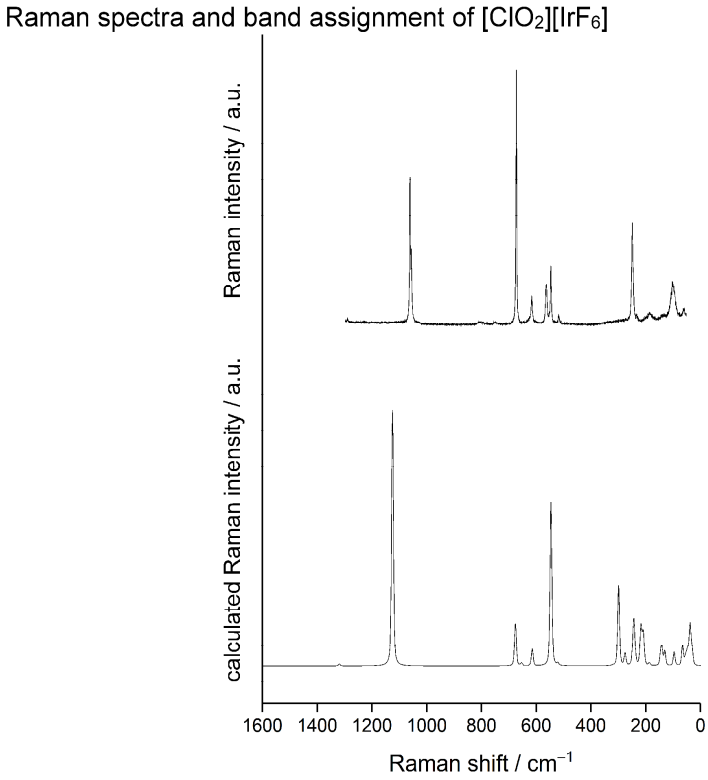

Figure S9. Comparison of the experimental high-resolution and calculated solid-state (DFT-PBE0/TZVP) Raman spectra of $[ClO_2][IrF_6]$. Raman intensities are given in arbitrary units, a.u..

Table S26. Band assignments for the calculated Raman spectrum (>300 cm^{-1}) of $[ClO_2][IrF_6]$. The notation for band assignments is the following: ν – stretching, δ – deformation, s – symmetric, as – asymmetric.

ν (calculated) / cm^{-1}	ν (experimental) / cm^{-1}	Assignment
1319	1290	$\nu_{as}(ClO_2)$ – Asymmetric stretching of the O atoms of the $[ClO_2]^+$ cation
1125	1061, 1056	$\nu_s(ClO_2)$ – Symmetric stretching of the O atoms of the $[ClO_2]^+$ cation
676, 657, 653, 614, 546, 545	672, 617, 562, 546	$\nu(IrF_6)$ – Stretching of F atoms of the $[IrF_6]^-$ anion
521	518	$\delta(ClO_2)$ – Scissoring of the O atoms of the $[ClO_2]^+$ cation

Raman spectra and band assignment of $[ClO_2][SnF_5]$

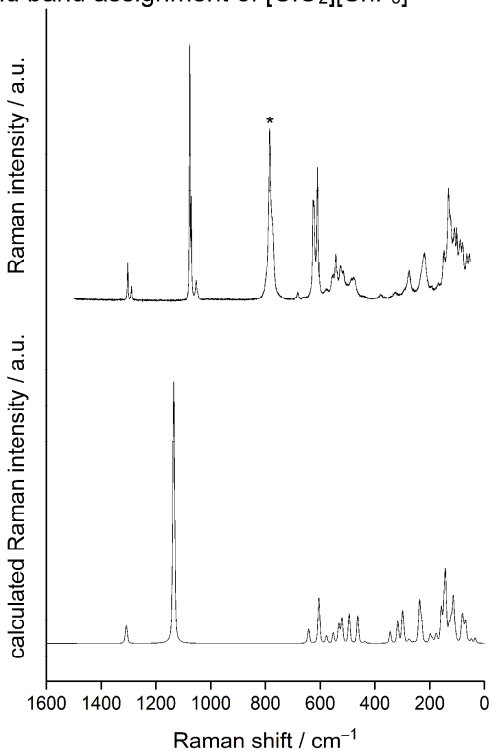

Figure S10. Comparison of the experimental high-resolution and calculated solid-state (DFT-PBE0/TZVP) Raman spectra of $[ClO_2][SnF_5]$. The asterisk denotes a band (at 783 cm^{-1}) that is likely caused by a ClF_2^+-containing impurity, likely $[ClF_2][SnF_5]$.[10] Raman intensities are given in arbitrary units, a.u..

Table S27. Band assignments for the calculated Raman spectrum (>300 cm^{-1}) of $[ClO_2][SnF_5]$. The notation for band assignments is the following: ν – stretching, δ – deformation, s – symmetric, as – asymmetric.

ν (calculated) / cm^{-1}	ν (experimental) / cm^{-1}	Assignment
1310, 1306	1303, 1289	$\nu_{as}(ClO_2)$ – Asymmetric stretching of the O atoms of the $[ClO_2]^+$ cation
1136, 1135	1076, 1071, 1052	$\nu_s(ClO_2)$ – Symmetric stretching of the O atoms of the $[ClO_2]^+$ cation
652, 642	682	$\nu(SnF_6)$ – Stretching of the axial F atoms
605, 601	624, 610	$\nu_s(SnF_6)$ – Symmetric stretching of F atoms
577, 552	577, 553, 542	$\nu(SnF_6)$ – Out-of-phase stretching of F atoms
532, 530, 520	525, 515	$\delta(ClO_2)$ + $\nu(SnF_6)$ – Scissoring of the O atoms of the $[ClO_2]^+$ cation coupled with out-of-phase stretching of F atoms
463	484	$\nu_s(SnF_6)$ – Symmetric stretching of μ-bridging F atoms
437	476	$\nu_{as}(SnF_6)$ – Asymmetric stretching of μ-bridging F atoms
344, 316, 299	379, 325	$\delta(SnF_6)$ – Wagging of SnF_6 units

Raman spectra and band assignment of $[ClO_2][Ti_2F_9]$

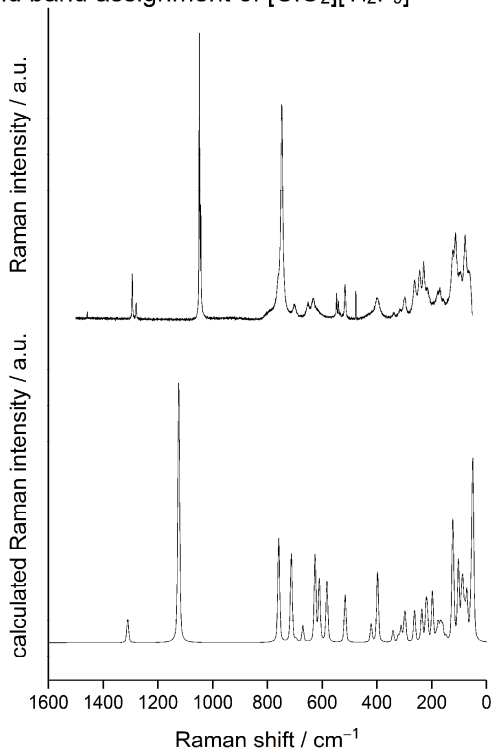

Figure S11. Comparison of the experimental high-resolution and calculated solid-state (DFT-PBE0/TZVP) Raman spectra of $[ClO_2][Ti_2F_9]$. Raman intensities are given in arbitrary units, a.u..

Table S28. Band assignments for the calculated Raman spectrum (>300 cm^{-1}) of $[ClO_2][Ti_2F_9]$. The notation for band assignments is the following: ν – stretching, δ – deformation, s – symmetric, as – asymmetric.

ν (calculated) / cm^{-1}	ν (experimental) / cm^{-1}	Assignment
1310	1293, 1280	$\nu_{as}(ClO_2)$ – Asymmetric stretching of the O atoms of the $[ClO_2]^+$ cation
1124	1049, 1044	$\nu_s(ClO_2)$ – Symmetric stretching of the O atoms of the $[ClO_2]^+$ cation
758	747	$\nu_s(TiF_6)$ – Symmetric stretching of F atoms of TiF_6 units
713, 695	700	$\nu(TiF_6)$ – In-phase stretching of terminal F atoms of TiF_6 units
670, 626, 610	652, 633	$\nu(TiF_6)$ – Out-of-phase stretching of terminal F atoms of TiF_6 units
583	545, 540	$\nu(TiF_6)$ – Stretching of terminal and μ-bridging F atoms of TiF_6 units
516	517	$\delta(ClO_2)$ – Scissoring of the O atoms of the $[ClO_2]^+$ cation
421, 398	477, 399	$\nu_{as}(TiF_6)$ – Asymmetric stretching of μ-bridging F atoms of TiF_6 units
397, 341, 322, 312, 301	335, 314, 298	$\delta(TiF_6)$ – Wagging of TiF_6 units

Raman spectra and band assignment of $[ClO_2][Nb_3F_{16}]$

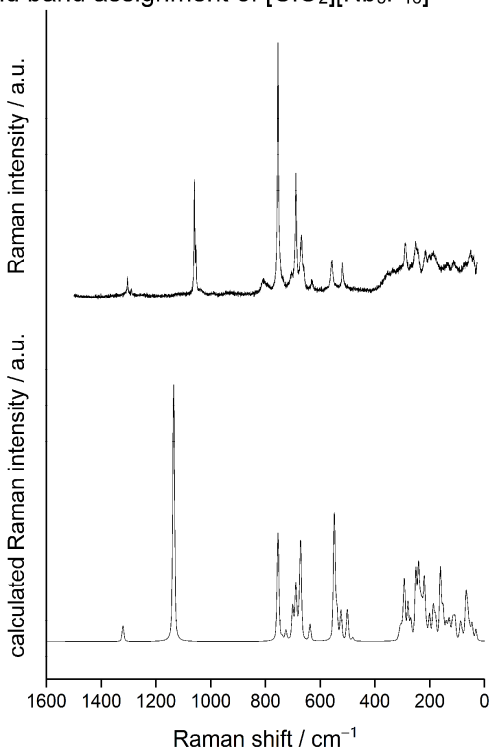

Figure S12. Comparison of the experimental high-resolution and calculated solid-state (DFT-PBE0/TZVP) Raman spectra of $[ClO_2][Nb_3F_{16}]$. Raman intensities are given in arbitrary units, a.u..

Table S29. Band assignments for the calculated Raman spectrum (>300 cm^{-1}) of $[ClO_2][Nb_3F_{16}]$. The notation for band assignments is the following: ν – stretching, δ – deformation, s – symmetric, as – asymmetric.

ν (calculated) / cm^{-1}	ν (experimental) / cm^{-1}	Assignment
1320	1304, 1291	$\nu_{as}(ClO_2)$ – Asymmetric stretching of the O atoms of the $[ClO_2]^+$ cation
1135	1060, 1054	$\nu_s(ClO_2)$ – Symmetric stretching of the O atoms of the $[ClO_2]^+$ cation
754, 753, 739, 725, 710, 701, 699, 689, 679, 671, 665, 637, 548, 539	754, 705, 689, 668, 630, 557	$\nu(NbF_6)$ –Stretching of terminal F atoms of NbF_6 units
524	519	$\delta(ClO_2)$ – Scissoring of the O atoms of the $[ClO_2]^+$ cation
501	not observed	$\nu_s(NbF_6)$ –Symmetric stretching of μ-bridging F atoms of NbF_6 units
481	not observed	$\nu_{as}(NbF_6)$ – Asymmetric stretching of μ-bridging F atoms of NbF_6 units
313, 307	290	$\delta(NbF_6)$ – Wagging of NbF_6 units

Raman spectra and band assignment of $[ClO_2][Mo_3O_3F_{13}]$

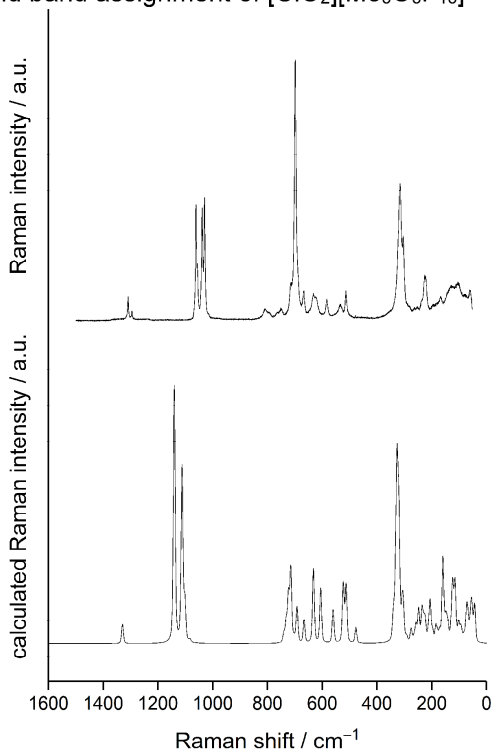

Figure S13. Comparison of the experimental high-resolution and calculated solid-state (DFT-PBE0/TZVP) Raman spectra of $[ClO_2][Mo_3O_3F_{13}]$. Raman intensities are given in arbitrary units, a.u..

Table S30. Band assignments for the calculated Raman spectrum (>300 cm^{-1}) of $[ClO_2][Mo_3O_3F_{13}]$. The notation for band assignments is the following: ν – stretching, δ – deformation, s – symmetric, as – asymmetric.

ν (calculated) / cm^{-1}	ν (experimental) / cm^{-1}	Assignment
1329	1309, 1294	$\nu_{as}(ClO_2)$ – Asymmetric stretching of the O atoms of the $[ClO_2]^+$ cation
1140	1061, 1056	$\nu_s(ClO_2)$ – Symmetric stretching of the O atoms of the $[ClO_2]^+$ cation
1112, 1102, 1083	1039, 1030	$\nu(MoOF_4)$ –Stretching of O atoms of $MoOF_4$ units
742, 739, 731, 723, 715, 702, 692, 666, 632, 605	714, 698, 667, 632, 624, 583	$\nu(MoOF_4)$ –Stretching of terminal F atoms of $MoOF_4$ units
560	534	$\nu(MoOF_4)$ –Stretching of μ-bridging F atoms of $MoOF_4$ units
523, 513	513	$\delta(ClO_2)$ – Scissoring of the O atoms of the $[ClO_2]^+$ cation
477	not observed	$\nu(MoOF_4)$ –Stretching of μ-bridging F atoms of $MoOF_4$ units
340, 333, 329	316	$\delta(MoOF_4)$ – Wagging of $MoOF_4$ units
326, 323, 320, 318	304	$\delta(MoOF_4)$ – Scissoring of O and F atoms of $MoOF_4$ units

Raman spectra and band assignment of $[ClO_2][Re_3O_6F_{10}]$

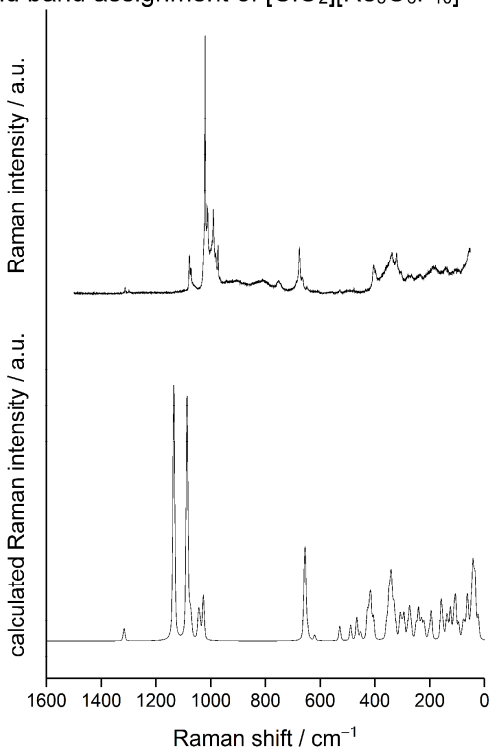

Figure S14. Comparison of the experimental high-resolution and calculated solid-state (DFT-PBE0/TZVP) Raman spectra of $[ClO_2][Re_3O_6F_{10}]$. Raman intensities are given in arbitrary units, a.u..

Table S31. Band assignments for the calculated Raman spectrum (>300 cm^{-1}) of $[ClO_2][Re_3O_6F_{10}]$. The notation for band assignments is the following: ν – stretching, δ – deformation, s – symmetric, as – asymmetric.

ν (calculated) / cm^{-1}	ν (experimental) / cm^{-1}	Assignment
1316	1312, 1298	$\nu_{as}(ClO_2)$ – Asymmetric stretching of the O atoms of the $[ClO_2]^+$ cation
1135	1078, 1072	$\nu_s(ClO_2)$ – Symmetric stretching of the O atoms of the $[ClO_2]^+$ cation
1086, 1076, 1071	1020, 1010, 990, 981, 973	$\nu_s(ReO_2F_4)$ – Asymmetric stretching of O atoms of ReO_2F_4 units
1044, 1039, 1027		$\nu_s(ReO_2F_4)$ – Symmetric stretching of O atoms of ReO_2F_4 units
659, 657, 654, 646, 636, 620	676, 665	$\nu(ReO_2F_4)$ –Stretching of terminal F atoms of ReO_2F_4 units
528	527	$\delta(ClO_2)$ – Scissoring of the O atoms of the $[ClO_2]^+$ cation
489, 466, 453	not observed	$\nu(ReO_2F_4)$ –Stretching of bridging F atoms of ReO_2F_4 units
428, 420, 415, 406	404	$\delta(ReO_2F_4)$ – Scissoring of O atoms of ReO_2F_4 units
357, 350, 346, 342, 338	338, 321	$\delta(ReO_2F_4)$ – Scissoring of F atoms of ReO_2F_4 units
331, 325, 308, 301	303	$\delta(ReO_2F_4)$ – Wagging of ReO_2F_4 units

References

[1] A. J. Karttunen, T. Tynell, M. Karppinen, *J. Phys. Chem. C* **2015**, *119*, 13105–13114.
[2] V. Sivchik, R. K. Sarker, Z.-Y. Liu, K.-Y. Chung, E. V. Grachova, A. J. Karttunen, P.-T. Chou, I. O. Koshevoy, *Chem. Eur. J.* **2018**, *24*, 11475–11484.
[3] G. Sansone, L. Maschio, D. Usvyat, M. Schütz, A. Karttunen, *J. Phys. Chem. Lett.* **2016**, *7*, 131–136.
[4] N. Glebko, I. Aleksandrova, G. C. Tewari, T. S. Tripathi, M. Karppinen, A. J. Karttunen, *J. Phys. Chem. C* **2018**, *122*, 26835–26844.
[5] B. Metz, H. Stoll, M. Dolg, *J. Chem. Phys.* **2000**, *113*, 2563–2569.
[6] F. Weigend, R. Ahlrichs, *Phys. Chem. Chem. Phys.* **2005**, *7*, 3297–3305.
[7] R. Ahlrichs, M. Bär, M. Häser, H. Horn, C. Kölmel, *Chem. Phys. Lett.* **1989**, *162*, 165–169.
[8] R. E. Stene, B. Scheibe, C. Pietzonka, A. J. Karttunen, W. Petry, F. Kraus, *J. Fluorine Chem.* **2018**, *211*, 171–179.
[9] B. Scheibe, A. J. Karttunen, F. Weigend, F. Kraus, *Chem. - Eur. J.* **2020**, DOI 10.1002/chem.202003629.
[10] A. I. Popov, A. V. Scharabarin, V. F. Sukhoverkhov, N. A. Tchumaevsky, *Z. Anorg. Allg. Chem.* **1989**, *576*, 242–254.

7.6. The $[U_2F_{12}]^{2-}$ Anion of $Sr[U_2F_{12}]$

Benjamin Scheibe, Clemens Pietzonka, Otto Mustonen, Maarit Karppinen, Antti J. Karttunen, Mihail Atanasov, Frank Neese, Matthias Conrad, Florian Kraus

Angew. Chem. **2018**, *130*, 2964–2968
Angew. Chem. Int. Ed. **2018**, 57, 2914–2918.
DOI: 10.1002/ange.201800743
DOI: 10.1002/anie.201800743

© 2018 Wiley-VCH Verlag GmbH & Co. KGaA, Weinheim

Reproduced with permission of John Wiley and Sons; permission conveyed through Copyright Clearance Center, Inc. (License number: 4885931363231).

GDCh Communications Angewandte International Edition Chemie

Uranium

International Edition: DOI: 10.1002/anie.201800743
German Edition: DOI: 10.1002/ange.201800743

The $[U_2F_{12}]^{2-}$ Anion of $Sr[U_2F_{12}]$

*Benjamin Scheibe, Clemens Pietzonka, Otto Mustonen, Maarit Karppinen, Antti J. Karttunen, Mihail Atanasov, Frank Neese, Matthias Conrad, and Florian Kraus**

Dedicated to Professor Wolfgang Schnick on the occasion of his 60th birthday

Abstract: *The D_{2h}-symmetric dinuclear complex anion $[U_2F_{12}]^{2-}$ of pastel green $Sr[U_2F_{12}]$ shows a hitherto unknown structural feature: The coordination polyhedra around the U atoms are edge-linked monocapped trigonal prisms, the U^V atoms are therefore seven-coordinated. This leads to a U–U distance of 3.8913(6) Å. A weak U^V–U^V interaction is observed for the dinuclear $[U_2F_{12}]^{2-}$ complex and described by the antiferromagnetic exchange J_{exp} of circa $-29.9\ cm^{-1}$. The crystalline compound can be easily prepared from SrF_2 and β-UF_5 in anhydrous hydrogen fluoride (aHF) at room temperature. It was studied by means of single crystal X-ray diffraction, IR, Raman and UV/VIS spectroscopy, magnetic measurements, and by molecular as well as by solid-state quantum chemical calculations.*

Compounds containing a central atom with coordination number seven may exhibit in principle three different idealized geometric ligand arrangements.[1–3] These are the monocapped octahedron (C_{3v}, 1/3/3 arrangement), the monocapped trigonal prism (C_{2v}, 1/4/2 arrangement), and the pentagonal bipyramid (D_{5h}, 1/5/1 arrangement). Binary main-group species seem to prefer the 1/5/1 arrangement, which was reported for $[XeF_7]^+$, IF_7, $[TeF_7]^-$, and $[SbF_7]^{2-}$, but also some transition-metal compounds show this motif, such as ReF_7, $[Re(CN)_7]^{3-}$, and $[U(N_3)_7]^{3-}$.[4–9] The 1/4/2 arrangement is observed for the anions $[NbF_7]^{2-}$, $[TaF_7]^{2-}$, $[Nb(N_3)_7]^{2-}$, and $[Ta(N_3)_7]^{2-}$, but also by $[XeF_7]^-$ in $[Xe_2F_{13}]^-$.[10–12] The 1/3/3 arrangement is featured in the homoleptic complex anions $[MoF_7]^-$, $[WF_7]^-$, $[Mo(CH_3)_7]^-$, and $[U(N_3)_7]^{3-}$.[9,13,14]

To our knowledge, there are so far only two reported cases with condensed homoleptic complex anions exhibiting a coordination number of seven for their central atoms. One being the $[Zr_2F_{12}]^{4-}$ anion (*Ci* symmetry) in $[Co(en)_3]_2[Zr_2F_{12}]$-$[SiF_6]\cdot 4H_2O$, which can be described as a distorted edge-linked pentagonal bipyramid.[15] The other case can be described as an association of two $[IF_6]^-$ anions in $[N(Me)_4]$-$[IF_6]$, forming a $[I_2F_{12}]^{2-}$ anion, which consists of edge-sharing monocapped trigonal prisms (*Ci* symmetry). However, the I-(μ-F) distances are very different as a result of the sterically active lonepairs of the I atoms.[16] An example for a compound with a condensed heteroleptic complex anion and coordination number seven for the central atoms is $K[HF_2]\cdot 2IF_5$, for which an infinite chain structure is observed in which HF_2^- ions are bridged by IF_5 molecules.[17]

Herein we describe the synthesis and properties of the salt $Sr[U_2F_{12}]$, strontium di-μ-fluorido decafluoridodiuranate(V). The bulk phase of the compound appears pastel green, for a photograph see Figure S1 in the Supporting Information, while single crystals are yellowish. It can be synthesized from the reaction of SrF_2 and β-UF_5 in anhydrous hydrogen fluoride (aHF) at room temperature, see Equation (1) and

$$SrF_2 + 2\,UF_5 \xrightarrow{aHF} Sr[U_2F_{12}] \quad (1)$$

the Supporting Information for details. During the course of the synthesis the HF solution turns bluish, which is characteristic for the solvated $[UF_6]^-$ ion.[18] $Sr[U_2F_{12}]$ was always obtained together with a small percentage (1–3%) of crystalline, paramagnetic $Sr[UF_5(FHF)_2]$ as an impurity. This compound will be reported elsewhere.

However, unlike other hexafluoridouranates(V), such as $NO[UF_6]$ or KUF_6, which contain isolated $[UF_6]^-$ ions or more complex anionic structure motifs, $Sr[U_2F_{12}]$ contains the highly symmetric di-μ-fluorido-decafluoridodiuranate(V) anion, $[U_2F_{12}]^{2-}$ (Figure 1), in its solid-state structure as evidenced by single crystal X-ray diffraction.[19–21] The compound crystallizes in the tetragonal space group type *I*4/*mcm* with $a = 9.2149(13)$, $c = 11.361(2)$ Å, $V = 964.7(3)$ Å^3, and $Z = 4$ at $T = 100$ K. Further crystallographic details are available from Table S1.

The anion can be formally described as a dimer of $[UF_6]^-$ ions. The coordination sphere around each U atom is then best described as a monocapped trigonal prism with C_{2v} symmetry for these formal "UF_7" subunits. Linkage via the edge (see Figure 1, the F(3) atoms) leads to the $[U_2F_{12}]^{2-}$ anion with ideal D_{2h} symmetry. Their arrangement in the crystal structure is shown in Figure S2.

To our knowledge, such a coordination polyhedron has not been observed for complex anions containing homoleptic ligands, previously. Furthermore, the anion is the first example of a dinuclear fluoridouranate(V) complex. There

[*] M. Sc. B. Scheibe, C. Pietzonka, Dr. M. Conrad, Prof. Dr. F. Kraus
Fachbereich Chemie
Philipps-Universität Marburg
Hans-Meerwein-Strasse 4, 35032 Marburg (Germany)
E-mail: florian.kraus@chemie.uni-marburg.de
Homepage: https://www.uni-marburg.de/fb15/ag-kraus

M. Sc. O. Mustonen, Prof. Dr. M. Karppinen, Prof. Dr. A. J. Karttunen
Department of Chemistry, Aalto University
00076 Aalto (Finland)

Prof. Dr. M. Atanasov, Prof. Dr. F. Neese
Max-Planck Institute for Chemical Energy Conversion
Stiftstrasse 34–36, 45470 Mülheim an der Ruhr (Germany)

Supporting information and the ORCID identification number(s) for the author(s) of this article can be found under: https://doi.org/10.1002/anie.201800743.

 © 2018 Wiley-VCH Verlag GmbH & Co. KGaA, Weinheim

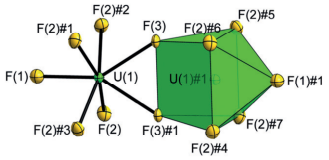

Figure 1. A section of the crystal structure of $Sr[U_2F_{12}]$ showing the $[U_2F_{12}]^{2-}$ anion. The green coordination polyhedron highlights the first coordination sphere of a uranium atom. Displacement ellipsoids are set at 70% probability at 100 K. Selected interatomic distances in [Å] and angles [°]: U(1)–F(1) 2.079(10), U(1)–F(2) 2.081(4), U(1)–F(3) 2.281(4), U(1)–U(1)#1 3.8913(10); F(1)-U(1)-F(2) 81.23(12), F(1)-U-(1)-F(3) 148.54(17), F(2)-U(1)-F(2)#1 162.5(2), F(3)-U(1)-F(3)#1 62.9-(3), U(1)-F(3)-U(1)#1 117.1(3). See the Supporting Information for crystallographic details. Further details on the crystal structure investigation(s) may be obtained from the Fachinformationszentrum Karlsruhe, 76344 Eggenstein-Leopoldshafen, Germany (fax: (+49) 7247-808-666; e-mail: crysdata@fiz-karlsruhe.de), on quoting the depository number CSD–433765.

are three crystallographically different kinds of fluorido ligands, of which F(1) and F(2) are terminal ligands with almost equal U–F distances of 2.079(10) and 2.081(4) Å, respectively. Such distances are in good agreement with the literature.[19,22] In comparison, the μ-bridging fluorido ligand F(3) shows an increased distance to the U atoms with 2.281(4) Å, which is expected due to its higher coordination number. With 3.8913-(10) Å, the U–U distance within the dinuclear complex is small for a U^V fluoride compound. In comparison, α-UF_5 shows a U–U interchain distance of circa 4.5 Å and β-UF_5 shows U–U distances of 4.5 and 4.6 Å.[23,24]

If the centers of gravity of the $[U_2F_{12}]^{2-}$ anions are thought of as an atom (B), then, together with the Sr atoms (A), a simple AB structure type results, where each of the A and B atoms shows a distorted cubic coordination sphere. Therefore, $Sr[U_2F_{12}]$ can be derived from the simple CsCl structure type. The crystallographic relation is shown in Scheme S1. The surrounding of the Sr atoms by F atoms is square-antiprismatic and is shown in Figure S3.

Quantum chemical calculations using a well-established protocol within the ab initio ligand-field theory implemented in the program ORCA were carried out to elucidate the antibonding effect of the F^- ligands on the 5f orbitals of the uranium atoms, which also leads to the ligand field splitting and gives rise to the f–f absorption spectra.[25–27] From a chemical perspective this can be done by using the angular overlap model (AOM), which defines the antibonding effects on f-orbitals for well aligned orbitals of the U and F atoms with overlap of σ- and π-symmetry (see Supporting Information for details).[28,29] These effects are quantified by the AOM parameters e_σ and e_π, which depend on the nature of the ligand and the metal–ligand bond length. The trend of the U–F distances correlates with the computed AOM parameters for the three inequivalent fluoride donors, which classify the relative σ- and π-donor strength—the F(1) atom being the strongest, the F(2) atom weaker, and the μ-F(3) atom the weakest σ- and π-donor towards the uranium atom, see Figure 2. Population analyses, carried out for the bulk phase of $Sr[U_2F_{12}]$ using quantum chemical solid state calculations within the CRYSTAL 14 program package on the PBE0-TZVP level of theory (see the Supporting Information),[44,45] also suggest such a trend with the μ-F(3) atoms being the most ionic ones.

The vibrational spectra of the compound show three different regions: At approximately 610 cm^{-1} the symmetric U–F stretching modes, at circa 450 cm^{-1} the asymmetric U–F stretching modes and at circa 270 cm^{-1} the F-U-F deformation modes are observed. Using quantum chemical solid state calculations within the CRYSTAL14 program package, the experimentally obtained Raman and IR spectra of $Sr[U_2F_{12}]$ were nicely reproduced and allowed the assignment of the observed bands (the spectra and irreducible representations are given in the Supporting Information). Overall, the observed bands are in good agreement with other hexafluoridouranate(V) salts.[19,20]

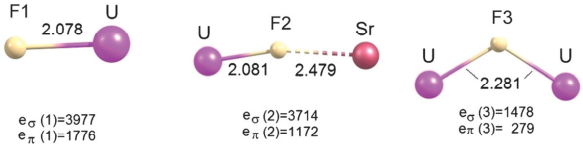

Figure 2. σ- and π-donor character of the three types of fluoride ligands as given by the AOM parameters e_σ and e_π (in cm^{-1}) and their correlation with the number and strength of their interactions with their nearest neighbors in the crystal structure of $Sr[U_2F_{12}]$.

Additionally, we were interested in the absorption spectrum of the highly symmetric $[U_2F_{12}]^{2-}$ anion, in which the uranium(V) atoms have the electron configuration $[Rn]5f^1$, where on-site f–f electron interaction is absent and thus only a few absorptions can be observed.[21,30] We recorded the solid state absorption spectrum and performed Complete Active Space Self-Consistent Field (CASSCF) calculations for the $[U_2F_{12}]^{2-}$ anion and a hypothetical $[UF_7]^{2-}$ subunit, see Figure 3. The calculations for the $[U_2F_{12}]^{2-}$ anion were carried out for D_{2h} symmetry and are in excellent agreement with the recorded spectrum regarding relative intensities and computed energies. Upon comparison of the two calculated anions, the f–f transitions for the hypothetical $[UF_7]^{2-}$ anion change strongly both in energy and intensity when going to the dinuclear $[U_2F_{12}]^{2-}$ anion, showing the effect of f^1–f^1 pair interactions on the f–f transitions. Thus, from the eight possible f–f excitations stemming from the lowest $\Gamma_5 \rightarrow \Gamma_5$ excitation within each $[UF_7]^{2-}$ subunit only two, $A_g \rightarrow B_{3u'}$ and $A_g \rightarrow B_{2u'}$, are computed to appear with an appreciable intensity (Figure 3, right). For the $[U_2F_{12}]^{2-}$ anion we calculated eight possible f–f transitions, of which six could be observed in the spectrum. Comparing the spectrum with the spectra of $Cs[UF_6]$, $NO[UF_6]$, or $RbUF_6$, the distinctive ligand field effects of the surroundings of the U^V atoms become visible.[19,31,32] This is characteristic for the actinides,

 © 2018 Wiley-VCH Verlag GmbH & Co. KGaA, Weinheim

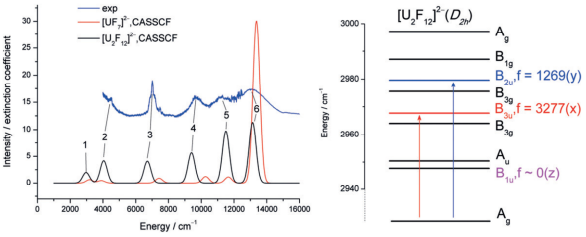

Figure 3. Left: Experimental (blue) and simulated (black; CASSCF, Gaussians with half width at half maximum of 500 cm^{-1}) absorption spectra arising from f–f transitions of $[U_2F_{12}]^{2-}$ and the computed spectrum of the formal $[UF_7]^{2-}$ subunit with the same geometry and charge as the dimer (red lines). Based on CASSCF calculations (see Supporting Information for further details) assignment of the six parity allowed transitions 1, 2, 3, 4, 5, and 6 are assigned as $A_g \rightarrow B_{2u}$, B_{3u}; $A_g \rightarrow B_{1u}$, B_{2u}, B_{3u}; $A_g \rightarrow B_{1u}$, B_{2u}, B_{3u}; $A_g \rightarrow B_{1u}$, B_{2u}; $A_g \rightarrow B_{1u}$, B_{2u}, B_{3u}; and $A_g \rightarrow B_{1u}$, B_{2u}, B_{3u}, respectively. Symmetry notations refer to spin-orbit wavefunctions classified according to the irreducible representations of the D_{2h} point group. Right: Eight possible f–f transitions of $[U_2F_{12}]^{2-}$ arising from the coupling of the lowest two Γ_5 electronic states within each $[UF_7]^{2-}$ subunit with respective irreducible representations from CASSCF calculations and additionally the oscillator strengths f are shown.

where ligand-field splitting and spin-orbit coupling can be in the same order of magnitude.[21]

There are scarce reports on the magnetic properties of homoleptic uranium(V) fluorido complexes.[19,33–36] However, several heteroleptic dinuclear uranium(V) complexes have been magnetically characterized and most of them show antiferromagnetic coupling with susceptibility maxima in the range of 5 to 70 K.[37–42] To our knowledge, no magnetic data for a homoleptic dinuclear uranium(V) complex, such as in $Sr[U_2F_{12}]$, have been reported as of yet. We carried out DC magnetic measurements on $Sr[U_2F_{12}]$ and also computed data for the $[U_2F_{12}]^{2-}$ anion with the CASSCF and N-Electron Valence Perturbation Theory to second order (NEVPT2) methods (Figure 4, left) for χ versus T data (additional details are given in the Supporting Information, for field-dependent magnetic data see Figure S4). The paramagnetic $Sr[UF_5(FHF)_2]$ impurity leads to an increase of the molar susceptibility at temperatures below 5 K. The compound $Sr[U_2F_{12}]$ shows molecular antiferromagnetic behavior, with a maximum of the molar susceptibility at approximately $T_{max} = 26$ K.

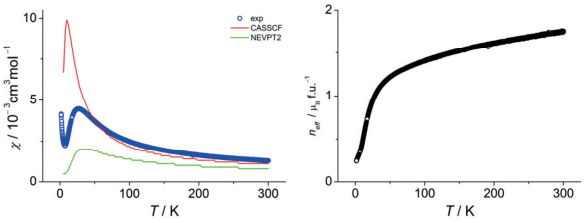

Figure 4. Left: χ versus T data of $Sr[U_2F_{12}]$ at 1 T (blue) and computed data (red: CASSCF; green: NEVPT2) for $[U_2F_{12}]^{2-}$. The presence of the paramagnetic impurity $Sr[UF_5(FHF)_2]$ is also indicated, see the ascent below 5 K and the Figures S6 and S8. Right: Temperature dependence of the effective magnetic moment per $Sr[U_2F_{12}]$ formula unit.

This temperature should not be regarded as a Néel temperature, as the $[U_2F_{12}]^{2-}$ anions are separated by the Sr cations which results in a very large inter-dimer separation with next-nearest U–U distances of 4.9672(7) Å. This large separation and the very ionic nature of the Sr–F bond causes only very weak inter-dimer interactions.

The magnetic data were fitted with a modified Heisenberg-Dirac-van-Vleck model, in which the paramagnetic impurity was considered (see Figure S7 and the Supporting Information for further details). The exchange coupling parameter J_{exp}, which indicates the strength of the antiferromagnetic coupling of the U^V atoms, is determined as -29.86 cm^{-1}, whereas the CASSCF calculations lead to -10.74 cm^{-1} and the NEVPT2 calculations to -38.22 cm^{-1}.

Furthermore, temperature independent paramagnetism (van Vleck paramagnetism) is observed for $Sr[U_2F_{12}]$, and this behavior is also predicted by our calculations. Field-dependent measurements at 15 K yield a molar susceptibility of $3.8300(5) \times 10^{-3}$ $cm^3 mol^{-1}$ for $Sr[U_2F_{12}]$. In the temperature region between 50 and 300 K, the data was fitted with a modified Curie–Weiss law (Figure S5) resulting in an effective magnetic moment of 1.02(1) μ_B per uranium atom and a Weiss constant of $-32(2)$ K, which also demonstrates the antiferromagnetic interaction of the U^V atoms. In Figure 4 (right) the temperature dependence of the effective magnetic moment per $Sr[U_2F_{12}]$ formula unit is shown. A strong influence of the temperature below 50 K can be observed, while a linear course of the data above 100 K is found. The effective magnetic moment approaches a non-zero value at very low temperatures, which is common for uranium(III) and uranium(V) compounds.[33]

In general, the magnetic exchange J depends on the overlap of the magnetic orbitals on the U^V centers which is controlled by the U-L-U angle (α) and the nature of the bridging ligand L. For angles close to 90° this overlap is weak resulting in a ferromagnetic exchange. For the complex reported here a significant deviation of the U-F-U bridging angle from 90° with $\alpha = 117.1(3)°$ is observed. This results in a significant overlap and leads to antiferromagnetic exchange as Figure 5 shows for the lowest pair of singly occupied molecular orbitals—the lowest MO, being an almost non-bonding orbital, and the antibonding one which is 2304 cm^{-1} higher in energy. Equation (2) shows the approximation of

$$J = J_{af} \cos^2 \alpha \qquad (2)$$

J by the antiferromagnetic contribution J_{af} only. As an approximation, the ferromagnetic contribution to J was neglected as the deviation of α from 90° is very large.[43]

Values of experimentally obtained J_{exp} and calculated $|J_{af}|$ for other dinuclear U^V complexes with the same bridging topology but with μ-oxido and μ-imido ligands are shown in Table 1. To

 © 2018 Wiley-VCH Verlag GmbH & Co. KGaA, Weinheim

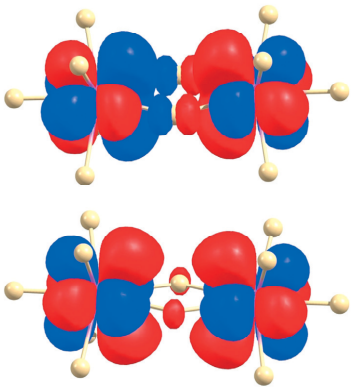

Figure 5. Contour plot of molecular orbitals for the U–U bonding interaction ^2A_g (energy 0 cm^{-1}, bottom) and the U–U antibonding interaction $^2B_{1u}$ (energy 2304 cm^{-1}, top). Contour plots have been constructed using the (hypothetical) one-electron oxidized analogue of $[U_2F_{12}]^{2-}$, that is, the mixed-valence $[U_2F_{12}]^{-}$ with the structure data of $Sr[U_2F_{12}]$. The diagram has been constructed using contour isovalues of 0.015 electron/$Bohr^3$. Color codes: red: positive; blue: negative.

eliminate the differences of J_{exp} due to the different bridging angles of these complexes, J_{af} has been calculated from the reported J values by normalization with $\cos^2\alpha$. This allows us to compare the $|J_{af}|$ values and formulate the following sequence of ligands with regards to their super exchange abilities: $O^{2-} > NR_2^{-} > F^{-}$. This observed trend is likely due to the higher iconicity of the U–F bond in comparison to a U–N or a U–O bond.

To conclude, we reported the compound $Sr[U_2F_{12}]$, which contains the highly symmetric and hitherto unknown dinuclear $[U_2F_{12}]^{2-}$ anion. The coordination polyhedra around the U atoms are in the shape of edge-sharing mono-capped trigonal prisms. The different kinds of U–F bonding, with the bridging μ-F atoms being clearly the most ionic ones, could be interpreted within the angular overlap model and with population analyses. The magnetic and spectroscopic properties of $Sr[U_2F_{12}]$ were nicely reproduced and explained utilizing molecular as well as solid-state quantum chemical calculations. The $[U_2F_{12}]^{2-}$ anion shows molecular antiferromagnetism caused by the coupling of the U^V atoms, mediated by the bridging fluorido ligands. As a result of the beautiful simplicity of this $[U_2F_{12}]^{2-}$ anion and its D_{2h} symmetry, we expect it to be the ideal benchmark species for future quantum chemical studies on the U^V–U^V interaction. Investigations of other fluoridouranates(V) with divalent cations, such as $Sr[UF_5(FHF)_2]$, are in progress.

Table 1: Dinuclear U^V complexes and their calculated (mean) negative J_{af} values given as the modulus of J_{af}. L stands for the μ-bridging atoms F^-, NR_2^-, and O^{2-}. The ligand Z is a polypyrrolic macrocycle.[40]

U^V complexes	$d(U_1\text{-}L)$ [Å]	$d(U_2\text{-}L)$ [Å]	α [°]	T_{max} [K]	J_{exp} [cm^{-1}]	$\lvert J_{af}\rvert$ [cm^{-1}]
$[\{U(\mu\text{-}F)F_5\}_2]^{2-}$	2.281(4)	2.281(4)	117.1(3)	26	−29.9	144
$[\{U(\mu\text{-}NtBu)_2(I)(tBu_2bpy)\}_2]$[39]	2.067(5)	2.387(5)	106.7(2)	13	−14.4	176
	2.380(5)	2.078(5)	106.5(2)			
$[(Me_3SiOUO)_2(Z)]$[40]	2.099(4)	2.085(4)	106.3(2)	17	−33.0	412
	2.098(4)	2.094(4)	106.6(2)			
$[\{((^{nP,Me}ArO)_3tacn)U\}_2(\mu\text{-}O)_2]$[42]	2.206(2)	2.066(2)	109.18(7)	70	−77.8	721

Acknowledgements

We thank the Deutsche Forschungsgemeinschaft (DFG) for generous funding, Prof. Dr. Willner, Wuppertal, for the initial donation of UF_6, Solvay for the donation of fluorine, Dr. Harms, Marburg, for X-ray measurement time. A.J.K. thanks the Academy of Finland for funding (grant 294799) and CSC, the Finnish IT Center for Science, for computational resources.

Conflict of interest

The authors declare no conflict of interest.

Keywords: fluorine · hexafluoridouranate(V) · magnetic properties · quantum chemical calculations · uranium

How to cite: *Angew. Chem. Int. Ed.* **2018**, *57*, 2914 2918
Angew. Chem. **2018**, *130*, 2964–2968

[1] R. J. Gillespie, *VSEPR Model of Molecular Geometry*, Dover Publications, Mineola, **2013**.
[2] R. Hoffmann, B. F. Beier, E. L. Muetterties, A. R. Rossi, *Inorg. Chem.* **1977**, *16*, 511–522.
[3] A.-R. Mahjoub, T. Drews, K. Seppelt, *Angew. Chem. Int. Ed. Engl.* **1992**, *31*, 1036–1039; *Angew. Chem.* **1992**, *104*, 1047–1050.
[4] K. O. Christe, D. A. Dixon, J. C. P. Sanders, G. J. Schrobilgen, W. W. Wilson, *J. Am. Chem. Soc.* **1993**, *115*, 9461–9467.
[5] R. D. Burbank, F. N. Bensey, *J. Chem. Phys.* **1957**, *27*, 981–982.
[6] G. W. Drake, D. A. Dixon, J. A. Sheehy, J. A. Boatz, K. O. Christe, *J. Am. Chem. Soc.* **1998**, *120*, 8392–8400.
[7] T. Vogt, A. N. Fitch, J. K. Cockcroft, *Science* **1994**, *263*, 1265–1267.
[8] M. V. Bennett, J. R. Long, *J. Am. Chem. Soc.* **2003**, *125*, 2394–2395.
[9] M.-J. Crawford, A. Ellern, P. Mayer, *Angew. Chem. Int. Ed.* **2005**, *44*, 7874–7878; *Angew. Chem.* **2005**, *117*, 8086–8090.
[10] J. L. Hoard, *J. Am. Chem. Soc.* **1939**, *61*, 1252–1259.
[11] R. Haiges, J. A. Boatz, M. Yousufuddin, K. O. Christe, *Angew. Chem. Int. Ed.* **2007**, *46*, 2869–2874; *Angew. Chem.* **2007**, *119*, 2927–2932.
[12] A. Ellern, A.-R. Mahjoub, K. Seppelt, *Angew. Chem. Int. Ed. Engl.* **1996**, *35*, 1123–1125; *Angew. Chem.* **1996**, *108*, 1198–1200.
[13] S. Giese, K. Seppelt, *Angew. Chem. Int. Ed. Engl.* **1994**, *33*, 461–463; *Angew. Chem.* **1994**, *106*, 473–475.

 © 2018 Wiley-VCH Verlag GmbH & Co. KGaA, Weinheim

[14] B. Roessler, K. Seppelt, *Angew. Chem. Int. Ed.* **2000**, *39*, 1259–1261; *Angew. Chem.* **2000**, *112*, 1326–1329.
[15] Y. Du, M. Yang, J. Yu, Q. Pan, R. Xu, *Angew. Chem. Int. Ed.* **2005**, *44*, 7988–7990; *Angew. Chem.* **2005**, *117*, 8202–8204.
[16] A. R. Mahjoub, K. Seppelt, *Angew. Chem. Int. Ed. Engl.* **1991**, *30*, 323–324; *Angew. Chem.* **1991**, *103*, 309–311.
[17] A. R. Mahjoub, D. Leopold, K. Seppelt, *Eur. J. Solid State Inorg. Chem.* **1992**, *29*, 635–647.
[18] G. D. Sturgeon, R. A. Penneman, F. Kruse, L. B. Asprey, *Inorg. Chem.* **1965**, *4*, 748–750.
[19] B. Scheibe, S. Lippert, S. S. Rudel, M. R. Buchner, O. Burghaus, C. Pietzonka, M. Koch, A. J. Karttunen, F. Kraus, *Chem. Eur. J.* **2016**, *22*, 12145–12153.
[20] J. Selbin, J. D. Ortego, *Chem. Rev.* **1969**, *69*, 657–671.
[21] *The Chemistry of the Actinide and Transactinide Elements* (Eds.: L. R. Morss, N. M. Edelstein, J. Fuger, J. J. Katz), Springer, Dordrecht, **2006**.
[22] A. Rosenzweig, D. T. Cromer, *Acta Crystallogr.* **1967**, *23*, 865–867.
[23] P. G. Eller, A. C. Larson, *Inorg. Chim. Acta* **1979**, *37*, 129–133.
[24] R. R. Ryan, R. A. Penneman, L. B. Asprey, R. T. Paine, *Acta Crystallogr. Sect. B* **1976**, *32*, 3311–3313.
[25] M. Atanasov, D. Ganyushin, K. Sivalingam, F. Neese in *Molecular Electronic Structures of Transition Metal Complexes II* (Eds.: D. M. P. Mingos, P. Day, J. P. Dahl), Springer Berlin Heidelberg, Berlin, **2011**, pp. 149–220.
[26] F. Neese, *WIREs Comput. Mol. Sci.* **2012**, *2*, 73–78.
[27] F. Neese, *WIREs Comput. Mol. Sci.* **2017**, e1327.
[28] C. E. Schäffer, C. K. Jørgensen, *Mol. Phys.* **1965**, *9*, 401–412.
[29] W. Urland, *Chem. Phys.* **1976**, *14*, 393–401.
[30] S. T. Liddle, *Angew. Chem. Int. Ed.* **2015**, *54*, 8604–8641; *Angew. Chem.* **2015**, *127*, 8726–8764.
[31] M. J. Reisfeld, G. A. Crosby, *Inorg. Chem.* **1965**, *4*, 65–70.
[32] H.-D. Amberger, W. Grape, E. Stumpp, *J. Less-Common Met.* **1983**, *95*, 181–190.
[33] D. R. Kindra, W. J. Evans, *Chem. Rev.* **2014**, *114*, 8865–8882.
[34] J. Mulak, Z. Zolnierek, *Bull. Acad. Pol. Sci. Ser. Sci. Chim.* **1972**, *20*, 1081–1086.
[35] W. Rüdorff, H. Leutner, *Justus Liebigs Ann. Chem.* **1960**, *632*, 1–7.
[36] N. Nguyen-Hoang, A. J. Dianoux, H. Marquet-Ellis, P. Plurien, *C. R. Hebd. Seances Acad. Sci.* **1965**, *260*, 1963–1966.
[37] R. K. Rosen, R. A. Andersen, N. M. Edelstein, *J. Am. Chem. Soc.* **1990**, *112*, 4588–4590.
[38] G. Nocton, P. Horeglad, J. Pécaut, M. Mazzanti, *J. Am. Chem. Soc.* **2008**, *130*, 16633–16645.
[39] L. P. Spencer, E. J. Schelter, P. Yang, R. L. Gdula, B. L. Scott, J. D. Thompson, J. L. Kiplinger, E. R. Batista, J. M. Boncella, *Angew. Chem. Int. Ed.* **2009**, *48*, 3795–3798; *Angew. Chem.* **2009**, *121*, 3853–3856.
[40] P. L. Arnold, G. M. Jones, S. O. Odoh, G. Schreckenbach, N. Magnani, J. B. Love, *Nat. Chem.* **2012**, *4*, 221–227.
[41] D. M. King, F. Tuna, E. J. L. McInnes, J. McMaster, W. Lewis, A. J. Blake, S. T. Liddle, *Science* **2012**, *337*, 717–720.
[42] A.-C. Schmidt, F. W. Heinemann, W. W. Lukens, K. Meyer, *J. Am. Chem. Soc.* **2014**, *136*, 11980–11993.
[43] O. Kahn, *Molecular Magnetism*, Wiley-VCH, New York, **2001**.
[44] R. Dovesi, R. Orlando, A. Erba, C. M. Zicovich-Wilson, B. Civalleri, S. Casassa, L. Maschio, M. Ferrabone, M. De La Pierre, P. D'Arco, Y. Noel, M. Causa, M. Rerat, B. Kirtman, *Int. J. Quantum Chem.* **2014**, *114*, 1287–1317.
[45] R. Dovesi, V. R. Saunders, C. Roetti, R. Orlando, C. M. Zicovich-Wilson, F. Pascale, B. Civalleri, K. Doll, N. M. Harrison, I. J. Bush, P. D'Arco, M. Llunell, M. Causà, Y. Noël, CRYSTAL14 User's Manual, University of Torino, Torino, **2014**.

Manuscript received: January 18, 2018
Accepted manuscript online: January 24, 2018
Version of record online: February 14, 2018

 © 2018 Wiley-VCH Verlag GmbH & Co. KGaA, Weinheim

Angewandte Chemie
Eine Zeitschrift der Gesellschaft Deutscher Chemiker

Supporting Information

The $[U_2F_{12}]^{2-}$ Anion of $Sr[U_2F_{12}]$

*Benjamin Scheibe, Clemens Pietzonka, Otto Mustonen, Maarit Karppinen, Antti J. Karttunen, Mihail Atanasov, Frank Neese, Matthias Conrad, and Florian Kraus**

anie_201800743_sm_miscellaneous_information.pdf

Supporting Information

Experimental Section

General: All operations were performed in either stainless steel (316L) or monel metal Schlenk lines, which were passivated with 100% fluorine at various pressures before use. Preparations were carried out in an atmosphere of dry and purified argon (5.0, Praxair). Hydrogen fluoride (99%, Hoechst) was dried over K_2NiF_6 prior to its use. β-UF_5 was prepared by photoreduction of UF_6 with CO in a fused quartz apparatus, according to a literature procedure.[1,2]

Preparation of $Sr[U_2F_{12}]$: In a typical reaction β-UF_5 (251.7 mg, 756 µmol) and SrF_2 (47.39 mg, 377 µmol) were placed in a FEP reaction tube and approximately 3 mL of anhydrous HF were added to the mixture. Reaction took place at room temperature and a light blue solution was obtained after a few minutes reaction time. Pastel green crystals of $Sr[U_2F_{12}]$ (see Figure S1) were obtained from this solution by slow distillation of HF into a separate FEP tube.

Figure S1. A sample of $Sr[U_2F_{12}]$ sealed in a quartz tube.

Single-crystal X-ray diffraction: X-ray structure analysis of single crystals of $Sr[U_2F_{12}]$ was carried out with a IPDS 2T diffractometer (STOE & Cie) with monochromated molybdenum radiation (MoK_α, λ = 0.71073 Å) and an image plate detector. Evaluation and integration of the diffraction data was carried out by using the Stoe & Cie X-Area software, and an absorption correction was applied (integration).[3] The structure was solved by using Direct Methods (SHELXT) in the space group type *I*4/*mcm* (140), and refined against F^2 (SHELXLE).[4,5] All atoms were located by difference Fourier synthesis and refined anisotropically. Representations of the crystal structure were created by using the Diamond software.[6] Further details of the crystal structure investigation can be obtained from the Fachinformationszentrum Karlsruhe, 76344 Eggenstein-Leopoldshafen, Germany (fax: (+49) 7247-808-666; email: crysdata@fiz-karlsruhe.de, http://www.fiz-karlsruhe.de/request_for_deposited_data.html) on quoting the depository number CSD-433765.

IR and Raman Spectroscopy: The IR spectrum was measured on an FTIR spectrometer (Bruker alpha) by using a diamond ATR unit under an Ar atmosphere in a glovebox. The spectrum was processed with the OPUS software package.[7] The Raman spectrum was collected by using a Labram HR800 (JobinYvon) instrument equipped with a 25 mW He/Ne laser tube (λ = 632.817 nm). The collected data were handled with the LabSpec software.[8]

Absorption spectroscopy: The absorption spectrum was measured with a Cary 5000 UV/VIS/NIR spectrometer (Agilent Technologies). For the measurement, a Praying Mantis (Harrick Scientific Prodcuts) was used. The air-tight chamber was loaded with the sample in a glove box. The spectrum was

measured with a reduced slit height at room temperature with a resolution of 1 nm and a scan rate of 2 nm/s. A zero- and baseline correction was applied.

Magnetic measurements: DC-magnetic data of $Sr[U_2F_{12}]$ were collected with the aid of the VMS option of a physical property measurement system (ppms) of LOT-Quantum Design. Field- and temperature dependent magnetic data were recorded, the former in the range of −9 to 9 T at constant temperatures of 1.8, 5, 10 and 15 K, the latter in the range from 1.8 K to 300 K with an applied field of 0.1 T.
The collected data were corrected with respect to the diamagnetic moment of the sample holder, as well as to the diamagnetic contribution ($\chi_{dia} = -2.085 \cdot 10^{-4}$ cm^3mol^{-1}) of the sample derived from Pascal constants taking into account the composition of $Sr[U_2F_{12}]$, the result being the net paramagnetic data.[9]

Crystallographic data of $Sr[U_2F_{12}]$

Further details of the crystal structure investigation can be obtained from the Fachinformationszentrum Karlsruhe, 76344 Eggenstein-Leopoldshafen, Germany (fax: (+49) 7247-808-666; E-Mail: crysdata@fiz-karlsruhe.de, http://www.fiz-karlsruhe.de/request_for_deposited_data.html) on quoting the depository number CSD-433765.

Due to the high absorption coefficient of 39.15 mm^{-1} (Mo-K_α) for $Sr[U_2F_{12}]$, for comparison: organic compounds usually have a μ of <1 mm^{-1} (Mo-K_α), a high residual electron density remains, even after absorption correction.

Table S1. Selected crystallographic data for $Sr[U_2F_{12}]$, CSD-433765.

	$Sr[U_2F_{12}]$
Empirical formula	$F_{12}SrU_2$
Color and appearance	yellowish block
Crystal size / mm^3	0.18 · 0.15 · 0.09
Molar mass / $g \cdot mol^{-1}$	791.68
Crystal system	tetragonal
Space group type (No.)	*I*4/*mcm* (140)
a / Å	9.2149(13)
c / Å	11.361(2)
V / $Å^3$	964.7(3)
Z	4
$\rho_{calcd.}$ / $g \cdot cm^{-3}$	5.45
λ / Å	0.71073 (Mo-K_α)
T / K	100(2)
μ / mm^{-1}	39.15 (Mo-K_α)
θ_{max}	34.90
hkl_{max}	$-14 \leq h \leq 13$
	$-14 \leq k \leq 14$
	$-18 \leq l \leq 18$
R_{int}, R_σ	0.097, 0.038
$R(F)$ ($I \geq 2\sigma(I)$, all data)	0.045, 0.045
$wR(F^2)$ ($I \geq 2\sigma(I)$, all data)	0.100, 0.100
S (all data)	1.34
Data, parameter, restraints	591, 25, 0
$\Delta\rho_{max}$, $\Delta\rho_{min}$ / $e \cdot Å^{-3}$	5.84, −4.00

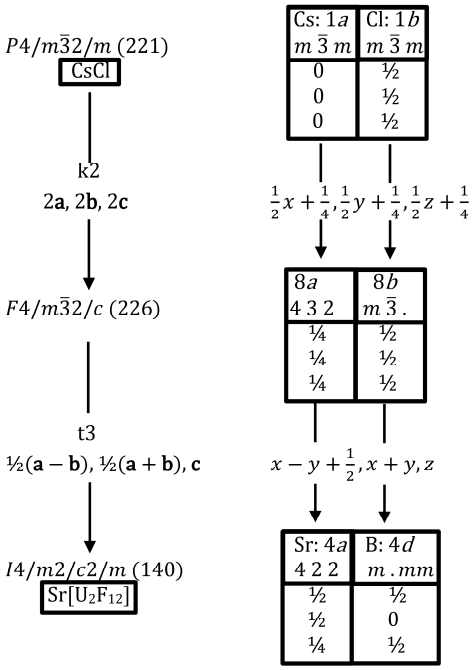

Scheme S1. Bärnighausen-Tree for $Sr[U_2F_{12}]$ showing its structural relationship to the CsCl structure type. The center of gravity of the anion is regarded as “B”.

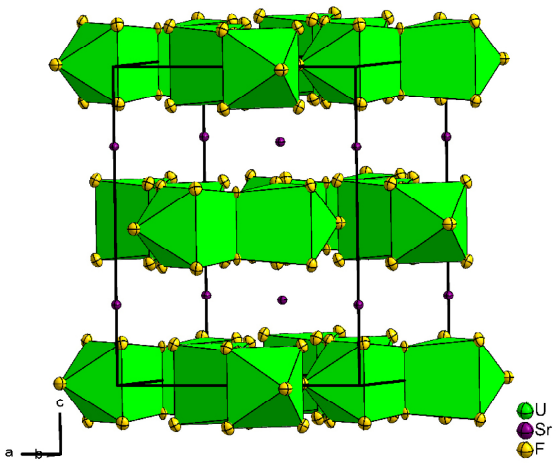

Figure S2. The crystal structure of $Sr[U_2F_{12}]$. Displacement ellipsoids are shown at a 70% probability level at 100 K, the first coordination sphere of the U atoms are shown as green polyhedra.

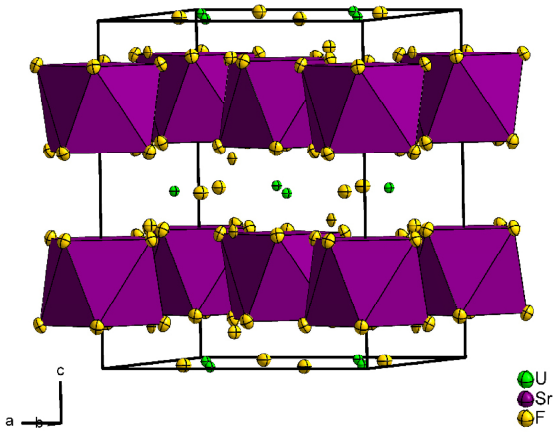

Figure S3. Section of the crystal structure of $Sr[U_2F_{12}]$. Displacement ellipsoids are shown at a 70% probability level at 100 K, the first coordination sphere of the Sr atoms are shown as purple polyhedra.

Magnetic measurements

The measured sample of $Sr[U_2F_{12}]$ shows an antiferromagnetic behavior. The field dependent measurement shows magnetic saturation up to 10 K (Figure S4). At 15 K a linear course with the molar susceptibility of $\chi_m = 3.8300(5)\cdot10^{-3}$ cm^3mol^{-1} was determined from the slope of the magnetization data versus the applied field.

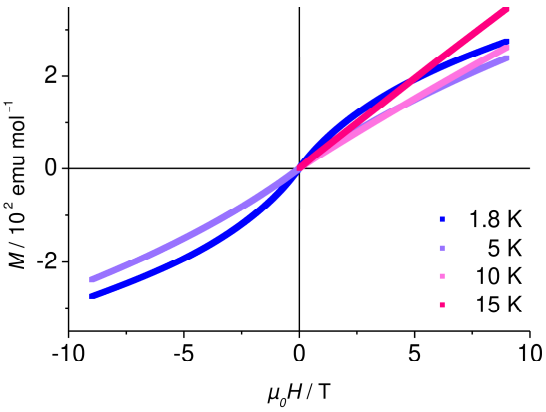

Figure S4. Field dependent magnetic data of $Sr[U_2F_{12}]$ at different temperatures.

In order to receive unbiased susceptibility data, the temperature dependent magnetization was recorded with an applied field of 0.1 T, were magnetic saturation may be neglected. The magnetic susceptibility shows a maximum at 26.4 K, see Figure S5.

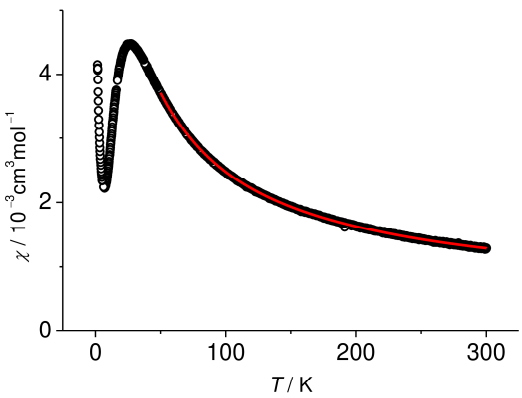

Figure S5. Molar susceptibility versus temperature plot of $Sr[U_2F_{12}]$, measured with an applied field of 0.1 T and a Curie-Weiss-fitting curve (red).

To obtain information on the effective magnetic moment (μ_{eff}), temperature independent paramagnetism (*TIP*) and the Weiss constant (Θ), a modified Curie-Weiss law (Equation 1) was used to fit the data in the temperature range of 50 to 300 K.

$$\chi_{tot} = \chi_{TIP} + \chi_{CW} \tag{1}$$

With χ_{CW} being expressed by the Curie-Weiss law (Equation 2).

$$\chi_{CW} = \frac{C}{T - \Theta} \tag{2}$$

Wherein C represents the Curie constant (Equation 3).

$$C = \frac{n_{\mathrm{eff}}^2 \; N_A \; \mu_0 \; \mu_B^2}{3 \; k_B} \tag{2}$$

Where n_{eff} is the number of effective magnetic moments in units of Bohr magnetons, N_A is Avogadro's number, the magnetic constant is denoted by μ_0, μ_B represents the Bohr magneton and k_B the Boltzmann constant. By converting Equation 1, data from the reciprocal susceptibility versus temperature curve, or the χT versus T curve, have also been used to calculate the mentioned parameters above. Figure S6 shows data of the temperature dependent scan in different representations as well as the corresponding fitting curves. The resulting values being $TIP = 4.90(9) \cdot 10^{-4}$ cm^3 mol^{-1}, $n_{eff} = 1.02(1)$ μ_B per uranium atom and $\Theta = -32(2)$ K. The negative value for Θ indicates an antiferromagnetic interaction between the uranium atoms within the $[U_2F_{12}]^{2-}$ ion.

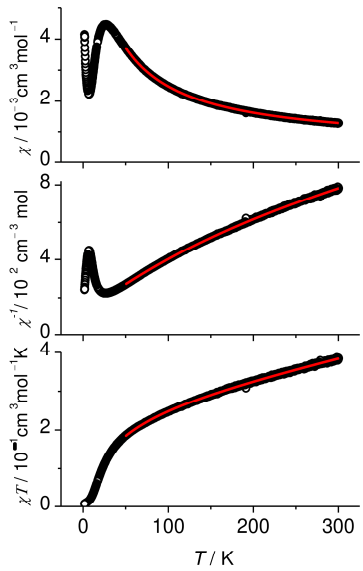

Figure S6. Temperature dependent scan of $Sr[U_2F_{12}]$ at an applied field of 0.1 T and corresponding fitting curves (red).

The temperature dependent development of the effective magnetic moment per formula unit in Bohr magnetons is shown in Figure 4 of the main text. Assuming the spin state $S = 1/2$ for each U(V) atom in the dinuclear complex $[U_2F_{12}]^{2-}$, based on the Heisenberg–Dirac-van Vleck operator (Equation 4), the following Equation 5 allows to fit the temperature dependent molar susceptibility using the parameters J_K, g, χ_0 and x_{mon}, which is a weighting factor for the monomeric part.

$$\hat{H}_{HDvV} = -\sum_{i<j} J_{ij}\, S_i S_j \tag{4}$$

Where J_K represents the exchange interaction energy in Kelvin, g the Landé factor, χ_0 a temperature independent contribution to the susceptibility and x_{mon} is the amount of a contribution of mononuclear U(V) impurities to the susceptibility. A fitting of the χ_m vs T data, based on Equation 5, is shown in Figure S7.

$$\chi_m = (1 - x_{mon}) \cdot 2 \frac{N_A \mu_B^2}{k_B T} g^2 \frac{\exp\left\{\frac{J_K}{T}\right\}}{1 + 3\exp\left\{\frac{J_K}{T}\right\}} + x_{mon} \frac{N_A \mu_B^2}{3\, k_B T} n_{eff}^2 + \chi_0 \tag{5}$$

The significant paramagnetic contribution to the susceptibility may be attributed to the additional phase $Sr[UF_5(FHF)_2]$, which will be reported elsewhere. The amount of this phase (χ_{mon}) is depending on the assumed n_{eff}, which is used in the second term of Equation 5. For $n_{eff} = 2.535\ \mu_B$, which is the theoretical value, χ_0 might be a contribution due to van Vleck temperature-independent paramagnetism originated from excited-state mixing.[10] The following results for the above mentioned parameters are obtained $J_k = -29.86(5)\ cm^{-1}$, $g = 1.014(1)$, $\chi_0 = 7.00(3) \cdot 10^{-4}\ cm^3\ mol^{-1}$ and $x_{mon} = 0.00808(3)$. Using the value from the Curie-Weiss-fit, $n_{eff} = 1.02(1)\ \mu_B$ per uranium atom, leads to $J_k = -29.86(5)\ cm^{-1}$, $g = 1.036(1)$, $\chi_0 = 7.00(3) \cdot 10^{-4}\ cm^3\ mol^{-1}$ and $x_{mon} = 0.0499(2)$.

This means the content of $Sr[UF_5(FHF)_2]$ is in the range of 1 to 5%. A similar treatment was used in the case of an imido diuranium complex, containing uranium (V) atoms.[11,12] The uranium atoms in the dimeric uranium (V) complex, $[\{U(NtBu)_2(I)(tBu_2bpy)\}_2]$, being similarly connected like the ones in the $[U_2F_{12}]^{2-}$ ion.[10]

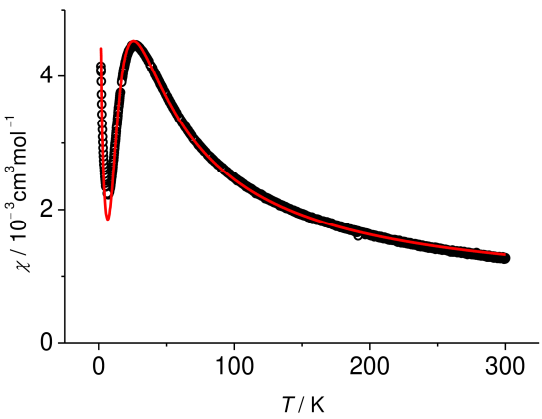

Figure S7. Molar susceptibility of $Sr[U_2F_{12}]$ measured with an applied field of 0.1 T and a HDvV-fitting curve (red).

An alternative route to estimate the amount of the monomeric impurity, exists in analyzing the field dependent data at low temperatures, which are displayed in Figure S4. Assuming the magnetization of the antiferromagnetic phase of $Sr[U_2F_{12}]$ behaves linear with the applied field, the magnetic saturation, which is observed from 1.8 to 10 K, originates from the secondary phase of $Sr[UF_5(FHF)_2]$. To explain the magnetic behavior in the mentioned temperature range, a suitable modified Brillouin-function was applied (Equation 6).

$$M_m = x_{mon}\, M_m^{\infty}\, B_J(\alpha) + B\, \chi_{AF} \tag{6}$$

With $B_J(\alpha)$ being defined in Equation 7, α in Equation 8 and M_m^{∞} in Equation 9.

$$B_J(\alpha) = \left\{\frac{2J+1}{2J}\ \coth\left(\left(\frac{2J+1}{2J}\right)\alpha\right) - \frac{1}{2J}\ \coth\left(\frac{\alpha}{2J}\right)\right\} \tag{7}$$

$$\alpha = \frac{g_J\, J\, \mu_B\, B}{k_B\, T} \tag{8}$$

$$M_m^{\infty} = N_A\, g_J\, J\, \mu_B \tag{9}$$

Where the used parameters are the following, M_m being the molar magnetization depending on external field and temperature, M_m^{∞} is the molar magnetic saturation, $B_J(\alpha)$ denotes the Brillouin term within the total angular momentum quantum number J, B is the external applied field, T the temperature, g_J the Landé factor depending on J, μ_B the Bohr magneton, k_B is the Boltzmann constant, χ_{AF} marks the molar susceptibility of $Sr[U_2F_{12}]$ at the relevant temperature and x_{mon} the amount of the secondary phase. Figure S8 shows the fitting lines to the molar magnetization data at 1.8 and 5 K.

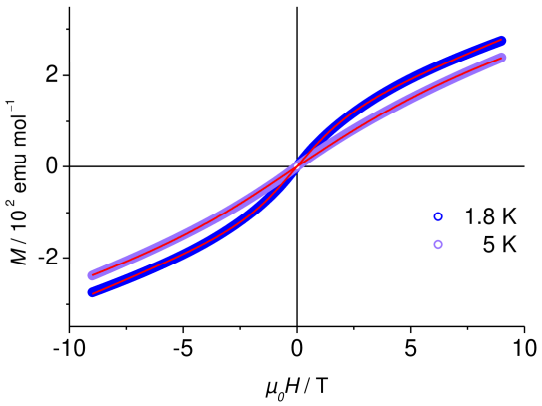

Figure S8. Field dependent data of $Sr[U_2F_{12}]$ with fitting lines (red) resulting from applying the modified Brillouin function (Equation 6).

Giving J and g_J the theoretical values of $\frac{5}{2}$ and $\frac{6}{7}$, appropriate to the $^2F_{5/2}$ ground state, and the relevant temperature to T, the following values for x_{mon} were obtained: 0.008 at 1.8 K and 0.011 at 5 K. This is in the same order like the results from the HDvV-calculations. The same method was used to calculate the amount of paramagnetic impurities incorporated in nonmagnetic Sr_2YIrO_6 single crystals.[13]

Quantum chemical solid-state calculations on $Sr[U_2F_{12}]$.

Computational details

We carried out periodic quantum chemical calculations on $Sr[U_2F_{12}]$ using the PBE0 hybrid density functional method (DFT).[14,15] We applied a triple-zeta-valence (TZVP) level basis set for U and a split-valence + polarization (SVP) level basis for the other atoms. The basis sets for U and F, derived from the Karlsruhe def2 basis sets, were taken from our previous study on $NOUF_6$.[16,17] The basis set for Sr was derived from the def2-SVP basis set for this study (details and full basis set listing below). All calculations were carried out using the CRYSTAL14 program package.[18,19] The reciprocal space was sampled using a 3x3x3 Monkhorst-Pack-type *k*-point grid. All calculations were run as spin-unrestricted (the magnetic ground state is described in detail below). For the evaluation of the Coulomb and exchange integrals (TOLINTEG), tight tolerance factors of 8, 8, 8, 8, and 16 were used. Both the atomic positions and lattice constants were fully optimized within the constraints imposed by the space group symmetry. Default optimization convergence thresholds and an extra large integration grid (XLGRID) for the DFT part were applied in all calculations.

The harmonic vibrational frequencies were obtained by using the computational scheme implemented in CRYSTAL.[20,21] The Raman intensities were obtained using the scheme implemented in CRYSTAL14.[22,23] The predicted spectra are based on the harmonic approximation and the wavenumbers have been scaled by a factor of 0.95 to account for the overestimation typical for predicted harmonic frequencies.[24] The Raman intensities have been calculated for a polycrystalline powder sample (total isotropic intensity in arbitrary units). The Raman final spectrum was obtained by using pseudo-Voigt peak profile (50:50 Lorenzian:Gaussian) and FWHM of 8 cm^{-1}. When simulating the Raman spectrum, the temperature and laser wavelength were set to values corresponding to the experimental setup (T = 298.15 K, λ = 632.8 nm). For the IR spectrum, a Lorentzian lineshape and a FWHM of 8 cm^{-1} was used. The peak assignment was carried out by visual inspection of the normal modes (Jmol program package).[25]

Magnetic ground state of $Sr[U_2F_{12}]$

Each U atom in the $[U_2F_{12}]^{2-}$ anion of $Sr[U_2F_{12}]$ has one unpaired f-electron. We investigated spin configurations where the spins on the two U atoms are 1) both α (ferromagnetic, / FM); 2) α and β (antiferromagnetic / AFM). The ferromagnetic case could be studied in the original space group *I*4/*mcm* (140) but for the antiferromagnetic case, the symmetry had to be decreased as *I*4/*mcm* (140) -> *Ibam* (72) -> *Ima*2 (46). When the symmetry is decreased, the number of symmetry operations decreases from 16 to 4 and the Wyckoff position 8*h* occupied by the U atoms splits to 4*b* + 4*b* in the orthorhombic subgroup *Ima*2. This symmetry breaking and splitting of the Wyckoff position enables the antiferromagnetic spin configuration. We investigated different initial f-orbital occupation schemes (keyword FDOCCUP), but the majority of the calculations converged in the lowest energy spin configuration and few calculations ended up in states with significantly higher energy (> 100 kJ/mol).

The AFM configuration turned out to be the magnetic ground state, the ferromagnetic state being 67 cm^{-1} higher in energy. This energy difference is in a reasonable agreement with the energy difference of 75.7 cm^{-1} predicted by the much more sophisticated NEVPT2 multi-configuration *ab initio* method discussed below. The spin density of the AFM ground state, arising from the unpaired f-electrons of the uranium atoms, is illustrated in Figure S9. The results discussed below have been obtained for the antiferromagnetic ground state.

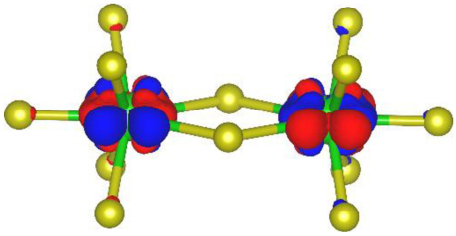

Figure S9. Spin density of the antiferromagnetic ground state of the $[U_2F_{12}]^{2-}$ anion in $Sr[U_2F_{12}]$. α and β spin density are shown as blue and red isosurface, respectively (isodensity value 0.01 a.u.). Only a section of the crystal structure with one $[U_2F_{12}]^{2-}$ anion is shown. Green = U, yellow = F.

Optimized structural parameters of $Sr[U_2F_{12}]$

Full geometry optimization of $Sr[U_2F_{12}]$ in the orthorhombic subgroup *Ima*2 results in lattice parameters *a* = *b* = 9.10 Å and *c* = 11.57 Å in terms of the tetragonal space group *I*4/*mcm* (optimized geometry included below). The deviation from ideal tetragonal symmetry is less than 0.03%. The optimized structure is in reasonable agreement with the experimental X-Ray structure, the differences in the lattice parameters *a* and *c* being –1.2% and 1.8%. The predicted U–F distances are 2.07, 2.08, and 2.27 Å, in very good agreement with the the corresponding X-ray distances of 2.08, 2.08, and 2.28 Å. The predicted U−F−U angle of 117.3° is also in good agreement with the experimental value of 117.1°.

To get a qualitative picture of the bonding in $Sr[U_2F_{12}]$, we investigated the partial atomic charges with the Hirshfeld and Mulliken schemes. The Hirshfeld partial atomic charges (e^-) are: U = +2.6, Sr = +1.4, F(1) = –0.6, F(2) = –0.5, F(3) = –0.6. The Mulliken partial atomic charges (e^-) are: U = +2.2, Sr = +1.4, F(1) = F(2) = F(3) = –0.5. The predicted charges are in agreement with each other and also in line with the electronegativities and oxidation states of the atoms. The Mulliken overlap populations between various atoms are as follows (in e^- units): U–F(terminal) = 0.13, U–F(bridging) = 0.08, and Sr–F = 0.05. The overlap populations should be considered only in a qualitative way, but they suggest that the U–F bonds are rather ionic, as expected. The U–F(bridging) bonds are possibly slightly more ionic in comparison to the non-bridging U–F bonds. The results of the population analyses are very well in line with the results previously obtained for $UF_5 \cdot 2HCN$.[26]

DFT-PBE0 Raman and IR spectra of $Sr[U_2F_{12}]$

The DFT-PBE0 Raman and IR spectra of $Sr[U_2F_{12}]$ are shown in Figure S10 and Figure S11 together with the experimental spectra, the observed bands are listed in Table S2. The predicted Raman spectrum corresponds well to the experimental spectrum, enabling the interpretation of the spectral data (Table S3). In the case of the IR spectrum, only the first few peaks a properly resolved in the experiments, hindering the comparison between theory and experiment.

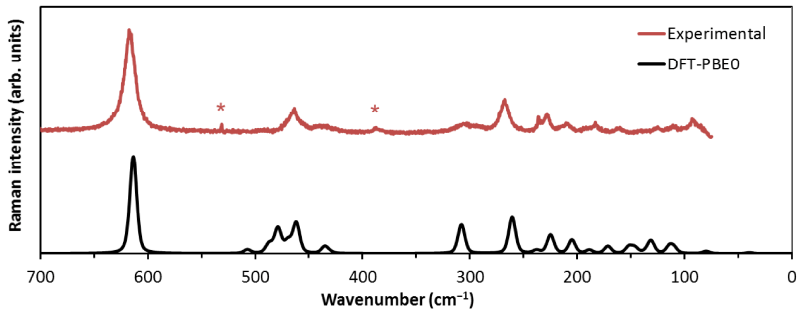

Figure S10. Measured and predicted Raman spectrum of polycrystalline $Sr[U_2F_{12}]$ at room temperature. Asterisks denote artifact signals or signals of FEP.

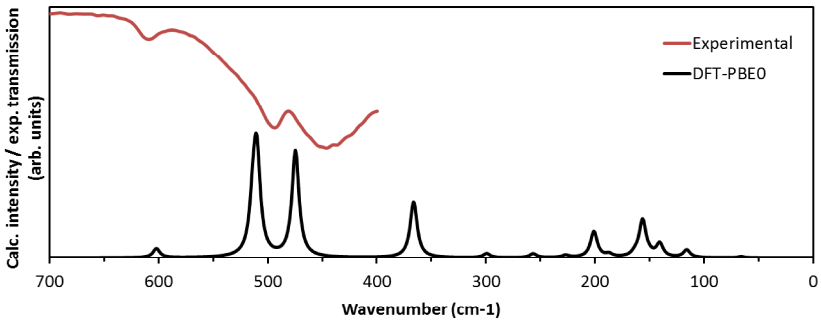

Figure S11. Measured room temperature ATR-IR spectrum and predicted IR spectrum of $Sr[U_2F_{12}]$.

Table S2. Observed peaks in the measured IR and Raman spectra. All values are given in cm^{-1}.

Raman active mode	IR active mode	Assignment
619	612	Symmetric U−F stretch
464, 436	493, 445	Antisymmetric U−F stretch
304, 267	-	U−F bending

Table S3. Peak assignment for the Raman and IR spectra. The data have been calculated for the AFM ground state (space group *Ima*2). The irreducible representations have been converted to the original space group (*I*4/*mcm* with point group D_{4h}).

Freq. (cm-1)	IR intensity (arb. units)	Raman intensity (arb. units)	Assignment	irrep (D_{4h})
620	0.1	13.4	Symmetric U-F stretch for F1 and F2. Same phase for U atoms.	B2g
614	0.1	1000.0	Symmetric U-F stretch for F1 and F2. Same phase for U atoms.	A1g
602	100.0	0.5	Symmetric U-F stretch for F1, F2, F3. Different phase for U atoms.	Eu
602	106.1	0.0	Symmetric U-F stretch for F1, F2, F3. Different phase for U atoms.	Eu
555	0.0	0.0	Antisymmetric U-F stretch for F2. Different phase for U atoms.	A1u
518	2.1	0.0	Antisymmetric U-F stretch for F2. Different phase for U atoms.	A2g
513	549.9	0.0	Antisymmetric U-F stretch for F1 and F2. Same phase for U atoms.	Eu
513	575.4	0.1	Antisymmetric U-F stretch for F1 and F2. Same phase for U atoms.	Eu
510	2068.5	0.4	Antisymmetric U-F stretch for F2. Same phase for U atoms.	A2u
507	38.6	17.6	Antisymmetric U-F stretch for F2. Different phase for U atoms.	Eg
507	0.0	20.6	Antisymmetric U-F stretch for F2. Different phase for U atoms.	Eg
494	0.0	0.0	Antisymmetric U-F stretch for F2. Same phase for U atoms.	B1u
487	0.1	91.9	Antisymmetric U-F stretch for F2. Different phase for U atoms.	B1g
478	30.4	244.8	Antisymmetric U-F stretch for F1 and F3. Same phase for U atoms	A1g
474	1157.8	6.1	Antisymmetric U-F stretch for F1, F3, F2. Different phase for U atoms	Eu
474	1185.5	1.9	Antisymmetric U-F stretch for F1, F3, F2. Different phase for U atoms	Eu
469	20.0	114.9	Antisymmetric U-F stretch for F1 and F2. Same phase for U atoms	B2g
462	0.0	153.4	Antisymmetric U-F stretch for F2. Same phase for U atoms.	Eg
461	0.0	156.8	F3 stretching/bending, also F2. Same phase for U atoms.	Eg
436	0.0	75.5	Antisymmetric U-F stretch for F2. Different phase for U atoms.	A1g
435	0.2	0.1	F3 stretching/bending, also F2. Same phase for U atoms.	B2u
431	0.0	9.5	Antisymmetric U-F stretch for F2. Different phase for U atoms.	B2g
367	630.5	0.0	F2 stretching/bending	Eu
367	623.4	0.0	F2 stretching/bending	Eu
318	0.0	0.0	F2 stretching/bending	B1u
309	0.0	147.6	F2 stretching/bending	Eg
309	0.0	148.6	F2 stretching/bending	Eg
301	93.3	0.0	F2 stretching/bending	A2u
262	0.0	0.0	U-F bending, at low energies, coupled with Sr atoms	B1u
261	0.1	368.7	U-F bending, at low energies, coupled with Sr atoms	B1g
258	49.0	3.0	U-F bending, at low energies, coupled with Sr atoms	Eg
258	0.0	0.7	U-F bending, at low energies, coupled with Sr atoms	Eg
257	37.7	0.1	U-F bending, at low energies, coupled with Sr atoms	Eu
257	0.0	0.7	U-F bending, at low energies, coupled with Sr atoms	Eu
241	0.0	0.2	U-F bending, at low energies, coupled with Sr atoms	A2g
238	0.0	35.4	U-F bending, at low energies, coupled with Sr atoms	B2g
229	27.4	0.0	U-F bending, at low energies, coupled with Sr atoms	Eu
228	3.6	170.2	U-F bending, at low energies, coupled with Sr atoms	A1g
227	19.8	17.9	U-F bending, at low energies, coupled with Sr atoms	Eu
224	5.7	0.0	U-F bending, at low energies, coupled with Sr atoms	A2u
210	0.4	2.9	U-F bending, at low energies, coupled with Sr atoms	B2u

207	0.0	63.7	U-F bending, at low energies, coupled with Sr atoms	Eg
205	0.0	73.9	U-F bending, at low energies, coupled with Sr atoms	Eg
203	275.4	0.5	U-F bending, at low energies, coupled with Sr atoms	Eu
203	285.0	0.0	U-F bending, at low energies, coupled with Sr atoms	Eu
195	0.3	0.1	U-F bending, at low energies, coupled with Sr atoms	A2g
189	2.1	33.3	U-F bending, at low energies, coupled with Sr atoms	A2g
188	56.2	0.0	U-F bending, at low energies, coupled with Sr atoms	A2u
184	1.9	0.1	U-F bending, at low energies, coupled with Sr atoms	Eg
184	0.0	0.1	U-F bending, at low energies, coupled with Sr atoms	Eg
181	0.0	0.4	U-F bending, at low energies, coupled with Sr atoms	A1u
175	0.0	72.5	U-F bending, at low energies, coupled with Sr atoms	B2g
166	17.3	0.1	Tilting and twisting of the [U2F12]2- anions. At low energies, coupled with Sr atoms	Eu
164	0.5	0.1	Tilting and twisting of the [U2F12]2- anions. At low energies, coupled with Sr atoms	Eu
163	28.9	0.0	Tilting and twisting of the [U2F12]2- anions. At low energies, coupled with Sr atoms	Eu
162	69.7	0.2	Tilting and twisting of the [U2F12]2- anions. At low energies, coupled with Sr atoms	Eu
160	370.1	0.3	Tilting and twisting of the [U2F12]2- anions. At low energies, coupled with Sr atoms	Eu
158	378.9	0.0	Tilting and twisting of the [U2F12]2- anions. At low energies, coupled with Sr atoms	Eu
154	6.6	31.4	Tilting and twisting of the [U2F12]2- anions. At low energies, coupled with Sr atoms	Eg
154	0.0	27.7	Tilting and twisting of the [U2F12]2- anions. At low energies, coupled with Sr atoms	Eg
151	84.2	4.0	Tilting and twisting of the [U2F12]2- anions. At low energies, coupled with Sr atoms	A2u
151	2.0	52.0	Tilting and twisting of the [U2F12]2- anions. At low energies, coupled with Sr atoms	B1g
146	0.0	0.0	Tilting and twisting of the [U2F12]2- anions. At low energies, coupled with Sr atoms	A2g
145	0.1	0.0	Tilting and twisting of the [U2F12]2- anions. At low energies, coupled with Sr atoms	B1u
142	249.3	0.2	Tilting and twisting of the [U2F12]2- anions. At low energies, coupled with Sr atoms	A2u
138	0.0	4.6	Tilting and twisting of the [U2F12]2- anions. At low energies, coupled with Sr atoms	A2g
138	0.9	0.0	Tilting and twisting of the [U2F12]2- anions. At low energies, coupled with Sr atoms	Eg
135	0.0	1.2	Tilting and twisting of the [U2F12]2- anions. At low energies, coupled with Sr atoms	Eg
132	0.0	19.1	Tilting and twisting of the [U2F12]2- anions. At low energies, coupled with Sr atoms	A1g
132	0.0	0.0	Tilting and twisting of the [U2F12]2- anions. At low energies, coupled with Sr atoms	B1u
131	0.0	95.9	Tilting and twisting of the [U2F12]2- anions. At low energies, coupled with Sr atoms	B2g
119	0.0	0.4	Tilting and twisting of the [U2F12]2- anions. At low energies, coupled with Sr atoms	A1u
117	83.0	4.8	Tilting and twisting of the [U2F12]2- anions. At low energies, coupled with Sr atoms	Eu
114	111.4	0.4	Tilting and twisting of the [U2F12]2- anions. At low energies, coupled with Sr atoms	Eu
113	3.9	62.7	Tilting and twisting of the [U2F12]2- anions. At low energies, coupled with Sr atoms	B1g
113	0.2	26.7	Tilting and twisting of the [U2F12]2- anions. At low energies, coupled with Sr atoms	Eg
112	0.0	24.6	Tilting and twisting of the [U2F12]2- anions. At low energies, coupled with Sr atoms	Eg
90	0.0	0.1	Tilting and twisting of the [U2F12]2- anions. At low energies, coupled with Sr atoms	Eg
89	0.0	0.0	Tilting and twisting of the [U2F12]2- anions. At low energies, coupled with Sr atoms	Eg
84	0.2	0.0	Tilting and twisting of the [U2F12]2- anions. At low energies, coupled with Sr atoms	B2u
79	0.1	29.9	Tilting and twisting of the [U2F12]2- anions. At low energies, coupled with Sr atoms	B1g
70	0.0	0.0	lattice vibrations (low frequency modes spanning the whole lattice)	B1u
67	13.1	0.1	lattice vibrations (low frequency modes spanning the whole lattice)	Eu
66	11.3	0.0	lattice vibrations (low frequency modes spanning the whole lattice)	Eu
40	0.0	5.0	lattice vibrations (low frequency modes spanning the whole lattice)	Eg
40	0.0	4.6	lattice vibrations (low frequency modes spanning the whole lattice)	Eg
31	0.0	0.1	lattice vibrations (low frequency modes spanning the whole lattice)	A2g

Details for the Sr basis set

The Karlsruhe def2-SVP basis set was used as a starting point (28 core electrons described by a pseudopotential).[16] The most diffuse s- and p-type functions were removed (exponents 0.026 and 0.033, respectively). The exponent of the remaining outermost s-type function (0.062) was increased to 0.13 by dividing the second outermost s-exponent of 0.338 by a factor of 2.6. The exponent of the remaining outermost p-type function (0.10) was increased to 0.13 and the outermost s and p functions were combined into a single sp-type function to increase the efficiency of the CRYSTAL code. The most diffuse d function (0.036) was removed and the d-primitives with exponents 0.104 and 0.27 were combined into one primitive with an exponent of 0.22 (geometric mean).

```
Full basis set listing for Sr in CRYSTAL input format
238 6
INPUT
10. 0 2 2 2 1 0
7.400074 135.479430 0
3.606379 17.534463 0
6.484868 88.359709 0
3.288053 15.394372 0
4.622841 29.888987 0
2.246904 6.659414 0
4.633975 -15.805992 0
0 0 3 2.0 1.0
  5.9276428767      0.19698765364
  3.0691274814     -0.64852205985
  0.70675488028     0.62064729022
0 0 1 0.0 1.0
 0.33824024280      1.0000000000
0 1 1 0.0 1.0
 0.13             1.0 1.0
0 2 4 6.0 1.0
  2.4324720000     -0.37145059848
  1.6642340000      0.37856824234
  0.59455471858     0.59874487803
  0.26152621998     0.35314019512
0 3 2 0.0 1.0
  3.6180810000     -0.75010000000E-02
  0.99665600000     0.10809800000
0 3 1 0.0 1.0
  0.22              1.0
```

Optimized structure of $Sr[U_2F_{12}]$ (DFT-PBE0, antiferromagnetic ground state)

Please note that in the orthorhombic subgroup *Ima*2, *a* and *c* axes are interchanged in comparison to the tetragonal space group *I*4/*mcm* (symmetry is reduced to allow the antiferromagnetic ground state).

```
46 (space group)
11.56674238 9.09792373 9.10041995 (lattice constants)
10 (number of atoms in the asymmetric unit, followed by fractional coordinates of each atom)
292   2.500000000000E-01   1.507326167353E-01  -9.924766381289E-02
292  -2.500000000000E-01   3.492673056199E-01   9.924766167527E-02
238   6.807177274890E-18  -1.162459293474E-17   2.499999513460E-01
9     2.500000000000E-01   3.115171642935E-01   6.121535489089E-02
9    -2.500000000000E-01   1.884826308937E-01  -6.121528534439E-02
9     1.268568311829E-01   2.896798339634E-01  -1.907049019763E-01
9     1.268567998658E-01  -2.896796781356E-01  -3.092950332310E-01
9    -1.268285859120E-01   4.405139729972E-01  -3.977262953725E-02
9     3.731714387891E-01   5.948585839323E-02   3.977255561433E-02
9     3.520844120905E-01   5.732608536842E-08  -2.500000002472E-01
```

Ab initio Studies on the Electronic Structure, Magnetic Properties and Optical Spectra of $[U_2F_{12}]^{2-}$

I. Computational details

I.1 Correlated electronic structure calculations of the magnetic and optical properties of $[U_2F_{12}]^{2-}$ and its $[UF_7]^{2-}$ subunit

CASSCF and NEVPT2 calculations on $[U_2F_{12}]^{2-}$ and $[UF_7]^{2-}$ have been carried out using the multireference module of ORCA employing geometries as reported by the X-ray data.[27,28] The Complete Active Space Self-Consistent Field (CASSCF) method is a multi-configuration quantum chemistry method in which the wave function is expanded over all electronic configurations corresponding to a given number of electrons distributed over a given number of orbitals.[29] The so determined set of orbitals and electrons defines the complete active space (CAS), and typically contains the orbitals and electrons responsible for the magnetic and optical properties of the considered molecule. In the case of actinide complexes, it is usually recommended to include all 5f orbitals and associated electrons in the active space. The CASSCF method is known to provide an accurate description of both the ground state and the excited states, and to incorporate all of the non-dynamical correlation, but lacks most of the dynamical correlation. The latter effects can however be added a posteriori using second order perturbation theory (PT2). In this approach, the electronic energies are corrected for dynamical correlation by accounting, in a perturbative scheme by exciting electrons from (to) doubly occupied (empty, virtual) orbitals into (from) the active space orbitals.
Here we make use of the N-Electron Valence Perturbation Theory (NEVPT2) method in its strongly contracted form (SC-NEVPT2) including all electrons (i.e. with no Frozen-Core approximation).[30–33] This is of prime importance for spin-orbit coupling calculations which are affected by the core electrons, having thus an impact on all related properties (i.e. *g*-factors, zero-field tensors and associated magnetic properties). The strongly contracted or "SC" scheme is called so because it makes use of strongly contracted CSFs which form a compact and orthogonal basis, avoiding thus time-consuming orthogonalization steps. In a last step, spin-orbit coupling (SOC) and other scalar relativistic effects are introduced by means of the second order scalar relativistic Douglas-Kroll-Hess Hamiltonian formalism (DKH2) in a mean-field approach using Quasi-Degenerate Perturbation Theory (QDPT).[34–36] In other words, the multiplets stemming from the SO-free CASSCF states (before relativistic treatment) are mixed by the Spin-Orbit Mean Field (SOMF) operator while the NEVPT2 corrected energies replace the diagonal of the QDPT matrix. Herein, all CASSCF/NEVPT2 + SOC calculations always include all states from all spin multiplicities. This is done in a state-average fashion, with all states equally weighted in the CASSCF wavefunction. All SO-free states are thus always included in the QDPT treatment. In all calculations the SARC2 basis sets have been used for U and the DEF2-TZVPP basis set for the fluorine orbitals.[37] The present DEF2-TZVPP basis set is an adapted version of the DEF2 basis set from the Karlsruhe group (i.e. Ahlrichs basis set), which is provided in the Turbomole basis set library.[38,39] It retains the original DEF2 exponents but with only one contracted function per angular momentum, and with contraction coefficients suitable for the DKH scalar relativistic Hamiltonian. In addition, the AUTOAUX feature was used in order to automatically generate auxiliary basis sets for the resolution of identity approximation.[40,41]

II. Results from the electronic structure calculations

II.1. Anisotropic exchange and magnetic susceptibility of $[U_2F_{12}]^{2-}$

The two unpaired f-electrons of $[U_2F_{12}]^{2-}$ give rise to 91 triplets (S = 1) and 105 singlet (S = 0) states. State averaged CASSCF and NEVPT2 calculations accounting for all states yield a singlet ground state and a triplet excited state 20.2 cm^{-1}(CASSCF) and 75.7 cm^{-1}(NEVPT2) above the ground state. Under the influence of spin-orbit coupling the ground state Kramers doublets of the two $U^V(f^1)$ centers yield four sublevels with energies and symmetries plotted in Figure S12. With an exchange coupling between the electrons localized on the two U centers described by the Heisenberg-Dirac-van Vleck Hamiltonian H_{exc} of the form of Equation 10 ($\hat{\mathbf{S}}_1$ and $\hat{\mathbf{S}}_2$ – the local spin-operators on each $U^V(f^1)$ center).

$$\hat{H}_{HDvVleck} = -J\hat{\mathbf{S}}_1\hat{\mathbf{S}}_2 \tag{10}$$

Our results predict an antiferromagnetic U(f^1)-U(f^1) exchange coupling parameter J = −20.2 (CASSCF) and −75.7 cm^{-1} (NEVPT2). Spin-orbit coupling accounted for using quasidegenerate perturbation theory (QDPT) leads to relativistic mixing of the S = 0 ground state with the S = 1 excited state and splitting and mixing among the M_s = 1, 0, −1 sublevels of the triplet described by the zero field splitting Hamiltonian of Equation 11 with the $\hat{S}_z^2, \hat{S}_x^2$ and $\hat{S}_y^2$ total spin operators acting on the S = 1 state manifold:

$$\hat{H}_{ZFS} = D(\hat{S}_z^2 - 2/3) + E(\hat{S}_x^2 - \hat{S}_y^2) \tag{11}$$

Spin-orbit energies of the four spin-obit coupling states (0.0, 8.4, 11.5, 12.4 cm^{-1} (CASSCF); 0.0, 37.8, 38.4, 38.5 cm^{-1} (NEVPT2)) allow to extract the isotropic J, the pseudo-axial D and the orthorhombic E anisotropic zero-field splitting parameters (Table S4). Starting from local s = 1/2 spins on the two U(f^1) centers, the parameters of the anisotropic Hamiltonian of Equation 12, J_{xx}, J_{yy} and J_{zz}, have been derived using Equations 13-15, giving the relations between the two set of parameters. They are listed in Table S4 and reflect quite a pronounced magnetic anisotropy of exchange type.

$$\hat{H}_{aniso} = -J_{xx}\hat{S}_x^1\hat{S}_x^2 - J_{yy}\hat{S}_y^1\hat{S}_y^2 - J_{zz}\hat{S}_z^1\hat{S}_z^2 \tag{12}$$

$$J_{xx} = J + \frac{2}{3}D - 2E \tag{13}$$

$$J_{yy} = J + \frac{2}{3}D + 2E \tag{14}$$

$$J_{zz} = J - \frac{4}{3}D \tag{15}$$

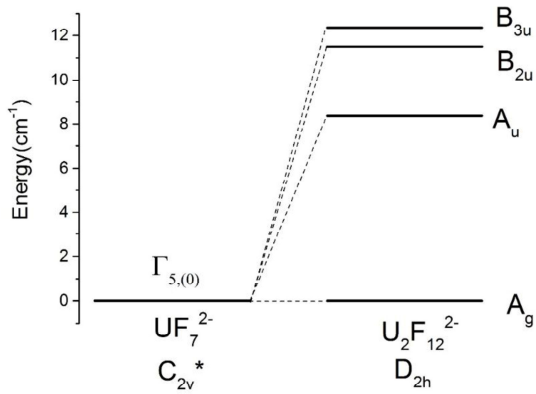

Figure S12. Pair states of $[U_2F_{12}]^{2-}$ resulting from anisotropic exchange coupling between the ground state Kramers doublets of the two $[UF_7]^{2-}$ subunits $\Gamma_{5,0}(a)\sigma(a)\Gamma_{5,0}(b)\sigma(b);\sigma(a),\sigma(b) = \pm 1/2$ of the $[F_5U(a)(\mu\text{-}F)_2U(b)F_5]^{2-}$ anion. Symmetry notations pertain to the C_{2v} and D_{2h} point groups of $[UF_7]^{2-}$ and $[U_2F_{12}]^{2-}$, respectively.

Table S4. Isotropic and anisotropic exchange parameters (in cm^{-1}) for $[U_2F_{12}]^{2-}$ from CASSCF and NEVPT2 calculations.

Method	*J*	*D*	*E*	J_{xx}	J_{yy}	J_{zz}
CASSCF	−10.74	3.54	0.44	−9.25	−7.51	−15.47
NEVPT2	−38.22	0.70	0.025	−37.80	−37.70	−39.16

Computed magnetic susceptibilities (χ) vs *T*, using CASSCF and NEVPT wavefunctions, compare well with the experimentally measured ones (Figure S13) showing a maximum expected for a weakly coupled antiferromagnetic pair of the two spins localized on each UF_7^{2-}; experimental data points are found between the curves predicted by CASSCF and NEVPT2, showing the tendency of the two methods to correspondingly overestimate (underestimate) χ. Surprisingly, a better quantitative agreement between theory and experiment emerges from a χT vs *T* plot in the case of the CASSCF results. The linear range in the χT vs *T* dependence for $T > 75$ K, shown by both the computed and experimental data reflects temperature independent (van Vleck) paramagnetism, suggestive for the mixing of ground state wave functions via the magnetic field.

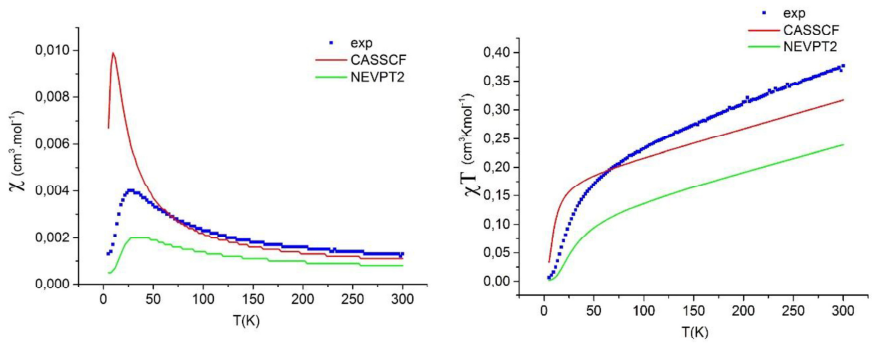

Figure S13. Computed vs experimental χ vs *T* (left) and χT vs *T* dependencies for $[U_2F_{12}]^{2-}$.

II.2. Electronic structure and the f-f absorption spectrum $[U_2F_{12}]^{2-}$

CASSCF (NEVPT2) calculations have been carried out on the two equivalent $[UF_7]^{2-}$ (f^1) fragments within the dimer. In these calculations the geometry as reported by the X-ray crystal structure of C_{2v} symmetry was adopted. The f^1 configuration of U gives rise to seven non-degenerate non-relativistic levels [CASSCF: 0, 1716, 2802, 2977, 5675, 7231 and 8582 cm^{-1}; NEVPT2: 0, 1860, 3136, 3196, 6203, 8089, 9494 cm^{-1}]. Spin-orbit coupling greatly modifies the energies of the seven non-relativistic $s = 1/2$ states and leads to seven Kramers doublets, the ground state $\Gamma_{5,0}$ and the six excited states $\Gamma_{5,i}$ ($i = 1$-6). From these computations we find that under the influence of spin orbit coupling the energies of the six f-f transitions shift to higher energies by almost a factor of two: 3182, 3899, 7426, 10262, 11650, 13372 cm^{-1} (CASSCF results, Figure S14). Exchange coupling between each possible pair of f^1 states, each located on a different $[UF_7]^{2-}$ center each of C_{2v} symmetry (denoted here after as *a* and *b*), leads to a multitude of $S = 0$ and $S = 1$. Focusing on the $\Gamma_{5,0,\sigma}(a)$ and $\Gamma_{5,0,\sigma}(b)$ ground states ($\sigma = \pm 1/2$), the weak exchange coupling leads to four sublevels shown in Figure S14 with A_g as the ground state. Exchange coupling of the $\Gamma_{5,0,\sigma}$ ground state on one $U^V(f^1)$ center with say the lowest electronic excited state on the other center, leads to eight wave functions of the type of Equation 16. These states are of different parity and are of A_g, B_{1g}, B_{2g}, B_{3g}, A_u, B_{1u}, B_{2u} and B_{3u} symmetries classified according to the irreducible representations of the D_{2h} point group.

$$1/\sqrt{2}\left[\Gamma_{5,0,\sigma}(a)\Gamma_{5,1,\sigma}(b) \pm \Gamma_{5,0,\sigma}(b)\Gamma_{5,1,\sigma}(a)\right] \quad (16)$$

In Figure S15 we compare the energy and oscillator strength of the lowest electronic transition of $[UF_7]^{2-}$ with the computed energies and oscillator strengths (f) of the corresponding electronic transitions within the exchange coupled pair. Out of the eight transitions from the A_g ground state of the dimer only two, $A_g \rightarrow B_{2u}$ and $A_g \rightarrow B_{3u}$, are symmetry allowed. Comparing their oscillator strengths with the one of the corresponding transition in $[UF_7]^{2-}$ we can conclude that there is a dramatic enhancement of intensity of f-f transitions when going from $[UF_7]^{2-}$ to the $[U_2F_{12}]^{2-}$ ion. Table S5 illustrates a perfect agreement between experimental and computed spectrum and provides at the same time assignment of the transitions in the spectrum of $[U_2F_{12}]^{2-}$ pertaining to the D_{2h} point group of the complex.

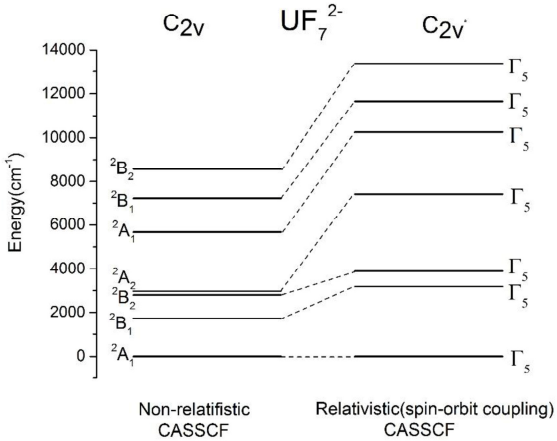

Figure S14. Energy levels for $[UF_7]^{2-}$ (f^1) from a CASSCF calculation without (left) and accounting for (right) spin-orbit coupling effects; symmetry notations follow the irreducible representations of the non-relativistic C_{2v} (left) and the relativistic C_{2v}^* double group (right).

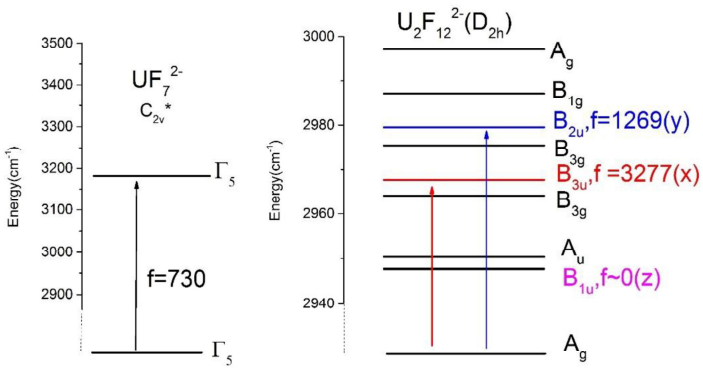

Figure S15. Energy und oscillator strengths for the lowest f^1 electronic transition of $[UF_7]^{2-}$: $\Gamma_5 \rightarrow \Gamma_5$ (C_{2v}^* point group) and eight resulting transitions in $[U_2F_{12}]^{2-}$ (D_{2h} point group) from CASSCF calculations of $[UF_7]^{2-}$ and $[U_2F_{12}]^{2-}$ utilizing CAS(1,7) and CAS(2,14) active spaces, respectively.

Table S5. Energies (cm^{-1}) (oscillator strengths $f \cdot 10^{10}$) of spectroscopic terms of $[UF_7]^{2-}$ and $[U_2F_{12}]^{2-}$ from CASSCF calculations in comparison with the experimentally observed f-f transitions in the absorption spectrum of $[U_2F_{12}]^{2-}$ and their assignment to transition from the ground state into ligand field–spin orbit coupled eigenstates in the D_{2h} point group.

$[UF_7]^{2-}$				$[U_2F_{12}]^{2-}$		
Non-relativistic (C_{2v})		Relativistic (SOC, C_{2v}*)		Relativistic (SOC)		Exp.
Term (C_{2v})	Energy(f)	Term (C_{2v}*)	Energy(f)	Term (D_{2h})	Energy(f)	
$^2A_1$	0	Γ_5	0	A_g	0	-
$^2B_1$	1860(1760)	Γ_5	3182(730)	B_{3u} B_{2u}	2970(3227) 2982(1263)	-
$^2B_2$	3136(0)	Γ_5	3899(537)	B_{1u} B_{3u} B_{2u}	4032(1848) 4053(1893) 4060(5883)	3570
$^2A_2$	3196(20)	Γ_5	7426(1032)	B_{1u} B_{3u} B_{2u}	6710(5145) 6724(3767) 6727(438)	6280
$^2A_1$	6203(2253)	Γ_5	10263(1404)	B_{2u} B_{1u}	9414(6168) 9415(6854)	9140
$^2B_1$	8089(4501)	Γ_5	11650(1308)	B_{1u} B_{2u} B_{3u}	11485(173) 11500(2299) 11513(19797)	10850
$^2B_2$	9494(32898)	Γ_5	13372(34679)	B_{1u} B_{3u} B_{2u}	13136(5633) 13137(5165) 13150(15233)	12830

II.3. Chemical bonding in $[U_2F_{12}]^{2-}$

CASSCF calculations using the $[UF_7]^{2-}$ complex with the X-ray structure, yields a wave function which allows to extract the parameters of the ligand field, the 7x7 matrix V_{LF} of Equation 17 and the value of the spin-orbit coupling parameter $\zeta = 2049$ cm^{-1}.

$$V_{LF} = \begin{bmatrix} -122 & 0 & -2358 & 0 & 882 & 0 & 288 \\ 0 & -817 & 0 & -442 & 0 & -1099 & 0 \\ -2358 & 0 & 2957 & 0 & 776 & 0 & -710 \\ 0 & -442 & 0 & -2004 & 0 & 1395 & 0 \\ 882 & 0 & 756 & 0 & -1820 & 0 & -2616 \\ 0 & -1099 & 0 & 1395 & 0 & 2324 & 0 \\ 288 & 0 & -710 & 0 & -2616 & 0 & -518 \end{bmatrix} \quad (17)$$

The ligand field matrix of Equation 17 has been written down based on real f-orbitals, implying U and F orbital interactions of proper alignment, to form φs,δs,πs,σ, πc,δc and φc bonds with U. The large off-diagonal matrix elements of V_{LF} reflect the low C_{2v} symmetry at each U-site of the dimer. Parametrization of the matrix elements of Equation 17 in terms of the angular overlap model was done under the following assumption: i) neglecting φs ,δs, δc and φc bonds; ii) approximating the F-ligand as forming linear π-bonds with U ($e_{\pi c} = e_{\pi s} = e_{\pi}$) and iii) assuming three different sets of parameters of F-atoms completing the coordination sphere of U: the terminal F (F(1)), the U-F-Sr bridging (F(2)) and the U-F-U bridging (F(3)); iv) assuming, as usually done when parameterizing the ligand field, additivity of the contributions to V_{LF} from the F(1), F(2) and F(3) ligands. Furthermore, adopting the X-ray structure for $[UF_7]^{2-}$ we parameterized each matrix element $\langle f_i | V_{LF} | f_j \rangle, i, j = 1:7$ of Equation 17 in the form of Equation 18.

$$\langle f_i | V_{LF} | f_j \rangle = c_\sigma^{ij}(1)e_\sigma(1) + c_\pi^{ij}(1)e_\pi(1) + c_\sigma^{ij}(2)e_\sigma(2) + c_\pi^{ij}(2)e_\pi(2) + c_\sigma^{ij}(3)e_\sigma(3) + c_\pi^{ij}(3)e_\pi(3) \quad (18)$$

A least squares fit was possible, yielding an impressive consistency between ab-initio ligand field matrix elements (Equation 17) and matrix elements computed using the best fit parameter values and Equation 18 (standard deviation of only 69 cm^{-1}, see Figure S16 for computed vs ab initio ligand field matrix elements).

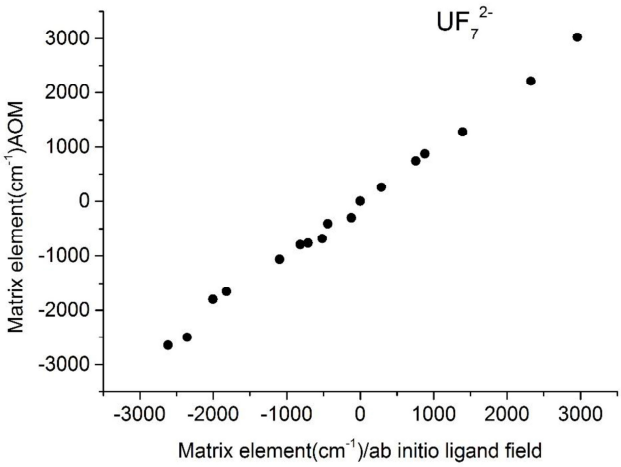

Figure S16. Ab-initio angular overlap matrix elements (*y*-axis) computed using angular overlap parameters from a best fit of these parameters to ab initio ligand field matrix elements from a CASSCF calculation (plotted on the *x*-axis) using the structure of $[UF_7]^{2-}$ from X-ray data.

On the basis of these results the single terminal F(1) can be characterized as the strongest donor [$e_\sigma(1)$ = 3977 cm^{-1}, $e_\pi(1)$ = 1776 cm^{-1}; d(U(1)-F(1)) = 2.078 Å] followed by the weaker σ and π-donating four equivalent F(2) ligands being shared between one U^V and one Sr^{2+} nearest lattice neighbor [$e_\sigma(2)$ = 3714 cm^{-1}, $e_\pi(2)$ = 1172 cm^{-1}, d(U(1)-F(2)) = 2.081 Å]. As chemically expected, the two F(3) ligands bridging the two $U^V(f^1)$ centers impose the weakest ligand field toward U [$e_\sigma(3)$ = 1478 cm^{-1}, $e_\pi(3)$ = 279 cm^{-1}] and this correlates with the longest X-ray reported U-F distance [d(U(1)-F(3)) = 2.281 Å]. The results demonstrate the variability of the ratio e_π/e_σ (usually postulated as 1/4 or 1/3) for the different fluoride ligands and the *non-transferability* of the angular overlap model parameters e_σ and e_π between F of different bonding type.

References

[1] G. W. Halstead, P. G. Eller, L. B. Asprey, K. V. Salazar, *Inorg. Chem.* **1978**, *17*, 2967–2969.
[2] G. W. Halstead, P. G. Eller, R. T. Paine, in *Inorg. Synth.* (Ed.: J.P. Fackler), John Wiley & Sons, Inc., Hoboken, NJ, USA, **1982**, pp. 162–167.
[3] *X-Area*, STOE & Cie GmbH, Darmstadt, Deutschland, **2011**.
[4] G. M. Sheldrick, *Acta Crystallogr. Sect. Found. Adv.* **2015**, *71*, 3–8.
[5] C. B. Hübschle, G. M. Sheldrick, B. Dittrich, *J. Appl. Crystallogr.* **2011**, *44*, 1281–1284.
[6] K. Brandenburg, H. Putz, *Diamond - Crystal and Molecular Structure Visualization*, Crystal Impact GbR, Bonn, **2017**.
[7] *OPUS*, Bruker Optik GmbH, Ettlingen (Germany), **2009**.
[8] *Labspec Spectroscopy Suit Software*, HORIBA Scientific, **2000**.
[9] K.-H. Hellwege, A. M. Hellwege, Eds., *Magnetic Properties of Coordination and Organometallic Transition Metal Compounds*, Springer-Verlag, Berlin/Heidelberg, **1979**.
[10] L. P. Spencer, E. J. Schelter, P. Yang, R. L. Gdula, B. L. Scott, J. D. Thompson, J. L. Kiplinger, E. R. Batista, J. M. Boncella, *Angew. Chem. Int. Ed.* **2009**, *48*, 3795–3798.
[11] R. K. Rosen, R. A. Andersen, N. M. Edelstein, *J. Am. Chem. Soc.* **1990**, *112*, 4588–4590.
[12] J. D. Rinehart, T. D. Harris, S. A. Kozimor, B. M. Bartlett, J. R. Long, *Inorg. Chem.* **2009**, *48*, 3382–3395.
[13] L. T. Corredor, G. Aslan-Cansever, M. Sturza, K. Manna, A. Maljuk, S. Gass, T. Dey, A. U. B. Wolter, O. Kataeva, A. Zimmermann, et al., *Phys. Rev. B* **2017**, *95*, 064418.
[14] J. P. Perdew, K. Burke, M. Ernzerhof, *Phys. Rev. Lett.* **1996**, *77*, 3865–3868.
[15] C. Adamo, V. Barone, *J.Chem.Phys.* **1999**, *110*, 6158–6170.
[16] F. Weigend, R. Ahlrichs, *Phys.Chem.Chem.Phys.* **2005**, *7*, 3297–3305.
[17] B. Scheibe, S. Lippert, S. S. Rudel, M. R. Buchner, O. Burghaus, C. Pietzonka, M. Koch, A. J. Karttunen, F. Kraus, *Chem. - Eur. J.* **2016**, *22*, 12145–12153.
[18] R. Dovesi, R. Orlando, A. Erba, C. M. Zicovich-Wilson, B. Civalleri, S. Casassa, L. Maschio, M. Ferrabone, M. De La Pierre, P. D'Arco, et al., *Int. J. Quantum Chem.* **2014**, *114*, 1287–1317.
[19] R. Dovesi, V. R. Saunders, C. Roetti, R. Orlando, C. M. Zicovich-Wilson, F. Pascale, B. Civalleri, K. Doll, N. M. Harrison, I. J. Bush, et al., **2014**.
[20] F. Pascale, C. M. Zicovich-Wilson, F. Lopez, B. Civalleri, R. Orlando, R. Dovesi, *J Comput Chem* **2004**, *25*, 888–897.
[21] C. M. Zicovich-Wilson, F. Pascale, C. Roetti, V. R. Saunders, R. Orlando, R. Dovesi, *J. Comput. Chem.* **2004**, *25*, 1873–1881.
[22] L. Maschio, B. Kirtman, M. Rérat, R. Orlando, R. Dovesi, *J. Chem. Phys.* **2013**, *139*, 164101.
[23] L. Maschio, B. Kirtman, M. Rérat, R. Orlando, R. Dovesi, *J. Chem. Phys.* **2013**, *139*, 164102.
[24] A. P. Scott, L. Radom, *J. Phys. Chem.* **1996**, *100*, 16502–16513.
[25] *Jmol: An Open-Source Java Viewer for Chemical Structures in 3D. http://www.jmol.org/.*
[26] B. Scheibe, S. S. Rudel, M. R. Buchner, A. J. Karttunen, F. Kraus, *Chem. - Eur. J.* **2017**, *23*, 291–295.
[27] F. Neese, *Wiley Interdiscip. Rev. Comput. Mol. Sci.* **2012**, *2*, 73–78.
[28] F. Neese, *Wiley Interdiscip. Rev. Comput. Mol. Sci.* **2017**, e1327.
[29] B. O. Roos, P. R. Taylor, P. E. M. Siegbahn, *Chem. Phys.* **1980**, *48*, 157–173.
[30] C. Angeli, B. Bories, A. Cavallini, R. Cimiraglia, *J. Chem. Phys.* **2006**, *124*, 054108.
[31] C. Angeli, R. Cimiraglia, J.-P. Malrieu, *J. Chem. Phys.* **2002**, *117*, 9138–9153.
[32] C. Angeli, R. Cimiraglia, S. Evangelisti, T. Leininger, J.-P. Malrieu, *J. Chem. Phys.* **2001**, *114*, 10252–10264.
[33] C. Angeli, R. Cimiraglia, J.-P. Malrieu, *Chem. Phys. Lett.* **2001**, *350*, 297–305.
[34] T. Nakajima, K. Hirao, *Chem. Rev.* **2012**, *112*, 385–402.
[35] M. Reiher, *Wiley Interdiscip. Rev. Comput. Mol. Sci.* **2012**, *2*, 139–149.
[36] F. Neese, *J. Chem. Phys.* **2005**, *122*, 034107.
[37] D. A. Pantazis, F. Neese, *J. Chem. Theory Comput.* **2011**, *7*, 677–684.
[38] F. Weigend, F. Furche, R. Ahlrichs, *J. Chem. Phys.* **2003**, *119*, 12753–12762.
[39] F. Weigend, R. Ahlrichs, *Phys. Chem. Chem. Phys.* **2005**, *7*, 3297–3305.
[40] G. L. Stoychev, A. A. Auer, F. Neese, *J. Chem. Theory Comput.* **2017**, *13*, 554–562.
[41] F. Neese, *J. Comput. Chem.* **2003**, *24*, 1740–1747.

7.7. UF_4 and the High-Pressure Polymorph HP-UF_4

Benjamin Scheibe, Jörn Bruns, Gunter Heymann, Malte Sachs, Antti J. Karttunen, Clemens Pietzonka, Sergei I. Ivlev, Hubert Huppertz, Florian Kraus

Chem. Eur. J. **2019**, *25*, 7366–7374.
DOI: 10.1002/chem.201900639

© 2019 Wiley-VCH Verlag GmbH & Co. KGaA, Weinheim

Reproduced with permission of John Wiley and Sons; permission conveyed through Copyright Clearance Center, Inc. (License number: 4885910436677).

ChemPubSoc Europe
DOI: 10.1002/chem.201900639
CHEMISTRY A European Journal Full Paper
Check for updates

Uranium |Hot Paper|

UF_4 and the High-Pressure Polymorph HP-UF_4

Benjamin Scheibe,[a] Jörn Bruns,[b] Gunter Heymann,[c] Malte Sachs,[a] Antti J. Karttunen,[d] Clemens Pietzonka,[a] Sergei I. Ivlev,[a] Hubert Huppertz,[c] and Florian Kraus*[a]

Abstract: A laboratory-scale synthesis of UF_4 is presented that utilizes the reduction of UF_6 with sulfur in anhydrous hydrogen fluoride. An excess of sulfur can be removed by vacuum sublimation, yielding pure UF_4, as shown by powder X-ray diffraction, micro X-ray fluorescence analysis, infrared and Raman spectroscopy, as well as magnetic measurements. Furthermore, a single-crystalline, high-pressure modification of UF_4 was obtained in a multi-anvil press at elevated temperatures. The high-pressure polymorph HP-UF_4 was characterized by means of single-crystal and powder X-ray diffraction, as well as by magnetic measurements, and presents a novel crystal structure type. Quantum-chemical calculations show the HP-modification to be 10 kJ mol^{-1} per formula unit higher in energy compared to UF_4.

Introduction

The first synthesis of uranium tetrafluoride was likely published in 1861, starting from U_3O_8 and hydrofluoric acid, yielding UF_4 and UO_2F_2 (Equation 1).[1]

$$U_3O_8 + 8HF \rightarrow UF_4 + 2UO_2F_2 + 4H_2O \quad (1)$$

Since the Manhattan Project, uranium tetrafluoride has been a key intermediate in the enrichment of the ^{235}U isotope, which is used for the production of nuclear weapons and fuels.[2–5] UF_4 is commonly referred to as "green salt", which is converted by various fluorination agents to volatile UF_6 for the enrichment process. The ^{235}U isotope is then enriched, for example, by gas centrifugation, reconverted to UF_4 and usually further processed to UO_2, which is a common nuclear fuel.[3] Uranium tetrafluoride can be reduced with Ca or Mg for the production of uranium metal.[4–6] Enriched uranium metal, or its alloys with aluminium, are also used as targets for the production of ^{99}Mo, which decays to the valuable ^{99m}Tc isotope, which is used in medical diagnostics.[7] Furthermore, enriched UF_4 can be used in Generation IV reactors, most notably in Molten Salt Reactors (MSR) or in the advanced Molten Salt Fast Reactors (MSFR).[8,9]

Various methods for the synthesis and technical production of UF_4 have been reported and extensively reviewed.[3,4,10] Thus, only a short overview will be given here. In principle, there are two main approaches for the synthesis of UF_4, a wet and a dry chemical process. The first is based on the reduction of an uranyl(VI) salt in aqueous medium to U^{IV}, followed by the precipitation of uranium tetrafluoride hydrates upon addition of hydrofluoric acid. Suitable reducing agents are for example tin(II) chloride, sodium dithionite, $Na_2S_2O_4$, or sulfur dioxide in the presence of Cu^{2+} ions.[10–12] To obtain neat UF_4, the UF_4 hydrates have to be dried either under vacuum, or in a stream of hydrogen fluoride at temperatures of up to 500 °C. So, due to hydrolysis (by the H_2O molecules of crystallization), usually UO_2 is obtained as a side product that cannot be easily separated from UF_4.[3,10]

The most important process for the production of UF_4 is probably the dry-chemical hydrofluorination of UO_2 (Equation 2).[3,6]

$$UO_2 + 4HF \rightleftharpoons UF_4 + 2H_2O \quad (2)$$

The reaction is carried out at temperatures between 250 and 600 °C and water released during the reaction is constantly removed to prevent the hydrolysis of UF_4. The obtained UF_4 usually contains a small percentage of UO_2 and UO_2F_2, the latter due to UO_3 impurities in the starting material (Equation 3).[3] By adding a few percent of H_2 to the gas stream, U^{VI} as well as oxidic impurities can be significantly reduced.

$$UO_3 + 2HF \rightarrow UO_2F_2 + H_2O \quad (3)$$

The synthesis of UF_4 is also possible through the reduction of UF_6, which, however, has been of little technical interest.[3,13]

[a] B. Scheibe, M. Sachs, C. Pietzonka, Dr. S. I. Ivlev, Prof. Dr. F. Kraus
Fachbereich Chemie, Philipps-Universität Marburg
Hans-Meerwein-Straße 4, 35032 Marburg (Germany)
E-mail: f.kraus@uni-marburg.de
Homepage: https://www.uni-marburg.de/fb15/ag-kraus

[b] Dr. J. Bruns
Institut für Anorganische Chemie, Universität zu Köln
Greinstr. 6, 50939 Köln (Germany)

[c] Prof. Dr. G. Heymann, Prof. Dr. H. Huppertz
Institut für Allgemeine, Anorganische und Theoretische Chemie
Universität Innsbruck, Innrain 80–82, 6020 Innsbruck (Austria)

[d] Prof. Dr. A. J. Karttunen
Department of Chemistry and Materials Science, Aalto University
Kemistintie 1, 02150 Espoo (Finland)

Supporting information and the ORCID identification number(s) for the author(s) of this article can be found under: https://doi.org/10.1002/chem.201900639.

© 2019 Wiley-VCH Verlag GmbH & Co. KGaA, Weinheim

ChemPubSoc Europe
CHEMISTRY A European Journal
Full Paper

Suitable reducing agents are for example, H_2, HCl, HBr, N_2H_4, and NH_3. On a small scale H_2 has been used in a technical process for the reduction of depleted UF_6 to UF_4 and HF. The UF_4 is then further reacted with oxides like B_2O_3 or SiO_2 producing valuable BF_3 or SiF_4 and uranium oxides (Equation 4).[13]

$$3UF_4 + 2B_2O_3 \rightarrow 3UO_2 + 4BF_3 \quad (4)$$

Based on a report from 1911 on the reaction of pure UF_6 with sulfur, yielding US_2, UF_4 and possibly SF_4, we investigated the reduction of UF_6 with sulfur in anhydrous HF (aHF), which yields UF_4.[14] The obtained UF_4 was further reacted in a multi-anvil press under high temperature and pressure to obtain a single crystalline high pressure modification of UF_4.

Results and Discussion

The reaction of UF_6 with an excess amount of S_8 in aHF proceeds quickly at the melting point of aHF (−83.37 °C). Initially, a bluish supernatant HF solution is formed, indicating the presence of the $[UF_6]^-$ ion.[15] After a few minutes of reaction time at room temperature, a brown supernatant HF solution is obtained that is accompanied by the precipitation of a greyish solid, which indicates the formation of mixed uranium(IV/V) fluorides, such as U_2F_9 and U_4F_{17} (see Figure S1 in the Supporting Information).[3] After two to three days of reaction time at room temperature, a green solid and a colourless supernatant HF solution results.

The fluorination process of sulfur in this reaction is probably quite complex, with the possible intermediate formation of sulfur difluoride, SF_2, thio-thionyl fluoride, SSF_2, and disulfur difluoride, S_2F_2.[16,17] These low-valent sulfur fluorides are either unstable towards disproportionation in the presence of aHF, or unstable at room temperature (S_2F_2).[16,17] Uranium hexafluoride is also known to oxidize H_2S at 25 °C in the gas phase, or when liquid H_2S is used both as a solvent and reactant.[18] In both cases UF_4, SF_4, and HF are formed. Besides that, it has been reported that no reaction between UF_6 and SF_4 takes place at temperatures up to 300 °C.[19] At a temperature of 500 °C the formation of SF_6 has been observed. In comparison to that, it has been shown that PuF_6 reacts with SF_4 at 30 °C.[19] Furthermore, the reaction between gaseous UF_6 and sulfur was reported to be slow up to at least 130 °C, with SF_4 being the fluorination product.[20] This reaction could be accelerated by increasing the pressure with N_2, but in both cases several heating cycles had to be performed to obtain quantitative yields. It is likely from the aforementioned reactions that SF_4 is the main product of the reaction between S_8 and UF_6 in the presence of aHF. The overall reaction can then be described by Equation 5.

$$2UF_6 + \frac{1}{8}S_8 \rightarrow 2UF_4 + SF_4 \quad (5)$$

The removal of HF and other volatiles from the reaction mixture using vacuum distillation yields sulfur-containing UF_4, due to the excess of sulfur used. The remaining sulfur was removed under vacuum at 350 °C. The phase purity of the UF_4 was checked by a Rietveld refinement of a powder X-ray diffraction (PXRD) pattern recorded at 293 K (see Figure 1 and Table S1). The following lattice parameters were refined: $a = 12.815(1)$, $b = 10.806(1)$, $c = 8.3804(2)$ Å, $\beta = 126.26(1)°$, $V = 935.71(3)$ Å^3, $C2/c$ (no. 15), $mS60$, β-ZrF_4 structure type.[21] The determined values are in good agreement with so far reported data; see Table 1. Based on X-ray diffraction, UF_4 was obtained as a phase-pure product.

We attempted the detection of a potential sulfur content of our powder samples by micro X-ray fluorescence analysis (μXRF). No sulfur-containing impurities (like S_8 or US_2) were detected in the sample after the sublimation. Furthermore, infrared and Raman spectra were recorded (see Figure S2 and Figure S3). In the measured IR spectrum, a weak band at 612 cm^{-1} and a partly resolved broad band with a maximum at approximately 430 cm^{-1} can be seen, which are in agreement with previous reports on UF_4.[27,28] Possible oxygen-containing species like UO_2, UO_3, and UO_2F_2 show bands at 450,

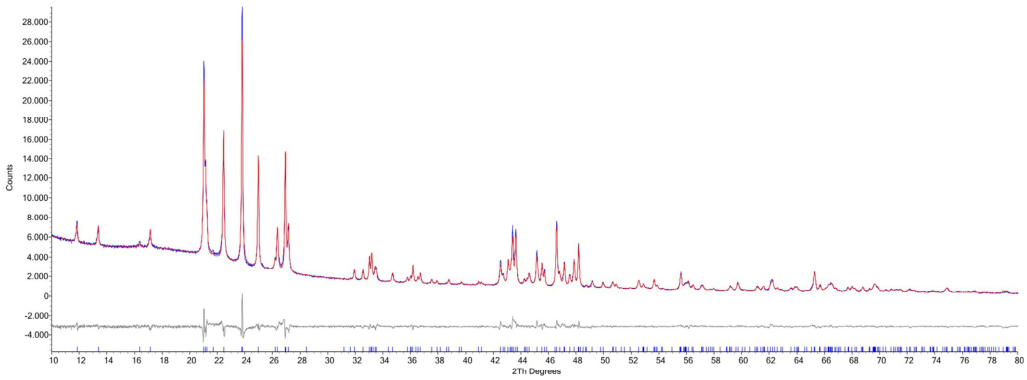

Figure 1. Observed and calculated powder X-ray diffraction patterns of ZrF_4-type UF_4 after Rietveld refinement. The observed pattern is shown in blue, the calculated one in red. The calculated reflection positions are indicated by the vertical bars below the patterns. The curve at the bottom represents the difference between the observed and calculated intensity. Profile *R*-factors: $R_p = 3.15$ %, $wR_p = 4.51$ %, GOF = 2.13. Further details on the structure determination are available from the Supporting Information.

© 2019 Wiley-VCH Verlag GmbH & Co. KGaA, Weinheim

ChemPubSoc Europe

CHEMISTRY A European Journal Full Paper

Table 1. Reported lattice parameters of ZrF_4-type UF_4. RT stands for room temperature.

Radiation type	T [K]	a [Å]	b [Å]	c [Å]	β [°]	Reference
Neutron	300	12.7941(2)	10.7901(2)	8.3687(2)	126.25(2)	[22]
X-ray	RT	12.79(6)	10.72(5)	8.39(5)	126.2(5)	[23]
X-ray	RT	12.73(1)	10.753(7)	8.404(8)	126.33(5)	[24]
X-ray	RT	12.760(4)	10.768(2)	8.399(2)	126.32(2)	[25]
X-ray	RT	12.801(1)	10.799(1)	8.374(1)	126.30(1)	[26]
X-ray	293	12.815(1)	10.806(1)	8.3804(2)	126.26(1)	this work

700–950, and 1020 cm^{-1}, respectively.[3,29] Such bands are absent.

The Raman spectra of UF_4 obtained at different excitation wavelengths show bands at 473, 219, and 151 cm^{-1}. The intensities of these bands are relatively low and UF_4 seems to be a very weak Raman scatterer.[28,30,31] In the Raman spectra, no bands attributable to sulfur species, such as S_8, which is a strong Raman scatterer, could be observed.[32] Furthermore, no bands attributable to oxygen-containing species like UO_2, UO_3, and UO_2F_2 could be observed in the Raman spectra.[3,33,34]

We were furthermore interested in obtaining a crystalline, high-pressure modification of UF_4 since it had only been scarcely studied under high-pressure conditions.[30,35,36] The only reported crystal structure for ambient-pressure UF_4 to date is that of the β-ZrF_4 type, which is a structure type observed for several transition metals, as well as for some lanthanoid and actinoid tetrafluorides MF_4 (M=Hf, Ce, Tb, Th, Pa, Np, Pu, Am, Cm, Bk).[22,23,37–41] In this structure type, each metal cation is coordinated by eight F atoms in a square-antiprismatic shape. The ZrF_8 coordination polyhedra share corners, which results in a 3D network that can be described with the Niggli formula $^3_\infty[ZrF_{8/2}]$. In contrast to UF_4, there are several reports of crystallographic studies on high-temperature and high-pressure modifications of single-crystalline ZrF_4. The high-temperature modification α-ZrF_4 has been obtained by sublimation of β-ZrF_4 under an argon atmosphere with a temperature gradient of 1020→580 K.[42] It crystallizes in space group $P4_2/m$ (no. 84), $tP40$, with a=7.896(1), c=7.724(1) Å, V=481.6 $Å^3$, Z=8 (T=not reported).[42] Each Zr atom is coordinated by eight fluorine atoms, forming a polyhedron of square-antiprismatic shape. The ZrF_8 polyhedra share corners and edges, resulting in a 3D framework, which can be described with the Niggli formula $^3_\infty[ZrF_{8/2}]$. The high-pressure modification γ-ZrF_4 has been obtained by heating β-ZrF_4 at temperatures of 1173 to 1273 K under pressures of 4 to 8 GPa.[43,44] It crystallizes in the space group $P2_1/c$ (no. 14), $mP20$, with a=5.554(2), b=5.639(2), c=7.973(3) Å, β=105.98(5)°, V=240.1 Å, Z=4 (T=not reported).[43,44] The Zr atom has a similar coordination environment to α-ZrF_4, with edge and corner sharing ZrF_8 square-antiprisms, $^3_\infty[ZrF_{8/2}]$.

Up to now, only a few high-pressure studies on UF_4 have been published. It is reported that a hexagonal modification of UF_4 has been obtained by shock compression. Based on powder X-ray diffraction data recorded on a film, the authors assigned this modification to the Cu_3P type structure ($hP26$, $P6_3mc$) with a=7.05 and c=7.27 Å, and a site occupation factor of $^3/_4$ for the uranium position. We note that this modification would be isotypic to UF_3, and the given composition UF_4 is only generated by an under-occupancy of U.[35,45] A cubic modification of UF_4 with a=6.34(5) Å and V=254.8 $Å^3$ (T=not reported) has been obtained by explosive compression, utilizing RDX (hexogen) as an explosive under conditions of 16 to 50 GPa and 400 to 1600 °C.[36] However, no further structural data were reported. Furthermore, a Raman spectroscopic study was conducted on UF_4 at a pressure of 4.7 GPa, assigning a phase transition at 2.2 GPa. The phase transition was observed by powder X-ray diffraction.[30]

Green HP-UF_4 single-crystals, with essentially the same colour as regular UF_4, were obtained in this study under a pressure of 9.5 GPa and a temperature of 600 °C in a multi-anvil press. HP-UF_4 is metastable at room temperature and all characterizations have been carried out under ambient pressure. This high-pressure modification of UF_4, called HP-UF_4, crystallizes in the monoclinic space group $P2_1/m$ (no. 11) with four formula units per unit cell, $mP20$. To the best of our knowledge, HP-UF_4 is a new structure type. See Table 2 for crystallographic details. The crystal structure of HP-UF_4 is shown in Figure 2.

There are two symmetry-independent uranium atoms U(1) and U(2) in the structure of HP-UF_4, both occupy the Wyckoff position 2e (m). U(1) is coordinated by eleven fluorine atoms, which form a polyhedron best described as a distorted monocapped pentagonal antiprism; see Figure 3 and Figure 4. U(2) is coordinated by nine fluorine atoms, forming a polyhedron that can be described as a prismatoid composed of a penta-

Table 2. Selected crystallographic data and details of the single-crystal structure determination of HP-UF_4.

	HP-UF_4
empirical formula	UF_4
colour and appearance	green plate
crystal size [mm]	0.02×0.03×0.03
molar mass [g mol^{-1}]	314.02
crystal system	monoclinic
space group (No.)	$P2_1/m$ (11)
a [Å]	4.6015(2)
b [Å]	6.9786(3)
c [Å]	7.6271(3)
β [°]	101.013(2)
V [$Å^3$]	240.41(2)
Z	4
ρ_{calcd} [g cm^{-3}]	8.676
λ (MoK_α) [Å]	0.71073
T [K]	183
μ [mm^{-1}]	67.395
θ_{max}	39.47
range of Miller indices	$-8 \le h \le 8$
	$-12 < k < 12$
	$-13 \le l \le 13$
R_{int}, R_σ	0.037, 0.015
$R(F)$ ($I \ge 2\sigma(I)$, all data)	0.015, 0.019
$wR(F^2)$ ($I \ge 2\sigma(I)$, all data)	0.028, 0.029
S (all data)	1.16
data, parameter, restraints	1530, 53, 0
$\Delta\rho_{max}$, $\Delta\rho_{min}$ [e $Å^{-3}$]	2.83, −2.12

© 2019 Wiley-VCH Verlag GmbH & Co. KGaA, Weinheim

ChemPubSoc Europe

CHEMISTRY A European Journal
Full Paper

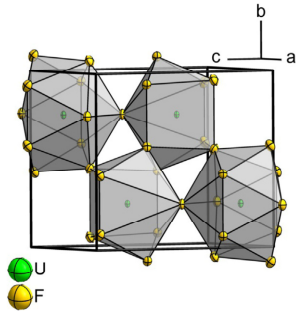

Figure 2. Crystal structure of HP-UF_4. Displacement ellipsoids are shown at the 90% probability level at 183 K.

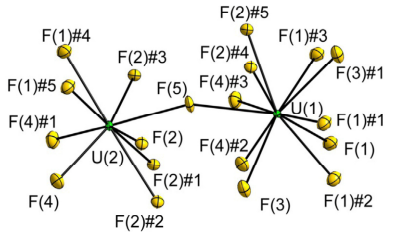

Figure 3. A section of the crystal structure of HP-UF_4. Displacement ellipsoids are shown at the 90% probability level at 183 K. Symmetry transformations for the generation of equivalent atoms: F(1): #1 $-x$, $-1/2+y$, $2-z$; #2 x, $3/2-y$, z; #3 $-x$, $2-y$, $2-z$; #4 x, y, $-1+z$; #5 x, $3/2-y$, $-1+z$; F(2): #1 $1-x$, $1/2+y$, $1-z$; #2 $1-x$, $1-y$, $1-z$; #3 x, $3/2-y$, z; #4 $-x$, $1-y$, $1-z$; #5 $-x$, $1/2+y$, $1-z$; F(3): #1 $-1+x$, y, z. F(4): #1 x, $3/2-y$, z; #2 $1-x$, $1-y$, $1-z$; #3 $1-x$, $1/2+y$, $1-z$.

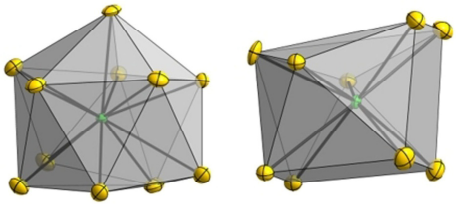

Figure 4. Coordination environment of the two symmetry-independent uranium atoms in HP-UF_4. Left: U(1) with eleven neighbouring fluorine atoms; Right: U(2) with nine neighbouring fluorine atoms. Uranium atoms are depicted in green and fluorine atoms in yellow. Displacement ellipsoids are shown at the 90% probability level at 183 K.

gon and quadrangle in parallel orientation. The coordination spheres of the uranium atoms can also be described by the Niggli formulas ${}^{3}_{\infty}\{[UF_{6/3}F_{5/2}]^{0.5}\}$ for U(1) and ${}^{3}_{\infty}\{[UF_{6/3}F_{3/2}]^{0.5}\}$ for U(2), respectively. Atom coordinates and the isotropic displacement parameters are available in Table 3, anisotropic displacement parameters in Table S2. Selected atomic distances, d, and angles, $\measuredangle$, are given in Table 4.

Table 3. Atomic coordinates and equivalent isotropic displacement parameters, U_{eq}, for HP-UF_4 at 183 K.

Atom	Wyckoff position	x	y	z	U_{eq} [Å^2]
U(1)	2*e*	0.03554(3)	3/4	0.82749(2)	0.00233(3)
U(2)	2*e*	0.45712(3	3/4	0.34398(2)	0.00229(3)
F(1)	4*f*	0.2048(4)	0.9198(3)	0.0933(2)	0.0064(3)
F(2)	4*f*	0.2975(4)	0.4259(2)	0.3961(2)	0.0046(3)
F(3)	2*e*	0.5525(6)	3/4	0.8844(3)	0.0068(4)
F(4)	4*f*	0.7764(4)	0.5546(3)	0.2513(2)	0.0068(3)
F(5)	2*e*	0.1582(5)	3/4	0.5410(3)	0.0056(4)

Table 4. Selected interatomic distances d of HP-UF_4.

	d [Å]	Multiplicity
U(1)–F(1)	2.349(2)	2
U(1)–F(1)	2.674(2)	2
U(1)–F(2)	2.401(2)	2
U(1)–F(3)	2.335(3)	1
U(1)–F(3)	2.344(2)	1
U(1)–F(4)	2.414(2)	2
U(1)–F(5)	2.359(2)	1
U(2)–F(1)	2.358(2)	2
U(2)–F(2)	2.420(2)	2
U(2)–F(2)	2.434(2)	2
U(2) F(4)	2.217(2)	2
U(2)–F(5)	2.222(2)	1

The fluorine atoms F(3), F(4), and F(5) are μ_2-bridging between the uranium atoms with U–F distances in the range of 2.217(2) to 2.414(2) Å and U-F-U angles from 155.8(1) to 159.0(2)°. The fluorine atoms F(1) and F(2) are μ_3-bridging between both uranium atoms with increased U–F distances of 2.349(2) to 2.674(2) Å and decreased U-F-U angles of 117.2(1) to 123.1(1)°, which may be explained by the different coordination numbers. Such μ_3-bridging fluorine atoms are also present in U^{IV} containing fluorido complexes like $RbUF_5$ and RbU_3F_{13}.[46] The average U–F distance for U(1) is 2.429 Å and for U(2) 2.342 Å.

For comparison, in the structure of ZrF_4-type UF_4, both uranium atoms are coordinated by eight fluorine atoms, forming distorted square antiprisms.[21] All fluorine atoms in this modification are μ_2-bridging between the uranium atoms with distances in the range of 2.230 to 2.354 Å. The average U–F distance for U(1) in ZrF_4-type UF_4 is 2.290 Å and for U(2) it is 2.266 Å. Comparing the average U–F distances of both modifications, those in HP-UF_4 are increased due to the higher coordination numbers, which is generally observed in high-pressure modifications.[47]

The overall structure of HP-UF_4 is a 3D network structure in which the UF_9 and UF_{11} polyhedra share corners and edges. The UF_9 polyhedra are surrounded by two UF_9 and seven UF_{11} polyhedra; the UF_{11} polyhedra are surrounded by seven UF_9 and four UF_{11} polyhedra. In HP-UF_4 the F···F distances are observed in a range from circa 2.37 to 2.89 Å and are thus shorter compared to ZrF_4-type UF_4 (2.56 to 3.08 Å). The nearest U–U distances in HP-UF_4 are in the range of 4.045(1) to 4.602(1) Å, those in ZrF_4-type UF_4 are between 4.468 and 4.584 Å. The

© 2019 Wiley-VCH Verlag GmbH & Co. KGaA, Weinheim

ChemPubSoc Europe
CHEMISTRY A European Journal
Full Paper

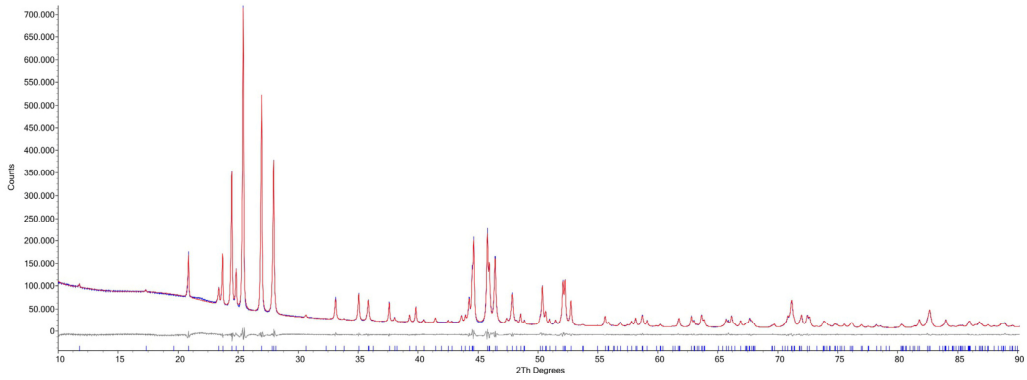

Figure 5. Observed and calculated powder X-ray diffraction patterns of HP-UF_4 after Rietveld refinement. The observed pattern is shown in blue, the calculated one in red. The calculated reflection positions are indicated by the vertical bars below the patterns. The curve at the bottom represents the difference between the observed and calculated intensity. Profile *R* factors: $R_p = 1.98\%$, $wR_p = 2.69\%$, GOF = 5.31. Further details on the structure determination are available from the Supporting Information.

average U–U distances for the nearest U atoms are 4.382 Å for U(1) and 4.284 Å for U(2) in HP-UF_4, the ones in ZrF_4-type UF_4 are 4.507 Å for U(1) and 4.504 Å for U(2). These observations are in line with the expectations for a high-pressure structure.

The U atoms in HP-UF_4 are approximately hexagonal close packed with the hexagonal layers perpendicular to the *b*-axis. However, the F atoms occupy neither octahedral nor tetrahedral voids, but reside either on the faces (μ_3-F) or on the edges (μ_2-F) of these polyhedra.

The phase purity of the obtained HP-UF_4 was checked by powder X-ray diffraction; see Figure 5. No additional reflections resulting from crystalline impurities, such as the ambient pressure modification of ZrF_4-type UF_4 or Pt from the container material used during the synthesis, were observed. Thus, HP-UF_4 was prepared phase-pure based on powder X-ray diffraction. The following cell parameters were obtained after a Rietveld refinement fit: $a = 4.6080(1)$, $b = 6.9955(1)$, $c = 7.6364(1)$ Å, $\beta = 101.07(1)^\circ$, $V = 241.58(1)$ Å^3, $T = 293$ K. The lattice parameters obtained at 293 K show a good agreement with the single-crystal data obtained at 183 K, with a slight difference due to the different measurement temperatures and X-ray wavelengths.

The magnetic properties of ZrF_4-type UF_4 and HP-UF_4 were investigated by means of temperature-dependent DC-magnetic measurements in a temperature range between 300 and 5 K. The magnetic susceptibilities are shown in Figure 6. At temperatures between 100 to 300 K, the susceptibilities of both compounds can be fitted with a Curie–Weiss law ($C/(T-\Theta)$). An effective moment, μ_{eff}, of 3.67(1) μ_B and 3.61(1) μ_B per formula unit and a paramagnetic Curie constant Θ of −160.8(7) K and −147.1(2) K resulted from the fits of ZrF_4-type UF_4 and HP-UF_4, respectively.

The effective moments for ambient pressure UF_4 and HP-UF_4 are of similar magnitude. The obtained values resemble the effective atomic moment of 3.58 μ_B of a [Rd]$5f^2$ U^{4+} cation with a $^3H_4$ ground state indicating that crystal-field effects contribute only to a small extent within this temperature region. This behaviour is found for many U^{IV} systems.[46,48–50] The negative values of Θ of both compounds indicate an antiferromagnetic interaction between the U^{IV} ions, although the course of the susceptibility at low temperatures does not display an explicit magnetic ordering.

The low temperature magnetic susceptibilities of ZrF_4-type UF_4 and HP-UF_4 are given in Figure 7. The susceptibilities of both compounds exhibit saturation effects. However, the saturation is more pronounced for HP-UF_4. A saturation of the susceptibility at low temperatures is often observed in compounds containing U^{IV} cations.[46,48–50] This effect is discussed in terms of crystal-field effects that should stabilize a singlet ground state, which is populated with decreasing temperature. In case of ZrF_4-type UF_4, heat capacity,[51] magnetic,[52] and spectroscopic measurements[53] reveal an energy difference Δ between the ground state and the first excited state of about 10 cm^{-1}. Due to the small energy difference, the saturation of the susceptibility, and therefore the deviation from the Curie–Weiss law, occurs only at low temperatures, for example, $k_BT \approx \Delta$. Leask and co-workers suggested the following fitting function (Equation 6) for the magnetic susceptibility of ZrF_4-type UF_4 below 20 K, assuming, in line with spectroscopic measurements,[53] that only the first exited state is accessible within this temperature range.[52]

$$\chi(T) = p \cdot \frac{8N_A\mu_B^2}{k_B} \cdot \frac{1}{\Delta} \cdot \frac{1-\exp(-\Delta/T)}{1+\exp(-\Delta/T)} + \mu_0 \qquad (6)$$

In the equation, N_A is the Avogadro constant, μ_B the Bohr magneton, and k_B the Boltzmann constant. The factor *p* accounts for a reduction of the magnetic susceptibility due to antiferromagnetic coupling, Δ is the energy difference in K between the ground state and the first excited state and μ_0 is the temperature-independent susceptibility. Applying Equation 6 to our data, we can reproduce the results of previous studies,

© 2019 Wiley-VCH Verlag GmbH & Co. KGaA, Weinheim

ChemPubSoc Europe
CHEMISTRY A European Journal
Full Paper

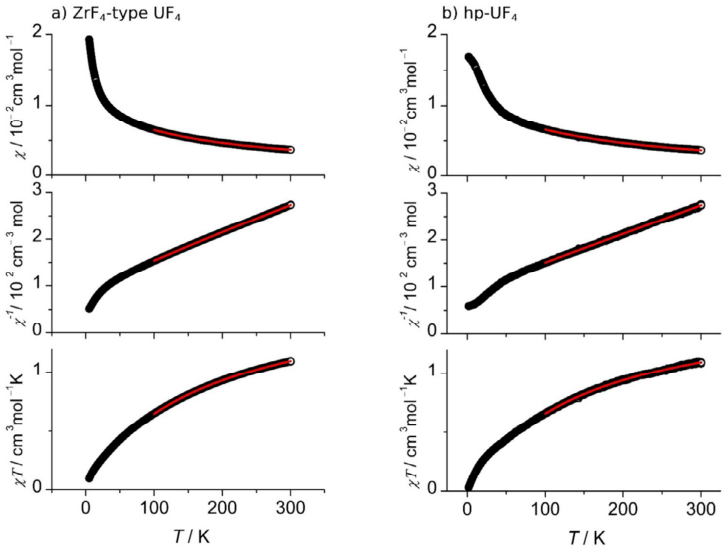

Figure 6. Section of the molar susceptibility of ZrF_4-type UF_4 (o) and HP-UF_4 (Δ) at low temperatures measured with a field of 0.1 T. The data was fitted with Equation 6.

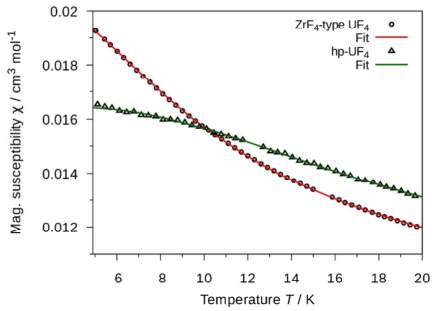

Figure 7. Different plots of the temperature dependence of the molar susceptibility of a) ZrF_4-type UF_4 and b) HP-UF_4 with an applied field of 0.1 T. The temperature range used for the Curie–Weiss fits is shown in red.

finding an energy gap Δ of 10.6(1) cm^{-1} (see Figure 7). In the case of HP-UF_4, we determine an energy gap Δ of 21.9(2) cm^{-1}, almost twice the value of ZrF_4-type UF_4. This is in line with the expected increase of crystal-field effects as the average coordination number of the uranium atoms increases from eight in ZrF_4-type UF_4 to nine and eleven (ten in average) in HP-UF_4. Due to the higher energy difference between the ground state and the first excited state of HP-UF_4 the saturation of the magnetic susceptibility is more pronounced as in ZrF_4-type UF_4 (see Figure 7).

Using quantum chemical calculations, we optimized the structures of ZrF_4-type UF_4 and HP-UF_4 with density functional theory (DFT) applying the hybrid functional PBE0. The results of the structural optimization of the magnetic ground state of ZrF_4-type UF_4 and a comparison with experimental data are collected in Table S3 and Table S4 in the Supporting Information. The data concerning HP-UF_4 is summarized in Table S5 and Table S6. The calculated lattice parameters of the two compounds agree well with the experimental results. The difference is in the order of 1%. The experimental U–F distances (in the following given in brackets) are also well reproduced by the DFT calculations. In case of ZrF_4-type UF_4, the calculated U–F distances range from 2.21 Å (2.230) to 2.34 Å (2.354).[21] The average distance of U(1) and U(2) to their coordinating fluorine atoms is calculated as 2.27 Å (2.290 and 2.266, respectively). In case of HP-UF_4, the calculated U–F distances range from 2.18 Å (2.217(2)) to 2.68 Å (2.414(2)). The average U–F distance of U(1) is 2.43 Å (2.429) and of U(2) 2.32 Å (2.342). This demonstrates that PBE0 calculations can reproduce the experimental structures of ZrF_4-type UF_4 and HP-UF_4 reasonably well.

We estimated the magnetic ground states of ZrF_4-type UF_4 and HP-UF_4 performing single-point calculations with different starting spin-orientations. Details concerning the calculations are given in the Experimental Section. The results of the calculations are summarized in Table 5 and Table 6. We find an antiferromagnetic ground state for both structures in line with the negative paramagnetic Curie-temperatures determined from experiment. Comparing the two ground state energies, ZrF_4-type UF_4 is about 10 kJ mol^{-1} per formula unit more stable than HP-UF_4. This is expected from our experiments finding the ZrF_4-type UF_4 to be the stable polymorph under normal conditions.

© 2019 Wiley-VCH Verlag GmbH & Co. KGaA, Weinheim

ChemPubSoc Europe

CHEMISTRY A European Journal
Full Paper

Table 5. Energy difference of different magnetic structures of ZrF_4-UF_4 (*C*2/*c*, *mP*60) (DFT-PBE0/TZVP). Magnetic ordering: AF (antiferromagnetic), FR (ferrimagnetic), F (ferromagnetic).

Magnetic space group	Magnetic ordering	ΔE [meV] and per formula unit	Spin arrangement[a]
P_c2/c (13.74)	AF	0	↓↑↓↑↓↑↓↑↓↑
$C2'/c''$ (15.89)	FR	12	↑↑↑↑↑↑↑↑↓↓↓↓
P_c2/c (13.74)	AF	13	↓↑↓↑↑↓↑↓↓↑↓↑
non magnetic	–	1313	–

[a] The atomic positions of the corresponding uranium atoms are listed in Table S7 in the Supporting Information.

Table 6. Energy difference of different magnetic structures of HP-UF_4 ($P2_1/m$, *mP*20) (PBE0/TZVP). Magnetic ordering: AF (antiferromagnetic), FR (ferrimagnetic), F (ferromagnetic).

Magnetic space group	Magnetic ordering	ΔE [meV] and per formula unit	Spin arrangement[a]
$P2_1'/m$ (11.54)	AF	0	↑↑↓↓
$P2_1'/m$ (11.52)	AF	11	↓↑↓↑
$P2_1'/m$ (11.54)	F	21	↑↑↑↑
non magnetic	–	1358	–

[a] The atomic positions of the corresponding uranium atoms are listed in Table S8 in the Supporting Information.

For both structures, the energy difference of the ground state magnetic structures to magnetic structures higher in energy is in the order of 10 to 20 meV. These small energy differences point to only weak antiferromagnetic coupling between the uranium atoms, reflecting that experimentally no magnetic ordering is found in the investigated temperature range between 5 and 300 K.

As pointed out above, U^{IV} systems are often discussed as having a singlet ground state. However, our calculations reveal a triplet ground state with a spin magnetic moment of approximately 2 μ_B per uranium atom. This discrepancy could stem from neglecting spin-orbit interactions in our calculations. The typical magnitudes of spin-orbit effects are discussed to be around 300 meV for actinoid ions.[54] It is thus likely that the degeneracy of the triplet ground state can be lifted by including spin-orbit interactions in our calculations driving UF_4 to the experimentally indicated singlet ground state.

Conclusion

Based on powder X-ray diffraction, micro X-ray fluorescence analysis, IR and Raman spectroscopy, a route for the synthesis of UF_4 free from oxygen-containing impurities has been developed. The magnetic behaviour was re-examined and shown to be consistent with previously reported values. A high-pressure modification HP-UF_4 was synthesized in a multi-anvil press. The compound is metastable under ambient temperature and pressure and its structure was determined by single-crystal X-ray diffraction. HP-UF_4 has a complex 3D network structure that is structurally not related to high-pressure modifications of ZrF_4. To the best of our knowledge, it presents a novel structure type. The coordination numbers of the uranium atoms are nine and eleven, respectively. The magnetic behaviour at high temperatures is similar to that of ambient pressure ZrF_4-type UF_4. The magnetic susceptibility shows saturation effects at low temperatures that are often observed for U^{IV} systems. Quantum chemical solid-state calculations indicate HP-UF_4 to be 10 kJ mol^{-1} per formula unit less stable than ZrF_4-type UF_4.

Experimental Section

General: All operations were performed in either stainless steel (316L) or Monel metal Schlenk lines, which were passivated with 100% fluorine at various pressures before use. Preparations were carried out in an atmosphere of dry and purified argon (5.0, Praxair). Hydrogen fluoride (99%, Hoechst) was dried over K_2NiF_6 prior to its use. The well-educated reader is aware that F_2, HF, and UF_6 can be dangerous if not properly handled. Uranium compounds are radioactive and should therefore not be ingested. Sulfur is safe at ambient conditions.

Preparation of UF_4 from the reaction of sulfur with UF_6: In a typical reaction, sublimed S_8 (455 mg, 14.2 mmol) was placed in a perfluorinated ethylene propylene copolymer (FEP) reaction tube and heated several times under vacuum. Approximately 2 mL of anhydrous HF were added by vacuum distillation. The suspension was frozen with liquid nitrogen and UF_6 (3.27 g, 9.29 mmol) was distilled onto it. The reaction mixture was slowly warmed, and reaction began at the melting point of HF. The supernatant solution turned bluish for a few seconds, then brown with the formation of a greyish solid. After two to three days of reaction time at room temperature, a green solid formed, with a colourless supernatant HF solution (see Figure S1 in the Supporting Information). The solvent and volatile reaction products were distilled into a separate FEP reaction tube and the crude product was transferred into a flame-dried glass Schlenk tube. The tube was attached to a vacuum line and residual S_8 was sublimed off in a fine vacuum at approximately 350 °C. The yield of UF_4 is quantitative with respect to UF_6.

Preparation of the high-pressure modification of UF_4: UF_4 was filled in crucibles, which are made of hexagonal boron nitride (HeBoSint® P100, Henze BNP GmbH, Kempten, Germany) and lined with a platinum foil (thickness 0.027 mm, Ögussa GmbH, Vienna, Austria). For the heating process the boron nitride crucible was surrounded by two thin graphite tubes, which are employed as a graphite resistance heater. The assembly was then placed inside the octahedral pressure medium made from 5% magnesium chromite doped magnesium oxide (Ceramic Substrates & Components Ltd., Isle of Wight, UK). In order to transfer the uniaxial load of the press onto the eight octahedral faces of the magnesium oxide octahedron, eight tungsten carbide cubes (ha-7%Co, Hawedia, Marklkofen, Germany) were used. As soon as the compression process (300 min) of the Walker-module to a maximum pressure of 9.5 GPa was finished, the sample was heated to $T = 873$ K within 10 min. After keeping this temperature constant for 15 min, the sample was steadily cooled to room temperature within 40 min. The completed heating process was followed by a decompression to ambient pressure within 700 minutes. Under strictly inert conditions, the surrounding crucible material has been easily removed from the crystalline sample. Further information about the multi-anvil technique and the construction of the various assemblies can be obtained from numerous references.[55–59]

Powder X-ray diffraction: Powder X-ray diffraction patterns were obtained with a StadiMP diffractometer (Stoe) using $Cu_{K\alpha}$ radiation

© 2019 Wiley-VCH Verlag GmbH & Co. KGaA, Weinheim

ChemPubSoc Europe

CHEMISTRY A European Journal Full Paper

($\lambda = 1.54059$ Å), a germanium monochromator and a Mythen1K detector. The compounds were placed on adhesive tape (Scotch Tape, 3M) and measured in transmission geometry. The data were handled within the WINXPOW software.[60] Rietveld refinement was performed with the TOPAS program suite.[61]

Single-crystal X-ray diffraction: X-ray structure analysis of a single-crystal of HP-UF_4 was carried out with a D8 QUEST PHOTON 100 diffractometer (Bruker) with monochromated molybdenum radiation ($\lambda = 0.71073$ Å). Evaluation and integration of the diffraction data was carried out with the Bruker software package.[62] An empirical multi-scan absorption correction was applied. The structure was solved with Direct Methods (SHELXT 2014/5) in the space group $P2_1/m$ (No. 11) and refined against F^2 (SHELXL 2014/7).[63,64] All atoms were refined anisotropically. Representations of the crystal structure were created with the Diamond software.[65] CCDC 1896463 contains the supplementary crystallographic data for this paper. These data are provided free of charge by The Cambridge Crystallographic Data Centre.

Micro X-ray fluorescence: Micro X-ray fluorescence spectra were obtained with a Tornado M4 µXRF spectrometer (Bruker). A tungsten X-ray tube was used for the measurements.

IR and Raman Spectroscopy: The IR spectra were measured inside a glovebox on an ALPHA FTIR spectrometer (Bruker) equipped with a PLATINUM-ATR unit with a diamond window. The spectra were processed with the OPUS software package.[66] The Raman spectra were collected with an InVia Qontor Raman microscope (Renishaw) equipped with laser wavelengths of 457, 532, 633 and 785 nm. The collected data were handled with the WiRE software.[67]

Magnetic measurements: DC-magnetic data were collected with the aid of the VSM option of a physical property measurement system (ppms) of LOT-Quantum Design. Temperature dependent magnetic data were recorded in the range from 1.8 to 300 K with an applied field of 0.1 T.

The collected data were corrected with respect to the diamagnetic moment of the sample holder, as well as to the diamagnetic contribution ($\chi_{dia} = -7.9 \times 10^{-5}\ cm^3 mol^{-1}$) of the sample, derived from Pascal constants taking into account the composition of UF_4, the result being the net paramagnetic data.[68]

Quantum-chemical calculations: We performed periodic density functional theory (DFT) calculations to calculate the energy difference of the two UF_4 modifications. We further wanted to estimate the magnetic ground state of these structures. The calculations were performed with the software package CRYSTAL17 that uses Gaussian-type atom-centred basis functions.[69] We applied the PBE0 hybrid functional and triple-zeta-valence+ polarization (TZVP) level basis sets for the uranium and fluorine atoms.[70–72] The basis sets derived from the molecular Karlsruhe def2 basis sets were taken from our previous studies.[73] We applied a 5×5×5 Monkhorst–Pack-type *k*-points grid for the reciprocal space integration. For the evaluation of the Coulomb and exchange integrals (TOLINTEG) we used tightened tolerance factors of 8, 8, 8, 8, and 16. We performed the structural optimizations of the atomic positions and lattice constants within the constraints imposed by the respective space group symmetry and the default optimization convergence thresholds. We applied spin-unrestricted formalism using an antiferromagnetic spin orientation. We expect only minor effects of different spin orientations on the results of the optimization.

We estimated the magnetic ground states, performing single-point calculations with different starting spin-orientations using the optimized structure obtained as above as input. For each UF_4 modification, we calculated a non-magnetic, a ferromagnetic, and two antiferromagnetic starting configurations. In case of ZrF_4-type UF_4, we could not find a stable ferromagnetic solution as the calculations always converged in a ferrimagnetic state. The antiferromagnetic spin-orientations were derived from the maximal magnetic subgroups of the space groups of the paramagnetic phases using a single magnetic propagation vector along the crystallographic *b*-axis. For that, we used the MAXMAGN-toolkit from the *Bilbao Crystallographic Server*.[74] The starting magnetizations were set with the input keyword FDOCCUP that defines initial f-orbital starting occupations. We found that for both spin orientations an initial occupation of (0 0 0 0 0 1 1) converged to the lowest energy.

Acknowledgements

F.K. thanks the Deutsche Forschungsgemeinschaft DFG for funding and Solvay for generous donations of F_2. J.B. is thankful for a research stipend (BR5269/1) donated by the DFG. We thank Prof. Willner, Wuppertal, for UF_6 donations and Dr. Conrad, Marburg, for helpful discussions. A.J.K. thanks CSC, the Finnish IT Center for Science, for computational resources.

Conflict of interest

The authors declare no conflict of interest.

Keywords: actinoids · fluorine · high-pressure chemistry · magnetic properties · uranium

[1] H. Hermann, Ueber Einige Uran-Verbindungen, Universität Göttingen, **1861**.
[2] B. C. Reed, *The History and Science of the Manhattan Project*, Springer, Heidelberg (Germany), **2013**.
[3] W. Bacher, E. Jacob, *Gmelin Handbuch Der Anorganischen Chemie, Uran Ergänzungsband C8*, Springer, Berlin (Germany), **1980**.
[4] *The Chemistry of the Actinide and Transactinide Elements* (Eds.: L. R. Morss, N. M. Edelstein, J. Fuger, J. J. Katz), Springer, Dordrecht (The Netherlands), **2006**.
[5] F. Kraus, *Nachr. Chem.* **2008**, *56*, 1236 – 1240.
[6] C. R. Edwards, A. J. Oliver, *JOM* **2000**, *52*, 12 – 20.
[7] National Research Council (US), *Medical Isotope Production without Highly Enriched Uranium*, National Academies Press, Washington, DC (USA), **2009**.
[8] J. Serp, M. Allibert, O. Beneš, S. Delpech, O. Feynberg, V. Ghetta, D. Heuer, D. Holcomb, V. Ignatiev, J. L. Kloosterman, et al., *Prog. Nucl. Energy* **2014**, *77*, 308 – 319.
[9] M. Brovchenko, D. Heuer, E. Merle-Lucotte, M. Allibert, V. Ghetta, A. Laureau, P. Rubiolo, *Nucl. Sci. Eng.* **2013**, *175*, 329 – 339.
[10] J. J. Katz, E. Rabinowitch, *The Chemistry of Uranium*, McGraw-Hill, New York (USA), **1951**.
[11] I. V. Tananaev, N. S. Nikolaev, Y. A. Luk'yanychev, A. A. Opalovskii, *Russ. Chem. Rev.* **1961**, *30*, 654 – 671.
[12] R. J. Allen, H. G. Petrow, P. J. Magno, *Ind. Eng. Chem.* **1958**, *50*, 1748 – 1749.
[13] E. P. Magomedbekov, S. V. Chizhevskaya, O. M. Klimenko, A. V. Davydov, A. V. Zhukov, A. M. Chekmarev, G. A. Sarychev, *At. Energy* **2012**, *111*, 282 – 287.
[14] O. Ruff, A. Heinzelmann, *Z. Anorg. Chem.* **1911**, *72*, 63 – 84.
[15] G. D. Sturgeon, R. A. Penneman, F. H. Kruse, L. B. Asprey, *Inorg. Chem.* **1965**, *4*, 748 – 750.
[16] F. Seel, H. D. Gölitz, *Z. Anorg. Allg. Chem.* **1964**, *327*, 32 – 50.
[17] R. Brown, G. Pez, *Aust. J. Chem.* **1967**, *20*, 2305.
[18] L. E. Trevorrow, J. Fischer, W. H. Gunther, *Inorg. Chem.* **1963**, *2*, 1281 – 1284.

© 2019 Wiley-VCH Verlag GmbH & Co. KGaA, Weinheim

ChemPubSoc Europe

CHEMISTRY A European Journal Full Paper

[19] C. E. Johnson, J. Fischer, M. J. Steindler, *J. Am. Chem. Soc.* **1961**, *83*, 1620 – 1622.
[20] L. B. Asprey, E. M. Foltyn, *J. Fluorine Chem.* **1982**, *20*, 277 – 280.
[21] A. C. Larson, R. B. Roof, D. T. Cromer, *Acta Crystallogr.* **1964**, *17*, 555 – 558.
[22] S. Kern, J. Hayward, S. Roberts, J. W. Richardson, F. J. Rotella, L. Soderholm, B. Cort, M. Tinkle, M. West, D. Hoisington, G. H. Lander, *J. Chem. Phys.* **1994**, *101*, 9333 – 9337.
[23] W. H. Zachariasen, *Acta Crystallogr.* **1949**, *2*, 388 – 390.
[24] T. K. Keenan, L. B. Asprey, *Inorg. Chem.* **1969**, *8*, 235 – 238.
[25] L. B. Asprey, R. G. Haire, *Inorg. Nucl. Chem. Lett.* **1973**, *9*, 1121 – 1128.
[26] P. Souček, O. Beneš, B. Claux, E. Capelli, M. Ougier, V. Tyrpekl, J.-F. Vigier, R. J. M. Konings, *J. Fluorine Chem.* **2017**, *200*, 33 – 40.
[27] M. Goldstein, R. J. Hughes, W. D. Unsworth, *Spectrochim. Acta Part A* **1975**, *31*, 621 – 624.
[28] W. Krasser, H. W. Nürnberg, *Spectrochim. Acta Part A* **1970**, *26*, 1059 – 1062.
[29] G. C. Allen, N. R. Holmes, *Appl. Spectrosc.* **1994**, *48*, 525 – 530.
[30] M. J. Lipp, Z. Jenei, J. Park-Klepeis, W. J. Evans, *LLNL-TR-522251*, Lawrence Livermore National Laboratory, **2011**.
[31] E. Villa-Aleman, M. S. Wellons, *J. Raman Spectrosc.* **2016**, *47*, 865 – 870.
[32] B. A. Trofimov, L. M. Sinegovskaya, N. K. Gusarova, *J. Sulfur Chem.* **2009**, *30*, 518 – 554.
[33] R. Böhler, A. Quaini, L. Capriotti, P. Çakır, O. Beneš, K. Boboridis, A. Guiot, L. Luzzi, R. J. M. Konings, D. Manara, *J. Alloys Compd.* **2014**, *616*, 5 – 13.
[34] D. M. L. Ho, A. E. Jones, J. Y. Goulermas, P. Turner, Z. Varga, L. Fongaro, T. Fanghänel, K. Mayer, *Forensic Sci. Int.* **2015**, *251*, 61 – 68.
[35] S. S. Batsanov, Y. M. Kiselev, L. I. Kopaneva, *Russ. J. Inorg. Chem.* **1980**, *25*, 1987 – 1988.
[36] A. A. Deribas, E. D. Ruchkin, V. S. Filatkina, L. A. Khripin, *Combust. Explos. Shock Waves (Engl. Transl.)* **1966**, *2*, 91 – 93.
[37] G. Benner, B. G. Müller, *Z. Anorg. Allg. Chem.* **1990**, *588*, 33 – 42.
[38] R. Schmidt, B. G. Müller, *Z. Anorg. Allg. Chem.* **1999**, *625*, 605 – 608.
[39] D. H. Templeton, C. H. Dauben, *J. Am. Chem. Soc.* **1954**, *76*, 5237 – 5239.
[40] L. B. Asprey, F. H. Kruse, R. A. Penneman, *Inorg. Chem.* **1967**, *6*, 544 – 548.
[41] S. E. Nave, R. G. Haire, P. G. Huray, *Phys. Rev. B* **1983**, *28*, 2317 – 2327.
[42] R. Papiernik, D. Mercurio, B. Frit, *Acta Crystallogr. Sect. B* **1982**, *38*, 2347 – 2353.
[43] R. Papiernik, B. Frit, B. Gaudreau, *Rev. Chim. Miner.* **1986**, *23*, 400 – 436.
[44] J.-P. Laval, *Acta Crystallogr. Sect. C* **2014**, *70*, 742 – 748.
[45] I. Oftedal, *Z. Phys. Chem. Sect. B* **1929**, *5*, 272 – 291.
[46] J. Yeon, M. D. Smith, J. Tapp, A. Möller, H.-C. zur Loye, *Inorg. Chem.* **2014**, *53*, 6289 – 6298.
[47] W. Kleber, *Krist. Tech.* **1967**, *2*, 13 – 14.
[48] T. Yoshimura, C. Miyake, S. Imoto, *Bull. Chem. Soc. Jpn.* **1974**, *47*, 515 – 518.
[49] D. R. Kindra, W. J. Evans, *Chem. Rev.* **2014**, *114*, 8865 – 8882.
[50] V. V. Klepov, J. B. Felder, H.-C. zur Loye, *Inorg. Chem.* **2018**, *57*, 5597 – 5606.
[51] J. H. Burns, D. W. Osborne, E. F. Westrum, *J. Chem. Phys.* **1960**, *33*, 387 – 394.
[52] M. J. M. Leask, D. W. Osborne, W. P. Wolf, *J. Chem. Phys.* **1961**, *34*, 2090 – 2099.
[53] W. T. Carnall, G. K. Liu, C. W. Williams, M. F. Reid, *J. Chem. Phys.* **1991**, *95*, 7194 – 7203.
[54] *Handbook on the Physics and Chemistry of the Actinides*, North-Holland Physics Publishing, Elsevier, Amsterdam (The Netherlands), **1986**.
[55] H. Huppertz, G. Heymann, U. Schwarz, M. R. Schwarz, in *Handbook of Solid State Chemistry* (Eds.: R. Dronskowski, S. Kikkawa, A. Stein), Wiley-VCH, Weinheim (Germany), **2017**, pp. 23 – 48.
[56] H. Huppertz, *Z. Kristallogr. Cryst. Mater.* **2004**, *219*, 330 – 338.
[57] D. Walker, M. A. Carpenter, C. M. Hitch, *Am. Mineral.* **1990**, *75*, 1020 – 1028.
[58] D. Walker, *Am. Mineral.* **1991**, *76*, 1092 – 1100.
[59] D. C. Rubie, *Phase Transitions* **1999**, *68*, 431 – 451.
[60] STOE & Cie, *WinXPOW*, STOE & Cie GmbH, Hilpertstrasse 10, 64295 Darmstadt (Germany), **2015**.
[61] A. A. Coelho, *J. Appl. Crystallogr.* **2018**, *51*, 210 – 218.
[62] *APEX2*, Bruker AXS Inc., Madison, Wisconsin, USA, **2014**.
[63] G. M. Sheldrick, *Acta Crystallogr. Sect. A* **2015**, *71*, 3 – 8.
[64] C. B. Hübschle, G. M. Sheldrick, B. Dittrich, *J. Appl. Crystallogr.* **2011**, *44*, 1281 – 1284.
[65] K. Brandenburg, H. Putz, *Diamond – Crystal and Molecular Structure Visualization*, Crystal Impact GbR, Bonn (Germany), **2017**.
[66] *OPUS*, Bruker Optik GmbH, Ettlingen (Germany), **2009**.
[67] *WiRE (Windows-Based Raman Environment)*, Renishaw Plc., New Mills, Kingswood, Wotton-under-Edge GL12 8JR (UK), **2018**.
[68] *Magnetic Properties of Coordination and Organometallic Transition Metal Compounds* (Eds.: K.-H. Hellwege, A. M. Hellwege), Springer, Berlin/Heidelberg (Germany), **1979**.
[69] R. Dovesi, A. Erba, R. Orlando, C. M. Zicovich-Wilson, B. Civalleri, L. Maschio, M. Rérat, S. Casassa, J. Baima, S. Salustro, et al., *WIREs Comput. Mol. Sci.* **2018**, *8*, e1360.
[70] C. Adamo, V. Barone, *J. Chem. Phys.* **1999**, *110*, 6158 – 6170.
[71] F. Weigend, R. Ahlrichs, *Phys. Chem. Chem. Phys.* **2005**, *7*, 3297 – 3305.
[72] F. Weigend, *Phys. Chem. Chem. Phys.* **2006**, *8*, 1057 – 1065.
[73] B. Scheibe, C. Pietzonka, O. Mustonen, M. Karppinen, A. J. Karttunen, M. Atanasov, F. Neese, M. Conrad, F. Kraus, *Angew. Chem. Int. Ed.* **2018**, *57*, 2914 – 2918; *Angew. Chem.* **2018**, *130*, 2964 – 2968.
[74] M. I. Aroyo, A. Kirov, C. Capillas, J. M. Perez-Mato, H. Wondratschek, *Acta Crystallogr. Sect. A* **2006**, *62*, 115 – 128.

Manuscript received: February 11, 2019
Accepted manuscript online: March 26, 2019
Version of record online: May 3, 2019

 © 2019 Wiley-VCH Verlag GmbH & Co. KGaA, Weinheim

CHEMISTRY
A European Journal

Supporting Information

UF_4 and the High-Pressure Polymorph HP-UF_4

Benjamin Scheibe,[a] Jörn Bruns,[b] Gunter Heymann,[c] Malte Sachs,[a] Antti J. Karttunen,[d] Clemens Pietzonka,[a] Sergei I. Ivlev,[a] Hubert Huppertz,[c] and Florian Kraus*[a]

chem_201900639_sm_miscellaneous_information.pdf

Content

Pictures of the reaction of UF_6 and sulfur 2
Selected crystallographic data of ZrF_4-type UF_4 and hp-UF_4 3
IR spectra of ZrF_4-type UF_4 4
Raman spectra of ZrF_4-type UF_4 5
Crystallographic details of hp-UF_4 6
Quantum Chemical calculations 7
References 9

Pictures of the reaction of UF_6 and sulfur

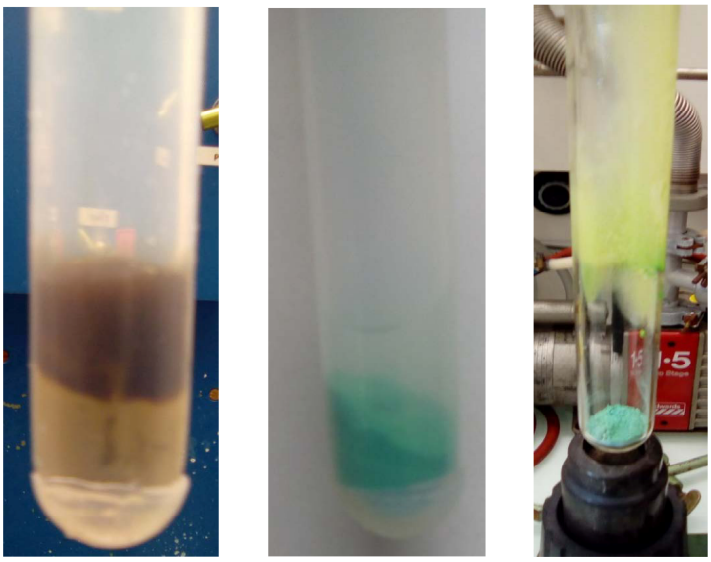

Figure S1. Left: Reaction mixture of UF_6 and S_8 in aHF after a few minutes reaction time at room temperature. Middle: Formed UF_4 after three days reaction time at room temperature. Right: Sublimation of excessive S_8 in vacuo at elevated temperatures.

Selected crystallographic data of ZrF_4-type UF_4 and hp-UF_4

The Rietveld refinements were carried out with the TOPAS program suite.[1] The structure model of ZrF_4-type UF_4 was taken from the literature and for hp-UF4 from our single-crystal structure determination.[2] The background was corrected with Chebyshev polynomials. The peak shapes were described with TCHZ pseudo-Voigt functions. Anisotropic broadening was refined by the model of Stephens.[3] For hp-UF_4 preferred orientation was corrected by spherical harmonics. For ZrF_4-type UF_4 the isotropic atomic displacement parameters were fixed to an arbitrary value, the cell parameters and atom coordinates were refined. For hp-UF_4 the isotropic atomic displacement parameters of the F atoms were fixed to an arbitrary value, the isotropic atomic displacement parameters of the U atoms, the cell parameters and atom coordinates were refined.

Table S1. Selected crystallographic data and refinement details of ZrF_4-type UF_4 and hp-UF_4.

	ZrF_4-type UF_4 (PXRD)	hp-UF_4 (PXRD)
Empirical formula	F_4U_1	F_4U_1
Color and appearance	green powder	green powder
Molar mass / g·mol^{-1}	314.02	314.02
Crystal system	monoclinic	monoclinic
Space group (No.)	$C2/c$ (no. 15)	$P2_1/m$ (no. 11)
a / Å	12.815(1)	4.6080(1)
b / Å	10.806(1)	6.9955(1)
c / Å	8.3804(2)	7.6364(1)
β / °	126.26(1)	101.07(1)
V / Å^3	935.71(3)	241.58(1)
Z	12	4
$\rho_{calcd.}$ / g·cm^{-3}	6.6873(2)	8.6339(2)
λ / Å	1.540598 (Cu-$K_{\alpha1}$)	1.540598 (Cu-$K_{\alpha1}$)
T / K	293	293
2θ range measured (min, max, increment) / °	10.000, 95.005, 0.015	10.000, 90.130, 0.015
2θ range refined (min, max) / °	10.000, 80.000	10.000, 90.130
R_p, wR_p, R_{exp}	0.0315, 0.0451, 0.0212	0.0198, 0.0269, 0.0051
GOF	2.13	5.31
R_{Bragg} (I)	0.0201	0.0066
Data, parameter, restraints, constraints	4666, 59, 0, 9	5342, 82, 0, 5

IR spectra of ZrF_4-type UF_4

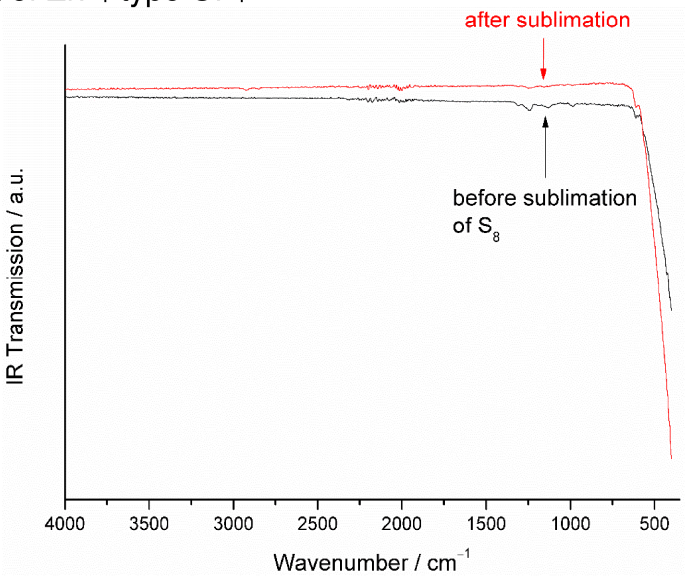

Figure S2. ATR-IR spectra of the ZrF_4-type UF_4 obtained from the reduction of UF_6. In black the spectrum before the sublimation of excessive sulfur is shown, in red after the sublimation of sulfur in vacuo. The signals in the range of 1800-2250 cm^{-1} are caused by the diamond window of the ATR unit.

Raman spectra of ZrF_4-type UF_4

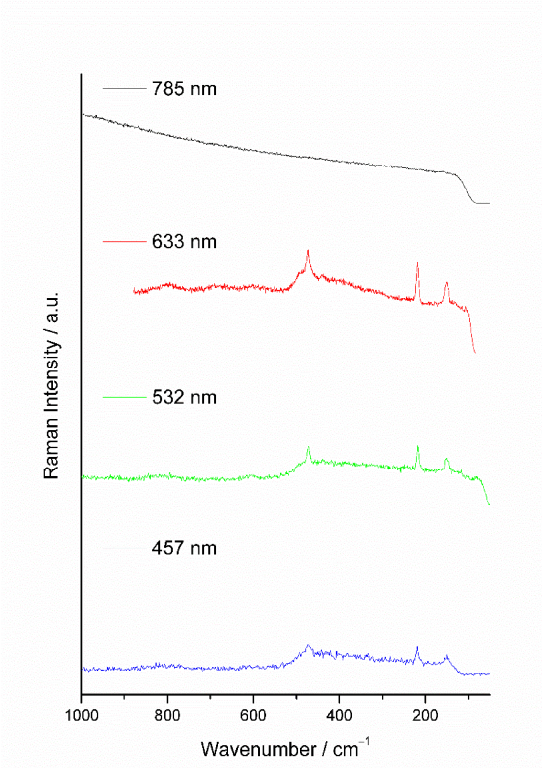

Figure S3. Raman spectra of ZrF_4-type UF_4 obtained with different excitation wavelengths. With a wavelength of 785 nm strong fluorescence was observed and no bands could be resolved.

Crystallographic details of hp-UF_4

Table S2. Anisotropic displacement parameters of hp-UF_4 at 183 K.

Atom	U^{11} / Å^2	U^{22} / Å^2	U^{33}/ Å^2	U^{23} / Å^2	U^{13} / Å^2	U^{12} / Å^2
U(1)	0.00181(5)	0.00338(5)	0.00184(5)	0	0.00044(4)	0
U(2)	0.00249(5)	0.00266(5)	0.00196(5)	0	0.00100(4)	0
F(1)	0.0060(7)	0.0078(7)	0.0051(6)	-0.0008(5)	0.0000(5)	0.0010(5)
F(2)	0.0039(6)	0.0055(6)	0.0044(6)	-0.0003(5)	0.0006(5)	-0.0007(5)
F(3)	0.0071(10)	0.0071(10)	0.0074(10)	0	0.0041(8)	0
F(4)	0.0068(7)	0.0073(6)	0.0067(6)	-0.0007(6)	0.0025(5)	0.0014(6)
F(5)	0.0066(9)	0.0061(9)	0.0054(9)	0	0.0044(7)	0

Quantum Chemical calculations

Table S3: Comparison of experimental cell parameters of ZrF_4-type UF_4 (*C*2/*c*, *mS*60) at 293 K with the results of DFT structure optimization (DFT-PBE0/TZVP) at 0 K.

	Experiment	DFT	Difference Δ / %
a / Å	12.816(1)	12.79	−0.2
b / Å	10.807(1)	10.70	−1.0
c / Å	8.3813(7)	8.35	−0.4
ß / °	126.262(6)	126.10	−0.1
V / Å³	936.0(2)	923.20	−1.3

Table S4: Comparison of experimental atomic positions in fractional coordinates of ZrF_4-type UF_4 (*C*2/*c*, *mS*60) with the results of DFT structure optimization (PBE0/TZVP) at 0 K.

Atom	Wyckoff	Site symmetry		*x*	*y*	*z*
U(1)	4*e*	2	Exp.	0	0.2131(2)	1/4
			DFT	0	0.211	1/4
U(2)	8*f*	1	Exp.	0.2044(1)	0.4277(1)	0.8307(2)
			DFT	0.203	0.428	0.829
F(1)	4*c*	$\bar{1}$	Exp.	1/4	1/4	0
			DFT	1/4	1/4	0
F(2)	4*e*	2	Exp.	0	0.6041(2)	1/4
			DFT	0	0.605	1/4
F(3)	8*f*	1	Exp.	0.8935(2)	0.2937(2)	0.9315(3)
			DFT	0.894	0.293	0.929
F(4)	8*f*	1	Exp.	0.8800(2)	0.0543(2)	0.0432(3)
			DFT	0.878	0.052	0.043
F(5)	8*f*	1	Exp.	0.7887(2)	0.5303(2)	0.8952(3)
			DFT	0.795	0.530	0.899
F(6)	8*f*	1	Exp.	0.6182(2)	0.1211(2)	0.7813(4)
			DFT	0.619	0.122	0.788
F(7)	8*f*	1	Exp.	0.6252(2)	0.3472(2)	0.6526(4)
			DFT	0.628	0.349	0.661

Table S5: Comparison of experimental cell parameters of hp-UF_4 ($P2_1/m$, *mP*20) at 183 K with the results of DFT structure optimization (DFT-PBE0/TZVP) at 0 K.

	Experiment	DFT	Difference Δ / %
a / Å	4.6015(2)	4.57	−0.7
b / Å	6.9786(3)	6.94	−0.5
c / Å	7.6271(3)	7.64	+0.2
ß / °	101.013(2)	101.28	+0.3
V / Å³	240.411(18)	237.34	−1.3

Table S6: Comparison of experimental atomic positions in fractional coordinates of hp-UF_4 ($P2_1/m$, $mP20$) at 183 K with the results of DFT structure optimization (DFT-PBE0/TZVP) at 0 K.

Atom	Wyckoff	Site symmetry		*x*	*y*	*z*
U(1)	*2e*	*m*	Exp.	0.03554(3)	3/4	0.82749(2)
			DFT	0.046	3/4	0.830
U(2)	*2e*	*m*	Exp.	0.45712(3)	3/4	0.34398(2)
			DFT	0.455	3/4	0.348
F(1)	4f	1	Exp.	0.2048(4)	0.9198(3)	0.0933(2)
			DFT	0.207	0.920	0.094
F(2)	4f	1	Exp.	0.2975(4)	0.4259(2)	0.3961(2)
			DFT	0.301	0.425	0.394
F(3)	*2e*	*m*	Exp.	0.5525(6)	3/4	0.8844(3)
			DFT	0.549	3/4	0.882
F(4)	4f	1	Exp.	0.7764(4)	0.5546(3)	0.2513(2)
			DFT	0.779	0.569	0.252
F(5)	*2e*	*m*	Exp.	0.1582(5)	3/4	0.5410(3)
			DFT	0.156	3/4	0.541

Table S7: Atomic positions of the magnetic uranium atoms in the crystallographic unit cell of ZrF_4-type UF_4 ($C2/c$, $mS60$) from DFT structure optimization (PBE0/TZVP).

Atom	*x*	*y*	*z*
U1	-2.025812360064E-01 -	4.279394338636E-01	1.713934186831E-01
U2	2.977204330399E-01	7.164525727251E-02	1.715764021913E-01
U3	2.014408686332E-01 -	4.277700338751E-01	3.266649137127E-01
U4	-2.989441634133E-01	7.268654040022E-02	3.266675002657E-01
U5	2.032982416777E-01	4.277963123136E-01	-1.712626810382E-01
U6	-2.966706288189E-01	-7.191720929750E-02	-1.705875268037E-01
U7	-2.013368717084E-01	4.277156303464E-01	-3.272528167438E-01
U8	2.982978851207E-01	-7.249700659936E-02	-3.279700110002E-01
U9	-4.985983791647E-01	-2.894450931139E-01	2.522031501758E-01
U10	2.777442930952E-04	2.107139405926E-01	2.508244624342E-01
U11	-4.997350775920E-01	2.891758627377E-01	-2.501562994115E-01
U12	-3.412936060106E-04	-2.107431602974E-01	-2.510659070890E-01

Table S8: Atomic positions of the magnetic uranium atoms in the crystallographic unit cell of hp-UF_4 ($P2_1/m$, $mP20$) from DFT structure optimization (PBE0/TZVP).

Atom	*x*	*y*	*z*
U1	4.586298665850E-01	-1.734668183328E+00	-1.275194279585E+00
U2	-4.542727350410E-01	1.734668183328E+00	1.289077508462E+00
U3	1.567248602702E+00	-1.734668183328E+00	2.600325169785E+00
U4	-1.559838813908E+00	1.734668183328E+00	-2.585971034342E+00

References

[1] A. A. Coelho, *J. Appl. Crystallogr.* **2018**, *51*, 210–218.
[2] A. C. Larson, R. B. Roof, D. T. Cromer, *Acta Crystallogr.* **1964**, *17*, 555–558.
[3] P. W. Stephens, *J. Appl. Crystallogr.* **1999**, *32*, 281–289.

7.8. Synthesis and Crystal Structures of Transition Metal(II) Fluoridometallate(IV) Hydrates of Neptunium and Plutonium: $A^{II}M^{IV}F_6 \cdot 3H_2O$ (A^{II} = Mn, Zn; M^{IV} = Np, Pu)

Benjamin Scheibe, Juliane März, Moritz Schmidt, Thorsten Stumpf, Florian Kraus

Eur. J. Inorg. Chem. **2020**, *2020*, 2279-2284.
DOI: 10.1002/ejic.202000298

© 2020 The Authors. Published by Wiley-VCH Verlag GmbH & Co. KGaA.

Open access article distributed under the Creative Commons CC BY 4.0 license.
The original licensed material is shown.
(https://creativecommons.org/licenses/by/4.0/legalcode)

EurJIC
European Journal of Inorganic Chemistry

Full Paper
doi.org/10.1002/ejic.202000298

Np and Pu Fluoridometallates

Synthesis and Crystal Structures of Transition Metal(II) Fluoridometallate(IV) Hydrates of Neptunium and Plutonium: $A^{II}M^{IV}F_6 \cdot 3H_2O$ (A^{II} = Mn, Zn; M^{IV} = Np, Pu)

Benjamin Scheibe,[a] Juliane März,[b] Moritz Schmidt,[b] Thorsten Stumpf,*[b] and Florian Kraus*[a]

Abstract: Transition metal(II) fluoridometallates(IV) $A^{II}M^{IV}F_6 \cdot 3H_2O$ (A^{II} = Mn, Zn; M^{IV} = Np, Pu) were synthesized from NpO_2 or PuO_2 and the respective transition metal chlorides from hydrofluoric acid under mild conditions. The olive-green (Np) or orange (Pu) compounds were obtained as single-crystals and the respective structures were determined by single-crystal X-ray diffraction. In the isotypic compounds, chains of edgesharing tricapped trigonal prismatic polyhedra $^{2}_{\infty}[M^{IV}F_{8/2}(H_2O)_{1/1}]$, are present and an overall three-dimensional network structure is observed in which the A^{II} and M^{IV} atoms are arranged according to the simple NaCl structure type. Within the respective U–Pu series of the Zn and Mn salts the cell volumes and the M^{IV}–F distances decrease due to the actinoid contraction.

Introduction

With fluoride ion donors like alkali metal fluorides, *A*F, lanthanoid or actinoid tetrafluorides, $M^{IV}F_4$ (M^{IV} is e.g. Ce, Tb, Th, U), can form ternary compounds of manifold compositions such as $AM^{IV}F_5$, $AM^{IV}{}_2F_9$, $AM^{IV}{}_3F_{13}$, and $A_7M^{IV}{}_6F_{31}$.[1–4] Furthermore, various fluoridometallate(IV) hydrates containing divalent transition metal cations, A^{II}, have been described, which have compositions like $A^{II}M^{IV}F_6 \cdot 3H_2O$ (A^{II} = Mn, Ni, Zn; M^{IV} = U, Np) and $A^{II}M^{IV}{}_2F_{10} \cdot 8H_2O$ (A^{II} = Co, Ni; M^{IV} = U, Np).[5–8] The uranium compounds $A^{II}U^{IV}F_6 \cdot 3H_2O$ (A^{II} = Mn, Ni, Zn) were synthesized under hydrothermal conditions at 200 °C.[5,6] Such a synthetic approach utilizes an in situ-reduction of the uranyl acetate precursor and hydrofluoric acid as both the solvent and fluoride ion source. Similar hydrothermal reaction conditions have been used for the synthesis of a variety of single-crystalline ternary and quaternary fluoridometallates(IV) of Th–Pu.[4,9–16] Whereas for the synthesis of the hexafluoridoneptunates(IV) $A^{II}Np^{IV}F_6 \cdot 3H_2O$ (A^{II} = Mn, Fe, Co, Ni, Zn), neptunium tetrafluoride, the transition metal fluoride $A^{II}F_2$, 40 % hydrofluoric acid and much harsher conditions of 750 K and a pressure of 2000 bar were used.[7,8] The single-crystal structure of $CoNpF_6 \cdot 3H_2O$ was determined and the space group was assigned as *C*2 (No. 5).[7,8] This structure model was then used for the calculation of the Sternheimer quadrupole antishielding factor, γ_∞, of Np^{IV} in the series $A^{II}Np^{IV}F_6 \cdot 3H_2O$ (A^{II} = Mn, Fe, Co, Ni, Zn).[17,18] Overall, the fluoridometallates(IV) of transuranium elements have been investigated far less than the respective uranium or thorium systems, thus synthetic pathways and detailed crystallographic investigations of fluoridometallates(IV), especially of plutonium, are lacking.[1]

Here, we present the synthesis of transition metal(II) fluoridometallate(IV) hydrates of Np and Pu and their crystal structures.

Results and Discussion

The transition metal fluoridometallate(IV) hydrates with the composition $A^{II}M^{IV}F_6 \cdot 3H_2O$ (A^{II} = Mn, Zn; M^{IV} = Np, Pu), manganese(II) hexafluoridoneptunate(IV) trihydrate (abbreviated as **MnNp**), manganese(II) hexafluoridoplutonate(IV) trihydrate (**MnPu**), zinc(II) hexafluoridoneptunate(IV) trihydrate (**ZnNp**), and zinc(II) hexafluoridoplutonate(IV) trihydrate (**ZnPu**), have been synthesized from hydrofluoric acid suspensions starting from the oxides (NpO_2 or PuO_2) and a transition metal dichloride ($MnCl_2 \cdot 4H_2O$ or $ZnCl_2$), see Equation (1).

$$6\,HF_{(aq)} + A^{II}Cl_{2(aq)} + M^{IV}O_{2(s)} + H_2O \xrightarrow{HF_{(aq)}} A^{II}M^{IV}F_6 \cdot 3H_2O_{(s)} + 2\,HCl_{(aq)} \quad (1)$$

A^{II} = Mn, Zn
M^{IV} = Np, Pu

Single-crystals of the olive-green (Np) or orange (Pu) compounds could be obtained from the suspensions after a few

[a] B. Scheibe M.Sc., Prof. Dr. F. Kraus
Fachbereich Chemie, Philipps-Universität Marburg,
Hans-Meerwein-Straße 4, 35032 Marburg, Germany
E-mail: f.kraus@uni-marburg.de
[b] Dr. J. März, Dr. M. Schmidt, Prof. Dr. T. Stumpf
Institut für Ressourcenökologie, Helmholtz-Zentrum Dresden-Rossendorf,
Bautzner Landstraße 400, 01328 Dresden, Germany
E-mail: t.stumpf@hzdr.de
Supporting information and ORCID(s) from the author(s) for this article are available on the WWW under https://doi.org/10.1002/ejic.202000298.
© 2020 The Authors. Published by Wiley-VCH Verlag GmbH & Co. KGaA. · This is an open access article under the terms of the Creative Commons Attribution License, which permits use, distribution and reproduction in any medium, provided the original work is properly cited.

© 2020 The Authors. Published by Wiley-VCH Verlag GmbH & Co. KGaA, Weinheim

EurJIC
European Journal of Inorganic Chemistry

Full Paper
doi.org/10.1002/ejic.202000298

Chemistry Europe
European Chemical Societies Publishing

days of crystallization time at room temperature (**MnNp** and **MnPu**) or at 60 °C (**ZnNp** and **ZnPu**), see Figure 1 for photographs of the crystals of **MnNp** and **ZnPu**. The crystal structures of the obtained compounds were determined by means of single-crystal X-ray diffraction.

The salts are isotypic and crystallize in the monoclinic space group *C*2/*c* (No. 15) with four formula units per unit cell, *mS*44, 15, f^4e^2d (H atoms neglected for Pearson symbol and Wyckoff sequence). See Table 1 for select crystallographic data and details of the structure determinations. Atom coordinates and

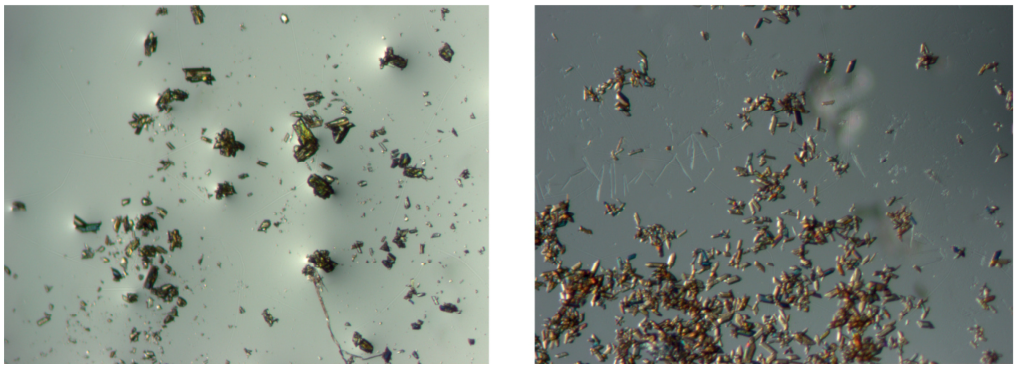

Figure 1. Left: Picture of olive-green crystals of the compound MnNp. The largest crystals were approximately 0.15 mm long. Right: Picture of orange crystals of the compound ZnPu. The largest crystals were approximately 0.15 mm long.

Table 1. Selected crystallographic data and details of the structure determinations of the compounds $AMF_6{\cdot}3H_2O$ (*A* = Mn, Zn; *M* = Np, Pu).

	MnNp	**MnPu**	**ZnNp**	**ZnPu**
Formula	$MnNpF_6{\cdot}3H_2O$	$MnPuF_6{\cdot}3H_2O$	$ZnNpF_6{\cdot}3H_2O$	$ZnPuF_6{\cdot}3H_2O$
Molar mass /g mol^{-1}	459.97	464.97	470.42	475.42
Space group (No.)	*C*2/*c* (15)	*C*2/*c* (15)	*C*2/*c* (15)	*C*2/*c* (15)
a /Å	12.2729(5)	12.2436(9)	12.0846(9)	12.0429(9)
b /Å	6.9548(3)	6.9641(5)	6.9154(5)	6.9110(5)
c /Å	8.0105(3)	7.9707(6)	7.9236(6)	7.8825(6)
β /°	92.9860(10)	93.149(2)	92.800(3)	93.039(3)
V /Å^3	682.81(5)	678.60(9)	661.38(8)	655.13(8)
Z	4	4	4	4
Pearson symbol	*mS*44	*mS*44	*mS*44	*mS*44
$\rho_{calc.}$ /g cm^{-3}	4.48	4.55	4.72	4.82
μ /mm^{-1}	17.07	11.57	19.34	13.72
Color	olive green	orange	olive green	orange
Crystal habitus	block	block	block	block
Crystal size /mm^3	0.045×0.059×0.076	0.054×0.087×0.219	0.047×0.091×0.112	0.032×0.061×0.124
T /K	100	100	100	100
λ /Å	0.71073 (Mo-K_α)	0.71073 (Mo-K_α)	0.71073 (Mo-K_α)	0.71073 (Mo-K_α)
No. of reflections	36885	24596	19872	59570
θ range /°	3.32–37.78	3.33–37.76	3.38–37.82	3.39–45.45
Range of Miller indices	$-20 \le h \le 20$	$-21 \le h \le 20$	$-20 \le h \le 20$	$-24 \le h \le 24$
	$-11 \le k \le 11$	$-12 \le k \le 11$	$-11 \le k \le 11$	$-13 \le k \le 13$
	$-13 \le l \le 13$	$-13 \le l \le 13$	$-13 \le l \le 12$	$-15 \le l \le 15$
Absorption correction	multi-scan	multi-scan	multi-scan	multi-scan
T_{min}, T_{max}	0.31, 0.41	0.11, 0.21	0.17, 0.26	0.21, 0.35
R_{int}, R_σ	0.027, 0.010	0.037, 0.015	0.047, 0.022	0.038, 0.012
Completeness of the data set	0.990	0.990	0.997	1.000
No. of unique reflections	1810	1803	1768	2756
No. of parameters	66	66	66	66
No. of restraints	0	0	0	0
No. of constraints	0	0	0	0
S (all data)	1.36	1.18	1.08	1.15
$R(F)$ [$I \ge 2\sigma(I)$, all data]	0.010, 0.010	0.010, 0.011	0.016, 0.017	0.011, 0.012
$wR(F^2)$ [$I \ge 2\sigma(I)$, all data]	0.022, 0.023	0.024, 0.024	0.036, 0.037	0.023, 0.023
Extinction coefficient	0.00235(8)	0.00384(12)	0.00352(13)	0.00351(7)
$\Delta\rho_{max}$, $\Delta\rho_{min}$ /e Å^{-3}	0.83, −0.73	0.87, −0.88	1.90, −1.21	1.49, −0.92

© 2020 The Authors. Published by Wiley-VCH Verlag GmbH & Co. KGaA, Weinheim

EurJIC
European Journal of Inorganic Chemistry

Full Paper
doi.org/10.1002/ejic.202000298

Chemistry Europe
European Chemical Societies Publishing

Table 2. Atomic coordinates and equivalent isotropic displacement parameters U_{iso} of $MnNpF_6{\cdot}3H_2O$ and $MnPuF_6{\cdot}3H_2O$.

Atom	Position	$MnNpF_6{\cdot}3H_2O$				$MnPuF_6{\cdot}3H_2O$			
		x	*y*	*z*	U_{iso} /Å^2	*x*	*y*	*z*	U_{iso} /Å^2
M^{IV}(1)	4*e*	1/2	0.48050(2)	1/4	0.00300(2)	1/2	0.48099(2)	1/4	0.00423(3)
Mn(1)	4*c*	3/4	3/4	1/2	0.00483(4)	3/4	3/4	1/2	0.00646(5)
F(1)	8*f*	0.43161(7)	0.36997(12)	−0.00662(10)	0.00841(14)	0.43327(7)	0.36949(13)	−0.00649(11)	0.01038(15)
F(2)	8*f*	0.61502(7)	0.71306(12)	0.33447(10)	0.00783(13)	0.61549(7)	0.71150(13)	0.33145(11)	0.00960(14)
F(3)	8*f*	0.66669(7)	0.64464(12)	0.70309(10)	0.00760(13)	0.66574(7)	0.64610(13)	0.70356(11)	0.00939(14)
O(1)	4*e*	1/2	0.1191(2)	1/4	0.0150(3)	1/2	0.1185(2)	1/4	0.0176(3)
O(2)	8*f*	0.67913(9)	1.02977(16)	0.56677(15)	0.01001(17)	0.67918(10)	1.03000(16)	0.56453(17)	0.01177(19)
H(1)	8*f*	0.544(2)	0.051(4)	0.214(4)	0.024(7)	0.547(3)	0.050(4)	0.214(4)	0.020(7)
H(2)	8*f*	0.713(3)	1.081(5)	0.630(4)	0.033(8)	0.712(3)	1.073(5)	0.635(4)	0.023(7)
H(3)	8*f*	0.652(3)	1.110(5)	0.516(4)	0.034(8)	0.656(3)	1.112(5)	0.511(4)	0.039(9)

Table 3. Atomic coordinates and equivalent isotropic displacement parameters U_{iso} of $ZnPuF_6{\cdot}3H_2O$ and $ZnPuF_6{\cdot}3H_2O$.

Atom	Position	$ZnPuF_6{\cdot}3H_2O$				$ZnPuF_6{\cdot}3H_2O$			
		x	*y*	*z*	U_{iso} /Å^2	*x*	*y*	*z*	U_{iso} /Å^2
M^{IV}(1)	4*e*	1/2	0.48128(2)	1/4	0.00317(4)	1/2	0.48183(2)	1/4	0.00253(1)
Zn(1)	4*c*	3/4	3/4	1/2	0.00516(6)	3/4	3/4	1/2	0.00469(3)
F(1)	8*f*	0.43071(11)	0.36674(19)	−0.00686(16)	0.0082(2)	0.43236(6)	0.36659(11)	−0.00721(9)	0.00795(11)
F(2)	8*f*	0.61869(11)	0.71263(18)	0.33833(16)	0.0073(2)	0.61898(6)	0.71136(11)	0.33564(9)	0.00706(10)
F(3)	8*f*	0.66962(10)	0.64449(18)	0.69891(16)	0.0074(2)	0.66880(6)	0.64552(11)	0.69958(9)	0.00721(10)
O(1)	4*e*	1/2	0.1184(4)	1/4	0.0148(5)	1/2	0.1189(2)	1/4	0.0164(3)
O(2)	8*f*	0.68105(15)	1.0185(2)	0.5661(2)	0.0086(3)	0.68107(8)	1.01901(13)	0.56450(13)	0.00854(12)
H(1)	8*f*	0.534(4)	0.058(7)	0.206(6)	0.029(12)	0.545(3)	0.044(5)	0.209(5)	0.035(9)
H(2)	8*f*	0.718(3)	1.072(6)	0.630(5)	0.015(9)	0.720(2)	1.075(5)	0.632(4)	0.021(7)
H(3)	8*f*	0.655(5)	1.105(9)	0.512(7)	0.047(15)	0.651(3)	1.104(5)	0.506(4)	0.031(8)

Table 4. Select atomic distances in Å and bond multiplicities of the compounds $A^{II}M^{IV}F_6{\cdot}3H_2O$ (A^{II} = Mn, Zn; M^{IV} = U,[5] Np, Pu).

Multiplicity	Distance	$MnUF_6{\cdot}3H_2O$[5]	$MnNpF_6{\cdot}3H_2O$	$MnPuF_6{\cdot}3H_2O$	$ZnUF_6{\cdot}3H_2O$[5]	$ZnNpF_6{\cdot}3H_2O$	$ZnPuF_6{\cdot}3H_2O$
2	M^{IV}(1)–F(1)	2.318(2)	2.3112(8)	2.2949(9)	2.3143(11)	2.3031(13)	2.2876(7)
2	M^{IV}(1)–F(1)	2.431(2)	2.3994(8)	2.3860(9)	2.4040(12)	2.3822(13)	2.3641(8)
2	M^{IV}(1)–F(2)	2.238(2)	2.2287(8)	2.2129(9)	2.2461(11)	2.2380(12)	2.2187(7)
2	M^{IV}(1)–F(3)	2.284(2)	2.2724(8)	2.2629(9)	2.2947(11)	2.2810(13)	2.2695(7)
1	M^{IV}(1)–O(1)	2.585(5)	2.5131(16)	2.5247(17)	2.536(2)	2.509(2)	2.5079(15)
2	A^{II}–F(2)	2.093(2)	2.0831(8)	2.0847(9)	2.0079(11)	2.0068(12)	2.0057(7)
2	A^{II}–F(3)	2.103(2)	2.0981(8)	2.0987(9)	2.0278(11)	2.0272(13)	2.0287(7)
2	A^{II}–O(2)	2.199(3)	2.2084(11)	2.2063(11)	2.1090(15)	2.1117(16)	2.1092(9)

equivalent isotropic displacement parameters are given in Table 2 and Table 3. Anisotropic displacement parameters are reported in the Supporting Information. Selected atomic distances of the obtained compounds and of the isotypic uranium compounds, $MnUF_6{\cdot}3H_2O$ and $ZnUF_6{\cdot}3H_2O$, are given in Table 4.[5] Within the isotypic compounds the M^{IV} atom occupies Wyckoff position 4*e* (site symmetry 2) and is coordinated by eight fluorine atoms and one water molecule, forming a coordination polyhedron that can be described as a tricapped trigonal prism, which is shown for compound MnNp in Figure 2. The coordination number of nine and the tricapped trigonal prismatic coordination polyhedron are commonly observed for actinoid atoms of fluoridometallates(IV), such as in LiMF$_5$ (M = U–Pu), α-$NaUF_5{\cdot}H_2O$, β-$NaUF_5{\cdot}H_2O$, β-$NaUF_5$, KU_2F_9, $Rb_3Th_3F_{13}$ and $CsTh_6F_{25}$.[4,15,16,19–21]

In the $A^{II}M^{IV}F_6{\cdot}3H_2O$ structure type the fluorine atom F(1) acts μ_2-bridging between the actinoid atoms M^{IV} and the atoms F(2) and F(3) are μ_2-bridging between the A^{II} and M^{IV} atoms, respectively. The oxygen atom O(1) is bound terminally to the actinoid atom. Two different M^{IV}–F(1) distances are observed in this structure type, a shorter one to the two F(1) atoms which are part of the trigonal prism and a longer one to the two "capping" F(1) atoms of the trigonal prism. The M^{IV}–F distances lie in the following ranges for the Mn^{II} salts (T = 100 K): 2.238(2)–2.431(2) Å ($MnUF_6{\cdot}3H_2O$), 2.2287(8)–2.3994(8) Å (**MnNp**), 2.2129(9)–2.3860(9) Å (**MnPu**). For the Zn^{II} salts (T = 100 K) the ranges are 2.2461(11)–2.4040(12) Å ($ZnUF_6{\cdot}3H_2O$), 2.2380(12)–2.3822(13) Å (**ZnNp**) and 2.2187(7)–2.3641(8) Å (**ZnPu**). The order of the M^{IV}–F distances for the respective Mn^{II} and Zn^{II} salts is also shown in the Figures S1 and S2 in the Supporting Information. For both salt series the M^{IV}–F distances decrease when going from U to Pu. This is most likely caused by the decrease of the ionic radii of the actinoid ions with increasing Z (i.e. the actinoid contraction). Thus, the increasing effective charge of the M^{IV} ion causes a shortening of interatomic M^{IV}–F distances and a stronger M^{IV}–F interaction. The actinoid contraction has also been observed for other actinoid systems in different oxidation states such as $[M^{III}(H_2O)_9](CF_3SO_3)_3$ (M^{III} = U–Cm, Cf), $[M^{III}(H_2O)_9]^{3+}$(aq) (M^{III} = U–Cf), $M^{IV}(^{Ar}acnac)$ (M^{IV} = Th–Pu; $^{Ar}acnac$ = 3,5-

© 2020 The Authors. Published by Wiley-VCH Verlag GmbH & Co. KGaA, Weinheim

EurJIC
European Journal of Inorganic Chemistry

Full Paper
doi.org/10.1002/ejic.202000298

Chemistry Europe
European Chemical Societies Publishing

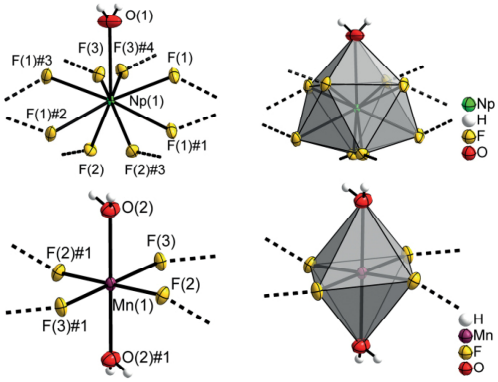

Figure 2. Top left: A section of the crystal structure of compound MnNp showing the coordination environment of Np(1) (M^{IV}). Symmetry transformations for the generation of equivalent atoms: #1 1 − *x*, 1 − *y*, −*z*; #2 *x*, 1 − *y*, 1/2 + *z*; #3 1 − *x*, *y*, 1/2 − *z*; #4: *x*, 1 − *y*, −1/2 + *z*. Top right: A section of the crystal structure of compound **MnNp** showing the coordination polyhedron of the Np(1) atom (M^{IV}). Bottom left: A section of the crystal structure of compound **MnNp** showing the coordination environment of the Mn(1) atom. Symmetry transformations for the generation of equivalent atoms: #1 3/2 − *x*, 3/2 − *y*, 1 − *z*. Bottom right: A section of the crystal structure of compound **MnNp** showing the coordination polyhedron of the Mn(1) atom. The displacement ellipsoids are shown at the 90 % probability level at 100 K. Hydrogen atoms are shown with arbitrary radii. Contacts to neighboring atoms are depicted as dashed bonds.

t$Bu_2C_6H_3$*N*C(Ph)CHC(Ph)*O*), or $[M^{VI}O_2][B_8O_{11}(OH)_4]$ (M^{VI} = U–Pu), as well as in a theoretical study on DFT level of the $[(M^{IV}O_2)(CO_3)_3]^{4-}$ anion (M^{IV} = U–Cm).[1,22–26]

The cell volume is another indicator for the actinoid contraction, as shown by the Mn^{II} salts, which have decreasing cell volumes along the U–Pu series at 100 K [U: 695.9(4) Å^3, Np: 682.81(5) Å^3, Pu: 678.60(9) Å^3]. A similar trend is also observed for the Zn^{II} salts at 100 K, which have the following cell volumes: 668.05(6) Å^3 (U), 661.38(8) Å^3 (Np) and 655.13(8) Å^3 (Pu).[5]

A comparison of the M^{IV}–O(1) distances in the Mn^{II} salts, where the longest distance of 2.585(5) Å is observed in $MnUF_6{\cdot}3H_2O$, the shortest 2.5131(16) Å in compound **MnNp** and an intermediate distance of 2.5247(17) Å in compound **MnPu**, shows that the same trend as for the M^{IV}–F distances is not obeyed. A further indication for "inconsistent" M^{IV}–O(1) distances can be seen in the Zn^{II} compounds: 2.536(2) Å (U), 2.509(2) Å (Np), 2.5079(15) Å (Pu). The M^{IV}–O(1) distances of compounds **ZnNp** and **ZnPu** are equal within the tripled standard uncertainties.

The M^{IV}–F(1)–M^{IV} angles show only small or no differences within the Mn^{II} and Zn^{II} series within the tripled standard uncertainties, the values being 116.97(3)° for $MnUF_6{\cdot}3H_2O$, 116.89(3)° for compound **MnNp**, 117.13(4)° for compound **MnPu** and 115.85(5)° for $ZnUF_6{\cdot}3H_2O$, 115.85(5)° for compound **ZnNp** and 116.19(3)° for compound **ZnPu**.

The A^{II} atom in the $A^{II}M^{IV}F_6{\cdot}3H_2O$ structure type occupies the Wyckoff position 4*c* (site symmetry $\bar{1}$) and is coordinated by four equatorial fluorine atoms and two water molecules in *trans* position, forming an octahedron-like coordination polyhedron shown in Figure 2. The A^{II}–F(2), A^{II}–F(3), and A^{II}–O(2) distances show no or only small differences within the tripled standard uncertainties for both the Mn^{II} and Zn^{II} series, thus the different actinoid atoms of the compounds have no substantial effect on them.

In the $A^{II}M^{IV}F_6{\cdot}3H_2O$ structure type, the H_2O molecules form hydrogen bonds to both O and F atoms, hydrogen bond lengths are reported in Table S1 and sections of the crystal structure of **MnNp** with hydrogen bonds are shown in Figure S1 and S2 in the SI. The water molecule $H_2O(1)$ shows short contacts to $H_2O(2)$ molecules of neighboring $[A^{II}F_4(H_2O)]$ polyhedra. The O(1)···O(2) distances for the Mn^{II} salts are the following: 2.976(4) Å (U), 2.8976(13) Å (**MnNp**), 2.9023(15) Å (**MnPu**) – for the Zn^{II} salts they are: 2.8662(19) Å (U), 2.849(2) Å (**ZnNp**), 2.8531(11) Å (**ZnPu**). The water molecule $H_2O(2)$ shows short contacts to the F atoms F(1), F(2) and F(3) of both neighboring $[A^{II}F_4(H_2O)]$ and $[M^{IV}F_8(H_2O)]$ polyhedra. These distances fall into the following ranges for the Mn^{II} salts: 2.743(4)–2.981(4) Å (U), 2.6933(14)–2.9313(14) Å (**MnNp**), 2.7000(16)–2.9253(15) Å (**MnPu**) – for the Zn^{II} salts the ranges are: 2.683(2)–2.986(2) Å (U), 2.675(2)–2.973(2) Å (**ZnNp**), 2.6712(12)–2.9612(12) Å (**ZnPu**). The differences between these short contacts are small and do not indicate a similar trend as for the M^{IV}–F distances. The angles of these short contacts are equal within the tripled standard uncertainties for the respective series, which indicates that the different actinoid atoms have a minor effect on the hydrogen bonding.

The global crystal structures of the isotypic compounds can be described as layer structures. They are made up of alternating layers of $[A^{II}F_4(H_2O)_2]$ and $[M^{IV}F_8(H_2O)]$ polyhedra parallel to the *bc* plane and stacked along the *a* direction, see Figure 3. The $[M^{IV}F_8(H_2O)]$ polyhedra are *trans*-connected to adjacent $[M^{IV}F_8(H_2O)]$ polyhedra via edges, forming infinite chains along the *c* direction. Within these chains the orientation of the $[M^{IV}F_8(H_2O)]$ polyhedra varies by 180°, so that the H_2O molecules of the polyhedra are arranged *trans* to each other. These chains with the Niggli formula ${}^1_\infty[M^{IV}F_{8/2}(H_2O)_{1/1}]$ are then interconnected via the ${}^0_\infty[A^{II}F_{4/2}(H_2O)_{2/1}]$ polyhedra – resulting in a three-dimensional network structure. The global structure de-

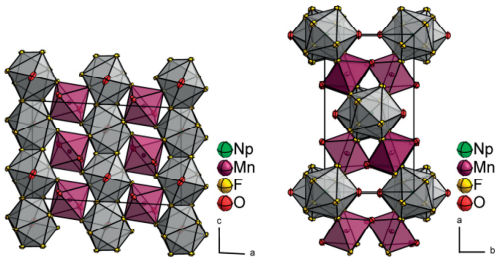

Figure 3. Left: Crystal structure of **MnNp** projected along the *b* axis. Right: Crystal structure of **MnNp** projected along the *c* axis. Hydrogen atoms are omitted for clarity. The coordination polyhedra of Mn atoms are shown in purple and of Np atoms in grey. The displacement ellipsoids are shown at the 90 % probability level at 100 K.

© 2020 The Authors. Published by Wiley-VCH Verlag GmbH & Co. KGaA, Weinheim

EurJIC
European Journal of Inorganic Chemistry

Full Paper
doi.org/10.1002/ejic.202000298

Chemistry Europe
European Chemical Societies Publishing

scription holds some surprises: The nearest A^{II}•••A^{II} distances are around 5.3 Å. If these atoms are connected, tetragonal close packed layers which are AB stacked along the *a* axis result. If, however, A^{II}•••A^{II} distances up to approximately 7.2 Å are considered, a distorted cuboctahedral coordination polyhedron is obtained that is typical for cubic close packing. Thus, the A^{II} atoms of the compounds reported here are arranged like the Cu atoms in the Cu structure type. The M^{IV} atoms are located close to the tetragonal faces of the cuboctahedra which represent the octahedral voids of the cubic close packing. Thus, the coordination polyhedron around the A^{II} atom is a distorted octahedron $[A^{II}M^{IV}_6]$, as is the case for the M^{IV} atoms, $[M^{IV}A^{II}_6]$. The M^{IV} atoms are surrounded by M^{IV} atoms also in the shape of a distorted cuboctahedron with A^{II} atoms close to the octahedral voids. Thus, the A^{II} atoms and the M^{IV} atoms of the compounds presented here are arranged according to the atom positions of the NaCl structure type.

Conclusion

The transition metal(II) fluoridometallate(IV) hydrates of the composition $A^{II}M^{IV}F_6{\cdot}3H_2O$ (A^{II} = Mn, Zn; M^{IV} = Np, Pu) were synthesized from the oxides NpO_2 and PuO_2 and the transition metal chlorides in hydrofluoric acid. The compounds can be obtained in single-crystalline form at room temperature (**MnNp** and **MnPu**) or elevated temperature after a few days of crystallization time (**ZnNp** and **ZnPu**). The compounds are isotypic to the respective uranium compounds, belonging to the $A^{II}M^{IV}F_6{\cdot}3H_2O$ structure type. Within the U–Pu series of the Zn and Mn salts the actinoid contraction is observed in the cell volumes and the M^{IV}–F atomic distances, indicating a stronger interaction between M^{IV} and F atoms with increasing *Z*. In contrast, the M^{IV}–O distances of the coordinating H_2O molecules show no such correlation with *Z*.

Experimental Section

General: Experiments with ^{237}Np and ^{242}Pu were carried out in a laboratory designed for handling radioactive materials at the Institute of Resource Ecology (Helmholtz-Zentrum Dresden-Rossendorf, Dresden, Germany). All experiments were carried out in negative pressure glove boxes equipped with HEPA filters. Np and Pu compounds as well as hydrofluoric acid may be dangerous if not properly handled. Hydrofluoric acid (48 %, suprapur, Carl Roth Karlsruhe) was used for the experiments.

Synthesis: $MnNpF_6{\cdot}3H_2O$ (**MnNp**): 2.4 mg (0.0089 mmol) $^{237}NpO_2$ and 4.8 mg (0.024 mmol) $MnCl_2{\cdot}4H_2O$ were placed in a polypropylene reaction vessel and covered with 0.25 mL hydrofluoric acid. The color of the resulting suspension changed quickly from brown to green. Olive green crystals of **MnNp** were obtained after a few days of crystallization time at room temperature. $MnPuF_6{\cdot}3H_2O$ (**MnPu**): 1.3 mg (0.0047 mmol) $^{242}PuO_2$ and 5.8 mg (0.029 mmol) $MnCl_2{\cdot}4H_2O$ were placed in a polypropylene reaction vessel and covered with 0.25 mL hydrofluoric acid. The color of the resulting suspension changed quickly from brown to orange. Orange crystals of **MnPu** were obtained after a few days of crystallization time at room temperature. $ZnNpF_6{\cdot}3H_2O$ (**ZnNp**): 2.0 mg (0.0074 mmol) $^{237}NpO_2$ and 8.7 mg (0.064 mmol) $ZnCl_2$ were placed in a polypropylene reaction vessel and covered with 0.25 mL of 48 % hydrofluoric acid. The color of the resulting suspension changed quickly from brown to green. Olive green crystals of **ZnNp** were obtained after heating the suspension for 4 days to 60 °C on a sand bath. $ZnPuF_6{\cdot}3H_2O$ (**ZnPu**): 1.4 mg (0.0051 mmol) $^{242}PuO_2$ and 7.8 mg (0.057 mmol) $ZnCl_2$ were placed in a polypropylene reaction vessel and covered with 0.25 mL hydrofluoric acid. The color of the resulting suspension changed quickly from brown to orange. Orange crystals of **ZnPu** were obtained after heating the suspension for 4 days to 60 °C on a sand bath.

Single-Crystal X-ray Diffraction: Crystals of the compounds were always covered with water and/or perfluorinated oil before removing them from the glove box. The crystals were then selected under perfluorinated oil and mounted on a MiTeGen loop. Intensity data of suitable crystals were recorded with a D8 VENTURE diffractometer (Bruker). The diffractometer was operated with Mo-K_α radiation (0.71073 Å, multi-layered optics) and equipped with a PHOTON 100 CMOS detector. Evaluation, integration and reduction of the diffraction data was carried out with the APEX3 software suite.[27] The diffraction data was corrected for absorption utilizing the multiscan method of SADABS within the APEX3 software suite. The structures were solved with dual-space methods (SHELXT) and refined against F^2 (SHELXL) in the space group *C*2/*c* (No. 15).[28,29] Although systematic absence violations are observed for space group *C*2/*c*, their intensities are very weak. Solution and refinement of the structures in the crystallographic subgroups *Cc* (No. 9) and *C*2 (No. 5) showed correlation between atoms and non-positive definite displacement parameters for some atoms. Subsequently, space group *C*2/*c* was chosen, which was also indicated by the Addsym feature of the program package PLATON.[30,31] Non-hydrogen atoms were refined with anisotropic displacement parameters. Hydrogen atoms were located from the difference density maps and allowed for free refinement with isotropic displacement parameters. The highest residual electron density after the final refinement of **MnNp** was 0.53 Å distant from atom O(2), of **MnPu** was 1.37 Å distant from atom H(3), of **ZnNp** was 0.59 Å distant from atom Np(1) and of **ZnPu** was 0.74 Å distant from atom Pu(1). Representations of the crystal structures were created with the Diamond software.[32]

Deposition Number(s) 1993125–1993128 (**MnNp**, **ZnNp**, **ZnPu**, **MnPu**) contain(s) the supplementary crystallographic data for this paper. These data are provided free of charge by the joint Cambridge Crystallographic Data Centre and Fachinformationszentrum Karlsruhe Access Structures service www.ccdc.cam.ac.uk/structures.

Acknowledgments

We thank the Deutsche Forschungsgemeinschaft for generous funding.

Keywords: Actinides · Neptunium · Plutonium · Fluorides · Structure elucidation

[1] L. R. Morss, N. M. Edelstein (Eds.: J. Fuger, J. J. Katz), *The Chemistry of the Actinide and Transactinide Elements*, Springer, Dordrecht, **2006**.
[2] A. Grzechnik, C. C. Underwood, J. W. Kolis, K. Friese, *J. Fluorine Chem.* **2013**, *156*, 124–129.
[3] G. Brunton, *Acta Crystallogr.* **1966**, *21*, 814–817.
[4] J. Yeon, M. D. Smith, J. Tapp, A. Möller, H.-C. zur Loye, *Inorg. Chem.* **2014**, *53*, 6289–6298.
[5] J. Felder, J. Yeon, M. Smith, H.-C. zur Loye, *Inorg. Chem. Front.* **2017**, *4*, 368–377.

© 2020 The Authors. Published by Wiley-VCH Verlag GmbH & Co. KGaA, Weinheim

EurJIC
European Journal of Inorganic Chemistry

Full Paper
doi.org/10.1002/ejic.202000298

Chemistry Europe
European Chemical Societies Publishing

[6] A. C. Bean, T. A. Sullens, W. Runde, T. E. Albrecht-Schmitt, *Inorg. Chem.* **2003**, *42*, 2628–2633.
[7] H. Abazli, Dissertation, Université Pierre et Marie Curie, Paris, **1984**.
[8] H. Abazli, A. Cousson, J. Jové, M. Pagès, M. Gasperin, *J. Less-Common Met.* **1984**, *96*, 23–33.
[9] P. M. Almond, L. Deakin, A. Mar, T. E. Albrecht-Schmitt, *J. Solid State Chem.* **2001**, *158*, 87–93.
[10] P. M. Almond, L. Deakin, A. Mar, T. E. Albrecht-Schmitt, *Inorg. Chem.* **2001**, *40*, 886–890.
[11] V. V. Klepov, J. B. Felder, H.-C. zur Loye, *Inorg. Chem.* **2018**, *57*, 5597–5606.
[12] J. Yeon, M. D. Smith, J. Tapp, A. Möller, H.-C. zur Loye, *J. Am. Chem. Soc.* **2014**, *136*, 3955–3963.
[13] J. Yeon, M. D. Smith, G. Morrison, H.-C. zur Loye, *Inorg. Chem.* **2015**, *54*, 2058–2066.
[14] V. V. Klepov, G. Morrison, H.-C. zur Loye, *Cryst. Growth Des.* **2019**, *19*, 1347–1355.
[15] A. T. Chemey, C. Celis-Barros, J. M. Sperling, D. Páez-Hernández, T. E. Albrecht-Schmitt, *Inorg. Chem.* **2019**, *58*, 14790–14799.
[16] C. J. Windorff, A. T. Chemey, J. M. Sperling, B. E. Klamm, T. E. Albrecht-Schmitt, *Inorg. Chem.* **2020**, https://doi.org/10.1021/acs.inorgchem.0c00360.
[17] T. Thevenin, A. Cousson, *J. Solid State Chem.* **1987**, *67*, 254–258.
[18] J. Jové, A. Cousson, H. Abazli, A. Tabuteau, T. Thévenin, M. Pagès, *Hyperfine Interact.* **1988**, *39*, 1–16.
[19] A. Fischer, Z. Szabó, *Acta Crystallogr., Sect. E:. Crystallogr. Commun.* **2004**, *60*, i45–i46.
[20] A. T. Chemey, J. M. Sperling, T. E. Albrecht-Schmitt, *RSC Adv.* **2018**, *8*, 28642–28648.
[21] C. C. Underwood, C. D. McMillen, J. W. Kolis, *J. Chem. Crystallogr.* **2012**, *42*, 606–610.
[22] C. Apostolidis, B. Schimmelpfennig, N. Magnani, P. Lindqvist-Reis, O. Walter, R. Sykora, A. Morgenstern, E. Colineau, R. Caciuffo, R. Klenze, et al., *Angew. Chem. Int. Ed.* **2010**, *49*, 6343–6347; *Angew. Chem.* **2010**, *122*, 6487–6491.
[23] P. D'Angelo, F. Martelli, R. Spezia, A. Filipponi, M. A. Denecke, *Inorg. Chem.* **2013**, *52*, 10318–10324.
[24] D. D. Schnaars, A. J. Gaunt, T. W. Hayton, M. B. Jones, I. Kirker, N. Kaltsoyannis, I. May, S. D. Reilly, B. L. Scott, G. Wu, *Inorg. Chem.* **2012**, *51*, 8557–8566.
[25] S. Wang, E. V. Alekseev, W. Depmeier, T. E. Albrecht-Schmitt, *Chem. Commun.* **2011**, *47*, 10874.
[26] J.-B. Liu, G. P. Chen, W. Huang, D. L. Clark, W. H. E. Schwarz, J. Li, *Dalton Trans.* **2017**, *46*, 2542–2550.
[27] *APEX3*, Bruker AXS Inc., Madison, Wisconsin, USA, **2018**.
[28] G. M. Sheldrick, *Acta Crystallogr., Sect. A: Found. Adv.* **2015**, *71*, 3–8.
[29] G. M. Sheldrick, *Acta Crystallogr., Sect. C: Struct. Chem.* **2015**, *71*, 3–8.
[30] A. L. Spek, *PLATON - A Multipurpose Crystallographic Tool*, Utrecht University, Utrecht, The Netherlands, **2019**.
[31] A. L. Spek, *Acta Crystallogr., Sect. D: Biol. Crystallogr.* **2009**, *65*, 148–155.
[32] K. Brandenburg, H. Putz, *Diamond - Crystal and Molecular Structure Visualization*, Crystal Impact GbR, Bonn, **2019**.

Received: March 27, 2020

 © 2020 The Authors. Published by Wiley-VCH Verlag GmbH & Co. KGaA, Weinheim

EurJIC European Journal of Inorganic Chemistry

Supporting Information

Synthesis and Crystal Structures of Transition Metal(II) Fluoridometallate(IV) Hydrates of Neptunium and Plutonium: $A^{II}M^{IV}F_6 \cdot 3H_2O$($A^{II}$ = Mn, Zn; M^{IV} =Np, Pu)

Benjamin Scheibe, Juliane März, Moritz Schmidt, Thorsten Stumpf,* and Florian Kraus*

Contents

Selected crystallographic data of the compounds $A^{II}M^{IV}F_6{\cdot}3H_2O$ (A^{II} = Mn, Zn; M^{IV} = Np, Pu) 1

Progression of the M^{IV}–O and M^{IV}–F distances in the compounds $A^{II}M^{IV}F_6{\cdot}3H_2O$ (A^{II} = Mn, Zn; M^{IV} = Np, Pu) 3

Hydrogen bonding in the compounds $A^{II}M^{IV}F_6{\cdot}3H_2O$ (A^{II} = Mn, Zn; M^{IV} = Np, Pu) 5

References 7

Selected crystallographic data of the compounds $A^{II}M^{IV}F_6 \cdot 3H_2O$ (A^{II} = Mn, Zn; M^{IV} = Np, Pu)

Table S1. Anisotropic displacement parameters of $MnNpF_6 \cdot 3H_2O$.

Atom	U_{11} / Å²	U_{22} / Å²	U_{33} / Å²	U_{23} / Å²	U_{13} / Å²	U_{12} / Å²
Np(1)	0.00281(3)	0.00364(3)	0.00256(3)	0	0.00016(2)	0
Mn(1)	0.00426(10)	0.00606(10)	0.00418(10)	-0.00004(8)	0.00040(8)	-0.00081(7)
F(1)	0.0098(3)	0.0104(3)	0.0050(3)	-0.0011(3)	0.0006(3)	-0.0041(3)
F(2)	0.0082(3)	0.0078(3)	0.0073(3)	-0.0004(3)	-0.0013(3)	-0.0025(2)
F(3)	0.0056(3)	0.0100(3)	0.0072(3)	0.0017(3)	0.0013(3)	-0.0013(2)
O(1)	0.0144(7)	0.0067(6)	0.0249(8)	0	0.0105(6)	0
O(2)	0.0103(4)	0.0085(4)	0.0109(4)	0.0012(3)	-0.0021(3)	-0.0015(3)

Table S2. Anisotropic displacement parameters of $MnPuF_6 \cdot 3H_2O$.

Atom	U_{11} / Å²	U_{22} / Å²	U_{33} / Å²	U_{23} / Å²	U_{13} / Å²	U_{12} / Å²
Pu(1)	0.00394(3)	0.00480(3)	0.00394(3)	0	0.00017(2)	0
Mn(1)	0.00583(10)	0.00767(11)	0.00590(11)	-0.00010(8)	0.00047(8)	-0.00091(8)
F(1)	0.0116(4)	0.0125(4)	0.0070(3)	-0.0010(3)	0.0006(3)	-0.0045(3)
F(2)	0.0097(3)	0.0101(3)	0.0088(4)	-0.0006(3)	-0.0012(3)	-0.0030(3)
F(3)	0.0073(3)	0.0118(4)	0.0092(3)	0.0017(3)	0.0019(3)	-0.0016(3)
O(1)	0.0181(7)	0.0080(6)	0.0281(9)	0	0.0128(7)	0
O(2)	0.0125(5)	0.0096(4)	0.0129(5)	0.0014(3)	-0.0020(4)	-0.0021(3)

Table S3. Anisotropic displacement parameters of $ZnNpF_6 \cdot 3H_2O$.

Atom	U_{11} / Å²	U_{22} / Å²	U_{33} / Å²	U_{23} / Å²	U_{13} / Å²	U_{12} / Å²
Np(1)	0.00292(5)	0.00359(5)	0.00300(5)	0	0.00002(3)	0
Zn(1)	0.00449(13)	0.00627(12)	0.00471(13)	0.00013(9)	0.00018(10)	-0.00108(9)
F(1)	0.0086(5)	0.0098(5)	0.0064(5)	-0.0008(4)	0.0011(4)	-0.0035(4)
F(2)	0.0069(5)	0.0083(5)	0.0066(5)	-0.0005(4)	-0.0014(4)	-0.0023(4)
F(3)	0.0061(5)	0.0088(5)	0.0074(5)	0.0011(4)	0.0012(4)	-0.0009(4)
O(1)	0.0140(11)	0.0070(8)	0.0246(13)	0	0.0117(10)	0
O(2)	0.0086(6)	0.0071(5)	0.0098(7)	0.0002(5)	-0.0016(5)	-0.0004(4)

Table S4. Anisotropic displacement parameters of $ZnPuF_6 \cdot 3H_2O$.

Atom	U_{11} / Å^2	U_{22} / Å^2	U_{33} / Å^2	U_{23} / Å^2	U_{13} / Å^2	U_{12} / Å^2
Pu(1)	0.00234(2)	0.00302(2)	0.00223(2)	0	0.00015(1)	0
Zn(1)	0.00420(6)	0.00571(6)	0.00416(6)	0.00003(4)	0.00034(4)	-0.00106(4)
F(1)	0.0088(3)	0.0100(3)	0.0052(2)	-0.0012(2)	0.00067(19)	-0.0035(2)
F(2)	0.0067(2)	0.0075(3)	0.0068(2)	-0.00019(19)	-0.00124(19)	-0.00217(19)
F(3)	0.0056(2)	0.0089(3)	0.0072(3)	0.0022(2)	0.00133(19)	-0.00102(19)
O(1)	0.0176(6)	0.0058(5)	0.0271(8)	0	0.0141(5)	0
O(2)	0.0085(3)	0.0067(3)	0.0103(3)	0.0005(2)	-0.0009(2)	-0.0007(2)

Progression of the M^{IV}–O and M^{IV}–F distances in the compounds $A^{II}M^{IV}F_6 \cdot 3H_2O$ (A^{II} = Mn, Zn; M^{IV} = Np, Pu)

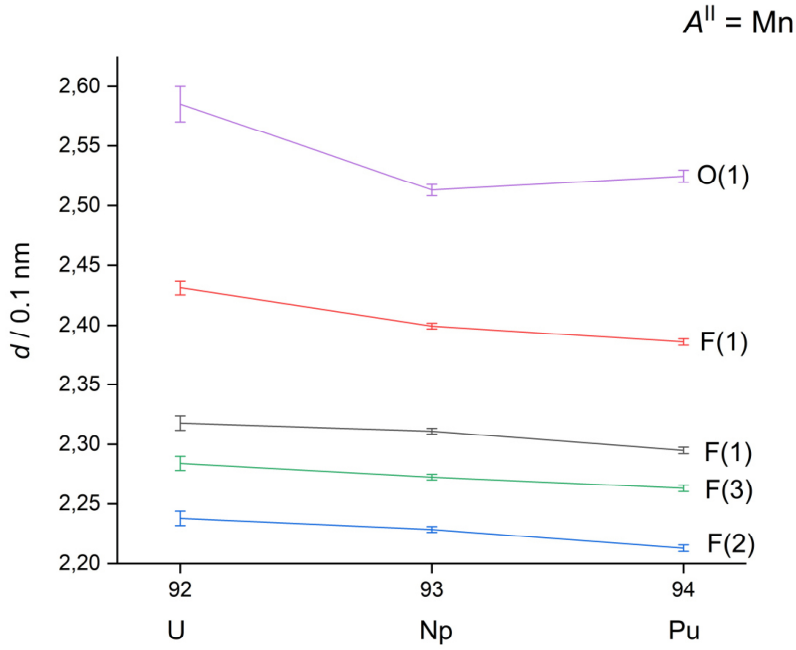

Figure S1. Progression of the M^{IV}–O and M^{IV}–F distances within the U-Pu series of the Mn^{II} salts at 100 K.[1] The error bars indicate the threefold standard uncertainty.

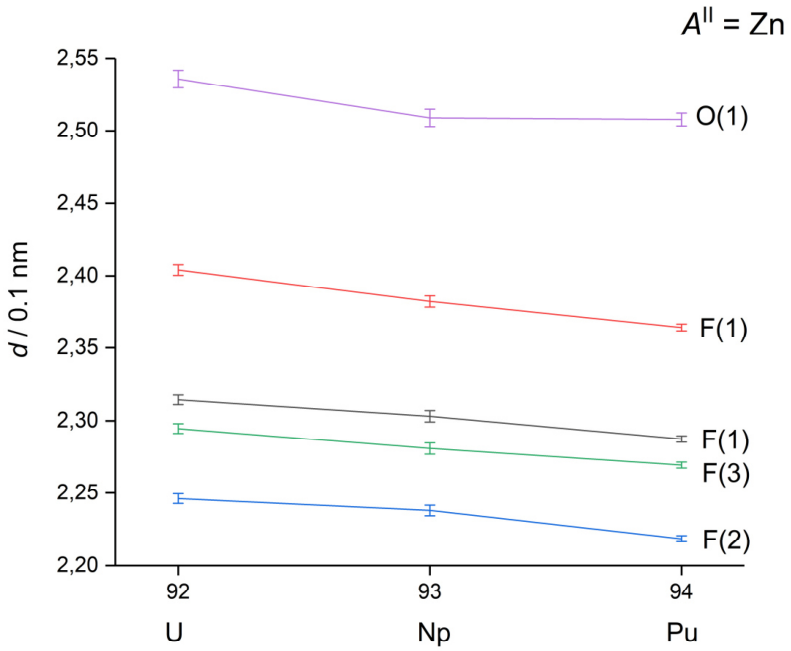

Figure S2. Progression of the M^{V}–O and M^{V}–F distances within the U-Pu series of the Zn^{II} salts at 100 K.[1] The error bars indicate the threefold standard uncertainty.

4

Hydrogen bonding in the compounds $A^{II}M^{V}F_6 \cdot 3H_2O$ (A^{II} = Mn, Zn; M^{V} = Np, Pu)

Table S5. Details of the hydrogen bonds *D*−H···*A* in $MnUF_6 \cdot 3H_2O$.[1]

D−H···*A*	*D*−H / Å	H···*A* / Å	*D*···*A* / Å	∡*D*−H···*A* / °
O(1)−H(1)···O(2)	0.90(6)	2.16(7)	2.976(4)	149(6)
O(2)−H(3)···F(1)	0.78(8)	2.04(8)	2.766(4)	155(7)
O(2)−H(2)···F(2)	0.82(7)	2.48(7)	2.981(4)	121(6)
O(2)−H(2)···F(3)	0.82(7)	1.96(7)	2.743(4)	159(7)

Table S6. Details of the hydrogen bonds *D*−H···*A* in $MnNpF_6 \cdot 3H_2O$.

D−H···*A*	*D*−H / Å	H···*A* / Å	*D*···*A* / Å	∡*D*−H···*A* / °
O(1)−H(1)···O(2)	0.78(3)	2.16(3)	2.8976(13)	157(3)
O(2)−H(3)···F(1)	0.76(3)	2.08(3)	2.7585(14)	149(3)
O(2)−H(2)···F(2)	0.73(4)	2.53(3)	2.9313(14)	116(3)
O(2)···H(2)···F(3)	0.73(4)	1.99(3)	2.6933(14)	162(4)

Table S7. Details of the hydrogen bonds *D*−H···*A* in $MnPuF_6 \cdot 3H_2O$.

D−H···*A*	*D*−H / Å	H···*A* / Å	*D*···*A* / Å	∡*D*−H···*A* / °
O(1)−H(1)···O(2)	0.81(3)	2.14(3)	2.9023(15)	158(3)
O(2)−H(3)···F(1)	0.76(4)	2.10(4)	2.7621(14)	146(3)
O(2)−H(2)···F(2)	0.74(3)	2.52(3)	2.9253(15)	117(3)
O(2)−H(2)···F(3)	0.74(3)	1.98(3)	2.7000(16)	164(3)

Table S8. Details of the hydrogen bonds *D*−H···*A* in $ZnUF_6 \cdot 3H_2O$.[1]

D−H···*A*	*D*−H / Å	H···*A* / Å	*D*···*A* / Å	∡*D*−H···*A* / °
O(1)−H(1)···O(2)	0.81(4)	2.11(4)	2.8662(19)	154(4)
O(2)−H(3)···F(1)	0.80(4)	2.09(4)	2.7881(19)	145(4)
O(2)−H(2)···F(2)	0.77(4)	2.52(3)	2.986(2)	121(3)
O(2)−H(2)···F(3)	0.77(4)	1.94(4)	2.683(2)	163(4)

Table S9. Details of the hydrogen bonds *D*−H···*A* in $ZnNpF_6 \cdot 3H_2O$.

D−H···*A*	*D*−H / Å	H···*A* / Å	*D*···*A* / Å	∡*D*−H···*A* / °
O(1)−H(1)···O(2)	0.69(5)	2.20(5)	2.849(2)	156(5)
O(2)−H(3)···F(1)	0.80(6)	2.08(6)	2.790(2)	148(5)
O(2)−H(2)···F(2)	0.76(4)	2.56(4)	2.973(2)	116(4)
O(2)−H(2)···F(3)	0.76(4)	1.94(4)	2.675(2)	165(4)

Table S10. Details of the hydrogen bonds *D*−H···*A* in $ZnPuF_6 \cdot 3H_2O$.

D−H···*A*	*D*−H / Å	H···*A* / Å	*D*···*A* / Å	∡*D*−H···*A* / °
O(1)−H(1)···O(2)	0.82(3)	2.09(3)	2.8531(11)	153(3)
O(2)−H(3)···F(1)	0.82(3)	2.07(3)	2.7883(12)	146(3)
O(2)−H(2)···F(2)	0.79(3)	2.54(3)	2.9612(12)	115(3)
O(2)−H(2)···F(3)	0.79(3)	1.90(3)	2.6712(12)	165(3)

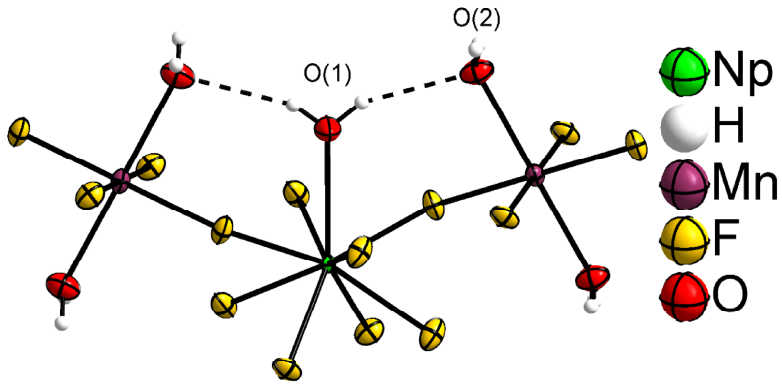

Figure S3. A section of the crystal structure of $MnUF_6 \cdot 3H_2O$ showing the hydrogen bonds between donor O(1)H(1) and acceptor O(2). The hydrogen bonds are drawn as dashed bonds. The displacement ellipsoids are shown at the 90 % probability level at 100 K. Hydrogen atoms are shown with arbitrary radii.

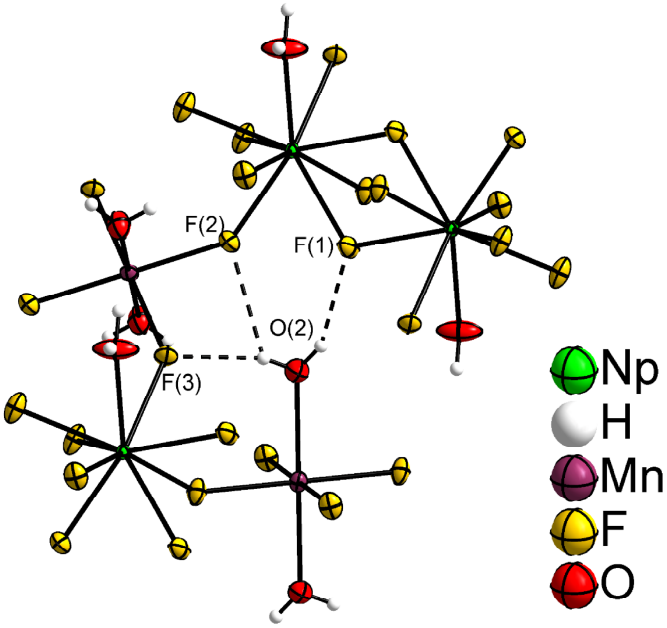

Figure S4. A section of the crystal structure of $MnUF_6 \cdot 3H_2O$ showing the hydrogen bonds between donor O(2)H(3) and acceptor F(1), as well as donor O(2)H(2) and acceptors F(2) and F(3). The hydrogen bonds are drawn as dashed bonds. The displacement ellipsoids are shown at the 90 % probability level at 100 K. Hydrogen atoms are shown with arbitrary radii.

References

[1] J. Felder, J. Yeon, M. Smith, H.-C. zur Loye, *Inorg. Chem. Front.* **2017**, *4*, 368–377.

7.9. A Molecular Octafluoridoneptunate(IV) Anion in $(NH_4)_4[NpF_8]$ and Theoretical Investigations of the $[MF_8]^{4-}$ System (*M* = Th - Bk)

Benjamin Scheibe, Michael Patzschke, Juliane März, Matthias Conrad, Florian Kraus

Eur. J. Inorg. Chem. **2020**
DOI: 10.1002/ejic.202000565

© 2020 The Authors. Published by Wiley-VCH Verlag GmbH & Co. KGaA.

Open access article distributed under the Creative Commons CC BY 4.0 license.
The original licensed material is shown.
(https://creativecommons.org/licenses/by/4.0/legalcode)

EurJIC
European Journal of Inorganic Chemistry

Full Paper
doi.org/10.1002/ejic.202000565

Actinide Fluoridometallates

A Molecular Octafluoridoneptunate(IV) Anion in $(NH_4)_4[NpF_8]$ and Theoretical Investigations of the $[MF_8]^{4-}$ System (M = Th – Bk)

Benjamin Scheibe,[a] Michael Patzschke,[b] Juliane März,[b] Matthias Conrad,[a] and Florian Kraus*[a]

Abstract: Olive-green single crystals of ammonium octafluoridoneptunate(IV), $(NH_4)_4[NpF_8]$, were obtained by converting NpO_2 to a green neptunium tetrafluoride hydrate with hydrofluoric acid and subsequent treatment of the fluoride with an aqueous NH_4F solution. The crystal structure of the compound was determined by single-crystal X-ray diffraction and observed to be isotypic to the uranium analogue. In $(NH_4)_4[NpF_8]$, molecular $[NpF_8]^{4-}$ anions, which can either be described as a distorted square-antiprism or a bicapped trigonal prism, are present which are bound to the NH_4^+ ions via N–H···F hydrogen bonds. Quantum-chemical calculations of $[MF_8]^{4-}$ anions show that the M–F bonds are highly ionic and the energy differences between different ligand arrangements likely can be overcome by lattice energies of different crystal structures in the solid state.

Introduction

The actinide tetrafluorides MF_4 (M = Th – Cm) can act as fluoride-ion acceptors and form ternary fluoridometallates(IV) with e.g. the alkali metal fluorides, AF.[1] A variety of compounds have been reported with compositions such as AMF_5, AM_2F_9, AM_3F_{13} and $A_7M_6F_{31}$, of which many were already studied during the Manhattan Project.[1,2] In these ternary fluorides the anions usually form layer or network structures such as for example ${}^{2}_{\infty}[UF_{3/3}F_{4/2}F_{2/1}]^-$ in $RbUF_5$ or ${}^{3}_{\infty}[UF_{8/2}F_{1/1}]^-$ in $LiUF_5$.[3] In recent years single-crystal structure determinations of ternary fluoridometallates(IV) have mainly been carried out for Th and U compounds, whereas such studies and thus detailed structural parameters for compounds of the transuranium elements are lacking.[3–7] For the latter, usually only data obtained from powder diffraction studies have been reported, with the exception of a few single-crystal structure determinations.[1,2,8–13]

The coordination number of the actinide atom in ternary fluoridometallates(IV) is usually nine, with a tricapped-trigonal prismatic arrangement of the fluorido ligands.[3,4] Compounds with a coordination number of eight of the actinide atom are scarce for fluoridometallates(IV), examples being $Li_4[UF_8]$, $(NH_4)_4[UF_8]$, $Li_4[PuF_8]$ and K_5ThF_9.[6,11,14–16] In these compounds the complex anions are spatially separated and not connected to each other. For coordination number eight commonly four different ligand arrangements are observed – the ideal polyhedra being either a cube (O_h), a square antiprism (D_{4d}), a snub disphenoid (D_{2d}, Johnson solid J_{84}) or a bicapped trigonal prism (C_{2v}).[17–19] The energy differences of the different configurations are usually small.[17] However, in the solid state, these ideal arrangements are usually not observed but rather more-or-less distorted ones. This makes the classification in some cases ambiguous, for example for distorted square-antiprismatic and bicapped trigonal-prismatic arrangements. Many examples for coordination number eight stem from fluorine chemistry, since high oxidation states and/or high coordination numbers in such anions are more likely achieved with the small and chemically very hard fluorine atoms.

A cubic arrangement of ligands in molecular homoleptic complex anions has so far only been observed for the actinide compounds $Na_3[PaF_8]$ and $Na_2[UF_8]$.[20,21] The square-antiprismatic arrangement has been observed in many more compounds, such as in $Na_3[TaF_8]$, $(NO)_2[WF_8]$, $(NO)_2[UF_8]$, $A_2[ReF_8]$ (A = K, NO, NO_2), $[Li(OEt_2)]_2[Re(CH_3)_8]$, $Cs[ReF_8]$, $(N(CH_3)_4)[IF_8]$, $(NO)(NOF)_2[IF_8]$, $(NO)_2[XeF_8]$ and $Cs_2[XeF_8]\cdot 4BrF_5$.[22–29] The snub disphenoid arrangement is observed in cyanido complexes such as $K_4[M(CN)_8]\cdot 2H_2O$ (M = Mo, W), $(M(H_2O)_4)[W(CN)_8]$ (M = Ho, Er, Tm, Lu) and $(M(H_2O)_5)[W(CN)_8]$ (M = La, Pr, Nd, Eu, Gd).[30–32] The bicapped trigonal-prismatic arrangement is observed in $Li_4[MF_8]$ (M = Zr, Ce, Tb, U).[33–36]

Border cases are $(NH_4)_4[UF_8]$ and K_5ThF_9, in which the $[MF_8]^{4-}$ anions are distorted and could either be classified as a square-antiprism or a bicapped trigonal prism.[6,15,16] This is probably also the case for $(NH_4)_4[MF_8]$ (M = Ce, Pa, Np, Pu) but only powder diffraction or EXAFS (Np) data has been reported so far and the single-crystal structures have not yet been deter-

[a] B. Scheibe, Dr. M. Conrad, Prof. Dr. F. Kraus
Fachbereich Chemie, Philipps-Universität Marburg,
Hans-Meerwein-Straße 4, 35032 Marburg, Germany
E-mail: f.kraus@uni-marburg.de
https://www.uni-marburg.de/de/fb15/arbeitsgruppen/ag-kraus
[b] Dr. M. Patzschke, Dr. J. März
Institut für Ressourcenökologie, Helmholtz-Zentrum Dresden-Rossendorf,
Bautzner Landstraße 400, 01328 Dresden, Germany
Supporting information and ORCID(s) from the author(s) for this article are available on the WWW under https://doi.org/10.1002/ejic.202000565.
© 2020 The Authors. Published by Wiley-VCH GmbH. · This is an open access article under the terms of the Creative Commons Attribution License, which permits use, distribution and reproduction in any medium, provided the original work is properly cited.

 © 2020 The Authors published by Wiley-VCH GmbH

EurJIC
European Journal of Inorganic Chemistry

Full Paper
doi.org/10.1002/ejic.202000565

Chemistry Europe
European Chemical Societies Publishing

mined.[37–40] In comparison to $(NH_4)_4[UF_8]$, the Th compound $(NH_4)_4ThF_8$ does not show molecular anions, but a more complex anion with the Niggli formula $^1_\infty[ThF_{4/2}F_{5/1}]^{3-}$.[41,42]

In the NH_4F-MF_4 system (M = U, Np, Pu) several ternary compounds are known, such as $(NH_4)MF_5$, $(NH_4)_2MF_6$, $(NH_4)M_3F_{13}$, $(NH_4)_7M_6F_{31}$, which have also been obtained for U and Pu by thermal decomposition of $(NH_4)_4[MF_8]$.[1,40,43–45] The final product of the decomposition being the anhydrous tetrafluoride. In the case of Pu it is also possible to obtain anhydrous PuF_3 through the decomposition of ammonium fluoridoplutonates(IV) in a closed system.[46]

Here, we report on the synthesis and crystal structure of $(NH_4)_4[NpF_8]$, as well as on theoretical investigations of the chemical bonding, the energy differences of different ligand arrangements, and a selection of bond properties of the $(NH_4)_4[MF_8]$ (M = Th – Bk) system.

Results and Discussion

The compound ammonium octafluoridoneptunate(IV), $(NH_4)_4[NpF_8]$, was synthesized starting from brown NpO_2, which was treated with hydrofluoric acid in an autoclave at 190 °C to give a green solid – which is likely a neptunium tetrafluoride hydrate, $NpF_4{\cdot}xH_2O$ – see Equation (1). The green solid was then treated with an approximately 21 mol/L aqueous NH_4F solution. From the suspension olive-green crystals of $(NH_4)_4[NpF_8]$ were obtained after a few days of crystallization time at room temperature, see Equation (2). Other approaches for the synthesis of ammonium octafluoridometallates(IV) include the reaction of either the oxide or tetrafluoride (U, Pu) with $NH_4[HF_2]$ at elevated temperatures.[6,40,46]

In the case of similar protactinium compounds, PaF_4 and NH_4F have been used at elevated temperatures and in the case of americium compounds, $Am(OH)_4$ and aqueous NH_4F solutions were used as starting materials.[38,47]

$$4\,HF_{(aq)} + NpO_{2(s)} + x\,H_2O \xrightarrow{HF_{(aq)},\ 190\,°C} NpF_4 \cdot xH_2O_{(s)} + 2\,H_2O \quad (1)$$

$$4\,NH_4F_{(aq)} + NpF_4 \cdot xH_2O_{(s)} \xrightarrow{H_2O} (NH_4)_4[NpF_8]_{(s)} + x\,H_2O \quad (2)$$

The crystal structure of $(NH_4)_4[NpF_8]$ was determined by single-crystal X-ray diffraction. The compound crystallizes in the monoclinic space group $C2/c$ (No. 15) with four formula units per unit cell, Pearson symbol $mS52$, Wyckoff sequence 15, f^6e^1 (hydrogen atoms omitted) and is isotypic to the U compound.[6,15] See Table 1 for crystallographic data and details of the structure determination. Selected atomic distances of $(NH_4)_4[NpF_8]$ and of the isotypic uranium compound are given in Table 2. Atomic coordinates, equivalent isotropic displacement parameters and anisotropic displacement parameters are reported in the Supporting Information.

Table 1. Selected crystallographic data and details of the structure determination of $(NH_4)_4[NpF_8]$.

Formula	$(NH_4)_4[NpF_8]$
Molar mass / g mol^{-1}	461.14
Space group (No.)	$C2/c$ (15)
a / Å	13.0951(8)
b / Å	6.6359(4)
c / Å	13.0668(8)
β / °	117.297(2)
V / Å^3	1009.03(11)
Z	4
Pearson symbol	$mS52$ (without H atoms)
$\rho_{calc.}$ / g cm^{-3}	3.04
μ / mm^{-1}	10.39
Color	olive green
Crystal morphology	plate
Crystal size / mm^3	0.049 × 0.074 × 0.17
T / K	100
λ / Å	0.71073 (Mo-K_α)
No. of reflections	30328
θ range / °	3.50–37.82
Range of Miller indices	$-22 \le h \le 22$
	$-11 \le k \le 11$
	$-22 \le l \le 22$
Absorption correction	multi-scan
T_{max}, T_{min}	0.63, 0.27
R_{int}, R_σ	0.040, 0.018
Completeness of the data set	1.000
No. of unique reflections	2727
No. of parameters	93
No. of restrains	0
No. of constrains	0
S (all data)	1.12
$R(F)$ ($I \ge 2\sigma(I)$, all data)	0.017, 0.018
$wR(F^2)$ ($I \ge 2\sigma(I)$, all data)	0.035, 0.036
Extinction coefficient	0.00198(9)
$\Delta\rho_{max}$, $\Delta\rho_{min}$ / e Å^{-3}	1.25, –1.11

Table 2. Selected atomic distances in Å and bond multiplicities in the compounds $(NH_4)_4[UF_8]$[6] (T = 150 K) and $(NH_4)_4[NpF_8]$ (T = 100 K).

Multiplicity	Bond	$(NH_4)_4[UF_8]$[6]	$(NH_4)_4[NpF_8]$
2	M^{IV}(1)–F(1)	2.257(1)	2.253(1)
2	M^{IV}(1)–F(2)	2.335(1)	2.308(1)
2	M^{IV}(1) F(3)	2.286(1)	2.276(1)
2	M^{IV}(1)–F(4)	2.281(1)	2.262(1)

The Np(1) atom occupies Wyckoff position 4e (site symmetry 2) and is coordinated by eight fluorine atoms, forming a coordination polyhedron that can either be described as a distorted quadratic antiprism or as a distorted bicapped trigonal prism, see Figure 1. The $[NpF_8]^{4-}$ anions are mononuclear complexes which are unusual and commonly not observed for ternary actinide fluoridometallates(IV) where in most cases condensed coordination polyhedra are observed.

For example, in compounds such as AMF_5, AM_2F_9 or AM_3F_{13} (A is e.g. Li, Na, and M is e.g. Th, U) complex anions forming infinite layers or networks, respectively, are observed.[1,3–5]

The Np–F distances in $[NpF_8]^{4-}$ are observed in the range of 2.253(1) to 2.308(1) Å, whereas in $[UF_8]^{4-}$ the U–F distances at 150 K lie in between 2.257(1) and 2.335(1) Å.[6] An EXAFS study of $(NH_4)_4[NpF_8]$ at room temperature gave an average Np–F distance of 2.26(1) Å which nicely agrees with our results. The

© 2020 The Authors published by Wiley-VCH GmbH

EurJIC
European Journal of Inorganic Chemistry

Full Paper
doi.org/10.1002/ejic.202000565

Chemistry Europe
European Chemical Societies Publishing

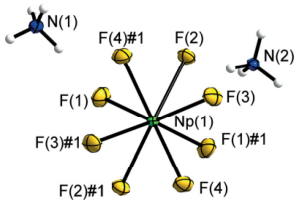

Figure 1. A section of the crystal structure of $(NH_4)_4[NpF_8]$. Symmetry transformations: #1: 1 – *x*, *y*, 1/2 – *z*. The displacement ellipsoids are shown at the 90 % probability level at 100 K. Hydrogen atoms are shown with arbitrary radii.

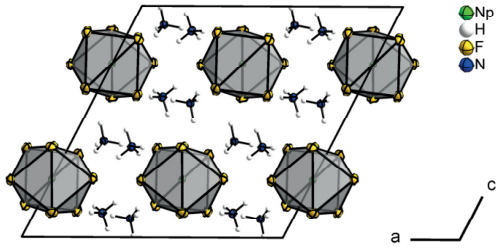

Figure 3. Crystal structure of $(NH_4)_4[NpF_8]$ projected along the *b* axis. The $[NpF_8]^{4-}$ anions are shown as transparent grey polyhedra. The displacement ellipsoids are shown at the 90 % probability level at 100 K. Hydrogen atoms are shown with arbitrary radii.

Np–F distances are shorter than the U–F distances, which can both be attributed to the different measurement temperatures and/or the actinide contraction. In comparison, the Pu–F distances in the $[PuF_8]^{4-}$ anion of $Li_4[PuF_8]$ lie in the range of 2.216(7) to 2.354(5) Å at 296 K.[11]

The F–Np–F angles in the $[NpF_8]^{4-}$ anion lie in the range of 71.13(4) to 145.14(4)° and the F–U–F angles in $[UF_8]^{4-}$ at 150 K are in between 70.81(4) and 145.31(4)°.[6]

The ammonium ions form N–H···F hydrogen bonds to the $[NpF_8]^{4-}$ anions, see Figure 2 and the Supporting Information for further details. The H atoms are either coordinated by one or two F atoms. Both ammonium ions are surrounded tetrahedrally by four $[NpF_8]^{4-}$ anions.

The donor···acceptor distances within the N–H···F hydrogen bonds are in the range of 2.720(2) to 3.036(2) Å for $N(1)H_4^+$ and 2.757(2) to 3.062(2) Å for $N(2)H_4^+$ in the Np compound. In the uranium compound the respective distances are in the range of 2.723(2) to 3.050(2) Å for $N(1)H_4^+$ and 2.758(2) to 3.068(2) Å for $N(2)H_4^+$. Thus, the N–H···F distances of the U and Np compounds are similar.

The arrangement of the ammonium cations and the $[NpF_8]^{4-}$ anions in the unit cell is shown in Figure 3. The $[NpF_8]^{4-}$ anions are surrounded by 16 NH_4^+ ions forming a distorted square orthobicupola (similar to Johnson solid J_{28}) with approximate Np–N distances of 4.33 to 4.93 Å.[19]

The Np atoms are surrounded by ten further Np atoms in the shape of a staggered dodecahedron (SDD-10, Figure S1 in the SI) when Np–Np distances of approximately 6.6 to 7.4 Å are considered.[48] Such a coordination environment is also observed for the Pu atoms in γ-Pu.[49,50] However, four more Np atoms belong topologically to the packing so that coordination number 14 results when Np–Np distances up to 8.6 Å are considered. The ammonium ions reside close to the positions of the tetrahedral and octahedral voids of the Np–Np coordination SDD-10 polyhedron.

In order to gain insight into the bonding situation for actinide(IV) fluorido complexes we performed a series of DFT calculations on the $[MF_8]^{4-}$ anions (with *M* ranging from Th to Bk) using density functional theory. The appropriate spin state was chosen for all compounds and the results compared to published multi-reference calculations on $[PuF_8]^{4-}$.[11] The good agreement with published bond parameters makes us confident, that the DFT results are valid for our series.[6,11] We do expect to find longer bond lengths in comparison with experimental values from e.g. single-crystal X-ray diffraction, as the calculations were carried out for the gas-phase and thus interactions present in the solid state, e.g. electrostatic interaction with the cations, are lacking.

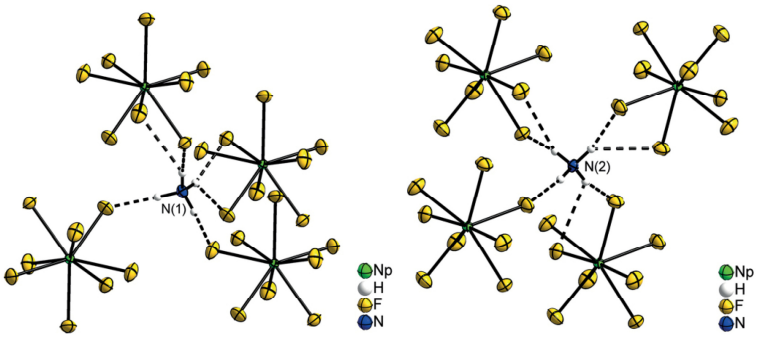

Figure 2. Sections of the crystal structure of $(NH_4)_4[NpF_8]$ showing the N–H···F hydrogen bonds of $N(1)H_4^+$ (left) and $N(2)H_4^+$ (right). The displacement ellipsoids are shown at the 90 % probability level at 100 K. Hydrogen atoms are shown with arbitrary radii. N–H···F hydrogen bonds are depicted as dashed bonds.

 © 2020 The Authors published by Wiley-VCH GmbH

EurJIC
European Journal of Inorganic Chemistry

Full Paper
doi.org/10.1002/ejic.202000565

Chemistry Europe
European Chemical Societies Publishing

Table 3. Comparison of calculated M–F distances (M = Th – Bk) in Å obtained for the complexes in D_{4d}, D_{2d}, O_h symmetries as well as the global minimum symmetry of $[MF_8]^{4-}$ anions.

Anion	M–F distances D_{4d} symmetry	D_{2d} symmetry	O_h symmetry	global minimum M–F distances	Average M–F distance	Symmetry
$[ThF_8]^{4-}$	2.4138	2.4068, 2.4231	2.4167	2.4138	2.4138	D_2
$[PaF_8]^{4-}$	2.3906	2.3613, 2.4206	2.4158	2.3601, 2.4222	2.3911	D_2
$[UF_8]^{4-}$	2.3664	2.3147, 2.4265	2.2272	2.3388, 2.3660, 2.3664, 2.4062	2.3680	C_2
$[NpF_8]^{4-}$	2.3518	2.1550, 2.2345	2.3553	2.3514, 2.3521	2.3517	D_2
$[PuF_8]^{4-}$	2.3384	2.3199, 2.3645	2.3572	2.3195, 2.3650	2.3422	D_2
$[AmF_8]^{4-}$	2.3335	2.2756, 2.4030	2.3562	2.3335	2.3335	D_2
$[CmF_8]^{4-}$	2.3509	2.3397, 2.3550	2.3554	2.3466	2.3466	D_2
$[BkF_8]^{4-}$	2.3131	2.2971, 2.3331	2.3261	2.3131	2.3131	D_2

In order to check possible structures and their relative energies all anions were optimized with cubic, square antiprismatic and snub-disphenoid coordination spheres (point groups O_h, D_{4d} and D_{2d} respectively). It was then checked whether the resulting structures constituted true minima. Where this was not the case, the structure was relaxed in the directions of the imaginary frequencies. Some basic points about the resulting structures is summarized in Table 3.

Two surprising results are the short Np–F and U–F bond lengths observed for the $[NpF_8]^{4-}$ anion in D_{2d} and for the $[UF_8]^{4-}$ anion in O_h symmetry. These structures are much higher in energy than the D_{4d}-symmetric ones. In fact, none of the D_{2d}- or O_h-symmetric structures are local minima on the potential hyper surface, but all D_{4d}-symmetric structures are. Having a look at the square antiprisms shows that the bond lengths in all cases are larger than the sum of the respective ionic radii. The largest deviation is obtained for $[CmF_8]^{4-}$ with 0.11 Å. The average deviation is 0.09 Å and is due to substantial repulsion between the fluorido ligands in the D_{4d}-symmetric structures. For all considered actinide complexes, except those of Pa, U, and Pu, the square-antiprismatic structures are the lowest local minima we found for the starting symmetries D_{4d}, D_{2d}, and O_h. The lowest-energy structures of the Pa, U, and Pu complexes are derived from the cubic O_h-symmetric ones by distortion along imaginary frequencies. For the uranium complex, a structure with four distinctive pairs of U–F distances is observed, resulting in the lowest-energy point group C_2, also a true minimum. The resulting structure of the anion is similar to the one contained in the published crystal structure, albeit with larger bond lengths.[6]

In case of the Pa and Pu complexes, lowest-energy structures with two different bond lengths were obtained resembling a square antiprismatic structure with alternating bond lengths as a global minimum. Finally, for Np only a very small deviation from the perfect square antiprismatic structure was necessary to reach a global minimum of lower energy on the potential hyper surface. The energy differences between the square antiprismatic local minima structures and the global minima of lower energy are not large though (11 kJ/mol for Pa, 18 kJ/mol for U and 29 kJ/mol for Pu) and may easily be compensated by the lattice energies of different crystal structures. Relative stabilities and structural data for the minima are given in Table 4. For the relative energies, all structures were relaxed to the Abelian subgroup D_2 in which only doubly occupied MO's occur. For the uranium complex the subgroup C_2 had to be used to find a global minimum.

Table 4. Energies relative to the square-antiprismatic (D_{4d}) coordination sphere in kJ/mol. The minimum energies are the Gibbs energies including vibrational and rotational corrections in kJ/mol.

Anion	D_{2d} symmetry	O_h symmetry	Minimum energy (symmetry)
$[ThF_8]^{4-}$	3.81	37.00	−1.74 (D_2)
$[PaF_8]^{4-}$	−6.47	37.82	−9.53 (D_2)
$[UF_8]^{4-}$	−10.26	57.06	−18.77 (C_2)
$[NpF_8]^{4-}$	135.97	35.61	−16.73 (D_2)
$[PuF_8]^{4-}$	−20.25	3.10	−29.04 (D_2)
$[AmF_8]^{4-}$	−12.82	8.44	−6.55 (D_2)
$[CmF_8]^{4-}$	−8.35	3.85	−28.00 (D_2)
$[BkF_8]^{4-}$	4.67	53.05	−1.72 (D_2)

To get a better insight into the bonding situation, we performed an NBO (natural bond order) analysis and looked at the actinide ion charges and populations. The results are displayed in Figure 4. The average actinide ion charge is +2.23, but we see a deviation from that charge along the series. Comparing s, p, d and f populations it becomes clear that the effect of an f overpopulation results from back-bonding of the fluorido ligands. Fluorine is a good π donor and hence increases the

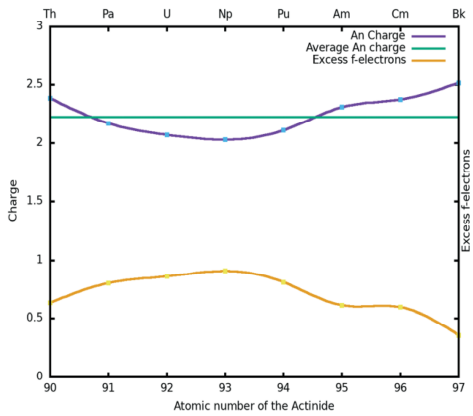

Figure 4. Charges of actinide ions (An) and f-occupations from NBO analysis of the actinide ions in $[MF_8]^{4-}$ anions.

© 2020 The Authors published by Wiley-VCH GmbH

EurJIC
European Journal of Inorganic Chemistry

Full Paper
doi.org/10.1002/ejic.202000565

Chemistry Europe
European Chemical Societies Publishing

Table 5. Bond parameters for the energetic minima of the $[MF_8]^4$ anions (M = Th – Bk). Z – LI is the atomic number Z minus the localization index LI, which is a measure for the oxidation state of the metal cation. DI is the delocalization index, given for the M–F bonds and as an average over all M–F bonds. The IQA (interacting quantum atoms) energies are averaged and given per average bond in kJ/mol. The percentage of covalency, calculated as the fraction of exchange-correlation interaction and total potential energy between the actinide ion and the fluoride ion, is also averaged.

Anion	Symmetry	Z – LI	DI (M–F)	Average DI	IQA Energy	[%]Covalency
$[ThF_8]^{4-}$	D_2	4.51	0.35	0.35	1733	10.7
$[PaF_8]^{4-}$	D_2	4.51	0.39, 0.34	0.37	1707	11.5
$[UF_8]^{4-}$	C_2	4.49	0.40, 0.38, 0.38, 0.35	0.38	1680	12.0
$[NpF_8]^{4-}$	D_2	4.48	0.39, 0.39	0.39	1654	12.4
$[PuF_8]^{4-}$	D_2	4.45	0.41, 0.37	0.39	1628	12.6
$[AmF_8]^{4-}$	D_2	4.41	0.39	0.39	1602	12.8
$[CmF_8]^{4-}$	D_2	4.30	0.38	0.38	1523	12.9
$[BkF_8]^{4-}$	D_2	4.39	0.38	0.38	1628	12.2

f-population of the actinide atoms. We see a maximum for the Np and then a drop to the Bk complex, which has a lower f-overpopulation than the Th complex. This fits well with the general concept that early actinides behave transition-metal like and employ their orbitals more in bonding than the late actinides. To understand these trends in more detail, we performed QTAIM (quantum theory of atoms in molecules) calculations also using IQA (interacting quantum atom) theory. These calculations yielded localisation and delocalisation indices and through IQA even a measure of the degree of covalency of the M–F bonds.

Another property to look at is the localization index (LI) subtracted from the atomic number (i.e. Z – LI). For rather ionic species, this gives an estimation of the oxidation state for the less electronegative part.[51] This number lies above four in all cases for the actinide atom, showing a strong ionic interaction, as could be expected (Table 5). The values change only little over the whole series. The delocalization index (DI), a property related to the bond order, shows an increase in bonding up to Np and then a decline. This is similar to the f-overpopulation, but with a slightly later maximum in the series. The changes in the DI however are rather small. The IQA interaction energy decreases from Th to Cm but rises again somewhat for Bk. The larger drop for Cm can be explained by the larger Cm–F distance in the minimum structure. The percentage of covalency increases to Cm and then drops again for Bk. Looking at the total energy in the covalent bonds, one sees a maximum for Np and Pu again in good agreement with DI and NBO charges. The covalent part of the bond interaction amounts to approximately 200 kJ/mol. This can be compared to a covalent energy contribution in the LiF molecule of 166 kJ/mol, determined by the same approach, which here amounts to 20.1 % covalency. This last result compares extremely well with the covalent character of the LiF bond, which is 20.5 %, using the electronegativity of the elements.[52]

Conclusions

Ammonium octafluoridoneptunate(IV), $(NH_4)_4[NpF_8]$, was obtained in single-crystalline form from the reaction of $NpF_4 \cdot xH_2O$ with an aqueous NH_4F solution. The structure is isotypic to its uranium analogue. In the crystal structure molecular, mononuclear $[NpF_8]^{4-}$ anions are observed which can either be described as distorted square-antiprisms or bicapped trigonal prisms. The structural parameters of the $[NpF_8]^{4-}$ anions are similar to known $[UF_8]^{4-}$ anions resulting in comparable parameters of the N–H···F hydrogen bonds in these closely related compounds. The M–F bonding interactions in the series of $[MF_8]^{4-}$ anions (M = Th – Bk) are strongly ionic with some backbonding from the fluorido ligands. We find a maximum in bonding with f-participation around the Np complex. The different coordination spheres of the $[MF_8]^{4-}$ anions do not differ extremely in energy and the observed differences can be counterbalanced by the lattice energies of different crystal structures.

Experimental Section

General: Experiments with ^{237}Np were carried out in a laboratory designed for handling radioactive materials at the Institute of Resource Ecology (Helmholtz Zentrum Dresden Rossendorf, Dresden, Germany). All experiments were carried out in negative pressure glove boxes equipped with HEPA filters. Np compounds as well as hydrofluoric acid may be dangerous if not handled properly. Hydrofluoric acid (48 %, Supra-quality, Carl Roth Karlsruhe) was used for the experiments.

Synthesis: 6.0 mg (0.022 mmol) $^{237}NpO_2$ and 0.2 mL 48 % hydrofluoric acid were placed in the PTFE liner (V = 6 mL) of a Parr Instrument acid digestion vessel (Model 4749). The sealed vessel was placed in an aluminum casing on a heating plate inside the glove box and heated to 190 °C for 22 hours. The heating plate was then turned off and the vessel was cooled to room temperature. After that, the vessel was opened, the obtained green solid was washed several times with deionized water and transferred to a 2 mL polypropylene reaction vessel. The reaction vessel was charged with 154.7 mg (4.18 mmol) NH_4F and 0.2 mL deionized water. Olive-green crystals of $(NH_4)_4[NpF_8]$ were obtained after a few days of crystallization time.

Single-crystal X-ray diffraction: Crystals of $(NH_4)_4[NpF_8]$ were covered with perfluorinated oil before removing them from the glove box. The crystals were then selected under perfluorinated oil and mounted on a MiTeGen loop. Intensity data of a suitable crystal were recorded with a D8 VENTURE diffractometer (Bruker). The diffractometer was operated with Mo-K_α radiation (0.71073 Å, multi layered optics) and equipped with a PHOTON 100 CMOS detector. Evaluation, integration and reduction of the diffraction data was carried out with the APEX3 software suite.[53] The diffraction data were corrected for absorption utilizing the multi-scan method of SADABS within the APEX3 software suite. The structure was solved with dual-space methods (SHELXT) and refined against F^2 (SHELXL)

© 2020 The Authors published by Wiley-VCH GmbH

EurJIC
European Journal of Inorganic Chemistry

Full Paper
doi.org/10.1002/ejic.202000565

Chemistry Europe
European Chemical Societies Publishing

in the space group $C2/c$ (No. 15).[54,55] Eight systematic absence violations [$I > 3\sigma(I)$] were observed for space group $C2/c$, but their intensities were close to three sigma. Solution and refinement of the structures in the crystallographic subgroups Cc (No. 9) and $C2$ (No. 5) resulted in correlations between atomic coordinates and non-positive definite displacement parameters for some atoms. Subsequently, space group $C2/c$ was chosen, which was also indicated by the Addsym feature of the program package PLATON.[56,57] Non-hydrogen atoms were refined with anisotropic displacement parameters. Hydrogen atoms were located from the difference density maps and allowed for free refinement with isotropic displacement parameters. The highest residual electron density after the final refinement was 1.00 Å distant from the Np atom. Representations of the crystal structures were created with the Diamond software package.[58] Deposition Number 1939940 contains the supplementary crystallographic data for this paper. These data are provided free of charge by the joint Cambridge Crystallographic Data Centre and Fachinformationszentrum Karlsruhe Access Structures service www.ccdc.cam.ac.uk/structures.

Computational Methods: All DFT calculations were performed with Turbomole version 7.3.1.[59] The functional PBE0 was used throughout.[60,61] PBE0 as hybrid functional contains 25 % exact exchange, ensuring a positive HOMO-LUMO gap for actinide systems. Def-TZVPP basis sets were used for all elements.[62–64] The core electrons of the actinides were treated with a small core ECP, thus removing 60 core electrons per actinide and including scalar relativistic effects in the process.[65] To reduce computational time, the RI-J approximation with appropriate auxiliary basis sets was employed.[66] The highest possible spin-state was taken as the ground state. After the optimization HOMO-LUMO gaps were checked and then symmetry restrictions were relaxed and the single point energy was calculated. The optimizations were further checked by calculation of vibrational frequencies. In case imaginary frequencies were found, the system was distorted following the imaginary modes and a new optimization done. This was repeated until only real frequency values remained, hereby ensuring that a local minimum on the potential hyper surface was found. Optimizations were performed starting with D_{4d}, D_{2d} and O_h symmetry. Based on the minimum-energy structures NBO (natural bond orbital) charges were calculated with Turbomole. All minimum-energy structures were subjected to a QTAIM (Quantum theory of atoms in molecules) analysis using the AIMAll program.[67,68] From these calculations the localization and delocalization indices as well as the IQA (interacting quantum atoms) energies were extracted.[69] IQA makes it possible to partition the total energy of a system into contributions from the atomic basins and their interactions. We are here interested in the potential energy contribution to the pairwise interaction energies, or the potential energy contribution to the bond between the atoms in the pair. This contribution can be written as the sum of four terms, electron-nuclear interactions between atom A and B, nuclear-electron interactions between A and B, nuclear-nuclear repulsion and electron-electron repulsion. It is possible to split up this interaction in a different way as the sum of the coulombic interaction and the exchange-correlation interaction between the basins of atom A and B. In this form the coulombic part represents the ionic part of the interaction energy and the exchange-correlation part is the covalent contribution.

Acknowledgments

We thank the Deutsche Forschungsgemeinschaft (DFG) for generous funding. Open access funding enabled and organized by Projekt DEAL.

Keywords: Actinides · Density functional calculations · Neptunium · Fluorine · Single-crystal X-ray diffraction

[1] L. R. Morss, N. M. Edelstein, J. Fuger, J. J. Katz, Eds., *The Chemistry of the Actinide and Transactinide Elements*, Springer, Dordrecht, **2006**.
[2] W. H. Zachariasen, *J. Am. Chem. Soc.* **1948**, *70*, 2147–2151.
[3] J. Yeon, M. D. Smith, J. Tapp, A. Möller, H.-C. zur Loye, *Inorg. Chem.* **2014**, *53*, 6289–6298.
[4] V. V. Klepov, J. B. Felder, H.-C. zur Loye, *Inorg. Chem.* **2018**, *57*, 5597–5606.
[5] A. T. Chemey, J. M. Sperling, T. E. Albrecht-Schmitt, *RSC Adv.* **2018**, *8*, 28642–28648.
[6] A. T. Chemey, C. Celis-Barros, K. Huang, J. M. Sperling, C. J. Windorff, R. E. Baumbach, D. E. Graf, D. Páez-Hernández, M. Ruf, D. E. Hobart, T. E. Albrecht-Schmitt, *Inorg. Chem.* **2019**, *58*, 637–647.
[7] A. Oudahmane, M. El-Ghozzi, L. Jouffret, D. Avignant, *J. Solid State Chem.* **2015**, *232*, 73–78.
[8] W. H. Zachariasen, *The Crystal Chemistry of Fluorides of Thorium, Uranium, Neptunium, and Plutonium.* Report: MDDC-1151, Argonne National Laboratory, **1947**.
[9] W. H. Zachariasen, *X-ray Diffraction Studies of Fluorides of Plutonium and Neptunium: Chemical Identity and Crystal Structure*, Report: MDDC-1396, Argonne National Laboratory, **1947**.
[10] T. K. Keenan, *Inorg. Nucl. Chem. Lett.* **1966**, *2*, 153–156.
[11] A. T. Chemey, C. Celis-Barros, J. M. Sperling, D. Páez-Hernández, T. E. Albrecht-Schmitt, *Inorg. Chem.* **2019**, *58*, 14790–14799.
[12] A. T. Chemey, J. M. Sperling, C. J. Windorff, D. E. Hobart, T. E. Albrecht-Schmitt, *Cryst. Growth Des.* **2020**, *20*, 2998–3006.
[13] B. Scheibe, J. März, M. Schmidt, T. Stumpf, F. Kraus, *Eur. J. Inorg. Chem.* **2020**, *2020*, 2279–2284.
[14] G. Brunton, *J. Inorg. Nucl. Chem.* **1967**, *29*, 1631–1636.
[15] A. Rosenzweig, D. T. Cromer, *Acta Crystallogr., Sect. A* **1970**, *26*, 38–44.
[16] R. R. Ryan, R. A. Penneman, *Acta Crystallogr., Sect. B* **1971**, *27*, 829–833.
[17] M. Kaupp, *Angew. Chem. Int. Ed.* **2001**, *40*, 3534; *Angew. Chem.* **2001**, *113*, 3642.
[18] J. K. Burdett, R. Hoffmann, R. C. Fay, *Inorg. Chem.* **1978**, *17*, 2553–2568.
[19] N. W. Johnson, *Can. J. Math.* **1966**, *18*, 169–200.
[20] S. M. De Sio, R. E. Wilson, *Inorg. Chem.* **2014**, *53*, 1750–1755.
[21] J. G. Malta, H. Selig, S. Siegel, *Inorg. Chem.* **1966**, *5*, 130–132.
[22] V. Langer, Ľ. Smrčok, M. Boča, *Acta Crystallogr., Sect. C: Cryst. Struct. Commun.* **2010**, *66*, i85–i86.
[23] S. Adam, A. Ellern, K. Seppelt, *Chem. Eur. J.* **1996**, *2*, 398–402.
[24] I.-C. Hwang, K. Seppelt, *J. Fluorine Chem.* **2000**, *102*, 69–72.
[25] P. A. Koz'min, *J. Struct. Chem.* **1964**, *5*, 60–65.
[26] V. Pfennig, K. Seppelt, N. Robertson, *Angew. Chem. Int. Ed. Engl.* **1997**, *36*, 1350–1352; *Angew. Chem.* **1997**, *109*, 1410.
[27] A.-R. Mahjoub, K. Seppelt, *Angew. Chem. Int. Ed.* **1991**, *30*, 876–878; *Angew. Chem.* **1991**, *103*, 844–845.
[28] A. Ellern, K. Seppelt, *Z. Anorg. Allg. Chem.* **2001**, *627*, 234–237.
[29] S. W. Peterson, J. H. Holloway, B. A. Coyle, J. M. Williams, *Science* **1971**, *173*, 1238–1239.
[30] I. V. Saramaga, V. V. Dovgei, I. V. Yarovets, B. I. Cherniak, *Ukr. Khim. Zh.* **1998**, *64*, 34–39.
[31] J. L. Hoard, H. H. Nordsieck, *J. Am. Chem. Soc.* **1939**, *61*, 2853–2863.
[32] A.-H. Yuan, P. D. Southon, D. J. Price, C. J. Kepert, H. Zhou, W.-Y. Liu, *Eur. J. Inorg. Chem.* **2010**, *2010*, 3610–3614.
[33] P. Dugat, M. El Ghozzi, J. Métin, D. Avignant, *J. Solid State Chem.* **1995**, *120*, 187–196.
[34] A. T. Chemey, T. E. Albrecht-Schmitt, *Acta Crystallogr., Sect. E, Crystallogr. Commun.* **2019**, *75*, 139–141.
[35] A. Delaigue, J. C. Cousseins, *Rev. Chim. Miner.* **1972**, *9*, 789–798.
[36] M. El-Ghozzi, D. Avignant, J. C. Cousseins, *Eur. J. Solid State Inorg. Chem.* **1992**, *29*, 981–992.
[37] R. A. Penneman, A. Rosenzweig, *Inorg. Chem.* **1969**, *8*, 627–630.
[38] L. B. Asprey, F. H. Kruse, R. A. Penneman, *Inorg. Chem.* **1967**, *6*, 544–548.
[39] F. Poineau, C. M. Silva, C. B. Yeamans, G. S. Cerefice, A. P. Sattelberger, K. R. Czerwinski, *Inorg. Chim. Acta* **2016**, *448*, 93–96.
[40] R. Benz, R. M. Douglass, F. H. Kruse, R. A. Penneman, *Inorg. Chem.* **1963**, *2*, 799–803.

 © 2020 The Authors published by Wiley-VCH GmbH

EurJIC
European Journal of Inorganic Chemistry

Full Paper
doi.org/10.1002/ejic.202000565

Chemistry Europe
European Chemical Societies Publishing

[41] R. A. Penneman, R. R. Ryan, A. Rosenzweig, *Chem. Commun.* **1968**, 990.
[42] R. R. Ryan, R. A. Penneman, A. Rosenzweig, *Acta Crystallogr., Sect. B* **1969**, *25*, 1958–1962.
[43] W. Bacher, E. Jacob, *Gmelin Handbuch der Anorganischen Chemie - System-Nummer 55: U Uran. Ergänzungsband C 8: Verbindungen mit Fluor*, Springer-Verlag, Berlin Heidelberg New York, **1980**.
[44] B. N. Wani, S. J. Patwe, U. R. K. Rao, K. S. Venkateswarlu, *J. Fluorine Chem.* **1989**, *44*, 177–185.
[45] C. N. A. Che Zainul Bahri, A. F. Ismail, A. Ab. Majid, *Nucl. Eng. Technol.* **2019**, *51*, 792–799.
[46] B. Claux, O. Beneš, E. Capelli, P. Souček, R. Meier, *J. Fluorine Chem.* **2016**, *183*, 10–13.
[47] L. B. Asprey, R. A. Penneman, *Inorg. Chem.* **1962**, *1*, 134–136.
[48] A. Ruiz-Martínez, S. Alvarez, *Chem. Eur. J.* **2009**, *15*, 7470–7480.
[49] W. H. Zachariasen, *The Crystal Structure of Gamma Plutonium. Report: LA-1325*, Los Alamos Scientific Laboratory, **1951**.
[50] W. H. Zachariasen, F. H. Ellinger, *Acta Crystallogr.* **1955**, *8*, 431–433.
[51] A. Kerridge, *RSC Adv.* **2014**, *4*, 12078–12086.
[52] N. B. Hannay, C. P. Smyth, *J. Am. Chem. Soc.* **1946**, *68*, 171–173.
[53] *APEX3*, Bruker AXS Inc., Madison, Wisconsin, USA, **2018**.
[54] G. M. Sheldrick, *Acta Crystallogr., Sect. A: Found. Adv.* **2015**, *71*, 3–8.
[55] G. M. Sheldrick, *Acta Crystallogr., Sect. C: Struct. Chem.* **2015**, *71*, 3–8.
[56] A. L. Spek, *PLATON - A Multipurpose Crystallographic Tool*, Utrecht University, Utrecht, The Netherlands, **2019**.
[57] A. L. Spek, *Acta Crystallogr., Sect. D: Biol. Crystallogr.* **2009**, *65*, 148–155.
[58] K. Brandenburg, H. Putz, *Diamond - Crystal and Molecular Structure Visualization*, Crystal Impact GbR, Bonn, **2019**.
[59] *TURBOMOLE V7.3.1*, a Development of University of Karlsruhe and Forschungszentrum Karlsruhe GmbH, 1989–2007, TURBOMOLE GmbH, since 2007, **2018**.
[60] J. P. Perdew, K. Burke, M. Ernzerhof, *Phys. Rev. Lett.* **1996**, *77*, 3865–3868.
[61] J. P. Perdew, M. Ernzerhof, K. Burke, *J. Chem. Phys.* **1996**, *105*, 9982–9985.
[62] F. Weigend, R. Ahlrichs, *Phys. Chem. Chem. Phys.* **2005**, *7*, 3297–3305.
[63] X. Cao, M. Dolg, *THEOCHEM* **2004**, *673*, 203–209.
[64] X. Cao, M. Dolg, H. Stoll, *J. Chem. Phys.* **2003**, *118*, 487–496.
[65] W. Küchle, M. Dolg, H. Stoll, H. Preuss, *J. Chem. Phys.* **1994**, *100*, 7535–7542.
[66] F. Weigend, *Phys. Chem. Chem. Phys.* **2002**, *4*, 4285–4291.
[67] R. F. W. Bader, *Atoms in Molecules: A Quantum Theory*, Clarendon Press, Oxford, **1994**.
[68] T. A. Keith, *AIMAll*, TK Gristmill Software, Overland Park KS, USA, **2017**.
[69] M. A. Blanco, A. Martín Pendás, E. Francisco, *J. Chem. Theory Comput.* **2005**, *1*, 1096–1109.

Received: June 16, 2020

 © 2020 The Authors published by Wiley-VCH GmbH

EurJIC European Journal of Inorganic Chemistry

Supporting Information

A Molecular Octafluoridoneptunate(IV) Anion in $(NH_4)_4[NpF_8]$ and Theoretical Investigations of the $[MF_8]^{4-}$ System (M = Th – Bk)

Benjamin Scheibe, Michael Patzschke, Juliane März, Matthias Conrad, Florian Kraus*

Supporting Information

Content

Selected crystallographic data of $(NH_4)_4[NpF_8]$ 1
Comparison of the hydrogen bonding in $(NH_4)_4[UF_8]$ and $(NH_4)_4[NpF_8]$ 1
Surrounding of a Np atom by other Np atoms in $(NH_4)_4[NpF_8]$ 2
XYZ coordinates of the optimized structures of $[MF_8]^{4-}$ anions 2
References 8

Selected crystallographic data of $(NH_4)_4[NpF_8]$

Table S1. Atomic coordinates and equivalent isotropic displacement parameters U_{iso} of $(NH_4)_4[NpF_8]$ at 100 K.

Atom	Position	*x*	*y*	*z*	U_{iso} / Å^2
Np(1)	4*e*	1/2	0.42470(2)	1/4	0.00410(3)
N(1)	8*f*	0.74069(14)	0.5930(2)	0.60802(14)	0.0101(2)
N(2)	8*f*	0.62234(14)	−0.1326(2)	0.08192(13)	0.0092(2)
F(1)	8*f*	0.56636(10)	0.65453(18)	0.39286(10)	0.01153(19)
F(2)	8*f*	0.65685(10)	0.57721(17)	0.24668(10)	0.00911(18)
F(3)	8*f*	0.55246(10)	0.22005(18)	0.14238(10)	0.01121(19)
F(4)	8*f*	0.34154(10)	0.26961(19)	0.11524(10)	0.01133(19)
H(1A)	8*f*	0.687(3)	0.624(5)	0.536(3)	0.020(8)
H(1B)	8*f*	0.783(3)	0.487(6)	0.609(3)	0.024(9)
H(1C)	8*f*	0.712(3)	0.565(5)	0.652(3)	0.013(7)
H(1D)	8*f*	0.781(3)	0.696(5)	0.635(3)	0.020(8)
H(2A)	8*f*	0.606(3)	−0.024(5)	0.099(3)	0.011(7)
H(2B)	8*f*	0.575(3)	−0.160(5)	0.007(3)	0.008(6)
H(2C)	8*f*	0.613(3)	−0.219(5)	0.126(3)	0.013(7)
H(2D)	8*f*	0.695(3)	−0.142(5)	0.096(3)	0.018(8)

Table S2. Anisotropic displacement parameters of $(NH_4)_4[NpF_8]$ at 100 K.

Atom	U_{11} / Å^2	U_{22} / Å^2	U_{33} / Å^2	U_{23} / Å^2	U_{13} / Å^2	U_{12} / Å^2
Np(1)	0.00352(4)	0.00467(4)	0.00399(4)	0	0.00160(3)	0
N(1)	0.0103(6)	0.0098(6)	0.0099(6)	−0.0003(5)	0.0042(5)	−0.0020(5)
N(2)	0.0089(6)	0.0096(5)	0.0099(6)	0.0003(5)	0.0050(5)	0.0008(5)
F(1)	0.0113(5)	0.0123(5)	0.0092(4)	−0.0042(4)	0.0032(4)	−0.0005(4)
F(2)	0.0075(4)	0.0104(4)	0.0105(4)	−0.0006(3)	0.0050(4)	−0.0021(3)
F(3)	0.0097(5)	0.0124(4)	0.0123(4)	−0.0048(4)	0.0057(4)	−0.0001(4)
F(4)	0.0074(4)	0.0138(5)	0.0115(4)	−0.0044(4)	0.0033(4)	−0.0026(4)

Comparison of the hydrogen bonding in $(NH_4)_4[UF_8]$ and $(NH_4)_4[NpF_8]$

Table S3. Details of the N−H···F hydrogen bonds in $(NH_4)_4[UF_8]$ at 150 K.[1]

N−H···F	N−H / Å	H···F / Å	N···F / Å	∡N−H···F / °
N(1)−H(1A)···F(1)	0.93(3)	1.81(3)	2.7340(17)	172(3)
N(1)−H(1D)···F(1)	0.86(4)	2.43(4)	3.0499(17)	130(3)
N(1)−H(1D)···F(2)	0.86(4)	2.00(4)	2.8021(17)	154(3)
N(1)−H(1C)···F(2)	0.87(3)	1.92(3)	2.7543(17)	160(3)
N(1)−H(1C)···F(3)	0.87(3)	2.45(3)	2.9886(17)	120(2)
N(1)−H(1B)···F(4)	0.96(4)	1.79(4)	2.7227(18)	163(3)
N(2)−H(2C)···F(1)	0.85(3)	2.42(3)	3.0188(17)	127(2)
N(2)−H(2D)···F(2)	0.84(3)	2.58(3)	3.0682(16)	118(3)
N(2)−H(2C)···F(2)	0.85(3)	1.96(3)	2.7653(17)	157(3)
N(2)−H(2A)···F(3)	0.86(3)	1.91(3)	2.7578(17)	170(3)
N(2)−H(2B)···F(3)	0.92(3)	1.93(3)	2.8386(16)	171(3)
N(2)−H(2B)···F(4)	0.92(3)	2.45(3)	2.9723(16)	116(2)
N(2)−H(2D)···F(4)	0.84(3)	1.97(3)	2.7875(16)	163(3)

Table S4. Details of the N−H···F hydrogen bonds in $(NH_4)_4[NpF_8]$ at 100 K.[1]

N−H···F	N−H / Å	H···F / Å	N···F / Å	∡N−H···F / °
N(1)−H(1A)···F(1)	0.90(4)	1.83(4)	2.720(2)	171(3)
N(1)−H(1D)···F(1)	0.84(4)	2.41(4)	3.036(2)	132(3)
N(1)−H(1D)···F(2)	0.84(4)	2.04(4)	2.8034(19)	152(3)
N(1)−H(1C)···F(2)	0.84(4)	1.94(3)	2.755(2)	163(3)
N(1)−H(1C)···F(3)	0.84(4)	2.48(3)	2.972(2)	118(3)
N(1)−H(1B)···F(4)	0.89(4)	1.86(4)	2.725(2)	165(4)
N(2)−H(2C)···F(1)	0.86(3)	2.40(3)	2.993(2)	127(3)
N(2)−H(2D)···F(2)	0.89(4)	2.54(3)	3.062(2)	118(3)
N(2)−H(2C)···F(2)	0.86(3)	1.95(3)	2.7670(19)	157(3)
N(2)−H(2A)···F(3)	0.81(3)	1.95(3)	2.757(2)	173(3)
N(2)−H(2B)···F(3)	0.91(3)	1.94(3)	2.831(2)	168(3)
N(2)−H(2B)···F(4)	0.91(3)	2.43(3)	2.967(2)	118(2)
N(2)−H(2D)···F(4)	0.89(4)	1.91(4)	2.776(2)	166(3)

Surrounding of a Np atom by other Np atoms in $(NH_4)_4[NpF_8]$

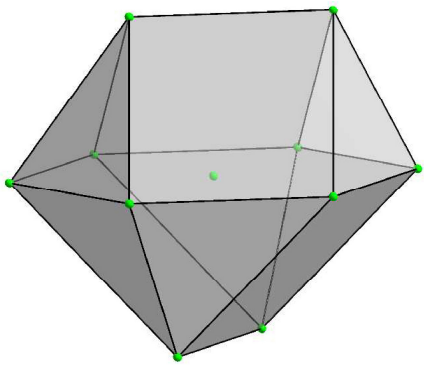

Figure S1. Surrounding of a Np atom by other Np atoms in $(NH_4)_4[NpF_8]$ when Np−Np distances of approximately 6.61-7.34 Å are considered.

XYZ coordinates of the optimized structures of $[MF_8]^{4-}$ anions

$[ThF_8]^{4-}$ O_h-symmetry

```
Th   0.0000000   0.0000000   0.0000000
F    1.3952899   1.3952899   1.3952899
F   −1.3952899   1.3952899   1.3952899
F   −1.3952899  −1.3952899   1.3952899
F    1.3952899  −1.3952899   1.3952899
F    1.3952899  −1.3952899  −1.3952899
F    1.3952899   1.3952899  −1.3952899
F   −1.3952899   1.3952899  −1.3952899
F   −1.3952899  −1.3952899  −1.3952899
```

$[ThF_8]^{4-}$ D_{4d}-symmetry

Th	0.0000000	0.0000000	0.0000000
F	1.8545570	−0.7681827	−1.3405053
F	0.7681827	1.8545570	−1.3405053
F	1.8545570	0.7681827	1.3405053
F	0.7681827	−1.8545570	1.3405053
F	−0.7681827	1.8545570	1.3405053
F	−1.8545570	0.7681827	−1.3405053
F	−0.7681827	−1.8545570	−1.3405053
F	−1.8545570	−0.7681827	1.3405053

$[ThF_8]^{4-}$ D_{2d}-symmetry

Th	0.0000000	0.0000000	0.0000000
F	1.6151976	1.6151976	0.7583266
F	−1.6151976	−1.6151976	0.7583266
F	1.6151976	−1.6151976	−0.7583266
F	−1.6151976	1.6151976	−0.7583266
F	1.0540908	1.0540908	−1.9102732
F	−1.0540908	−1.0540908	−1.9102732
F	1.0540908	−1.0540908	1.9102732
F	−1.0540908	1.0540908	1.9102732

$[ThF_8]^{4-}$ D_2-symmetry

Th	0.0000000	0.0000000	0.0000000
F	1.8547972	−0.7676236	−1.3405585
F	0.7676236	1.8547972	−1.3405585
F	1.8547972	0.7676236	1.3405585
F	0.7676236	−1.8547972	1.3405585
F	−0.7676236	1.8547972	1.3405585
F	−1.8547972	0.7676236	−1.3405585
F	−0.7676236	−1.8547972	−1.3405585
F	−1.8547972	−0.7676236	1.3405585

$[PaF_8]^{4-}$ O_h-symmetry

Pa	0.0000000	0.0000000	0.0000000
F	−1.3947442	−1.3947442	1.3947442
F	−1.3947442	−1.3947442	−1.3947442
F	1.3947442	−1.3947442	−1.3947442
F	1.3947442	−1.3947442	1.3947442
F	1.3947442	1.3947442	1.3947442
F	−1.3947442	1.3947442	1.3947442
F	−1.3947442	1.3947442	−1.3947442
F	1.3947442	1.3947442	−1.3947442

$[PaF_8]^{4-}$ D_{4d}-symmetry

Pa	0.0000000	0.0000000	0.0000000
F	1.8421491	−0.7630431	−1.3187938
F	0.7630431	1.8421491	−1.3187938
F	1.8421491	0.7630431	1.3187938
F	0.7630431	−1.8421491	1.3187938
F	−0.7630431	1.8421491	1.3187938
F	−1.8421491	0.7630431	−1.3187938
F	−0.7630431	−1.8421491	−1.3187938
F	−1.8421491	−0.7630431	1.3187938

$[PaF_8]^{4-}$ D_{2d}-symmetry

Pa	0.0000000	0.0000000	0.0000000
F	1.5938208	1.5938208	0.7037329
F	−1.5938208	−1.5938208	0.7037329
F	1.5938208	−1.5938208	−0.7037329
F	−1.5938208	1.5938208	−0.7037329
F	1.0304310	1.0304310	−1.9327958
F	−1.0304310	−1.0304310	−1.9327958
F	1.0304310	−1.0304310	1.9327958
F	−1.0304310	1.0304310	1.9327958

$[PaF_8]^{4-}$ D_2-symmetry

Pa	0.0000000	0.0000000	0.0000000
F	1.9188607	−0.8661216	−1.1977633
F	0.7045903	1.7363226	−1.4349022
F	1.9188607	0.8661216	1.1977633
F	0.7045903	−1.7363226	1.4349022
F	−0.7045903	1.7363226	1.4349022
F	−1.9188607	0.8661216	−1.1977633
F	−0.7045903	−1.7363226	−1.4349022
F	−1.9188607	−0.8661216	1.1977633

$[UF_8]^{4-}$ O_h-symmetry

U	0.0000000	0.0000000	0.0000000
F	−1.2858872	−1.2858872	1.2858872
F	−1.2858872	−1.2858872	−1.2858872
F	1.2858872	−1.2858872	−1.2858872
F	1.2858872	−1.2858872	1.2858872
F	1.2858872	1.2858872	1.2858872
F	−1.2858872	1.2858872	1.2858872
F	−1.2858872	1.2858872	−1.2858872
F	1.2858872	1.2858872	−1.2858872

$[UF_8]^{4-}$ D_{4d}-symmetry

U	0.0000000	0.0000000	0.0000000
F	1.8404065	−0.7623213	−1.2772614
F	0.7623213	1.8404065	−1.2772614
F	1.8404065	0.7623213	1.2772614
F	0.7623213	−1.8404065	1.2772614
F	−0.7623213	1.8404065	1.2772614
F	−1.8404065	0.7623213	−1.2772614
F	−0.7623213	−1.8404065	−1.2772614
F	−1.8404065	−0.7623213	1.2772614

$[UF_8]^{4-}$ D_{2d}-symmetry

U	0.0000000	0.0000000	0.0000000
F	1.5592343	1.5592343	0.7036921
F	−1.5592343	−1.5592343	0.7036921
F	1.5592343	−1.5592343	−0.7036921
F	−1.5592343	1.5592343	−0.7036921
F	1.0482639	1.0482639	−1.9210358
F	−1.0482639	−1.0482639	−1.9210358
F	1.0482639	−1.0482639	1.9210358
F	−1.0482639	1.0482639	1.9210358

$[UF_8]^{4-}$ C_2-symmetry

U	0.0000000	0.0000000	0.0078541
F	−1.2016531	−1.5773108	−1.2992958
F	−1.6077578	1.1508470	−1.2973983
F	1.2016531	1.5773108	−1.2992958
F	1.6077578	−1.1508470	−1.2973983
F	1.8710777	0.2799336	1.3671411
F	0.3055053	−2.0385058	1.2334801
F	−1.8710777	−0.2799336	1.3671411
F	−0.3055053	2.0385058	1.2334801

$[NpF_8]^{4-}$ O_h-symmetry

Np	0.0000000	0.0000000	0.0000000
F	−1.3598215	−1.3598215	1.3598215
F	−1.3598215	−1.3598215	−1.3598215
F	1.3598215	−1.3598215	−1.3598215
F	1.3598215	−1.3598215	1.3598215
F	1.3598215	1.3598215	1.3598215
F	−1.3598215	1.3598215	1.3598215
F	−1.3598215	1.3598215	−1.3598215
F	1.3598215	1.3598215	−1.3598215

$[NpF_8]^{4-}$ D_{4d}-symmetry

Np	0.0000000	0.0000000	0.0000000
F	1.8321364	−0.7588958	−1.2642056
F	0.7588958	1.8321364	−1.2642056
F	1.8321364	0.7588958	1.2642056
F	0.7588958	−1.8321364	1.2642056
F	−0.7588958	1.8321364	1.2642056
F	−1.8321364	0.7588958	−1.2642056
F	−0.7588958	−1.8321364	−1.2642056
F	−1.8321364	−0.7588958	1.2642056

$[NpF_8]^{4-}$ D_{2d}-symmetry

Np	0.0000000	0.0000000	0.0000000
F	1.4549228	1.4549228	0.6406748
F	−1.4549228	−1.4549228	0.6406748
F	1.4549228	−1.4549228	−0.6406748
F	−1.4549228	1.4549228	−0.6406748
F	0.9474700	0.9474700	−1.7881452
F	−0.9474700	−0.9474700	−1.7881452
F	0.9474700	−0.9474700	1.7881452
F	−0.9474700	0.9474700	1.7881452

$[NpF_8]^{4-}$ D_2-symmetry

Np	0.0000000	0.0000000	0.0000000
F	1.8053582	−0.7355462	−1.3160064
F	0.7700087	1.8284810	−1.2621089
F	1.8053582	0.7355462	1.3160064
F	0.7700087	−1.8284810	1.2621089
F	−0.7700087	1.8284810	1.2621089
F	−1.8053582	0.7355462	−1.3160064
F	−0.7700087	−1.8284810	−1.2621089
F	−1.8053582	−0.7355462	1.3160064

$[PuF_8]^{4-}$ O_h-symmetry

Pu	0.0000000	0.0000000	0.0000000
F	−1.3609286	−1.3609286	1.3609286
F	−1.3609286	−1.3609286	−1.3609286
F	1.3609286	−1.3609286	−1.3609286
F	1.3609286	−1.3609286	1.3609286
F	1.3609286	1.3609286	1.3609286
F	−1.3609286	1.3609286	1.3609286
F	−1.3609286	1.3609286	−1.3609286
F	1.3609286	1.3609286	−1.3609286

$[PuF_8]^{4-}$ D_{4d}-symmetry

Pu	0.0000000	0.0000000	0.0000000
F	1.7968702	−0.7442880	−1.2982158
F	0.7442880	1.7968702	−1.2982158
F	1.7968702	0.7442880	1.2982158
F	0.7442880	−1.7968702	1.2982158
F	−0.7442880	1.7968702	1.2982158
F	−1.7968702	0.7442880	−1.2982158
F	−0.7442880	−1.7968702	−1.2982158
F	−1.7968702	−0.7442880	1.2982158

$[PuF_8]^{4-}$ D_{2d}-symmetry

Pu	0.0000000	0.0000000	0.0000000
F	1.5592293	1.5592293	0.8534187
F	−1.5592293	−1.5592293	0.8534187
F	1.5592293	−1.5592293	−0.8534187
F	−1.5592293	1.5592293	−0.8534187
F	1.0495999	1.0495999	−1.7828081
F	−1.0495999	−1.0495999	−1.7828081
F	1.0495999	−1.0495999	1.7828081
F	−1.0495999	1.0495999	1.7828081

$[PuF_8]^{4-}$ D_2-symmetry

Pu	0.0000000	0.0000000	0.0000000
F	0.9467620	−1.7766049	−1.1520574
F	−1.6683266	−0.8515805	−1.4439121
F	−0.9467620	1.7766049	−1.1520574
F	1.6683266	0.8515805	−1.4439121
F	0.9467620	1.7766049	1.1520574
F	1.6683266	−0.8515805	1.4439121
F	−0.9467620	−1.7766049	1.1520574
F	−1.6683266	0.8515805	1.4439121

$[AmF_8]^{4-}$ O_h-symmetry

Am	0.0000000	0.0000000	0.0000000
F	−1.2725538	−1.2725538	1.2725538
F	−1.2725538	−1.2725538	−1.2725538
F	1.2725538	−1.2725538	−1.2725538
F	1.2725538	−1.2725538	1.2725538
F	1.2725538	1.2725538	1.2725538
F	−1.2725538	1.2725538	1.2725538
F	−1.2725538	1.2725538	−1.2725538
F	1.2725538	1.2725538	−1.2725538

$[AmF_8]^{4-}$ D_{4d}-symmetry

Am	0.0000000	0.0000000	0.0000000
F	1.7935881	−0.7429285	−1.2947491
F	0.7429285	1.7935881	−1.2947491
F	1.7935881	0.7429285	1.2947491
F	0.7429285	−1.7935881	1.2947491
F	−0.7429285	1.7935881	1.2947491
F	−1.7935881	0.7429285	−1.2947491
F	−0.7429285	−1.7935881	−1.2947491
F	−1.7935881	−0.7429285	1.2947491

$[AmF_8]^{4-}$ D_{2d}-symmetry

Am	0.0000000	0.0000000	0.0000000
F	1.5569679	1.5569679	0.5746853
F	−1.5569679	−1.5569679	0.5746853
F	1.5569679	−1.5569679	−0.5746853
F	−1.5569679	1.5569679	−0.5746853
F	0.9822379	0.9822379	−1.9608077
F	−0.9822379	−0.9822379	−1.9608077
F	0.9822379	−0.9822379	1.9608077
F	−0.9822379	0.9822379	1.9608077

$[AmF_8]^{4-}$ D_2-symmetry

Am	0.0000000	0.0000000	0.0000000
F	1.7937626	−0.7427954	−1.2945577
F	0.7427956	1.7937629	−1.2945575
F	1.7937626	0.7427954	1.2945577
F	0.7427956	−1.7937629	1.2945575
F	−0.7427956	1.7937629	1.2945575
F	−1.7937626	0.7427954	−1.2945577
F	−0.7427956	−1.7937629	−1.2945575
F	−1.7937626	−0.7427954	1.2945577

$[CmF_8]^{4-}$ O_h-symmetry

Cm	0.0000000	0.0000000	0.0000000
F	−1.3598854	−1.3598854	1.3598854
F	−1.3598854	−1.3598854	−1.3598854
F	1.3598854	−1.3598854	−1.3598854
F	1.3598854	−1.3598854	1.3598854
F	1.3598854	1.3598854	1.3598854
F	−1.3598854	1.3598854	1.3598854
F	−1.3598854	1.3598854	−1.3598854
F	1.3598854	1.3598854	−1.3598854

$[CmF_8]^{4-}$ D_{4d}-symmetry

Cm	0.0000000	0.0000000	0.0000000
F	1.8160597	−0.7522366	−1.2895189
F	0.7522366	1.8160597	−1.2895189
F	1.8160597	0.7522366	1.2895189
F	0.7522366	−1.8160597	1.2895189
F	−0.7522366	1.8160597	1.2895189
F	−1.8160597	0.7522366	−1.2895189
F	−0.7522366	−1.8160597	−1.2895189
F	−1.8160597	−0.7522366	1.2895189

$[CmF_8]^{4-}$ D_{2d}-symmetry

Cm	0.0000000	0.0000000	0.0000000
F	1.5250647	1.5250647	0.9069894
F	−1.5250647	−1.5250647	0.9069894
F	1.5250647	−1.5250647	−0.9069894
F	−1.5250647	1.5250647	−0.9069894
F	1.1105801	1.1105801	−1.7548208
F	−1.1105801	−1.1105801	−1.7548208
F	1.1105801	−1.1105801	1.7548208
F	−1.1105801	1.1105801	1.7548208

$[CmF_8]^{4-}$ D_2-symmetry

Cm	0.0000000	0.0000000	0.0000000
F	1.7116649	−0.9257524	−1.3113214
F	0.9257524	1.7116649	−1.3113214
F	1.7116649	0.9257524	1.3113214
F	0.9257524	−1.7116649	1.3113214
F	−0.9257524	1.7116649	1.3113214
F	−1.7116649	0.9257524	−1.3113214
F	−0.9257524	−1.7116649	−1.3113214
F	−1.7116649	−0.9257524	1.3113214

$[BkF_8]^{4-}$ O_h-symmetry

Bk	0.0000000	0.0000000	0.0000000
F	−1.3429649	−1.3429649	1.3429649
F	−1.3429649	−1.3429649	−1.3429649
F	1.3429649	−1.3429649	−1.3429649
F	1.3429649	−1.3429649	1.3429649
F	1.3429649	1.3429649	1.3429649
F	−1.3429649	1.3429649	1.3429649
F	−1.3429649	1.3429649	−1.3429649
F	1.3429649	1.3429649	−1.3429649

$[BkF_8]^{4-}$ D_{4d}-symmetry

Bk	0.0000000	0.0000000	0.0000000
F	1.7821696	−0.7381988	−1.2764379
F	0.7381988	1.7821696	−1.2764379
F	1.7821696	0.7381988	1.2764379
F	0.7381988	−1.7821696	1.2764379
F	−0.7381988	1.7821696	1.2764379
F	−1.7821696	0.7381988	−1.2764379
F	−0.7381988	−1.7821696	−1.2764379
F	−1.7821696	−0.7381988	1.2764379

$[BkF_8]^{4-}$ D_{2d}-symmetry

Bk	0.0000000	0.0000000	0.0000000
F	1.5434559	1.5434559	0.7156422
F	−1.5434559	−1.5434559	0.7156422
F	1.5434559	−1.5434559	−0.7156422
F	−1.5434559	1.5434559	−0.7156422
F	1.0046990	1.0046990	−1.8504955
F	−1.0046990	−1.0046990	−1.8504955
F	1.0046990	−1.0046990	1.8504955
F	−1.0046990	1.0046990	1.8504955

$[BkF_8]^{4-}$ D_2-symmetry

Bk	0.0000000	0.0000000	0.0000000
F	1.7824113	−0.7380363	−1.2762447
F	0.7380363	1.7824115	−1.2762447
F	1.7824113	0.7380363	1.2762447
F	0.7380363	−1.7824115	1.2762447
F	−0.7380363	1.7824115	1.2762447
F	−1.7824113	0.7380363	−1.2762447
F	−0.7380363	−1.7824115	−1.2762447
F	−1.7824113	−0.7380363	1.2762447

References

[1] A. T. Chemey, C. Celis-Barros, K. Huang, J. M. Sperling, C. J. Windorff, R. E. Baumbach, D. E. Graf, D. Páez-Hernández, M. Ruf, D. E. Hobart, T. E. Albrecht-Schmitt, *Inorg. Chem.* **2019**, *58*, 637–647.

8. Anhang

8.1. Atomkoordinaten und kristallographische Daten

8.1.1. Verbindungen aus Abschnitt 4.3

8.1.1.1. $(ClOF_2)_2[CrF_6]$

Tabelle 35. Ausgewählte Daten und Details der Strukturbestimmung von $(ClOF_2)_2[CrF_6]$.

Diffraktometer	IPDS2
Formel	$Cr_1Cl_2O_2F_{10}$
molare Masse / g·mol^{-1}	346,54
Raumgruppe (Nr.)	*C*2/*m* (12)
a / Å	9,2613(15)
b / Å	6,7573(7)
c / Å	7,2877(11)
β / °	117,190(11)
V / Å^3	405,68(11)
Z	2
Pearsonsymbol	*mS*30
$\rho_{calc.}$ / g·cm^{-3}	2,837
μ / mm^{-1}	2,232
Farbe	pink
Kristallmorphologie	Block
Kristallgröße / mm^3	0,03×0,04×0,04
T / K	100
λ / Å	0,71073 (Mo-K_α)
Anzahl der Reflexe	3941
θ-Bereich / °	3,143 - 31,505
Bereich der Miller-Indizes	$-13 \leq h \leq 13$
	$-9 \leq k \leq 9$
	$-10 \leq l \leq 10$
Absorptionskorrektur	Integration
$Trans._{max}$, $Trans._{min}$	0,8153, 0,6697
R_{int}, R_σ	0,0366, 0,0267
Vollständigkeit des Datensatzes	1,000
Anzahl der einzigartigen Reflexe	727
Anzahl der Parameter	44
Anzahl der Restraints	0
Anzahl der Constraints	0
S (alle Daten)	1,164
$R(F)$ ($I \geq 2\sigma(I)$, alle Daten)	0,0407, 0,0574
$wR(F^2)$ ($I \geq 2\sigma(I)$, alle Daten)	0,0906, 0,0980
Extinktionskoeffizient	-
$\Delta\rho_{max}$, $\Delta\rho_{min}$ / e·Å^{-3}	0,825, −1,195

Tabelle 36. Atomkoordinaten und äquivalente isotrope Auslenkungsparameter, U_{iso}, der Verbindung $(ClOF_2)_2[CrF_6]$ bei 100 K.

Atom	Position	*x*	*y*	*z*	U_{iso} / Å^2
Cr(1)	2*c*	1/2	1/2	1/2	0,0110(2)
Cl(1)	4*i*	0,21105(14)	1/2	0,73307(17)	0,0216(3)
O/F(1)	8*j*	0,3160(2)	0,6756(3)	0,8301(3)	0,0193(7)
F(2)	4*i*	0,1082(4)	1/2	0,8543(4)	0,0213(6)
F(3)	4*i*	0,2964(3)	1/2	0,4782(4)	0,0185(6)
F(4)	4*i*	0,4172(3)	1/2	0,2280(4)	0,0186(6)
F(5)	4*h*	1/2	0,7760(4)	1/2	0,0192(6)

Tabelle 37. Anisotrope Auslenkungsparameter, U_{ij}, der Verbindung $(ClOF_2)_2[CrF_6]$ bei 100 K.

Atom	U_{11} / Å^2	U_{22} / Å^2	U_{33} / Å^2	U_{23} / Å^2	U_{13} / Å^2	U_{12} / Å^2
Cr(1)	0,0109(4)	0,0096(5)	0,0107(5)	0	0,0035(4)	0
Cl(1)	0,0165(5)	0,0323(7)	0,0118(5)	0	0,0029(4)	0,000
O/F(1)	0,0194(11)	0,0129(10)	0,0200(11)	−0,0031(8)	0,0041(8)	−0,0024(8)
F(2)	0,0217(14)	0,0263(16)	0,0170(14)	0	0,0096(12)	0
F(3)	0,0118(12)	0,0264(15)	0,0169(13)	0	0,0063(10)	0
F(4)	0,0154(12)	0,0275(15)	0,0110(12)	0	0,0043(10)	0
F(5)	0,0177(13)	0,0095(12)	0,0221(14)	0	0,0021(11)	0

8.1.1.2. $(ClOF_2)_2[RhF_6]$

Tabelle 38. Ausgewählte Daten und Details der Strukturbestimmung von $(ClOF_2)_2[RhF_6]$.

Diffraktometer	IPDS2
Formel	$Rh_1Cl_2O_2F_{10}$
molare Masse / g·mol^{-1}	395,72
Raumgruppe (Nr.)	*C*2/*m* (12)
a / Å	9,3751(11)
b / Å	6,8244(7)
c / Å	7,3202(9)
β / °	116,542(9)
V / Å^3	418,98(9)
Z	2
Pearsonsymbol	*mS*30
$\rho_{calc.}$ / g·cm^{-3}	3,137
μ / mm^{-1}	2,828
Farbe	farblos
Kristallmorphologie	Block
Kristallgröße / mm^3	0,04×0,08×0,08
T / K	100
λ / Å	0,71073 (Mo-K_α)
Anzahl der Reflexe	3830
θ-Bereich / °	3,111 - 32,003
Bereich der Miller-Indizes	$-13 \leq h \leq 13$
	$-10 \leq k \leq 10$
	$-10 \leq l \leq 10$
Absorptionskorrektur	Integration
$Trans._{max}$, $Trans._{min}$	0,6854, 0,4696
R_{int}, R_σ	0,0694, 0,0359
Vollständigkeit des Datensatzes	1,000
Anzahl der einzigartigen Reflexe	783
Anzahl der Parameter	44
Anzahl der Restraints	0
Anzahl der Constraints	0
S (alle Daten)	1,192
$R(F)$ ($I \geq 2\sigma(I)$, alle Daten)	0,0430, 0,0447
$wR(F^2)$ ($I \geq 2\sigma(I)$, alle Daten)	0,1089, 0,1108
Extinktionskoeffizient	-
$\Delta\rho_{max}$, $\Delta\rho_{min}$ / e·Å^{-3}	1,683, −1,941

Tabelle 39. Atomkoordinaten und äquivalente isotrope Auslenkungsparameter, U_{iso}, der Verbindung $(ClOF_2)_2[RhF_6]$ bei 100 K.

Atom	Position	*x*	*y*	*z*	U_{iso} / Å^2
Rh(1)	2*c*	1/2	1/2	1/2	0,01191(18)
Cl(1)	4*i*	0,21300(17)	1/2	0,7338(2)	0,0218(3)
O/F(1)	8*j*	0,3139(4)	0,6744(5)	0,8266(5)	0,0214(9)
F(2)	4*i*	0,1116(5)	1/2	0,8581(7)	0,0251(9)
F(3)	4*i*	0,2892(4)	1/2	0,4777(6)	0,0222(8)
F(4)	4*i*	0,4170(5)	1/2	0,2156(6)	0,0247(9)
F(5)	4*h*	1/2	0,7804(6)	1/2	0,0258(9)

Tabelle 40. Anisotrope Auslenkungsparameter, U_{ij}, der Verbindung $(ClOF_2)_2[RhF_6]$ bei 100 K.

Atom	U_{11} / Å^2	U_{22} / Å^2	U_{33} / Å^2	U_{23} / Å^2	U_{13} / Å^2	U_{12} / Å^2
Rh(1)	0,0089(3)	0,0118(3)	0,0103(3)	0	0,0000(2)	0
Cl(1)	0,0121(6)	0,0358(9)	0,0123(6)	0	0,0008(5)	0
O/F(1)	0,0172(14)	0,0158(14)	0,0209(15)	−0,0034(11)	−0,0007(11)	−0,0030(10)
F(2)	0,0182(17)	0,038(2)	0,0184(19)	0	0,0079(15)	0
F(3)	0,0088(14)	0,039(2)	0,0161(17)	0	0,0030(13)	0
F(4)	0,0154(17)	0,044(3)	0,0086(15)	0	0,0002(13)	0
F(5)	0,0186(17)	0,0117(16)	0,030(2)	0	−0,0041(15)	0

8.1.1.3. $(ClOF_2)_2[GeF_6]$

Tabelle 41. Ausgewählte Daten und Details der Strukturbestimmung von $(ClOF_2)_2[GeF_6]$.

Diffraktometer	IPDS2T
Formel	$Ge_1Cl_2O_2F_{10}$
molare Masse / g·mol^{-1}	366,29
Raumgruppe (Nr.)	*C*2/*m* (12)
a / Å	9,2914(19)
b / Å	6,7050(13)
c / Å	7,2694(14)
β / °	116,75(3)
V / Å^3	404,41(17)
Z	2
Pearsonsymbol	*mS*30
$\rho_{calc.}$ / g·cm^{-3}	3,008
μ / mm^{-1}	4,610
Farbe	farblos
Kristallmorphologie	Block
Kristallgröße / mm^3	0,05×0,05×0,09
T / K	100
λ / Å	0,71073 (Mo-K_α)
Anzahl der Reflexe	3836
θ-Bereich / °	3,138 - 32,555
Bereich der Miller-Indizes	$-14 \leq h \leq 14$
	$-10 \leq k \leq 9$
	$-11 \leq l \leq 9$
Absorptionskorrektur	Integration
$Trans._{max}$, $Trans._{min}$	0,5431, 0,4484
R_{int}, R_σ	0,0332, 0,0196
Vollständigkeit des Datensatzes	1,000
Anzahl der einzigartigen Reflexe	794
Anzahl der Parameter	45
Anzahl der Restraints	0
Anzahl der Constraints	0
S (alle Data)	1,092
$R(F)$ ($I \geq 2\sigma(I)$, alle Daten)	0,0335, 0,0381
$wR(F^2)$ ($I \geq 2\sigma(I)$, alle Daten)	0,0825, 0,0848
Extinktionskoeffizient	0,013(2)
$\Delta\rho_{max}$, $\Delta\rho_{min}$ / e·Å^{-3}	0,727, −1,548

Tabelle 42. Atomkoordinaten und äquivalente isotrope Auslenkungsparameter, U_{iso}, der Verbindung $(ClOF_2)_2[GeF_6]$ bei 100 K.

Atom	Position	*x*	*y*	*z*	U_{iso} / Å^2
Ge(1)	2*c*	1/2	1/2	1/2	0.01277(17)
Cl(1)	4*i*	0.21644(10)	1/2	0.73735(12)	0.0222(2)
O/F(1)	8*j*	0.31817(19)	0.6772(2)	0.8326(2)	0.0196(5)
F(2)	4*i*	0.1116(3)	1/2	0.8580(3)	0.0219(4)
F(3)	4*i*	0.3004(2)	1/2	0.4811(3)	0.0175(4)
F(4)	4*i*	0.4176(2)	1/2	0.2294(3)	0.0181(4)
F(5)	4*h*	1/2	0.7708(3)	1/2	0.0184(4)

Tabelle 43. Anisotrope Auslenkungsparameter, U_{ij}, der Verbindung $(ClOF_2)_2[GeF_6]$ bei 100 K.

Atom	U_{11} / Å^2	U_{22} / Å^2	U_{33} / Å^2	U_{23} / Å^2	U_{13} / Å^2	U_{12} / Å^2
Ge(1)	0,0128(2)	0,0120(2)	0,0122(2)	0	0,00446(16)	0
Cl(1)	0,0160(4)	0,0346(5)	0,0133(3)	0	0,0043(3)	0
O/F(1)	0,0200(8)	0,0156(8)	0,0191(8)	−0,0031(6)	0,0052(6)	−0,0029(5)
F(2)	0,0224(10)	0,0273(11)	0,0188(10)	0	0,0118(8)	0
F(3)	0,0124(8)	0,0221(10)	0,0172(9)	0	0,0059(7)	0
F(4)	0,0173(9)	0,0227(10)	0,0117(8)	0	0,0041(7)	0
F(5)	0,0187(9)	0,0107(8)	0,0210(9)	0	0,0046(7)	0

8.1.1.4. $(ClOF_2)_2[PdF_6]$

Tabelle 44. Ausgewählte Daten und Details der Strukturbestimmung von $(ClOF_2)_2[PdF_6]$.

Diffraktometer	IPDS2
Formel	$Pd_1Cl_2O_2F_{10}$
molare Masse / g·mol^{-1}	399,30
Raumgruppe (Nr.)	*Pnnm* (58)
a / Å	7,4491(15)
b / Å	9,4636(19)
c / Å	5,9111(12)
V / Å^3	416,70(15)
Z	2
Pearsonsymbol	*oP*30
$\rho_{calc.}$ / g·cm^{-3}	3,182
μ / mm^{-1}	3,022
Farbe	orange
Kristallmorphologie	Nadel
Kristallgröße / mm^3	0,02×0,02×0,13
T / K	100
λ / Å	0,71073 (Mo-K_α)
Anzahl der Reflexe	5271
θ-Bereich / °	3,481 - 28,278
Bereich der Miller-Indizes	$-9 \leq h \leq 9$
	$-12 \leq k \leq 12$
	$-7 \leq l \leq 7$
Absorptionskorrektur	Integration
$Trans._{max}$, $Trans._{min}$	0,6774, 0,4832
R_{int}, R_σ	0,1253, 0,0500
Vollständigkeit des Datensatzes	1,000
Anzahl der einzigartigen Reflexe	568
Anzahl der Parameter	41
Anzahl der Restraints	0
Anzahl der Constraints	0
S (alle Daten)	1,075
$R(F)$ ($I \geq 2\sigma(I)$, alle Daten)	0,0349, 0,0537
$wR(F^2)$ ($I \geq 2\sigma(I)$, alle Daten)	0,0754, 0,0832
Extinktionskoeffizient	-
$\Delta\rho_{max}$, $\Delta\rho_{min}$ / e·Å^{-3}	0,748, −0,746

Tabelle 45. Atomkoordinaten und äquivalente isotrope Auslenkungsparameter, U_{iso}, der Verbindung $(ClOF_2)_2[PdF_6]$ bei 100 K.

Atom	Position	*x*	*y*	*z*	U_{iso} / Å^2
Pd(1)	2*b*	1/2	1/2	0	0,0136(2)
Cl(1)	4*g*	0,5510(2)	0,74861(19)	1/2	0,0246(4)
O(1)	4*g*	0,3773(6)	0,6822(4)	1/2	0,0241(7)
F(1)	8*h*	0,5376(3)	0,8577(3)	0,6954(5)	0,0141(9)
F(2)	8*h*	0,6507(3)	0,5798(3)	0,2253(5)	0,0181(6)
F(3)	4*g*	0,3631(5)	0,6689(4)	0	0,0186(8)

Tabelle 46. Anisotrope Auslenkungsparameter, U_{ij}, der Verbindung $(ClOF_2)_2[PdF_6]$ bei 100 K.

Atom	U_{11} / Å^2	U_{22} / Å^2	U_{33} / Å^2	U_{23} / Å^2	U_{13} / Å^2	U_{12} / Å^2
Pd(1)	0,0113(3)	0,0139(3)	0,0157(3)	0	0	0,0002(3)
Cl(1)	0,0199(8)	0,0243(7)	0,0296(9)	0	0	0,0067(6)
O(1)	0,0110(19)	0,0139(19)	0,017(2)	0	0	−0,0053(16)
F(1)	0,0210(16)	0,0223(13)	0,0290(15)	−0,0055(12)	0,0046(12)	0,0010(10)
F(2)	0,0134(12)	0,0215(13)	0,0194(13)	−0,0020(11)	−0,0023(10)	0,0000(10)
F(3)	0,0147(18)	0,0182(17)	0,023(2)	0	0	0,0026(13)

8.1.1.5. $(ClOF_2)_2[PtF_6]$

Tabelle 47. Ausgewählte Daten und Details der Strukturbestimmung von $(ClOF_2)_2[PtF_6]$.

Diffraktometer	IPDS2
Formel	$Pt_1Cl_2O_2F_{10}$
molare Masse / g·mol^{-1}	487,99
Raumgruppe (Nr.)	*Pnnm* (58)
a / Å	7,4807(15)
b / Å	9,4651(19)
c / Å	5,9950(12)
V / Å^3	424,48(15)
Z	2
Pearsonsymbol	*oP*30
$\rho_{calc.}$ / g·cm^{-3}	3,818
μ / mm^{-1}	17,309
Farbe	orange
Kristallmorphologie	Block
Kristallgröße / mm^3	0,03×0,04×0,04
T / K	100
λ / Å	0,71073 (Mo-K$_\alpha$)
Anzahl der Reflexe	8073
θ-Bereich / °	3,471 - 33,295
Bereich der Miller-Indizes	$-11 \leq h \leq 11$
	$-14 \leq k \leq 14$
	$-9 \leq l \leq 9$
Absorptionskorrektur	Integration
$Trans._{max}$, $Trans._{min}$	0,8094, 0,5108
R_{int}, R_σ	0,0707, 0,0281
Vollständigkeit des Datensatzes	1,000
Anzahl der einzigartigen Reflexe	892
Anzahl der Parameter	41
Anzahl der Restraints	0
Anzahl der Constraints	0
S (alle Daten)	1,065
$R(F)$ ($I \geq 2\sigma(I)$, alle Daten)	0,0295, 0,0367
$wR(F^2)$ ($I \geq 2\sigma(I)$, alle Daten)	0,0749, 0,0774
Extinktionskoeffizient	-
$\Delta\rho_{max}$, $\Delta\rho_{min}$ / e·Å^{-3}	2,004, −2,474

Tabelle 48. Atomkoordinaten und äquivalente isotrope Auslenkungsparameter, U_{iso}, der Verbindung $(ClOF_2)_2[PtF_6]$ bei 100 K.

Atom	Position	*x*	*y*	*z*	U_{iso} / Å^2
Pt(1)	2*b*	1/2	1/2	0	0,01684(11)
Cl(1)	4*g*	0,5533(2)	0,74793(18)	1/2	0,0275(3)
O(1)	4*g*	0,3802(5)	0,6808(4)	1/2	0,0223(8)
F(1)	8*h*	0,5383(4)	0,8559(3)	0,6913(6)	0,0299(6)
F(2)	8*h*	0,6516(3)	0,5809(3)	0,2272(4)	0,0216(4)
F(3)	4*g*	0,3634(4)	0,6722(4)	0	0,0231(7)

Tabelle 49. Anisotrope Auslenkungsparameter, U_{ij}, der Verbindung $(ClOF_2)_2[PtF_6]$ bei 100 K.

Atom	U_{11} / Å^2	U_{22} / Å^2	U_{33} / Å^2	U_{23} / Å^2	U_{13} / Å^2	U_{12} / Å^2
Pt(1)	0,01533(16)	0,01656(14)	0,01864(15)	0	0	0,00005(9)
Cl(1)	0,0255(6)	0,0245(6)	0,0326(7)	0	0	0,0058(6)
O(1)	0,0181(18)	0,0214(19)	0,0272(19)	0	0	−0,0029(14)
F(1)	0,0300(12)	0,0238(12)	0,0359(15)	−0,0071(11)	0,0034(12)	−0,0014(11)
F(2)	0,0194(10)	0,0237(10)	0,0219(10)	−0,0025(9)	−0,0037(8)	−0,0009(8)
F(3)	0,0197(16)	0,0208(16)	0,0289(16)	0	0	0,0048(12)

8.1.1.6. $(ClOF_2)_2[SnF_6]$

Tabelle 50. Ausgewählte Daten und Details der Strukturbestimmung von $(ClOF_2)_2[SnF_6]$.

Diffraktometer	D8 Quest
Formel	$Sn_1Cl_2O_2F_{10}$
molare Masse / g·mol^{-1}	411,59
Raumgruppe (Nr.)	*Pnnm* (58)
a / Å	7,5859(4)
b / Å	9,7473(5)
c / Å	6,0864(3)
V / Å^3	450,04(4)
Z	2
Pearsonsymbol	*oP*30
$\rho_{calc.}$ / g·cm^{-3}	3,037
μ / mm^{-1}	3,576
Farbe	farblos
Kristallmorphologie	Block
Kristallgröße / mm^3	0,06×0,07×0,08
T / K	100
λ / Å	0,71073 (Mo-K$_\alpha$)
Anzahl der Reflexe	7790
θ-Bereich / °	3,403 - 40,333
Bereich der Miller-Indizes	$-7 \leq h \leq 13$
	$-16 \leq k \leq 17$
	$-9 \leq l \leq 11$
Absorptionskorrektur	Multi-scan
$Trans._{max}$, $Trans._{min}$	0,750, 0,634
R_{int}, R_σ	0,0308, 0,0238
Vollständigkeit des Datensatzes	0,981
Anzahl der einzigartigen Reflexe	1491
Anzahl der Parameter	42
Anzahl der Restraints	0
Anzahl der Constraints	0
S (alle Daten)	1,068
$R(F)$ ($I \geq 2\sigma(I)$, alle Daten)	0,0270, 0,0360
$wR(F^2)$ ($I \geq 2\sigma(I)$, alle Daten)	0,0644, 0,0685
Extinktionskoeffizient	1,068
$\Delta\rho_{max}$, $\Delta\rho_{min}$ / e·Å^{-3}	2,305, −2,620

Tabelle 51. Atomkoordinaten und äquivalente isotrope Auslenkungsparameter, U_{iso}, der Verbindung $(ClOF_2)_2[SnF_6]$ bei 100 K.

Atom	Position	*x*	*y*	*z*	U_{iso} / Å^2
Sn(1)	2*b*	1/2	1/2	0	0,00845(6)
Cl(1)	4*g*	0,53927(9)	0,75314(8)	1/2	0,02154(13)
O(1)	4*g*	0,3698(2)	0,67782(19)	1/2	0,0130(3)
F(1)	8*h*	0,51524(17)	0,85360(13)	0,6912(3)	0,0210(2)
F(2)	8*h*	0,63752(14)	0,59330(12)	0,2276(2)	0,01454(19)
F(3)	4*g*	0,3351(2)	0,65380(16)	0	0,0147(3)

Tabelle 52. Anisotrope Auslenkungsparameter, U_{ij}, der Verbindung $(ClOF_2)_2[SnF_6]$ bei 100 K.

Atom	U_{11} / Å^2	U_{22} / Å^2	U_{33} / Å^2	U_{23} / Å^2	U_{13} / Å^2	U_{12} / Å^2
Sn(1)	0,00632(8)	0,00924(9)	0,00981(9)	0	0	0,00057(6)
Cl(1)	0,0143(2)	0,0195(3)	0,0308(4)	0	0	0,0079(2)
O(1)	0,0065(6)	0,0144(7)	0,0182(8)	0	0	−0,0029(5)
F(1)	0,0205(6)	0,0160(5)	0,0267(6)	−0,0075(5)	0,0055(5)	−0,0001(4)
F(2)	0,0119(4)	0,0171(4)	0,0146(5)	−0,0035(4)	−0,0023(4)	−0,0013(3)
F(3)	0,0108(6)	0,0137(6)	0,0195(8)	0	0	0,0046(5)

8.1.1.7. $ClOF_2SnF_5$

Tabelle 53. Ausgewählte Daten und Details der Strukturbestimmung von $ClOF_2SnF_5$.

Diffraktometer	IPDS2T
Formel	$Sn_1Cl_1O_1F_7$
molare Masse / g·mol^{-1}	303,14
Raumgruppe (Nr.)	*C*2 (5)
a / Å	15,828(3)
b / Å	5,0614(10)
c / Å	7,4425(15)
β / °	111,25(3)
V / Å^3	555,7(2)
Z	4
Pearsonsymbol	*mS*40
$\rho_{calc.}$ / g·cm^{-3}	3,623
μ / mm^{-1}	5,169
Farbe	farblos
Kristallmorphologie	Block
Kristallgröße / mm^3	0,08×0,11×0,12
T / K	100
λ / Å	0,71073 (Mo-K$_\alpha$)
Anzahl der Reflexe	3926
θ-Bereich / °	2,761 - 29,540
Bereich der Miller-Indizes	$-21 \leq h \leq 21$
	$-7 \leq k \leq 7$
	$-10 \leq l \leq 9$
Absorptionskorrektur	Integration
$Trans._{max}$, $Trans._{min}$	0,4858, 0,3687
R_{int}, R_σ	0,0628, 0,0452
Vollständigkeit des Datensatzes	0,972
Anzahl der einzigartigen Reflexe	1508
Anzahl der Parameter	92
Anzahl der Restraints	1
Anzahl der Constraints	0
S (alle Daten)	1,117
$R(F)$ ($I \geq 2\sigma(I)$, alle Daten)	0,0371, 0,0398
$wR(F^2)$ ($I \geq 2\sigma(I)$, alle Daten)	0,0966, 0,0984
Extinktionskoeffizient	0,0080(15)
Flackparameter	−0,04(6)
$\Delta\rho_{max}$, $\Delta\rho_{min}$ / e·Å^{-3}	1,145, −1,580

Tabelle 54. Atomkoordinaten und äquivalente isotrope Auslenkungsparameter, U_{iso}, der Verbindung $ClOF_2SnF_5$ bei 100 K.

Atom	Position	*x*	*y*	*z*	U_{iso} / Å^2
Sn(1)	4*c*	0,65117(3)	0,30505(2)	0,45767(7)	0,0152(2)
Cl(1)	4*c*	0,59373(14)	0,8092(9)	0,8163(3)	0,0218(4)
O(1)	4*c*	0,5392(5)	0,6051(16)	0,8474(12)	0,0227(15)
F(1)	4*c*	0,6051(5)	1,0066(14)	0,9851(10)	0,0272(14)
F(2)	4*c*	0,6921(4)	0,7052(14)	0,9002(10)	0,0268(14)
F(3)	4*c*	0,5954(4)	0,6125(12)	0,5276(9)	0,0199(11)
F(4)	4*c*	0,5403(4)	0,1068(12)	0,3347(10)	0,0219(12)
F(5)	4*c*	0,6714(4)	0,1642(12)	0,7118(9)	0,0211(12)
F(6)	4*c*	0,6474(4)	0,4480(12)	0,2186(9)	0,0198(11)
F(7)	4*c*	0,7269(4)	-0,0011(13)	0,4192(9)	0,0179(11)

Tabelle 55. Anisotrope Auslenkungsparameter, U_{ij}, der Verbindung $ClOF_2SnF_5$ bei 100 K.

Atom	U_{11} / Å^2	U_{22} / Å^2	U_{33} / Å^2	U_{23} / Å^2	U_{13} / Å^2	U_{12} / Å^2
Sn(1)	0,0157(3)	0,0137(3)	0,0178(3)	0,0001(4)	0,0080(2)	0,0003(3)
Cl(1)	0,0284(9)	0,0169(8)	0,0206(8)	0,001(2)	0,0097(7)	0,0014(18)
O(1)	0,019(3)	0,025(4)	0,023(3)	−0,003(3)	0,007(3)	−0,007(3)
F(1)	0,034(3)	0,024(3)	0,026(3)	−0,003(3)	0,013(3)	0,002(3)
F(2)	0,023(3)	0,029(3)	0,028(3)	0,003(3)	0,009(3)	0,004(2)
F(3)	0,021(3)	0,017(3)	0,025(3)	−0,004(2)	0,013(2)	0,003(2)
F(4)	0,015(2)	0,021(3)	0,027(3)	−0,004(3)	0,005(2)	−0,004(2)
F(5)	0,027(3)	0,021(3)	0,018(3)	0,003(2)	0,012(2)	−0,002(2)
F(6)	0,024(3)	0,025(3)	0,012(2)	0,003(2)	0,008(2)	0,000(2)
F(7)	0,015(2)	0,016(2)	0,023(3)	−0,002(2)	0,006(2)	0,008(2)

8.1.1.8. $ClOF_2PbF_5$

Tabelle 56. Ausgewählte Daten und Details der Strukturbestimmung von $ClOF_2PbF_5$.

Diffraktometer	D8 Quest
Formel	$Pb_1Cl_1O_1F_7$
molare Masse / g·mol^{-1}	391,64
Raumgruppe (Nr.)	*C*2 (5)
a / Å	16,1838(12)
b / Å	5,1546(4)
c / Å	7,5376(5)
β / °	111,932(2)
V / Å^3	583,29(7)
Z	4
Pearsonsymbol	*mS*40
$\rho_{calc.}$ / g·cm^{-3}	4,460
μ / mm^{-1}	29,468
Farbe	farblos
Kristallmorphologie	Nadel
Kristallgröße / mm^3	0,03×0,03×0,14
T / K	100
λ / Å	0,71073 (Mo-K$_\alpha$)
Anzahl der Reflexe	5279
θ-Bereich / °	2,714 - 33,272
Bereich der Miller-Indizes	$-24 \leq h \leq 21$
	$-7 \leq k \leq 7$
	$-11 \leq l \leq 11$
Absorptionskorrektur	Multi-scan
$Trans._{max}$, $Trans._{min}$	0,5086, 0,2657
R_{int}, R_σ	0,042, 0,0235
Vollständigkeit des Datensatzes	0,989
Anzahl der einzigartigen Reflexe	2170
Anzahl der Parameter	93
Anzahl der Restraints	1
Anzahl der Constraints	0
S (alle Daten)	0,861
$R(F)$ ($I \geq 2\sigma(I)$, alle Daten)	0,0178, 0,0211
$wR(F^2)$ ($I \geq 2\sigma(I)$, alle Daten)	0,0333, 0,0341
Extinktionskoeffizient	0,00189(11)
Flackparameter	0,022(11)
$\Delta\rho_{max}$, $\Delta\rho_{min}$ / e·Å^{-3}	2,199, −1,211

Tabelle 57. Atomkoordinaten und äquivalente isotrope Auslenkungsparameter, U_{iso}, der Verbindung $ClOF_2PbF_5$ bei 100 K.

Atom	Position	*x*	*y*	*z*	U_{iso} / Å^2
Pb(1)	4*c*	0,35168(2)	0,25187(11)	0,54138(2)	0,00573(5)
Cl(1)	4*c*	0,40795(7)	0,7483(6)	0,18061(15)	0,0096(2)
O(1)	4*c*	0,4625(3)	0,9442(9)	0,1537(6)	0,0124(9)
F(1)	4*c*	0,3925(3)	0,5546(7)	0,0083(5)	0,0153(8)
F(2)	4*c*	0,3099(2)	0,8523(7)	0,0925(6)	0,0159(8)
F(3)	4*c*	0,2768(2)	0,5684(7)	0,5865(5)	0,0099(7)
F(4)	4*c*	0,3564(2)	0,1004(7)	0,7863(5)	0,0122(7)
F(5)	4*c*	0,4051(2)	-0,0661(7)	0,4632(5)	0,0131(7)
F(6)	4*c*	0,3287(2)	0,3946(7)	0,2803(5)	0,0107(7)
F(7)	4*c*	0,4673(2)	0,4486(7)	0,6698(6)	0,0129(7)

Tabelle 58. Anisotrope Auslenkungsparameter, U_{ij}, der Verbindung $ClOF_2PbF_5$ bei 100 K.

Atom	U_{11} / Å^2	U_{22} / Å^2	U_{33} / Å^2	U_{23} / Å^2	U_{13} / Å^2	U_{12} / Å^2
Pb(1)	0,00538(8)	0,00561(8)	0,00627(8)	−0,0002(2)	0,00225(5)	0,00006(19)
Cl(1)	0,0128(5)	0,0087(5)	0,0065(4)	0,0006(13)	0,0028(4)	−0,0004(13)
O(1)	0,011(2)	0,015(2)	0,009(2)	0,0040(17)	0,0023(16)	−0,0045(17)
F(1)	0,021(2)	0,0160(19)	0,0082(17)	−0,0042(15)	0,0048(15)	−0,0007(16)
F(2)	0,0090(16)	0,0150(18)	0,020(2)	0,0035(15)	0,0008(14)	0,0033(13)
F(3)	0,0089(16)	0,0083(16)	0,0113(17)	−0,0027(14)	0,0023(13)	0,0004(13)
F(4)	0,0135(17)	0,0159(18)	0,0055(16)	0,0037(14)	0,0016(14)	0,0006(14)
F(5)	0,0142(17)	0,0136(17)	0,0111(18)	−0,0025(14)	0,0043(14)	0,0057(14)
F(6)	0,0117(16)	0,0128(17)	0,0071(16)	0,0038(14)	0,0028(13)	−0,0007(14)
F(7)	0,0054(15)	0,0127(17)	0,0187(19)	0,0001(15)	0,0023(14)	−0,0031(13)

8.1.1.9. $ClOF_2[BF_4]$

Tabelle 59. Ausgewählte Daten und Details der Strukturbestimmung von $ClOF_2[BF_4]$.

Diffraktometer	D8 Quest
Formel	$B_1Cl_1O_1F_6$
molare Masse / g·mol^{-1}	176,62
Raumgruppe (Nr.)	*Pnma* (62)
a / Å	9,4367(4)
b / Å	5,5593(3)
c / Å	8,8592(4)
V / Å^3	464,77(4)
Z	4
Pearsonsymbol	*oP*36
$\rho_{calc.}$ / g·cm^{-3}	2,524
μ / mm^{-1}	0,885
Farbe	farblos
Kristallmorphologie	Block
Kristallgröße / mm^3	0,12×0,19×0,36
T / K	100
λ / Å	0,71073 (Mo-K_α)
Anzahl der Reflexe	7622
θ-Bereich / °	3,154 - 34,948
Bereich der Miller-Indizes	$-15 \leq h \leq 15$
	$-8 \leq k \leq 8$
	$-14 \leq l \leq 14$
Absorptionskorrektur	Multi-scan
$Trans._{max}$, $Trans._{min}$	0,747, 0,633
R_{int}, R_σ	0,0285, 0,0177
Vollständigkeit des Datensatzes	0,999
Anzahl der einzigartigen Reflexe	1101
Anzahl der Parameter	51
Anzahl der Restraints	0
Anzahl der Constraints	0
S (alle Daten)	1,079
$R(F)$ ($I \geq 2\sigma(I)$, alle Daten)	0,0323, 0,0369
$wR(F^2)$ ($I \geq 2\sigma(I)$, alle Daten)	0,0818, 0,0851
Extinktionskoeffizient	0,024(5)
$\Delta\rho_{max}$, $\Delta\rho_{min}$ / e·Å^{-3}	1,093, −0,870

Tabelle 60. Atomkoordinaten und äquivalente isotrope Auslenkungsparameter, U_{iso}, der Verbindung $ClOF_2[BF_4]$ bei 100 K.

Atom	Position	*x*	*y*	*z*	U_{iso} / Å^2
B(1)	4*c*	0,51587(19)	3/4	0,3332(2)	0,0114(3)
Cl(1)	4*c*	0,26167(4)	3/4	0,60668(5)	0,01986(13)
O/F(1)	8*d*	0,18440(9)	0,53743(16)	0,54836(10)	0,0188(2)
F(2)	4*c*	0,21316(12)	3/4	0,77213(12)	0,0160(2)
F(3)	8*d*	0,56338(8)	0,54452(14)	0,25864(9)	0,01697(17)
F(4)	4*c*	0,36736(11)	3/4	0,33855(13)	0,0155(2)
F(5)	4*c*	0,56644(13)	3/4	0,48078(13)	0,0201(2)

Tabelle 61. Anisotrope Auslenkungsparameter, U_{ij}, der Verbindung $ClOF_2[BF_4]$ bei 100 K.

Atom	U_{11} / Å^2	U_{22} / Å^2	U_{33} / Å^2	U_{23} / Å^2	U_{13} / Å^2	U_{12} / Å^2
B(1)	0,00894(17)	0,0375(3)	0,01310(18)	0	0,00168(12)	0
Cl(1)	0,0102(6)	0,0119(7)	0,0122(6)	0	−0,0003(5)	0
O/F(1)	0,0190(4)	0,0186(4)	0,0188(4)	−0,0045(3)	0,0018(3)	−0,0055(3)
F(2)	0,0167(5)	0,0195(5)	0,0119(4)	0	0,0038(4)	0
F(3)	0,0166(3)	0,0150(3)	0,0193(3)	−0,0040(3)	0,0024(3)	0,0024(3)
F(4)	0,0101(4)	0,0169(5)	0,0195(5)	0	0,0025(4)	0
F(5)	0,0218(5)	0,0248(6)	0,0137(4)	0	−0,0042(4)	0

8.1.1.10. $ClOF_2[Mo_3O_3F_{13}]$

Tabelle 62. Ausgewählte Daten und Details der Strukturbestimmung von $ClOF_2[Mo_3O_3F_{13}]$.

Diffraktometer	IPDS 2T
Formel	$Mo_3Cl_1O_4F_{15}$
molare Masse / g·mol^{-1}	672,27
Raumgruppe (Nr.)	$P\bar{1}$ (2)
a / Å	8,6464(4)
b / Å	8,6704(4)
c / Å	9,9748(4)
α / °	66,074(3)
β / °	81,794(3)
γ / °	87,833(3)
V / Å^3	676,37(5)
Z	2
Pearsonsymbol	$aP46$
$\rho_{calc.}$ / g·cm^{-3}	3,301
μ / mm^{-1}	3,129
Farbe	farblos
Kristallmorphologie	Block
Kristallgröße / mm^3	0,10×0,11×0,37
T / K	100
λ / Å	0,71073 (Mo-K$_\alpha$)
Anzahl der Reflexe	19132
θ-Bereich / °	3,043 - 34,072
Bereich der Miller-Indizes	$-13 \leq h \leq 13$
	$-13 \leq k \leq 13$
	$-15 \leq l \leq 14$
Absorptionskorrektur	Integration
$Trans._{max}$, $Trans._{min}$	0,7366, 0,3942
R_{int}, R_σ	0,0197, 0,0164
Vollständigkeit des Datensatzes	0,997
Anzahl der einzigartigen Reflexe	5536
Anzahl der Parameter	209
Anzahl der Restraints	0
Anzahl der Constraints	0
S (alle Daten)	1,090
$R(F)$ ($I \geq 2\sigma(I)$, alle Daten)	0,0215, 0,0279
$wR(F^2)$ ($I \geq 2\sigma(I)$, alle Daten)	0,0542, 0,0566
Extinktionskoeffizient	0,0035(3)
$\Delta\rho_{max}$, $\Delta\rho_{min}$ / e·Å^{-3}	0,822, −1,009

Tabelle 63. Atomkoordinaten und äquivalente isotrope Auslenkungsparameter, U_{iso}, der Verbindung $ClOF_2[Mo_3O_3F_{13}]$ bei 100 K.

Atom	Position	*x*	*y*	*z*	U_{iso} / Å^2
Mo(1)	2*i*	0,67382(2)	0,82389(2)	0,38178(2)	0,00953(4)
Mo(2)	2*i*	0,69858(2)	0,71630(2)	0,83001(2)	0,00996(4)
Mo(3)	2*i*	0,81999(2)	0,22133(2)	0,89850(2)	0,01014(4)
Cl(1)	2*i*	0,81562(5)	0,31630(6)	0,43806(6)	0,01751(9)
O(1)	2*i*	0,78591(17)	0,36714(19)	0,28531(15)	0,0137(2)
O(2)	2*i*	0,64916(18)	0,8661(2)	0,20935(17)	0,0179(3)
O(3)	2*i*	0,70219(18)	0,6669(2)	1,00872(16)	0,0176(3)
O(4)	2*i*	0,86090(18)	0,02244(18)	0,93343(18)	0,0170(3)
F(1)	2*i*	0,85707(16)	0,13386(16)	0,49387(16)	0,0209(3)
F(2)	2*i*	0,98032(13)	0,39621(15)	0,41629(14)	0,0159(2)
F(3)	2*i*	0,72825(16)	0,59703(16)	0,43389(15)	0,0187(2)
F(4)	2*i*	0,62555(14)	1,03135(15)	0,38287(14)	0,0154(2)
F(5)	2*i*	0,88408(14)	0,87729(17)	0,34890(15)	0,0175(2)
F(6)	2*i*	0,47038(14)	0,74453(16)	0,47075(15)	0,0176(2)
F(7)	2*i*	0,70494(15)	0,76342(16)	0,60512(13)	0,0178(2)
F(8)	2*i*	0,90719(14)	0,77734(17)	0,76509(15)	0,0185(2)
F(9)	2*i*	0,64169(16)	0,93553(16)	0,77435(16)	0,0189(2)
F(10)	2*i*	0,50129(14)	0,63787(17)	0,84257(14)	0,0183(2)
F(11)	2*i*	0,76703(15)	0,49397(15)	0,84200(15)	0,0192(2)
F(12)	2*i*	0,81440(17)	0,21766(18)	1,08399(14)	0,0210(3)
F(13)	2*i*	0,81367(16)	0,29794(17)	0,69436(14)	0,0191(2)
F(14)	2*i*	0,60614(14)	0,20889(18)	0,92485(16)	0,0212(3)
F(15)	2*i*	1,02010(14)	0,31328(16)	0,84895(15)	0,0193(2)

Tabelle 64. Anisotrope Auslenkungsparameter, U_{ij}, der Verbindung $ClOF_2[Mo_3O_3F_{13}]$ bei 100 K.

Atom	U_{11} / Å^2	U_{22} / Å^2	U_{33} / Å^2	U_{23} / Å^2	U_{13} / Å^2	U_{12} / Å^2
Mo(1)	0,00896(6)	0,00972(6)	0,00994(7)	−0,00418(5)	−0,00086(5)	0,00034(4)
Mo(2)	0,00974(6)	0,01016(6)	0,01080(7)	−0,00512(5)	−0,00148(5)	0,00072(4)
Mo(3)	0,01076(6)	0,00989(6)	0,00988(7)	−0,00400(5)	−0,00194(5)	0,00083(5)
Cl(1)	0,01216(17)	0,0231(2)	0,0231(2)	−0,01668(18)	0,00239(15)	−0,00269(15)
O(1)	0,0166(6)	0,0178(6)	0,0086(5)	−0,0067(5)	−0,0032(5)	−0,0002(5)
O(2)	0,0205(7)	0,0209(7)	0,0138(6)	−0,0082(5)	−0,0033(5)	0,0004(5)
O(3)	0,0194(7)	0,0218(7)	0,0127(6)	−0,0082(5)	−0,0019(5)	−0,0003(5)
O(4)	0,0192(6)	0,0124(6)	0,0201(7)	−0,0068(5)	−0,0048(5)	0,0017(5)
F(1)	0,0234(6)	0,0140(5)	0,0256(7)	−0,0081(5)	−0,0049(5)	0,0016(4)
F(2)	0,0114(5)	0,0170(5)	0,0199(6)	−0,0086(5)	0,0002(4)	−0,0038(4)
F(3)	0,0223(6)	0,0120(5)	0,0215(6)	−0,0074(5)	−0,0014(5)	0,0040(4)
F(4)	0,0161(5)	0,0115(5)	0,0197(6)	−0,0075(4)	−0,0021(4)	0,0015(4)
F(5)	0,0102(5)	0,0216(6)	0,0200(6)	−0,0081(5)	−0,0004(4)	−0,0011(4)
F(6)	0,0109(5)	0,0187(5)	0,0223(6)	−0,0085(5)	0,0023(4)	−0,0029(4)
F(7)	0,0216(6)	0,0206(6)	0,0118(5)	−0,0067(4)	−0,0037(4)	0,0013(4)
F(8)	0,0114(5)	0,0239(6)	0,0227(6)	−0,0125(5)	0,0000(4)	−0,0021(4)
F(9)	0,0215(6)	0,0134(5)	0,0242(6)	−0,0092(5)	−0,0060(5)	0,0042(4)
F(10)	0,0126(5)	0,0225(6)	0,0192(6)	−0,0077(5)	−0,0020(4)	−0,0038(4)
F(11)	0,0253(6)	0,0120(5)	0,0218(6)	−0,0081(5)	−0,0055(5)	0,0053(4)
F(12)	0,0294(7)	0,0227(6)	0,0126(5)	−0,0084(5)	−0,0043(5)	0,0007(5)
F(13)	0,0265(6)	0,0198(6)	0,0117(5)	−0,0069(4)	−0,0047(4)	0,0051(5)
F(14)	0,0124(5)	0,0249(6)	0,0279(7)	−0,0126(5)	−0,0014(5)	0,0001(4)
F(15)	0,0129(5)	0,0176(5)	0,0248(6)	−0,0060(5)	−0,0022(4)	−0,0015(4)

8.1.1.11. $(ClOF_2[OsO_3F_3])_2OsF_6$

Der gemessene Kristall war ein nicht-meroedrischer Zwilling mit zwei Komponenten.

Tabelle 65. Ausgewählte Daten und Details der Strukturbestimmung von $(ClOF_2[OsO_3F_3])_2OsF_6$.

Diffraktometer	D8 Quest
Formel	$Os_3Cl_2O_4F_{16}$
molare Masse / g·mol^{-1}	1073,50
Raumgruppe (Nr.)	$P\bar{1}$ (2)
a / Å	5,6262(4)
b / Å	7,4973(5)
c / Å	10,2444(6)
α / °	106,076(2)
β / °	97,064(2)
γ / °	96,846(2)
V / Å^3	406,72(5)
Z	1
Pearsonsymbol	$aP29$
$\rho_{calc.}$ / g·cm^{-3}	4,383
μ / mm^{-1}	23,909
Farbe	orange
Kristallmorphologie	Block
Kristallgröße / mm^3	0,05×0,07×0,18
T / K	100
λ / Å	0,71073 (Mo-K$_\alpha$)
Anzahl der Reflexe	90049
θ-Bereich / °	2,865 - 36,474
Bereich der Miller-Indizes	$-9 \leq h \leq 9$
	$-12 \leq k \leq 12$
	$-16 \leq l \leq 17$
Absorptionskorrektur	Multi-scan
$Trans._{max}$, $Trans._{min}$	0,274, 0,087
R_{int}, R_σ	0,0228, 0,0271
Vollständigkeit des Datensatzes	0,997
Anzahl der einzigartigen Reflexe	3990
Anzahl der Parameter	133
Anzahl der Restraints	0
Anzahl der Constraints	0
S (alle Daten)	1,063
$R(F)$ ($I \geq 2\sigma(I)$, alle Daten)	0,0252, 0,0325
$wR(F^2)$ ($I \geq 2\sigma(I)$, alle Daten)	0,0514, 0,0535
Extinktionskoeffizient	-
$\Delta\rho_{max}$, $\Delta\rho_{min}$ / e·Å^{-3}	3,809, −2,569

Tabelle 66. Atomkoordinaten und äquivalente isotrope Auslenkungsparameter, U_{iso}, der Verbindung $(ClOF_2[OsO_3F_3])_2OsF_6$ bei 100 K.

Atom	Position	*x*	*y*	*z*	U_{iso} / Å^2
Os(1)	2*i*	0,60779(2)	0,57027(2)	0,22531(2)	0,01357(3)
Os(2)	1*a*	0	0	0	0,01868(4)
Cl(1)	2*i*	0,2128(2)	0,7346(1)	0,5166(1)	0,0219(2)
O(1)	2*i*	0,4518(4)	0,8107(3)	0,6041(3)	0,0153(4)
O(2)	2*i*	0,5568(5)	0,3289(3)	0,1519(3)	0,0184(5)
O(3)	2*i*	0,3863(5)	0,6320(4)	0,1230(3)	0,0208(5)
O(4)	2*i*	0,8597(5)	0,6295(4)	0,1564(3)	0,0181(5)
F(1)	2*i*	0,1853(4)	0,8539(3)	0,4208(2)	0,0210(4)
F(2)	2*i*	0,0414(4)	0,8224(3)	0,6187(2)	0,0209(4)
F(3)	2*i*	0,3763(4)	0,5297(3)	0,3487(2)	0,0189(4)
F(4)	2*i*	0,6659(4)	0,8156(3)	0,3580(2)	0,0196(4)
F(5)	2*i*	0,8334(4)	0,5248(3)	0,3782(2)	0,0171(4)
F(6)	2*i*	0,1943(4)	−0,0080(3)	0,1554(2)	0,0229(4)
F(7)	2*i*	0,0199(4)	0,2495(3)	0,0735(3)	0,0245(5)
F(8)	2*i*	0,2650(4)	0,0376(3)	−0,0798(3)	0,0234(5)

Tabelle 67. Anisotrope Auslenkungsparameter, U_{ij}, der Verbindung $(ClOF_2[OsO_3F_3])_2OsF_6$ bei 100 K.

Atom	U_{11} / Å^2	U_{22} / Å^2	U_{33} / Å^2	U_{23} / Å^2	U_{13} / Å^2	U_{12} / Å^2
Os(1)	0,01301(5)	0,01160(5)	0,01567(6)	0,00411(4)	0,00148(4)	0,00104(4)
Os(2)	0,01841(8)	0,02214(9)	0,01371(8)	0,00380(6)	0,00183(6)	0,00075(6)
Cl(1)	0,0271(4)	0,0117(3)	0,0246(4)	0,0015(3)	0,0083(3)	−0,0011(3)
O(1)	0,0156(10)	0,0135(9)	0,0145(10)	0,0050(8)	−0,0033(8)	−0,0026(8)
O(2)	0,0191(11)	0,0132(10)	0,0210(12)	0,0030(9)	0,0043(9)	−0,0005(8)
O(3)	0,0174(11)	0,0250(12)	0,0221(13)	0,0108(10)	0,0000(9)	0,0056(9)
O(4)	0,0162(11)	0,0178(11)	0,0225(12)	0,0088(9)	0,0069(9)	0,0008(8)
F(1)	0,0224(10)	0,0189(10)	0,0237(11)	0,0109(8)	0,0011(8)	0,0023(8)
F(2)	0,0226(10)	0,0194(10)	0,0214(11)	0,0043(8)	0,0078(8)	0,0058(8)
F(3)	0,0192(10)	0,0169(9)	0,0230(10)	0,0065(8)	0,0109(8)	0,0032(7)
F(4)	0,0217(10)	0,0127(8)	0,0208(10)	0,0000(7)	0,0051(8)	−0,0009(7)
F(5)	0,0160(9)	0,0173(9)	0,0179(9)	0,0083(7)	−0,0011(7)	−0,0008(7)
F(6)	0,0219(11)	0,0234(10)	0,0219(11)	0,0077(9)	−0,0031(9)	0,0028(8)
F(7)	0,0242(11)	0,0177(10)	0,0301(13)	0,0044(9)	0,0058(9)	0,0022(8)
F(8)	0,0199(10)	0,0202(10)	0,0316(13)	0,0087(9)	0,0091(9)	0,0019(8)

8.1.1.12. $(ClOF_2)_2[AuF_4][SbF_6]$

Tabelle 68. Ausgewählte Daten und Details der Strukturbestimmung von $(ClOF_2)_2[AuF_4][SbF_6]$.

Diffraktometer	D8 Quest
Formel	$Au_1Sb_1Cl_2O_2F_{14}$
molare Masse / g·mol^{-1}	687,62
Raumgruppe (Nr.)	$P2_1/c$ (14)
a / Å	5,8201(3)
b / Å	9,2247(5)
c / Å	11,5058(6)
β / °	103,299(2)
V / Å^3	601,17(6)
Z	2
Pearsonsymbol	$mP40$
$\rho_{calc.}$ / g·cm^{-3}	3,799
μ / mm^{-1}	15,058
Farbe	gelb
Kristallmorphologie	Block
Kristallgröße / mm^3	0,06×0,08×0,10
T / K	100
λ / Å	0,71073 (Mo-K$_\alpha$)
Anzahl der Reflexe	35179
θ-Bereich / °	2,861 - 33,825
Bereich der Miller-Indizes	$-9 \leq h \leq 9$
	$-14 \leq k \leq 14$
	$-18 \leq l \leq 17$
Absorptionskorrektur	Multi-scan
$Trans._{max}$, $Trans._{min}$	0,341, 0,220
R_{int}, R_σ	0,0273, 0,0113
Vollständigkeit des Datensatzes	0,999
Anzahl der einzigartigen Reflexe	2409
Anzahl der Parameter	94
Anzahl der Restraints	0
Anzahl der Constraints	0
S (alle Daten)	1,124
$R(F)$ ($I \geq 2\sigma(I)$, alle Daten)	0,0215, 0,0271
$wR(F^2)$ ($I \geq 2\sigma(I)$, alle Daten)	0,0529, 0,0552
Extinktionskoeffizient	-
$\Delta\rho_{max}$, $\Delta\rho_{min}$ / e·Å^{-3}	2,373, −1,238

Tabelle 69. Atomkoordinaten und äquivalente isotrope Auslenkungsparameter, U_{iso}, der Verbindung $(ClOF_2)_2[AuF_4][SbF_6]$ bei 100 K.

Atom	Position	*x*	*y*	*z*	U_{iso} / Å^2
Au(1)	2*c*	0	1/2	0	0,01186(5)
Sb(1)	2*a*	1	1/2	1/2	0,00995(5)
Cl(1)	4*e*	0,58136(13)	0,67315(8)	0,18507(7)	0,02017(13)
O(1)	4*e*	0,5209(5)	0,7378(3)	0,0689(2)	0,0241(5)
F(1)	4*e*	0,4266(5)	0,7523(2)	0,2577(2)	0,0267(5)
F(2)	4*e*	0,8170(4)	0,75232(19)	0,2438(2)	0,0240(4)
F(3)	4*e*	0,2799(4)	0,50215(19)	0,1262(2)	0,0235(4)
F(4)	4*e*	0,1894(4)	0,50674(19)	−0,1155(2)	0,0229(4)
F(5)	4*e*	0,7187(4)	0,5241(2)	0,3814(2)	0,0271(5)
F(6)	4*e*	0,8225(4)	0,4622(3)	0,6121(2)	0,0266(4)
F(7)	4*e*	1,0007(4)	0,6987(2)	0,5351(2)	0,0262(4)

Tabelle 70. Anisotrope Auslenkungsparameter, U_{ij}, der Verbindung $(ClOF_2)_2[AuF_4][SbF_6]$ bei 100 K.

Atom	U_{11} / Å^2	U_{22} / Å^2	U_{33} / Å^2	U_{23} / Å^2	U_{13} / Å^2	U_{12} / Å^2
Au(1)	0,01156(7)	0,00893(7)	0,01494(7)	−0,00077(5)	0,00274(4)	0,00005(5)
Sb(1)	0,01109(10)	0,00577(10)	0,01314(10)	−0,00026(8)	0,00310(8)	−0,00042(7)
Cl(1)	0,0176(3)	0,0171(3)	0,0244(3)	0,0011(3)	0,0019(2)	0,0014(2)
O(1)	0,0244(12)	0,0255(12)	0,0222(11)	0,0068(9)	0,0049(9)	0,0023(9)
F(1)	0,0307(11)	0,0211(11)	0,0320(12)	−0,0012(7)	0,0151(9)	0,0075(7)
F(2)	0,0235(10)	0,0213(10)	0,0263(10)	0,0002(7)	0,0040(8)	−0,0075(7)
F(3)	0,0183(9)	0,0221(10)	0,0248(10)	0,0051(7)	−0,0057(7)	−0,0042(7)
F(4)	0,0265(10)	0,0205(10)	0,0269(10)	0,0009(7)	0,0165(8)	0,0015(7)
F(5)	0,0188(9)	0,0301(11)	0,0288(11)	0,0072(8)	−0,0023(8)	−0,0028(8)
F(6)	0,0280(10)	0,0280(10)	0,0286(11)	0,0038(9)	0,0167(9)	−0,0008(9)
F(7)	0,0322(11)	0,0091(8)	0,0384(11)	−0,0041(8)	0,0108(8)	−0,0005(7)

8.1.2. Verbindungen aus Abschnitt 5.3

8.1.2.1. NH_4PuF_5

Die N−H-Bindungslängen wurden mit dem Befehl DFIX auf 0,87(1) Å und die äquivalenten isotropen Auslenkungsparameter der H-Atome auf den 1,2-fachen Wert des N(1)-Atoms festgesetzt.

Tabelle 71. Ausgewählte Daten und Details der Strukturbestimmung von NH_4PuF_5.

Diffraktometer	D8 Venture
Formel	$Pu_1N_1F_5H_4$
molare Masse / g·mol^{-1}	355,04
Raumgruppe (Nr.)	$P2_1/c$ (14)
a / Å	7,6965(5)
b / Å	7,0413(5)
c / Å	8,6402(6)
β / °	115,982(2)
V / Å^3	420,92(5
Z	4
Pearsonsymbol	mP28 (ohne H-Atome)
$\rho_{calc.}$ / g·cm^{-3}	5,603
μ / mm^{-1}	15,661
Farbe	orange
Kristallmorphologie	Block
Kristallgröße / mm^3	0,08×0,10×0,11
T / K	100
λ / Å	0,71073 (Mo-K$_\alpha$)
Anzahl der Reflexe	40148
θ-Bereich / °	3,906 - 40,249
Bereich der Miller-Indizes	$-13 \leq h \leq 13$
	$-12 \leq k \leq 12$
	$-15 \leq l \leq 15$
Absorptionskorrektur	Multi-scan
$Trans._{max}$, $Trans._{min}$	0,283, 0,176
R_{int}, R_σ	0,0618, 0,0222
Vollständigkeit des Datensatzes	1,000
Anzahl der einzigartigen Reflexe	2638
Anzahl der Parameter	77
Anzahl der Restraints	4
Anzahl der Constraints	0
S (alle Daten)	1,204
$R(F)$ ($I \geq 2\sigma(I)$, alle Daten)	0,0170, 0,0184
$wR(F^2)$ ($I \geq 2\sigma(I)$, alle Daten)	0,0401, 0,0406
Extinktionskoeffizient	0,0138(3)
$\Delta\rho_{max}$, $\Delta\rho_{min}$ / e·Å^{-3}	1,629, −1,509

Tabelle 72. Atomkoordinaten und äquivalente isotrope Auslenkungsparameter, U_{iso}, der Verbindung NH_4PuF_5 bei 100 K.

Atom	Position	*x*	*y*	*z*	U_{iso} / Å^2
Pu(1)	4*e*	0,57552(2)	0,34752(2)	0,35449(2)	0,00308(3)
N(1)	4*e*	0,0390(3)	0,0711(4)	0,3224(3)	0,0104(3)
H(1)	4*e*	0,086(7)	0,123(6)	0,258(5)	0,012
H(2)	4*e*	0,027(8)	0,172(4)	0,376(6)	0,012
H(3)	4*e*	−0,062(4)	0,000(6)	0,275(6)	0,012
H(4)	4*e*	0,130(5)	0,003(6)	0,399(5)	0,012
F(1)	4*e*	0,3282(2)	0,1392(2)	0,2176(2)	0,0073(2)
F(2)	4*e*	0,3308(2)	0,4290(2)	0,4285(2)	0,0071(2)
F(3)	4*e*	0,3382(2)	0,5260(2)	0,14438(19)	0,0069(2)
F(4)	4*e*	0,6262(2)	0,2969(2)	0,1149(2)	0,0078(2)
F(5)	4*e*	0,8879(2)	0,3217(2)	0,4749(2)	0,0093(3)

Tabelle 73. Anisotrope Auslenkungsparameter, U_{ij}, der Verbindung NH_4PuF_5 bei 100 K.

Atom	U_{11} / Å^2	U_{22} / Å^2	U_{33} / Å^2	U_{23} / Å^2	U_{13} / Å^2	U_{12} / Å^2
Pu(1)	0,00334(4)	0,00322(4)	0,00291(4)	−0,00006(2)	0,00158(3)	0,00011(2)
N(1)	0,0079(7)	0,0137(9)	0,0093(8)	0,0019(7)	0,0036(6)	0,0018(7)
F(1)	0,0062(6)	0,0073(6)	0,0088(6)	−0,0013(5)	0,0038(5)	−0,0008(4)
F(2)	0,0073(5)	0,0071(6)	0,0076(6)	−0,0015(4)	0,0039(5)	0,0001(4)
F(3)	0,0076(6)	0,0055(5)	0,0063(5)	0,0001(4)	0,0019(5)	−0,0008(4)
F(4)	0,0109(6)	0,0068(6)	0,0070(6)	−0,0012(5)	0,0052(5)	−0,0006(5)
F(5)	0,0049(6)	0,0110(6)	0,0098(6)	−0,0022(5)	0,0013(5)	−0,0001(5)

8.1.2.2. $TlNpF_5$

Tabelle 74. Ausgewählte Daten und Details der Strukturbestimmung von $TlNpF_5$.

Diffraktometer	D8 Venture
Formel	$Np_1Tl_1F_5$
molare Masse / $g \cdot mol^{-1}$	536,37
Raumgruppe (Nr.)	$P2_1/c$ (14)
a / Å	8,0218(4)
b / Å	7,0653(3)
c / Å	8,7431(4)
β / °	117,1510(10)
V / $Å^3$	440,92(4)
Z	4
Pearsonsymbol	$mP44$
$\rho_{calc.}$ / $g \cdot cm^{-3}$	4,813
μ / mm^{-1}	31,367
Farbe	olivgrün
Kristallmorphologie	Block
Kristallgröße / mm^3	0,04×0,05×0,08
T / K	293
λ / Å	0,71073 (Mo-K_α)
Anzahl der Reflexe	23048
θ-Bereich / °	2,854 - 34,971
Bereich der Miller-Indizes	$-12 \leq h \leq 12$
	$-11 \leq k \leq 11$
	$-14 \leq l \leq 14$
Absorptionskorrektur	Multi-scan
$Trans._{max}$, $Trans._{min}$	0,147, 0,069
R_{int}, R_σ	0,0403, 0,0175
Vollständigkeit des Datensatzes	0,999
Anzahl der einzigartigen Reflexe	1936
Anzahl der Parameter	65
Anzahl der Restraints	0
Anzahl der Constraints	0
S (alle Daten)	1,146
$R(F)$ ($I \geq 2\sigma(I)$, alle Daten)	0,0179, 0,0195
$wR(F^2)$ ($I \geq 2\sigma(I)$, alle Daten)	0,0367, 0,0373
Extinktionskoeffizient	0,00551(15)
$\Delta\rho_{max}$, $\Delta\rho_{min}$ / $e \cdot Å^{-3}$	2,456, −3,392

Tabelle 75. Atomkoordinaten und äquivalente isotrope Auslenkungsparameter, U_{iso}, der Verbindung $TlNpF_5$ bei 293 K.

Atom	Position	*x*	*y*	*z*	U_{iso} / Å^2
Np(1)	4*e*	0,92079(2)	0,65431(2)	0,64082(2)	0,00891(4)
Tl(1)	4*e*	0,42560(3)	0,88306(3)	0,65817(2)	0,02972(6)
F(1)	4*e*	0,8460(3)	0,9764(3)	0,6439(3)	0,0163(4)
F(2)	4*e*	0,8371(3)	0,4243(3)	0,4276(3)	0,0161(4)
F(3)	4*e*	0,8298(3)	0,3589(3)	0,7147(3)	0,0154(4)
F(4)	4*e*	0,8719(4)	0,7016(3)	0,8794(3)	0,0193(4)
F(5)	4*e*	0,6189(3)	0,6766(4)	0,5133(3)	0,0231(5)

Tabelle 76. Anisotrope Auslenkungsparameter, U_{ij}, der Verbindung $TlNpF_5$ bei 293 K.

Atom	U_{11} / Å^2	U_{22} / Å^2	U_{33} / Å^2	U_{23} / Å^2	U_{13} / Å^2	U_{12} / Å^2
Np(1)	0,01104(6)	0,00836(6)	0,00783(6)	−0,00027(3)	0,00473(4)	0,00015(4)
Tl(1)	0,02383(9)	0,03957(11)	0,02640(9)	0,00883(7)	0,01201(7)	0,00623(7)
F(1)	0,0169(10)	0,0138(9)	0,0146(9)	−0,0017(7)	0,0039(8)	0,0021(8)
F(2)	0,0170(10)	0,0167(9)	0,0164(9)	−0,0053(8)	0,0091(8)	−0,0026(8)
F(3)	0,0146(9)	0,0140(9)	0,0181(10)	0,0024(7)	0,0078(8)	0,0004(7)
F(4)	0,0293(12)	0,0175(10)	0,0150(10)	−0,0024(8)	0,0135(9)	−0,0013(9)
F(5)	0,0137(10)	0,0259(12)	0,0266(12)	−0,0057(10)	0,0064(9)	0,0001(9)

8.1.2.3. $TlPuF_5$

Tabelle 77. Ausgewählte Daten und Details der Strukturbestimmung von $TlPuF_5$.

Diffraktometer	D8 Venture
Formel	$Pu_1Tl_1F_5$
molare Masse / g·mol^{-1}	541,37
Raumgruppe (Nr.)	$P2_1/c$ (14)
a / Å	8,0129(17)
b / Å	7,0041(15)
c / Å	8,676(3)
β / °	116,966(6)
V / Å^3	433,97(19)
Z	4
Pearsonsymbol	$mP44$
$\rho_{calc.}$ / g·cm^{-3}	8,286
μ / mm^{-1}	52,130
Farbe	orange
Kristallmorphologie	Block
Kristallgröße / mm^3	0,04×0,04×0,08
T / K	289
λ / Å	0,71073 (Mo-K_α)
Anzahl der Reflexe	19840
θ-Bereich / °	2,852 - 36,298
Bereich der Miller-Indizes	$-13 \leq h \leq 13$
	$-11 \leq k \leq 11$
	$-14 \leq l \leq 14$
Absorptionskorrektur	Multi-scan
$Trans._{max}$, $Trans._{min}$	0,274, 0,176
R_{int}, R_σ	0,0424, 0,0212
Vollständigkeit des Datensatzes	1,000
Anzahl der einzigartigen Reflexe	2111
Anzahl der Parameter	65
Anzahl der Restraints	0
Anzahl der Constraints	0
S (alle Daten)	1,220
$R(F)$ ($I \geq 2\sigma(I)$, alle Daten)	0,0200, 0,0227
$wR(F^2)$ ($I \geq 2\sigma(I)$, alle Daten)	0,0384, 0,0391
Extinktionskoeffizient	0,00350(12)
$\Delta\rho_{max}$, $\Delta\rho_{min}$ / e·Å^{-3}	3,132, −1,648

Tabelle 78. Atomkoordinaten und äquivalente isotrope Auslenkungsparameter, U_{iso}, der Verbindung $TlPuF_5$ bei 289 K.

Atom	Position	*x*	*y*	*z*	U_{iso} / Å^2
Pu(1)	4*e*	0,92045(2)	0,65368(2)	0,64057(2)	0,00730(4)
Tl(1)	4*e*	0,42404(3)	0,88314(3)	0,65756(3)	0,02795(6)
F(1)	4*e*	0,8471(4)	0,9751(3)	0,6442(3)	0,0149(4)
F(2)	4*e*	0,8385(4)	0,4248(4)	0,4281(3)	0,0149(4)
F(3)	4*e*	0,8313(4)	0,3584(3)	0,7146(3)	0,0143(4)
F(4)	4*e*	0,8735(4)	0,7004(4)	0,8805(3)	0,0180(5)
F(5)	4*e*	0,6208(4)	0,6762(4)	0,5144(4)	0,0220(5)

Tabelle 79. Anisotrope Auslenkungsparameter, U_{ij}, der Verbindung $TlPuF_5$ bei 289 K.

Atom	U_{11} / Å^2	U_{22} / Å^2	U_{33} / Å^2	U_{23} / Å^2	U_{13} / Å^2	U_{12} / Å^2
Pu(1)	0,01039(6)	0,00648(6)	0,00563(6)	−0,00021(4)	0,00414(4)	0,00024(4)
Tl(1)	0,02323(9)	0,03696(12)	0,02432(9)	0,00855(7)	0,01136(7)	0,00592(7)
F(1)	0,0179(12)	0,0113(10)	0,0124(10)	−0,0015(8)	0,0041(9)	0,0013(8)
F(2)	0,0170(11)	0,0159(11)	0,0138(10)	−0,0050(8)	0,0087(9)	−0,0028(9)
F(3)	0,0163(11)	0,0113(9)	0,0168(11)	0,0019(8)	0,0086(9)	−0,0004(8)
F(4)	0,0299(14)	0,0150(10)	0,0148(11)	−0,0024(9)	0,0151(10)	−0,0016(10)
F(5)	0,0137(12)	0,0252(14)	0,0240(13)	−0,0044(11)	0,0059(10)	−0,0001(10)

8.1.2.4. $NaPu_2F_9$

Tabelle 80. Ausgewählte Daten und Details der Strukturbestimmung von $NaPu_2F_9$.

Diffraktometer	D8 Venture
Formel	$Pu_2Na_1F_9$
molare Masse / g·mol^{-1}	677,99
Raumgruppe (Nr.)	*Pnma* (62)
a / Å	8,5121(4)
b / Å	10,9891(5)
c / Å	6,8845(3)
V / Å^3	643,98(5)
Z	4
Pearsonsymbol	*oP*48
$\rho_{calc.}$ / g·cm^{-3}	6,890
μ / mm^{-1}	20,485
Farbe	orange
Kristallmorphologie	Block
Kristallgröße / mm^3	0,06×0,07×0,07
T / K	100
λ / Å	0,71073 (Mo-K_α)
Anzahl der Reflexe	22499
θ-Bereich / °	3,492 - 36,407
Bereich der Miller-Indizes	$-14 \leq h \leq 14$
	$-18 \leq k \leq 18$
	$-11 \leq l \leq 11$
Absorptionskorrektur	Multi-scan
$Trans._{max}$, $Trans._{min}$	0,182, 0,097
R_{int}, R_σ	0,0317, 0,0144
Vollständigkeit des Datensatzes	0,999
Anzahl der einzigartigen Reflexe	1636
Anzahl der Parameter	59
Anzahl der Restraints	0
Anzahl der Constraints	0
S (alle Daten)	1,186
$R(F)$ ($I \geq 2\sigma(I)$, alle Daten)	0,0138, 0,0155
$wR(F^2)$ ($I \geq 2\sigma(I)$, alle Daten)	0,0318, 0,0324
Extinktionskoeffizient	0,00152(8)
$\Delta\rho_{max}$, $\Delta\rho_{min}$ / e·Å^{-3}	2,307, −2,008

Tabelle 81. Atomkoordinaten und äquivalente isotrope Auslenkungsparameter, U_{iso}, der Verbindung $NaNp_2F_9$ bei 100 K.

Atom	Position	*x*	*y*	*z*	U_{iso} / Å^2
Np(1)	8*d*	0,32747(2)	0,45210(2)	0,15923(2)	0,00265(3)
Na(1)	4*c*	0,4603(3)	0,250000	0,6589(3)	0,0250(4)
F(1)	8*d*	0,50066(16)	0,60369(13)	0,0829(2)	0,0095(2)
F(2)	8*d*	0,30140(17)	0,39926(13)	0,4851(2)	0,0093(2)
F(3)	8*d*	0,29386(18)	0,61072(14)	0,3656(2)	0,0097(2)
F(4)	8*d*	0,06923(17)	0,41427(15)	0,2090(2)	0,0103(2)
F(5)	4*c*	0,3274(2)	0,250000	0,1687(3)	0,0090(4)

Tabelle 82. Anisotrope Auslenkungsparameter, U_{ij}, der Verbindung $NaNp_2F_9$ bei 100 K.

Atom	U_{11} / Å^2	U_{22} / Å^2	U_{33} / Å^2	U_{23} / Å^2	U_{13} / Å^2	U_{12} / Å^2
Np(1)	0,00246(4)	0,00277(4)	0,00272(4)	−0,00001(2)	0,00010(2)	−0,00009(2)
Na(1)	0,0401(11)	0,0112(7)	0,0239(9)	0	−0,0160(7)	0
F(1)	0,0101(6)	0,0089(6)	0,0095(6)	−0,0009(5)	0,0015(5)	−0,0012(5)
F(2)	0,0104(6)	0,0084(6)	0,0091(6)	−0,0008(5)	−0,0001(5)	0,0008(5)
F(3)	0,0117(6)	0,0088(6)	0,0086(6)	−0,0003(5)	0,0012(5)	−0,0003(5)
F(4)	0,0073(6)	0,0125(6)	0,0111(6)	0,0003(5)	0,0014(5)	0,0003(5)
F(5)	0,0117(9)	0,0056(8)	0,0097(9)	0	−0,0001(6)	0

8.1.2.5. KPu_2F_9

Tabelle 83. Ausgewählte Daten und Details der Strukturbestimmung von KPu_2F_9.

Diffraktometer	D8 Venture
Formel	$Pu_2K_1F_9$
molare Masse / g·mol^{-1}	694,10
Raumgruppe (Nr.)	*Pnma* (62)
a / Å	8,6013(7)
b / Å	11,3374(9)
c / Å	6,9113(5)
V / Å^3	673,97(9)
Z	4
Pearsonsymbol	*oP*48
$\rho_{calc.}$ / g·cm^{-3}	6,841
μ / mm^{-1}	20,128
Farbe	orange
Kristallmorphologie	Block
Kristallgröße / mm^3	0,05×0,07×0,10
T / K	100
λ / Å	0,71073 (Mo-K_α)
Anzahl der Reflexe	23838
θ-Bereich / °	3,452 - 36,716
Bereich der Miller-Indizes	$-14 \leq h \leq 14$
	$-19 \leq k \leq 18$
	$-11 \leq l \leq 11$
Absorptionskorrektur	Multi-scan
$Trans._{max}$, $Trans._{min}$	0,344, 0,204
R_{int}, R_σ	0,0667, 0,0285
Vollständigkeit des Datensatzes	0,985
Anzahl der einzigartigen Reflexe	1726
Anzahl der Parameter	59
Anzahl der Restraints	0
Anzahl der Constraints	0
S (alle Daten)	1,097
$R(F)$ ($I \geq 2\sigma(I)$, alle Daten)	0,0205, 0,0232
$wR(F^2)$ ($I \geq 2\sigma(I)$, alle Daten)	0,0479, 0,0490
Extinktionskoeffizient	0,00199(12)
$\Delta\rho_{max}$, $\Delta\rho_{min}$ / e·Å^{-3}	3,431, −2,123

Tabelle 84. Atomkoordinaten und äquivalente isotrope Auslenkungsparameter, U_{iso}, der Verbindung KPu_2F_9 bei 100 K.

Atom	Position	*x*	*y*	*z*	U_{iso} / Å^2
Pu(1)	8*d*	0,32627(2)	0,45015(2)	0,15186(2)	0,00220(5)
K(1)	4*c*	0,46824(11)	0,250000	0,63570(13)	0,00775(15)
F(1)	8*d*	0,4944(2)	0,59903(17)	0,0764(3)	0,0063(3)
F(2)	8*d*	0,2907(2)	0,40465(16)	0,4715(3)	0,0062(3)
F(3)	8*d*	0,2819(2)	0,60712(17)	0,3545(2)	0,0061(3)
F(4)	8*d*	0,0648(2)	0,41932(19)	0,1964(3)	0,0074(3)
F(5)	4*c*	0,3252(3)	0,250000	0,1640(4)	0,0090(5)

Tabelle 85. Anisotrope Auslenkungsparameter, U_{ij}, der Verbindung KPu_2F_9 bei 100 K.

Atom	U_{11} / Å^2	U_{22} / Å^2	U_{33} / Å^2	U_{23} / Å^2	U_{13} / Å^2	U_{12} / Å^2
Pu(1)	0,00215(6)	0,00260(6)	0,00187(6)	0,00000(3)	0,00012(3)	−0,00004(3)
K(1)	0,0082(4)	0,0060(4)	0,0091(3)	0	−0,0029(3)	0,000
F(1)	0,0071(7)	0,0063(7)	0,0054(7)	−0,0010(6)	0,0006(6)	−0,0016(6)
F(2)	0,0072(7)	0,0065(8)	0,0050(7)	−0,0003(6)	−0,0005(6)	0,0011(6)
F(3)	0,0082(8)	0,0050(8)	0,0051(7)	−0,0001(5)	0,0008(6)	−0,0008(6)
F(4)	0,0048(7)	0,0108(8)	0,0066(7)	0,0002(7)	0,0007(6)	−0,0003(6)
F(5)	0,0136(14)	0,0065(12)	0,0069(12)	0	−0,0006(9)	0

8.1.3. Verbindungen aus Abschnitt 5.4

8.1.3.1. $Sr[UF_5(HF_2)_2]$

Tabelle 86. Ausgewählte Daten und Details der Strukturbestimmung von $Sr[UF_5(HF_2)_2]$.

Diffraktometer	IPDS2T
Formel	$U_1Sr_1F_9H_2$
molare Masse / $g \cdot mol^{-1}$	498,67
Raumgruppe (Nr.)	$P2_1/c$ (14)
a / Å	5,9752(5)
b / Å	11,1917(9)
c / Å	10,3409(9)
β / °	95,649(7)
V / Å^3	688,17(10)
Z	4
Pearsonsymbol	mP44 (ohne H-Atome)
$\rho_{calc.}$ / $g \cdot cm^{-3}$	4,813
μ / mm^{-1}	31,367
Farbe	hellblau
Kristallmorphologie	Block
Kristallgröße / mm^3	0,24×0,25×0,27
T / K	100
λ / Å	0,71073 (Mo-K_α)
Anzahl der Reflexe	6074
θ-Bereich / °	3,426 - 31,496
Bereich der Miller-Indizes	$-8 \leq h \leq 8$
	$-16 \leq k \leq 16$
	$-15 \leq l \leq 14$
Absorptionskorrektur	Integration
$Trans._{max}$, $Trans._{min}$	0,0896, 0,0166
R_{int}, R_σ	0,0510, 0,0406
Vollständigkeit des Datensatzes	0,999
Anzahl der einzigartigen Reflexe	2290
Anzahl der Parameter	101
Anzahl der Restraints	0
Anzahl der Constraints	0
S (alle Daten)	1,107
$R(F)$ ($I \geq 2\sigma(I)$, alle Daten)	0,0452, 0,0482
$wR(F^2)$ ($I \geq 2\sigma(I)$, alle Daten)	0,1238, 0,1273
Extinktionskoeffizient	0,0016(4)
$\Delta\rho_{max}$, $\Delta\rho_{min}$ / $e \cdot Å^{-3}$	4,949, −2,675

Tabelle 87. Atomkoordinaten und äquivalente isotrope Auslenkungsparameter, U_{iso}, der Verbindung $Sr[UF_5(HF_2)_2]$ bei 100 K.

Atom	Position	*x*	*y*	*z*	U_{iso} / Å^2
U(1)	4*e*	0,68515(4)	0,76026(3)	0,48206(2)	0,00773(14)
Sr(1)	4*e*	1,20470(11)	0,92417(6)	0,76769(6)	0,00853(17)
F(1)	4*e*	0,5824(8)	0,5784(4)	0,3877(5)	0,0129(9)
F(2)	4*e*	0,7935(11)	0,4100(5)	0,4783(5)	0,0213(11)
F(3)	4*e*	0,3695(8)	0,7729(4)	0,3543(5)	0,0101(8)
F(4)	4*e*	0,1501(9)	0,9589(5)	0,3012(6)	0,0188(10)
F(5)	4*e*	0,4835(8)	0,8318(5)	0,6145(5)	0,0139(9)
F(6)	4*e*	0,6941(8)	0,9300(4)	0,3980(5)	0,0114(8)
F(7)	4*e*	0,9752(8)	0,8244(5)	0,5881(5)	0,0127(9)
F(8)	4*e*	0,9133(8)	0,7172(5)	0,3500(5)	0,0145(9)
F(9)	4*e*	0,7306(8)	0,6247(4)	0,6244(4)	0,0121(8)

Tabelle 88. Anisotrope Auslenkungsparameter, U_{ij}, der Verbindung $Sr[UF_5(HF_2)_2]$ bei 100 K.

Atom	U_{11} / Å^2	U_{22} / Å^2	U_{33} / Å^2	U_{23} / Å^2	U_{13} / Å^2	U_{12} / Å^2
U(1)	0,00576(19)	0,00774(19)	0,00920(19)	0,00014(7)	−0,00172(11)	0,00011(7)
Sr(1)	0,0068(3)	0,0082(3)	0,0100(3)	0,0001(2)	−0,0023(2)	0,0001(2)
F(1)	0,013(2)	0,009(2)	0,016(2)	0,0001(16)	−0,0031(16)	0,0002(16)
F(2)	0,030(3)	0,021(3)	0,013(2)	−0,001(2)	0,0021(19)	0,014(2)
F(3)	0,007(2)	0,011(2)	0,012(2)	−0,0005(17)	−0,0010(16)	−0,0001(15)
F(4)	0,014(2)	0,014(2)	0,028(3)	0,004(2)	0,002(2)	0,0063(18)
F(5)	0,012(2)	0,012(2)	0,017(2)	−0,0009(17)	0,0003(16)	0,0025(16)
F(6)	0,011(2)	0,010(2)	0,013(2)	0,0021(15)	0,0010(16)	0,0005(16)
F(7)	0,011(2)	0,014(2)	0,012(2)	−0,0032(17)	−0,0032(16)	−0,0014(16)
F(8)	0,008(2)	0,017(2)	0,018(2)	0,0023(19)	0,0012(17)	0,0007(17)
F(9)	0,014(2)	0,011(2)	0,0105(19)	0,0017(16)	−0,0043(15)	0,0010(16)

8.1.3.2. $Ba(HF)_2U_2F_{12}$

Tabelle 89. Ausgewählte Daten und Details der Strukturbestimmung von $Ba(HF)_2U_2F_{12}$.

Diffraktometer	IPDS2T
Formel	$U_2Ba_1F_{14}H_2$
molare Masse / g·mol^{-1}	881,42
Raumgruppe (Nr.)	*Pnma* (62)
a / Å	8,5422(2)
b / Å	12,9933(5)
c / Å	9,5306(3)
V / Å^3	1057,81(6)
Z	4
Pearsonsymbol	*oP*68 (ohne H-Atome)
$\rho_{calc.}$ / g·cm^{-3}	5,535
μ / mm^{-1}	34,400
Farbe	gelb
Kristallmorphologie	Block
Kristallgröße / mm^3	0,08×0,11×0,11
T / K	100
λ / Å	0,71073 (Mo-K_α)
Anzahl der Reflexe	13850
θ-Bereich / °	3,136 - 31,491
Bereich der Miller-Indizes	$-19 \leq h \leq 19$
	$-12 \leq k \leq 12$
	$-13 \leq l \leq 14$
Absorptionskorrektur	Integration
$Trans._{max}$, $Trans._{min}$	0,4305, 0,1143
R_{int}, R_σ	0,0366, 0,0174
Vollständigkeit des Datensatzes	0,999
Anzahl der einzigartigen Reflexe	1828
Anzahl der Parameter	87
Anzahl der Restraints	0
Anzahl der Constraints	0
S (alle Daten)	1,130
$R(F)$ ($I \geq 2\sigma(I)$, alle Daten)	0,0259, 0,0303
$wR(F^2)$ ($I \geq 2\sigma(I)$, alle Daten)	0,0575, 0,0590
Extinktionskoeffizient	0,00027(6)
$\Delta\rho_{max}$, $\Delta\rho_{min}$ / e·Å^{-3}	1,384, −1,709

Tabelle 90. Atomkoordinaten und äquivalente isotrope Auslenkungsparameter, U_{iso}, der Verbindung $Ba(HF)_2U_2F_{12}$ bei 100 K.

Atom	Position	*x*	*y*	*z*	U_{iso} / Å^2
U(1)	8*d*	0,35057(2)	0,47759(2)	0,33953(2)	0,00840(7)
Ba(1)	4*c*	−0,01971(6)	0,250000	0,53384(5)	0,00940(10)
F(1)	8*d*	0,4935(5)	0,4065(3)	0,5166(4)	0,0159(7)
F(2)	8*d*	0,4246(4)	0,3628(3)	0,2083(4)	0,0133(7)
F(3)	8*d*	0,1557(4)	0,4790(3)	0,2028(4)	0,0134(7)
F(4)	8*d*	0,4155(4)	0,5965(3)	0,2071(4)	0,0150(7)
F(5)	8*d*	0,2144(5)	0,3654(3)	0,4350(4)	0,0195(8)
F(6)	8*d*	0,2030(5)	0,5791(3)	0,4407(4)	0,0186(8)
F(7)	4*c*	−0,3282(10)	0,250000	0,4359(11)	0,049(2)
F(8)	4*c*	−0,1432(9)	0,250000	0,8114(8)	0,046(2)

Tabelle 91. Anisotrope Auslenkungsparameter, U_{ij}, der Verbindung $Ba(HF)_2U_2F_{12}$ bei 100 K.

Atom	U_{11} / Å^2	U_{22} / Å^2	U_{33} / Å^2	U_{23} / Å^2	U_{13} / Å^2	U_{12} / Å^2
U(1)	0,00595(10)	0,01164(10)	0,00762(10)	0,00088(7)	−0,00023(6)	0,00001(7)
Sr(1)	0,0116(2)	0,00732(18)	0,00934(19)	0	0,00147(16)	0
F(1)	0,0142(17)	0,0134(15)	0,0202(17)	−0,0003(14)	−0,0071(14)	0,0007(13)
F(2)	0,0099(16)	0,0153(15)	0,0147(15)	−0,0032(13)	0,0000(13)	0,0011(13)
F(3)	0,0077(15)	0,0211(17)	0,0116(15)	−0,0011(14)	−0,0029(12)	0,0029(13)
F(4)	0,0119(16)	0,0179(16)	0,0154(15)	0,0071(14)	0,0004(14)	−0,0013(14)
F(5)	0,0135(17)	0,029(2)	0,0127(16)	−0,0052(15)	−0,0002(14)	0,0055(15)
F(6)	0,0108(16)	0,031(2)	0,0166(17)	0,0116(16)	0,0012(14)	−0,0061(15)
F(7)	0,030(4)	0,029(4)	0,087(7)	0	−0,011(4)	0
F(8)	0,027(4)	0,099(8)	0,013(3)	0	−0,002(3)	0

8.1.3.3. $(N_2H_6)U_2F_{10}(HF_2)_2$

Tabelle 92. Ausgewählte Daten und Details der Strukturbestimmung von $(N_2H_6)U_2F_{10}(HF_2)_2$.

Diffraktometer	D8 Quest
Formel	$U_2N_2F_{14}H_8$
molare Masse / g·mol^{-1}	456,50
Raumgruppe (Nr.)	*C*2/*c* (15)
a / Å	16,1264(8)
b / Å	9,7986(5)
c / Å	8,4047(4)
β / °	118,530(2)
V / Å^3	1166,81(10)
Z	4
Pearsonsymbol	*mS*72 (ohne H-Atome)
$\rho_{calc.}$ / g·cm^{-3}	4,430
μ / mm^{-1}	27,893
Farbe	hellblau
Kristallmorphologie	Block
Kristallgröße / mm^3	0,11×0,13×0,13
T / K	100
λ / Å	0,71073 (Mo-K$_\alpha$)
Anzahl der Reflexe	63897
θ-Bereich / °	2,527 - 39,535
Bereich der Miller-Indizes	$-28 \leq h \leq 28$
	$-17 \leq k \leq 17$
	$-15 \leq l \leq 15$
Absorptionskorrektur	Multi-scan
$Trans._{max}$, $Trans._{min}$	0,279, 0,183
R_{int}, R_σ	0,0411, 0,0142
Vollständigkeit des Datensatzes	0,999
Anzahl der einzigartigen Reflexe	3514
Anzahl der Parameter	99
Anzahl der Restraints	0
Anzahl der Constraints	0
S (alle Daten)	1,109
$R(F)$ ($I \geq 2\sigma(I)$, alle Daten)	0,0124, 0,0149
$wR(F^2)$ ($I \geq 2\sigma(I)$, alle Daten)	0,0219, 0,0223
Extinktionskoeffizient	0,00131(2)
$\Delta\rho_{max}$, $\Delta\rho_{min}$ / e·Å^{-3}	2,352, −1,440

Tabelle 93. Atomkoordinaten und äquivalente isotrope Auslenkungsparameter, U_{iso}, der Verbindung $(N_2H_6)U_2F_{10}(HF_2)_2$ bei 100 K.

Atom	Position	*x*	*y*	*z*	U_{iso} / Å^2
U(1)	8*f*	0,28436(2)	0,58752(2)	0,87933(2)	0,00469(2)
N(1)	8*f*	0,03663(9)	0,69418(14)	0,34345(18)	0,0085(2)
F(1)	8*f*	0,33593(7)	0,77193(9)	1,06502(13)	0,00867(15)
F(2)	8*f*	0,28180(7)	0,45796(10)	0,67012(13)	0,00906(15)
F(3)	8*f*	0,19544(7)	0,69654(10)	0,65559(13)	0,01158(17)
F(4)	8*f*	0,39005(7)	0,45356(10)	1,04121(14)	0,01129(16)
F(5)	8*f*	0,39120(7)	0,67557(10)	0,84628(15)	0,01234(17)
F(6)	8*f*	0,17087(7)	0,46127(10)	0,83100(14)	0,01082(16)
F(7)	8*f*	0,46614(8)	0,90549(11)	1,06535(16)	0,01522(19)
H(1)	8*f*	0,058(2)	0,775(4)	0,375(4)	0,039(9)
H(2)	8*f*	0,079(2)	0,636(3)	0,351(4)	0,024(7)
H(3)	8*f*	0,016(2)	0,664(3)	0,417(4)	0,022(7)
H(4)	8*f*	0,431(2)	0,863(4)	1,078(5)	0,041(9)

Tabelle 94. Anisotrope Auslenkungsparameter, U_{ij}, der Verbindung $(N_2H_6)U_2F_{10}(HF_2)_2$ bei 100 K.

Atom	U_{11} / Å^2	U_{22} / Å^2	U_{33} / Å^2	U_{23} / Å^2	U_{13} / Å^2	U_{12} / Å^2
U(1)	0,00578(2)	0,00492(2)	0,00422(2)	−0,00067(2)	0,00307(2)	−0,00089(2)
N(1)	0,0075(5)	0,0095(5)	0,0084(5)	0,0009(4)	0,0039(4)	0,0012(4)
F(1)	0,0088(4)	0,0085(4)	0,0094(4)	−0,0013(3)	0,0050(3)	−0,0015(3)
F(2)	0,0126(4)	0,0086(4)	0,0074(4)	−0,0016(3)	0,0059(3)	−0,0006(3)
F(3)	0,0145(4)	0,0109(4)	0,0079(4)	0,0020(3)	0,0042(3)	0,0046(3)
F(4)	0,0121(4)	0,0122(4)	0,0094(4)	0,0028(3)	0,0050(3)	0,0034(3)
F(5)	0,0143(4)	0,0125(4)	0,0154(5)	−0,0043(3)	0,0112(4)	−0,0064(3)
F(6)	0,0102(4)	0,0121(4)	0,0120(4)	−0,0025(3)	0,0067(3)	−0,0050(3)
F(7)	0,0170(5)	0,0167(5)	0,0176(5)	−0,0063(4)	0,0128(4)	−0,0086(4)

8.1.4. Verbindungen aus Abschnitt 5.5

8.1.4.1. $Rb[UF_7]$

Tabelle 95. Ausgewählte Daten und Details der Strukturbestimmung von $Rb[UF_7]$.

Diffraktometer	IPDS2
Formel	$U_1Rb_1F_7$
molare Masse / $g \cdot mol^{-1}$	456,50
Raumgruppe (Nr.)	$P2_1/c$ (14)
a / Å	5,0825(10)
b / Å	10,594(2)
c / Å	10,755(2)
β / °	95,15(3)
V / Å^3	576,8(2)
Z	4
Pearsonsymbol	$mP36$
$\rho_{calc.}$ / $g \cdot cm^{-3}$	5,257
μ / mm^{-1}	36,589
Farbe	farblos
Kristallmorphologie	Block
Kristallgröße / mm^3	0,01×0,03×0,08
T / K	100
λ / Å	0,71073 (Mo-K_α)
Anzahl der Reflexe	10037
θ-Bereich / °	2,704 - 33,408
Bereich der Miller-Indizes	$-7 \leq h \leq 7$
	$-16 \leq k \leq 14$
	$-14 \leq l \leq 16$
Absorptionskorrektur	Integration
$Trans._{max}$, $Trans._{min}$	0,5285, 0,1440
R_{int}, R_σ	0,0880, 0,0503
Vollständigkeit des Datensatzes	0,996
Anzahl der einzigartigen Reflexe	2232
Anzahl der Parameter	82
Anzahl der Restraints	0
Anzahl der Constraints	0
S (alle Daten)	1,029
$R(F)$ ($I \geq 2\sigma(I)$, alle Daten)	0,0310, 0,0367
$wR(F^2)$ ($I \geq 2\sigma(I)$, alle Daten)	0,0744, 0,0744
Extinktionskoeffizient	-
$\Delta\rho_{max}$, $\Delta\rho_{min}$ / $e \cdot Å^{-3}$	3,758, −2,718

Tabelle 96. Atomkoordinaten und äquivalente isotrope Auslenkungsparameter, U_{iso}, der Verbindung $Rb[UF_7]$ bei 100 K.

Atom	Position	*x*	*y*	*z*	U_{iso} / Å^2
U(1)	4*e*	0,47678(4)	0,22048(2)	0,47600(2)	0,01157(7)
Rb(1)	4*e*	1,00939(10)	0,49547(4)	0,27748(4)	0,01470(10)
F(1)	4*e*	0,1041(7)	0,2013(3)	0,3862(3)	0,0189(7)
F(2)	4*e*	0,2886(7)	0,1554(3)	0,6206(3)	0,0190(6)
F(3)	4*e*	0,7714(7)	0,3020(4)	0,5883(4)	0,0221(7)
F(4)	4*e*	0,5242(7)	0,1117(3)	0,3199(3)	0,0168(6)
F(5)	4*e*	0,6119(8)	0,3437(3)	0,3517(3)	0,0206(7)
F(6)	4*e*	0,2918(7)	0,3849(3)	0,5205(3)	0,0204(6)
F(7)	4*e*	0,7166(7)	0,0725(3)	0,5373(3)	0,0186(6)

Tabelle 97. Anisotrope Auslenkungsparameter, U_{ij}, der Verbindung $Rb[UF_7]$ bei 100 K.

Atom	U_{11} / Å^2	U_{22} / Å^2	U_{33} / Å^2	U_{23} / Å^2	U_{13} / Å^2	U_{12} / Å^2
U(1)	0,01091(11)	0,01193(9)	0,01187(10)	0,00016(5)	0,00107(6)	−0,00084(6)
Rb(1)	0,0158(2)	0,0139(2)	0,01448(18)	−0,00037(17)	0,00181(14)	−0,00104(16)
F(1)	0,0141(16)	0,0227(15)	0,0193(15)	−0,0044(12)	−0,0027(12)	0,0021(12)
F(2)	0,0212(17)	0,0195(15)	0,0168(14)	0,0047(12)	0,0046(11)	−0,0015(13)
F(3)	0,0154(17)	0,0270(16)	0,0232(16)	−0,0092(14)	−0,0020(12)	−0,0024(13)
F(4)	0,0203(16)	0,0150(13)	0,0153(13)	−0,0019(11)	0,0028(11)	−0,0003(12)
F(5)	0,0274(19)	0,0180(14)	0,0171(14)	0,0014(12)	0,0068(12)	−0,0074(13)
F(6)	0,0202(17)	0,0133(13)	0,0281(16)	−0,0025(13)	0,0049(13)	0,0015(13)
F(7)	0,0144(16)	0,0181(14)	0,0231(15)	0,0035(12)	0,0009(11)	−0,0004(12)

8.2. Basissatzdetails und optimierte Strukturen (CRYSTAL17)

8.2.1. Basissatzdetails für Cr, Pd und Rh

Die Basissätze wurden von Prof. Dr. Antti Karttunen (Aalto-Universität, Espoo, Finnland) von def-TZVP oder def2-TZVP-Basissätzen abgeleitet.[244]

Cr:

The starting point was the molecular Karlsruhe def-TZVP basis set.[244] The diffuse outermost s-exponents were increased from 0.03 and 0.09 to 0.13 and 0.27, respectively. The exponent of the p-type polarization function was changed from 0.12 to 0.13 and the outermost s and p functions were then combined into a single sp-type function. The exponents of the outermost d-functions were increased from 0.16 and 0.54 to 0.25 and 0.62, respectively.

Basis set in CRYSTAL input format:

```
23 12
0 0 8 2.0 1.0
  254477.80704     .23386945693E-03
  38131.797054     .18142601800E-02
  8675.2930607     .94363925721E-02
  2455.0099848     .38343639367E-01
  799.16217787     .12459194837
  286.90021489     .29489696029
  111.25413232     .41846149607
  43.864152636     .21633763420
0 0 4 2.0 1.0
  279.32669173    -.23450908111E-01
  86.274732376    -.11080370027
  13.555756113     .53028965842
  5.6978112751     .51603516947
0 0 2 2.0 1.0
  8.5636582615    -.38109545675
  1.3988296768     1.1991591436
0 0 1 2.0 1.0
 0.57288171116     1.0000000000
0 0 1 0.0 1.0
  0.27            1.0
0 1 1 0.0 1.0
  0.13            1.0 1.0
0 2 6 6.0 1.0
  1306.4398864     .24277326185E-02
  309.25311441     .19544041017E-01
  98.996273963     .90651794553E-01
  36.756916451     .25699279154
  14.566657077     .40935504891
  5.8739937432     .23729388849
0 2 3 6.0 1.0
```

22.890999695 -.28166026613E-01

3.0855001822 .56034120148

1.2132329118 .98119019650

0 2 1 0.0 1.0

0.44931680699 1.0000000000

0 3 4 4.0 1.0

43.720074476 .13622964026E-01

12.391242652 .78935180133E-01

4.2639442006 .23833840000

1.5525221790 .39526851122

0 3 1 0.0 1.0

0.53761929485 1.0

0 3 1 0.0 1.0

0.26 1.0

Pd:

The starting point was the molecular Karlsruhe def2-TZVP basis set.[244] The diffuse outermost s-exponents were increased from 0.04 and 0.10 to 0.13 and 0.26, respectively. The most diffuse p-function with an exponent of 0.04 was removed and the exponents of the outermost p-type polarization functions were changed from 0.11 and 0.41 to 0.13 and 0.27, respectively. The outermost s and p functions were then combined into two sp-type functions. The exponent of the outermost d-function was increased from 0.15 to 0.21 and the f-type polarization function was removed.

Basis set in CRYSTAL input format:

246 10

INPUT

18. 0 2 2 2 2 0

12.430000 240.229040 0

6.170759 35.171943 0

11.080000 170.417276 0

5.829554 28.472133 0

9.510000 69.013845 0

4.139781 11.750862 0

13.270000 -31.929554 0

6.630000 -5.398217 0

0 0 2 2.0 1.0

18.000000000 -0.16605388598

14.662134308 0.34899955055

0 0 1 2.0 1.0

5.6388709265 1.0000000000

0 0 1 0.0 1.0

1.3198953252 1.0000000000

0 0 1 0.0 1.0

0.57817908509 1.0000000000

0 1 1 0.0 1.0

0.29 1.0 1.0

0 1 1 0.0 1.0

0.14 1.0 1.0

0 2 4 6.0 1.0

12.552899300 0.61728998206E-01

7.2444496380 -0.24178626753

1.8905941078 0.49453200915

0.90737168760 0.50454362626

0 3 4 8.0 1.0

22.357457575 0.39559479546E-02

10.682526382 -0.14039011601E-01

2.4858232550 0.24219476776

1.0735333903 0.42580283281

0 3 1 0.0 1.0

0.42613842853 1.0000000000

0 3 1 0.0 1.0

0.21 1.0000000000

Rh:

The starting point was the molecular Karlsruhe def2-TZVP basis set.[244] The diffuse outermost s-exponents were increased from 0.04 and 0.10 to 0.14 and 0.29, respectively. The most diffuse p-function with an exponent of 0.04 was removed and the exponents of the outermost p-type polarization functions were changed from 0.12 and 0.38 to 0.13 and 0.26, respectively. The outermost s and p functions were then combined into two sp-type functions. The exponent of the outermost d-functions were increased from 0.14 and 0.38 to 0.20 and 0.40, respectively. The f-type polarization function was removed.

Basis set in CRYSTAL input format:

245 10

INPUT

17. 0 2 2 2 2 0

11.720000 225.347754 0

5.820000 32.823189 0

10.420000 158.709412 0

5.450000 26.444100 0

8.820000 62.758626 0

3.870000 10.978719 0

12.310000 -30.093456 0

6.160000 -5.218482 0

0 0 2 2.0 1.0

17.000000000 -0.16690803139

13.910581694 0.34235001652

0 0 1 2.0 1.0

5.2481265288 1.0000000000

0 0 1 0.0 1.0

1.2262575928 1.0000000000

0 0 1 0.0 1.0

0.53930216349 1.0000000000

```
0 1 1 0.0 1.0
 0.26              1.0 1.0
0 1 1 0.0 1.0
 0.13              1.0 1.0
0 2 4 6.0 1.0
  11.767103631      0.59494859388E-01
  6.7485133083     -0.23735853477
  1.7502679834      0.49019334303
 0.84321166133      0.50623933751
0 3 4 7.0 1.0
  19.857830136      0.66960778187E-02
  10.061378139     -0.21981738213E-01
  2.2619546477      0.37918706236
 0.97098845035      0.67289976592
0 3 1 0.0 1.0
 0.40              1.0000000000
0 3 1 0.0 1.0
 0.2               1.0000000000
```

8.2.2. Strukturen der Verbindungen aus Abschnitt 4.3

8.2.2.1. $(ClOF_2)_2[CrF_6]$

Aufgrund der symmetriebedingt O/F-mischbesetzten Lage in der Kristallstruktur von $(ClOF)_2[CrF_6]$, wurde ein Modell der Struktur mit vollbesetzten Lagen in der Untergruppe *C*2 (Nr. 5) konstruiert und optimiert.
Ein paramagnetischer Grundzustand wurde als Startwert gesetzt, nach der Optimierung lag ein diamagnetischer Zustand mit einem magnetischen Moment von −0,041 μ_B für das Cr(IV)-Atom und 0,00 μ_B für das $[CrF_6]^{2-}$-Anion vor.
Shrinking-Faktor: 4×4×3
Raumgruppe *C*2(Nr. 5)
a = 9,34004950 Å, *b* = 6,79343168 Å, *c* = 7,19469172 Å, *β* = 114,804653°, *V* = 414,39421600 Å^3

Tabelle 98. Atomkoordinaten der optimierten Struktur von $(ClOF_2)_2[CrF_6]$.

Atom	*x*	*y*	*z*
Cr	−2,775557561563E−17	2,865020296304E−03	−5,000000000000E−01
Cl	−2,872119040352E−01	−1,876175895387E−02	−2,726231891252E−01
F	−1,904445323790E−01	1,842446545814E−01	−1,744956501439E−01
F	−2,775557561563E−17	−2,615472324274E−01	−5,000000000000E−01
F	−2,040184571813E−01	9,090203209945E−03	4,909118835973E−01
F	8,056725906245E−02	1,754253224638E−02	−2,301408594772E−01
F	−3,941885610524E−01	6,775838329743E−03	−1,399458949171E−01
F	−2,775557561563E−17	2,807674084968E−01	−5,000000000000E−01
O	−1,843373185043E−01	−1,756840675965E−01	−1,731141228957E−01

8.2.2.2. $(ClOF_2)_2[RhF_6]$

Aufgrund der symmetriebedingt O/F-mischbesetzten Lage in der Kristallstruktur von $(ClOF)_2[RhF_6]$, wurde ein Modell der Struktur mit vollbesetzten Lagen in der Untergruppe *C*2 (Nr. 5) konstruiert und optimiert.
Ein paramagnetischer Grundzustand wurde als Startwert gesetzt, nach der Optimierung lag ein paramagnetischer Zustand mit einem magnetischen Moment von 0,75 μ_B für das Rh(IV)-Atom und 1,00 μ_B für das $[RhF_6]^{2-}$-Anion vor.
Shrinking-Faktor: 4×4×3
Raumgruppe *C*2(Nr. 5)
a = 9,46786671 Å, *b* = 6,85358524 Å, *c* = 7,27778510 Å, *β* = 114,517349°, *V* = 429,66713535 Å^3

Tabelle 99. Atomkoordinaten der optimierten Struktur von $(ClOF_2)_2[RhF_6]$.

Atom	*x*	*y*	*z*
Rh	−2,775557561563E−17	1,020151409704E−02	−5,000000000000E−01
Cl	−2,865163200118E−01	−1,091419380158E−02	−2,709189927684E−01
F	8,082129101376E−02	1,711789109971E−02	−2,159054932308E−01
F	−2,775557561563E−17	2,940615107664E−01	−5,000000000000E−01
F	2,108554649808E−01	1,457107074241E−02	−4,877115610877E−01
F	−5,551115123126E−17	−2,679403433043E−01	−5,000000000000E−01
F	3,902298866724E−01	1,552245443829E−02	1,371429864556E−01
F	1,899130818045E−01	1,895308530865E−01	1,757137099124E−01
O	1,867030464966E−01	−1,683794163449E−01	1,754409648252E−01

8.2.2.3. $(ClOF_2)_2[GeF_6]$

Aufgrund der symmetriebedingt O/F-mischbesetzten Lage in der Kristallstruktur von $(ClOF)_2[GeF_6]$, wurde ein Modell der Struktur mit vollbesetzten Lagen in der Untergruppe *C*2 (Nr. 5) konstruiert und optimiert.

Shrinking-Faktor: 4×4×3

Raumgruppe *C*2(Nr. 5)

a = 9,21269738 Å, *b* = 6,72255393 Å, *c* = 7,26660841 Å, *β* = 115,685508°, *V* = 405,57168024 Å^3

Tabelle 100. Atomkoordinaten der optimierten Struktur von $(ClOF_2)_2[GeF_6]$.

Atom	*x*	*y*	*z*
Ge	0,000000000000E+00	4,603429996633E−02	−5,000000000000E−01
Cl	−2,868148635880E−01	6,510809023055E−02	−2,671036761345E−01
F	0,000000000000E+00	3,143162528737E−01	−5,000000000000E−01
F	8,213088136837E−02	3,708772548725E−02	−2,324258365211E−01
F	−5,551115123126E−17	−2,326491893548E−01	−5,000000000000E−01
F	−2,018345084047E−01	3,687486199467E−02	4,874718486936E−01
F	−3,985717885121E−01	4,017968320732E−02	−1,429540868223E−01
F	−1,864025495557E−01	−1,379076633736E−01	−1,652961395914E−01
O	−1,822319610048E−01	2,243566207112E−01	−1,685060116691E−01

8.2.2.4. $(ClOF_2)_2[PdF_6]$

Ein diamagnetischer Grundzustand wurde für das System gesetzt.

Shrinking-Faktor: 3×3×4

Raumgruppe *Pnnm* (Nr. 58)

a = 7,52506107 Å, *b* = 9,45224215 Å, *c* = 5,96601984 Å, *V* = 424,355232 Å^3

Tabelle 101. Atomkoordinaten der optimierten Struktur von $(ClOF_2)_2[PdF_6]$.

Atom	*x*	*y*	*z*
Pd	5,000000000000E−01	−5,000000000000E−01	0,000000000000E+00
Cl	−4,528427445780E−01	−2,615341637050E−01	−5,000000000000E−01
F	−4,590183000620E−01	−1,406534605859E−01	−3,037882562843E−01
F	−3,523393810514E−01	−4,154957435751E−01	2,269094568661E−01
F	3,607837994880E−01	−3,303466069686E−01	0,000000000000E+00
O	3,751304805389E−01	−3,214675063942E−01	−5,000000000000E−01

8.2.2.5. $(ClOF_2)_2[PtF_6]$

Ein diamagnetischer Grundzustand wurde für das System gesetzt.

Shrinking-Faktor: 3×3×4

Raumgruppe *Pnnm* (Nr. 58)

a = 7,54888325 Å, *b* = 9,48654534 Å, *c* = 5,99464725 Å, *V* = 424,355232 Å^3

Tabelle 102. Atomkoordinaten der optimierten Struktur von $(ClOF_2)_2[PtF_6]$.

Atom	*x*	*y*	*z*
Pt	−5,000000000000E−01	−5,000000000000E−01	−6,479973123678E−20
Cl	−4,495833521926E−01	−2,612718256078E−01	−5,000000000000E−01
F	−4,559313367158E−01	−1,406854955933E−01	−3,047832681064E−01
F	−3,485045764144E−01	−4,145197137979E−01	2,298955449960E−01
F	3,614184041547E−01	−3,254419355278E−01	−6,479973123678E−20
O	3,788019292960E−01	−3,209935519315E−01	−5,000000000000E−01

8.2.2.6. $(ClOF_2)_2[SnF_6]$

Shrinking-Faktor: 4×4×4

Raumgruppe *Pnnm* (Nr. 58)

a = 7,60717571 Å, *b* = 9,70295915 Å, *c* = 6,13222728 Å, *V* = 452,632666 Å^3

Tabelle 103. Atomkoordinaten der optimierten Struktur von $(ClOF_2)_2[SnF_6]$.

Atom	*x*	*y*	*z*
Sn	−5,000000000000E−01	5,000000000000E−01	0,000000000000E+00
Cl	−4,694324495326E−01	−2,607419648916E−01	5,000000000000E−01
F	−4,867220830841E−01	−1,433849354689E−01	−3,089005846633E−01
F	−3,665092617247E−01	−4,005065761491E−01	2,301985446380E−01
F	3,303429530313E−01	−3,493160956939E−01	0,000000000000E+00
O	3,648488184713E−01	−3,270450353242E−01	5,000000000000E−01

8.2.2.7. $ClOF_2SnF_5$

Shrinking-Faktor: 4×4×3

Raumgruppe *C*2 (Nr. 5)

a = 15,85057481 Å, *b* = 5,05933828 Å, *c* = 7,54578367 Å, *β* = 111,617678°, *V* = 562,55963232 Å^3

Tabelle 104. Atomkoordinaten der optimierten Struktur von $ClOF_2SnF_5$.

Atom	*x*	*y*	*z*
Sn	1,506320638287E−01	−1,971005495097E−01	4,599837299248E−01
Cl	8,946509563488E−02	3,067545569028E−01	−1,915733758284E−01
F	1,067992857272E−01	−4,820530025664E−01	−1,742687497619E−02
F	1,942106051104E−01	2,049801943969E−01	−9,881549961138E−02
F	9,519656209454E−02	1,112656038053E−01	−4,638466459366E−01
F	3,770125203233E−02	−3,955124289911E−01	3,392354873956E−01
F	1,708716076180E−01	−3,435092491314E−01	−2,912633970133E−01
F	1,450772243233E−01	−4,335832346312E−02	2,249530428881E−01
F	2,253271378006E−01	4,941084114568E−01	4,163726612550E−01
O	3,673525841564E−02	1,043747870998E−01	−1,551306136763E−01

8.2.2.8. $ClOF_2PbF_5$

Shrinking-Faktor: 4×4×3

Raumgruppe *C*2 (Nr. 5)

a = 16,33880735 Å, *b* = 5,18135653 Å, *c* = 7,69535099 Å, *β* = 112,812006°, *V* = 600,51028779 Å^3

Tabelle 105. Atomkoordinaten der optimierten Struktur von $ClOF_2PbF_5$.

Atom	*x*	*y*	*z*
Pb	−1,478442335351E−01	−2,450843429393E−01	−4,615423128878E−01
Cl	−8,964421685165E−02	2,459640769779E−01	1,899015251158E−01
O	−3,638984395807E−02	4,393736564368E−01	1,570665506050E−01
F	−1,087717049137E−01	4,093208079329E−02	1,613197024537E−02
F	−1,914342861799E−01	3,531502252059E−01	9,302921274779E−02
F	−2,221855855214E−01	7,133417956215E−02	−4,119658088668E−01
F	−1,392343460382E−01	−4,056647739372E−01	−2,197271471198E−01
F	−9,426651184632E−02	4,373761949273E−01	4,520381865327E−01
F	−1,724753389781E−01	−9,465832173446E−02	2,815333240256E−01
F	−2,971698173852E−02	−4,555297529240E−02	−3,361087316952E−01

8.2.2.9. $ClOF_2[BF_4]$

Aufgrund der symmetriebedingt O/F-mischbesetzten Lage in der Kristallstruktur von $ClOF_2[BF_4]$, wurde ein Modell der Struktur mit vollbesetzten Lagen in der Untergruppe *Pna*2$_1$ (Nr. 33) konstruiert und optimiert.

Shrinking-Faktor: 3×3×5

Raumgruppe *Pna*2$_1$ (Nr. 33)

a = 9,18862261 Å, *b* = 9,00476847 Å, *c* = 5,51984241 Å, *V* = 456,719594 Å^3

Tabelle 106. Atomkoordinaten der optimierten Struktur von $ClOF_2[BF_4]$.

Atom	*x*	*y*	*z*
B	4,844742843371E−01	−3,436250203286E−01	−4,940043874716E−01
Cl	−2,618321141356E−01	4,017837731070E−01	−4,648630264864E−01
F	−2,118137899963E−01	2,316285998090E−01	4,979081079308E−01
F	−1,776292739824E−01	4,532330469201E−01	2,890697876765E−01
F	4,388963717872E−01	−2,673695167096E−01	−2,898948147969E−01
F	4,348931958265E−01	−4,883295014720E−01	−4,901519691902E−01
F	−3,623218026181E−01	−3,454069458131E−01	4,945974353076E−01
F	4,302843006040E−01	−2,720276165800E−01	2,963946309132E−01
O	−1,761620864280E−01	4,561224754701E−01	−2,721557638830E−01

8.2.2.10. $ClOF_2[Mo_3O_3F_{13}]$

Shrinking-Faktor: 3×3×3

Raumgruppe $P\bar{1}$ (Nr. 2)

a = 8,56045035 Å, b = 8,63077933 Å, c = 10,03771679 Å, α = 65,654528°, β = 80,738356°, γ = 86,958688°,

V = 666,791546 Å^3

Tabelle 107. Atomkoordinaten der optimierten Struktur von $ClOF_2[Mo_3O_3F_{13}]$.

Atom	*x*	*y*	*z*
Mo	−3,231478408814E−01	−1,685233317002E−01	3,806349659431E−01
Mo	−2,994906616986E−01	−2,836390522882E−01	−1,706080600014E−01
Mo	−1,776491850572E−01	2,146992490488E−01	−1,072830508410E−01
Cl	−1,929979066350E−01	3,300646564731E−01	4,296032976741E−01
O	−2,153157951472E−01	3,721837421588E−01	2,828591533426E−01
O	−3,436915303715E−01	−1,214866133217E−01	2,064402781265E−01
O	−2,890856995104E−01	−3,297603624694E−01	5,300515317957E−03
O	−1,329809036799E−01	1,456663407829E−02	−7,550583784795E−02
F	−1,421179557695E−01	1,315912980919E−01	4,975106596747E−01
F	−1,577638245131E−02	3,945961829254E−01	4,229616775497E−01
F	−2,683230265122E−01	−4,011261868340E−01	4,305051044373E−01
F	−1,089413807992E−01	−1,200792222752E−01	3,515694651073E−01
F	−3,742433925457E−01	4,101064985823E−02	3,836439395163E−01
F	−3,017845090332E−01	−2,374498944439E−01	−3,958264536210E−01
F	4,676197886800E−01	−2,509584622373E−01	4,670785789870E−01
F	−3,558243628336E−01	−5,788202648374E−02	−2,318595754021E−01
F	−8,764417539291E−02	−2,243692129116E−01	−2,475445979528E−01
F	4,955500857275E−01	−3,568785894952E−01	−1,510556228518E−01
F	−2,358492166416E−01	4,908605374364E−01	−1,592951626517E−01
F	−1,971777409184E−01	2,961732014198E−01	−3,095588872666E−01
F	−1,720118813951E−01	2,122892324144E−01	7,701611127305E−02
F	−3,961855675984E−01	2,024771434218E−01	−6,691141027033E−02
F	2,331756416300E−02	3,153836287356E−01	−1,704195377792E−01

8.2.2.11. $(ClOF_2[OsO_3F_3])_2OsF_6$

Ein paramagnetischer Grundzustand wurde als Startwert gesetzt, nach der Optimierung lag ein paramagnetischer Zustand mit einem magnetischen Moment von 1,46 μ_B für das Os(VI)-Atom und 2,00 μ_B für das OsF_6-Molekül vor.

Shrinking-Faktor: 4×3×2

Raumgruppe $P\bar{1}$ (Nr. 2)

a = 5,57081238 Å, b = 7,42786790 Å, c = 10,69442020 Å, α = 104,552193°, β = 97,929011°, γ = 95,605827°,

V = 420,173581 Å^3

Tabelle 108. Atomkoordinaten der optimierten Struktur von $(ClOF_2[OsO_3F_3])_2OsF_6$.

Atom	*x*	*y*	*z*
Os	3,955424771977E−01	4,259484557284E−01	−2,247677635946E−01
Os	2,233439266562E−37	3,793833323233E−20	−1,880790961316E−37
Cl	−2,342843279444E−01	2,819442038420E−01	4,813468453051E−01
F	−1,663299969164E−01	1,347646591716E−01	−4,321394987091E−01
F	−6,372621433103E−02	1,895695599369E−01	3,740967866248E−01
F	−3,388681231843E−01	4,587750600868E−01	−3,363543321517E−01
F	3,652161174540E−01	1,801068559551E−01	−3,486853783690E−01
F	−1,959558235623E−01	1,063341694588E−02	−1,510945167258E−01
F	2,765731571814E−01	4,601229891888E−02	−7,470874183723E−02
F	−1,818880367512E−02	−2,583007651246E−01	−6,673786045287E−02
F	1,920993008192E−01	4,618495714684E−01	−3,963096092464E−01
O	−4,772330760429E−01	2,166810881193E−01	4,163753846007E−01
O	−3,981976856845E−01	3,725735010737E−01	−1,132830320802E−01
O	1,265472563216E−01	3,688337115911E−01	−1,789287634190E−01
O	4,345700628744E−01	−3,360108895283E−01	−1,765579890611E−01

8.2.2.12. $(ClOF_2)_2[AuF_4][SbF_6]$

Shrinking-Faktor: 4×3×2

Raumgruppe $P2_1/c$ (Nr. 14)

a = 5,84221362 Å, b = 9,20688225 Å, c = 11,32100829 Å, β = 104,387130°, V = 589,843883 Å^3

Tabelle 109. Atomkoordinaten der optimierten Struktur von $(ClOF_2)_2[AuF_4][SbF_6]$.

Atom	*x*	*y*	*z*
Au	2,325886033057E−20	−5,000000000000E−01	7,222237291452E−35
Sb	2,775557561563E−17	−5,000000000000E−01	−5,000000000000E−01
Cl	−4,129579525239E−01	3,217532263836E−01	1,797444791028E−01
O	−4,757744248007E−01	2,551796969198E−01	6,361421884056E−02
F	4,336159175919E−01	2,379712999824E−01	2,613360636622E−01
F	2,907840648164E−01	4,896389900287E−01	1,303722018404E−01
F	−1,687082420206E−01	2,409128781928E−01	2,512999478230E−01
F	−1,880973557898E−01	−4,992867405202E−01	1,208450690395E−01
F	−2,863633840248E−01	4,704097681502E−01	3,776061999060E−01
F	1,129018036807E−02	2,980193320321E−01	−4,622548621736E−01
F	−1,759590148400E−01	−4,656322033406E−01	−3,846861215382E−01

8.2.3. Strukturen der Verbindungen aus Abschnitt 5.5

8.2.3.1. $Rb[UF_7]$

Shrinking-Faktor: 4×4×3

Raumgruppe $P2_1/c$ (Nr. 14)

a = 5,09162440 Å, b = 10,66868085 Å, c = 10,92822727 Å, β = 95,132601°, V = 591,251043 Å^3

Tabelle 110. Atomkoordinaten der optimierten Struktur von $Rb[UF_7]$.

Atom	*x*	*y*	*z*
Rb	1,195953899044E−02	4,954295019545E−01	2,814497682249E−01
U	4,797535984937E−01	2,138374591476E−01	4,770183606157E−01
F	1,030151450320E−01	1,951568433632E−01	3,918966530881E−01
F	3,003408063743E−01	1,543851147448E−01	−3,757034505506E−01
F	−4,774646672218E−01	1,094853525968E−01	3,200222665007E−01
F	−2,247606471703E−01	2,929811199395E−01	−4,112124340417E−01
F	2,981220145860E−01	3,798882989400E−01	−4,805421595537E−01
F	−3,824254902387E−01	3,378064997722E−01	3,557778043769E−01
F	−2,816418274788E−01	6,349660944793E−02	−4,656735786304E−01

8.2.4. Mulliken-Populationsanalysen der optimierten Strukturen

Tabelle 111. Berechnete durchschnittliche Mulliken-Ladungen der *M*-, Cl-, O- und F-Atome der Kationen und Anionen in Difluorooxychloronium(V)-Verbindungen. Die Mulliken-Populationsanalysen basieren auf den mit CRYSTAL17 optimierten Strukturen (DFT-PBE0/TZVP).[246] (*M*: Zentralatom des Anions)

Verbindung	durchschnittliche Ladung / *e*						Quelle
	M	Cl	O	F($ClOF_2^+$)	F	μ-F	
$ClOF_2[PF_6]$	+1,80	+1,40	−0,18	−0,20	−0,42	−0,46	a, [296]
$ClOF_2[AsF_6]$	+1,62	+1,39	−0,18	−0,20	−0,38	−0,42	a, [296]
$ClOF_2[VF_6]$	+1,82	+1,41	−0,20	−0,22	−0,39	−0,47	a, [296]
$ClOF_2[RuF_6]$	+1,96	+1,40	−0,19	−0,21	−0,42	−0,49	a, [296]
$ClOF_2[IrF_6]$	+1,68	+1,39	−0,19	−0,21	−0,38	−0,44	a, [296]
$ClOF_2[OsF_6]$	+1,84	+1,41	−0,18	−0,22	−0,41	−0,46	a, [296]
$ClOF_2[SbF_6]$	+2,14	+1,40	−0,18	−0,21	−0,47	−0,51	a, [296]
$ClOF_2[NbF_6]$[b]	+2,36	+1,42	−0,20	−0,22	−0,49	−0,55	a, [296]
$ClOF_2[TaF_6]$[b]	+2,50	+1,42	−0,19	−0,22	−0,53	−0,57	a, [296]
$(ClOF_2)_2[CrF_6]$[b]	+1,78	+1,40	−0,21	−0,25	−0,50	−0,54	a
$(ClOF_2)_2[RhF_6]$[b]	+1,64	+1,39	−0,20	−0,25	−0,50	−0,52	a
$(ClOF_2)_2[GeF_6]$[b]	+1,57	+1,39	−0,20	−0,24	−0,50	−0,50	a
$(ClOF_2)_2[PdF_6]$	+1,59	+1,39	−0,21	−0,23	-	−0,50	a
$(ClOF_2)_2[PtF_6]$	+1,46	+1,39	−0,22	−0,23	-	−0,48	a
$(ClOF_2)_2[SnF_6]$	+1,80	+1,40	−0,22	−0,24	-	−0,53	a
$ClOF_2SnF_5$	+1,81	+1,40	−0,21	−0,22	−0,49	−0,53, −0,49[c]	a
$ClOF_2PbF_5$	+1,70	+1,40	−0,21	−0,23	−0,44	−0,50, −0,48[c]	a
$ClOF_2[BF_4]$[b]	+1,03	+1,39	−0,20	−0,20	−0,45	−0,45	a
$ClOF_2[Mo_3O_3F_{13}]$	+2,02	+1,33	−0,14, −0,39[d]	−0,20	−0,41	−0,46, −0,53[c]	a
$(ClOF_2[OsO_3F_3])_2OsF_6$	+1,90[e], +1,97[f]	+1,40	−0,20, −0,42[d]	−0,25	−0,42[e], −0,32[f]	−0,47[e]	a
$(ClOF_2)_2[AuF_4][SbF_6]$	+1,23[g], +2,04[h]	+1,40	−0,21	−0,22	−0,47[h]	−0,47[g], −0,49	a

a: diese Arbeit; b: Modell ohne O/F-Fehlordnung; c: μ-verbrückend zwischen Zentralatomen des Anions; d: An das Zentralatom des Anions gebunden; e: $[OsO_3F_3]^-$-Anion; f: OsF_6-Molekül; g: $[AuF_4]^-$-Anion; h: $[SbF_6]^-$-Anion.

8.3. Abbildungsverzeichnis

Abbildung 1. Lewis-Formeln der Halogenmonofluoride sowie davon abgeleiteter Ionen. Freie Elektronenpaare (Doppelpunkte) sind nur für das zentrale Halogenatom gezeigt. 3
Abbildung 2. Lewis-Formeln der Halogentrifluoride sowie davon abgeleiteter Ionen. Freie Elektronenpaare (Doppelpunkte) sind nur für das zentrale Halogenatom gezeigt. 4
Abbildung 3. Ausschnitte aus den Kristallstrukturen von $[Br_2F_5][SbF_6]$ (links) und $[Br_3F_8][SbF_6]$ (rechts), es sind jeweils die Kationen gezeigt.[34] 6
Abbildung 4. Strukturen der $[X_2F_7]^-$- (X = Au, Br) bzw. $[X_3F_{10}]^-$-Anionen (X = Cl, Br).[41,42,119] 7
Abbildung 5. Die beiden Konstitutionsisomere des $[Br_4F_{13}]^-$-Anions.[43] Beim linken Anion ist eines der Fluoratome fehlgeordnet und das Fluoratom mit dem kleineren Besetzungsfaktor transparent dargestellt. 8
Abbildung 6. Lewis-Formeln der Halogenpentafluoride sowie davon abgeleiteter Ionen. Freie Elektronenpaare sind nur für das zentrale Halogenatom gezeigt. 9
Abbildung 7. Verschiedene mehrkernige Fluoridoiodate(V): $[I_3F_{16}]^-$ (1), $[I_2F_{12}(HF_2)_2]^{2-}$ (2) $[I_4F_{24}]^{4-}$ (3) und ein Ausschnitt aus einem polymeren Anion (4) mit verbrückenden $[HF_2]^-$-Anionen.[51,55,56] 10
Abbildung 8. Lewis-Formeln des bekannten Halogenheptafluorids sowie davon abgeleiteter Ionen. 11
Abbildung 9. Lewis-Formeln der bekannten Halogenoxidtrifluoride sowie davon abgeleiteter Ionen. Freie Elektronenpaare sind nur für das zentrale Halogenatom gezeigt. 13
Abbildung 10. Ausschnitt aus dem komplexen Anion der Verbindung $NO_2Br_3O_2F_{10}$.[189] Die Fluoratome der $[BrF_4]^-$-Anionen sind μ_2- oder μ_3-verbrückend. 15
Abbildung 11. Lewis-Formeln der bekannten Halogendioxidfluoride sowie davon abgeleiteter Ionen. Freie Elektronenpaare sind nur für das zentrale Halogenatom gezeigt. 15
Abbildung 12. Die mehrkernigen $[BrCl_2O_6]^+$- und $[Br_3O_6]^+$-Kationen.[137] 16
Abbildung 13. Lewis-Formeln des bekannten Halogenoxidtetrafluorids sowie des davon abgeleiteten Anions. 17
Abbildung 14. Lewis-Formeln der bekannten Halogendioxidtrifluoride sowie davon abgeleiteter Ionen. 18
Abbildung 15. Lewis-Formeln der bekannten Halogentrioxidfluoride sowie des davon abgeleiteten Anions. 19
Abbildung 16. Konstruktionsskizze eines PFA- oder FEP-Reaktionsgefäßes, bestehend aus einem 3/4“-Kunststoffrohr, Faltenbalgventil und entsprechenden Adaptern.[217] Die Bemaßung ist in Millimetern angegeben. 21
Abbildung 17. Schematischer Aufbau der Metallanlage für die Handhabung von Chlortrifluorid, die Abbildung wurde von Dr. Sergei Ivlev (Philipps-Universität Marburg) erstellt. 1: Trocknungsrohr, gefüllt mit P_2O_5; 2: Monel- und Edelstahlgefäß mit definiertem Volumen; 3: Beheizbare Monelspirale; 4: U-Rohre aus PFA; 5: Graduierter Kühlfinger aus PFA; 6: Monelzylinder; 7: Reaktionsgefäß aus PFA oder FEP; 8: Beheizbarer Natronkalk(„Sodalime“)-Absorber; 9: Kühlfalle aus PFA; Ar: Argon der Qualität 5.0; P1: Monel-Rohrfedermanometer (AIR PRODUCTS); P2: Edelstahl-Rohrfedermanometer (UNION CARBIDE); P3: Kapazitätsmanometer Baratron 627F (MKS Instruments Deutschland GmbH; P4: Monel-Rohrfedermanometer (Acco); P5: Pirani-Manometer VD84 (Thyracont Vacuum Instruments

GmbH); V: Faltenbalgventil aus Edelstahl oder Monel (Typ SS- oder M-4BRW, Swagelok) oder Membranventil aus Monel (4600er Serie, HOKE); Vakuum: Zweistufige Drehschieberpumpe (Typ RV5F mit perfluoriertem Öl und Fluorelastomeren als Dichtungen, Edwards). 22
Abbildung 18. Schematischer Aufbau der Metallanlage für die Handhabung von Fluor und flüchtigen Fluoriden.[217] 24
Abbildung 19. Schematischer Aufbau der Metallanlage für die Handhabung von wasserfreiem Fluorwasserstoff. (Abbildung verändert nach [217]) 25
Abbildung 20. Aufbau des verwendeten UV-Reaktors.[217] 26
Abbildung 21. Kristallpräparationseinheit für temperatur- und luftempfindliche Kristalle.[236] 29
Abbildung 22. Ausschnitte aus der Kristallstruktur von $[ClOF_2]_2[CrF_6]$. Links ist das $ClOF_2^+$-Kation mit verbrückenden Fluoratomen abgebildet, rechts das $[CrF_6]^{2-}$-Anion. Die gestrichelten Bindungen stehen für kurze Kontakte der Form Cl···μ-F verbrückender Fluoratome des Anions mit den Chloratomen. Die Auslenkungsellipsoide sind mit 70% Aufenthaltswahrscheinlichkeit bei 100 K dargestellt. Symmetrietransformationen (links): #1 x, 1 − y, z; #2 1/2 − x, 3/2 − y, 1 − z; (rechts): #1 1 − x, y, 1 − z; #2 1 − x, 1 − y, 1 − z. Die Verbindungen $(ClOF_2)_2[MF_6]$ (M = Rh, Ge) kristallisieren isotyp zur Chromverbindung. 46
Abbildung 23. Kristallstruktur von $(ClOF_2)_2[CrF_6]$, projiziert entlang der *b*-Achse (links) oder der *c*-Achse (rechts). Die ersten Koordinationssphären der Chloratome sind als grüne und die der Chromatome als graue Polyeder dargestellt. Die Atome sind mit willkürlichen Radien abgebildet. Die Verbindungen $(ClOF_2)_2[MF_6]$ (M = Rh, Ge) kristallisieren isotyp zur Chromverbindung. 47
Abbildung 24. Links: Niedrigaufgelöstes Raman-Spektrum (532 nm Laser) von festem $(ClOF_2)_2[GeF_6]$. Rechts: Hochaufgelöstes (oben, 532 nm Laser) und berechnetes (unten) Raman-Spektrum von festem $(ClOF_2)_2[GeF_6]$. Das berechnete Spektrum basiert auf einem geordneten Modell von $(ClOF_2)_2[GeF_6]$ in der Raumgruppe *C*2 (Nr. 5), siehe Abschnitt 8.2.2.3. Die Banden bei circa 1000 und 800 cm^{-1} stellen vermutlich Kombinationsbanden oder Obertöne dar. Die Raman-Intensitäten sind in willkürlichen Einheiten (a.u.) angegeben. 48
Abbildung 25. Ausschnitte aus der Kristallstruktur von $[ClOF_2]_2[SnF_6]$. Links ist das $ClOF_2^+$-Kation mit verbrückenden Fluoratomen abgebildet, rechts das $[SnF_6]^{2-}$-Anion. Die gestrichelten Bindungen stehen für kurze Kontakte der Form Cl···μ-F verbrückender Fluoratome des Anions mit den Chloratomen. Die Auslenkungsellipsoide sind mit 70% Aufenthaltswahrscheinlichkeit bei 100 K dargestellt. Symmetrietransformationen (links): #1 x, y, 1 − z; (rechts): #1 1 − x, 1 − y, z; #2 1 − x, 1 − y, −z; #3 x, y, −z. Die Verbindungen $(ClOF_2)_2[MF_6]$ (M = Pd, Pt) kristallisieren isotyp zur Zinnverbindung. 52
Abbildung 26. Kristallstruktur von $[ClOF_2]_2[SnF_6]$, projiziert entlang der *c*-Achse. Die ersten Koordinationssphären der Chloratome sind als grüne und die der Zinnatome als graue Polyeder dargestellt. Die Atome sind mit willkürlichen Radien abgebildet. Die Verbindungen $(ClOF_2)_2[MF_6]$ (M = Pd, Pt) kristallisieren isotyp zur Zinnverbindung. 53
Abbildung 27. Links: Niedrigaufgelöstes Raman-Spektrum (532 nm Laser) von festem $(ClOF_2)_2[PtF_6]$. Rechts: Hochaufgelöstes (oben, 532 nm Laser) und berechnetes (unten) Raman-Spektrum von festem $(ClOF_2)_2[PtF_6]$. Die Raman-Intensitäten sind in willkürlichen Einheiten (a.u.) angegeben. 55

Abbildung 28. Links: Niedrigaufgelöstes Raman-Spektrum (532 nm Laser) von festem $(ClOF_2)_2[SnF_6]$. Rechts: Hochaufgelöstes (oben, 532 nm Laser) und berechnetes (unten) Raman-Spektrum von festem $(ClOF_2)_2[SnF_6]$. Die Raman-Intensitäten sind in willkürlichen Einheiten (a.u.) angegeben. 56
Abbildung 29. Ausschnitte aus der Kristallstruktur von $ClOF_2SnF_5$. Links ist das $ClOF_2^+$-Kation mit verbrückenden Fluoratomen abgebildet, rechts die Koordinationssphäre des Sn(1)-Atoms. Die gestrichelten Bindungen stehen für kurze Kontakte der Form Cl···μ-F verbrückender Fluoratome des Anions mit den Chloratomen oder zu weiteren Zinnatomen verbrückender Fluoratome (F(7)). Die Auslenkungsellipsoide sind mit 70% Aufenthaltswahrscheinlichkeit bei 100 K dargestellt. Symmetrietransformation (rechts): #1 3/2 − *x*, 1/2 + *y*, 1 − *z*. $ClOF_2PbF_5$ kristallisiert isotyp zur Zinnverbindung. 59
Abbildung 30. Kristallstruktur von $ClOF_2SnF_5$, projiziert entlang der *b*-Achse (links) oder auf die (101)-Ebene (rechts). Die ersten Koordinationssphären der Chloratome sind als grüne und die der Zinnatome als graue Polyeder dargestellt. Die Atome sind mit willkürlichen Radien abgebildet. 61
Abbildung 31. Links: Niedrigaufgelöstes Raman-Spektrum (532 nm Laser) von festem $ClOF_2PbF_5$. Rechts: Hochaufgelöstes (oben, 532 nm Laser) und berechnetes (unten) Raman-Spektrum von festem $ClOF_2PbF_5$. Die Raman-Intensitäten sind in willkürlichen Einheiten (a.u.) angegeben. 62
Abbildung 32. Ausschnitte aus der Kristallstruktur von $ClOF_2[BF_4]$. Links ist das $ClOF_2^+$-Kation mit verbrückenden Fluoratomen abgebildet, rechts das $[BF_4]^-$-Anion. Die gestrichelten Bindungen stehen für kurze Kontakte der Form Cl···μ-F verbrückender Fluoratome des Anions mit den Chloratomen. Die Auslenkungsellipsoide sind mit 70% Aufenthaltswahrscheinlichkeit bei 100 K dargestellt. Die Besetzungsfaktoren der gemischtbesetzten Lage sind: O(0,44(2))/F(0,56). Symmetrietransformationen (links): #1 *x*, 3/2 − *y*, *z*; #2 1 − *x*, 1/2 + *y*, 1 − *z*; (rechts): #1 *x*, 3/2 − *y*, *z*. 65
Abbildung 33. Kristallstruktur von $ClOF_2[BF_4]$, projiziert entlang der *b*-Achse (links) oder der *c*-Achse (rechts). Die ersten Koordinationssphären der Chloratome sind als grüne und die der Boratome als graue Polyeder dargestellt. Die Atome sind mit willkürlichen Radien abgebildet. 66
Abbildung 34. Infrarotspektren (links) und Raman-Spektren (rechts, 532 nm Laser) von festem $ClOF_2[BF_4]$. Oben ist jeweils das gemessene Spektrum und unten das berechnete abgebildet. Die berechneten Spektren basieren auf einem geordneten Modell von $ClOF_2[BF_4]$ in der Raumgruppe $Pna2_1$ (Nr. 33), siehe Abschnitt 8.2.2.9. Die berechnete IR-Absorption und die Raman-Intensitäten sind in willkürlichen Einheiten angegeben (a.u.). 67
Abbildung 35. Ausschnitte aus der Kristallstruktur von $ClOF_2[Mo_3O_3F_{13}]$. Links ist das $ClOF_2^+$-Kation mit verbrückenden Fluoratomen abgebildet, rechts das $[Mo_3O_3F_{13}]^-$-Anion. Die gestrichelten Bindungen stehen für kurze Kontakte der Form Cl···μ-F verbrückender Fluoratome des Anions mit den Chloratomen. Die Auslenkungsellipsoide sind mit 70% Aufenthaltswahrscheinlichkeit bei 100 K dargestellt. 71
Abbildung 36. Dimeres $ClOF_2[Mo_3O_3F_{13}]$, welches durch die Berücksichtigung der Cl···μ-F-Kontakte erhalten wird. 72
Abbildung 37. Infrarotspektren (links) und Raman-Spektren (rechts, 532 nm Laser) von festem $ClOF_2[Mo_3O_3F_{13}]$. Oben ist jeweils das gemessene Spektrum und unten das berechnete abgebildet. Die

berechnete IR-Absorption und die Raman-Intensitäten sind in willkürlichen Einheiten angegeben (a.u.). 73
Abbildung 38. Ausschnitte aus der Kristallstruktur von $(ClOF_2[OsO_3F_3])_2OsF_6$. Links ist das $ClOF_2^+$-Kation mit verbrückenden Fluoratomen abgebildet, in der Mitte das $[OsO_3F_3]^-$-Anion und rechts das OsF_6-Molekül. Die gestrichelten Bindungen stehen für kurze Kontakte der Form Cl···μ-F verbrückender Fluoratome des Anions mit den Chloratomen. Die Auslenkungsellipsoide sind mit 70% Aufenthaltswahrscheinlichkeit bei 100 K dargestellt. Symmetrietransformationen (links): #1 −1 + *x*, *y*, *z*; (rechts): #1 −*x*, −*y*, −*z*..... 77
Abbildung 39. Kristallstruktur von $(ClOF_2[OsO_3F_3])_2OsF_6$, projiziert entlang der *b*-Achse (links) oder der *a*-Achse (rechts). Die ersten Koordinationssphären der Chloratome sind als grüne, die des Os(1)-Atoms ($[OsO_3F_3]^-$) als graue und die des Os(2)-Atoms (OsF_6) als pflaumenfarbene Polyeder dargestellt. Die Atome sind mit willkürlichen Radien abgebildet. 78
Abbildung 40. Links: Niedrigaufgelöstes Raman-Spektrum (523 nm Laser) von festem $(ClOF_2[OsO_3F_3])_2OsF_6$. Rechts: Hochaufgelöstes (oben, 532 nm Laser) und berechnetes (unten) Raman-Spektrum von festem $(ClOF_2[OsO_3F_3])_2OsF_6$. Die Raman-Intensitäten sind in willkürlichen Einheiten (a.u.) angegeben. 79
Abbildung 41. Ausschnitte aus der Kristallstruktur von $(ClOF_2)_2[AuF_4][SbF_6]$. Links ist das $ClOF_2^+$-Kation mit verbrückenden Fluoratomen abgebildet, in der Mitte das $[AuF_4]^-$-Anion und rechts das $[SbF_6]^-$-Anion. Die gestrichelten Bindungen stehen für kurze Kontakte der Form Cl···μ-F verbrückender Fluoratome des Anions mit den Chloratomen. Die Auslenkungsellipsoide sind mit 70% Aufenthaltswahrscheinlichkeit bei 100 K dargestellt. Symmetrietransformationen (Mitte): #1 −*x*, 1 − *y*, −*z*; (rechts): #1 2 − *x*, 1 − *y*, 1 − *z*. 83
Abbildung 42. Kristallstruktur von $(ClOF_2)_2[AuF_4][SbF_6]$, projiziert entlang der *a*-Achse (links) oder der *b*-Achse (rechts). Die ersten Koordinationssphären der Chloratome sind als grüne, die der Goldatome als orange und die der Antimonatome als graue Polyeder dargestellt. Die Atome sind mit willkürlichen Radien abgebildet. 84
Abbildung 43. Niedrigaufgelöstes (oben, 532 nm Laser) und berechnetes (unten) Raman-Spektrum von festem $(ClOF_2)_2[AuF_4][SbF_6]$. Die Raman-Intensitäten sind in willkürlichen Einheiten (a.u.) angegeben. 85
Abbildung 44. Niedrigste unbesetzte Molekülorbitale (LUMO) des freien $ClOF_2^+$-Kations.[296] Fluoratome sind in gelb, Chloratome in grün und Sauerstoffatome in rot dargestellt. 87
Abbildung 45. Übersicht über die durch Reaktionen mit Chlortrifluorid dargestellten Verbindungen. Die Reaktionen sind der Übersichtlichkeit halber nicht ausgeglichen. 93
Abbildung 46. Ausschnitte aus der Kristallstruktur von $TlPuF_5$. Links ist die Umgebung des Plutoniumatoms dargestellt und rechts das Koordinationspolyeder mit umgebenden Plutoniumatomen. Links sind die Auslenkungsellipsoide mit 70% Aufenthaltswahrscheinlichkeit bei 289 K dargestellt. Rechts sind die Atome mit willkürlichen Radien abgebildet. Symmetrietransformationen: #1 2 − *x*, −1/2 + *y*, 3/2 − *z*; #2 2 − *x*, 1 −*y*, 1 − *z*; #3 2 − *x*, 1/2 + *y*, 3/2 − *z*; #4 *x*, 3/2 −*y*, −1/2 + *z*. Die Verbindungen NH_4PuF_5 und $TlNpF_5$ und kristallisieren isotyp zu $TlPuF_5$..... 110

Abbildung 47. Kristallstruktur von $TlPuF_5$, projiziert entlang der *a*-Achse (links) oder der *c*-Achse (rechts). Die Atome sind mit willkürlichen Radien abgebildet. Die Verbindungen NH_4PuF_5 und $TlNpF_5$ kristallisieren isotyp zu $TlPuF_5$. 111
Abbildung 48. 3^2.4.3.4-Netz, welches von den Metallatomen (*M* = Np, Pu) im $TlMF_5$ parallel zur *bc*-Ebene aufgespannt wird. 111
Abbildung 49. Wasserstoffbrückenbindungen der Form N−H···F des Ammoniumions in NH_4PuF_5. Die Auslenkungsellipsoide sind mit 70% Aufenthaltswahrscheinlichkeit bei 100 K dargestellt. Wasserstoffatome (weiß) sind isotrop mit willkürlichen Radien abgebildet. Symmetrietransformationen: #1 *x*, 1/2 − *y*, 1/2 + *z*; #2 −1 + *x*, *y*, *z*. 112
Abbildung 50. Ausschnitte aus der Kristallstruktur von KPu_2F_9. Links ist die Umgebung des Plutoniumatoms dargestellt und rechts das Koordinationspolyeder mit umgebenden Plutoniumatomen. Links sind die Auslenkungsellipsoide mit 70% Aufenthaltswahrscheinlichkeit bei 100 K dargestellt. Rechts sind die Atome mit willkürlichen Radien abgebildet. Symmetrietransformationen: #1 1 − *x*, 1 − *y*, −*z*; #2 1/2 − *x*, 1 −*y*, −1/2 + *z*; #3 1/2 + *x*, *y*, 1/2 − *z*. Die Verbindung $NaPu_2F_9$ kristallisiert isotyp zu KPu_2F_9. 115
Abbildung 51. Kristallstruktur von KPu_2F_9, projiziert entlang der *b*-Achse (links) oder der *c*-Achse (rechts). Die Atome sind mit willkürlichen Radien abgebildet. Die Verbindung $NaPu_2F_9$ kristallisiert isotyp zu KPu_2F_9. 116
Abbildung 52. 3^2.4.3.4-Netz, welches von den Plutoniumatomen in APu_2F_9 (*A* = Na, K) parallel zur *ac*-Ebene aufgespannt wird. 116
Abbildung 53. Ausschnitte aus der Kristallstruktur von $Sr[UF_5(HF_2)_2]$. Links ist das $[UF_5(HF_2)_2]^-$-Anion dargestellt und rechts ein Strukturausschnitt mit der ersten Koordinationssphären der Uranatome als graue Polyeder. Links sind die Auslenkungsellipsoide mit 70% Aufenthaltswahrscheinlichkeit bei 100 K dargestellt. Rechts sind die Atome mit willkürlichen Radien abgebildet. 118
Abbildung 54. Infrarotspektrum von festem $Sr[UF_5(HF_2)_2]$. 119
Abbildung 55. Ausschnitte aus der Kristallstruktur von $Ba(HF)_2U_2F_{12}$. Links ist die Umgebung des Bariumkations dargestellt und rechts die Umgebung des Uranatoms. Die Auslenkungsellipsoide sind mit 70% Aufenthaltswahrscheinlichkeit bei 100 K dargestellt. Gestrichelte Bindungen stehen für Bindungen zu weiteren Uranatomen der verbrückenden Fluoratome. Symmetrietransformationen (links): #1 1/2 + *x*, 1/2 − *y*, 3/2 − *z*; (rechts): #1 1 − *x*, 1 − *y*, 1 − *z*; #2 1/2 + *x*, *y*, 1/2 − *z*. 121
Abbildung 56. Kristallstruktur von $Ba(HF)_2U_2F_{12}$, projiziert entlang der *c*-Achse (links) oder der *b*-Achse (rechts). Die ersten Koordinationssphären der Uranatome sind als graue Polyeder dargestellt. Die Atome sind mit willkürlichen Radien abgebildet. 122
Abbildung 57. Ausschnitte aus der Kristallstruktur von $(N_2H_6)U_2F_{10}(HF_2)_2$. Links ist das Hydrazinium(2+)-Kation dargestellt und rechts die Umgebung des Uranatoms. Die Auslenkungsellipsoide sind mit 70% Aufenthaltswahrscheinlichkeit bei 100 K dargestellt. Wasserstoffatome (weiß) sind isotrop mit willkürlichen Radien abgebildet. Gestrichelte Bindungen stehen für Wasserstoffbrückenbindungen der Formen F−H···F und N−H···F oder Bindungen zu weiteren Uranatomen der verbrückenden Fluoratome. Symmetrietransformationen (links): #1 −*x*, *y*, 1/2 − *z*; #2 −1/2 + *x*, 1/2 + *y*, −1 + *z*; #3 −*x*, 1 − *y*, 1 − *z*; #4 1/2 − *x*, 3/2 − *y*, 1 − *z*; (rechts): #1 1/2 − *x*, 3/2 − *y*, 2 − *z*; #2 *x*, 1 − *y*, 1/2 + *z*. 124

Abbildung 58. Kristallstruktur von $(N_2H_6)U_2F_{10}(HF_2)_2$, projiziert entlang der *a*-Achse (links) oder der *c*-Achse (rechts). Die Atome sind mit willkürlichen Radien abgebildet. Gestrichelte Bindungen stehen für Wasserstoffbrückenbindungen der Form F−H···F. 126
Abbildung 59. Ausschnitte aus der Kristallstruktur von $Rb[UF_7]$. Links ist das $[UF_7]^-$-Anion dargestellt und rechts ein Strukturausschnitt mit der ersten Koordinationssphären der Uranatome als graue Polyeder. Links sind die Auslenkungsellipsoide mit 70% Aufenthaltswahrscheinlichkeit bei 100 K dargestellt. Rechts sind die Atome mit willkürlichen Radien abgebildet. 129
Abbildung 60. Die möglichen Ligandenanordnungen für Koordinationszahl sieben. (Abbildung verändert nach [396]). 129
Abbildung 61. Hochaufgelöstes (oben, 532 nm Laser) und berechnetes (unten) Raman-Spektrum von $Rb[UF_7]$. Die Raman-Intensitäten sind in willkürlichen Einheiten (a.u.) angegeben. 131
Abbildung 62. Übersicht über die dargestellten und charakterisierten Verbindungen mit Fluoridouranat(V)-Anionen. Die Reaktionen sind der Übersichtlichkeit halber nicht ausgeglichen. ... 132
Abbildung 63. Erste Koordinationssphären der beiden kristallographisch-unabhängigen Uranatome in HP-UF_4. 134
Abbildung 64. Übersicht über die dargestellten und charakterisierten Fluoridoneptunate(IV) und -plutonate(IV). Die Reaktionen sind der Übersichtlichkeit halber nicht ausgeglichen. 134

8.4. Tabellenverzeichnis

Tabelle 1. Bisher beschriebene Halogenfluoride und formal durch Fluoridionenabstraktion abgeleitete Kationen oder Fluoridionenaufnahme abgeleitete Anionen. Zusätzlich ist die Klassifikation der Spezies nach dem VSEPR-Modell angegeben (bei mehrkernigen Spezies für Halogenatome ungleich Fluor). Dabei steht *A* für das Zentralatom, *B* für die Liganden und *E* für ein freies Elektronenpaar. 1

Tabelle 2. Bisher beschriebene Halogenoxidfluoride und durch Fluoridionenabstraktion abgeleitete Kationen und durch Fluoridionenaufnahme abgeleitete Anionen. Zusätzlich ist die Klassifikation der Spezies nach dem VSEPR-Modell angegeben. Dabei steht *A* für das Zentralatom, *B* für die Liganden und *E* für ein freies Elektronenpaar. 12

Tabelle 3. Verwendete Basissätze für die quantenchemischen Festkörperrechnungen mit dem Programmpaket CRYSTAL17. 31

Tabelle 4. Gitterparameter, Zellvolumina und Besetzungsfaktoren (S.O.F.) der O/F-mischbesetzten Lage der isotypen Verbindungen $(ClOF_2)_2[MF_6]$ (*M* = Cr, Rh, Ge) 45

Tabelle 5. Bandenlagen und -zuordnungen der Raman-Spektren von $(ClOF_2)_2[GeF_6]$, basierend auf dem berechneten Raman-Spektrum. (> 300 cm^{-1}) Das berechnete Spektrum basiert auf einem geordneten Modell von $(ClOF_2)_2[GeF_6]$ in der Raumgruppe *C*2 (Nr. 5), siehe Abschnitt 8.2.2.3. (*v*: Streckschwingung, *δ*: Deformationsschwingung, *π*: Inversionsschwingung, *s*: Symmetrisch, *as*: Asymmetrisch) 49

Tabelle 6. Gitterparameter und Zellvolumina der isotypen Verbindungen $(ClOF_2)_2[MF_6]$ (*M* = Pd, Pt, Sn) 51

Tabelle 7. Bandenlagen und -zuordnungen der Raman-Spektren von $(ClOF_2)_2[PtF_6]$, basierend auf dem berechneten Raman-Spektrum. (> 300 cm^{-1}) (*v*: Streckschwingung, *δ*: Deformationsschwingung, *π*: Inversionsschwingung, *s*: Symmetrisch, *as*: Asymmetrisch) 55

Tabelle 8. Bandenlagen und -zuordnungen der Raman-Spektren von $(ClOF_2)_2[SnF_6]$, basierend auf dem berechneten Raman-Spektrum. (> 300 cm^{-1}) (*v*: Streckschwingung, *δ*: Deformationsschwingung, *π*: Inversionsschwingung, *s*: Symmetrisch, *as*: Asymmetrisch) 56

Tabelle 9. Gitterparameter und Zellvolumina der isotypen Verbindungen $ClOF_2MF_5$ (*M* = Sn, Pb) 59

Tabelle 10. Bandenlagen und -zuordnungen der Raman-Spektren von $ClOF_2PbF_5$, basierend auf dem berechneten Raman-Spektrum. (> 300 cm^{-1}) (*v*: Streckschwingung, *δ*: Deformationsschwingung, *π*: Inversionsschwingung, *s*: Symmetrisch, *as*: Asymmetrisch) 63

Tabelle 11. Bandenlagen und -zuordnungen der Infrarotspektren von festem $ClOF_2[BF_4]$, basierend auf dem berechneten Spektrum. (> 400 cm^{-1}) Das berechnete Spektrum basiert auf einem geordneten Modell von $ClOF_2[BF_4]$ in der Raumgruppe $Pna2_1$ (Nr. 33), siehe Abschnitt 8.2.2.9. (*v*: Streckschwingung, *δ*: Deformationsschwingung, *π*: Inversionsschwingung, *s*: Symmetrisch, *as*: Asymmetrisch, n.b.: nicht beobachtet) 68

Tabelle 12. Bandenlagen und -zuordnungen der Raman-Spektren von festem $ClOF_2[BF_4]$, basierend auf dem berechneten Spektrum. (> 300 cm^{-1}) Das berechnete Spektrum basiert auf einem geordneten Modell von $ClOF_2[BF_4]$ in der Raumgruppe $Pna2_1$ (Nr. 33), siehe Abschnitt 8.2.2.9. (*v*: Streckschwingung, *δ*: Deformationsschwingung, *π*: Inversionsschwingung, *s*: Symmetrisch, *as*: Asymmetrisch, n.b.: nicht beobachtet) 69

Tabelle 13. Bandenlagen und -zuordnungen der Infrarotspektren von $ClOF_2[Mo_3O_3F_{13}]$, basierend auf dem berechneten Spektrum. (> 400 cm^{-1}) (*v*: Streckschwingung, *δ*: Deformationsschwingung, *π*: Inversionsschwingung, *s*: Symmetrisch, *as*: Asymmetrisch, n.b.: nicht beobachtet)..... 74
Tabelle 14. Bandenlagen und -zuordnungen der Raman-Spektren von $ClOF_2[Mo_3O_3F_{13}]$, basierend auf dem berechneten Spektrum. (> 300 cm^{-1}) (*v*: Streckschwingung, *δ*: Deformationsschwingung, *π*: Inversionsschwingung, *s*: Symmetrisch, *as*: Asymmetrisch) 75
Tabelle 15. Bandenlagen und -zuordnungen der Raman-Spektren von $(ClOF_2[OsO_3F_3])_2OsF_6$, basierend auf dem berechneten Spektrum. (> 300 cm^{-1}) (*v*: Streckschwingung, *δ*: Deformationsschwingung, *π*: Inversionsschwingung, *s*: Symmetrisch, *as*: Asymmetrisch, n.b.: nicht beobachtet)..... 80
Tabelle 16. Raman-aktive Streck- und Scherschwingungen des $[OsO_3F_3]^-$-Anions verschiedener $[OsO_3F_3]^-$-Salze. (>300 cm^{-1}) (*v*: Streckschwingung, *δ*: Scherschwingung) 81
Tabelle 17. Raman-aktive Streck- und Scherschwingungen des OsF_6-Moleküls. (*v*: Streckschwingung, *δ*: Scherschwingung, s: Symmetrisch, as: Asymmetrisch) 81
Tabelle 18. Bandenlagen und -zuordnungen der Raman-Spektren von $(ClOF_2)_2[AuF_4][SbF_6]$, basierend auf dem berechneten Spektrum. (> 300 cm^{-1}) (*v*: Streckschwingung, *δ*: Deformationsschwingung, *π*: Inversionsschwingung, *s*: Symmetrisch, *as*: Asymmetrisch, n.b.: nicht beobachtet)..... 86
Tabelle 19. Raman-aktive Streck- und Scherschwingungen des $[AuF_4]^-$-Anions in Tetrafluoridoauraten(III). (*v*: Streckschwingung, *δ*: Scherschwingung, s: Symmetrisch, as: Asymmetrisch)..... 86
Tabelle 20. Raman-aktive Streck- und Scherschwingungen des $[SbF_6]^-$-Anions in Hexafluoridoantimonaten(V). (*v*: Streckschwingung, *δ*: Scherschwingung) 86
Tabelle 21. Gemessene und berechnete Cl−O-, Cl−F- und Cl···F-Abstände in Difluorooxychloronium(V)-Verbindungen. Die berechneten Abstände stammen aus den mit CRYSTAL17 optimierten Strukturen (DFT-PBE0/TZVP). 88
Tabelle 22. Ausgewählte gemessene und berechnete Winkel in Difluorooxychloronium(V)-Verbindungen. Die berechneten Winkel stammen aus den mit CRYSTAL17 optimierten Strukturen (DFT-PBE0/TZVP). 90
Tabelle 23. Vergleich der Raman-aktiven Banden (Bandenlagen in cm^{-1}) des $ClOF_2^+$-Kations in verschiedenen Difluorooxychloronium(V)-Verbindungen. (*v*: Streckschwingung, *δ*: Scherschwingung, *π*: Inversionsschwingung, s: Symmetrisch, as: Asymmetrisch, n.b: nicht beobachtet)..... 92
Tabelle 24. Übersicht über die Strukturmotive, die Art der Verbrückung des Anions und die Niggli-Formeln der charakterisierten ClF_2^+-Verbindungen. Die Koordinationszahl der Chloratome beträgt in allen aufgelisteten Verbindungen 2+2. 95
Tabelle 25. Übersicht über die Strukturmotive und die Niggli-Formeln der in dieser Arbeit beschriebenen $ClOF_2^+$-Verbindungen. Die Koordinationszahl der Chloratome beträgt in allen aufgelisteten Verbindungen 3+3. 96
Tabelle 26. Übersicht über die Koordinationszahlen der Chloratome (KZ(Cl)), der Strukturmotive und der Niggli-Formeln der in dieser Arbeit beschriebenen ClO_2^+-Verbindungen. 97

Tabelle 27. Gitterparameter und Zellvolumina der isotypen Verbindungen NH_4MF_5 (*M* = U, Pu) und $TlMF_5$ (*M* = Th, Np, Pu). 109
Tabelle 28. Vergleich der *M*−F-Abstände in NH_4MF_5 (*M* = U, Pu) und $TlMF_5$ (*M* = Th, Np, Pu) des *β*-NH_4UF_5-Typs.[334] 110
Tabelle 29. Gitterparameter und Zellvolumina der isotypen Verbindungen NaM_2F_9 (*M* = U, Np, Pu) und KM_2F_9 (*M* = Th, U, Pu) des KU_2F_9-Typs.[353] 114
Tabelle 30. Vergleich der *M*−F-Abstände in NaM_2F_9 (*M* = U, Np, Pu) und KM_2F_9 (*M* = Th, U, Pu) des KU_2F_9-Typs.[353] 115
Tabelle 31. Details zu den N−H···F-Wasserstoffbrückenbindungen in $(N_2H_6)U_2F_{10}(HF)_2$. 126
Tabelle 32. Gitterparameter der kubischen Modifikationen der Heptafluoridouranate $A[UF_7]$ (*A* = Na, K, Rb, Cs, NO) bei Raumtemperatur.[395] 128
Tabelle 33. Moleküle (ReF_7 und IF_7) und homoleptische Komplexe mit Koordinationszahl sieben für das Zentralatom. (1/4/2-Anordnung: einfach überkapptes trigonales Prisma; 1/3/3-Anordnung: einfach überkapptes Oktaeder; 1/5/1-Anordnung: pentagonale Bipyramide) 129
Tabelle 34. Bandenlagen und -zuordnungen der Raman-Spektren von Heptafluoridouranaten(VI). (>240 cm^{-1}) (*v*: Streckschwingung, *δ*: Scherschwingung, s: Symmetrisch, as: Asymmetrisch) 131
Tabelle 35. Ausgewählte Daten und Details der Strukturbestimmung von $(ClOF_2)_2[CrF_6]$. 420
Tabelle 36. Atomkoordinaten und äquivalente isotrope Auslenkungsparameter, U_{iso}, der Verbindung $(ClOF_2)_2[CrF_6]$ bei 100 K. 421
Tabelle 37. Anisotrope Auslenkungsparameter, U_{ij}, der Verbindung $(ClOF_2)_2[CrF_6]$ bei 100 K. 421
Tabelle 38. Ausgewählte Daten und Details der Strukturbestimmung von $(ClOF_2)_2[RhF_6]$. 422
Tabelle 39. Atomkoordinaten und äquivalente isotrope Auslenkungsparameter, U_{iso}, der Verbindung $(ClOF_2)_2[RhF_6]$ bei 100 K. 423
Tabelle 40. Anisotrope Auslenkungsparameter, U_{ij}, der Verbindung $(ClOF_2)_2[RhF_6]$ bei 100 K. 423
Tabelle 41. Ausgewählte Daten und Details der Strukturbestimmung von $(ClOF_2)_2[GeF_6]$. 424
Tabelle 42. Atomkoordinaten und äquivalente isotrope Auslenkungsparameter, U_{iso}, der Verbindung $(ClOF_2)_2[GeF_6]$ bei 100 K. 425
Tabelle 43. Anisotrope Auslenkungsparameter, U_{ij}, der Verbindung $(ClOF_2)_2[GeF_6]$ bei 100 K. 425
Tabelle 44. Ausgewählte Daten und Details der Strukturbestimmung von $(ClOF_2)_2[PdF_6]$. 426
Tabelle 45. Atomkoordinaten und äquivalente isotrope Auslenkungsparameter, U_{iso}, der Verbindung $(ClOF_2)_2[PdF_6]$ bei 100 K. 427
Tabelle 46. Anisotrope Auslenkungsparameter, U_{ij}, der Verbindung $(ClOF_2)_2[PdF_6]$ bei 100 K. 427
Tabelle 47. Ausgewählte Daten und Details der Strukturbestimmung von $(ClOF_2)_2[PtF_6]$. 428
Tabelle 48. Atomkoordinaten und äquivalente isotrope Auslenkungsparameter, U_{iso}, der Verbindung $(ClOF_2)_2[PtF_6]$ bei 100 K. 428
Tabelle 49. Anisotrope Auslenkungsparameter, U_{ij}, der Verbindung $(ClOF_2)_2[PtF_6]$ bei 100 K. 429
Tabelle 50. Ausgewählte Daten und Details der Strukturbestimmung von $(ClOF_2)_2[SnF_6]$. 429
Tabelle 51. Atomkoordinaten und äquivalente isotrope Auslenkungsparameter, U_{iso}, der Verbindung $(ClOF_2)_2[SnF_6]$ bei 100 K. 430
Tabelle 52. Anisotrope Auslenkungsparameter, U_{ij}, der Verbindung $(ClOF_2)_2[SnF_6]$ bei 100 K. 430

Tabelle 53. Ausgewählte Daten und Details der Strukturbestimmung von $ClOF_2SnF_5$. 431
Tabelle 54. Atomkoordinaten und äquivalente isotrope Auslenkungsparameter, U_{iso}, der Verbindung $ClOF_2SnF_5$ bei 100 K. 432
Tabelle 55. Anisotrope Auslenkungsparameter, U_{ij}, der Verbindung $ClOF_2SnF_5$ bei 100 K. 432
Tabelle 56. Ausgewählte Daten und Details der Strukturbestimmung von $ClOF_2PbF_5$. 433
Tabelle 57. Atomkoordinaten und äquivalente isotrope Auslenkungsparameter, U_{iso}, der Verbindung $ClOF_2PbF_5$ bei 100 K. 434
Tabelle 58. Anisotrope Auslenkungsparameter, U_{ij}, der Verbindung $ClOF_2PbF_5$ bei 100 K. 434
Tabelle 59. Ausgewählte Daten und Details der Strukturbestimmung von $ClOF_2[BF_4]$. 435
Tabelle 60. Atomkoordinaten und äquivalente isotrope Auslenkungsparameter, U_{iso}, der Verbindung $ClOF_2[BF_4]$ bei 100 K. 436
Tabelle 61. Anisotrope Auslenkungsparameter, U_{ij}, der Verbindung $ClOF_2[BF_4]$ bei 100 K. 436
Tabelle 62. Ausgewählte Daten und Details der Strukturbestimmung von $ClOF_2[Mo_3O_3F_{13}]$. 437
Tabelle 63. Atomkoordinaten und äquivalente isotrope Auslenkungsparameter, U_{iso}, der Verbindung $ClOF_2[Mo_3O_3F_{13}]$ bei 100 K. 438
Tabelle 64. Anisotrope Auslenkungsparameter, U_{ij}, der Verbindung $ClOF_2[Mo_3O_3F_{13}]$ bei 100 K. 439
Tabelle 65. Ausgewählte Daten und Details der Strukturbestimmung von $(ClOF_2[OsO_3F_3])_2OsF_6$. 440
Tabelle 66. Atomkoordinaten und äquivalente isotrope Auslenkungsparameter, U_{iso}, der Verbindung $(ClOF_2[OsO_3F_3])_2OsF_6$ bei 100 K. 441
Tabelle 67. Anisotrope Auslenkungsparameter, U_{ij}, der Verbindung $(ClOF_2[OsO_3F_3])_2OsF_6$ bei 100 K. 441
Tabelle 68. Ausgewählte Daten und Details der Strukturbestimmung von $(ClOF_2)_2[AuF_4][SbF_6]$. 442
Tabelle 69. Atomkoordinaten und äquivalente isotrope Auslenkungsparameter, U_{iso}, der Verbindung $(ClOF_2)_2[AuF_4][SbF_6]$ bei 100 K. 443
Tabelle 70. Anisotrope Auslenkungsparameter, U_{ij}, der Verbindung $(ClOF_2)_2[AuF_4][SbF_6]$ bei 100 K. 443
Tabelle 71. Ausgewählte Daten und Details der Strukturbestimmung von NH_4PuF_5. 444
Tabelle 72. Atomkoordinaten und äquivalente isotrope Auslenkungsparameter, U_{iso}, der Verbindung NH_4PuF_5 bei 100 K. 445
Tabelle 73. Anisotrope Auslenkungsparameter, U_{ij}, der Verbindung NH_4PuF_5 bei 100 K. 445
Tabelle 74. Ausgewählte Daten und Details der Strukturbestimmung von $TlNpF_5$. 446
Tabelle 75. Atomkoordinaten und äquivalente isotrope Auslenkungsparameter, U_{iso}, der Verbindung $TlNpF_5$ bei 293 K. 447
Tabelle 76. Anisotrope Auslenkungsparameter, U_{ij}, der Verbindung $TlNpF_5$ bei 293 K. 447
Tabelle 77. Ausgewählte Daten und Details der Strukturbestimmung von $TlPuF_5$. 448
Tabelle 78. Atomkoordinaten und äquivalente isotrope Auslenkungsparameter, U_{iso}, der Verbindung $TlPuF_5$ bei 289 K. 449
Tabelle 79. Anisotrope Auslenkungsparameter, U_{ij}, der Verbindung $TlPuF_5$ bei 289 K. 449
Tabelle 80. Ausgewählte Daten und Details der Strukturbestimmung von $NaPu_2F_9$. 450

Tabelle 81. Atomkoordinaten und äquivalente isotrope Auslenkungsparameter, U_{iso}, der Verbindung $NaNp_2F_9$ bei 100 K. 451
Tabelle 82. Anisotrope Auslenkungsparameter, U_{ij}, der Verbindung $NaNp_2F_9$ bei 100 K. 451
Tabelle 83. Ausgewählte Daten und Details der Strukturbestimmung von KPu_2F_9. 452
Tabelle 84. Atomkoordinaten und äquivalente isotrope Auslenkungsparameter, U_{iso}, der Verbindung KPu_2F_9 bei 100 K. 453
Tabelle 85. Anisotrope Auslenkungsparameter, U_{ij}, der Verbindung KPu_2F_9 bei 100 K. 453
Tabelle 86. Ausgewählte Daten und Details der Strukturbestimmung von $Sr[UF_5(HF_2)_2]$. 454
Tabelle 87. Atomkoordinaten und äquivalente isotrope Auslenkungsparameter, U_{iso}, der Verbindung $Sr[UF_5(HF_2)_2]$ bei 100 K. 455
Tabelle 88. Anisotrope Auslenkungsparameter, U_{ij}, der Verbindung $Sr[UF_5(HF_2)_2]$ bei 100 K. 455
Tabelle 89. Ausgewählte Daten und Details der Strukturbestimmung von $Ba(HF)_2U_2F_{12}$. 456
Tabelle 90. Atomkoordinaten und äquivalente isotrope Auslenkungsparameter, U_{iso}, der Verbindung $Ba(HF)_2U_2F_{12}$ bei 100 K. 457
Tabelle 91. Anisotrope Auslenkungsparameter, U_{ij}, der Verbindung $Ba(HF)_2U_2F_{12}$ bei 100 K. 457
Tabelle 92. Ausgewählte Daten und Details der Strukturbestimmung von $(N_2H_6)U_2F_{10}(HF_2)_2$. 458
Tabelle 93. Atomkoordinaten und äquivalente isotrope Auslenkungsparameter, U_{iso}, der Verbindung $(N_2H_6)U_2F_{10}(HF_2)_2$ bei 100 K. 459
Tabelle 94. Anisotrope Auslenkungsparameter, U_{ij}, der Verbindung $(N_2H_6)U_2F_{10}(HF_2)_2$ bei 100 K. 459
Tabelle 95. Ausgewählte Daten und Details der Strukturbestimmung von $Rb[UF_7]$. 460
Tabelle 96. Atomkoordinaten und äquivalente isotrope Auslenkungsparameter, U_{iso}, der Verbindung $Rb[UF_7]$ bei 100 K. 461
Tabelle 97. Anisotrope Auslenkungsparameter, U_{ij}, der Verbindung $Rb[UF_7]$ bei 100 K. 461
Tabelle 98. Atomkoordinaten der optimierten Struktur von $(ClOF_2)_2[CrF_6]$. 466
Tabelle 99. Atomkoordinaten der optimierten Struktur von $(ClOF_2)_2[RhF_6]$. 466
Tabelle 100. Atomkoordinaten der optimierten Struktur von $(ClOF_2)_2[GeF_6]$. 467
Tabelle 101. Atomkoordinaten der optimierten Struktur von $(ClOF_2)_2[PdF_6]$. 467
Tabelle 102. Atomkoordinaten der optimierten Struktur von $(ClOF_2)_2[PtF_6]$. 468
Tabelle 103. Atomkoordinaten der optimierten Struktur von $(ClOF_2)_2[SnF_6]$. 468
Tabelle 104. Atomkoordinaten der optimierten Struktur von $ClOF_2SnF_5$. 468
Tabelle 105. Atomkoordinaten der optimierten Struktur von $ClOF_2PbF_5$. 469
Tabelle 106. Atomkoordinaten der optimierten Struktur von $ClOF_2[BF_4]$. 469
Tabelle 107. Atomkoordinaten der optimierten Struktur von $ClOF_2[Mo_3O_3F_{13}]$. 470
Tabelle 108. Atomkoordinaten der optimierten Struktur von $(ClOF_2[OsO_3F_3])_2OsF_6$. 471
Tabelle 109. Atomkoordinaten der optimierten Struktur von $(ClOF_2)_2[AuF_4][SbF_6]$. 471
Tabelle 110. Atomkoordinaten der optimierten Struktur von $Rb[UF_7]$. 472
Tabelle 111. Berechnete durchschnittliche Mulliken-Ladungen der *M*-, Cl-, O- und F-Atome der Kationen und Anionen in Difluorooxychloronium(V)-Verbindungen. Die Mulliken-Populationsanalysen basieren auf den mit CRYSTAL17 optimierten Strukturen (DFT-PBE0/TZVP).[246] (*M*: Zentralatom des Anions) 473